Virchows Arch (2010) 456:1–12
DOI 10.1007/s00428-009-0824-9

REVIEW AND PERSPECTIVE

Precursors of endometrial and ovarian carcinoma

Robert J. Kurman · Thomas G. McConnell

Received: 28 April 2009 / Revised: 29 June 2009 / Accepted: 17 August 2009 / Published online: 27 October 2009
© Springer-Verlag 2009

Abstract This review discusses precursor lesions of endometrial and ovarian carcinoma with an emphasis on the unique molecular alterations that have led to the development of binary classification schemes for tumors of both the endometrium and ovary. While such a system is well established for endometrial carcinoma, only recently has a binary classification scheme been proposed for ovarian carcinoma. For both, the morphologic and molecular genetic-defining characteristics of their respective precursor lesions are described in detail. Furthermore, similarities and differences of the precursor lesions of specific tumors of these two genital tract organs are also addressed with a brief discussion of the clinical implications of their diagnosis.

Keywords Carcinoma precursors · Endometrial carcinoma · Ovarian carcinoma · Endometrial intraepithelial carcinoma · Tubal intraepithelial carcinoma · p53 signature

The precursors of the most common type of endometrial carcinoma, endometrioid carcinoma, have been recognized for the last several decades whereas the precursors of the most common type of ovarian carcinoma, serous carcinoma, have only recently been elucidated. It is of interest that despite obvious differences in the nature of these lesions, there are some striking parallels. Accordingly, in this review, we will attempt to compare their similarities and differences as they offer important insights into the pathogenesis of these two malignancies which in turn is important for the development of new methods of early detection and novel approaches to treatment. We will begin with a discussion of the precursors of endometrial carcinoma followed by a discussion of ovarian cancer precursors.

In discussing endometrial and ovarian carcinoma and their respective precursors, it becomes clear that certain conceptual homologies exist between the two. In both, there are distinct clinical and pathologic features that allow for a division into two broad groupings. This dualistic model is now well accepted for endometrial carcinoma and a similar model has recently been proposed for ovarian carcinoma [1–3]. In the case of endometrial carcinoma, the two groupings, designated type I and type II, were first based on clinical features, followed and bolstered by histomorphologic features, and finally solidified by the discovery of specific molecular genetic alterations that correspond to the clinical and pathologic features. For ovarian tumors, the recent dualistic model proposed by Shih and Kurman is similar; it correlates clinicopathologic features and behavior with specific molecular alterations, allowing for a dualistic classification system that accommodates all of the surface epithelial tumors [2].

Precursors for any given carcinoma should be morphologically recognizable lesions that are reproducible thereby permitting early clinical intervention. Defining such lesions by morphology alone, however, is often imperfect and frequently suffers from significant interobserver disagreement. Our understanding of the underlying molecular events in carcinogenesis [4] has confirmed morphologic

R. J. Kurman
Departments of Gynecology and Obstetrics, and Pathology,
The Johns Hopkins University School of Medicine and Hospital,
Baltimore, MD, USA

T. G. McConnell
Department of Pathology,
The Johns Hopkins University School of Medicine and Hospital,
Baltimore, MD, USA
e-mail: tmcconnell@pathgroup.com

R. J. Kurman (✉)
Department of Pathology, The Johns Hopkins Hospital,
Weinberg 2242, 401 N. Broadway,
Baltimore, MD 21231, USA
e-mail: rkurman@jhmi.edu

observations indicating that what were thought to be precursors are indeed precursor lesions, by demonstrating that such lesions harbor the identical genetic alterations detected in the corresponding invasive carcinoma. In modern surgical pathology, such molecular genetic analysis serves as the underpinning for defining histologically reproducible precursor lesions. The goal, ultimately, is that the histologic recognition of these lesions will lead to early identification and possible curative intervention prior to the development of overtly malignant disease.

Endometrial carcinoma

Endometrial carcinoma is the most common gynecologic malignancy in industrialized nations. In the USA, it is estimated that in 2008, there were approximately 40,000 new cases and over 7,300 women died of the disease [5]. Based on clinical characteristics, tumor histomorphology and more recently, distinct molecular findings, the majority of endometrial carcinomas can be segregated into two broad categories, designated type I and type II [6]. Although overlap exists and certain histologic variants do not neatly fit into either category, type I carcinomas represent approximately 80% of all cases with most resembling the nonmalignant endometrium and therefore termed "endometrioid", though they can also show other types of histologic differentiation. Patients with type I tumors frequently share common clinical features including obesity, anovulation, and the use of estrogen medications that lead to unopposed estrogenic stimulation of the endometrium. These tumors are typically less aggressive compared to type II tumors with a 5-year survival (all stages) of 85% [5]. In contrast, type II tumors are unrelated to unopposed estrogenic stimulation and are highly aggressive. They resemble serous carcinoma of the ovary/fallopian tube and tend to arise in women that are at least 5 to 10 years older than those with type I tumors. For type I tumors, a significant body of literature exists suggesting that these tumors develop in an orderly progression from proliferative endometrium to endometrial hyperplasia and atypical hyperplasia before progressing to well-differentiated endometrioid carcinoma. Molecularly, they share one of a few specific mutations that are distinct from type II tumors [7]. On the other hand, the progression model and putative precursor lesion of endometrial serous carcinoma is not as well understood.

Type I endometrial carcinoma precursors

Type I endometrial carcinomas are the most common type of endometrial carcinoma, accounting for up to 80% of cases [8, 9]. The overwhelming number of cases are classified as "endometrioid", though distinct variants exist, including mucinous and secretory carcinomas (Fig. 1). These carcinomas can, for the most part, be regarded as estrogen-dependent tumors. A sizable body of literature exists that correlates hyperestrogenism of various etiologies, from endogenous (persistent anovulatory menstrual cycles, obesity, estrogen-producing tumors) and exogenous (estrogen only hormone replacement therapy) sources, with the development of endometrial hyperplasia and endometrial carcinoma [10]. The age range for most patients developing a type I carcinoma is 50 to 70 years, peaking around 60 years. There is, however, a wide age range from young premenopausal women under 30 years to older postmenopausal women over 70 years.

In a well-accepted progression model for type I tumors, unopposed estrogen results in endometrial hyperplasia which becomes progressively more complex architecturally and that may or may not be associated with cytologic atypia. In some instances, the atypical hyperplastic lesions, when left untreated, can develop into carcinoma. Which hyperplasias progress to carcinomas and which do not was the subject of a landmark study by Kurman et al. [11], the findings of which now provide the underlying morphologic basis for the most widely accepted classification that was adopted by the WHO in 1994. This classification system subdivides endometrial hyperplasias into two categories based on the presence or absence of cytologic atypia and then further segregates lesions based on their architectural complexity (simple and complex hyperplasia; Fig. 2). In addition to defining the concept of simple and complex hyperplasia (both architectural aberrations), this study also demonstrated that it is cytologic atypia that is the single

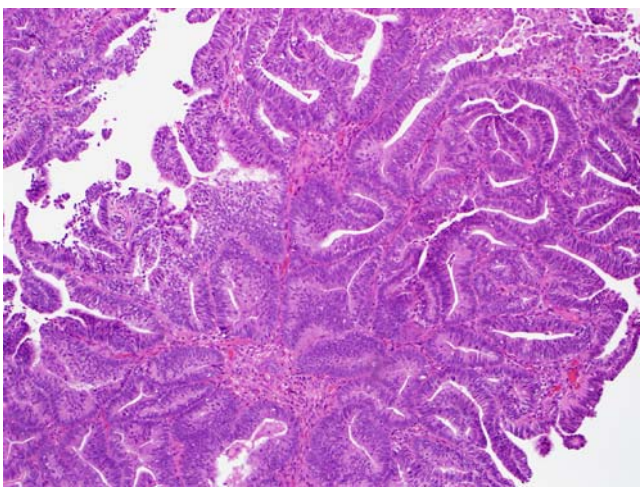

Fig. 1 Endometrioid carcinoma. Well-differentiated endometrioid carcinoma (FIGO grade 1) is characterized by a desmoplastic or "altered" stroma comprised of a fibroblastic stroma, a complex confluent gland pattern, and low-grade nuclei in the neoplastic glands

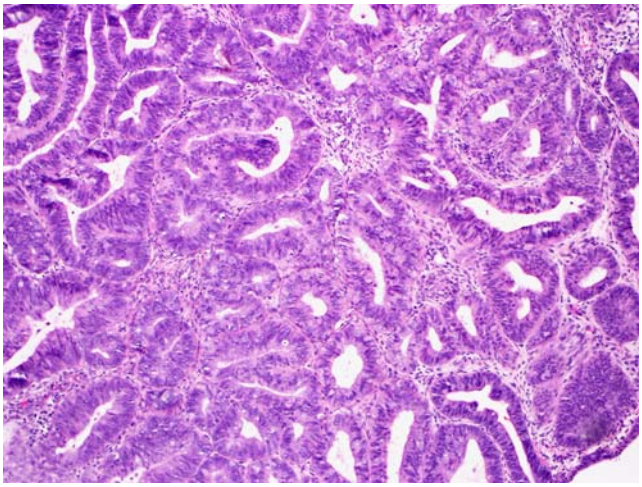

Fig. 2 Complex atypical hyperplasia. Each of the closely packed irregular glands is encompassed by intervening stroma. Nuclear stratification is evident

most important prognostic indicator for progression from hyperplasia to carcinoma. Unfortunately, what constitutes cytologic atypia is subject to significant interobserver reproducibility [12–14]. The morphologic features of cytologic atypia involve alterations in the nuclei including stratification, loss of polarity, enlargement, rounding, coarsening of chromatin, and the presence of prominent nucleoli (Fig. 3). Mitotic activity is variable and there is frequently an eosinophilic cytoplasmic alteration (eosinophilic metaplasia). These atypical features should be readily apparent and involve the majority of the cells in any given gland. Complex glandular architecture, defined as back-to-back crowding with minimal intervening stroma, almost always occurs when cytologic atypia is present. Simple hyperplasia is only rarely associated with cytologic atypia.

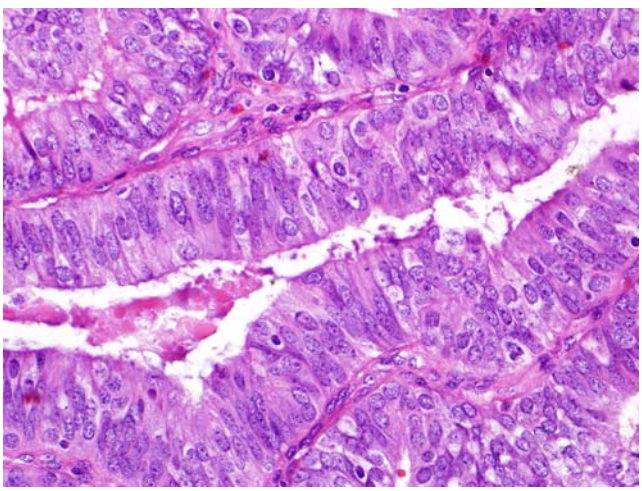

Fig. 3 Complex atypical hyperplasia. At ×400 magnification, the nuclei are predominantly rounded with vesicular nuclei containing clumped chromatin and enlarged irregular nucleoli. These changes are considered diagnostic of "atypia"

Recently, some investigators have attempted to improve the accuracy of the diagnosis of hyperplasia by utilizing a system (endometrial intraepithelial neoplasia (EIN) system) initially based on the computerized morphometric analyses of Baak et al. and further refined and advanced predominantly by Mutter and colleagues [15–18]. However, this approach has not been validated in large studies using diagnoses rendered by general pathologists, and a recent large comparison study of the EIN system versus the WHO system showed similarly increased risks of progression to carcinoma for diagnoses of EIN and atypical hyperplasia [19]. Furthermore, most clinicians are unfamiliar with it. Thus, the practical utility of this classification has not been established.

Advances in molecular genetics have increased our knowledge of the underlying genetic events that lead to the development of both endometrial hyperplasia and endometrial carcinoma. While no single genetic alteration is present in all endometrioid carcinomas, a handful of specific mutations are commonly found in most type I tumors. The most commonly altered gene is phosphatase and tensin homolog (*PTEN*) occurring in up to 83% of rigorously defined cases of endometrioid carcinomas [20, 21]. Located at 10q23 and encoding for a phosphatase (tyrosine kinase) in the AKT signal transduction pathway, *PTEN* functions as a tumor suppressor gene with an important role in cell survival and with possible roles in both cellular migration and adhesion [7, 22]. *PTEN* mutations are considered early events in type I tumorigenesis as they are found in up to 20% of endometrial hyperplasias (with and without atypia) [23–25]. Loss of PTEN function occurs not only by mutation/deletion but also via epigenetic mechanisms, specifically promoter methylation which can be found in up to 20% of tumors with loss of PTEN function [23]. PTEN immunohistochemical expression patterns have been reported to have utility as a biomarker for those hyperplastic lesions but large scale confirmatory studies have failed to show that loss of PTEN expression has the specificity and reproducibility to be clinically useful [20, 26, 27].

Additional significant and common genetic alterations in type I tumorigenesis include microsatellite instability (MSI) occurring in 20–45% of cases, *K-ras* mutation occurring in 10–30% of cases, and *beta-catenin* mutation in up to 20% cases (with or without associated e-*cadherin* mutations) [28–33]. *p53* mutations are uncommon in endometrioid carcinomas; however, when present, they tend to correlate with high histologic grade, being uncommon in FIGO grade 1 carcinomas and found in nearly 20% of FIGO grade 3 tumors; *p53* mutations rarely coexist with *PTEN* mutations [34]. *K-ras* mutations, as with *PTEN* mutations, are early events as they can also be found in simple hyperplasias [35]. Similarly, MSI, known to frequently be associated

with *PTEN* mutation, is also likely to be an early event in carcinogenesis since it is found in both the hyperplasia and subsequent carcinomas [36]. It is evident that due to the genetic heterogeneity of type I endometrial carcinoma, a single progression model based on molecular genetic mechanisms is not likely to be applicable to all cases. Furthermore, attempts to correlate the varied morphologic appearances of type I tumors with specific genetic alterations have, to date, not shown any utility.

Thus, while molecular genetics has improved our ability to define clinically significant endometrial precursor lesions, namely atypical hyperplasias, the progression model is still a work in progress. Light microscopic morphologic analysis remains the standard means of evaluating endometrial lesions, and the most widely accepted classification scheme, the WHO classification, is the best approach to classifying endometrial adenocarcinoma precursors.

Type II endometrial carcinoma and the putative precursor lesion

Serous carcinoma of the endometrium was first identified by Lauchlan [37] in a brief report and further characterized clinicopathologically by Hendrickson et al. [38]. Serous carcinoma is a distinctive highly aggressive carcinoma and is considered the prototypic type II tumor (Fig. 4). At this time, there are insufficient data to determine whether clear cell carcinoma and malignant mixed Müllerian tumors also belong in this group. In general, putative precursor lesions to invasive serous carcinoma of the endometrium are less well understood than those for type I tumors. The term endometrial intraepithelial carcinoma (EIC), briefly introduced by Sherman et al. in 1992 and formalized by Ambros et al in 1995, is defined as a noninvasive endometrial surface lesion with cytologic features identical to invasive serous carcinoma (Fig. 5) [39, 40]. In the Sherman and Ambros studies, EIC was found adjacent to invasive serous carcinoma of the endometrium in nearly 90% of cases and was also frequently present in foci not in continuity with the invasive carcinoma, giving credence to the concept that this intraepithelial lesion represented a precursor of uterine serous carcinoma. In a subsequent study by Sherman et al., similar p53 immunohistochemical expression patterns in both EIC and synchronous serous carcinoma further supported the view that EIC is a precursor of invasive serous carcinoma [41].

Molecular biologic studies of uterine serous carcinoma have demonstrated mutations in the *p53* gene in up to 90% of uterine serous carcinoma cases [42]. p53 protein is a transcription factor that functions as a tumor suppressor. It is a ubiquitous protein with important roles in response to DNA damage, minimizing the risk of genomic instability, cell-cycle arrest, and, importantly, apoptosis [43]. In 1997, Tashiro et al. demonstrated that in four of five cases with synchronous EIC and invasive serous carcinoma, the EIC and invasive serous carcinoma had identical *p53* mutations [42]. Furthermore, in three of four cases of EIC without invasive carcinoma, *p53* mutations were also demonstrated providing further confirmation that EIC was the precursor of invasive serous carcinoma. Additionally, all isolated EIC cases and 16 of 21 invasive serous carcinomas had strong diffuse nuclear p53 immunohistochemical expression, thus correlating strong diffuse p53 immunohistochemical expression with *p53* mutation in both EIC and invasive serous carcinoma.

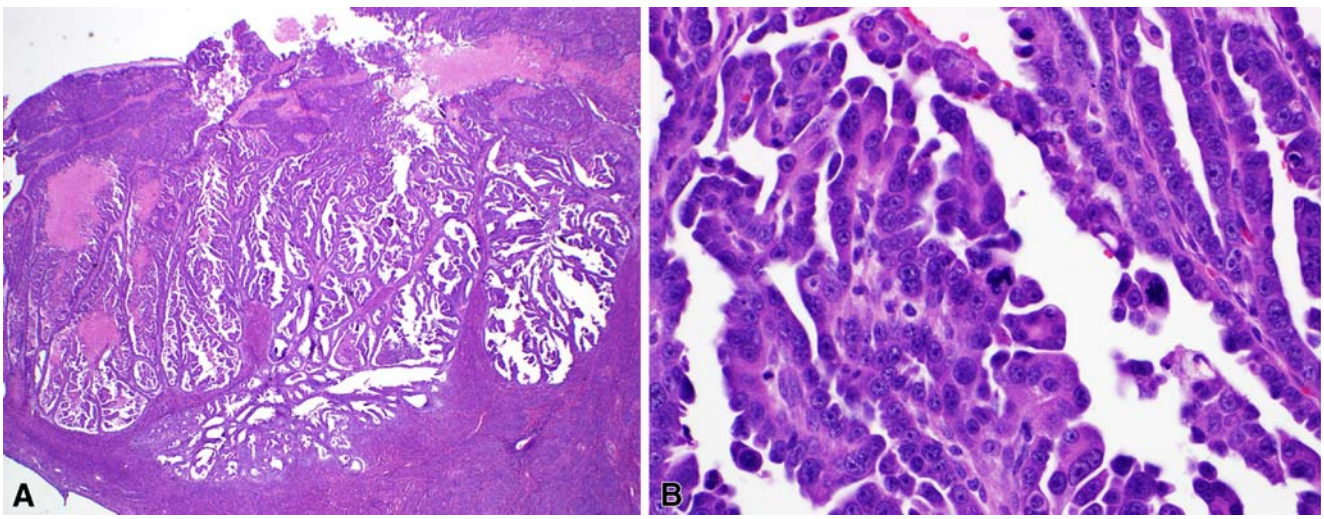

Fig. 4 Serous carcinoma of the endometrium. **a** At low magnification, this tumor is characterized by numerous papillary tufts arising from arborizing papillae. **b** Higher magnification shows characteristic grade 3 nuclear atypia with high nuclear to cytoplasmic ratio, macronucleoli, numerous mitoses, and marked pleomorphism. Note the occasional free-floating cell clusters

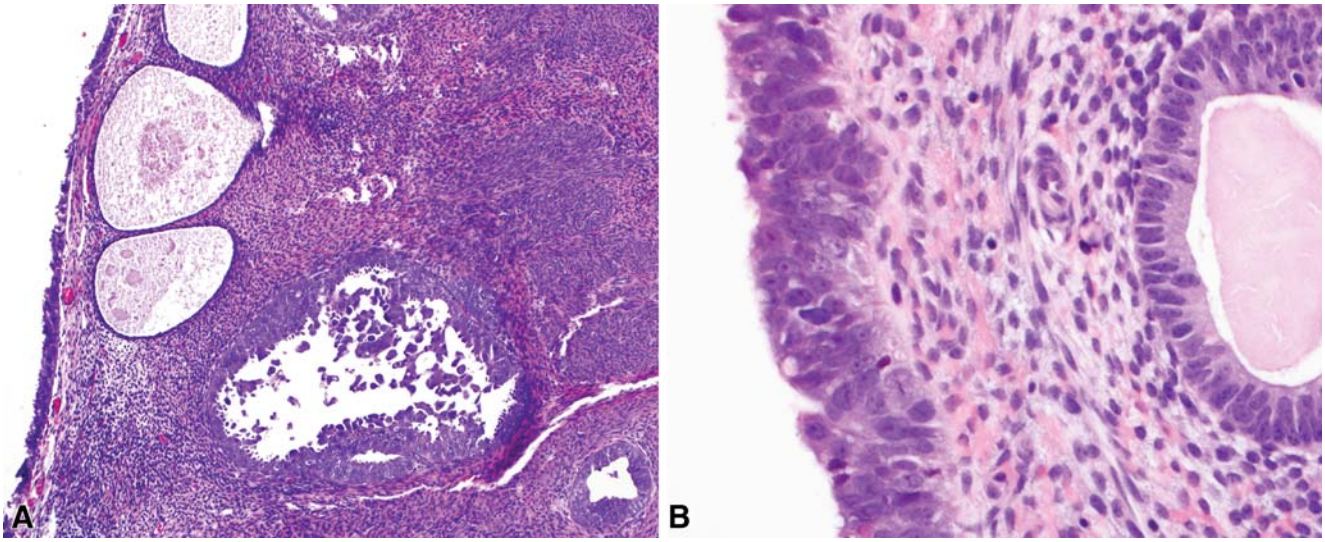

Fig. 5 Endometrial intraepithelial carcinoma. **a** Several glands, as well as the surface epithelium, are lined by malignant cells with high-grade nuclei (**b**) exhibiting marked nuclear enlargement, clumped and smudged chromatin, and prominent cherry-red nucleoli. Interspersed among the involved glands are atrophic and mildly dilated benign glands

Although numerous cases of isolated noninvasive EIC have been reported, most reported cases of EIC demonstrate synchronous invasive endometrial serous carcinoma and some are associated with intraperitoneal disease without identifiable invasive disease in the corpus [39, 44–46]. The finding of extrauterine disease concurrently with isolated EIC does not preclude the use of the term "intraepithelial" for the lesion found in the endometrium. The cells of EIC are loosely cohesive and would appear to be easily shed permitting intratubal spread to the peritoneal cavity even in the absence of invasion in the uterine corpus. Serous carcinoma is highly aggressive and appears to have the capacity to spread rapidly from an initial molecular perturbation (*p53* mutation) to a morphologically identifiable intraepithelial lesion to a frankly invasive and metastatic carcinoma. The traditional cancer progression paradigm of an in situ carcinoma giving rise to a locally invasive carcinoma with dominant mass formation then metastatic spread does not apply to the vast majority of serous carcinomas of the female genital tract, as serous carcinoma metastasizes early in its development. That EIC is only occasionally found exclusive of an invasive component is in keeping with the rapid progression of serous carcinogenesis.

In an attempt to further refine the concept of a precursor lesion to endometrial serous carcinoma, Zheng and colleagues in a morphologic and molecular study of invasive uterine serous carcinoma and EIC have suggested that a "dysplastic" lesion termed "endometrial glandular dysplasia" (EmGD) with serous-like differentiation and atypical cytology of a lesser degree than that of serous EIC is frequently seen in association with uterine serous carcinoma and serous EIC, but not with endometrioid carcinoma [47, 48]. Additionally, according to these investigators, these dysplastic lesions mostly show "intermediate" levels of p53 immunohistochemical expression based on an arbitrary level of expression without correlative *p53* mutational analysis. However, molecular analyses of these lesions frequently show LOH at 17p (TP53 locus), often in a concordant pattern with a paired serous EIC or serous carcinoma [47]. In a more recent molecular analysis of uterine serous neoplasia with multiple foci of EmGD [47, 49], an elevated frequency of p53 mutations (43%) was found; however, correlation of the p53 immunohistochemical expression level in the foci of EmGD with and without *p53* mutations was not performed. It was also found that in six of 14 cases with synchronous EmGD and either serous carcinoma or EIC that at least one identical *p53* mutation was detected in both the EmGD and the synchronous serous neoplastic lesion. While these findings are suggestive that some foci of EmGD may be precursor lesions to endometrial serous carcinoma, it is more likely that the morphologic changes that precede frankly invasive endometrial serous carcinoma show a spectrum of cytologic alterations, with the well-established morphologic features of EIC being at the more extreme end of that spectrum and perhaps some of lesions of the type designated as EmGD at the opposite end. However, since the molecular hallmark of serous carcinogenesis is *p53* mutation and there is a growing body of evidence that, at least in serous neoplasia of the distal fallopian tube, *p53* mutation precedes even subtle morphologic alterations, such a low level of *p53* mutation in EmGD (43%), an already morphologically recognizable lesion, raises concern that such an entity, even if diagnostically reproducible, is at best a heterogeneous lesion that in some instances may represent the earliest

recognizable cytologic alterations of *p53* mutation and hence serous carcinogenesis, but is not specific enough to assist in clinical decision making. Furthermore, it is unclear from the available literature what "intermediate" p53 immunohistochemical expression of serous-like endometrial lesions actually represents in regard to *p53* gene mutation. In fact, p53 immunohistochemical expression of less than strong diffuse nuclear staining has not been systematically studied and/or correlated with the presence or absence of *p53* gene mutations. Virtually all classically defined serous EIC lesions demonstrate strong diffuse p53 immunohistochemical expression, and this expression pattern has been strongly correlated with *p53* mutations [41, 42]. It should be noted, however, that on occasion, a case with entirely negative p53 immunohistochemical expression harbors a *p53* mutation. These lesions have been molecularly analyzed and have been shown to have p53 mutations (often nonsense mutations) that likely lead to truncated proteins that are presumed to be either non-immunoreactive or are unstable [42]. Little is known about precursors to rarer histologic subtypes of type II adenocarcinomas. Endometrial clear cell carcinoma is an uncommon high-grade malignancy, and thus, any attempt to define a possible unique and diagnostically reproducible precursor lesion is hindered by its rarity. Though attempts to define a putative precursor lesion for endometrial clear cell carcinoma have been made [50], the findings are as yet inconclusive and suffer from lack of molecular genetic analysis.

Ovarian carcinoma

Ovarian carcinoma, though morphologically more diverse, has significant similarities to endometrial carcinoma. A recently proposed model of ovarian carcinogenesis, similar to the dualistic system for endometrial tumors delineated above, divides surface epithelial tumors into two broad groups based on clinicopathologic and molecular genetic analyses [2]. The dualistic model of ovarian carcinogenesis accommodates the diverse nature of serous carcinomas of the ovary as well as other histologic types. In this proposed system, type I tumors are comprised, for the most part, of cytologically low-grade indolent neoplasms that include low-grade micropapillary serous carcinoma (MPSC), as well as most mucinous endometrioid and clear cell carcinomas. It should be noted that clear cell carcinoma, which is almost always high grade, is an exception to type I tumors being low grade. Generally, these neoplasms are associated with well-accepted and histologically type-specific precursor lesions and are considered to be genetically stable tumors. Type II tumors are highly aggressive rapidly progressive neoplasms with less well-characterized precursor lesions and have a high level of genetic instability. They predominately include high-grade serous carcinoma, but also encompass rarer lesions such as malignant mesodermal mixed tumor and undifferentiated carcinoma. In addition to the obvious differences in clinicopathologic presentation and histomorphology, these two groups of neoplasms have distinct genetic alterations. Utilizing this dualistic model for ovarian carcinogenesis as a conceptual framework, the remainder of the review will focus on precursors to ovarian carcinoma, with an emphasis on both low-grade and high-grade serous carcinoma precursors.

Precursors of type I tumors

Precursors of low-grade ovarian serous carcinoma

A series of detailed clinicopathologic studies of serous borderline tumors performed at our institution has helped to define two distinct morphologies [51, 52]. The more common usual type serous borderline tumor exhibits hierarchical branching and is a benign neoplasm, but is now recognized as being the precursor to noninvasive low-grade micropapillary serous carcinoma. We prefer the designation atypical proliferative serous tumor (APST) for this neoplasm to emphasize its benign behavior and to distinguish it from the less common morphologic appearance of serous borderline tumors, showing nonhierarchical branching, termed MPSC, an entity that some other authors refer to as serous borderline tumor with micropapillary architecture. Morphologic and molecular biologic studies have shown that MPSC is the immediate precursor of invasive low-grade carcinoma (Figs. 6 and 7) [53–55]. At times, invasive low-grade serous carcinomas are associated with APSTs without micropapillary architecture; however, it is conceivable that occult foci of MPSC were not sampled. Invasive MPSC is characterized by small nests and micropapillae haphazardly infiltrating the stroma, psammoma bodies are common, but frank necrosis is almost never observed. Extra-ovarian involvement by either noninvasive or invasive MPSC can be in the form of either noninvasive or invasive implants; however, we consider invasive implants associated with MPSC to be metastases and are diagnosed as such. Not uncommonly, APSTs also have associated extra-ovarian disease and even lymph node involvement. These lesions are virtually always noninvasive and may or may not be etiologically directly related one to the other.

Thus, based largely on molecular genetic studies of noninvasive serous tumors (both APST and noninvasive MPSC), the precursor to noninvasive and invasive MPSC is the APST itself. Supporting this relationship is that both

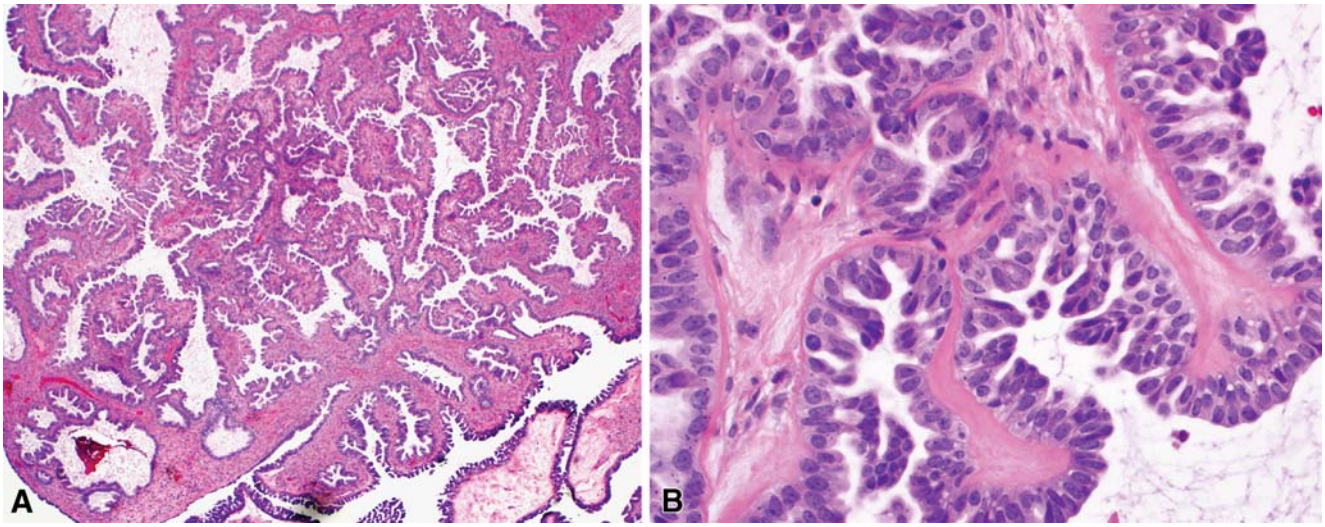

Fig. 6 Atypical proliferative serous tumor. **a** At low magnification, tumor exhibits a hierarchical branching pattern with progressively smaller papillae. The elongated to partially rounded nuclei (**b**) show mild pleomorphism, small nucleoli, and only infrequent mitotic figures (none shown). The tips of the papillae frequently terminate in small cellular clusters that detach and appear to be free-floating

APST and MPSC are characterized by an identical group of mutations, namely sequence mutations in *KRAS*, *BRAF*, and less commonly *ERBB2* [1, 56–62]. These mutations perturb the mitogen-activated protein kinase signal transduction pathway and lead to neoplastic transformation. They are considered early events in low-grade serous carcinogenesis as identical alterations can be found in morphologically benign serous cystadenomas and their associated APST. Although greater allelic imbalance is found in MPSC [58] as compared with APST, the specific underlying molecular etiology of why a specific subset of APST develops micropapillary growth and evolves into MPSC is the subject of ongoing research and has not been clearly elucidated.

Precursors of mucinous ovarian carcinoma

Primary mucinous tumors of the ovary are much less common than serous tumors and although some clinicopathologic similarities exist, there are notable differences in the development of benign and malignant mucinous ovarian neoplasms. It has been recognized for many years that benign mucinous epithelium in both mucinous cystadenomas and atypical proliferative mucinous tumors (APMT) is often found concurrently with primary invasive mucinous carcinomas of the ovary. In fact, it is not uncommon to find a spectrum of morphologic and cytologic changes from cystadenoma to APMT with and without intraepithelial carcinoma to invasive mucinous carcinoma occurring in the same tumor. These findings strongly suggest that mucinous carcinoma develops slowly in a stepwise fashion from benign precursors like the other type I tumors. Molecular genetic analyses support this concept as identical *KRAS* mutations have been found in mucinous carcinomas and its associated/adjacent benign mucinous epithelium (in both cystadenoma and APMT) [61, 63, 64]. To date, mutations other than those of *KRAS* have not been observed in mucinous carcinoma or its precursor lesions.

Precursors of endometrioid and clear cell carcinoma

Ovarian endometrioid carcinomas represent approximately 6% of ovarian surface epithelial neoplasms and 18% of all ovarian carcinomas. The majority of ovarian endometrioid carcinomas are well differentiated and 43% are diagnosed in stage I. Numerous clinicopathologic studies have shown an increased risk of developing endometrioid and clear cell carcinoma in those patients with endometriosis. Furthermore, it is well accepted that endometriosis is considered a precursor lesion for both these specific histologic types of ovarian carcinoma with nearly 30 % of ovarian endometrioid and 50% of ovarian clear cell carcinomas associated with endometriosis [65]. In fact, a morphologically identifiable transition from benign endometriotic foci to an associated endometrioid and clear cell carcinoma has been reported in approximately one third of carefully evaluated cases [66–69]. In a recent study of clear cell carcinoma, 62% of cystic clear cell carcinomas arising in association with endometriosis showed an identifiable transition (atypical endometriosis/intraepithelial carcinoma) from benign to malignant [70]. Similar to APMTs, endometrioid borderline tumors (atypical proliferative endometrioid tumors, APETs) can also be found in association with ovarian endometrioid carcinoma and thus are also considered precursor lesions, a concept bolstered by molecular genetic studies showing the identical mutation in the carcinoma and its associated

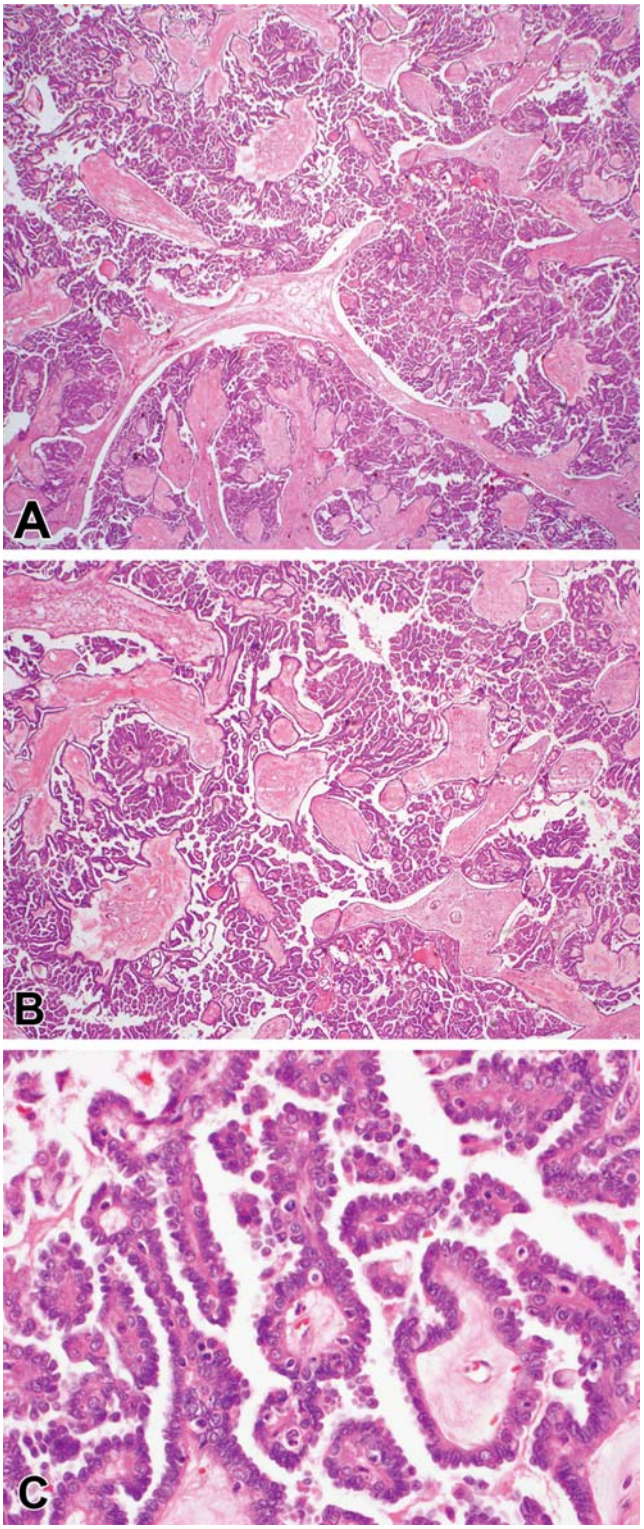

◀ **Fig. 7** Micropapillary serous carcinoma, noninvasive. **a**–**c** Broad papillae give rise to a highly complex epithelial proliferation without significant hierarchical arborization. This case shows many narrow micropapillae, some with stromal cores, emanating from broad-based papillae. Higher magnification shows distinctly rounded cells with obvious nucleoli. In comparison to APSTs, there is more nuclear atypia with a higher nuclear to cytoplasmic ratio, more pleomorphism, and more frequent mitotic figures

APET [71]. The same is likely true for the much rarer atypical proliferative clear cell tumors, but definitive molecular genetic analysis linking the two is lacking. The stepwise progression hypothesized for the development of mucinous carcinoma from cystadenoma to APMT to carcinoma is also applicable to at least a subset of ovarian endometrioid carcinomas that arise in association with an APET. Several studies have reported similar genetic alterations, including LOH at 10q23 and *PTEN* mutations, in both endometrioid carcinoma and associated morphologically benign appearing endometriosis within the same specimen [72–74]. Although only a limited number of molecular genetic studies of endometriosis and endometrioid carcinoma have been reported in the literature, certain genetic alterations are common in these lesions. Namely, similar to those mutations found in uterine endometrioid carcinoma, *PTEN* alterations are found in 20% of ovarian endometrioid carcinomas and *KRAS* and *BRAF* mutations have been found in nearly 10% [72–75]. Interestingly, one study has reported *beta-catenin* mutations in up to 60% of both ovarian endometrioid carcinoma and their associated APETs [71]. Thus, for ovarian endometrioid carcinoma, the molecular genetic alterations, typical well-differentiated histology, and less aggressive behavior support its inclusion as a type I ovarian tumor. Although a recent molecular genetic analysis of clear cell carcinoma has shown a high percentage of cases with *PIK3CA* mutations [76], a finding not commonly seen in other ovarian neoplasms, further study is necessary to confirm this finding and to more precisely define any other unique molecular genetic changes associated with ovarian atypical proliferative clear cell tumors and carcinomas. Presently, for clear cell carcinoma, its inclusion in the recently proposed dualistic model of ovarian carcinogenesis as type I or II is less well established than for serous, mucinous, and endometrioid tumors.

Precursors of type II tumors

Precursors of high-grade serous carcinoma

High-grade serous carcinoma accounts for the overwhelming majority of malignant serous neoplasms of the ovary. Molecular genetic studies have shown that most high-grade serous carcinomas harbor *p53* mutations, similar to uterine serous carcinoma [77–79]. The precursor lesion to this highly aggressive malignancy is less well characterized than that for low-grade serous carcinoma of the ovary and more controversial than the precursor to uterine serous carcinoma. The most widely accepted progression model

for high-grade serous carcinoma involves malignant transformation of ovarian surface epithelium or ovarian cortical inclusion cysts, most likely via *p53* mutation, followed in rapid succession by stromal invasion and peritoneal metastasis. However, ovarian surface epithelium and cortical inclusion cysts only rarely exhibit foci of noninvasive cytologically malignant alteration and such alterations are even less often found without a frankly invasive associated serous carcinoma [80–82]. Thus, lack of an obvious and reproducible precursor lesion led to the initial proposal that serous carcinomas arose de novo. Yet, occasional foci of preinvasive change in surface epithelium and cortical inclusion cysts have been identified, molecularly analyzed, and shown to have identical mutations to concurrent invasive serous carcinoma [81, 83]. Recently, based on the earlier work of Piek et al. [84], Crum and colleagues have proposed that high-grade serous carcinoma may originate from the distal fallopian tube via an intraepithelial carcinoma (tubal intraepithelial carcinoma, TIC; Fig. 8) [85–87]. This group has shown that cytologically malignant intraepithelial lesions with diffuse p53 immunohistochemical expression (most with *p53* mutations) can be associated with metastatic high-grade serous carcinoma. These studies have also led to the demonstration of a putative precursor lesion with no to minimal morphologic alterations originating in the secretory-type epithelial cells that presumably precedes TIC, termed the "p53 signature" (Fig. 8) [88]. These lesions were initially found in patients undergoing risk-reduction salpingo-oophorectomies for breast cancer (BRCA) mutations, but subsequently were also found in women without BRCA mutations. These lesions are comprised of morphologically benign tubal epithelial cells, often with subtle nuclear alterations but lacking stratification. There is evidence of DNA damage and they demonstrate strong diffuse p53 immunohistochemical expression; in nearly 60%, there are *p53* mutations. Clearly not all of these lesions will progress to serous carcinoma or even TIC, but some probably do. No matter what their site of origin, the balance of molecular genetic evidence suggests that *p53* mutations are likely early events in high-grade serous carcinogenesis and that such mutations can precede distinct morphologic alterations. However, because of the rapid development and early metastasis of serous carcinoma, the exact origin of precursors to serous carcinoma will likely remain difficult to conclusively prove.

Summary

The goal of defining specific cancer precursors is to facilitate early detection of lesions with a high risk of development into invasive carcinoma. While this approach is firmly established for some gynecologic malignancies with well-characterized precursor lesions and obvious early clinical manifestations such as atypical endometrial hyperplasia and endometrioid carcinoma, detection of high-grade ovarian serous carcinomas prior to the development of widespread invasive disease remains particularly elusive. Thus, a more realistic approach to the early detection of carcinomas of the female genital tract, specifically high-grade serous carcinoma and uterine serous carcinoma, may

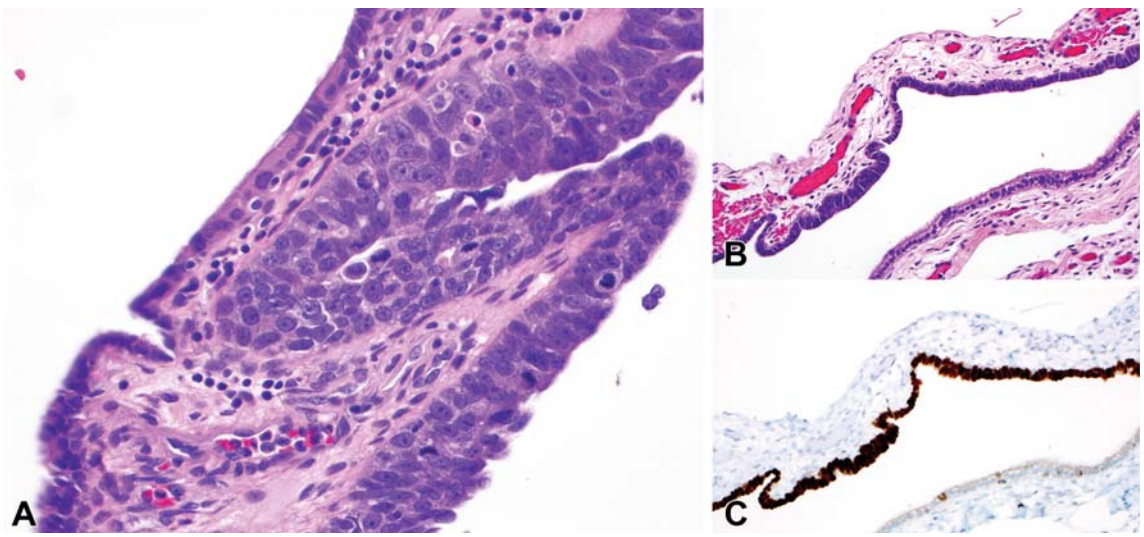

Fig. 8 Tubal intraepithelial carcinoma and the p53 signature. **a** TIC is characterized by the replacement of the native tubal epithelium by cytologically malignant cells with marked nuclear pleomorphism, loss of polarity, and a high nuclear to cytoplasmic ratio (compare to normal tubal epithelium present). These cells show strong diffuse nuclear expression for p53 and in most cases exhibit *p53* mutations. **b**, **c** The p53 signature shows no, or as in this case minimal, cytologic alteration of tubal epithelial cells of the secretory-type (nonciliated). The cells exhibit strong diffuse nuclear p53 expression

be to focus on the development of assays for biomarkers linked to specific genetic aberrations, thus bypassing the obvious anatomic impediment to the early diagnosis of these diseases.

Conflict of interest statement We declare that we have no conflict of interest.

References

1. Singer G, Stohr R, Cope L et al (2005) Patterns of p53 mutations separate ovarian serous borderline tumors and low- and high-grade carcinomas and provide support for a new model of ovarian carcinogenesis: a mutational analysis with immunohistochemical correlation. Am J Surg Pathol 29:218–224
2. Shih I, Kurman RJ (2004) Ovarian tumorigenesis: a proposed model based on morphological and molecular genetic analysis. Am J Pathol 164:1511–1518
3. Kurman RJ, Shih I (2008) Pathogenesis of ovarian cancer: lessons from morphology and molecular biology and their clinical implications. Int J Gynecol Pathol 27:151–160
4. Vogelstein B, Fearon ER, Hamilton SR et al (1988) Genetic alterations during colorectal-tumor development. N Engl J Med 319:525–532
5. Jemal A, Siegel R, Ward E et al (2008) Cancer statistics, 2008. CA Cancer J Clin 58:71–96
6. Bokhman JV (1983) Two pathogenetic types of endometrial carcinoma. Gynecol Oncol 15:10–17
7. Lax SF (2004) Molecular genetic pathways in various types of endometrial carcinoma: from a phenotypical to a molecular-based classification. Virchows Arch 444:213–223
8. Cirisano FD Jr, Robboy SJ, Dodge RK et al (1999) Epidemiologic and surgicopathologic findings of papillary serous and clear cell endometrial cancers when compared to endometrioid carcinoma. Gynecol Oncol 74:385–394
9. Cirisano FD Jr, Robboy SJ, Dodge RK et al (2000) The outcome of stage I–II clinically and surgically staged papillary serous and clear cell endometrial cancers when compared with endometrioid carcinoma. Gynecol Oncol 77:55–65
10. Ronnett BM, Zaino R, Ellenson LH, Kurman R (2002) Endometrial carcinoma. In: Kurman RJ (ed) Blaustein's pathology of the female genital tract. Springer, New York, pp 501–559
11. Kurman RJ, Kaminski PF, Norris HJ (1985) The behavior of endometrial hyperplasia. A long-term study of "untreated" hyperplasia in 170 patients. Cancer 56:403–412
12. Bergeron C, Nogales FF, Masseroli M et al (1999) A multicentric European study testing the reproducibility of the WHO classification of endometrial hyperplasia with a proposal of a simplified working classification for biopsy and curettage specimens. Am J Surg Pathol 23:1102–1108
13. Kendall BS, Ronnett BM, Isacson C et al (1998) Reproducibility of the diagnosis of endometrial hyperplasia, atypical hyperplasia, and well-differentiated carcinoma. Am J Surg Pathol 22:1012–1019
14. Sherman ME, Ronnett BM, Ioffe OB et al (2008) Reproducibility of biopsy diagnoses of endometrial hyperplasia: evidence supporting a simplified classification. Int J Gynecol Pathol 27:318–325
15. Baak JP, Kurver PH, Diegenbach PC et al (1981) Discrimination of hyperplasia and carcinoma of the endometrium by quantitative microscopy—a feasibility study. Histopathology 5:61–68
16. Baak JP (1986) Further evaluation of the practical applicability of nuclear morphometry for the prediction of the outcome of atypical endometrial hyperplasia. Anal Quant Cytol Histol 8:46–48
17. Mutter GL (2000) Endometrial intraepithelial neoplasia (EIN): will it bring order to chaos? The Endometrial Collaborative Group. Gynecol Oncol 76:287–290
18. Mutter GL, Zaino RJ, Baak JP et al (2007) Benign endometrial hyperplasia sequence and endometrial intraepithelial neoplasia. Int J Gynecol Pathol 26:103–114
19. Lacey JV Jr, Mutter GL, Nucci MR et al (2008) Risk of subsequent endometrial carcinoma associated with endometrial intraepithelial neoplasia classification of endometrial biopsies. Cancer 113:2073–2081
20. Mutter GL, Lin MC, Fitzgerald JT et al (2000) Altered PTEN expression as a diagnostic marker for the earliest endometrial precancers. J Natl Cancer Inst 92:924–930
21. Mutter GL (2001) Pten, a protean tumor suppressor. Am J Pathol 158:1895–1898
22. Myers MP, Pass I, Batty IH et al (1998) The lipid phosphatase activity of PTEN is critical for its tumor supressor function. Proc Natl Acad Sci U S A 95:13513–13518
23. Levine RL, Cargile CB, Blazes MS et al (1998) PTEN mutations and microsatellite instability in complex atypical hyperplasia, a precursor lesion to uterine endometrioid carcinoma. Cancer Res 58:3254–3258
24. Yoshinaga K, Sasano H, Furukawa T et al (1998) The PTEN, BAX, and IGFIIR genes are mutated in endometrial atypical hyperplasia. Jpn J Cancer Res 89:985–990
25. Maxwell GL, Risinger JI, Gumbs C et al (1998) Mutation of the PTEN tumor suppressor gene in endometrial hyperplasias. Cancer Res 58:2500–2503
26. Zaino RJ (2000) Endometrial hyperplasia: is it time for a quantum leap to a new classification? Int J Gynecol Pathol 19:314–321
27. Cirpan T, Terek MC, Mgoyi L et al (2006) Immunohistochemical evaluation of PTEN protein in patients with endometrial intraepithelial neoplasia compared to endometrial adenocarcinoma and proliferative phase endometrium. Eur J Gynaecol Oncol 27:389–392
28. Burks RT, Kessis TD, Cho KR et al (1994) Microsatellite instability in endometrial carcinoma. Oncogene 9:1163–1166
29. Caduff RF, Johnston CM, Frank TS (1995) Mutations of the Ki-ras oncogene in carcinoma of the endometrium. Am J Pathol 146:182–188
30. Enomoto T, Inoue M, Perantoni AO et al (1991) K-ras activation in premalignant and malignant epithelial lesions of the human uterus. Cancer Res 51:5308–5314
31. Kobayashi K, Sagae S, Nishioka Y et al (1999) Mutations of the beta-catenin gene in endometrial carcinomas. Jpn J Cancer Res 90:55–59
32. MacDonald ND, Salvesen HB, Ryan A et al (2000) Frequency and prognostic impact of microsatellite instability in a large population-based study of endometrial carcinomas. Cancer Res 60:1750–1752
33. Saegusa M, Hashimura M, Yoshida T et al (2001) beta-Catenin mutations and aberrant nuclear expression during endometrial tumorigenesis. Br J Cancer 84:209–217
34. Lax SF, Kendall B, Tashiro H et al (2000) The frequency of p53, K-ras mutations, and microsatellite instability differs in uterine endometrioid and serous carcinoma: evidence of distinct molecular genetic pathways. Cancer 88:814–824
35. Duggan BD, Felix JC, Muderspach LI et al (1994) Early mutational activation of the c-Ki-ras oncogene in endometrial carcinoma. Cancer Res 54:1604–1607
36. Duggan BD, Felix JC, Muderspach LI et al (1994) Microsatellite instability in sporadic endometrial carcinoma. J Natl Cancer Inst 86:1216–1221

37. Lauchlan SC (1981) Tubal (serous) carcinoma of the endometrium. Arch Pathol Lab Med 105:615–618
38. Hendrickson M, Ross J, Eifel P et al (1982) Uterine papillary serous carcinoma: a highly malignant form of endometrial adenocarcinoma. Am J Surg Pathol 6:93–108
39. Ambros RA, Sherman ME, Zahn CM et al (1995) Endometrial intraepithelial carcinoma: a distinctive lesion specifically associated with tumors displaying serous differentiation. Hum Pathol 26:1260–1267
40. Sherman ME, Bitterman P, Rosenshein NB et al (1992) Uterine serous carcinoma. A morphologically diverse neoplasm with unifying clinicopathologic features. Am J Surg Pathol 16:600–610
41. Sherman ME, Bur ME, Kurman RJ (1995) p53 in endometrial cancer and its putative precursors: evidence for diverse pathways of tumorigenesis. Hum Pathol 26:1268–1274
42. Tashiro H, Isacson C, Levine R et al (1997) p53 gene mutations are common in uterine serous carcinoma and occur early in their pathogenesis. Am J Pathol 150:177–185
43. Harris CC, Hollstein M (1993) Clinical implications of the p53 tumor-suppressor gene. N Engl J Med 329:1318–1327
44. Carcangiu ML, Chambers JT (1992) Uterine papillary serous carcinoma: a study on 108 cases with emphasis on the prognostic significance of associated endometrioid carcinoma, absence of invasion, and concomitant ovarian carcinoma. Gynecol Oncol 47:298–305
45. Goff BA, Kato D, Schmidt RA et al (1994) Uterine papillary serous carcinoma: patterns of metastatic spread. Gynecol Oncol 54:264–268
46. Lee KR, Belinson JL (1992) Papillary serous adenocarcinoma of the endometrium: a clinicopathologic study of 19 cases. Gynecol Oncol 46:51–54
47. Liang SX, Chambers SK, Cheng L et al (2004) Endometrial glandular dysplasia: a putative precursor lesion of uterine papillary serous carcinoma. Part II: molecular features. Int J Surg Pathol 12:319–331
48. Zheng W, Liang SX, Yu H et al (2004) Endometrial glandular dysplasia: a newly defined precursor lesion of uterine papillary serous carcinoma. Part I: morphologic features. Int J Surg Pathol 12:207–223
49. Jia L, Liu Y, Yi X et al (2008) Endometrial glandular dysplasia with frequent p53 gene mutation: a genetic evidence supporting its precancer nature for endometrial serous carcinoma. Clin Cancer Res 14:2263–2269
50. Fadare O, Liang SX, Ulukus EC et al (2006) Precursors of endometrial clear cell carcinoma. Am J Surg Pathol 30:1519–1530
51. Burks RT, Sherman ME, Kurman RJ (1996) Micropapillary serous carcinoma of the ovary. A distinctive low-grade carcinoma related to serous borderline tumors. Am J Surg Pathol 20:1319–1330
52. Seidman JD, Kurman RJ (1996) Subclassification of serous borderline tumors of the ovary into benign and malignant types. A clinicopathologic study of 65 advanced stage cases. Am J Surg Pathol 20:1331–1345
53. Longacre TA, McKenney JK, Tazelaar HD et al (2005) Ovarian serous tumors of low malignant potential (borderline tumors): outcome-based study of 276 patients with long-term (> or =5-year) follow-up. Am J Surg Pathol 29:707–723
54. McKenney JK, Balzer BL, Longacre TA (2006) Lymph node involvement in ovarian serous tumors of low malignant potential (borderline tumors): pathology, prognosis, and proposed classification. Am J Surg Pathol 30:614–624
55. Seidman JD, Kurman RJ (2000) Ovarian serous borderline tumors: a critical review of the literature with emphasis on prognostic indicators. Hum Pathol 31:539–557
56. Nakayama K, Nakayama N, Kurman RJ et al (2006) Sequence mutations and amplification of PIK3CA and AKT2 genes in purified ovarian serous neoplasms. Cancer Biol Ther 5:779–785
57. Sieben NL, Macropoulos P, Roemen GM et al (2004) In ovarian neoplasms, BRAF, but not KRAS, mutations are restricted to low-grade serous tumours. J Pathol 202:336–340
58. Singer G, Kurman RJ, Chang HW et al (2002) Diverse tumorigenic pathways in ovarian serous carcinoma. Am J Pathol 160:1223–1228
59. Singer G, Shih I, Truskinovsky A et al (2003) Mutational analysis of K-ras segregates ovarian serous carcinomas into two types: invasive MPSC (low-grade tumor) and conventional serous carcinoma (high-grade tumor). Int J Gynecol Pathol 22:37–41
60. Singer G, Oldt R III, Cohen Y et al (2003) Mutations in BRAF and KRAS characterize the development of low-grade ovarian serous carcinoma. J Natl Cancer Inst 95:484–486
61. Mayr D, Hirschmann A, Lohrs U et al (2006) KRAS and BRAF mutations in ovarian tumors: a comprehensive study of invasive carcinomas, borderline tumors and extraovarian implants. Gynecol Oncol 103:883–887
62. Ho CL, Kurman RJ, Dehari R et al (2004) Mutations of BRAF and KRAS precede the development of ovarian serous borderline tumors. Cancer Res 64:6915–6918
63. Enomoto T, Weghorst CM, Inoue M et al (1991) K-ras activation occurs frequently in mucinous adenocarcinomas and rarely in other common epithelial tumors of the human ovary. Am J Pathol 139:777–785
64. Gemignani ML, Schlaerth AC, Bogomolniy F et al (2003) Role of KRAS and BRAF gene mutations in mucinous ovarian carcinoma. Gynecol Oncol 90:378–381
65. Russell P (1979) The pathological assessment of ovarian neoplasms. I: introduction to the common 'epithelial' tumours and analysis of benign 'epithelial' tumours. Pathology 11:5–26
66. Fukunaga M, Nomura K, Ishikawa E et al (1997) Ovarian atypical endometriosis: its close association with malignant epithelial tumours. Histopathology 30:249–255
67. McMeekin DS, Burger RA, Manetta A et al (1995) Endometrioid adenocarcinoma of the ovary and its relationship to endometriosis. Gynecol Oncol 59:81–86
68. de la Sainz CR, Eichhorn JH, Rice LW et al (1996) Histologic transformation of benign endometriosis to early epithelial ovarian cancer. Gynecol Oncol 60:238–244
69. Vercellini P, Parazzini F, Bolis G et al (1993) Endometriosis and ovarian cancer. Am J Obstet Gynecol 169:181–182
70. Veras E, Mao TL, Ayse A et al (2009) Cystic and adenofibromatous clear cell carcinomas of the ovary: distinctive tumors that differ in their pathogenesis and behavior: a clinicopathologic analysis of 122 cases. Am J Surg Pathol 33:844–853
71. Oliva E, Sarrio D, Brachtel EF et al (2006) High frequency of beta-catenin mutations in borderline endometrioid tumours of the ovary. J Pathol 208:708–713
72. Obata K, Morland SJ, Watson RH et al (1998) Frequent PTEN/MMAC mutations in endometrioid but not serous or mucinous epithelial ovarian tumors. Cancer Res 58:2095–2097
73. Sato N, Tsunoda H, Nishida M et al (2000) Loss of heterozygosity on 10q23.3 and mutation of the tumor suppressor gene PTEN in benign endometrial cyst of the ovary: possible sequence progression from benign endometrial cyst to endometrioid carcinoma and clear cell carcinoma of the ovary. Cancer Res 60:7052–7056
74. Thomas EJ, Campbell IG (2000) Molecular genetic defects in endometriosis. Gynecol Obstet Invest 50(Suppl 1):44–50
75. Cuatrecasas M, Erill N, Musulen E et al (1998) K-ras mutations in nonmucinous ovarian epithelial tumors: a molecular analysis and clinicopathologic study of 144 patients. Cancer 82:1088–1095
76. Kuo K-T, Mao TL, Jones S et al (2009) Frequent activating mutations of PIK3CA in ovarian clear cell carcinoma. Am J Pathol 174:1597–1601

77. Kohler MF, Marks JR, Wiseman RW et al (1993) Spectrum of mutation and frequency of allelic deletion of the p53 gene in ovarian cancer. J Natl Cancer Inst 85:1513–1519
78. Kupryjanczyk J, Thor AD, Beauchamp R et al (1993) p53 gene mutations and protein accumulation in human ovarian cancer. Proc Natl Acad Sci U S A 90:4961–4965
79. Salani R, Kurman RJ, Giuntoli R et al (2008) Assessment of TP53 mutation using purified tissue samples of ovarian serous carcinomas reveals a higher mutation rate than previously reported and does not correlate with drug resistance. Int J Gynecol Cancer 18:487–491
80. Bell DA, Scully RE (1994) Early de novo ovarian carcinoma. A study of fourteen cases. Cancer 73:1859–1864
81. Hutson R, Ramsdale J, Wells M (1995) p53 protein expression in putative precursor lesions of epithelial ovarian cancer. Histopathology 27:367–371
82. Werness BA, Parvatiyar P, Ramus SJ et al (2000) Ovarian carcinoma in situ with germline BRCA1 mutation and loss of heterozygosity at BRCA1 and TP53. J Natl Cancer Inst 92:1088–1091
83. Balkwill F, Bast RC, Berek J et al (2003) Current research and treatment for epithelial ovarian cancer. A position paper from the Helene Harris Memorial Trust. Eur J Cancer 39:1818–1827
84. Piek JM, van Diest PJ, Zweemer RP et al (2001) Dysplastic changes in prophylactically removed fallopian tubes of women predisposed to developing ovarian cancer. J Pathol 195:451–456
85. Crum CP, Drapkin R, Miron A et al (2007) The distal fallopian tube: a new model for pelvic serous carcinogenesis. Curr Opin Obstet Gynecol 19:3–9
86. Jarboe E, Folkins A, Nucci MR et al (2008) Serous carcinogenesis in the fallopian tube: a descriptive classification. Int J Gynecol Pathol 27:1–9
87. Medeiros F, Muto MG, Lee Y et al (2006) The tubal fimbria is a preferred site for early adenocarcinoma in women with familial ovarian cancer syndrome. Am J Surg Pathol 30:230–236
88. Folkins AK, Jarboe EA, Saleemuddin A et al (2008) A candidate precursor to pelvic serous cancer (p53 signature) and its prevalence in ovaries and fallopian tubes from women with BRCA mutations. Gynecol Oncol 109:168–173

Virchows Arch (2010) 456:13–21
DOI 10.1007/s00428-009-0847-2

REVIEW AND PERSPECTIVE

Genome-scale approaches to the epigenetics of common human disease

Andrew P. Feinberg

Received: 22 June 2009 / Revised: 22 September 2009 / Accepted: 5 October 2009 / Published online: 21 October 2009
© Springer-Verlag 2009

Abstract Traditionally, the pathology of human disease has been focused on microscopic examination of affected tissues, chemical and biochemical analysis of biopsy samples, other available samples of convenience, such as blood, and noninvasive or invasive imaging of varying complexity, in order to classify disease and illuminate its mechanistic basis. The molecular age has complemented this armamentarium with gene expression arrays and selective analysis of individual genes. However, we are entering a new era of epigenomic profiling, i.e., genome-scale analysis of cell-heritable nonsequence genetic change, such as DNA methylation. The epigenome offers access to stable measurements of cellular state and to biobanked material for large-scale epidemiological studies. Some of these genome-scale technologies are beginning to be applied to create the new field of epigenetic epidemiology.

Keywords Epigenetics · Epidemiology · DNA methylation

Epigenetics

The term epigenetics was coined by the Cambridge University embryologist Conrad Waddington in a series of monographs, and he used it to describe his original view of developmental biology that the morphological and functional properties of an organism arise sequentially under a program defined by the genome under the influence of the organism's environment [1]. The modern definition of epigenetics is modifications of the DNA or associated proteins, other than DNA sequence variation itself, that carry information content during cell division [2], although a few scientists take a more relaxed or stricter view, either including RNA modification or limiting to vertical (generational) transmission. Remarkably, the modern definition and Waddington's have converged. That is because the epigenetic state of an organism progresses from gamete to zygote to somatic tissue, all of which have profoundly different epigenomes, while the DNA is the same. Furthermore, given that the developmental state of a cell can be completely reprogrammed by somatic cell nuclear transfer, or by specific genes in combination, the information specifying cell state is not the DNA alone but the epigenetic program layered on top of this genetic code and is heritable during cell division but ultimately reprogrammable.

The focus of this review is the specific epigenetic modification involving DNA methylation (DNAm), a covalent addition of a methyl (CH_3) group to the nucleotide cytosine. DNAm is the only epigenetic modification whose mechanism for propagation is well understood biochemically. CpG dinucleotides show heritable methylation during cell division because the complementary strand shows the same sequence, and both cytosines are normally methylated. During DNA replication, the two daughter strands contain *hemimethylated* DNA, i.e., the parent strand is methylated and the daughter strand is not. The enzyme DNA methyltransferase I (DNMT1) has high affinity for this hemimethylated strand and adds a methyl group to the newly synthesized daughter cytosine at that site, likely within the same DNA replication complex. Dietary methionine and a cofactor synthesized from folic acid are necessary for the success of methylation maintenance, providing a strong link between the environment and the

A. P. Feinberg (✉)
Center for Epigenetics and Department of Medicine,
Johns Hopkins University School of Medicine,
855 N. Wolfe St., Rangos 570,
Baltimore, MD 21205, USA
e-mail: afeinberg@jhu.edu

epigenome. Indeed in animals, the epigenome and gene expression can be modified by dietary manipulation of methylation precursors, and dietary deprivation of methionine leads to liver cancer in animals [3].

"CpG islands" are regions rich in CpG dinucleotides (formally defined as G + C content≥0.5 and CpG_{obs}/CpG_{exp}≥0.6)[4], and they are often described as uniformly unmethylated in normal cells, with the exception of the inactive X chromosome, and are near imprinted genes [5, 6]. However, the assumption that autosomal CpG islands (except for imprinted genes) are never methylated is clearly not the case [7–10]. It is also important to note that functionally important DNAm information is often not within conventionally defined CpG islands, e.g., the *H19* and insulin-like growth factor II gene (*IGF2*) differentially methylated regions (DMRs) that regulate imprinting of *IGF2* [11, 12].

Epigenetics of human disease

How can one identify disease-specific epigenetic differences? One would like to know that the epigenome varies normally in the population, is associated in particular ways with disease, and does not always simply reflect normal tissue-specific differences in gene expression. Individual gene data in support of this epigenetic variation were first reported in the 1980s [13]. Other genomic regions showing epigenetic variation in the population include X inactivation [14] and both familial and environmental determinants of *IGF2*/*H19* imprinting, or parent of origin-specific gene silencing [14].

A common theme of disease epigenetics is the role of defects in phenotypic plasticity, the ability of cells to change their behavior in response to internal or external environmental cues; this was reviewed recently in detail [15]. For example, hereditary disorders of the epigenetic apparatus lead to developmental defects, a dramatic example being the Rett syndrome. This disorder involves loss of function of methyl-CpG-binding protein 2 (MeCP2), which recognizes DNAm. Children with Rett syndrome develop normally until 6–12 months and then gradually lose developmental milestones over years, due to a failure to maintain gene silencing in the brain. This process of delayed onset of disease is also a hallmark of bipolar disorder and schizophrenia.

The study of epigenetic changes in human cancers began with the discovery of widespread hypomethylation [16]. Cancer involves both hypomethylation and hypermethylation, attendant overexpression of oncogenes, silencing of tumor suppressor genes, and loss of imprinting. Here too, the mechanism by which epigenetic changes leads to cancer appears to involve disruption of normal phenotypic plasticity, in this case of the programming that leads a cell to differentiate normally within a given tissue compartment [2]. Moreover, epigenetic changes that arise constitutionally are associated with increased risk of common disease, such as loss of imprinting of the *IGF2* gene in cancer, which has been shown in both human [17] and mouse [18, 19] studies. Prospective or nested case–control studies are needed to establish a cause and effect relationship in colorectal cancer.

Epigenetic alterations have long been linked to human disease, originally through disorders of genomic imprinting [20]. Defects in the epigenetic machinery also lead to developmental abnormalities, such as MeCP2 mutations in Rett syndrome [21] and DNMT3B mutations in immunodeficiency, centromeric region instability, and facial anomalies (ICF) syndrome [21].

Epigenetic alterations may also contribute to neuropsychiatric disease. Bipolar disorder shows several features consistent with an epigenetic contribution: lack of complete concordance in monozygotic twins; onset of illness in adolescence or adulthood rather than childhood, the often episodic nature of the illnesses, and the apparent relationship to environmental factors, such as stress [22, 23]. Stress has been shown to alter epigenetic marks including DNAm and histone modifications in the brain in animal models [24, 25]. Interestingly, three important bipolar disorder medications, the mood stabilizer valproate [24, 25], the antidepressant imipramine [25], and the antipsychotic haloperidol [26], have also been shown to induce epigenetic changes in the brain. More direct evidence in support of an epigenetic effect in bipolar disorder: is based on the identification of an excess of maternal transmission in some pedigrees [27]. The mounting evidence for epigenetic involvement in autism includes relationships with related phenotypes as well as direct evidence. For example, imprinted genes on the X chromosome are thought to be involved in social skills in girls because defects in these skills are found in Turner syndrome and in children lacking the paternal X chromosome but not the maternal X chromosome [28]. Both fragile X, a disorder with known phenotype overlap with autism, and ICF syndrome arise from malfunctions in the establishment of normal DNAm patterns [29, 30]. Rett syndrome, also associated with autistic features, is caused by mutations in the gene encoding DNA methyl-binding protein MeCP2, a protein important for interpreting DNAm and controlling the repression of gene transcription [31]. Patients with these three disorders exhibit mental retardation, demonstrating the importance for proper DNAm in the regulation of cognitive function. Furthermore, one mechanistic study has shown that abnormally hypomethylated CNS neurons were impaired functionally and were selected against in postnatal development [32]. Another suggests that neuronal activity can drive the transcription of genes important for controlling neurotransmitter release by regulating their DNAm status [33].

The potential for imprinting of autism-related genes could explain the lack of Mendelian inheritance in autism and the inconstant results across linkage and association studies that do not account for these features. Direct evidence for this idea comes from a study of the gene for contactin-associated protein-like 2 (*CNTNAP2*), identified by multiple studies as associated with autism spectrum disorders (ASD) [34–38]. In one of these studies, risk for ASD associated with the identified single nucleotide polymorphism (SNP) showed parent-of-origin specificity suggesting a role for imprinting [36].

Epigenetics of aging

Increasing evidence supports a role for epigenetics in the biology of aging. X-inactivated genes in the mouse show an increased frequency of reactivation with aging, consistent with age-related epigenetic change [39, 40]. The frequency of epigenetic changes in mice may be one to two orders of magnitude greater than the rate of somatic DNA mutation [41]. This fits with a role of epigenetics in late-onset disorders such as frailty, a syndrome of decreased resiliency and reserves, in which a mutually exacerbating cycle of declines across multiple systems results in negative energy balance, sarcopenia, and diminished strength and tolerance for exertion [42]. Accumulation of DNA sequence changes might not occur at enough high rate during the lifespan to induce common disease, but epigenetic changes may occur at a frequency that could contribute to this effect. Very few studies have demonstrated epigenetic changes in humans with age due to technical and biosample limitations. A recent study has shown differences in local and global methylation by age by examining the similarity in methylation patterns between MZ twins aged 3 years old and MZ twins aged 50. Although these analyses were not in the same individuals (the same twins were not followed longitudinally), the similarity in methylation patterns between young twins compared to the dissimilar patterns among older twins argues strongly for age-related changes in the epigenome [43]. Direct evidence comes from a recent study showing changes in DNA methylation in the same individual over time, described in more detail below.

Epigenomics

Epigenomics refers to genome-scale analysis of epigenetic marks. The term "methylome," or genome-wide state of DNAm, was first introduced by the author in 2001 [44]. Despite the availability of an essentially complete genome sequence for several years, understanding the methylome has progressed more slowly, largely due to limitations in technology affecting sensitivity, specificity, throughput, quantitation, and cost among the previously used detection methods. All of the available methods involve trade-offs among these variables. Furthermore, all of these variables are themselves moving targets, particularly cost. The rule in genomic science generally is that increased demand substantially reduces cost because of three factors: fierce competition in the biotechnology sector; production efficiencies as methods are automated; and continued technological advances. It is also important to define clearly what is meant by genome scale. The term is commonly applied to any method not limited to specific predefined genes, but no epigenomic method in common use examines the entire epigenome. For the sake of this article, the discussion will be limited to DNAm analysis because of its particular suitability for pathological and epidemiological studies due to its stability in biobanked specimens.

The human genome contains $\sim 3 \times 10^9$bp of DNA, of which there are $\sim 3 \times 10^7$ CpG dinucleotides, and half of that is nonrepetitive single- or low-copy sequence [45]. CpG dinucleotides are the sites that can be methylated and the methylation in turn replicated faithfully during cell division by DNA methyltransferase 1. While non-CpG methylation exists, it is not currently considered epigenetic information since no mechanism is known for its propagation during DNA replication.

What are the methods in common practice for measuring genome-scale DNAm? While this review naturally is written from the perspective of our own approaches, there are several other excellent reviews of epigenomics [46, 47]. Most investigators are drawn to commercially available methods, particularly those that can be performed as a service, with only DNA needing to be prepared by the investigator. However, these methods are not necessarily the most comprehensive or most accurate. A method similar to array-based SNP analysis is the Illumina GoldenGate methylation assay [48], or its more recent cousin, the Illumina Infinium methylation platform. Both methods involve bisulfite conversion of unmethylated DNA to uracil, followed by polymerase chain reaction (PCR) which propagates a thymine residue at the converted base [49]. Methylated cytosine is unconverted and thus read as cytosine. Thus, the methylation state ($C/^mC$) is transformed to a pseudopolymorphism (T/C, respectively). The readout is then as for any SNP and is semiquantitative, accurate within ~17% for the GoldenGate assay [50]. The major limitation of this approach is the relatively poor coverage of the genome by both methods, only ~1,500 CpG by GoldenGate and ~27,000 CpG by Infinium, thus representing 0.01% to 0.18% of the single-copy methylome. A second limitation is the choices involved in selecting CpG sites for analysis. The chips are designed based in part on the idea that functional CpG methylation lies within

canonical gene promoters and CpG islands. CpG islands are defined algorithmically, i.e., based on a formula given above. The major rationale for this choice is literature showing hypermethylation of CpG islands in cancer. Yet, those studies are largely self-referential in design, and recent studies described below suggest that most variable DNAm occurs outside of these islands. Nevertheless, great advances have been made possible by these reagents and methods, and they show the promise of increasing efforts by many laboratories to improve the resolution of genome-scale technology.

Furthermore, there are comparatively few data supporting the choice specifically of promoters and CpG islands for studies of other diseases, or normal population variation. Indeed, a relatively small scale but very comprehensive study was performed by Stephan Beck at the Sanger Center on ~1.8 Mb of DNA including ~40,000 CpG sites across 12 tissues [10]. The study showed that most methylation variation was not at transcriptional start site-associated CpGs or at CpG islands [10]. One encouraging result from that study, for those who wish to use CpG chips as described above, was a high degree of correlation between CpG site methylation within a few hundred base pairs. However, the choice of one or two CpGs per candidate region seems precariously underrepresented.

A second approach in common practice is hybridization of antibody-purified methylated DNA to high-density genome arrays [51]. For example, NimbleGen offers of methylated DNA immunoprecipitation (MeDIP) to a ~2-Mb array tiled through gene promoters and CpG islands. The coverage of this array is much greater than the SNP-based arrays described above. However, choice of selection is still a significant issue given that complete tiling of the genome would currently require ten arrays, which is cost-prohibitive for large-scale epidemiological studies. Furthermore, MeDIP shows significant limitations in discriminating methylation differences in regions of medium- to low-density CpG content [52], and our recent study shows that that is exactly where many or most significant variation in DNAm occurs [53]. Another method focused on CpG islands is restriction landmark genome scanning [54]. There are emerging alternatives for methylation fractionation, including affinity purification of methylated DNA on methyl-CpG-binding protein [55], or affinity purification of unmethylated DNA [56].

Two promising methods for genome-scale analysis use methylated DNA fractionation based on restriction endonuclease digestion. One of these, developed by John Greally and colleagues at Albert Einstein College of Medicine in New York, is termed HELP for HpaII-tiny fragment Enrichment by Ligation-mediated PCR [57]. It takes advantage of the difference in sizes of Hpa-II fragments, which are generated from unmethylated DNA, and Msp-I fragments, which recognize the same cleavage site but are methylation-independent. While initial specificity was relatively limited, recent improvements involve additional methylcytosine sensitive endonucleases and allow representation of >98% of CpG islands and >90% of refSeq promoters, and it can also be combined with next generation sequencing for readout [58]. A second involves fractionation of the unmethylated component with McrBC, which recognizes methylated DNA if there are two methylcytosines preceded by purines and separated by ~40–100 b, an easy condition to meet for methylated DNA except at very low CpG density. This approach was first applied to specific chromosome analysis [59] but was subsequently extended to study of human cancer [60].

Rafael Irizarry and I with our colleagues developed an array-based readout method that is independent of methylation fractionation method and can be applied equally to McrBC, HELP, or antibody-based methods. This approach, termed CHARM for comprehensive high-throughput array-based relative methylation analysis, involves two essential components. First, the array is agnostic to presuppositions about the location of differential methylation and tiles through regions based only on the relative CpG content in decreasing abundance [52]. It, therefore, includes all CpG islands, but that represents only 38% of the CpG "real estate," or available oligonucleotide probe positions for analysis on the array. One could use additional arrays or soon to be released higher density arrays to increase coverage, which is now about one fourth of the entire nonrepetitive methylome. The second component is genome-weighted smoothing, or correction for the hybridization properties of the target (i.e., sample) genome at each location, which is in turn calculated from empirical measurements of hybridization efficiency with regard to GC content, CpG density, and length of fragments [52]. A statistical suite of postprocessing algorithms, written in R, is termed CharmR and is continually revised. The arrays and CharmR are open access and open source (http://www.biostat.jhsph.edu/~maryee/charmR/). Thus, while not commercially available, this technology is readily transportable to core laboratories that have statistical and programming support.

Although my colleagues and I have developed one of the current approaches to epigenomic analysis, we gladly welcome the advent of second generation sequencing technology for DNAm analysis. There are multiple competing commercial platforms for massively parallel sequencing on slides, with throughput per machine >300 Gb per run at <1% of the cost of conventional automated sequencing [61, 62]. A particular advantage of sequencing-based methylation analysis is the ability to ascertain allele-specific methylation by virtue of DNA polymorphisms within the same sequencing read. This is particularly true as longer reads become cost-effective.

Nevertheless, whole genome bisulfite sequencing applied to humans is not presently cost-effective for epidemiological studies. Costs are in the many tens of thousands of dollars, compared to hundreds of dollars per sample for alternative less comprehensive methods. Therefore, sequencing-based methods all involve significant trade-offs. One method involves "reduced representation," using restriction enzymes to limit the sequenced target to regions within CpG islands [63], which may miss significant normal variation in patient populations or across tissues [53]. Single molecule sequencing detection, such as in development by Pacific Biosystems, or other methods not widely discussed publicly, might reduce costs to the point of making whole genome shotgun sequencing inexpensive compared to other methods for epigenomic profiling. Until that day comes, however, a great deal can be learned about the methylome of human normal and disease populations using array or chip-based approaches.

The first genome-scale epigenetic analysis of human cancer: CpG island shores

We recently exploited CHARM methodology to perform the first genome-scale analysis of the human cancer methylome and to compare it to the normal tissue-varying methylome. A comparison was first made of DNA from five autopsy specimens, three matched tissues each representing the three embryonic lineages, brain, liver, and spleen. Surprisingly, most tissue-specific DNAm was not at CpG islands but at regions of intermediate CpG density located up to 2 kb from the islands, and which we termed "CpG island shores" [53]. Even though CpG islands accounted for 33% of the CpG real estate on the arrays, they only accounted for 6% of these tissue-varying differentially methylated regions, or T-DMRs. In contrast 76% of T-DMRs were in CpG island shores. Furthermore, the T-DMRs were located for the most part outside of promoters (96%), and more than half were >2 kb from the nearest annotated gene [53].

Next, comparing 13 colorectal cancers to matched normal mucosa from the same patients, 2,707 regions were identified showing cancer-specific differentially methylated regions, or C-DMRs, under a false discovery rate of 5%. These, too, were highly enriched at CpG island shores (67%), and islands were comparatively underrepresented (8% compared to 38% on the arrays). The data were highly reproducible, being validated by independent quantitative bisulfite pyrosequencing on a replicate set of 50 colon cancers and matched normal mucosa [53].

Remarkably, there was a comparable amount of hypermethylation as hypomethylation, even though the cancer literature is heavily biased toward the former. That may be because the CpG islands, even though underrepresented for C-DMRs overall, show hypermethylation when methylation is altered in cancer, while the shores away from the islands tend toward relative hypomethylation. In retrospect, this is not surprising, since CpG islands are *protected* against normal DNA methylation, and thus, the only direction they can commonly change in disease is toward relative hypermethylation. In any case, the common dictum that cancer shows repetitive DNA hypomethylation and gene-specific hypermethylation appears to be false. While the former is true, single genes are numerically comparably altered by hypomethylation and hypermethylation in cancer [53]. These results are illustrated in Fig. 1.

This comparative methylome analysis also showed that C-DMRs and T-DMRs largely overlap (65% using an *F* statistic). Indeed, if one performs supervised clustering to identify the C-DMRs that distinguish colorectal cancer from normal mucosa, those same DMRs in *unsupervised* clustering completely discriminate spleen from liver from brain [53]. Thus, the DMRs that regulate normal differentiation are involved in aberrant methylation in cancer, and this may occur *generally* across cancer, since they even distinguish tissues not of the type from which the cancer derives.

What do CpG island shores do? This is of great relevance to any investigator interested in the disease epigenome, since they were previously unapparent yet obviously at the heart of

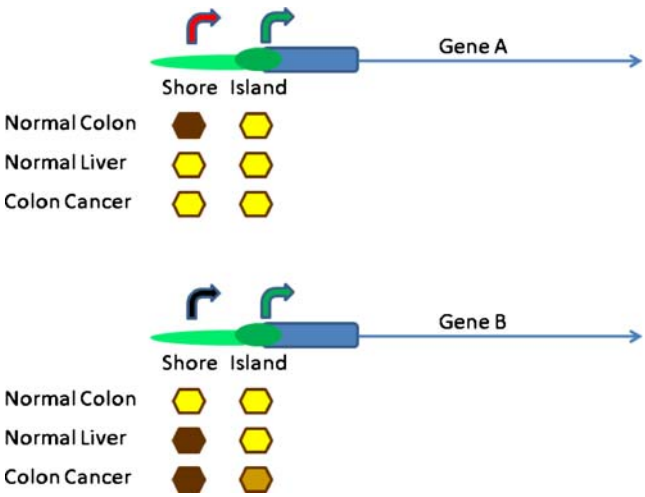

Fig. 1 Altered DNA methylation of CpG island shores in human colon cancer. Shown are an example of hypomethylation (*Gene A*, *top*) and hypermethylation (*Gene B*, *bottom*) in cancer revealed by a genome-scale analysis of the cancer methylome. *Gene A* is normally methylated at the shore and not at the island, and it acquires a hypomethylated pattern at the shore in colon cancer, resembling that of the normal liver. Aberrant expression at an alternate promoter, or for an untranslated RNA, is activated at the shore. *Gene B* is normally unmethylated at both shore and island, and it acquires a hypermethylated island at the shore, resembling the normal liver, and potentially at the island as well. Aberrant silencing ensues at the shore and potentially at the canonical promoter

normal and abnormal variation. One clue comes from their localization, as they appear to be enriched in alternative transcriptional start sites for annotated genes, as well as unannotated RNAs. This localization was functionally supported by rapid amplification of complementary DNA ends experiments showing that hypomethylated CpG island shores in cancer show activation of alternative transcriptional start sites within them in the same tumor showing hypomethylation at these sites [53].

The new field of epigenetic epidemiology

Epidemiology is the study of disease in populations, and genetic epidemiology, or the relationship of genetic variation to disease, has exploded by taking advantage of the data generated by the HapMap project, a consortium effort to identify six million common polymorphisms across the genome and in the major human population groupings [64]. Genome-wide association studies have become the mainstay of human genetics research and have identified nearly 100 loci for over 40 diseases [65]. Concomitant copy number variant (CNV) analysis which can be performed on the same chip platform has also identified insertions or deletions that contribute to common disease [66]. However, epigenomics has not yet been integrated into the routine search for variation contributing to human disease susceptibility.

The new field of *epigenetic epidemiology* will measure and catalog such epigenetic variation within and across populations and to characterize the correlation properties of methylation, similar to the catalog of SNP/CNV variation and linkage disequilibrium. Epigenetic epidemiology can also provide a unique perspective on the environmental factors contributing to common disease. Several examples of environmentally mediated epigenetic effects have been documented, including the influence of methyl donors and folate from diet on methylation levels, smoking influence on methylation, and the effects of metallotoxins [67, 68]. DNA methylation occurs by homocysteine conversion to methionine, which is then converted to S-adenosylmethionine, the common methyl donor for DNAm. Animal work has shown that folate-deprived rats become hypomethylated locally, at particular genes [69, 70] and globally [71]. Human cell work has shown that specific genes may be hyper- or hypomethylated with reduced folate [72]. Also, clinical studies have shown a correlation between serum folate levels and hypomethylation [73], and epidemiologic interventions show older women put on folate-depleted diets result in increased plasma homocysteine and decreased methylation [74, 75]. A hypomethylation defect was associated with assisted reproductive technology in the conception of children with Beckwith–Wiedemann syndrome, a disorder of prenatal overgrowth, birth defects, and cancer [76], which has been borne out by several other groups [77, 78]. Thus, prenatal exposure can act through an epigenetic mechanism.

The prior focus of epigenomics on the simple interface between epigenetics and human disease phenotype variation has prepared us now to address the more complex task of including genetic variation in genome-scale analysis. Going forward, it is critical to develop genome-wide tools to determine the relationship between genetic variation, epigenetic variation, and disease simultaneously. This area of overlap, the hashed area in Fig. 2, is deliberately drawn as the larger fraction of the overlap between genetics and phenotype to emphasize that most genetic findings must be considered in an epigenetic context and to highlight that the full value of typical genetic epidemiology studies cannot be realized until the complementary epigenetic measures and statistical tools are developed and performed on these samples.

Fallin, Bjornsson, and I have proposed a common disease genetic and epigenetic (CDGE) model for human disease, which states that DNA sequence variation (traditional genetics), environment, and epigenetic mechanisms interact to cause or accelerate common disease, especially those of later onset [23, 79]. CDGE provides a model for understanding how one might integrate epigenetics into traditional studies genetics and the environment. For example, epigenetic marks such as DNAm may influence disease risk, either directly (such as aberrant DNAm turning a gene on/off inappropriately) or indirectly (through masking/unmasking DNA sequence variation that has disease consequences). This type of DNA variation, whose penetrance is dependent on epigenetic context, is denoted "g_{dep}," since it is only one risk factor in the context of

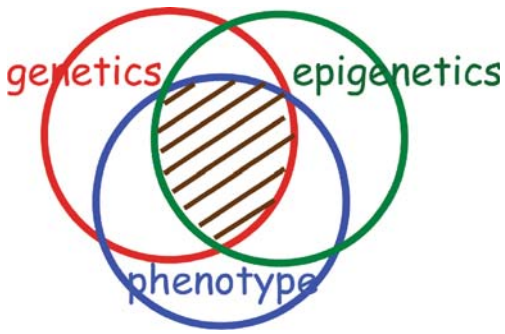

Fig. 2 Epigenetic epidemiology. New genome-scale tools for epigenetic analysis will allow us to determine the relationship between genetic variation, epigenetic variation, and disease simultaneously. The *area of overlap* is deliberately drawn as the larger fraction of the overlap between genetics and phenotype to emphasize that most genetic findings must be considered in an epigenetic context and to highlight that the full value of typical genetic epidemiology studies cannot be realized until the complementary epigenetic measures and statistical tools are developed and performed on these samples

certain epigenetic patterns. This type of sequence variation would be difficult to discover in traditional genetic association approaches, without knowledge of the epigenetic background. Parent-of-origin analyses in genetic epidemiology are aimed at accommodating this problem in the context of imprinting, but this is often low-powered and only addresses one kind of epigenetic model. Whether epigenotype (e.g., DNAm) acts directly or indirectly on disease risk, factors that control epigenotype are themselves critical risk factors. DNA variation that controls epigenotype such as DNAm may be located, for example, in genes that encode proteins in the one-carbon transfer pathway and may affect the cell's ability to maintain DNAm. This type of risk-related DNA variation is denoted "g_{epg}" to indicate that the multiple effects manifest through an epigenetic mechanism. With these thoughts in mind, at least three models can be considered for how DNA variation may contribute to risk: (1) independently of epigenetic mechanisms (g_{ind}), (2) as genetic mediators of epigenetic modifications of other genes (g_{epg}), or (3) where the effect of the genetic variant depends on its epigenetic context (g_{dep}). Only the first of these would be easily detected in current genetic association studies. Current genetic studies might have reduced power to detect g_{epg} without epigenotype measures or knowledge of the factors that contribute to epigenotype. Current genetic studies would have virtually no power to detect g_{dep} without epigenetic measurement [23, 79].

A critical clue to CDGE comes from a global genome-scale measurement of DNAm termed luminometric methylation assay (LUMA), a precise quantitative measure of Hpa II site methylation. Using LUMA, intraindividual change in DNA methylation was found over time with familial clustering. DNA from 111 participants in the AGES Reykjavik Study [80] was first analyzed. In this cohort, 8.1% of individuals showing changes greater than 20% in Hpa II methylation over time, and these were approximately equally divided between gains and losses of DNAm. Permutation analysis showed that the change observed was much greater than by chance ($P<0.0001$) [81]. Next examined was a second cohort of 126 individuals from a collection of Utah pedigrees that had been sampled twice over an average of 16 years. In this group, 11% of individuals show changes greater than 20% in Hpa II methylation over time. The Utah pedigrees showed high heritability, with a heritability estimate of 0.99 ($P<0.0001$) [81]. The familial clustering of methylation changes raises the possibility that methylation changes could be directly related to genetic variation, as suggested by CDGE. Another recent study shows associations of single nucleotide polymorphisms with nearby differences in DNA methylation [82], consistent with CDGE.

Future needs for epigenetic epidemiology will require advances in three areas. First, we must develop scalable, cost-effective approaches for population-level epigenetic profiling. This includes technical advances in measurement and quantification of DNAm. We must also develop even more comprehensive coverage of the epigenome. This can be done by increasing real estate on the arrays, in part perhaps by reducing coverage of highly comparable adjacent sequences on the tiled regions, or by increasing array density as will occur this year. A substantial advance will come from combining array-based advances with second generation sequencing technology. For example, one could capture the relevant epigenome target (identified by studies on arrays) using arrays or molecular inversion probe or other solution-based technologies and then perform bisulfite-based shotgun sequencing for single nucleotide resolution.

Second, we must further develop the statistical tools and concepts that are necessary to analyze, interpret, and compare population-level epigenetic data. A critical requirement for epidemiological analyses is the transformation of granular individual epigenotypes into the higher-level epidemiological data types without significant information loss. This will include developing new statistical tools for identifying the subset of variable DNAm regions relevant to human disease and developing methods to simplify granular methylation patterns into epigenetic "barcodes," similar to the work by Irizarry on gene expression [83].

Third, we must integrate conventional genetic epidemiology with these epigenetic data to fully develop epigenetic epidemiology. We must answer fundamental questions about type, frequency, and properties of epigenetic variation within and across individuals, families, and populations. This can be done by relating genetic variation to epigenetic variation in normal populations, or by investigating epigenetic differences among monozygotic twins. A critical question is whether epigenetic marks are transmitted intact from parent to offspring and whether DNAm is allele-specific and covaries with allele-specific gene expression. For example, can we develop an epigenetic transmission test comparable to the transmission disequilibrium test used in genetic epidemiology? Finally, and most excitingly, we must begin to examine the epigenome comprehensively in large population-based epidemiological studies of disease. Such studies will greatly enhance cancer risk assessment and prevention and are already showing promise in better understanding common neuropsychiatric disease.

References

1. Van Speybroeck L (2002) From epigenesis to epigenetics: the case of C. H. Waddington. Ann N Y Acad Sci 981:61–81
2. Feinberg AP, Tycko B (2004) The history of cancer epigenetics. Nat Rev Cancer 4:143–153

3. Poirier LA (2002) The effects of diet, genetics and chemicals on toxicity and aberrant DNA methylation: an introduction. J Nutr 132:2336S–2339S
4. Gardiner-Garden M, Frommer M (1987) CpG islands in vertebrate genomes. J Mol Biol 196:261–282
5. Bird AP (1986) CpG-rich islands and the function of DNA methylation. Nature 321:209–213
6. Riggs AD, Pfeifer GP (1992) X-chromosome inactivation and cell memory. Trends Genet 8:169–174
7. Strichman-Almashanu LZ, Lee RS, Onyango PO et al (2002) A genome-wide screen for normally methylated human CpG islands that can identify novel imprinted genes. Genome Res 12:543–554
8. Song F, Smith JF, Kimura MT et al (2005) Association of tissue-specific differentially methylated regions (TDMs) with differential gene expression. Proc Natl Acad Sci USA 102:3336–3341
9. Shiota K, Kogo Y, Ohgane J et al (2002) Epigenetic marks by DNA methylation specific to stem, germ and somatic cells in mice. Genes Cells 7:961–969
10. Eckhardt F, Lewin J, Cortese R et al (2006) DNA methylation profiling of human chromosomes 6, 20 and 22. Nat Genet 38:1378–1385
11. Hark AT, Schoenherr CJ, Katz DJ et al (2000) CTCF mediates methylation-sensitive enhancer-blocking activity at the H19/Igf2 locus. Nature 405:486–489
12. Cui H, Niemitz EL, Ravenel JD et al (2001) Loss of imprinting of insulin-like growth factor-II in Wilms' tumor commonly involves altered methylation but not mutations of CTCF or its binding site. Cancer Res 61:4947–4950
13. Silva AJ, White R (1988) Inheritance of allelic blueprints for methylation patterns. Cell 54:145–152
14. Sandovici I, Naumova AK, Leppert M et al (2004) A longitudinal study of X-inactivation ratio in human females. Hum Genet 115:387–392
15. Feinberg AP (2007) Phenotypic plasticity and the epigenetics of human disease. Nature 447(7143):433–440
16. Feinberg AP, Vogelstein B (1983) Hypomethylation of ras oncogenes in primary human cancers. Biochem Biophys Res Commun 111:47–54
17. Cui H, Cruz-Correa M, Giardiello FM et al (2003) Loss of IGF2 imprinting: a potential marker of colorectal cancer risk. Science 299:1753–1755
18. Sakatani T, Kaneda A, Iacobuzio-Donahue CA et al (2005) Loss of imprinting of Igf2 alters intestinal maturation and tumorigenesis in mice. Science 307:1976–1978
19. Kaneda A, Wang CJ, Cheong R, et al (2007) Enhanced sensitivity to IGF-II signaling links loss of imprinting of IGF2 to increased cell proliferation and tumor risk. Proc Natl Acad Sci USA 104:20926–20931
20. Horsthemke B, Buiting K (2008) Genomic imprinting and imprinting defects in humans. Adv Genet 61:225–246
21. Bestor TH (2000) The DNA methyltransferases of mammals. Hum Mol Genet 9:2395–2402
22. Petronis A, Gottesman II, Crow TJ et al (2000) Psychiatric epigenetics: a new focus for the new century. Mol Psychiatry 5:342–346
23. Bjornsson HT, Fallin MD, Feinberg AP (2004) An integrated epigenetic and genetic approach to common human disease. Trends Genet 20:350–358
24. Weaver IC, Cervoni N, Champagne FA et al (2004) Epigenetic programming by maternal behavior. Nat Neurosci 7:847–854
25. Tsankova NM, Berton O, Renthal W et al (2006) Sustained hippocampal chromatin regulation in a mouse model of depression and antidepressant action. Nat Neurosci 9:519–525
26. Shimabukuro M, Jinno Y, Fuke C et al (2006) Haloperidol treatment induces tissue- and sex-specific changes in DNA methylation: a control study using rats. Behav Brain Funct 2:37
27. McMahon FJ, Stine OC, Meyers DA et al (1995) Patterns of maternal transmission in bipolar affective disorder. Am J Hum Genet 56:1277–1286
28. Skuse DH, James RS, Bishop DV et al (1997) Evidence from Turner's syndrome of an imprinted X-linked locus affecting cognitive function. Nature 387:705–708
29. Hansen RS, Wijmenga C, Luo P et al (1999) The DNMT3B DNA methyltransferase gene is mutated in the ICF immunodeficiency syndrome. Proc Natl Acad Sci USA 96:14412–14417
30. Sutcliffe JS, Nelson DL, Zhang F et al (1992) DNA methylation represses FMR-1 transcription in fragile X syndrome. Hum Mol Genet 1:397–400
31. Amir RE, Van den Veyver IB, Wan M et al (1999) Rett syndrome is caused by mutations in X-linked MECP2, encoding methyl-CpG-binding protein 2. Nat Genet 23:185–188
32. Fan G, Beard C, Chen RZ et al (2001) DNA hypomethylation perturbs the function and survival of CNS neurons in postnatal animals. J Neurosci 21:788–797
33. Nelson ED, Kavalali ET, Monteggia LM (2008) Activity-dependent suppression of miniature neurotransmission through the regulation of DNA methylation. J Neurosci 28:395–406
34. Roohi J, Montagna C, Tegay DH et al (2008) Disruption of contactin 4 in 3 subjects with autism spectrum disorder. J Med Genet 46(3):176–182
35. Bakkaloglu B, O'Roak BJ, Louvi A et al (2008) Molecular cytogenetic analysis and resequencing of contactin associated protein-like 2 in autism spectrum disorders. Am J Hum Genet 82:165–173
36. Arking DE, Cutler DJ, Brune CW et al (2008) A common genetic variant in the neurexin superfamily member CNTNAP2 increases familial risk of autism. Am J Hum Genet 82:160–164
37. Alarcon M, Abrahams BS, Stone JL et al (2008) Linkage, association, and gene-expression analyses identify CNTNAP2 as an autism-susceptibility gene. Am J Hum Genet 82:150–159
38. Strauss KA, Puffenberger EG, Huentelman MJ et al (2006) Recessive symptomatic focal epilepsy and mutant contactin-associated protein-like 2. N Engl J Med 354:1370–1377
39. Wareham KA, Lyon MF, Glenister PH et al (1987) Age related reactivation of an X-linked gene. Nature 327:725–727
40. Brown S, Rastan S (1988) Age-related reactivation of an X-linked gene close to the inactivation centre in the mouse. Genet Res 52:151–154
41. Bennett-Baker PE, Wilkowski J, Burke DT (2003) Age-associated activation of epigenetically repressed genes in the mouse. Genetics 165:2055–2062
42. Bandeen-Roche K, Xue QL, Ferrucci L et al (2006) Phenotype of frailty: characterization in the women's health and aging studies. J Gerontol A Biol Sci Med Sci 61:262–266
43. Fraga MF, Ballestar E, Paz MF et al (2005) Epigenetic differences arise during the lifetime of monozygotic twins. Proc Natl Acad Sci USA 102:10604–10609
44. Feinberg AP (2001) Methylation meets genomics. Nat Genet 27:9–10
45. Fazzari MJ, Greally JM (2004) Epigenomics: beyond CpG islands. Nat Rev Genet 5:446–455
46. Esteller M (2007) Cancer epigenomics: DNA methylomes and histone-modification maps. Nat Rev Genet 8:286–298
47. Illingworth RS, Bird AP (2009) CpG islands—'a rough guide'. FEBS Lett 583:1713–1720
48. Bibikova M, Fan JB (2009) GoldenGate assay for DNA methylation profiling. Methods Mol Biol 507:149–163
49. Clark SJ, Harrison J, Paul CL et al (1994) High sensitivity mapping of methylated cytosines. Nucleic Acids Res 22:2990–2997

50. Bibikova M, Lin Z, Zhou L et al (2006) High-throughput DNA methylation profiling using universal bead arrays. Genome Res 16:383–393
51. Weber M, Davies JJ, Wittig D et al (2005) Chromosome-wide and promoter-specific analyses identify sites of differential DNA methylation in normal and transformed human cells. Nat Genet 37:853–862
52. Irizarry RA, Ladd-Acosta C, Carvalho B et al (2008) Comprehensive high-throughput arrays for relative methylation (CHARM). Genome Res 18:780–790
53. Irizarry RA, Ladd-Acosta C, Wen B et al (2009) The human colon cancer methylome shows similar hypo- and hypermethylation at conserved tissue-specific CpG island shores. Nat Genet 41:178–186
54. Costello JF, Smiraglia DJ, Plass C (2002) Restriction landmark genome scanning. Methods 27:144–149
55. Jorgensen HF, Adie K, Chaubert P et al (2006) Engineering a high-affinity methyl-CpG-binding protein. Nucleic Acids Res 34:e96
56. Illingworth R, Kerr A, Desousa D et al (2008) A novel CpG island set identifies tissue-specific methylation at developmental gene loci. PLoS Biol 6:e22
57. Khulan B, Thompson RF, Ye K et al (2006) Comparative isoschizomer profiling of cytosine methylation: the HELP assay. Genome Res 16:1046–1055
58. Oda M, Glass JL, Thompson RF et al (2009) High-resolution genome-wide cytosine methylation profiling with simultaneous copy number analysis and optimization for limited cell numbers. Nucleic Acids Res 37(12):3829–3839
59. Yamada Y, Watanabe H, Miura F et al (2004) A comprehensive analysis of allelic methylation status of CpG islands on human chromosome 21q. Genome Res 14:247–266
60. Ordway JM, Bedell JA, Citek RW et al (2006) Comprehensive DNA methylation profiling in a human cancer genome identifies novel epigenetic targets. Carcinogenesis 27:2409–2423
61. Margulies M, Egholm M, Altman WE et al (2005) Genome sequencing in microfabricated high-density picolitre reactors. Nature 437:376–380
62. Shendure J, Porreca GJ, Reppas NB et al (2005) Accurate multiplex polony sequencing of an evolved bacterial genome. Science 309:1728–1732
63. Meissner A, Gnirke A, Bell GW et al (2005) Reduced representation bisulfite sequencing for comparative high-resolution DNA methylation analysis. Nucleic Acids Res 33:5868–5877
64. Frazer KA, Ballinger DG, Cox DR et al (2007) A second generation human haplotype map of over 3.1 million SNPs. Nature 449:851–861
65. Manolio TA, Brooks LD, Collins FS (2008) A HapMap harvest of insights into the genetics of common disease. J Clin Invest 118:1590–1605
66. Cooper GM, Nickerson DA, Eichler EE (2007) Mutational and selective effects on copy-number variants in the human genome. Nat Genet 39:S22–S29
67. Sutherland JE, Costa M (2003) Epigenetics and the environment. Ann N Y Acad Sci 983:151–160
68. Van den Veyver IB (2002) Genetic effects of methylation diets. Annu Rev Nutr 22:255–282
69. Pogribny IP, Basnakian AG, Miller BJ et al (1995) Breaks in genomic DNA and within the p53 gene are associated with hypomethylation in livers of folate/methyl-deficient rats. Cancer Res 55:1894–1901
70. Pogribny IP, Miller BJ, James SJ (1997) Alterations in hepatic p53 gene methylation patterns during tumor progression with folate/methyl deficiency in the rat. Cancer Lett 115:31–38
71. Wainfan E, Poirier LA (1992) Methyl groups in carcinogenesis: effects on DNA methylation and gene expression. Cancer Res 52:2071s–2077s
72. Jhaveri MS, Wagner C, Trepel JB (2001) Impact of extracellular folate levels on global gene expression. Mol Pharmacol 60:1288–1295
73. Fowler BM, Giuliano AR, Piyathilake C et al (1998) Hypomethylation in cervical tissue: is there a correlation with folate status? Cancer Epidemiol Biomarkers Prev 7:901–906
74. Jacob RA, Gretz DM, Taylor PC et al (1998) Moderate folate depletion increases plasma homocysteine and decreases lymphocyte DNA methylation in postmenopausal women. J Nutr 128:1204–1212
75. Rampersaud GC, Kauwell GP, Hutson AD et al (2000) Genomic DNA methylation decreases in response to moderate folate depletion in elderly women. Am J Clin Nutr 72:998–1003
76. DeBaun MR, Niemitz EL, Feinberg AP (2003) Association of in vitro fertilization with Beckwith–Wiedemann syndrome and epigenetic alterations of LIT1 and H19. Am J Hum Genet 72:156–160
77. Gicquel C, Gaston V, Mandelbaum J et al (2003) In vitro fertilization may increase the risk of Beckwith–Wiedemann syndrome related to the abnormal imprinting of the KCN1OT gene. Am J Hum Genet 72:1338–1341
78. Niemitz EL, Feinberg AP (2004) Epigenetics and assisted reproductive technology: a call for investigation. Am J Hum Genet 74:599–609
79. Bjornsson HT, Cui H, Gius D et al (2004) The new field of epigenomics: implications for cancer and other common disease research. Cold Spring Harb Symp Quant Biol 69:447–456
80. Harris TB, Launer LJ, Eiriksdottir G et al (2007) Age, gene/environment susceptibility—Reykjavik study: multidisciplinary applied phenomics. Am J Epidemiol 165:1076–1087
81. Bjornsson HT, Sigurdsson MI, Fallin MD et al (2008) Intra-individual change in DNA methylation over time with familial clustering. JAMA 299(24):2877–2883
82. Boks MP, Derks EM, Weisenberger DJ et al (2009) The relationship of DNA methylation with age, gender and genotype in twins and healthy controls. PLoS ONE 4:e6767
83. Zilliox MJ, Irizarry RA (2007) A gene expression bar code for microarray data. Nat Methods 4:911–913

Virchows Arch (2010) 456:23–29
DOI 10.1007/s00428-009-0867-y

ORIGINAL ARTICLE

Comparison of histopathological and gene expression-based typing of cancer of unknown primary

Lars Morawietz · Arno Floore · Lisette Stork-Sloots · Gunnar Folprecht · Reinhard Buettner · Anja Rieger · Manfred Dietel · Gerdt Huebner

Received: 30 June 2009 / Revised: 14 September 2009 / Accepted: 19 November 2009 / Published online: 10 December 2009
© Springer-Verlag 2009

Abstract For the clinical diagnosis and appropriate therapy of patients with cancer of unknown primary (CUP), biopsies of the tumor metastases are generally examined histopathologically and by immunohistochemistry (IHC). Gene expression profiling (GEP) is a new diagnostic technique that might further contribute to tumor specification. Biopsies of 43 CUP cases underwent a retrospective central histopathological and immunohistochemical review and centrally performed GEP using CupPrint™. Two samples could not be evaluated by IHC due to small biopsy size or loss of immunoreactivity. One of these and 17 other samples were not suited for GEP due to RNA degradation. In 13 out of the remaining 24 cases (54%), the same primary was proposed by IHC and GEP and was supported by the clinical findings, furthermore leading to the doubtless identification of the primary in four out of these. In seven cases, there was discordance between IHC and GEP, with the clinical picture being more in line with IHC in three and with GEP in four cases. Four cases had to remain undecided because the primary tumors suggested by IHC and GEP were not supported. In conclusion, overlap between IHC and GEP results and the clinical presentation was noted in the majority of those true CUP cases that were evaluable with both techniques. Therefore, GEP can be a complementary diagnostic technique assisting immunohistochemical profiling of cancer biopsies with unknown primary.

Keywords Cancer of unknown primary · Immunohistochemistry · Gene expression profiling · CUP

L. Morawietz (✉) · A. Rieger · M. Dietel
Institute of Pathology, Charité University Hospital Berlin,
Charitéplatz 1,
10117 Berlin, Germany
e-mail: lars.morawietz@charite.de

A. Floore · L. Stork-Sloots
Agendia BV,
Science Park 406,
1098 XH Amsterdam, The Netherlands

G. Folprecht
University Hospital Carl Gustav Carus,
Fetscherstr. 74,
01307 Dresden, Germany

R. Buettner
Institute of Pathology, University of Bonn Medical School,
Sigmund Freud Allee 25,
53125 Bonn, Germany

G. Huebner
Department Hematology and Oncology,
Sana Kliniken Ostholstein,
Muhlenkamp 5,
23758 Oldenburg-Holstein, Germany

Introduction

Five percent of cancer cases present primarily as metastases, for example in biopsies of enlarged lymph nodes, lesions of the liver, or the lung. The finding of a metastasis usually results in a diagnostic workup, aiming at the detection of the primary tumor and defining the extent of disease. This includes radiological, laboratory, endoscopic, and other examinations as well as profound immunohistochemical profiling of a biopsy [1, 2].

If no primary can be defined or diagnosed, the tumor will be characterized as cancer of unknown primary (CUP). This is not a rare condition. CUP is one of the ten most frequent malignancies worldwide, and it constitutes 3% to 5% of all cancers [3]. In Germany, the mortality rate for CUP is 15 in 100,000 both in women and men and is

similar to the mortality rates reported for gastric, pancreatic, or ovarian cancer [4].

In the majority of patients, the disease has spread to several organs at the time of diagnosis. A systemic therapy, e.g., cytostatic chemotherapy, is needed in most of these cases. The decision for a specific regimen in CUP is problematic because the primary and, therefore, the tumor entity and TNM stage are unclear. Nevertheless, some CUP sub-entities have been defined that can be treated according to the most likely primary. For example, metastases of adenocarcinoma in axillary lymph nodes in women will be treated as metastasized breast cancer, and metastases of squamous cell carcinoma in cervical lymph nodes will be treated as head and neck cancer [5, 6]. For other CUPs that do not belong to a defined subcategory, standardized chemotherapeutic regimens have been proposed, too [3, 7, 8]. This is a pragmatic approach, since at one point, it is required to begin therapy and cease redundant search for the unknown primary, which will be diagnosed during the further course of disease in only 7% of patients [9].

However, before defining a tumor as CUP, both the oncologist and the patient want to benefit from all feasible tests that modern diagnostics can provide. Tissue analysis has made some advancement during the last 10 years. Immunohistochemistry (IHC) has become a routine procedure, and a large spectrum of antibodies has been developed, which are by themselves or in combination more or less specific for certain tumors [2, 10]. For example, the thyroidal transcription factor (TTF-1) is expressed in carcinoma of the thyroid and in adenocarcinoma and neuroendocrine carcinoma of the lung in many cases, and for further differentiation, surfactant protein A which is restricted to adenocarcinoma of the lung can be used as a diagnostic marker. However, for some tumor entities, especially tumors of the upper gastrointestinal tract, such specific markers are not yet established [11]. Poorly differentiated carcinoma may exhibit a marker profile that is discordant with published literature or may exhibit discordant expression or loss of site-specific markers.

Recently, the development of array technologies like microarray-based gene expression profiling (GEP) has shown promising results in identifying primary tumors. Microarrays allow the simultaneous analysis of hundreds or thousands of genes within a single test, requiring only a small amount of RNA [12–15]. Based on 635 individual tumors representing 30 carcinoma and 17 non-carcinoma classes, an expression profile of 495 genes was designed to predict tumor origin and was further developed into a standardized test (CupPrint TM) [16]. A great overlap between gene expression profiles in fresh frozen and formalin-fixed, paraffin-embedded samples of the same tumor was observed, and the correct classification of metastases by GEP in cases with known primary was reported [17, 18]. Therefore, it seems adequate to perform GEP on formalin-fixed, paraffin-embedded biopsies from CUP cases in order to define the primary tumor more accurately.

The aim of the present study was to compare results and feasibility of GEP with results from an experienced histopathological institute utilizing a broad spectrum of immunohistochemical markers on patients with true CUP syndrome.

Material and methods

Patients

This retrospective study was conducted on samples from patients with "Adeno- or Undifferentiated Carcinoma of Unknown Primary" who had been enrolled in a "prospective randomized phase II trial of Paclitaxel and Carboplatin versus Gemcitabine and Vinorelbine" executed by the Working Group Oncology of the German Cancer Society, carried out between 2001 and 2004 [7]. Ethics approval was given by the Ärztekammer Rheinland Pfalz, Mainz, Germany, and written informed consent was obtained. Of 92 patients enrolled, we were able to analyze 43 tissue samples. The mean patient age was 61.2 years; 19 patients were female and 24 were male. Further study details were published previously [7].

Histopathological examination

From all patients, a biopsy of the metastatic tumor site was taken and examined by the local pathologist. For the present study, participating institutes sent the paraffin blocks to the Institute of Pathology at the University Hospital Charité for central pathology review. Since the present study was undertaken in the year 2006, the samples were 2 to 5 years old. The blocks were accompanied by a shipment sheet, including the patients' initials, date of birth, gender, a three-digit code number, and site of biopsy. No further information was provided, so that the reference pathologists were blinded to the clinical diagnoses.

From each paraffin block, 20 sections of 1 to 2 μm thickness were cut and mounted onto SuperFrost Plus glass slides. Two slides were stained with hematoxylin and eosin (H&E) and periodic acid Schiff (PAS), respectively, and the remaining 18 slides were used for IHC. There was no predefined antibody panel; in fact, the appropriate stainings were selected based on the differential diagnoses that appeared most applicable after review of the H&E and PAS slides.

Antibodies were directed against different cytokeratins (CK5/6, CK7, CK8, CK20) and p63 to differentiate squamous

cell carcinoma, adenocarcinoma, and mesothelioma, antibodies against calretinin to identify mesothelioma, TTF-1 and thyroglobulin for thyroid carcinoma, surfactant protein A and TTF-1 to identify lung tumors, CDX2 and villin for gastrointestinal, especially colonic tumors, HepPar1 for liver, S100 protein, melanoma cell (clone HMB45) and melan A for melanoma, alpha-fetoprotein and placental alkaline phosphatase for germ cell tumors, prostate-specific antigen (PSA) and androgen receptor for prostate carcinoma, CD56, chromogranin A and synaptophysin for neuroendocrine tumors, gross cystic disease fluid protein 15 and mammaglobin for breast cancer, estrogen and progesterone receptor for breast and other gynecologic tumors, and CA125 for ovarian carcinoma. In singular cases, other antibodies were used or some of the above antibodies in a different context, like melan A as a marker for adrenal cortical carcinoma.

All IHC stainings were performed on automated staining systems (Benchmark XT, Ventana Medical Systems, Tucson, USA), using heat induced antigen retrieval, commercially available antibodies (Dako, Glostrup, Denmark and Zytomed Systems GmbH, Berlin, Germany), and standardized detection systems (UltraView Red, Ventana). The evaluation was done by two pathologists (L.M. and M.D.) experienced in tumor pathology, using standard light microscopes from ×25 to ×400 magnification (DM RBE, Leitz, Wetzlar, Germany). If possible, a specific tumor was diagnosed, such as adenocarcinoma of the lung when IHC was positive for CK7 and surfactant A. Cases positive solely for CK7 and CK20 were classified adenocarcinoma of the upper gastrointestinal tract. In these cases, based on histomorphologic features such as presence of signet ring cells, ductular structures, or desmoplastic stroma, it was tried to propose a most likely gastrointestinal primary site. This may give the impression that a specific primary tumor could be diagnosed by IHC and histomorphology. However, these diagnoses resemble "educated guesses." These had to be made in order to obtain a distinct result that could be compared with the GEP results.

Gene expression profiling

Three to five microsections of 5 μm thickness were prepared at the Institute of Pathology from the same tissue blocks as above and shipped to the laboratory for GEP (Agendia B.V., Amsterdam, The Netherlands).

H&E staining was done to determine if enough tumor cells were present. If necessary and possible, microdissection was performed for enrichment of the tumor cells. Total RNA was extracted and amplified in a two-round amplification using a commercially available kit (Paradise kit, Aviara DX, San Diego, CA USA). During the second round, 5-[3-aminoallyl]uridine 5′-triphosphate is incorporated; Cy3 mono ester was coupled to this active group following the standard protocol from the Paradise kit. The labeled cRNA was hybridized on the diagnostic CupPrint array against a universal reference using standard protocols (Agilent Technologies, Santa Clara, USA). This array harbors eight identical mini arrays, each containing 1,900 features, among which are 495 signature genes, normalization genes, negative control features, and print control features. Expression levels from the 495 signature genes were compared to the CupPrint database comprising of more than 600 tumors and representing 49 tumor types. Each tumor in the database received a similarity score (k-nearest neighbor); this value positively correlated with an increase in consistency of tumor types [16]. In order to achieve comparability with the IHC results and the clinical data, not all five nearest neighbors were taken into account, but only the most likely primary tumor was suggested. In case that this tumor could also be caused by biopsy site interference, an alternative was suggested as well.

Results

Tissue blocks were available from 43 patients. Of note, the analysis for these samples was done 2 to 5 years after biopsies were taken. Therefore, due to small sample size or loss of immunoreactivity, two samples could not properly be evaluated histopathologically, and due to RNA degradation, one of these and another 17 tumor blocks could not be evaluated by GEP. Therefore, a complete set of results from IHC, GEP, and clinical evaluation was available for 24 cases.

In a consensus meeting, results from the independent methods were disclosed and discussed. The appraisal of the different methods was difficult since clinical picture, histopathology, and GEP delivered different kind of information. The clinical information was mainly the location of the tumor masses, based on computed tomography, ultrasound, and, in some cases, endoscopic examinations, and gender of the patient. The histopathological information was a suggestion of one or two tumor types, based on the World Health Organization (WHO) classification of tumors. The GEP resulted in a proposal of one or two diagnoses out of 49 predefined tumor categories.

By definition, it could not be doubtlessly decided if a certain result was right or wrong as the primary tumor remained unknown in all cases. All patients had died by the time this retrospective trial was carried out, and autopsy was performed only in one case and did not reveal a doubtless primary tumor. During the consensus meeting, we discussed and agreed upon, if all diagnoses for one case were well in line, if they were contradictory, or if the histopathological diagnosis or the GEP was more helpful in light of the clinical situation.

Results from the consensus meeting, histopathological examination and gene expression profiling of the 24 cases are summarized in Table 1.

We came to a consensus on the most likely primary tumor in 13 cases (54%). In nine out of these cases, we agreed that after extensive workup, these still had to be classified as adenocarcinomas of unknown primary, probably with gastrointestinal origin, but with no doubtlessly assignable primary tumor. These nine cases were immunoreactive only for unspecific markers such as CK7, CK20, and CDX-2 but negative for more specific markers. Remarkably, in four cases (18, 52, 73, 88), the results allowed the identification of the specific histogenesis of the primary tumor: Two samples (52 and 73) expressed surfactant protein A and were classified as lung tumors by GEP, which was well in line with the clinical tumor manifestation. One tumor (18) was positive for CK5/6 and CA125 and was classified as squamous cell carcinoma of the cervix uteri by GEP, which was concordant with the clinical picture. And one tumor (88) was positive for CA125 and estrogen receptor and was classified as serous ovarian carcinoma by GEP, which was supported by the clinical tumor manifestation (Table 2).

Four cases (7, 11, 24, 47) had to remain undecided, because neither the immunohistochemical nor the gene expression-based suggestion could be supported by the clinical finding. In two cases (7 and 47), IHC and GEP pointed to the same primary (lung and colon, respectively), but no such tumor had been detected by clinical examination. In one case (11), a tumor with cribriform appearance, monomorphous nuclei with prominent nucleoli and positivity only for CK8 with no CK7/CK20 expression was diagnosed a prostate cancer, although PSA and androgen receptor were negative. GEP suggested hepatocellular carcinoma in this case, but when reviewing the clinical data, there was neither a prostatic nor a hepatic tumor.

In seven cases, there was disagreement between the histopathological diagnosis and GEP. In four out of these (8, 62, 72, 90), the clinical picture supported the diagnosis

Table 1 Synopsis of clinical tumor manifestation, histopathology and gene expression profiling

ID	Biopsy site	Gender	Histopathological diagnosis	Gene expression profile	Clinical picture in line with	Appraisal
6	Liver	m	ACUP upper GI, possibly pancreas	Pancreas	HCC/CCC	Consensus
7	Liver	m	Small cell lung cancer	Seminoma or SCC of lung	No lung or testicular tumor	Undecided
8	Bone	m	ACUP upper GI, possibly pancreas	CCC	CCC	Pro GEP
11	Lymph node	m	Prostate carcinoma	HCC	No primary	Undecided
15	Peritoneum	m	Urothelial carcinoma or CCC	CCC or mesothelioma	CCC	Consensus
18	Soft tissue	f	SCC or AC of cervix uteri	SCC of cervix uteri	Cervix uteri	No CUP
22	Liver	f	ACUP upper GI, primarily CCC	CCC	CCC	Consensus
24	Lymph node	m	ACUP upper GI, possibly stomach	Skin or oral cavity	No primary. Not skin	Undecided
37	Liver	f	ACUP upper GI	Colon or CCC	Pancreas	Consensus
47	Lymph node	m	Neuroendocrine carcinoma of colon	Colon	No tumor in colonoscopy	Undecided
52	Lymph node	m	Adenocarcinoma of lung	Lung	Lung	No CUP
54	Liver	f	ACUP upper GI, possibly pancreas	Colon or gallbladder	Biliopancreatic system	Consensus
57	Liver	m	ACUP upper GI, possibly stomach	HCC	Upper GI or lung	Pro IHC
59	Liver	m	ACUP upper GI, biliopancreatic	Colon or gallbladder	CCC	Consensus
61	Liver	f	ACUP upper GI	Upper GI	CCC	Consensus
62	Liver	f	Adenocarcinoma of colon	HCC or colon	Upper GI or HCC	Pro GEP
64	Pancreas	m	ACUP upper GI, possibly pancreas	Pancreas, lung, mesothelioma	Pancreas	Pro IHC
72	Pleura	m	Chromophobe renal cell carcinoma	Upper GI, CCC	CCC	Pro GEP
73	Lymph node	m	Adenocarcinoma of lung	Lung	Lung	No CUP
74	Liver	f	ACUP upper GI, biliopancreatic	Biliopancreatic	Biliopancreatic system	Consensus
83	Lymph node	m	ACUP upper GI, possibly stomach	Breast or head and neck	Lung or stomach	Pro IHC
88	Peritoneum	f	Serous ovarian carcinoma	Serous ovarian carcinoma	Serous ovarian carcinoma	No CUP
90	Lymph node	m	ACUP GI, possibly colon	HCC	HCC	Pro GEP
92	Liver	m	ACUP upper GI, biliopancreatic	CCC	CCC	Consensus

ID patient identification number, *f* female, *m* male, *ACUP* adenocarcinoma of unknown primary, *GI* gastrointestinal tract, *SCC* squamous cell carcinoma, *HCC* hepatocellular carcinoma, *CCC* cholangiocellular carcinoma, *IHC* immunohistochemistry, *GEP* gene expression profiling

Table 2 Comprehensive comparison of the GEP and IHC results

	True CUP, IHC=GEP	Primary detected, IHC=GEP	True CUP, GEP>IHC	True CUP, IHC>GEP	Undecided
N=(% of 24)	9 (38%)	4 (17%)	4 (17%)	3 (13%)	4 (17%)

that was based on GEP, which favored hepatocellular and cholangiocellular carcinoma in two cases each. In three cases (57, 64, 83), the clinical tumor spread was better in line with the IHC results, which favored adenocarcinoma of the stomach in two and pancreas carcinoma in one case.

Summarizing the above, 20 out of the 24 cases remained true CUP after extensive immunohistochemical workup and GEP, while in the remaining four cases, the histogenesis of the primary tumor could be revealed.

Discussion

Selection of an appropriate therapy regimen for CUP patients provides a challenge, because there is no definite information on the primary tumor regarding both entity and stage. After failure of the initial extensive diagnostic workup to identify, a primary a case has to be assigned as CUP.

The results of our study show that with advanced radiological, immunohistochemical, and molecular techniques, over 50% of cases can be further classified, and a most likely primary tumor can be defined. In 17% of cases (four out of 24), the results even allowed the identification of the primary tumor in our series.

More than half of the cases (14 out of 24, 58%) were histopathologically diagnosed as adenocarcinoma of unknown primary with a probable origin in the upper gastrointestinal tract. Further differentiation by IHC is limited in these tumors, because to date, no specific markers exist that are able to differentiate between intra- and extrahepatic cholangiocarcinoma, carcinoma of the stomach, pancreas, or small bowel [11]. These are the entities in which GEP might be most helpful—if it can reliably differentiate between these localizations. In fact, GEP yielded specific suggestions in the majority of these cases. However, the major drawback of the present study design is that it does not allow for a definite appraisal of either the IHC- or the GEP-based diagnosis, since in 20 cases, the primary tumor remained undetected. Except for those four cases with a specific immunoprofile, concordant GEP result, and matching clinical picture, we were not able to doubtlessly define if the proposed diagnoses were right or wrong. Hence, our data will need validation by a prospective study guided by the results of IHC and GEP.

A study by Horlings et al., using the same microarray assay, came to comparable results. While in a set of 84 cases with known primary, they came to a correct classification in 83%, and in another set of 16 cases with initial (later detected) CUP, the correct classification was made in 94%, the number of valuable information given by GEP to a third set, consisting of 22 true CUP cases, was only 14 cases (64%) [18]. This number is similar to our GEP results, which were supported by IHC and/or clinical findings in 13 out of 20 unsolved CUP cases (65%).

Both detailed histopathological review with the extensive use of IHC and GEP showed their advantages and disadvantages. GEP is a statistical method that transforms differential RNA levels into suggestions of most closely matching tumor types. It is independent of the observer's experience or other subjective factors as investigators expectations and can distinguish tumors that histopathologically look similar, such as cholangiocarcinoma from ductal pancreatic adenocarcinoma. The commercially available CupPrint test assesses 49 tumor categories—which are much less than defined in the WHO classification of tumors. However, GEP spans the most important and most likely tumor types when looking for an unknown primary. For microarray analysis, the use of high-quality buffered formalin and highly pure paraffin and proper fixation time are important to avoid degradation of RNA during storage. Our results indicate that GEP is more susceptible to shortcomings in specimen fixation and handling than IHC because out of 43 external tissue blocks, only two were not assessable by IHC in our institute, but 18 could not be evaluated by GEP. We suggest that the lack of intact RNA is also caused by the time of 2 to 5 years between biopsy and execution of the present study. If fixation and embedding is done according to standard operating protocols and analysis is performed within reasonable time after biopsy, the success rate can exceed 90%, as has been reported by independent working groups, using the same microarray assay [18, 19]. Furthermore, the group of Horlings et al. compared samples from different years and found out that the success rate dropped to three out of eight cases when the tissue blocks were as old as 14 years [18]. The samples in our present study were only 2 to 5 years old, so we suggest that the comparably low success rate is also due to the fact that the samples came from different laboratories and had been embedded using numerous different reagents and procedures.

Another limiting factor was the small size of the tumor infiltrates in many punch biopsy samples. While a histopathological diagnosis can in principle be made with

as little as one neoplastic gland—if it expresses tumor-specific markers—GEP requires a minimum of RNA that can be hybridized on the microarray.

In a retrospective study by Bridgewater et al. on 21 true CUP cases, using the same microarray assay, 18 GEP results (86%) were well in line with clinical tumor presentation and histopathology, and in 12 out of these, the GEP results might have had influence on the treatment strategy if it had been known initially [20]. The superiority of GEP over IHC in that study might be explained by the fact that apparently, it was not enforced to make a specific diagnosis by IHC; at least, the methods section of that publication does not describe how detailed histopathological diagnostics were carried out.

Besides the CUPPrint assay, further gene expression-based tests are commercially available for CUP. The assay by Veridex LLC (Raritan, NJ USA) is based on ten genes, the expression of which is analyzed by quantitative reverse-transcriptase polymerase chain reaction [21, 22]. The training set consisted of 260 cases with known primary, and the algorithm was then applied to 37 CUP cases, of which 28 were correctly identified by the assay (76%). Out of 11 true CUP cases, the Veridex assay made a valuable proposition in eight (73%).

The comparability of the published study is limited because of great variance regarding inclusion criteria, intensity of immunohistochemical workup, sample size, sample quality, and GEP assay and because in true CUP, the final diagnosis remains enigmatic. What we believe we can deduce from our and from published studies is that GEP supports the histopathological diagnosis if the results are concordant and that GEP offers a new differential diagnosis, if results are discordant.

Prognostic tumor characteristics like differentiation grade, growth fraction, blood or lymph vessel invasion, or extension of necrosis can only be evaluated by histopathology and IHC. Therefore, a thorough histopathological evaluation will always be required to guide the clinician to the most likely primary tumor site or sites, to give reason to further specific examinations, for example endoscopy, and to deliver important information about the tumor that may have influence on the prognosis and possibly the choice of therapy and improvement of clinical outcome [21]. If no primary tumor is found, the task of the histopathological evaluation is to assign the tumor to one of the defined CUP subcategories such as ACUP or CUP with neuroendocrine differentiation.

In this complicated clinical situation, the CupPrint test could contribute additional information. However, a clinical trial comparing standard workup followed by empirical therapy with an approach of GEP/IHC-guided therapy followed by the site-specific chemotherapy for the most likely tumor will be necessary to show if this approach is superior for the clinical outcome of the patient. The French CUP group announced to conduct such a study [19]. As long as results are not available, we suggest a thorough histopathological and immunohistochemical examination. GEP is a promising complementary technique that can give additional and supporting information. In the majority of cases (15 out of 24 in this study), GEP supported the histopathological diagnosis and could have strengthened the treatment decision. A combined approach might help to identify more primaries in CUP patients and allow a more targeted therapy with a consecutive improvement in survival.

Acknowledgments We would like to acknowledge Iris Simon for reviewing and rewriting the manuscript and Arenda Schuurman for collecting the CupPrint data.

Conflict of interest statement Lisette Stork-Sloots and Arno Floore are employed by Agendia.

References

1. Freudenberg LS, Rosenbaum-Krumme SJ, Bockisch A et al (2008) Cancer of unknown primary. Recent Results Cancer Res 170:193–202
2. Varadhachary GR, Abbruzzese JL, Lenzi R (2004) Diagnostic strategies for unknown primary cancer. Cancer 100:1776–1785
3. Pavlidis N, Fizazi K (2005) Cancer of unknown primary (CUP). Crit Rev Oncol Hematol 54:243–250
4. Dachdokumentation Krebs (2003) Available via http://www.rki.de/cln_091/nn_204078/DE/Content/GBE/DachdokKrebs/krebs__node.html?__nnn=true. Accessed 15 May 2009
5. Hauswald H, Lindel K, Rochet N et al (2008) Surgery with complete resection improves survival in radiooncologically treated patients with cervical lymph node metastases from cancer of unknown primary. Strahlenther Onkol 184:150–156
6. Patel J, Nemoto T, Rosner D et al (1981) Axillary lymph node metastasis from an occult breast cancer. Cancer 47:2923–2927
7. Huebner G, Link H, Kohne CH et al (2009) Paclitaxel and carboplatin vs gemcitabine and vinorelbine in patients with adeno- or undifferentiated carcinoma of unknown primary: a randomised prospective phase II trial. Br J Cancer 100:44–49
8. Pentheroudakis G, Greco FA, Pavlidis N (2009) Molecular assignment of tissue of origin in cancer of unknown primary may not predict response to therapy or outcome: A systematic literature review. Cancer Treat Rev 35:221–227
9. Greco FA, Spigel DR, Yardley DA et al (2009) Unknown primary cancer (UPC): Accuracy of tissue of origin prediction by molecular profiling. J Clin Oncol 27(suppl):11070
10. Kaufmann O, Fietze E, Dietel M (2002) Immunohistochemical diagnosis in cancer metastasis of unknown primary tumor. Pathologe 23:183–197
11. Morawietz L, Dietel M (2007) Der unbekannte Primarius – eine diagnostische Herausforderung. Im Fokus Onkologie 5:59–64
12. Ramaswamy S, Tamayo P, Rifkin R et al (2001) Multiclass cancer diagnosis using tumor gene expression signatures. Proc Natl Acad Sci USA 98:15149–15154
13. Shedden KA, Taylor JM, Giordano TJ et al (2003) Accurate molecular classification of human cancers based on gene

expression using a simple classifier with a pathological tree-based framework. Am J Pathol 163:1985–1995
14. Su AI, Welsh JB, Sapinoso LM et al (2001) Molecular classification of human carcinomas by use of gene expression signatures. Cancer Res 61:7388–7393
15. Tothill RW, Kowalczyk A, Rischin D et al (2005) An expression-based site of origin diagnostic method designed for clinical application to cancer of unknown origin. Cancer Res 65:4031–4040
16. van Laar RK, Ma XY, de Jong D et al (2009) Implementation of a novel microarray-based diagnostic test for cancer of unknown primary. Int J Cancer 125(6):1390–1397
17. Frank M, Döring C, Metzler D et al (2007) Global gene expression profiling of formalin-fixed paraffin-embedded tumor samples: a comparison to snap-frozen material using oligonucleotide microarrays. Virchows Arch 450:699–711
18. Horlings HM, van Laar RK, Kerst JM et al (2008) Gene expression profiling to identify the histogenetic origin of metastatic adenocarcinomas of unknown primary. J Clin Oncol 26:4435–4441
19. Loriot Y, Gross-Goupil M, Lesimple T et al (2009) Identifying the primary site using gene expression profiling in patients with carcinoma of an unknown primary (CUP): a feasibility study from the GEFCAPI. J Clin Oncol 27(suppl):22168
20. Bridgewater J, van Laar R, Floore A et al (2008) Gene expression profiling may improve diagnosis in patients with carcinoma of unknown primary. Br J Cancer 22(98):1425–1430
21. Varadhachary GR, Raber MN, Matamoros A et al (2008) Carcinoma of unknown primary with a colon-cancer profile - changing paradigm and emerging definitions. Lancet Oncol 9:596–599
22. Talantov D, Baden J, Jatkoe T et al (2006) A quantitative reverse transcriptase-polymerase chain reaction assay to identify metastatic carcinoma tissue of origin. J Mol Diagn 8:320–329

Virchows Arch (2010) 456:31–37
DOI 10.1007/s00428-009-0862-3

ORIGINAL ARTICLE

Clinicopathologic characteristics of pleomorphic carcinoma of the breast

Jing Zhao · Ronggang Lang · Xiaojing Guo · Ling Chen · Feng Gu · Yu Fan · Xilin Fu · Li Fu

Received: 24 June 2009 / Revised: 8 November 2009 / Accepted: 10 November 2009 / Published online: 16 December 2009
© Springer-Verlag 2009

Abstract Pleomorphic carcinoma of the breast is considered a rare variant of high-grade ductal NOS carcinoma (NOS-IDC), and the prognosis is poor. However, its clinicopathologic features are not well-characterized. Using the criteria delineated in the World Health Organization breast tumor classification of 2003, ten cases of pleomorphic carcinoma were identified from 9794 NOS-IDC in our archived materials that were originally diagnosed as high-grade infiltrating ductal carcinoma of breast. To investigate the clinicopathologic characteristics and to elucidate the histologic diagnosis and differential diagnosis of this entity, we reviewed the pathology manifestations and clinical features of these cases and examined the tumor expression of ER, PR, PCNA, AE_1/AE_3, p53, S-100, C-erbB-2, EMA, p63, and Bcl-2 by immunohistochemistry.

Keywords Breast · Carcinoma · Pleomorphic carcinoma · Histological classification · Clinicopathologic feather · Morphology

Introduction

In 2003, World Health Organization (WHO) breast tumor classification separated pleomorphic carcinoma from the infiltrating ductal carcinoma, NOS type, because of its unique morphologic manifestation and unfavorable prognosis [1]. It was considered a rare variant of the high-grade infiltrating ductal NOS carcinoma (NOS-IDC) and was morphologically characterized by proliferation of pleomorphic and bizarre tumor giant cells comprising more than 50% of the total neoplastic proliferation in a background of adenocarcinoma with spindle and squamous differentiation. Due to its rarity, there have been so far only few cases reported in the literature. We reviewed our archived materials of breast cancer and identified ten of such cases. The purpose of this study is to further characterize the clinicopathologic features and to discuss the differential diagnosis of the tumor.

J. Zhao and R. Lang are both the first authors of this paper

J. Zhao · R. Lang · X. Guo · L. Chen · F. Gu · Y. Fan · X. Fu · L. Fu (✉)
Department of Breast Cancer Pathology and Research Laboratory, State Key Laboratory of Breast Cancer Research, Cancer Institute & Hospital, Tianjin Medical University, Tianjin 300060, People's Republic of China
e-mail: fulijyb@hotmail.com

Materials and methods

Histopathologic diagnosis and clinical information

Nine thousand seven hundred ninety-four cases of NOS-IDC were retrieved from a total of 12,641 cases of breast cancer diagnosed from January 2001 to December 2006 in the archives of the Department of Breast Cancer Pathology and Research Laboratory, Cancer Hospital of Tianjin Medical University (Tianjin, China). In every case, the entire tumor was blocked at intervals of 3 mm, and two sections were cut from each paraffin-embedded samples. Histopathology of the tumors was reviewed independently by three pathologists, and the proportion of pleomorphic giant tumor cells was assessed in each case. Using the criteria described in the WHO breast tumor classification of 2003 [1], ten of the 9,794 cases were re-classified as pleomorphic carcinoma where the pleomorphic and bizarre tumor giant cells comprised >50% of the integral tumor. Histological grade was assessed using Elston and Ellis grading system. All the diagnostic materials were obtained

prior to any treatment, and the patients were treated in the Department of Breast Cancer of the institution. Follow-up was available in all the patients, and data used for calculation were collected from the date of initial diagnosis to the patient's death or the most recent censorship.

Immunohistochemical study

Immunohistochemistry (IHC) was performed using the labeled streptavidin–biotin technique with mouse monoclonal antibodies against ER, PR, PCNA, AE_1/AE_3, p53, S-100, C-erbB-2, EMA, p63, and Bcl-2. Briefly, 4-μm sections of tumor tissue were deparaffinized and rehydrated through a series of xylene and alcohol. Antigen retrieval by citrate buffer (0.01 M; pH 6.0) and blocking endogenous peroxidase activity using normal serum were performed. Optimal incubation and concentration of primary antibodies were determined via serial dilutions of each of the following primary antibodies (Zymed, San Fransisco, CA): ER (1:40), PR (1:40), PCNA(1:100), AE_1/AE_3 (1:400), p53 (1:50), S-100 (1:800), C-erbB-2 (1:400), EMA (1:200), p63 (1:100), and Bcl-2 (1:40). Phosphate-buffered saline (PBS) was used instead of primary antibody in the incubation step as a negative control, and the positive controls for each marker were used according to the manufacture's recommendation. After incubation with anti-mouse secondary antibody for 20 min at 37°C and streptavidin–horseradish peroxidase (Zymed) for 20 min at 37°C, color was developed by incubation with 3, 3-diaminobenzidine tetra-hydrochloride. The sections were counterstained with hematoxylin. All steps were preceded by rinsing with PBS (pH 7.6).

Assessment of ER, PR, p53, PCNA, and p63 were based on protein staining in the nuclei of tumor cells. AE_1/AE_3, Bcl-2, S-100, and EMA expressions were indicated by cytoplasm staining. The IHC stain was scored as positive if >15% tumor cells expressed the antigen and strongly positive if >50% of tumor cells demonstrated expression. C-erbB-2 protein expression was scored as positive if >10% of tumor cells showed moderate to strong complete membrane immunoreactivity.

Results

Clinical data

The characteristics of the ten cases are summarized in Table 1. All the patients were females, and five of them were pre-menopausal. The patients' age ranged from 33 to 76 years with a median age of 50. Except for one case diagnosed by mammography, all the patients presented with a palpable mass. Four cases of tumors were located in the left breast and six in the right. The tumor sizes ranged from 1 to 15 cm (mean, 4.3 cm). The largest tumor (case 3, Table 1) occupied the whole breast with skin edema. In terms of the pTNM staging, eight of the patients were in stage II, and the remaining two were in stages I and IIIb, respectively. Nine patients underwent radical mastectomy or modified radical mastectomy, and the remaining one received conservative surgery. Eight patients were followed up for longer than 60 months, and four of them had cancer recurrence or progression of disease within 5 years. Among these four patients, one developed local recurrence and metastasis to lumbar vertebrae within 26 months after the initial diagnosis and died of disease 9 months after the detection of metastases. Another developed liver metastasis 33 months after the diagnosis and died 7 months later. In the remaining two cases, lung and thoracic bone metastases were found at 42 and 44 months, respectively, and were alive with disease at the last follow-up of 64 and 69 months, respectively. The other four patients were alive without evidence of tumor progression at last follow-up. The remaining two cases had short follow-up (27 and 46 months, respectively), and no evidence of disease was identified.

Imaging studies

All patients received examinations of mammography and/or ultrasound before surgery. In three of eight patients' mammography demonstrated breast lesions that were well-circumscribed without evidence of calcification, and ultrasound examination showed low echo tumors with distinct circumscription and well-distributed internal echo in three of eight patients examined. The impressions of image studies on these cases included benign breast tumors, fibroadenoma, malignant phyllodes tumor, and inflammatory conditions, incongruous with the final pathological diagnoses. Mammography and ultrasound study each separately made the diagnosis of carcinoma or suspicious for carcinoma in five of eight patients examined.

Histopathological manifestation

Macroscopy

Most of the tumors were solid and firm with gray-yellow to gray-tan color. Six tumors were circumscribed with a homogeneous cut surface. Necrosis and hemorrhage were identified in the largest tumor.

Histology

All the tumors were histological grade III. They displayed various morphological patterns with pleomorphic giant cells consisting of more than 50% of the tumor cells and

Table 1 Clinicopathological parameters of pleomorphic carcinoma in ten cases

Number	Age (years)	Tumor size (cm)	TNM stage	Mammographic diagnosis	Ultrasound diagnosis	Rate of pleomorphic tumor giant cells (%)	Positive axillary nodes/ total	Follow-up outcome (follow-up period)
1	33	2.5	IIB	Benign	Carcinoma	>80	1/35	Died of metastasis (39 months)
2	44	4.0	IIA	Benign	–	>50	0/28	Alive (46 months)
3	50	15.0	IIIB(skin and pectoralis involved)	–	Adenofibroma or cystosarcoma phyllodes	>60	0/43	Died of metastasis (35 months)
4	41	1.0	I	Benign	Adenofibroma	>50	0/17	Alive (90 months)
5	50	4.5	IIA	/	Carcinoma	>50	0/20	alive (81 months)
6	55	4.0	IIA	Carcinoma	Inflammation	>50	0/17	Alive (27 months)
7	57	3.5	IIA	Suspect of malignant	Carcinoma	>60	1/21	alive with lung metastasis (64 months)
8	42	2.5	IIB	carcinoma	/	>50	1/18	Alive (70 months)
9	76	2.5	IIB	Carcimona	Carcinoma	>60	3/13	Alive with thoracic bone metastasis (69 months)
10	52	4.0	IIB	Suspect of malignant	Carcinoma	>50	0/15	Alive (77 months)

up to over 80% in one case (Fig. 1). In two tumors, the bizarre giant cells were immersed within the spindle and/or squamous components. The tumor giant cells had nuclei with size up to tenfold greater than that of the mononuclear tumor cells and manifested hyperchromasia, coarsely clumped chromatin, and multiple prominent nucleoli. In addition, high mitotic rate (>20 mitotic figures/10 HPFs) with abnormal mitosis was also frequently found. Tumor metastasis to axillary lymph nodes was identified in four cases after thorough axillary dissections (numbers of the lymph nodes removed per cases ranged from 13 to 42 with a mean of 22.7). One tumor extended to the overlying skin and to the pectoralis muscles.

Immunohistochemical analysis

All the tumors were negative for ER and PR. In contrast, tumor expression of PCNA and AE_1/AE_3 were identified in every case, and a strongly positive stain was noted in eight of the ten tumors. Positive immunoreactivity for p53 was found in six tumors and for EMA in eight tumors. Four tumors were positive for S-100 and six tumors expressed C-erbB-2, whereas low level of Bcl-2 expression was noted in only one of the cases. P63 expression was identified in two tumors where the stain was predominantly located in tumor cells with spindle shape and/or squamous differentiation; meanwhile, majority of the pleomorphic and bizarre tumor cells were lack of the immunoreactivity (Fig. 2a–h).

Discussion

In 1989, Douglas-Jones and Barr [2] reported a case of breast carcinoma with bizarre malignant multinucleated giant cells in fine needle aspiration materials. Gupta et al. [3, 4] later reported five cases of breast carcinoma with pleomorphic tumor cell population in cytology materials, which also included a lactating patient. In their report, a proportion of the bizarre malignant giant cells within a tumor was not deliberately assessed. Silver and Tavassoli [5] in 2000 described 26 cases of unusual high-grade ductal carcinoma with histologically pleomorhic or anaplastic features and first proposed the term of pleomorphic carcinoma of the breast. They made the diagnosis when ≥50% of the tumor manifested a pleomorphic cell population, and tumors of lobular origin were excluded. Although clinical analysis indicated that the tumor was a prognostically unfavorable lesion, it was not the author's intention to advocate it as a specific subtype of mammary carcinoma, rather to believe that it represented the extreme end of the morphological spectrum of grade III infiltrating ductal carcinoma. The WHO classification of breast tumors in 2003 adopted the terminology and defined it as a rare variant of high-grade ductal NOS carcinoma characterized by proliferation of pleomorphic and bizarre tumor giant cells comprising >50% of the tumor cells in a background of adenocarcinoma or adenocarcinoma with spindle and squamous differentiation. So far, very few cases have been

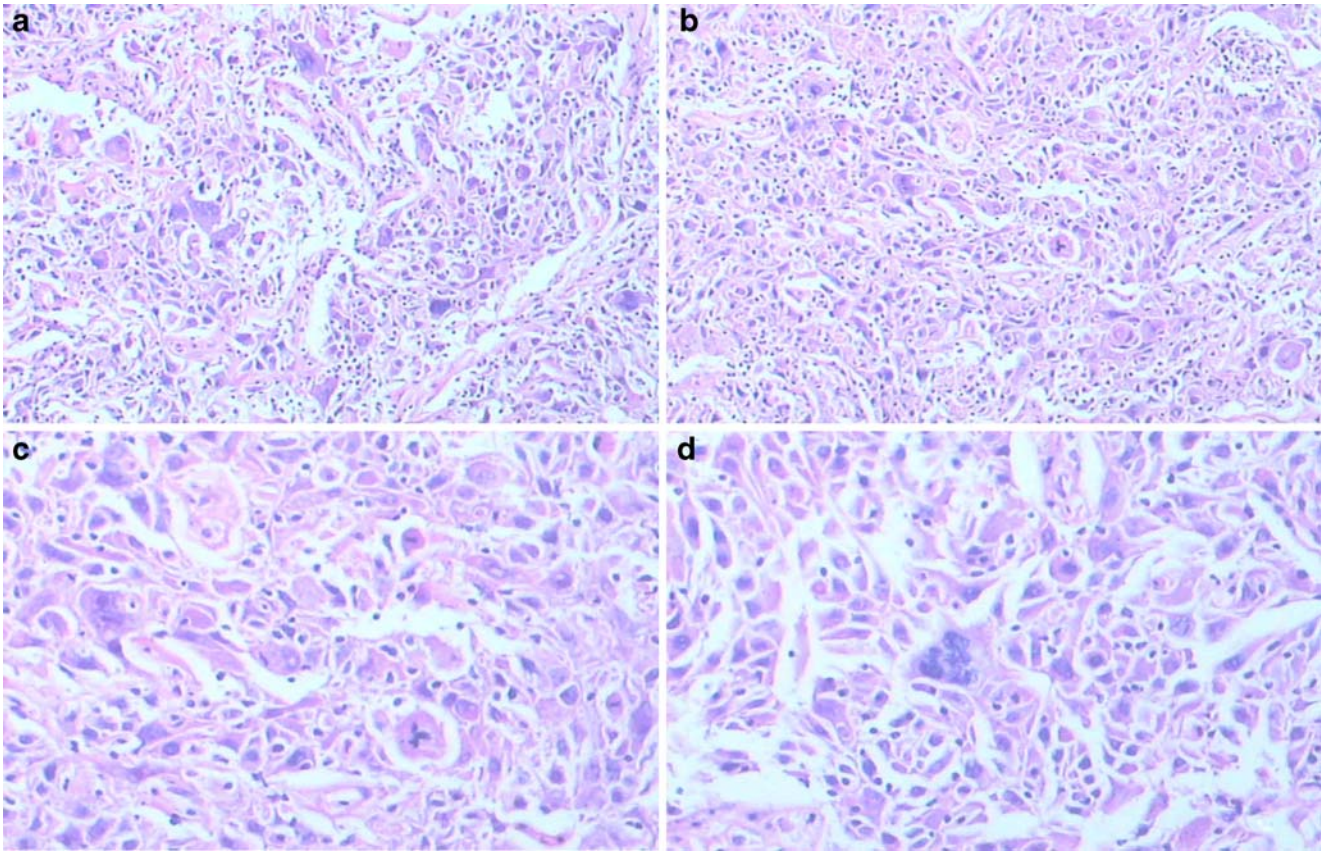

Fig. 1 Pleomorphic carcinoma of the breast (**a**, **b** HE ×100; **c**, **d** HE ×200) pleomorphics and bizarre tumor giants cells containing more than 50%, frequently with greater than a tenfold nuclear size variation in a given lesion and a high mitotic rate in pleomorphic carcinoma

reported in the literature and data accumulation is required to further characterize the tumor and to explore the nature of this unusual carcinoma of breast.

Using the morphologic criteria set in the 2003 WHO classification of breast tumors, we identified ten cases of pleomorphic carcinoma in a total of 9,794 NOS-IDC (0.1%) and 12,641 patients (0.08%) with breast cancer at our institution in a period of 6 years. Similar to most breast cancers, pleomorphic carcinoma may occur at any age in women and tends to occur in the perimenopausal period. Among our patients, the youngest one was 33 years old and the oldest one was 76, with a median age of 50. Five of them were premenopausal. Silver and Tavassoli [5] reported that the most frequent (65%) presentation of the tumor was a palpable mass of variable duration ranging from a few weeks to 2 years, and many of the neoplasm were reported to be rapidly enlarging or relatively stable in size with recent enlargement. Twelve percent of their patients presented with distant metastasis (stage IV), and tumor metastasis to axillary lymph nodes was identified in 12 of the 23 cases. In our study, tumor metastasis to axillary nodes was found in four patients, and tumor involving the overlying skin and extending to the pectoralis muscles occurred in another patient. No distant metastasis was identified in our patients. No imaging study of their patients was reported by Silver and Tavassoli [5]. However, the preoperation mammography and ultrasound study failed to recognize the tumors as carcinoma in three of eight patients, respectively, due to lack of the classic carcinoma features.

Pleomorphic carcinoma is immunohistochemically positive for EMA and AE_1/AE_3, generally negative for Bcl-2, ER, and PR. p53 and S-100 express in about two thirds and one thirdof the cases, respectively. We have demonstrated a similar immunoprofile in this group of tumors that were positive for PCNA, negative for ER and PR in all the cases, and positive for p53 and S-100 in 60% and 40% of cases.

Fig. 2 Immunohistochemical analysis for C-erbB-2, PCNA, p53, EMA, AE_1/AE_3, S-100, and Bcl-2 in the pleomorphic carcinoma. **a** C-erbB-2 protein expression is positive on membrane immunoreactivity. (SP ×400). **b**, **c** PCNA and p53 are positive on cell nuclei of the pleomorphic carcinoma of the breast (SP ×200). **d**, **e** The staining of EMA and AE_1/AE are dispersed in the cytoplasm of the pleomorphic carcinoma (SP ×200). **f**, **g** Positive immunostaining of S-100 in pleomorphic carcinoma cell cytoplasm(SP ×200), while weakly cytoplasmatic immunoreactivity of Bcl-2 (SP ×400). **h** the staining of p63 on cell nuclei of the pleomorphic carcinoma (SP ×200)

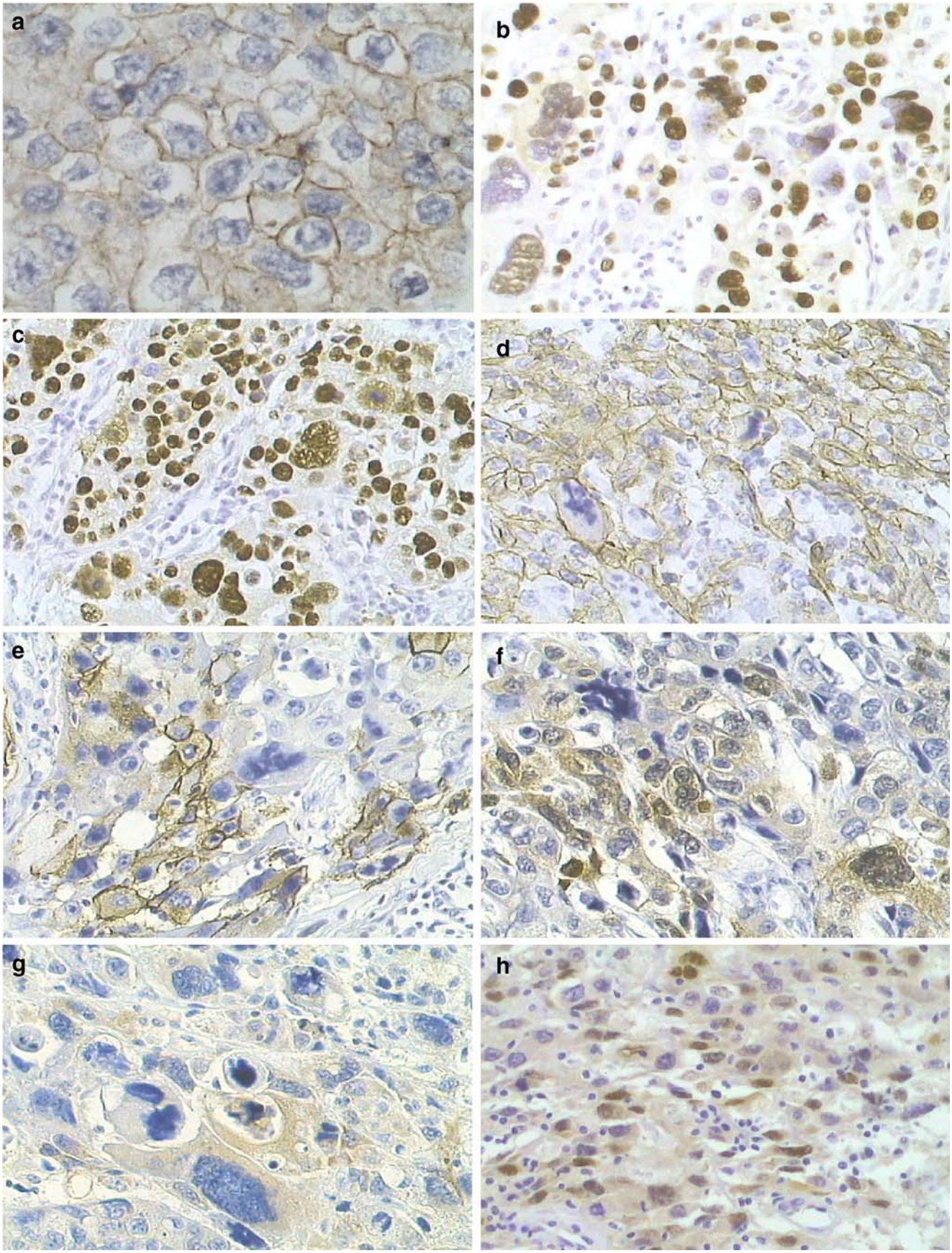
a
b
c
d
e
f
g
h

Expressions of C-erbB-2, PCNA, S-100, EMA, and p53 have been associated with promotion of tumor cell growth and metastasis through different modes of actions and therefore linking with poor prognosis [6–9]. Moreover, the lack of expression of ER, PR, and Bcl-2 intends to occur in tumors with high histological grade [10]. Besides known as a marker for myoepithelial cells, p63 has recently been found useful in diagnosing mammary metaplastic carcinomas with a sensitivity of 65%, a specificity of 96%, and a positive predictive value of 96% [11]. Koker and Kleer [12] demonstrated strong p63 expression in 86.7% of metaplastic carcinomas, and a universal staining pattern was noted in the areas with spindle cell and squamous differentiation. Similar finding was also noted in two of our cases, and the immunoreactivity in the small areas with spindle and squamous differentiation seems to suggest that a metaplastic component can exist in pleomorphic carcinoma. However pleomorphic giant cells remained to be the predominant feature of the tumors that allowed the correct diagnosis of pleomorphic carcinoma.

Pleomorphic tumor cells can be present in other breast tumors, such as invasive pleomorphic lobular carcinoma (IPLC), carcinoma with osteoclastic giant cells, mammary sarcoma, and metastatic tumors. It is important to differentiate these tumors from pleomorphic carcinoma of the breast. In the report by Silver and Tavassoli [5], nine of the 26 cases of pleomorphic carcinoma were originally misdiagnosed as sarcoma, probable sarcoma or carcinosarcoma. In addition, if a transitional ductal carcinoma within the tumor is absent, it can be easily misdiagnosed as metastatic tumor, especially when tumors manifest defined margins. Although bizarre giant cells can be detected in sarcoma, the epithelial morphology of other components of the tumor is usually missing. A panel of IHC for epithelial and mesenchymal marker would determine the essential epithelial nature of pleomorphic carcinoma. Metastatic carcinoma to breast is a rare event and intends to be multicentric. Precaution should be excised when making a diagnosis of pleomorphic carcinoma in a patient with history of other primary tumors. Careful examination of the tumor morphology with necessary help of IHC studies should lead to a correct diagnosis. Breast carcinoma containing osteoclastic giant cells can also be mistakenly interpreted as pleomorphic carcinoma. However, the osteoclast-type giant cells were generally present admixed with inflammatory cells, fibroblasts, hypervascular stroma with extravasated red blood cells, lymphocytes, monocytes, and histiocyes with binucleation. Comparing with those in pleomorphic carcinoma, the osteoclastic giant cells are often regular, and the nuclei are round to ovoid in shape and are not hyperchromatic. Although the pattern of fibroblasts may simulate spindle cell differentiation of carcinoma, all the fibroblasts and osteoclastic giant cells are negative immunohistochemically for epithelial markers [13]. IPLC is a distinctive, aggressive subtype of invasive lobular carcinomas (ILC) [14]. Similar to pleomorphic carcinoma, it presented enlarged nuclei with hyperchromasia, irregularities, and marked plemorphism. It also often present as histoloci grades II and III tumor. However, the IPLC intends to remain as the typical growth pattern of ILC, where individual tumor cells disperse through fibrous connective tissue or arrange in a single linear Indian file. Immunohistochemical study would characterize its profile negative for E-cadherin protein and often positive for ER [15].

Patients with pleomorphic carcinoma of the breast have an unfavorable prognosis. According to the report of Silver and Tavassoli [5], of the 16 patients with follow-up, six were disease-free (mean, 74 months), four alive with disease (mean, 33 months) and six dead of disease at a mean of 22 months. In their patients with metastasis, liver was the most common site followed by lung, pleura, and bone. In our study, four of the eight patients followed up for 5 years or more developed cancer recurrence or progression, and two of them died of the disease. The prognosis appeared better than that reported by Silver and Tavossoli [5]; however, it could be due to the fact that the diagnosis was made at an earlier stage of the tumors and the limitations of this small study. Further studies, including molecular study, are warranted to explore the biologic behavior of this rare variant breast carcinoma with unique morphologic feature and to address the question: Is it truly a variant of NOS-IDC or an independent subtype of breast carcinoma?

Acknowledgment We thank Prof. Vincenzo Eusebi, M.D., Director and Professor of Anatomic and Cytopatholofy section of Pathology "M, Malpighi", University of Bologna, Bologna, Italy and Xinmin Zhang, M.D., Department of Pathology and Laboratory Medicine, Temple University Hospital, Philadelphia, USA for their critical review for this manuscript. This study was supported by fundings from Science Foundation of Tianjin Medical University(2006KY24) and National Natural Science Foundation of China (30600225 and 30470667), Program for Changjiang Scholars and Innovative Research Team in University (IRT0743), National "863" Program of China (2006AA02A249), and National "973" Program of China (2009CB521700).

Conflict of interest statement We declare that we have no conflict of interest.

References

1. Tavassoli FA, Devilee P (2003) Pathology and genetica of tumors of the breast and female genital organs. World Health Organization Classification of Tumors. IARC, Lyon
2. Douglas-Jones AG, Barr WT (1989) Breast carcinoma with tumor giant cells. Report of a case with fine needle aspiration cytology. Acta Cytol 33:109–114

3. Gupta RK, Wakefield SJ, Lallu S et al (1992) Aspiration cytodiagnosis of breast carcinoma in pregnancy and lactation with immunohistochemical and electron microscopic study of an unusual mammary malignancy with plomorphic giant cells. Diagn Cytopathol 8:352–356
4. Gupta RK (1996) Aspiration cytodiagnosis of a rare carcinoma of breast with bizarre malignant giant cells. Diagn Cytopathol 15:66–69
5. Silver SA, Tavassoli FA (2000) Pleomorphic carcinoma of the breast: clinicopathological analysis of 26 cases of an unusual high-grade phenotype of ductal carcinoma. Histopathology 36:505–514
6. Kushlinskii NE, Orinovskii MB, Gurevich LE et al (2004) Expression of biomolecular markers (Ki-67, PCNA, Bc1–2, BAX, BclX, VEGF) in breast tumors. Bull Exp Biol Med 137:182–185
7. Donato R (2001) S100: a multigenic family of calcium-modulated protein of the EF-hand type with intracellular and extracellular functional roles. Int J Biochem Cell Biol 33:637–668
8. Agrawal AK, Jeleń M, Rudnicki J et al (2008) Molecular markers (c-erbB-2, p53) in breast cancer. Folia Histochem Cytobiol 46:449–455
9. van der Vegt B, de Roos MA, Peterse JL et al (2007) The expression pattern of MUC1 (EMA) is related to tumour characteristics and clinical outcome of invasive ductal breast carcinoma. Histopathology 51:322–335
10. Kymionis GD, Dimitrakakis CE, Konstadoulakis MM et al (2001) Can expression of apoptosis genes, bcl-2 and bax, predict survival and responsiveness to chemotherapy in node-negative breast cancer patients? J Surg Res 99:161–168
11. Tse GM, Tan PH, Chaiwun B et al (2006) p63 is useful in the diagnosis of mammary metaplastic carcinomas. Pathology 38:16–20
12. Koker MM, Kleer CG (2004) p63 expression in breast cancer: a highly sensitive and specific marker of metaplastic carcinoma. Am J Surg Pathol 28:1506–1512
13. Eusebi V, Magalhaes F, Azzopardi JG (1992) Pleomorphic lobular carcinoma of the breast: an aggressive tumor showing apocrine differentiation. Hum Pathol 23:655–62
14. Tavassoli FA, Eusebi V (2009) Tumors of the breast. American Registry of Pathology/AFIP, Washington
15. Wahed A, Connelly J, Reese T (2002) E-cadherin expression in pleomorphic lobular carcinoma: an aid to differentiation from ductal carcinoma. Ann Diagn Cytopathol 6:349–51

Virchows Arch (2010) 456:39–44
DOI 10.1007/s00428-009-0855-2

ORIGINAL ARTICLE

DcR1 expression in endometrial carcinomas

Jordi Tarragona · Nuria Llecha · Maria Santacana · Susana Lopez · Sonia Gatius · David Llobet · Xavier Dolcet · Victor Palomar-Asenjo · Francisco Javier Gonzalez-Tallada · Xavier Matias-Guiu

Received: 9 June 2009 / Revised: 21 September 2009 / Accepted: 22 October 2009 / Published online: 20 November 2009
© Springer-Verlag 2009

Abstract The tumor necrosis factor-related apoptosis-inducing ligand (TRAIL) is a member of the TNF family, which mediates apoptosis by the extrinsic pathway. Up-regulation of decoy receptors, DcR1 and DcR2, may result in diminished binding of TRAIL to their functional receptors. DcR1 expression was assessed in normal endometrial tissue (NE) and endometrial carcinoma (EC) samples by immunohistochemistry (IHC) and quantitative real-time polymerase chain reaction (PCR). IHC was performed in two tissue microarrays; one composed of 80 samples of NE and a second one constructed from paraffin-embedded blocks of 62 EC. For quantitative real-time RT-PCR analysis, RNA was obtained from 19 NE and 28 EC samples using Trizol®. mRNA expression of DcR1 was assessed with Taqman®-based assays in an Abi-Prism 700 SDS. Results were correlated with stage, histological type, and grade. By IHC, cytoplasmic expression of DcR1 was frequently seen in NE (79.6%) and varied according to the menstrual cycle. Positive DcR1 immunostaining was also detected in EC (98.1% of the cases) without any specific statistical association with histological type, grade, and stage. By quantitative real-time PCR, all NE had similar levels of DcR1expression (0.8–1.7 RQ), which were considered the basal levels of DcR1 expression in NE. Increased DcR1 expression (≥5-fold higher than the basal levels) was detected in 13 of 28 EC (46.4%). High DcR1 expression levels were found in ECs of different stages: IA, four of 12 (33%); IB, two of four (50%); IC, four of six (66%); and IIA and IIB three of six (50%). Results suggest that DcR1 expression occurs in a subset of EC and may contribute to resistance to TRAIL-induced apoptosis.

Keywords Endometrial carcinoma · DcR1 · Tissue microarray · Apoptosis resistance

FIS PI060577, FIS PI070276, SAF2002-10529-E, SAF2004-05250, Marató de TV3 2005-47, and RD06/0020/134. X. D. holds a postdoctoral fellowship from Fondo de Investigaciones Sanitarias, Ministerio de Sanidad y Consumo (CO05/00028). Tumor samples were obtained from Xarxa catalana de Bancs de Tumors and the Tumor Banc Platform of RTICC.

J. Tarragona · N. Llecha · M. Santacana · S. Lopez · S. Gatius · D. Llobet · X. Dolcet · V. Palomar-Asenjo · X. Matias-Guiu (✉)
Department of Pathology and Molecular Genetics,
Hospital Universitari Arnau de Vilanova, University of Lleida
IRBLLEIDA,
Av Alcalde Rovira Roure 80,
25198 Lleida, Spain
e-mail: xmatias@arnau.scs.es

J. Tarragona
e-mail: tarragona@gss.scs.e

F. J. Gonzalez-Tallada
Department of Gynecology, Hospital Universitari
Arnau de Vilanova, University of Lleida, IRBLLEIDA,
Lleida, Spain

Introduction

There are some evidences indicating that apoptosis resistance may play an important role in development and progression of endometrial carcinoma (EC) [1–4]. Cells resistant to apoptosis are likely to be resistant to therapy and be responsible for relapses.

Apoptosis can be initiated by two main mechanisms: the intrinsic pathway, which has its origin in the mitochondria and the extrinsic apoptotic pathway, triggered by the activation of death receptors situated in the cell surface [5]. A final common feature for execution of the apoptotic program is the activation of a cascade of caspases, which are proteases that have a cysteine containing active site that

cleaves protein substrates at specific amino acid motifs containing an aspartic acid residue.

The extrinsic pathway is activated by the members of the tumor necrosis factor (TNF) superfamily [6–8]. After ligand binding, the activated receptors recruit an adaptor protein called Fas-Associated protein with Dead Domain (FADD). FADD binds to the receptor through interactions with pro-caspase-8 to form a complex at the receptor called DISC. In turn, active caspase-8 activates effector caspases, such as caspase-3, causing the cell to undergo apoptosis. The tumor necrosis factor-related apoptosis-inducing ligand (TRAIL) and the Fas ligand belong to the pro-apoptotic cytokines of the TNF superfamily. TRAIL induces apoptosis in many types of cancer cells. However, some neoplastic cells are resistant to TRAIL [9]. TRAIL can bind four different receptors DR4/TRAIL-R1, DR5/TRAIL-R2, DcR1/TRAIL-R3, and DcR2/TRAIL-R4. DR4 and DR5 are functional receptors that induce apoptosis upon ligation with TRAIL. DcR1 and DcR2 (TRAILR3 and TRAILR4), known as decoy receptors, lack the intracellular domains required to induce apoptosis [10].

The different steps of the apoptotic process are deregulated in cancer [11, 12]. Down-regulation of death receptors, such as Fas, and loss-of-function mutations and deletions on receptors DR4 and DR5 have been detected in some tumors. Moreover, up-regulation of decoy receptors (DcR1 and DcR2) that compete with the functional receptors for the ligand binding may result in a diminished binding of TRAIL to their functional receptors [10]. Such a mechanism has been suggested as a potential cause for apoptosis resistance in some types of tumor.

The main aim of the present study was to assess the expression of DcR1 (TRAILR3) in a series of normal endometrium (NE) and EC in order to assess the possible role of DcR1 expression in apoptosis resistance in EC.

Materials and methods

Tissues

The material was composed of formalin-fixed, paraffin-embedded tissue samples from 142 patients for immunohistochemical evaluation and an independent series of fresh frozen tissue samples from 47 patients for quantitative reverse transcription-polymerase chain reaction (RT-PCR) analysis.

Tissue microarrays

Two tissue microarrays (TMA) were constructed. The first TMA was constructed from 80 paraffin-embedded samples of NE in different phases of the menstrual cycle (20 proliferative, 50 secretory, ten menstrual) obtained from the surgical pathology files from Hospital Universitari Arnau de Vilanova de Lleida. The second TMA was composed of 62 EC obtained from the surgical pathology files of Hospital Universitari Arnau de Vilanova de Lleida and Hospital de Sant Pau, Barcelona, Spain. The specimens were collected between 2003 and 2006; they were consecutively obtained, without any criteria for selection. They included 22 endometrioid carcinomas (EEC) grade I, 24 EEC grade II, seven EEC grade III, three mixed endometrioid and non-endometrioid carcinomas (all of them with a serous component, which in one case also coexisted with clear cell elements), two non-endometrioid carcinomas (NEEC; all of them serous carcinomas) grade III, and the epithelial components of four malignant mixed Müllerian tumors (all of them with a non-endometrioid component of serous type). Forty-three tumors were stage I, 11 were stage II, and eight were stage III. Staging information was complete in all cases.

The study was approved by the local ethics committee, and the samples were obtained with a specific consent.

A tissue arrayer device (Beecher Instrument, MD) was used to construct the TMA. Briefly, all the samples were histologically reviewed, and representative areas were marked in the corresponding paraffin blocks. Two selected cylinders (0.6 mm in largest diameter) from two different areas were included in each case. Control normal tissues from the same EC specimens were also included.

Immunohistochemical study

TMA blocks were sectioned at a thickness of 3 μm, dried for 16 h at 56º before being dewaxed in xylene and rehydrated through a graded ethanol series, and washed with phosphate-buffered saline. Antigen retrieval was achieved by heat treatment in a pressure cooker for 2 min in EDTA (pH 8.9). Before staining the sections, endogenous peroxidase was blocked. A DcR1 polyclonal rabbit antibody was used (1:100 dilution; PA1-21270, Affinity Bioreagents). After incubation, the reaction was visualized with the EnVision Detection Kit (DAKO) using diaminobenzidine chromogen as a substrate. Sections were counterstained with hematoxylin. Appropriate positive and negative controls were also tested. Immunohistochemical results were evaluated by two pathologists, by following uniform preestablished criteria. DcR1 immunostaining was graded semiquantitatively by considering the percentage and intensity of the staining. A histological score was obtained from each sample, which ranged from 0 (no immunoreaction) to 300 (maximum immunoreactivity). The score was obtained by applying the following formula, Histoscore $= 1 \times$ (% light staining) $+ 2 \times$ (% moderate staining) $+ 3 \times$ (% strong staining). The reliability of such score for interpretation of

immunohistochemical staining in EC TMAs has been shown previously [2–4, 13, 14]. Since each TMA included two different tumor cylinders from each case, immunohistochemical evaluation was done after examining both samples.

Endometrial epithelial tissue explant isolation

Fresh frozen (normal and neoplastic) endometrial tissue was analyzed. The normal endometrial tissue samples were classified according to the phase in the menstrual cycle (six proliferative, 12 secretory, one inactive). Moreover, 28 tumor samples were obtained from patients with EC; they corresponded to 24 EEC and four NEEC. Ten tumors were grade I, 13 were grade II, and five were grade III. Twelve tumors were stage IA, four were stage IB, six were stage IC, and six were stage II. Age of the patients ranged from 49 to 88 years of age (mean, 68.4 years). The samples were collected in Dulbecco's Modified Eagle Medium (DMEM), chopped in 1-mm pieces, and incubated with collagenase in DMEM for 1.5 h at 37°C with periodic mixing. Afterwards, tissue was mechanically dissociated through a 10-ml pipette and a 1-ml blue tip and resuspended in 2 ml of fresh DMEM medium. To separate endometrial epithelial cells from the stromal fraction, the dissociated tissue was seeded on top of 8 ml of DMEM medium, and tissue was allowed to sediment by gravity. This step was repeated three times. Finally, tissue explants were resuspended in DMEM supplemented with 10% fetal bovine serum, 1 mM sodium pyruvate, 2 mM L-glutamine, and 1% of penicillin/streptomycin (Sigma) at 37°C with saturating humidity and 5% CO2. They were frozen until use. Immunostaining for keratin was used to confirm that the resulting tissue explants were exclusively composed of epithelial cells.

Real-time PCR analysis

Total cellular RNA was extracted using Trizol reagent (Life Technologies, Switzerland) and 1 μg of total RNA was retrotranscribed into cDNA using Taqman Reverse Transcription Reagents (P/N N808-0234). The RT reaction was then used as template for a 25-μl reaction for real-time detection of DcR1 using TaqMan Technology on an Applied Biosystems 7000 sequence detection system. Applied Biosystems assays-on-demand primers and TaqMan MGB probes (FAM™ dye-labeled reporter and no fluorescent quencher) for the target gene and predeveloped glyceraldehyde 3-phosphate dehydrogenase (GAPDH) (VIC-dye-labeled probe) were used. Gene expression quantification was performed in separate tubes (singleplex) for both the target gene and endogenous control gene using the primer and probe sequences for DcR1 and GAPDH (assay ID: HS 00174949 m1 and HS 99999905 m1, Applied Biosystems). The thermal cycler conditions were UNG activation 2 min at 50°C, AmpliTaq activation 95°C for 10 min, denaturation 95°C for 15 s, and annealing/extension 60°C for 1 min (repeated 40 times). Duplicate control values from two independent RNA extractions were analyzed with quantitative relative software using the comparative CT (ΔΔCT) method as described by the manufacturer. The amount of target $\left(2^{-\Delta\Delta CT}\right)$ was obtained by normalizing to an endogenous reference (GAPDH) and relative to a calibrator.

Statistical analysis

Statistical analysis was performed on a database using SPSS for Windows (version 11.5; SPSS Inc., Chicago, Ill). Immunohistochemical results were compared by the Mann–Whitney U and Student's *t* tests when applicable. Associations between qualitative variables were assessed by χ^2 or Fisher exact tests. Correlations between quantitative variables were established through Pearson's and Spearman's rho tests. Statistical significance was set at $p \leq 0.05$.

Results

Immunohistochemistry

In NE, DcR1 was evaluated in 64 cases. Three cases were excluded because there was no representative normal tissue left during the construction of the array. Moreover, the number of cylinders missed in the construction of the TMA was thirteen. Overall, positive DcR1 cytoplasmic staining was demonstrated in 51 cases (79.6%), and the H score varied from ten to 200 (mean, 90). DcR1 immunostaining varied according to the different phases of the menstrual cycle. DcR1 immunoexpression was significantly higher in the secretory phase (mean H score, 82.4; Fig. 1) than in the proliferative endometrium (mean H score, 31.3; Fig. 2; $p < 0.001$, Fig. 1). The staining was cytoplasmic.

In EC, DcR1 was evaluated in 54 of the 62 cases (Fig. 3). Two cases were excluded because there was no representative tumor tissue in the TMA sections (only non-neoplastic stromal tissue or necrosis was present), and six cases were missed in the TMA construction. Overall, DcR1 cytoplasmic immunostaining was detected in 53 of the 54 cases (98.1%). The staining was cytoplasmic and heterogeneous, and the H score ranged from five to 290 (mean, 83.4).

Overall, there was no significant correlation between DcR1 immunostaining between NE (all phases during the endometrial cycle) and EC ($p=0.215$). However, when we compared the differences between EC and the proliferative endometrium, we found that the mean H scores were different (83.4 and 31.3, respectively) and that difference had statistical significance ($p=0.001$)

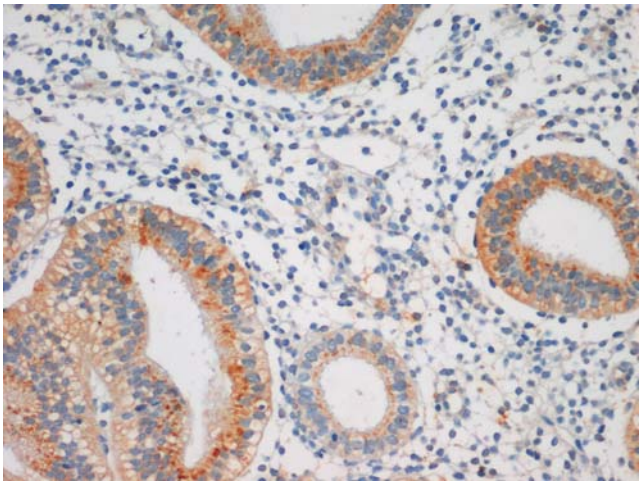

Fig. 1 DcR1 expression in normal endometrium during the secretory phase (early stage)

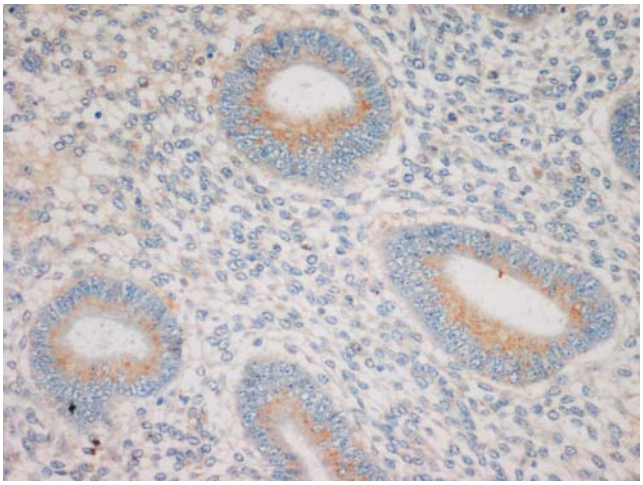

Fig. 2 DcR1 immunostaining in normal endometriun during the proliferative phase

No significant differences were seen between DcR1 expression and histological type, grade, and stage. The mean H score for EEC and NEEC were 93.6 (range, 5–290), and 39.28 (range, 15–70), respectively, and such difference did not reach statistical significance ($p=0.231$). Moreover, mean H scores were 94 for grade I tumors (range, 5–220), 92.1 for grade II tumors (range, 20–290), and 51.3 for grade III tumors (range, 15–125), and such a difference was not statistically significant ($p=0.107$). Finally, there was no significant difference between DcR1 expression and stage. Mean H scores were 91 (range, 30–180) for stage IA, 81.8 (range. 30–2220) for stage IB, 85 (range, 5–240) for stage IC, 146.6 (range, 20–290) for stage IIA, 78.7 (range, 15–150) for stage IIB, and 74.2 (range, 15–170) for stage IIIA.

Quantitative RT-PCR

By quantitative real-time PCR, all normal endometrial tissues (proliferative, secretory, or inactive) had similar levels of DcR1expression (0.8–1.7 RQ), which were considered the basal levels of DcR1 expression in normal tissue. Increased DcR1 expression (≥5-fold higher than the basal levels) was detected in 13 of 28 EC (46.4%). High DcR1 expression levels were found in ECs of different stages: IA, four of 12 (33%); IB, two of four (50%); IC, four of six (66%); and IIA and IIB, three of six (50%; Table 1). No statistical significance was obtained when evaluating DcR1 expression with clinicopathological parameters, such as histological type, grade, or stage. However, EC infiltrating the myometrium deeply (stage IC) showed the highest proportion of positivity for DcR1. Moreover, it was clear that one third of the EC samples exhibited increased DCR1 mRNA levels in comparison with normal endometrial tissue.

Discussion

Deregulation of apoptosis plays an important role in development and progression of cancer [9, 11, 12]. Moreover, cells resistant to apoptosis are likely to escape the immune surveillance, but they may also be resistant to therapy. The “extrinsic pathway” is activated by ligand-bound death receptors such as TNF, Fas, or TRAIL receptors [5–8]. Different steps of the extrinsic apoptotic pathway have been found to be deregulated in many tumors. Down-regulation of death receptors, like Fas, has been detected in colorectal and hepatocellular carcinomas; and loss-of-function mutations and deletions on receptors DR4 and DR5 occur in metastatic breast carcinomas and lung carcinomas. In other tumors, there is up-regulation of decoy receptors (DcR1 and DcR2) that compete with the functional receptors for the ligand binding and may result in

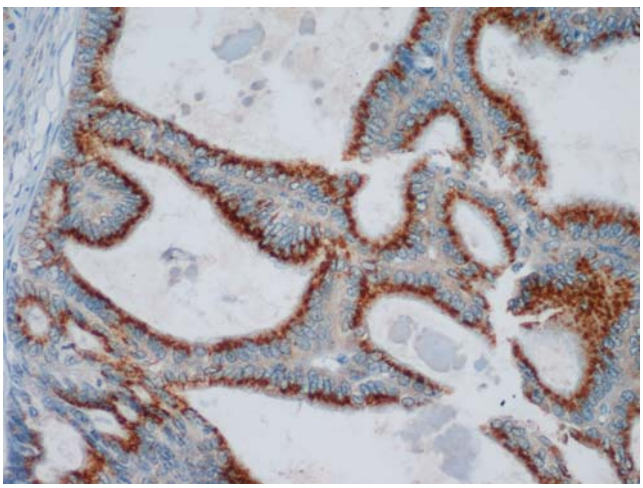

Fig. 3 DcR1 immunohistochemical staining in endometrial carcinoma

Table 1 DcR1 expression by QRT-PCR

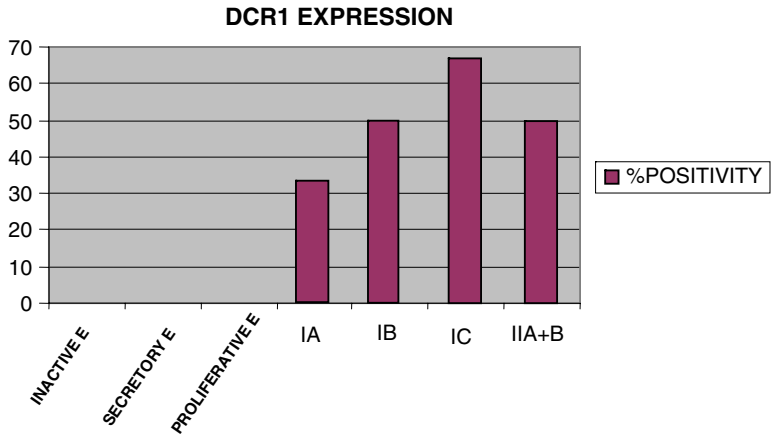

a diminished binding of TRAIL to their functional receptors and decreased apoptosis [10].

ECs can be classified into two main clinicopathological variants: type I, EEC and type II, NEEC [15]. Recent molecular studies have shown that these two forms of EC follow different molecular pathways [15]. Type I, EEC, characteristically shows five different molecular alterations that may coexist in some cases: microsatellite instability [16] and mutations of the *PTEN* [17–19], *PIK3CA* [20, 21], *K-RAS* [22], and β-catenin genes [23]. In contrast, type II, NEEC, is usually associated with mutations in the p53 tumor suppressor gene and loss of heterozygosity at many different loci [24, 25].

There are many evidences suggesting that alteration of apoptosis is important in development and progression of endometrioid adenocarcinomas of the endometrium. They frequently show activation of the PI3K pathway, either by inactivating mutations in PTEN [17–19] or by activating mutations in the *PIK3CA* gene [20, 21]. Activation of the PI3K pathway may lead to enhanced survival by different mechanisms that ultimately cause phosphorylation of BAD, inhibition of caspase-9, or down-regulation of Fas ligand. p53 alterations, which are characteristic of non-endometrioid carcinomas, may also occur in endometrioid tumors, particularly in those neoplasms showing overlapping features between types I and II tumors, and they may have an impact in apoptosis at several different levels [24, 25]. Also, members of the Bcl-2 family of genes, like *BAX* [1] and other proteins involved in apoptotic control, like NF-kB or survivin, are involved in endometrial carcinoma [2, 3]. Moreover, an important protein responsible for apoptosis resistance in endometrial carcinoma is FLICE-like inhibitory protein (FLIP), which shares a high degree of homology with caspase-8 but lacks protease activity and [4]. FLIP is frequently expressed in endometrial carcinomas and is regulated by CK2 [13, 26]. However, it is evident that FLIP overexpression does not explain, alone, by itself, resistance of TRAIL-induced apoptosis in endometrial carcinoma. For that reason, it is reasonable to look for other proteins involved in such a phenomenon.

Decoy receptors (DcR1 and DcR2) can bind TRAIL but are deficient in signaling to caspase-8. Up-regulation of decoy receptors (DcR1 and DcR2) competing with the functional receptors for the ligand binding and resulting in a diminished binding of TRAIL to their functional receptors has been regarded as a mechanism of inhibition of TRAIL-induced apoptosis in cancer cells [10]. However, it has recently been suggested that, rather than competing for binding for TRAIL, decoy receptors may inhibit the apoptotic signal by forming ligand-independent protein complexes, which would be deficient in mediating a robust death signal [27]. Moreover, in one study, formation of these heterocomplexes was ligand-dependent but correlated with reduced TRAIL-mediated cell death [28].

In this study, we have tried to assess the expression in DcR1 in normal endometrial tissue and endometrial carcinoma. By immunohistochemistry, DcR1 expression was higher in the secretory phase in comparison with the proliferative phase. This is not unusual for a protein which may be responsible for resistance for TRAIL-induced apoptosis, since the many proteins involved in the negative control of apoptotic cell death show elevated levels during the secretory phase. Moreover, DcR1 was also frequently expressed in endometrial carcinoma. Although there was no significant difference between endometrial carcinoma and normal endometrium, when considering all phases of the menstrual cycle, there were some differences between endometrial carcinoma and the normal endometrial tissue during the proliferative phase, which is probably the best control among normal endometrial tissues. When we checked the samples by quantitative real-time RT-PCR, there was a significant difference between normal endometrial tissue and endometrial carcinoma, and the levels of DcR1 in endometrial carcinoma showed some correlation with stage, since myoinvasive tumors (stage IC) showed the

highest proportion of high DCR1 expression. Interestingly, in normal endometrium, we did not see differences in mRNA DcR1 among the different phases of the menstrual cycle. Lack of correlation between mRNA levels and protein expression are not unusual when evaluating gene expression in tumor samples. Technical problems could be responsible for the lack of correlation between mRNA and protein levels, but they have been minimized by the design of the methodological strategy. It is worth mentioning that mRNA was evaluated in tissue explants that were exclusively composed of epithelial cells, minimizing the possibility of stromal contamination that would interfere with the molecular interpretation. The discrepancy between the data obtained by immunohistochemistry with that of quantitative RT-PCR could be also explained by the presence of posttranslational processing of DcR1, which would modify protein expression. In summary, the results suggest that DcR1 expression occurs in normal endometrium and endometrial carcinoma and could play a role in resistance to TRAIL-induced apoptotic cell death during menstrual cycle and endometrial carcinoma tumor progression.

The study has some limitations. For example, it is not possible to assess the effect of DCR1 on apoptosis by correlating its expression with the apoptotic index or the expression of some apoptotic markers. It has long been observed that, frequently, those tumors that show higher levels of apoptosis resistance are precisely those that exhibit higher apoptotic indexes. Such a paradox is due to the fact that apoptosis resistance is usually associated with high grade and high cell proliferation, and these two features are, by themselves, associated with high apoptotic indexes. Moreover, further functional studies assessing cell viability after DCR1 down-regulation by transfection with DCR1 siRNA will be required to confirm the role of DCR1 on apoptosis resistance in endometrial carcinoma.

Conflict of interest statement We declare that we have no conflict of interest.

References

1. Catasus L, Matias-Guiu X, Machín P et al (1998) BAX somatic frameshift mutations in endometrioid adenocarcinomas of the endometrium. Lab Invest 78:1439–1444
2. Pallares J, Martínez-Guitarte JL, Dolcet X et al (2004) Abnormalities in NF-κB family and related proteins in endometrial carcinoma. J Pathol 204:569–577
3. Pallares J, Martínez-Guitarte JL, Dolcet X et al (2005) Survivin expression in endometrial carcinoma. Int J Gynecol Pathol 24:247–253
4. Dolcet X, Llobet D, Pallares J et al (2005) FLIP is frequently expressed in endometrial carcinoma and has a role in resistance to TRAIL-induced apoptosis. Lab Invest 85:885–894
5. Gupta S (2003) Molecular signaling in death receptor and mitochondrial pathways of apoptosis. Int J Oncol 22(1):15–20
6. Baud V, Karin M (2001) Signal transduction by tumor necrosis factor and its relatives. Trends Cell Biol 11(9):372–377
7. Thorburn A (2004) Death receptor induced cell killing. Cell Signal 16:139–144
8. Zörnig M, Hueber A, Baum W et al (2001) Apoptosis regulators and their role in tumorigenesis. Biochim Biophys Acta 1551:F1–F37
9. Zhang L, Fang B (2005) Mechanisms of resistance to TRAIL-induced apoptosis in cancer. Cancer Gene Ther 12:228–237
10. Ashkenazi A (2002) Targeting death and decoy receptors of the tumour-necrosis factor superfamily. Nat Rev Cancer 2:420–428
11. Igney FH, Krammer PH (2003) Death and anti-death: tumour resistance to apoptosis. Nat Rev Cancer 2:277–288
12. Kaufmann SH, Vaux DL (2003) Alterations in the apoptotic machinery and their potential role in anticancer drug resistance. Oncogene 22:7414–743
13. Pallares J, Llobet D, Santacana M et al (2009) CK2beta is expressed in endometrial carcinoma and has a role in apoptosis resistance and cell proliferation. Am J Pathol 174:287–296
14. Pallares J, Velasco A, Eritja N et al (2008) Promoter hypermethylation and reduced expression of RASSF1A are frequent molecular alterations of endometrial carcinoma. Mod Pathol 21:691–699
15. Matias-Guiu X, Catasus L, Bussaglia E, Lagarda H, Garcia A, Pons C, Muñoz J, Arguelles R, Machin P, Prat J (2001) Molecular pathology of endometrial hyperplasia and carcinoma. Hum Pathol 32:569–577
16. Catasus L, Machin P, Matias-Guiu X et al (1998) Microsatellite instability in endometrial carcinomas: clinicopathologic correlations in a series of 42 cases. Hum Pathol 29:1160–1164
17. Kanamori Y, Kigawa J, Itamochi H et al (2001) Correlation between loss of PTEN expression and Akt phosphorylation in endometrial carcinoma. Clin Cancer Res 7:892–895
18. Bussaglia E, del Rio E, Matias-Guiu X et al (2000) PTEN mutations in endometrial carcinomas. A molecular and clinicopathologic analysis of 38 cases. Hum Pathol 31:312–317
19. Tashiro H, Blazes MS, Wu R et al (1997) Mutations in PTEN are frequent in endometrial carcinoma but rare in other common gynecological malignancies. Cancer Res 57:3935–3940
20. Oda K, Stokoe D, Taketani Y et al (2005) High frequency of coexistent mutations of PIK3CA and PTEN genes in endometrial carcinoma. Cancer Res 65:10669–10673
21. Velasco A, Bussaglia E, Pallares J et al (2006) PIK3CA gene mutations in endometrial carcinoma: correlation with PTEN and K-RAS alterations. Hum Pathol 37:1465–1472
22. Lagarda H, Catasus L, Arguelles R, Matias-Guiu X, Prat J (2001) K-ras mutations in endometrial carcinomas with microsatellite instability. J Pathol 193:193–9
23. Machin P, Catasus L, Pons C, Muñoz J, Matias-Guiu X, Prat J (2002) CTNNB1 mutations and beta-catenin expression in endometrial carcinomas. Human Pathol 33:206–212
24. Tashiro H, Isacson C, Levine R et al (1997) p53 gene mutations are common in uterine serous carcinoma and occurs early in their pathogenesis. Am J Pathol 150:177–185
25. Sherman ME, Bur ME, Kurman RJ (1995) p53 in endometrial cancer and its putative precursors: evidence for diverse pathways of tumorigenesis. Human Pathol 26:1268–1274
26. Llobet D, Eritja N, Encinas M et al (2008) CK2 controls TRAIL and Fas sensitivity by regulating FLIP levels in endometrial carcinoma cells. Oncogene 27:2513–24
27. Clancy L, Mruk K, Archer K et al (2005) Preligand assembly domain-mediated ligand-independent association between TRAIL receptor 4 (TR4) and TR2 regulates TRAIL-induced apoptosis. Proc Natl Acad Sci USA 102:18099–18104
28. Mérino D, Lalaoui N, Morizot A et al (2006) Differential inhibition of TRAIL-mediated DR5-DISC formation by decoy receptors 1 and 2. Mol Cell Biol 26:7046–7055

Virchows Arch (2010) 456:45–51
DOI 10.1007/s00428-009-0860-5

ORIGINAL ARTICLE

Tissue transglutaminase 2 as a biomarker of cervical intraepithelial neoplasia (CIN) and its relationship to $p16^{INK4A}$ and nuclear factor κB expression

Ruchi Gupta · Radhika Srinivasan · Raje Nijhawan · Vanita Suri

Received: 8 July 2009 / Revised: 29 October 2009 / Accepted: 3 November 2009 / Published online: 25 November 2009
© Springer-Verlag 2009

Abstract Tissue transglutaminase 2 (TG2) is a recently identified molecule with multifunctional physiological roles. This is the first report of the expression of TG2 in cervical intraepithelial neoplasia (CIN) and invasive squamous cell carcinoma (SCC). For comparison, the expression of p16, a known surrogate biomarker of HPV infection, was evaluated. The expression of nuclear factor kappa B (NF-κB), a molecule crucial to inflammation and neoplasia, was also determined to explore its possible linkage with TG2 expression. Twenty cases each with normal cervical histology, CIN1, CIN2, CIN3, and invasive SCC were analyzed for TG2, p16, and NF-κB expression by immunohistochemistry. Intergroup differences were analyzed by Friedman ANOVA. Cytoplasmic as well as nuclear TG2 expression was observed in the epithelial cells. As compared to normal controls, CIN1 showed markedly increased cytoplasmic TG2 expression (p=0.006). In CIN2/3, additional nuclear TG2 expression was seen (p=0.009 and 0.031, respectively). Marked extracellular stromal upregulation of TG2 was noted in CIN3/SCC versus normal controls (p=0.054; p=0.003). There was no relationship of TG2 with either p16 of NF-κB expression. Combining TG2 immunoreactivity with p16 increased the immunolabeling of dysplasia from 35% to 100% in CIN1, 45% to 60% in CIN2, and 60% to 85% in CIN3. TG2 serves as an additional biomarker for all grades of cervical dysplasia, especially for low-grade dysplasia.

Keywords Tissue transglutaminase 2 · CIN · p16 · Cervical cancer · Nuclear factor κB · Biomarker

R. Gupta
Department of Pathology,
Postgraduate Institute of Medical Education and Research,
Chandigarh, India

R. Srinivasan (✉) · R. Nijhawan
Department of Cytology and Gynecological Pathology,
Postgraduate Institute of Medical Education and Research,
Chandigarh, India 160012
e-mail: drsradhika@gmail.com

V. Suri
Department of Obstetrics and Gynecology,
Postgraduate Institute of Medical Education and Research,
Chandigarh, India

Introduction

Carcinoma of the uterine cervix is one of the foremost causes of cancer-related mortality in women with an estimated 493,000 new cases and 274,000 deaths occurring worldwide [1]. Invasive squamous cell carcinoma of the cervix progresses through a well-recognized pre-cancer stage termed cervical intraepithelial neoplasia or CIN. It is now well established that persistent infection with high-risk human papilloma virus (HPV) infection is necessary for the development of the high-grade precursor lesions encompassing CIN2 and CIN3 [2, 3]. Consequent to the genomic integration of these viral genes, there is altered cellular expression of several proteins resulting in disordered cellular signaling. One such protein is tissue transglutaminase 2, a molecule which has only recently been shown to play a significant role in cancer development. It is a cytosolic protein, belonging to a family of calcium dependent enzymes [4]. It catalyzes the formation of a covalent bond between gamma carboxamide group of peptide bound glutamine residue and primary amino group of a wide variety of proteins leading to their post-translation modification [5]. Initial studies have revealed that TG2 is overexpressed in breast cancer [6], malignant melanoma

[7], and orthotopic glioblastoma [8]. This study is the first to examine the role of TG2 in pre-cancer and invasive squamous cancer of the uterine cervix.

p16INK4A or p16 is a well-established surrogate biomarker of HPV infection in the cervical epithelium and is known to be overexpressed in cervical intraepithelial neoplasia and squamous cell carcinoma [9–12]. The protein p16 is integral to pRb (retinoblastoma) mediated control of the G1-S phase transition of the cell cycle. p16 puts a brake on the cell cycle by inactivating the cyclin-dependent kinases that phosphorylate Rb protein. A reciprocal relationship between p16 and pRb expression has been observed [13]. In cervical cancer, the disruption of pRb by HPV E7 results in the upregulation of p16 through negative feedback regulation. Furthermore, accumulation of the E2F, a transcription factor regulated by pRb, in turn induces the overexpression of p16 [13]. On the other hand, the retinoblastoma protein is also one of the major targets of TG2-induced polyamination, thereby protecting it from caspase-mediated cleavage [5]. In a study by Jeon et al. [14], HPV E7 has also been found to be one of the target proteins, polyaminated by TG2. Consequent to this polyamination, the interaction of HPV E7 and pRb, a major step for cervical carcinogenesis, gets disrupted. They thus concluded that TG2 protects pRb, thereby promoting anti-apoptotic properties [14]. Thus the interaction of p16 and TG2 is intriguing and complex and was explored in this study.

A key molecule that integrates the pathways of inflammation and neoplasia is the nuclear factor kappa B (NF-κB), which also plays a pivotal role in cell cycle regulation [15]. Mann et al. [16] have demonstrated a direct relationship of TG2 expression with the transcription factor NF-κB or NF-κB activation in pancreatic ductal carcinoma samples. Further, inhibition of endogenous TG2 activity inhibits constitutive NF-κB activation in cell culture systems. In a recently established link to oncogenic HPV, functional NF-kB binding site has been identified within the HPV16 LCR (long control region). Further, it was demonstrated that HR-HPV E7 inhibits NF-κB activation by targeting the IKK complex. In addition, HR-HPV E6 seems to inhibit NF-κB (p65)-dependent transcriptional activity within the nucleus. This implies that NF-κB could be one of the targets through which these HPVs could interfere with the transcriptional control in cervical carcinogenesis [17, 18].

Hence, in this study, we evaluated the complex relationship of these three proteins viz, TG2, NF-κB, and p16, in cervical carcinogenesis by comparison of their expression in the cervical pre-cancer and invasive cancer.

Materials and methods

This was a retrospective analysis of 100 paraffin-embedded cervical biopsies, including 20 cases each, in the category of normal cervical histology, CIN1, CIN2, CIN3, and invasive squamous cell carcinoma diagnosed in 2004–2006. NF-κB expression was evaluated in a subset of 70 of these cases, with 14 cases of normal histology, 15 CIN1, 10 CIN2, 14 CIN3, and 17 cases of squamous cell carcinoma. Serial sections were obtained on poly-L-lysine coated slides, from the paraffin blocks for immunohistochemical analysis. Antigen retrieval was carried out by pressure cooker method for p16 and microwave for TG2 and NF-κB, using 0.01 M citrate solution at pH 6.0. p16 mouse monoclonal antibody (clone 6H12, Novacastra, Newcastle Upon Tyne, UK) was applied at 1:20 dilution (diluted in Bovine serum albumin). Primary rabbit polyclonal antibody against TG2 (clone H-237) and a mouse monoclonal antibody against NFκB (F-6) was obtained from Santa Cruz Biotech Inc, Santa Cruz, CA, USA. Both were applied in a 1:40 dilution. The streptavidin–biotin peroxidase secondary antibody (Novocastra, Newcastle upon Tyne, UK) consisting of the secondary biotinylated rabbit antimouse or goat anti-rabbit antibody was applied at 1:100 dilution in bovine serum albumin for 30 min followed by streptavidin conjugated with horseradish peroxidase for another 30 min. Finally, the color was developed by treatment with diaminobenzidine solution (Sigma-Aldrich, St. Louis, MO, USA) and hydrogen peroxide. Sections were counter-stained with hematoxylin and then dehydrated, cleared with xylene, and mounted in DPX. The final brown reaction product was evaluated by light microscopy.

Controls for immunohistochemistry

The cases of squamous cell carcinoma served as positive control slides for p16 and NF-κB immunostaining. The negative control slides in each batch consisted of omission of the primary antibody and substitution by the buffer. For TG2 immunostaining, the positive control consisted of cases of metastatic breast cancer in lymph nodes and slides of pancreatic adenocarcinomas. These slides were kindly provided by Dr Kapil Mehta of M.D. Anderson Cancer Centre, USA.

Evaluation of immunohistochemical staining

TG2, NF-kB, and p16 immunoreactivity was evaluated, taking into account the percentage positivity of tumor cells and staining intensity. Positivity was seen as a brown reaction product staining the nucleus and/or cytoplasm. Scoring of percentage positive tumor cells was carried out as follows: 0% staining as negative, 0–5% as 1+, 5–25% as 2+, and >25% as 3+. Intensity of immunostaining was scored as 1+ (weak), 2+ (moderate), and 3+ (strong) depending upon the degree of positivity. The immunohis-

tochemistry score (IHC score) was obtained as a product of percentage positive tumor cells (0–3) and staining intensity score (0–3). Thus, the IHC score could range from 0 to 9. The results of immunohistochemistry were analyzed and scored independently by two pathologists.

Statistical analysis

Data were analyzed using the statistical package SPSS version 10.0 for MS-Windows (SPSS Inc., Chicago, IL, USA). Differences between means of continuous variables and categorical variables were analyzed using Friedman and chi-square tests where applicable. The significance of TG2, NF-kB, and p16 expression between and within the individual groups was analyzed using the Friedman ANOVA test and post hoc test of Scheffe, respectively. The relationship between TG2, NF-kB, and p16 expression was ascertained using Spearman's correlation test. Significance was assumed at a p value less than 0.05. Interobserver agreement for immunohistochemical analyses was assessed using interclass correlation coefficients. The correlation coefficient was 0.85, implying an excellent agreement.

Results

TG2 immunohistochemistry

TG2 was expressed in the cervical epithelium, stroma, and the vasculature, but at variable levels. In the cervical epithelium, the expression was nuclear, cytoplasmic, or both (Fig. 1). The stromal cells, including fibroblasts, extracellular matrix, endothelium, and chronic inflammatory cells, also showed immunoreactivity. The intensity of staining of the stroma was variable in different groups as well as within the same group. Vascular smooth muscle cells also consistently stained positive for TG2.

Table 1 summarizes the TG2 expression in the different groups. In the normal cervical histology group, a majority (n=14/20) of the cases showed weak cytoplasmic immunostaining, and in four cases, there was no expression (Fig. 1a). Additional weak nuclear immunoreactivity was seen in two cases (10%). In contrast, all cases of CIN1 showed strong cytoplasmic positivity (Fig. 1b). Additional nuclear reactivity was observed in four cases of CIN1 (20%). The expression of TG2 in CIN1 was either restricted to the basal one third or was present as diffuse full thickness expression. In CIN2/3, the expression of TG2 was predominantly nuclear. In CIN2, 10 cases were positive with either nuclear expression (n=3/20) cases or nucleo-cytoplasmic positivity (n=7/20). In CIN3, similar nucleo-cytoplasmic expression of TG2 was seen in seven out of 20 cases (33.3%; Fig. 1c), whereas two cases (9.5%) showed only nuclear positivity. In invasive squamous cell carcinoma, a heterogeneous staining pattern was observed (Fig. 1d). In contrast to the higher-grade CINs, squamous cell carcinomas displayed a predominant cytoplasmic immunoreactivity (n=14/20). Only two cases showed nucleo-cytoplasmic positivity.

Stromal TG2 expression was scored separately from epithelial reactivity. Strong stromal TG2 was seen in higher grades of CIN and invasive cancer as compared to the normal cervix (Fig. 1e).Occasionally, we observed increased TG2 cytoplasmic expression at the stromal–epithelial interface (Fig. 1f) and in foci of neoangiogenesis (Fig. 1e, inset).

The variations in TG2 expression among the various groups is depicted in the box plot graph (Fig. 2). Cytoplasmic TG2 expression was markedly upregulated in CIN1 as compared to normal cervical epithelium (p=0.006); however, there was no significant difference between cytoplasmic TG2 expression when normal histology and CIN3 (p=0.053) or invasive carcinoma were compared. On the other hand, there was a significant nuclear expression of TG2 in the CIN2 and CIN3 groups as compared to normal epithelium (p=0.009 and 0.031, respectively). The expression of TG2 in the stroma was evaluated separately, and it was observed that there was mild upregulation of stromal TG2 expression in CIN3 (P=0.054) and marked upregulation in invasive squamous cell carcinoma (p=0.003) as compared to the normal cervix (Fig. 3).

Comparison of TG2 with p16 and NF-κB expression

We compared the expression of TG2 with p16 and NF-κB expression determined immunohistochemically on serial sections. The expression of p16 in the CIN1 cases was predominantly cytoplasmic (8/10) with nuclear positivity in one and nucleo-cytoplasmic in another. In contrast, a majority of CIN2 (n=9/20), CIN3 (n=12/20), and SCC (n=18/20) showed both nuclear and/or nucleo-cytoplasmic positivity. There was a significant difference of p16 expression between the groups (p=0.000). On the other hand, NF-κB immunohistochemistry showed a mild increase in its expression in CIN1, CIN2, and SCC as compared to the expression in the normal epithelium, which is depicted in box plots (Fig. 4); the difference between groups was however not statistically significant (p=0.537). Further, logistic regression test and Spearman correlation test were applied to discern the inter-relationship between expression of all the three molecules. There was no correlation between TG2 and NF-κB expression or between p16 and NFκB expression. An interesting observation was made with respect to TG2 and p16 expression. Although

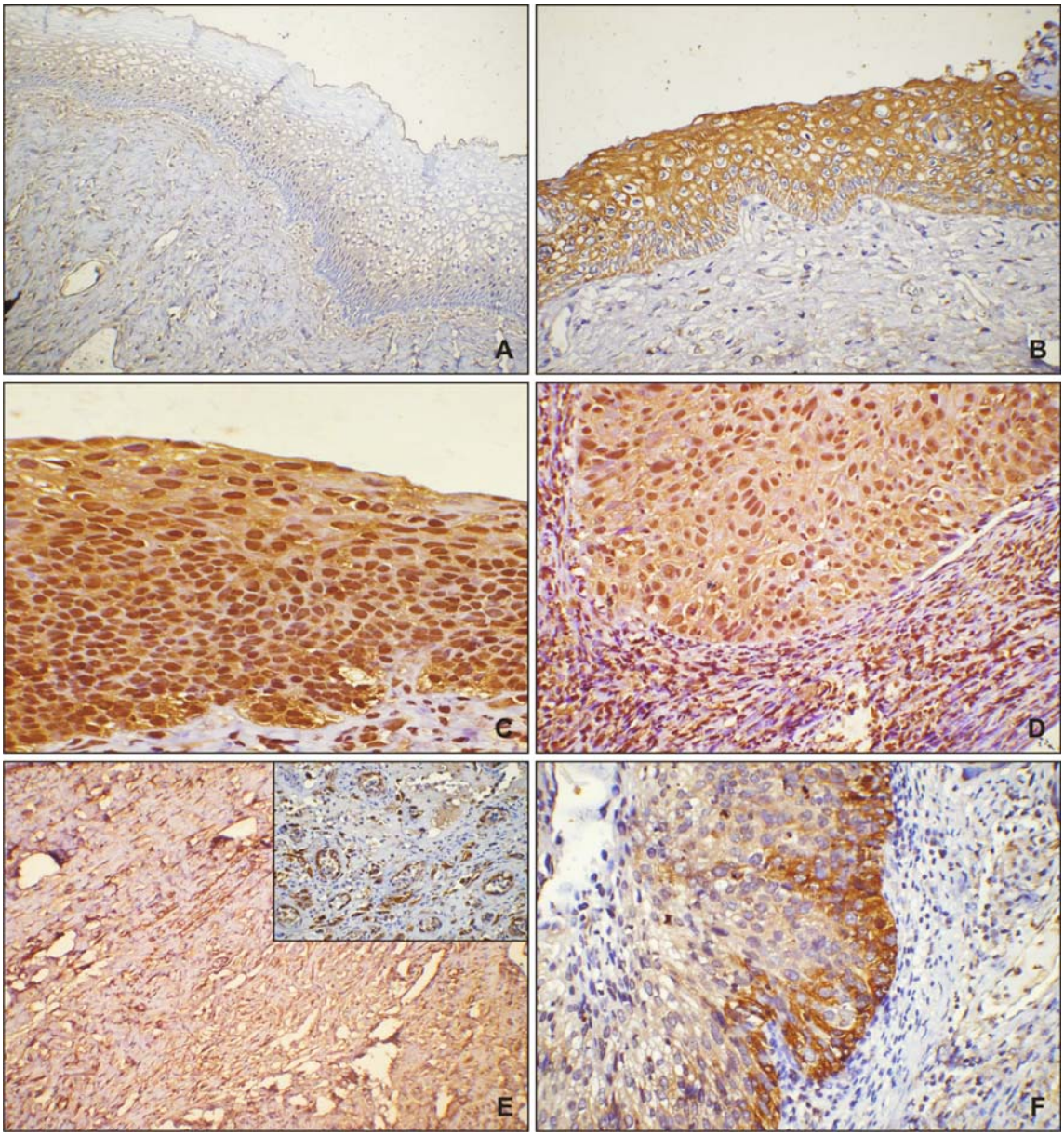

Fig. 1 TG2 expression in normal cervix, CIN (1–3), and SCC. **a** Weak cytoplasmic positivity in normal cervix; **b** CIN1 with 2+ to 3+ cytoplasmic positivity; **c** and **d** nucleo-cytoplasmic positivity in CIN2 and CIN3, respectively; **e** SCC showing strong stromal expression with a focus of neoangiogenesis *highlighted in the inset*; **f** SCC, positivity in the epithelial–stromal interface. (Original magnification ×400; streptavidin–biotin immunoperoxidase)

Table 1 Tissue transglutaminase2 expression in normal cervix, CIN, and invasive cancer

Immunoreactivity	Normal *N*=20	CIN1 *N*=20	CIN2 *N*=20	CIN3 *N*=20	SCC *N*=20
Negative	4	0	2	3	5
Positive	16	20	18	17	15
Cytoplasmic	14	16	8	8	14
Nucleo-cytoplasmic	2	3	7	7	1
Nuclear	0	1	3	2	0

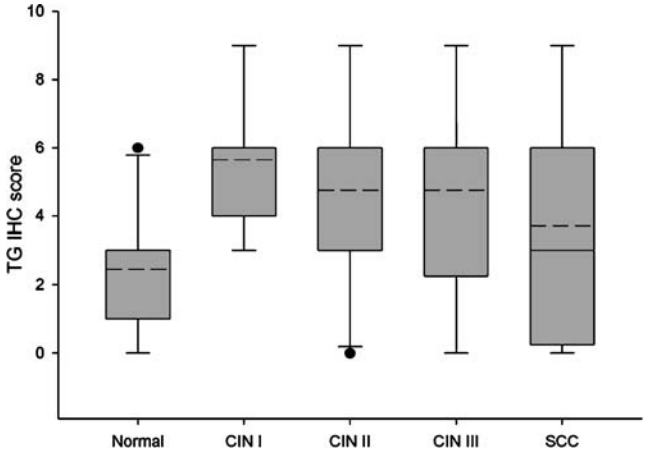

Fig. 2 Box plot representing the range of TG2 IHC score in each category along with the median value (*solid line*) and mean value (*dashed line*). The *dots* represent the cases which fall out of the 90th percentile range. In normal, CIN1, CIN2, and CIN3 cases, the median falls out of the 25th to 75th percentile and hence is not depicted

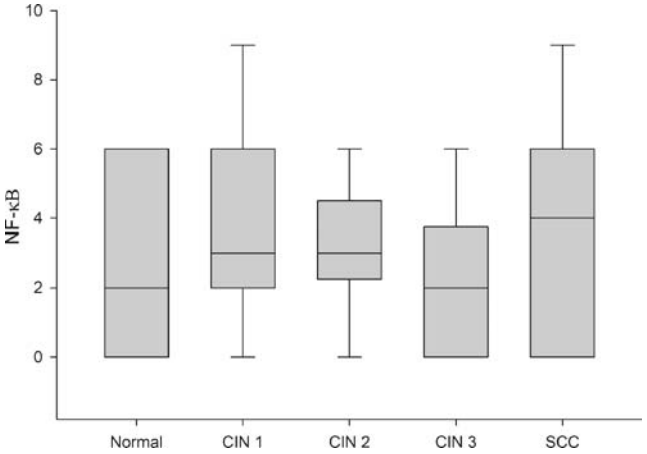

Fig. 4 Box plot representing the range of NF-κB IHC score in each category along with the median value (*solid line*)

there was no direct correlation between TG2 and p16 expression, high-grade CIN lesions (CIN2 and CIN3) showed nuclear immunoreactivity for both TG2 and p16. In contrast, in invasive squamous cell carcinoma, p16 continued to show nuclear positivity, whereas TG2 again showed cytoplasmic positivity. This is depicted graphically in Fig. 5.

We further examined if TG2 could serve as a biomarker of cervical dysplasia in addition to the well-established marker p16. The combinatorial expression of TG2 and p16 is depicted in Table 2. Thus, whereas TG2 uniformly labels all cases of CIN1, diffuse nucleo-cytoplasmic positivity for p16 was seen only in 30% cases. In CIN2 and CIN3, combining TG2 with p16 increased the immunolabeling of dysplastic cells from 45–60% to 60–85%. Hence TG2 can serve as an additional marker for cervical dysplasia.

Discussion

The cervical epithelium undergoes a series of morphological changes following HPV infection. Newer molecules are constantly being explored to detect these changes as early as possible and predict the lesions, which are likely to evolve into higher grades and, further, carcinoma. TG2 is one such recently studied protein, in relation to various cancers like breast carcinoma [19], pancreatic adenocarcinomas [20], and glioblastoma multiforme [8], with positive results. Ours is the first study to have evaluated its role in the pathogenesis of cervical cancer.

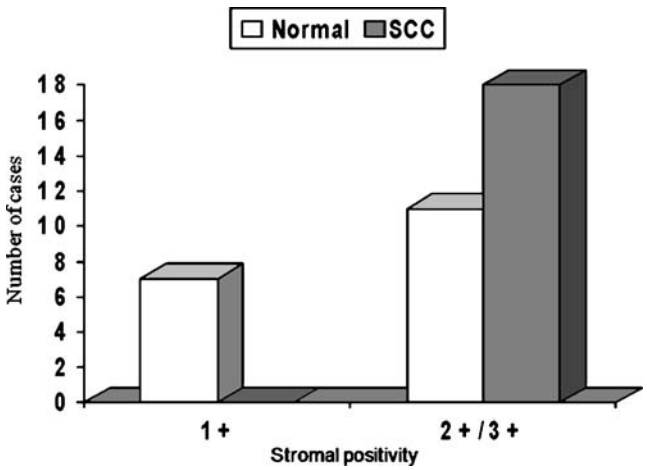

Fig. 3 Stromal TG2 expression invasive in squamous cell carcinoma versus normal cervix

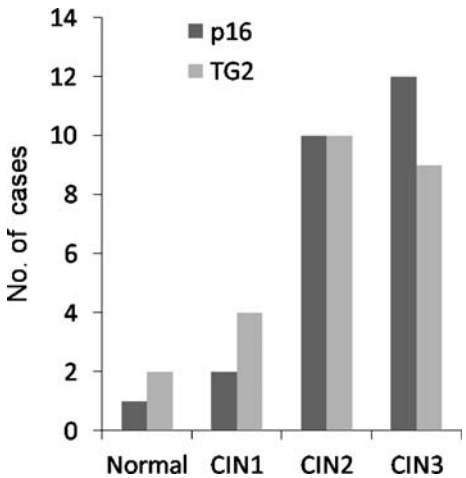

Fig. 5 Nuclear/nucleo-cytoplasmic TG2 expression in comparison to p16 expression in different grades of CIN

Table 2 Comparison of TG2 and p16 immunoreactivity in CIN

Immunoreactivity	CIN1 *N*=20	CIN2 *N*=20	CIN3 *N*=20
p16+/TG2+	6	7	3
p16+/TG2−	0	2	9
p16−/TG2+	14	3	5
p16−/TG2−	0	8	3
p16 positivity	6 (30%)	9 (45%)	12 (60%)
p16 or TG2 positivity	20 (100%)	12 (60%)	17 (85%)

Tissue transglutaminase 2 has a predominant cytosolic expression as was seen in normal cervical squamous epithelium. The extracellular matrix (ECM) also showed immunoreactivity for TG2 protein indicating a role for it in the ECM. The most striking observation was the overall increased expression of TG2 in the dysplastic epithelium as compared to the normal cervical lining epithelium. It may be speculated here that TG2 protein may be one of the early proteins, which is affected by the HPV infection and could have consequences on viral and cellular proteins as well. The presence of high levels of TG2 in CIN1 may thus reflect cellular response to inflammation and HPV infection, which may facilitate cell survival by its interaction with proteins involved in cell proliferation and cell death. In CIN2 and CIN3, the immunoreactivity for TG2 remains at moderately high levels with specifically nuclear expression, in comparison to CIN1. This nuclear translocation of TG2 in the high-grade CIN is intriguing. In a recent report by Mann et al. [16], this nuclear expression has been linked to NF-κB activation. TG2 can activate NF-κB by cross-linking and resultant polymerization or by destabilizing the association of p65/p50 (NF-κB) complex with IκB [16]. In fact, confocal microscopy has revealed co-localization of the activated NF-κB with TG2 in the nucleus of the cancer cell. Hence we also explored the association between NF-κB and TG2 expression. Our study failed to establish any such association based on immunohistochemical analysis.

Hence, more advanced molecular techniques are required to simultaneously analyze the dynamic cellular profiles of TG2 and NF-κB following HPV infection to delineate their role in cervical carcinogenesis.

In the nucleus, the other protein that has been found to interact with TG2 is the tumor suppressor protein pRb (retinoblastoma protein). TG2 protects pRb from caspase-mediated apoptosis, thereby promoting cell survival [5]. Thus, overall in CIN2 and CIN3, the increased nuclear expression of TG2 can tilt the delicate balance in favor of cell survival or confer the cell with anti-apoptotic phenotype and therefore aid the progression or persistence of the CIN lesion. Further studies on tissue samples and at the molecular and cellular level taking into account the inter- and intraobserver variation are indicated in this regard.

The significance of the upregulated expression of TG2 in the stroma of invasive cancer also warrants further investigation. In recent experimental studies by Mangala et al. [6] and Mehta et al. [21] on MCF-7 breast cancer cells, TG2 expression was shown to promote cell surface interaction with fibronectin, protect cells from apoptosis, and lead to the development of metastasis and a drug-resistant phenotype. Hettasch et al. [22] have made similar observations in the human breast cancer. Experiments have also shown its ability to cross-link proteins and promote cell adhesion and spreading [23, 24]. The presence of intense TG2 expression observed at the stromal–epithelial interface supports the previous observation of its role in cell migration, invasiveness, and metastasis [16, 21, 25]. Stromal TG2 expression was also present in the endothelium of the newly formed blood vessels (neoangiogenesis), which was in tune with the findings of Dardik et al. [26]. In invasive squamous cell carcinoma, the upregulated TG2 therefore holds promise as another therapeutic target.

p16INK4A, a well-recognized biomarker of HPV infection has found a place in diagnostic surgical pathology for labeling cervical dysplasia. TG2 is a potentially useful marker for low-grade dysplasia or CIN1 lesions. In fact, the difference in immunostaining between normal epithelium and CIN1 epithelium was even more remarkable than p16 immunoreactivity. In high-grade CIN lesions, p16 positivity was lower than expected. Although the p16 positivity in CIN2/3 lesions is well over 90% in several studies [11, 27], a few recent studies have shown a somewhat lower positivity rate of 60–75% in CIN2 and a positivity of 72–91% in CIN3 [10, 28, 29]. Differences in the HPV genotypes causing CIN could be one possible reason for the lower positivity rate although this aspect was not examined in our study. Therefore, in our setup, additional biomarkers of cervical dysplasia may be useful. The nuclear/nucleo-cytoplasmic staining of TG2 in high-grade dysplasia (CIN2/3), not observed in normal cervical epithelium or generally in CIN1 lesions, could represent one potential additional biomarker. As is evident from Table 2, the addition of TG2 immunostaining can supplement p16 immunostaining for identification of cervical precancerous lesions.

Thus, we conclude that tissue transglutaminase 2 is a unique enzyme and has diverse roles. Biologically, this molecule could represent the critical link between inflammation on the one hand and carcinogenesis on the other. It is hoped that a better understanding of this molecule can translate into a significant improvement in the management of cervical cancer and its precursor lesions.

Conflict of interest statement We declare that we have no conflict of interest.

References

1. Ferlay J, Bray F, Pisani P et al (2004) GLOBOCAN 2002 cancer incidence. Mortality and prevalence worldwide. IARC, Lyon IARC Press Cancer Base No. 5 version 2.0
2. Winer RL, Kiviat NB, Hughes JP et al (2005) Development and duration of human papillomavirus lesions, after initial infection. J Infect Dis 191:731–738
3. Castle PE, Ashfaq R, Ansari F et al (2005) Immunohistochemical evaluation of heat shock proteins in normal and preinvasive lesions of the cervix. Cancer Lett 229:245–252
4. Peng X, Zhang Y, Zhang H et al (1999) Interaction of tissue transglutaminase with nuclear transport protein importin-alpha3. FEBS Lett 446:35–39
5. Boehm JE, Singh U, Combs C et al (2002) Tissue transglutaminase protects against apoptosis by modifying the tumor suppressor protein p110. Rb J Biol Chem 277:20127–20130
6. Mangala LS, Fok JY, Zorrilla-Calancha IR et al (2006) Tissue transglutaminase expression promotes cell attachment, invasion and survival in breast cancer cells. Oncogene 26:2459–2470
7. Fok JY, Ekmekcioglu S, Mehta K (2006) Implications of tissue transglutaminase expression in malignant melanoma. Mol Cancer Ther 5:1493–1503
8. Yuan L, Siegel M, Choi K et al (2006) Transglutaminase 2 inhibitor, KCC009, disrupts fibronectin assembly in the extracellular matrix and sensitizes orthotopic glioblastomas to chemotherapy. Oncogene 26:2563–2573
9. Klaes R, Friedrich T, Spitkovsky D et al (2001) Overexpression of p16(INK4A) as a specific marker for dysplastic and neoplastic epithelial cells of the cervix uteri. Int J Cancer 92:276–284
10. Kang S, Kim J, Kim HB et al (2006) Methylation of p16INK4a is a non-rare event in cervical intraepithelial neoplasia. Diagn Mol Pathol 15:74–82
11. Kalof AN, Cooper K (2006) p16INK4a immunoexpression: surrogate marker of high-risk HPV and high-grade cervical intraepithelial neoplasia. Adv Anat Pathol 13:190–194
12. Ishikawa M, Fujii T, Saito M et al (2006) Overexpression of p16 INK4a as an indicator for human papillomavirus oncogenic activity in cervical squamous neoplasia. Int J Gynecol Cancer 16:347–353
13. Masumoto N, Fujii T, Ishikawa M et al (2003) P16 overexpression and human papillomavirus infection in small cell carcinoma of the uterine cervix. Hum Pathol 34:778–783
14. Jeon JH, Choi KH, Cho SY et al (2003) Transglutaminase 2 inhibits Rb binding of human papillomavirus E7 by incorporating polyamine. EMBO J 22:5273–5282
15. Shishodia S, Aggarwal BB (2002) Nuclear factor-kappaB activation: a question of life or death. J Biochem Mol Biol 35:28–40
16. Mann AP, Verma A, Sethi G et al (2006) Overexpression of tissue transglutaminase leads to constitutive activation of nuclear factor-{kappa}B in cancer cells: delineation of a novel pathway. Cancer Res 66:8788–8795
17. Spitkovsky D, Hehner SP, Hofmann TG et al (2002) The human papillomavirus oncoprotein E7 attenuates NF-kappa B activation by targeting the Ikappa B kinase complex. J Biol Chem 277:25576–25582
18. Fontaine V, van der Meijden E, de Graaf J et al (2000) A functional NF-kappaB binding site in the human papillomavirus type 16 long control region. Virology 272:40–49
19. Herman JF, Mangala LS, Mehta K (2006) Implications of increased tissue transglutaminase (TG2) expression in drug-resistant breast cancer (MCF-7) cells. Oncogene 25:3049–3058
20. Verma A, Wang H, Manavathi B et al (2006) Increased expression of tissue transglutaminase in pancreatic ductal adenocarcinoma and its implications in drug resistance and metastasis. Cancer Res 66:10525–10533
21. Mehta K, Fok JY, Mangala LS (2006) Tissue transglutaminase: from biological glue to cell survival cues. Front Biosci 11:173–185
22. Hettasch JM, Bandarenko N, Burchette JL et al (1996) Tissue transglutaminase expression in human breast cancer. Lab Invest 75:637–645
23. Zemskov EA, Janiak A, Hang J et al (2006) The role of tissue transglutaminase in cell–matrix interactions. Front Biosci 11:1057–1076
24. Akimov SS, Krylov D, Fleischman LF et al (2000) Tissue transglutaminase is an integrin-binding adhesion coreceptor for fibronectin. J Cell Biol 148:825–838
25. Akimov SS, Belkin AM (2001) Cell surface tissue transglutaminase is involved in adhesion and migration of monocytic cells on fibronectin. Blood 98:1567–1576
26. Dardik R, Inbal A (2006) Complex formation between tissue transglutaminase II (tTG) and vascular endothelial growth factor receptor 2 (VEGFR-2): proposed mechanism for modulation of endothelial cell response to VEGF. Exp Cell Res 312:2973–2982
27. Yildiz IZ, Usubutun A, Firat P et al (2007) Efficiency of immunohistochemical p16 expression and HPV typing in cervical squamous intraepithelial lesion grading and review of the p16 literature. Pathol Res Pract 203:445–449
28. Branca M, Ciotti M, Santini D et al (2004) p16(INK4A) expression is related to grade of cin and high-risk human papillomavirus but does not predict virus clearance after conization or disease outcome. Int J Gynecol Pathol 23:354–365
29. Agoff SN, Lin P, Morihara J et al (2003) p16(INK4a) expression correlates with degree of cervical neoplasia: a comparison with Ki-67 expression and detection of high-risk HPV types. Mod Pathol 16(7):665–673

Virchows Arch (2010) 456:53–63
DOI 10.1007/s00428-009-0861-4

ORIGINAL ARTICLE

Expression of resistin-like molecule beta in gastric cancer: its relationship with clinicopathological parameters and prognosis

Liduan Zheng · Mixia Weng · Jun He · Xiuping Yang · Guosong Jiang · Qiangsong Tong

Received: 12 October 2009 / Revised: 5 November 2009 / Accepted: 6 November 2009 / Published online: 5 December 2009
© Springer-Verlag 2009

Abstract Resistin-like molecule beta (RELMβ), an intestinal goblet cell-specific protein, is a biomarker of intestinal metaplasia in Barrett's esophagus and over-expressed in colon cancer. Since gastric adenocarcinomas can arise through a process of intestinalization, we hypothesized that RELMβ might be aberrantly expressed in gastric cancer. This study was undertaken to examine the RELMβ expression in gastric cancer and correlate it with clinical outcome. One hundred and thirty-six gastric cancer patients were evaluated for the RELMβ expression by immunohistochemistry. The RELMβ transcripts were measured by real-time quantitative PCR. In normal gastric mucosa, RELMβ expression was absent, whereas areas of intestinal metaplasia revealed RELMβ reactivity. Eighty-nine patients of gastric cancer (65.4%) were positive for RELMβ expression. In a subtotal of 20 patients, RELMβ transcripts were positively correlated with protein levels in gastric cancer tissues, but absent in normal gastric mucosa. The expression rate of RELMβ was higher in intestinal-type carcinomas than in diffuse-type carcinomas ($P<0.001$). RELMβ positivity in gastric cancer was positively correlated with tumor differentiation ($P=0.001$) and inversely correlated with tumor infiltration ($P=0.007$), lymph node metastasis ($P=0.035$), and heparanase expression ($P<0.001$), without correlation with age, gender, tumor location and size, tumor-node metastasis stages, and Ki-67 expression. Patients showing positive RELMβ expression had a significantly longer overall survival than those with negative expression ($P=0.001$). These results provide evidences that the RELMβ expression in gastric cancer is correlated with clinicopathological features and may be a useful prognostic factor for predicting the outcome of gastric cancer patients.

Keywords Resistin-like molecule beta · Gastric cancer · Gene expression

L. Zheng (✉) · M. Weng · J. He · X. Yang
Department of Pathology, Union Hospital of Tongji Medical College, Huazhong University of Science and Technology, Wuhan 430022, Hubei Province, China
e-mail: ld_zheng@hotmail.com

G. Jiang · Q. Tong
Department of Surgery, Union Hospital of Tongji Medical College, Huazhong University of Science and Technology, Wuhan 430022, Hubei Province, China

Introduction

Gastric cancer is the leading cause of cancer death in China and the third cause of cancer-related death in North America and Western Europe [1]. Biological parameters are being utilized for their diagnostic and prognostic values in the management of gastric cancer patients. A series of studies indicate that mucin 2 (MUC2) and intestinal trefoil factor (ITF), both goblet cell-derived proteins, aberrantly express and serve as prognostic biomarkers in gastric cancer [2–4]. Alterations of MUC2 are considered to be relevant to the abnormal behavior of cancer cells, such as altered cell adhesion or metastasis, and to the avoidance of immunological defense [5]. In addition, ITF expression has been found in many cancers, including colon cancer, breast cancer, lung cancer, and prostate cancer [6–9]. Antisense ITF suppresses growth and tumorigencity of gastric cancer cells in vitro through induction of apoptosis [10]. Furthermore, blocking the expression of ITF induces chemosensitivity to adriamycin in human gastric cancer cells [10]. These results suggest that goblet cell-specific proteins may participate in the genetic events of gastric cancer, which is potentially of great clinical importance.

Resistin-like molecule beta (RELMβ) is a recently described goblet cell-specific protein that belongs to the resistin-like molecules/found in inflammatory zone (RELM/FIZZ) gene family [11, 12]. RELMβ is produced by goblet cells specifically in the colon and is secreted apically into the colonic lumen where it exists intact, at high concentrations, as a homodimer in the stool of both mice and humans [13]. Indeed, although their sequences are unrelated, ITF and RELMβ exhibit some structural similarities. Both are relatively small proteins secreted by goblet cells that have multiple cysteine residues, one of which is critical for homodimer formation [14, 15]. It has been demonstrated that RELMβ functions as a critical immune-effector molecule in the expulsion of gastrointestinal tract nematodes by disrupting the ability of nematodes to optimally sense the gastrointestinal tract microenvironment [12]. Our previous studies indicate that RELMβ is over-expressed in a majority of human colon cancer, and there is an association between clinicopathological features of colon cancer and RELMβ expression [16]. In addition, we demonstrate that the goblet cell-specific protein RELMβ is expressed in the metaplastic epithelium of Barrett's esophagus (BE) and enhanced in dysplasia, which can be served as a potential biomarker for the correct diagnosis of BE [17]. These evidences suggest the role of RELMβ in cancer cell biology.

Since gastric adenocarcinomas can arise through a process of intestinalization [18], combined with the evidences that RELMβ is expressed in intestinal metaplasia [17], we hypothesized that RELMβ might be aberrantly expressed in human gastric cancer. In the current study, immunohistochemical staining was performed to examine the expression of RELMβ in gastric cancer patients and to correlate its expression with clinicopathological parameters, tumor invasion and metastasis, tumor proliferative capacity, and patients' survival. We demonstrated, for the first time, that RELMβ was absent in normal gastric mucosa and aberrantly expressed in a majority (65.4%) of gastric cancer, and the expression was limited to the cytoplasm of cancer cells and goblet cells of intestinal metaplasia. Our report on RELMβ expression in gastric cancer suggests that further investigation is warranted to explore the emerging role of this goblet-specific protein in human gastric cancer.

Methods and materials

Clinical material

Approval to conduct this study was obtained from the Institutional Review Board of Tongji Medical College. We retrospectively evaluated specimens of surgically resected primary gastric carcinoma from 136 patients at Union Hospital of Tongji Medical College between January 1999 and December 2001. This period was selected to provide a sufficient period of follow-up to determine patient prognosis. None of these patients underwent either chemotherapy or radiotherapy before surgery. Their pathological diagnosis and histological types were proven by at least two pathologists, according to the World Health Organization (WHO) and Laurén classification [19, 20]. Tumors that were histologically papillary were designated "well differentiated", whereas those that were signet ring cell and mucinous were considered "poorly differentiated" [21]. Adjacent gastric mucosa that contained no macroscopic tumor was also obtained, and the non-neoplastic areas were subsequently verified by microscopic histology to be free of tumor infiltration. Tumor staging was assessed using the tumor-node metastasis (TNM) system according to the International Union Against Cancer (UICC) [22]. For purposes of statistical analysis, stage I and II tumors were combined, as were stage III and IV tumors. Ninety of the gastric cancer patients were men (66.2%) and 46 were women (33.8%), with a mean age of 62.7 years (range, 42–83 years). Other patient characteristics were listed in Table 1. The patients were followed up for an interval of 24 to 80 months, with a mean of 53 months. All deaths were attributable to gastric cancer.

Immunohistochemistry

Harvested specimens were fixed in 10% formalin and embedded in paraffin, then slid into 4-μm-thick slides. Tissue sections were dewaxed in ethanol and rehydrated in a graded series of ethanol. Antigen retrieval was performed by boiling the sections in 10 mmol/L of sodium citrate solution (pH 6.0) for 5 min in a microwave. Then the sections were allowed to cool down for 20 min. After rinsing in phosphate-buffered saline (PBS), endogenous peroxidase activity was quenched with 1% (*v*/*v*) hydrogen peroxide in methanol. Nonspecific binding sites were blocked using 5% (*v*/*v*) normal goat serum. The sections were then incubated with affinity purified rabbit polyclonal antibodies for human RELMβ (Abcam Inc, Cambridge, MA, USA) and Ki-67 (Santa Cruz Biotechnology) and monoclonal antibody for human heparanase (HPA; InSight Company, Rehovot, Israel) at 1:200 dilutions overnight at 4°C. After washing with 1× PBS (0.01 M, pH 7.4), the slides were incubated with a horseradish peroxidase (DAKO, Glostrup, Denmark) and stained with 3,3′-diaminobenzidine (DAKO). Following counterstaining with hematoxylin and dehydration in ethanol and xylene, the slides were mounted. Negative controls included parallel sections treated with omission of the primary antibody, in addition to an adjacent section of the same block in which the primary antibody was

Table 1 Correlation between RELMβ expression and clinicopathologic factors

Clinicopathologic factor	Total	Positive RELMβ expression	
	n (%)	*n* (%)	*P* value
Age (years)			
≤60	35 (25.7)	22 (62.9)	0.709
>60	101 (74.3)	67 (66.3)	
Sex			
Male	90 (66.2)	58 (64.4)	0.732
Female	46 (33.8)	31 (67.4)	
Location			
Cardia	24 (17.6)	16 (66.7)	0.997
Corpus	42 (30.9)	27 (64.3)	
Antrum	55 (40.4)	36 (65.5)	
Whole	15 (11.1)	10 (66.7)	
Size (diameter)			
≤6 cm	98 (72.1)	65 (66.3)	0.727
>6 cm	38 (27.9)	24 (63.2)	
Laurén classification			
Intestinal type	83 (61.1)	65 (78.3)	<0.001
Diffuse type	53 (38.9)	24 (45.3)	
WHO classification			
Papillary	6 (2.2)	4 (66.7)	0.743
Tubular	115 (86.8)	77 (66.9)	
Signet ring cell	10 (9.6)	5 (50.0)	
Mucinous	5 (1.4)	3 (60.0)	
WHO grade			
Well differentiated	34 (25.0)	31 (91.2)	0.001
Moderately differentiated	47 (34.6)	30 (63.8)	
Poorly differentiated	55 (40.4)	28 (50.9)	
Gastric wall invasion			
T1/T2	40 (29.4)	33 (82.5)	0.007
T3/T4	96 (70.6)	56 (58.3)	
Lymph node metastasis			
Negative	48 (35.3)	37 (77.1)	0.035
Positive	88 (64.7)	52 (59.1)	
Distant metastasis			
Negative	121 (88.9)	82 (67.8)	0.105
Positive	15 (11.1)	7 (46.7)	
TNM stage			
I/II	54 (39.7)	33 (61.1)	0.389
III/IV	82 (60.3)	56 (68.3)	

Pearson's χ^2 test was done to determine the statistical significance of the relationship of RELMβ expression with various variables

replaced by rabbit polyclonal IgG or mouse monoclonal IgG (Abcam Inc) as an isotype control or PBS.

Staining results determinant

The reactivity degree of RELMβ, HPA, and Ki-67 in each tissue section was assessed by at least two pathologists without knowledge of clinicopathological features of the tumor or patient survival. The degree of positivity was initially classified according to the percentage of positive tumor cells as follows: (−) <5% cells positive, (1+) 6–25% cells positive, (2+) 26–50% cells positive, and (3+) >50% cells positive. Slices with moderate positive (2+) or strong positive (3+) reactivity were classified as having a "high expression," whereas slices with negative (−) or weak positive (1+) reactivity were classified as having a "low expression".

Real-time quantitative PCR

The tumor specimens and distant normal gastric mucous tissues (>5 cm from the margin of the tumor) of 20 gastric cancer patients were collected and stored at −80°C until use. Total RNA was isolated with RNeasy Mini Kit (Qiagen Inc., Valencia, CA, USA). The reverse transcription reactions were conducted with Transcriptor First Strand cDNA Synthesis Kit (Roche, Indianapolis, IN, USA). The PCR primers were designed by Premier Primer 5.0 software as the follows: for human RELMβ 5′-ATGGGGCCGTCCTCTTGCCTCC-3′ and 5′-TCAGGTCAGGTGGCAGCAGCG-3′ amplifying a 336-bp fragment and for human α-tubulin 5′-CTCATCA CAGGCAAGGAAGAT-3′ and 5′-TTAAGGTAAGTG TAGGTTGGG-3′ amplifying a 410-bp fragment. Real-time PCR with SYBR Green PCR Master Mix (Applied Biosystems, Foster City, CA, USA) was performed using ABI Prism 7700 Sequence Detector (Applied Biosystems). The fluorescent signals were collected during extension phase, Ct values of the sample were calculated, and RELMβ transcript levels were analyzed by $2^{-\Delta\Delta Ct}$ method.

Statistics analysis

The SPSS 12.0 statistical software was applied for statistical analysis. The χ^2 analysis and Fisher exact probability analysis were applied for comparison among expression of RELMβ, HPA and Ki-67, and individual clinicopathological features. Pearson's coefficient correlation was applied to analyze the relationship between RELMβ protein and transcripts. The Kaplan–Meier method was used to estimate survival rates, and the log-rank test was used to assess survival differences

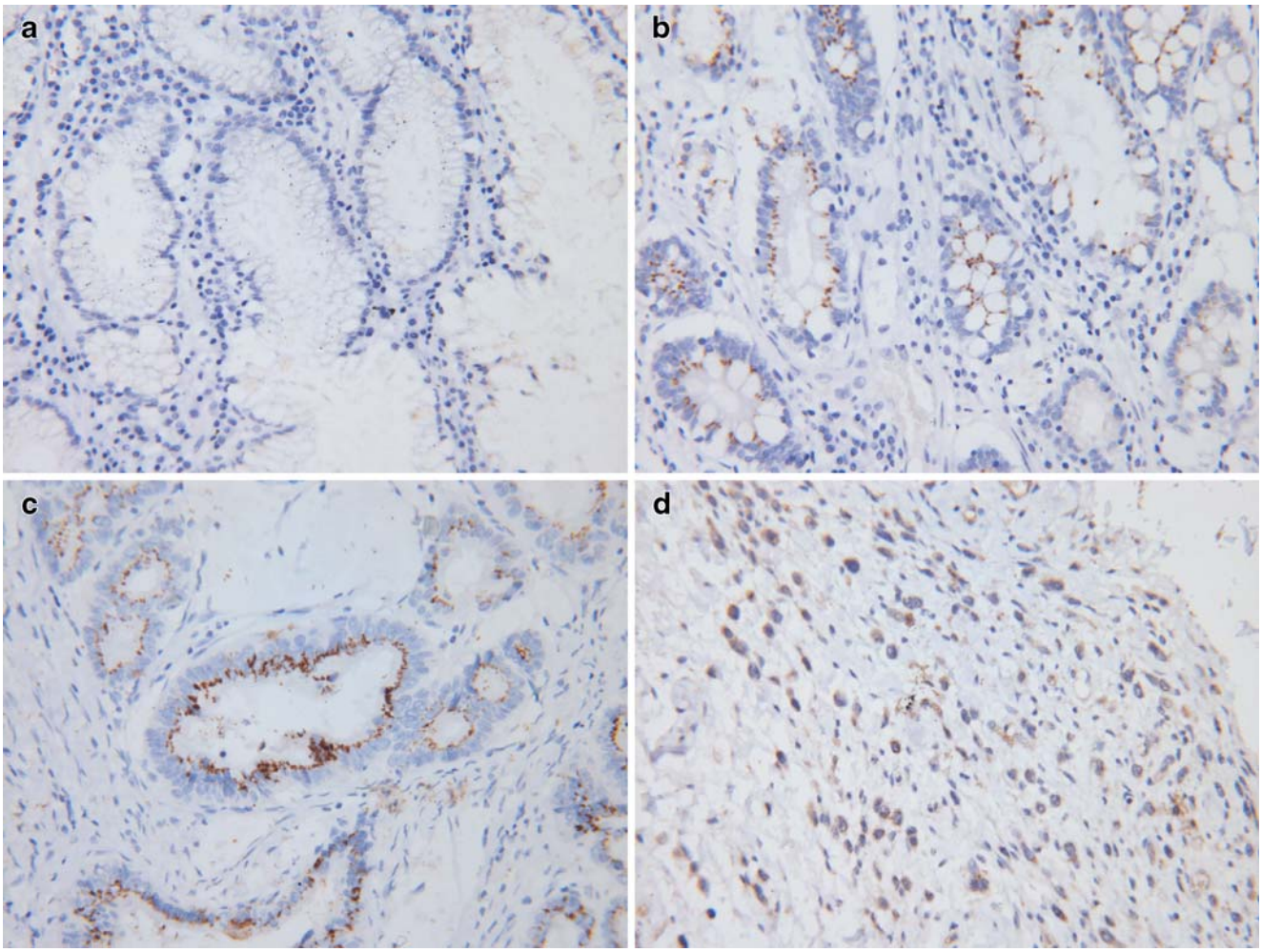

Fig. 1 Expression patterns of RELMβ in normal gastric mucosa and gastric cancer tissues. Sections of normal (non-neoplastic) gastric mucosa and gastric cancer tissue specimens were processed for immunostaining of RELMβ expression. **a** No RELMβ immunoreactivity was detected in the normal gastric mucosa. **b** Diffusely distributed RELMβ expression was noted in the goblet cells of intestinal metaplasia. **c** In intestinal-type carcinoma, RELMβ expression was distributed as coarse granules at the luminal border of gland-like tubular structures in the tumor. **d** In diffuse-type carcinoma, RELMβ was expressed diffusely as fine granules in the cytoplasm or occasionally on one side of the cytoplasm of tumor cells. Original magnification, ×400

between groups. The Cox proportional hazards model was applied for multivariate survival analysis. In all of the tests, a two-sided $P<0.05$ was defined as statistically significant.

Results

RELMβ expression in non-neoplastic gastric mucosa

As shown in Fig. 1a, normal gastric mucosa without intestinal metaplasia showed no RELMβ reactivity. In gastric mucosa adjacent to malignant tumor, no RELMβ expression was observed either. Of 136 specimens, 81 (59.6%) contained areas of intestinal metaplasia. In all glands exhibiting intestinal metaplasia, diffusely distributed RELMβ immunoreactivity was detected in the cytoplasm of goblet cells (Fig. 1b). The specificity of staining is supported by negligible background staining in the stromal elements and also through the employment of negative controls (incubation with rabbit polyclonal IgG or mouse monoclonal IgG as an isotype control or PBS; data not shown).

RELMβ expression in gastric cancer

Two patterns of RELMβ expression were noted in gastric cancer. In intestinal-type carcinoma, RELMβ expression was distributed as coarse granules at the luminal border of gland-like tubular structures in the tumor (Fig. 1c). In diffuse-type carcinoma, RELMβ was expressed diffusely as fine granules in the cytoplasm or occasionally on one side of the cytoplasm of tumor cells (Fig. 1d). Positive RELMβ expression was found in 89 of 136 cases (65.4%) of gastric cancer examined, including papillary/tubular carcinoma, mucinous carcinoma, and signet ring cell carcinoma (Fig. 2), while it was negative in the remaining 47 cases (34.6%; Table 1). However, no significant difference was found in the expression rates of RELMβ among the different types of gastric carcinomas (χ^2 test, $P=0.743$;

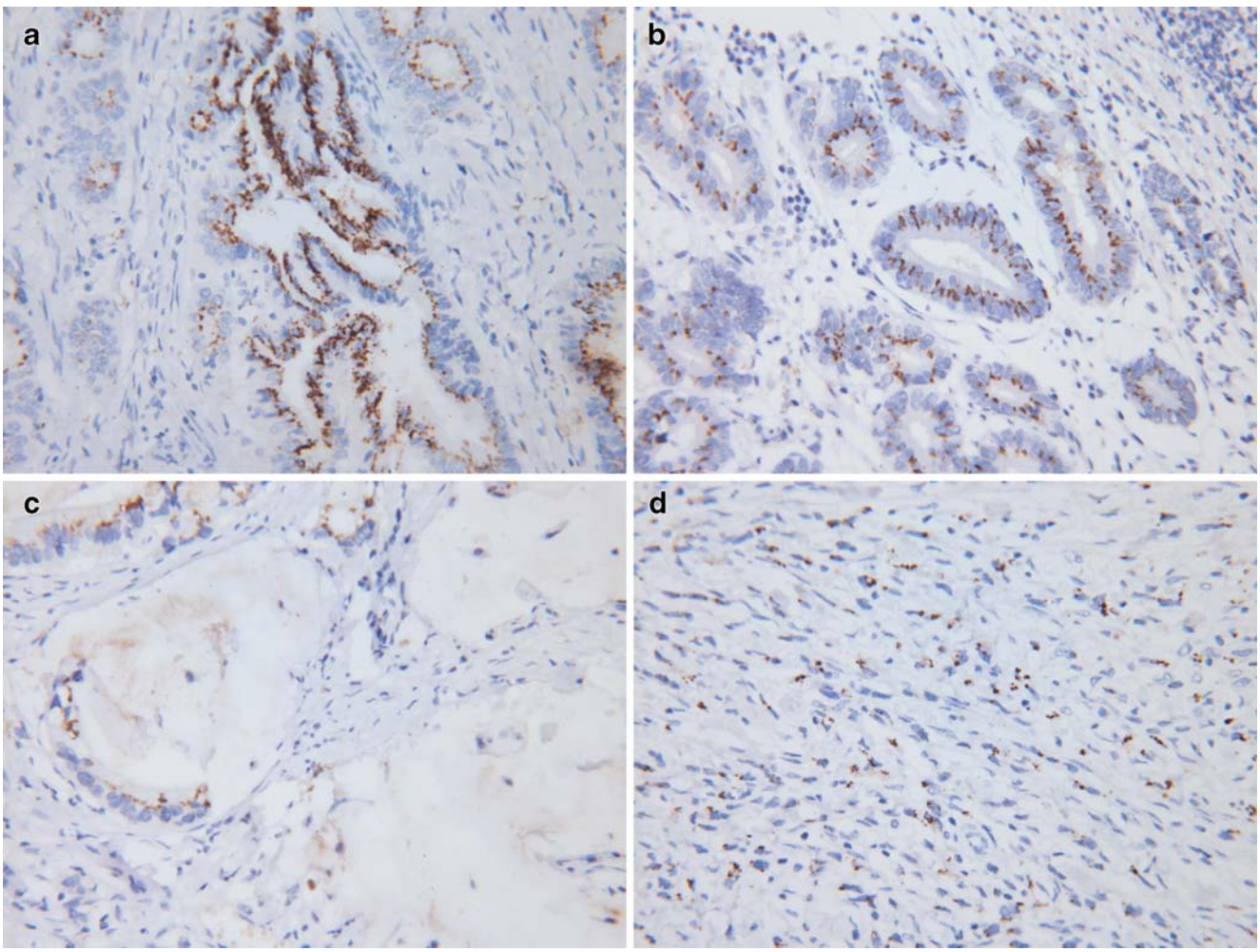

Fig. 2 Expression patterns of RELMβ in different tumor types of gastric cancer. Positive RELMβ expression was found in all types of gastric cancer examined, including papillary carcinoma (**a**), tubular carcinoma (**b**), mucinous carcinoma (**c**), and signet ring cell carcinoma (**d**). Original magnification, ×400

Table 1). The intensity of RELMβ immunostaining in positive gastric cancer cases was mild in 21 of 89 (23.6%), moderate in 32 of 89 (36.0%), and intense in 36 of 89 (40.4%) cases. In subtotal 20 patients, RELMβ transcripts were detected in gastric cancer tissues (Fig. 3a), but absent in normal gastric mucosa free of tumor infiltration as verified by microscopic histology. In addition, in gastric cancer tissues examined, the RELMβ transcripts were positively correlated with protein levels ($P<0.001$; Fig. 3b).

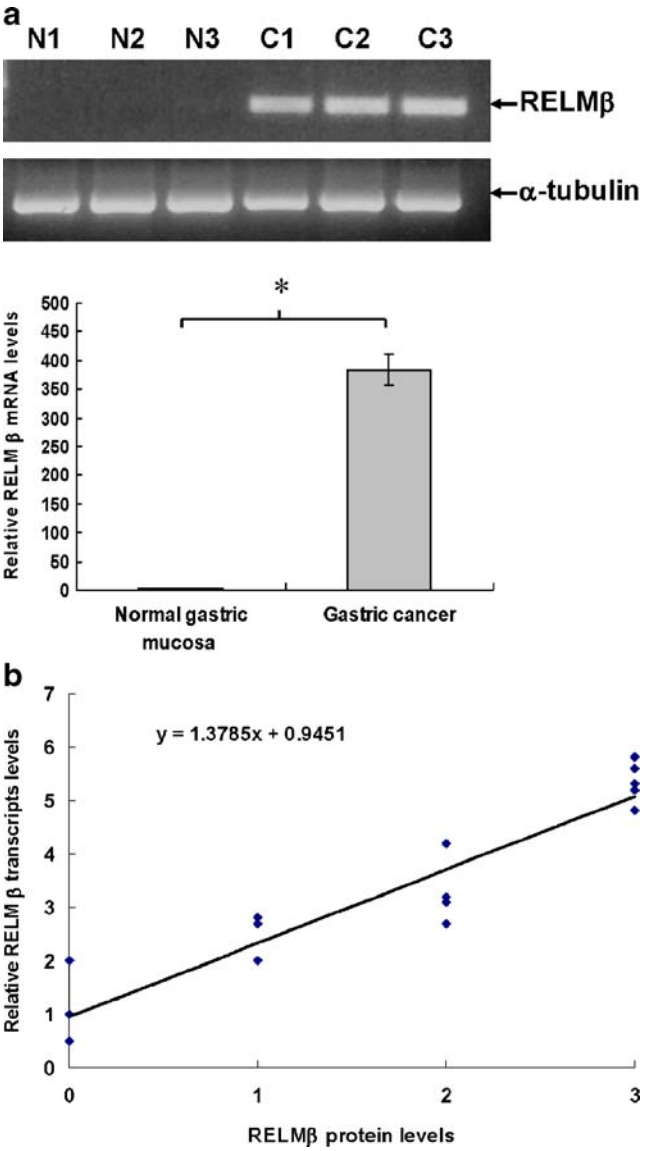

Fig. 3 RELMβ transcripts in normal gastric mucosa and gastric cancer tissues. In a subtotal of 20 patients, tumor specimens and adjacent gastric mucosa that contained no macroscopic tumor were obtained, and the non-neoplastic areas were subsequently verified by microscopic histology to be free of tumor infiltration. Real-time quantitative PCR was performed to measure the RELMβ transcripts. **a** RELMβ transcripts were detected in gastric cancer tissues, but absent in normal gastric mucosa free of tumor infiltration. *C* gastric cancer tissues, *N* normal gastric mucosa. **b** In gastric cancer tissues examined, the RELMβ transcripts were positively correlated with RELMβ protein levels detected by immunohistochemistry. The different RELMβ staining grades (negative, weak, moderate, and strong) were indicated as *0*, *1*, *2*, and *3*, respectively. There was a significant difference between normal gastric mucosa and gastric cancer (*$P<0.05$). Triplicate experiments were performed with essentially identical results

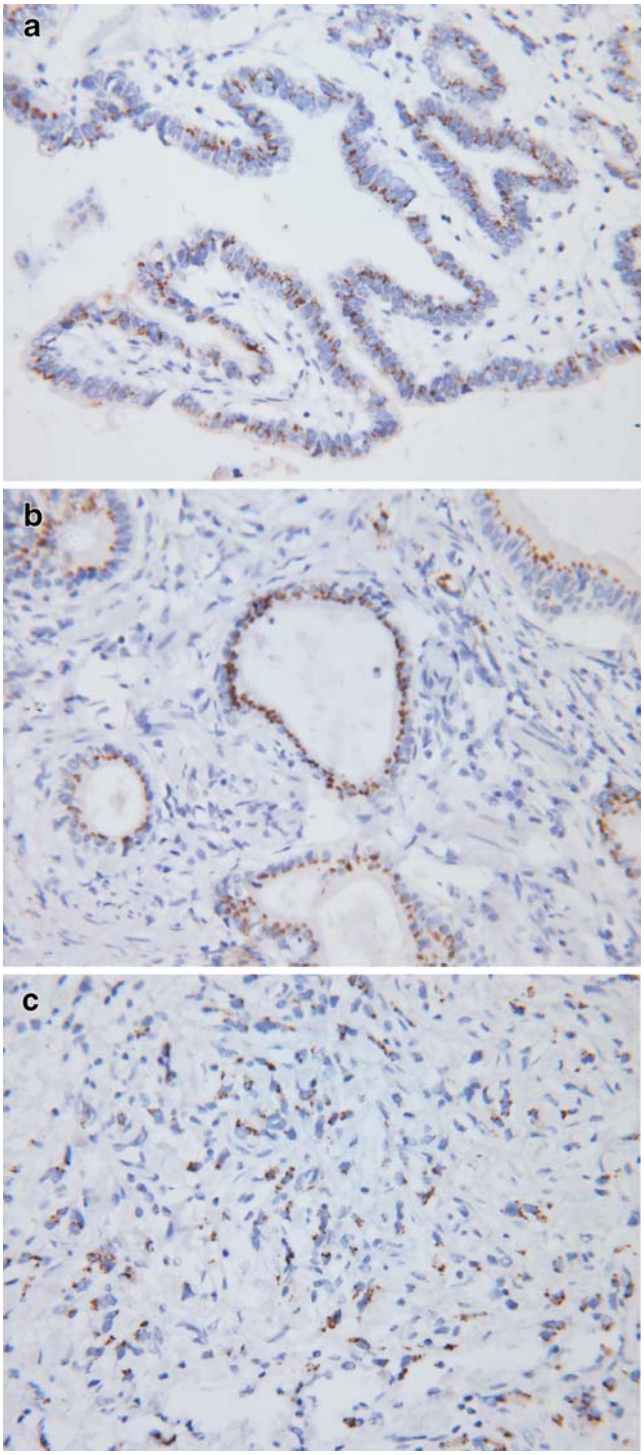

Fig. 4 Expression of RELMβ in gastric cancer of different differentiation. In the gastric cancer cases examined, higher RELMβ expression of statistical difference was found concerning histological grade: well (**a**) and moderately differentiated (**b**) versus poorly differentiated (**c**) carcinomas. Original magnification, ×400

RELMβ expression in relation to clinicopathological features

The relationship between RELMβ expression and clinicopathological features was summarized in Table 1. The RELMβ expression was not affected by demographic factors, such as age and gender (χ^2 test, P=0.709, P=0.732; Table 1) or by tumor location and size (χ^2 test, P=0.997, P=0.727; Table 1), distant metastasis (χ^2 test, P=0.105; Table 1), and clinical stage (χ^2 test, P=0.389; Table 1). Of note, in the gastric cancer cases examined, the expression rate of RELMβ was higher in intestinal-type carcinomas than in diffuse-type

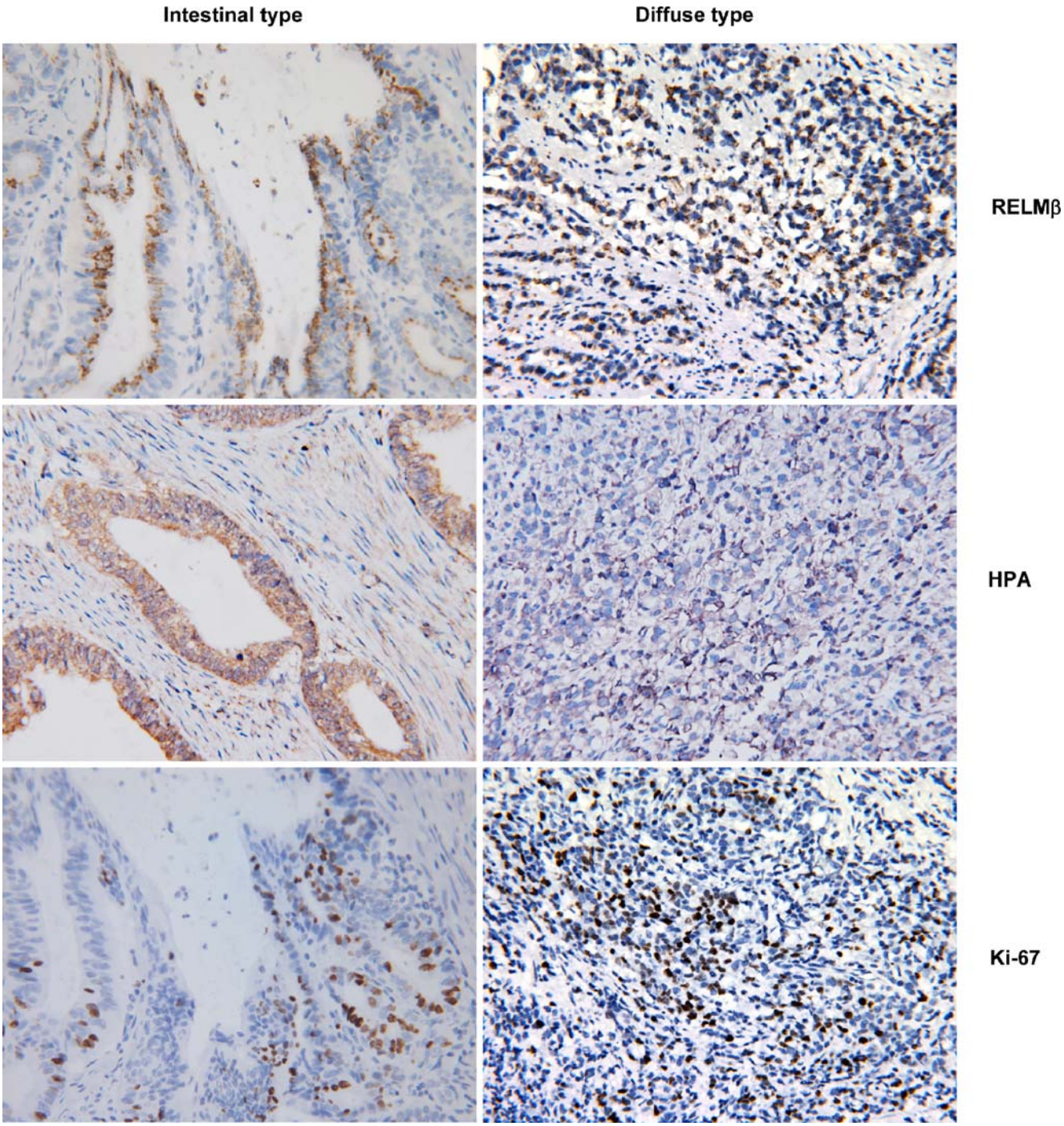

Fig. 5 Expression of RELMβ, HPA, and Ki-67 in gastric cancer tissues. Gastric cancer tissue specimens were processed for immunostaining of RELMβ, HPA, and Ki-67. The cytoplasmic expression of RELMβ and HPA was detected in both intestinal- and diffuse-type carcinomas. Nuclear immunostaining of Ki-67 was also observed in different histological types (intestinal and diffuse) of gastric carcinoma. Original magnification, ×400

carcinomas (χ^2 test, $P<0.001$; Table 1). RELMβ positivity in gastric cancer was positively correlated with tumor differentiation (χ^2 test, $P=0.001$; Fig. 4 and Table 1) and inversely correlated with tumor infiltration (χ^2 test, $P=0.007$; Table 1) and lymph node metastasis (χ^2 test, $P=0.035$; Table 1).

RELMβ expression in relation to metastatic and proliferative index

Since the above results indicate that RELMβ expression correlated with the tumor invasion and metastasis, we further investigated the relationship between expression of RELMβ and HPA, one of the key enzymes involved in the invasion and metastasis of malignant tumors [23], in human gastric cancers by immunohistochemical staining. A cytoplasmic HPA expression was demonstrated in the advanced stage gastric carcinoma. In accordance with the depth of invasion, the carcinomas beyond the proper muscle demonstrated more frequent HPA expression than carcinomas limited within the proper muscle (data not shown). However, the HPA expression was negatively correlated with RELMβ expression in the gastric cancer cases examined (χ^2 test, $P<0.001$, Fig. 5 and Table 2). Since previous studies reported that RELMβ expression was abundant in proliferative epithelia and dramatically extinguished in the nonproliferating differentiated epithelia [11], we further observed the correlation between RELMβ expression and proliferative index in gastric cancer. However, we found that the expression of Ki-67, a proliferative index, was not statistically correlated with RELMβ expression ($P=0.628$; Fig. 5 and Table 2).

RELMβ expression in relation to patient survival

The median postoperative survival time (44.1 months) of RELMβ-positive patients was significantly longer than that (26.4 months) of RELMβ-negative patients ($P=0.001$; Fig. 6 and Table 3). RELMβ expression was associated with increased survival durations ($P=0.001$; Table 3). Additionally, all other factors, except patient age and tumor size, significantly influenced patient survival in univariate analyses (Table 3), including lymph node metastasis ($P<0.001$), differentiation ($P<0.001$), and TNM stage ($P<0.001$). In addition, multivariate analysis using the Cox proportional hazards model showed that lymph node metastasis ($P=0.033$), differentiation ($P=0.012$), TNM stage ($P=0.001$), and RELMβ expression ($P=0.023$) were independent prognostic factors of gastric carcinoma (Table 3).

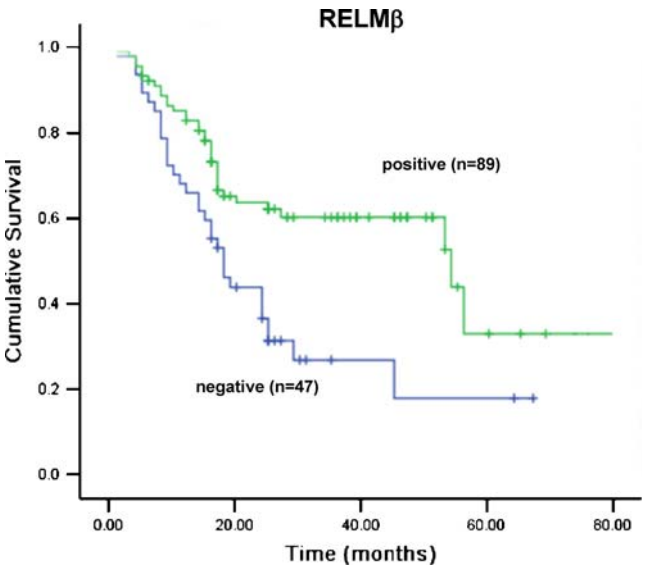

Fig. 6 Kaplan–Meier curves of survival durations in patients with gastric cancer according to the RELMβ expression. Survival durations were significantly longer in patients with positive expression of RELMβ (median survival, 44.1 months) than in those with negative expression of RELMβ (median survival, 26.4 months; $P=0.001$)

Table 2 Correlations among the expressions of RELMβ, HPA, and Ki-67

	HPA			Ki-67		
	Low	High	*P* value	Low	High	*P* value
RELMβ						
Low	22	47	<0.001	21	48	0.628
High	48	19		23	44	
HPA						
Low				23	47	0.897
High				21	45	

Pearson's χ^2 test was done to determine the statistical significance of the relationship among various variables

Discussion

In recent years, Steppan et al. described an intestinal goblet cell-specific protein, RELMβ, a member of the RELM/FIZZ gene family, which is characterized by a signature carboxyl terminus sequence containing 10 completely conserved cysteine residues with invariant spacing [11]. Although most studies of RELMβ have focused on its function in intestinal defense against parasitic nematode infections of the intestine and colonic inflammation [24–28], a role of RELMβ in tumor biology is receiving increasing attention. First, RELMβ mRNA was markedly increased in tumors of the *min* mice, which harbor a mutation of the APC gene and thus develop intestinal tumors similar to humans with familial adenomatous polyposis [11]. Second, RELMβ expression was enhanced in a majority of human colon cancer tissues and correlated

Table 3 Univariate and multivariate analysis of prognostic factors in gastric cancer patients

Variables	*n*	Univariate analysis			Multivariate analysis		
		Median survival (months)	95% CI	*P*	RR	95% CI	*P*
Age (years)							
≤60	35	28.5	21.3–35.5	0.055	0.787	0.453–1.562	0.243
>60	100	41.7	33.7–49.9				
Tumor size (diameter)							
≤6 cm	98	38.4	30.1–46.9	0.630	1.128	0.687–2.561	0.395
<6 cm	38	36.8	28.6–44.8				
Lymph node							
N_0	48	70.3	60.3–80.5	<0.001	3.565	2.835–4.293	0.033
N_1	41	26.6	18.3–34.7				
N_2	32	14.2	10.7–17.9				
N_3	15						
WHO grade							
Well differentiated	34	56.8	45.3–68.1	<0.001	3.224	2.012–5.432	0.012
Moderately differentiated	47	46.4	39.2–53.4				
Poorly differentiated	55	20.7	14.5–27.3				
TNM stage							
I/II	54	58.2	36.5–79.7	<0.001	2.543	1.435–4.252	0.001
III/IV	82	25.3	18.3–31.9				
RELMβ expression							
Negative	47	26.4	18.5–34.1	0.001	0.251	0.149–0.421	0.023
Positive	89	44.1	37.5–50.9				

Log-rank test and Cox proportional hazards model were applied for univariate and multivariate analysis

n number of patients, *RR* relative risk, 95% CI 95% confidence interval

with clinicopathological features [16]. Third, RELMβ expression was detected in the metaplastic epithelium of Barrett's esophagus (BE) and enhanced in dysplasia, a premalignant lesion of esophagus cancer [17]. It is not known whether other types of epithelial cancers can also express RELMβ. Furthermore, no study has yet examined large enough numbers of specimens to permit meaningful correlations between RELMβ expression and clinicopathological features of gastric cancer.

The present study was conducted to investigate the frequency and clinicopathological relationships of RELMβ in well-characterized primary gastric adenocarcinomas. We demonstrated, for the first time, that RELMβ was aberrantly expressed in gastric cancer tissues, and the expression was limited to the cytoplasm of cancer cells and goblet cells of intestinal metaplasia. Human gastric carcinomas have been classified into the intestinal and diffuse types according to the Laurén classification [20, 29]. It has generally been concluded that intestinal-type (differentiated type) carcinomas arise from areas of intestinal metaplasia, whereas diffuse type (undifferentiated type) lesions originate from normal gastric mucosa [29]. However, contrary to this hypothesis, histological and cytochemical markers of intestinal epithelia have been detected in gastric cancers of both intestinal and diffuse types [30, 31]. On the other hand, a high incidence of intestinal-type gastric cancers show gastric phenotypic markers, with a phenotypic shift from gastric to intestinal-type expression in tumors manifesting greater depth of invasion [32, 33]. Thus, the exact original of different types of gastric carcinoma still remains largely unknown. Because RELMβ is strongly expressed by goblet cells in normal small and large intestine [11], it seemed like a useful marker to shed more light on the issue of gastric cancer histogenesis. However, in our study, RELMβ expression was not only restricted to the intestinal type but also detected in the diffuse-type gastric carcinoma, which was consistent with previous reports that intestinal-type properties were not only specifically associated with intestinal-type carcinomas but also detected in diffuse-type carcinomas [30, 31]. The present study would therefore support the notion that dedifferentiation of intestinal to diffuse carcinoma may be another histogenic pathway according to the histological heterogeneity of tumor cells, which was demonstrated in the carcinomas containing moderately and poorly differentiated components with similar morphological appearance and diffuse distribution [34].

By analyzing the relationship between RELMβ expression and clinicopathological features of gastric cancer, we demonstrated that RELMβ expression was positively correlated with the degree of differentiation of gastric adenocarcinoma. In addition, we found that RELMβ expression was negatively associated with tumor infiltration and lymph node metastasis. Although the RELMβ expression was lower in specimens with distant metastasis, no statistical significance was found due to limited cases. Furthermore, the RELMβ expression was unrelated to tumor location and size. So far, the relationship between RELMβ expression and cell proliferation remains controversial. In previous studies, in situ hybridization indicated the restriction of RELMβ mRNA in proliferative epithelia at the bases of crypts, but not in the nonproliferating differentiated epithelia of colonic mucosa [11]. However, immunohistochemical analysis demonstrated that RELMβ protein expression was well represented in nature (likely end stage) goblet cells [12]. We believe that these differences may be due to the varied methods for gene expression analysis. In this study, our evidences showed the lack of correlation between RELMβ expression and Ki-67 proliferative index in gastric cancer, which was consistent with our similar findings in colon cancer [16]. Importantly, RELMβ expression in gastric cancer was associated with a better survival regardless of tumor stage. These results demonstrate an association between clinicopathological features of gastric cancer and RELMβ expression. We believe that RELMβ may be a useful prognostic factor for predicting the outcome of gastric cancer patients. However, further investigation is still needed to explore the exact function of RELMβ in gastric carcinogenesis.

HPA, an endo-h-D-glucuronidase, is one of the key enzymes involved in the invasion and metastasis of malignant tumors [23]. Under normal physiological conditions, HPA expression is detectable in endothelial cells, smooth muscle cells, cytotrophoblasts, keratinocytes, platelets platelets, neutrophils, and activated T lymphocytes [23]. However, HPA expression is up-regulated in many tumor cells including esophageal carcinoma, pancreatic carcinoma, melanoma, bladder cancer, and prostate cancer [35–39]. In gastric cancer, the frequency of HPA expression was significantly correlated with histopathological parameters reflecting invasive and metastatic potentials and prognosis [40, 41]. Therefore, we want to investigate the relationship between expression of RELMβ and HPA in human gastric cancers. We found that in gastric cancer tissues, RELMβ expression is negatively correlated with that of HPA. Integrating our recent studies that transfection of RELMβ gene attenuated the migration and invasion of cultured gastric cancer cells in vitro (data not shown), we speculate that RELMβ may participate in the invasion and metastasis of gastric cancer, which warrants our further investigation.

In summary, we demonstrate, for the first time, that the goblet cell-specific protein RELMβ was absent in normal gastric mucosa and aberrantly expressed in a majority of human gastric cancer tissues, and RELMβ expression in gastric cancer was associated with clinicopathological parameters and prognosis. In addition, our preliminary data indicated the similar expression patterns of RELMβ and MUC2 in gastric carcinoma (data not shown), suggesting a close relationship between RELMβ and other intestinal markers, which warrants our further investigation. Moreover, further in vitro and in vivo experiments are warranted to elucidate the underlying mechanism for the induction of RELMβ in gastric cancer and the viability of RELMβ as a therapeutic target of gastric cancer.

Acknowledgment This work was supported by the National Natural Science Foundation of China (no. 30200284, no. 30600278, and no. 30772359), Program for New Century Excellent Talents in University of China (NCET-06-0641), and Scientific Research Foundation for the Returned Overseas Chinese Scholars, State Education Ministry (2008889).

Conflict of interest statement We declare that we have no conflict of interest.

References

1. Parkin DM, Bray F, Ferlay J et al (2005) Global cancer statistics, 2002. CA Cancer J Clin 55:74–108
2. Mitsuuchi M, Hinoda Y, Itoh F et al (1999) Expression of MUC2 gene in gastric regenerative, metaplastic, and neoplastic epithelia. J Clin Lab Anal 13:259–265
3. Lee HW, Yang DH, Kim HK et al (2007) Expression of MUC2 in gastric carcinomas and background mucosae. J Gastroenterol Hepatol 22:1336–1343
4. Yamachika T, Werther JL, Bodian C et al (2002) Intestinal trefoil factor: a marker of poor prognosis in gastric carcinoma. Clin Cancer Res 8:1092–1099
5. Aksoy N, Akinci OF (2004) Mucin macromolecules in normal, adenomatous, and carcinomatous colon: evidence for the neotransformation. Macromol Biosci 4:483–496
6. Babyatsky M, Lin J, Yio X et al (2009) Trefoil factor-3 expression in human colon cancer liver metastasis. Clin Exp Metastasis 26:143–151
7. May FE, Westley BR (1997) Expression of human intestinal trefoil factor in malignant cells and its regulation by oestrogen in breast cancer cells. J Pathol 182:404–413
8. May FE, Westley BR (1997) Trefoil proteins: their role in normal and malignant cells. J Pathol 183:4–7
9. Garraway IP, Seligson D, Said J et al (2004) Trefoil factor 3 is overexpressed in human prostate cancer. Prostate 61:209–214
10. Chan MW, Chan VY, Leung WK et al (2005) Anti-sense trefoil factor family-3 (intestinal trefoil factor) inhibits cell growth and induces chemosensitivity to adriamycin in human gastric cancer cells. Life Sci 76:2581–2592
11. Steppan CM, Brown EJ, Wright CM et al (2001) A family of tissue-specific resistin-like molecules. PNAS 98:502–506
12. Artis D, Wang ML, Keilbaugh SA et al (2004) RELM{beta}/FIZZ2 is a goblet cell-specific immune-effector molecule in the gastrointestinal tract. PNAS 101:13596–13600

13. He W, Wang ML, Jiang HQ et al (2003) Bacterial colonization leads to the colonic secretion of RELMbeta/FIZZ2, a novel goblet cell-specific protein. Gastroenterology 125:1388–1397
14. Banerjee RR, Lazar MA (2001) Dimerization of resistin and resistin-like molecules is determined by a single cysteine. J Biol Chem 276:25970–25973
15. Kinoshita K, Taupin DR, Itoh H et al (2000) Distinct pathways of cell migration and antiapoptotic response to epithelial injury: structure-function analysis of human intestinal trefoil factor. Mol Cell Biol 20:4680–4690
16. Zheng LD, Tong QS, Weng MX et al (2009) Enhanced expression of resistin-like molecule beta in human colon cancer and its clinical significance. Dig Dis Sci 54:274–281
17. Zheng L, Tong Q, Weng M et al (2010) Expression of resistin-like molecule beta in Barrett's esophagus: a novel biomarker for metaplastic epithelium. Dig Dis Sci 55. doi:10.1007/s10620-009-0719-2
18. Cassaro M, Rugge M, Gutierrez O et al (2000) Topographic patterns of intestinal metaplasia and gastric cancer. Am J Gastroenterol 95:1431–1438
19. Fenoglio-Preiser C, Correa P, Guilford P et al (2000) WHO histological classification of gastric tumours. In: Hamilton SR AL, Hamilton SRAL (eds) World health organization classification of tumors. Pathology and genetics of tumors of the digestive system. IARC, Lyon, p 38
20. Lauren P (1965) The two histological main types of gastric carcinoma: diffuse and so-called intestinal-type carcinoma. an attempt at a histo-clinical classification. Acta Pathol Microbiol Scand 64:31–49
21. Fenoglio-Preiser CM, Noffsinger AE, Stemmermann GN et al (2008) The neoplastic stomach. Gastrointestinal pathology: an atlas and text. Lippincott Williams & Wilkins, Philadelphia, pp 254–255
22. Sobin LH, Wittekind CH (1997) TNM classification of malignant tumors, ed 5. Wiley-Liss, New York, pp 59–62
23. Nakajima M, Irimura T, Di Ferrante N et al (1984) Metastatic melanoma cell heparanase. Characterization of heparan sulfate degradation fragments produced by B16 melanoma endoglucuronidase. J Biol Chem 259:2283–2290
24. Munitz A, Seidu L, Cole ET et al (2009) Resistin-like molecule alpha decreases glucose tolerance during intestinal inflammation. J Immunol 182:2357–2363
25. Nair MG, Guild KJ, Du Y et al (2008) Goblet cell-derived resistin-like molecule beta augments CD4+ T cell production of IFN-gamma and infection-induced intestinal inflammation. J Immunol 181:4709–4715
26. Krimi RB, Kotelevets L, Dubuquoy L et al (2009) Resistin-like molecule beta regulates intestinal mucous secretion and curtails TNBS-induced colitis in mice. Inflamm Bowel Dis 14:931–941
27. Barnes SL, Vidrich A, Wang ML et al (2007) Resistin-like molecule beta (RELMbeta/FIZZ2) is highly expressed in the ileum of SAMP1/YitFc mice and is associated with initiation of ileitis. J Immunol 179:7012–7020
28. Hogan SP, Seidu L, Blanchard C et al (2006) Resistin-like molecule beta regulates innate colonic function: barrier integrity and inflammation susceptibility. J Allergy Clin Immunol 118:257–268
29. Ribeiro MM, Sarmento JA, Sobrinho Simoes MA et al (1981) Prognostic significance of Lauren and Ming classifications and other pathologic parameters in gastric carcinoma. Cancer 47:780–784
30. Furihata C, Tatematsu M, Miki K et al (1984) Gastric- and intestinal-type properties of human gastric cancers transplanted into nude mice. Cancer Res 44:727–733
31. Fiocca R, Villani L, Tenti P et al (1988) Widespread expression of intestinal markers in gastric carcinoma: a light and electron microscopic study using BD-5 monoclonal antibody. J Clin Pathol 41:178–187
32. Yoshikawa A, Ki I, Yamachika T et al (1998) Phenotypic shift in human differentiated gastric cancers from gastric to intestinal epithelial cell type during disease progression. Gastric Cancer 1:134–141
33. Yamachika T, Inada K, Fujimitsu Y et al (1997) Intestinalization of gastric signet ring cell carcinomas with progression. Virchows Arch 431:103–110
34. Zheng HC, Li XH, Hara T et al (2008) Mixed-type gastric carcinomas exhibit more aggressive features and indicate the histogenesis of carcinomas. Virchows Arch 452:525–534
35. Ikeguchi M, Fukuda K, Yamaguchi K et al (2003) Quantitative analysis of heparanase gene expression in esophageal squamous cell carcinoma. Ann Surg Oncol 10:297–304
36. Kim AW, Xu X, Hollinger EF et al (2003) Human heparanase-1 gene expression in pancreatic adenocarcinoma. J Gastrointest Surg 6:167–172
37. Rivera RS, Nagatsuka H, Siar CH et al (2008) Heparanase and vascular endothelial growth factor expression in the progression of oral mucosal melanoma. Oncol Rep 19:657–661
38. Gohji K, Okamoto M, Kitazawa S et al (2001) Heparanase protein and gene expression in bladder cancer. J Urol 166:1286–1290
39. Stadlmann S, Moser PL, Pollheimer J et al (2003) Heparanase-1 gene expression in normal, hyperplastic and neoplastic prostatic tissue. Eur J Cancer 39:2229–2233
40. Wang Z, Xu H, Jiang L et al (2004) Positive association of heparanase expression with tumor invasion and lymphatic metastasis in gastric carcinoma. Mod Pathol 18:205–211
41. Takaoka M, Naomoto Y, Ohkawa T et al (2003) Heparanase expression correlates with invasion and poor prognosis in gastric cancers. Lab Invest 83:613–622

Virchows Arch (2010) 456:65–70
DOI 10.1007/s00428-009-0864-1

ORIGINAL ARTICLE

Primary choriocarcinoma of the liver: a clinicopathological study of five cases in males

Huaiyin Shi · Dengfeng Cao · Lixin Wei · Lu Sun · Aitao Guo

Received: 8 October 2009 / Revised: 13 November 2009 / Accepted: 14 November 2009 / Published online: 16 December 2009
© Springer-Verlag 2009

Abstract Primary choriocarcinomas of the liver are rare. Previous reported cases were mostly in infants with only rare adult cases. Here, we presented five adult cases. The patients were all males, with an average age of 41.6 years (from 36 to 48 years). Clinical presentations included right upper abdominal pain or abdominal distension. All patients presented with a large hepatic mass on ultrasonography that measured 11 cm on average in the greatest diameter. Elevated serum human chorionic gonadotropin (HCG) levels were noted in all cases. At presentation, the tumor was confined to the liver in two patients and therefore surgically resected. The other three patients presented with extrahepatic metastases on imaging study and therefore only received chemotherapy. All five patients died from the tumor within 2 to 8 months. Autopsy was performed for all five cases. The autopsy confirmed that the choriocarcinoma was confined to the liver in two surgically resected cases. The other three patients had metastatic choriocarcinoma in the lung (two patients), peritoneum (one patient), adrenal glands (one patient), and brain (one patient). None of the patients had any evidence of a testicular tumor or scar after examination of the entirely submitted testes. No tumor was observed in central nervous system, mediastinum, or other organs other than described above. Grossly, the primary tumors were large, soft, hemorrhagic, and with foci of necrosis. Histologically, the tumors were composed of mononucleated trophoblastic cells with round nuclei, clear cytoplasm, and prominent nucleoli admixed with large, multinucleated syncytiotrophoblastic cells. Immunohistochemically, tumor cells were strongly positive for keratin, HCG, and focally positive for human placental lactogen. Ki-67 proliferation index was high (mean 75%) in the mononucleated trophoblastic cells. Our series is the largest one to document primary hepatic choriocarcinoma in adults. Although these tumors are rare, they behave in a very aggressive fashion.

Keywords Choriocarcinoma · Extragonadal germ cell tumors · Liver

H. Shi (✉) · L. Wei · L. Sun · A. Guo
Department of Pathology, The Chinese PLA General Hospital,
Fuxing Road 28#,
Beijing 100853, China
e-mail: shihuaiyin@sina.com

D. Cao
Department of Pathology and Immunology, School of Medicine,
Washington University,
Saint Louis, MO, USA

Introduction

Choriocarcinoma typically occurs in the gonad (testis and ovary) and uterus. Less commonly, choriocarcinoma can occur in extragonadal sites (other than uterus, testes, and ovary) [1–21]. However, there is still some controversy regarding the existence of such extragonadal choriocarcinoma, especially in males. One school thought that such choriocarcinoma in males may represent metastases from small testicular tumors that have gone clinically undetected [1, 2, 22, 23]. For this reason, a specific criterion has been proposed for accepting an extragonadal choriocarcinoma in males as a primary tumor, namely the demonstration of absence of tumor within the gonads by serial sectioning of the testes [1]. Similarly, in females, one has to exclude a uterine or ovarian choriocarcinoma before

making a primary choriocarcinoma in other organs. In spite of these strict criteria, there are indeed still some extragonadal (other than uterine, testes, and ovary) choriocarcinomas [1–21]. Most reported primary extragonadal choriocarcinomas were in the mediastinum [1, 7, 8, 14, 16, 20, 21] and stomach [13], and only very rarely such choriocarcinomas occur in liver [3–5, 24]. Most reported primary hepatic choriocarcinomas were of infantile type (their origin was still controversial, and they may represent metastasis from occult placental choriocarcinoma) [5, 24], and there were only two well-documented cases in adults [3, 4]. In this study, we report five adult primary hepatic choriocarcinomas. All five patients were adult males (mean age 41.6 years, range 36 to 48 years old). Two of these five cases were diagnosed on surgical resection specimens but also with subsequent autopsy. The other three cases were diagnosed only on autopsy.

Materials and methods

This study was approved by the ethnic committee of the Chinese General PLA Hospital. The autopsy files of the Chinese PLA General Hospital and its two affiliated branch hospitals were searched for primary hepatic tumors. Of these primary tumors, five choriocarcinomas were identified. Hematoxylin-and-eosin (H&E)-stained sections were available for review in all five cases. Formalin-fixed paraffin-embedded tissue blocks containing tumor were retrieved for generating 4-μm-thick unstained slides for immunohistochemical staining on an automatic staining machine with the following antibodies: carcinoembryonic antigen (CEA; catalog number M7072, dilution 1:200; Dako, Carpinteria, CA, USA), cytokeratin (CK) AE1/AE3 (AE1/AE3, catalog number M3515, dilution 1:80; Dako, Carpinteria, CA, USA), human chorionic gonadotropin (HCG; polyclonal, dilution 1: 200; Dako, Carpinteria, CA, USA), alpha-fetoprotein (AFP; catalog number A0008, dilution 1:100; Dako, Carpinteria, CA, USA), human placental lactogen (HPL; polyclonal, 1:800; Dako, Carpinteria, CA, USA), hepatocyte paraffin 1 (Hepar1; catalog number OCH1E5.2.10, dilution 1:50; Dako, Carpinteria, CA, USA), OCT4 (clone C20, dilution 1:500, Santa Cruz Biotechnology), CD117 (IgG, dilution 1:50; Oncogene, Boston, MA, USA), CD30 (Clone BerH2, dilution 1:20; Dako, Carpinteria, CA, USA), placental-like alkaline phosphatase (PLAP; clone A268, dilution 1:100; Dako, Carpinteria, CA, USA), and Ki-67 (clone MM1, dilution 1: 50; Novocastra, Norwell, MA, USA). Appropriate positive and negative controls were included for each run of immunostaining. Clinical data were retrieved from the medical records.

Results

Clinical presentations

The clinical features in our patients are presented in Table 1. All patients were men, with an average age of 41.6 years (from 36 to 48 years). Clinically, they presented with symptoms of right upper abdominal pain (all five patients) or abdominal distension (one patient). The two patients with lung and brain metastasis also presented with headache, nausea, cough, hemoptysis, and shortness of breath. On ultrasonography, all five patients had a solitary mass (mean size 11 cm, ranging from 9 to 13 cm) in the liver. On further imaging studies, two of five patients had tumor confined to the liver, and the other three had tumors in other sites (multiple lung nodules in two patients, solitary brain nodule in one patient, peritoneum in one patient, and adrenal glands in one patient). One of these three patients had abdominal distension and ascites. Elevated serum HCG level was noted in all five cases (mean 5,300 mIU/ml, range 560~16,500 mIU/ml); however, the serum levels of AFP (available in five patients), CEA (available in five patients), and CA19–9 (available in three patients) were not elevated in any patient.

Pathologic findings on surgical resected specimens and needle biopsies

Surgical resection was performed for the two patients with tumor confined to the liver but without ascites. Grossly, the resected tumor measured 12 and 9 cm, respectively. On cut surface, both tumors were large, soft, hemorrhagic, and partially necrotic (Fig. 1). The resected tumors in both cases were solitary, and no satellite nodules were noted in the surrounding liver. The margins of the specimen were negative for tumor. Microscopically, the tumor cells in both patients were adjacent to the surrounding nonneoplastic liver parenchyma (Fig. 2a) and consisted of a dual cell population composed of mononucleated trophoblastic cells with uniform round nuclei and clear cytoplasm admixed with large multinucleated syncytiotrophoblastic cells with abundant amphophilic to eosinophilic cytoplasm (Fig. 2b). Numerous atypical mitoses and nuclear atypia were observed in the mononucleated trophoblastic cells (Fig. 2c). These two components were intimately admixed and were often found in association with extensive areas of hemorrhage and necrosis (Fig. 2d). With the diagnosis of choriocarcinoma, both patients received postsurgical chemotherapy.

For other three patients, due to extrahepatic tumor spread on imaging study, no surgery was performed. Instead, the diagnosis was made on liver needle core biopsies. The diagnosis from needle biopsies was poorly differentiated

Table 1 The clinicopathologic information of the five autopsy cases of primary hepatic choriocarcinoma

Case no.	Age (years)/ sex	Clinical presentation	Imaging findings	Treatment	Survival (months)	Autopsy findings
1	39/male	UAP	12 cm mass in the liver on ultrasonography	Resection and chemotherapy (EMA/CO)	6	Choriocarcinoma confined to the liver
2	45/male	UAP, headache, nausea, cough, shortness of breath	11 cm mass in the liver on ultrasonography, multiple small nodules in both lungs (0.8 to 2.5 cm in size), and solitary brain nodule (1 cm in size) on CT examination	Chemotherapy (DDP + 5FU)	2	Choriocarcinoma in the liver, lung, and brain; no tumor seen in the testis, mediastinum, or central nervous system or other sites
3	48/male	UAP, AD, and ascites	13 cm mass in the liver on ultrasonography, nodules in bilateral adrenal glands (2.0 cm in the left and 4.0 cm in the right) on CT examination	Chemotherapy (DDP + 5FU)	3	Choriocarcinoma in the liver with multiple metastases in peritoneum and bilateral adrenal glands; no tumor seen in the testis, mediastinum, or central nervous system or other sites
4	36/male	UAP, hemoptysis	10 cm mass in the liver on ultrasonography, multiple left lung nodules (size range 0.5 to 3 cm) on CT examination	Chemotherapy (DDP + 5FU)	5	Choriocarcinoma in the liver with multiple metastases in the lung (left lung); no tumor seen in the testis, mediastinum, or central nervous system or other sites
5	40/male	UAP	9 cm in the liver on ultrasonography	Resection and chemotherapy (CTX/CF)	8	Choriocarcinoma confined to the liver; no tumor seen in the testis, mediastinum, or central nervous system or other sites

UAP upper abdominal pain, *AD* abdominal distension, *DDP* dichlorodiammine platinum, *CTX* cyclophosphamide, *CF* cisplatin and 5-fluorouracil, *5FU* 5-fluorouracil, *EMA/CO* etoposide–methotrexate–actinomycin D–cyclophosphamide–vincristine

carcinoma in two cases and poorly differentiated carcinoma probably representing metastatic choriocarcinoma in one case. Chemotherapy was then administrated for these three patients (Table 1).

Fig. 1 The gross appearance of primary hepatic choriocarcinoma. The tumor has a fleshy appearance with extensive hemorrhage in the center

Autopsy findings

In spite of aggressive chemotherapy, all five patients died from their disease within 2 to 8 months (mean 4.8 months). Autopsy was performed for all five patients.

On autopsy, a solitary hepatic tumor (size ranged from 10 to 13 cm, mean size 11.3 cm) was seen in the three patients who did not received surgical resection. On cut surface, these tumors were largely hemorrhagic with necrosis. The tumor cells showed typical morphology of choriocarcinoma, i.e., consisted of a dual population of mononucleated trophoblastic cells and syncytiotrophoblastic cells. One patient (case 2) had multiple small foci of metastatic choriocarcinoma in his lung (both sides, the largest nodule measuring 2.5 cm) and brain (solitary nodule in left frontal lobe measuring approximately 1 cm). Multiple small foci of metastatic choriocarcinoma were seen in the peritoneum and bilateral adrenal glands in another patient (case 3). In the last case (case 4), the metastases (multiple with the largest one measuring about 3 cm in diameter) were only seen in his left lung. In the two patients who had prior surgical resection, no residual tumor was seen in the liver (case 1 and case 5).

For all five patients, the testes were not enlarged. The testes were serial sectioned and submitted entirely for

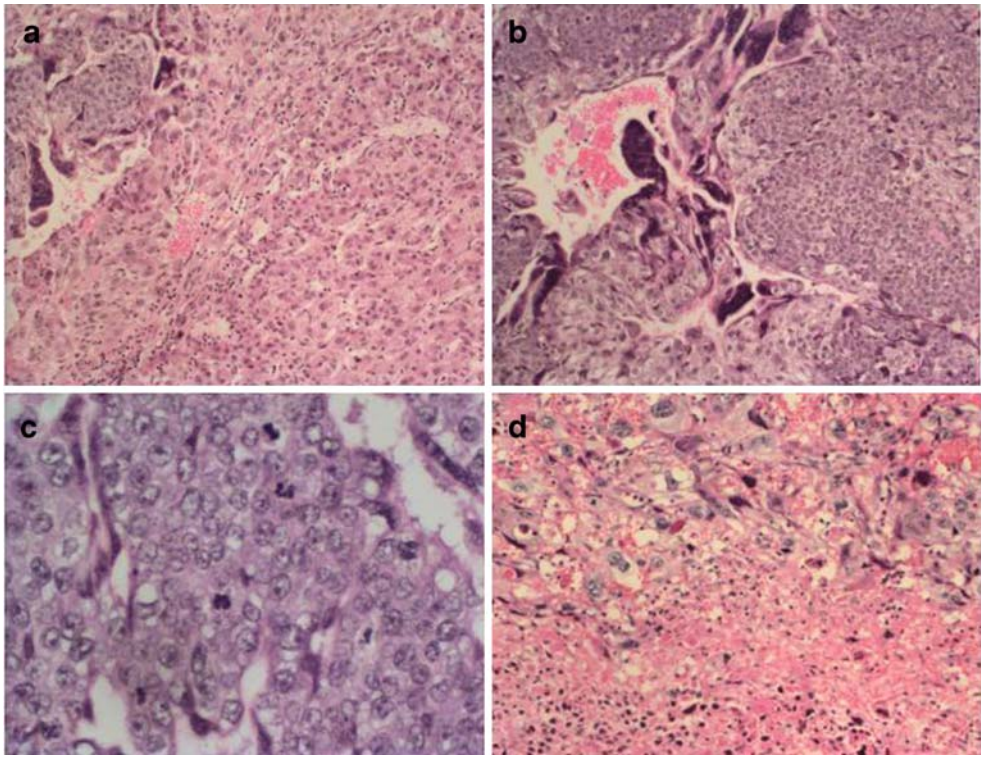

Fig. 2 Histologic features of primary hepatic choriocarcinoma. **a** The tumor (*upper left*) was seen adjacent to the surrounding liver (*lower right*; H&E ×100). **b** The tumor disclosed a dual cell population composed of mononucleated trophoblastic cells with large multinucleated syncytiotrophoblastic cells in a plexiform pattern (H&E ×100). **c** Mitotic figures were easily found in the mononucleated trophoblastic cells (H&E ×400). **d** There was prominent hemorrhage and necrosis within the tumor (H&E ×200)

histologic examination. Microscopically, there was no scar formation or other pathologic features that were often associated with germ cell tumor regression [25]. There was no tumor or necrosis in any other organs except those described above.

Immunohistochemical staining

Immunohistochemical studies were performed in all five cases (on surgically resected tumor in case 1 and case 5, on autopsy material in other 3 cases). The tumors showed

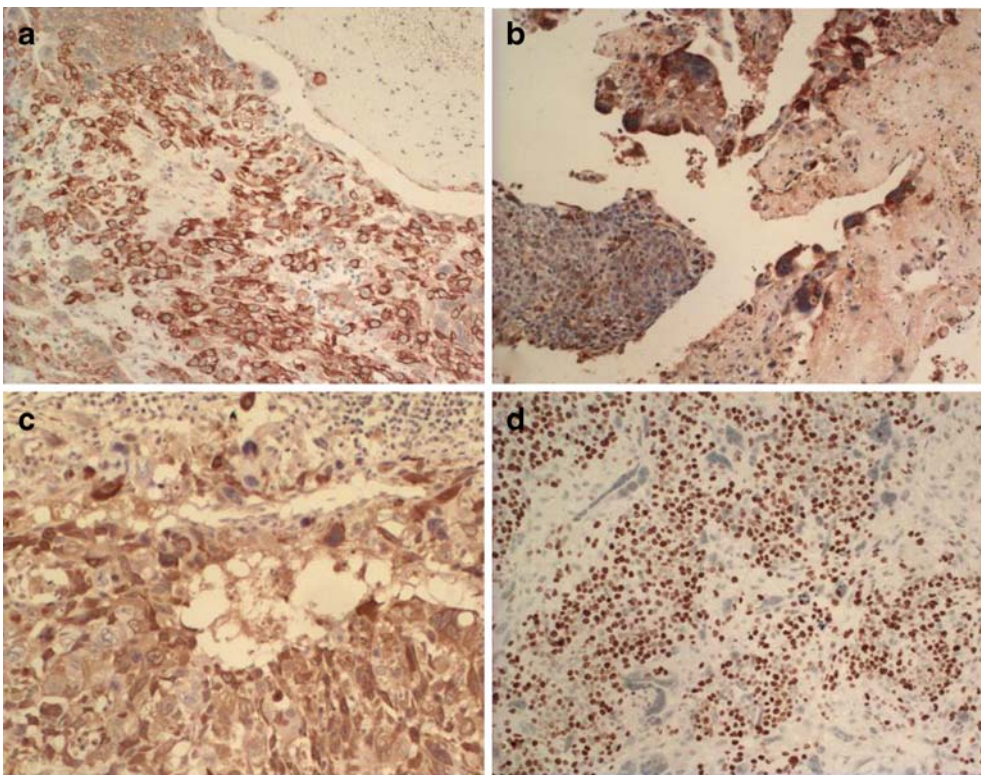

Fig. 3 Immunohistochemical staining of primary hepatic choriocarcinoma. **a** The tumor cells were strongly positive for cytokeratin. **b** The syncytiotrophoblastic cells were positive for beta-HCG. **c** Focal positivity for HPL was noted in the mononucleated trophoblastic cells. **d** Ki-67 proliferation index was high in the mononucleated trophoblastic cells

strong positive CK staining in both mononucleated and syncytial trophoblastic cells (Fig. 3a). Positive HCG staining was seen in the large syncytiotrophoblastic cells (Fig. 3b). Focal strong immunoreactivity for HPL in the mononucleated trophoblastic cells was also noted (Fig. 3c). Ki-67 proliferation index was high in the mononucleated trophoblastic cells (Fig. 3d), ranging from 65% to 80% (average 75%). Stains for CEA, AFP, hepatocyte paraffin 1, CD117, CD30, OCT-4, and PLAP were uniformly negative in the tumor cells in all five cases.

Discussion

Extragonadal germ cell tumors are rare, and most of them occur in the midline structures such as sacrum, mediastinum, and the central nervous system. Only very rarely extragonadal germ cell tumors occur in the liver. In the literature, there are less than 30 cases of primary hepatic germ cell tumors reported including yolk sac tumor [26–28], mixed germ cell tumors [6, 29], and choriocarcinomas [3, 4, 24]. Among the primary choriocarcinomas of the liver, the vast majority of them were of infantile type (some of which may represent metastases from occult placental choriocarcinoma) [24, 30]. In previous studies, only two well-documented adult cases have been reported [3, 4]. In this study, we reported five additional primary hepatic choriocarcinoma in adult patients. All these five patients were males, and their mean age was 41.6 years old (range 36 to 48). Two of these cases were diagnosed on surgically resected specimens, and the other three were diagnosed only on autopsy material. In spite of aggressive therapy, they all died from the tumor within 2 to 8 months.

One major issue regarding diagnosing primary hepatic choriocarcinoma is to exclude a metastasis from other sites notably from testis in males. It is well known that primary testicular germ cell tumors can undergo spontaneous regression whereas the patients present with distant metastases [1, 2, 22, 23, 25]. In all five cases in our study, the testes were serially sectioned and submitted entirely for histologic examination. There was no tumor or scar or other features associated with germ cell tumor regression seen in the testes [25]. In our study, two patients had choriocarcinoma limited to the liver, supporting the diagnosis of a primary hepatic choriocarcinoma. In the remaining three cases, choriocarcinoma was also present outside the liver (lung, brain, peritoneum, and adrenal glands). Although one may question the hepatic tumor in these three cases that represent metastasis, the presence of a solitary tumor in the liver and multiple small nodules in the lung, adrenal glands, and peritoneum were more consistent with a primary hepatic choriocarcinoma with metastasis to the latter sites rather than the opposite. In addition, some carcinomas such as rectal adenocarcinoma [31], gastric adenocarcinoma [32], and lung adenocarcinoma [33] can have choriocarcinomatous differentiation. Theoretically, the choriocarcinomatous component can metastasize to the liver. In our study, all five patients did not have such a history or nonchoriocarcinomatous carcinoma in any organ.

The morphologic diagnosis (other than determining origin) of choriocarcinoma in the liver is usually not an issue on surgically resected specimen. However, due to the rarity of choriocarcinoma in the liver, the diagnosis may be difficult on small needle biopsies as seen in our study. Three of our five patients had only needle biopsies, and a poorly differentiated carcinoma was initially rendered instead of a more specific diagnosis of choriocarcinoma. There are few tumors that may mimic choriocarcinoma. Giant cell variant of poorly differentiated hepatocellular carcinoma can mimic choriocarcinoma. Metastasis from a tumor with trophoblastic-like giant cells may also mimic choriocarcinoma. However, metastasis to the liver typically presented with multiple liver nodules. In difficult cases, immunostains to include beta-HCG, PLAP, HPL, and Hepar1, etc. might be helpful. However, one must keep in mind that none of these markers is entirely specific as some carcinomas can aberrantly produce HCG. One has to correlate immunohistochemical findings with morphologic features.

Finally, the prognosis of primary hepatic choriocarcinoma appeared to be dismal. In the two cases reported before, both patients died from tumor [3, 4]. One patient received chemotherapy but with no satisfactory response [4]. In our study, two of five patients received chemotherapy used for choriocarcinoma, but the response was poor. In the remaining three patients, the chemotherapy was against poorly differentiated carcinoma, but again the response was poor. All five patients in our study died from tumor within 2 to 8 months.

In summary, we reported five primary hepatic choriocarcinomas in adult patients. These tumors are rare in the liver, but they behave very aggressively.

Acknowledgment The author thanks Xin Song, Wei Chen, Enping Bai, Shiming Zan, Chao Guo, and Xia Tian for their excellent technical assistance.

Conflict of interest statement We declare that we have no conflict of interest.

References

1. Moran CA, Suster S (1997) Primary mediastinal choriocarcinomas: a clinicopathologic and immunohistochemical study of eight cases. Am J Surg Pathol 21:1007–1012
2. Greenwood SM, Goodman JR, Schneider G et al (1971) Choriocarcinoma in a man. Am J Med 51:416–422

3. Arai M, Oka K, Nihei T et al (2001) Primary hepatic choriocarcinoma —a case report. Hepatogastroenterology 48:424–426
4. Fernández Alonso J, Sáez C et al (1992) Primary pure choriocarcinoma of the liver. Pathol Res Pract 188:375–377
5. van der Hoef M, Niggli FK, Willi UV et al (2004) Solitary infantile choriocarcinoma of the liver: MRI findings. Pediatr Radiol 34:820–823
6. Theegarten D, Reinacher A, Graeven U et al (1998) Mixed malignant germ cell tumour of the liver. Virchows Arch 433:93–96
7. Candes FP, Ajinkya MS (1987) Primary mediastinal choriocarcinoma (case report). J Postgrad Med 33:219–221
8. Yamashita S, Ohyama C, Nakagawa H et al (2002) Primary choriocarcinoma in the posterior mediastinum. J Urol 167:1789
9. McKenney JK, Heerema-McKenney A, Rouse RV (2007) Extragonadal germ cell tumors: a review with emphasis on pathologic features, clinical prognostic variables, and differential diagnostic considerations. Adv Anat Pathol 14:69–92
10. Vegh GL, Szigetvári I, Soltesz I et al (2008) Primary pulmonary choriocarcinoma: a case report. J Reprod Med 53:369–372
11. Bell DM, Porras G, Tortoledo ME et al (2009) Primary sinonasal choriocarcinoma. Ann Diagn Pathol 13:96–100
12. Minei S, Matsui T, Obinata D et al (2008) Primary choriocarcinoma of the urinary bladder. Hinyokika Kiyo 54:293–296
13. Kobayashi A, Hasebe T, Endo Y et al (2005) Primary gastric choriocarcinoma: two case reports and a pooled analysis of 53 cases. Gastric Cancer 8:178–185
14. Yun EJ, Chung JY, Han HS (2005) Primary mediastinal choriocarcinoma. Int J Gynaecol Obstet 88:158–159
15. Dehner LP (1990) Germ cell tumors of the mediastinum. Semin Diagn Pathol 7:266–284
16. Dulmet EM, Macchiarini P, Suc B et al (1993) Germ cell tumors of the mediastinum. Cancer 72:1894–1901
17. Lack EE, Weinstein HJ, Welch KJ (1985) Mediastinal germ cell tumors in childhood: a clinical and pathological study of 21 cases. J Thorac Cardiovasc Surg 89:826–835
18. Sato K, Takeuchi H, Kubota T (2009) Pathology of intracranial germ cell tumors. Prog Neurol Surg 23:59–75
19. Ragam A, Apichai S, Radhakrishnan A et al (2008) Extragonadal choriocarcinoma in ulcerative colitis. J Clin Oncol 26:5813–5814
20. Kathuria S, Jablokov VR (1987) Primary choriocarcinoma of liver with immunohistochemical study and review of the literature. J Surg Oncol 34:39–42
21. Kersh RC, Constable WC, Hahn SS et al (1990) Primary malignant extragonadal germ cell tumors: an analysis of the effect of radiotherapy. Cancer 65:2681–2685
22. Jacobsen GK, Barlebo H, Olsen J et al (1984) Testicular germ cell tumours in Denmark 1976–1980. Pathology of 1058 consecutive cases. Acta Radiol Oncol 23:239–247
23. Powell S, Hendry WF, Peckham MJ (1983) Occult germ-cell testicular tumours. Br J Urol 55:440–444
24. Yoon JM, Burns RC, Malogolowkin MH et al (2007) Treatment of infantile choriocarcinoma of the liver. Pediatr Blood Cancer 49:99–102
25. Balzer BL, Ulbright TM (2006) Spontaneous regression of testicular germ cell tumors: an analysis of 42 cases. Am J Surg Pathol 30:858–865
26. Wong NA, D'Costa H, Barry RE et al (1998) Primary yolk sac tumour of the liver in adulthood. J Clin Pathol 51:939–940
27. Lenci I, Tariciotti L, Baiocchi L et al (2008) Primary yolk sac tumor of the liver: incidental finding in a patient transplanted for hepatocellular carcinoma. Transpl Int 21:598–601
28. Toumi N, Chaumette-Plankaert MT, Cherqui D et al (2004) Germ cell tumors. Case 3. Primary yolk sac tumor of the liver. J Clin Oncol 22:1756–1758
29. Verma M, Agarwal S, Mohta A (2003) Primary mixed germ cell tumour of the liver—a case report. Indian J Pathol Microbiol 46:658–659
30. Kim SN, Chi JG, Kim YW et al (1993) Neonatal choriocarcinoma of liver. Pediatr Pathol 13:723–730
31. Verbeek W, Schulten HJ, Sperling M et al (2004) Rectal adenocarcinoma with choriocarcinomatous differentiation: clinical and genetic aspects. Hum Pathol 35:1427–1430
32. Granier G, Marty-Double C (2007) Gastrointestinal adenocarcinomas with a choriocarcinomatous component: 2 cases and a review of 120 cases in the literature. Gastroenterol Clin Biol 31:854–857
33. Yamamoto S, Tanaka H, Takeo H et al (2006) Primary pulmonary choriocarcinoma combined with adenocarcinoma. Pathol Int 56:402–407

Virchows Arch (2010) 456:71–76
DOI 10.1007/s00428-009-0859-y

ORIGINAL ARTICLE

Multinucleated floret-like giant cells in sporadic and NF1-associated neurofibromas: a clinicopathologic study of 94 cases

Gaetano Magro · Paolo Amico · Giada Maria Vecchio · Rosario Caltabiano · Marine Castaing · Denisa Kacerovska · Dmitry V. Kazakov · Michal Michal

Received: 22 September 2009 / Revised: 28 October 2009 / Accepted: 1 November 2009 / Published online: 25 November 2009
© Springer-Verlag 2009

Abstract Multinucleated floret-like giant cells (MNFGCs), similar to those commonly observed in pleomorphic lipoma and giant cell fibroblastoma, have been occasionally reported in gynecomastia and neurofibromas from patients affected by neurofibromatosis type 1 (NF1). Accordingly, it has been suggested that their detection, especially in an otherwise typical neurofibroma, could be a morphological clue to diagnosis of NF1. The aim of the present study was the identification of MNFGCs in a large series (94 cases) of sporadic and NF1-associated neurofibromas, to assess if their presence may indeed be a morphological marker of NF1. Numerous MNFGCs, namely, those that were easily apparent at low magnification (×50 and ×100), were identified only in 5.3% of cases. In 18.1% of cases, a low number of these cells could be observed but only after a careful search, especially at higher magnification (×200 and ×400). Immunohistochemically, all MNFGCs were stained with vimentin and CD34, but not with S-100 protein. Interestingly, there was no statistically significant correlation between MNFGCs (presence or absence) and NF1 (p=0.73), gender (p=0.59), age (p=0.43), and site of tumor (cutaneous vs deep-seated soft tissue; p=0.27). Our clinicopathologic findings suggest that MNFGCs in an otherwise typical neurofibroma are not a reliable marker of NF1, likely representing a morphological reactive change of the indigenous dermal or endoneurial fibroblasts or dendritic cells in response to unknown microenvironmental stimuli.

Keywords Neurofibroma · Neurofibromatosis type I · Multinucleated floret-like cells · CD34

G. Magro (✉) · P. Amico · G. M. Vecchio · R. Caltabiano
Dipartimento G.F. Ingrassia, Policlinico Universitario G. Rodolico,
Anatomia Patologica, Università di Catania,
Via S. Sofia 87,
Catania, Italy
e-mail: g.magro@unict.it

M. Castaing
G.F Ingrassia Department, Integrated Tumor Registry
of Messina-Catania-Siracusa, Hygiene and Public Health Institute,
Via S. Sofia 87,
Catania, Italy

D. Kacerovska · D. V. Kazakov · M. Michal
Sikl's Department of Pathology,
Charles University Medical Faculty Hospital,
Pilsen, Czech Republic

Introduction

Neurofibroma is a relatively common benign peripheral nerve sheath tumor which can occur both sporadically or as part of neurofibromatosis type I (NF1) [1, 2]. Several histologic variants have been recognized over time, including classic, plexiform, cellular, epithelioid, myxoid, hyalinized, pacinian, pigmented, and granular cell variant [3–5]. In addition, some cases of neurofibroma with epithelial, rhabdomyomatous and lipomatous differentiation, or dendritic cells with pseudorosette formation have also been described [1, 6–8]. Although neurofibroma may present a wide morphological spectrum, only the plexiform neurofibroma, a tumor mass grossly consisting of tortuous expanded nerved branches, is virtually pathognomonic of NF1 [1, 2]. Apart plexiform neurofibroma, which is present in up 30% of cases of NF1 patients [9], most neurofibromas occurring in the context of this syndrome exhibit a morphology indistinguishable from those usually encountered in sporadic cases.

One of us (GM) first reported the presence of numerous multinucleated floret-like giant cells (MNFGCs), similar to those typically observed in pleomorphic lipoma and giant

cell fibroblastoma, in a diffuse type, cutaneous neurofibroma from a patient affected by NF1 [10]. This unusual finding was subsequently confirmed in other three neurofibromas from patients with NF1 [11–13]. Notably, one of these patients presented MNFGCs in all 20 cutaneous neurofibromas which had been surgically excised at different periods [13]. The same study also documented occasional MNFGCs in sporadic neurofibromas, raising the question whether the presence of such cells in an otherwise typical neurofibroma may represent a reliable morphological marker of NF1 [13]. To the best of our knowledge, there is no study in the literature, which compares the presence of MNFGCs in sporadic neurofibromas versus NF1-associated neurofibromas. Accordingly, the aim of the present study was the identification of MNFGCs in a series of 94 cases of neurofibromas occurring either sporadically or in NF1 patients to establish if these cells could serve as a morphological clue to diagnosis of NF1. Moreover, a clinicopathologic correlation between the presence of MNFGCs with age, gender, site, histological type, and malignant peripheral nerve sheath tumors (MPNSTs) arising from a pre-existing neurofibroma is provided.

Materials and methods

A retrospective review of all lesions coded as "neurofibroma" have been selected from the surgical pathology files at the Anatomic Pathology, Department G.F. Ingrassia, University of Catania, Catania, Italy and Sikl's Department of Pathology, Charles University Hospital, Pilsen, Czech Republic and Bioptical Laboratory, Pilsen, Czech Republic. All available slides stained with hematoxylin and eosin were reviewed. For all cases, the clinical data were obtained from pathology reports. Neurofibromas manifested a wide anatomic distribution including arm, forearm, wrist, breast, head, eyelid, neck, knee, back, scalp, abdomen, chest, thigh, vulva, and paravertebral region.

All sections were meticulously scrutinized for the presence of MNFGCs, namely, medium-sized to large cells exhibiting multiple nuclei arranged either randomly or in a wreath-like configuration, similar to floret-like cells typically observed in pleomorphic lipoma and giant cell fibroblastoma [1]. Their quantification was performed semiquantitatively, and the cases examined were arbitrarily divided into two groups: "neurofibromas with high number of MNGFCs" and "neurofibromas with low number of MNGFCs." In the former group, MNFGCs were readily apparent at low magnification (×50 and ×100), whereas in the latter group, they were identified only after a careful search, especially at higher magnification (×200 and ×400).

In addition, according to the site of their origin, neurofibromas of the present series were divided into cutaneous or deep-seated soft tissue neurofibromas. The former lesions were superficially located, with involvement of dermis and/or subcutis and were further histologically subdivided into diffuse or nodular type, according to the growth pattern exhibited by tumor [1]. The deep-seated soft tissue neurofibromas were represented by nodular masses with no evidence of skin or subcutis involvement.

Representative paraffin-embedded tissue blocks from all cases (22 of 94) containing MNFGCs were cut and processed for immunohistochemical analyses. One of these cases was previously published as case report [10]. Immunohistochemical studies were performed with the labeled streptavidin–biotin peroxidase detection system using the Ventana automated immunostainer (Ventana Medical Systems, Tucson, AZ). The antibodies used included vimentin (clone V9; dilution 1:50), CD34 (Clone Q Bend-10; dilution 1:50), S-100 protein (polyclonal; 1:5000), epithelial membrane antigen (clone GP1.4; dilution: 1:50), pancytokeratins (MNF116: dilution 1:100), and CD68 (clone KP1; dilution: 1:50; all purchased from DakoCytomation, Glostrup, Denmark).

Correlations between MNFGCs and the characteristics of the study population were performed through chi-square test and exact Fisher test when requested. p values<0.05 were considered statistically significant.

Results

All relevant clinical features in our patients are summarized in Table 1. There were 41 men and 50 women. Gender was not available in three cases. The patients ranged in age from 10 to 88 years, with an average age of 45.1. Age was not available in seven cases. Most neurofibromas (62.8%) were cutaneous, exhibiting a nodular or a diffuse pattern in 14.9% and 47.9% of the cases, respectively (Table 1). Deep-seated soft tissue neurofibromas represented 37.2% of the cases, and among these, a plexiform pattern was observed in 17.1% of cases.

An established history of NF1 was known in 50 patients (53.2%), while the remaining 44 patients (46.8%) had no clinical signs of this syndrome (Table 1). All patients without history of NF1 clinically presented with a single lesion. On the contrary, multiple cutaneous lesions (ranging from two to five) were available in three cases of patients with NF1. The six cases of plexiform type, deep-seated soft tissue neurofibromas were all associated with NF1.

Histologically, all tumors of the present study shared the typical morphological features of neurofibroma, namely, a proliferation of spindle-shaped cells with scant cytoplasm and elongated, often wavy nuclei. Extracellular matrix varied greatly from myxoid to fibrous. Among the NF1 patients, a MPNST was identified in eight cases (8.5%;

Table 1 Selected characteristics of the study population

	Patients (total number=94)	
	n	Percentage
Gender		
Men	41	43.6
Women	50	53.2
Missing	3	3.2
Age (years)		
<45	46	48.9
≥45	41	43.6
Missing	7	7.5
NF1		
No	44	46.8
Yes	50	53.2
MNFGCs		
High number	5	5.3
Low number	17	18.1
Absence	72	76.6
Site of tumor		
Diffuse cutaneous	45	47.9
Nodular cutaneous	14	14.9
Deep-seated soft tissues	35	37.2
MPNST		
No	86	91.5
Yes	8	8.5

n number of patients, *NF1* neurofibromatosis type I, *MNFGCs* multinucleated floret-like giant cells, *MPNST* malignant peripheral nerve sheath tumors

Table 1). In all these cases, a pre-existing neurofibroma could be histologically identified, with a plexiform pattern detected in three cases. All MPNSTs but one were histologically classified as high grade, according to World Health Organization classification [2].

MNFGCs were identified in 23.4% of the cases (Table 1). Neurofibromas which contained high or low number of MNFGCs represented 5.3% and 18.1% of the series, respectively (Table 1; Figs. 1 and 2). MNFGCs were morphologically similar both in sporadic and NF1-associated neurofibromas (Fig. 3a, b). They were found to be intermingling with neurofibroma tumor cells, from which they were easily distinguished by the presence of multiple nuclei arranged randomly or in a wreath-like configuration (Fig. 3a, b). Some of the nuclei were large in size, vesicular, and with a prominent nucleolus (Fig. 4). MNFGCs had a relatively abundant eosinophilic cytoplasm with dendritic-like processes (Figs. 3a, b and 4). Notably, one case of NF1-associated neurofibroma focally exhibited areas with numerous MNFGCs which lined pseudovascular spaces, namely, optically empty spaces without erythrocytes, evoking

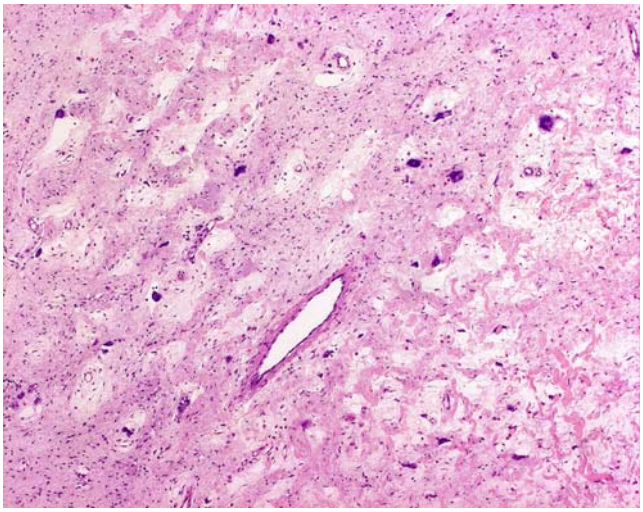

Fig. 1 Neurofibroma from a NF1 patient: numerous MNFGCs are easily identified at low magnification

a giant cell fibroblastoma (Fig. 5). Immunohistochemically, MNFGCs were stained with vimentin and CD34, while no immunoreactivity was obtained with all other antibodies. CD34 staining highlighted the dendritic-like cytoplasmic processes of the tumor cells (Fig. 6).

Correlations between clinicopathologic features and MNFGCs are summarized in Table 2. Interestingly, there was no statistically significant association between NF1 and MNFGCs (high, low number, or absence; $p=0.93$; Table 2). Similar results were obtained with the dichotomization, presence or absence of MNFGCs ($p=0.73$; not shown). Only in one of the three cases of NF1-associated neurofibromas with multiple cutaneous lesions was a low number of MNFGCs found in all surgically excised samples (two cutaneous neurofibromas, diffuse type). The remaining two cases were devoid of MNFGCs.

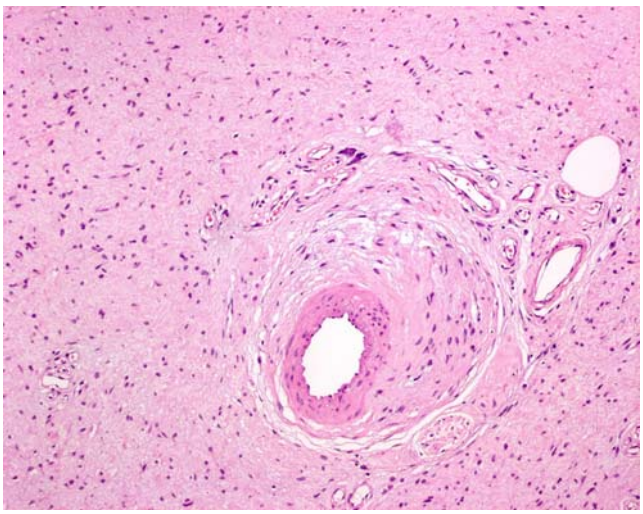

Fig. 2 Neurofibroma from a NF1 patient: only rarely MNFGCs are evident at higher magnification

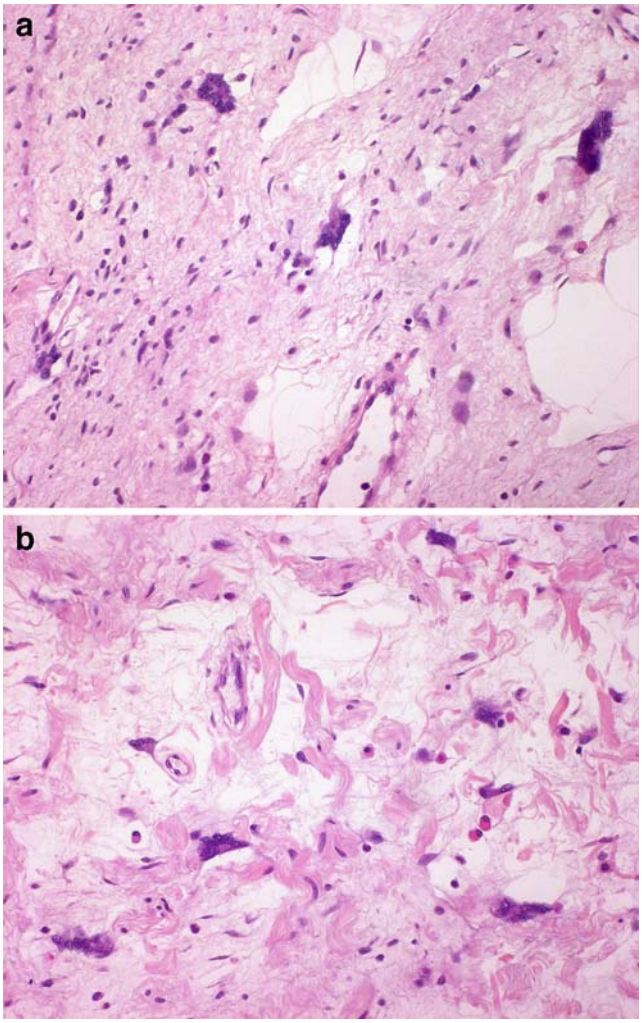

Fig. 3 MNFGCs are morphologically similar in both sporadic neurofibromas (**a**) and NF1-associated neurofibromas (**b**): large-sized cells with eosinophilic cytoplasm and multiple nuclei with a floret-like arrangement

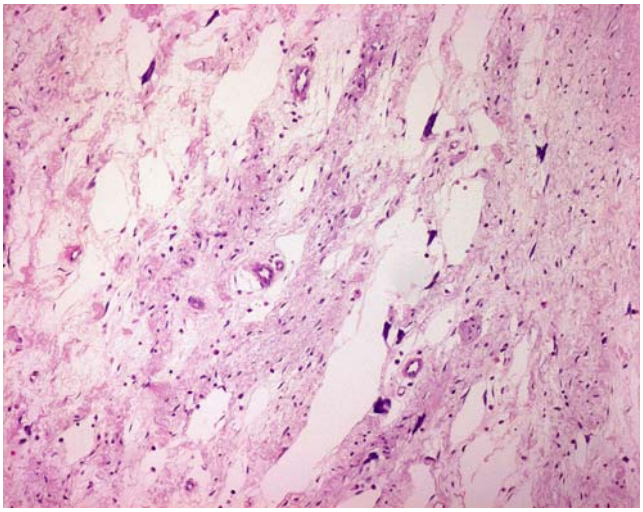

Fig. 5 Neurofibroma from a NF1 patient: area with pseudovascular spaces lined by MNFGCs, closely reminiscent of giant cell fibroblastoma

With regard to clinical features, no correlation was found between MNFGCs and gender (p=0.59), age (<45 vs ≥45; p=0.43), and site of tumor (cutaneous vs deep-seated soft tissues; p=0.27; Table 2). Similarly, analyzing the presence or absence of MNFGCs, the association between MPNSTs and MNFGCs in pre-existing neurofibroma was not statistically significant, with only in one out of eight cases (p=0.68; not shown), containing a low number of these cells.

It was noteworthy that among cutaneous neurofibromas, only diffuse type contained MNFGCs, whereas such cells were lacking in all cases of nodular type neurofibromas (not shown). In the former, MNFGCs were identified in 33.3% of the cases (not shown), with an associated NF1 history in 60% of cases (not shown). Only 20% of deep-seated soft tissue neurofibromas contained MNFGCs (Table 2), and

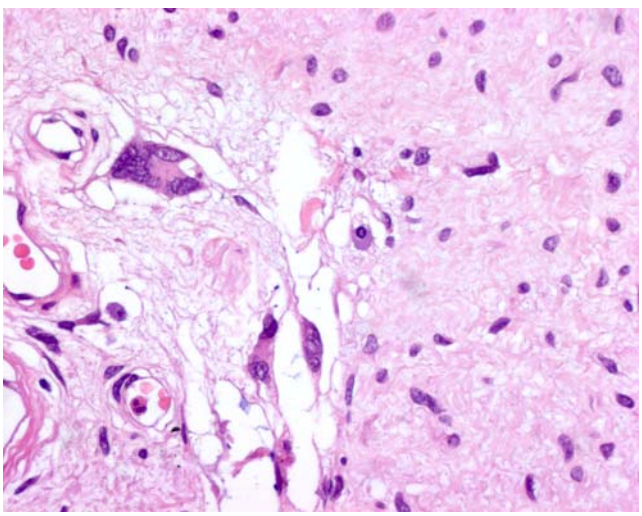

Fig. 4 Sporadic neurofibroma. MNFGCs exhibiting vesicular nuclei with a prominent nucleolus

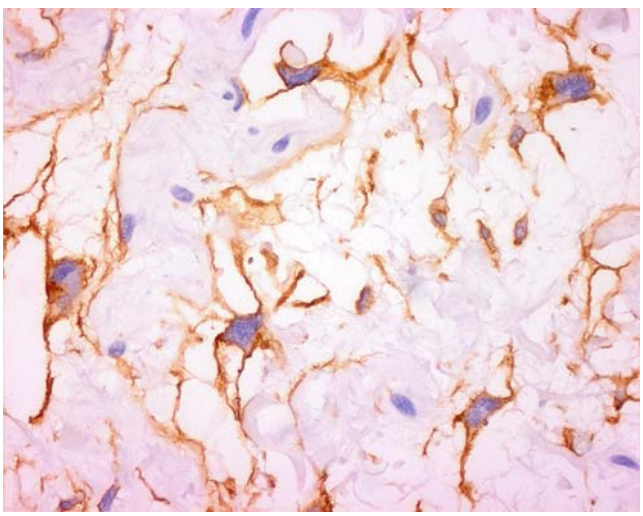

Fig. 6 Immunostaining with CD34 highlighting cytoplasmic dendritic-like processes

Table 2 Correlations between MNFGCs and characteristics of the study population

	Patients (total number=94)			
	High number of MNFGCs (n=5)	Low number of MNFGCs (n=17)	Absence of MNFGCs (n=72)	p
	n (%)	n (%)	n (%)	
Gender				
Men	3 (60)	9 (52.9)	29 (40.3)	0.59
Women	2 (40)	8 (47.1)	40 (55.6)	
Missing	0	0	3 (4.2)	
Age (years)				
<45	2 (40)	7 (41.2)	37 (51.4)	0.43
≥45	3 (60)	10 (58.8)	28 (38.9)	
Missing	0	0	7 (9.7)	
NF1				
No	2 (40)	9 (64.3)	33 (45.8)	0.93
Yes	3 (60)	8 (35.7)	39 (54.2)	
Site of tumor				
Cutaneous	2 (40)	13 (76.5)	44 (61.1)	0.27
Deep-seated soft tissues	3 (60)	4 (23.5)	28 (38.9)	

n number of patients, *NF1* neurofibromatosis type I, *MNFGCs* multinucleated floret-like giant cells, *MPNST* malignant peripheral nerve sheath tumors

among these, 28.6% of cases were associated with NF1 (not shown).

Discussion

MNFGCs cells have been well documented in the stroma of several anatomic locations, including lower female genital tract, testis, urinary bladder, anus, breast, and skin [14–17]. Similar cells have also been described as part of some soft tissue tumors, including pleomorphic lipoma, giant cell fibroblastoma, giant cell collagenoma, and giant cell angiofibroma/solitary fibrous tumor [1]. Interestingly, MNFGCs have been occasionally reported in gynecomastia from patients bearing NF1, suggesting the possibility that their detection could help in recognizing patients with this syndrome [18, 19]. The possibility of a link between MNFGCs and NF1 was also supported by the detection of these cells and also in some cases of neurofibromas from NF1 patients [10–13]. This latter finding led some authors to postulate that MNFGCs in an otherwise typical neurofibroma could be a morphological marker of NF1 [13]. To confirm this hypothesis, we first studied the incidence and quantification of MNFGCs in a large series of NFs occurring either sporadically or in the context of NF1.

Our results showed that the occurrence of MNFGCs in neurofibromas is relatively low, being found in 23.4% (22 of 94) of cases. Among these cases, most (17 of 22) were represented by neurofibromas containing only a few numbers of MNFGCs which would likely have been easily overlooked in daily practice. In fact, these cells could be identified only after a meticulous search, especially at higher magnification (×200 and ×400). Only in 5.3% of the series were MNFGCs found to be numerous and readily identifiable at low magnification (×50 and ×100). A previous study showed that 20 neurofibromas, all surgically excised from a 54-year-old patient affected by NF1, contained numerous MNFGCs [13]. This intriguing finding was compared with a series of 53 sporadic neurofibromas (NF1-associated neurofibromas were not included) [13]. The authors found MNFGCs in 5.6% of sporadic tumors, and interestingly, these cells were lower in number (i.e., identified only after a careful scrutiny), when compared with those found in the single patient with NF1 [13]. Therefore, it was suggested that a high number of these cells might be a clue to the presence of NF1 [13].

Based on the results of our study, we were not able to confirm this hypothesis. By comparing sporadic versus NF1-associated neurofibromas, there is no statistically significant association between MNFGCs and NF1. Moreover, the high number of MNFGCs is a reliable feature in distinguishing between NF1 and non-NF1 patients, because the cells were found in three versus two cases with or without NF1, respectively. In contrast to a previous report [13], our study failed to confirm the presence of numerous MNFGCs in multiple neurofibromas excised from the same NF1 patient. In addition, by analyzing other clinicopathologic characteristics, the presence of MNFGCs did not significantly correlate with patients' age, gender, site (cutaneous vs deep-seated soft tissues), and MPNSTs arising from pre-existing neurofibroma.

The histogenesis of MNFGCs in neurofibroma is still to be established. The present study shows that these cells are not integral part of neurofibroma, as they are significantly identified only in 5.3% (five of 94) of cases, without differences between sporadic and NF1-associated cases. Morphologically similar, if not identical, MNFGCs have been described in the stroma of benign fibroepithelial neoplasms of the breast, mesodermal fibroepithelial polyps of the lower female genital tract, fibroepithelial polyps of anus, allergic-type nasal polyps, and bladder with inflammatory or neoplastic (urothelial carcinoma) diseases [15, 17, 20, 21]. As previously suggested for the above mentioned pathological conditions [17], it is likely to postulate that MNFGCs occasionally encountered in neurofibromas may merely represent a morphological reactive change of the indigenous dermal or endoneurial fibroblasts or dendritic cells in response to unknown stimuli. Immunohistochemical

analysis, revealing exclusively vimentin and CD34 expression, would support the fibroblastic or dendritic nature of MNFGCs. Interestingly, some authors noted a close relationship between mast cells and MNFGCs, suggesting a potential role of the former in the formation of the latter cells [17]. Whether the well-known presence of mast cells in neurofibromas [1] could be closely related to that of MNFGCs is an intriguing hypothesis that deserves further clarification which is beyond the scope of the present paper.

Although not statistically significant, it was noteworthy that MNFGCs in our series were more frequently found in cutaneous versus deep-soft tissue neurofibromas. Among cutaneous neurofibromas, only diffuse type contained MNFGCs, whereas no case of nodular-type neurofibroma exhibited such cells. This finding would suggest that the type of growth pattern, namely, diffuse rather than nodular, may induce native dermal CD34+ fibroblasts/dendritic cells to acquire a multinucleated and floret-like appearance.

In conclusion, the presence of MNFGCs in an otherwise typical neurofibroma is not a significant indicator of NF1. Awareness that neurofibromas may contain MNFGCs is important for pathologist to avoid confusion with other tumors, especially giant cell fibroblastoma. Although the occasional presence of numerous MNSFCs in a neurofibroma may represent an alarming feature, these cells should not be misinterpreted as atypical tumor cells suggesting the possibility of atypical neurofibroma or MPNSTs arising from a pre-existing neurofibroma [1, 22]. This potential confusion should be raised because atypical tumor cells in a neurofibroma or MPNST may occasionally have multinucleation [1, 23]. Unlike MNSFCs, however, atypical tumor cells have hyperchromatic and irregular nuclei and may also exhibit prominent intranuclear pseudoinclusions [1, 23]. The presence of numerous atypical tumor cells uniformly distributed in a neurofibroma, in association with an increased cellularity and mitotic figures, is a reliable indicator of malignant transformation [1, 23]. Lastly, immunohistochemistry, showing a vimentin^{+}/CD34^{+}/S100^{-}/CD68^{-} profile in MNSFCs, is helpful in ruling out atypical tumor cells which are characteristically S-100 protein positive.

Conflict of interest The authors declare that they have no conflict of interest.

References

1. Weiss SW, Goldblum JR (2008) Enzinger and Weiss's soft tissue tumors. Mosby, St Louis
2. Scheithauer BW, Louis DN, Hunter S et al (2000) Malignant peripheral nerve sheath tumour (MPNST). In: Louis DN, Ohgaki H, Webster OD, Cavenee WK (eds) Pathology and genetics. Tumours of the central nervous system. IARC, Lyon, pp 155–162
3. Megahed M (1994) Histopathologic variants of neurofibroma: a study of 114 lesions. Am J Dermatopathol 16:486
4. Gonzalez-Vela MC, Val-Bernal JF, Gonzalez-Lopez MA et al (2006) Pure sclerotic neurofibroma: a neurofibroma mimicking sclerotic fibroma. J Cutan Pathol 33:47
5. MacLennan SE, Melin-Aldana H, Yakuboff KP (1999) Pacinian neurofibroma of the hand: a case report and literature review. J Hand Surg [Am] 24:413–416
6. Val-Bernal JF, Gonzales-Vela MC (2005) Cutaneous lipomatus neurofibroma: characterization and frequency. J Cutan Pathol 32:274–279
7. Plaza JA, Wakely PE, Suster S (2006) Lipoblastic nerve sheath tumors. Report of a distinctive variant of neural soft tissue neoplasm with adipocytic differentiation. Am J Surg Pathol 30:337–344
8. Kazakov DV, Vanecek T, Sima R et al (2005) Dendritic cell neurofibroma with pseudorosettes lacks mutations in exons 1–15 of the neurofibromatosis type 2 gene. Am J Dermatopathol 27:286
9. Ferner RE (2007) Neurofibromatosis 1 and neurofibromatosis 2: a twenty first century perspective. Lancet Neurol 6:340
10. Magro G, Scavo S, Ruggieri M (2002) Floretlike multinucleated giant cell in a neurofibroma from a patient with NF1: an unusual finding for such a tumor. Virchows Arch 441:525–526
11. Shaktawat SS, Golka D (2007) Floret-like multinucleated giant cells in neurofibroma. Diagn Pathol 8:2–47
12. Swick BL (2008) Floret-like multinucleated giant cells in a neurofibromatosis type 1-associated neurofibroma. Am J Dermatopathol 30:632–634
13. Taungjaruwinai WM, Golbert LJ (2009) Multinucleate giant cells in neurofibromas: a clue to the diagnosis of neurofibromatosis. J Cutan Pathol
14. Groisman GM, Amar M, Polak-Charcon S (2000) Multinucleated stromal cells of the anal mucosa: a common finding. Histopathology 36:224–228
15. Groisman GM, Polak-Charcon S (1998) Fibroepithelial polyps of the anus: a histologic, immunohistochemical, and ultrastructural study, including comparison with the normal anal subepithelial layer. Am J Surg Pathol 22:70–76
16. Ohtsuki Y, Furihata M, Iwata J et al (2000) Multinucleated giant cells in submucosal layer of human urinary bladder: an immunohistochemical and electron microscopic study. Pathol Res Pract 196:293–298
17. Pitt MA, Roberts IS, Agbamu DA et al (1993) The nature of atypical multinucleated stromal cells: a study of 37 cases from different sites. Histopathology 23:137–145
18. Damiani S, Eusebi V (2001) Gynecomastia in type-1 neurofibromatosis with features of pseudoangiomatous stromal hyperplasia with giant cells. Report of two cases. Virchows Arch 438:513–516
19. Zamecnik M, Michal M, Gogora M et al (2002) Gynecomastia with pseudoangiomatous stromal hyperplasia and multinucleated giant cells. Association with neurofibromatosis type 1. Virchows Arch 441:85–87
20. Powell CM, Cranor ML, Rosen PP (1994) Multinucleated stromal giant cell in mammary fibroepithelial neoplasm. A study of 11 patients. Arch Pathol Lab Med 118:912–916
21. Ryska A, Reynolds C, Keeney GL (2001) Benign tumors of the breast with multinucleated stromal giant cell. Immunohistochemical analysis of six cases and review of the literature. Virchows Arch 439:768–775
22. Lin BT, Weiss LM, Medeiros LJ (1997) Neurofibroma and cellular neurofibroma with atypia: a report of 14 tumors. Am J Surg Pathol 21:1443–1449
23. Jokinen CJ, Argenyi ZB (2009) Atypical neurofibroma of the skin and subcutaneous tissue: clinicopathologic analysis of 11 cases. J Cutan Pathol. doi:10.1111/j.1600-0560.2009.01293.x

Virchows Arch (2010) 456:77–84
DOI 10.1007/s00428-009-0871-2

ORIGINAL ARTICLE

Renal cell carcinoma with mixed features of papillary and clear cell cytomorphology: a fluorescent in situ hybridization study

Kien T. Mai · Hamidreza Faraji · Darren Desantis · Susan J. Robertson · Eric C. Belanger · Joelle Levac

Received: 21 September 2009 / Revised: 30 November 2009 / Accepted: 3 December 2009 / Published online: 22 December 2009
© Springer-Verlag 2009

Abstract We performed fluorescent in situ hybridization (FISH) to investigate the numeric change of chromosomes 7, 17, and Y and loss of chromosome 3p in "papillary renal cell carcinomas (RCC) with extensive clear cell changes (CCC)." Consecutive cases of RCC over a 12-year period were reviewed to identify "papillary RCC with extensive CCC." Immunostaining for cytokeratin 7 and alpha-methylacyl-CoA racemase (AMACR) and FISH for chromosomes 7, 17, Y, and 3p were applied. Of the total of 521 RCC retrieved, there were 49 RCC with papillary architecture and clear cell areas that could be divided into: Group 1 (12 cases), typical clear cell RCC with focal areas of papillary formation; Group 2 (28 cases), focal typical papillary RCC having papillary architecture with extensive CCC; and Group 3 (nine cases), RCC with an admixture of eosinophilic/clear cytoplasm and solid/papillary architecture. Group 1 showed negative immunoreactivity for CK7 and AMACR and absence of numeric chromosomal gain or loss of chromosomes 7/17 and Y. Groups 2 and 3 showed variable reactivity for CK7 and AMACR. Tumors in group 2 and five in group 3 showed trisomies of chromosomes 7 and/or 17 with or without loss of chromosome Y. Loss of small arm 3p was observed in groups 1 and 3 but not in group 2 tumors. In conclusion, papillary RCC may show phenotypical CCC mimicking clear cell RCC. In a small number of cases with mixed histopathological features, FISH is helpful in subtyping RCC.

Keywords Kidney · Carcinoma · Clear · Papillary

K. T. Mai · H. Faraji · D. Desantis · S. J. Robertson · E. C. Belanger · J. Levac
Department of Pathology and Laboratory Medicine, The Ottawa Hospital and University of Ottawa, Ottawa, ON, Canada

K. T. Mai (✉)
Anatomical Pathology, The Ottawa Hospital, General Campus, 501 Smyth Rd, Ottawa, ON K1H 8L6, Canada
e-mail: ktmai@ottawahospital.on.ca

Introduction

Clear cell renal cell carcinoma (CRCC) is the most common type of renal cell carcinoma (70%), and papillary subtype (PRCC) accounts for 10–20%. CRCC are often characterized cytogenetically by the deletion of one small arm of chromosome 3, and loss/malfunction of VHL/FHIT gene located at p25/p14 loci, respectively, of the remaining 3p arm. Histopathologically, CRCC consist frequently of cells with clear and abundant cytoplasm and are frequently associated with vascular invasion and distant metastasis [1-12]. PRCC are characterized by trisomy 7 or 17 and loss of the Y chromosome [13-16]. Microscopically, they often display papillary structures with chromophil cells and foamy macrophages. These carcinomas may be multifocal and are associated with a greater rate of loco-regional invasion with lymph node metastasis than vascular invasion and distant metastasis. Recent studies have demonstrated that PRCC with clear cytomorphology are associated with deletion of 3p without trisomy of the 7 or 17 chromosomes [17, 18]. Furthermore, some CRCC have been associated with trisomies 7/17 [19, 20].

Immunohistochemically, most CRCC have demonstrated negative immunoreactivity for cytokeratin 7 (CK7) and alpha-methylacyl-coenzyme A racemase (AMACR) in while most PRCC displayed positive immunoreactivity for

these antisera [21-25]. In a previous study at our institution, it was demonstrated that there is a group of RCC displaying hybrid cytomorphological and immunohistochemical properties with areas displaying features of CRCC or PRCC, respectively [26]. In the current study, we performed in situ hybridization (FISH) of chromosomes 7, 17, and Y and loci 3p25 and 3p14 on hybrid RCC.

Materials and methods

Consecutive cases of nephrectomy or local resection for RCC were retrieved from our Anatomical Pathology files dating from January 1993 until June 2005. Cases with areas displaying admixtures of typical PRCC of types 1 or 2 with or without oncocytic features, displaying papillary structures or solid areas with glomeruloid structures, and cases with admixtures of typical CRCC with clear cells forming solid, glandular or alveolar patterns, and foci of PRCC were identified. In these neoplasms, areas characteristic of PRCC and characteristic of CRCC were searched and identified. Areas of tumor displaying features intermediate between PRCC with chromophil cytoplasm and CRCC with clear cytoplasm were designated as displaying clear cell changes (CCC). Each surgical specimen was represented by three to 12 sections of 4-μm thickness, stained with hematoxylin–phloxin–saffron or H&E. For each case, two to five samples of representative tumor tissue, 3 mm in diameter, were removed from the paraffin block and re-embedded with other tumor samples to produce a tissue microarray paraffin block that contained up to 12 different samples. Areas with uncommon features such as papillary in CRCC, areas of clear cell in papillary RCC as well as areas transitional between typical uncommon features were carefully selected for sampling. Normal tissue was also sampled from non-tumoral tissue distant from the tumor. The tissue arrays were submitted for immunohistochemical studies and FISH.

Immunostaining was performed on formalin-fixed tissue sections using the avidin–biotin peroxidase complex (ABC) method with an ABC kit (Vector Laboratories, Burlingame, CA, USA) for cytokeratin 7 (CK7) (Dako, Carpenteria, USA, dilution 1:200) and AMACR (Dako).

For FISH, three separate sets of tests were performed for chromosomes 7/17, XY, and loci 3p14/25. For chromosomes 7/17 and XY, kits CEP7 (labeled in orange) and CEP17 (labeled in green), and kits X (labeled in orange) and Y (labeled in green; inter Medico, Abbott Molecular Inc., Mississauga, Ontario, Canada) were used. For 3p14/25 probes, human bacterial artificial chromosome probes for VHL and FHIT genes were obtained from The Centre for Applied Genomics Genetics and Genomics Biology, The Hospital for Sick Children (Toronto, Canada). The RP11-438 J1 labeled in orange corresponds to VHL gene and the RP11-94D19 labeled in green hybridizes to the proximal end of the FHIT gene. Both genes are in the small arm of the chromosome 3. Hybridization was performed on 3-μm thick sections using HYBtite set for 73°C for 5 min denaturation, followed by 37°C for 16–18 h hybridization. The cut slides were dried overnight at 37°C, then deparaffinized, rinsed in water dehydrated, and hybridized with a mixture of probes, CEP buffer (Inter Medico), and Cot-1 DNA (Inter Medico). Cot-1 was used to reduce the background in FISH experiments for 3p14/25 probes. The slides were visualized under fluorescent light. For each case, 200 tumor cells with nuclei were visualized to identify the probe signals. Care was taken for distinguishing stromal from epithelial cells. For FISH for 3p14/25, nuclei with one signal (red or green) or one red and one green signals separated by a distance less than 0.5 mm (presumably in the same small arm 3p) were recorded as having one 3p chromosome visualized. Nuclei with two red/ two green signals or two red and one green/one red and two green signals and one red and one green signals separated by a distance of more than 0.5 mm were considered as having two small arms 3p (no loss of chromosome 3p). The number of tumor nuclei without signals/total number of tumor cells with nuclei and the number of tumor nuclei with one 3p signal/total number of tumor nuclei with signals were recorded in percentage, respectively

Statistical analysis was performed using the Fisher exact test. Trisomy of chromosomes 7/17 was defined as the proportion of nuclei having three signals of the same chromosome higher than that in the normal tissue (see below). Similarly, loss of chromosome Y and the small arm 3p was defined as the proportion of nuclei having signal lower than that in the normal tissue (see below). Loss of the small arm 3p was defined as the proportion of nuclei having signals from 3p below that seen in normal control tissue and equal to that seen in control CRCC cases.

Results

Among a total of 521 RCC including CRCC, PRCC, chromophobe RCC, collecting duct RCC, and unclassifiable RCC, we identified 68 RCC that displayed the cytohistopathological admixture of clear and chromophil cells along with solid and papillary or glomeruloid architectures. The patients' age ranged from 41 to 81 years (58±10) with a male to female ratio of 3:1.

We classified these tumors as follows (Tables 1 and 2):

1. Group 1: CRCC with areas of papillary RCC (15 cases). Gender ratio, male/female was 11:4 and patient ages were of 56±8 years. The carcinomas were not encapsulated, measured 5–14 cm (6.3±7.4 cm), had a Fuhrman nuclear

Table 1 Clinical data and histopathological findings of study cases

	#	M/F ratio	Age	Size	Grade	Stage	VI	LN	DM	Sarcom change	DOD
Group 1 CRCC, papillary	15	11:4	56±8	0.5–14 6.3±7.4	2–4 (3.2)	1–4 (3.05)	14 (9)	0	7	3 [1]	9
Group 2 PRCC CCC	25	19:6	58±10	2.6–6.6 4.6±2.0	1–3 (2.6)	1–3 (2.3)	3 (2)	3	2	2 [2]	2
Group 3 RCC, mixed	26	20:6	58±9	2–14 6.8±6.8	2–4 (3.10)	1–4 (3.10)	7 (3)	1	5	7 [3]	6
Total	68						24 (14)	4	14	12 [6]	17

VI difference between CRCC and mixed and between CRCC and PRCC with CCC were statistically significant, $p<0.05$

M/F male to female ratio, *VI* venous invasion, *()* renal vein invasion, *sarcom* sarcomatous, *LN* lymph node metastasis, *DM* distant metastasis, *DOD* dead of disease, *[]* focal sarcomatous change

grades of 2 to 4 and often showed tumoral necrosis and venous invasion. Areas of papillary architecture were extensive (up to 90% of the carcinoma) or focal. The tumor showed negative immunoreactivity for CK7 and AMACR. (Fig. 1a–c).

2. Group 2 (25 cases): RCC with papillary architecture formed by clear cells with absence of the solid areas typical of CRCC. Gender ratio, male/female was 19:6, and patient ages were of 58±10 years. The carcinomas showed encapsulation with frequent capsular penetration and measured from 2.6 to 6.6 cm (mean 4.6± 2.0 cm). The architecture often consisted of papillae having clear cells with or without cells with varying degrees of foamy cytoplasm. The tumor frequently showed positive immunoreactivity for CK7 and AMACR in areas of typical PRCC and decreased to negative immunoreactivity for CK7 and AMACR in areas with CCC with or without foamy cytoplasm (Fig. 2a–c).
3. Group 3 (26 cases): RCC with admixture of areas of group 2 or typical PRCC and areas of solid CRCC. Gender ratio, male/female was 20:6, and patient ages were of 58±9 years. The carcinomas were frequently not encapsulated and measured from 2.0 to 14 cm (mean 6.8±2=6.8 cm). The tumor frequently showed positive immunoreactivity for CK7 and AMACR in areas of typical PRCC and negative immunoreactivity for CK7 and AMACR in areas of typical CRCC (Fig. 3a–e).

The non-neoplastic renal tissue distant from the carcinoma shows positive reactivity for CK7 only in distal tubules, atrophic or regenerative renal epithelial cells and collecting ducts, and positive reactivity for AMACR in proximal and distal tubules with dark cytoplasm and negative reactivity for collecting ducts.

For FISH studies, normal renal tissue (a total of 12 samples) was examined. Nuclei with signals (per total tumoral nuclei) for chromosomes 7 or 17 were 59–72% (67±5), and nuclei with double signals (per total number of nuclei with signals) for chromosomes 7 or 17 were 25–47% (36±6) and 22–41% (33±7), respectively. For chromosome 3p, nuclei with signals (per total tumoral nuclei) were 60–72% (68±6) and nuclei with double chromosome 3p (per total number of

Table 2 Summary of immunohistochemical and FISH findings

	Immunoreactivity		Loss of Y in male	Trisomy of chromosome		Loss of 3p14/25
	CK7	AMACR		7	17	
Group 1 CRCC, papillary (15 cases)	Neg	Neg	No	No	No	Yes
Group 2 PRCC+CCC (25 cases)						
Areas of PRCC	Pos	Pos	Yes	Yes: 23/25	12/25	No
Areas of CCC	Neg/Pos	Neg/Pos	Yes	Yes: 23/25	12/25	No
Group 3 RCC, mixed (26 cases)	Neg					
Areas of PRCC	Pos	Pos	Yes	Yes: 26/26	Yes: 7/26	No
Areas of CRCC	Neg	Neg	Yes	Yes: 26/26	Yes: 7/26	Yes

CK7 cytokeratin 7, *AMACR* alpha-methylacyl-CoA racemase, *Neg* negative, *Pos* positive, *Neg/Pos* weakly positive

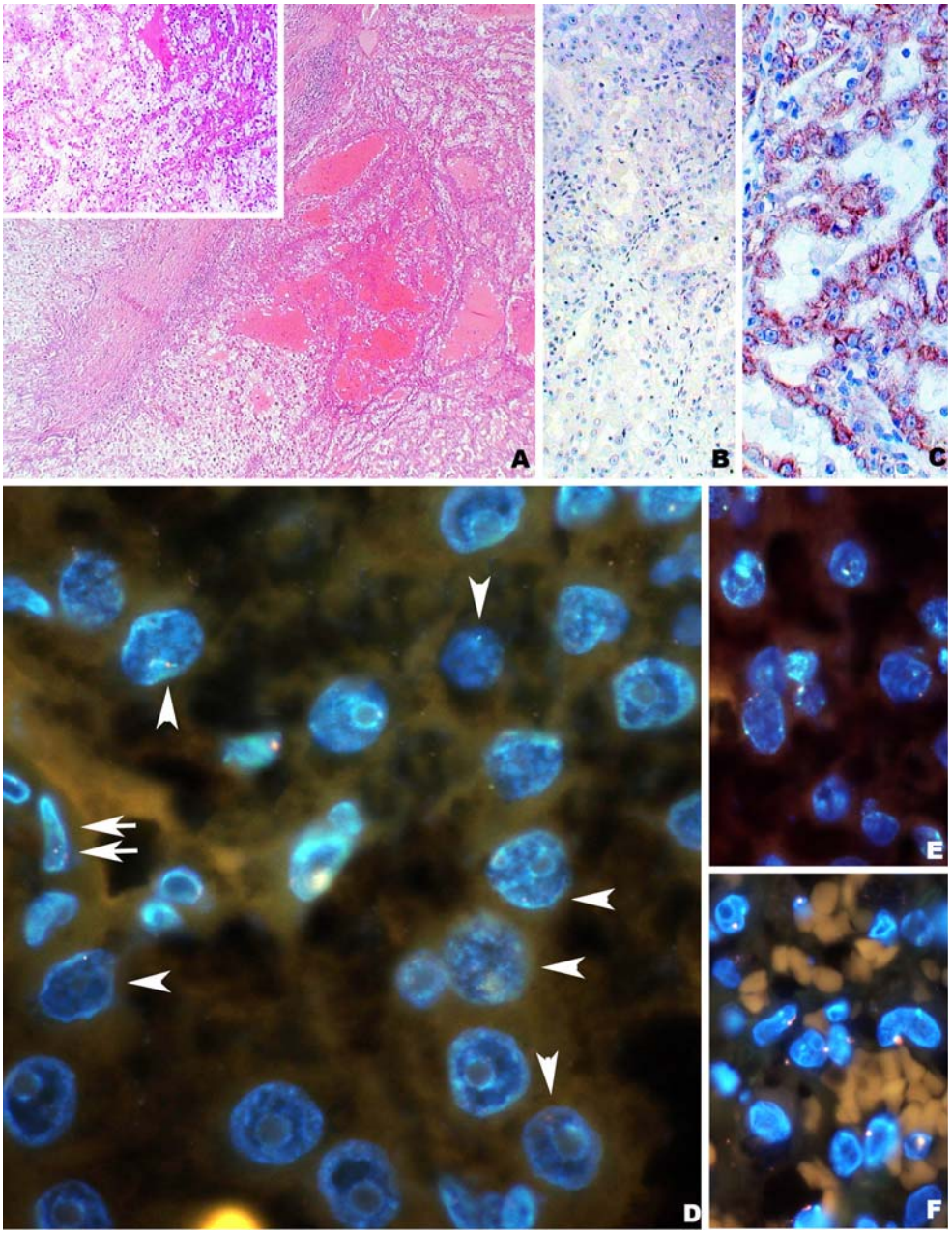

Fig. 1 **a** CRCC with focal papillary architecture forming a distinct nodule. *Inset* High magnification showing transitional change from solid CRCC to PCRCC. **b** Immunostaining for CK7 showing negative reactivity in both solid and papillary areas of RCC. **c** Immunostaining for AMACR showing positive reactivity in papillary areas of RCC and negative reactivity in areas with alveolar architecture. **d** Interphase FISH study for 3p25 (*red*) and 3p14 (*green*) show signals from single 3p arm (red and green signals were located at a distance of less than 0.5 mm; *arrowheads*). Note one stromal cell with signals from two 3p arms (*double arrows*). **e** Interphase FISH study for chromosomes 7 (*red*) and 17 (*green*) shows absence of trisomy for chromosomes 7/17. **f** Interphase FISH study for chromosomes X (*red*) and Y (*green*) shows the presence of chromosome Y

nuclei with signals) were 36–61% (46±7). For control cases of PRCC (30 cases), nuclei with triple signals (per total number of nuclei with signals) for chromosomes 7 or 17 were 15–34% (22±8) in 17 of 20 cases and 17–28% (23±7) in 19/20 cases, respectively. Loss of Y was observed 50 to 90% of cells in 14/15 male patients and with trisomies of 7 and/or 17 and/or loss of Y in male patients in 20/20 cases. For CRCC (grades 2–3/4), the proportion of tumoral nuclei with signals was 46–65% and nuclei with double 3p in 0–12% of total number of nuclei with signals.

In all Group 1 cases, FISH showed loss of one copy of 3p14/25 and absence of trisomies 7/17 and presence of Y in all samples including areas with papillary architecture (Fig. 1d–f). Group 3 tumors were associated with trisomies 7 and/or 17 and/or loss of Y in male patients in all areas in all tumors including areas with CCC and with features of typical CRCC. Trisomy of chromosome 7 was present in all 26 cases, trisomy of chromosome 17 was present in five cases, and there is loss of chromosome Y in all 20 male patients. In addition, loss of 3p25/3p14 was detected in areas of typical CRCC in all cases. There was no loss of 3p arm in areas of PRCC with CCC and in areas of typical PRCC in all cases (Fig. 3f–k). In Group 2 tumors, FISH demonstrated trisomy of chromosomes 7/17 17 (12–28% nuclei with signals) and loss of chromosome Y in all male patients in all samples. There was no loss of loci 14/25 of chromosome 3p

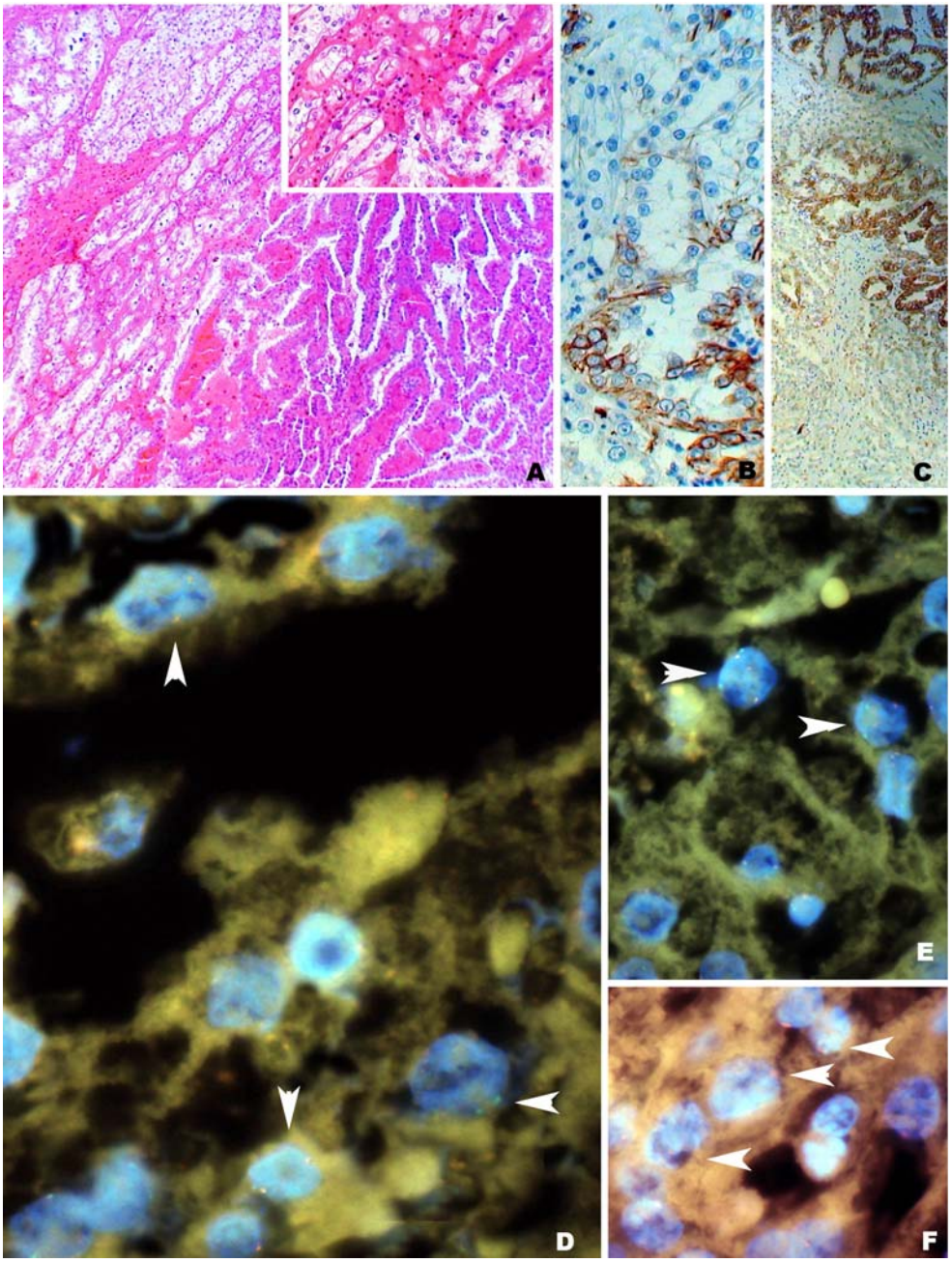

Fig. 2 **a** PRCC with focal CCC. Note the clear cell changes in the areas of papillary architecture and tubular architecture. *Inset* CCC in area of tubular architecture. **b** Immunostaining for CK7 showing strong positive reactivity in the areas with chromophil cytoplasm and weaker of negative reactivity in the clear cytoplasm. **c** Immunostaining for AMACR showing strong positive reactivity in the areas with chromophil cytoplasm and weaker or negative reactivity in the clear cytoplasm. **d** Interphase FISH study for 3p25 (*red*) and 3p14 (*green*) show signals from both 3p arms (red and green signals were located in a distance of less than 0.5 mm in the same 3p arm and greater than 0.5 mm in two different 3p arms; *arrowheads*). Note one stromal cell with signals from two 3p arms (*double arrows*). **e** Interphase FISH study for chromosome 7 (*red*) and 17 (*green*) shows trisomy for chromosomes 7/17 (*arrowheads*). **f** Interphase FISH study for chromosome X (*red*) and Y (*green*) shows the loss of chromosome Y (*arrowheads*)

in areas of PRCC with CCC or in areas of typical PRCC (Fig. 2d–f).

Discussion

Cytogenetic and molecular alterations have been considered pivotal in the classification of RCC. In CRCC, it has been demonstrated that there is alteration of the VHL gene located on the small arm of chromosome 3. The VHL gene is a tumor suppressor gene, and its loss, as seen in deletion of the 3p, is responsible for the VHL syndrome. In addition, the fragile histidine triad gene located in the proximal part of chromosome 3p has been proven to be associated with CRCC. Cytogenetic studies have demonstrated that in both inherited and sporadic CRCC, there is a loss of the small arm 3p with a break point at regions 3p11–3p21 or at the centromere in a majority of cases. In studies on VHL gene, the remaining VHL allele genes often become inactive due to molecular mutation with complete loss of VHL function in about one half of cases. Hypermethylation accounts for the inactivation in the remaining half of cases (1–12). Therefore, in FISH studies, the loss of one arm of 3p or inability to identify two copies of VHL/FHIT is suggestive

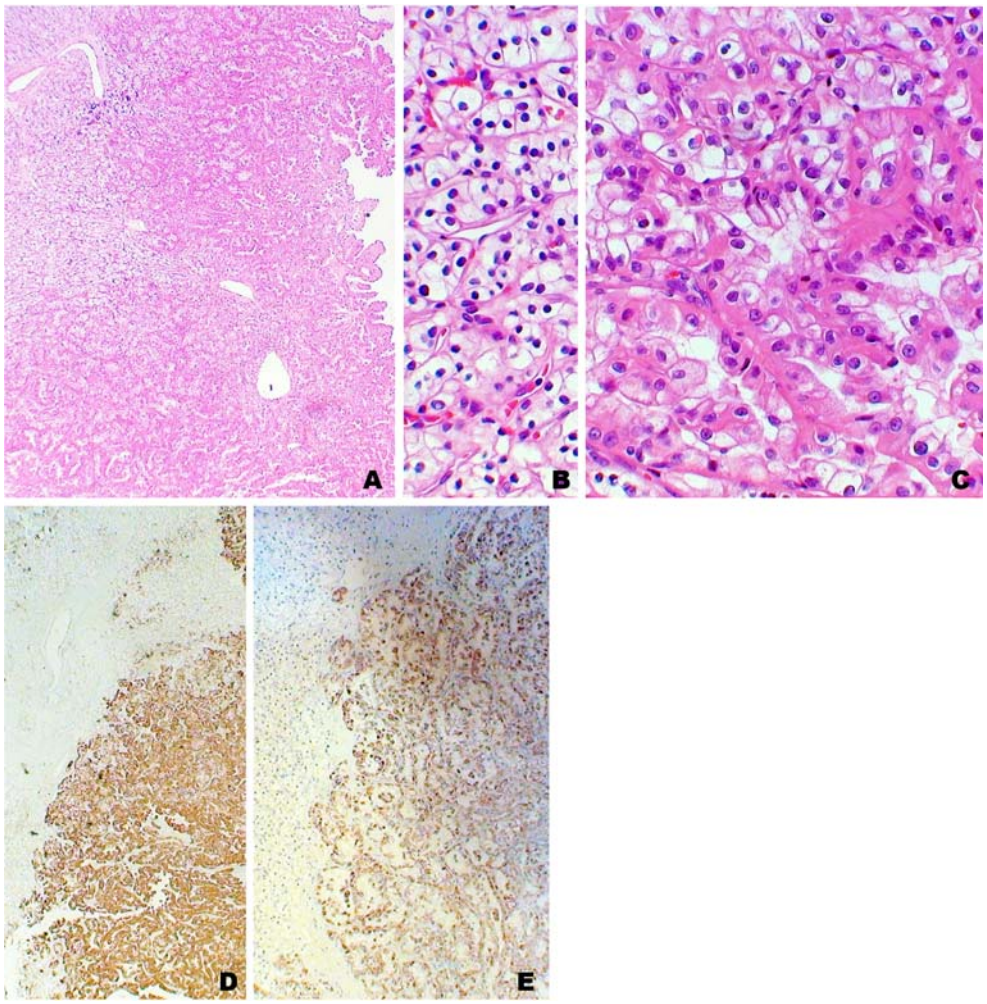

Fig. 3 PRCC with CCC and areas of solid CRCC. **a** Area of mixed clear cell alveolar RCC and PRCC with papillary architecture. **b** Solid area with features of alveolar CRCC. **c** Transitional zones between papillary areas with and without CCC. **d** Immunostaining for CK7 showing positive reactivity in area without CCC and negative area with CCC and area of alveolar CRCC. **e** Immunostaining for AMACR showing positive reactivity in area without CCC and negative area with CCC and area of alveolar CRCC. **f** Interphase FISH study for chromosome 7 (*red*) and 17 (*green*) of the areas with papillary architecture shows trisomy for chromosomes 7/17 (*arrowheads*). **g** Interphase FISH study for chromosome X (*red*) and Y (*green*) of the areas with papillary architecture shows the loss of chromosome Y. **h** Interphase FISH study for 3p25 (*red*) and 3p14 (*green*) of the areas with papillary architecture shows signals from both 3p arms (red and green signals were located at a distance of less than 0.5 mm in the same 3p arm and greater than 5 mm in two different 3p arms; *double arrowheads*). **i** Interphase FISH study for 3p25 (*red*) and 3p14 (*green*) of the areas of alveolar CRCC show signals from only one 3p arm (red and green signals were located at a distance of less than 0.5 mm in the same 3p arm; *double arrowheads*). Note stromal cells with signals from two 3p arms (*double arrows*). **j** Interphase FISH study for chromosome 7 (*red*) and 17 (*green*) of the areas of alveolar CRCC shows trisomy for chromosomes 7/17. **k** Interphase FISH study for chromosome X (*red*) and Y (*green*) of the areas of alveolar CRCC shows the loss of chromosome Y

of cytogenetic alterations diagnostic of CRCC. The second copy of VHL/FHIT genes that are inactive may or may not be visualized.

In this study, Group 1 RCC represents CRCC with focal or extensive papillary structures. CRCC with extensive papillary structures in this group were associated with the alteration of 3p and the absence of trisomy 7 or 17. The tumors represent the CRCC with secondary papillary architectures as described in two previous reports [17, 18].

Group 2 represents PRCC having typical cytogenetic alterations of PRCC with secondary CCC as evidenced by focal chromosomal changes of CRCC occasionally identified. Group 3 represents the combined areas of PRCC and CRCC.

Recent interests of the cytogenetic and molecular studies have led to the new classification of RCC. Knowledge on the molecular alterations of the clear cell PRCC is limited in a small number of study cases. Furthermore, RCC is

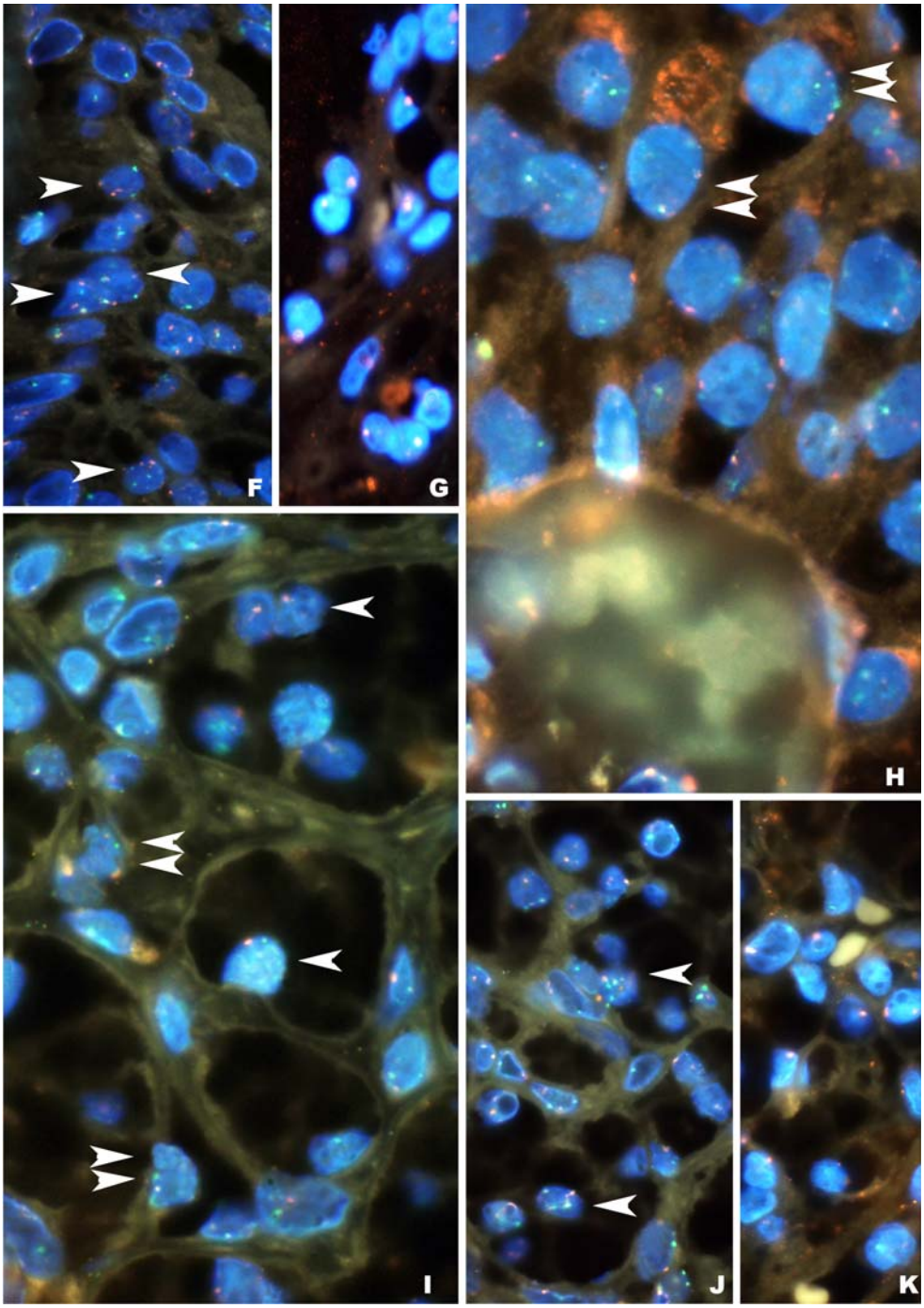

Fig. 3 (continued)

usually not homogeneous, expressing different histopathological pattern within the same tumor. It is well known that there is molecular heterogeneity in the primary as well as metastatic RCC [27, 28]. Cytogenetic and molecular studies revealed that alteration of the small arms of the chromosome 3 characteristic of CRCC do not preclude further chromosomal changes with trisomy of chromosomes 7, 17, and Y and vice versa. Therefore, hypothetical alterations at loci p25 and p14 of the chromosome 3 likely represent the subsequent alterations seen in the pathway of cytogenetic changes in PRCC.

Our findings in the present study have been reported in other studies detecting loss of loci 3p25 in some PRCC with clear cell component and trisomies 7/17or loss of chromosome Y in some CRCC [19, 20, 28, 29]. In addition, we were able to locate the areas associated with loss of loci

in 3p and areas with trisomies 7/17 and/or loss of chromosome Y, respectively. The presence of chromosomal changes characteristic of PRCC in areas histopathologically and immunohistochemically typical of CRCC, and the absence of loss of 3p in areas of PRCC in Group 3 tumors are suggestive of the interesting histopathogenesis of some CRCC. Since CRCC is often associated with more aggressive biological behavior and higher mortality rate than PRCC, it is reasonable to believe that some CRCC develop from papillary renal neoplasms.

In conclusion, it is important to recognize this type of tumor with hybrid morphological features of typical PRCC and CRCC due to its more aggressive biological behavior compared to classical PRCC. Its recognition may also facilitate the classification of RCC with ambiguous morphologies. The identification of CRCC in a tumor with typical PRCC may have the therapeutic application associated with CRCC [30, 31]

Conflict of interest statement We declare that we have no conflict of interest

References

1. Erlandsson R, Boldog F, Sümegi J et al (1988) Do human renal cell carcinomas arise by a double-loss mechanism? Cancer Genet Cytogenet 36:197–202
2. Kovacs G, Erlandsson R, Boldog F et al (1988) Consistent chromosome 3p deletion and loss of heterozygosity in renal cell carcinoma. Proc Natl Acad Sci USA 85:1571–1575
3. Maher ER, Yates JR, Ferguson-Smith MA (1990) Statistical analysis of the two stage mutation model in von Hippel-Lindau disease, and in sporadic cerebellar haemangioblastoma and renal cell carcinoma. J Med Genet 27:311–314
4. Latif F, Tory K, Gnarra J et al (1993) Identification of the von Hippel-Lindau disease tumor suppressor gene. Science 260:1317–1320
5. Foster K, Prowse A, van den Berg A et al (1994) Somatic mutations of the von Hippel-Lindau disease tumour suppressor gene in non-familial clear cell renal carcinoma. Hum Mol Genet 3:2169–2173
6. Yoshida MA, Ohyashiki K, Ochi H et al (1986) Rearrangement of chromosome 3 in renal cell carcinoma. Cancer Genet Cytogenet 19:351–354
7. Yoshida MA, Ohyashiki K, Ochi H et al (1986) Cytogenetic studies of tumor tissue from patients with nonfamilial renal cell carcinoma. Cancer Res 46(Pt 2):2139–2147
8. Gnarra JR, Tory K, Weng Y et al (1994) Mutations of the VHL tumour suppressor gene in renal carcinoma. Nat Genet 7:85–90
9. Herman JG, Latif F, Weng Y et al (1994) Silencing of the VHL tumor-suppressor gene by DNA methylation in renal carcinoma. Proc Natl Acad Sci USA 91:9700–9704
10. Receveur AO, Couturier J, Molinié V et al (2005) Characterization of quantitative chromosomal abnormalities in renal cell carcinomas by interphase four-color. Cancer Genet Cytogenet 158:110–118
11. van den Berg A, Buys CH (1997) Involvement of multiple loci on chromosome 3 in renal cell cancer development. Genes Chromosomes Cancer 19:59–76, Review
12. Murphy WM, Beckwith JB, Farrow GM (1994) Tumours of the kidney, bladder, and related urinary structures, 3rd Series. Armed Force Institute of Pathology, Washington, DC, pp 92–136
13. Kocacs G, Akhtar M, Beckwith BJ et al (1997) The Hidelberg classification of renal cell tumours. J Pathol 183:131–133
14. Kovacs G (1989) Papillary renal cell carcinoma. A morphologic and cytogenetic study of 11 cases. Am J Pathol 134:27–34
15. Kovacs G, Fuzesi L, Emanual A et al (1991) Cytogenetics of papillary renal cell tumors. Genes Chromosomes Cancer 3:249–255
16. Kovacs G (1993) Molecular differential pathology of renal cell tumours. Histopathology 22:1–8, Review
17. Fuzesi L, Gunawan B, Bergmann F (1999) Papillary renal cell carcinoma with clear cell cytomorphology and chromosomal loss of 3p. Histopathology 35:157–161
18. Salama ME, Worsham MJ, DePeralta-Venturina M (2003) Malignant papillary renal tumors with extensive clear cell change: a molecular analysis by microsatellite analysis and fluorescence in situ hybridization. Arch Pathol Lab Med 127:1176–1181
19. Klatte T, Rao PN, de Martino M et al (2009) Cytogenetic profile predicts prognosis of patients with clear cell renal cell carcinoma. J Clin Oncol 5:746–753
20. Gobbo S, Eble JN, Grignon DJ et al (2008) Clear cell papillary renal cell carcinoma: a distinct histopathologic and molecular genetic entity. Am J Surg Pathol 32:1239–1245
21. Mazal PR, Stichenwirth M, Koller A et al (2005) Expression of aquaporins and PAX-2 compared to CD10 and cytokeratin 7 in renal neoplasms: a tissue microarray study. Mod Pathol 18:535–540
22. Avery AK, Beckstead J, Renshaw AA et al (2000) Use of antibodies to RCC and CD10 in the differential diagnosis of renal neoplasms. Am J Surg Pathol 24:203–210
23. Shen SS, Krishna B, Chirala R et al (2005) Kidney-specific cadherin, a specific marker for the distal portion of the nephron and related renal neoplasms. Mod Pathol 18:933–940
24. McGregor DK, Khurana KK, Cao C et al (2001) Diagnosing primary and metastatic renal cell carcinoma: the use of the monoclonal antibody 'Renal Cell Carcinoma Marker'. Am J Surg Pathol 12:1485–1492
25. Mai KT, Kohler DM, Roustan Delatour NL et al (2006) Cytohistopathologic hybrid renal cell carcinoma with papillary and clear cell features. Pathol Res Pract 202:863–868
26. Ljungberg B (1986) DNA content in renal cell carcinoma. A clinical study with special reference to tumor heterogeneity and prognosis. Scand J Urol Nephrol Suppl 100:1–47
27. Ljungberg B, Stenling R, Roos G (1986) DNAcontent and prognosis in renal cell carcinoma. A comparison between primary tumors and metastases. Cancer 57:2346–2350
28. Höglund M, Gisselsson D, Soller M et al (2004) Dissecting karyotypic patterns in renal cell carcinoma: an analysis of the accumulated cytogenetic data. Cancer Genet Cytogenet 153:1–9
29. Granata P, Portentoso P, Minelli E et al (1992) Clonal chromosome changes in renal carcinoma do not correlate with clinical stages and histopathologic grades. Cancer Genet Cytogenet 64:30–34
30. Requena MJ, Carrasco JC, Alvarez-Kindelan J (2008) Role of molecular markers in diagnosis and prognosis of renal cell carcinoma. APAnal Quant Cytol Histol. 30:336-7. Comment on: (2007). Anal Quant Cytol Histol 29:41–49
31. Pospihalj B, Zamparese R, Mazzucchelli R, Morichetti D (2007) Kidney cancer: not a single disease. Anal Quant Cytol Histol 29:377–379

Virchows Arch (2010) 456:85–89
DOI 10.1007/s00428-009-0868-x

ORIGINAL ARTICLE

Can renal oncocytoma be distinguished from chromophobe renal cell carcinoma by the presence of fibrous capsule?

Alma Demirović · Sanja Cesarec · Borislav Spajić · Davor Tomas · Stela Bulimbašić · Milan Milošević · Zlatko Marušić · Božo Krušlin

Received: 13 October 2009 / Revised: 20 November 2009 / Accepted: 23 November 2009 / Published online: 19 December 2009
© Springer-Verlag 2009

Abstract The most important differential diagnosis of chromophobe renal cell carcinoma (CRCC) is renal oncocytoma. Due to overlapping morphological characteristics of renal oncocytoma and CRCC, particularly its eosinophilic variant, making a correct diagnosis can be challenging. To date, no data are available on the presence of the tumor fibrous capsule as a diagnostic feature in differentiating these tumors. The main purpose of this study was to establish the presence and compare the thickness of the tumor fibrous capsule between two tumor groups. A total of 37 tumors—18 cases of CRCC (three eosinophilic and 15 classic) and 19 cases of renal oncocytoma—were analyzed. Four slides of each tumor stained with hematoxylin and eosin were first scanned at low-power magnification (×40) to assess the presence of the capsule. If present, the capsule was measured in three different thickest areas at higher magnification (×200). The mean value of capsule thickness was calculated and taken into consideration. The capsule was present in 12 (66.7%) cases of CRCCs and in only two (10.5%) cases of renal oncocytomas. Statistical analysis showed significant difference between the presence of fibrous capsule in these two observed tumor groups (P=0.001). Average thickness of capsule in CRCCs was 337.7 μm, and 115.4 μm in renal oncocytomas, but the median was not statistically significant (P=0.198). Studies with a larger number of cases are needed to conclude if this characteristic could be a low-cost, reliable microscopic feature in differentiating between CRCC and renal oncocytoma.

Keywords Chromophobe renal cell carcinoma · Renal oncocytoma · Capsule · Morphometry

A. Demirović · D. Tomas · Z. Marušić · B. Krušlin (✉)
Ljudevit Jurak University, Department of Pathology,
Sestre Milosrdnice University Hospital,
Vinogradska cesta 29,
Zagreb, Croatia
e-mail: bkruslin@kbsm.hr

S. Cesarec · D. Tomas · B. Krušlin
School of Medicine, University of Zagreb,
Zagreb, Croatia

B. Spajić
Department of Urology, Sestre Milosrdnice University Hospital,
Zagreb, Croatia

S. Bulimbašić
Department of Pathology, University Hospital Dubrava,
Zagreb, Croatia

M. Milošević
School of Public Health Andrija Štampar,
Zagreb, Croatia

Introduction

In the current World Health Organization (WHO) classification of renal tumors, chromophobe renal cell carcinoma (CRCC) is recognized as a malignant renal cell neoplasm derived from the intercalated cell of the collecting duct, which accounts for 5% of renal epithelial tumors [1]. Two main variants are classic and eosinophilic CRCC. Although considered less aggressive than other renal cell carcinomas, CRCC has a metastatic potential and may undergo sarcomatoid transformation, which is associated with more aggressive behavior [1]. Renal oncocytoma is a benign tumor, which shares a common cellular origin with CRCC and represents 3% to 9% of all primary renal tumors [1]. Due to overlapping morphological characteristics of renal oncocytoma and CRCC, particularly its eosinophilic variant with the abundant granular eosinophilic cytoplasm, making a correct diagnosis can be challenging. In recent years, much effort has been made to identify immunohistochemical markers that could be useful in

differentiating between CRCC and renal oncocytoma [2–6]. However, final decision about the appropriate panel of immunohistochemical markers for the differential diagnosis of CRCC and renal oncocytoma is still being discussed. Hale's iron stain can be particularly useful in differentiating these tumors, but many laboratories have found this stain to be technically challenging and present with variable results [3]. Other authors have attempted to make the distinction on account of nuclear morphometric measurements and features, with the conclusion that a combination of hyperchromatic wrinkled nuclei and perinuclear halos is more often associated with CRCC [7–10]. CRCC is, like cases of clear cell renal carcinoma, according to our experience, in the majority of cases surrounded by a fibrous capsule, separates the tumor tissue from the surrounding renal parenchyma. Unlike CRCC, renal oncocytoma, despite being a benign tumor, lacks the fibrous capsule in a number of cases. The main purpose of this study was to establish the presence and compare the thickness of the tumor fibrous capsule between two tumor groups. According to the English literature, there are no data on similar research in this field.

Patients and methods

Patients

The files from two Departments of Pathology (Ljudevit Jurak University Department of Pathology, Sestre Milosrdnice University Hospital and Department of Pathology, University Hospital Dubrava, Zagreb) from the period between 1999 and 2008 were searched for cases of histologically confirmed CRCC and renal oncocytoma. All cases were reviewed and diagnosis of CRCC, and renal oncocytoma was established according to the criteria proposed by 2004 WHO for classification of renal tumors [11]. There were 37 cases in total: 18 (three eosinophilic and 15 classic) CRCCs and 19 renal oncocytomas. Four slides of each tumor, stained with hematoxylin and eosin, were analyzed. Among patients with CRCC, ten were females, and eight were males. Patients' age ranged from 34 to 76 years (mean, 56.9). Tumor size ranged from 1.7 to 17 cm (mean, 7.9). Nuclear grade for CRCC was assessed according to the Fuhrman classification system [12]. There were ten CRCCs with G2, seven with G3, and one with G4 nuclear grade. Among patients with renal oncocytoma, 12 were females, and seven were males. Patients' age ranged from 47 to 80 years (mean, 65.2). Tumor size ranged from 0.9 to 8 cm (mean, 3.6).

Methods

We analyzed the presence of the tumor fibrous capsule and measured its thickness in the cases of CRCCs and renal oncocytomas. Four slides of each tumor were first scanned at low-power magnification (×40) to assess the presence of tumor fibrous capsule. If present, capsule was measured in three different thickest areas at higher magnification (×200). Morphometric measurements of capsule were done by computerized morphometry system with an Olympus microscope BX51, QuickPHOTO Pro software, and an Olympus Camedia C-5050 camera and were expressed in micrometers. The mean value of capsule thickness was calculated and taken into consideration**.** All samples were examined independently by three observers, and any difference was resolved by a joint review. Statistical analysis was performed using Chi-square test, Spearman's correlation test, Fisher's exact test, and Mann–Whitney test. The level of statistical significance was set as $P<0.05$.

Results

The main clinical and morphometric findings are summarized in Tables 1 and 2. Capsule was present in 12 cases (66.7%) of CRCCs and in only two cases (10.5%) of renal oncocytomas (Fig. 1). Statistical analysis showed significant difference between the presence of fibrous capsule in these two observed tumor groups ($P=0.001$). The capsule in CRCCs was found to encompass the whole tumor circumference on the examined slides, while in cases of renal oncocytomas with capsule, it was formed only partially. Seven cases (36.8%) of renal oncocytomas featured a grossly visible star-shaped central scar, but there was no surrounding fibrous capsule in any of them. Average thickness of capsule in CRCCs was 337.7 μm, and 115.4 μm in renal oncocytomas, but the median was not statistically significant ($P=0.198$). The correlation between tumor size, nuclear grade, and capsular presence in CRCCs showed no statistically significant differences ($P=0.616$, $P=0.091$, respectively). When comparing capsule thickness with tumor size and nuclear grade in CRCCs, no statistically significant differences were found ($P=0.688$, $P=0.533$, respectively). Mean tumor size was higher in CRCCs (7.9 cm) than in renal oncocytomas (3.6 cm). Patients with renal oncocytoma were significantly older compared to patients with CRCC ($P=0.021$). Significant difference in distribution of these two tumor types between male and female was not found ($P=0.743$).

Discussion

The most important differential diagnosis of CRCC is renal oncocytoma. Their distinction is essential since CRCC has malignant potential whereas renal oncocytoma is a benign tumor. Moreover, cases of sarcomatoid transformation of

Table 1 Clinical, histological, and morphometric findings in chromophobe renal cell carcinoma

Case	Age	Gender	Tumor size (cm)	Type	Nuclear grade	Capsule	Capsule thickness (μm)
1	55	F	6.5	Classic	G2	+	83.2
2	53	F	12	Classic	G2	+	295
3	60	F	12	Classic	G2	+	175.7
4	63	M	10	Eosinophilic	G2	+	85.1
5	47	F	1.7	Classic	G3	+	380.4
6	46	M	5.5	Classic	G3	+	218.4
7	60	F	7	Eosinophilic	G2	+	507.9
8	47	F	17	Eosinophilic	G4	+	562.2
9	58	M	3	Classic	G2	+	551.4
10	51	F	8	Classic	G2	−	
11	66	M	6.2	Classic	G3	+	238.5
12	76	M	4.5	Classic	G2	−	
13	49	F	7.5	Classic	G3	+	565.5
14	75	M	11	Classic	G3	+	623.6
15	34	F	12	Classic	G3	−	
16	52	M	6	Classic	G2	−	
17	56	F	5.5	Classic	G2	−	
18	76	M	7.2	Classic	G3	−	

CRCC emphasize the importance of making the accurate diagnosis due to more aggressive behavior of this type of CRCC [1, 13–15]. CRCCs and renal oncocytomas have overlapping morphologic, immunohistochemical, histochemical, and ultrastructural characteristics. Preoperative physical and radiographic examinations are not reliable in distinguishing renal oncocytoma from CRCC, which makes the accurate diagnosis for pathologists even more complicated [16, 17]. Also, the conclusions of studies concerning fine-needle aspiration biopsy results in differentiating these tumors are inconsistent [18–20]. Thus, in the majority of cases, the final diagnosis is made after a histopathological

Table 2 Clinical and morphometric findings in renal oncocytoma

Case	Age	Gender	Tumor size (cm)	Capsule	Capsule thickness (μm)
1	70	F	1.5	+	120.7
2	54	F	3	+	110.1
3	79	F	2.5	−	
4	57	M	4	−	
5	68	F	2.2	−	
6	62	F	3	−	
7	68	M	3	−	
8	70	F	6.5	−	
9	77	M	0.9	−	
10	61	F	1.7	−	
11	55	F	8	−	
12	80	F	6	−	
13	47	M	4.3	−	
14	74	F	2.6	−	
15	52	M	6	−	
16	72	M	3.5	−	
17	69	F	2	−	
18	66	M	3	−	
19	58	F	4.2	−	

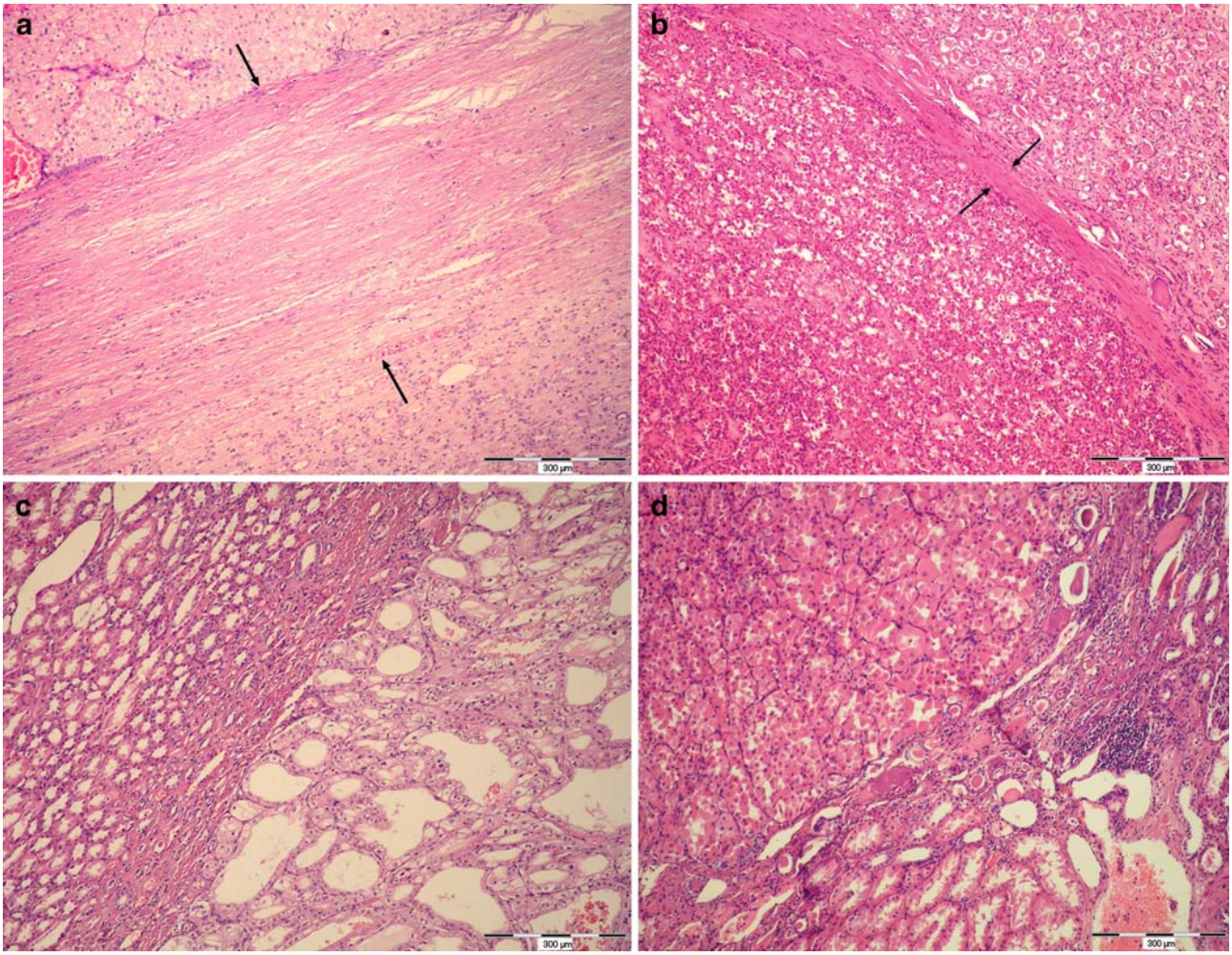

Fig. 1 Chromophobe renal cell carcinoma (**a**) and renal oncocytoma (**b**) surrounded by fibrous capsule. Chromophobe renal cell carcinoma (**c**) and renal oncocytoma (**d**) without fibrous capsule (×100, HE)

evaluation. Under the light microscope, the most important discriminating characteristics are nuclear and cytologic features. Renal oncocytoma has homogeneous nuclear size, round nuclear contours, common binucleation, and discrete nucleoli. However, CRCC in some cases can also have similar appearance although more often with hyperchromatic wrinkled nuclei and perinuclear halos [10]. Entrapped normal tubules in the central or peripheral parts of the tumor could also be the clue to the diagnosis of renal oncocytoma [2]. In the majority of cases, however, a definitive diagnosis can still not be rendered based on these criteria under the light microscope evaluation only. Much effort has been made to identify immunohistochemical markers that could be useful in differentiating between CRCC and renal oncocytoma, such as caveolin-1, CD63, antimitochondrial antibody, cytokeratin 14, cytokeratin 7, vimentin, glutathione S-transferase α, CD10, CD117, claudin-7, claudin-8, and kidney-specific cadherin [2–6]. Antimitochondrial antibodies and parvalbumin are considered to be excellent markers for differentiating between these tumors [21–23]. Also, the combination of three immunohistochemical markers: vimentin, glutathione S-transferase α, and epithelial cell adhesion molecule is highly sensitive and specific for the differential diagnosis of CRCC and renal oncocytoma [4]. Hale's iron stain continues to be a useful histochemical marker in differentiating between these tumors, but many laboratories have found it technically challenging and with variable results [3]. Brunelli et al. [24] analyzed a group of ten renal oncocytomas and 19 CRCCs by fluorescence in situ hybridization to clarify the genetic lesions of these tumors and revealed that detection of losses of chromosomes 2, 6, 10, and 17 could support the diagnosis of CRCC over a renal oncocytoma. These conclusions will hopefully lead to a better understanding of different patterns of genetic anomalies and facilitate the differential diagnosis between CRCC and renal oncocytoma. According to our experience, in a number of cases, CRCC was found to be surrounded by

a fibrous capsule, which separates the tumor tissue from adjacent renal parenchyma. When compared with renal oncocytoma, statistically significant difference in the presence of the fibrous capsule in the two observed tumor groups was striking. Even though the capsule in oncocytomas, when present, was less thick than in CRCCs, the median was not statistically significant due to a small number of cases. In somewhat older literature, surrounding capsule of variable thickness was reported to be a feature of typical oncocytoma [25]. However, in the last WHO classification of kidney tumors, oncocytomas are defined as well-circumscribed, nonencapsulated neoplasms [11]. Interestingly, no data are available on the presence of the tumor fibrous capsule as a diagnostic feature in differentiating these tumors. Shimasaki et al. [26] studied the participation of myofibroblasts in the capsular formation of renal cell carcinomas, with only two cases of CRCC, and concluded that myofibroblasts may participate in the capsular formation of conventional and CRCC. To date, there are no data on similar research regarding renal oncocytoma and comparative analysis with CRCC. Our results show that the capsule is significantly more common and thicker in CRCCs compared to renal oncocytomas. Studies with a larger number of cases are needed to conclude if this characteristic could be a low-cost, reliable microscopic feature in differentiating between CRCC and renal oncocytoma.

Acknowledgment This work was supported in part by the Ministry of Science, Education and Sports, Croatia, project number 108-1081870-1884 and 134-0000000-3381.

Conflict of interest The authors declare that they have no conflict of interest.

References

1. Lopez-Beltran A, Scarpelli M, Montironi R, Kirkali Z (2006) 2004 WHO Classification of the renal tumors of the adults. Eur Urol 49:798–805
2. Mete O, Kilicaslan I, Gulluoglu MG, Uysal V (2005) Can renal oncocytoma be differentiated from its renal mimics? The utility of anti-mitochondrial, caveolin 1, CD63 and cytokeratin 14 antibodies in the differential diagnosis. Virchows Arch 447:938–946
3. Garcia E, Li M (2006) Caveolin-1 immunohistochemical analysis in differentiating chromophobe renal cell carcinoma from renal oncocytoma. Am J Clin Pathol 125:392–398
4. Liu L, Qian J, Singh H, Meiers I, Zhou X, Bostwick DG (2007) Immunohistochemical analysis of chromophobe renal cell carcinoma, renal oncocytoma, and clear cell carcinoma. Arch Pathol Lab Med 131:1290–1297
5. Osunkoya AO, Cohen C, Lawson D, Picken MM, Amin MB, Young AN (2009) Claudin -7 and claudin-8: immunohistochemical markers for the differential diagnosis of chromophobe renal cell carcinoma and renal oncocytoma. Hum Pathol 40:206–210
6. Mazal PR, Exner M, Haitel A et al (2005) Expression of kidney-specific cadherin distinguishes chromophobe renal cell carcinoma from renal oncocytoma. Hum Pathol 36:22–28
7. Castren JP, Kuopio T, Nurmi MJ, Collan YU (1995) Nuclear morphometry in differential diagnosis of renal oncocytoma and renal cell carcinoma. J Urol 154:1302–1306
8. Okon K, Sinczak-Kuta A (2008) Nuclear morphometry as a tool of limited capacity for distinguishing renal oncocytoma from chromophobe carcinoma. Pol J Pathol 59:9–13
9. Tickoo SK, Amin MB (1998) Discriminant nuclear features of renal oncocytoma and chromophobe renal cell carcinoma. Analysis of their potential utility in the differential diagnosis. Am J Clin Pathol 110:782–787
10. Abrahams NA, Tamboli P (2005) Oncocytic renal neoplasms: diagnostic considerations. Clin Lab Med 25:317–339
11. Eble JN, Sauter G, Epstein JI, Sesterhenn IA (2004) World Health Organization classification of tumours. Pathology and genetics of tumours of the urinary system and male genital organs. IARC Press, Lyon
12. Fuhrman SA, Lasky LC, Limas C (1982) Prognostic significance of morphologic parameters in renal cell carcinoma. Am J Surg Pathol 6:655–663
13. Shannon BA, Cohen RJ (2003) Rhabdoid differentiation of chromophobe renal cell carcinoma. Pathology 35:228–330
14. Cheville JC, Lohse CM, Zincke H et al (2004) Sarcomatoid renal cell carcinoma: an examination of underlying histologic subtype and an analysis of associations with patient outcome. Am J Surg Pathol 28:435–441
15. Delahunt B (2009) Advances and controversies in grading and staging of renal cell carcinoma. Mod Pathol 22:S24–S36
16. Choudhary S, Rajesh A, Mayer NJ, Mulcahy KA, Haroon A (2009) Renal oncocytoma: CT features cannot reliably distinguish oncocytoma from other renal neoplasms. Clin Radiol 64:517–522
17. Chao DH, Zisman A, Pantuck AJ, Freedland SJ, Said JW, Belldegrun AS (2002) Changing concepts in the management of renal oncocytoma. Urology 59:635–642
18. Brierly RD, Thomas PJ, Harrison NW, Fletcher MS, Nawrocki JD, Ashton-Key M (2000) Evaluation of fine-needle aspiration cytology for renal masses. BJU Int 85:14–18
19. Wiatrowska BA, Zakowski MF (1999) Fine-needle aspiration biopsy of chromophobe renal cell carcinoma and oncocytoma. Comparison of cytomorphologic features. Cancer Cytopathol 87:161–167
20. Liu J, Fanning CV (2001) Can renal oncocytomas be distinguished from renal cell carcinoma on fine-needle aspiration specimens? A study of conventional smears in conjunction with ancillary studies. Cancer Cytopathol 93:390–397
21. Abrahams NA, Maclennan GT, Khoury JD et al (2004) Chromophobe renal cell carcinoma: a comparative study of histological, immunohistochemical and ultrastructural features using high throughput tissue microarray. Histopathology 45:593–602
22. Martignoni G, Pea M, Chilosi M et al (2001) Parvalbumin is constantly expressed in chromophobe renal carcinoma. Mod Pathol 14:760–767
23. Tickoo SK, Amin MB, Linden MD et al (1997) Antimitochondrial antibody (113–1) in the differential diagnosis of granular cell tumors. Am J Surg Pathol 21:922–930
24. Brunelli M, Eble JN, Zhang S, Martignoni G, Delahunt B, Cheng L (2005) Eosinophilic and classic chromophobe renal cell carcinoma have similar frequent losses of multiple chromosomes from among chromosomes 1, 2, 6, 10 and 17, and this pattern of genetic abnormality is not present in renal oncocytoma. Mod Pathol 18:161–169
25. Petersen RO (1986) Urologic pathology, 2nd edn. J.B. Lippincott Co, Philadelphia
26. Shimasaki N, Kuroda N, Guo L et al (2005) The participation of myofibroblasts in the capsular formation of human conventional and chromophobe renal cell carcinomas. Histol Histopathol 20:67–73

Virchows Arch (2010) 456:91–96
DOI 10.1007/s00428-009-0865-0

ORIGINAL ARTICLE

Thoracic vasculitis presenting as surgical problems

Michael Jansen · Sheikh Saleh · Margot Bolster · Aonghus O'Donnell · Thomas Ahern · Liam Spence · Mary N. Sheppard · Louise Burke

Received: 10 June 2009 / Revised: 13 October 2009 / Accepted: 17 November 2009 / Published online: 10 December 2009
© Springer-Verlag 2009

Abstract We present four patients with vasculitis manifesting with unusual clinical or pathological features, generating surgical problems. Two cases presented with pulmonary hypertension, with investigations and radiological evidence prompting clinical suspicion of pulmonary thrombo-embolic disease. First case, with an antecedant history of Wegener's granulomatosis (WG), demonstrated following "embolectomy", WG involving the large pulmonary elastic arteries. The second case of inoperable "pulmonary thrombo-embolic disease" was subsequently found at limited post mortem to have giant cell arteritis, which affected widespread small peripheral pulmonary arterial vessels. The other two cases were of aortitis occurring in the background of immune-mediated disease, which had been treated with aggressive immunosuppression regimens. The first of these was a case of Cogan's syndrome complicated by descending aortitis, a rarely reported phenomenon, with co-existent acute endocarditis of the aortic valve leaflets. Most cases of endocarditis in this context occur secondary to and in continuity with ascending aortitis. That this case, and a case of ascending aortitis occurring in the context of relapsing polychondritis occurred in the face of aggressive immunosuppression with an apparent clinical response, underscores the need to not accept a clinical picture at face value. This has implications for clinical management, particularly in the follow-up of surgical prosthetic devices such as grafts which may be used in these cases. All four cases emphasise the continued importance of histology and the post-mortem examination in elucidating previously undetected or unsuspected disease.

Keywords Vascular disease · Valve disease · Pulmonary arteries · Aorta/aortic inflammation

M. Jansen (✉) · L. Burke
Department of Histopathology, Cork University Hospital,
Wilton,
Cork, Eire, Ireland
e-mail: jansmichael@gmail.com

S. Saleh
Department of Histopathology, Royal Chesterfield Hospital,
Chesterfield, UK

M. Bolster
Department of Pathology, University College Cork,
Cork,
Eire, Ireland

A. O'Donnell · T. Ahern
Department of Cardiothoracic Surgery, Cork University Hospital,
Wilton,
Cork, Eire, Ireland

L. Spence
Department of Radiology, Cork University Hospital,
Wilton,
Cork, Eire, Ireland

M. N. Sheppard
Histopathology, Royal Brompton and Harefield Trusts,
London, UK

Introduction

Vasculitis both as an isolated phenomenon, or as part of a syndrome affecting multiple tissue types, has protean manifestations and may affect any size vessel. Vasculitis affecting large vessels is notable for its ability to cause significant vascular compromise. Vasculitic disease is also known to mimic other forms of inflammatory disease; a diagnostic problem that can be compounded when well-characterised disease entities present in a nonstereotypic

fashion. Additionally, less common forms of vasculitis resulting from autoimmunity, like that in Cogan's syndrome (CS), remain unusual entities where the full spectrum of disease is still being explored. In this context, the unusual individual case of vasculitis may yet inform and expand our knowledge of disease. Immunosuppression is frequently utilised to retard the inappropriate inflammatory activity, with the effectiveness of therapy being quantified by clinical response and monitoring of serological markers of inflammation. In many autoimmune diseases where vasculitis is a possibility, the cardiovascular system is not routinely monitored and involvement can be missed.

With this backdrop, we present four cases of thoracic vasculitis presenting with or displaying unusual clinical features, each eventually coming to surgery and/or autopsy with material subsequently available for histologic examination. The pivotal role of histology and the autopsy is highlighted, illustrating its ability to reveal previously unsuspected disease. Two cases presented with pulmonary hypertension, prompting strong clinical suspicion of pulmonary thrombo-embolic disease with subsequent surgical intervention to remove the "emboli". The other two cases are those of an aortitis occurring in the background of an immune-mediated disease process ultimately requiring surgery in spite of aggressive immunosuppression.

Materials and results

Case 1

A 34-year-old female, with a known diagnosis of Wegener's granulomatosis (WG), presented in early 2001 with a history of increasing dyspnoea without chest pain or haemoptysis. A histologically proven diagnosis of WG was made in 1993 with an initial presentation of persistent nasal obstruction. Antineutrophil cytoplasmic antibody, antiproteinase 3 had been documented as positive on multiple occasions and her therapy included intravenous cyclophosphamide, azathioprine, corticosteroids and various antibiotics. Echocardiogram revealed an elevated pulmonary artery pressure estimated at 90 mmHg with right ventricular and atrial dilatation and tricuspid regurgitation. Computed tomography pulmonary angiography showed smooth soft tissue filling defects within the right and left main pulmonary arteries (MPA) with extension from the origin of the right MPA into the upper and lower lobe branches. In the left MPA, only focal severe stenosis was seen. These features were interpreted as evidence of thrombo-embolism and a surgical pulmonary "embolectomy" was performed. At surgery, hard adherent tissue was seen within the proximal pulmonary artery and this was submitted for histopathology.

Microscopically, the specimen showed vasculitis of the pulmonary artery (see Fig. 1). There was a mixed inflammatory cell infiltrate with abundant lymphocytes, plasma cells and occasionally foamy histiocytes within the artery wall (see Fig. 2) with areas of basophilic geographic necrosis surrounded by palisading histiocytes and multinucleate giant cells. Stains for mycobacteria and fungi were negative. The appearances were of a giant cell vasculitis with features in keeping with Wegener's granulomatosis affecting the main pulmonary artery.

Case 2

A 45-year-old female with a history of Crohn's disease and systemic hypertension presented in 1995 with shortness of breath and was transferred to the Royal Brompton Hospital, London, with a clinical diagnosis of thrombo-embolic pulmonary hypertension. An angiogram performed on admission revealed occlusion of the right upper lobe, right middle lobe, left upper lobe and left lingula pulmonary arteries. She was treated with insertion of a Greenfield inferior vena cava filter and anticoagulated using Warfarin. Her lupus anticoagulant and anticardiolipin antibodies were strongly positive. 15 months later, she represented with worsening shortness of breath and marked exercise intolerance. Although surgical intervention was attempted, the thrombi occluding the arteries were too peripherally lodged to permit removal. She died shortly after surgery in right-sided heart failure. Post-mortem examination revealed that the left and right main pulmonary arteries showed slightly raised atherosclerotic plaques. The lobar branches were normal. All segmental arteries showed focal narrowing and abrupt occlusion of branches by thrombi and occlusion of peripheral vessels by firm white fibrotic tissue with subpleural scarring. Histology of the segmental arterial

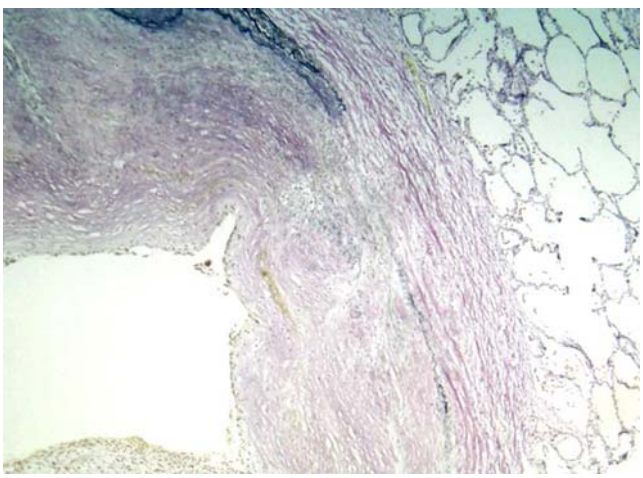

Fig. 1 Muscularized small pulmonary artery from Case 1 showing intimal proliferation and destruction of the elastic lamina with replacement by fibrosis. Elastic von Gieson ×5

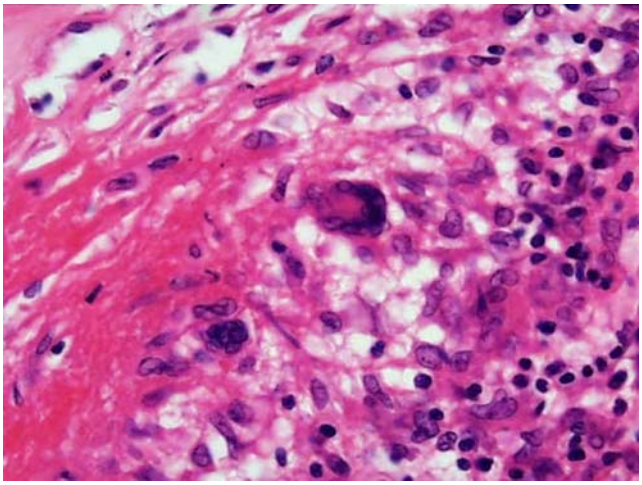

Fig. 2 High power photomicrograph of the same artery from Case 1 in Fig. 1 showing histiocytes and giant cells with accompanying mononuclear inflammatory infiltrate HE ×20

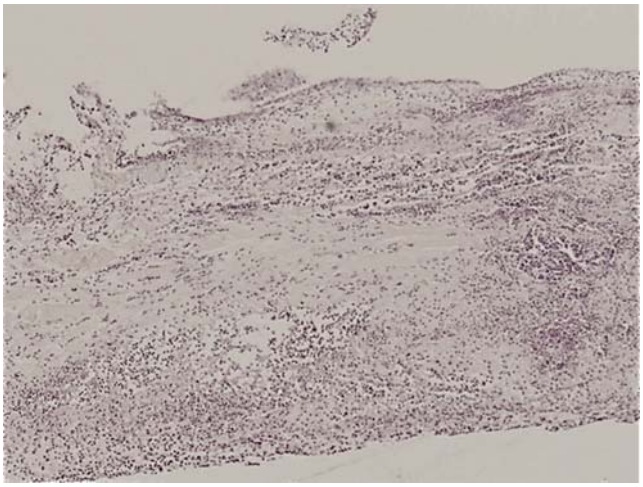

Fig. 3 Aortic valve cusp from Case 3 showing extensive acute inflammation HE ×4

branches showed a giant cell vasculitis with destruction of the media complicated by thrombosis with luminal occlusion. Smaller muscular vessels throughout the lung parenchyma showed luminal occlusion by fibrous tissue with evidence of recanalisation and replacement of vessel wall by fibrosis. There was no evidence of granulomas in the lung parenchyma, heart or lymph node and no evidence of generalised vasculitis in the coronary vessels, the aorta and its branches. The features were those of a giant cell arteritis with associated thrombosis. Because the autopsy was limited to the chest, it was not possible to assess if there was vasculitis affecting other organs.

Case 3

A 38-year-old female with a diagnosis of Cogan's syndrome made 3 months earlier developed palpitations. Echocardiogram showed good left ventricle function with mild to moderate aortic regurgitation and mild mitral regurgitation. An initially normal cardiovascular exam was documented. Blood tests showed raised ESR and CRP, an autoimmune serology screen was negative. Abdominal imaging revealed an aneurysmal dilation of the descending aorta with a maximal measurement of 4 cm. in the antero-posterior dimension. Immunosuppression was increased and included steroids and cyclophosphamide. One month later, she was admitted to hospital with biventricular failure and severe acute aortic regurgitation and an immediate salvage aortic valve replacement was performed. One cusp was sent for microbiological culture and failed to grow an organism. At histology, the other two cusps grossly showed tiny cream-coloured foci on the surface. Microscopically, there was severe acute endocarditis with microabscess formation and fibrinoid necrosis (see Fig. 3). Special stains for organisms were negative. She died shortly after surgery from an intracerebral haemorrhage. At post-mortem examination, the ascending aorta and the great vessels of the head and neck were normal. Distal to the origin of the left subclavian artery the thoracic aorta was dilated with a circumference of 70 mm. The intima showed a “cobble-stoned” appearance and the wall was thickened (see Fig. 4). There was no ulceration or thrombosis in the aorta. Microscopic examination of the ascending aorta and aortic arch vessels was normal. The descending aorta distal to the subclavian artery origin showed marked aortitis with intimal proliferation and fibrosis, as well as infiltration of the intima and adjacent media by neutrophil leukocytes surrounding areas of medial necrosis with focal transmural destruction in the upper abdominal aorta. The vasa vasorum extended into the media and were surrounded by a chronic inflammatory,

Fig. 4 Aorta from Case 3 showing marked wall thickening with intima showing a cobblestoned appearance

predominantly lymphocytic, infiltrate. Macrophages were prominent, with very occasional giant cells noted. These changes extended from the descending thoracic aorta into the upper and lower abdominal aorta and involved the mesenteric vessels and the iliac vessels, with sparing of the renal vessels. The brain was not examined at the family request. The features were those of a florid acute on chronic aortitis with aortic valve endocarditis complicating Cogan's syndrome.

Case 4

A 54-year-old woman was diagnosed with relapsing polychondritis with involvement of ear and nasal cartilage as well as scleritis. An echocardiogram revealed mild aortic regurgitation. In 1999, she experienced a flare up of her disease, with scleritis, worsened aortic regurgitation and elevation of serological markers of inflammatory activity. She was managed with increased immunosuppression with steroids and azathioprine. Subsequent echocardiogram revealed worsening aortic regurgitation with dilation of the aortic root and an ascending aortic aneurysm, prompting the introduction of cyclophosphamide to her immunosuppressant regime. Her ESR was decreased from 90 to 24 mm/h over 4 months, and her immunosuppressant dose was reduced. At this stage magnetic resonance imaging of the chest showed an aneurysm of the ascending aorta extending from the sinotubular junction to beyond the right innominate artery. One month later, aortic valve replacement and aortic root replacement were performed. Pathological examination of the aorta showed a thickened wall measuring 5 mm with pronounced irregularity of the intimal surface (see Fig. 5). Histologically, intimal fibrosis and infiltration by acute and chronic inflammatory cells was noted. The medial elastic tissue was destroyed and replaced by vascular granulation tissue and focal necrosis. The vasa vasorum extended throughout the aortic wall, with surrounding chronic inflammation and endothelial swelling. Neutrophil leukocyte aggregates forming microabscesses were present in the media and intima. The adventitia showed focal lymphoid infiltration and fibrosis. Special stains for bacteria and fungi were negative. No giant cells, granulomas or eosinophils were present. The features were consistent with an aortitis associated with polychondritis.

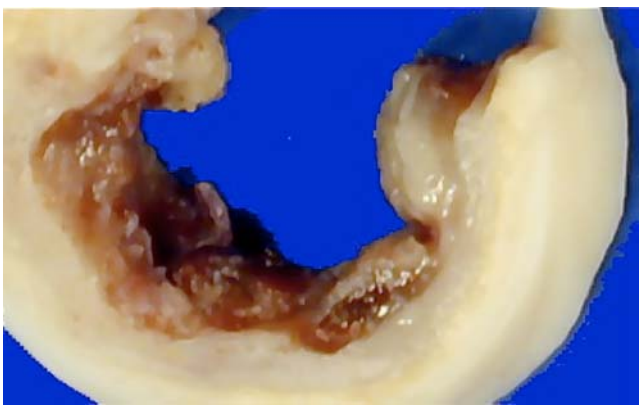

Fig. 5 Aorta from Case 4 showing marked intimal thickening and wall fibrosis

Discussion

Vasculitic disorders can present in many ways as highlighted by these thoracic cases and recognition of these diverse manifestations is important. Vasculitides are classified according to the size of the involved vessels. The pathological patterns of large vessel vasculitides are Buerger's disease, temporal arteritis, Takayasu's disease, Behcet's disease, infectious arteritides and rheumatologic diseases [1]. Buerger's disease is a thrombotic arteriopathy with no arterial wall involvement. Temporal arteritis and Takayasu's disease belong to the group of giant cell arteritides. In temporal arteritis, the inflammation is prominent in the internal part of the media with intimal thickening and subsequent occlusion. In Takayasu's disease, the external part of the media is prominently involved with fibrous thickening of the arterial wall with stenosis. Rheumatologic diseases usually result in giant cell aortitis with aortic valve incompetence. The first two cases illustrate that vasculitis involving the pulmonary arteries can mimic thrombo-embolism with progression to surgery in both cases. Vasculitis of the pulmonary artery has been attributed to either Takayasu's arteritis [2, 3], or giant cell arteritis [4], with patients presenting with evidence of pulmonary artery obstruction mimicking thrombo-embolic disease, pulmonary hypertension and severe haemoptysis. WG does not usually involve the large elastic arteries and to our knowledge this is the first reported case of WG affecting the main pulmonary arteries, here presenting clinically as a mimic of pulmonary thrombo-embolic disease. There has been one case report of a link between Wegener's granulomatosis and Takayasu's aortitis found in an autopsy case [5] and an overlap with giant cell arteritis has been reported in atypical presentations of Wegener's granulomatosis [6]. In case 2, the history of Crohn's disease may be important since this is linked to granulomatous lesions in airways and elsewhere [7] but again there has been no previous link to pulmonary artery vasculitis. As in the WG case, there has one case report linking Crohn's disease to aortitis [8]. The finding of antiphospholipid antibody pointed to thrombosis with microvascular angiopathy in the lung but there is no link to giant cell vasculitis. There has been one previous report of similar giant cell vasculitis involving the pulmonary artery and aorta in a

young woman presenting with signs and symptoms of chronic thrombo-embolic pulmonary hypertension who also underwent pulmonary thrombo-endarterectomy with concomitant coronary artery bypass [9]. It is important to differentiate forms of vasculitis from chronic thrombo-embolic pulmonary hypertension because management of these differ considerably. The outcome for both the above patients could have been different if vasculitis had been considered.

Granulomatous vasculitis due to infection is always an important diagnosis to exclude, particularly in patients treated with immunosuppressive agents.

The two cases of aortitis emphasise that involvement of large vessels occurs in these rare autoimmune diseases of Cogan's syndrome and relapsing polychondritis, and that vasculitis can progress despite diagnosis and therapy, requiring surgery in both cases. These two cases also emphasise that both acute and chronic inflammatory cells are seen in blood vessels in these conditions.

Typical CS is a disease of young adults consisting of flares of interstitial keratitis and vestibuloauditory dysfunction with deafness. The demonstration of autoantibodies to inner ear and endothelial antigens [10] indicates that autoimmunity could initiate or perpetuate an abnormal immune response. The prognosis of typical CS is excellent but life-threatening aortic insufficiency develops in 10% of reported cases [11]. The features of our case of CS are noteworthy for several reasons. The acute aortic valve endocarditis occurred in the background of intensive immunosuppressive therapy, making the exclusion of infective aetiology mandatory. Also, despite therapy, there was florid acute and chronic inflammation in both the aortic valve leaflets and the aortic wall. Most valve lesions mentioned in case reports of CS, occur with a contiguous ascending aortitis, a feature not present in this case. Involvement of the aortic cusps, with an uninvolved ascending aorta and an acute descending and abdominal aortitis has not been described before.

Relapsing polychondritis (RP) is a rare multisystem autoimmune disease of unknown origin characterised by recurrent episodes of inflammation and progressive destruction of cartilaginous tissues. Additionally proteoglycan-rich structures of the eye, heart, blood vessels or inner ear may all be affected. In most patients, RP manifests in a fluctuating but progressive course. An immunological basis is hypothesised following the demonstration of serum antibodies to type II collagen in up to two thirds of cases. Cardiovascular complications are documented in 25% of patients and include aortic and mitral regurgitation, aortic aneurysm, aortic dissection, myocarditis, pericarditis, atrioventricular block and systemic vasculitis [12]. The aortitis is usually lymphocytic infiltration around the vasa vasorum of the media accompanied by fragmentation and loss of the elastic tissue with fibrous replacement. Of special interest in this case is the presence of florid acute inflammation of all three layers of the aortic wall with microabscess formation despite aggressive immunosuppression with clinical improvement and a documented decline in serological markers of inflammatory activity, highlighting the importance of careful cardiological follow up in these cases. Therefore, we recommend close and prolonged follow-up: firstly because there can be early paravalvular prosthetic leakage due to the friability of the tissue to which it has been anchored in all cases of aortitis; secondly because aortic aneurysms occur frequently in relapsing polychondritis, may be multiple, may involve all parts of the aorta and result in fatal rupture even in asymptomatic patients; and thirdly because there can be a fatal outcome due to other organ involvement, like airway obstruction, acute glomerulonephritis or systemic vasculitis.

In conclusion, this paper reports four unusual cardiopulmonary vascular complications of four different diseases, all with an autoimmune basis, leading to surgery in each case. Two of these cases presented clinically and radiologically with evidence of pulmonary thrombo-embolic disease. One of the cases, with an antecedent history of Wegener's granulomatosis, was shown following “embolectomy”, to have a WG lesion affecting the large pulmonary elastic arteries, a finding heretofore not reported in the literature. The second case of “pulmonary thrombo-embolic disease” was found at limited post mortem to have giant cell arteritis affecting widespread small peripheral pulmonary arterial vessels. The association with positive serology for anticardiolipin antibodies, a finding suggestive of primary antiphospholipid syndrome, has also previously not been reported. We further reported a case of Cogan's syndrome, complicated by descending aortitis, a rarely reported phenomenon, with co-existent acute endocarditis of the aortic valve leaflets. This scenario, too, has not been previously reported, with the occasional cases with aortic valve inflammation usually arising consequent to and in continuity with ascending aortitis. That this case and the ascending aortitis occurring in relapsing polychondritis described above occurred in the face of an aggressive immunosuppressive regimen including cyclophosphamide with an apparent clinical response, again underscores the need to not accept a clinical picture at face value. A similar point can be made with the WG case where the patient developed pulmonary vasculitis despite therapy. If patients develop new symptoms related to the cardiovascular system they should be clinically investigated. These cases emphasise the need for the surgeon to be aware of these rare entities and plan his surgery accordingly and also emphasise the importance of histology and the post-mortem examination in elucidating previously undetected or unsuspected disease.

Conflicts of interest statement We declare that we have no conflicts of interest.

References

1. Bruneval P (1999) Pathology of large vessel vasculitides. Rev Med Interne 20:875–887
2. Koyabu S, Isaka N, Yada T et al (1993) Severe respiratory failure caused by recurrent pulmonary hemorrhage in Takayasu's arteritis. Chest 104:1905–1906
3. Elsasser S, Soler M, Bolliger C et al (2000) Takayasu disease with predominant pulmonary involvement. Respiration 67:213–215
4. Chassagne P, Gligorov J, Dominique S (1995) Pulmonary artery obstruction and giant cell arteritis. Ann Intern Med 122:732
5. Mejia-Hernandez C, Alvarez-Mendoza A, DeLeon-Bojorge B (1999) Takayasu's arteritis coexisting with Wegener's granulomatosis in a teenager with renal insufficiency: case report. Pediatr Dev Pathol 2:385–388
6. Leavitt RY, Fauci AS (1992) Less common manifestations and presentations of Wegener's granulomatosis. Curr Opin Rheumatol 4:16–22
7. Rogler G, Scholmerich J (2004) Extraintestinal manifestations of inflammatory bowel disease. Med Klin (Munich) 99:123–130
8. Wackerlin A, Zund G, Maggiorini M et al (1997) Aortic valve insufficiency in Crohn disease. Schweiz Med Wochenschr 127:935–939
9. Brister SJ, Wilson-Yang K, Lobo FV et al (2002) Pulmonary thromboendarterectomy in a patient with giant cell arteritis. Ann Thorac Surg 73:1977–1979
10. Lunardi C, Bason C, Leandri M et al (2002) Autoantibodies to inner ear and endothelial antigens in Cogan's syndrome. Lancet 360:915–921
11. Haynes BF, Kaiser-Kupfer MI, Mason P et al (1980) Cogan syndrome: studies in thirteen patients, long-term follow-up, and a review of the literature. Medicine (Baltimore) 59:426–441
12. Del Rosso A, Petix NR, Pratesi M et al (1997) Cardiovascular involvement in relapsing polychondritis. Semin Arthritis Rheum 26:840–844

Virchows Arch (2010) 456:97–103
DOI 10.1007/s00428-009-0863-2

ORIGINAL ARTICLE

Morphological and immunophenotypic features of primary and metastatic giant cell tumour of bone

M. Alberghini · K. Kliskey · T. Krenacs · P. Picci · L. Kindblom · R. Forsyth · N. A. Athanasou

Received: 7 September 2009 / Revised: 10 November 2009 / Accepted: 16 November 2009 / Published online: 15 December 2009
© Springer-Verlag 2009

Abstract Giant cell tumour of bone (GCTB) is a primary tumour of bone that may rarely, in the absence of malignant cytological features, produce metastatic lesions, most commonly in the lungs. Whether these lung nodules represent true neoplastic secondaries or implants derived from the primary tumour is not certain. In this study, we have analysed the morphological and immunophenotypic features of 19 conventional GCTBs and corresponding lung nodules for expression of macrophage, osteoclast, proliferation and tumour-associated markers. A striking morphological feature of all GCTBs that produced lung secondaries was the presence of large areas of haemorrhage and thrombus formation; mononuclear and multinucleated cells of GCTB were frequently found within these areas of haemorrhage and thrombus. A similar pattern of CD14, CD33, HLA-DR and CD51 expression was seen in macrophages and giant cells in primary and secondary tumours. Smooth muscle actin expression was frequently noted in primary GCTBs that recurred and metastasised. No difference was seen in the expression of p53, p63, Ki-67, cyclin D1 or Bcl-2 in primary and secondary tumours. Our findings suggest that most lung nodules associated with primary conventional GCTBs are implants derived from tumour emboli formed in areas of haemorrhage and thrombus formation within the primary tumour.

Keywords Giant cell · Bone tumour · Osteoclast · Metastasis

M. Alberghini · P. Picci
Istituto Ortopedico Rizzoli,
Bologna, Italy

K. Kliskey · N. A. Athanasou (✉)
Nuffield Department of Orthopaedics,
Rheumatology and Musculoskeletal Sciences,
University of Oxford,
Nuffield Orthopaedic Centre,
Oxford OX3 7LD, UK
e-mail: nick.athanasou@ndorms.ox.ac.uk

T. Krenacs
1st Department of Pathology and Experimental Cancer Research,
Semmelweis University,
Budapest, Hungary

L. Kindblom
Royal Orthopaedic Hospital,
Birmingham, UK

R. Forsyth
N. Goormaghtigh Institute of Pathology,
Ghent, Belgium

Introduction

Giant cell tumour of bone (GCTB) is a primary tumour of bone characterised by the presence of numerous osteoclast-like giant cells and a mononuclear component that includes proliferating mononuclear stromal cells and infiltrating macrophages [1, 2]. GCTB has a variable and unpredictable course, in most cases behaving as a benign, but progressively enlarging lesion which can extend through the bone cortex into surrounding soft tissues. GCTB frequently recurs following curettage and can produce metastatic lesions, most commonly in the lungs in approximately 2–3% of patients [3–8].

Lung metastases of conventional GCTB are reported to grow slowly and show some morphological resemblance to the original primary tumour [1–3, 5, 6]. These tumours are distinct from lung secondaries of a primary GCTB which has undergone sarcomatous transformation and contains malignant tumour cells. Metastatic lung nodules associated with conventional GCTB can present at the time of initial

surgery or develop many years after the appearance of the primary tumour. Although these lung nodules do not exhibit cytological features of malignancy, it is not certain whether they represent tumour implants rather than true neoplastic secondaries.

Radiologically aggressive (Enneking stage III) GCTBs are more prone to develop lung metastases, and these lung nodules develop more commonly in patients who have been treated for recurrent tumours [4–6, 9]. As a consequence, it has been suggested that the lung nodules could represent tumour emboli induced by repeated surgery [10]. Vascular invasion by GCTB has been reported in up to 30% of cases, although its precise incidence is unclear [2, 6, 10, 11], and no clear association has been established between vascular invasion in primary conventional GCTB and the development of lung nodules [2, 6, 9, 10].

In this study, we have analysed the morphological and immunophenotypic features of a large series of primary conventional GCTBs that metastasised to the lung, as well as corresponding features in the metastatic lung nodules. We have examined the expression of macrophage, osteoclast and stromal cell markers as well as expression of proliferation, apoptosis and tumour-associated antigens in these tumours. These findings have also been compared to a series of primary (non-recurrent/non-metastatic) GCTBs. Our aim has been to determine whether identification of specific morphological and immunophenotypic features in primary and metastatic GCTBs may provide a clue as to the pathogenetic mechanism which leads to lung metastasis in these tumours.

Materials and methods

Tumour specimens were obtained from Istituto Ortopedico Rizzoli, Bologna, Nuffield Orthopaedic Centre, Oxford and Royal Orthopaedic Hospital, Birmingham; ethical approval for analysis of the tissues from all these cases was obtained. Clinical details of these cases are shown in Table 1.

Morphological findings in haematoxylin–eosin-stained sections of 19 primary cases of conventional giant cell tumour which metastasised to the lung were examined. In 17 of these cases, histology of the lung nodules derived from these tumours was also available for examination. A tissue microarray (TMA) containing 70 sample cores (2 mm) of these primary and secondary GCTBs was made using a computer-guided instrument TMA Master (3DHistech Ltd, Budapest, Hungary), and sections of the TMA were cut and processed for immunohistochemistry. A TMA containing 80 sample cores of 40 primary GCTBs which had neither recurred nor metastasised was similarly made and processed.

The immunophenotypic features of primary and secondary tumours were studied using a panel of monoclonal antibodies directed against macrophage (CD14, human leucocyte antigen-DR (HLA-DR)), osteoclast (CD51), blood vessel endothelial cell (CD31, CD34, factor 8), lymphatic endothelial cell (podoplanin and LYVE-1), smooth muscle actin (SMA) and proliferation (Ki-67), apoptosis (bcl-2) and tumour-associated (cyclin D1 p53, p63,) markers. Immunohistochemistry was carried out using a NovoLink (Leica-NovoCastra) polymer peroxidise detection kit. Monoclonal antibodies used in this study are shown in Table 2. Immunostained TMA slides were taken to whole-slide scanning using a Mirax Scan (3DHistech), and spots as digital slides linked with patient data were scored and analysed. All markers were scored as weak (+), moderate (++) and strong (+++), depending on the number of positive mononuclear cells and their intensity, setting up threshold values as <5%, 5–20% and >20%, respectively (Table 3).

Results

Morphological findings in primary and secondary GCTBs

Morphologically, all primary and recurrent GCTBs which produced lung nodules contained both giant cell and mononuclear cell components typical of GCTB. Morphological features varied not only between tumours but also in different areas of the primary tumour. In general, osteoclast-like cells were numerous and widely scattered throughout the tumour. Focally, areas of spindle-shaped mononuclear stromal cells predominated and were associated with a variable degree of collagen formation; in some areas, proliferating stromal cells were disposed in a storiform pattern. Osteoid and/or woven bone formation by mononuclear stromal cells was seen, and spindle-shaped mononuclear cells showed variable, occasionally frequent typical mitotic activity (one to 15 mitotic figures per 10 high-power fields (HPF)); none of the tumours showed marked cytological atypia or features suggestive of malignancy. Aneurysmal bone cyst formation was seen in five of the tumours. The tumours were highly vascular and frequently contained dilated thin-walled blood vessels.

A prominent feature in all primary GCTBs which produced lung nodules was the presence of large areas of haemorrhage with formation of thrombus that in some cases was undergoing organisation and contained both giant cell and mononuclear components of the tumour (Fig. 1a, b). Vascular invasion at the periphery of the tumour was seen in three of the 19 tumours.

GCTB lung nodules were generally small. They contained a variable number of osteoclast-like giant cells and a proliferation of mononuclear cells which showed typical mitotic activity but no nuclear atypia (Fig. 1c). In general, the number of giant cells was fewer than in the primary tumours. Cytologically, the metastatic lung nodules

Table 1 Details of metastatic giant cell tumour cases

Sex/age at diagnosis	Site	Onset of lung metastasis (months)	Follow-up
F/25	Radius distal	11	Alive at 6 years
F/37	Femur distal	37	Alive at 17 years
F/19	Radius distal	48	Alive at 9 years
F/16	Vertebra	15	Alive 6 years
F/23	Radius distal	14	Alive at 6 years
M/22	Vertebra	14	Died from causes related to growth of primary GCTB
M/62	Femur distal	23	Alive at 10 years
F/32	Ischium	25	Alive at 27 months
M/27	Humerus proximal	11	Alive at 12 years
M/39	Fibula proximal	At diagnosis	Died from causes other than GCTB at 66 months
F/23	Femur distal	44	Alive at 8 years
M/22	Radius distal	14	Alive at 17 years
F/29	Femur distal	33	Alive at 13 years
F/27	Femur distal	5	Alive at 39 months
M/30	Femur distal	At diagnosis	Alive at 62 months
M/40	Femur distal	13	Alive at 30 months
M/41	Femur distal	72	Alive at 12 years
F/24	Tibia distal	At diagnosis	Alive at 12 years
F/27	Vertebra L4	At diagnosis	Alive at 8 years

were relatively bland, and there was no marked nuclear atypia. None of the lung nodules exhibited a high mitotic rate or showed cytological features of malignancy.

In the TMAs of the control group of 40 primary GCTBs which neither recurred nor metastasised, osteoclast-like giant cells were generally numerous, and there was a variable proliferation of mononuclear stromal cells and

Table 2 Monoclonal antibodies used in this study

Antigen	Antibody	Source	Dilution
CD14	NCL-CD14	Novocastra	1:50
CD51	NCL-CD51	Novocastra	1:150
HLA-DR	CR3/43	Dako	1:20
Ki-67	Mib-1	Dako	1:200
CD68	KP1	Dako	1:1,000
bcl2 oncoprotein	124	Dako	1:40
SMA	1A4	Dako	1:50
p53	Do7	Novocastra	1:200
p63	A4A	Thermo Lab Vision	1:150
Her2	CB11	Thermo Lab vision	1:200
Cyclin D1	SP4	Thermo Lab Vision	1:100
CD34	Q Bend 10	Dako	1:20
CD31	JC 70	Dako	1:20
LYVE-1	Anti-LYVE-1	IMM Oxford	1:250
Podoplanin	D 240	Sigma	1:100
CD33	WM-54	Dako	1:25

Table 3 Antigenic phenotype of mononuclear and multinucleated cells in primary and secondary giant cell tumours of bone

Antigen	Mononuclear cells	Multinucleated cells
CD14	++/+++	–
CD51	+	+++
HLA-DR	+++	–
Ki-67	+/++	–
CD68	+/++	+++
bcl2	+	+
SMA	++/+++	–
p53	+	–
p63	+	–
Her2	–	–
cyclinD1	+	+
CD34	+[a]	–
CD31	+[a]	–
LYVE-1	–	–
Podoplanin	–	–
CD33	++/+++	+++

A similar immunophenotypic reaction was seen in all primary and secondary GCTBs

+ weak reaction, ++ moderate reaction, +++ strong reaction

[a] Blood vessel endothelial cell staining only

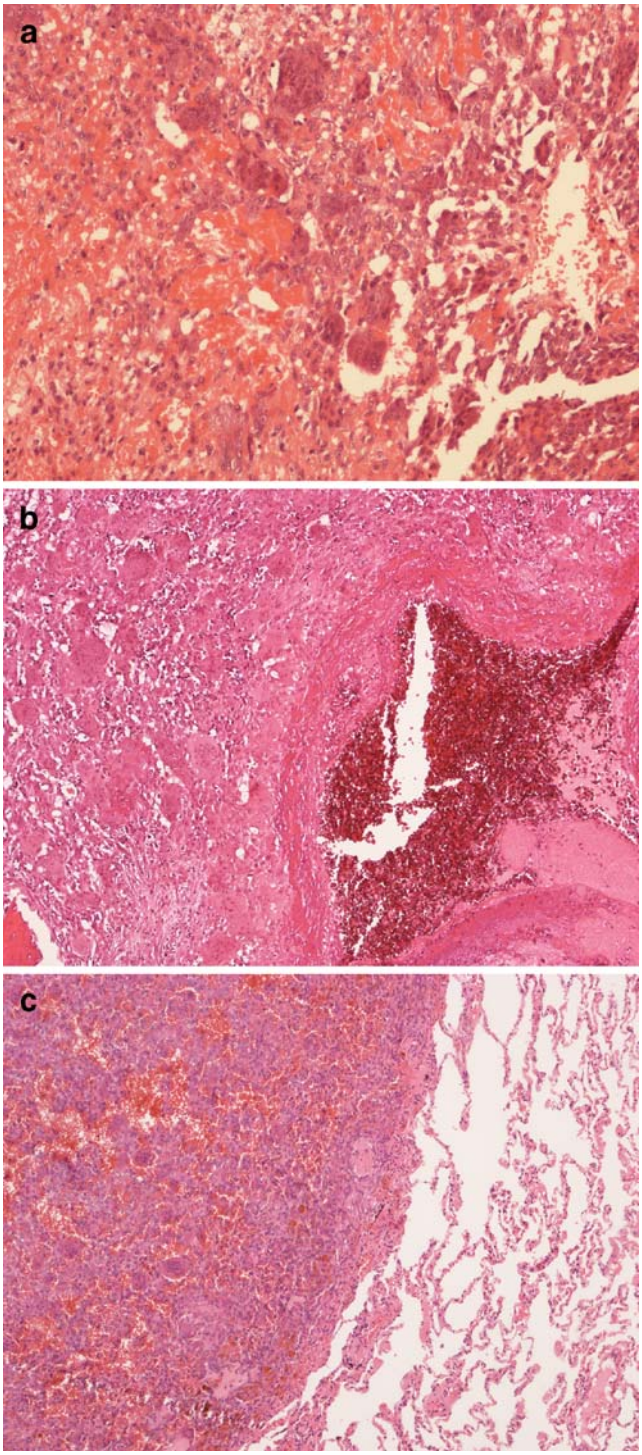

Fig. 1 Areas of **a** haemorrhage and **b** thrombus formation containing mononuclear and multinucleated cells in a primary conventional GCTB and **c** corresponding lung nodule in this case

collagen within these tumours. The number of mitotic figures per 10 HPF was highly variable, with some tumours containing up to 10 mitotic figures per HPF. Small areas of haemorrhage were seen in 16 of these tumours, but none of the tumours contained large areas of haemorrhage; no evidence of thrombus formation was seen in any of the control group tumours.

Immunophenotypic features of primary and secondary GCTBs

Results of immunohistochemical studies are shown in Table 3. Mononuclear stromal cells in both primary and secondary GCTBs strongly expressed HLA-DR and SMA (Figs. 2 and 3). SMA expression by mononuclear cells was variable in primary GCTBs, but in some tumours, particularly recurrent GCTBs, SMA was strongly expressed. Frequently, the same degree of HLA-DR and SMA expression was seen in both primary tumours and lung nodules (Fig. 3). Expression of the proliferation-associated marker Ki67 and the proto-oncogene cyclin D1 was noted in mononuclear cells in both primary and secondary tumours. No difference was seen in the expression of p53, p63 and bcl-2 in primary and secondary tumours; no appreciable Her2 membrane staining for the epidermal growth factor receptor type 2 was noted in any of the cases tested.

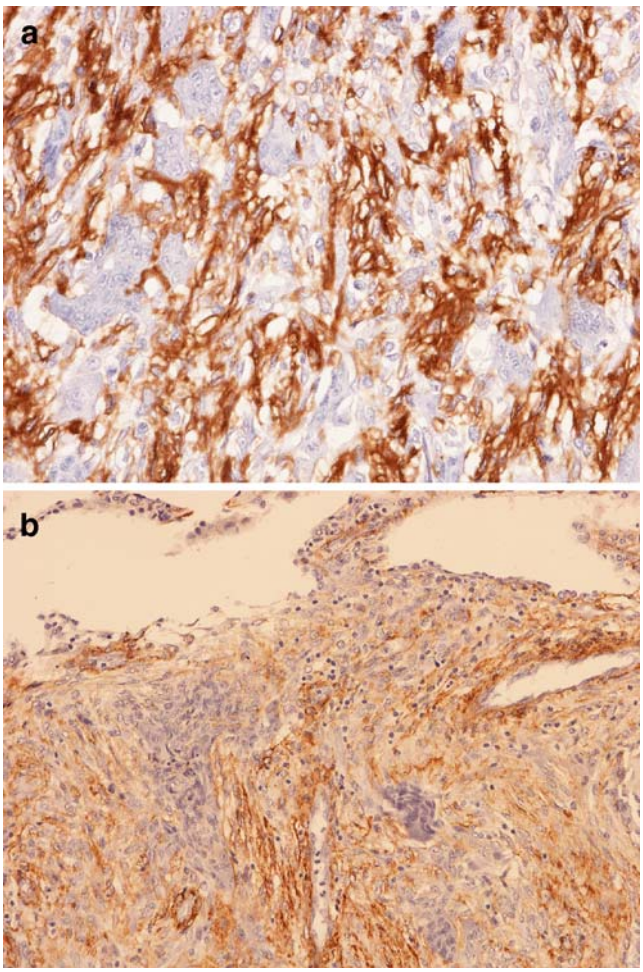

Fig. 2 Expression of SMA by mononuclear cells in **a** primary GCT and **b** corresponding lung nodule

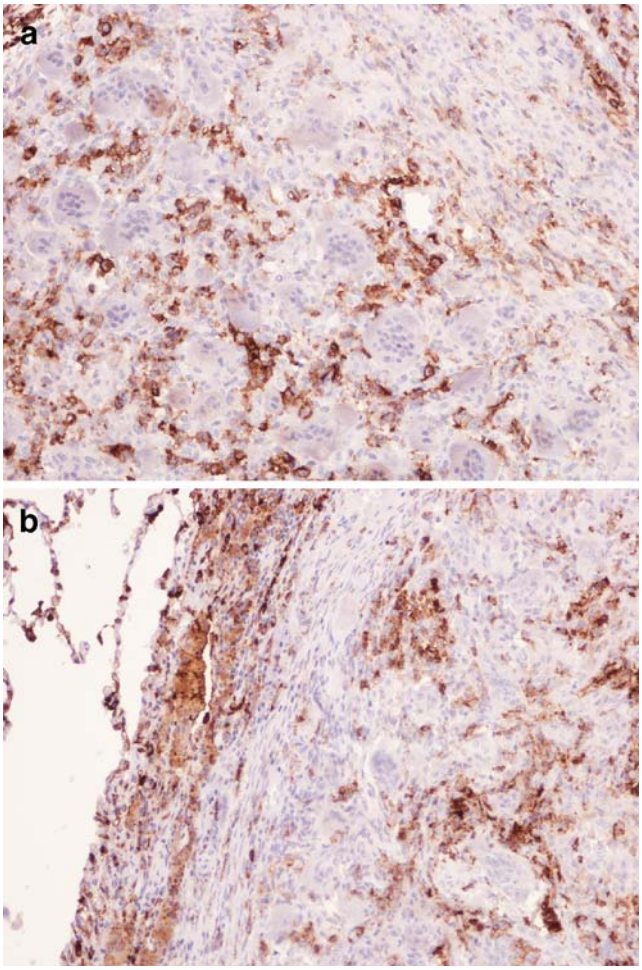

Fig. 3 Expression of HLA-DR in **a** primary GCTB and **b** corresponding lung nodule

As previously noted [12, 13], macrophage-like mononuclear cells in primary GCTB expressed CD14, CD33 and HLA-DR and the osteoclast-like giant cells in GCTB expressed CD51 and CD33 but did not express CD14 or HLA-DR. Fewer mononuclear cells expressed CD51 compared with CD14 and CD33. Mononuclear and multinucleated cells in lung nodules showed a similar pattern of expression of macrophage and osteoclast markers (Figs. 3 and 4).

Both primary and secondary tumours were highly vascular and contained numerous small blood vessels which were lined by endothelial cells that expressed CD31 and CD34. There was no expression of the lymphatic endothelial cell markers, LYVE1 or podoplanin in primary GCTBs.

An identical pattern of expression of HLA-DR, SMA, p53, p63 and bcl2 was seen in mononuclear stromal cells in the control group of 40 primary (non-metastatic, non-recurrent) GCTBs. Giant cells in these tumours, as expected, expressed an osteoclast phenotype (CD51+/CD33+/CD14−/HLA-DR−). A similar pattern of vascular endothelial marker expression was also noted in these tumours.

Discussion

It is known that the pulmonary metastases that develop in patients with conventional GCTBs are usually solitary or few in number and that these tumours grow slowly and have a long doubling time [4–7]. Surgically unresected lung metastases in such cases have been reported to remain stationary or even spontaneously regress without therapy [5, 6, 14]. These observations have been interpreted by some investigators to support the concept of "benign metastasis" whereby the lung nodules are thought to result from implantation of tumour emboli that have seeded to the lung from a primary GCTB [7, 10, 11]. The morphological and immunophenotypic findings in the primary GCTBs and corresponding lung nodules that we examined in this study would be in keeping with this pathogenetic mechanism of metastasis from a conventional GCTB.

A striking morphological feature of all the primary GCTBs which were associated with lung secondaries was the presence of numerous large areas of haemorrhage

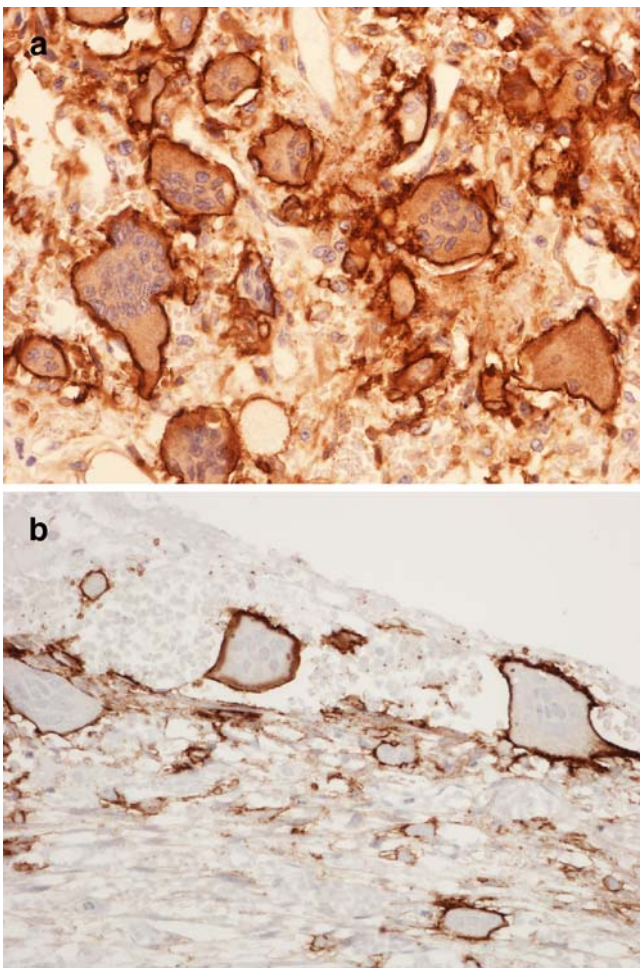

Fig. 4 Expression of CD51 in **a** primary GCTB and **b** corresponding lung nodule

within the tumour. Morphologically, in all the cases of primary GCTB that we examined, there were areas of haemorrhage and thrombus formation; these thrombi were at various stages of organisation; in some early thrombi, there was prominent ingrowth of fibrous and granulation tissue into the thrombus, and both mononuclear stromal cells and giant cells were commonly seen in or around small vessels within this reparative tissue. These areas of haemorrhage and thrombus formation were distinct from blood-filled spaces associated with aneurysmal bone cyst change, which was a prominent feature in only a minority of the primary GCTBs we examined. In contrast to the group of primary GCTBs which had metastasised, the control group of primary (non-metastatic, non-recurrent) GCTBs did not show thrombus formation. There has been no systematic analysis of haemorrhage and thrombus formation in GCTB. Secondary changes, including areas of haemorrhage and ABC change, have been reported by some observers to be frequent and noted in up to 15% of cases [15].

Pathogenetic mechanisms which have been proposed for the formation of lung nodules that develop in the context of conventional GCTB include proliferation of a subpopulation of neoplastic cells which have metastatic potential in an otherwise benign or locally aggressive tumour and origin from tumour emboli derived from the primary GCTB [9–11, 14]. It has been noted that most metastatic GCTBs are detected a year or more after initial surgery to the primary [4, 6, 7, 14]. As surgery would result in haemorrhage and thrombus formation within the bone, it has been proposed that any residual GCTB not removed at the time of surgery could grow into this thrombus and then break off, in this way leading to an embolic metastasis in the lungs [10, 11].

Some support for this concept of benign metastasising GCTBs, initially proposed by Huvos [10], is provided by our immunophenotypic findings in which we found that the immunophenotype of mononuclear stromal cells in lung metastases of GCTB recapitulated that of the primary tumours from which they were presumably derived. Mononuclear stromal cells in both primary and secondary GCTBs showed a similar expression of SMA and HLA-DR. We also found no significant difference in the expression of proliferation, apoptosis and tumour-associated markers by mononuclear cells in primary GCTBs and the corresponding lung nodules which developed in these patients. p63 has been proposed as a specific marker for GCTB [16], and our findings show that it was expressed weakly by some but not all mononuclear cells in primary and secondary GCTBs. Most primary and secondary GCTBs are diploid [17]; only a minority of GCTB cases have been found to show cytogenetic abnormalities, and no clear consistent genetic abnormality has been identified in conventional GCTBs associated with lung metastasis [17–19]. Telomeric associations can be identified in most cases of GCTBs [20], and it has been proposed that disturbed telomere maintenance may play a role in the pathogenesis and behaviour of GCTBs. It has been concluded on the basis of an analysis of doubling time and flow cytometry data that most cases of GCTB and their pulmonary metastases are of spontaneous regression or growth cessation type. These metastatic tumours show less expression of the proliferation marker Ki-67 than continuous slow-growing and rapidly growing metastases. Other studies, however, have reported no consistent difference in the mitotic index [1, 2, 15] or in expression of proliferation and other tumour markers in primary and recurrent GCTBs associated with lung metastasis [21–25]. We noted that the immunophenotype of giant cells in primary (non-metastatic and metastatic) GCTBs and lung nodules was identical, indicating that the osteoclasts are essentially reactive cells recruited by receptor activator of nuclear factor-κB ligand-expressing mononuclear stromal cells [13]; the role of osteoclast specific proteases, such as cathepsin K [26], in lung nodule formation has not been determined, but it would be expected that this enzyme would be similarly expressed by osteoclasts in primary and secondary GCTBs.

The presence of organising thrombus and invasion of granulation tissue by mononuclear and giant cell components of GCTB was a consistent finding in the primary GCTBs which metastasised. This finding suggests that most lung nodules associated with primary conventional GCTB are implants derived from tumour emboli that originate from thrombi in areas of haemorrhage within the primary tumour. These tumour thrombi could propagate and grow into venous channels of small- to medium-sized arteries and thus account for the finding of tumour within vessels at the periphery of GCTBs. It is possible that, in some cases, thrombus-containing GCTB becomes detached and enters the circulation, resulting in one or more emboli that become implanted within the lungs. Such tumour implants would presumably form in the same way as they do in other benign/locally aggressive tumours that exhibit vascular invasion and are associated with lung nodule formation (e.g. chondroblastoma). No lymphatic vessels were found within primary tumours, thus indicating that lymphatic spread of GCTB does not occur.

Lung metastases of conventional GCTB have been shown to occur more commonly in aggressive tumours with soft tissue extension or local recurrence and are rarely seen at initial presentation, appearing on average 3.5 years after diagnosis [4, 5, 14]. True malignant GCTBs account for less than 5% of cases in most series and in 70% of cases are radiation-induced sarcomas [1–3]. Our finding that the lung nodules do not morphologically show malignant features and have the same immunophenotypic features as primary GCTBs accords with the suggestion of Huvos that these lesions may be iatrogenically produced following curettage [10]. Noting the presence of numerous large areas

of haemorrhage within the primary tumour, in addition to the cytological features of the mononuclear cells, should be useful in the assessment of lung nodules that develop in GCTB.

Acknowledgement The authors are members of EuroBoNet, a European Network of Excellence studying the pathology and genetics of bone tumours. The authors thank Chris Lowe for typing the manuscript.

Conflict of interest We declare that we have no conflict of interest.

References

1. Reid R, Bareyce SS, Sciot R (2002) Giant cell tumour. In: Fletcher C, Unni K, Mertens F (eds) Pathology and genetics of tumours of soft tissue and bone. IARC, Lyon, pp 310–312
2. Unni K, Inwards C, Bridge J et al (2005) Tumours of the bones and joints. AFIP Atlas of Tumour Pathology Fourth Series, AFIP, pp 281–298
3. Geshickter CF, Copeland MM (1930) Recurrent and so-called metastatic giant cell tumour. Arch Surg 20(5):714–755
4. Turcotte RE (2006) Giant cell tumour of bone. Orthop Clin N Am 32:35–51
5. Bertoni F, Present D, Sudanese A et al (1988) Giant cell tumour of bone with pulmonary metastases. Clin Orthop 237:275–285
6. Rock MG, Pritchard DJ, Unni KK (1984) Metastases from histologically benign giant-cell tumour of bone. J Bone Joint Surg 66N:269–273
7. Tubbs WS, Brown LR, Beabout JW et al (1992) Benign giant-cell tumour of bone with pulmonary metastases. AJR 158:331–334
8. Faisham WI, Zulmi W, Saim AH et al (2004) Pulmonary metastases of giant cell tumour of the bone. Med J Malaysia 59 (Suppl F):78–81
9. Maloney WJ, Vaughan LM, Jones HH et al (1989) Benign metastasizing giant cell tumour of bone. Clin Orthop 243:208–215
10. Huvos AG (1991) Bone tumours: diagnosis, treatment and prognosis. Saunders, Philadelphia, pp 429–467
11. Mirra JM, Ulich T, Magidson J et al (1982) A case of probable benign pulmonary "metastases" or implants arising from a giant cell tumour of bone. Clin Orthop 162:245–254
12. Forsyth RG, De Boeck G, Baeide JJ et al (2009) CD33+ CD14− phenotype is characteristic of multinuclear osteoclast-like cells in giant cell tumour of bone. J Bone Miner Res 24:70–77
13. Lau YS, Sabokbar A, Gibbons CL et al (2005) Phenotypic and molecular studies of giant-cell tumours of bone and soft tissue. Hum Pathol 36:945–954
14. Bertoni F, Present D, Enneking WF (1985) Giant-cell tumour of bone with pulmonary metastases. J Bone Joint Surg 67A:890–900
15. Forest M (1988) Orthopaedic surgical pathology: diagnosis of tumours and pseudotumoral lesions of bone and joint. Churchill Livingstone, New York, pp 423–428
16. Dickson BC, Li SQ, Wunder JS et al (2008) Gene expression profiling identifies p63 as a diagnostic marker for giant cell tumour of the bone. Mod Pathol 21:531–539
17. Ladanyi M, Traganos F, Huvos AG (1989) Benign metastasizing giant cell tumours of bone. A DNA flow cytometric study. Cancer 64:1521–1526
18. Osaka S, Toriyama M, Taira K et al (1997) Analysis of giant cell tumour of bone with pulmonary metastases. Clin Orthop 335:253–261
19. Osaka S, Sugita H, Osaka E et al (2004) Clinical and immunohistochemical characteristics of benign giant cell tumour of bone with pulmonary metastases: case series. Orthop Surg 12:55–62
20. Forsyth RG, De Boeck G, Bekaert S et al (2008) Telomere biology in giant cell tumour of bone. J Pathol 214:555–563
21. de Souza PE, Paim JF, Carvalhais JN et al (1999) Immunohistochemical expression of p53, MDM2, Ki-67 and PCNA in central giant cell granuloma and giant cell tumour. J Oral Pathol Med 28:54–58
22. Ueda Y, Dockhorn-Dworniczak B, Blasius S et al (1993) Analysis of mutant p53 protein in osteosarcomas and other malignant and benign lesions of bone. J Cancer Res Clin Oncol 119:172–178
23. Rao UN, Goodman M, Chung WW et al (2005) Molecular analysis of primary and recurrent giant cell tumours of bone. Cancer Genet Cytogenet 158:126–136
24. Masui F, Ushigome S, Fujii K (1998) Giant cell tumour of bone: a clinicopathologic study of prognostic factors. Pathol Int 48:723–729
25. Sulh MA, Greco MA, Jiang T et al (1996) Proliferation index and vascular density of giant cell tumours of bone: are they prognostic markers? Cancer 77:2044–2051
26. Lindeman JH, Hanemaaijer R, Mulder A et al (2004) Cathepsin K is the principal protease in giant cell tumour of bone. Am J Pathol 165:593–600

Virchows Arch (2010) 456:105–106
DOI 10.1007/s00428-009-0870-3

LETTER TO THE EDITOR

Intraductal fibroadenoma and intraductal phyllodes tumour—a part of the spectrum of the breast ductal adenoma?

Joško Bezić

Received: 9 November 2009 / Accepted: 28 November 2009 / Published online: 16 December 2009
© Springer-Verlag 2009

Dear editor

I have read with great interest the article of Cummings MC et al., published in the recent issue of *Virchows Archiv*, where two cases of intraductal fibroepitelial proliferation similar to fibroadenoma and phyllodes tumour were described. Both cases were composite intraductal lesions with varying proportions of fibroepithelial and papillomatous proliferation involving several ducts, with occasional admixture of the both components within the one duct. The authors concluded that the cases with such overlapping features might suggest that fibroadenoma and intraduct papilloma could share a common pathogenesis [1].

These described cases of intraductal fibroepitelial proliferation, in my opinion, have some similarities with patohistological entity of ductal adenoma. Presenting the similar case of intraductal fibroadenomatosis, Chung et al. concluded that this type of intraductal proliferation had overlap features of papillomas, fibroadenomas, benign phyllodes tumour, and intraductal adenomas [2].

J. Bezić (✉)
Institute of Pathology, Cytology and Forensic Medicine,
Clinical Hospital Split,
Spinčićeva 1,
21000 Split, Croatia
e-mail: jb@mefst.hr

First described by Azzopardi and Salm in 1984, ductal adenoma is defined as a well-circumscribed benign glandular proliferation located, at least in partly, within a duct lumen [3, 4]. Usually single or multiple adenomatous nodules with proliferating tubules composed of luminal cells and basal myoepithelium are seen, surrounded by fibrous tissue [4, 5]. Epithelial and stromal changes are frequent (apocrine metaplasia of the luminal cells, peripheral, or central fibrosis with tubular distortion, stromal myxoid change) [4, 6].

Although some authors believe that ductal adenoma evolve by sclerosis of intraductal papillomas, intraluminal epithelial proliferation without papillary formation cannot be excluded in their pathogenesis [5, 6]. Carney and Toorkey suggest that ductal papilloma and ductal adenoma are related lesions with different type of epithelial intraluminal proliferation, one papillary and common (ductal papilloma), the other tubular and uncommon (ductal adenoma) [6].

The term ductal adenoma defines primarily intraductal location of this entity, but it is less informative concerning its histological picture. Some ductal adenomas with extensive myxoid and cartilagionous stromal changes resemble breast pleomorphic adenomas, and some with myoepithelial hyperplasia can be included in the category of adenomyoepitheliomas. Cases with central sclerosis and elastosis with tubular distortion may be similar to radial sclerosing lesions. The cases described by Cummings et al. may represent cases of ductal adenomas with extensive

stromal proliferation giving fibroadenomatous and phyllodes tumour appearance, extending the morphological spectrum of this entity.

References

1. Cummings MC, da Silva L, Papadimos DJ, Lakhani SR (2009) Fibroadenoma et intraduct papilloma—a common pathogenesis? Virchows Arch 455:271–275
2. Chung A, Scharre K, Wilson M (2008) Intraductal fibroadenomatosis: an unusual variant of fibroadenoma. Breast J 14:193–195
3. Azzopardi JG, Salm R (1984) Ductal adenoma of the breast: a lesion which can mimic carcinoma. J Pathol 144:15–23
4. Tavassoli FA, Devilee P (eds) (2003) World health organization of tumours: pathology and genetics of tumours of the breast and female genital organs. IARC Press, Lyon
5. Lammie GA, Millis RR (1989) Ductal adenoma of the breast—a review of fifteen cases. Hum Pathol 20:903–908
6. Carney JA, Toorkey BC (1991) Ductal adenoma of the breast with tubular features. A probable component of the complex of myxomas, spotty pigmentation, endocrine overactivity and schwannomas. Am J Surg Path 15:722–731

Virchows Arch (2010) 456:107–109
DOI 10.1007/s00428-009-0875-y

INVITED EDITORIAL

Soft tissue sarcomas: introduction to the Virchows Archiv review issue

Louis Guillou · Pancras C. W. Hogendoorn · Fred T. Bosman

Received: 15 December 2009 / Accepted: 15 December 2009 / Published online: 18 February 2010
© The Author(s) 2010. This article is published with open access at Springerlink.com

Soft tissue sarcomas constitute a heterogeneous category of neoplasms composed mostly of uncommon tumours of different histology, different biology, and different outcome. Thirty years ago, the diagnosis of these neoplasms was mainly based on morphology coupled with some classical histochemical stains such as periodic acid-Schiff, reticulin, and trichrome stains. In the last 15 years, thanks to the substantial development of immunohistochemistry, cytogenetics and molecular genetic analysis significant improvements have been made regarding the classification and diagnosis of these tumors, with direct implications for clinical management and prognosis [1, 2]. Many new entities were recognized of which desmoplastic small round cell tumor and intimal sarcomas are examples. Other sarcoma entities gradually disappeared or lost in importance (e.g., the so-called malignant fibrous histiocytoma [3], hemangiopericytoma [4], and fibrosarcoma categories). During the same period of time, molecular ancillary techniques (including a vast array of polymerase chain reaction-based techniques, fluorescence in situ hybridization (FISH), conventional and array-based comparative genomic hybridization, expression arrays, direct genome sequencing, and DNA methylation analysis to name a few) allowed detailed analysis of these tumors and the resulting data facilitated better understanding of their biology (Fig. 1). In addition, thanks to improvements in nucleic acid preservation and isolation, many molecular techniques provided new parameters important for diagnostics and/or prognosis and were modified to be applicable on formalin-fixed, paraffin-embedded material (e.g., FISH, polymerase chain reaction-based techniques). This is all condensed in a substantial revision of the World Health Organization classification which combined histology with genetics [2]. Methodological advances thus allowed better understanding of biology, within turn novel classifications based upon new histogenetic concepts and robust diagnostic methods.

This review issue focuses on the pathobiology of soft tissue sarcomas. In the introductory paper, Bovée and Hogendoorn introduced to the reader the most significant molecular acquisitions that occurred in the domain of sarcomas and their implications for the patient in terms of diagnosis, prognosis, and clinical management [5]. The genomic characteristics of soft tissue sarcomas are exposed in an article of Mertens and coworkers [6]. Here, the authors discuss how the genomic characterization of soft tissue sarcomas has not only provided cell biologists with decisive information on the parts of the genome that may harbor genes that are essential for tumor development, but also given the clinicians involved in the management of these patients a valuable diagnostic tool. Beck et al. share with us the "state of the art" of gene expression profiling in soft tissue sarcomas and how this technique has led to advancements in the understanding of sarcoma pathobiology, the identification of clinically useful biomarkers, and the refinement of sarcoma classification schemes, with hopefully significant benefits to patients [7].

There are two intriguing and highly relevant questions in sarcoma pathobiology: the first one is "why do some people develop sarcomas?" and the second is "from which cells do sarcomas develop?". Recent studies in model systems as

L. Guillou · F. T. Bosman
Department of Pathology, University of Lausanne,
Centre Hospitalier Universitaire Vaudois, Pathology,
Lausanne, Switzerland

P. C. W. Hogendoorn (✉)
Department of Pathology, Leiden University Medical Center,
P.O. Box 9600, L1-Q, 2300 RC Leiden, The Netherlands
e-mail: p.c.w.hogendoorn@lumc.nl

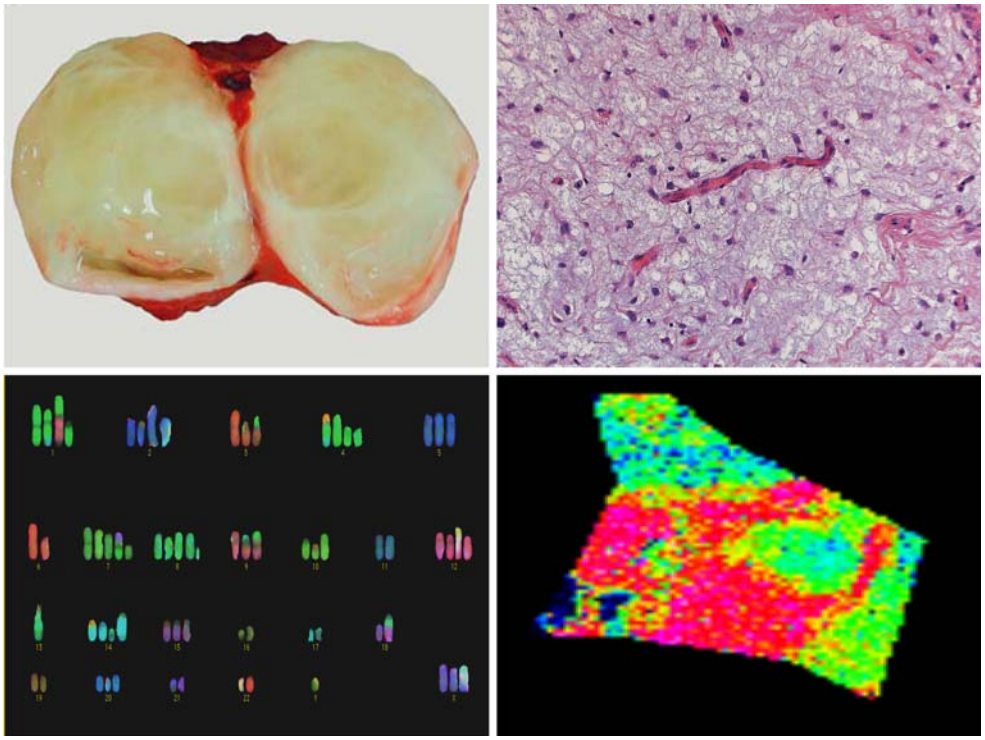

Fig. 1 Unraveling soft tissue tumors from macroscopy via histology to proteinprofiling and genetics: Macroscopic image of a myxoid soft tissue tumour characterized by its abundant jelly ("myxoid") extracellular matrix on cut surface; histology of grade I myxofibrosarcoma showing sparse tumour cells with slight nuclear atypia in a background of myxoid extracellular matrix with curvilinear bloodvessels (×400); imaging mass spectrometry on a tissue slide of grade I myxofibrosarcoma illustrating the heterogeneity in lipid profiles related to their spatial distribution; and combined binary ratio fluorescence in situ hybridization of grade III myxofibrosarcoma with numeric and structural karyotypic aberrations

well as on human tumors have provided some answers to these questions and undoubtedly, in the years to come, much of the secrets of mesenchymal stem cells, how they differentiate and how dysregulation of proliferation and differentiation in this system leads to which type of sarcoma [8–15].

Roughly, soft tissue sarcomas can be divided in two categories, those with simple karyotypes and those with complex karyotypes [16]. Of the soft tissue sarcomas (with relatively simple karyotypes), 15-20% bear specific reciprocal translocations which can be used as diagnostic markers. Some others are characterized by specific somatic mutations (e.g., KIT and platelet-derived growth factor receptor alpha in gastrointestinal stromal tumor (GIST) [17]) or specific amplifications (e.g., MDM2 and CDK4 amplification in the well-differentiated/dedifferentiated liposarcoma category [18]).

For the purposes of this review, sarcomas with specific translocations have been separated into two groups, those involving the Ewing's sarcoma (EWS) gene and those that do not involve the EWS gene. Sarcomas involving EWS translocations (e.g., Ewing's sarcoma, desmoplastic small round cell tumor, etc.) are reviewed by Dei Tos and Romeo [19], whereas genetic and clinicopathological features of soft tissue sarcomas with non EWS translocations (e.g., synovial sarcoma, alveolar rhabdomyosarcoma, etc.) are presented in a comprehensive way by Fisher [20].

In the last 10 years, improvements have been accomplished regarding the diagnosis and pathobiology of well-differentiated/dedifferentiated liposarcomas. Coindre and coworkers summarize for us the most significant advances that occurred in this domain, including the discovery of new promising therapeutic targets [21].

Soft tissue sarcomas with complex karyotypes account for about 50% of sarcomas. This sarcoma category includes most of spindle cell/pleomorphic sarcomas (myxofibrosarcoma, pleomorphic liposarcoma, etc.) as well as leiomyosarcomas, malignant peripheral nerve sheath tumors, and many other neoplasm's. Guillou and Aurias review their cytogenetic, molecular genetics, and main clinicopathologic characteristics [22]. Most recently, progress in the field of protein chemistry led to a new conceptual approach in order to try to unravel aspecific terms like myxoid matrix (see also Fig. 1). Attempts were made to characterize this matrix [23, 24] which turned out to be heterogeneous at the protein level, while morphologically the hallmark of an array of tumor types [25]. Willems et al. discuss the usefulness of such an approach for myxoid matrix containing tumors if explored [26]. Dr. Liegl and coworkers finally discuss the progress made in the understanding of the pathobiology, morphologic evaluation and mechanisms of resistance to tyrosine kinase inhibition in GIST [27]. Gist is one of the examples in oncopathology where the understanding of the genetics of the tumour have lead to major changes in treatment following the development of specific tyrosine kinase blockers [28]. Now we have reached the moment that the subsequent resistant mechanisms which develop in the course of the treatment are of keen interest for

molecular pathologist and of importance for the patients which have gained years of live quality after treatment of this in the past so aggressive tumor.

For those interested in sarcomas, these are exciting times. We are getting closer to understanding their biology; our diagnoses are better and grow closer to what clinicians need to adequately treat patients. Much remains to be done. We hope that this review issue on the pathobiology of soft tissue sarcomas meets the expectations of the readers of Virchows Archiv. The guest editors warmly thank all the contributors for their effort, willingness, and invaluable input to this work.

Open Access This article is distributed under the terms of the Creative Commons Attribution Noncommercial License which permits any noncommercial use, distribution, and reproduction in any medium, provided the original author(s) and source are credited.

References

1. Hogendoorn PCW, Collin F, Daugaard S et al (2004) Changing concepts in the pathological basis of soft tissue and bone sarcoma treatment. Eur J Cancer 40:1644–1654
2. Fletcher CDM, Unni KK, Mertens F (2002) WHO classification of tumours. Pathology and genetics of tumours of soft tissue and bone. IARC Press, Lyon
3. Fletcher CDM (1992) Pleomorphic malignant fibrous histiocytoma: fact or fiction? A critical reappraisal based on 159 tumors diagnosed as pleomorphic sarcoma. Am J Surg Pathol 16:213–228
4. Fletcher CDM (1994) Haemangiopericytoma—a dying breed? Reappraisal of an 'entity' and its variants: a hypothesis. Curr Diagn Pathol 1:19–23
5. Bovee JVMG, Hogendoorn PCW (2010) Molecular pathology of sarcomas: concepts and clinical implications. Virchows Arch. doi:10.1007/s00428-009-0828-5
6. Mertens F, Panagopoulos I, Mandahl N (2010) Genomic characteristics of soft tissue sarcomas. Virchows Arch. doi:10.1007/s00428-009-0736-8
7. Beck AH, West RB, Van de Rijn M (2010) Gene expression profiling for the investigation of soft tissue sarcoma pathogenesis and the identification of diagnostic, prognostic, and predictive biomarkers. Virchows Arch. doi:10.1007/s00428-009-0774-2
8. Mohseny AB, Szuhai K, Romeo S et al (2009) Osteosarcoma originates from mesenchymal stem cells in consequence of aneuploidization and genomic loss of Cdkn2. J Pathol 219:294–305
9. Cironi L, Provero P, Riggi N et al (2009) Epigenetic features of human mesenchymal stem cells determine their permissiveness for induction of relevant transcriptional changes by SYT-SSX1. PLoS ONE 4:e7904
10. Riggi N, Cironi L, Provero P et al (2005) Development of Ewing's sarcoma from primary bone marrow-derived mesenchymal progenitor cells. Cancer Res 65:11459–11468
11. Riggi N, Cironi L, Suva ML et al (2007) Sarcomas: genetics, signalling, and cellular origins. Part 1: the fellowship of TET. J Pathol 213:4–20
12. Riggi N, Cironi L, Provero P et al (2006) Expression of the FUS-CHOP fusion protein in primary mesenchymal progenitor cells gives rise to a model of myxoid liposarcoma. Cancer Res 66:7016–7023
13. Riggi N, Suva ML, Suva D et al (2008) EWS-FLI-1 expression triggers a Ewing's sarcoma initiation program in primary human mesenchymal stem cells. Cancer Res 68:2176–2185
14. Suva ML, Cironi L, Riggi N et al (2007) Sarcomas: genetics, signalling, and cellular origins. Part 2: TET-independent fusion proteins and receptor tyrosine kinase mutations. J Pathol 213:117–130
15. Suva ML, Riggi N, Stehle JC et al (2009) Identification of cancer stem cells in Ewing's sarcoma. Cancer Res 69:1776–1781
16. Ladanyi M (1995) The emerging molecular genetics of sarcoma translocations. Diagn Mol Pathol 4:162–173
17. Hirota S, Isozaki K, Moriyama Y et al (1998) Gain-of-function mutations in c-kit in human gastrointestinal stromal tumors. Science 279:577–580
18. Dei Tos AP (2001) Lipomatous tumours. Curr Diagn Pathol 7:8–16
19. Romeo S, Dei Tos AP (2010) Soft tissue tumors associated with EWSR1 translocation. Virchows Arch. doi:10.1007/s00428-009-0854-3
20. Fisher C (2010) Soft tissue sarcomas with non-EWS translocations: molecular genetic features and pathologic and clinical correlations. Virchows Arch. doi:10.1007/s00428-009-0776-0
21. Coindre JM, Pedeutour F, Aurias A (2010) Well-differentiated and dedifferentiated liposarcomas. Virchows Arch. doi:10.1007/s00428-009-0815-x
22. Guillou L, Aurias A (2010) Soft tissue sarcomas with complex genomic profiles. Virchows Arch. doi:10.1007/s00428-009-0853-4
23. Willems SM, Schrage YM, Baelde JJ et al (2008) Myxoid tumours of soft tissue: the so-called myxoid extracellular matrix is heterogeneous in composition. Histopathology 52:465–474
24. Willems SM, Mohseny AB, Balog C et al (2009) Cellular/intramuscular myxoma and grade I myxofibrosarcoma are characterized by distinct genetic alterations and specific composition of their extracellular matrix. J Cell Mol Med 7:1301
25. Graadt van Roggen JF, Hogendoorn PCW, Fletcher CDM (1999) Myxoid tumours of soft tissue. Histopathology 35:291–312
26. Willems SM, Wiweger M, Frans Graadt van Roggen J et al. (2010) Running GAGs: myxoid matrix revisited. What's in it for the pathologist? Virchows Arch. doi:10.1007/s00428-009-0822-y
27. Liegl-Atzwanger B, Fletcher JA, Fletcher CMD (2010) Gastrointestinal stromal tumors. Virchows Arch. doi:10.1007/s00428-010-0891-y
28. Verweij J, van Oosterom A, Blay JY et al (2003) Imatinib mesylate (STI-571 Glivec(R), Gleevec) is an active agent for gastrointestinal stromal tumours, but does not yield responses in other soft-tissue sarcomas that are unselected for a molecular target. Results from an EORTC Soft Tissue and Bone Sarcoma Group phase II study. Eur J Cancer 39:2006–2011

Virchows Arch (2010) 456:111–127
DOI 10.1007/s00428-010-0891-y

REVIEW AND PERSPECTIVE

Gastrointestinal stromal tumors

Bernadette Liegl-Atzwanger · Jonathan A. Fletcher · Christopher D. M. Fletcher

Received: 28 January 2010 / Accepted: 29 January 2010 / Published online: 18 February 2010
© Springer-Verlag 2010

Abstract Gastrointestinal stromal tumors (GISTs) have emerged from being poorly defined, treatment-resistant tumors to a well-recognized, well-understood, and treatable tumor entity within only one decade. The understanding of GIST biology has made this tumor a paradigm for molecularly targeted therapy in solid tumors and provides informative insights into the advantages and limitations of so-called targeted therapeutics. Approximately 85% of GISTs harbor activating mutations in *KIT* or the homologous receptor tyrosine kinase *PDGFRA* gene. These mutations are an early event in GIST development and the oncoproteins serve as a target for the small molecule tyrosine kinase inhibitors imatinib and sunitinib. The existing and emerging treatment options demand exact morphologic classification and risk assessment. Although, KIT (CD117) immunohistochemistry is a reliable diagnostic tool in the diagnosis of GIST, KIT-negative GISTs, GISTs showing unusual morphology as well as GISTs which progress during or after treatment with imatinib/sunitinib can be a challenge for pathologists and clinicians. This review focuses on GIST pathogenesis, morphologic evaluation, promising new immunohistochemical markers, risk assessment, the role of molecular analysis, and the increasing problem of secondary imatinib resistance and its mechanisms.

Keywords Gastrointestinal stromal tumor · GIST · Imatinib · Sunitinib · Tyrosine kinase inhibitors · Resistance · KIT · PDGFRA

B. Liegl-Atzwanger · J. A. Fletcher · C. D. M. Fletcher
Department of Pathology, Brigham and Women's Hospital and Harvard Medical School,
Boston, MA, USA

B. Liegl-Atzwanger
Department of Pathology, Medical University of Graz,
Graz, Austria

C. D. M. Fletcher (✉)
Department of Pathology, Brigham and Women's Hospital,
75 Francis Street,
Boston, MA 02115, USA
e-mail: cfletcher@partners.org

Introduction

Gastrointestinal stromal tumors (GISTs) are the most common mesenchymal tumors in the gastrointestinal (GI) tract. Malignant examples of this tumor type were once viewed as the most treatment-refractory sarcomas, with fewer than 10% of patients showing clinical response to conventional chemo- or radiation therapies [1, 2]. For decades, prior to the late 1990s, these mesenchymal tumors arising in the GI tract were most often classified as smooth muscle tumors or neural tumors [3]. In 1983, Mazur and Clark introduced the term "stromal tumor" [4], but it was not widely accepted until the early 1990s, when CD34 was discovered as a marker for stromal tumors arising in the gastrointestinal tract, at that time being regarded as relatively specific [5]. In the 1990s, investigators noted similarities between GIST cells and the interstitial cells of Cajal, a group of cells located in the muscularis propria and around the myenteric plexus throughout the GI tract, serving as pacemakers for peristaltic contraction [6–10]. Studies revealed that interstitial cells of Cajal express KIT and are developmentally dependent on stem cell factor which is regulated through the KIT kinase [7, 11]. In 1998, a groundbreaking publication by Hirota and colleagues, showed activating mutations in the *KIT* receptor tyrosine kinase (RTK) gene in GIST as well as expression of KIT

protein by immunohistochemistry [6]. These insights, together with the subsequent introduction of highly effective tyrosine kinase inhibitor (TKI) treatments, led to immense research interest in GIST. Subsequent studies confirmed these findings; and in 2003, Heinrich and colleagues [12] additionally identified platelet-derived growth factor receptor alpha (*PDGFRA)* gene mutations as an alternative pathogenetic event in GISTs lacking *KIT* gene mutations. To date, approximately 85% of GISTs are reported to harbor activating mutations in *KIT* or the homologous RTK gene, *PDGFRA* [12–14], and KIT immunohistochemistry has proven to be a reliable and sensitive tool in GIST diagnosis [8, 15, 16]. With the possibility of inhibiting the activated oncoproteins KIT and PDGFRA with TKI therapies (imatinib and sunitinib), inoperable or metastatic GISTs are now treatable, and a number of additional alternative drugs are already in clinical trials. Increased understanding of GIST biology has made this tumor a paradigm of molecularly targeted therapy in solid tumors and provides informative insights into the advantages and limitations of so-called targeted therapeutics.

Oncogenic *KIT* and *PDGFRA* mutations and signaling pathways in GIST

The *KIT* and *PDGFRA* genes map to chromosome 4q12 [17]. Both encode type III receptor tyrosine kinases sharing closely related structural features. These kinases are composed of an extracellular (EC) ligand-binding region containing five immunoglobulin-like repeats, a transmembrane sequence, a juxtamembrane domain (JM), and two cytoplasmic kinase domains (TK[I]: ATP-binding pocket; and TK[II]: kinase activation loop; Fig. 1) [18, 19].

KIT and PDGFRA are activated by binding of their respective ligands, stem cell factor and PDGFA, to the EC region. Ligand binding results in receptor homodimerization and subsequent cross-phosphorylation of cytoplasmic tyrosines which serve as binding sites for various signaling proteins, leading to phosphorylation cascades with activation of signaling substrates regulating cell proliferation, adhesion, motility, and survival [20] (Fig. 2). KIT tyrosine kinase activity is regulated by its JM domain, which inhibits KIT kinase activity in the absence of KIT ligand [21]. Overall, KIT activation has been shown to regulate important cell functions including proliferation, apoptosis, adhesion, and chemotaxis, [22–25] and KIT is critical for the development and maintenance of several cell types, e.g., germ cells, hematopoietic cells, mast cells, melanocytes, and interstitial cells of Cajal [20, 26, 27].

In GISTs, *KIT* or *PDGFRA* mutations cause constitutive oncogenic signaling in the absence of their ligands. The uncontrolled RTK activity results in the activation of the PI3K-AKT and MEK-MAPK pathways accompanied by relatively low level signal transducer and activation of transcription (STAT)1 and STAT3 activation [25, 28, 29], leading to alterations in cell cycle, protein translation, metabolism, and apoptosis (Fig. 2).

Mutations in the *KIT* or *PDGFRA* gene involve two main regions, the receptor regulatory domains (dimerization domain in the EC region and JM domain) and the enzymatic domains (TK[I] and TK[II]). In GISTs most *KIT* mutations (~65%) involve the JM domain (exon 11) followed by mutations involving the EC dimerization

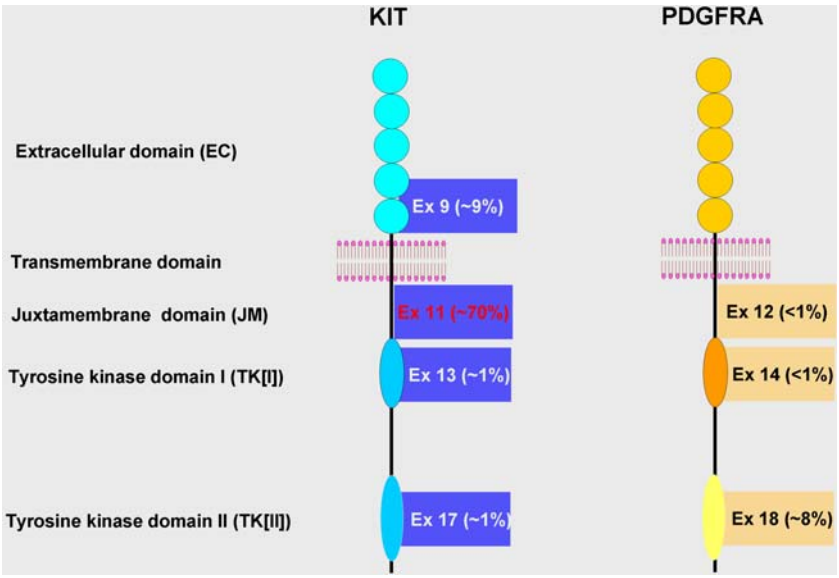

Fig. 1 Schematic structure of KIT and PDGFRA receptor tyrosine kinases and distribution of KIT mutations in GIST

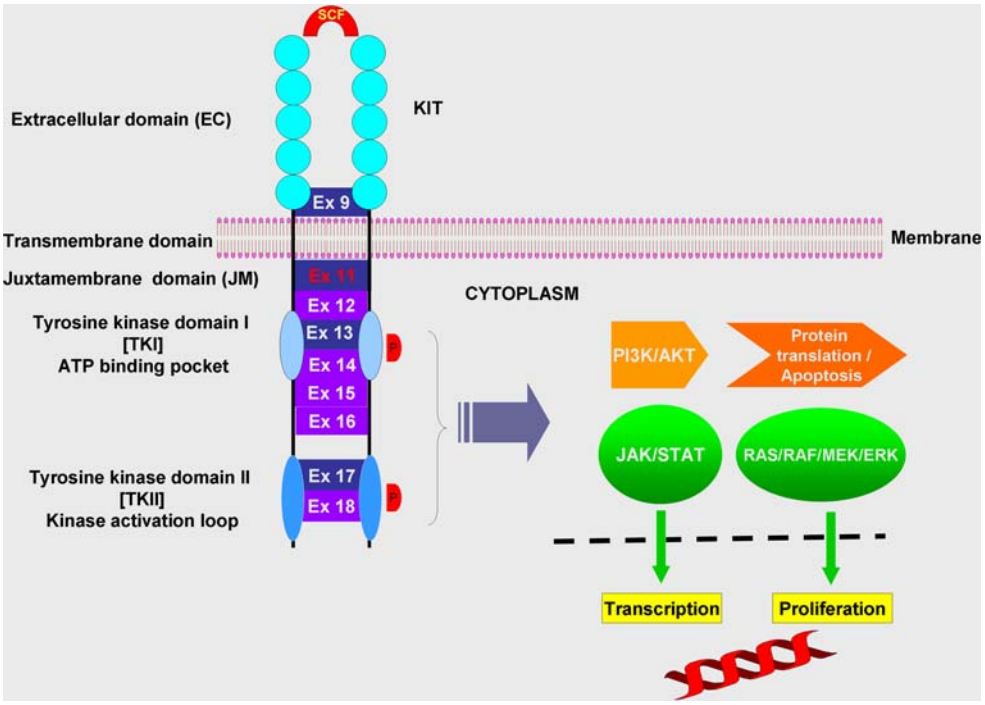

Fig. 2 Summary of the major signaling pathways activated by KIT

domain (exon 9) which are seen in about 9% of cases [13, 14]. Primary *KIT* mutations can also occur in exon 13 (TK [I]: ATP binding pocket) and exon 17 (TK[II]: kinase activation loop), but these mutations are rare (~2%) and data are quite limited.

GISTs harboring an exon 11 mutation can occur throughout the GI tract. Various types of mutation can be found in exon 11 including missense mutations, insertions, and deletions. Tandem repeat mutations are infrequently seen in the distal part of *KIT* exon 11. These changes were predominantly found in female stomach and have been proposed to be associated with a quite indolent clinical course [30–33]. More controversial are GISTs with deletion mutations in and around *KIT* exon 11 codon 557–558. Some studies have shown an aggressive clinical course and poor prognosis, but these findings have not been confirmed by others [30, 32, 33]. Loss of heterozygosity in the *KIT* locus has been associated with high proliferative activity and increased metastatic potential [31, 32].

GISTs with an exon 9 mutation arise most commonly in the small intestine and are frequently high-risk tumors [31, 34, 35]. In the vast majority of cases, exon 9 mutations are characterized by insertion of six base pairs, a duplication of Ala and Tyr and are found in primary as well as relapsed or advanced GISTs [32, 36]. According to a recent study, *KIT* exon 13 and exon 17 mutant GISTs are slightly over-represented among the intestinal group of GISTs, and if tumors with an exon 13 mutation occur in the stomach, they tend to be slightly larger and more aggressive than "average"gastric GISTs. The majority of *KIT* exon 13 and 17 mutations are substitutions and, in small intestinal GISTs, these mutations have no substantial impact on clinicopathologic features when compared to the "average" small intestinal GIST [37].

PDGFRA mutations, identified in approximately 8% of GISTs, involve mainly (~6–7%) either exon 18 (TK[II]: kinase activation loop) or exon 14 (TK[I]: ATP-binding pocket) and rarely (less than 1%) exon 12 (JM) [12, 38–40]. Mutations in *PDGFRA* exon 14 and 18 are mostly missense mutations. The subset of GISTs with a *PDGFRA* mutation that is associated with a commonly benign clinical course is limited to the stomach and omentum, lack KIT expression by immunohistochemistry (IHC), and preferentially shows epithelioid morphology [41, 42]. GISTs with a mutation D842V in exon 18 of *PDGFRA* are resistant to imatinib and sunitinib [13, 43–45].

Mutations in the JM domain impair its auto-inhibitory functions, causing kinase activation [46, 47], whereas mutations in the EC region may lead to ligand-independent receptor dimerization [13]. *KIT* and *PDGFRA* mutations are mutually exclusive.

Most recently, *BRAF* exon 15 V600E mutations were identified in 7–13% of adult wild-type GISTs [48–50]. GISTs with *BRAF* mutation seem to show a predilection for the small bowel [49, 50]; however, the association with high-risk malignancy is controversial as yet [48–50].

Role of cytogenetics in GIST progression

KIT or *PDGFRA* mutations are an early event in GIST development. Mutations are found irrespective of tumor

size. They are observed in "silent" microscopic and multiple incidental GISTs detected in gastrectomies, performed for other causes, and in 10–20% of normal patients over the age of 60 [51, 52]. These findings underscore that mutations per se are involved in the oncogenesis and proliferation of GISTs, but seem to be of little importance in malignant transformation [53]. Therefore, additional genetic hits are important in clinical tumor progression. Approximately two-thirds of *KIT* and *PDGFRA* mutant GISTs show either monosomy 14 or partial loss of 14q [12, 54, 55]. Two 14q regions, 14q11.2–q12 and 14q23–q24, seem to harbor tumor suppressor genes important in early GIST development [54, 56]. Another common event, seen in approximately 50% of GISTs, is loss of the long arm of chromosome 22. This finding is associated with progression to borderline/malignant GIST [54, 57–59]. Less frequently observed are losses on chromosomes 1p, 9q, 11p, 17q, and gains on chromosomes 8q and 17q, which are also associated with malignant behavior [56, 57, 59–61]. GISTs without mutations in *KIT*, *PDGFRA* or *BRAF*, whether pediatric or adult, have been shown to exhibit a much lower level of cytogenetic progression than observed in mutant GISTs [10, 62] underscoring that mechanisms leading to tumor progression are different in mutant and wild-type GISTs.

Epidemiology

The exact incidence of GIST in the USA and Europe is hard to determine, as GISTs have only been properly recognized and uniformly diagnosed as an entity since the late 1990s. Recent population-based studies performed in Sweden [63], Holland [64] and Iceland [65] found incidences of approximately 14.5, 12.7, and 11 cases/million/year, respectively. These findings would translate into an annual incidence in Europe of ~8,000-9,000 cases and in the USA of ~4,000-5,000 cases a year. Nevertheless, the prevalence of GIST is higher, as many patients live with the disease for many years or develop small GISTs only detected at autopsy or if a gastrectomy is performed for another cause. A German study performed on consecutive autopsies revealed small GISTs (1-10 mm) in 22.5% of individuals over the age of 50 years [66]. These minute GISTs are immunoreactive for KIT and often contain an oncogenic mutation in the *KIT* or *PDGFRA* gene [66]. Similar findings have been reported by other groups [51–53, 67]. These findings suggest that small GISTs do not progress often (or rapidly) into large tumors despite the presence of *KIT* or *PDGFRA* mutations.

At the time of diagnosis, the majority of patients with GIST are between 40 and 80 years old, with a median age of approximately 60 years; GISTs have no clear gender predilection [68]. Rarely, GISTs occur in children and young adults. Pediatric GISTs are considered a separate clinicopathologic entity (see below) and occur predominantly in the second decade [10, 69, 70]. Most GISTs are sporadic, but families with germ-line *KIT* mutations and GISTs are well described [71–79]. Furthermore, hereditary syndromes such as neurofibromatosis type I [80–82], Carney's triad (gastric GIST, paraganglioma, and pulmonary chondroma) [83, 84], and Carney's dyad (paraganglioma, gastric GIST) [78] can be associated with the development of GISTs.

Clinical and pathological aspects

Clinical features

GISTs occur throughout the GI tract and are most commonly seen in the stomach (60%), jejunum and ileum (30%), duodenum (5%), colorectum (4%), and rarely the esophagus and appendix [35, 68, 70, 85]. Tumors lacking any association with the bowel wall are known as extra-gastrointestinal stromal sarcomas and more often occur in the omentum, mesentery, or retroperitoneum [86, 87]. Clinical symptoms associated with GIST include abdominal pain, fatigue, dysphagia, satiety, and obstruction. Patients may present with chronic GI bleeding (causing anemia) or acute GI bleeding (caused by erosion through the gastric or bowel mucosa) or rupture into the abdominal cavity causing life-threatening intraperitoneal hemorrhage. Previously, a population-based study revealed that approximately 70% of GISTs were associated with clinical symptoms, 20% were not, and 10% were detected at autopsy [63]. The median tumor size in each of these categories was 8.9, 2.7, and 3.4 cm, respectively [63]. Small GISTs mainly present as incidental findings during endoscopy, surgery, or radiologic studies for other reasons, whereas patients with malignant GIST often present with disseminated disease. Metastases can quite often occur 10-15 years after initial surgery, and therefore long-term follow-up is required. Metastases develop primarily in the abdominal cavity and liver, rarely in the soft tissue and skin, and exceptionally rarely in lymph nodes or in the lung [85]. Clinically, it is essential to differentiate metastatic GIST from multifocal GISTs observed in patients with germline *KIT* or *PDGFRA* mutations, in patients with neurofibromatosis 1 and multiple sporadic GISTs, mainly occurring in the proximal stomach [88]. The pathogenesis of multiple sporadic GISTs is poorly understood; however, these GISTs have been shown to harbor different *KIT* mutations in separate individual lesions from the same patient [88]. Generally speaking, the clinical history, clinical presentation (see below), morphology, mitotic activity and, in rare cases, mutational analysis should allow exact precise classification.

Macroscopic features

GISTs present most often as well-circumscribed, highly vascular tumors associated with the stomach or the intestine. On gross examination, these tumors appear fleshy pink or tan-white and may show hemorrhagic foci, central cystic degenerative changes, or necrosis (Fig. 3).

Microscopic features

Morphologic evaluation reveals three principal subtypes of GIST depending on the cytomorphology. Spindle cell GIST (Fig. 4a), accounting for approximately 70% of cases, is composed of cells with palely eosinophilic fibrillary cytoplasm, ovoid nuclei, and ill-defined cell borders, often with a syncytial appearance, arranged in short fascicles or whorls. GIST with epithelioid cell morphology (Fig. 4b), accounting for approximately 20%, is composed of round cells with eosinophilic to clear cytoplasm arranged in sheets and nests. Finally, approximately 10% of GISTs show mixed morphology, being composed of both spindle and epithelioid cells (Fig. 4c). Variable cellularity as well as sclerotic, collagenous, or myxoid stromal changes can be seen in each subtype. Spindle cell GISTs can show nuclear palisading (Fig. 4d) or a storiform growth pattern as well as prominent paranuclear vacuolation (Fig. 4e), a morphologic feature formerly proposed to be suggestive of smooth muscle origin but far more commonly seen in GISTs. Overall, GISTs are characterized as uniform and monotonous tumors; however, pleomorphic GISTs [89] and dedifferentiated GISTs are seen very occasionally (Fig. 4f) [90].

GISTs after treatment with TKI may show a dramatic decrease in tumor cellularity and marked sclerosis (Fig. 5a) or prominent stromal alterations including myxoid change (Fig. 5b). In the majority of cases, the cytomorphology remains comparable with the primary tumor. However, changes from spindle to purely epithelioid cytomorphology, a pseudopapillary epithelioid growth pattern [91] as well as, in very rare cases, rhabdomyosarcomatous differentiation (Fig. 5c, d), has been reported after TKI treatment [92]. These findings can cause major diagnostic problems especially if the tumor also loses KIT expression. Under such circumstances, mutational analyses facilitate the diagnosis, as these tumors still retain their primary *KIT* or *PDGFRA* mutation after treatment [91, 92]. Although reports about these unusual findings are limited to date, the use of several different TKIs or other drugs over a longer period may predispose to the development of treatment-resistant tumor clones showing unusual morphology. A somewhat surprising observation in this context is that tumors showing these unusual morphologic alterations generally lack secondary *KIT* mutations [91, 92], the most common cause for secondary TKI treatment resistance. Interestingly, in one case, a metastatic peritoneal nodule showed a *BRAF* mutation in addition to the primary *PDGFRA* mutation after treatment with Imatinib [49].

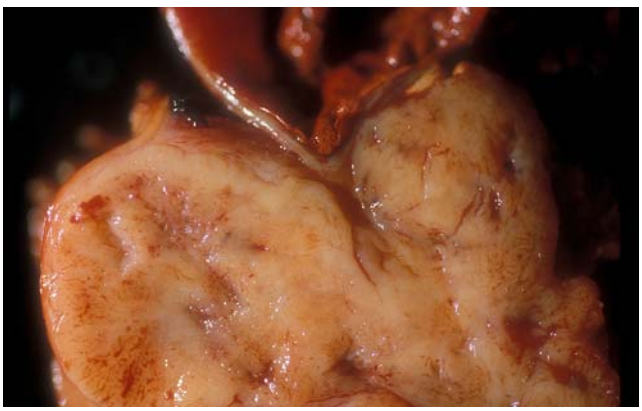

Fig. 3 Typically fleshy tan-white surface of a large gastric serosal GIST

GIST and neurofibromatosis type I

The occurrence of multiple small GISTs in the small bowel, other than in the setting of disseminated sporadic GIST, is significantly associated with neurofibromatosis type I (NF1). These GISTs show spindle cell morphology, are usually mitotically inactive, and express KIT, usually in the absence of *KIT* and *PDGFRA* mutations [80–82]. Clinically, they are usually benign. In rare cases, clinically malignant GISTs in association with multiple benign tumor nodules have been described [35].

Pediatric GISTs

Approximately 1-2% of GISTs occur in the pediatric age group, predominantly in the second decade. Pediatric GISTs are associated with a marked female predominance, are preferentially located in the stomach, and show mainly epithelioid morphology [10, 69, 70]. Although these tumors consistently express KIT protein, the majority lack *KIT* or *PDGFRA* mutations [10, 69, 70]. Unlike adult GISTs, these tumors quite often spread to lymph nodes. Interestingly, pediatric *KIT* wild-type GISTs lack the typical cytogenetic deletions seen in adult *KIT*-mutant GISTs and progress to malignancy without acquiring large-scale chromosomal aberrations [10]. The difference between pediatric *KIT* wild-type and adult GISTs of the stomach is further demonstrated by their separate clustering by gene expression profiling [69], and it is very likely that these tumors are a separate clinicopathologic entity. In the pediatric wild-

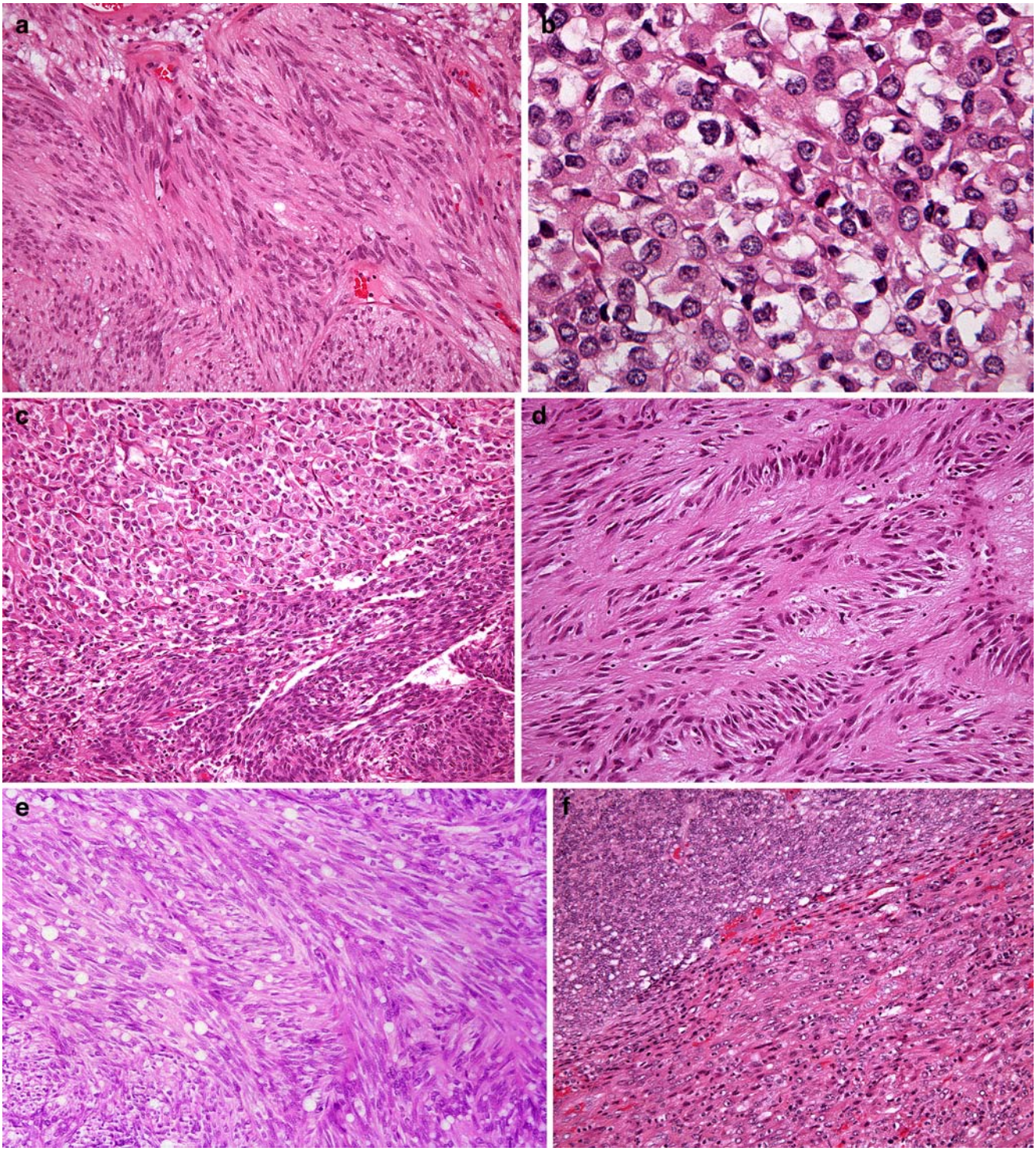

Fig. 4 **a** GIST composed of spindle cells with uniform ovoid or tapering nuclei and palely eosinophilic fibrillary cytoplasm with ill-defined cell borders. **b** GIST composed of epithelioid cells with eosinophilic or clear cytoplasm. **c** GIST with mixed spindle cell and epithelioid cytomorphology. **d** Spindle cell GIST showing prominent nuclear palisading (tumors such as this were often formerly labeled as GANT). **e** Spindle cell GIST showing prominent paranuclear cytoplasmic vacuolation. **f** Dedifferentiated GIST showing abrupt transition from conventional GIST to undifferentiated sarcoma composed of much larger epithelioid and spindle cells, which were KIT-negative

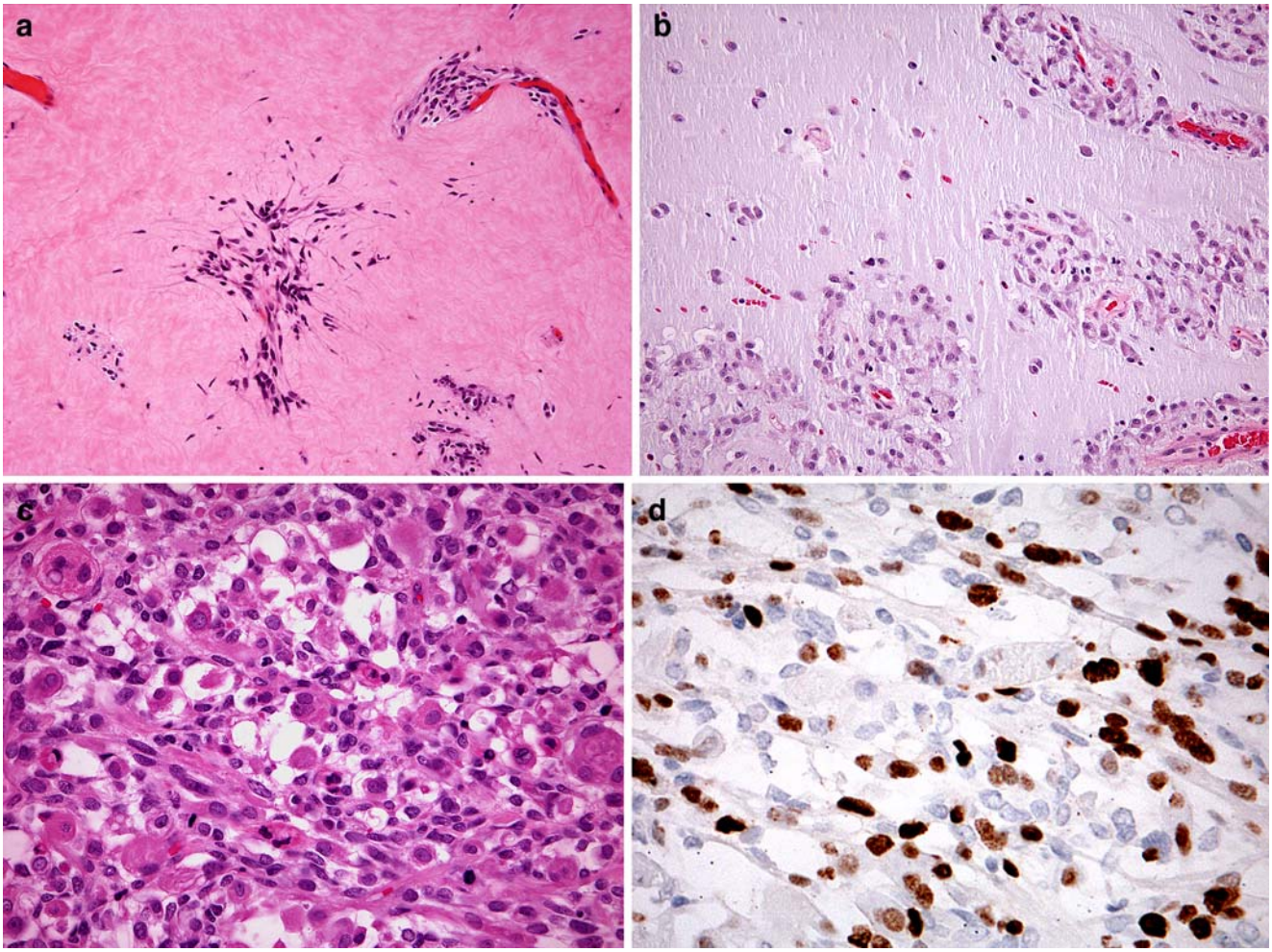

Fig. 5 **a** Treated GIST with marked stromal sclerosis and reduced cellularity. **b** Treated GIST showing myxoid stromal change. **c** Treated GIST showing heterologous rhabdomyosarcomatous differentiation. **d** Strong nuclear expression of myf-4 (myogenin) in a GIST showing heterologous rhabdomyosarcomatous differentiation

type GIST group, time to tumor progression was significantly longer on sunitinib than on prior imatinib treatment, indicating that this patient group could benefit from sunitinib as first-line treatment [93, 94].Sometimes pediatric GISTs are associated with pulmonary chondromas and/or paragangliomas referred to as Carney's triad [83]. In the pediatric age group, Carney's triad should be considered in any patient with GIST, especially if patients also present with lung nodules.

Familial GISTs

Heritable mutations in *KIT* and *PDGFRA* have been reported in some families [71–79]. The penetrance in these kindreds is high, and most affected family members will develop one or more GISTs during their life span. The mean age of onset (44 years) is younger than that of sporadic GISTs (around 60 years) without gender differences. Most of these GISTs follow a benign course, and their morphology does not differ from that of their sporadic counterparts. Interestingly, patients harboring a heritable *KIT* exon 13 or 17 mutation develop multiple GISTs, whereas patients harboring a heritable *KIT* exon 11 mutation can also develop skin hyperpigmentation and mast cell disease [71–75].

GISTs in association with Carney's triad and Carney's dyad (Carney-Stratakis syndrome)

GISTs are part of Carney's triad (gastric GIST, paraganglioma, and pulmonary chondroma) [83, 84] and Carney's dyad (paraganglioma, gastric GIST) [78], and these GISTs are *KIT/PDGFRA* wild-type. The genetic basis for Carney's triad is not known, although it is thought to be sporadic rather than familial. In both conditions, the presence of multiple gastric GISTs is common. Carney's

dyad is transmitted as an autosomal dominant trait, and recently Pasini et al. demonstrated, in a subset of these GISTs, germline mutations of the genes coding for succinate dehydrogenase subunits B, C, or D, implying that other molecular mechanisms, rather than *KIT/PDGFRA* mutations, may play a role in the pathogenesis of GISTs in this setting [78]. Recently, Zhang et al. reported a study of 104 GISTs in Carney triad, emphasizing the differences from sporadic GISTs [95]. The clinical features of the triad include occurrence at a young age, female predilection, tumor multifocality, slow growth, frequent metastasis (often to lymph nodes), lack of response to imatinib treatment, and sometimes fatal outcome. In addition, this subset of GISTs occurs mainly in the gastric antrum, shows predominantly epithelioid morphology, and lacks *KIT*, *PDGFRA*, or *SDH* mutations [95]. Interestingly, there is no correlation between conventional risk assessment and tumor behavior and, even with metastatic disease, clinical behavior is unpredictable [95].

Immunohistochemical markers in the diagnosis of GIST

KIT has been demonstrated to be a very specific and sensitive marker in the differential diagnosis of mesenchymal tumors in the GI tract, and around 95% of GISTs express KIT [6, 8, 16, 96]. Different KIT-staining patterns can be observed [16]. Most GISTs show strong and diffuse cytoplasmic KIT staining (Fig. 6a) often associated with dot-like ("Golgi-pattern") staining. Only in a minority of cases is an exclusively dot-like or even a membranous staining pattern observed. The extent and patterns of KIT staining do not correlate with the type of *KIT* mutation and have no impact on the likelihood of response to imatinib. However, GISTs showing weak or focal KIT expression and those GISTs completely negative for KIT are more likely *KIT* wild-type or *PDGFRA* mutant GISTs [38, 39]. Approximately, 4-5% of GISTs are KIT negative [38, 39]. KIT-negative GISTs preferentially occur in the stomach and usually show pure epithelioid or mixed (spindle and epithelioid) cytomorphology.

Other commonly expressed but less sensitive and specific markers are CD34, h-caldesmon, and SMA. CD34 is expressed in approximately 80% of gastric tumors, 50% of those in the small intestine, and 95% of GISTs in the esophagus and rectum [35, 97], whereas h-caldesmon is expressed in more than two-thirds of GISTs [86, 98] and SMA in 30%. S-100 and cytokeratin are only infrequently expressed in GISTs. Desmin expression has been reported rarely in GISTs, but in our experience approximately 30% of KIT-negative GISTs, especially those located in the stomach and showing epithelioid morphology, are desmin positive (Fig. 6b) [99]. In this context, it should be noted

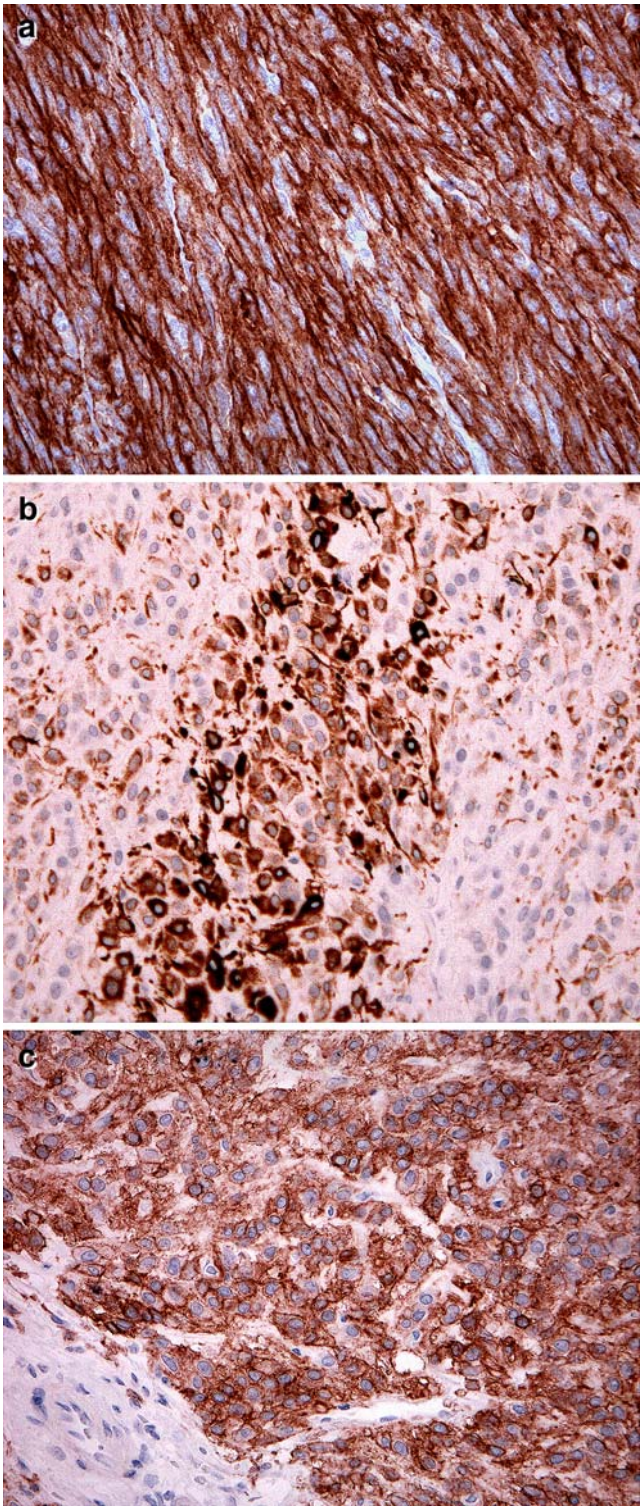

Fig. 6 **a** Spindle-cell GIST showing strong and diffuse cytoplasmic KIT expression. **b** Desmin staining in a KIT-negative epithelioid GIST (with *PDGFRA* mutation). **c** Cytoplasmic and membranous DOG1.1 staining in a KIT-negative GIST

that KIT negativity by no means justifies denying patients therapy with TKI (imatinib or sunitinib), as some wild-type GISTs as well as some tumors with *PDGFRA* mutations respond to treatment with TKI (see below).

In recent years, alternative antibodies for the diagnosis of GIST have emerged. These immunomarkers were mainly identified through molecular studies and are of special interest in the subgroup of KIT-negative GISTs.

One promising marker is discovered on GIST (DOG1), also known as TMEM16A, which is a transmembrane protein recently shown to be up-regulated in GISTs by gene expression profiling [100]. Two recent studies have suggested that antibodies against DOG1 have greater sensitivity and specificity than KIT (CD117) and CD34, and that these antibodies could serve as specific immunohistochemical markers for GIST irrespective of the underlying *KIT/PDGFRA* mutation or KIT expression by IHC [100, 101]. In our own experience, DOG1.1 is a very sensitive marker for GIST, works well on paraffin-embedded tissue, and is highly expressed in *KIT* mutant GISTs as well as in unusual subtypes of GIST lacking *KIT/PDGFRA* mutations, namely pediatric GISTs and GISTs associated with NF1 [99]. Although, DOG1.1 stains about one-third of KIT-negative GISTs (Fig. 6c), in our experience the remaining two-thirds, while often being morphologically typical, are difficult to validate immunohistochemically [99]. Depending on the DOG1 antibody used in different studies, staining in normal gastric epithelium, carcinomas, germ cell tumors, melanomas, and rarely in some mesenchymal tumors has been reported [101, 102].

Protein kinase C (PKC)-theta is a member of the protein kinase C family and is expressed in virtually all GISTs and is very specific, at least by Western blots. Immunohistochemical staining for PKC-theta has been reported in GIST; however in our experience, the commercially available antibodies to this protein show high background staining and limited specificity and are therefore of limited diagnostic utility [28, 103, 104].

PDGFRA alpha is a receptor tyrosine kinase closely related to KIT. Antibodies to this kinase have been proposed to be of use in the identification of KIT-negative GISTs harboring a *PDGFRA* mutation [105–108]. However, in our experience (and that of other major centers), the commercially available antibodies to PDGFRA do not show reproducible immunohistochemical results in paraffin sections.

Nestin, an intermediate filament protein, has been proposed to be expressed in GISTs as well as in a subset of glial, epithelial, melanocytic, and vascular tumors [109] and the intensity of staining has been suggested to correlate with risk stratification [109]. Although, our personal experience is limited with this marker, it seems to work well on paraffin-embedded tissue. Further evaluation of this antibody, especially on KIT-negative GISTs, will be necessary to determine its potential use in routine diagnosis.

Carbonic anhydrase II (CA II) has been proposed as a novel biomarker in GIST [110]. Independent of mutational status, 95% of GISTs express CA II and, interestingly, 50% of KIT negative cases show strong CA II expression [110]. In addition CA II expression also seems to be associated with a better disease-specific survival rate compared to low or no expression [110]. Although, we do not have personal experience with this marker, the results are promising that CA II could be used as an additional diagnostic as well as prognostic marker.

Despite these developments, a subset of KIT-negative tumors remains a diagnostic challenge, at least in terms of immunohistochemical verification; and mutational analysis should be strongly considered under these circumstances.

Recently, a PCR-based assay based on the identification of a single gene set identified through top scoring pair analysis (a method able to identify a gene pair where the relative expression is reversed between two cancers) has been proposed to be highly accurate to differentiate GISTs from leiomyosarcomas as well as to accurately identify KIT-negative GISTs and GISTs with weak or heterogeneous KIT expression [111]. Price et al. proposed an estimated accuracy for this test of around 98% [111]. Although, such testing appears to be promising, it has not yet been evaluated by independent groups.

Differential diagnosis

The main differential diagnoses of spindle-cell GIST that should be considered are smooth muscle tumors, desmoid fibromatosis, schwannoma, inflammatory myofibroblastic tumor, inflammatory fibroid polyp, and solitary fibrous tumor. Smooth muscle tumors show brightly eosinophilic cytoplasm with defined cell borders rather than the syncytial appearance typically seen in GIST. Although SMA and caldesmon are expressed in both tumor types, desmin expression is relatively specific for smooth muscle tumors and rarely positive in spindle-cell GISTs. However, in our experience, desmin expression is mainly seen in epithelioid GISTs located in the stomach and lacking KIT expression [99]. Schwannomas occurring in the gastrointestinal tract typically show a distinctive peripheral cuff of lymphocytes and express S-100 protein and GFAP [112]. Intraabdominal desmoid fibromatosis is morphologically characterized by long sweeping fascicles of fibroblastic/myofibroblastic spindle cells set within a collagenous matrix. Immunohistochemistry reveals nuclear beta-catenin positivity in approximately 75% of cases [113, 114]. In the absence of antigen retrieval, KIT positivity in desmoid fibromatoses is infrequent [115]. Inflammatory myofibroblastic tumors mainly occur in children and young adults. They are cellular, fascicular, fibroblastic/myofibroblastic

tumors with a prominent inflammatory infiltrate composed mainly of plasma cells. ALK expression by immunohistochemistry can facilitate the diagnosis [116] but is seen in at most 50% of cases (mostly in children). Inflammatory fibroid polyp (IFP) has a collagenous or more myxoid granulation tissue-like stroma containing fibroblasts in a pattern-less array and inflammatory cells, including numerous eosinophils. Perivascular fibrosis is commonly seen. The fibroblasts usually express CD34. PDGFRA expression by immunohistochemistry and mutations in *PDGFRA* has been reported in IFPs [117, 118]. However, in contrast to GIST, IFPs do not express KIT and DOG1 [101, 102]. The differential diagnosis for epithelioid GIST includes neuroendocrine carcinoma, glomus tumor, malignant melanoma, epithelioid leiomyosarcoma, epithelioid MPNST, and clear cell sarcoma. Neuroendocrine carcinomas are characterized by cytokeratin, synaptophysin, and chromogranin positivity. Glomus tumors are rarely seen in the GI tract and are morphologically and immunohistochemically identical to glomus tumors in other locations. Melanoma, clear cell sarcoma, and epithelioid malignant peripheral nerve sheath tumor (MPNST) express S-100 protein; the first two may also express second-line melanoma markers that are not expressed in MPNST. Furthermore, clear cell sarcomas are characterized by *EWSR1–CREB1* or *−ATF1* gene fusions [119, 120].

Morphologic risk assessment in GIST

Although the vast majority of GISTs smaller than 2 cm are essentially clinically benign, occasional patients develop metastases sometimes 5 years or more after primary excision. Therefore, older classifications using the terminology "benign" or "malignant" GIST have been replaced by stratification schemata to help predict the risk of aggressive clinical behavior. The first widely accepted scheme to predict the risk of aggressive clinical behavior in GIST was published in 2002 by Fletcher and colleagues after a consensus workshop held at the National Institutes of Health [3, 121]. The proposed risk assessment was based on tumor size and mitotic activity [per 50 high power fields (HPF)], with the most important cut-offs being tumor size of 5 cm and 5 mitoses/50 HPF as indicators of aggressive clinical behavior. According to the 2002 consensus guidelines, all GISTs may have malignant potential. In 2005 and 2006, Miettinen and colleagues from the AFIP presented two very large studies of gastric GISTs and jejunal/ileal GISTs [35, 68], providing strong evidence that GISTs located in the stomach have a much lower rate of aggressive behavior than jejunal and ileal GISTs of similar size and mitotic activity. Based on these publications, anatomic location is now included as an additional parameter in risk assessment for GIST according to the recently updated consensus NCCN guidelines from 2007 [1] (for summary, see Table 1, adapted from Miettinen et al [122]). According to the new guidelines, GISTs smaller than 2 cm can be regarded as essentially benign. In addition to these widely accepted and preferentially used risk assessment schemes, additional schemes have also been proposed by Joensuu and Woodall et al [123, 124]. Of interest is the prognostic nomogram for recurrence-free survival after complete surgical resection of localized primary GISTs using size, mitotic index and site to predict the probability of 2- and 5-year recurrence-free survival [125]. This nomogram may potentially be of help in stratifying patients for adjuvant TKI treatment.

Other proposed prognostic markers in GISTs

The tumor suppressor gene *CDKN2A* (p16) on chromosome 9p is an important inhibitor of the cell cycle and has been demonstrated to be inactivated in a significant proportion of malignant GISTs [126–130]. Evaluation of p16 by immunohistochemistry has been proposed, and downregulation of p16

Table 1 Risk stratification of primary GIST by mitotic index, size and anatomic location

Risk stratification of primary GIST					
Tumor parameter		Risk of progressive disease[a]			
Mitotic index	Size	Gastric	Duodenum	Jejunum/ileum	Rectum
≤5/50 HPF	≤2 cm	None	None	None	None
≤5/50 HPF	>2≤5 cm	Very low (1.9%)	Low (8.3%)	Low (4.3%)	Low (8.5%)
≤5/50 HPF	>5≤10 cm	Low (3.6%)	-[c]	Moderate (24%)	-[c]
≤5/50 HPF	>10 cm	Moderate (10%)	High (34%)	High (52%)	High (57%)
>5/50 HPF	≤2 cm	None[b]	-[c]	High[b]	High (54%)
>5/50 HPF	>2≤5 cm	Moderate (16%)	High (50%)	High (73%)	High (52%)
>5/50 HPF	>5≤10 cm	High (55%)	-[c]	High (85%)	-[c]
>5/50 HPF	>10 cm	High (86%)	High (86%)	High (90%)	High (71%)

[a] Defined as metastasis or tumor-related death

[b] Limited number of cases

[c] Insufficient data

The table is based on Miettinen et al, Semin Diagn Pathol, 2006 [122]. Data based on long-term follow-up of 1,055 gastric, 629 small intestinal, 144 duodenal, and 111 rectal GISTs [35, 68].

has been shown to correlate with aggressive behavior, even in tumors classified as low risk according [40] to the standard morphologic evaluation [127, 128, 130]. However, most recently, Steigen et al. demonstrated contrary results [131].

The p27 cell cycle inhibitor can also be downregulated in malignant GISTs and upregulation of cell cycle regulatory proteins (cyclins B1,D, and E; cdc2, CDK2, CDK4, and CDK6), as well as increased expression of p53, RB, and cyclinA by immunohistochemistry, have been proposed to be detected more commonly in high-risk GISTs [128, 130, 132–136]. In addition to the markers mentioned above, an increasing list of prognostic factors has been reported in GIST for example Ezrin, Raf kinase inhibitor protein, COX-2, bcl-2, CA II [110, 136–139]. However, standardized protocols for staining and interpretation of these markers have not been established as yet.

Role of molecular testing with regard to prognosis and treatment

Objective clinical response to imatinib has been shown to depend on the underlying RTK mutation, and a molecular classification of GISTs has been proposed [14]. Based on four clinical trials (phase I-III) investigating more than 700 genotyped GISTs, the objective response rates for *KIT* exon 11 mutant GISTs, *KIT* exon 9 mutant GISTs, and wild-type GISTs are 72-86%, 38-48%, and up to 28%, respectively [1, 13, 43, 140–142]. Primary resistance to imatinib has been likewise demonstrated in 5% of GISTs showing *KIT* exon 11 mutation and in 16% and 23% of *KIT* exon 9 mutant and *KIT* wild-type GISTs, respectively. *PDGFRA* mutant GISTs have been shown to respond to imatinib, with the exception of the exon 18 D842V mutation [13, 43–45]. Overall, the best response rates to imatinib {the longest median time to tumor progression (~24 months) and longest median survival (~63 months)} [13, 43, 140] are seen in GISTs harboring a *KIT* exon 11 mutation. In these patients, the median time to tumor progression is more than 1 year longer than for *KIT* exon 9 mutant or other common genotypic subsets.

Generally, patients with *KIT* exon 11 mutant GISTs are treated with 400 mg imatinib/day, and dose escalation to 800 mg/day is recommended if patients progress on 400 mg. Clinical data did not reveal a significant benefit for *KIT* exon 11 mutant GISTs whether treated initially with 400 or 800 mg of imatinib [140]. However, patients with *KIT* exon 9 mutations have better progression-free survival if treated with imatinib 800 mg/day than 400 mg [36, 43]. This observation provides the rationale for recent consensus that *KIT* mutation status be evaluated routinely in inoperable GISTs, and with imatinib dose escalated immediately to 800 mg/day if a *KIT* exon 9 mutation is found.

To date, routine mutational testing on all GISTs remains very controversial, as most institutions treat patients with imatinib as a first-line therapy, irrespective of mutational status. Nevertheless, scientific data coming from major academic institutions in Europe and the USA, where molecular analysis of GISTs is routinely performed, suggest that mutational testing should be performed for unresectable and metastatic GISTs, such that patients with *KIT* exon 9 mutants can be dose-escalated to 800 mg/day.

Mutational testing could additionally be considered before adjuvant imatinib treatment for primary "intermediate-high risk" GISTs [1, 143]. Adjuvant treatment with imatinib has been reported to extend progression-free survival in patients with high-risk primary GISTs [144, 145]. Recent study results provide encouraging data on imatinib as an adjuvant therapy. In the ACOSOG Z9001, a phase III randomized trial, 778 patients with localized GIST, who underwent complete surgical resection, were treated for 1 year with imatinib (400 mg/day) versus placebo. The patients were only stratified by tumor size. Adjuvant imatinib treatment significantly improved recurrence-free survival in the imatinib group versus the placebo group as well as in all tumor size stratification groups. The greatest difference between the treatment and the placebo arm was observed in high risk patients (tumor size ≥10 cm). However, the overall survival in the imatinib and placebo group was the same [146]. Based on these results, imatinib was approved as adjuvant therapy for GIST by the US Federal Drug Administration and the European Medicines Agency. Although, an overall consensus as to which patients should receive adjuvant treatment does not exist yet, it is widely accepted that patients with high-risk GISTs should definitely get adjuvant imatinib treatment.

Although state-of-the-art first-line treatment for all patients with metastatic/unresectable GIST is imatinib, it is likely that this treatment regimen will change in the future based on the underlying mutational status [36, 94].

Supportive arguments for routine mutational testing of all GISTs are also based on data that *KIT* exon 9 mutant GISTs in the small intestine and colon are more aggressive than tumors with a *KIT* exon 11 mutation [31, 34], whereas tumors with a *PDGFRA* mutation are less aggressive than those harboring a *KIT* mutation [41, 147].

Resistance mechanisms in GIST

The vast majority of patients with unresectable or metastatic GIST show a response to imatinib. Treatment response can be seen on CT scan as reduction of the tumor mass or as decreased FDG uptake on a PET scan. In a subset of cases, the tumor remains stable under treatment, whereas, in the minority of cases, tumor re-growth is noted within

the first 6 months. Tumor progression within the first 6 months of imatinib treatment is referred to as primary resistance. In this group, *KIT* exon 9 and *KIT* wild-type tumors are over-represented compared with exon 11 mutant tumors [13, 43]. The majority of patients showing initially good response or stable disease will develop tumor progression in one or more lesions usually after 12-36 months, referred to as secondary resistance. Secondary resistance is most commonly caused by secondary (acquired) mutations in the *KIT* kinase domain, and rarely other resistance mechanisms including *KIT/PDGFRA* genomic amplification and activation of alternative oncogenes have been reported [148–150]. Secondary *KIT* kinase mutations are non-randomly distributed single nucleotide substitutions affecting codons in the ATP binding pocket (exons 13 and 14) and the kinase activation loop (exon 17 and 18). Several studies have demonstrated resistance mutations in 44-67% of GISTs progressing after imatinib therapy [142, 151–153]. Sunitinib, the second-line TKI used after imatinib failure, has been shown to be effective against secondary mutations located in the ATP binding pocket (exon 13 and 14) but not against mutations in the kinase activation loop (exon 17 and 18) based on in vitro and in vivo studies [36, 94].

We demonstrated substantial inter- and intralesional heterogeneity in TKI resistance mutations in patients treated with imatinib alone or imatinib and sunitinib: 83% of patients in this study had secondary drug-resistant *KIT* mutations, including 67% with two to five different secondary mutations in separate metastases, and 34% with two secondary *KIT* mutations in the same metastasis [150]. The most frequent secondary resistance mutation in patients whose GISTs have primary *KIT* exon 11 mutations and who eventually progress during imatinib treatment is the V654A point mutation in the ATP-binding pocket [142, 154]. Interestingly, the V654A mutation, which is sunitinib-sensitive based on in vitro studies [94], was found in ~27% of our samples after clinical progression on sunitinib [150]. In addition, these same samples showed minimal-to-low morphologic evidence of treatment response. Such observations suggest that sunitinib is cytostatic rather than cytocidal in GISTs with secondary V654A mutations, in keeping with the clinical evidence from a randomized, placebo-controlled, multicenter trial demonstrating that stable GIST was the best overall tumor response on sunitinib treatment [155]. The presence of low-level TKI resistance mutations on the same *KIT* alleles encoding the V654A may also account for persistence of V654A alleles during sunitinib therapy.

New treatment options in GISTs

Imatinib currently remains the standard first-line treatment option for patients with unresectable and metastatic GISTs, especially those harboring an exon 11 mutation. However, accumulating evidence suggests that sunitinib could be effective as a first-line treatment for GISTs harboring *KIT* exon 9 mutation and for *KIT/PDGFRA* wild-type GISTs (including pediatric GISTs) [36, 94, 152]. Sunitinib is effective against secondary imatinib-resistance mutations in the ATP-binding pocket [94]. However, the substantial heterogeneity of resistance mutations (as discussed above) highlights the therapeutic challenges involved in salvaging patients, especially after clinical progression on TKI monotherapies. With regard to treatment approaches, the role of newer generation KIT and PDGFRA kinase inhibitors (e.g., nilotinib, dasatinib, etc.) remains to be determined in GIST patients who are multiply resistant, i.e., after imatinib and sunitinib treatment, to TKIs. Nilotinib has been shown to be effective in advanced imatinib- and sunitinib-resistant GISTs [156]. Using nilotinib 400 mg twice a day, the median progression-free survival and the median overall survival were 12 and 34 weeks, respectively [156]. In vitro data, using cell lines expressing imatinib-resistant *PDGFRA* (D842V) mutants, suggest that dasatinib, a dual SRC/ABL kinase inhibitor, and IPI-504, a heat shock protein 90 inhibitor, may be a therapeutic option for patients with a GIST harboring the *PDGRA* (D842V9) mutation [157]. Histone deacetylase inhibitors (HDACI) alone or in combination with imatinib show inhibition of cell proliferation, KIT activity and expression as well as activation of downstream pathways in KIT-positive cell lines, providing preclinical evidence that HDACI may expand the treatment options in KIT-positive GISTs [158]. IGFR inhibitors in combination with imatinib have been proposed as a treatment option mainly for wild-type GISTs which tend to be less responsive to imatinib-based therapies. The rational for this treatment is based on detected amplification of IGF1R and protein over-expression predominantly in WT and pediatric GISTs [159, 160].

It seems clear that multi-agent treatment modalities are needed in the future. Combination therapies with various such inhibitors could prolong GIST remissions, in a manner analogous to treatment approaches used in HIV, by suppressing a broader spectrum of tumor clones from the outset of therapy. Similarly, therapeutic options less dependent on specific molecular mechanisms of KIT or PDGFRA activation are needed to overcome the substantial heterogeneity of secondary *KIT* kinase mutations responsible for treatment failure in the vast majority of patients. Such treatment options include inhibition of the KIT chaperone HSP90 [161], which may result in KIT oncoprotein degradation, irrespective of the TKI-resistance mutations present, or the use of flavopiridol, which acts as a *KIT* transcriptional repressor and is not expected to be altered by any nucleotide mutation in the

KIT coding sequence [162]. Compelling data has been presented recently by demonstrating the effects of bortezomib on imatinib-sensitive and imatinib-resistant cell lines. The results are especially promising as this drug has been shown to be effective against GIST cells harboring various resistance mutations and preliminary in vitro data confirm the potency of bortezomib in transgenic mice [163].

Other broadly relevant therapeutic strategies include blockage of crucial KIT-mediated signaling pathways, as might be accomplished via PI3-K [164], PKC-theta [165], MEK, or AKT-inhibitors [142].

Conclusion

This review provides an overview of GIST pathogenesis, morphologic evaluation, new diagnostically promising immunohistochemical markers, risk assessment, the role of molecular analyses as well as the increasing problem of secondary imatinib resistance and its mechanisms. The review demonstrates that within just one decade, GISTs have emerged from being poorly defined, treatment-resistant tumors to a well-recognized, well-understood, and treatable tumor entity. The small molecule tyrosine kinase inhibitors imatinib and sunitinib have fundamentally changed the overall survival for patients with metastatic GIST. However, the increased understanding of GIST biology has also provided informative insights into the limitations of so-called targeted therapeutics and highlights the upcoming problem of secondary resistance. Exact morphologic classification and risk assessment are an essential part of optimal patient care. Although, the precise role of molecular analysis is controversial to date, the potential value of molecular testing in at least a subset of GISTs is clear.

Conflict of interest statement We declare that we have no conflict of interest.

References

1. Demetri GD, Benjamin RS, Blanke CD et al (2007) NCCN Task force report: management of patients with gastrointestinal stromal tumor (GIST)—update of the NCCN clinical practice guidelines. J Natl Compr Canc Netw 5(Suppl 2):S1–S29
2. Edmonson JH, Marks RS, Buckner JC et al (2002) Contrast of response to dacarbazine, mitomycin, doxorubicin, and cisplatin (DMAP) plus GM-CSF between patients with advanced malignant gastrointestinal stromal tumors and patients with other advanced leiomyosarcomas. Cancer Investig 20(5–6):605–612
3. Fletcher CD, Berman JJ, Corless C et al (2002) Diagnosis of gastrointestinal stromal tumors: a consensus approach. Human Pathol 33:459–465
4. Mazur MT, Clark HB (1983) Gastric stromal tumors. Reappraisal of histogenesis. Am J Surg Pathol 7(6):507–519
5. Miettinen M, Virolainen M, Maarit Sarlomo R (1995) Gastrointestinal stromal tumors—value of CD34 antigen in their identification and separation from true leiomyomas and schwannomas. Am J Surg Pathol 19(2):207–216
6. Hirota S, Isozaki K, Moriyama Y et al (1998) Gain-of-function mutations of c-kit in human gastrointestinal stromal tumors. Science 279(5350):577–580
7. Huizinga JD, Thuneberg L, Kluppel M et al (1995) W/kit gene required for interstitial cells of Cajal and for intestinal pacemaker activity. Nature 373(6512):347–349
8. Kindblom L, Ramotti H, Aldenborg F et al (1998) Gastrointestinal pacemaker cell tumor (GIPACT): gastrointestinal stromal tumors show phenotypic characteristics of the interstitial cells of Cajal. Am J Pathol 152:1259–1269
9. Robinson TL, Sircar K, Hewlett BR et al (2000) Gastrointestinal stromal tumors may originate from a subset of CD34-positive interstitial cells of Cajal. Am J Pathol 156(4):1157–1163
10. Janeway KA, Liegl B, Harlow A et al (2007) Pediatric KIT wild-type and platelet-derived growth factor receptor alpha wild-type gastrointestinal stromal tumors share KIT activation but not mechanisms of genetic progression with adult gastrointestinal stromal tumors. Cancer Res 67(19):9084–9088
11. Isozaki K, Hirota S, Nakama A et al (1995) Disturbed intestinal movement, bile reflux to the stomach, and deficiency of c-kit-expressing cells in Ws/Ws mutant rats. Gastroenterology 109 (2):456–464
12. Heinrich MC, Corless CL, Duensing A et al (2003) PDGFRA-activating mutations in gastrointestinal stromal tumors. Science 299(5607):708–710
13. Heinrich MC, Corless CL, Demetri GD et al (2003) Kinase mutations and imatinib response in patients with metastatic gastrointestinal stromal tumor. J Clin Oncol 21(23):4342–4349
14. Corless CL, Fletcher JA, Heinrich MC (2004) Biology of gastrointestinal stromal tumors. J Clin Oncol 22(18):3813–3825
15. Hornick JL, Fletcher CD (2002) Immunohistochemical staining for KIT (CD117) in soft tissue sarcomas is very limited in distribution. Am J Clin Pathol 117(2):188–193
16. Hornick JL, Fletcher CD (2007) The role of KIT in the management of patients with gastrointestinal stromal tumors. Human Pathol 38(5):679–687
17. Stenman G, Eriksson A, Claesson-Welsh L (1989) Human PDGFA receptor gene maps to the same region on chromosome 4 as the KIT oncogene. Genes Chromos Cancer 1(2):155–158
18. Hubbard SR (2004) Juxtamembrane autoinhibition in receptor tyrosine kinases. Nat Rev Mol Cell Biol 5(6):464–471
19. Pawson T (2002) Regulation and targets of receptor tyrosine kinases. Eur J Cancer 38(Suppl 5):S3–S10
20. Blume-Jensen P, Claesson-Welsh L, Siegbahn A et al (1991) Activation of the human c-kit product by ligand-induced dimerization mediates circular actin reorganization and chemotaxis. Embo J 10(13):4121–4128
21. O'Farrell AM, Abrams TJ, Yuen HA et al (2003) SU11248 is a novel FLT3 tyrosine kinase inhibitor with potent activity in vitro and in vivo. Blood 101(9):3597–3605
22. Casteran N, De Sepulveda P, Beslu N et al (2003) Signal transduction by several KIT juxtamembrane domain mutations. Oncogene 22(30):4710–4722
23. Duensing A, Medeiros F, McConarty B et al (2004) Mechanisms of oncogenic KIT signal transduction in primary gastrointestinal stromal tumors (GISTs). Oncogene 23(22):3999–4006
24. Kitayama H, Kanakura Y, Furitsu T et al (1995) Constitutively activating mutations of c-kit receptor tyrosine kinase confer factor-independent growth and tumorigenicity of factor-dependent hematopoietic cell lines. Blood 85(3):790–798

25. Rossi F, Ehlers I, Agosti V et al (2006) Oncogenic Kit signaling and therapeutic intervention in a mouse model of gastrointestinal stromal tumor. Proc Natl Acad Sci U S A 103(34):12843–12848
26. Lev S, Blechman J, Nishikawa S et al (1993) Interspecies molecular chimeras of kit help define the binding site of the stem cell factor. Mol Cell Biol 13(4):2224–2234
27. Maeda H, Yamagata A, Nishikawa S et al (1992) Requirement of c-kit for development of intestinal pacemaker system. Development 116(2):369–375
28. Duensing A, Joseph NE, Medeiros F et al (2004) Protein kinase C theta (PKCtheta) expression and constitutive activation in gastrointestinal stromal tumors (GISTs). Cancer Res 64 (15):5127–5131
29. Rubin BP, Singer S, Tsao C et al (2001) KIT activation is a ubiquitous feature of gastrointestinal stromal tumors. Cancer Res 61(22):8118–21
30. Corless CL, Heinrich MC (2008) Molecular pathobiology of gastrointestinal stromal sarcomas. Annu Rev Pathol 3:557–586
31. Lasota J, Dansonka-Mieszkowska A, Stachura T et al (2003) Gastrointestinal stromal tumors with internal tandem duplications in 3′ end of KIT juxtamembrane domain occur predominantly in stomach and generally seem to have a favorable course. Mod Path 16(12):1257–1264
32. Lasota J, Miettinen M (2008) Clinical significance of oncogenic KIT and PDGFRA mutations in gastrointestinal stromal tumours. Histopathology 53(3):245–266
33. Wardelmann E, Losen I, Hans V et al (2003) Deletion of Trp-557 and Lys-558 in the juxtamembrane domain of the c-kit protooncogene is associated with metastatic behavior of gastrointestinal stromal tumors. Int J Cancer 106(6):887–895
34. Antonescu CR, Sommer G, Sarran L et al (2003) Association of KIT exon 9 mutations with nongastric primary site and aggressive behavior: KIT mutation analysis and clinical correlates of 120 gastrointestinal stromal tumors. Clin Cancer Res 9 (9):3329–3337
35. Miettinen M, Makhlouf H, Sobin LH et al (2006) Gastrointestinal stromal tumors of the jejunum and ileum: a clinicopathologic, immunohistochemical, and molecular genetic study of 906 cases before imatinib with long-term follow-up. Am J Surg Pathol 30(4):477–489
36. Heinrich MC, Owzar K, Corless CL et al (2008) Correlation of kinase genotype and clinical outcome in the North American intergroup phase III trial of imatinib mesylate for treatment of advanced gastrointestinal stromal tumor: CALGB 150105 study by Cancer and Leukemia Group B and Southwest Oncology Group. J Clin Oncol 26(33):5360–5367
37. Lasota J, Corless CL, Heinrich MC et al (2008) Clinicopathologic profile of gastrointestinal stromal tumors (GISTs) with primary KIT exon 13 or exon 17 mutations: a multicenter study on 54 cases. Mod Path 21(4):476–484
38. Debiec-Rychter M, Wasag B, Stul M et al (2004) Gastrointestinal stromal tumours (GISTs) negative for KIT (CD117 antigen) immunoreactivity. J Pathol 202(4):430–438
39. Medeiros F, Corless CL, Duensing A et al (2004) KIT-negative gastrointestinal stromal tumors: proof of concept and therapeutic implications. Am J Surg Pathol 28(7):889–894
40. Wardelmann E, Hrychyk A, Merkelbach-Bruse S et al (2004) Association of platelet-derived growth factor receptor alpha mutations with gastric primary site and epithelioid or mixed cell morphology in gastrointestinal stromal tumors. J Mol Diagn 6 (3):197–204
41. Lasota J, Dansonka-Mieszkowska A, Sobin LH et al (2004) A great majority of GISTs with PDGFRA mutations represent gastric tumors of low or no malignant potential. Lab Invest 84 (7):874–883
42. Lasota J, Stachura J, Miettinen M (2006) GISTs with PDGFRA exon 14 mutations represent subset of clinically favorable gastric tumors with epithelioid morphology. Lab Invest 86(1):94–100
43. Debiec-Rychter M, Sciot R, Le Cesne A et al (2006) KIT mutations and dose selection for imatinib in patients with advanced gastrointestinal stromal tumours. Eur J Cancer 42(8):1093–1103
44. Corless CL, Schroeder A, Griffith D et al (2005) PDGFRA mutations in gastrointestinal stromal tumors: frequency, spectrum and in vitro sensitivity to imatinib. J Clin Oncol 23(23):5357–5364
45. Hirota S, Ohashi A, Nishida T et al (2003) Gain-of-function mutations of platelet-derived growth factor receptor alpha gene in gastrointestinal stromal tumors. Gastroenterology 125(3):660–667
46. Mendel DB, Laird AD, Xin X et al (2003) In vivo antitumor activity of SU11248, a novel tyrosine kinase inhibitor targeting vascular endothelial growth factor and platelet-derived growth factor receptors: determination of a pharmacokinetic/pharmacodynamic relationship. Clin Cancer Res 9(1):327–337
47. Ma Y, Cunningham ME, Wang X et al (1999) Inhibition of spontaneous receptor phosphorylation by residues in a putative alpha-helix in the KIT intracellular juxtamembrane region. J Biol Chem 274(19):13399–13402
48. Agaimy A, Terracciano LM, Dirnhofer S et al (2009) V600E BRAF mutations are alternative early molecular events in a subset of KIT/PDGFRA wild-type gastrointestinal stromal tumours. J Clin Pathol 62(7):613–616
49. Agaram NP, Wong GC, Guo T et al (2008) Novel V600E BRAF mutations in imatinib-naive and imatinib-resistant gastrointestinal stromal tumors. Genes Chromos Cancer 47(10):853–859
50. Hostein I, Faur N, Primois C et al (2010) BRAF mutation status in gastrointestinal stromal tumors. Am J Clin Pathol 133(1):141–148
51. Agaimy A, Wunsch PH, Dirnhofer S et al (2008) Microscopic gastrointestinal stromal tumors in esophageal and intestinal surgical resection specimens: a clinicopathologic, immunohistochemical, and molecular study of 19 lesions. Am J Surg Pathol 32(10):1553–1559
52. Kawanowa K, Sakuma Y, Sakurai S et al (2006) High incidence of microscopic gastrointestinal stromal tumors in the stomach. Human Pathol 37(12):1527–1535
53. Corless CL, McGreevey L, Haley A et al (2002) *KIT* mutations are common in incidental gastrointestinal stromal zumors one centimeter or less in size. Am J Pathol 160(5):1567–1572
54. Debiec-Rychter M, Lasota J, Sarlomo-Rikala M et al (2001) Chromosomal aberrations in malignant gastrointestinal stromal tumors: correlation with c-KIT gene mutation. Cancer Genet Cytogenet 128(1):24–30
55. Fukasawa T, Chong JM, Sakurai S et al (2000) Allelic loss of 14q and 22q, NF2 mutation, and genetic instability occur independently of c-kit mutation in gastrointestinal stromal tumor. Jpn J Cancer Res 91(12):1241–1249
56. El-Rifai W, Sarlomo-Rikala M, Miettinen M et al (1996) DNA copy number losses in chromosome 14: an early change in gastrointestinal stromal tumors. Cancer Res 56(14):3230–3233
57. Bergmann FGB, Hermanns B et al (1998) Cytogenetic and morphologic characteristics of gastrointestinal stromal tumors. Recurrent rearrangement of chromosome 1 and losses of chromosomes 14 and 22 as common anomalies. Verh Dtsch Ges Pathol 82:275–278
58. Kim NG, Kim JJ, Ahn JY et al (2000) Putative chromosomal deletions on 9P, 9Q and 22Q occur preferentially in malignant gastrointestinal stromal tumors. Int J Cancer 85(5):633–638
59. Lasota J, vel Dobosz AJ, Wasag B et al (2007) Presence of homozygous KIT exon 11 mutations is strongly associated with malignant clinical behavior in gastrointestinal stromal tumors. Lab Invest 87(10):1029–1041
60. El-Rifai W, Sarlomo-Rikala M, Andersson LC et al (2000) High-resolution deletion mapping of chromosome 14 in stromal

tumors of the gastrointestinal tract suggests two distinct tumor suppressor loci. Genes Chromos Cancer 27(4):387–391
61. Schurr P, Wolter S, Kaifi J et al (2006) Microsatellite DNA alterations of gastrointestinal stromal tumors are predictive for outcome. Clin Cancer Res 12(17):5151–5157
62. Belinsky MG, Skorobogatko YV, Rink L et al (2009) High density DNA array analysis reveals distinct genomic profiles in a subset of gastrointestinal stromal tumors. Genes Chromos Cancer 48(10):886–896
63. Nilsson B, Bumming P, Meis-Kindblom JM et al (2005) Gastrointestinal stromal tumors: the incidence, prevalence, clinical course, and prognostication in the preimatinib mesylate era-a population-based study in western Sweden. Cancer 103 (4):821–829
64. Goettsch WG, Bos SD, Breekveldt-Postma N et al (2005) Incidence of gastrointestinal stromal tumours is underestimated: results of a nationwide study. Eur J Cancer 41(18):2868–2872
65. Tryggvason G, Gislason HG, Magnusson MK et al (2005) Gastrointestinal stromal tumors in Iceland, 1990-2003: the icelandic GIST study, a population-based incidence and pathologic risk stratification study. Int J Cancer 117(2):289–293
66. Agaimy A, Wunsch PH, Hofstaedter F et al (2007) Minute gastric sclerosing stromal tumors (GIST tumorlets) are common in adults and frequently show c-KIT mutations. Am J Surg Pathol 31(1):113–120
67. Abraham SC, Krasinskas AM, Hofstetter WL et al (2007) "Seedling" mesenchymal tumors (gastrointestinal stromal tumors and leiomyomas) are common incidental tumors of the esophagogastric junction. Am J Surg Pathol 31(11):1629–1635
68. Miettinen M, Sobin LH, Lasota J (2005) Gastrointestinal stromal tumors of the stomach: a clinicopathologic, immunohistochemical, and molecular genetic study of 1,765 cases with long-term follow-up. Am J Surg Pathol 29(1):52–68
69. Prakash S, Sarran L, Socci N et al (2005) Gastrointestinal stromal tumors in children and young adults: a clinicopathologic, molecular, and genomic study of 15 cases and review of the literature. J Pediatr Hematol Oncol 27(4):179–187
70. Miettinen M, Lasota J, Sobin LH (2005) Gastrointestinal stromal tumors of the stomach in children and young adults: a clinicopathologic, immunohistochemical, and molecular genetic study of 44 cases with long-term follow-up and review of the literature. Am J Surg Pathol 29(10):1373–1381
71. Beghini A, Tibiletti MG, Roversi G et al (2001) Germline mutation in the juxtamembrane domain of the kit gene in a family with gastrointestinal stromal tumors and urticaria pigmentosa. Cancer 92(3):657–662
72. Isozaki K, Terris B, Belghiti J et al (2000) Germline-activating mutation in the kinase domain of KIT gene in familial gastrointestinal stromal tumors. Am J Pathol 157(5):1581–1585
73. Kang DY, Park CK, Choi JS et al (2007) Multiple gastrointestinal stromal tumors: clinicopathologic and genetic analysis of 12 patients. Am J Surg Pathol 31(2):224–232
74. Maeyama H, Hidaka E, Ota H et al (2001) Familial gastrointestinal stromal tumor with hyperpigmentation: association with a germline mutation of the c-kit gene. Gastroenterology 120(1):210–215
75. Nishida T, Hirota S, Taniguchi M et al (1998) Familial gastrointestinal stromal tumours with germline mutation of the KIT gene. Nat Genet 19(4):323–324
76. O'Riain C, Corless CL, Heinrich MC et al (2005) Gastrointestinal stromal tumors: insights from a new familial GIST kindred with unusual genetic and pathologic features. Am J Surg Pathol 29(12):1680–1683
77. Kleinbaum EP, Lazar AJ, Tamborini E et al (2008) Clinical, histopathologic, molecular and therapeutic findings in a large kindred with gastrointestinal stromal tumor. Int J Cancer 122 (3):711–718
78. Pasini B, McWhinney SR, Bei T et al (2008) Clinical and molecular genetics of patients with the Carney-Stratakis syndrome and germline mutations of the genes coding for the succinate dehydrogenase subunits SDHB, SDHC, and SDHD. Eur J Hum Genet 16(1):79–88
79. Li FP, Fletcher JA, Heinrich MC et al (2005) Familial gastrointestinal stromal tumor syndrome: phenotypic and molecular features in a kindred. J Clin Oncol 23(12):2735–2743
80. Andersson J, Sihto H, Meis-Kindblom JM et al (2005) NF1-associated gastrointestinal stromal tumors have unique clinical, phenotypic, and genotypic characteristics. Am J Surg Pathol 29 (9):1170–1176
81. Maertens O, Prenen H, Debiec-Rychter M et al (2006) Molecular pathogenesis of multiple gastrointestinal stromal tumors in NF1 patients. Hum Mol Genet 15(6):1015–1023
82. Miettinen M, Fetsch JF, Sobin LH et al (2006) Gastrointestinal stromal tumors in patients with neurofibromatosis 1: a clinicopathologic and molecular genetic study of 45 cases. Am J Surg Pathol 30(1):90–96
83. Carney JA (1999) Gastric stromal sarcoma, pulmonary chondroma, and extra-adrenal paraganglioma (Carney triad): natural history, adrenocortical component, and possible familial occurrence. Mayo Clin Proc 74(6):543–552
84. Carney JA, Stratakis CA (2002) Familial paraganglioma and gastric stromal sarcoma: a new syndrome distinct from the Carney triad. Am J Med Genet 108(2):132–139
85. DeMatteo RP, Lewis JJ, Leung D et al (2000) Two hundred gastrointestinal stromal tumors: recurrence patterns and prognostic factors for survival. Ann Surg 231(1):51–58
86. Miettinen M, Monihan JM, Sarlomo-Rikala M et al (1999) Gastrointestinal stromal tumors/smooth muscle tumors (GISTs) primary in the omentum and mesentery: clinicopathologic and immunohistochemical study of 26 cases. Am J Surg Pathol 23 (9):1109–1118
87. Reith JD, Goldblum JR, Lyles RH et al (2000) Extragastrointestinal (soft tissue) stromal tumors: an analysis of 48 cases with emphasis on histologic predictors of outcome. Mod Path 13 (5):577–585
88. Agaimy A, Markl B, Arnholdt H et al (2009) Multiple sporadic gastrointestinal stromal tumours arising at different gastrointestinal sites: pattern of involvement of the muscularis propria as a clue to independent primary GISTs. Virchows Arch 455(2):101–108
89. Verma P, Corless C, Medeiros F et al (2005) Pleomorphic gastrointestinal stromal tumors: diagnostic and therapeutic implications. Mod Pathol 18(suppl 1):121A, abstract
90. Antonescu CR, Hornick JL, Nielsen GP et al (2007) Dedifferentiation in gastrointestinal stromal tumor (GIST) to an anaplastic KIT-negative phenotype—a diagnostic pitfall. Mod Pathol 20 (suppl 2):11A, abstract
91. Pauwels P, Debiec-Rychter M, Stul M et al (2005) Changing phenotype of gastrointestinal stromal tumours under imatinib mesylate treatment: a potential diagnostic pitfall. Histopathology 47(1):41–47
92. Liegl B, Hornick JL, Antonescu C et al (2009) Rhabdomyosarcomatous differentiation in gastrointestinal stromal tumors after tyrosine kinase inhibitor therapy: a novel form of tumor progression. Am J Surg Pathol 33(2):218–226
93. Janeway KA, Albritton KH, Van Den Abbeele AD et al (2009) Sunitinib treatment in pediatric patients with advanced GIST following failure of imatinib. Pediatr Blood Cancer 52(7):767–771
94. Heinrich MC, Maki RG, Corless CL et al (2008) Primary and secondary kinase genotypes correlate with the biological and clinical activity of sunitinib in imatinib-resistant gastrointestinal stromal tumor. J Clin Oncol 26(33):5352–5359

95. Zhang L, Smyrk TC, Young WF Jr et al (2010) Gastric stromal tumors in Carney triad are different clinically, pathologically, and behaviorally from sporadic gastric gastrointestinal stromal tumors: findings in 104 cases. Am J Surg Pathol 34(1):53–64
96. Sarlomo-Rikala M, Kovatich A, Barusevicius A et al. (1998). CD117: a sensitive marker for gastrointestinal stromal tumors that is more specific than CD34. Mod Path (11):728–734
97. Miettinen M, Lasota J (2005) KIT (CD117): a review on expression in normal and neoplastic tissues, and mutations and their clinicopathologic correlation. Appl Immunohistochem Mol Morphol 13(3):205–220
98. Orosz Z, Tornoczky T, Sapi Z (2005) Gastrointestinal stromal tumors: a clinicopathologic and immunohistochemical study of 136 cases. Pathol Oncol Res 11(1):11–21
99. Liegl B, Hornick JL, Corless C et al (2009) Monoclonal antibody DOG 1.1 shows higher sensitivity than KIT in the diagnosis of Gastrointestinal stromal tumors, including unusual subtypes. Am J Surg Pathol 33(3):437–446
100. West RB, Corless CL, Chen X et al (2004) The novel marker, DOG1, is expressed ubiquitously in gastrointestinal stromal tumors irrespective of KIT or PDGFRA mutation status. Am J Pathol 165(1):107–113
101. Espinosa I, Lee CH, Kim MK et al (2008) A novel monoclonal antibody against DOG1 is a sensitive and specific marker for gastrointestinal stromal tumors. Am J Surg Pathol 32(2):210–218
102. Miettinen M, Wang ZF, Lasota J (2009) DOG1 antibody in the differential diagnosis of gastrointestinal stromal tumors: a study of 1,840 cases. Am J Surg Pathol 33(9):1401–1408
103. Blay P, Astudillo A, Buesa JM et al (2004) Protein kinase C theta is highly expressed in gastrointestinal stromal tumors but not in other mesenchymal neoplasias. Clin Cancer Res 10(12 Pt 1):4089–4095
104. Lee HE, Kim MA, Lee HS et al (2008) Characteristics of KIT-negative gastrointestinal stromal tumours and diagnostic utility of protein kinase C theta immunostaining. J Clin Pathol 61(6):722–729
105. Rossi G, Valli R, Bertolini F et al (2005) PDGFR expression in differential diagnosis between KIT-negative gastrointestinal stromal tumours and other primary soft-tissue tumours of the gastrointestinal tract. Histopathology 46(5):522–531
106. Peterson MR, Piao Z, Weidner N et al (2006) Strong PDGFRA positivity is seen in GISTs but not in other intra-abdominal mesenchymal tumors: immunohistochemical and mutational analyses. Appl Immunohistochem Mol Morphol 14(4):390–396
107. Zheng S, Chen LR, Wang HJ et al (2007) Analysis of mutation and expression of c-kit and PDGFR-alpha gene in gastrointestinal stromal tumor. Hepatogastroenterology 54(80):2285–2290
108. Miselli F, Millefanti C, Conca E et al (2008) PDGFRA immunostaining can help in the diagnosis of gastrointestinal stromal tumors. Am J Surg Pathol 32(5):738–743
109. Yang XH, Wu QL, Yu XB et al (2008) Nestin expression in different tumours and its relevance to malignant grade. J Clin Pathol 61(4):467–473
110. Parkkila S, Lasota J, Fletcher J A et al. (2010) Carbonic anhydrase II. A novel biomarker for gastrointestinal stromal tumors. Mod Pathol (in press)
111. Price ND, Trent J, El-Naggar AK et al (2007) Highly accurate two-gene classifier for differentiating gastrointestinal stromal tumors and leiomyosarcomas. Proc Natl Acad Sci U S A 104 (9):3414–9
112. Sarlomo-Rikala M, Miettinen M (1995) Gastric schwannoma—a clinicopathological analysis of six cases. Histopathology 27 (4):355–360
113. Carlson JW, Fletcher CD (2007) Immunohistochemistry for beta-catenin in the differential diagnosis of spindle cell lesions: analysis of a series and review of the literature. Histopathology 51(4):509–514
114. Montgomery E, Torbenson MS, Kaushal M et al (2002) Beta-catenin immunohistochemistry separates mesenteric fibromatosis from gastrointestinal stromal tumor and sclerosing mesenteritis. Am J Surg Pathol 26(10):1296–1301
115. Lucas DR, al-Abbadi M, Tabaczka P et al (2003) C-Kit expression in desmoid fibromatosis. Comparative immunohistochemical evaluation of two commercial antibodies. Am J Clin Pathol 119(3):339–345
116. Cessna MH, Zhou H, Sanger WG et al (2002) Expression of ALK1 and p80 in inflammatory myofibroblastic tumor and its mesenchymal mimics: a study of 135 cases. Mod Path 15(9):931–938
117. Lasota J, Wang ZF, Sobin LH et al (2009) Gain-of-function PDGFRA mutations, earlier reported in gastrointestinal stromal tumors, are common in small intestinal inflammatory fibroid polyps. A study of 60 cases. Mod Path 22(8):1049–56
118. Schildhaus HU, Cavlar T, Binot E et al (2008) Inflammatory fibroid polyps harbour mutations in the platelet-derived growth factor receptor alpha (PDGFRA) gene. J Pathol 216(2):176–182
119. Antonescu CR, Nafa K, Segal NH et al (2006) EWS-CREB1: a recurrent variant fusion in clear cell sarcoma—association with gastrointestinal location and absence of melanocytic differentiation. Clin Cancer Res 12(18):5356–5362
120. Lyle PL, Amato CM, Fitzpatrick JE et al (2008) Gastrointestinal melanoma or clear cell sarcoma? Molecular evaluation of 7 cases previously diagnosed as malignant melanoma. Am J Surg Pathol 32(6):858–866
121. Fletcher CD, Berman JJ, Corless C et al (2002) Diagnosis of gastrointestinal stromal tumors: a consensus approach. Int J Surg Pathol 10(2):81–89
122. Miettinen M, Lasota J (2006) Gastrointestinal stromal tumors: pathology and prognosis at different sites. Semin Diagn Pathol 23(2):70–83
123. Joensuu H (2008) Risk stratification of patients diagnosed with gastrointestinal stromal tumor. Human Pathol 39(10):1411–1419
124. Woodall CE 3rd, Brock GN, Fan J et al (2009) An evaluation of 2,537 gastrointestinal stromal tumors for a proposed clinical staging system. Arch Surg 144(7):670–678
125. Gold JS, Gonen M, Gutierrez A et al (2009) Development and validation of a prognostic nomogram for recurrence-free survival after complete surgical resection of localised primary gastrointestinal stromal tumour: a retrospective analysis. Lancet Oncol 10(11):1045–1052
126. Perrone F, Tamborini E, Dagrada GP et al (2005) 9p21 locus analysis in high-risk gastrointestinal stromal tumors characterized for c-kit and platelet-derived growth factor receptor alpha gene alterations. Cancer 104(1):159–169
127. Ricci R, Arena V, Castri F et al (2004) Role of p16/INK4a in gastrointestinal stromal tumor progression. Am J Clin Pathol 122 (1):35–43
128. Sabah M, Cummins R, Leader M et al (2004) Loss of heterozygosity of chromosome 9p and loss of p16INK4A expression are associated with malignant gastrointestinal stromal tumors. Mod Pathol 17(11):1364–1371
129. Schneider-Stock R, Boltze C, Lasota J et al (2003) High prognostic value of p16INK4 alterations in gastrointestinal stromal tumors. J Clin Oncol 21(9):1688–1697
130. Schneider-Stock R, Boltze C, Lasota J et al (2005) Loss of p16 protein defines high-risk patients with gastrointestinal stromal tumors: a tissue microarray study. Clin Cancer Res 11(2 Pt 1):638–645
131. Steigen SE, Bjerkehagen B, Haugland HK et al (2008) Diagnostic and prognostic markers for gastrointestinal stromal tumors in Norway. Mod Path 21(1):46–53
132. Feakins RM (2005) The expression of p53 and bcl-2 in gastrointestinal stromal tumours is associated with anatomical site, and p53 expression is associated with grade and clinical outcome. Histopathology 46(3):270–279

133. Nemoto Y, Mikami T, Hana K et al (2006) Correlation of enhanced cell turnover with prognosis of gastrointestinal stromal tumors of the stomach: relevance of cellularity and p27kip1. Pathol Int 56(12):724–731
134. Pruneri G, Mazzarol G, Fabris S et al (2003) Cyclin D3 immunoreactivity in gastrointestinal stromal tumors is independent of cyclin D3 gene amplification and is associated with nuclear p27 accumulation. Mod Path 16(9):886–892
135. Tornillo L, Duchini G, Carafa V et al (2005) Patterns of gene amplification in gastrointestinal stromal tumors (GIST). Lab Invest 85(7):921–931
136. Romeo S, Debiec-Rychter M, Van Glabbeke M et al (2009) Cell cycle/apoptosis molecule expression correlates with imatinib response in patients with advanced gastrointestinal stromal tumors. Clin Cancer Res 15(12):4191–4198
137. Martinho O, Gouveia A, Silva P et al (2009) Loss of RKIP expression is associated with poor survival in GISTs. Virchows Arch 455(3):277–284
138. Turkoz HK, Alkan I, Sisman S et al (2009) Cyclooxygenase-2 expression and connection with tumor recurrence and histopathologic parameters in gastrointestinal stromal tumors. APMIS 117 (11):825–830
139. Wei YC, Li CF, Yu SC et al (2009) Ezrin overexpression in gastrointestinal stromal tumors: an independent adverse prognosticator associated with the non-gastric location. Mod Path 22 (10):1351–1360
140. Blanke CD, Demetri GD, von Mehren M et al (2008) Long-term results from a randomized phase II trial of standard- versus higher-dose imatinib mesylate for patients with unresectable or metastatic gastrointestinal stromal tumors expressing KIT. J Clin Oncol 26(4):620–625
141. Blanke CD, Rankin C, Demetri GD et al (2008) Phase III randomized, intergroup trial assessing imatinib mesylate at two dose levels in patients with unresectable or metastatic gastrointestinal stromal tumors expressing the kit receptor tyrosine kinase: S0033. J Clin Oncol 26(4):626–632
142. Heinrich MC, Corless CL, Blanke CD et al (2006) Molecular correlates of imatinib resistance in gastrointestinal stromal tumors. J Clin Oncol 24(29):4764–4774
143. Casali PG, Jost L, Reichardt P et al (2008) Gastrointestinal stromal tumors: ESMO clinical recommendations for diagnosis, treatment and follow-up. Ann Oncol 19(Suppl 2):ii35–ii38
144. DeMatteo R, Owzar K, Antonescu C R, et al. (2008). Efficacy of adjuvant imatinib mesylate following complete resection of localized, primary gastrointestinal stromal tumor (GIST) at high risk of recurrence: the US intergroup phase II trial ACOSOG Z9000. Gastrointestinal Cancer Symposium, Orlando, Florida. Proceedings No. 8, p73
145. DeMatteo RPACR, Chadaram V, et al. (2005). Adjuvant imatinib mesylate in patients with primary high risk gastrointestinal stromal tumors (GIST) following complete resection: Safety results from the U.S. Intergroup Phase II trial ACOSOG Z9000. J Clin Oncol 23(ASCO Annual Meeting Proceedings. No. 16S, Part I of II (June 1 Supplement))
146. DeMatteo RP, Ballman KV, Antonescu CR et al (2009) Adjuvant imatinib mesylate after resection of localised, primary gastrointestinal stromal tumour: a randomised, double-blind, placebo-controlled trial. Lancet 373(9669):1097–1104
147. Lasota J, Miettinen M (2006) KIT and PDGFRA mutations in gastrointestinal stromal tumors (GISTs). Semin Diagn Pathol 23 (2):91–102
148. Fletcher J, Corless C, Dimitrijevic S et al. (2003) Mechanisms of resistance to imatinib mesylate (IM) in advanced gastrointestinal stromal tumors (GIST). Proc Am Soc Clin Oncol (22):3275–3277
149. Debiec-Rychter M, Cools J, Dumez H et al (2005) Mechanisms of resistance to imatinib mesylate in gastrointestinal stromal tumors and activity of the PKC412 inhibitor against imatinib-resistant mutants. Gastroenterology 128(2):270–279
150. Liegl B, Kepten I, Lee C et al (2008) Heterogeneity of kinase inhibitor resistance mechanisms in GIST. J Pathol 216(1):64–74
151. Agaram NP, Besmer P, Wong GC et al (2007) Pathologic and molecular heterogeneity in imatinib-stable or imatinib-responsive gastrointestinal stromal tumors. Clin Cancer Res 13(1):170–181
152. Prenen H, Cools J, Mentens N et al (2006) Efficacy of the kinase inhibitor SU11248 against gastrointestinal stromal tumor mutants refractory to imatinib mesylate. Clin Cancer Res 12(8):2622–2627
153. Wardelmann E, Merkelbach-Bruse S, Pauls K et al (2006) Polyclonal evolution of multiple secondary KIT mutations in gastrointestinal stromal tumors under treatment with imatinib mesylate. Clin Cancer Res 12(6):1743–1749
154. Antonescu CR, Besmer P, Guo T et al (2005) Acquired resistance to imatinib in gastrointestinal stromal tumor occurs through secondary gene mutation. Clin Cancer Res 11(11):4182–4190
155. Demetri GD, van Oosterom AT, Garrett CR et al (2006) Efficacy and safety of sunitinib in patients with advanced gastrointestinal stromal tumour after failure of imatinib: a randomised controlled trial. Lancet 368(9544):1329–1338
156. Montemurro M, Schoffski P, Reichardt P et al (2009) Nilotinib in the treatment of advanced gastrointestinal stromal tumours resistant to both imatinib and sunitinib. Eur J Cancer 45 (13):2293–2297
157. Dewaele B, Wasag B, Cools J et al (2008) Activity of dasatinib, a dual SRC/ABL kinase inhibitor, and IPI-504, a heat shock protein 90 inhibitor, against gastrointestinal stromal tumor-associated PDGFRAD842V mutation. Clin Cancer Res 14 (18):5749–5758
158. Muhlenberg T, Zhang Y, Wagner AJ et al (2009) Inhibitors of deacetylases suppress oncogenic KIT signaling, acetylate HSP90, and induce apoptosis in gastrointestinal stromal tumors. Cancer Res 69(17):6941–6950
159. Pantaleo MA, Astolfi A, Di Battista M et al (2009) Insulin-like growth factor 1 receptor expression in wild-type GISTs: a potential novel therapeutic target. Int J Cancer 125(12):2991–2994
160. Tarn C, Rink L, Merkel E et al (2008) Insulin-like growth factor 1 receptor is a potential therapeutic target for gastrointestinal stromal tumors. Proc Natl Acad Sci U S A 105(24):8387–92
161. Bauer S, Yu LK, Demetri GD et al (2006) Heat shock protein 90 inhibition in imatinib-resistant gastrointestinal stromal tumor. Cancer Res 66(18):9153–9161
162. Sambol EB, Ambrosini G, Geha RC et al (2006) Flavopiridol targets c-KIT transcription and induces apoptosis in gastrointestinal stromal tumor cells. Cancer Res 66(11):5858–5866
163. Bauer S, Parry JA, Muhlenberg T et al (2010) Proapoptotic activity of bortezomib in gastrointestinal stromal tumor cells. Cancer Res 70(1):150–159
164. Bauer S, Duensing A, Demetri GD et al (2007) KIT oncogenic signaling mechanisms in imatinib-resistant gastrointestinal stromal tumor: PI3-kinase/AKT is a crucial survival pathway. Oncogene 26(54):7560–7568
165. Ou WB, Zhu MJ, Demetri GD et al (2008) Protein kinase C-theta regulates KIT expression and proliferation in gastrointestinal stromal tumors. Oncogene 18:5624–5634

Virchows Arch (2010) 456:129–139
DOI 10.1007/s00428-009-0736-8

REVIEW AND PERSPECTIVE

Genomic characteristics of soft tissue sarcomas

Fredrik Mertens · Ioannis Panagopoulos · Nils Mandahl

Received: 20 September 2008 / Revised: 16 December 2008 / Accepted: 17 January 2009 / Published online: 3 February 2009
© Springer-Verlag 2009

Abstract Studies on the molecular mechanisms behind soft tissue sarcoma development have disclosed that these malignancies are as genetically heterogeneous as they are clinically and morphologically diverse. Much of the genetic information on soft tissue sarcomas is still limited to the genomic level, as detected by chromosome banding analysis or comparative genomic hybridization. Based on the results of such studies, soft tissue sarcomas may be broadly dichotomized into one group, accounting for approximately 20% of the cases, characterized by specific balanced translocations, and one group typically showing massive chromosomal rearrangements leading to recurrent, but non-specific, structural and numerical rearrangements. As summarized in this review, the genomic characterization of soft tissue sarcomas has not only provided cell biologists with decisive information on the parts of the genome that may harbor genes that are essential for tumor development but also given the clinicians involved in the management of these patients a valuable diagnostic tool.

Keywords Soft tissue sarcoma · Cytogenetics · Comparative genomic hybridization · Gene fusion

Introduction

The hypothesis that human neoplasia is caused by acquired genomic changes is of long standing [1]. However, it was not until the introduction of the chromosome banding techniques in the early 1970 s that a detailed and systematic assessment of the genomic distribution of these changes could be initiated. As metaphase spreads were easier to obtain from cells cultured in suspension, much more attention was initially paid to the hematologic malignancies than to the more common solid tumors, and it was rapidly demonstrated that most types of leukemia and lymphoma display clearly non-random patterns of chromosome aberrations [2]. Furthermore, from these studies, it became apparent that different chromosome aberrations play different roles during tumor development; some are primary, tumor-initiating events, whereas others are secondary aberrations, occurring later in tumor development and possibly influencing tumor progression.

With the advent of better techniques for culturing cells, solid tumors, in particular those of mesenchymal derivation, also became available for cytogenetic analyses, soon revealing a scenario very similar to that in the hematologic malignancies, i.e., a non-random association between the karyotype and a number of other biological properties of the tumors, such as malignancy grade and morphologic subtype. Still, solid tumors remain less well investigated at the chromosome level, making up only some 30% of the more than 54,000 neoplasms with clonal chromosomal changes that have been reported in the literature [3].

During the last two decades, the ability to identify and characterize acquired chromosomal rearrangements has been improved significantly by the development of fluorescence in situ hybridization (FISH) and comparative genomic hybridization (CGH). With FISH, metaphase as well as interphase nuclei can be analyzed using probes specific for chromosomes, parts of chromosomes, or unique DNA sequences (Figs. 1 and 2). CGH is a technique for revealing regions of the genome that are gained or lost in tumor cells. It cannot detect balanced rearrangements, but a

F. Mertens (✉) · I. Panagopoulos · N. Mandahl
Department of Clinical Genetics, Lund University Hospital,
221 85 Lund, Sweden
e-mail: Fredrik.mertens@med.lu.se

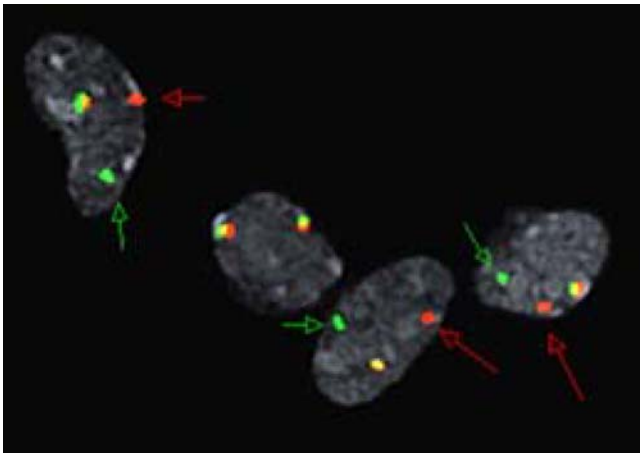

Fig. 1 Clinical usefulness of FISH. Interphase nuclei from a fine-needle biopsy of a synovial sarcoma analyzed with a dual color probe specific for the *SS18* gene in 18q11. This gene is rearranged due to the translocation t(X;18)(p11;q11) in almost all synovial sarcomas. The intact gene yields a yellow (combined red and green) signal, whereas the allele involved in the translocation is seen as separated red and green signals (indicated by *red and green arrows*, respectively)

great advantage with CGH over cytogenetic banding analysis is that it is not dependent on dividing cells. Hence, archival material, such as frozen samples or paraffin-embedded, formalin-fixed tumors can be used. CGH is now increasingly performed by hybridizing DNA to large numbers of defined DNA sequences, so-called array CGH, potentially yielding information on genomic imbalances at the single exon level (Fig. 2) [4].

In parallel, spectacular improvements on molecular genetic techniques have made it possible not only to obtain highly accurate and detailed information on the consequences of chromosome aberrations at the gene level but also to study in one experiment a large number of genes, even entire genomes. Undoubtedly, these technical breakthroughs will, within only a few years, have a tremendous impact on our understanding of the genetic changes underlying tumor development.

Still, most of the information that we have on sarcomas comes from cytogenetic analyses, supplemented by CGH studies and molecular investigations of recurrent balanced chromosomal rearrangements. The present review will provide a general overview of the genomic changes that have been detected in soft tissue sarcomas.

Two different patterns of genomic changes in soft tissue sarcomas

Soft tissue sarcomas include a wide variety of histopathologic entities that clinically cover the spectrum from slowly growing, rarely metastasizing lesions to highly aggressive malignancies. Cytogenetic analyses of close to 1,500 cases have shown that the clinical and biological variation among these neoplasms is reflected in their karyotypes [3, 5], which may be broadly dichotomized into one group characterized by specific, balanced translocations and one group typically showing more extensive chromosomal rearrangements leading to recurrent, but non-specific, chromosomal gains and losses. The former group, which constitutes approximately 20% of all soft tissue sarcomas [2], presently includes 12 different tumor types in which a total of 30 different gene fusions have been identified (Table 1). This subset of sarcomas has, for several reasons, been the focus of much attention. First, the strict association between most of these translocations and specific morphologic subtypes makes them, and their consequences at the gene level, excellent diagnostic tools. Second, as many of them often occur as the sole cytogenetic aberration, they are likely to constitute critical steps in tumorigenesis. The subgroup characterized by more complex karyotypes comprises the majority of the sarcomas, including, e.g., leiomyosarcoma, malignant peripheral nerve sheath tumors, and myxofibrosarcoma. Although no tumor-specific aberration has been detected among these sarcomas, they all show non-random, but largely overlapping, patterns of chromosomal gains and losses. Only for a few of the recurrent imbalances has the crucial molecular consequence been pinpointed, but, as for the other tumor types, it is assumed that repeatedly deleted regions indicate the location of tumor suppressor genes and that frequently amplified regions harbor dominantly acting oncogenes [6]. It should also be kept in mind that the number of investigated cases is still small and that the karyotypes, due to a combination of high complexity and poor technical quality, often contain many unresolved marker chromosomes. Furthermore, not only balanced translocations but also various unbalanced rearrangements, such as interstitial deletions, may result in gene fusions. Thus, the presence of gene fusions also in this set of sarcomas should not be ruled out.

Most soft tissue sarcomas are of unknown cellular origin, but depending on their more or less pronounced resemblance to normal mesenchymal cells they are in the current WHO classification grouped according to line of differentiation [5]. Adhering to this classification, but excluding sarcomas primarily arising in bone or parenchymatous organs and adding dermatofibrosarcoma protuberans and malignant peripheral nerve sheath tumor, a short summary of salient genomic features in entities that have been sufficiently analyzed is presented below.

Adipocytic tumors

Irrespective of site of origin, atypical lipomatous tumors have the same morphologic appearance and genetic

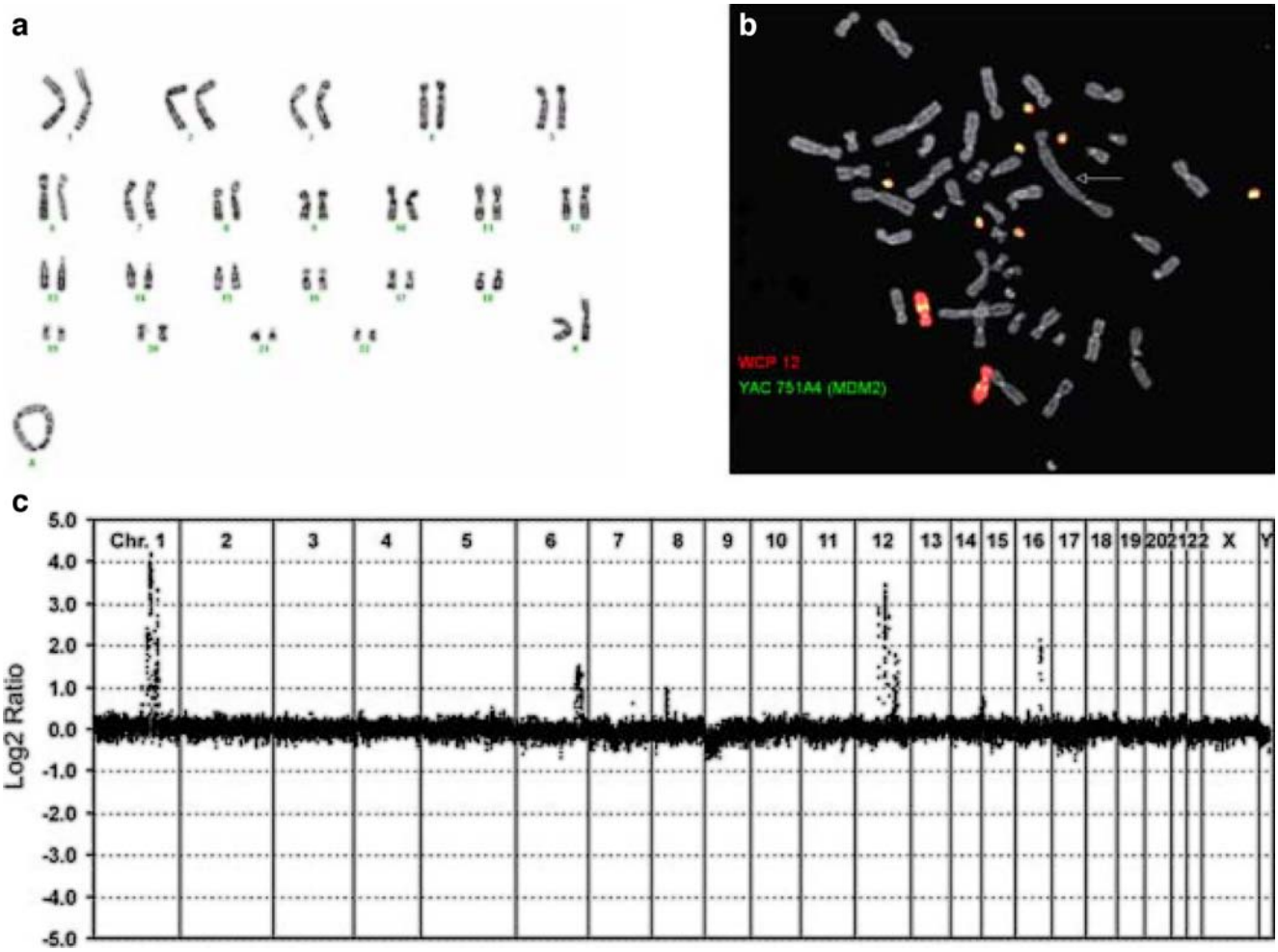

Fig. 2 Genomic changes in three well-differentiated liposarcomas. **a** Karyogram showing a supernumerary ring chromosome as the sole aberration. Note that this characteristic chromosome aberration is common also in other sarcomas, such as dermatofibrosarcoma protuberans and myxoinflammatory fibroblastic sarcoma, and that the different contents of the ring chromosomes in these sarcomas cannot be seen at G-banding analysis. **b** Metaphase-FISH analysis of ring chromosomes using whole chromosome painting and locus-specific probes, revealing that small rings are composed of material from chromosome 12, with amplification of the *MDM2* gene. The *arrow* indicates a telomeric association, a common finding in well-differentiated liposarcomas. **c** Array CGH analysis showing amplicons in 12q, as well as at other sites of the genome

characteristics. However, when located in the trunk wall or extremities, they almost always behave like conventional lipomas, albeit with a higher risk for local recurrence [7], whereas mediastinal and retroperitoneal lesions often dedifferentiate and kill the patient. Thus, the former type is often referred to as atypical lipomas and the latter kind as well-differentiated liposarcomas [5]. Cytogenetically, they are characterized by one or more supernumerary ring chromosomes and/or giant marker chromosomes in mostly near-diploid karyotypes. Although the contents of the rings/markers vary between as well as within tumors, they invariably harbor material from the long arm of chromosome 12, with a few exceptions including segments from 12q12-q23 and with high-level amplification being restricted to 12q13-21 (Fig. 2). Several potential targets for the amplification have been identified, including *CDK4* and *HMGA2* in 12q14 and *MDM2* in 12q15, but other oncogenes, such as *GLI* and *SAS*, are also frequently co-amplified [8–12]. Other chromosomes, notably chromosome 1, are also often included in the rings/giant markers [13–16].

Dedifferentiated liposarcomas remain poorly investigated, but most of the published cases have displayed ring chromosomes composed of chromosome 12 material, confirming the biologic relationship with atypical lipomatous tumors [17]. In line with their more malignant behavior, secondary aberrations and polyploidy are, however, more common among the dedifferentiated liposarcomas [18].

The cytogenetic hallmark of myxoid liposarcoma, including tumors with round cell components, is the t(12;16)(q13;p11) [19]. Close to 100 cases have been reported, more than 80% of which have had a translocation

Table 1 Soft tissue sarcomas with characteristic chromosome aberrations

Sarcoma	Aberration	Molecular genetic consequence
Atypical lipomatous tumor	Ring chromosome/giant marker	Amplification of, e.g., *MDM2*, *CDK4*, *HMGA2*, *GLI* and *SAS*
Myxoid/round cell liposarcoma	t(12;16)(q13;p11)	*FUS–DDIT3*
	t(12;22)(q13;q12)	*EWSR1–DDIT3*
Solitary fibrous tumor/hemangiopericytoma	der(12)(q13-15)	Unknown
Inflammatory myofibroblastic tumor	t(1;2)(q21;p23)	*TPM3–ALK*
	inv(2)(p23q35)	*ATIC–ALK*
	t(2;2)(p23;q13)	*RANBP2–ALK*
	t(2;4)(p23;q21)	*SEC31A–ALK*
	t(2;11)(p23;p15)	*CARS–ALK*
	t(2;17)(p23;q23)	*CLTC–ALK*
	t(2;19)(p23;p13)	*TPM4–ALK*
Infantile fibrosarcoma	t(12;15)(p13;q25)	*ETV6–NTRK3*
Myxoinflammatory fibroblastic sarcoma	t(1;10)(p22;q24)	Deregulation of *FGF8* and *NPM3*
	Ring chromosome	Amplification of, e.g., *VGLL3*
Low-grade fibromyxoid sarcoma	t(7;16)(q33-34;p11)	*FUS–CREB3L2*
	t(11;16)(p11;p11)	*FUS–CREB3L1*
Dermatofibrosarcoma protuberans	Ring chromosome, t(17;22)(q21;q13), der(22)t(17;22)	*COL1A1–PDGFB*
Alveolar rhabdomyosarcoma	t(1;13)(p36;q14)	*PAX7–FOXO1A*
	t(2;2)(p23;q36)	*PAX3–NCOA1*
	t(2;13)(q36;q14)	*PAX3–FOXO1A*
	t(X;2)(q13;q36)	*PAX3–FOXO4*
Angiomatoid fibrous histiocytoma	t(2;22)(q33;q12)	*EWSR1–CREB1*
	t(12;16)(q13;p11)	*FUS–ATF1*
	t(12;22)(q13;q12)	*EWSR1–ATF1*
Synovial sarcoma	t(X;18)(p11;q11)	*SS18–SSX1, SS18–SSX2* or *SS18–SSX4*
	t(X;20)(p11;q13)	*SS18L1–SSX1*
Clear cell sarcoma	t(2;22)(q33;q12)	*EWSR1–CREB1*
	t(12;22)(q13;q12)	*EWSR1–ATF1*
Desmoplastic small round cell tumor	t(11;22)(p13;q12)	*EWSR1–WT1*
Extraskeletal myxoid chondrosarcoma	t(3;9)(q12;q22)	*TFG–NR4A3*
	t(9;15)(q22;q21)	*TCF12–NR4A3*
	t(9;17)(q22;q11)	*TAF15–NR4A3*
	t(9;22)(q22;q12)	*EWSR1–NR4A3*
Alveolar soft part sarcoma	t(X;17)(p11;q25)	*ASPSCR1–TFE3*

or variants thereof, between 12q13 and 16p11. A variant translocation, t(12;22)(q13;q12), has been seen in approximately 5% of the cases. The pathogenetic importance of these translocations is further emphasized by the fact that they are the sole anomalies in half of the cases. However, there is also a non-random set of secondary changes, the most common being trisomy 8. The molecular genetic consequences of the t(12;16) and t(12;22) are the formation of the fusion genes *FUS–DDIT3* and *EWSR1–DDIT3*, respectively [20–22].

Only a few pleomorphic liposarcomas have been analyzed cytogenetically. Most of them had highly complex karyotypic changes, none of which seems tumor-specific. A CGH analysis of more than 20 tumors has shown a recurrent gain of sequences from 1q and 5p, sometimes in the form of high-level amplification, and deletions on chromosome arms 2q, 10q, 11q, and 13q [18, 23].

Fibroblastic/myofibroblastic tumors

Solitary fibrous tumor (SFT) and hemangiopericytoma (HPC) are closely related histopathologically and have been suggested to represent different aspects of a single biological entity. No consistent aberrations have emerged among the approximately 20 cases of each type that have been investigated by chromosome banding analysis. However, one third of HPC and 10% of SFT have shown involvement of the 12q13-15 region. The molecular consequences of these rearrangements are unknown, but

the *GLI* oncogene, which is upregulated through a t(7;12)(p21-22;q13-15) in pericytomas [24], does not seem to be involved. CGH studies have also indicated that +8 and losses from 13q are present in a subset of the lesions [25].

Inflammatory myofibroblastic tumor was only recently recognized as a distinct histopathologic entity. Thus, the cytogenetic information is still scarce, but about half of the cases, especially when occurring in children and young adults, have translocations and other rearrangements of 2p22-24, often as the sole aberration [26]. The target for these rearrangements is the *ALK* gene in 2p23, which encodes a tyrosine kinase receptor, forming fusion genes with many different partners [27, 28]. All of them result in expression of the kinase domain of the ALK protein. Some of these chimeric genes are shared with anaplastic large cell lymphoma, but the *NPM–ALK* fusion, which predominates in lymphomas, has not yet been detected in any sarcoma.

At G-banding analysis, infantile fibrosarcomas typically display hyperdiploid karyotypes with trisomies for, in particular, chromosomes 8, 11, 17, and 20. FISH and molecular studies have, however, shown that most, if not all, of the cases also have a cytogenetically cryptic translocation between chromosomes 12 and 15, resulting in a fusion between the *ETV6* and *NTRK3* genes in 12p13 and 15q25, respectively [29, 30]. Presumably, this is the primary event in tumorigenesis. Interestingly, the same translocation and fusion gene have been found in several other tumor types, including mesoblastic nephroma, secretory breast carcinoma, and acute leukemia [2]. Adult fibrosarcomas, which are morphologically similar to infantile fibrosarcomas but much more aggressive, typically show complex karyotypes with multiple aberrations, and no specific aberration has emerged.

The published data on myxofibrosarcomas are difficult to evaluate, as the diagnostic criteria for this tumor have changed with time. Possibly, this could, at least in part, account for the heterogeneous spectrum of karyotypic abnormalities that has been observed. Most cases have had complex karyotypes, especially high-grade and recurrent lesions, often including cytogenetic signs of gene amplification [31–33]. The only recurrent gain involves chromosome 7, whereas losses primarily affect chromosomes 1, 3, 5, 6, 10, 12, 16, 17, and 19. An array CGH study of eight myxofibrosarcomas indicated another spectrum of imbalances, including frequent gain of the 12q15-21 region, but was in agreement with the cytogenetic findings concerning gain of 7q33-35 and loss of 10p13-14 [34].

Myxoinflammatory fibroblastic sarcoma is a recently described tumor entity in which two recurrent aberrations have been described: a t(1;10)(p22;q24) and supernumerary ring chromosomes. The former aberration results in deregulation of the *FGF8* and *NPM3* genes located close to the breakpoint in 10q, whereas the latter ones are associated with amplification of a less than 2 Mb segment of the short arm of chromosome 3 (Hallor et al., submitted for publication). The amplicon contains only a few genes, including *VGLL3* and *CHMP2BK*, both of which are overexpressed in tumors with amplification. The interplay between these aberrations, as well as their impact on tumor differentiation, remains to be elucidated; although usually occurring as mutually exclusive aberrations, they are sometimes present simultaneously. Furthermore, a seemingly identical t(1;10) has been described also in a hemosiderotic fibrolipomatous tumor, and ring chromosomes containing the same amplicon in 3p have been described in inflammatory malignant fibrous histiocytoma (Hallor et al., submitted for publication) [35].

Most low-grade fibromyxoid sarcomas have a near-diploid karyotype with a reciprocal t(7;16)(q33-34;p11) or a supernumerary ring chromosome (Fig. 3). Irrespective of

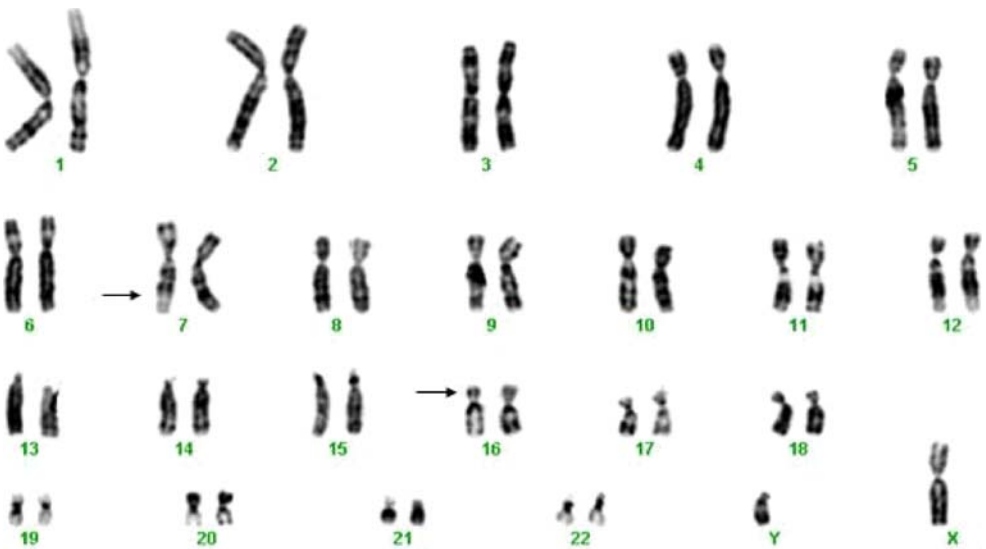

Fig. 3 Example of a sarcoma-specific chromosome aberration. The t(7;16)(q33-34;p11), resulting in a *FUS–CREB3L2* fusion gene, is strongly associated with low-grade fibromyxoid sarcoma

karyotypic background, however, almost all cases carry a chimeric *FUS–CREB3L2* gene [36, 37]; a single case had the related gene fusion *FUS–CREB3L1* [38]. The differential diagnosis of low-grade fibromyxoid sarcoma may be problematic, and it is thus of interest that the two fusion genes seem to be strongly associated with this tumor type, although a few exceptions, notably sclerosing epithelioid fibrosarcoma, have been reported [36–39].

The cytogenetic hallmark of dermatofibrosarcoma protuberans is the finding of one or more supernumerary ring chromosomes that by FISH and CGH analyses have been shown to contain material from chromosomes 17 and 22 [40–42]; occasionally, an unbalanced der(22)t(17;22)(q21-23;q13) is seen instead. The molecular consequence of both types of aberration is the overexpression of the platelet-derived growth factor beta (*PDGFB*) chain gene in chromosome 22 through fusion with the collagen gene *COL1A1* in chromosome 17 [43, 44]. The same fusion gene is shared with giant cell fibroblastoma and Bednar tumor, but at the chromosome level these two variants more often show a balanced or unbalanced t(17;22) than ring chromosomes. Dermatofibrosarcoma protuberans sometimes progresses into a high-grade fibrosarcoma, and FISH and CGH studies have indicated an association between an increased number of *COL1A1–PDGFB* copies and fibrosarcomatous changes in a subset of these cases [45, 46].

So-called fibrohistiocytic tumors

Arguably, malignant fibrous histiocytoma (MFH) is the most controversial diagnostic entity among soft tissue sarcomas. Once constituting the most prevalent subtype, it has become all but extinct; tumors previously diagnosed as MFH are now recognized to represent, e.g., dedifferentiated forms of adipocytic or myogenic sarcomas, myxofibrosarcomas, or metastatic carcinomas [17, 47–49]. Thus, much of the published genomic information on "MFH" probably concerns other tumor types.

Focusing only on the approximately 60 cases that have been described as pleomorphic, giant cell, or inflammatory MFH, one can conclude that the karyotypes are usually very complex and that complete descriptions of all aberrations most often cannot be obtained. Most likely, these tumors are genetically highly unstable, as suggested by extensive intercellular variation, frequent telomeric associations, and co-existence of several ploidy levels. Reasonably, CGH analysis should be a better way of obtaining useful information on the genomic changes underlying these tumors. Also such data are, however, disparate, but the combined information based on several studies indicates that sequence gains from 5p, 7p21, 1p21-pter, 1q21-22, and 12q13-15 and losses from 13q11-31, 9p21-pter, and 11q23-qter are particularly common [17, 50]. Combined with molecular analyses, these findings indicate involvement of either the CDKN2A/RB1 pathway or the TP53/MDM2 pathway in about 80% of MFH.

Smooth muscle tumors

Around 50 soft tissue leiomyosarcomas with chromosome aberrations have been reported; two thirds with polyploid chromosome numbers and about one third with cytogenetic signs of gene amplification. Adding to the complexity, they often show extensive intratumor heterogeneity [51, 52]. No specific structural or numerical aberration has been found, but a clustering of breakpoints in chromosomes 1, 3, and 7 and chromosome band 19q13 is seen. Recurrent imbalances include losses from chromosomes/chromosome arms 1p, 4q, 9p, 11, 13q, 14q, 18, 19, and 22q and gains of 1q, 7, and 20. The rare subtype inflammatory leiomyosarcoma seems to display a distinctly different cytogenetic profile; three of four karyotyped tumors have shown hyperhaploid stemline karyotypes [53]. CGH studies of leiomyosarcomas strongly support the importance of loss of material from 13q and 10q, each found in more than half of the cases, as well as gain of sequences from 1q, 5p, 8q, 16p, and 17p and losses from 2q, 11q, and 16q, imbalances present in 25–35% of the cases [54, 55]. CGH data also indicate that loss of 10q sequences and gain of 5p are associated with a more aggressive disease [56, 57].

Skeletal muscle tumors

About 100 alveolar rhabdomyosarcomas (ARMS) have been reported. The cytogenetic hallmarks of ARMS are the t(2;13)(q36;q14) and, much less frequently, t(1;13)(p36;q14) [58, 59]. Secondary numerical and structural aberrations are common, and the karyotypes are frequently moderately to highly complex. The molecular consequences of the translocations are the formation of chimeric genes involving *FOXO1A* (in 13q14) and either *PAX7* (in 1p36) or *PAX3* (in 2q36) [60]. The fusion products are strong transcriptional activators [61]. Roughly 60% of ARMS are *PAX3–FOXO1A*- positive and 20% are *PAX7–FOXO1A*-positive. In addition, two variants, *PAX3–FOXO4* and *PAX3–NCOA1*, have been identified in sporadic cases, but it remains possible that some tumors with classical ARMS morphology are fusion-gene-negative [62–64]. As other forms of rhabdomyosarcoma are negative for the gene fusions, RT-PCR and, bearing in mind the large number of different fusion genes involving *FOXO1A,* especially FISH analysis are valuable diagnostic tools. Preliminary studies indicate that tumors with the

PAX3–FOXO1A fusion are more aggressive and more likely to metastasize [65].

The majority of embryonal rhabdomyosarcomas have hypo- or hyperdiploid chromosome numbers. No recurrent structural aberration has been found, but many numerical changes and other imbalances are common: trisomy for chromosomes 2 and 8 are seen in half of the cases, and gain of material from 1q, 7q, 11q, and chromosomes 12 and 13 and loss of material from 9p, 15q, and 17 are all seen in 20–30% of the cases [59, 66]. Several CGH studies have revealed gains of chromosomes 2, 7, 8, 11, 12, and 13 and losses of distal 1p and 14q [67].

The less than ten cytogenetically characterized pleomorphic rhabdomyosarcomas reported have displayed highly complex karyotypic changes. The *PAX3–FOXO1A* fusion gene was found in one case. The genomic imbalances detected by CGH are more similar to those seen in MFH than to those in alveolar or embryonal rhabdomyosarcoma.

Vascular tumors

Benign as well as malignant vascular tumors remain poorly investigated, with karyotypic data on only a handful of angiosarcomas and Kaposi sarcomas. No consistent aberration has been detected among these cases. CGH analyses suggest that gains in 8q and 20p and losses in 22q are the most frequent genomic imbalances among angiosarcomas [68].

Nerve sheath tumors

Malignant peripheral nerve sheath tumors may be sporadic or occur through malignant transformation of large, usually plexiform, neurofibromas in patients with neurofibromatosis type 1 (NF1). In line with this association, molecular genetic investigations have revealed that both sporadic and NF1-associated tumors often display somatic loss or mutation of the *NF1* gene [69]. More than 100 cases with abnormal karyotypes have been reported, most of which display complex karyotypes, often with a chromosome number in the triploid or tetraploid range. No recurrent balanced rearrangement has been detected among them. Recurrent breakpoints are seen in chromosome arms 1p, 5p, 7p, 9p, 11q, 17p, 17q, 20q, and 22q, and frequent chromosomal imbalances include loss of material from chromosomes/chromosome arms1p, 3p, 5p, 6q, 7p, 9p, 10p, 11, 12, 16, 17, 19p, 20q, 22, and X, gain of chromosome 7, and amplification of several regions on 17q [70–75]. No difference in karyotypic profile between sporadic cases and NF1-associated tumors has been detected.

Tumors of uncertain differentiation

Angiomatoid fibrous histiocytomas (AFH) is a low-grade malignant tumor that is not in any way related to other "MFH" tumors. Most reported cases have had near-diploid karyotypes with simple balanced or moderately complex, unbalanced structural rearrangements. Based on the finding of recurrent breakpoints in chromosome bands 2q33, 12q13, and 22q12, RT-PCR analyses of larger series of AFH have revealed three fusion genes, in decreasing order of frequency: *EWSR1–CREB1*, *EWSR1–ATF1,* and *FUS–ATF1*, corresponding to t(2;22)(q33;q12), t(12;22)(q13;q12), and t(12;16)(q13;p11), respectively [76, 77]. Interestingly, the two former fusion genes have also been found in clear cell sarcoma, which is clinically and morphologically very different from AFH.

Synovial sarcoma is one of the more extensively analyzed sarcomas, with cytogenetic information on more than 200 cases, including monophasic, biphasic, and poorly differentiated lesions [78–81]. Typically, they have near-diploid karyotypes of low or moderate complexity, and in more than 90% a tumor-specific t(X;18)(p11;q11), or variants thereof, is present. Recurrent secondary changes, each seen in 10–15% of the cases, include gain of chromosomes/segments 2q13-21, 7, 8q22-24, 12, and 21 and losses of 3p12-p26, 11p, and 11q. CGH findings are largely consistent with these findings. The t(X;18) may result in the formation of one of three different fusion genes involving *SS18* in 18q11 (Fig. 1) and either of the physically and functionally related genes *SSX1*, *SSX2*, and *SSX4* in Xp11; *SS18–SSX1* is found in two thirds and *SS18–SSX2* in one third of the cases. *SS18–SSX4* and a fourth fusion gene variant with involvement of 20q13 and Xp11, *SS18L1–SSX1*, have been seen only in very occasional tumors. *SS18–SSX2*-positive tumors are, with few exceptions, monophasic and the vast majority of biphasic tumors are *SS18–SSX1*-positive [82–84]. The potential impact of the type of gene fusion on outcome has been investigated in more than 400 synovial sarcomas, but the results are not conclusive. In one series, the fusion type was the most significant prognostic factor among patients with localized disease at diagnosis, a finding that could not be corroborated in another equally large series [82, 83]. It has also been suggested that patients with tumors showing simple karyotypes and *SS18–SSX2* fusion have better clinical outcome than those with a complex tumor karyotype and *SS18–SSX1* fusion [80].

Clear cell sarcomas of soft tissue, also known as malignant melanomas of soft parts, have hypodiploid to hypertriploid karyotypes of moderate complexity [85, 86]. A characteristic t(12;22)(q13;q12) is present in 70% of the tumors and is thought to be the primary genetic event. However, extra copies of chromosome 8 or an isochromo-

some for 8q is as common as the t(12;22). The t(12;22) results in a fusion gene in which the 3′-part of *EWSR1* (in 22q12) is replaced by the 3′-part of the activating transcription factor 1, *ATF1* (in 12q13). A variant fusion gene, *EWSR1–CREB1*, has been found in clear cell sarcomas occurring preferentially in the gastrointestinal tract and with little or no melanocytic differentiation [87].

Cytogenetic data are available on only a few desmoplastic small round cell tumors. The karyotypes are usually near-diploid with few numerical and/or structural aberrations. Almost always a breakpoint in 22q is found, and most tumors also have a break in 11p13, in about two thirds of the cases resulting in a t(11;22)(p13;q11-13), in some tumors as the sole anomaly. Much larger series of DSRCT have been investigated by RT-PCR, detecting an *EWSR1-WT1* chimera in almost all of the cases [88]. Identification of t(11;22)(p13;q12) or the *EWSR1-WT1* transcript is useful in the differential diagnosis and may show higher sensitivity than immunohistochemical analyses [89].

The karyotypic information available on approximately 20 epithelioid sarcomas reveal considerable heterogeneity. Gain of 8q and a breakpoint in 22q11-12, often associated with loss of distal 22q, have been found in one third of the cases. Possibly, the genomic aberrations are different in the proximal type and the classic, peripheral epithelioid sarcomas; chromosome 22 aberrations, leading to deletion of the *SMARCB1* gene in 22q11 or inactivation at the protein level, and polyploidy seem to be more frequent among the former [90, 91].

Extraskeletal myxoid chondrosarcomas almost always have pseudodipoid or near-diploid chromosome numbers [92, 93]. One of four reciprocal translocations—t(3;9)(q12;q22), t(9;22)(q22;q12), t(9;17)(q22;q11), and t(9;15)(q22;q21)—is present, often as the sole change, in approximately 90% of the cases, with the t(9;22) being the more common. Secondary changes include gains of chromosomes 12, 7, 19, and 8. The four translocations all result in the formation of fusion genes involving *NR4A3* in 9q22-q31.1 and *EWSR1* in 22q12, *TAF15* in 17q11, *TCF12* in 15q21, or *TFG* in 3q12 [92–94]. Since these fusion genes have not yet been described in any other tumor type, they represent useful diagnostic markers, but the significance, if any, of the variation in gene fusions as prognostic factors remains unknown.

Chromosome banding data are available on a dozen alveolar soft part sarcomas, most of which have had near-diploid karyotypes with relatively few aberrations [95, 96]. Almost all tumors have a breakpoint in 17q25 and, in more than half of the cases, another one in Xp11. The recombination between those two chromosome bands is mostly seen as an unbalanced, non-reciprocal translocation, der(17)t(X;17)(p11;q25); only some 15% seem to have a balanced t(X;17). The translocation results in a fusion of the ubiquitously expressed *ASPSCR1* gene in 17q25 and the transcription factor gene *TFE3* in Xp11 [95]. The same gene fusion has been found also in a subset of pediatric renal cell carcinomas, but in these tumors the translocation is balanced.

Current status and future directions

Obviously, the characterization of genomic changes in soft tissue sarcomas has not only provided molecular geneticists and cell biologists with decisive information on the parts of the genome that may harbor genes that are essential for tumor development but has also given the clinicians involved in the management of these patients a valuable diagnostic tool (Table 1) [5]. Still, most soft tissue sarcomas remain poorly characterized; only for four subtypes is cytogenetic information on more than 100 cases available, and for many less than 10 cases have been analyzed. Furthermore, with the exception of a few of the translocations leading to gene fusions, the consequences at the transcript level are unknown for most recurrent genomic alterations.

Apart from the obvious relevance of specific genetic aberrations for establishing a correct diagnosis, which is a prominent prognostic parameter in itself, the importance of the genetic aberrations on clinical outcome is elusive. The currently used prognostication systems rely on relatively crude clinical parameters, such as tumor size, and histopathologic parameters such as morphologic subtype, grade, necrosis, vascular invasion, and growth pattern, all of which suffer from inter-observer variability. Although there is no shortage of published reports claiming an impact of particular genetic aberrations, be they on the chromosome or gene level, on outcome, these studies have more often than not been based on small series of patients. Furthermore, the proposed correlations have, with a few exceptions, not been corroborated in independent studies. Nevertheless, support for the notion that independent prognostic information may be gained from genomic analysis could be derived from a cytogenetic study of 278 high-grade soft tissue sarcomas. Four parameters were found to be significantly associated with metastasis risk: grade, size, breakpoints in the proximal part of chromosome 1, and gain of material from the short arm of chromosome 6 [97].

Thus, there is no reason to believe that the pattern of genetic aberrations should be of less importance for the management of soft tissue sarcomas than for that of leukemias and lymphomas, where genomic analyses today constitute an integral part of the routine diagnostic and prognostic profiling. However, there is clearly a need for

further analyses, using cytogenetic as well as high-resolution genomic techniques, on larger series of morphologically well-characterized tumors from patients with adequate follow-up to establish the spectrum of aberrations occurring within each type of soft tissue sarcoma, as well as to allow proper evaluation of the prognostic importance of characteristic genomic changes.

Acknowledgments The authors are supported by grants from the Swedish Cancer Society, the Swedish Children's Cancer Fund, and the Swedish Research Council.

Conflicts of interest We declare that we have no conflict of interest.

References

1. Boveri T (1914) Zur Frage der Entstehung maligner Tumoren. Gustav Fisher Verlag, Jena
2. Mitelman F, Johansson B, Mertens F (2007) The impact of translocations and gene fusions on cancer causation. Nat Rev Cancer 7:233–245
3. Mitelman F, Johansson B, Mertens F (Eds) (2008) Mitelman database of chromosome aberrations in cancer. http://cgap.nci.nih.gov/Chromosomes/Mitelman
4. Pinkel D, Albertson DG (2005) Array comparative genomic hybridization and its application in cancer. Nat Genet 37:S11–S17
5. Fletcher CDM, Unni KK, Mertens F (eds) (2002) World Health Organization classification of tumours. Pathology and genetics of tumours of soft tissue and bone. IARC, Lyon
6. Helman LJ, Meltzer P (2003) Mechanisms of sarcoma development. Nat Rev Cancer 3:685–694
7. Billing V, Mertens F, Domanski HD et al (2008) Deep-seated ordinary and atypical lipomas; histopathology, cytogenetics, clinical features, and outcome in 215 tumors of the extremity and trunk wall. J Bone Joint Surg Br 90:929–933
8. Berner J-M, Forus A, Elkahloun A et al (1996) Separate amplified regions encompassing CDK4 and MDM2 in human sarcomas. Genes Chromosomes Cancer 17:254–259
9. Dei Tos AP, Doglioni C, Piccinin S et al (2000) Coordinated expression and amplification of the MDM2, CDK4, and HMGI-C genes in atypical lipomatous tumors. J Pathol 190:531–536
10. Hostein I, Pelmus M, Aurias A et al (2004) Evaluation of MDM2 and CDK4 amplification by real-time PCR on paraffin wax-embedded material: a potential tool for the diagnosis of atypical lipomatous tumours/well-differentiated liposarcomas. J Pathol 202:95–102
11. Italiano A, Bianchini L, Keslair F et al (2008) HMGA2 is the partner of MDM2 in well-differentiated and dedifferentiated liposarcomas whereas CDK4 belongs to a distinct inconsistent amplicon. Int J Cancer 122:2233–2241
12. Singer S, Socci ND, Ambrosini G et al (2007) Gene expression profiling of liposarcoma identifies distinct biological types/subtypes and potential therapeutic targets in well-differentiated and dedifferentiated liposarcoma. Cancer Res 67:6626–6636
13. Meza-Zepeda LA, Forus A, Lygren BO et al (2002) Positional cloning identifies a novel cyclophilin as a candidate amplified oncogene in 1q21. Oncogene 21:2261–2269
14. Micci F, Teixeira MR, Bjerkehagen B et al (2002) Characterization of supernumerary rings and giant marker chromosomes in well-differentiated lipomatous tumors by a combination of G-banding, CGH, M-FISH, and chromosome- and locus-specific FISH. Cytogenet Genome Res 97:13–19
15. Nilsson M, Meza-Zepeda LA, Mertens F et al (2004) Amplification of chromosome 1 sequences in lipomatous tumors and other sarcomas. Int J Cancer 109:363–369
16. Pedeutour F, Forus A, Coindre J-M et al (1999) Structure of the supernumerary ring and giant rod chromosomes in adipose tissue tumors. Genes Chromosomes Cancer 24:30–41
17. Coindre J-M, Hostein I, Maire G et al (2004) Inflammatory malignant fibrous histiocytomas and dedifferentiated liposarcomas: histological review, genomic profile, and MDM2 and CDK4 status favour a single entity. J Pathol 203:822–830
18. Rieker RJ, Joos S, Bartsch C et al (2002) Distinct chromosomal imbalances in pleomorphic and in high-grade dedifferentiated liposarcomas. Int J Cancer 99:68–73
19. Turc-Carel C, Limon J, Dal Cin P et al (1986) Cytogenetic studies of adipose tissue tumors. II. Recurrent reciprocal translocation t(12;16)(q13;p11) in myxoid liposarcomas. Cancer Genet Cytogenet 23:291–299
20. Crozat A, Åman P, Mandahl N et al (1993) Fusion of CHOP to a novel RNA-binding protein in human myxoid liposarcoma. Nature 363:640–644
21. Rabbitts TH, Forster A, Larson R et al (1993) Fusion of the dominant negative transcription regulator CHOP with a novel gene FUS by translocation t(12;16) in malignant liposarcoma. Nat Genet 4:175–180
22. Panagopoulos I, Höglund M, Mertens F et al (1996) Fusion of the EWS and CHOP genes in myxoid liposarcoma. Oncogene 12:489–494
23. Idbaih A, Coindre J-M, Derré J et al (2005) Myxoid malignant fibrous histiocytoma and pleomorphic liposarcoma share very similar genomic imbalances. Lab Invest 85:176–181
24. Dahlén A, Fletcher CDM, Mertens F et al (2004) Activation of the GLI oncogene through fusion with the beta-actin gene (ACTB) in a group of distinctive pericytic neoplasms: pericytoma with t(7;12). Am J Pathol 164:1645–1653
25. Miettinen MM, el-Rifai W, Sarlomo-Rikala M et al (1997) Tumor size-related DNA copy number changes occur in solitary fibrous tumors but not in hemangiopericytomas. Mod Pathol 10:1194–1200
26. Griffin CA, Hawkins AL, Dvorak C et al (1999) Recurrent involvement of 2p23 in inflammatory myofibroblastic tumors. Cancer Res 59:2776–2780
27. Lawrence B, Perez-Atayde A, Hibbard MK et al (2000) TPM3–ALK and TPM4–ALK oncogenes in inflammatory myofibroblastic tumors. Am J Pathol 157:377–384
28. Patel AS, Murphy KM, Hawkins AL et al (2007) RANBP2 and CLTC are involved in ALK rearrangements in inflammatory myofibroblastic tumors. Cancer Genet Cytogenet 176:107–114
29. Knezevich SR, McFadden DE, Tao W et al (1998) A novel ETV6–NTRK3 gene fusion in congenital fibrosarcoma. Nat Genet 18:184–187
30. Rubin BP, Chen C-J, Morgan TW et al (1998) Congenital mesoblastic nephroma t(12;15) is associated with ETV6–NTRK3 gene fusion. Cytogenetic and molecular relationship to congenital (infantile) fibrosarcoma. Am J Pathol 153:1451–1458
31. Mertens F, Fletcher CDM, Dal Cin P et al (1998) Cytogenetic analysis of 46 pleomorphic soft tissue sarcomas and correlation with morphologic and clinical features: a report of the CHAMP Study Group. Genes Chromosomes Cancer 22:16–25
32. Örndal C, Rydholm A, Willén H et al (1994) Cytogenetic intratumor heterogeneity in soft tissue tumors. Cancer Genet Cytogenet 78:127–137
33. Willems SM, Debiec-Rychter M, Szuhai K et al (2006) Local recurrence of myxofibrosarcoma is associated with increase in

tumor grade and cytogenetic aberrations, suggesting a multistep tumour progression model. Mod Pathol 19:407–416
34. Ohguri T, Hisaoka M, Kawauchi S et al (2006) Cytogenetic analysis of myxoid liposarcoma and myxofibrosarcoma by array-based comparative genomic hybridisation. J Clin Pathol 59:978–983
35. Wettach GR, Boyd LJ, Lawce HJ et al (2008) Cytogenetic analysis of a hemosiderotic fibrolipomatous tumor. Cancer Genet Cytogenet 182:140–143
36. Panagopoulos I, Storlazzi CT, Fletcher CDM et al (2004) The chimeric FUS/CREB3L2 gene is specific for low-grade fibromyxoid sarcoma. Genes Chromosomes Cancer 40:218–228
37. Guillou L, Benhattar J, Gengler C et al (2007) Translocation-positive low-grade fibromyxoid sarcoma: clinicopathologic and molecular analysis of a series expanding the morphologic spectrum and suggesting potential relationship to sclerosing epithelioid fibrosarcoma. A study from the French sarcoma group. Am J Surg Pathol 31:1387–1402
38. Mertens F, Fletcher CDM, Antonescu CR et al (2005) Clinicopathologic and molecular genetic characterization of low-grade fibromyxoid sarcoma, and cloning of a novel FUS/CREB3L1 fusion gene. Lab Invest 85:408–415
39. Matsuyama A, Hisaoka M, Shimajiri S et al (2006) Molecular detection of FUS–CREB3L2 fusion transcripts in low-grade fibromyxoid sarcoma using formalin-fixed, paraffin-embedded tissue specimens. Am J Surg Pathol 30:1077–1084
40. Mandahl N, Heim S, Willén H et al (1990) Supernumerary ring chromosome as the sole cytogenetic abnormality in a dermatofibrosarcoma protuberans. Cancer Genet Cytogenet 49:273–275
41. Pedeutour F, Coindre J-M, Sozzi G et al (1994) Supernumerary ring chromosomes containing chromosome 17 sequences. A specific feature of dermatofibrosarcoma protuberans? Cancer Genet Cytogenet 76:1–9
42. O'Brien KP, Seroussi E, Dal Cin P et al (1998) Various regions within the alpha-helical domain of the COL1A1 gene are fused to the second exon of the PDGFB gene in dermatofibrosarcomas and giant-cell fibroblastomas. Genes Chromosomes Cancer 23:187–193
43. Simon M-P, Pedeutour F, Sirvent N et al (1997) Deregulation of the platelet-derived growth factor B-chain gene via fusion with collagen gene COL1A1 in dermatofibrosarcoma protuberans and giant-cell fibroblastoma. Nat Genet 15:95–98
44. Patel UK, Szabo SS, Hernandez VS et al (2008) Dermatofibrosarcoma protuberans COL1A1–PDGFB fusion is identified in virtually all dermatofibrosarcoma cases when investigated by newly developed multiplex reverse transcription polymerase chain reaction and fluorescence in situ hybridization assays. Hum Pathol 39:184–193
45. Kiuru-Kuhlefelt S, El-Rifai W, Fanburg-Smith J et al (2001) Concomitant DNA copy number amplification at 17q and 22q in dermatofibrosarcoma protuberans. Cytogenet Cell Genet 92:192–195
46. Abbott JJ, Erickson-Johnson M, Wang X et al (2006) Gains of COL1A1–PDGFB genomic copies occur in fibrosarcomatous transformation of dermatofibrosarcoma protuberans. Mod Pathol 19:1512–1518
47. Fletcher CDM, Gustafson P, Rydholm A et al (2001) Clinicopathologic re-evaluation of 100 malignant fibrous histiocytomas: prognostic relevance of subclassification. J Clin Oncol 19:3045–3050
48. Chibon F, Mariani O, Derré J et al (2002) A subgroup of malignant fibrous histiocytomas is associated with genetic changes similar to those of well-differentiated liposarcomas. Cancer Genet Cytogenet 139:24–29
49. Nakayama R, Nemoto T, Takahashi H et al (2007) Gene expression analysis of soft tissue sarcomas: characterization and reclassification of malignant fibrous histiocytoma. Mod Pathol 20:749–759
50. Simons A, Schepens M, Jeuken J et al (2000) Frequent loss of 9p21 ($p16^{INK4A}$) and other genomic imbalances in human malignant fibrous histiocytoma. Cancer Genet Cytogenet 118:89–98
51. Mandahl N, Fletcher CDM, Dal Cin P et al (2000) Comparative cytogenetic study of spindle cell and pleomorphic leiomyosarcomas of soft tissues: a report from the CHAMP Study Group. Cancer Genet Cytogenet 116:66–73
52. Wang R, Lu Y-J, Fisher C et al (2001) Characterization of chromosome aberrations associated with soft-tissue leiomyosarcomas by twenty-four-color karyotyping and comparative genomic hybridization analysis. Genes Chromosomes Cancer 31:54–64
53. Chang A, Schuetze SM, Conrad EU III et al (2005) So-called "inflammatory leiomyosarcoma": a series of 3 cases providing additional insights into a rare entity. Int J Surg Pathol 13:185–195
54. Larramendy ML, Kaur S, Svarvar C et al (2006) Gene copy number profiling of soft-tissue leiomyosarcomas by array-comparative genomic hybridization. Cancer Genet Cytogenet 169:94–101
55. Meza-Zepeda LA, Kresse SH, Barragan-Polania AH et al (2006) Array comparative genomic hybridization reveals distinct DNA copy number differences between gastrointestinal stromal tumors and leiomyosarcomas. Cancer Res 66:8984–8993
56. Hu J, Rao UNM, Jasani S et al (2005) Loss of DNA copy number of 10q is associated with aggressive behavior of leiomyosarcomas: a comparative genomic hybridization study. Cancer Genet Cytogenet 161:20–27
57. Wang R, Titley JC, Lu Y-J et al (2003) Loss of 13q14-q21 and gain of 5p14-pter in the progression of leiomyosarcoma. Mod Pathol 16:778–785
58. Douglass EC, Shapiro DN, Valentine M et al (1993) Alveolar rhabdomyosarcoma with the t(2;13): cytogenetic findings and clinicopathologic correlations. Med Pediatr Oncol 21:83–87
59. Gordon T, McManus A, Anderson J et al (2001) Cytogenetic abnormalities in 42 rhabdomyosarcoma: a United Kingdom Cancer Cytogenetics Group study. Med Pediatr Oncol 36:259–267
60. Xia SJ, Pressey JG, Barr FG (2002) Molecular pathology of rhabdomyosarcoma. Cancer Biol Therapy 1:97–104
61. Barr FG (2001) Gene fusions involving PAX and FOX family members in alveolar rhabdomyosarcoma. Oncogene 20:5736–5746
62. Barr FG, Qualman SJ, Macris MH et al (2002) Genetic heterogeneity in the alveolar rhabdomyosarcoma subset without typical gene fusions. Cancer Res 62:4704–4710
63. Davicioni E, Finckenstein FG, Shahbazian V et al (2006) Identification of a PAX-FKHR gene expression signature that defines molecular classes and determines the prognosis of alveolar rhabdomyosarcomas. Cancer Res 66:6936–6946
64. Wachtel M, Dettling M, Koscielniak E et al (2004) Gene expression signatures identify rhabdomyosarcoma subtypes and detect a novel t(2;2)(q35;p23) translocation fusing PAX3 to NCOA1. Cancer Res 64:5539–5545
65. Sorensen PHB, Lynch JC, Qualman SJ et al (2002) *PAX3–FKHR* and *PAX7–FKHR* gene fusions are prognostic indicators in alveolar rhabdomyosarcoma: a report from the Children's Oncology Group. J Clin Oncol 20:2672–2679
66. Kullendorff CM, Donnér M, Mertens F et al (1998) Chromosomal aberrations in a consecutive series of childhood rhabdomyosarcoma. Med Pediatr Oncol 30:156–159
67. Bridge JA, Liu J, Weibolt V et al (2000) Novel genomic imbalances in embryonal rhabdomyosacoma revealed by comparative genomic hybridization and fluorescence in situ hybridization: an intergroup rhabdomyosarcoma study. Genes Chromosomes Cancer 27:337–344

68. Baumhoer D, Gunawan B, Becker H et al (2005) Comparative genomic hybridization in four angiosarcomas of the breast. Gynecol Oncol 97:348–352
69. Bottillo I, Ahlquist T, Brekke H et al (2008) Germline and somatic NF1 mutations in sporadic and NF1-associated malignant peripheral nerve sheath tumours. J Pathol, in press
70. Berner J-M, Sorlie T, Mertens F et al (1999) Chromosome band 9p21 is frequently altered in malignant peripheral nerve sheath tumours: studies of CDKN2A and other genes of the pRB pathway. Genes Chromosomes Cancer 26:151–160
71. Bridge RS Jr, Bridge JA, Neff JR et al (2004) Recurrent chromosomal imbalances and structurally abnormal breakpoints within complex karyotypes of malignant peripheral nerve sheath tumour and malignant triton tumour: a cytogenetic and molecular cytogenetic study. J Clin Pathol 57:1172–1178
72. Jhanwar SC, Chen Q, Li FP et al (1994) Cytogenetic analysis of soft tissue sarcomas. Recurrent chromosome abnormalities in malignant peripheral nerve sheath tumors (MPNST). Cancer Genet Cytogenet 78:138–144
73. Mantripragada KK, Spurlock G, Kluwe L et al (2008) High-resolution DNA copy number profiling of malignant peripheral nerve sheath tumors using targeted microarray-based comparative genomic hybridization. Clin Cancer Res 14:1015–1024
74. Mertens F, Dal Cin P, De Wever I et al (2000) Cytogenetic characterization of peripheral nerve sheath tumours: a report of the CHAMP Study Group. J Pathol 190:31–38
75. Storlazzi CT, Brekke HR, Mandahl N et al (2006) Identification of a novel amplicon at distal 17q containing the BIRC5/SURVIVIN gene in malignant peripheral nerve sheath tumours. J Pathol 209:492–500
76. Antonescu CR, Dal Cin P, Nafa K et al (2007) EWSR1–CREB is the predominant gene fusion in angiomatoid fibrous histiocytoma. Genes Chromosomes Cancer 46:1051–1060
77. Hallor KH, Micci F, Meis-Kindblom JM et al (2007) Fusion genes in angiomatoid fibrous histiocytoma. Cancer Lett 251:158–163
78. Limon J, Mrozek K, Mandahl N et al (1991) Cytogenetics of synovial sarcoma: presentation of ten new cases and review of the literature. Genes Chromosomes Cancer 3:338–345
79. Mandahl N, Limon J, Mertens F et al (1995) Nonrandom secondary chromosome aberrations in synovial sarcomas with t (X;18). Int J Oncol 7:495–499
80. Panagopoulos I, Mertens F, Isaksson M et al (2001) Clinical impact of molecular and cytogenetic findings in synovial sarcoma. Genes Chromosomes Cancer 31:362–372
81. Turc-Carel C, Dal Cin P, Limon J et al (1987) Involvement of chromosome X in primary cytogenetic change in human neoplasia: nonrandom translocation in synovial sarcoma. Proc Natl Acad Sci USA 84:1981–1985
82. Ladanyi M, Antonescu CR, Leung DH et al (2002) Impact of SYT–SSX fusion type on the clinical behavior of synovial sarcoma: a multi-institutional retrospective study of 243 patients. Cancer Res 62:135–140
83. Guillou L, Benhattar J, Binichon F et al (2004) Histologic grade, but not SYT–SSX fusion type, is an important prognostic factor in patients with synovial sarcoma: a multicenter, retrospective analysis. J Clin Oncol 22:4040–4050
84. Amary MFC, Berisha F, Del Carlo Bernardi F et al (2007) Detection of SS18–SSX fusion transcripts in formalin-fixed paraffin-embedded neoplasms: analysis of conventional RT-PCR, qRT-PCR and dual color FISH as diagnostic tools for synovial sarcoma. Mod Pathol 20:482–496
85. Bridge JA, Borek DA, Neff JR et al (1990) Chromosomal abnormalities in clear cell sarcoma. Implications for histogenesis. Am J Clin Pathol 93:26–31
86. Panagopoulos I, Mertens F, Debiec-Rychter M et al (2002) Molecular genetic characterization of the EWS/ATF1 fusion gene in clear cell sarcoma of the tendons and aponeuroses. Int J Cancer 99:560–567
87. Antonescu CR, Nafa K, Segal NH et al (2006) EWS–CREB1: a recurrent variant fusion in clear cell sarcoma—association with gastrointestinal location and absence of melanocytic differentiation. Clin Cancer Res 12:5356–5362
88. Gerald WL, Haber DA (2005) The EWS–WT1 gene fusion in desmoplastic small round cell tumor. Semin Cancer Biol 15:197–205
89. Lae ME, Roche PC, Jin L et al (2002) Desmoplastic small round cell tumor. A clinicopathologic, immunohistochemical, and molecular study of 32 tumors. Am J Surg Pathol 26:823–835
90. Lualdi E, Modena P, Debiec-Rychter M et al (2004) Molecular cytogenetic characterization of proximal-type epithelioid sarcoma. Genes Chromosomes Cancer 41:283–290
91. Modena P, Lualdi E, Facchinetti F et al (2005) SMARCB1/INI1 tumor suppressor gene is frequently inactivated in epithelioid sarcomas. Cancer Res 65:4012–4019
92. Panagopoulos I, Mertens F, Isaksson M et al (2002) Molecular genetic characterization of the EWS/CHN and RBP56/CHN fusion genes in extraskeletal myxoid chondrosarcoma. Genes Chromosomes Cancer 35:340–352
93. Sjögren H, Meis-Kindblom JM, Örndal C et al (2003) Studies on the molecular pathogenesis of extraskeletal myxoid chondrosarcoma—cytogenetic, molecular genetic, and cDNA microarray analyses. Am J Pathol 162:781–792
94. Hisaoka M, Hashimoto H (2005) Extraskeletal myxoid chondrosarcoma: updated clinicopathological and molecular genetic characteristics. Pathol Int 55:453–463
95. Ladanyi M, Lui MY, Antonescu CR et al (2001) The der(17) t (X;17)(p11;q25) of human alveolar soft part sarcoma fuses the TFE3 transcription factor gene to ASPL, a novel gene at 17q25. Oncogene 20:48–57
96. Folpe AL, Deyrup AT (2006) Alveolar soft-part sarcoma: a review and update. J Clin Pathol 59:1127–1132
97. Mertens F, Strömberg U, Rydholm A et al (2006) Prognostic significance of chromosome aberrations in high-grade soft tissue sarcomas. J Clin Oncol 24:315–320

Virchows Arch (2010) 456:141–151
DOI 10.1007/s00428-009-0774-2

REVIEW AND PERSPECTIVE

Gene expression profiling for the investigation of soft tissue sarcoma pathogenesis and the identification of diagnostic, prognostic, and predictive biomarkers

Andrew H. Beck · Robert B. West · Matt van de Rijn

Received: 8 December 2008 / Revised: 31 March 2009 / Accepted: 14 April 2009 / Published online: 2 May 2009
© Springer-Verlag 2009

Abstract Soft tissue sarcomas are malignant neoplasms derived from mesenchymal tissues. Their pathogenesis is poorly understood and there are few effective treatment options for advanced disease. In the past decade, gene expression profiling has been applied to sarcomas to facilitate understanding of sarcoma pathogenesis and to identify diagnostic, prognostic, and predictive markers. In this paper, we review this body of work and discuss how gene expression profiling has led to advancements in the understanding of sarcoma pathobiology, the identification of clinically useful biomarkers, and the refinement of sarcoma classification schemes. Lastly, we conclude with a discussion of strategies to further optimize the translation of gene expression data into a greater understanding of sarcoma pathogenesis and improved clinical outcomes for sarcoma patients.

Keywords Gene expression profiling · Microarrays · Genomics · Bioinformatics · Tumor biology · Soft tissue tumors · Sarcomas · Biomarkers · Molecular pathology · Surgical pathology

A. H. Beck · R. B. West · M. van de Rijn (✉)
Pathology Department, Stanford University Medical Center,
300 Pasteur Drive,
Stanford, CA 94305, USA
e-mail: mrijn@stanford.edu

R. B. West
Pathology and Laboratory Service,
Palo Alto Veterans Affairs Health Care System,
Palo Alto, CA, USA

Introduction

Sarcomas are malignant neoplasms derived from mesenchymal tissues. They represent approximately 1% of malignancies diagnosed annually. Sarcomas are currently diagnosed based on histopathological evaluation supplemented with the use of immunohistochemistry and molecular diagnostic techniques in selected cases [1]. There are ~100 recognized histopathological subtypes of soft tissue tumors [2]. The rarity of these tumors and the large number of diagnostic entities make sarcomas a challenging area of investigation.

Currently, treatment for sarcomas consists of surgery with consideration for chemotherapy and radiotherapy. The growing importance of comprehensive treatment regimens involving neoadjuvant chemotherapy [3] and preoperative radiotherapy [4] emphasizes the importance of pathological analysis of preoperative biopsy material. The strongest predictor of patient outcome is stage at time of diagnosis. Treatment options are limited and few effective adjuvant therapies exist for advanced disease. Due to the poor prognosis and limited effective therapeutic options available for most sarcomas, there is a major clinical need for increased understanding of sarcoma pathogenesis to facilitate the development of new diagnostic markers and therapeutic agents [5, 6].

Gene expression microarray technology was developed in the mid-1990s to permit genome-wide monitoring of gene expression [7–9]. The principal types of array platforms used for gene expression monitoring involve the robotic deposition of DNA fragments onto a glass slide [7] or the in situ synthesis of oligonucleotides on high-density arrays using photolithography [10]. Each of these technologies is able to produce genome-wide measurements of expression to produce a "snap shot" of a tumor's gene expression at a specific point in time.

Standard molecular biology techniques (Southern blotting, Northern blotting, Western blotting, polymerase chain reaction, sequencing) and ancillary molecular techniques routinely utilized by pathologists (immunohistochemistry, fluorescence in situ hybridization), typically measure one biomarker at a time, and consequently relatively little statistical analysis is required to interpret the result. In contrast, a gene expression profiling experiment measures the expression of thousands (10,000–500,000) of transcripts in parallel. The enormous amount of quantitative data produced by a single sample measured on a gene expression microarray requires the application of statistical procedures to standardize the data and determine the significance of the observed findings [11]. In recent years, the statistical community has adopted recommendations for biomedical researchers working with these technologies [11, 12]. These recommendations hope to facilitate standardization of the primary steps of microarray data analysis (design, preprocessing, inference, classification, and validation). Following application of statistical procedures to the dataset, it is useful to apply additional analytic tools to integrate the findings with databases containing biomedical annotation to facilitate translation of the microarray data into biologically and clinically useful knowledge [13–16].

It is hoped that application of this technology to sarcomas will afford a greater understanding of their biology and facilitate the development of more effective diagnostic and treatment regimens to improve outcomes for sarcoma patients. The primary goals of gene expression profiling in sarcomas are to: (1) gain a deeper understanding of the aberrant biological pathways contributing to sarcomagenesis, (2) refine the classificatory scheme for sarcomas to better reflect the underlying biology of the tumors, and (3) identify markers to predict diagnosis, patient outcome, and response to therapy (Fig. 1) [17]. In the following sections, we review studies utilizing gene expression profiling in soft tissue sarcoma.

Synovial sarcoma

Synovial sarcomas compose 5–10% of all soft tissue sarcomas. They are aggressive sarcomas and distant metastasis is the major cause of mortality [18]. The tumors are defined molecularly by a specific t(X;18)(p11.2;q11.2) translocation which fuses *SS18* (*SYT*) on chromosome 18 with either *SSX1*, *SSX2*, or *SSX4* on the X chromosome [19, 20]. The aberrant pathways induced by this translocation are incompletely understood [21]. Due in part to limited understanding of synovial sarcoma pathogenesis, clinical management consists primarily of surgery and radiotherapy and no effective targeted therapies are currently available [18].

Gene expression profiling has been performed to better characterize the tumor's pathogenesis. In most profiling studies, synovial sarcomas showed a distinct pattern of gene expression and clustered together (Fig. 2) [22–27]. In several other reports, some synovial sarcomas showed a similar pattern of gene expression to malignant peripheral nerve sheath tumor, resulting in a subset of synovial sarcomas clustering with malignant peripheral nerve sheath tumors (MPNSTs) [28, 29]. Taken together, these studies support that synovial sarcoma represents a relatively homogenous sarcoma subtype, whose gene expression profile shows the most similarity to malignant peripheral nerve sheath tumor.

Several groups have published lists of genes highly expressed in synovial sarcoma. Francis et al. [27] examined 32 synovial sarcomas in a study that included 177 sarcomas spanning 13 histological subtypes. Of these 13 subtypes, they found that synovial sarcoma showed the most distinct gene expression signature. They identified 4,000 genes differentially expressed in synovial sarcoma (false discovery rate=11%), including the SS chromosome X breakpoint genes *SSX1* and *SSX3* and genes involved in: neural differentiation (*FNA1*, *NCAM1*, *NEDD5*, *NPDC1*, and *OLFM1*), the retinoic acid pathway (*RARA*, *RARG*, *MDK*, *MEIS1*, and *PRAME*), and the epidermal growth factor (EGF) and fibroblast growth factor (FGF) receptor signaling pathways (*ERBB2*, *FGFR1*, *FGFR3*, *FGF18*, and *FRAG1*). Nielsen et al. [22] performed gene expression profiling on eight monophasic synovial sarcomas in a study that contained a total of 41 soft tissue tumors spanning six histologic subtypes. They identified a cluster of genes (including *SSX*, retinoic acid pathway genes, and epidermal growth factor receptor (*EGFR*)) which showed high levels of expression in synovial sarcoma. Nielsen et al. subsequently validated these gene microarray findings on a tissue microarray and showed that most synovial sarcomas showed protein expression of EGFR and SALL2 [30]. This group subsequently showed that the marker TLE1, which was identified through gene expression profiling experiments, was an effective diagnostic immunohistochemical marker for synovial sarcoma [31]. Allander et al. performed gene expression profiling on 14 synovial sarcomas, four malignant fibrous histiocytomas, and one fibrosarcoma and found that synovial sarcomas showed increased expression of ERBB2 and IGFBP2 and IGF2 [26]. They validated and extended this finding by performing immunohistochemistry on a tissue microarray containing 37 synovial sarcomas. In this analysis, they noted that strong protein expression of ERBB2 and IGFBP2 localized to the glandular epithelial component of biphasic synovial sarcomas and to the solid epithelioid areas of some monophasic synovial sarcomas, suggesting that these proteins are involved in epithelial differentiation in synovial sarcoma [26]. Nagayama et al. [28] performed gene expression profiling on a total of 47

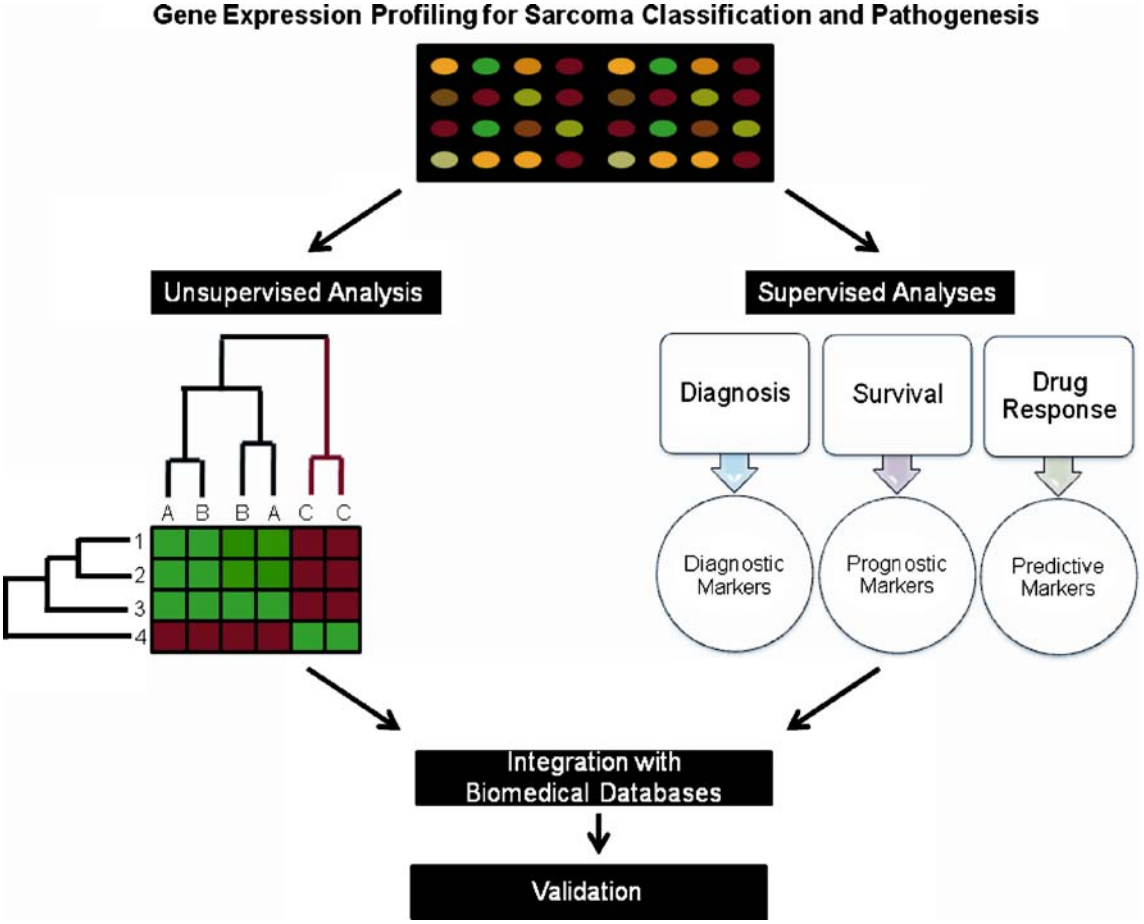

Fig. 1 Schematic overview of the use of gene expression profiling for the investigation of sarcoma pathogenesis and the identification of diagnostic, prognostic, and predictive biomarkers. Following collection of biological samples for analysis, gene expression microarray experiments begin with the hybridization of cDNA or cRNA to a microarray chip, producing tens of thousands of gene expression measurements per sample. Following data collection, the most commonly used data analysis techniques are: unsupervised two-way clustering of samples and genes to discover novel biologic pathways observed in sarcoma subtypes and to discover new relationships within and between sarcoma subtypes. Supervised analyses complement the unsupervised approaches and are used to identify gene expression signatures and biomarkers to predict particular clinical phenotypes, such as: diagnostic subtype, prognosis, and response to treatment. Due to the complexity of microarray data and the large gene lists typically produced by both unsupervised and supervised analyses, it is useful to integrate the data with repositories of biomedical annotation information to optimize the translation of the findings into biomedically useful knowledge. A final step of independent validation (ideally on an independent platform with independent samples) is essential to ensure the validity and reproducibility of the findings

sarcomas spanning six histologic subtypes and including 13 synovial sarcomas. They found that MPNST and SS clustered together and identified genes involved in neural differentiation shared by the two tumor types (including *EPHA4*, *EFNB3*). Interestingly, it has recently been shown that *SS18-SSX2* exerts part of its oncogenic effect by altering cytoskeletal architecture in an Eph-dependent manner [32]. YF Lee et al. performed gene expression profiling on nine synovial sarcomas, nine leiomyosarcomas, and nine pleomorphic sarcomas (malignant fibrous histiocytoma (MFH)) and identified 44 genes with significantly higher expression in synovial sarcoma [33]. This gene list includes genes involved in embryonic development (*FGF9*), transcriptional regulation (*SSX4*, *NCOA3*), cell signaling (*EFNB1*, *IGF2*), and cellular adhesion (*CDH1*, *ICAM1*) [33]. Fernebro et al. [34] identified a gene expression signature that discriminated between cases with the variant *SS18-SSX1* translocation as compared with *SS18-SSX2*. These data may provide insight into the potential association of the SS18-SSX1 variant with poorer prognosis, which has been suggested in several papers [20, 35], but not confirmed in subsequent studies [36, 37]. Taken together, the most consistent findings from these analyses are that overexpression of ERBB2, neural markers, and genes involved in retinoic acid and EGF and FGF signaling is seen in synovial sarcoma.

Based on the study by Nielsen et al. [22] that showed high levels of expression of EGFR (Her-1) in synovial

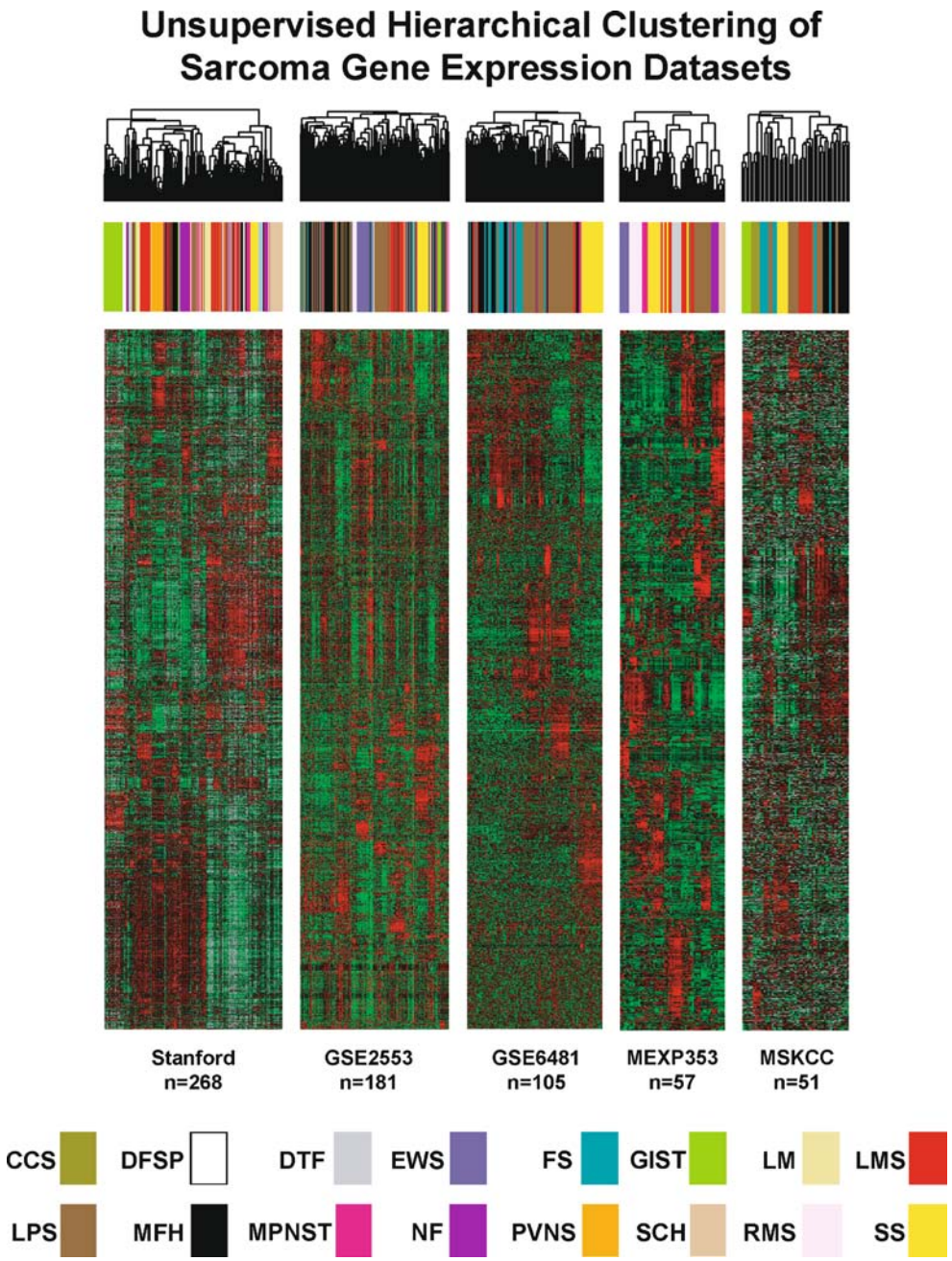

Fig. 2 Unsupervised hierarchical clustering of five sarcoma gene expression datasets. The cases are arranged along the *columns* and the genes along the *rows*. Within the heat map, *red* indicates relatively increased expression, *black* median expression, and *green* decreased expression. The *color bar* underlying the *dendrogram* indicates the diagnostic subtype of each case as indicated in the legend, which uses the following abbreviations: clear cell sarcoma (*CCS*), dermatofibrosarcoma protuberans (*DFSP*), desmoid-type fibromatosis (*DTF*), Ewing's sarcoma (*EWS*), fibrosarcoma (*FS*), gastrointestinal stromal tumor (*GIST*), leiomyoma (*LM*), leiomyosarcoma (*LMS*), liposarcoma (*LPS*), malignant fibrous histiocytoma/pleomorphic sarcoma (*MFH*), malignant peripheral nerve sheath tumor (*MPNST*), neurofibroma (*NF*), pigmented villonodular synovitis (*PVNS*), schwannoma (*SCH*), rhabdomyosarcoma (*RMS*), and synovial sarcoma (*SS*). The clustering pattern suggests that one subset of sarcomas (including GIST, SS, EWS) shows relatively homogenous gene expression patterns and a second subset of sarcomas (including LMS, LPS, and MFH) shows more heterogeneous patterns of gene expression. The gene expression data presented in this figure were downloaded from the Gene Expression Omnibus (http://www.ncbi.nlm.nih.gov/geo/), Stanford Microarray Database (http://genome-www5.stanford.edu/), ArrayExpress (http://www.ebi.ac.uk/microarray-as/ae/), and supplemental materials accompanying the paper by Segal et al. [25]. Prior to clustering, the genes were mean-centered. Clustering was performed with average linkage and correlation (uncentered) as the distance metric using Cluster 3.0 software (http://bonsai.ims.u-tokyo.ac.jp/~mdehoon/software/cluster/software.htm#ctv)

sarcoma, Ray-Coquard et al. [38] performed a phase II trial of gefitinib (an EGFR tyrosine kinase inhibitor) for the treatment of patients with synovial sarcomas expressing EGFR by immunohistochemistry that were refractory to standard chemotherapy regimens. In this trial, gefitinib failed to show significant therapeutic efficacy to warrant further evaluation in this setting. These negative results highlight the difficulty of translating findings from gene expression profiling into the oncology clinic and suggest the importance of considering other biologically important features (such as phosphorylation) in addition to messenger RNA and protein expression levels.

While most gene expression studies have focused on genes highly expressed in synovial sarcoma, Lubniecka et al. noted that a significant number of genes are down-regulated by the *SS18-SSX* fusion [39]. They investigated *EGR1*, which is a gene that shows low expression levels in synovial sarcoma, and showed that EGR1 expression is significantly inhibited by the SS18-SSX fusion. They then demonstrated that EGR1's expression can be reactivated in a synovial sarcoma cell model following treatment with the histone deacetylase inhibitor romidepsin, suggesting a potential mechanistic rationale for the use of histone deacetylase inhibitors in the treatment of synovial sarcoma [39]. There is a major clinical need for new targeted therapies for synovial sarcoma [18], and additional functional work will need to be performed using techniques such as animal modeling [21] to further delineate the pathways mediated by the by the *SS18*:*SSX* fusion and to identify effective targeted therapeutic agents.

Leiomyosarcoma

Leiomyosarcomas are malignant tumors of smooth muscle, which most frequently occur in the retroperitoneum or uterus and may also arise in large blood vessels and extremities [2]. The pathogenesis of leiomyosarcoma is not well understood. Retroperitoneal site and larger size predict poorer prognosis, and local recurrence and metastasis are common in leiomyosarcoma. Clinical management typically consists of surgery, radiation, and chemotherapy. There are currently no effective targeted therapies available for leiomyosarcoma.

Gene expression studies to date have shown inconsistent results regarding the variability within leiomyosarcoma. Most experiments have found that leiomyosarcomas show diverse patterns of gene expression, with a relatively homogenous subset of leiomyosarcomas clustering together while one or multiple separate groups of leiomyosarcoma cluster with pleomorphic sarcoma (MFH) [22, 27, 33]. In contrast, to these studies, Baird et al. found relatively homogenous patterns of gene expression among 17 LMS with all cases clustering together [24].

Several groups have identified lists of genes that show high expression in leiomyosarcomas, many of which are known to be involved in smooth muscle differentiation (for example: *CALD1*, *MYL4*, *SLMAP*) [22, 27]. Our laboratory has found that elevated expression of these muscle-associated genes is seen in a distinct subset of leiomyosarcoma; however, two other distinct subsets of leiomyosarcoma exist, which each show increased expression of distinct gene sets. Taken together, these findings suggest that in contradistinction to relatively homogenous sarcoma subtypes (such as synovial sarcoma and gastrointestinal stromal tumor), a significant amount of variability exists within leiomyosarcoma. It may well be that subsets of this entity can be found in which subsets of cases have dysregulation of specific pathways that could then be targeted for therapy. Much more work needs to be done to define these subgroups and identify gene targets.

Several studies have used microarrays to identify prognostic markers in leiomyosarcoma. YF Lee et al. performed a supervised analysis and identified a list of 335 genes significantly differentially expressed between 20 primary tumors and seven metastatic tumors [40]. They then clustered a set of 30 nonmetastatic tumors with this gene set and showed that the clustering classification strongly predicted the presence of concurrent metastasis and correlated with time to metastasis. Most of the genes from the metastasis signature showed increased expression in the cluster of cases with poorer prognosis and encoded proteins involved in cell cycle, signal transduction, and apoptosis. Future studies will need to be performed to assess whether this gene expression signature predicts metastatic outcome on an independent dataset.

In a recent study, CH Lee et al. performed gene microarray analysis on a series of leiomyosarcomas and identified highly variable expression levels of macrophage-associated genes within leiomyosarcoma [41]. This finding prompted the investigators to evaluate the protein expression of macrophage markers (CD163 and CD68) on a leiomyosarcoma tissue microarray with clinical follow-up data. This analysis revealed that increased macrophages within leiomyosarcoma are associated with poor outcome in nongynecological leiomyosarcoma. Further research will be needed to validate the prognostic findings in leiomyosarcoma. In addition, further data mining of the leiomyosarcoma datasets is necessary to further identify aberrant molecular pathways to permit the development of targeted therapies for leiomyosarcoma patients.

Liposarcoma

Liposarcomas represent ~20% of soft tissue sarcomas and are the single most prevalent subtype of soft tissue sarcoma

[2]. There are three principle histologic subtypes of liposarcoma (well differentiated/dedifferentiated, myxoid/round cell, and pleomorphic), which show distinct morphologic features and cytogenetic aberrations [42]. Several studies have performed gene expression profiling to assess the relationship between liposarcoma subsets, to provide insight into their pathogenesis, and to identify diagnostic and therapeutic markers.

Most studies have shown that myxoid/round cell liposarcoma, well-differentiated/dedifferentiated, and pleomorphic liposarcoma show distinct patterns of gene expression [24, 27, 29]. Singer et al. performed gene expression profiling to create a 142-gene classifier that distinguished between liposarcoma subtypes, lipoma, and normal fat on a training set of 80 samples and an independent test set of 49 samples [43]. They found that cell cycle and checkpoint pathways tended to be activated in well-differentiated/dedifferentiated liposarcoma and that Nutlin-3a, an antagonist of MDM2, preferentially induces apoptosis and growth arrest in dedifferentiated liposarcoma cells compared with normal adipocytes [43]. Other groups had previously shown that *MDM2* and *CDK4* are frequently amplified in atypical lipomatous tumor/well-differentiated liposarcoma and dedifferentiated liposarcoma [44]. To further characterize biological relationships between adipogenic tumors, Matushansky et al. created a developmental model of lipogenic sarcomagenesis by first defining gene expression profiles of stages of differentiation during in vitro differentiation of human mesenchymal stem cells into adipose tissues. They then created a differentiation-based classifier to correlate each of the major liposarcoma subtypes (dedifferentiated, well differentiated, round cell, and pleomorphic) to one of the stages of differentiation [45]. This novel approach provides additional insight into the relationship between liposarcoma subtypes. Taken together, these findings show that the liposarcoma subtypes show distinct gene expression profiles, which may be characteristic of particular stages of mesenchymal stem cell differentiation along an adipogenic path.

Despite the fact that liposarcoma is the most common single sarcoma subtype, few gene expression studies have been performed to identify prognostic or predictive markers for this entity, making this an important area for future investigation.

Pleomorphic sarcoma/MFH

Pleomorphic sarcoma, previously known as MFH, remains one of the most frequently diagnosed sarcoma types, despite the fact that leading sarcoma experts question the validity and usefulness of this diagnostic category [46]. The diagnostic term was first proposed in the mid-1960s when it was thought that cultured fibroblasts adopted phagocytic qualities resembling histiocytes [47]. The diagnostic category was seriously called into question following a careful analysis of 159 lesions identified by morphology as MFH. This analysis revealed that most cases could be recategorized as specific types of pleomorphic sarcoma and only 13% were morphologically compatible with the MFH category [48]. In a subsequent study, Fletcher et al. [49] implemented a combination of morphological, immunohistochemical, and ultrastructural criteria and showed that myogenic differentiation was associated with worse prognosis in cases that had previously been diagnosed as MFH. In the most recent World Health Organization (WHO) classification system, the term pleomorphic MFH has been replaced with undifferentiated pleomorphic sarcoma [2]. This is thought to be a rare entity that accounts for no more than 5% of soft tissue sarcomas [50].

Motivated in part by uncertainty concerning the biological basis for this diagnostic category, several gene expression studies have been performed to characterize patterns of gene expression in pleomorphic sarcoma/MFH. Unsupervised hierarchical clustering analyses have suggested that pleomorphic sarcoma/MFH may not represent a distinct biological entity but may instead represent a heterogeneous collection of high-grade sarcomas that shares patterns of gene expression with other high-grade karyotypically complex sarcomas [22–27].

While there is evidence for great heterogeneity in this group of tumors, they appear to have shared characteristics as well as evidenced by the work of Matushansky et al. [51]. To evaluate the pathogenesis and patterns of gene expression in pleomorphic sarcoma/MFH, Matushansky et al. [51] first defined a stem cell gene signature and showed that the stem cell signature was highly and specifically expressed by pleomorphic sarcoma/MFH. Using functional studies, they showed that expression of DKK1, which is known to be involved in embryonic development through inhibition of the WNT signaling pathway, inhibits mesenchymal stem cell differentiation via the Wnt2/β-catenin pathway and that mesenchymal stem cells can be transformed via inhibition of WNT signaling to form pleomorphic sarcoma-like tumors in nude mice. These findings suggest a particular cell of origin for pleomorphic sarcoma/MFH and suggest that alteration of WNT signaling pathway may provide a potential therapeutic strategy.

Taken together, most gene expression studies on pleomorphic sarcoma/MFH fail to show significant homogeneity within the tumor types; however, the novel technique employed by Matushansky et al. provides interesting insight into the pathogenesis of pleomorphic sarcoma/MFH. Future work will need to be undertaken to evaluate this hypothesis and to identify new therapeutic targets in this malignancy.

GIST

Gastrointestinal stromal tumors (GIST) are mesenchymal neoplasms that arise in the wall of the gastrointestinal tract and that compose approximately 1–3% of gastrointestinal neoplasms [52]. The majority of GISTs show activation of the KIT or PDGFRa receptor tyrosine kinase proteins, and imatinib, a tyrosine kinase inhibitory with activity against GIST, shows therapeutic efficacy in these tumors [53]. Heinrich and colleagues [54] have shown that specific mutations in *KIT* or *PDGFRa* correlate with biologic features of the tumor and predict response to therapy. In contrast, the protein expression of CD34, KIT (CD117), α-smooth muscle actin, and desmin has shown no association with survival in GIST patients treated with imatinib [55].

Several large sarcoma gene expression studies included significant numbers of GIST, and these studies all show that GISTs have a distinct and homogenous gene expression pattern and tend to all group together in unsupervised hierarchical clustering [22, 24, 27, 29]. Subramanian et al. [56] performed gene expression profiling on 26 GISTs with known *KIT* and *PDGFRa* status and identified gene expression profiles characteristic of different mutation types. A small percentage of GISTs do not show expression of KIT (CD117) by immunohistochemistry, and these tumors represent a diagnostic challenge. West et al. [57] identified DOG1 as a promising marker for CD117-negative GIST. This study was recently validated using a novel monoclonal antibody against DOG1 [58]. Yang et al. [59] recently showed that DOG1 (TMEM16A) is a calcium-activated chloride channel. Both DOG1 and KIT are expressed at high levels in cells of Cajal in the myenteric plexus from which GIST originates. Price et al. [60] performed gene expression profiling on a large collection of GISTs and leiomyosarcoma and created a two-gene classifier that was highly discriminant between the two diagnoses. Taken together, these studies show that GISTs show relatively homogenous patterns of gene expression with relatively little variability within this diagnostic category.

Small round blue cell tumors

Small round blue cell tumors encompass several diagnostic categories, including: primitive neuroectodermal tumor (PNET/Ewing's), rhabdomyosarcoma, neuroblastoma, and desmoplastic small round cell tumor. In an early and widely cited gene expression profiling experiment, Khan et al. used gene expression profiling and artificial neural networks to create a highly accurate gene-expression-based classifier to differentiate between neuroblastoma, rhabdomyosarcoma, non-Hodgkin lymphoma, and the Ewing family of tumors [61]. Gene expression studies have been performed to predict poor prognosis in the Ewing family of tumors [62, 63]. Ferreira et al. performed gene expression profiling to identify distinct genomic instability patterns associated with DNA repair and cell cycle checkpoint pathways in Ewing's sarcoma [64]. Multiple studies have looked at the oncogenic profile of the *EWS-FLI1* fusion. In a recent meta-analysis, Hancock et al. identified a core *EWS-FLI1* signature that supports the hypothesis that these tumors are derived from mesenchymal stem cells [65].

Most alveolar rhabdomyosarcomas are characterized by the t(2;13) translocation, which results in the generation of the PAX3-FKHR oncogenic fusion protein. Several gene expression studies have been performed to identify a PAX-FKHR gene expression signature [66–69]. Ren et al. showed that rhabdomyosarcomas may originate from mesenchymal stem cells, and the PAX3-FKHR fusion product induces skeletal muscle differentiation [70]. Several gene expression studies have been performed to identify predictive [71] and prognostic markers in rhabdomyosarcoma [66].

Low-grade fibroblastic tumors

The diagnostic category of low-grade fibroblastic tumors includes a large number of diagnostic entities, which are comprised of tumors characterized by a proliferation of spindle cells with fibroblastic features. Gene expression profiling has been performed on several low-grade fibroblastic tumor subsets to better define their pathogenesis, to identify prognostic markers, and to discover novel patterns of fibroblastic gene expression that may provide insight into stromal reaction patterns in the carcinoma microenvironment.

Dermatofibrosarcoma protuberans (DFSP) is an aggressive spindle cell neoplasm that frequently involves subcutaneous soft tissues. The tumor is associated with the t(17:22) chromosomal translocation, which fuses the *COL1A1* and *PDGFb* genes. DFSP have been shown to have a characteristic gene expression signature [72]. Gene expression profiling of DFSP led to the identification of APOD as an immunohistochemical marker expressed at high levels in DFSP, which may prove to be clinically useful as a diagnostic marker for differentiating DFSP from fibrous histiocytoma [73].

Desmoid-type fibromatosis (DTF) is a fibroblastic neoplasm that arises in the deep soft tissues and show infiltrative local growth with frequent recurrence, although they do not metastasize. DTFs can occur in association with familial cancer syndromes, such as familial adenomatous

polyposis and familial infiltrative fibromatosis, both of which result from germ line mutations in the *APC* gene. Beta-catenin dysregulation is a common finding in sporadic fibromatosis, and specific mutations in the beta-catenin gene (*CTNNB1*) predict recurrence risk [74]. DTF have been shown to have a distinct gene expression profile, characterized by high levels of expression of genes involved in extracellular matrix structure and function, including collagens, collagen binding, cell–cell adhesion, and cell-surface receptor-linked signal transduction regulation [75–77]. Gene signatures have been identified that differentiate DTF from nodular fasciitis [77] as well as solitary fibrous tumor [76]. West and colleagues have utilized DTF's gene expression signature to provide insight into a stromal reaction pattern consistently observed in ~25% of breast carcinomas and which correlates with improved prognosis [75, 76]. Currently, no effective therapies exist to prevent recurrence in desmoid-type fibromatosis, although imatinib has recently been shown to be an active agent in the treatment of some advanced fibromatosis [78]. Increased molecular understanding of this neoplasm is essential to permit the further development of more efficacious therapies [79].

Low-grade "fibrohistiocytic" tumors

Pigmented villonodular synovitis (PVNS) and tenosynovial giant cell tumor (TGCT) are related tumors, which are characterized by a proliferation of synovial-like mononuclear cells interspersed with multinucleate giant cells and inflammatory cells [2]. These tumors are classified as benign "fibrohistiocytic tumors" in the WHO classification of soft tissue tumors [2]. West et al. [80] evaluated the expression of a series of type III receptor tyrosine kinases on a large soft tissue tumor tissue microarray and identified increased expression of colony stimulating factor 1 (CSF1) and its receptor (CSF1R) in PVNS/TGCT. This finding led the investigators to identify a translocation that fuses *CSF1* on 1p13 to *COL6A3* on 2q35, resulting in the overexpression of CSF1 in a minority of tumor cells and the recruitment of CSF1R-expressing macrophages that compose the majority of the tumor mass in PVNS/TGCT [80]. The identification of the important role of the CSF1–CSF1R pathway in the pathogenesis of PVNS/TGCT suggests that inhibition of this pathway through the use of small-molecule inhibitors (such as SU11248) [81] could be effective for management of aggressive/recurrent PVNS/TGCT. It has recently been shown that the CSF1 response signature observed in PVNS/TGCT is seen in a subset (~25%) of breast carcinomas and is associated with higher grade, decreased hormone receptor expression, and increased *TP53* mutations [82].

Future directions

Over the past decade, many sarcoma types have been profiled with gene microarrays. However, we are still in the early stages of translating these data into deeper understanding of sarcomagenesis to facilitate the identification of predictive diagnostic markers and effective therapeutic regimens.

A first step towards this goal is increased utilization of the great wealth of sarcoma gene expression data that have been placed in public repositories, such as Gene Expression Omnibus [83] and Array Express [84]. A gene expression meta-analysis utilizing these datasets in conjunction with novel bioinformatics analytic techniques [15, 85–91] may prove useful for more fully understanding the aberrant biological pathways contributing to sarcomagenesis and for identifying and designing effective drugs to treat these conditions. Several investigators have utilized large-scale meta-analyses to identify common core biological pathways that are seen across diverse cancer types [13, 14, 92, 93]. This technique has not yet been applied systematically to sarcomas. Several studies have utilized gene expression profiles to guide chemotherapy, [16, 94, 95] and increased utilization of bioinformatics tools and publically available datasets may permit the development of clinical studies to assess the efficacy of gene expression profiling to guide chemotherapy in sarcoma.

A second step towards increased utilization of sarcoma gene microarray data is to encourage integration of these data with other sources of biomedical information measured with emerging molecular biology techniques, such as ultrahigh-throughput sequencing, array comparative genomic hybridization, and micro-RNA profiling [96]. It is hoped that the integration of these technologies with clinical and functional data will facilitate a deeper understanding of sarcoma biology and the development of diagnostic and therapeutic tools to improve the survival of sarcoma patients.

The final step towards translating these data into clinical practice will be developing techniques for measuring the most useful biomarkers using tools widely available in diagnostic pathology laboratories. A promising approach to achieving this goal is by analyzing data produced by massively parallel high-throughput genome-wide technologies (such as microarrays) to identify sparse sets of potentially clinically useful biomarkers, which can then be tested on large numbers of patient samples using tissue microarrays [97]. The ultimate goal is to allow measurement of a set of validated prognostic and predictive markers in routine clinical practice with tools available in diagnostic pathology laboratories, such as immunohistochemistry, fluorescent in situ hybridization, and polymerase-chain-reaction-based DNA/RNA analyses.

Conflict of interest statement We declare that we have no conflict of interest.

References

1. Weiss SW, Goldblum JR (2008) Enzinger and Weiss's soft tissue tumors, 5th edn. Mosby/Elsevier, Philadelphia
2. Fletcher CDM, Unni KK, Mertens F et al (2002) Pathology and genetics of tumours of soft tissue and bone. IARC Press, Lyon
3. Wendtner CM, Abdel-Rahman S, Krych M et al (2002) Response to neoadjuvant chemotherapy combined with regional hyperthermia predicts long-term survival for adult patients with retroperitoneal and visceral high-risk soft tissue sarcomas. J Clin Oncol 20:3156–3164
4. O'Sullivan B, Davis AM, Turcotte R et al (2002) Preoperative versus postoperative radiotherapy in soft-tissue sarcoma of the limbs: a randomised trial. Lancet 359:2235–2241
5. Borden EC, Baker LH, Bell RS et al (2003) Soft tissue sarcomas of adults: state of the translational science. Clin Cancer Res 9:1941–1956
6. Judson I (2008) State-of-the-art approach in selective curable tumours: soft tissue sarcoma. Ann Oncol 19(Suppl 7):vii166–vii169
7. Schena M, Shalon D, Davis RW et al (1995) Quantitative monitoring of gene expression patterns with a complementary DNA microarray. Science 270:467–470
8. Brown PO, Botstein D (1999) Exploring the new world of the genome with DNA microarrays. Nat Genet 21:33–37
9. Lockhart DJ, Winzeler EA (2000) Genomics, gene expression and DNA arrays. Nature 405:827–836
10. Fodor SP, Rava RP, Huang XC et al (1993) Multiplexed biochemical assays with biological chips. Nature 364:555–556
11. Allison DB, Cui X, Page GP et al (2006) Microarray data analysis: from disarray to consolidation and consensus. Nat Rev Genet 7:55–65
12. Butte A (2002) The use and analysis of microarray data. Nat Rev Drug Discov 1:951–960
13. Rhodes DR, Chinnaiyan AM (2004) Bioinformatics strategies for translating genome-wide expression analyses into clinically useful cancer markers. Ann N Y Acad Sci 1020:32–40
14. Rhodes DR, Kalyana-Sundaram S, Tomlins SA et al (2007) Molecular concepts analysis links tumors, pathways, mechanisms, and drugs. Neoplasia 9:443–454
15. Segal E, Friedman N, Kaminski N et al (2005) From signatures to models: understanding cancer using microarrays. Nat Genet 37 (Suppl):S38–S45
16. Potti A, Dressman HK, Bild A et al (2006) Genomic signatures to guide the use of chemotherapeutics. Nat Med 12:1294–1300
17. Tschoep K, Kohlmann A, Schlemmer M et al (2007) Gene expression profiling in sarcomas. Crit Rev Oncol Hematol 63:111–124
18. Eilber FC, Dry SM (2008) Diagnosis and management of synovial sarcoma. J Surg Oncol 97:314–320
19. Clark J, Rocques PJ, Crew AJ et al (1994) Identification of novel genes, SYT and SSX, involved in the t(X;18)(p11.2;q11.2) translocation found in human synovial sarcoma. Nat Genet 7:502–508
20. Kawai A, Woodruff J, Healey JH et al (1998) SYT-SSX gene fusion as a determinant of morphology and prognosis in synovial sarcoma. N Engl J Med 338:153–160
21. Haldar M, Randall RL, Capecchi MR (2008) Synovial sarcoma: from genetics to genetic-based animal modeling. Clin Orthop Relat Res 466:2156–2167
22. Nielsen TO, West RB, Linn SC et al (2002) Molecular characterisation of soft tissue tumours: a gene expression study. Lancet 359:1301–1307
23. Nakayama R, Nemoto T, Takahashi H et al (2007) Gene expression analysis of soft tissue sarcomas: characterization and reclassification of malignant fibrous histiocytoma. Mod Pathol 20:749–759
24. Baird K, Davis S, Antonescu CR et al (2005) Gene expression profiling of human sarcomas: insights into sarcoma biology. Cancer Res 65:9226–9235
25. Segal NH, Pavlidis P, Antonescu CR et al (2003) Classification and subtype prediction of adult soft tissue sarcoma by functional genomics. Am J Pathol 163:691–700
26. Allander SV, Illei PB, Chen Y et al (2002) Expression profiling of synovial sarcoma by cDNA microarrays: association of ERBB2, IGFBP2, and ELF3 with epithelial differentiation. Am J Pathol 161:1587–1595
27. Francis P, Namlos HM, Muller C et al (2007) Diagnostic and prognostic gene expression signatures in 177 soft tissue sarcomas: hypoxia-induced transcription profile signifies metastatic potential. BMC Genomics 8:73
28. Nagayama S, Katagiri T, Tsunoda T et al (2002) Genome-wide analysis of gene expression in synovial sarcomas using a cDNA microarray. Cancer Res 62:5859–5866
29. Henderson SR, Guiliano D, Presneau N et al (2005) A molecular map of mesenchymal tumors. Genome Biol 6:R76
30. Nielsen TO, Hsu FD, O'Connell JX et al (2003) Tissue microarray validation of epidermal growth factor receptor and SALL2 in synovial sarcoma with comparison to tumors of similar histology. Am J Pathol 163:1449–1456
31. Terry J, Saito T, Subramanian S et al (2007) TLE1 as a diagnostic immunohistochemical marker for synovial sarcoma emerging from gene expression profiling studies. Am J Surg Pathol 31:240–246
32. Barco R, Hunt LB, Frump AL et al (2007) The synovial sarcoma SYT-SSX2 oncogene remodels the cytoskeleton through activation of the ephrin pathway. Mol Biol Cell 18:4003–4012
33. Lee YF, John M, Edwards S et al (2003) Molecular classification of synovial sarcomas, leiomyosarcomas and malignant fibrous histiocytomas by gene expression profiling. Br J Cancer 88:510–515
34. Fernebro J, Francis P, Eden P et al (2006) Gene expression profiles relate to SS18/SSX fusion type in synovial sarcoma. Int J Cancer 118:1165–1172
35. Ladanyi M, Antonescu CR, Leung DH et al (2002) Impact of SYT-SSX fusion type on the clinical behavior of synovial sarcoma: a multi-institutional retrospective study of 243 patients. Cancer Res 62:135–140
36. Guillou L, Benhattar J, Bonichon F et al (2004) Histologic grade, but not SYT-SSX fusion type, is an important prognostic factor in patients with synovial sarcoma: a multicenter, retrospective analysis. J Clin Oncol 22:4040–4050
37. Takenaka S, Ueda T, Naka N et al (2008) Prognostic implication of SYT-SSX fusion type in synovial sarcoma: a multi-institutional retrospective analysis in Japan. Oncol Rep 19:467–476
38. Ray-Coquard I, Le Cesne A, Whelan JS et al (2008) A phase II study of gefitinib for patients with advanced HER-1 expressing synovial sarcoma refractory to doxorubicin-containing regimens. Oncologist 13:467–473
39. Lubieniecka JM, de Bruijn DR, Su L et al (2008) Histone deacetylase inhibitors reverse SS18-SSX-mediated polycomb silencing of the tumor suppressor early growth response 1 in synovial sarcoma. Cancer Res 68:4303–4310
40. Lee YF, John M, Falconer A et al (2004) A gene expression signature associated with metastatic outcome in human leiomyosarcomas. Cancer Res 64:7201–7204
41. Lee CH, Espinosa I, Vrijaldenhoven S et al (2008) Prognostic significance of macrophage infiltration in leiomyosarcomas. Clin Cancer Res 14:1423–1430
42. Dei Tos AP (2000) Liposarcoma: new entities and evolving concepts. Ann Diagn Pathol 4:252–266

43. Singer S, Socci ND, Ambrosini G et al (2007) Gene expression profiling of liposarcoma identifies distinct biological types/subtypes and potential therapeutic targets in well-differentiated and dedifferentiated liposarcoma. Cancer Res 67:6626–6636
44. Sirvent N, Coindre JM, Maire G et al (2007) Detection of MDM2-CDK4 amplification by fluorescence in situ hybridization in 200 paraffin-embedded tumor samples: utility in diagnosing adipocytic lesions and comparison with immunohistochemistry and real-time PCR. Am J Surg Pathol 31:1476–1489
45. Matushansky I, Hernando E, Socci ND et al (2008) A developmental model of sarcomagenesis defines a differentiation-based classification for liposarcomas. Am J Pathol 172:1069–1080
46. Tos AP (2006) Classification of pleomorphic sarcomas: where are we now? Histopathology 48:51–62
47. Ozzello L, Stout AP, Murray MR (1963) Cultural characteristics of malignant histiocytomas and fibrous xanthomas. Cancer 16:331–344
48. Fletcher CD (1992) Pleomorphic malignant fibrous histiocytoma: fact or fiction? A critical reappraisal based on 159 tumors diagnosed as pleomorphic sarcoma. Am J Surg Pathol 16:213–228
49. Fletcher CD, Gustafson P, Rydholm A et al (2001) Clinicopathologic re-evaluation of 100 malignant fibrous histiocytomas: prognostic relevance of subclassification. J Clin Oncol 19:3045–3050
50. Fletcher CD (2006) The evolving classification of soft tissue tumours: an update based on the new WHO classification. Histopathology 48:3–12
51. Matushansky I, Hernando E, Socci ND et al (2007) Derivation of sarcomas from mesenchymal stem cells via inactivation of the Wnt pathway. J Clin Invest 117:3248–3257
52. Miettinen M, Lasota J (2006) Gastrointestinal stromal tumors: review on morphology, molecular pathology, prognosis, and differential diagnosis. Arch Pathol Lab Med 130:1466–1478
53. Joensuu H, Roberts PJ, Sarlomo-Rikala M et al (2001) Effect of the tyrosine kinase inhibitor STI571 in a patient with a metastatic gastrointestinal stromal tumor. N Engl J Med 344:1052–1056
54. Heinrich MC, Corless CL, Demetri GD et al (2003) Kinase mutations and imatinib response in patients with metastatic gastrointestinal stromal tumor. J Clin Oncol 21:4342–4349
55. Sciot R, Debiec-Rychter M, Daugaard S et al (2008) Distribution and prognostic value of histopathologic data and immunohistochemical markers in gastrointestinal stromal tumours (GISTs): an analysis of the EORTC phase III trial of treatment of metastatic GISTs with imatinib mesylate. Eur J Cancer 44:1855–1860
56. Subramanian S, West RB, Corless CL et al (2004) Gastrointestinal stromal tumors (GISTs) with KIT and PDGFRA mutations have distinct gene expression profiles. Oncogene 23:7780–7790
57. West RB, Corless CL, Chen X et al (2004) The novel marker, DOG1, is expressed ubiquitously in gastrointestinal stromal tumors irrespective of KIT or PDGFRA mutation status. Am J Pathol 165:107–113
58. Espinosa I, Lee CH, Kim MK et al (2008) A novel monoclonal antibody against DOG1 is a sensitive and specific marker for gastrointestinal stromal tumors. Am J Surg Pathol 32:210–218
59. Yang YD, Cho H, Koo JY et al (2008) TMEM16A confers receptor-activated calcium-dependent chloride conductance. Nature 455:1210–1215
60. Price ND, Trent J, El-Naggar AK et al (2007) Highly accurate two-gene classifier for differentiating gastrointestinal stromal tumors and leiomyosarcomas. Proc Natl Acad Sci U S A 104:3414–3419
61. Khan J, Wei JS, Ringner M et al (2001) Classification and diagnostic prediction of cancers using gene expression profiling and artificial neural networks. Nat Med 7:673–679
62. Ohali A, Avigad S, Zaizov R et al (2004) Prediction of high risk Ewing's sarcoma by gene expression profiling. Oncogene 23:8997–9006
63. Cheung IY, Feng Y, Danis K et al (2007) Novel markers of subclinical disease for Ewing family tumors from gene expression profiling. Clin Cancer Res 13:6978–6983
64. Ferreira BI, Alonso J, Carrillo J et al (2008) Array CGH and gene-expression profiling reveals distinct genomic instability patterns associated with DNA repair and cell-cycle checkpoint pathways in Ewing's sarcoma. Oncogene 27:2084–2090
65. Hancock JD, Lessnick SL (2008) A transcriptional profiling meta-analysis reveals a core EWS-FLI gene expression signature. Cell Cycle 7:250–256
66. Davicioni E, Finckenstein FG, Shahbazian V et al (2006) Identification of a PAX-FKHR gene expression signature that defines molecular classes and determines the prognosis of alveolar rhabdomyosarcomas. Cancer Res 66:6936–6946
67. Ebauer M, Wachtel M, Niggli FK et al (2007) Comparative expression profiling identifies an in vivo target gene signature with TFAP2B as a mediator of the survival function of PAX3/FKHR. Oncogene 26:7267–7281
68. Lae M, Ahn EH, Mercado GE et al (2007) Global gene expression profiling of PAX-FKHR fusion-positive alveolar and PAX-FKHR fusion-negative embryonal rhabdomyosarcomas. J Pathol 212:143–151
69. Wachtel M, Dettling M, Koscielniak E et al (2004) Gene expression signatures identify rhabdomyosarcoma subtypes and detect a novel t(2;2)(q35;p23) translocation fusing PAX3 to NCOA1. Cancer Res 64:5539–5545
70. Ren YX, Finckenstein FG, Abdueva DA et al (2008) Mouse mesenchymal stem cells expressing PAX-FKHR form alveolar rhabdomyosarcomas by cooperating with secondary mutations. Cancer Res 68:6587–6597
71. Schaefer KL, Eisenacher M, Braun Y et al (2008) Microarray analysis of Ewing's sarcoma family of tumours reveals characteristic gene expression signatures associated with metastasis and resistance to chemotherapy. Eur J Cancer 44:699–709
72. Linn SC, West RB, Pollack JR et al (2003) Gene expression patterns and gene copy number changes in dermatofibrosarcoma protuberans. Am J Pathol 163:2383–2395
73. West RB, Harvell J, Linn SC et al (2004) Apo D in soft tissue tumors: a novel marker for dermatofibrosarcoma protuberans. Am J Surg Pathol 28:1063–1069
74. Lazar AJ, Tuvin D, Hajibashi S et al (2008) Specific mutations in the {beta}-catenin gene (CTNNB1) correlate with local recurrence in sporadic desmoid tumors. Am J Pathol 173:1518–1527
75. Beck AH, Espinosa I, Gilks CB et al (2008) The fibromatosis signature defines a robust stromal response in breast carcinoma. Lab Invest 88:591–601
76. West RB, Nuyten DS, Subramanian S et al (2005) Determination of stromal signatures in breast carcinoma. PLoS Biol 3:e187
77. Bacac M, Migliavacca E, Stehle JC et al (2006) A gene expression signature that distinguishes desmoid tumours from nodular fasciitis. J Pathol 208:543–553
78. Heinrich MC, McArthur GA, Demetri GD et al (2006) Clinical and molecular studies of the effect of imatinib on advanced aggressive fibromatosis (desmoid tumor). J Clin Oncol 24:1195–1203
79. Kotiligam D, Lazar AJ, Pollock RE et al (2008) Desmoid tumor: a disease opportune for molecular insights. Histol Histopathol 23:117–126
80. West RB, Rubin BP, Miller MA et al (2006) A landscape effect in tenosynovial giant-cell tumor from activation of CSF1 expression by a translocation in a minority of tumor cells. Proc Natl Acad Sci U S A 103:690–695
81. Murray LJ, Abrams TJ, Long KR et al (2003) SU11248 inhibits tumor growth and CSF-1R-dependent osteolysis in an experimental breast cancer bone metastasis model. Clin Exp Metastasis 20:757–766

82. Beck AH, Espinosa I, Edris B et al (2009) The macrophage colony-stimulating factor 1 response signature in breast carcinoma. Clin Cancer Res 15:778–787
83. Edgar R, Domrachev M, Lash AE (2002) Gene expression omnibus: NCBI gene expression and hybridization array data repository. Nucleic Acids Res 30:207–210
84. Parkinson H, Sarkans U, Shojatalab M et al (2005) ArrayExpress—a public repository for microarray gene expression data at the EBI. Nucleic Acids Res 33:D553–D555
85. Bild AH, Potti A, Nevins JR (2006) Linking oncogenic pathways with therapeutic opportunities. Nat Rev Cancer 6:735–741
86. Hu P, Bader G, Wigle DA et al (2007) Computational prediction of cancer-gene function. Nat Rev Cancer 7:23–34
87. Lamb J, Crawford ED, Peck D et al (2006) The connectivity map: using gene-expression signatures to connect small molecules, genes, and disease. Science 313:1929–1935
88. Lamb J (2007) The connectivity map: a new tool for biomedical research. Nat Rev Cancer 7:54–60
89. Dennis G Jr, Sherman BT, Hosack DA et al (2003) DAVID: Database for Annotation, Visualization, and Integrated Discovery. Genome Biol 4:P3
90. von Mering C, Jensen LJ, Kuhn M et al (2007) STRING 7—recent developments in the integration and prediction of protein interactions. Nucleic Acids Res 35:D358–D362
91. Subramanian A, Tamayo P, Mootha VK et al (2005) Gene set enrichment analysis: a knowledge-based approach for interpreting genome-wide expression profiles. Proc Natl Acad Sci U S A 102:15545–15550
92. Segal E, Friedman N, Koller D et al (2004) A module map showing conditional activity of expression modules in cancer. Nat Genet 36:1090–1098
93. Rhodes DR, Yu J, Shanker K et al (2004) Large-scale meta-analysis of cancer microarray data identifies common transcriptional profiles of neoplastic transformation and progression. Proc Natl Acad Sci U S A 101:9309–9314
94. Bonnefoi H, Potti A, Delorenzi M et al (2007) Validation of gene signatures that predict the response of breast cancer to neoadjuvant chemotherapy: a substudy of the EORTC 10994/BIG 00-01 clinical trial. Lancet Oncol 8:1071–1078
95. Dressman HK, Berchuck A, Chan G et al (2007) An integrated genomic-based approach to individualized treatment of patients with advanced-stage ovarian cancer. J Clin Oncol 25:517–525
96. Subramanian S, Lui WO, Lee CH et al (2008) MicroRNA expression signature of human sarcomas. Oncogene 27:2015–2026
97. Camp RL, Neumeister V, Rimm DL (2008) A decade of tissue microarrays: progress in the discovery and validation of cancer biomarkers. J Clin Oncol 26:5630–5637

Virchows Arch (2010) 456:153–166
DOI 10.1007/s00428-009-0776-0

REVIEW AND PERSPECTIVE

Soft tissue sarcomas with non-EWS translocations: molecular genetic features and pathologic and clinical correlations

Cyril Fisher

Received: 21 January 2009 / Revised: 27 March 2009 / Accepted: 14 April 2009 / Published online: 28 April 2009
© Springer-Verlag 2009

Abstract Many soft tissue sarcoma subtypes have consistent chromosomal translocations with novel fusion genes, which result in disordered cellular function. The microscopic appearances, immunophenotype and behaviour of such tumours relate to the genetic events to a variable extent. This paper reviews the molecular pathology and related morphological and clinical features of sarcomas with non-EWS translocations. These include synovial sarcoma, alveolar rhabdomyosarcoma, alveolar soft part sarcoma, dermatofibrosarcoma protuberans, low-grade fibromyxoid sarcoma, infantile fibrosarcoma and inflammatory myofibroblastic tumour.

Keywords Translocation · Soft tissue sarcoma · Molecular genetics

Introduction

Increasing numbers of soft tissue sarcoma subtypes are found to have consistent chromosomal translocations with formation of fusion genes whose products and interactions affect cell proliferation, growth and survival. The initiating factors for most gene fusions are unknown [1]. However, the genetic rearrangements and fusion gene products are now routinely demonstrable in fixed tissue using fluorescence in situ (FISH) and reverse transcription polymerase chain reaction (RT-PCR) techniques, and the patterns of gene activation can be displayed by gene expression profiling. These developments have led to improved diagnosis and to an increasing influence of genetic findings on clinical management of these rare tumours.

Sarcomas with non-EWS translocations are spindle, polygonal or small round cell tumours with varying behaviour, which mostly occur in children or young adults. They include synovial sarcoma, alveolar rhabdomyosarcoma, alveolar soft part sarcoma, dermatofibrosarcoma protuberans, low-grade fibromyxoid sarcoma, infantile fibrosarcoma and inflammatory myofibroblastic tumour. This paper reviews the molecular genetic findings in these sarcoma types and their relationship with morphological, immunohistochemical and clinical features.

Synovial sarcoma

Synovial sarcoma does not arise from or differentiate towards synovium and the name is a historical error [2]. This tumour is extremely rare within joints [3–5] and generally arises in periarticular connective tissue and most commonly around the knee. Identification of the t(X;18) by cytogenetic or molecular means, however, has confirmed that synovial sarcoma occurs in almost any anatomical location [2]. Occasional cases have arisen in the field of therapeutic irradiation for other lesions [6–8].

C. Fisher
Department of Pathology, Royal Marsden NHS Foundation Trust, London, UK

C. Fisher (✉)
Royal Marsden Hospital,
203 Fulham Road,
London, SW3 6JJ, UK
e-mail: cyril.fisher@rmh.nhs.uk

Genetic features

Over 90% of synovial sarcomas have a reciprocal balanced translocation t(X;18)(p11.2:q11.2) in which eight amino acids at the carboxy terminal of the *SYT (SS18)* gene on chromosome 18 are replaced with 78 amino acids of the carboxy terminal of the *SSX* gene on the X chromosome. The *SSX* gene has five variants of which *SSX1* (in about two thirds of cases) or *SSX2* are the usual components of the fusion gene [9], with a very small number involving *SSX4* [10]. Molecular variants within the fusion genes [11–13] and a t(X;20) translocation involving *SS18L* [14] have been described in single cases. The fusion gene seems to locate to a different nuclear domain from either of its components [15–17].

The functions of the gene products are unknown. The normal SYT protein is widely expressed, whereas *SSX* genes encode histone-binding proteins that are normally mainly expressed in the testis. In synovial sarcoma, cyclin D1 activity is increased, with induction of p21 (cyclin-dependent kinase inhibitor) but the oncogenic effect of the fusion is not clear, and other events might be required for sarcomagenesis. Alterations in other genes include expression of *ERBB2* in epithelial areas, upregulation of *IGF2*, repression of *CD44*, *PTEN* inactivation and mutations in genes associated with the Wnt pathway, notably *APC* and the genes encoding E-cadherin and beta-catenin [18]. Gene expression profiling has shown variably high expression of *ERBB2*, *IGFBP2* and *IGF2* in synovial sarcomas [19, 20], several differences in gene expression for *SYT-SSX1* and *SYT-SSX2* fusion types [21] and a possible genetic signature related to development of metastases [21].

Pathologic features

Microscopically, biphasic, monophasic spindle cell, poorly differentiated, calcifying/ossifying and myxoid subtypes have been described. The monophasic variant (Fig. 1) is the most common and has spindle cells, which are identical to those in biphasic tumours but can vary in shape from rounded to longer and more spindled. Poorly differentiated synovial sarcoma (Fig. 2) is characterised by frequent mitoses and necrosis, with rounding of cells, and can be focal or involve the whole tumour, which then resembles other small round cell sarcomas [22, 23] or less commonly carcinoma. All histological types of synovial sarcoma are focally immunoreactive for epithelial markers (cytokeratins in cytoplasm and epithelial membrane antigen on cell membrane) in over 90% of cases. There is diffuse immunoreactivity for bcl2 [24] and at least focal positivity for CD99 (which is more often cytoplasmic than membranous [25]), S100 protein, CD56 and calponin in many cases [26–28]. Calretinin [29] and beta-catenin [30] are also sometimes detectable in tumour cell nuclei. New antibodies selected based on data from gene profiling studies, such as TLE1 [31], or antibodies to fusion gene components such as SYT [32], though not wholly specific, might prove useful in diagnosis.

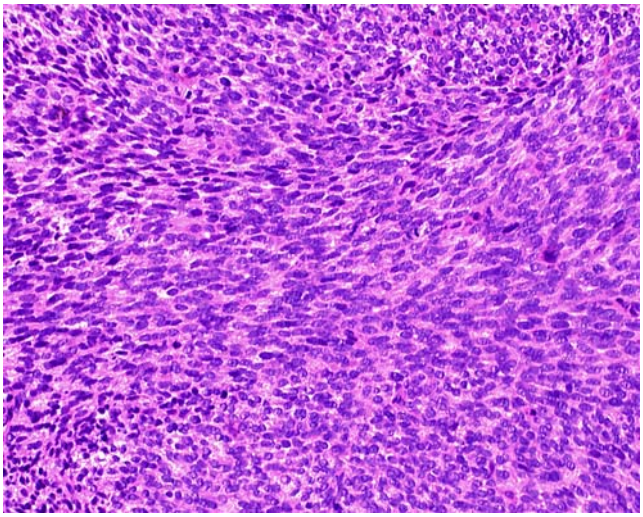

Fig. 1 Monophasic synovial sarcoma, showing fascicles of short uniform spindle cells with scanty cytoplasm

All histologic subtypes, regardless of immunophenotype, and those related to previous irradiation have the same range of genetic findings [7, 23, 33]. However, there is a relationship between degree of epithelial differentiation and type of fusion gene. Almost all biphasic tumours have the *SYT-SSX1* fusion [34, 35], whereas monophasic synovial sarcoma can display either fusion. The genetic changes are specific to synovial sarcoma [36, 37]. Thus, demonstration

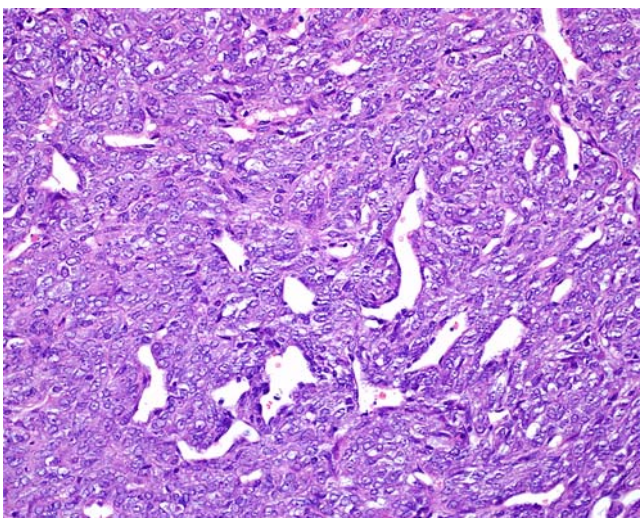

Fig. 2 Poorly differentiated synovial sarcoma composed of closely packed rounded cells with mitotic activity. There is a hemangiopericytic pattern

of the translocation or fusion gene transcripts is diagnostic and can distinguish synovial sarcoma from morphologically similar sarcomas, including malignant peripheral nerve sheath tumour and Ewing sarcoma/PNET.

Clinical features

Typically, synovial sarcoma is a tumour of young adults (mean age of 34), with nearly half the cases presenting in patients younger than 30 years [38]. There is a slight male predominance, and while cases with SYT-SSX1 fusion genes show an equal sex distribution, two thirds of those with *SYT-SSX2* gene rearrangement are found in females [38]. Primary tumours with *SYT-SSX1* fusion gene type tend to be more often located in the extremities [39].

Synovial sarcoma metastasizes in up to 50% of cases, to lung, bone and sometimes lymph node [38]. The 5- and 10-year survival figures are 36–76% and 20–63%, respectively [40–43]. Advanced stage, proximal location, male sex, age >40 years, tumour size >5 cm, poorly differentiated histology and Ki67 index [44] have been identified as adverse prognostic factors [42, 45]. Conversely, the outcome is more favourable in childhood, in very small sarcomas and in those with ossification. There may be a relationship between fusion type and prognosis although this is not straightforward [39]. Tumours with SYT-SSX1 have a higher proliferation rate and a lower 5-year metastasis-free survival compared with those with SYT-SSX2 [46], and it has been suggested that synovial sarcomas localised at time of diagnosis, which have the *SSX2* gene rearrangement, have a better outcome [38, 47]. However, this has not been confirmed in subsequent studies as a factor independent of grade [48] or tumour size [49]. The use of gene expression profiling for predicting metastasis has yet to be assessed [21].

About 55% of synovial sarcomas overexpress EGFR as detected by immunohistochemistry [50] and 73% express ERBB2 as shown by quantitative RT-PCR [50] and cDNA microarray analysis [20], raising the possibility of therapeutic interventions directed at receptor tyrosine kinases [51, 52] but results have so far been disappointing.

Alveolar rhabdomyosarcoma

Alveolar rhabdomyosarcoma is the second most common subtype of rhabdomyosarcoma after embryonal rhabdomyosarcoma [53]. It occurs principally in patients aged 10–25 years, with a median age of 16, with sporadic examples occurring in younger patients and older adults. The most common sites are the deep muscles of the extremities, but the tumour can also arise in the head and neck (nasal cavity, nasopharynx and paranasal sinuses, orbit, ear canal and oral cavity, including tongue), trunk, retroperitoneum and pelvis [54].

Genetic features

Approximately 75–90% of tumours categorised histologically as alveolar rhabdomyosarcomas have translocations which fuse the 5′ end (amino-terminal DNA-binding domain) of members of the *PAX* gene family, involved in formation of skeletal muscle satellite cells, with the 3′ end (C-terminal transactivation domain) of *FKHR (FOXO1)*, a gene which regulates myoblast differentiation [55–59]. About 70% harbour a t(2;13)(q35;q14), creating a *PAX3-FKHR* fusion, 15% have the t(1;13)(p36;q14) with formation of the *PAX7-FKHR* fusion, and occasional variants are reported in single cases [58, 60]. The fusion proteins are powerful transcription factors, and *PAX3-FKHR* expression has been shown to enhance cellular proliferation and invasion in rhabdomyosarcoma cell lines [61]. Additional changes, including those in *INK4a/ARF* and *TP53* pathways, may be needed for oncogenesis [62].

Pathological features

The typical microscopic pattern is one of nests of medium-sized rounded cells set within dense collagenous stroma (Fig. 3). The nests show central discohesion forming pseudoalveolar spaces, with a peripheral adherent layer of cells lining the ‘space’. The cells have ovoid hyperchromatic nuclei and scanty eosinophilic cytoplasm, and multinucleated cells with peripheral (‘wreath-like’) rings of nuclei are common. Rarely, there is increased clear

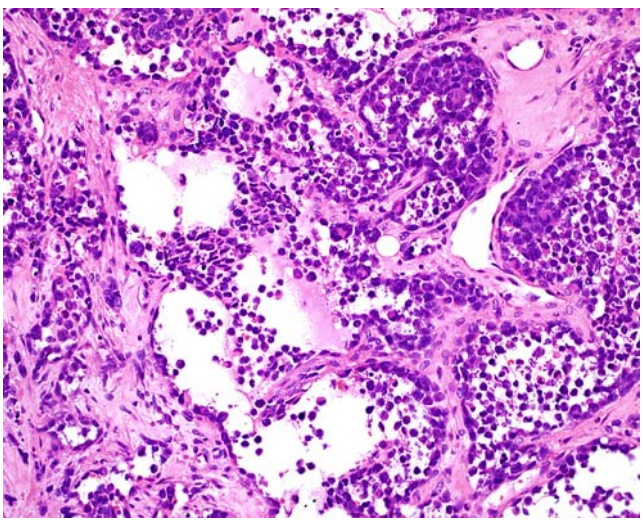

Fig. 3 Alveolar rhabdomyosarcoma showing nests of discohesive rounded cells, with rounded rhabdomyoblasts and multinucleated forms, in cellular fibrous stroma

cytoplasm due to glycogen accumulation, indicating designation as clear cell rhabdomyosarcoma [63–65]. Solid alveolar rhabdomyosarcoma [66, 67] is composed of sheets or large nests of rounded cells with hyperchromatic or vesicular nuclei, scanty cytoplasm and rare rhabdomyoblasts (Fig. 4). Solid variants of alveolar rhabdomyosarcoma are more often fusion negative than those with typical morphology [68]. There is otherwise no correlation between microscopic appearance and molecular abnormalities.

Immunohistochemistry for desmin is positive in almost all alveolar rhabdomyosarcomas in a high proportion of cells, and rhabdomyoblastic differentiation is confirmed by nuclear positivity for products of myogenic regulatory genes, including myogenin (myf4) and MyoD1(myf3). pRB immunoreactivity, related to allelic imbalance in the *RB1* gene, is more frequently detected in embryonal rhabdomyosarcoma than in alveolar rhabdomyosarcoma and may be an additional aid in differential diagnosis [69]. In some cases, genetic analysis is required to make this distinction.

Clinical features

Alveolar rhabdomyosarcoma is aggressive and metastasizes to lymph node, bone marrow, lung and other organs. Not uncommonly, especially with a head and neck or deep-seated primary tumour, the patient presents with an enlarged lymph node or with effects of marrow involvement such as leucoerythroblastic anaemia. Tumours with *PAX7-FKHR* fusion are less aggressive than those with *PAX3-FKHR*. They arise more often in the extremities, tend to remain localised and are associated with longer event-free survival [70] and longer overall survival in both locoregional [71] and metastatic disease [59]. Gene expression profiling can distinguish alveolar and embryonal rhabdomyosarcoma [72], has shown different profiles for fusion-positive and fusion-negative tumours [73] and has also identified molecular risk groups with varying outcome related to different gene signatures [74].

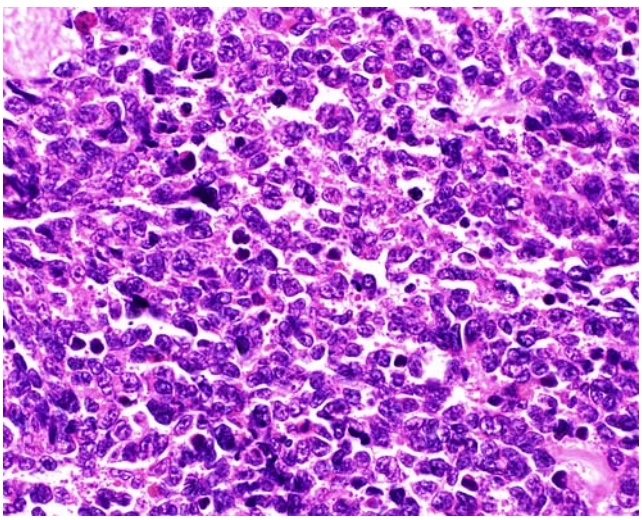

Fig. 4 Alveolar rhabdomyosarcoma, solid variant, composed of small round cells without obvious rhabdomyoblastic differentiation

Alveolar soft part sarcoma

Alveolar soft part sarcoma is a translocation sarcoma that does not correspond to any specific lineage. It is a rare tumour, accounting for <1% of all soft tissue sarcomas [75]. Its peak incidence is between 15 and 35 years of age, with a female predominance. The most frequent sites are the deep muscles of the thigh [76], especially the quadriceps, with sporadic cases in a variety of somatic and visceral locations, including bladder [77], cervix, vagina, uterus [78], mediastinum, heart [79] and GI tract. Head and neck locations, including tongue [80] and orbit [81], are common in childhood cases.

Genetic features

This tumour is characterised by an unbalanced (non-reciprocal) translocation, der(17)t(X;17)(p11;q25) [82, 83]. This results in fusion of the *TFE3* transcription factor gene (which contains a basic helix-loop-helix DNA-binding domain and a leucine zipper dimerization domain) on chromosome X with *ASPL* (*ASPSCR1*) on chromosome 17, which encodes a widely expressed protein of unknown function, to form aberrant transcription factors of two types that differ by one exon [84]. The fusion protein remains within the nucleus and can be demonstrated by immunohistochemistry using a specific antibody to the carboxy terminus of *TFE3* [85]. The same fusion is present in Xp11 (balanced) translocation-associated renal cell carcinomas, a category of papillary renal tumours occurring primarily in children and young adults [86, 87]. TFE3 nuclear immunoreactivity can also be demonstrated in some PEComas [88] and granular cell tumours [85] but whether that indicates a genetic abnormality of *TFE3* in those tumours is presently unclear.

Pathological features

Microscopically, there are nests of cells separated by fibrous septa and further delineated by thin-walled blood vessels (Fig. 5). The tumour cells are polygonal with distinct cell boundaries and contain rounded uniform vesicular nuclei and abundant finely granular or focally vacuolated cytoplasm. In childhood cases, there is often a

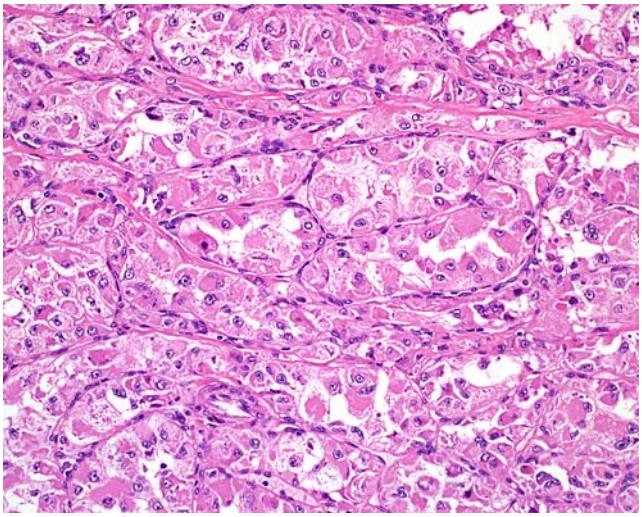

Fig. 5 Alveolar soft part sarcoma with nested pattern of polygonal cells with abundant cytoplasm

more solid pattern with the cells forming solid sheets or small closely packed nests and with reduced vascularity. No genetic differences between adult and childhood histological patterns have been identified.

The cytoplasm contains membrane bound rhomboidal crystals, which ultrastructurally display lattice-like filaments 4–6 nm in diameter with a periodicity of 10 nm [89, 90] and pre-crystalline granules. The latter contain monocarboxylate transporter 1, a proton-linked transporter for monocarboxylates (e.g. lactate and pyruvate) found in abundance in skeletal and cardiac muscle and its interacting partner CD147 (neurothelin) [91].

Immunohistochemistry using a specific antibody to the carboxy terminus of *TFE3* [85] is positive in nuclei of alveolar soft part sarcoma and also in translocation-associated renal cell carcinomas [86], some PEComas [88] and granular cell tumours [85].

Clinical features

Alveolar soft part sarcoma is relatively aggressive and metastasizes to lung, brain and bone but patients with localised disease can have a very prolonged course with survival of 77% at 2 years, 60% at 5 years, 38% at 10 years and 15% at 20 years (median 6 years) [76]. Patients presenting with metastatic disease have a median survival of 40 months and a 5-year survival of 20% [92]. Young adult [76] patients and those with small tumours have a better outcome, and childhood cases have a markedly better prognosis, especially for head and neck disease, with up to 100% 5-year survival [93]. There are no known genetic features, which predict behaviour or response to therapy, although a recent data showing activation of MET by the ASPL-TFE3 fusion protein have provided a rationale for examining MET kinase inhibitors in this setting [94].

Dermatofibrosarcoma protuberans

This is a relatively common neoplasm [95], which is more frequent in males, with a peak age incidence of 25–45 years, and also occurs in childhood and congenitally [96]. Dermatofibrosarcoma occurs mostly on the trunk and upper limbs as well as, to a lesser extent, other locations. The tumour begins as a dermal plaque or nodule and grows slowly, sometimes becoming multinodular. There are several morphologic variants, including pigmented dermatofibrosarcoma, giant cell fibroblastoma [97–100] and fibrosarcoma arising in dermatofibrosarcoma [101–106].

Genetic features

Dermatofibrosarcoma has a reciprocal translocation, t(17;22)(q22;q13.1) resulting in fusion of the genes *COL1A* (encoding the alpha 1 chain of collagen type 1, a heterotrimer) on 17q21-22 and *PDGFB1* (encoding the beta chain of platelet-derived growth factor, a homodimer) at 22q13 [107–111]. The same fusion is also seen in supernumerary ring chromosomes derived from t(17;22) [112], which are found in adult cases of dermatofibrosarcoma. Identical genetic changes have also been shown in morphologic variants, including the pigmented (Bednar tumour) [113] and granular cell [114] types, in the juvenile version giant cell fibroblastoma [114] (which more commonly has the linear translocation derivative than the ring chromosome [110]) and in examples of fibrosarcoma arising in dermatofibrosarcoma [115–117]. COL1A1-PDGFB fusion transcripts have also been identified in superficial CD34-positive fibrosarcomas without an antecedent or coexistent component of dermatofibrosarcoma [116]. The fusion gene transcripts can be detected by RT-PCR in paraffin-embedded material [96, 118]; this is not usually required for diagnosis but might be useful in guiding therapy, especially for superficial fibrosarcomas. Other rearrangements, including t(2;17) and t(9;22), are found rarely [119]. Gene expression profiling has shown high expression of a group of genes, which include *PDGFB*, osteonectin and apolipoprotein D [120, 121].

Pathological features

The typical lesion is composed of uniform elongated thin spindle cells with minimal cytoplasm and indistinct margins, in a striking and monotonous storiform pattern (Fig. 6). The tumour forms a nodule or ill-defined dermal

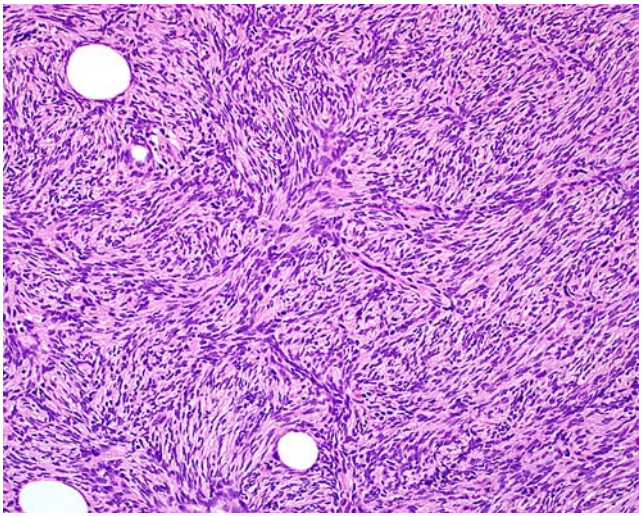

Fig. 6 Dermatofibrosarcoma demonstrating regular storiform pattern. The tumour infiltrates subcutaneous fat

plaque, which extends into subcutaneous fat with a characteristic honeycomb pattern, including layers of infiltrating tumour parallel to the skin surface. The lesional cells are diffusely positive for CD34. Apolipoprotein D, a glycoprotein component of high density lipoprotein, has been advocated as a diagnostic immunohistochemical marker [122], but is not specific for this tumour type [123].

Clinical features

Dermatofibrosarcoma recurs, especially if incompletely excised, but metastasis occurs in fewer than 5% of cases and usually follows multiple recurrences. Exceptionally, there is fibrosarcomatous (Fig. 7) or (very rarely) pleomorphic sarcomatous transformation, which can be regarded as a form of dedifferentiation.

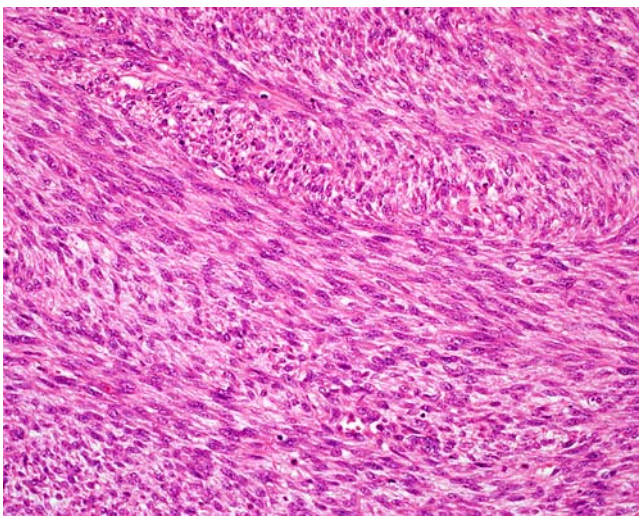

Fig. 7 Fibrosarcoma in dermatofibrosarcoma has a fascicular or herring bone pattern and frequent mitoses

PDGFR is a receptor tyrosine kinase, which in dermatofibrosarcoma is constitutively activated by autocrine or paracrine mechanisms as a result of overproduction of its ligand PDGFB [124], leading to cellular proliferation [125]. This has suggested the use of the tyrosine kinase inhibitors imatinib [126] and more recently sunitinib or sorafenib in locally advanced or metastatic disease [127–131], but fibrosarcomatous variants without the translocation do not respond [132, 133] so that genetic analysis is indicated before targeted therapy.

Low-grade fibromyxoid sarcoma

This fibrosarcoma variant has been recognised for over 20 years [134] but has recently been defined by specific genetic features, which have allowed appreciation of its wider range of microscopic appearances. This includes the tumour originally designated as hyalinizing spindle cell tumour with giant rosettes [135]. Low-grade fibromyxoid sarcoma presents as a well-defined mass in deeper soft tissues of extremities (especially the thigh), trunk and rarely other locations, including viscera, in young adults of either sex [136–142]. Examples located superficially have a higher incidence in childhood [143].

Genetic features

A t(7;16) translocation was initially reported in a hyalinizing spindle cell tumour [144] and a ring chromosome derived from the same chromosomes in metastatic low-grade fibromyxoid sarcoma [145]. Subsequently, a consistent balanced translocation, t(7;16)(q34;p11) in which the 5′ part of *FUS* from chromosome 16p11 fuses with 3′ part of *CREB3L2* (also known as *BBF2H7*), on chromosome 7q34, has been described in both low-grade fibromyxoid sarcoma and hyalinizing spindle cell tumour [146–148]. The breakpoints are mostly at exon 6 (and rarely 7) of *FUS* and exon 5 of *CREB3L2* [147–149]. *CREB3L2* is a member of the CREB3 family of transcription factors, which contain DNA binding and leucine zipper dimerization domains, and the fusion gene has increased transcriptional activity [150]. A smaller number have t(11,16)(p11;p11) with a FUS-CREB3L1 fusion gene consisting of the first nine exons of FUS and exons 5–12 from *CREB3L1* [148]. These findings have demonstrated that this sarcoma is morphologically heterogeneous and can be highly cellular or pleomorphic. No relationship has yet been shown, however, between genetic findings and microscopic appearances.

Pathological features

Histologically, low-grade fibromyxoid sarcoma shows fibrous and focally myxoid areas with a vaguely whorled pattern (Fig. 8). An abrupt transition to the myxoid foci is characteristic. Recurrent tumours can show increased cellularity, pleomorphism and mitotic activity. Up to 30% of cases have large rosette-like fibrous nodules bordered by more rounded tumour cells (Fig. 9). This variant was originally termed hyalinizing spindle cell tumour with giant rosettes [135] but is now known to be genetically identical to low-grade fibromyxoid sarcoma [146]. A relationship between low-grade fibromyxoid sarcoma and sclerosing epithelioid fibrosarcoma has been suggested [151].

The spindle cells in low-grade fibromyxoid sarcoma are often immunoreactive for EMA, at least focally [143, 151] and mostly negative for SMA, S100 protein and CD34. These must be distinguished from perineurioma, which has a mostly superficial location, elongated spindle cells with extended bipolar processes, perivascular whorls and immunoreactivity for claudin-1, GLUT1 and often CD34, as well as a characteristic ultrastructure. The genetic features of low-grade fibromyxoid sarcoma can be detected in paraffin section using FISH, RT-PCR [149, 151] or DNA-based PCR [152], with a sensitivity of over 80%, which is of diagnostic value.

Clinical features

Low-grade fibromyxoid sarcoma is a histologically low-grade sarcoma with metastatic potential. Reported rates of recurrence and metastasis were high in the early reports [136], which were retrospective studies of cases previously diagnosed as other tumours, with long follow-up. More recent studies indicate recurrence rates of 9–21% [137, 151]. In genetically confirmed cases, the metastatic rate was 27%, but more than 80% of metastases appeared after 9 years, indicating the need for long-term follow-up [151]. Superficial examples have a lower recurrence rate of 12%, and none has been reported to metastasize [143]. The finding at presentation of foci of higher grade sarcoma appears not to be prognostically adverse. No relationship has been shown between genetic findings and outcome.

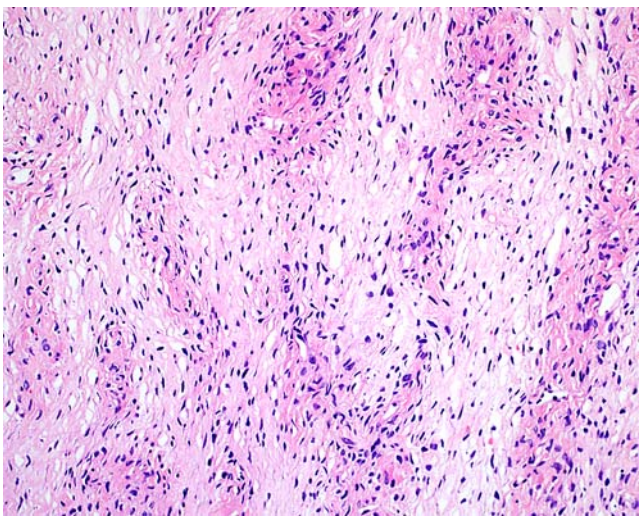

Fig. 8 Low-grade fibromyxoid sarcoma with alternating myxoid and fibrous areas. Note minimally pleomorphic spindle cells

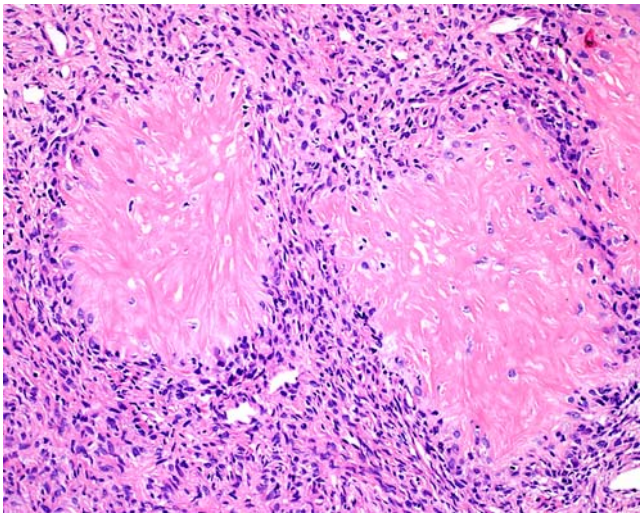

Fig. 9 'Giant' collagenous rosettes in low-grade fibromyxoid sarcoma. The cells adjacent to the collagenous zones tend to be more rounded

Infantile fibrosarcoma

This tumour occurs predominantly in the first 4 years of life, with a peak in the first 3 months, and presents as a rapidly growing mass, which can reach a large size. It arises in deep soft tissue, in limbs, where it can erode bone, and less commonly involves the trunk or head and neck region.

Genetic features

The majority of cases are diploid but reported cytogenetic abnormalities include trisomy 11, random gains of chromosomes 8, 11, 17 and 20 [153], deletion of the long arm of 17 [154] and a t(12;13) translocation [155]. Most cases of infantile fibrosarcoma have a specific translocation t (12;15)(p13;q25) [156–158] leading to fusion of *ETV6 (TEL)*, a member of the ets family of transcription factors,

on chromosome 12p13, and *NTRK3 (TRKC)*, which encodes a receptor tyrosine kinase for neurotropin-3 [159, 160] on chromosome 15q25. The helix–loop–helix dimerization domain of *ETV6* fuses to the protein tyrosine kinase domain of *NTRK3*. The fusion protein results in ligand-independent chimeric protein tyrosine kinase activity with autophosphorylation. This leads to constitutive activation of Ras-MAPK and P13K-AKT pathways via insulin receptor substrate-1, which is tyrosine-phosphorylated [161–163], and through the activation of *c-Src* [164]. The fusion protein also associates with TGF-betaII receptor, which can be oncogenic by leading to inhibition of TGF-beta receptor signals that mediate tumour suppression [165].

Identical genetic findings have been reported in the cellular variant of congenital mesoblastic nephroma, a microscopically similar tumour of the kidney [166, 167], and in secretory carcinoma of breast [168] and acute myeloid leukaemia [169], implying oncogenesis by lineage-independent activation of kinase-related signalling pathways.

Pathological features

Infantile fibrosarcoma is composed of uniform ovoid mitotically active spindle cells arranged in sheets or herringbone fascicles (Fig. 10). There is sometimes an apparently primitive round cell component but, as with other translocation sarcomas, cytologic atypia and pleomorphism are typically absent. A proportion of cases show positivity for SMA or desmin, with occasional expression of cytokeratin, CD34 and S100 protein. No relationship has been described between histologic appearances and genetic findings. However, the distinction from other sarcomas (especially synovial sarcoma and malignant peripheral nerve sheath tumour) can, when required, be made by genetic analysis, as well as careful attention to morphology and demonstration of the relevant immunophenotype.

Clinical features

Unlike adult fibrosarcoma, this is a tumour of intermediate malignancy: [170] About a third of cases recur but very few (0–5%) metastasize [171], and the 5-year survival exceeds 90% [172–174]. Most deaths from this disease are due to local complications. Complete excision is the treatment of choice [175]. Cases treated with pre-operative chemotherapy [171] or with chemotherapy alone [176] have done well. Axial tumours seem to behave more aggressively [177], but there are no histological or genetic predictors of behaviour.

Inflammatory myofibroblastic tumour

Inflammatory myofibroblastic tumour commonly arises in the abdomen, especially retroperitoneum or mesentery, where it can be solitary or multicentric, and rarely in other soft tissue sites [178, 179]. Similar tumours have been described in the lung under a variety of terms. The peak incidence is in the first decade of life, followed by adolescence, although examples occur in older adults. Patients present with symptoms relating to the mass lesion or with systemic features, including fever, anaemia and leukocytosis. A distinct subset arises in the urinary tract [180, 181], especially in the bladder; these are more frequent in males with a peak in the fifth decade, and

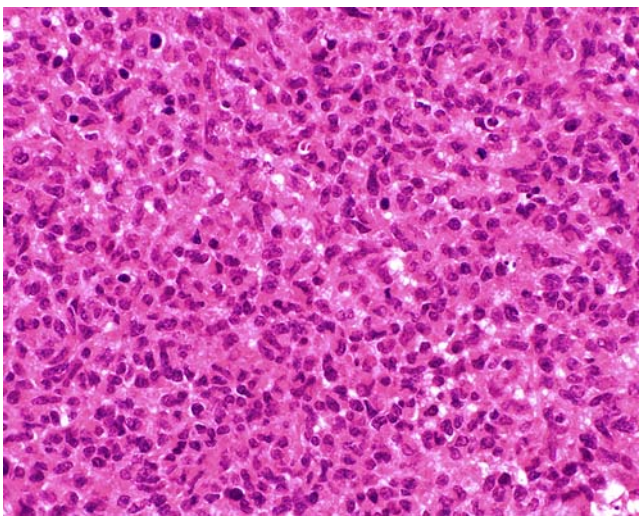

Fig. 10 Infantile fibrosarcoma is composed of uniform short spindle cells arranged in sheets or fascicles

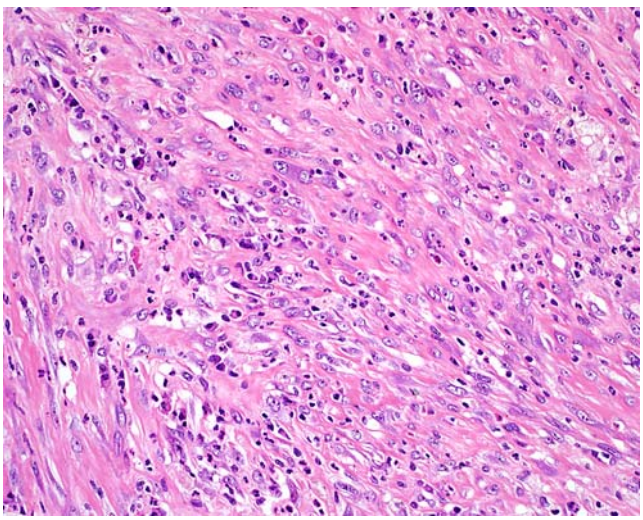

Fig. 11 Inflammatory myofibroblastic tumour displaying fasciitis-like and fascicular patterns with a marked admixture of plasma cells

about a quarter of the cases are associated with prior instrumentation [182, 183].

Genetic features

Inflammatory myofibroblastic tumour has fusions involving the C-terminal kinase domain of anaplastic lymphoma kinase (*ALK*) gene, located on 2p23, which encodes a receptor tyrosine kinase of the insulin growth factor receptor family that is normally expressed only in the central nervous system [184]. The resultant fusion protein is a constitutively active kinase. In inflammatory myofibroblastic tumours in pulmonary and other locations, the *ALK* gene can be rearranged with one of several other genes, including the actin-binding cytoskeletal proteins tropomyosin-3 (N-terminal coiled coil domain) as *TPM3-ALK* or tropomyosin 4 (*TPM4-ALK*) [185]. Other partners include *CLTC* (clathrin heavy chain gene, localised to 17q23) [186], *ATIC* at 2q35 (in a bladder tumour) [187], *RANBP2* at 2q13, *CARS* at 11p15 [188] and *SEC31L1* at 4q21 [189]. Identical rearrangements involving *TPM3*, *CLTC* and *ATIC* occur in anaplastic large cell lymphoma.

Pathological features

This is a variably cellular, usually bland fibroblastic–myofibroblastic proliferation with admixed plasma cells and lymphocytes. The appearances vary within the same tumour, with fasciitis-like, fascicular and sclerosing areas (Fig. 11). Related to the genetic changes, there is immunoreactivity for *ALK* in 36% to 60% [190–193] of cases, mostly in intra-abdominal, visceral or pulmonary tumours, and especially in those occurring in childhood [180, 193]. The staining is usually diffuse and cytoplasmic but varies with some fusion types: It can be granular (*CTLC*) or show nuclear membranous accentuation (*RANPB2*). It should be noted that immunoreactivity for *ALK* has also been reported in other tumours, including examples of malignant peripheral nerve sheath tumour, rhabdomyosarcoma and leiomyosarcoma [191, 194]. The *ALK* gene rearrangements can be detected in fixed tissue using FISH or PCR techniques [192, 195], which can be useful in diagnosis [183]; they are generally absent from the other sarcomas, which show sporadic ALK immunoreactivity [194].

Clinical features

About a third of cases recur after excision [196]. There is a relationship between *ALK* expression and morphology and behaviour of inflammatory myofibroblastic tumour: *ALK*-negative tumours occur more frequently in adults and display more nuclear pleomorphism and atypical mitoses, and in a recent series, all of six metastatic IMTs were *ALK* negative [193].

Conclusions

Non-EWS translocations are found in soft tissue sarcomas with a wide range of morphological manifestations and biological behaviour. Advances in knowledge of the genetics of these tumours are leading to more accurate diagnosis, by detection of translocations and gene fusions and by the use of new immunohistochemical reagents derived from specific fusion genes and their products or from gene profiling studies. The relationship between genetic changes and morphology is variable and mostly imprecise. The impact of genetic changes on behaviour is also variable within and between tumour types. There remain inconsistent findings in some prognostic studies, which are usually multifactorial.

Acknowledgement The author thanks Marc Ladanyi for comments on the manuscript.

Conflict of interest statement I declare that I have no conflict of interest.

References

1. Mitelman F, Johansson B, Mertens F (2007) The impact of translocations and gene fusions on cancer causation. Nat Rev Cancer 7:233–245
2. Fisher C (1998) Synovial sarcoma. Ann Diagn Pathol 2:401–421
3. McKinney CD, Mills SE, Fechner RE (1992) Intraarticular synovial sarcoma. Am J Surg Pathol 16:1017–1020
4. Fetsch JF, Meis JM (1992) Intra-articular synovial sarcoma. Mod Pathol 5:6A
5. Ishida T, Iijima T, Moriyama S et al (1996) Intra-articular calcifying synovial sarcoma mimicking synovial chondromatosis. Skeletal Radiol 25:766–769
6. van de Rijn M, Barr FG, Xiong QB et al (1997) Radiation-associated synovial sarcoma. Hum Pathol 28:1325–1328
7. Egger JF, Coindre JM, Benhattar J et al (2002) Radiation-associated synovial sarcoma: clinicopathologic and molecular analysis of two cases. Mod Pathol 15:998–1004
8. Deraedt K, Debiec-Rychter M, Sciot R (2006) Radiation-associated synovial sarcoma of the lung following radiotherapy for pulmonary metastasis of Wilms' tumour. Histopathology 48:473–475
9. Crew AJ, Clark J, Fisher C et al (1995) Fusion of SYT to two genes, SSX1 and SSX2, encoding proteins with homology to the Kruppel-associated box in human synovial sarcoma. Embo J 14:2333–2340
10. Agus V, Tamborini E, Mezzelani A et al (2001) Re: A novel fusion gene, SYT-SSX4, in synovial sarcoma. J Natl Cancer Inst 93:1347–1349
11. Otsuka S, Nishijo K, Nakayama T et al (2006) A variant of the SYT-SSX2 fusion gene in a case of synovial sarcoma. Cancer Genet Cytogenet 167:82–88

12. Krskova L, Sumerauer D, Stejskalova E et al (2007) A novel variant of SYT-SSX1 fusion gene in a case of spindle cell synovial sarcoma. Diagn Mol Pathol 16:179–183
13. Amary MF, Diss TC, Flanagan AM (2007) Molecular characterization of a novel variant of a SYT-SSX1 fusion transcript in synovial sarcoma. Histopathology 51:559–561
14. Storlazzi CT, Mertens F, Mandahl N et al (2003) A novel fusion gene, SS18L1/SSX1, in synovial sarcoma. Genes Chromosomes Cancer 37:195–200
15. Brett D, Whitehouse S, Antonson P et al (1997) The SYT protein involved in the t(X;18) synovial sarcoma translocation is a transcriptional activator localised in nuclear bodies. Hum Mol Genet 6:1559–1564
16. Thaete C, Brett D, Monaghan P et al (1999) Functional domains of the SYT and SYT-SSX synovial sarcoma translocation proteins and co-localization with the SNF protein BRM in the nucleus. Hum Mol Genet 8:585–591
17. Hashimoto N, Araki N, Yoshikawa H et al (2000) SYT-SSX fusion proteins in synovial sarcomas: detection and characterization with new antibodies. Cancer Lett 149:31–36
18. Saito T, Oda Y, Sakamoto A et al (2000) Prognostic value of the preserved expression of the E-cadherin and catenin families of adhesion molecules and of beta-catenin mutations in synovial sarcoma. J Pathol 192:342–350
19. Nielsen TO, West RB, Linn SC et al (2002) Molecular characterisation of soft tissue tumours: a gene expression study. Lancet 359:1301–1307
20. Allander SV, Illei PB, Chen Y et al (2002) Expression profiling of synovial sarcoma by cDNA microarrays: association of ERBB2, IGFBP2, and ELF3 with epithelial differentiation. Am J Pathol 161:1587–1595
21. Fernebro J, Francis P, Eden P et al (2006) Gene expression profiles relate to SS18/SSX fusion type in synovial sarcoma. Int J Cancer 118:1165–1172
22. Folpe AL, Schmidt RA, Chapman D et al (1998) Poorly differentiated synovial sarcoma: immunohistochemical distinction from primitive neuroectodermal tumors and high-grade malignant peripheral nerve sheath tumors. Am J Surg Pathol 22:673–682
23. van de Rijn M, Barr FG, Xiong QB et al (1999) Poorly differentiated synovial sarcoma: an analysis of clinical, pathologic, and molecular genetic features. Am J Surg Pathol 23:106–112
24. Pilotti S, Mezzelani A, Azzarelli A et al (1998) bcl-2 expression in synovial sarcoma. J Pathol 184:337–339
25. Machen SK, Fisher C, Gautam RS et al (1998) Utility of cytokeratin subsets for distinguishing poorly differentiated synovial sarcoma from peripheral primitive neuroectodermal tumour. Histopathology 33:501–507
26. Pelmus M, Guillou L, Hostein I et al (2002) Monophasic fibrous and poorly differentiated synovial sarcoma: immunohistochemical reassessment of 60 t(X;18)(SYT-SSX)-positive cases. Am J Surg Pathol 26:1434–1440
27. Fisher C, Montgomery E, Healy V (2003) Calponin and h-caldesmon expression in synovial sarcoma; the use of calponin in diagnosis. Histopathology 42:588–593
28. Olsen SH, Thomas DG, Lucas DR (2006) Cluster analysis of immunohistochemical profiles in synovial sarcoma, malignant peripheral nerve sheath tumor, and Ewing sarcoma. Mod Pathol 19:659–668
29. Miettinen M, Limon J, Niezabitowski A et al (2001) Calretinin and other mesothelioma markers in synovial sarcoma: analysis of antigenic similarities and differences with malignant mesothelioma. Am J Surg Pathol 25:610–617
30. Ng TL, Gown AM, Barry TS et al (2005) Nuclear beta-catenin in mesenchymal tumors. Mod Pathol 18:68–74
31. Terry J, Saito T, Subramanian S et al (2007) TLE1 as a diagnostic immunohistochemical marker for synovial sarcoma emerging from gene expression profiling studies. Am J Surg Pathol 31:240–246
32. He R, Patel RM, Alkan S et al (2007) Immunostaining for SYT protein discriminates synovial sarcoma from other soft tissue tumors: analysis of 146 cases. Mod Pathol 20:522–528
33. Winnepenninckx V, De Vos R, Debiec-Rychter M et al (2001) Calcifying/ossifying synovial sarcoma shows t(X;18) with SSX2 involvement and mitochondrial calcifications. Histopathology 38:141–145
34. Mancuso T, Mezzelani A, Riva C et al (2000) Analysis of SYT-SSX fusion transcripts and bcl-2 expression and phosphorylation status in synovial sarcoma. Lab Invest 80:805–813
35. Antonescu CR, Kawai A, Leung DH et al (2000) Strong association of SYT-SSX fusion type and morphologic epithelial differentiation in synovial sarcoma. Diagn Mol Pathol 9:1–8
36. van de Rijn M, Barr FG, Collins MH et al (1999) Absence of SYT-SSX fusion products in soft tissue tumors other than synovial sarcoma. Am J Clin Pathol 112:43–49
37. Tamborini E, Agus V, Perrone F et al (2002) Lack of SYT-SSX fusion transcripts in malignant peripheral nerve sheath tumors on RT-PCR analysis of 34 archival cases. Lab Invest 82:609–618
38. Ladanyi M, Antonescu CR, Leung DH et al (2002) Impact of SYT-SSX fusion type on the clinical behavior of synovial sarcoma: a multi-institutional retrospective study of 243 patients. Cancer Res 62:135–140
39. Ladanyi M (2005) Correlates of SYT-SSX fusion type in synovial sarcoma: getting more complex but also more interesting? J Clin Oncol 23:3638–3639 Author reply 3639–3640
40. Spillane AJ, A'Hern R, Judson IR et al (2000) Synovial sarcoma: a clinicopathologic, staging, and prognostic assessment. J Clin Oncol 18:3794–3803
41. Lewis JJ, Antonescu CR, Leung DH et al (2000) Synovial sarcoma: a multivariate analysis of prognostic factors in 112 patients with primary localized tumors of the extremity. J Clin Oncol 18:2087–2094
42. Trassard M, Le Doussal V, Hacene K et al (2001) Prognostic factors in localized primary synovial sarcoma: a multicenter study of 128 adult patients. J Clin Oncol 19:525–534
43. Mullen JR, Zagars GK (1994) Synovial sarcoma outcome following conservation surgery and radiotherapy. Radiother Oncol 33:23–30
44. Skytting BT, Bauer HC, Perfekt R et al (1999) Ki-67 is strongly prognostic in synovial sarcoma: analysis based on 86 patients from the Scandinavian Sarcoma group register [in process citation]. Br J Cancer 80:1809–1814
45. Bergh P, Meis-Kindblom JM, Gherlinzoni F et al (1999) Synovial sarcoma: identification of low and high risk groups. Cancer 85:2596–2607
46. Nilsson G, Skytting B, Xie Y et al (1999) The SYT-SSX1 variant of synovial sarcoma is associated with a high rate of tumor cell proliferation and poor clinical outcome. Cancer Res 59:3180–3184
47. Kawai A, Woodruff J, Healey JH et al (1998) SYT-SSX gene fusion as a determinant of morphology and prognosis in synovial sarcoma. N Engl J Med 338:153–160
48. Guillou L, Benhattar J, Bonichon F et al (2004) Histologic grade, but not SYT-SSX fusion type, is an important prognostic factor in patients with synovial sarcoma: a multicenter, retrospective analysis. J Clin Oncol 22:4040–4050
49. Takenaka S, Ueda T, Naka N et al (2008) Prognostic implication of SYT-SSX fusion type in synovial sarcoma: a multi-institutional retrospective analysis in Japan. Oncol Rep 19:467–476

50. Thomas DG, Giordano TJ, Sanders D et al (2005) Expression of receptor tyrosine kinases epidermal growth factor receptor and HER-2/neu in synovial sarcoma. Cancer 103:830–838
51. Blay JY, Ray-Coquard I, Alberti L et al (2004) Targeting other abnormal signaling pathways in sarcoma: EGFR in synovial sarcomas, PPAR-gamma in liposarcomas. Cancer Treat Res 120:151–167
52. Tschoep K, Kohlmann A, Schlemmer M et al (2007) Gene expression profiling in sarcomas. Crit Rev Oncol Hematol 63:111–124
53. GE NWA, Webber BL et al (1995) Classification of Rhabdomyosarcoma and related sarcomas. Pathologic aspects and proposal for a new classification. An intragroup rhabdomyosarcoma study. Cancer 76:1073–1085
54. Weiss SW, Goldblum JR (2008) Soft Tissue Tumors. Mosby Elsevier, Philadelphia, pp 595–632
55. Downing JR, Khandekar A, Shurtleff SA et al (1995) Multiplex RT-PCR assay for the differential diagnosis of alveolar rhabdomyosarcoma and Ewing's sarcoma. Am J Pathol 146:626–634
56. de Alava E, Ladanyi M, Rosai J et al (1995) Detection of chimeric transcripts in desmoplastic small round cell tumor and related developmental tumors by reverse transcriptase polymerase chain reaction. A specific diagnostic assay. Am J Pathol 147:1584–1591
57. Barr FG (2001) Gene fusions involving PAX and FOX family members in alveolar rhabdomyosarcoma. Oncogene 20:5736–5746
58. Barr FG, Qualman SJ, Macris MH et al (2002) Genetic heterogeneity in the alveolar rhabdomyosarcoma subset without typical gene fusions. Cancer Res 62:4704–4710
59. Sorensen PH, Lynch JC, Qualman SJ et al (2002) PAX3-FKHR and PAX7-FKHR gene fusions are prognostic indicators in alveolar rhabdomyosarcoma: a report from the children's oncology group. J Clin Oncol 20:2672–2679
60. Wachtel M, Dettling M, Koscielniak E et al (2004) Gene expression signatures identify rhabdomyosarcoma subtypes and detect a novel t(2;2)(q35;p23) translocation fusing PAX3 to NCOA1. Cancer Res 64:5539–5545
61. Anderson J, Ramsay A, Gould S et al (2001) PAX3-FKHR induces morphological change and enhances cellular proliferation and invasion in rhabdomyosarcoma. Am J Pathol 159:1089–1096
62. Keller C, Arenkiel BR, Coffin CM et al (2004) Alveolar rhabdomyosarcomas in conditional Pax3:Fkhr mice: cooperativity of Ink4a/ARF and Trp53 loss of function. Genes Dev 18:2614–2626
63. Begin LR, Schurch W, Lacoste J et al (1994) Glycogen-rich clear cell rhabdomyosarcoma of the mediastinum. Potential diagnostic pitfall. Am J Surg Pathol 18:302–308
64. Boman F, Champigneulle J, Schmitt C et al (1996) Clear cell rhabdomyosarcoma. Pediatr Pathol Lab Med 16:951–959
65. Chan JK, Ng HK, Wan KY et al (1989) Clear cell rhabdomyosarcoma of the nasal cavity and paranasal sinuses. Histopathology 14:391–399
66. Tsokos M, Webber BL, Parham DM et al (1992) Rhabdomyosarcoma. A new classification scheme related to prognosis. Arch Pathol Lab Med 116:847–855 [see comments]
67. Parham DM, Shapiro DN, Downing JR et al (1994) Solid alveolar rhabdomyosarcomas with the t(2;13). Report of two cases with diagnostic implications. Am J Surg Pathol 18:474–478
68. Parham DM, Qualman SJ, Teot L et al (2007) Correlation between histology and PAX/FKHR fusion status in alveolar rhabdomyosarcoma: a report from the Children's Oncology Group. Am J Surg Pathol 31:895–901
69. Kohashi K, Oda Y, Yamamoto H et al (2008) Alterations of RB1 gene in embryonal and alveolar rhabdomyosarcoma: special reference to utility of pRB immunoreactivity in differential diagnosis of rhabdomyosarcoma subtype. J Cancer Res Clin Oncol 134:1097–1103
70. Kelly KM, Womer RB, Sorensen PH et al (1997) Common and variant gene fusions predict distinct clinical phenotypes in rhabdomyosarcoma. J Clin Oncol 15:1831–1836
71. Kazanowska B, Reich A, Stegmaier S et al (2007) Pax3-fkhr and pax7-fkhr fusion genes impact outcome of alveolar rhabdomyosarcoma in children. Fetal Pediatr Pathol 26:17–31
72. Lae M, Ahn EH, Mercado GE et al (2007) Global gene expression profiling of PAX-FKHR fusion-positive alveolar and PAX-FKHR fusion-negative embryonal rhabdomyosarcomas. J Pathol 212:143–151
73. De Pitta C, Tombolan L, Albiero G et al (2006) Gene expression profiling identifies potential relevant genes in alveolar rhabdomyosarcoma pathogenesis and discriminates PAX3-FKHR positive and negative tumors. Int J Cancer 118:2772–2781
74. Davicioni E, Finckenstein FG, Shahbazian V et al (2006) Identification of a PAX-FKHR gene expression signature that defines molecular classes and determines the prognosis of alveolar rhabdomyosarcomas. Cancer Res 66:6936–6946
75. Folpe AL, Deyrup AT (2006) Alveolar soft-part sarcoma: a review and update. J Clin Pathol 59:1127–1132
76. Lieberman PH, Brennan MF, Kimmel M et al (1989) Alveolar soft-part sarcoma. A clinico-pathologic study of half a century. Cancer 63:1–13
77. Amin MB, Patel RM, Oliveira P et al (2006) Alveolar soft-part sarcoma of the urinary bladder with urethral recurrence: a unique case with emphasis on differential diagnoses and diagnostic utility of an immunohistochemical panel including TFE3. Am J Surg Pathol 30:1322–1325
78. Nielsen GP, Oliva E, Young RH et al (1995) Alveolar soft-part sarcoma of the female genital tract: a report of nine cases and review of the literature. Int J Gynecol Pathol 14:283–292
79. Luo J, Melnick S, Rossi A et al (2008) Primary cardiac alveolar soft part sarcoma. A report of the first observed case with molecular diagnostics corroboration. Pediatr Dev Pathol 11:142–147
80. Fanburg-Smith JC, Miettinen M, Folpe AL et al (2004) Lingual alveolar soft part sarcoma; 14 cases: novel clinical and morphological observations. Histopathology 45:526–537
81. Font RL, Jurco S 3rd, Zimmerman LE (1982) Alveolar soft-part sarcoma of the orbit: a clinicopathologic analysis of seventeen cases and a review of the literature. Hum Pathol 13:569–579
82. Joyama S, Ueda T, Shimizu K et al (1999) Chromosome rearrangement at 17q25 and xp11.2 in alveolar soft-part sarcoma: a case report and review of the literature. Cancer 86:1246–1250
83. Cullinane C, Thorner PS, Greenberg ML et al (1992) Molecular genetic, cytogenetic, and immunohistochemical characterization of alveolar soft-part sarcoma. Implications for cell of origin. Cancer 70:2444–2450
84. Ladanyi M, Lui MY, Antonescu CR et al (2001) The der(17) t(X;17)(p11;q25) of human alveolar soft part sarcoma fuses the TFE3 transcription factor gene to ASPL, a novel gene at 17q25. Oncogene 20:48–57
85. Argani P, Lal P, Hutchinson B et al (2003) Aberrant nuclear immunoreactivity for TFE3 in neoplasms with TFE3 gene fusions: a sensitive and specific immunohistochemical assay. Am J Surg Pathol 27:750–761
86. Argani P, Antonescu CR, Illei PB et al (2001) Primary renal neoplasms with the ASPL-TFE3 gene fusion of alveolar soft part sarcoma: a distinctive tumor entity previously included among renal cell carcinomas of children and adolescents. Am J Pathol 159:179–192

87. Bruder E, Passera O, Harms D et al (2004) Morphologic and molecular characterization of renal cell carcinoma in children and young adults. Am J Surg Pathol 28:1117–1132
88. Folpe AL, Mentzel T, Lehr HA et al (2005) Perivascular epithelioid cell neoplasms of soft tissue and gynecologic origin: a clinicopathologic study of 26 cases and review of the literature. Am J Surg Pathol 29:1558–1575
89. LP SFH, Foote FW, Stewart FW (1964) Ultrastructure of alveolar soft part sarcoma. Cancer 17:821–830
90. Ordonez NG, Ro JY, Mackay B (1989) Alveolar soft part sarcoma. An ultrastructural and immunocytochemical investigation of its histogenesis. Cancer 63:1721–1736
91. Ladanyi M, Antonescu CR, Drobnjak M et al (2002) The precrystalline cytoplasmic granules of alveolar soft part sarcoma contain monocarboxylate transporter 1 and CD147. Am J Pathol 160:1215–1221
92. Portera CA Jr, Ho V, Patel SR et al (2001) Alveolar soft part sarcoma: clinical course and patterns of metastasis in 70 patients treated at a single institution. Cancer 91:585–591
93. Casanova M, Ferrari A, Bisogno G et al (2000) Alveolar soft part sarcoma in children and adolescents: A report from the Soft-Tissue Sarcoma Italian Cooperative Group. Ann Oncol 11:1445–1449
94. Tsuda M, Davis IJ, Argani P et al (2007) TFE3 fusions activate MET signaling by transcriptional up-regulation, defining another class of tumors as candidates for therapeutic MET inhibition. Cancer Res 67:919–929
95. Criscione VD, Weinstock MA (2007) Descriptive epidemiology of dermatofibrosarcoma protuberans in the United States, 1973 to 2002. J Am Acad Dermatol 56:968–973
96. Maire G, Fraitag S, Galmiche L et al (2007) A clinical, histologic, and molecular study of 9 cases of congenital dermatofibrosarcoma protuberans. Arch Dermatol 143:203–210
97. Shmookler BM, Enzinger FM, Weiss SW (1989) Giant cell fibroblastoma. A juvenile form of dermatofibrosarcoma protuberans. Cancer 64:2154–2161
98. Alguacil-Garcia A (1991) Giant cell fibroblastoma recurring as dermatofibrosarcoma protuberans. Am J Surg Pathol 15:798–801
99. Allen PW, Zwi J (1992) Giant cell fibroblastoma transforming into dermatofibrosarcoma protuberans. Am J Surg Pathol 16:1127–1129
100. Goldblum JR (1996) Giant cell fibroblastoma: a report of three cases with histologic and immunohistochemical evidence of a relationship to dermatofibrosarcoma protuberans. Arch Pathol Lab Med 120:1052–1055
101. Wrotnowski U, Cooper PH, Shmookler BM (1988) Fibrosarcomatous change in dermatofibrosarcoma protuberans. Am J Surg Pathol 12:287–293
102. Ding J, Hashimoto H, Enjoji M (1989) Dermatofibrosarcoma protuberans with fibrosarcomatous areas. A clinicopathologic study of nine cases and a comparison with allied tumors. Cancer 64:721–729
103. Connelly JH, Evans HL (1992) Dermatofibrosarcoma protuberans. A clinicopathologic review with emphasis on fibrosarcomatous areas. Am J Surg Pathol 16:921–925
104. Diaz-Cascajo C, Weyers W, Borrego L et al (1997) Dermatofibrosarcoma protuberans with fibrosarcomatous areas: a clinicopathologic and immunohistochemic study in four cases. Am J Dermatopathol 19:562–567
105. Mentzel T, Beham A, Katenkamp D et al (1998) Fibrosarcomatous ("high-grade") dermatofibrosarcoma protuberans: clinicopathologic and immunohistochemical study of a series of 41 cases with emphasis on prognostic significance. Am J Surg Pathol 22:576–587
106. Abbott JJ, Oliveira AM, Nascimento AG (2006) The prognostic significance of fibrosarcomatous transformation in dermatofibrosarcoma protuberans. Am J Surg Pathol 30:436–443
107. Pedeutour F, Simon MP, Minoletti F et al (1996) Translocation, t(17;22)(q22;q13), in dermatofibrosarcoma protuberans: a new tumor-associated chromosome rearrangement. Cytogenet Cell Genet 72:171–174
108. Simon MP, Pedeutour F, Sirvent N et al (1997) Deregulation of the platelet-derived growth factor B-chain gene via fusion with collagen gene COL1A1 in dermatofibrosarcoma protuberans and giant-cell fibroblastoma. Nat Genet 15:95–98
109. Wang J, Hisaoka M, Shimajiri S et al (1999) Detection of COL1A1-PDGFB fusion transcripts in dermatofibrosarcoma protuberans by reverse transcription-polymerase chain reaction using archival formalin-fixed, paraffin-embedded tissues. Diagn Mol Pathol 8:113–119
110. Sirvent N, Maire G, Pedeutour F (2003) Genetics of dermatofibrosarcoma protuberans family of tumors: from ring chromosomes to tyrosine kinase inhibitor treatment. Genes Chromosomes Cancer 37:1–19
111. Sandberg AA, Bridge JA (2003) Updates on the cytogenetics and molecular genetics of bone and soft tissue tumors. Dermatofibrosarcoma protuberans and giant cell fibroblastoma. Cancer Genet Cytogenet 140:1–12
112. Nishio J, Iwasaki H, Ohjimi Y et al (2001) Supernumerary ring chromosomes in dermatofibrosarcoma protuberans may contain sequences from 8q11.2-qter and 17q21-qter: a combined cytogenetic and comparative genomic hybridization study. Cancer Genet Cytogenet 129:102–106
113. Nishio J, Iwasaki H, Ishiguro M et al (2001) Supernumerary ring chromosome in a Bednar tumor (pigmented dermatofibrosarcoma protuberans) is composed of interspersed sequences from chromosomes 17 and 22: a fluorescence in situ hybridization and comparative genomic hybridization analysis. Genes Chromosomes Cancer 30:305–309
114. Maire G, Martin L, Michalak-Provost S et al (2002) Fusion of COL1A1 exon 29 with PDGFB exon 2 in a der(22) t(17;22) in a pediatric giant cell fibroblastoma with a pigmented Bednar tumor component. Evidence for age-related chromosomal pattern in dermatofibrosarcoma protuberans and related tumors. Cancer Genet Cytogenet 134:156–161
115. Wang J, Morimitsu Y, Okamoto S et al (2000) COL1A1-PDGFB fusion transcripts in fibrosarcomatous areas of six dermatofibrosarcomas protuberans. J Mol Diagn 2:47–52
116. Sheng WQ, Hashimoto H, Okamoto S et al (2001) Expression of COL1A1-PDGFB fusion transcripts in superficial adult fibrosarcoma suggests a close relationship to dermatofibrosarcoma protuberans. J Pathol 194:88–94
117. Patel KU, Szabo SS, Hernandez VS et al (2008) Dermatofibrosarcoma protuberans COL1A1-PDGFB fusion is identified in virtually all dermatofibrosarcoma protuberans cases when investigated by newly developed multiplex reverse transcription polymerase chain reaction and fluorescence in situ hybridization assays. Hum Pathol 39:184–193
118. Terrier-Lacombe MJ, Guillou L, Maire G et al (2003) Dermatofibrosarcoma protuberans, giant cell fibroblastoma, and hybrid lesions in children: clinicopathologic comparative analysis of 28 cases with molecular data–a study from the French Federation of Cancer Centers Sarcoma Group. Am J Surg Pathol 27:27–39
119. Sonobe H, Furihata M, Iwata J et al (1999) Dermatofibrosarcoma protuberans harboring t(9;22)(q32;q12.2). Cancer Genet Cytogenet 110:14–18
120. Linn SC, West RB, Pollack JR et al (2003) Gene expression patterns and gene copy number changes in dermatofibrosarcoma protuberans. Am J Pathol 163:2383–2395

121. Nielsen TO (2006) Microarray Analysis of Sarcomas. Adv Anat Pathol 13:166–173
122. West RB, Harvell J, Linn SC et al (2004) Apo D in soft tissue tumors: a novel marker for dermatofibrosarcoma protuberans. Am J Surg Pathol 28:1063–1069
123. Lisovsky M, Hoang MP, Dresser KA et al (2008) Apolipoprotein D in CD34-positive and CD34-negative cutaneous neoplasms: a useful marker in differentiating superficial acral fibromyxoma from dermatofibrosarcoma protuberans. Mod Pathol 21:31–38
124. Shimizu A, O'Brien KP, Sjoblom T et al (1999) The dermatofibrosarcoma protuberans-associated collagen type Ialpha1/platelet-derived growth factor (PDGF) B-chain fusion gene generates a transforming protein that is processed to functional PDGF-BB. Cancer Res 59:3719–3723
125. Greco A, Fusetti L, Villa R et al (1998) Transforming activity of the chimeric sequence formed by the fusion of collagen gene COL1A1 and the platelet derived growth factor b-chain gene in dermatofibrosarcoma protuberans. Oncogene 17:1313–1319
126. Sjoblom T, Shimizu A, O'Brien KP et al (2001) Growth inhibition of dermatofibrosarcoma protuberans tumors by the platelet-derived growth factor receptor antagonist STI571 through induction of apoptosis. Cancer Res 61:5778–5783
127. Rubin BP, Schuetze SM, Eary JF et al (2002) Molecular targeting of platelet-derived growth factor B by imatinib mesylate in a patient with metastatic dermatofibrosarcoma protuberans. J Clin Oncol 20:3586–3591
128. Maki RG, Awan RA, Dixon RH et al (2002) Differential sensitivity to imatinib of 2 patients with metastatic sarcoma arising from dermatofibrosarcoma protuberans. Int J Cancer 100:623–626
129. Kasper B, Lossignol D, Gil T et al (2006) Imatinib mesylate in a patient with metastatic disease originating from a dermatofibrosarcoma protuberans of the scalp. Anticancer Drugs 17:1223–1225
130. McArthur GA (2006) Dermatofibrosarcoma protuberans: a surgical disease with a molecular savior. Curr Opin Oncol 18:341–346
131. Ostman A, Heldin CH (2007) PDGF Receptors as Targets in Tumor Treatment. Adv Cancer Res 97:247–274
132. McArthur GA, Demetri GD, van Oosterom A et al (2005) Molecular and clinical analysis of locally advanced dermatofibrosarcoma protuberans treated with imatinib: Imatinib Target Exploration Consortium Study B2225. J Clin Oncol 23:866–873
133. McArthur GA (2007) Molecular targeting of dermatofibrosarcoma protuberans: a new approach to a surgical disease. J Natl Compr Canc Netw 5:557–562
134. Evans HL (1987) Low-grade fibromyxoid sarcoma. A report of two metastasizing neoplasms having a deceptively benign appearance. Am J Clin Pathol 88:615–619
135. Lane KL, Shannon RJ, Weiss SW (1997) Hyalinizing spindle cell tumor with giant rosettes: a distinctive tumor closely resembling low-grade fibromyxoid sarcoma. Am J Surg Pathol 21:1481–1488
136. Evans HL (1993) Low-grade fibromyxoid sarcoma. A report of 12 cases. Am J Surg Pathol 17:595–600
137. Folpe AL, Lane KL, Paull G et al (2000) Low-grade fibromyxoid sarcoma and hyalinizing spindle cell tumor with giant rosettes: a clinicopathologic study of 73 cases supporting their identity and assessing the impact of high-grade areas. Am J Surg Pathol 24:1353–1360
138. Kim L, Yoon YH, Choi SJ et al (2007) Hyalinizing spindle cell tumor with giant rosettes arising in the lung: report of a case with FUS-CREB3L2 fusion transcripts. Pathol Int 57:153–157
139. Saito R, Kumabe T, Watanabe M et al (2008) Low-grade fibromyxoid sarcoma of intracranial origin. J Neurosurg 108:798–802
140. Jakowski JD, Wakely PE Jr (2008) Primary intrathoracic low-grade fibromyxoid sarcoma. Hum Pathol 39:623–628
141. Winfield HL, De Las Casas LE, Greenfield WW et al (2007) Low-grade fibromyxoid sarcoma presenting clinically as a primary ovarian neoplasm: a case report. Int J Gynecol Pathol 26:173–176
142. Park IJ, Kim HC, Yu CS et al (2007) Low-grade fibromyxoid sarcoma of the colon. Dig Liver Dis 39:274–277
143. Billings SD, Giblen G, Fanburg-Smith JC (2005) Superficial low-grade fibromyxoid sarcoma (Evans tumor): a clinicopathologic analysis of 19 cases with a unique observation in the pediatric population. Am J Surg Pathol 29:204–210
144. Bejarano PA, Padhya TA, Smith R et al (2000) Hyalinizing spindle cell tumor with giant rosettes–a soft tissue tumor with mesenchymal and neuroendocrine features. An immunohistochemical, ultrastructural, and cytogenetic analysis. Arch Pathol Lab Med 124:1179–1184
145. Mezzelani A, Sozzi G, Nessling M et al (2000) Low grade fibromyxoid sarcoma. a further low-grade soft tissue malignancy characterized by a ring chromosome. Cancer Genet Cytogenet 122:144–148
146. Reid R, de Silva MV, Paterson L et al (2003) Low-grade fibromyxoid sarcoma and hyalinizing spindle cell tumor with giant rosettes share a common t(7;16)(q34;p11) translocation. Am J Surg Pathol 27:1229–1236
147. Panagopoulos I, Storlazzi CT, Fletcher CD et al (2004) The chimeric FUS/CREB3l2 gene is specific for low-grade fibromyxoid sarcoma. Genes Chromosomes Cancer 40:218–228
148. Mertens F, Fletcher CD, Antonescu CR et al (2005) Clinicopathologic and molecular genetic characterization of low-grade fibromyxoid sarcoma, and cloning of a novel FUS/CREB3L1 fusion gene. Lab Invest 85:408–415
149. Matsuyama A, Hisaoka M, Shimajiri S et al (2006) Molecular detection of FUS-CREB3L2 fusion transcripts in low-grade fibromyxoid sarcoma using formalin-fixed, paraffin-embedded tissue specimens. Am J Surg Pathol 30:1077–1084
150. Panagopoulos I, Moller E, Dahlen A et al (2007) Characterization of the native CREB3L2 transcription factor and the FUS/CREB3L2 chimera. Genes Chromosomes Cancer 46:181–191
151. Guillou L, Benhattar J, Gengler C et al (2007) Translocation-positive low-grade fibromyxoid sarcoma: clinicopathologic and molecular analysis of a series expanding the morphologic spectrum and suggesting potential relationship to sclerosing epithelioid fibrosarcoma: a study from the French Sarcoma Group. Am J Surg Pathol 31:1387–1402
152. Matsuyama A, Hisaoka M, Shimajiri S et al (2008) DNA-based Polymerase chain reaction for detecting FUS-CREB3L2 in low-grade fibromyxoid sarcoma using formalin-fixed, paraffin-embedded tissue specimens. Diagn Mol Pathol 17:237–240
153. Schofield DE, Fletcher JA, Grier HE et al (1994) Fibrosarcoma in infants and children. Application of new techniques. Am J Surg Pathol 18:14–24
154. Gorman PA, Malone M, Pritchard J et al (1990) Deletion of part of the short arm of chromosome 17 in a congenital fibrosarcoma. Cancer Genet Cytogenet 48:193–198
155. Strehl S, Ladenstein R, Wrba F et al (1993) Translocation (12;13) in a case of infantile fibrosarcoma. Cancer Genet Cytogenet 71:94–96
156. Boulos BM, Dajuvone C, Azarnoff DL (1976) A new method for increasing the chemotherapeutic drug concentration in the tumor tissue. Panminerva Med 18:95–98
157. Knezevich SR, McFadden DE, Tao W et al (1998) A novel ETV6-NTRK3 gene fusion in congenital fibrosarcoma. Nat Genet 18:184–187
158. Sheng WQ, Hisaoka M, Okamoto S et al (2001) Congenital-infantile fibrosarcoma. A clinicopathologic study of 10 cases and

molecular detection of the ETV6-NTRK3 fusion transcripts using paraffin-embedded tissues. Am J Clin Pathol 115:348–355
159. Kaplan DR, Miller FD (1997) Signal transduction by the neurotrophin receptors. Curr Opin Cell Biol 9:213–221
160. Lannon CL, Martin MJ, Tognon CE et al (2004) A highly conserved NTRK3 C-terminal sequence in the ETV6-NTRK3 oncoprotein binds the phosphotyrosine binding domain of insulin receptor substrate-1: an essential interaction for transformation. J Biol Chem 279:6225–6234
161. Wai DH, Knezevich SR, Lucas T et al (2000) The ETV6-NTRK3 gene fusion encodes a chimeric protein tyrosine kinase that transforms NIH3T3 cells. Oncogene 19:906–915
162. Tognon C, Garnett M, Kenward E et al (2001) The chimeric protein tyrosine kinase ETV6-NTRK3 requires both Ras-Erk1/2 and PI3-kinase-Akt signaling for fibroblast transformation. Cancer Res 61:8909–8916
163. Martin MJ, Melnyk N, Pollard M et al (2006) The insulin-like growth factor I receptor is required for Akt activation and suppression of anoikis in cells transformed by the ETV6-NTRK3 chimeric tyrosine kinase. Mol Cell Biol 26:1754–1769
164. Jin W, Yun C, Hobbie A et al (2007) Cellular transformation and activation of the phosphoinositide-3-kinase-Akt cascade by the ETV6-NTRK3 chimeric tyrosine kinase requires c-Src. Cancer Res 67:3192–3200
165. Jin W, Kim BC, Tognon C et al (2005) The ETV6-NTRK3 chimeric tyrosine kinase suppresses TGF-beta signaling by inactivating the TGF-beta type II receptor. Proc Natl Acad Sci U S A 102:16239–16244
166. Knezevich SR, Garnett MJ, Pysher TJ et al (1998) ETV6-NTRK3 gene fusions and trisomy 11 establish a histogenetic link between mesoblastic nephroma and congenital fibrosarcoma. Cancer Res 58:5046–5048
167. Rubin BP, Chen CJ, Morgan TW et al (1998) Congenital mesoblastic nephroma t(12;15) is associated with ETV6-NTRK3 gene fusion: cytogenetic and molecular relationship to congenital (infantile) fibrosarcoma. Am J Pathol 153:1451–1458
168. Tognon C, Knezevich SR, Huntsman D et al (2002) Expression of the ETV6-NTRK3 gene fusion as a primary event in human secretory breast carcinoma. Cancer Cell 2:367–376
169. Eguchi M, Eguchi-Ishimae M, Tojo A et al (1999) Fusion of ETV6 to neurotrophin-3 receptor TRKC in acute myeloid leukemia with t(12;15)(p13;q25). Blood 93:1355–1363
170. Fletcher C, Unni K, Mertens F (eds) (2002) World Health Organization Classification of Tumours. Pathology and genetics of tumours of soft tissue and bone. IARC, Lyon.
171. Loh ML, Ahn P, Perez-Atayde AR et al (2002) Treatment of infantile fibrosarcoma with chemotherapy and surgery: results from the Dana-Farber Cancer Institute and Children's Hospital, Boston. J Pediatr Hematol Oncol 24:722–726
172. Chung EB, Enzinger FM (1976) Infantile fibrosarcoma. Cancer 38:729–739
173. Soule EH, Pritchard DJ (1977) Fibrosarcoma in infants and children: a review of 110 cases. Cancer 40:1711–1721
174. Coffin CM, Jaszcz W, O'Shea PA et al (1994) So-called congenital-infantile fibrosarcoma: does it exist and what is it? Pediatr Pathol 14:133–150
175. Cecchetto G, Carli M, Alaggio R et al (2001) Fibrosarcoma in pediatric patients: results of the Italian Cooperative Group studies (1979–1995). J Surg Oncol 78:225–231
176. Surico G, Muggeo P, Daniele RM et al (2003) Chemotherapy alone for the treatment of congenital fibrosarcoma: is surgery always needed? Med Pediatr Oncol 40:268–270
177. Blocker S, Koenig J, Ternberg J (1987) Congenital fibrosarcoma. J Pediatr Surg 22:665–670
178. Coden DJ, Hornblass A (1990) Orbital hemangiopericytoma. JAMA 264:1861
179. Coffin CM, Humphrey PA, Dehner LP (1998) Extrapulmonary inflammatory myofibroblastic tumor: a clinical and pathological survey. Semin Diagn Pathol 15:85–101
180. Montgomery EA, Shuster DD, Burkart AL et al (2006) Inflammatory myofibroblastic tumors of the urinary tract: a clinicopathologic study of 46 cases, including a malignant example inflammatory fibrosarcoma and a subset associated with high-grade urothelial carcinoma. Am J Surg Pathol 30:1502–1512
181. Hirsch MS, Dal Cin P, Fletcher CD (2006) ALK expression in pseudosarcomatous myofibroblastic proliferations of the genitourinary tract. Histopathology 48:569–578
182. Harik LR, Merino C, Coindre JM et al (2006) Pseudosarcomatous myofibroblastic proliferations of the bladder: a clinicopathologic study of 42 cases. Am J Surg Pathol 30:787–794
183. Sukov WR, Cheville JC, Carlson AW et al (2007) Utility of ALK-1 protein expression and ALK rearrangements in distinguishing inflammatory myofibroblastic tumor from malignant spindle cell lesions of the urinary bladder. Mod Pathol 20:592–603
184. Morris SW, Kirstein MN, Valentine MB et al (1994) Fusion of a kinase gene, ALK, to a nucleolar protein gene, NPM, in non-Hodgkin's lymphoma. Science 263:1281–1284
185. Lawrence B, Perez-Atayde A, Hibbard MK et al (2000) TPM3-ALK and TPM4-ALK oncogenes in inflammatory myofibroblastic tumors. Am J Pathol 157:377–384
186. Bridge JA, Kanamori M, Ma Z et al (2001) Fusion of the ALK gene to the clathrin heavy chain gene, CLTC, in inflammatory myofibroblastic tumor. Am J Pathol 159:411–415
187. Debiec-Rychter M, Marynen P, Hagemeijer A et al (2003) ALK-ATIC fusion in urinary bladder inflammatory myofibroblastic tumor. Genes Chromosomes Cancer 38:187–190
188. Debelenko LV, Arthur DC, Pack SD et al (2003) Identification of CARS-ALK fusion in primary and metastatic lesions of an inflammatory myofibroblastic tumor. Lab Invest 83:1255–1265
189. Panagopoulos I, Nilsson T, Domanski HA et al (2006) Fusion of the SEC31L1 and ALK genes in an inflammatory myofibroblastic tumor. Int J Cancer 118:1181–1186
190. Chan JK, Cheuk W, Shimizu M (2001) Anaplastic lymphoma kinase expression in inflammatory pseudotumors. Am J Surg Pathol 25:761–768
191. Cessna MH, Zhou H, Sanger WG et al (2002) Expression of ALK1 and p80 in inflammatory myofibroblastic tumor and its mesenchymal mimics: a study of 135 cases. Mod Pathol 15:931–938
192. Cook JR, Dehner LP, Collins MH et al (2001) Anaplastic lymphoma kinase (ALK) expression in the inflammatory myofibroblastic tumor: a comparative immunohistochemical study. Am J Surg Pathol 25:1364–1371
193. Coffin CM, Hornick JL, Fletcher CD (2007) Inflammatory myofibroblastic tumor: comparison of clinicopathologic, histologic, and immunohistochemical features including ALK expression in atypical and aggressive cases. Am J Surg Pathol 31:509–520
194. Li XQ, Hisaoka M, Shi DR et al (2004) Expression of anaplastic lymphoma kinase in soft tissue tumors: an immunohistochemical and molecular study of 249 cases. Hum Pathol 35:711–721
195. Coffin CM, Patel A, Perkins S et al (2001) ALK1 and p80 expression and chromosomal rearrangements involving 2p23 in inflammatory myofibroblastic tumor. Mod Pathol 14:569–576
196. Biselli R, Boldrini R, Ferlini C et al (1999) Myofibroblastic tumours: neoplasias with divergent behaviour. Ultrastructural and flow cytometric analysis. Pathol Res Pract 195:619–632

Virchows Arch (2010) 456:167–179
DOI 10.1007/s00428-009-0815-x

REVIEW AND PERSPECTIVE

Well-differentiated and dedifferentiated liposarcomas

Jean-Michel Coindre · Florence Pédeutour · Alain Aurias

Received: 4 March 2009 / Revised: 4 July 2009 / Accepted: 18 July 2009 / Published online: 18 August 2009
© Springer-Verlag 2009

Abstract Atypical lipomatous tumor or well-differentiated liposarcoma (ALT-WDLPS) and dedifferentiated liposarcoma (DDLPS) share the same basic genetic abnormality characterized by a simple genomic profile with a 12q14–15 amplification involving *MDM2* gene. These tumors are the most frequent LPS. This paper reviews the molecular pathology, general clinical and imaging features, histopathology, new diagnostic tools, and prognosis of ALT-WDLPS and DDLPS.

Keywords Well-differentiated liposarcoma · Dedifferentiated liposarcoma · MDM2 · CDK4

J.-M. Coindre
Department of Pathology and INSERM U916, Institut Bergonié, Bordeaux, France

J.-M. Coindre
Laboratory of Pathology, University Victor Ségalen, Bordeaux, France

F. Pédeutour
Laboratoire de Génétique Somatique des Tumeurs Solides, CHU de Nice et CNRS UMR 6543, Faculté de Médecine, Nice, France

A. Aurias
Genetics and Biology of Cancers and INSERM U830, Institut Curie, Paris, France

J.-M. Coindre (✉)
Department of Pathology, Institut Bergonié, 229, cours de l'Argonne, 33076 Bordeaux Cédex, France
e-mail: coindre@bergonie.org

Introduction

Liposarcoma (LPS) is one of the most frequent sarcoma of adult representing 25% of soft tissue sarcomas in a large European database (www.conticabase.org). According to its clinicopathological and molecular genetic characteristics, it can be subtyped in three categories [1]: atypical lipomatous tumor or well-differentiated LPS (ALT-WDLPS)/dedifferentiated LPS (DDLPS), myxoid/round cell LPS, and pleomorphic LPS. ALT-WDLPS/DDLPS is the most frequent LPS subtype and shows a simple genomic profile characterized by a 12q14–15 amplification involving the *MDM2* gene. Myxoid/round cell LPS is characterized by a specific reciprocal translocation t(12;16), leading to the fusion of *DDIT3* (*CHOP*) (12q13) and *FUS* (*TLS*) (16p11) genes. Pleomorphic LPS is the less frequent type and harbors a complex genomic profile with numerous gains and losses similar to the genomic profile seen in poorly differentiated sarcomas and particularly in myxofibrosarcomas [2].

During the last 10 years, the progressive identification of genomic abnormalities in DDLPS leads to a better understanding of these tumors as well as to the use of new criteria for the diagnosis. These genomic criteria are also very helpful for the diagnosis of ALT-WDLPS, which may be difficult to distinguish from benign adipocytic tumors. Moreover, a better knowledge of genomic aberrations seen in this category of LPS (ALT-WDLPS/DDLPS) suggests a multistep genetic process as recently reported in myxofibrosarcomas [3].

This paper reviews the cytogenetic and molecular genetic findings of ALT-WDLPS/DDLPS as well as their clinicopathological characteristics.

Genetics of atypical lipomatous tumor well-differentiated liposarcoma and dedifferentiated liposarcoma

Cytogenetics [4–6]

WDLPS and DDLPS show similar cytogenetic features. In most cases, there are one or two supernumerary rings or giant rod chromosomes. In most cases, these ring or giant chromosomes (also called "marker" chromosomes) are either the sole change, in addition of 46 apparently normal chromosomes, or may be associated with a few other numerical or structural abnormalities. Telomeric associations are frequently observed. Occasionally, especially in DDLPS, double minute chromosomes, multiple copies of the rings and giant markers, as well as genomic instability with random abnormalities from one cell to another can be observed (Fig. 1).

Molecular cytogenetics and genetics

Fluorescence in situ hybridization (FISH) and comparative genomic hybridization (CGH) studies have shown that these supernumerary chromosomes always contain amplified sequences of the region q14–15 of chromosome 12 [7] (Fig. 2). A large variety of other chromosomal regions, including 12q22 and 1q23 for the most frequently involved, have also been shown to be co-amplified in these supernumerary chromosomes. Surprisingly, there is usually no associated alteration on the corresponding chromosomes in the same cell. Molecular methods, such as Southern blotting and FISH analysis, showed that the *MDM2* gene, located at 12q15, was consistently amplified and could be considered as the target gene of this amplicon. More recently, it has been reported that the exons 1 and 2 of *HMGA2*, a gene located at 12q14.3 and known for being rearranged in ordinary lipomas, was consistently co-amplified with *MDM2* [8]. In addition, more centromeric genes, such as *CDK4* and *SAS/TSPAN31*, located at 12q14.1, belong to a separate amplicon that is co-amplified with *MDM2* and *HMGA2* in approximately 90% of cases. The *GLI* and *DDIT3* genes (12q13.3) are very rarely amplified. Another striking feature of the structure of supernumerary ring and giant chromosomes of ALT-WDLPS/DDLPS is that they most often lack alpha-satellite centromeric sequences [9, 10]. Instead, they contain a functional so-called neocentromere containing a high proportion of AT sequences and from variable chromosomal origin [11].

The detection of the amplification and overexpression of MDM2 in 100% of cases and of CDK4 in 90% of cases detected by FISH (Figs. 3 and 4) and immunohistochemistry (Fig. 5) represents nowadays an important tool for the diagnosis of ALT-WDLPS and DDLPS [12, 13].

In addition to the 12q14–15 amplicon, co-amplifications involving mainly 1p32 and 6q23 and also 2q14 (unpublished data) have been detected in DDLPS [14]. Co-amplifications of 1p32 and 6q23 are exclusive one of the other and never seen in WDLPS. Characterization by CGH array of the minimal region of amplification has shown that the target genes are *JUN* in the 1p32 band [15] and *ASK1* in the 6q23 band [16] (Fig. 6).

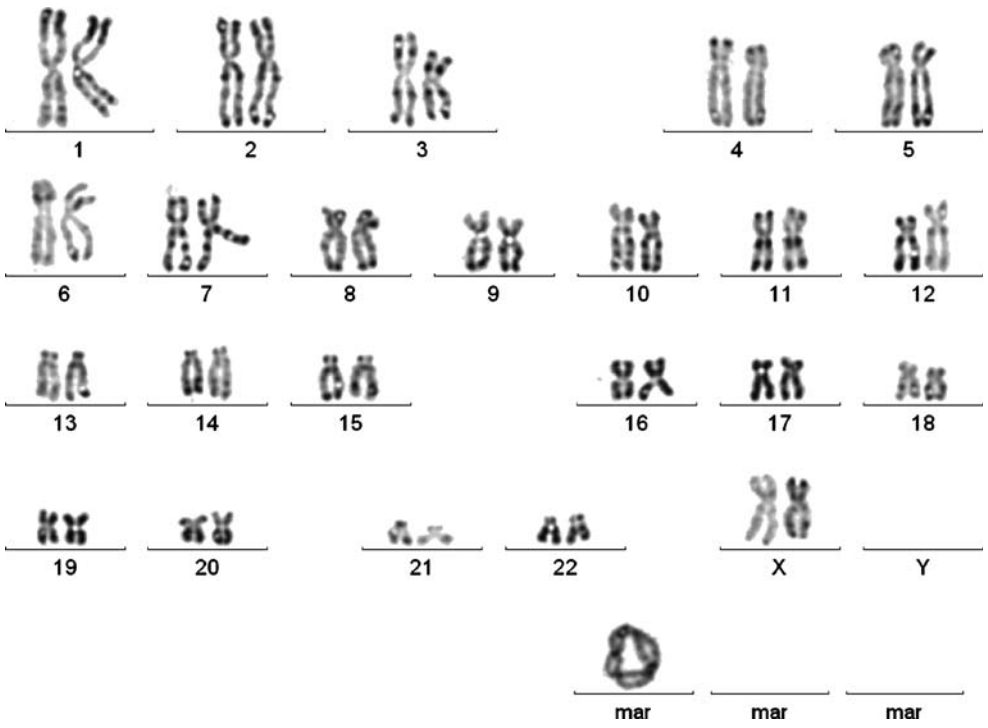

Fig. 1 Karyotype of an ALT-WDLPS in which the only rearrangement is a ring chromosome

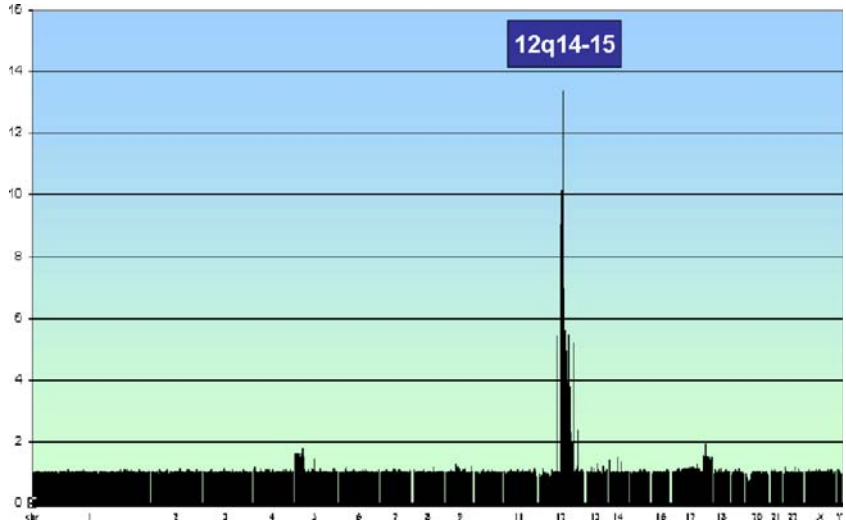

Fig. 2 Array CGH in an ALT-WDLPS showing an amplification of the 12q14–15 involving *MDM2* and *CDK4* genes

Mechanisms involved

MDM2 inhibits P53 and therefore decreases apoptosis and tends to increase cell survival [17]. CDK4 phosphorylates *Rb* gene product, which no longer interacts with E2F transcription factors, and the cell cycle proceeds through the G1-S checkpoint [18]. In summary, the biological consequence of the 12q14–15 amplicon is both to decrease apoptosis and to increase cell proliferation (Fig. 7).

ASK1 is a MAP3 kinase involved in the JNK signaling pathway [16]. Amplification and overexpression of *ASK1* activates JNK, which phosphorylates different target proteins, leading to the activation of some proteins, including JUN and inactivation of other proteins, in particular peroxisome proliferator-activated receptor (PPAR) gamma. It has been demonstrated that PPAR gamma plays a key role in adipocytic differentiation [19], and therefore, the amplification of *ASK1* inhibits adipocytic differentiation. *JUN* is an oncogene that also inhibits PPAR gamma via C/EBP beta [15]. Therefore, dedifferentiation in LPS might be explained by amplification and overexpression of *ASK1* or *JUN* genes. In summary, amplification of *MDM2* and *CDK4*, which are seen in both ALT-WDLPS and DDLPS, may be responsible for the malignant tumor process, whereas amplification of other genes such as *ASK1* and *JUN* may explain inhibition of adipocytic differentiation in DDLPS (Fig. 8).

Xenograft model on nude mice

The murine 3T3-L1 cell line is a highly relevant cellular model of human WDLPS and DDLPS. This cell line, which

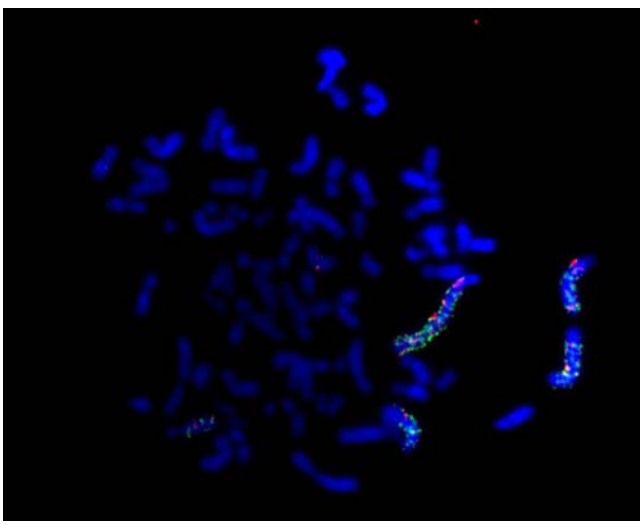

Fig. 3 FISH analysis on chromosomes showing that the ring chromosome is composed of *MDM2* genes copies

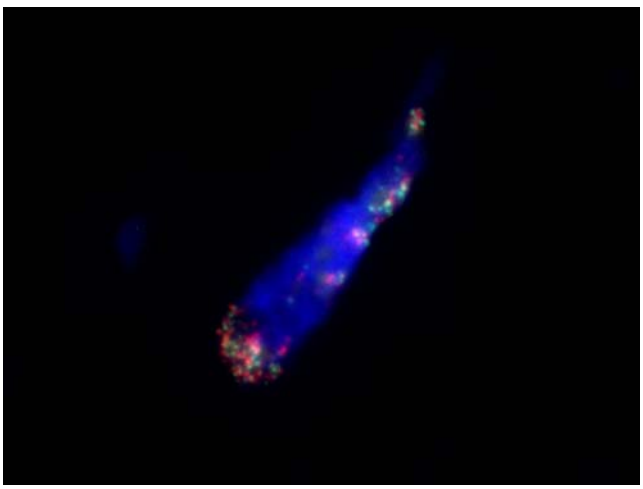

Fig. 4 FISH with MDM2 (red signal) and CDK4 (green signal) probes on formalin-fixed paraffin-embedded tissue from a DDLPS showing a high level amplification of both genes. Fluorescent signals are typically clustered

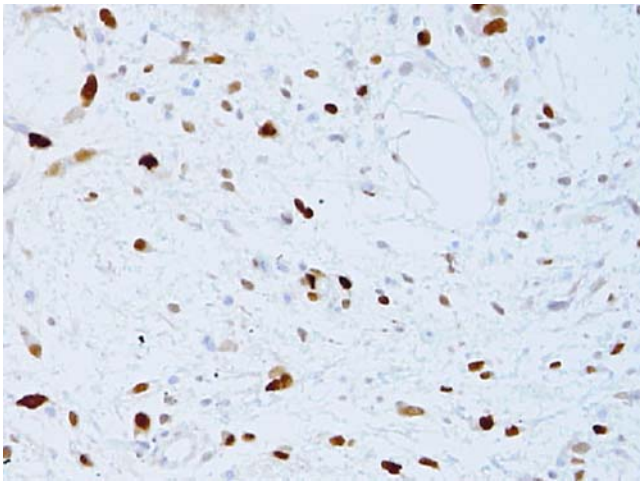

Fig. 5 Immunohistochemical staining for MDM2 (clone IF2) in a DDLPS. Many tumor cells show strong nuclear positivity

has often been used to define molecular events associated with adipogenesis, exhibits chromosomal features close to those of WDLPS and DDLPS with a high level MDM2 and CDK6 amplification in most cells associated with a high level amplification of the JUN locus in 1% of the cells [16]. CDK4 and CDK6 are closely related proteins, which play similar roles in cell-cycle progression.

3T3-L1 cells induce LPS in nude mice and recapitulate tumor progression from WDLPS at early fat pad stage to DDLPS at later stage. In this tumor model, high level amplification of JUN was observed in large nuclei from the undifferentiated areas of the tumor but not in nuclei from the well-differentiated areas, which exhibited only MDM2 and CDK6 amplification [16].

Potential therapeutic targets

Several proteins involved in the mechanism of DDLPS are potential therapeutic targets [20] (Figs. 7 and 8).

Nutlins are MDM2 antagonists that stabilize TP53 and induce apoptosis in cell lines with *MDM2* amplification but which have no effect on apoptosis in cell lines with no *MDM2* amplification [21]. Phase 1 studies are ongoing (http://clinicaltrials.gov/ct2/show/NCT00559533?term=R7112&rank=2 and http://clinicaltrials.gov/ct2/show/NCT00623870?term=R7112&rank=1)

Flavoperidol is a CDK4 inhibitor used in phases 1 [22] and 2 (http://www.clinicaltrials.gov/ct2/results?term=Flavopiridol+) studies.

Thioredoxin is an ASK1 antagonist, which induces adipocytic differentiation in a dedifferentiated cell line exhibiting *ASK1* amplification [16].

Aplidin is a cyclic depsipeptide isolated from a Mediterranean tunicate, which leads to apoptosis by JNK pathway activation [23]. The constitutive activation of this pathway in DDLPS could make Aplidin more efficient in these tumors.

Atypical lipomatous tumor well-differentiated liposarcoma

Definition, terminology, and epidemiology

ALT-WDLPS is a mesenchymal neoplasm composed either entirely or in part of a mature adipocytic proliferation usually showing nuclear atypia in stroma cells [24] and associated with an amplification of MDM2 gene [5, 6].

Definition of ALT-WDLPS is classically based on histologic aspects alone, but on both conceptual and practical points of view, the presence of the molecular genetic alteration described above is of great help for delineating this tumor [25].

The fact that WDLPS shows no potential for metastasis unless it contains a dedifferentiated component led to the introduction of atypical lipomatous tumor, particularly for lesions located in the limbs or in the trunk wall, since wide resection is usually curative. ALT and WDLPS are synonyms describing lesions, which are identical both morphologically and genetically and in terms of biological potential. “The choice of terminology is therefore best determined by the degree of reciprocal comprehension between the surgeon and the pathologist to prevent either inadequate or excessive treatment” [24].

ALT-WDLPS accounts for about 30–40% of all LPS and is the second most frequent category of LPS after DDLPS. They mostly occur during the sixth and seventh decades of life with a predilection for men [26].

Clinical features [24, 27]

ALT-WDLPS occurs in the deep soft tissue of the limbs, particularly in the thigh, the retroperitoneum, the paratesticular area, and the groin. It rarely occurs in other sites, such as the mediastinum, subcutaneous tissue, and miscellaneous parenchymal sites.

Symptoms depend on the location of the tumor. In the extremities, it usually presents as a painless, slowly growing, and deep-seated mass present for months or even several years and which can attain very large size. In the retroperitoneum, it is associated with the usual symptoms of intra-abdominal mass or may be found by chance. In this location, the tumor is often more 20 cm in size.

Imaging and gross features

MRI in the extremities and CT scan in the retroperitoneum show that the tumor has a fat density with zones of higher

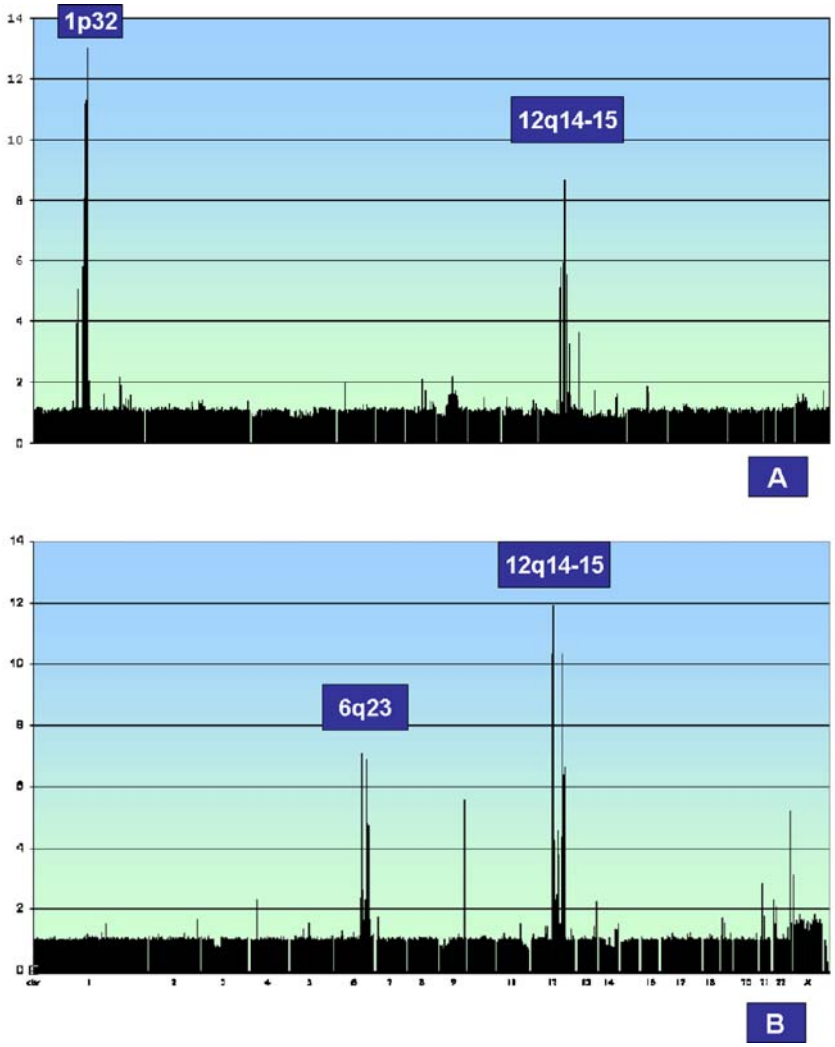

Fig. 6 Array CGH in two cases of DDLPS showing, in addition to the 12q14–15 amplification, a co-amplification of 1q32 in case A (**a**) and 6q23 in case B (**b**). These co-amplifications are exclusive one of the other and not seen in ALT-WDLPS

density corresponding to fibrous septa, sclerotic areas, or inflammatory component.

Grossly, ALT-WDLPS is usually a large, well-demarcated, and lobulated mass. In the retroperitoneum, there may be several separated masses. Color varies from yellow to white

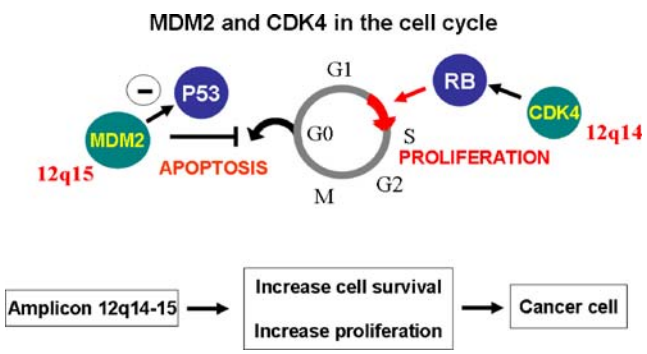

Fig. 7 Mechanism of action of *MDM2* and *CDK4* products on both cell survival and proliferation

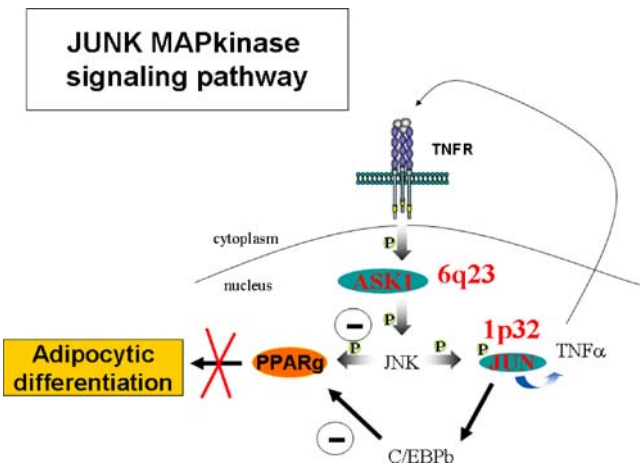

Fig. 8 Mechanism of dedifferentiation in LPS: amplification and overexpression of genes *ASK1* and *JUN* belonging to the JUN MAP kinase signaling pathway lead to inhibition of PPAR gamma, which plays a key role in adipocytic differentiation

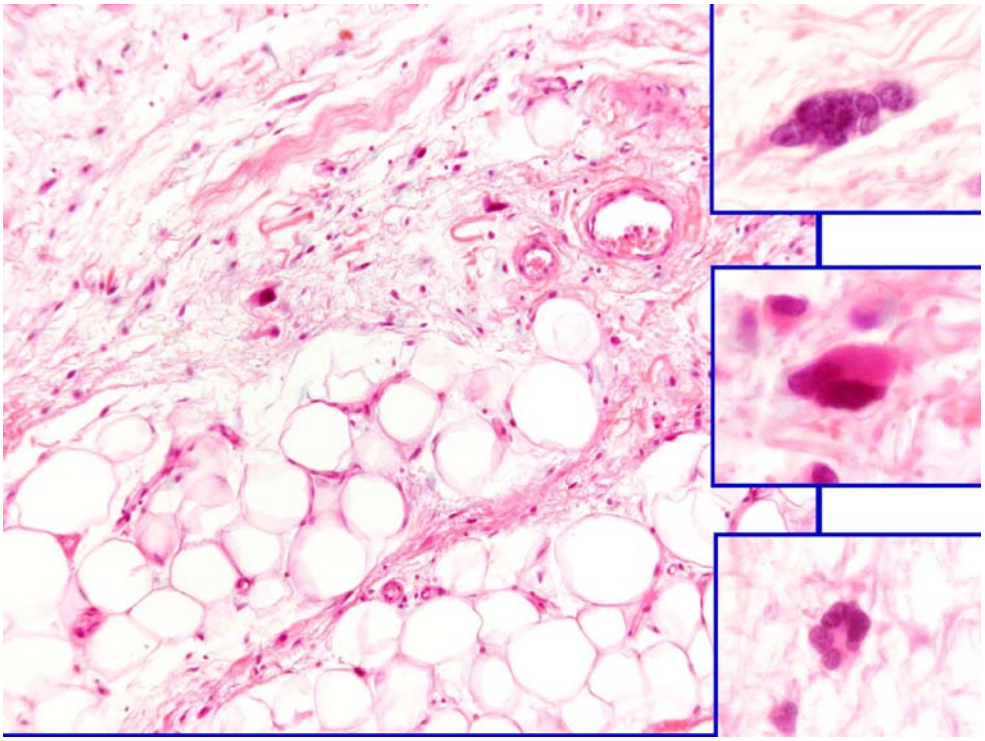

Fig. 9 ALT-WDLPS lipoma-like subtype is composed of mature adipocytic cells. The key for the diagnosis is the presence of atypical cells located in the fibrous septa

depending on the proportion adipocytic, fibrous, and myxoid component.

Histopathology [24, 27]

ALT-WDLPS can be subdivided into three main subtypes: lipoma-like, sclerosing, and inflammatory.

Many ALT-WDLPS combine areas of both lipoma-like and sclerosing subtypes in variable proportions. Therefore, the distinction between these two subtypes is often subjective and has no value in terms of diagnosis and prognosis.

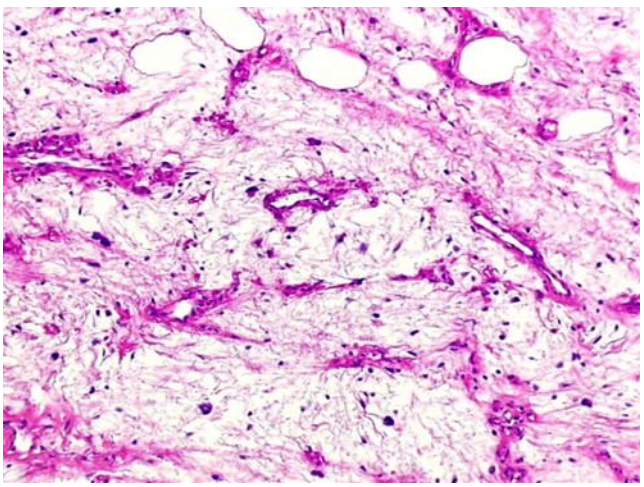

Fig. 10 ALT-WDLPS sclerosing subtype is composed of a myxofibrous background with scattered atypical cells and adipocytic cells

In the typical lipoma-like subtype, tumor is composed of mature adipocytic cells with a significant variation in size, associated with a variable number of atypical stromal cells, which constitute the key for the diagnosis of ALT-WDLPS. These cells tend to be more numerous in the fibrous septa where they should be looked for (Fig. 9). However, they could be so rare as to require extensive sampling. These atypical cells are spindle with hyperchromatic nuclear or multinucleated pleomorphic cells. Lipoblasts are rarely present and not required for the diagnosis of ALT-WDLPS.

The sclerosing subtype (Fig. 10) is most often seen in retroperitoneum or paratesticular region. It is composed of a fibrous or myxofibrous background with scattered stromal cells exhibiting nuclear hyperchromasia associated with multinuclear cells and sometimes rare multivacuolated lipoblasts. These sclerosing areas alternate with adipocytic areas, which can be limited in extent and sometimes missed particularly in small tissue samples. In this situation, analysis of *MDM2/CDK4* status is very helpful.

The inflammatory subtype is rare and occurs almost exclusively in the retroperitoneum [28]. It consists of a chronic inflammatory infiltrate superimposed on a lipoma-like or sclerosing form of ALT-WDLPS. This form may be easily confused with an inflammatory lesion or even a lymphoma. When dealing with a retroperitoneal lesion showing atypical stromal cells, we should always keep in mind the possibility of an ALT-WDLPS or DDLPS, and analysis of *MDM2/CDK4* status is regularly conclusive (Fig. 11).

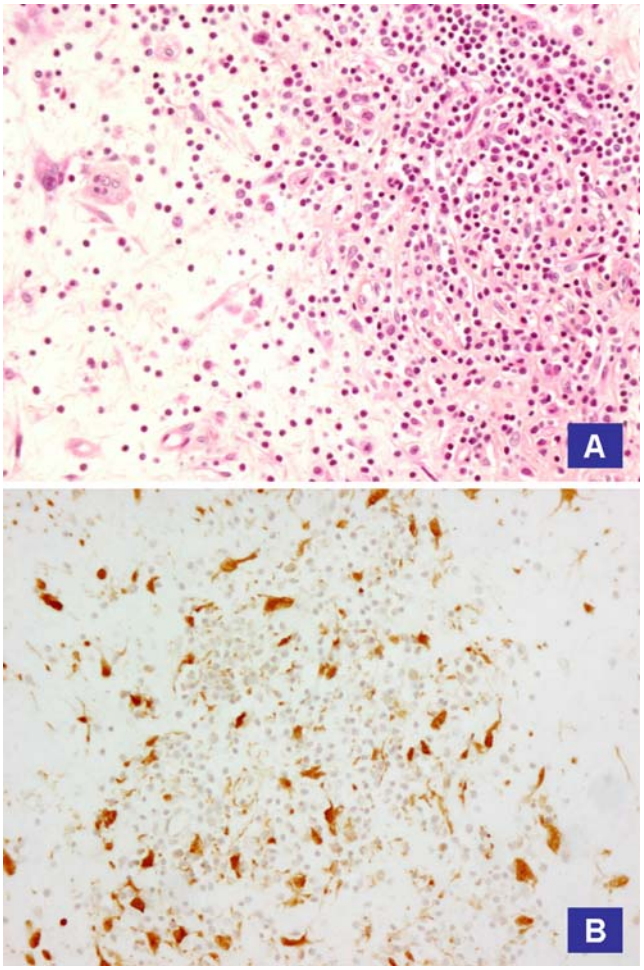

Fig. 11 ALT-WDLPS inflammatory subtype. Retroperitoneal tumor showing a chronic inflammatory infiltrate with a few atypical cells (**a**). Immunohistochemistry shows numerous cells positive for MDM2 and CDK4 (**b**)

Ancillary techniques

With the identification of 12q13–15 amplicon involving *MDM2*, *HMGA2*, and often *CDK4* genes in ALT-WDLPS, ancillary diagnostic tools can now be utilized to distinguish these tumors from benign lipomatous tumors. Immunohistochemistry showing overexpression of MDM2 and/or CDK4 may be used on first line to detect tumors with potential amplification of these genes. Clones IF2 for MDM2 and DCS-31 for CDK4 were respectively positive in 100% and 91% in ALT-WDLPS and also in 4% and 2% in benign lipomatous tumors [13]. Moreover, these antibodies may also stain the nuclei of histiocytes and reactive giant cells, which are often present in lipomas displaying inflammatory or necrotic changes. On the other hand, FISH showing amplification of *MDM2*, *HMGA2*, and *CDK4* is sensitive and specific for identifying ALT-WDLPS [12, 29].

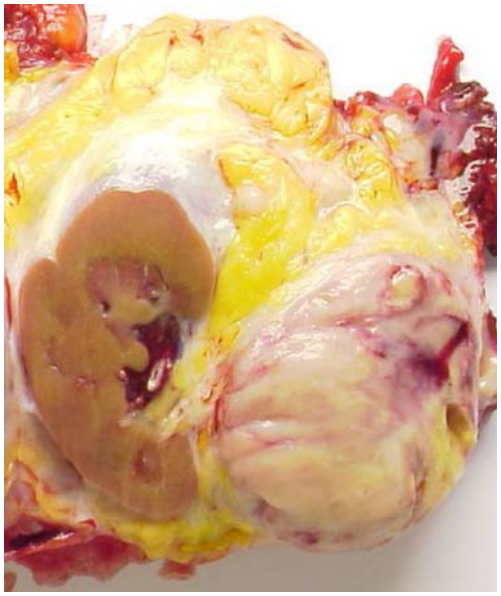

Fig. 12 Gross appearance of a retroperitoneal DDLPS showing areas of ALT-WDLPS and of DDLPS

Differential diagnosis [30–32]

One of the most frequent diagnostic problems revealed by second opinion practice is the distinction of ALT-WDLPS from benign lipomatous tumors. Deep lipomas with secondary changes may show irregular adipocytic size due to atrophic adipocytes admixed with inflammatory cells and histiocytes and reactive fibrous tissue with spindle cells mistaken for atypical cells and lipoblasts. Careful sampling, immunohistochemistry, and FISH for MDM2 and CDK4 are the keys for diagnosis. Normal fat with *Lochkern* (hole in the adipocyte nucleus), intramuscular lipoma with atrophic muscle, some spindle and pleomorphic cell lipomas, fat necrosis, atrophy of fat secondary to malnutrition or local trauma, silicone reaction due to injection of silicone for therapeutic or cosmetic purposes, and rare localized massive lymphoedema seen in morbid obesity can be mistaken for an ALT-WDLPS. In these situations, the use of immunohistochemistry and/or FISH for the detection of *MDM2* and *CDK4* amplification is frequently conclusive.

Prognosis

ALT-WDLPS are nonmetastasizing tumors for which the local recurrence rate is mainly dependant on their location. Tumors in the extremities have significantly lower rates of local recurrence than those in the retroperitoneum, which recur in almost 100% of cases and often cause the patient's death. The risk of dedifferentiation is time dependent and is probably more than 20% in retroperitoneum and less than 5% in extremities. Overall mortality ranges from 0% in the

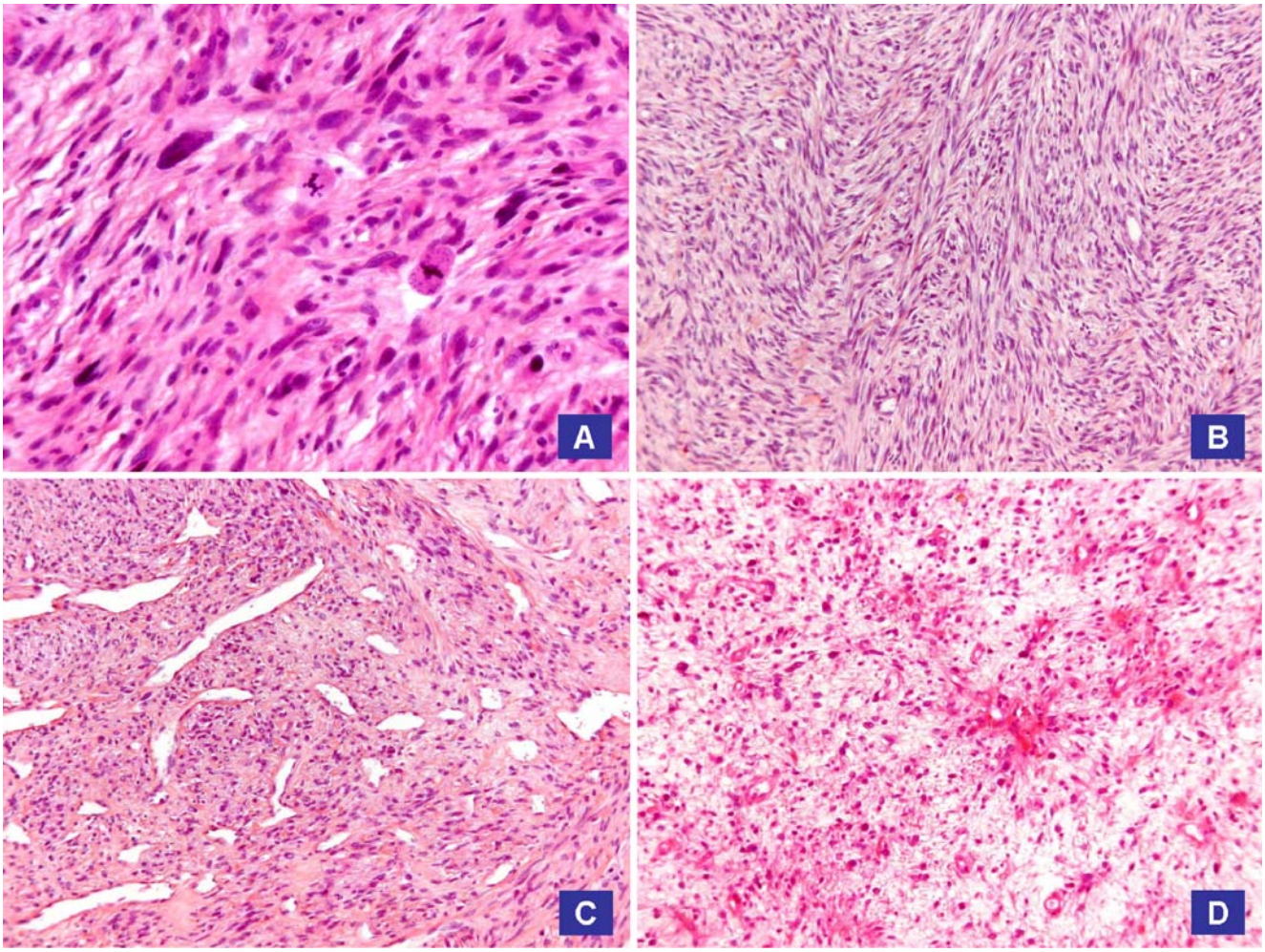

Fig. 13 Dedifferentiated component of DDLPS is usually composed of pleomorphic malignant fibrous histiocytoma (**a**), fibrosarcoma (**b**), malignant hemangiopericytoma (**c**) or high-grade myxofibrosarcoma-like areas (**d**)

limbs to more than 80% for cases occurring in the retroperitoneum for patients with a long follow-up.

Dedifferentiated liposarcoma

Definition, terminology, and epidemiology

DDLPS is a term first introduced by Evans in 1979 [33] to describe LPS containing ALT-WDLPS juxtaposed to areas of high-grade nonlipogenic sarcoma, usually resembling either high-grade pleomorphic sarcoma NOS or fibrosarcoma. DDLPS was believed to occur from ALT-WDLPS after several years. These traditional views have been modified by the description of exclusively low-grade dedifferentiated component and by the fact that most DDLPS arise in fact de novo and are diagnosed on the original excision [34]. Moreover, thanks to its specific genomic profile, DDLPS can now be identified in the absence of ALT-WDLPS areas [14]. Absence of ALT/WDLPS component may be explained by inappropriate sampling, disappearance of the ALT-WDLPS component, or even by absence of the well differentiated component in the initial tumor. The latter situation corresponds to undifferentiated LPS rather than to dedifferentiated LPS. Genomic abnormalities described in DDLPS support the fact that this tumor corresponds to a malignant adipocytic tumor showing progression from ALT-WDLPS to non-lipogenic sarcoma of variable aspect and grade [14–16]. About 90% of DDLPS arises de novo, while 10% occurs in recurrence. The risk of dedifferentiation is higher in deep-seated tumors, particularly in the retroperitoneum and is probably a time-dependent phenomenon. Numerous reports have supported the concept of DDLPS with two histological series of 32 [35] and 155 cases [34]. It represented 18% of LPS in a large series reported in 2006 [36], but we suspect a much more frequency due to the recent genomic criteria used for diagnosing cases without any ALT-WDLPS areas.

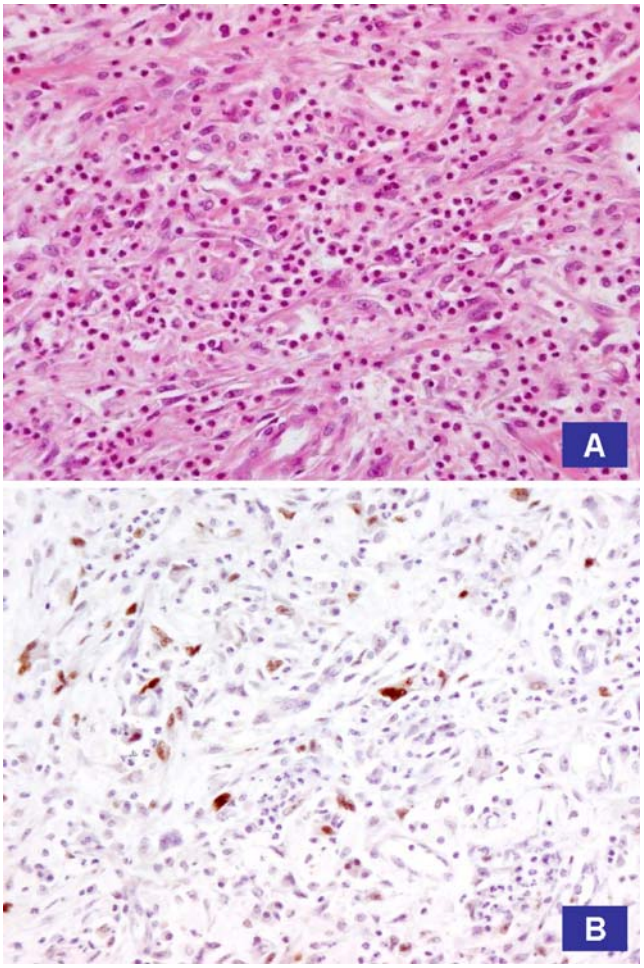

Fig. 14 Most so-called inflammatory malignant fibrous histiocytomas are in fact DDLPS. Typical aspect in **a** and strong nuclear positivity of tumor cells for MDM2 antibody in **b**

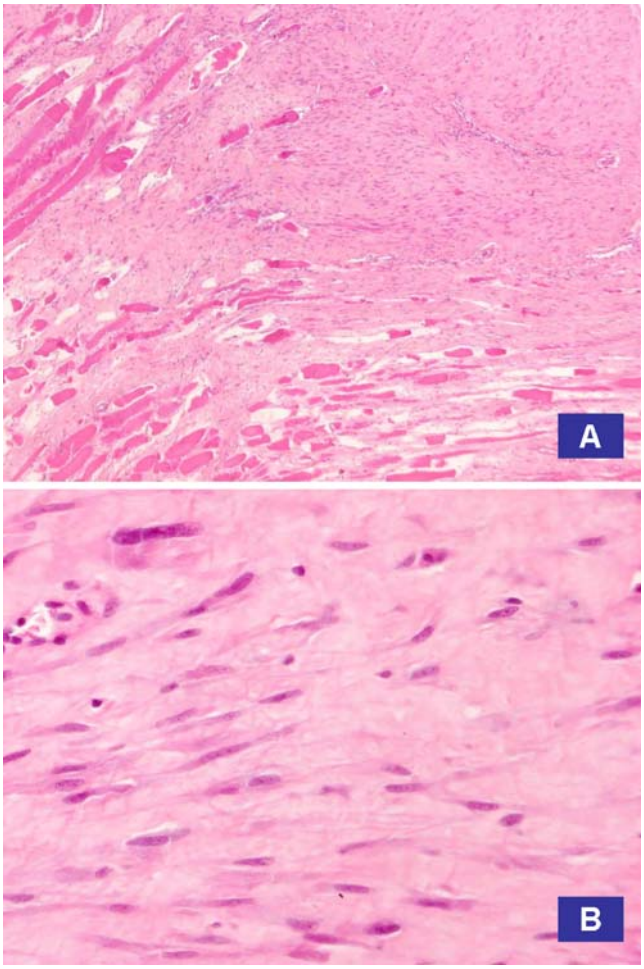

Fig. 15 Example of a low-grade dedifferentiated component in a DDLPS simulating a desmoid tumor with infiltration of the adjacent muscles in **a**. The tumor shows a fibrous background with moderately atypical spindle cells in **b**

Clinical features

DDLPS occur in late adult life with no sex predilection, most commonly in the retroperitoneum (more than 80% of cases), extremities, spermatic cord, and other sites of internal trunk. Occurrence in head and neck may be seen but is rare in subcutaneous tissue. In our experience, 60% of retroperitoneal sarcomas are LPS, two thirds of which are DDLPS. It usually presents as a large painless mass, which may be found by chance, particularly in the retroperitoneum.

Imaging and macroscopy

Radiological imaging may suggest the diagnosis by showing the coexistence of a fatty component with a non-fatty solid one.

The gross appearance of DDLPS is often helpful for the diagnosis. It usually consists of multinodular yellow (fatty) masses containing firm tan-gray areas corresponding to dedifferentiated foci (Fig. 12). Necrosis is often observed.

Histopathology [27, 37]

Histologically, DDLPS is traditionally defined by the association of ALT-WDLPS areas and a non-lipogenic sarcoma, usually with an abrupt transition, although in some cases, it can be gradual, and rarely the two components appear to be intermingled.

Dedifferentiated areas exhibit a wide morphological spectrum. Most cases show areas of high-grade poorly differentiated sarcoma resembling pleomorphic malignant fibrous histiocytoma, fibrosarcoma, malignant hemangiopericytoma, or high-grade myxofibrosarcoma (Fig. 13). It has been shown that most sarcomas diagnosed as poorly differentiated sarcoma and arising in the retroperitoneum are in fact dedifferentiated LPSs [38]. The keys of diagnosis are the presence of an ALT-WDLPS component easily

demonstrated by extensive sampling of the surrounding fat tissues and the positivity of immunohistochemistry for MDM2 and CDK4. Nowadays, these poorly differentiated sarcomas represent less than 10% of all sarcomas arising in retroperitoneum as well as in paratesticular areas and other internal trunk areas. Dedifferentiated areas resembling inflammatory malignant fibrous histiocytoma, characterized by numerous benign xanthomatous cells admixed with acute and chronic inflammatory cells and a variable number of atypical cells, have been associated with fever, weight loss, leukocytosis, eosinophilia, and leukemoid reaction. In fact, based on a combination of a careful histological review, *MDM2* and *CDK4* status, and genomic profiling, it has been showed that most so-called inflammatory malignant fibrous histiocytoma were, in fact, DDLPS [39] (Fig. 14).

The concept of low-grade dedifferentiation has increasingly been recognized [34]. Usually, low-grade areas coexist with areas of high-grade sarcomas, but in about 10% of cases, only low-grade areas are present [40–42]. These areas resemble low-grade myxofibrosarcoma, fibromatosis (Fig. 15), well-differentiated fibrosarcoma, and even dermatofibrosarcoma protuberans.

In about 5–10% of cases, the dedifferentiated component shows divergent differentiation featuring myogenic or osteochondromatous elements. An angiosarcomatous component has also been reported. Myosarcomatous differentiation is the most frequent but must be established with both morphological features and immunohistochemical profile, and specific muscle markers such as h-caldesmon and myogenin should be used given the non-specificity of markers such as smooth muscle actin and desmin and their frequent positivity in conventional DDLPS (Fig. 16). It has been recently reported that most tumors developed in the internal trunk and diagnosed as pleomorphic rhabdomyosarcoma or malignant mesenchymoma are actually DDLPS with a divergent differentiation. In this report, the presence of a divergent differentiation does not affect the clinical outcome [42].

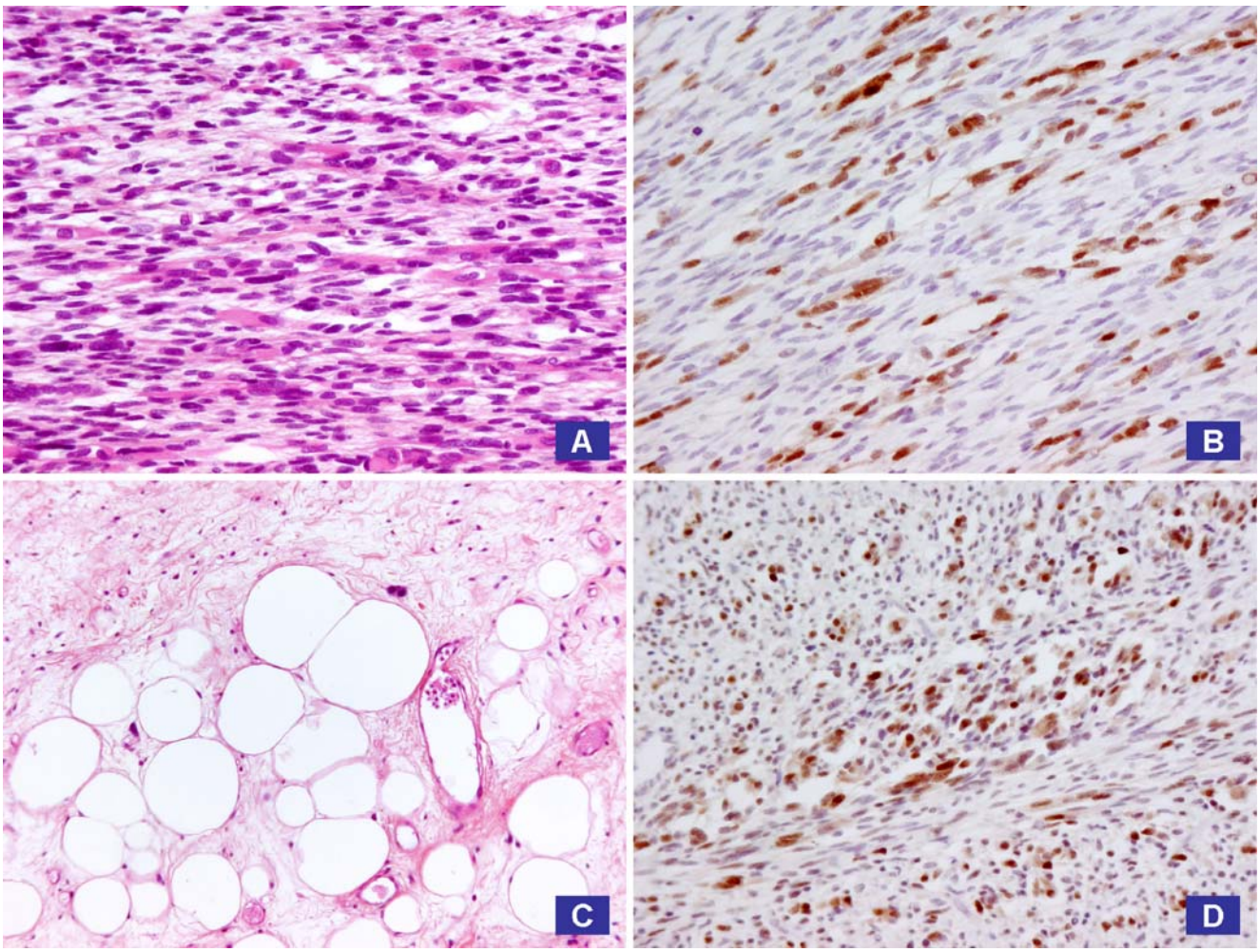

Fig. 16 DDLPS with a divergent differentiation. Histological aspect of a rhabdomyosarcoma (**a**) with a strong positivity for myogenin (**b**). Careful sampling shows an ALT-WDLPS component (**c**), and heterologous component is positive for MDM2 (**d**)

A number of unusual patterns are seen in DDLPS. A "neural-like" or "meningothelial-like" whorling pattern of differentiation often associated with ossification has been described [43, 44] (Fig. 17). Epithelial-like pattern composed of undifferentiated large round cells resembling a carcinoma or a melanoma, areas with dense amianthoid-like fibers, and areas composed of hibernoma-like cells have also been described [34].

Ancillary techniques

Immunohistochemistry for MDM2 and CDK4 is currently used for the diagnosis of DDLPS. Analysis of immunohistochemistry on a large number of sarcomas reported a sensitivity of 95% and 92% and a specificity of 81% and 95% for, respectively, MDM2 and CDK4 for the diagnosis of DDLPS [13]. In this report, 18.9% of various sarcomas, including malignant peripheral nerve sheath tumor, myxofibrosarcoma, embryonal rhabdomyosarcoma, poorly differentiated sarcoma leiomyosarcoma, and myxoid LPS, were also positive for MDM2. However, 90.2% of DDLPS were positive for both MDM2 and CDK4 as opposed to only 3.7% of other sarcomas. Moreover, due to the fact that there is no internal positive control for these antibodies, we should keep in mind that a non-immunoreactivity could correspond to a false negativity. These findings underline the importance of the clinical and morphological context as well as the need to use a panel of antibodies for achieving the right diagnosis.

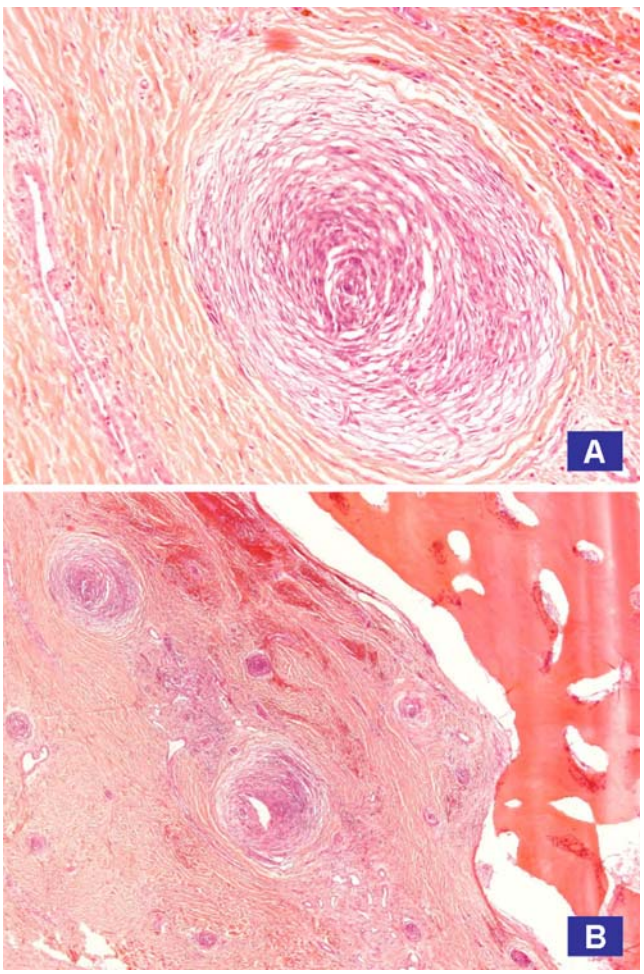

Fig. 17 DDLPS with a meningothelial-like-dedifferentiated component showing a whorling pattern (**a**) often associated with ossification (**b**)

Detection of *MDM2* and *CDK4* amplification by FISH or quantitative PCR is more efficient than immunohistochemistry for the diagnosis of DDLPS. FISH and quantitative PCR [12] gave concordant results but FISH was more powerful than quantitative PCR when tumor cells represented a minor component such as with inflammatory tumors and is more and more often use in the daily practice. In our experience, FISH is a powerful tool for the diagnosis of DDLPS, since it shows a true amplification with clustering of the signal. In addition, when a moderate gain of MDM2/CDK4 is detected, a complementary analysis with a centromeric probe for chromosome 12 can be performed. This helps to identify a polysomy 12 that has to be distinguished from a genuine amplification. As previously reported, a gain of *MDM2* or a polysomy can be seen in other sarcomas, particularly those with a complex genetics such as pleomorphic poorly differentiated sarcomas [29]. In these cases, fluorescent signals are not clustered, and the number of copies of centromere 12 is usually the same than the number of copies of *MDM2/CDK4*.

Multicolor FISH like COBRA has been reported to be helpful for difficult cases [45].

For difficult cases, the gold standard is array CGH, which shows a simple genomic profile with only a few amplicons, one in the 12q14.15 and usually another in the 1p32 or 6q23 chromosomal regions.

Differential diagnosis

Due to the histological complexity of DDLPS, many differential diagnoses may be raised on the morphological aspect alone: poorly differentiated sarcomas such as malignant fibrous histiocytoma, fibrosarcoma and malignant hemangiopericytoma, myxofibrosarcoma, pleomorphic rhabdomyosarcoma, and malignant mesenchymoma. In internal trunk areas, these diagnoses can be retained only after exclusion of a DDLPS, and in this situation, an extensive sampling should be performed in order to demonstrate an ALT-WDLPS component, and the MDM2-CDK4 status should be evaluated.

A DDLPS can be mistaken for an ALT-WDLPS because of minimal areas of dedifferentiation, which can be missed in case of insufficient sampling. According to Weiss and Goldblum, the presence of a macroscopically visible nodule

of dedifferentiation (>1.0 cm) should be demonstrated in an ALT-WDLPS for diagnosing a DDLPS [27].

Prognosis

Prognosis is mainly dominated by local recurrences (40–60%), particularly in the retroperitoneum, with a quite low metastatic potential (15–20%) [34, 35]. In fact, almost all retroperitoneal cases seem to locally recur if patients are followed for at least 10–20 years. Overall mortality range from 30% to 40% at 5 years. The most important prognostic factor is anatomic location with a poor prognosis for retroperitoneal tumors. Traditionally, neither histological grade nor extent of dedifferentiation is of prognostic value. However, a recent study on retroperitoneal LPSs suggested that grade and extent of dedifferentiation are predictors for event-free survival [46].

Conclusions

Advances in our knowledge about genetics of the ALT-WDLPS/DDLPS have led to significant improvements in the diagnostic approach of LPSs, especially by detection of MDM2 and CDK4 overexpression and/or amplification. Thanks to these new criteria, the distinction of ALT-WDLPS from challenging benign adipocytic tumors on one hand and identification of DDLPS among histologically poorly differentiated sarcomas on the other hand has become easier. More importantly, better understanding of the mechanisms involved in the development of DDLPS has led to the identification of new potential therapeutic targets.

References

1. Fletcher CDM, Unni KK, Mertens F (2002) Pathology and genetics. Tumours of soft tissue and bone. IARC, Lyon
2. Idbaih A, Coindre JM, Derré J et al (2005) Myxoid malignant fibrous histiocytoma and pleomorphic liposarcoma share very similar genomic imbalances. Lab Invest 85:176–181
3. Willems SM, Debiec-Rychter M, Szuhai K et al (2006) Local recurrence of myxofibrosarcoma is associated with increase in tumour grade and cytogenetic aberrations, suggesting a multistep tumour progression model. Mod Pathol 19:407–416
4. Rubin BP, Fletcher CDM (1997) The cytologenetics of lipomatous tumours. Histopathology 30:507–511
5. Pedeutour F, Marie G, Sirvent N (2004) De la cytogénétique à la cytogénomique des tumeurs adipocytaires. 2. Tumeurs adipocytaires malignes. Bull Cancer 91:317–323
6. Sandberg AA (2004) Updates on the cytogenetics and molecular genetics of bone and soft tissue tumors: liposarcoma. Cancer Genet Cytogenet 155:1–24
7. Pedeutour F, Suijkerbuijk RF, Forus A et al (1994) Complex composition and co-amplification of SAS and MDM2 in ring and giant rod marker chromosomes in well-differentiated liposarcomas. Genes Chromosomes Cancer 10:85–94
8. Italiano A, Blanchini L, Keslair F et al (2008) HMGA2 is the partner of MDM2 in well-differentiated and dedifferentiated liposarcomas whereas CDK4 belongs to a distinctive inconsistent amplicon. Int J Cancer 122:2233–2241
9. Sirvent N, Forus A, Lescaut W et al (2000) Characterization of centromere alterations in liposarcomas. Genes Chromosomes Cancer 29:117–129
10. Pedeutour F, Forus A, Coindre JM et al (1999) Structure of the supernumerary ring and giant rod chromosomes in adipose tissue tumors. Genes Chromosomes Cancer 24:30–41
11. Italiano A, Maire G, Sirvent N et al (2009) Variability of origin for the neocentromeric sequences in analphoid supernumerary marker chromosomes of well-differentiated liposarcomas. Cancer Lett 273:323–330
12. Sirvent N, Coindre JM, Marie G et al (2007) Detection of MDM2-CDK4 amplification by fluorescence in situ hybridization in 200 paraffin-embedded tumor samples: utility in diagnosing adipocytic lesions and comparison with immunohistochemistry and real-time PCR. Am J Surg Pathol 31:1476–1489
13. Bui Nguyen Binh M, Sastre-Garau X, Guillou L et al (2005) MDM2 and CDK4 immunostainings are useful adjuncts in diagnosing well-differentiated and dedifferentiated liposarcoma subtypes. A comparative analysis of 559 soft tissue neoplasms with genetic data. Am J Surg Pathol 29:1340–1347
14. Chibon F, Mariani O, Derré J et al (2002) A subgroup of malignant fibrous histiocytomas in associated with genetic changes similar to those of well-differentiated liposarcomas. Cancer Genet Cytogenet 139:24–29
15. Mariani O, Brennetot C, Coindre JM et al (2007) JUN oncogene amplification and overexpression block adipocytic differentiation in highly aggressive sarcomas. Cancer Cell 11:361–374
16. Chibon F, Mariani O, Derré J et al (2004) ASKI (MAP3K5) as a potential therapeutic target in malignant fibrous histiocytomas with 12q14–15 and 6q23 amplifications. Genes Chromosomes Cancer 40:32–37
17. Momand J, Wu HH, Dasgupta G (2000) MDM2-master regulator of the p53 tumor suppressor protein. Gene 242:15–29
18. Ortega S, Malumbres M, Barbacid M (2002) Cyclin D-dependent kinases, INK4 inhibitors and cancer. Biochim Biophys Acta 1602:73–87
19. Castriota G, Thompson GM, Lin Y et al (2007) Peroxisome proliferator-activited receptor gamma agonists inhibit adipocyte expression of alpha1-acid glycoprotein. Cell Biol Int 31:586–591
20. Singer S, Socci ND, Ambrosini G et al (2007) Gene expression profiling of liposarcoma identifies distinct biological types/subtypes and potential therapeutic targets in well-differentiated and dedifferentiated liposarcoma. Cancer Res 67:6626–6636
21. Müller CR, Paulsen EB, Noordhuis P et al (2007) Potential for treatment of liposarcomas with the MDM2 antagonist Nutlin-3A. Int J Cancer 121:199–205
22. Shapiro GI (2006) Cyclin-dependent kinase pathways as targets for cancer treatment. J Clin Oncol 24:1770–1783
23. Cuadrado A, Gnozalez L, Suarez Y et al (2004) JNK activation is critical for Aplidin-induced apoptosis. Oncogene 23:4673–4680
24. Dei Tos AP, Pedeutour F (2002) Atypical lipomatous tumour/well differentiated liposarcoma. In: Fletcher CDM, Unni KK, Mertens F (eds) Pathology and Genetics. Tumours of soft tissue and bone. IARC, Lyon, pp 35–37
25. Pilotti S, Della Torre G, Mezzelani A et al (2000) The expression of MDM2/CDK4 gene product in the differential diagnosis of well differentiated liposarcoma and large deep-seated lipoma. Br J Cancer 82:1271–1275

26. Dalal KM, Kattan MW, Antonescu CR et al (2006) Subtype specific prognostic nomogram for patients with primary liposarcoma of the retroperitoneum, extremity, or trunk. Ann Surg 244:381–391
27. Weiss SW, Goldblum JR (2008) Liposarcoma. In: Weiss SW, Goldblum JR (eds) Enzinger and Weiss's soft tissue tumors. Mosby, St Louis, pp 477–516
28. Kraus MD, Guillou L, Fletcher CD (1997) Well-differentiated inflammatory liposarcoma: an uncommon and easily overlooked variant of a common sarcoma. Am J Surg Pathol 1:37–50
29. Weaver J, Downs-Kelly E, Goldblum JR et al (2008) Fluorescence in situ hybridization for MDM2 gene amplification as a diagnostic tool in lipomatous neoplasms. Mod Pathol 21:943–949
30. Evans HL, Soule EH, Winkelman RK (1979) Atypical lipoma, atypical intramuscular lipoma, and well differentiated retroperitoneal liposarcoma. Cancer 43:574
31. Azumi N, Curtis J, Kempson RL et al (1987) Atypical and malignant neoplasms showing lipomatous differentiation: a study of 111 cases. Am J Surg Pathol 11:161
32. Weiss SW, Rao VK (1992) Well-differentiated liposarcoma (atypical lipoma) of deep soft tissue of the extremities, retroperitoneum and miscellaneous sites: a follow-up study of 92 cases with analysis of the incidence of "dedifferentiated". Am J Surg Pathol 16:1051
33. Evans HL (1979) Liposarcoma: a study of 55 cases with a reassessment of its classification. Am J Surg Pathol 3:507–523
34. Henricks WH, Chu YC, Goldblum JR et al (1997) Dedifferentiated liposarcoma. A clinicopathologic analysis of 155 cases with a proposal for an expanded definition of dedifferentiation. Am J Surg Pathol 21:271–281
35. McCormick D, Mentzel T, Beham A et al (1994) Dedifferentiated liposarcoma. Clinicopathologic analysis of 32 cases suggesting a better prognostic subgroup among pleomorphic sarcomas. Am J Surg Pathol 18:1213–1223
36. Dalal KM, Kattan MW, Antonescu CR et al (2006) Subtype specific prognostic nomogram for patients with primary liposarcoma of the retroperitoneum, extremity, or trunk. Ann Surg 244:381–391
37. Dei Tos AP, Pedeutour F (2002) Dedifferentiated liposarcoma. In: Fletcher CDM, Unni KK, Mertens F (eds) Pathology and genetics—tumours of soft tissue and bone. IARC, Lyon, pp 38–39
38. Coindre JM, Mariani O, Chibon F et al (2003) Most malignant fibrous histiocytomas developed in the retroperitoneum are dedifferentiated liposarcomas: a review of 25 cases initially diagnosed as malignant fibrous histiocytoma. Mod Pathol 16:256–262
39. Coindre JM, Hostein I, Maire G et al (2004) Inflammatory malignant fibrous histiocytomas and dedifferentiated liposarcomas: histological review, genomic profile, and MDM2 and CDK4 status favour a single entity. J Pathol 203:822–830
40. Tallini G, Erlandson RA, Brennan MF et al (1993) Divergent myosarcomatous differentiation in retroperitoneal liposarcoma. Am J Surg Pathol 17:546–556
41. Evans HL, Khurana KK, Kemp BL et al (1994) Heterologous elements in the dedifferentiated component of dedifferentiated liposarcoma. Am J Surg Pathol 18:1150–1157
42. Bui Nguyen Binh M, Guillou L, Hostein I et al (2007) Dedifferentiated liposarcomas with divergent myosarcomatous differentiation developed in the internal trunk. A study of 27 cases and comparison to conventional dedifferentiated liposarcomas and leiomyosarcomas. Am J Surg Pathol 31:1557–1566
43. Fanburg-Smith JC, Miettinen M (1998) Liposarcoma with meningothelial-like whorls: a study of 17 cases of a distinctive histological pattern associated with dedifferentiated liposarcoma. Histopathological 33:414–424
44. Nascimento AG, Kurtin PJ, Guillou L et al (1998) Dedifferentiated liposarcoma: a report of nine cases with a peculiar neurolike whorling pattern associated with metaplastic bone formation. Am J Surg Pathol 22:945–955
45. Willems SW, Szuhai K, Hartgrink H et al (2007) CT-guided, COBRA-FISH-assisted diagnosis of well-differentiated liposarcoma (inflammatory subtype) of the retroperitoneum. Histopathology 51:422–426
46. Mussi C, Collini P, Miceli R et al (2008) The prognostic impact of dedifferentiation in retroperitoneal liposarcoma: a series of surgically treated patients at a single institution. Cancer 113:1657–1665

Virchows Arch (2010) 456:181–192
DOI 10.1007/s00428-009-0822-y

REVIEW AND PERSPECTIVE

Running GAGs: myxoid matrix in tumor pathology revisited

What's in it for the pathologist?

Stefan M. Willems · Malgorzata Wiweger · J. Frans Graadt van Roggen · Pancras C. W. Hogendoorn

Received: 27 June 2009 / Accepted: 3 August 2009 / Published online: 25 August 2009
© The Author(s) 2009. This article is published with open access at Springerlink.com

Abstract Ever since Virchow introduced the entity myxoma, abundant myxoid extracellular matrix (ECM) has been recognized in various reactive and neoplastic lesions. Nowadays, the term "myxoid" is commonly used in daily pathological practice. But what do today's pathologists mean by it, and what does the myxoid ECM tell the pathologist? What is known about the exact composition and function of the myxoid ECM 150 years after Virchow? Here, we give an overview of the composition and constituents of the myxoid ECM as known so far and demonstrate the heterogeneity of the myxoid ECM among different tumors. We discuss the possible role of the predominant constituents of the myxoid ECM and attempt to relate them to differences in clinical behavior. Finally, we will speculate on the potential relevance of this knowledge in daily pathological practice.

Keywords Extracellular matrix · Glycosaminoglycans · Proteoglycan · Collagen · Myxofibrosarcoma · Intramuscular myxoma

Historical perspective

In his 1858 masterpiece *Cellularpathologie*, Rudolph Virchow introduced the term "myxoma" to describe a soft tissue tumor, histologically resembling the structure of the umbilical cord (Figs. 1 and 2) [1]. This description of myxoma was adopted in the seventh edition of the Medical Lexicon by Robley Dunglison who remarkably added that "[myxoma] was for the first time described in 1838 by Johannes Müller as Collonema" [2]. Müller used the term collonema (κολλα = glue) for "peculiar gelatinous tumours, consisting of a remarkably soft gelatiniform tissue, which trembles on being touched" [3]. Though this description is applicable to most myxoid tumors, it holds also for many nonmyxoid tumors and it is not particularly clear which tumor type Müller had in mind. Today, it has been generally accepted that it was indeed Virchow who introduced myxoma as an entity. The introduction of this new histological concept of tumors containing myxoid (μύξα = "mucus" and ειδος = "resemblance") areas soon led to the recognition of new entities, such as myxadenoma, myxochondroma, myxofibroma, and myxoneuroma [2]. The term myxosarcoma, introduced in 1802 by Bryant [4], became reserved for malignant tumors and defined as "a mucous transformation of round-celled sarcoma, malignant, and of large volume, usually attacking the omentum and the skin" [2]. Nowadays, myxoid changes/areas are recognized in both benign and malignant neoplasms (primarily classified as mesenchymal or epithelial) as well as non-neoplastic (reactive) lesions (Fig. 3).

In his first description, Virchow had already recognized the recurrent nature of some myxomatous tumors [1] and it became clear that it was difficult to predict the exact clinical behavior of these different tumors based on their myxoid morphology alone. Subsequently, the terms myxoma and myxosarcoma were used interchangeably till Arthur Stout recognized this as unwise [5] because "myxomas do not metastasize and there is no way to anticipate differences in their growth energy from their histopathology." Later studies confirmed the distinction between both entities on

S. M. Willems · M. Wiweger · P. C. W. Hogendoorn (✉)
Department of Pathology, Leiden University Medical Center, L1Q, P.O. Box 9600, 2300 RC Leiden, The Netherlands
e-mail: P.C.W.Hogendoorn@lumc.nl

J. F. G. van Roggen
Department of Pathology, Diaconessenhuis Hospital, Leiden, The Netherlands

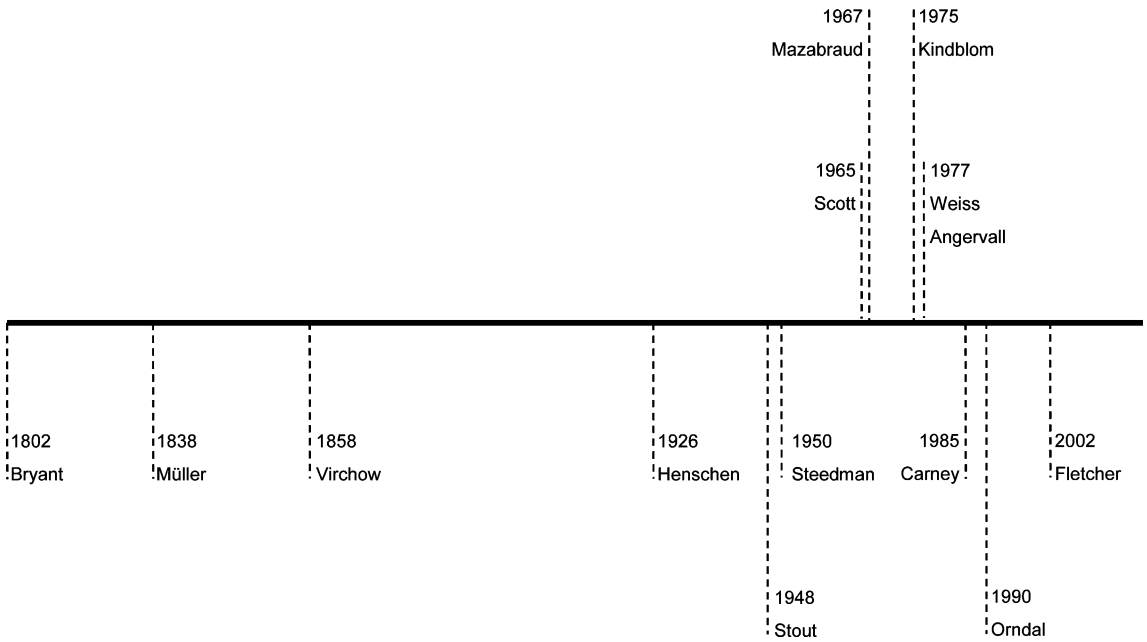

Fig. 1 Timetable with key events in studies on myxoid tumors of soft tissue. Though Müller already mentioned tumors with a macroscopically gelatinous appearance in 1838 [3], it was in 1858 when Virchow introduced the term myxoma to describe tumors which morphologically resembled the jelly structure of the umbilical cord [1]. Ever since, the term myxosarcoma, introduced by Bryant in 1802 was reserved for the malignant counterparts [4]. Because of their morphologically overlapping features, both terms were used interchangeably, which was mentioned by Stout in 1948 as unwise, warranting for macroscopical and microscopical criteria for the reliable differential diagnosis between the two entities [5]. The relationship between myxomas and fibrous dysplasia was first described in 1926 by Henschen [90], though it was Mazabraud who proposed it as a syndrome in 1967 [91]. The association of cardiac/cutaneous myxomas, hyperpigmentation of the skin, and endocrine overactivity was only recognized in 1985 by Carney [43]. Progress in the study of the myxoid ECM was made by the invention of the alcian blue staining in 1950 by Steedman [9], and Scott who developed the CEC method to distinguish the different GAGs in 1965 [10]. Based upon this technique, Kindblom showed in 1975 that different bone and soft tissue tumors (including myxoid ones) contained different GAGs [11]. From the late 1980s, it became clear that the ECM is a key player in tumor development and tumor progression, sustained by an exponentially growing number of publications [40]. As myxoid areas were now being recognized as an intrinsic part of a subset of tumors, Weiss and Angervall simultaneously described the myxoid variant of malignant fibrous histiocytoma/myxofibrosarcoma as a distinct entity [92, 93]. Parallel to morphological classification, an increasing number of myxoid tumors showed specific molecular genetics aberrations, such as (activating) mutations and translocations. The concept of malignant progression in myxoid tumors of soft tissue (i.e., myxoid liposarcoma) due to chromosomal instability and subsequent secondary genetic events was described in 1990 by Orndal et al. [94]. Nowadays, classification of myxoid tumors of soft tissues is based upon clinicopathological and molecular/cytogenetic aberrations as published in the 2002 WHO classification [7]

the basis of macroscopical and microscopical features (necrosis, nuclear atypia, and mitotic figures; Fig. 2) [6]. Today, myxoid tumors of soft tissue are classified according to the World Health Organization (WHO) formulation based on clinicopathological criteria and specific molecular/cytogenetic aberrations (Table 1) [7, 8]. So what is left of the term "myxoid" 150 years after Virchow? What do today's pathologists mean by it, and what does the myxoid extracellular matrix (ECM) tell the pathologist? What is the exact composition of this myxoid ECM and does it have a function? Here, we give an overview of the composition and constituents of the myxoid ECM as known so far and demonstrate the heterogeneity of the myxoid ECM among different tumors. We discuss the possible role of the predominant constituents of the myxoid ECM and attempt to relate them to differences in clinical behavior. Finally, we will speculate on the potential relevance of this knowledge in daily pathological practice.

Composition of the myxoid extracellular matrix

Glycosaminoglycans and proteoglycans

Substantial progress in the study of the myxoid ECM was made after the introduction of alcian blue staining in 1950 [9]. John Scott was one of the pioneers who used this histochemical stain to distinguish between the different glycosaminoglycans (GAGs) in tissue sections [10]. Kindblom et al. showed that the myxoid ECM of various (non)neoplastic tissues, i.e., Wharton's jelly and myxoid tumors of soft tissue, contained large amounts of GAGs

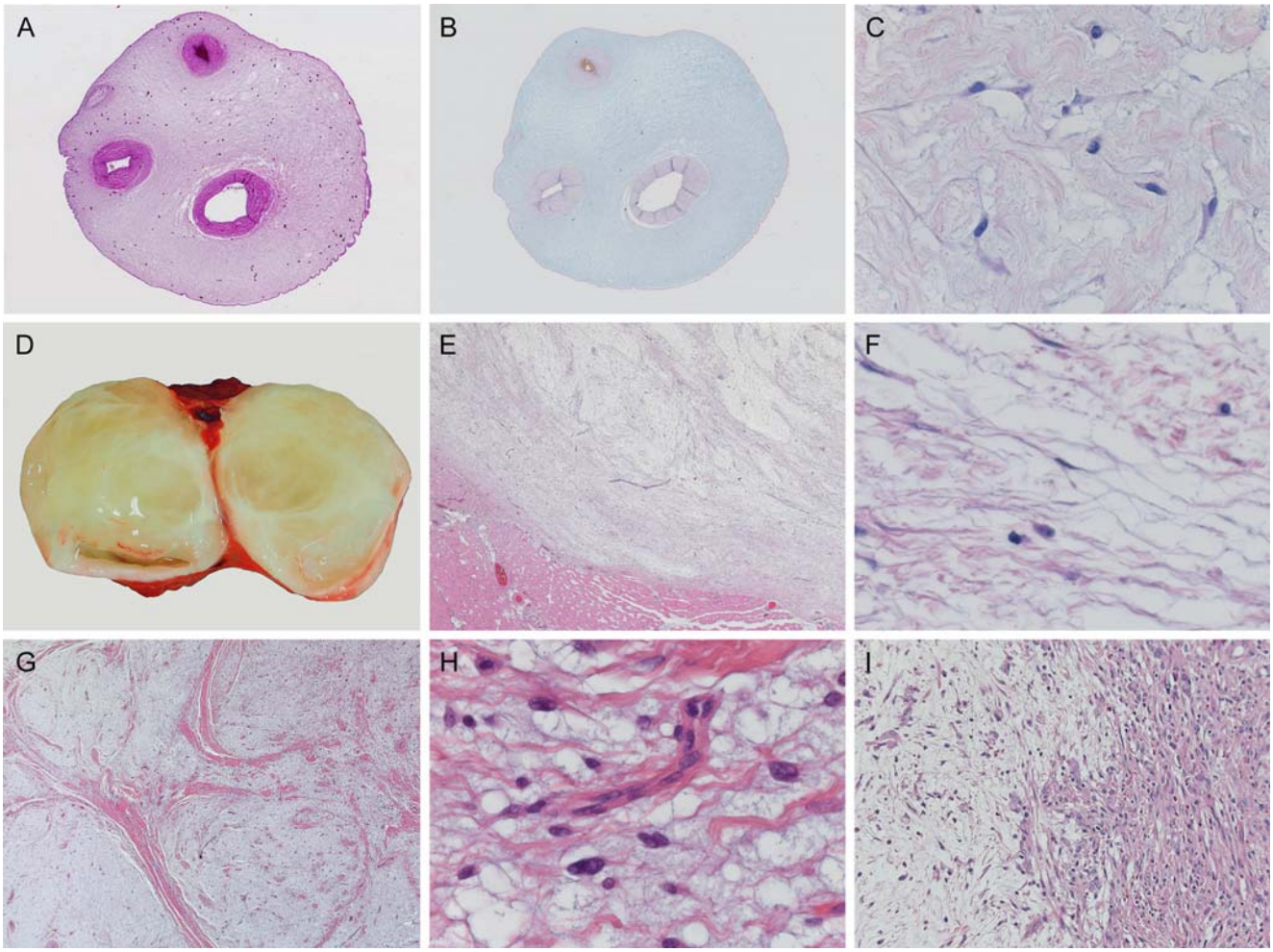

Fig. 2 Characteristic macroscopy and histomorphology of the myxoid ECM. Rudolph Virchow introduced the term myxoma for those tumors morphologically resembling Wharton's jelly of the umbilical cord (**a**), which contains large amounts of GAGs as detected by alcian blue (**b**). High-power image of Wharton's jelly showing abundant myxoid ECM containing fibrillary collagens, interspersed between myofibroblast-like stroma cells (**c**). Intramuscular myxoma characteristically has a gelatinous appearance on cut surface (**d**) and is well circumscribed towards its peripheral tissue (**e**). On higher magnification, it shows the same abundant myxoid ECM as the umbilical cord (**c**) and no significant atypia of the sparse tumor cells (**f**). Histological criteria are still a hallmark of diagnosis, showing characteristic lobulated, hypocellular morphology of grade I myxofibrosarcoma at low magnification (**g**).Curvilinear blood vessels are often seen in grade I myxofibrosarcoma (but are not diagnostic), whereas tumor cells show vesicular, slightly atypical nuclei compared to intramuscular myxoma (**h**). Another hallmark of myxofibrosarcoma is areas with abrupt transition of grade (**i**) which was already mentioned by Mentzel et al. [95]

(Figs. 1 and 2) [11]. GAGs are large macromolecules abundantly present in pericellular and extracellular matrices and consist of unbranched polysaccharide chains of disaccharides which are often sulfated. There are six different types of GAGs: hyaluronic acid (HA), keratin sulfate, chondroitin sulfate, dermatan sulfate, heparan sulfate, and heparin [12]. GAGs form proteoglycans (PGs) once covalently attached to specific core proteins. Core proteins of PGs are synthesized in the endoplasmic reticulum and post-translationally modified as they pass through the Golgi apparatus where hexuronic acid and hexosamine groups are attached. The exception is HA, which is synthesized directly under the cytoplasmic membrane by the hyaluronic acid synthetases 1, 2, and 3 [12]. The most common classification of the different PGs is based upon the properties of the core protein. The three main PG families present in the ECM are lecticans, small leucine-rich proteoglycans (SLRPs), and other ECM PG [13]. Lecticans always contain both a hyaluronan-binding domain and a C-type lectin domain. The lectican family includes: aggrecan, versican, neurocan, and brevican that can be found at different locations (Table 3) [12]. SLRPs can be found extracellularly and intracellularly and at the cell surface. They contain nine to 12 tandem repeats of leucine-rich motifs which involve their collagen-binding domains. The SLRP family includes decorin, biglycan, asporin, ECM

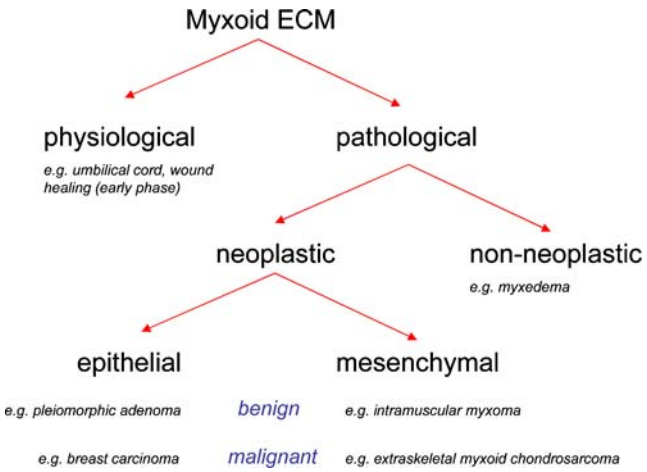

Fig. 3 Myxoid ECM is a ubiquitously histological feature in physiological and pathological conditions. Myxoid ECM is a morphological feature in physiological and pathological conditions, such as in myxedema due to increased production of HA. Myxoid areas/changes are also commonly present in tumors (both of epithelial and mesenchymal origin). In epithelial tumors, myxoid changes are often a secondary phenomenon, whereas in mesenchymal tumors, they are more frequently an intrinsic part of the tumor entity. This group of so-called myxoid tumors of soft tissues contains an increasing number of entities (e.g., myxofibrosarcoma, formerly called myxoid variant of malignant fibrous histiocytoma), sometimes sustained by specific distinct molecular/cytogenetic aberrations (e.g., myxoid liposarcoma)

protein 2, keratocan, proline/arginine-rich and leucine-rich repeat proteins, osteoadherin, lumican, fibromodulin, opticin, epiphycan, osteoglycin, podocan, chondroadherin, and nyctalopin [14]. ECM PGs do not show significant homology in the content of their core proteins. Perlecan, agrin, and collagen types XV and XVIII belong in this family [14]. Various GAGs and PGs have been identified in the myxoid ECM (Table 2): HA is the most common; none of them are specific for one particular lesion.

Collagens

One of the first papers addressing myxoma and its malignant counterpart ("myxosarcoma") mentioned the presence of fibrillary collagens as a hallmark for differential diagnosis [6]. Though this criterion did not last long, collagens (κολλα = glue; γηνε = that which produces) are a main component of the myxoid ECM. They are characterized by their regular, triple-stranded helix of so-called alpha-chains forming cord-like strands of 300 nm in length and 1.5 nm in diameter. A separate group of collagens is formed by the fibril-associated collagens with interrupted triple helices (FACIT) and includes collagen types XII and XIV. These collagens have several triple helical domains (collagen type domains [Col]) separated by nontriple helical domains (NC). All collagens contain large amounts of proline and glycine as well as hydroxyproline and hydroxylysine which are formed by post-translational modification. Based on their biochemical differences, more than 30 different types of collagens are recognized [15]. The most common types are I, II, III, and IV, which account for 90% of all collagens in humans. Except for collagen II, which is predominantly present in cartilage, collagen types I, III, and IV as well as VI, XII, and XIV may be found in the myxoid ECM (Table 2).

Other ECM molecules

Other structural molecules identified in the myxoid ECM are fibronectin and tenascin C (Table 2). Fibronectin is a fibril-forming glycoprotein existing in a dimeric or multimeric form. Each monomer contains several binding sites for fibrin, heparin, DNA, and cells. Fibronectin molecules consist of different repeats (types I, II, and III) and three different sites that can be alternatively spliced (EDA, EDB, and V). The dimeric, soluble form is produced by hepatocytes and lacks the alternative EDA and EDB variants. The multimeric form is extensively present in granulation tissue, basement membrane, and on cell surfaces and contains variable proportions of the EDA and EDB domains [16]. Until now, fibronectin has only been found in myxoid liposarcoma but might also be present in the ECM of other myxoid lesions (Table 2).

Tenascin C is a highly conserved glycoprotein of the ECM consisting of 300 kDa monomers, characteristically assembled in 1,800 kDa hexamers [17, 18]. It consists of several functionally independent domains of which the number is dramatically increased by alternative splicing. The N-terminal contains the cysteine-rich assembly domain, followed by EGF-like repeats, eight constant and up to nine alternatively spliced fibronectin type III repeats and a C-terminal fibrinogen-like globular domain [18]. Till today, its presence has only been shown in myxoid areas of epithelial but not (yet) in mesenchymal tumors (Table 2).

Functional role of the different constituents in the myxoid extracellular matrix

Glycosaminoglycans

GAGs have both biophysical and biochemical functions and play important roles in physiologic and neoplastic processes (Table 3) [19]. Due to their high content of sulfate and carboxyl groups, complex patterns of sulfation and uronic acid epimerizations, GAG chains confer upon PGs the diverse capacities to function as ideal physiological barriers, reservoirs for signaling proteins, and binding partners for structural macromolecules [13]. We have

Table 1 Myxoid tumors of soft tissue: overview of clinicopathological and genetic features

Myxoid tumors of soft tissue	Age	Sex	Predilection site	Molecular/cytogenetic aberrations	References
Benign					
Intramuscular myxoma (including its cellular variant)	Adults	F>M	Thigh, shoulder, buttocks, and rarely upper arm	GNAS1 mutations	[34]
Myxoid neurothekeoma	Young adults	F>M	Head, neck, and shoulders	Loss of 22q	[8]
Myxoid lipoma (myxolipoma)	Any age	F=M	Head and neck	Rearrangement of 13q and/or 16q	[8]
Myxoid chondroma	Adults	M>F	Hands and feet	Extra copies of chromosome 5 or 12q13–15 rearrangement	[8]
Myxoid neurofibroma	Any age	M=F	All over the body	NF1 mutations	[8]
Myxoid dermatofibroma	Young adults	F>M	Lower extremities	Unknown	[42]
Cardiac myxoma	Adults	F>M	Atria (predominantly left)	PRKAR1α mutations in Carney complex	[43]
Ossifying fibromyxoid tumor	Elderly	M>F	Extremities and trunk	Nonspecific cytogenetic aberrations	[8]
Cutaneous myxoid cyst	Any age	F>M	Distal and dorsal portions of fingers (and toes)	Unknown	[8]
Cutaneous myxoma (superficial angiomyxoma)	Adults	M>F	Trunk, lower extremities, head, and neck	PRKAR1α mutations in Carney complex	[43]
Myxoid nodular fasciitis	Young adults	M=F	Head, neck, and extremities	Nonspecific cytogenetic aberrations	[8, 44]
Locally aggressive					
Odontogenic myxoma	Young adults	F>M	Mandible and maxilla	PRKAR1α mutations in rare cases (not Carney complex)	[45]
Myxoinflammatory fibroblastic sarcoma	Adults	M=F	Feet, lower leg	t(1;10)(p22;q24) and amplification of chromosome 3	[46]
Aggressive angiomyxoma	Adults	F>>M	Inguinal region	Rearrangement of 12q13-15	[8]
Malignant					
Myxofibrosarcoma	Elderly	M=F	Extremities, thigh	Nonspecific cytogenetic aberrations	[47, 48]
Extraskeletal myxoid chondrosarcoma	Adults	M>F	Extremities and limb	t(9;22)(q22;q12), t(9;17)(q22;q11) or t (9;15)(q22;q21)	[49]
Low-grade fibromyxoid sarcoma	Young adults	M>F	Proximal extremities and trunk	t(7,16) (q33;p11)	[50]
Myxoid liposarcoma	Elderly	M>F	Lower extremities and thigh	t(12;16)(q13;p11) or t(12;22)(q13;q12)	[51]
Myxoid leiomyosarcoma of soft tissue	Adults	F>>M	Limbs, female genitalia, head, and neck	Nonspecific cytogenetic aberrations	[52]
Myxoid malignant peripheral nerve sheath tumor	Adults	F=M	Extremities, trunk	NF1 and TP53 mutations, P16 deletions	[8, 53]
Myxoid dermatofibrosarcoma	Adults	M=F	Trunk, groin, and extremities	t(17;22)(q22;q13)	[54]

shown that the myxoid ECM in soft tissue tumors is heterogeneous in composition and that the relative amount of each GAG is tumor-type- and tumor-grade-dependent [20]. Because of their negative charge, all GAGs, especially HA, are able to trap water molecules. Interestingly, HA is the common denominator in the myxoid ECM (Table 2). This suggests that HA is the major contributor to the edematous appearance of the myxoid ECM. As a result of the biophysical properties of GAGs (their high viscosity and low compressibility), they are ideal for tissue lubrication. On the other hand, their rigidity is responsible for the structural integrity of tissues facilitating diffusion of metabolites and cell migration [21]. The biochemical properties of GAGs are mediated by specific binding to other macromolecules. GAGs can bind to secreted proteases and antiproteases, growth factors, structural ECM proteins, and proteins expressed on (tumor) cells [22]. Chondroitin sulfate modulates cell fate as it appears to prevent apoptosis and is involved in cell proliferation. Since chondroitin sulfate is much more abundant in the ECM of extraskeletal myxoid chondrosarcoma compared to intramuscular myxoma and myxofibrosarcoma, it might, therefore, play a role in the more malignant behavior of this tumor [20]. Large multidomain ECM molecules such as collagen types I, III, V, and XIV and fibronectin contain at least one GAG binding site. This allows them to bind to heparan and chondroitin sulfates on cells or in the ECM, contributing to proper ECM formation.

Table 2 The composition of the myxoid ECM is heterogeneous but not lesion-specific

	Proteoglycans	Collagens (types)	Other ECM components	References
Non-neoplastic myxoid lesions				
Follicular mucinosis	HA			[55]
Myxedema	HA	I (III)		[56, 57]
Stenotic arteries	Versican, biglycan, perlecan, HA	I	TBFbeta1	[58, 59]
Pseudoaneurysm	Versican			[60]
Endocardiosis	HA			[61]
Valvular degeneration of the heart		I, III		[62]
Myxoid tumors of soft tissue				
Intramuscular myxoma	KS, HA, C4S, C6S	I, VI	Albumin, IgGs	[20, 34]
Myxofibrosarcoma	KS, HA, C4S, C6S	I, VI, XII, XIV	Thrombospondin Albumin, IgGs	[8, 20, 34]
Extraskeletal myxoid chondrosarcoma	C4S, C6S, HA (aggrecan)	I, III, VI (II, IV)	Albumin, IgGs	[20, 63]
Odontogenic myxoma	C4S, C6S, DS, KS, HS, aggrecan, versican, biglycan, decorin			[64]
Low-grade fibromyxoid sarcoma	HA			[65]
Myxoid neurothekeoma	HA			[66]
Myxoid lipoma (myxolipoma)	HA			[67]
Myxoid liposarcoma	HA		FN	[68]
Myxoid chondroma	HA, KS			[69]
Myxoid neurofibroma	HA, C4S, C6S			[69]
Chondromyxoid fibroma	Aggrecan	I, III, VI		[70]
Myxoid dermatofibroma	HA			[71]
Myxoid leiomyosarcoma	HA			[72]
Cardiac myxoma	C4S, C6S, (HA)			[73]
Ossifying fibromyxoid tumor		IV (II)		[74, 75]
Myxoinflammatory fibroblastic sarcoma			A1AT, A1ACT	[76]
Cutaneous myxoid cyst	HA			[77]
Aggressive angiomyxoma	HA			[78]
Cutaneous myxoma (superficial angiomyxoma)	HA			[79]
Myxoid areas in epithelial tumors				
Breast carcinoma	Aggrecan, versican, HA	I, II, IV		[80]
Pleiomorphic adenoma	Lumican, perlecan, aggrecan, C4S, C6S, DS, KS, HA	I, III, IV	FGF2, Tenascin, FN, ChM-I	[81–83]
Vulvar squamous cell carcinoma			CD44, TGF-beta3	[84]
Mixed tumor of skin		IV	Tenascin, FN	[85]
Cholangiocarcinoma	Perlecan			[86]
Miscellaneous tumors (nonsoft tissue, nonepithelial)				
Myxopapillary ependymoma	HA, CS, HS			[87]
Myxoid mesothelioma	HA			[88]
Myxoid meningioma	HA, CS			[89]

KS keratin sulfate, *HA* hyaluronic acid, *C4S* chondroitin sulfate, *C6S* chondroitin 6 sulfate, *DS* dermatan sulfate, *HS* heparan sulfate

Proteoglycans

PGs exhibit a wide variety of functions due to their structural diversity (Table 3). As PGs avidly bind proteins, they are involved in all cellular processes concerning cell–matrix, cell–cell, and ligand–receptor interactions. PGs are known to have affinity for a variety of ligands, including growth factors, cell adhesion molecules, ECM components,

Table 3 GAGs and PGs: their role in physiology and pathologic processes [19]

	Type and presence	Physiology	Pathology
C4S (CS-A)	Sulfated galactosaminoglycan; cartilage, skin and tendon	Binds Ca^{2+}, Cu^{2+} and Fe^{2+} ions; antioxidant (better then C6S and HA)	Decreased in OA, mediate adherence of plasmodium infected red blood cells
C6S (CS-C)	Sulfated galactosaminoglycan; cartilage, brain secretory granules	Reduces proinflammatory cytokines, MMPs, NO, and apoptosis	Laryngeal cancer, decreased in OA, increased in early atherosclerotic lesions
DS (CS-B)	Sulfated galactosaminoglycan; skin, blood vessels, heart, tendons, lungs	Regulation ECM integrity and cellular signaling; DS selectively activates heparin cofactor II that inactivates thrombin; carcinogenesis, wound repair, and fibrosis; DS binds water, coagulation	Dermatan sulfate accumulates abnormally in several of the mucopolysaccharidosis disorders and in myxomatous degeneration. Involved in cardiovascular disease, infection, fibrosis
HA	Lack sulfation and epimerization of glucuronic acid moiety to uronic acid, the only GAG synthesized in the cytoplasm at the plasma membrane and also the only GAG that is synthesized without core protein. Connective, epithelial and neural tissue. abundant in cartilage and bone	Early development, tissue organization, cell proliferation, facilitate migration and condensation of mesenchymal cells, participates in joint cavity formation, binds and immobilizes aggrecan, regulates osteoblast and osteoclast function. HA works as a scaffold for building PGs, suppresses cartilage degeneration and reduce pain perception, associated with cell adhesion and motility, suppresses prostaglandin E2 and IL-1 production, activates SRC, FAK, ERK and PKC whereas interaction with CD44 also regulates ERBB, PI3K, regu lates phosphorylation of BAD and hence promotes cell survival, contributes to cell proliferation and migration, bone turn over, involved in tissue repair in skin, binds to receptor CD44	Used for treatment of osteoarthritis
HS	Sulfated glucosaminoglycan; all types of cells, highly abundant in ECM of the skeleton	Coreceptors for morphogens, sequester growth factors and cytokines to regulate cell differentiation and growth, compose ECM scaffolds that make physical separation of the niche from cellular and signaling influence of surrounding environment, involved in skeletal patterning, differentiation, growth and homeostasis, critical for hematopoietic stem cell inch, Ndst1 mutation causes brain/skull defects and lung surfactant problems resulting in perinatal lethality, Ndst2 mutant have defective granule formation in mast cells, stimulates angiogenesis, osteocastogenesis, skeletal patterning, differentiation and homeostasis, coreceptor for morphogens, sequester growth factors and cytokines to regulate cell differentiation and growth, FGF-binding, binds fibronectin	Sequesters chemokines or FGF towards migrating tumor cells, promotes metastasis, multiple osteochondromas (MO)—benign bone cartilaginous tumor caused by mutant in EXT1 or EXT2, accumulated in mucopolysaccharidoses
KS	Sulfated glucosaminoglycan; N-glycan KSI or O-glycan KSII. Highly abundant in cornea and cartilage. Also found in epithelial tissue, central nervous system	Maintains proper special organization of the type I collagen fibrils and promotes transparency of cornea, cellular recognition of protein ligands, cell motility	Corneal opacity and corneal dystrophy (KS lacks GlcNAc sulfation), epithelial-derived carcinoma cells, alerted sulfation levels of KS was found in brain of Alzheimer patients
Aggrecan	O- and N-linked KSII, CS, DS, KS (HS absent), cartilage	Maintains tissue hydration, contributes to the mechanical properties of tissue, inhibits migration of neural crest cells, null mice show cartilage defects and delay in bone development	Chondrodystrophy, nanomelia, cartilage matrix deficiency (CMD), murine brachymorphism (bm), spondyloepimetaphyseal dysplasia enhanced expression in chondroblastoma, chondroma, chondrosarcoma, osteosarcoma, decreased in squamous cell carcinoma chondrodystrophy, nanomelia,

Table 3 (continued)

	Type and presence	Physiology	Pathology
			cartilage matrix deficiency, spondyloepimataphyseal dysplasia
Biglycan	CS, DS (HS absent), bone, cartilage, skin, connective tissue	Activates cell division, organization of collage fibers, increased in vascular injury, upregulates p27 and downregulates cyclin A and proliferating cell nuclear antigen, maintaining proper number of mature osteoblasts and survival of bone marrow stromal cells, organization of collagen fibers, regulator of cell cycle, binds TGF-beta	Overexpressed in pancreatic cancer and hyperplasic thymus osteoporosis
Decorin	CS, DS (HS absent), connective tissue, cornea	Inhibits collagen fiber formation by interaction with col I, col II, and col VI, inhibits cell division, adhesion, increased in vascular injury, downregulates Erbb2 and MAP kinases, upregulates p21 CDK inhibitor leading to inhibition of cell proliferation and specific induction of apoptosis in transformed cells. maintaining proper number of mature osteoblasts and maintaining survival of bone marrow stromal cells, bind nonfibril collagens XII and XIV, regulates cell proliferation, binds TGF-beta, mediates EGF signaling by binding to EGFR	Antiproliferative properties in tumor growth, overexpressed in colorectal carcinoma, colon adenocarcinoma, melanoma, osteosarcoma, basal cell carcinoma, inhibits migration of MG-63 osteosarcoma cells, reduced decorin levels were found in lung adenocarcinoma, squamous carcinoma, breast carcinoma, hepatocellular carcinoma and ovarian tumors, may regulate tumor angiogenesis, overexpression is often associated with shift from DS to CS, osteoporosis
Lumican	KS, cornea	Upregulates p27 and downregulates cyclin A and proliferating cell nuclear antigen, regulates collagen fibril organization and circumferential growth, corneal transparency, and epithelial cell migration and tissue repair	Upregulated in pancreatic, colorectal and breast cancers, stroma of salivary pleiotropic adenoma, reduced expression is correlated with progression of breast carcinoma
Perlecan	HS, CS, cartilage, limb bud mesenchyme, articular cartilage, bone marrow stroma, all basal membranes, vasculature	Growth factor signaling, collagen fibrillogenesis, structural stability, vasculogenesis, endorepellin, antiangiogenic factor, chondrocyte proliferation and differentiation, collagen I and II fibrillogenesis, vasculogenesis, mediator of Shh signaling, Wnt signaling, TGF-beta signaling in the skeleton, regulates FGF2 signaling	Schwartz–Jampel syndrome, dyssegmental dysplasia Silverman–Handmaker type (DDSH), perlecan-null embryo chondroplasia, prostate tumor metastasis
Versican	C6S>C4S>DS (HS, KS absent), connective tissue, aorta, brain; fibroblasts. important for vascular biology	Lipid retention, modification and accumulation, hydration of ECM, cell proliferation, migration, embryo development, binds HA, CD44, and chemokines	Promotes tumor growth and spread, expressed in the stroma of nearly all human cancers (prostate, breast, lung, ovarian cancers and odontogenic tumors, melanoma, brain tumors, pharyngeal squamous cell carcinoma, keratinocyte tumors, atherosclerosis)

enzymes, and enzyme inhibitors [22]. Lecticans bind other ECM proteins with its C-type lectin motif, facilitating the formation of networks permissive for cell growth [23]. For example, aggrecan and versican associate tightly with both HA, thereby maintaining tissue hydration. Due to the EGF-like repeats, lecticans are directly involved in growth control. Versican stimulates the proliferation of fibroblasts and is highly expressed by fast-growing cells and present in myxoid areas of both reactive and neoplastic (mesenchymal and epithelial) lesions (Table 2) [24].

Small leucine-rich proteoglycans

SLRPs are structurally and functionally related ECM molecules and abundantly expressed in connective tissues. Decorin and biglycan bind to collagen and influence collagen fibrillo-

genesis and ECM assembly in various ways: (a) due to its curved shape, decorin is able to bind to collagen types I, II, VI, and XIV linking them together and to fibronectin [25], (b) by decorating collagen fibers, decorin protects them from degradation by collagenases [25, 26], and (c) by its attached GAG chain, decorin is capable of modulating the activity of TGF-beta, which plays a central role in fibrogenesis [13, 25, 27]. Biglycan- and decorin-deficient mice show irregular and defective collagen fibrils, fragile skin, and a phenotype that closely resembles that of patients with Ehlers–Danlos syndrome [28]. In wound healing, there is a spatial temporal regulation of the expression of the different SLRPs (decorin, lumican, fibromodulin, and biglycan) tightly controlling the transformation of the myxoid ECM of granulation tissue towards fibrotic scar formation [29]. Myxoid areas in pleomorphic adenoma of the salivary gland and odontogenic myxoma lack expression of biglycan, lumican, and decorin, whereas these SLRPs are diffusely present in the fibrotic parts of the ECM of these tumors (Table 2). This suggests that the absence of SLRPs might contribute to impaired ECM formation resulting in a mere myxoid morphology.

Collagens

As form follows function [30], different collagens have different properties. In the initial phase of wound healing, collagen type I is quickly produced by fibroblasts and replaced by collagen type III in the later stage of scar formation [29]. The FACIT collagen types XII and XIV do not form collagen fibrils themselves but associate with fibrillary collagens, such as collagen type I, decorin, and GAGs, linking them together [31–33]. Collagen type XIV interacts with dermatan sulfate sequences on the single chondroitin sulfate/dermatan sulfate chain attached to decorin, thereby providing a link between the fibril-forming and the fibril-associated collagens [32]. Collagen type XIV is expressed significantly higher in grade I myxofibrosarcoma than in intramuscular myxoma (including its cellular variant) [34]. On one hand, this might have implications for ECM assembly and tumor development, thereby playing a potential role in the different biology and clinical behavior of these different entities; on the other hand, the effect of cell–ECM interaction in these tumors might work the other way around, as collagen XIV induces differentiation of fibroblastic cells [35]. Higher expression of collagen XIV in myxofibrosarcoma is associated with a more mature morphology of the tumor cells compared to intramuscular myxoma [5].

Other ECM molecules

Fibronectin plays a role in various biological processes, such as wound healing, host defense, regulation of ECM assembly, adhesion, and proliferation [36]. It is also a key molecule in cell–ECM signaling, and aberrant activation of fibronectin–ECM signaling has been described in many tumors [37]. Likewise, tenascin C is an ECM glycoprotein of which the spatial and temporal expression is tightly regulated during fetal development [38]. It has been shown that the tenascin C-encoding gene is upregulated in several pathologic conditions, such as wound healing, inflammation, and malignancies [38]. Elevated tenascin C expression has been found in epithelial and mesenchymal tumors, both in tumor and stromal cells, and is associated with unfavorable disease outcome (Table 2) [18]. Tenascin C attaches to cells via integrins, though the effect of this interaction on cellular signaling and tumor development is largely unknown [39].

Putative relevance for routine pathology practice

In routine general practice, one encounters a group of tumors, mesenchymal as well as epithelial, which may show variable degrees of myxoid appearance of their ECM. Myxoid tumors of soft tissue, the focus of this paper, encompass a heterogeneous group of lesions characterized by a marked abundance of extracellular mucoid/myxoid matrix (Table 1). This group of tumors exhibits a broad range of biological behavior varying from those which are entirely benign via locally aggressive (but nonmetastasizing) behavior to those which are frankly malignant; hence, accurate histopathological diagnosis is essential for appropriate clinical management. Till today, there have been no convincing data which demonstrate that the composition of the myxoid matrix significantly differ between tumors (both of mesenchymal and/or epithelial origin) and reactive lesions. From a biochemical point of view, the term “myxoid” is best considered a wastebasket of many different proteins and other (macro)molecules which might all have a different function (Tables 2 and 3). While determination of the different GAGs in myxoid tumors is interesting from a research point of view, Scott’s critical electrolyte concentration (CEC) method is no longer a routinely used technique by pathologists. Most myxoid tumors of soft tissue tumors contain HA (Table 2), and consequently, its detection is no longer regarded as discriminatory in differential diagnoses. Outside the academic setting (where recourse to sophisticated biochemical and molecular genetics techniques is generally not possible), when confronted with challenging myxoid lesions, the diagnostic process relies primarily on careful and discriminatory histopathological evaluation in order to reach a correct diagnosis. Routine histological criteria (e.g., tumor demarcation, growth and vascular pattern, and nuclear atypia) remain the hallmarks of diagnosis. (Immuno-) histochemistry may be useful as a adjunct in the setting of

certain differential diagnostic considerations, but is often not discriminatory and, therefore, not diagnostically useful [8]. Molecular cytogenetics is of increasing importance for diagnosis in difficult cases, as the genetic makeup of an increasing number of myxoid tumors of soft tissue is being elucidated (Table 1). Next to genetic causes (such as driver mutations, translocations, or gene amplifications), environmental factors have been shown to play an important role in tumorigenesis of both epithelial and mesenchymal tumors [40]. Virchow already mentioned the possible relationship between the histological appearance of the myxoid ECM of tumors and their differences in biological behavior [1]. It is very tempting to believe that GAGs and PGs play an important role in the biology of myxoid lesions rather than just being a byproduct of (myo)fibroblastic differentiation. Intramuscular myxoma expresses significantly less decorin and collagen VI and XIV (both protein and mRNA level) than grade I myxofibrosarcoma [34]. Next to decorin, liquid chromatography–mass spectrometry revealed other SLRPs (i.e., lumican, prolargin 4, biglycan) present in tumor lysates of grade I myxofibrosarcoma but not of intramuscular myxoma [34]. This suggest that ECM formation in intramuscular myxoma is impaired compared to grade I myxofibrosarcoma. Increased ECM rigidity activates integrins and subsequently leads to stimulation of the rho/Rock pathway and cell migration and invasion [41]. In this respect, the morphological similarity between the process of wound healing and myxoid changes/areas in (non)neoplastic lesions is rather striking. In the early phase, granulation tissue shows a loose, edematous/myxoid ECM rich in GAGs. In the subsequent phase, there is structural organization of the ECM with deposition of collagens produced by myofibroblasts which locally (de)differentiate from fibroblast/smooth muscle cells or are derived from the bone marrow. The term “myxoid” might not only be synonymous with (aberrant turnover and) the presence of GAGs, but also reflects the absence of proper ECM assembly or incomplete ECM formation. This might well explain that a myxoid morphology of the ECM is not specific at all and can be seen in reactive/non-neoplastic processes as well as in benign and malignant tumors (Fig. 3). As already extensively discussed in this paper, the ECM is dependent on the interplay of various macromolecules (polysaccharides and proteins) which determine its texture and consistency. It is becoming increasingly clear that, within this group of lesions, various tumor types may show differences in the biological composition of their myxoid matrix, as determined by differences in the relative proportions of the constituent macromolecules and the presence or absence of specific stromal constituents. Clearly, this is an important and highly relevant area for further research in order to identify tumor-specific markers and to consequently develop economically viable and user-friendly detection methods to facilitate the diagnostic process and ensure increasingly accurate histopathologic diagnosis.

Acknowledgements Stefan M. Willems was financially supported by a grant from The Netherlands Organization for Health Research and Development (project no. 920-03-403).

Conflict of interest statement We declare that we have no conflict of interest.

Open Access This article is distributed under the terms of the Creative Commons Attribution Noncommercial License which permits any noncommercial use, distribution, and reproduction in any medium, provided the original author(s) and source are credited.

References

1. Virchow R (1858) Die cellularpathologie in ihrer Begrundung auf physiologische und pathologische Gewebelehre. Hirschwald, Berlin
2. Dunglison R (1865) Medical lexicon. A dictionary of medical science. Blanchard and Lea, Philadelphia
3. Muller J (1838) Uber den feineren bau und die formen der krankhaften geschwulste. Haberling, Berlin
4. Bryant T (1802) Tumors and tumor formation. Churchill, New York.
5. Stout AP (1948) Myxoma, the tumor of primitive mesenchyme. Ann Surg 127:706–719
6. Sponsel KH, McDonald JR, Ghormley RK (1952) Myxoma and myxosarcoma of the soft tissues of the extremities. J Bone Joint Surg Am 34(A):820–826
7. Fletcher CDM, Unni KK, Mertens F (2002) WHO classification of tumours. Pathology and genetics of tumours of soft tissue and bone. IARC, Lyon
8. Graadt van Roggen JF, Hogendoorn PCW, Fletcher CDM (1999) Myxoid tumours of soft tissue. Histopathology 35:291–312
9. Steedman HF (1950) Alcian Blue 8 GS: a new stain for mucin. Q J Microsc Sci 3:477–479
10. Scott JE, Dorling J (1965) Differential staining of acid glycosaminoglycans (mucopolysaccharides) by alcian blue in salt solutions. Histochemie 5:221–233
11. Kindblom LG, Angervall L (1975) Histochemical characterization of mucosubstances in bone and soft tissue-tumors. Cancer 36:985–994
12. Gandhi NS, Mancera RL (2008) The structure of glycosaminoglycans and their interactions with proteins. Chem Biol Drug Des 72:455–482
13. Kresse H, Schonherr E (2001) Proteoglycans of the extracellular matrix and growth control. J Cell Physiol 189:266–274
14. Schaefer L, Iozzo RV (2008) Biological functions of the small leucine-rich proteoglycans: from genetics to signal transduction. J Biol Chem 283:21305–21309
15. Kadler KE, Hill A, Canty-Laird EG (2008) Collagen fibrillogenesis: fibronectin, integrins, and minor collagens as organizers and nucleators. Curr Opin Cell Biol 20:495–501
16. White ES, Baralle FE, Muro AF (2008) New insights into form and function of fibronectin splice variants. J Pathol 216:1–14
17. Bosman FT, Stamenkovic I (2003) Functional structure and composition of the extracellular matrix. J Pathol 200:423–428

18. Orend G, Chiquet-Ehrismann R (2006) Tenascin-C induced signaling in cancer. Cancer Lett 244:143–163
19. Lamoureux F, Baud'huin M, Duplomb L et al (2007) Proteoglycans: key partners in bone cell biology. BioEssays 29:758–771
20. Willems SM, Schrage YM, Baelde JJ et al (2008) Myxoid tumours of soft tissue: the so-called myxoid extracellular matrix is heterogeneous in composition. Histopathology 52:465–474
21. Almond A (2007) Hyaluronan. Cell Mol Life Sci 64:1591–1596
22. Rodgers KD, San Antonio JD, Jacenko O (2008) Heparan sulfate proteoglycans: a GAGgle of skeletal-hematopoietic regulators. Dev Dyn 237:2622–2642
23. Evanko SP, Angello JC, Wight TN (1999) Formation of hyaluronan- and versican-rich pericellular matrix is required for proliferation and migration of vascular smooth muscle cells. Arterioscler Thromb Vasc Biol 19:1004–1013
24. Zimmermann DR, Dours-Zimmermann MT, Schubert M et al (1994) Versican is expressed in the proliferating zone in the epidermis and in association with the elastic network of the dermis. J Cell Biol 124:817–825
25. McEwan PA, Scott PG, Bishop PN et al (2006) Structural correlations in the family of small leucine-rich repeat proteins and proteoglycans. J Struct Biol 155:294–305
26. Geng Y, McQuillan D, Roughley PJ (2006) SLRP interaction can protect collagen fibrils from cleavage by collagenases. Matrix Biol 25:484–491
27. Ferdous Z, Wei VM, Iozzo R et al (2007) Decorin-transforming growth factor- interaction regulates matrix organization and mechanical characteristics of three-dimensional collagen matrices. J Biol Chem 282:35887–35898
28. Danielson KG, Baribault H, Holmes DF et al (1997) Targeted disruption of decorin leads to abnormal collagen fibril morphology and skin fragility. J Cell Biol 136:729–743
29. Martinez DA, Vailas AC, Vanderby R et al (2007) Temporal extracellular matrix adaptations in ligament during wound healing and hindlimb unloading. Am J Physiol Regul Integr Comp Physiol 293:R1552–R1560
30. Sullivan LH (1896) The tall office building artistically considered. Lippincott's Magazine 57:403–409
31. Ehnis T, Dieterich W, Bauer M et al (1997) Localization of a binding site for the proteoglycan decorin on collagen XIV (undulin). J Biol Chem 272:20414–20419
32. Ehnis T, Dieterich W, Bauer M et al (1996) A chondroitin/dermatan sulfate form of CD44 is a receptor for collagen XIV (undulin). Exp Cell Res 229:388–397
33. Canty EG, Kadler KE (2005) Procollagen trafficking, processing and fibrillogenesis. J Cell Sci 118:1341–1353
34. Willems SM, Mohseny AB, Balog C et al (2009) Cellular/intramuscular myxoma and grade I myxofibrosarcoma are characterized by distinct genetic alterations and specific composition of their extracellular matrix. J Cell Mol Med 7:1291–1301
35. Ruehl M, Erben U, Schuppan D et al (2005) The elongated first fibronectin type III domain of collagen XIV is an inducer of quiescence and differentiation in fibroblasts and preadipocytes. J Biol Chem 280:38537–38543
36. Vakonakis I, Campbell ID (2007) Extracellular matrix: from atomic resolution to ultrastructure. Curr Opin Cell Biol 19:578–583
37. Larsen M, Artym VV, Green JA et al (2006) The matrix reorganized: extracellular matrix remodeling and integrin signaling. Curr Opin Cell Biol 18:463–471
38. Harty M, Neff AW, King MW et al (2003) Regeneration or scarring: an immunologic perspective. Dev Dyn 226:268–279
39. Jones FS, Jones PL (2000) The tenascin family of ECM glycoproteins: structure, function, and regulation during embryonic development and tissue remodeling. Dev Dyn 218:235–259
40. De Wever O, Mareel M (2003) Role of tissue stroma in cancer cell invasion. J Pathol 200:429–447
41. Berrier AL, Yamada KM (2007) Cell–matrix adhesion. J Cell Physiol 213:565–573
42. Fletcher CDM (1990) Benign fibrous histiocytoma of subcutaneous and deep soft tissue: a clinicopathologic analysis of 21 cases. Am J Surg Pathol 14:801–809
43. Carney JA, Gordon H, Carpenter PC et al (1985) The complex of myxomas, spotty pigmentation, and endocrine overactivity. Medicine (Baltimore) 64:270–283
44. Meng GZ, Zhang HY, Zhang Z et al (2009) Myofibroblastic sarcoma vs nodular fasciitis: a comparative study of chromosomal imbalances. Am J Clin Pathol 131:701–709
45. Perdigao PF, Stergiopoulos SG, De Marco L et al (2005) Molecular and immunohistochemical investigation of protein kinase a regulatory subunit type 1A (PRKAR1A) in odontogenic myxomas. Genes Chromosomes Cancer 44:204–211
46. Hallor KH, Sciot R, Staaf J et al (2009) Two genetic pathways, t(1;10) and amplification of 3p11–12, in myxoinflammatory fibroblastic sarcoma, haemosiderotic fibrolipomatous tumour, and morphologically similar lesions. J Pathol 217:716–727
47. Calonje E, Mentzel T, Fletcher CDM (1994) Cellular benign fibrous histiocytoma. Clinicopathologic analysis of 74 cases of a distinctive variant of cutaneous fibrous histiocytoma with frequent recurrence. Am J Surg Pathol 18:668–676
48. Willems SM, Debiec-Rychter M, Szuhai K et al (2006) Local recurrence of myxofibrosarcoma is associated with increase in tumour grade and cytogenetic aberrations, suggesting a multistep tumour progression model. Mod Pathol 19:407–416
49. Enzinger FM, Shiraki M (1972) Extraskeletal myxoid chondrosarcoma. An analysis of 34 cases. Hum Pathol 3:421–435
50. Evans HL (1993) Low-grade fibromyxoid sarcoma. A report of 12 cases. Am J Surg Pathol 17:595–600
51. Turc-Carel C, Limon J, Dal CP et al (1986) Cytogenetic studies of adipose tissue tumors. II. Recurrent reciprocal translocation t(12;16)(q13;p11) in myxoid liposarcomas. Cancer Genet Cytogenet 23:291–299
52. Rubin BP, Fletcher CDM (2000) Myxoid leiomyosarcoma of soft tissue, an underrecognized variant. Am J Surg Pathol 24:927–936
53. Brems H, Beert E, De Ravel RT et al (2009) Mechanisms in the pathogenesis of malignant tumours in neurofibromatosis type 1. Lancet Oncol 10:508–515
54. Pedeutour F, Simon MP, Minoletti F et al (1996) Translocation, t(17;22)(q22;q13), in dermatofibrosarcoma protuberans: a new tumor-associated chromosome rearrangement. Cytogenet Cell Genet 72:171–174
55. Kaya G, Augsburger E, Chavaz P et al (2006) CD44 and hyaluronate expression in follicular mucinosis. J Cutan Pathol 33:227–230
56. Alves MF, Filgueira AL, Lorena DE et al (1998) Type I and type III collagens in cutaneous mucinosis. Am J Dermatopathol 20:41–47
57. Lengyel J, Vertes B (1956) Hyaluronic acid studies of local myxedema and of the stroma of skin cancer. Dermatologica 113:219–225
58. Chung IM, Gold HK, Schwartz SM et al (2002) Enhanced extracellular matrix accumulation in restenosis of coronary arteries after stent deployment. J Am Coll Cardiol 40:2072–2081
59. Wight TN (2002) Versican: a versatile extracellular matrix proteoglycan in cell biology. Curr Opin Cell Biol 14:617–623
60. Burke AP, Jarvelainen H, Kolodgie FD et al (2004) Superficial pseudoaneurysms: clinicopathologic aspects and involvement of extracellular matrix proteoglycans. Mod Pathol 17:482–488
61. Black A, French AT, Dukes-McEwan J et al (2005) Ultrastructural morphologic evaluation of the phenotype of valvular interstitial cells in dogs with myxomatous degeneration of the mitral valve. Am J Vet Res 66:1408–1414

62. Nasuti JF, Zhang PJ, Feldman MD et al (2004) Fibrillin and other matrix proteins in mitral valve prolapse syndrome. Ann Thorac Surg 77:532–536
63. Aigner T, Oliveira AM, Nascimento AG (2004) Extraskeletal myxoid chondrosarcomas do not show a chondrocytic phenotype. Mod Pathol 17:214–221
64. Zhao M, Lu Y, Takata T, Mock D, Nikia H et al (1999) Immunohistochemical and histochemical characterization of the mucosubstances of odontogenic myxoma: histogenesis and differential diagnosis. Pathol Res Pract 195:391–397
65. Zamecnik M, Michal M (2000) Low-grade fibromyxoid sarcoma: a report of eight cases with histologic, immunohistochemical, and ultrastructural study. Ann Diagn Pathol 4:207–217
66. Gallager RL, Helwig EB (1980) Neurothekeoma—a benign cutaneous tumor of neural origin. Am J Clin Pathol 74:759–764
67. Hajdu SI (1979) Pathology of soft tissue Tumors. Lea and Febiger, Philadelphia
68. Fukuda T, Tsuneyoshi M (2000) Adhesion proteins, cellular morphology and fibrous components around the cell/extracellular-matrix interface in myxoid liposarcomas. J Cancer Res Clin Oncol 126:320–324
69. Mackenzie DH (1981) The myxoid tumors of somatic soft tissues. Am J Surg Pathol 5:443–458
70. Soder S, Inwards C, Muller S et al (2001) Cell biology and matrix biochemistry of chondromyxoid fibroma. Am J Clin Pathol 116:271–277
71. Calikoglu E, Chavaz P, Saurat JH et al (2003) Decreased CD44 expression and stromal hyaluronate accumulation in myxoid dermatofibroma. Dermatology 207:104–106
72. Yasui W, Oda N, Ito H et al (1991) Myxoid leiomyosarcoma of the stomach: a case report. Jpn J Clin Oncol 21:447–452
73. Lam RM, Hawkins ET, Roszka J (1984) Cardiac myxoma: histochemical and ultrastructural localization of glycosaminoglycans and proteoglycans. Ultrastruct Pathol 6:69–81
74. Folpe AL, Weiss SW (2003) Ossifying fibromyxoid tumor of soft parts: a clinicopathologic study of 70 cases with emphasis on atypical and malignant variants. Am J Surg Pathol 27:421–431
75. Yang P, Hirose T, Hasegawa T et al (1994) Ossifying fibromyxoid tumor of soft parts: a morphological and immunohistochemical study. Pathol Int 44:448–453
76. Hassanein AM, Atkinson SP, Al-Quran SZ et al (2008) Acral myxoinflammatory fibroblastic sarcomas: are they all low-grade neoplasms? J Cutan Pathol 35:186–191
77. Johnson WC, Graham JH, Helwig EB (1965) Cutaneous myxoid cyst. A clinicopathological and histochemical study. JAMA 191:15–20
78. Begin LR, Clement PB, Kirk ME et al (1985) Aggressive angiomyxoma of pelvic soft parts: a clinicopathologic study of nine cases. Hum Pathol 16:621–628
79. Calikoglu E, Augsburger E, Masouye I et al (2002) Hyaluronate accumulation and decreased CD44 expression in perifollicular solitary cutaneous myxoma. Dermatology 205:122–126
80. Kusafuka K, Muramatsu K, Kasami M et al (2008) Cartilaginous features in matrix-producing carcinoma of the breast: four cases report with histochemical and immunohistochemical analysis of matrix molecules. Mod Pathol 21:1282–1292
81. Kusafuka K, Ishiwata T, Sugisaki Y et al (2004) Lumican expression is associated with the formation of mesenchyme-like elements in salivary pleomorphic adenomas. J Pathol 203:953–960
82. Nara Y, Takeuchi J, Yoshida K et al (1991) Immunohistochemical characterisation of extracellular matrix components of salivary gland tumours. Br J Cancer 64:307–314
83. Kusafuka K, Hiraki Y, Shukunami C et al (2001) Cartilage-specific matrix protein chondromodulin-I is associated with chondroid formation in salivary pleomorphic adenomas: immunohistochemical analysis. Am J Pathol 158:1465–1472
84. Ambros RA, Kallakury BV, Malfetano JH et al (1996) Cytokine, cell adhesion receptor, and tumor suppressor gene expression in vulvar squamous carcinoma: correlation with prominent fibromyxoid stromal response. Int J Gynecol Pathol 15:320–325
85. Franchi A, Dini M, Paglierani M et al (1995) Immunolocalization of extracellular matrix components in mixed tumors of the skin. Am J Dermatopathol 17:36–41
86. Sabit H, Tsuneyama K, Shimonishi T et al (2001) Enhanced expression of basement-membrane-type heparan sulfate proteoglycan in tumor fibro-myxoid stroma of intrahepatic cholangiocarcinoma. Pathol Int 51:248–256
87. Giordana MT, Bertolotto A, Mauro A et al (1982) Glycosaminoglycans in human cerebral tumors. Part II. Histochemical findings and correlations. Acta Neuropathol 57:299–305
88. Shia J, Qin J, Erlandson RA et al (2005) Malignant mesothelioma with a pronounced myxoid stroma: a clinical and pathological evaluation of 19 cases. Virchows Arch 447:828–834
89. Harrison JD, Rose PE (1985) Myxoid meningioma: histochemistry and electron microscopy. Acta Neuropathol 68:80–82
90. Henschen F (1926) Fall von ostitis Fibrosa mit multiplen Tumoren in deer umgebenden Muskulatur. Verh Dtsch Ges Pathol 21:93–97
91. Mazabraud A, Semat P, Roze R (1967) A propos de l'association de fibromyxomes des tissus mous à la dysplasie fibreuse des os. Presse Med 75:2223–2228
92. Weiss SW, Enzinger FM (1977) Myxoid variant of malignant fibrous histiocytoma. Cancer 39:1672–1685
93. Angervall L, Kindblom LG, Merck C (1977) Myxofibrosarcoma. A study of 30 cases. Acta Pathol Microbiol Scand A 85A:127–140
94. Orndal C, Mandahl N, Rydholm A et al (1990) Chromosomal evolution and tumor progression in a myxoid liposarcoma. Acta Orthop Scand 61:99–105
95. Mentzel T, Calonje E, Wadden C et al (1996) Myxofibrosarcoma. Clinicopathologic analysis of 75 cases with emphasis on the low-grade variant. Am J Surg Pathol 20:391–405

Virchows Arch (2010) 456:193–199
DOI 10.1007/s00428-009-0828-5

REVIEW AND PERSPECTIVE

Molecular pathology of sarcomas: concepts and clinical implications

Judith V. M. G. Bovée · Pancras C. W. Hogendoorn

Received: 29 June 2009 / Revised: 18 August 2009 / Accepted: 24 August 2009 / Published online: 29 September 2009
© The Author(s) 2009. This article is published with open access at Springerlink.com

Abstract The molecular genetic changes that have been described in sarcomas over the past era have aided our understanding of their pathogenesis. The majority of sarcomas carry nonspecific genetic changes within a background of a complex karyotype. These constitute the challenges in sarcoma research for unraveling a putative multistep genetic model, such as for chondrosarcoma, and finding targets for therapeutic strategies. Approximately 15–20% of mesenchymal tumors carry a specific translocation within a relatively simple karyotype. The resulting fusion products act either as transcription factors upregulating genes responsible for tumor growth, as for instance in Ewing sarcoma, or translocate a highly active promoter in front of an oncogene driving tumor formation, as for instance in aneurysmal bone cyst. In addition, a small subset of mesenchymal tumors have specific somatic mutations driving oncogenesis. The specific genetic changes unraveled so far had great impact on the classification of bone and soft tissue tumors. In addition, these changes can assist the pathologist in the differential diagnosis of some of these entities, especially within the groups of small blue round cell tumors and spindle cell tumors, if performed in specialized centers. While a putative association between certain fusion products and outcome is still under debate, the role of predicting response of targeted therapy has been well established for KIT and PDGFRA mutations in gastrointestinal stromal tumors.

Keywords Bone neoplasm · Soft tissue tumours · Cytogenetics · Molecular pathology · Diagnostics

J. V. M. G. Bovée · P. C. W. Hogendoorn (✉)
Department of Pathology, Leiden University Medical Center,
P.O. Box 9600, L1-Q, 2300 RC Leiden, The Netherlands
e-mail: p.c.w.hogendoorn@lumc.nl

Introduction

More and more knowledge has become available aiding our understanding of the genetic background of cancer. Chromosomal translocations or gene mutations can give the cells in which they arise a growth advantage, ultimately leading to cancer. For bone and soft tissue tumors, an increasing amount of tumor-specific genetic data has become available. Approximately 15–20% of mesenchymal tumors carry a specific translocation [1] and have relatively simple karyotypes. These translocations are restricted to specific tumor types; in Ewing sarcoma, synovial sarcoma, and myxoid liposarcoma up to 90–95% of the tumors carry a tumor type-specific translocation. In addition, some tumors carry specific somatic gene mutations (e.g., KIT or PDGFRA mutations in gastrointestinal stromal tumors). In contrast, in the more frequent sarcomas such as osteosarcoma, chondrosarcoma, leiomyosarcoma, or high-grade pleomorphic sarcoma, more complex karyotypes are found with numerous gains and losses, without specific genetic alterations [2].

These molecular data help us to understand the pathogenesis of sarcomas. Moreover, they constitute the basis of the 2002 WHO classification of bone and soft tissue tumors, integrating morphology with genetics [3, 4]. Tumor-specific molecular changes have found their way in daily clinical practice as molecular diagnostic tools to assist the pathologist in diagnosing these lesions, but may also serve as markers to detect minimal residual disease and to predict clinical outcome, although the latter is still somewhat controversial. Finally, our increasing knowledge of the genetic background of sarcomas, including the ones without specific genetic changes, will hopefully enable the development of more types of targeted therapeutic strategies.

Clues about sarcoma pathogenesis

Sarcomas with specific reciprocal translocations

For translocation-derived sarcomas, such as Ewing sarcoma, the occurrence of the translocation is considered a very early step in tumorigenesis [5]. In many of the translocations in sarcomas, the EWSR1 or the FUS gene is involved. These promiscuous genes are strongly homologous and encode RNA-binding proteins. Most probably, EWSR1 and FUS have a similar effect when they are involved in a chromosomal translocation. The type of DNA-binding domain originating from the fusion partner probably determines the tumor type that is induced by the translocation.

These hybrid oncoproteins subsequently act as aberrant transcription factors dysregulating gene expression patterns initiating tumor formation. Target genes of the EWSR1-ETS fusion products were shown to stimulate cell proliferation (upregulation of PDGF-C, CCDN1, *c-MYC*), evade growth inhibition (downregulation of cyclin-dependent kinase inhibitors and TGF-beta receptor type II), escape from senescence (upregulation of hTERT), escape from apoptosis (repression of IGFBP-3 promoter), induce angiogenesis (VEGF), invasion and metastases (MMPs) [6].

Alternative to aberrant transcription factor activity of fusion products, some other mechanisms of translocation-based tumorigenesis have been described. One of the genes involved in a translocation can be placed under control of the other gene involved in the translocation, which usually leads to over expression. The growth factor PDGFB is placed under control of the COL1A1 promoter in the COL1A1-PDGFB fusion in dermatofibrosarcoma protuberans [7]. This leads to autocrine stimulation and tumor cell proliferation through the PDGF receptor [7, 8]. Similarly, in aneurysmal bone cyst, many different translocations have been described [9, 10], all resulting in oncogenic activation of the USP6 (TRE2 and TRE17) gene on chromosome 17p13 by placing it under transcriptional control of other, highly active promoters [11]. The mechanism by which upregulation of USP6, involved in actin remodeling [12], causes ABC formation is so far unknown. Finally, in congenital fibrosarcoma, the ETV6-NTRK3 fusion product represents a chimeric tyrosine kinase in itself leading to constitutively active Ras/MAPK mitogenic pathway and PI3K/Akt pathway-mediated cell survival [13].

Sarcomas with specific somatic mutations

In addition, some mesenchymal tumors carry specific somatic mutations that upon their discovery elucidated the pathogenesis of these tumors. For instance, KIT mutations in GIST revealed its relation with the interstitial cells of Cajal. Another example is fibrous dysplasia, a benign fibro-osseous lesion in the medulla of the bone. Polyostotic fibrous dysplasia can be associated with endocrine abnormalities and cafe au lait pigmentation in nonhereditary Mc Cune Albright Syndrome (Online Mendelian inheritance in man NCBI number MIM 174800). Fibrous dysplasia has for long been regarded a nonneoplastic process. Its neoplastic nature was suggested by the occurrence of clonal chromosomal abnormalities found in cytogenetic studies [14]. Fibrous dysplasia is characterized by activating mutations in the Gs alpha (GNAS1) gene localized on chromosome 20q12–q13.3, encoding the alpha subunit of the stimulatory guanine nucleotide-binding protein (G-protein) [15]. G-proteins couple extracellular receptors to intracellular effector enzymes and ion channels, mediating the cellular response to an external stimulus. The identification of GNAS1 mutations also in Mc Cune Albright syndrome (postzygotic) and nonskeletal-isolated endocrine lesions clarified that these disorders represent a spectrum of phenotypic expressions of the same basic disorder, probably reflecting different patterns of somatic mosaicism [15]. Moreover, GNAS1 mutations are also found in (intramuscular and cellular) myxomas [16] and the cooccurrence of fibrous dysplasia and myxomas is known as Mazabraud syndrome [17]. Interestingly, GNAS1 mutations are found in the cooccurring myxomas as well and are absent in a morphological mimic of myxoma: low-grade myxofibrosarcoma [18]. Finally, inactivating mutations of the hSNF5/INI1 gene are found in rhabdoid tumors. hSNF5 is a core member of the SWI/SNF chromatin remodeling complex and hSNF5 loss leads to epigenetically based changes in transcription resulting in cell cycle progression [19] and genomically stable tumors [20].

Sarcomas with more or less specific amplifications

While in principle not tumor specific, some sarcomas are characterized by a highly reproducible amplification such as in case of atypical lipomatous tumor/ well-differentiated liposarcoma/dedifferentiated liposarcoma the amplification of CDK4 and MDM2 [21–23]. While most if not all of the aforementioned tumors harbor such an amplification and as such it can be used to recognize a lipogenic origin in the dedifferentiated areas of dedifferentiated liposarcoma, it is by no means tumor specific as similar amplifications occur for instance in osteosarcoma or chondrosarcoma [24]. This genetic marker however is in context quite useful for diagnostic purposes.

Sarcomas with nonspecific complex karyotypes

The more frequent sarcomas, like high-grade pleomorphic sarcoma, myxofibrosarcoma [25] or leiomyosarcoma [26], have complex karyotypes lacking specific genetic aberrations.

For instance, for chondrosarcoma development, a multistep genetic model is presumed. Chondrosarcomas can be either central (arising in the medullar cavity of bone) or peripheral (at the surface of bone). Peripheral chondrosarcomas arise secondarily within the cartilaginous cap of a benign osteochondroma. Osteochondromas can occur within an autosomal dominantly inherited syndrome, Multiple Osteochondromas, in which mutations occur in either EXT1 or EXT2 [27]. These encode glycosyltransferases catalyzing heparan sulphate chain elongation on heparan sulphate proteoglycans, which are important for cellular signaling of Hedgehog, Fibroblast Growth Factor, Wnt, Bone Morphogenetic Protein and Transforming Growth Factor beta. Thus, while it is clear that inactivation of EXT underlies osteochondroma development [28, 29], so far, unidentified additional genetic changes are required for malignant transformation towards secondary peripheral chondrosarcoma, resulting in more complex karyotypes including near-haploidy and polyploidization [30, 31]. In contrast, in the more common central chondrosarcoma EXT is not involved [32]. Instead, complex karyotypes are found especially in high-grade chondrosarcoma [31, 33, 34], and 96% of them contains alterations at some level in the pRb pathway [35]. Thus, the genetic background of tumors without specific genetic aberrations is slowly being elucidated.

Classification of sarcomas

Since soft tissue tumors are relatively rare compared with epithelial malignancies, they are generally regarded difficult by surgical pathologists. Soft tissue tumors constitute a very heterogeneous group of tumors containing >100 histological types and subtypes. The considerable morphological overlap between the different diagnostic entities further adds to difficulties in classification [36]. Classification is however essential since these different entities require different treatment strategies and have a different outcome. In classifying tumors, the pathologist can be assisted by immunohistochemistry and molecular diagnostics [37]. Immunohistochemistry is used to confirm the line of differentiation, while molecular techniques can identify specific chromosomal translocations or mutations. The 2002 WHO classification of bone and soft tissue tumors is mainly based on the integration of morphology and genetics [36]. This classification is at present widely accepted and used.

Use of specific molecular changes in differential diagnosis

The differential diagnosis among the groups of small blue round cell tumors and spindle cell tumors can be very difficult for pathologists due to the high number of entities and their morphological overlap. Although the morphology and immunohistochemistry remain at the cornerstone of the diagnosis, the detection of specific genetic alterations, either translocations or somatic mutations, can be very helpful. Molecular diagnostics is especially important in those cases with unusual morphology, immunohistochemistry or clinical presentation.

The term “small blue round cell” tumor encompasses a heterogeneous group of tumors that share the presence of undifferentiated small round cells with scant cytoplasm at histology. The differential diagnosis includes Ewing sarcoma/PNET, neuroblastoma, non-Hodgkin lymphoma, poorly differentiated (round cell) synovial sarcoma, rhabdomyosarcoma, small cell osteosarcoma, desmoplastic round cell tumor, and mesenchymal chondrosarcoma (Table 1). Due to the absence of distinguishing morphological features, their distinction can be difficult. Using immunohistochemistry and conventional histochemical stainings, many of these entities can already be distinguished. In addition, molecular diagnostics can be used to detect specific reciprocal translocations in Ewing sarcoma, rhabdomyosarcoma, synovial sarcoma or desmoplastic small round cell tumor. Either (Real-Time) PCR [38] on RNA isolated from frozen or paraffin-embedded tumor tissue,or FISH on paraffin-embedded slides can be used to detect these translocations. Especially in case of poorly differentiated synovial sarcoma versus Ewing sarcoma / PNET the morphology and the immunohistochemical profile can be identical requiring the demonstration of a EWSR1 or SS18 rearrangement to come to a correct diagnosis and therapy.

Spindle cell tumors share, as their name implies, a spindle cell morphology of the tumor cells. The differential diagnosis includes monophasic synovial sarcoma, leiomyosarcoma, solitary fibrous tumor, malignant peripheral nerve sheath tumor, clear cell sarcoma, fibrohistiocytic tumors, dedifferentiated liposarcoma, spindle cell rhabdomyosarcoma, and in abdominal localization, gastrointestinal stromal tumor (Table 2). Monophasic synovial sarcoma and clear cell sarcoma carry specific chromosomal translocations that can be used. This is especially helpful in the distinction of MPNST and monophasic synovial sarcoma, which can be morphologically and immunohistochemically indistinguishable. KIT or PDGFRA mutation analysis can be helpful to diagnose gastrointestinal stromal tumor, especially in the small proportion in which CD117 is negative. The diagnosis of dedifferentiated liposarcoma especially if the well-differentiated liposarcoma component is not present at morphology can be facilitated by demonstrating the 12q13 amplification that is characteristic for these lesions, either by immunohistochemistry or FISH for amplification of MDM2 [39, 40].

Table 1 Distinguishing features in small blue round cell tumors

	Histochemical staining	Immunohistochemistry	Molecular diagnostics
Ewing sarcoma/PNET	PAS positive	CD99+	Translocation EWSR1
Neuroblastoma	–	CD99−, CD56+	MYCN amplification
Alveolar rhabdomyosarcoma	–	MYF4 (myogenin)+, Desmin+	Translocation FKHR (FOXO1A)
Non-Hodgkin lymphoma/leukemia	PAS negative	CD45+	Depending on subtype
Small cell carcinoma	–	Keratin+, neuroendocrine markers	–
(Poorly differentiated) synovial sarcoma	–	CD99+, BCL-2+	Translocation SS18 (SYT)
Small cell osteosarcoma	Deposition of bone (alkaline phosphatase)	–	–
Mesenchymal chondrosarcoma	Deposition of cartilage	–	–
Desmoplastic small round cell tumor	–	Coexpression keratin and desmin	Translocation EWSR1
Melanoma	–	Melanocytic markers+	–

Detection of minimal residual disease

Following exciting results in molecular screening of lymph nodes for micrometastases of colonic cancer and bone marrow for minimal residual disease after lymphoma treatment, efforts have been made to do the same for sarcomas harboring a tumor-specific translocation as for instance Ewing sarcomas [41, 42]. Presence of tumor cells in bone marrow but not in blood was claimed to be associated with adverse prognosis [43], while others showed an increased risk of systemic relapses associated with bone marrow micrometastasis and circulating tumor cells in localized Ewing tumor.[44]. Tumor cells were shown to be present in a subset of stem cell harvests of Ewings sarcoma patients and their persistence following transplantation was claimed to be associated with relapse. Large prospective multinational randomized trials have been designed such as the EuroEwing 99 trial to investigate these questions. Although this trial is now open for 10 years, still, the data are not mature to draw final conclusions with regard to this question, implying that when a difference is present, this should be minimal at best for the individual patient. For alveolar rhabdomyosarcoma, molecular markers have been advocated for early detection of tumor relapses as well as using a reverse transcriptase-polymerase chain reaction method [45].

Prediction of outcome

Some tumors like Ewing sarcoma or synovial sarcoma may carry individually one of a spectrum of tumor specific cytogenetic or molecular genetic abnormalities. In retrospective studies, it has been claimed that the prognoses for these tumor entities was influenced by the specific molecular-defined translocation type [46–48]. These appeared in these first studies a powerful prognostic indicator and in case of synovial sarcoma even a predictor of the biphasic versus the monophasic subtype. In due course however, based on either prospectively collected cases treated in the context of a clinical trial or large national sarcoma databases, the prognostic value of these subtypes of translocations has been questioned for both tumor types [49–52]. Next to the specific translocations, some sarcomas, especially well documented in Ewing sarcoma, harbor numerical chromosomal abnormalities,

Table 2 Distinguishing features in spindle cell tumors

	Histochemical stainings	Immunohistochemistry	Molecular diagnostics
Monophasic synovial sarcoma	–	EMA+, keratin+	Translocation SS18 (SYT)
Leiomyosarcoma	–	Smooth muscle markers+	–
Solitary fibrous tumor	–	CD34+	–
MPNST	Reticulin staining	S100 protein in a subset of cases	–
Clear cell sarcoma	–	Melanocytic markers+	Translocation EWSR1
GIST	–	CD117+, DOG1+	KIT/PDGFRA mutation
Dedifferentiated liposarcoma	–	MDM2, CDK4 over expression	MDM2 amplification

deletions of the p16 region or additional point mutations in p53 [53–57]. These abnormalities are most often grossly overlooked when applying an RT-PCR approach just focusing on the known fusion breakpoints. An important role in tumor progression and prognosis has been claimed for these additional, nontumor-specific events. In case of metastatic GIST, the prognosis is highly correlated to the response to tyrosine kinase-inhibiting drugs [58]. While also immunohistochemical phenotypic markers have been studied with potential prognostic impact [59], these failed to show prognostic impact in contrast to clinical [60] and morphological [61] parameters. Here, especially the type of mutation in KIT or PDGFRA appears to have an important impact on response to tyrosine kinase inhibition [62, 63] while additional molecular events superimposed to the original tumor-specific ones like those described earlier for Ewing sarcoma are increasingly more of interest in studying resistance [64,65] and tumor progression [66].

Identification of molecular targets for treatment

With the identification of some of the specific changes in sarcomas, therapeutic targets were disclosed. The most well-known example is KIT/PDGFRA mutations in gastrointestinal stromal tumors of which the constitutively active signaling and subsequent tumor growth can be inhibited using tyrosine kinase inhibitors such as imatinib (STI571, Gleevec) [67]. Also, specific translocations have revealed targets for therapy. The COL1A1-PDGFB fusion product in dermatofibrosarcoma protuberans signals through the PDGF receptor in an autocrine loop [8], of which the signaling can be blocked using tyrosine kinase inhibitors acting at PDGFR such as imatinib. Imatinib treatment of this superficially located low-grade sarcoma can be beneficial to reduce tumor size in otherwise inoperable tumors.

Conclusion

Molecular and cytogenetic studies performed over the past decades have been proven to have major impact in identification, classification, and in some cases, prognostication of a large variety of sarcomas. With regard to diagnosis, the use of molecular techniques for an array of tumor entities has found their way into routine clinicopathological practice. Like the treatment of sarcomas, the application of molecular techniques needs to be under strict protocol and in morphological context in order to avoid disastrous mistakes in tumor classification. Here, a need for vigorous (multi) national quality control assessments, centralization not only of treatment but also of (molecular) diagnosis and development of (multi) national guidelines [68–71] is a future view which needs attention of the pathology community as well as health-care decision makers.

Conflict of interest statement We declare that we have no conflicts of interest.

Open Access This article is distributed under the terms of the Creative Commons Attribution Noncommercial License which permits any noncommercial use, distribution, and reproduction in any medium, provided the original author(s) and source are credited.

References

1. Mitelman F, Johansson B, Mertens F (2007) The impact of translocations and gene fusions on cancer causation. Nat Rev Cancer 7:233–245
2. de Alava E (2007) Molecular pathology in sarcomas. Clin Transl Oncol 9:130–144
3. Fletcher CDM, Unni KK, Mertens F (2002) WHO Classification of tumours. Pathology and genetics of tumours of soft tissue and bone. IARC Press, Lyon
4. Hogendoorn PC, Collin F, Daugaard S et al (2004) Changing concepts in the pathological basis of soft tissue and bone sarcoma treatment. Eur J Cancer 40:1644–1654
5. Mitelman F, Johansson B, Mertens F (2007) The impact of translocations and gene fusions on cancer causation. Nat Rev Cancer 7:233–245
6. Janknecht R (2005) EWS-ETS oncoproteins: the linchpins of Ewing tumors. Gene 363:1–14
7. O'Brien KP, Seroussi E, Dal Cin P et al (1998) Various regions within the alpha-helical domain of the COL1A1 gene are fused to the second exon of the PDGFB gene in dermatofibrosarcomas and giant-cell fibroblastomas. Genes Chromosomes Cancer 23:187–193
8. Shimizu A, O'Brien KP, Sjoblom T et al (1999) The dermatofibrosarcoma protuberans-associated collagen type I alpha 1/platelet-derived growth factor (PDGF) B-chain fusion gene generates a transforming protein that is processed to functional PDGF-BB. Cancer Res 59:3719–3723
9. Oliveira AM, Hsi BL, Weremowicz S et al (2004) USP6 (Tre2) fusion oncogenes in aneurysmal bone cyst. Cancer Res 64:1920–1923
10. Oliveira AM, Perez-Atayde AR, Dal Cin P et al (2005) Aneurysmal bone cyst variant translocations upregulate USP6 transcription by promoter swapping with the ZNF9, COL1A1, TRAP150, and OMD genes. Oncogene 24(21):3419–3426
11. Oliveira AM, Chou MM, Perez-Atayde A et al (2006) Aneurysmal bone cyst: a neoplasm driven by upregulation of the USP6 oncogene. J Clin Oncol 24:e1
12. Masuda-Robens JM, Kutney SN, Qi H et al (2003) The TRE17 oncogene encodes a component of a novel effector pathway for Rho GTPases Cdc42 and Rac1 and stimulates actin remodeling. Mol Cell Biol 23:2151–2161
13. Jin W, Yun C, Hobbie A et al (2007) Cellular transformation and activation of the phosphoinositide-3-kinase-Akt cascade by the ETV6-NTRK3 chimeric tyrosine kinase requires c-Src. Cancer Res 67:3192–3200
14. Dal Cin P, Sciot R, Brys P et al (2000) Recurrent chromosome aberrations in fibrous dysplasia of the bone: a report of the CHAMP study group. CHromosomes and MorPhology. Cancer Genet Cytogenet 122:30–32
15. Bianco P, Riminucci M, Majolagbe A et al (2000) Mutations of the GNAS1 gene, stromal cell dysfunction, and osteomalacic

changes in non-McCune-Albright fibrous dysplasia of bone. J Bone Miner Res 15:120–128
16. Okamoto S, Hisaoka M, Ushijima M et al (2000) Activating Gs (alpha) mutation in intramuscular myxomas with and without fibrous dysplasia of bone. Virchows Arch 437:133–137
17. Faivre L, Nivelon-Chevallier A, Kottler ML et al (2001) Mazabraud syndrome in two patients: clinical overlap with McCune-Albright syndrome. Am J Med Genet 99:132–136
18. Willems SM, Mohseny AB, Balog C, Sewrajsing R, Briaire-de Bruijn IH, Knijnenburg J, Cleton-Jansen AM, Sciot R, Fletcher CD, Deelder AM, Szuhai K, Hensbergen PJ, Hogendoorn PCW (2009) Cellular/intramuscular myxoma and grade I myxofibrosarcoma are characterized by distinct genetic alterations and specific composition of their extracellular matrix. J Cell Mol Med 13 (7):1291–1301
19. Isakoff MS, Sansam CG, Tamayo P et al (2005) Inactivation of the Snf5 tumor suppressor stimulates cell cycle progression and cooperates with p53 loss in oncogenic transformation. Proc Natl Acad Sci U S A 102:17745–17750
20. McKenna ES, Sansam CG, Cho YJ et al (2008) Loss of the epigenetic tumor suppressor SNF5 leads to cancer without genomic instability. Mol Cell Biol 28:6223–6233
21. Dei Tos AP, Doglioni C, Piccinin S et al (2000) Coordinated expression and amplification of the MDM2, CDK4, and HMGI-C genes in atypical lipomatous tumours. J Pathol 190:531–536
22. Meis-Kindblom JM, Sjogren H, Kindblom LG et al (2001) Cytogenetic and molecular genetic analyses of liposarcoma and its soft tissue simulators: recognition of new variants and differential diagnosis. Virchows Arch 439:141–151
23. Sandberg AA (2004) Updates on the cytogenetics and molecular genetics of bone and soft tissue tumors: liposarcoma. Cancer Genet Cytogenet 155:1–24
24. Kanoe H, Nakayama T, Murakami H et al (1998) Amplification of the CDK4 gene in sarcomas: tumor specificity and relationship with the RB gene mutation. Anticancer Res 18:2317–2321
25. Willems SM, Debiec-Rychter M, Szuhai K et al (2006) Local recurrence of myxofibrosarcoma is associated with increase in tumour grade and cytogenetic aberrations, suggesting a multistep tumour progression model. Mod Pathol 19:407–416
26. Sreekantaiah C, Davis JR, Sandberg AA (1993) Chromosomal abnormalities in leiomyosarcomas. Am J Surg Pathol 142:293–305
27. Bovée JVMG (2008) Multiple osteochondromas. Orphanet J Rare Dis 3:3
28. Bovée JVMG, Cleton-Jansen AM, Wuyts W et al (1999) EXT-mutation analysis and loss of heterozygosity in sporadic and hereditary osteochondromas and secondary chondrosarcomas. Am J Hum Genet 65:689–698
29. Hameetman L, Szuhai K, Yavas A et al (2007) The role of EXT1 in non hereditary osteochondroma: identification of homozygous deletions. J Natl Cancer Inst 99:396–406
30. Bovée JVMG, Cleton-Jansen AM, Kuipers-Dijkshoorn N et al (1999) Loss of heterozygosity and DNA ploidy point to a diverging genetic mechanism in the origin of peripheral and central chondrosarcoma. Genes Chrom Cancer 26:237–246
31. Hallor KH, Staaf J, Bovée JVMG et al (2009) Genomic Profiling of Chondrosarcoma: Chromosomal Patterns in Central and Peripheral Tumors. Clin Cancer Res 15(8):2685–2694
32. Schrage YM, Hameetman L, Szuhai K et al (2009) Aberrant heparan sulfate proteoglycan localization, despite normal exostosin, in central chondrosarcoma. Am J Pathol 174:979–988
33. Tallini G, Dorfman H, Brys P et al (2002) Correlation between clinicopathological features and karyotype in 100 cartilaginous and chordoid tumours. A report from the chromosomes and morphology (CHAMP) collaborative study group. J Pathol 196:194–203
34. Bovée JVMG, Sciot R, Dal Cin P et al (2001) Chromosome 9 alterations and trisomy 22 in central chondrosarcoma: a cyto-genetic and DNA flow cytometric analysis of chondrosarcoma subtypes. Diagn Mol Pathol 10:228–236
35. Schrage YM, Lam S, Jochemsen AG et al. (2008). Central chondrosarcoma progression is associated with pRb pathway alterations; CDK4 downregulation and p16 overexpression inhibit cell growth in vitro. J Cell Mol Med
36. World Health Organization Classification of Tumours (2002) Pathology and genetics of tumours of soft tissue and bone. IARC Press, Lyon
37. Graadt van Roggen JF, Bovée JVMG, Morreau J et al (1999) Diagnostic and prognostic implications of the unfolding molecular biology of bone and soft tissue tumours. J Clin Pathol 52:481–489
38. Peter M, Gilbert E, Delattre O (2001) A multiplex real-time PCR assay for the detection of gene fusions observed in solid tumors. Lab Invest 81:905–912
39. Weaver J, Downs-Kelly E, Goldblum JR et al (2008) Fluorescence in situ hybridization for MDM2 gene amplification as a diagnostic tool in lipomatous neoplasms. Mod Path 21:943–949
40. Sirvent N, Coindre JM, Maire G et al (2007) Detection of MDM2-CDK4 amplification by fluorescence in situ hybridization in 200 paraffin-embedded tumor samples: utility in diagnosing adipocytic lesions and comparison with immunohistochemistry and real-time PCR. Am J Surg Pathol 31:1476–1489
41. Avigad S, Cohen IJ, Zilberstein J et al (2004) The predictive potential of molecular detection in the nonmetastatic Ewing family of tumors. Cancer 100:1053–1058
42. Fagnou C, Michon J, Peter M et al (1998) Presence of tumor cells in bone marrow but not in blood is associated with adverse prognosis in patients with Ewing's tumor. Societe Francaise d'Oncologie Pediatrique. J Clin Oncol 16:1707–1711
43. Schleiermacher G, Peter M, Oberlin O et al (2003) Increased risk of systemic relapses associated with bone marrow micrometastasis and circulating tumor cells in localized ewing tumor. J Clin Oncol 21:85–91
44. Yaniv I, Cohen IJ, Stein J et al (2004) Tumor cells are present in stem cell harvests of Ewings sarcoma patients and their persistence following transplantation is associated with relapse. Pediatr Blood Cancer 42:404–409
45. Athale UH, Shurtleff SA, Jenkins JJ et al (2001) Use of reverse transcriptase polymerase chain reaction for diagnosis and staging of alveolar rhabdomyosarcoma, Ewing sarcoma family of tumors, and desmoplastic small round cell tumor. J Pediatr Hematol Oncol 23:99–104
46. Ed A, Kawai A, Healy JH et al (1998) EWS-FL11 fusion transcript structure is an independent determinant of prognosis in Ewing's sarcoma. J Clin Oncol 16:1248–1255
47. Kawai A, Woodruff J, Healy JH et al (1998) SYT-SSX gene fusion as a determinant of morphology and prognosis in synovial sarcoma. N Engl J Med 338:153–160
48. Ladanyi M, Antonescu CR, Leung DH et al (2002) Impact of SYT-SSX fusion type on the clinical behavior of synovial sarcoma: a multi-institutional retrospective study of 243 patients. Cancer Res 62:135–140
49. Coindre JM, Pelmus M, Hostein I et al (2003) Should molecular testing be required for diagnosing synovial sarcoma? A prospective study of 204 cases. Cancer 98:2700–2707
50. Guillou L, Benhattar J, Terrier P et al (2003) SYT-SSX fusion type is not a prognostic factor in synovial sarcoma (SS) patients. A multi-institutional study of 182 cases. Mod Path 16:13A
51. Zoubek A, Dockhorn-Dworniczak B, Delattre O et al (1996) Does expression of different EWS chimeric transcripts define clinically distinct risk groups of Ewing tumor patients? J Clin Oncol 14:1245–1251
52. Le Deley M-C, Delattre O, Schaefer KL et al. (2009). Impact of EWS-ETS fusion type on disease progression in Ewing's sarcoma /

peripheral primitive neuroectodermal tumor: prospective results from the cooperative Euro-E.W.I.N.G.99 trial
53. Szuhai K, Ijszenga M, Tanke HJ et al (2006) Molecular cytogenetic characterization of four previously established and two newly established Ewing sarcoma cell lines. Cancer Genet Cytogenet 166:173–179
54. Wei G, Antonescu CR, de Alava E et al (2000) Prognostic impact of INK4A deletion in Ewing sarcoma. Cancer 89:793–799
55. Tsuchiya T, Sekine K, Hinohara S et al (2000) Analysis of the p16INK4, p14ARF, p15, TP53, and MDM2 genes and their prognostic implications in osteosarcoma and Ewing sarcoma. Cancer Genet Cytogenet 120:91–98
56. Ueda Y, Dockhorn-Dworniczak B, Blasius S et al (1993) Analysis of mutant p53 protein in osteosarcomas and other malignant and benign lesions of bone. J Cancer Res Clin Oncol 119:172–178
57. Armengol G, Tarkkanen M, Virolainen M et al (1997) Recurrent gains of 1q, 8 and 12 in the Ewing family of tumours by comparative genomic hybridization. Br J Cancer 75:1403–1409
58. Verweij J, Casali PG, Zalcberg J et al (2004) Progression-free survival in gastrointestinal stromal tumours with high-dose imatinib: randomised trial. Lancet 364:1127–1134
59. Sciot R, Debiec-Rychter M, Daugaard S et al (2008) Distribution and prognostic value of histopathologic data and immunohistochemical markers in gastrointestinal stromal tumours (GISTs): an analysis of the EORTC phase III trial of treatment of metastatic GISTs with imatinib mesylate. Eur J Cancer 44(13):1855–1860
60. Van Glabbeke M, Verweij J, Casali PG et al (2005) Initial and late resistance to imatinib in advanced gastrointestinal stromal tumors are predicted by different prognostic factors: a European organisation for research and treatment of cancer-Italian Sarcoma group-australasian gastrointestinal trials group study. J Clin Oncol 23:5795–5804
61. Fletcher CDM, Berman JJ, Corless C et al (2002) Diagnosis of gastrointestinal stromal tumors: a consensus approach. Hum Pathol 33:459–465
62. Heinrich MC, Corless CL, Demetri GD et al (2003) Kinase mutations and imatinib response in patients with metastatic gastrointestinal stromal tumor. J Clin Oncol 21:4342–4349
63. Debiec-Rychter M, Sciot R, Le Cesne A et al (2006) KIT mutations and dose selection for imatinib in patients with advanced gastrointestinal stromal tumours. Eur J Cancer 42:1093–1103
64. Heinrich MC, Corless CL, Blanke CD et al (2006) Molecular correlates of imatinib resistance in gastrointestinal stromal tumors. J Clin Oncol 24:4764–4774
65. Debiec-Rychter M, Cools J, Dumez H et al (2005) Mechanisms of resistance to imatinib mesylate in gastrointestinal stromal tumors and activity of the PKC412 inhibitor against imatinib-resistant mutants. Gastroenterology 128:270–279
66. Romeo S, Diebiec-Rychter M, Van Glabbeke M et al (2009) Cell cycle/apoptosis molecules expression correlates with Imatinib response in patients with advanced gastro-intestinal stromal tumours. Clin Cancer Res 15:4191–4198
67. Corless CL, Heinrich MC (2008) Molecular pathobiology of gastrointestinal stromal sarcomas. Annu Rev Pathol 3:557–586
68. Blay JY, Bonvalot S, Casali P et al (2005) Consensus meeting for the management of gastrointestinal stromal tumors. Report of the GIST consensus conference of 20–21 March 2004, under the auspices of ESMO. Ann Oncol 16:566–578
69. Paulussen M, Bielack S, Jurgens H et al (2008) Ewing's sarcoma of the bone: ESMO clinical recommendations for diagnosis, treatment and follow-up. Ann Oncol 19(Suppl 2):ii97–ii98
70. Bielack S, Carrle D, Jost L (2008) Osteosarcoma: ESMO clinical recommendations for diagnosis, treatment and follow-up. Ann Oncol 19(Suppl 2):ii94–ii96
71. Jansen-Landheer ML, Krijnen P, Oostindier MJ et al (2009) Improved diagnosis and treatment of soft tissue sarcoma patients after implementation of national guidelines: a population-based study. Eur J Surg Oncol. doi:10.1016/j.ejso.2009.05.002

Virchows Arch (2010) 456:201–217
DOI 10.1007/s00428-009-0853-4

REVIEW AND PERSPECTIVE

Soft tissue sarcomas with complex genomic profiles

Louis Guillou · Alain Aurias

Received: 12 July 2009 / Revised: 5 October 2009 / Accepted: 17 October 2009 / Published online: 13 November 2009
© Springer-Verlag 2009

Abstract Soft tissue sarcomas (STS) with complex genomic profiles (50% of all STS) are predominantly composed of spindle cell/pleomorphic sarcomas, including leiomyosarcoma, myxofibrosarcoma, pleomorphic liposarcoma, pleomorphic rhabdomyosarcoma, malignant peripheral nerve sheath tumor, angiosarcoma, extraskeletal osteosarcoma, and spindle cell/pleomorphic unclassified sarcoma (previously called spindle cell/pleomorphic malignant fibrous histiocytoma). These neoplasms show, characteristically, gains and losses of numerous chromosomes or chromosome regions, as well as amplifications. Many of them share recurrent aberrations (e.g., gain of 5p13-p15) that seem to play a significant role in tumor progression and/or metastatic dissemination. In this paper, we review the cytogenetic, molecular genetic, and clinicopathologic characteristics of the most common STS displaying complex genomic profiles. Features of diagnostic or prognostic relevance will be discussed when needed.

Keywords Soft tissue sarcoma · Karyotype · Genetics

L. Guillou (✉)
University Institute of Pathology,
Centre Hospitalier Universitaire Vaudois and University of Lausanne,
Rue du Bugnon 25,
1011 Lausanne, Switzerland
e-mail: louis.guillou@chuv.ch

A. Aurias
Genetics and Biology of Cancers, and INSERM U830,
Institut Curie,
Paris, France

Introduction

Soft tissue sarcoma (STS) is a heterogenous group of mesenchymal neoplasms showing high variations in their clinical presentation, morphology, immunoprofile, genetics, and behavior. Roughly, STS can divided into several categories, namely those bearing reciprocal translocations accounting for 15–20% of cases (e.g., synovial sarcoma, Ewing sarcoma), those with specific mutations (e.g., gastrointestinal stromal tumor (GIST)) or deletions (e.g., rhabdoid tumor), those with amplifications (e.g., well-differentiated liposarcoma), and those with complex genomic profiles (complex karyotypes). The latter category, which accounts for about 50% of STS, is mainly composed of spindle cell/pleomorphic tumors, including leiomyosarcoma, myxofibrosarcoma, pleomorphic liposarcoma (PLPS), pleomorphic rhabdomyosarcoma (PRMS), malignant peripheral nerve sheath tumor (MPNST), angiosarcoma, extraskeletal osteosarcoma, and spindle cell/pleomorphic unclassified sarcoma (previously called spindle cell/pleomorphic malignant fibrous histiocytoma (MFH)). High-grade dedifferentiated liposarcoma which is also characterized by complex karyotype shows, in addition, distinctive genomic abnormalities (giant chromosomes, supernumerary ring chromosomes, amplification of 12q13-q21), paralleling that observed in well-differentiated liposarcoma (see chapter on well-differentiated and dedifferentiated liposarcomas).

Leiomyosarcoma

Leiomyosarcoma (LMS) accounts for about 8–10% of adult soft tissue sarcomas [1–3]. These malignant neoplasms which show varying degree of smooth muscle differentia-

tion can develop anywhere in the body, as well as in visceral organs (prostate, urinary bladder, uterus, etc.).

Cytogenetics and molecular genetics

LMS usually show complex karyotypic alterations [4–6], and karyotypes differ generally from one tumor to another. Many LMS show chromosomal imbalances aberrations in the form of gains (chromosomes 1, 5, 6, 8, 15, 16, 17, 19, 20, 22, X), losses (chromosomes 1p, 2, 3, 4, 6q, 8, 9, 10p, 11p, 12q, 11q, 13, 16, 17p, 18 19, 22q), and amplifications (chromosomes 1, 5, 8, 12, 13, 17, 19, 20) [4, 6, 7].

Some gains and losses of chromosomal material, however, are more frequently observed and tend to correlate with poor outcome, large tumor size, and metastatic dissemination: loss of 1p12-pter, loss of 2p, loss of 13q14-q21 (targeting the Rb pathway) [8], loss of 10q (targeting PTEN) [9], and loss of 16q and gains of 17p, 8q, and 5p14 pter [8, 9]. LMS often show loss of RB1, correlating with the high frequency of LMS observed in hereditary retinoblastoma patients. The 5p13-p15 region is often amplified in several pleomorphic STS including LMS. Residing in this amplicon are three candidates genes which are overexpressed: TRIO, NKD2, and IRX2, of which TRIO seems to be particularly involved in tumor progression of LMS [10]. Activation of the PI3K–AKT pathway through different mechanisms (e.g., activation of IGFR, inactivation of PTEN, a negative regulator of the PI3K–AKT) also plays a crucial role in the development and maintenance of LMS [11]. This activation leads to the concomitant activation of downstream effectors such as mTOR and its targets (ß-catenin, pS6, p4E-BP1, etc.), as well as to MDM2 stabilization [11]. Recent clinical trials showed that analogs of rapamycin such as everolimus (RAD001), an mTOR inhibitor, have some efficacy in patients with LMS and PEComas [12, 13]. Gene and protein expression studies also identified genes/proteins that seem to be associated with unfavorable prognosis and high metastatic risk in leiomyosarcomas (see also chapter of Beck et al.) [14–16], including mutations in TP53 gene and inactivation of $p16^{INK4a}$ [17, 18], RASSF1A [19], and MGMT [20] secondary to promoter hypermethylation. A recent study on gene expression signature of 177 sarcomas identified a significant relationship between upegulation of several hypoxia-induced genes such as HIF1A and its targets and increased metastatic potential [21]. This was particularly true for STS with complex karyotypes, including LMS. This application of expression data would allow us to identify high-risk patients who might deserve specific therapy.

Recently, it has been realized that the more differentiated retroperitoneal leiomyosarcomas tend to behave more aggressively and that this aggressiveness was mainly dependent upon myocardin amplification/overexpression [22]. Myocardin is a transcriptional cofactor of SRF regulating smooth muscle differentiation. Pérot et al. [22] showed that inactivation of the myocardin pathway resulted in a significant reduction of smooth muscle differentiation, cell proliferation, and cell migration and was associated with less differentiated histology. These data suggest that myocardin might constitute a promising therapeutic target.

Some LMS which occur in children and some immunocompromised patients are associated with Epstein–Barr virus infection. EBV infection can be confirmed by in situ hybridization (using Epstein–Barr virus early RNA-EBER probes) or polymerase-chain-reaction-based methods [23], pointing to a potential role of EBV in leiomyosarcoma genesis. This was not observed in other neoplasms such as GIST [24].

Leiomyosarcomas of the uterus tend to parallel LMS of soft tissue in terms of karyotypic abnormalities. Most frequent losses by CGH include 10q, 11q, 13q, and 2p, whereas the most common gains are Xp, 1q, 5p, 8q, and 17p [4, 25]. Aberrations involving 1q21 seem to be more common and aberrations of 1p13 and 10q22 less common in soft tissue leiomyosarcomas [4, 5]. Losses involving 1q and 3p are more frequent among soft tissue LMS whereas losses of chromosomes 14 and 15 and of 22q12-qter are more frequent in non-soft-tissue LMS [4]. TP53 mutations, MDM2 stabilization, and inactivation of $p16^{INK4a}$ are observed in both soft tissue and uterine LMS and seem to be associated with LMS progression. Leiomyoma and LMS of the uterine corpus are two different diseases, and there is no evidence that the former originates from the latter [26]. For example, TP53 mutations and loss of heterozygosity for chromosome 10 are not observed in leiomyomas, while the t(12;14) (q15; q23-24) seen in many leiomyomas is not a feature of LMS [4, 25].

Clinical features

LMS are more common in middle-aged and elderly patients and rare in children. Clinical behavior depends mainly on tumor location [1, 2]. Leiomyosarcomas of the dermis are mostly observed in lower extremities of middle-aged to older male individuals. They are often small (<2 cm) and have an excellent prognosis. LMS of the somatic soft tissues often present as large (6 cm on average) lesions which tend to be situated in the extremities, especially the thigh, frequently connected to a small vein (one third of cases). About half of them develop in the subcutis and the remainder in muscle. Metastases develop in 40% to 45% of patients with a 5-year survival rate of 64% [2, 27].

LMS of the retroperitoneum, abdominal cavity, and mediastinum account for 50–65% of all LMS. They occur preferentially in women (two third of cases), presenting as

large (often >10 cm) multinodular masses which tend to infiltrate adjacent structures such as the kidney or pancreas. The prognosis of LMS of the abdominal cavity and retroperitoneum is markedly poor, with 70–90% of patients dying of their disease within 5 years [2, 27].

Epstein–Barr-virus-associated LMS tend to occur in children, to be multicentric, and to behave as low-grade tumors. They also occur in immunocompromised patients (e.g., transplanted patients and patients with acquired immunodeficiency syndrome) [23].

Pathologic features

Histologically, LMS is composed of a varying proportion of spindle and pleomorphic cells depending on the degree of differentiation. In well-differentiated lesions, the spindle cells are classically arranged in recognizable longitudinally oriented fascicles intersecting at right angles (Fig. 1). The cytoplasm of the cells is variably eosinophilic and fibrillary. In higher-grade tumors, cytologic atypia is common, associated with monster cells, normal and abnormal mitoses, foci of rhabdoid cytomorphology, and tumor necrosis. Several variants of LMS have been described, including the pleomorphic (10% of cases), myxoid, inflammatory, epithelioid, and osteoclast-like cell/giant-cell-rich LMS. EBV-associated LMS differs from classical LMS in several respects. They tend to be well differentiated and to exhibit reduced cytologic atypia, low mitotic activity, and numerous intratumoral lymphocytes.

Immunohistochemically, LMS show features of smooth muscle differentiation. Tumor cells are generally positive for muscle-specific actin (HHF-35), alpha smooth muscle actin, desmin, calponin, h-caldesmon, and smooth muscle myosin heavy chain and are negative for myogenin. A significant proportion of LMS (especially well-differentiated neoplasms) can be positive for EMA (10–30%), keratin (10–30%), and CD34 (30%). Extrauterine LMS are generally negative for estrogen and/or progesterone receptors.

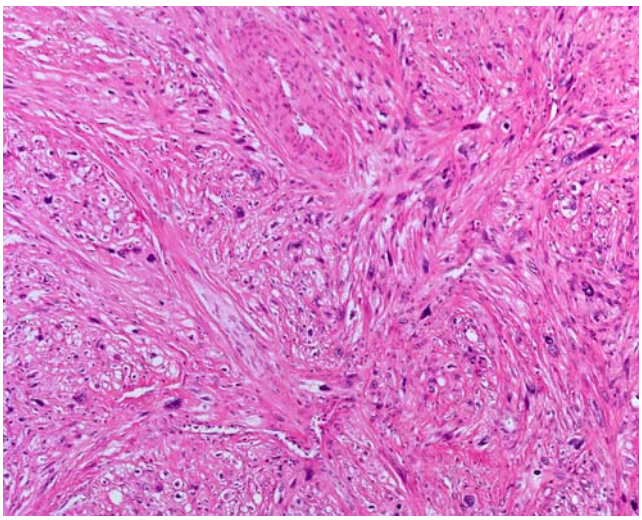

Fig. 1 Leiomyosarcoma. The tumor is moderately differentiated, composed of intersecting fascicles of spindle cells showing brightly eosinophilic cytoplasm and obvious nuclear atypia

Differential diagnosis

The differential diagnosis of LMS is quite large. Among benign lesions, inflammatory myofibroblastic tumor and all pseudosarcomatous (myo)fibroblastic reactive lesions (e.g., postoperative spindle cell nodule) are most likely to be confused with LMS. Spindle cell malignant neoplasms resembling LMS include myofibroblastic sarcoma, spindle cell rhabdomyosarcoma, pleomorphic rhabdomyosarcoma, high-grade undifferentiated pleomorphic sarcoma, gastrointestinal stromal tumor, sarcomatoid carcinoma, and spindle cell/pleomorphic melanoma.

Undifferentiated spindle/pleomorphic sarcoma (so-called storiform–pleomorphic MFH)

Undifferentiated high-grade spindle/pleomorphic sarcoma (undifferentiated pleomorphic sarcoma (UPS)) is now the preferred term to designate high-grade soft tissue sarcomas which fail to show any specific line of differentiation using currently available ancillary techniques and in which epithelial, melanotic, and lymphoid differentiations have been excluded [1, 28, 29]. It is a diagnosis of elimination. These neoplasms account for about 5–7% of sarcomas occurring in adults. Most were previously called “storiform–pleomorphic malignant fibrous histiocytomas”.

Cytogenetics and molecular genetics

UPS show complex cytogenetic rearrangements involving 30–35% of the genome, but no specific structural or numerical abnormalities have been proven, so far, to be useful for identification purposes [30] (Fig. 2). UPS and other pleomorphic sarcomas share many of the aberrations observed in LMS [31–33], including losses of 1q32.1, 2p25.3, 2q36-q37, 8p23, 9p, 10q21-q23, 11q22, 13q14-q21, 16q11, and 16q23, gains of 1p36-p31, 1q21-q24, 2p, 4p16, 5p, 5q34, 6q, 7p15-p22, 7q21-qter, 17q, 9q, 14q, 16p13, 17q, 19p13, 19q13.11-q13.2, 20q, and 21q, and high-level amplifications of loci 1p33-p34, 12q13-q15, 17cen-p11.2, and 17p13-pter (Figs. 3 and 4). Both tumor types share also very similar protein expression patterns [16, 34]. Loss of chromosome 13q is the most frequent genomic imbalance in UPS [35], leading to inactivation of the RB pathway [36]. Alterations within the TP53/ARF/

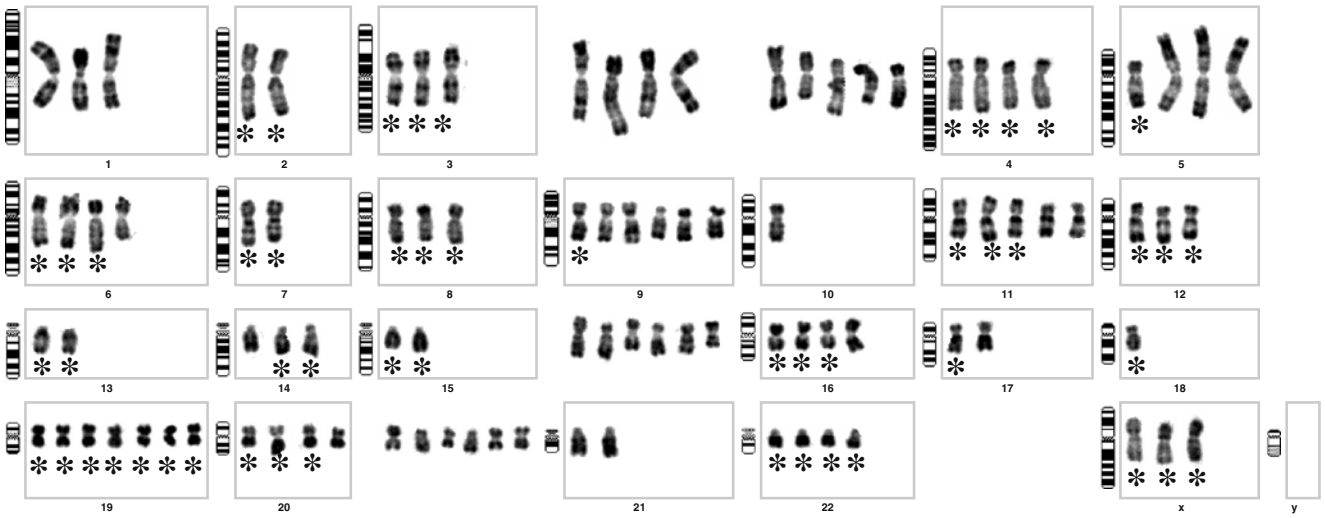

Fig. 2 Complex karyotype of an undifferentiated high-grade pleomorphic. sarcoma. Many chromosomes are abnormal and difficult to classify (*asterisk* indicates «apparently» normal (i.e., recognizable) chromosomes). Courtesy of Dr. F. Chibon, Bordeaux, France

MDM2 pathway are also frequent [32]. A recent gene expression analysis of 64 spindle and pleomorphic sarcomas showed that, when performing hierarchical clustering analyses, dedifferentiated liposarcoma, myxofibrosarcoma, leiomyosarcoma, malignant peripheral nerve sheath tumor, and adult-type fibrosarcoma formed their own clusters [37]. This study also showed that many of the so-called UPS/MFH had heterogeneous profiles and could be reclassified

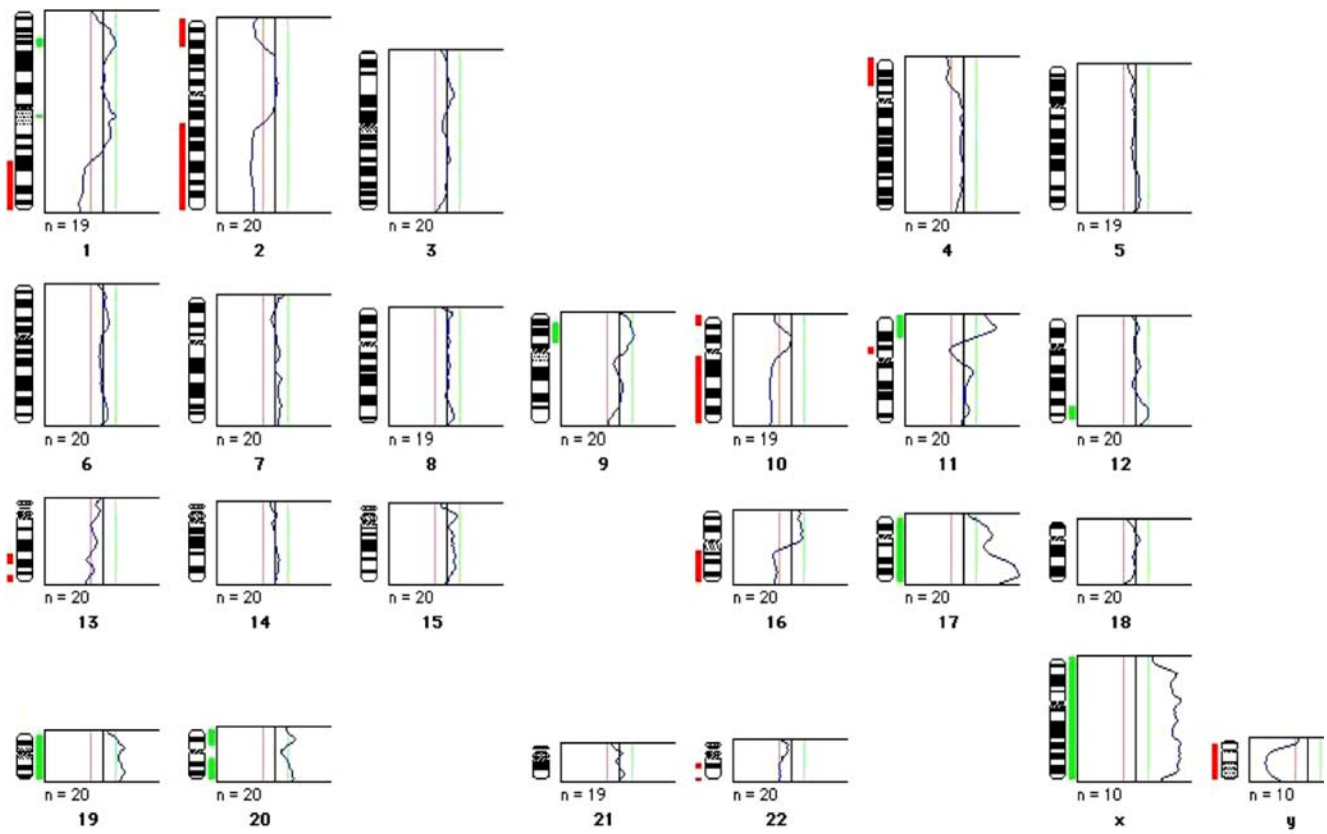

Fig. 3 Metaphase-based CGH of an undifferentiated high-grade pleomorphic sarcoma. Chromosomal imbalances are more easily depicted on CGH (chromosomal gains in *green*, losses in *red*) than on conventional karyotype. In this example, the tumor shows, among other rearrangements, gains of chromosomes 19 and 20 and losses of 1qter, 10q, 13q, and 16q. This cytogenetic profile is not specific for undifferentiated pleomorphic sarcomas and can also be observed in leiomyosarcomas. Courtesy of Dr. F. Chibon, Bordeaux, France

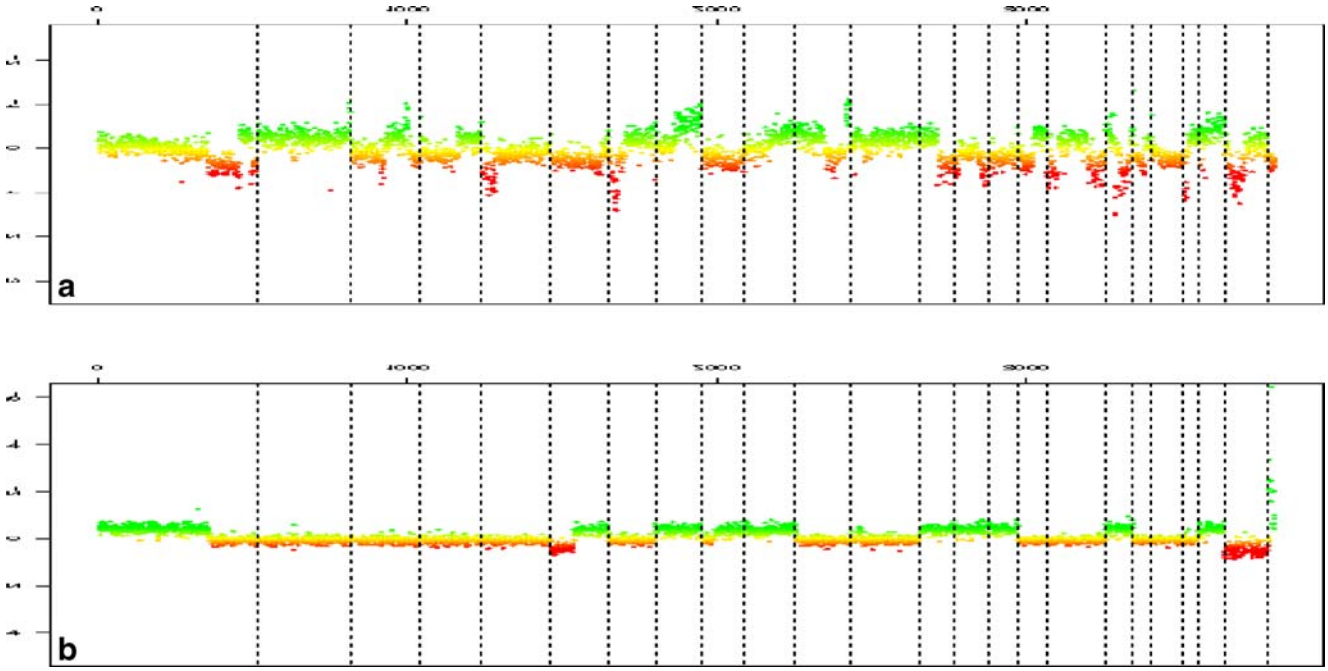

Fig. 4 Genomic profiles established by CGH BAC-array. This molecular approach allows us to identify rearranged chromosomal regions in undifferentiated pleomorphic sarcomas. Two types of genomic profiles are shown, one very complex (**a**) often associated with poor outcome and one less complex (**b**), associated (in the extremities) with better prognosis. Courtesy of Dr F. Chibon, Bordeaux, France

into other histologic subcategories of pleomorphic sarcomas, especially in the myxofibrosarcoma category. Interestingly and, in some way reassuring, the authors performed a histopathologic review after their molecular analysis, and they found that morphologic features were essentially in accordance with their molecular results [37].

Matrix-CGH studies showed that the gene TRIO, coding for a guanidine nucleotide exchange factor, is upregulated in pleomorphic sarcomas, correlating with copy number gains and high-level amplifications of the short arm of chromosome 5 [10]. TRIO is implicated in the control of cytoskeleton organization, transcription regulation, cell cycle progression, apoptosis, vesicle trafficking, and cell-to-cell adhesion, through activation of the Rho GTPase-mediated signaling pathway [10]. As in LMS, TRIO seems to play a significant role in UPS progression [10].

Along with LMS, pleomorphic sarcomas also show RASSF1A hypermethylation [19] (albeit less than in LMS) and upregulation of several hypoxia-related genes (e.g., HIF1A and its targets) as well as of several genes involved in cell proliferation, adhesion, and motility, correlating with increased aggressiveness and/or increased metastatic potential [21, 38]. A recent analysis of 49 UPS and LMS, which confirmed the strong similarities between the two histotypes in terms of genomic aberrations and gene expression patterns, identified two, so far unrecognized, prognostic factors. One, loss of 4q31 (a region which encompasses the SMAD1 gene involved in the TGF-beta pathway), was a significant predictor of metastasis in multivariate analysis for the entire group of UPS and LMS, and the other, loss of 18q22, was a favorable prognostic factor for the same group [32].

Ezrin (villin 2), a protein that serves as an intermediate between the plasma membrane and the actin cytoskeleton, is considered as a marker of cancer progression and a potential target for cancer therapy. It plays a key role in cell morphology, adhesion, migration, and organization. Ezrin is overexpressed in many neoplasms, and this overexpression was found to correlate with increased metastatic potential and reduced survival [39]. Not surprisingly, this was also the case for high-grade sarcomas including UPS [40, 41].

The cell of origin of STS is a matter of controversy. Recently, it has convincingly shown that mesenchymal stem cells are good progenitor candidates for Ewing [42] and myxoid liposarcoma [43] development. Mesenchymal stem cells seem also to be good progenitors for MFH development via inactivation of the Wnt pathway [44]. Recently, Matushansky et al. [44] nicely demonstrated that DKK1, a Wnt inhibitor and mediator of human mesenchymal stem cell proliferation is overexpressed in UPS/MFH and that human mesenchymal stem cells can be transformed via inhibition of the Wnt signaling to form UPS/MFH-like tumors in nude mice. This undifferentiation (or "dedifferentiation") can be reversed if the Wnt signaling pathway is appropriately reestablished.

Clinical features

UPS occurs most frequently in the limbs (especially lower limbs) and less often in the trunk of middle to advanced-aged adults, with a male predominance [1, 2]. Less than 10% are observed in the subcutaneous fat, most present as deep-seated masses. UPS are aggressive neoplasms; 30–50% of patients die within 5 years after diagnosis. Wide excision followed by irradiation is the treatment of choice. Adjuvant chemotherapy may be considered in selected cases (e.g., young patients). Myogenic differentiation is a negative prognostic factor in pleomorphic sarcomas [45, 46], with, however, the notable exception of dedifferentiated liposarcomas showing heterologous myogenic differentiation [47].

Pathologic features

UPS usually present as large (5–15 cm), well-circumscribed, deep-seated masses. Cut surface often show hemorrhagic, myxoid, and/or necrotic changes. The lesion is composed by an admixture of spindle and pleomorphic cells, set in a variably collagenized extracellular matrix (Fig. 5). Cellularity is variable, and cellular atypia, nuclear pleomorphism, mitoses, abnormal mitoses, areas of tumor necrosis, histiocyte-like cells, and foamy cells, as well as giant tumor cells with enlarged, polylobulated nuclei are commonly observed.

Immunohistochemically, it is common for undifferentiated high-grade pleomorphic sarcomas to show some limited foci of smooth muscle actin reactivity, but h-caldesmon, desmin, S100 protein, and epithelial markers are usually not expressed. If they are, the diagnosis of undifferentiated high-grade pleomorphic sarcoma should be questioned and a search for a specific line of differentiation pursued. UPS showing a significant amount of smooth muscle actin reactivity (and sometimes focal expression of desmin) but lacking the typical morphologic features of leiomyosarcoma are better classified as high-grade myofibrosarcomas (myofibroblastic sarcomas) or myosarcomas not otherwise specified [48, 49]. Histiocytic antigens (e.g., alpha-1-antitrypsin, alpha-1-antichymotrypsin, CD68, lysozyme) are of no utility. There are, by definition, no ultrastructural features of a specific lineage. Many tumor cells show features of fibroblasts, myofibroblast, or histiocytes.

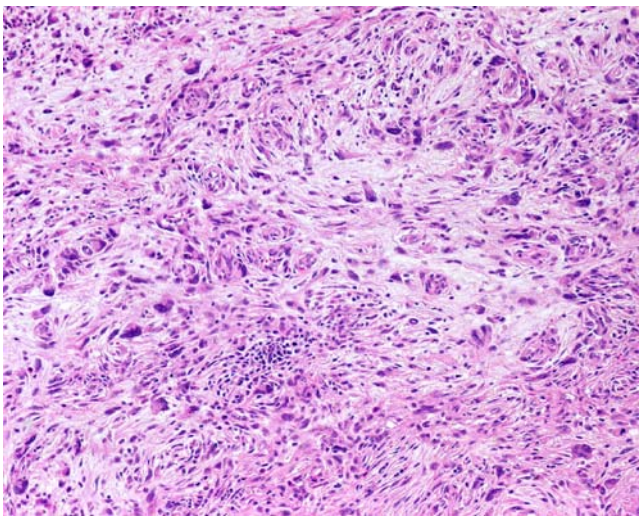

Fig. 5 Undifferentiated high-grade pleomorphic sarcoma. Proliferation of undifferentiated spindle and pleomorphic cells, set in variably collagenous background

Differential diagnosis

Undifferentiated high-grade pleomorphic sarcoma is a diagnosis of elimination [1, 28, 29]. Before giving such a diagnosis, all other potential mimics should have been ruled out, including metastatic carcinomas (lung, kidney), melanoma, lymphoma, pleomorphic rhabdomyosarcoma, pleomorphic leiomyosarcoma, pleomorphic liposarcoma, pleomorphic malignant peripheral nerve sheath tumor, liposarcoma with high-grade dedifferentiated areas, and high-grade myxofibrosarcoma. Extensive sampling, careful examination of slides (looking for lipoblasts or rhabdomyoblasts), and ancillary techniques (immunohistochemistry, electron microscopy, genetics) are critical in this context.

Myxofibrosarcoma

Myxofibrosarcoma, previously called myxoid malignant fibrous histiocytoma, is a relatively common sarcoma of older patients (median age 60 years) [1, 2, 50–53].

Cytogenetics and molecular genetics

Because myxofibrosarcoma has been, for a long time, included in the MFH category and because the separation between high-grade pleomorphic myxofibrosarcoma containing few (<10%) myxoid areas and undifferentiated pleomorphic sarcoma (UPS) is difficult and somewhat subjective [1, 51, 52], data on the cytogenetics and molecular genetics of myxofibrosarcoma are limited. Myxofibrosarcomas are generally associated with very complex karyotypes, sharing many of the aberrations observed in LMS and UPS [30, 37, 54]. A recent clinicopathologic and karyotype analysis of 32 myxofibrosarcomas showed that local recurrence was associated with increase in tumor grade and in cytogenetic aberrations [55]. Chromosomal aberrations were not restricted to higher-grade tumors but could also be observed in low-grade

myxofibrosarcomas, albeit less frequently. Normal karyotypes were also observed, independently of grade.

A CGH analysis of a series of 22 myxofibrosarcomas showed recurrent simple gains of the chromosome regions 19p and 19q, losses of chromosome 1q, 2q, 3p, 4q, 10q, 11q, and 13q, and high-level amplifications of the central regions of chromosomes 1, 5p, and 20q [54]. Loss of the 13q14-21 chromosomal region, encompassing the RB1 locus, was observed in all 22 cases examined. Of interest, gain of 5p and loss of 4q are not observed in low-grade myxofibrosarcomas as opposed to myxofibrosarcomas of higher grades, suggesting that these aberrations are late events in the oncogenesis of myxofibrosarcoma [54]. In their comparative study, the authors also found similar chromosomal aberrations in a series of nine pleomorphic liposarcomas, suggesting close relationship between myxofibrosarcoma and pleomorphic liposarcoma.

A recent gene expression analysis of 64 spindle and pleomorphic sarcomas showed that, when performing hierarchical clustering analyses, myxofibrosarcoma could be separated from other spindle cell/pleomorphic sarcomas, namely dedifferentiated liposarcoma, leiomyosarcoma, malignant peripheral nerve sheath tumor, and fibrosarcoma. This study also showed that many neoplasms which had initially been (mis)classified as UPS/MFH based on their morphology and immunoprofile could be reclassified as myxofibrosarcoma based on gene expression [37]. Two genes, GPR64 and TNXB, were particularly expressed by myxofibrosarcomas but not by UPS/MFH, thus allowing distinction between the two histotypes [37]. Separating a low-grade myxofibrosarcoma from a cellular myxoma can be difficult. A recent study showed that this can be done based on the differences in genetic alterations and in the composition of extracellular matrix [56].

Clinical features

Myxofibrosarcoma is mostly found in the deep dermis and subcutaneous fat of limbs (especially lower limbs) and limb girdles [1, 2, 50–53]. Thirty percent to 60% of the cases are deep-seated, developing in fascia and skeletal muscle. This is a slow-growing, often painless, tumor affecting men and women equally. Clinical behavior depends on tumor size, histologic grade (which includes tumor necrosis, mitotic rate, and amount of myxoid areas), and extent of resection [51, 52]. Local recurrences occur in about 50% of cases, often because of inadequate initial excisions. It is not unusual for recurrences to show signs of upgrading with an increase in cellularity, pleomorphism and mitotic activity, and, conversely, a reduction of the myxoid component. Metastases to lungs and bone are mostly observed in high-grade, large deep-seated tumors (20–35%); they are rare in low-grade lesions. The overall 5-year survival rate is 60–70%. A variant of myxofibrosarcoma showing distinctive epithelioid morphology and aggressive behavior has recently been individualized [57].

Pathologic features

Grossly, myxofibrosarcoma is typically ill-defined, heterogeneous, often multinodular, located in the subcutaneous fat, growing along fibrous septa and forming more or less gelatinous nodules. Large tumors are often deep-seated and partially necrotic and/or hemorrhagic. On microscopic examination, it is characterized by myxoid areas which are associated with cellular areas resembling undifferentiated pleomorphic sarcoma (Fig. 6). There is unfortunately no consensus on the extent of the myxoid areas required for the diagnosis of myxofibrosarcoma; whereas some authors require at least 50% [2] or 30% [52], 10% is enough for some others [51, 53]. Low-, intermediate-, and high-grade tumors have been described, depending on the amount of cellular atypia and on the respective proportions of myxoid and nonmyxoid components (the latter showing morphologic features of storiform–pleomorphic malignant fibrous histiocytoma) [2]. Low-grade myxofibrosarcomas are predominantly myxoid (≥50% myxoid) and hypocellular and contains distinctive curvilinear vessels (Fig. 7). Tumor cells, some of which have enlarged hyperchromatic nuclei, tend to aggregate around vessels. Vacuolated cells containing acid mucin and resembling lipoblasts are also found. Mitotic figures are rare. In high-grade lesions, the malignant fibrous histiocytoma-like component predominates: nuclear pleomorphism is evident, multinucleated giant cells and necrosis common, and mitotic figures, including abnormal mitoses, readily visible. Epithe-

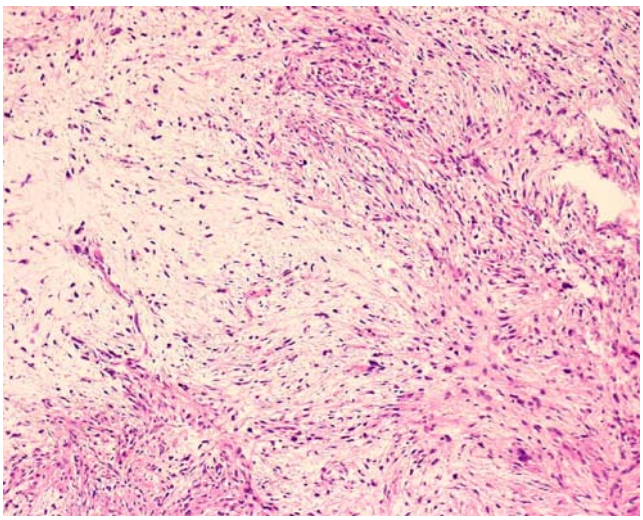

Fig. 6 Myxofibrosarcoma. This intermediate-grade myxofibrosarcoma is composed of an admixture of myxoid and cellular areas. Nuclear atypia are obvious

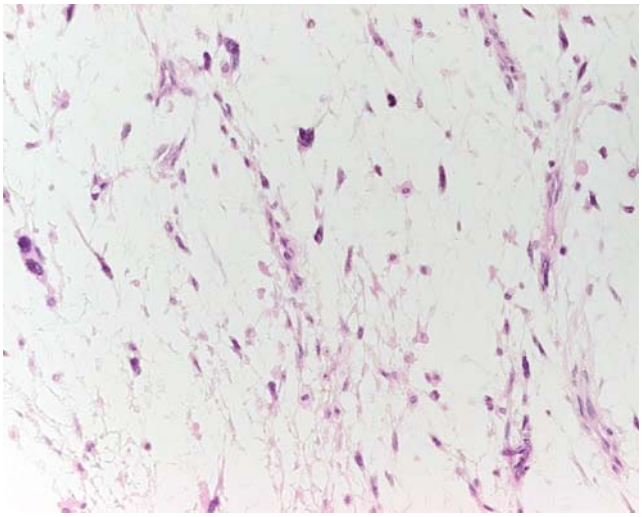

Fig. 7 Myxofibrosarcoma. This low-grade myxofibrosarcoma is paucicellular and contains an abundant myxoid extracellular matrix. Curvilinear vessels are readily visible. Despite low cellularity, nuclear atypia are always present

lioid myxofibrosarcomas are mostly high-grade tumors displaying prominent carcinoma-like or rhabdomyosarcoma-like appearances [57]. Intermediate-grade myxofibrosarcomas are more cellular than low-grade lesions and often contain minute solid areas showing frank pleomorphism.

Immunohistochemically, tumor cells stain diffusely for vimentin and occasionally for smooth muscle actin. They are negative for S100 protein and CD34. They show ultrastructural features of fibroblasts and, less frequently, of myofibroblasts.

Differential diagnosis

High-grade myxofibrosarcoma may be confused with any pleomorphic sarcoma including myxoinflammatory fibroblastic sarcoma (see below). Occurrence in the elderly, subcutaneous location, and the presence of small myxoid areas in an otherwise pleomorphic tumor should point to the diagnosis. Epithelioid myxofibrosarcoma should be distinguished from a poorly differentiated carcinoma, a melanoma, a pleomorphic liposarcoma, and a pleomorphic rhabdomyosarcoma [57].

Pleomorphic liposarcoma

PLPS is the less common variant of liposarcoma, accounting for less than 5% of all liposarcomas. It tends to occur in elderly people (median age 55–65 years) [1, 2, 58–60].

Cytogenetics and molecular genetics

Data on the cytogenetics and molecular genetics of PLPS are relatively limited. PLSP show, characteristically, high chromosome counts and complex structural arrangements, similar to that observed in UPS [61]. No specific genetic alterations have been attributed to PLPS. CGH analyses showed gains of 1p, 1q21-q32, 2q, 3p, 3q, 5p12-p15, 5q, 6p21, 7p, 7q22, 8q, 10q, 12q12-q24, 13q, 14q, 15q, 17p, 17q, 18p, 18q12, 19p12, 19q13, 20q, 22q, and Xq21-q27, and losses of 1q, 2q, 3p, 4q, 10q, 11q, 12p13, 13q14, 13q21-qter, 14q23-24, 16q22, 17p13, 17q11.2, and 22q13 [54, 62, 63]. Idbaih et al. [54] observed that chromosome imbalances encountered in PLPS were very similar to those observed in their series of myxofibrosarcoma, and that the two histotypes, taken together, can be distinguished from other pleomorphic sarcomas and more specifically from LMS. In the study of Schmidt et al. [62], patients with gains of 13q (i.e., 13q21, 13q22, 13q31, and 13q32) experienced shortened survivals as compared to those lacking these gains.

Deletion of 13q14.2-q14.3, targeting the RB1 pathway, is observed in about 60% of PLPS [63]. Other frequent events are loss of 17p13, spanning TP53, and loss of 17q11.2 containing the neurofibromatosis type 1 (NF1) gene [63]. Mutations of TP53 are frequent in PLPS [61]. Amplification of δ catenin on 5p and deregulation of genes involved in adipogenesis (C/EBPα and C/EBPγ on 19q, EP300 on 22q13) are also observed, and this may explain, in part, the propensity of PLPS to metastasize and to lose its adipocytic differentiation, respectively [63].

Despite their morphologic similarity, PLPS and high-grade dedifferentiated LPS show distinct chromosomal imbalances [64, 65]. Gains of 5p13-p15, 1p21, 1q21-q22, and 7q22 are more frequently observed in PLPS whereas high-level amplifications within chromosomal subregion 12q13-q21 were observed only in dedifferentiated LPS [64, 65]. Using a microarray-based gene expression profiling approach, Singer et al. [66] show that dedifferentiated and pleomorphic liposarcomas had different molecular signatures. Distinction between these two histotypes can be performed based on 15 differentially expressed genes, of which 12 (e.g., MDM2, CDK4) were located in the 12p13-p15 region [66]. Similar results were obtained by Fritz et al. in 2002 [65]. MAD2, a gene involved in the RB1 signaling pathway which is overexpressed by PLPS (and dedifferentiated LPS), might constitute a therapeutic target [66].

Recently, Matushansky et al. [67] proposed a nice hypothesis according to which soft tissue sarcomas, including LPS, could be categorized by their developmental/differentiation status from stem cell to mature tissue. Gene expression analyses were performed during in vitro differentiation of human mesenchymal stem cells into adipose tissue and results compared to gene expression in each of the four liposarcoma subtypes. The authors observed that some genes that were overexpressed in a given liposarcoma subtype were also overexpressed during given stages of normal adipocytic differentiation. In other

terms, each liposarcoma subtype profile would indicate the stage of differentiation arrest. After excluding markers of differentiation, the authors observed that cell cycle and purine metabolism pathways were upregulated in PLPS and MAPK kinase and insulin signaling pathways downregulated, suggesting that these pathways play significant role in PLPS tumorigenesis. Interestingly and unexpectedly, KRAS (a well-characterized oncogene) is overexpressed in PLPS as a marker of differentiation and not as a marker of tumorigenesis. They also observed that some liposarcoma subtypes do not parallel corresponding stages of adipocytic differentiation, suggesting additional molecular events [67].

Clinical features

PLPS occur predominantly in deep soft tissues (75% of cases) of the lower extremities, especially the thigh [1, 2, 58–60]. The limb girdles and the trunk (including the retroperitoneum) are each involved in 20% of cases. PLPS are high-grade tumors that recur locally in 35–50% and metastasize in 30–40% of cases. Five-year overall, metastasis-free and local recurrence-free survivals are 40–63%, 30–58%, and 25–75%, respectively [1, 2, 58, 59]. Tumor grade and morphologic features (except for epithelioid morphology) seem not to affect patient outcome [58–60]. Tumors >5 cm, deep-seated lesions, and truncal tumor location are adverse prognostic factors [58, 59]. Although rare, dermal PLPS have a much better prognosis as they are easily amenable to complete excision [68].

Pathological features

PLPS are composed of a varying combination of lipogenic and nonlipogenic areas (Fig. 8). Lipogenic areas are composed of malignant adipocytes and/or pleomorphic, often multivacuolated, lipoblasts with scalloped hyperchromatic nuclei. Nonlipogenic areas are characterized by malignant fibrous histiocytoma-like, leiomyosarcoma-like, round-cell-liposarcoma-like, and/or epithelioid/carcinoma-like features [1, 2, 58–60]. Areas showing hemangiopericytoma-like features are also occasionally observed [58, 59]. Tumor necrosis is common.

Immunohistochemically, lipogenic areas are often positive for S100 protein (35–50% of cases), whereas nonlipogenic areas show varying and often focal staining for smooth muscle actin, desmin, and CD34. Focal reactivity for keratins and/or EMA is occasionally observed, especially in PLPS containing epithelioid areas [58–60].

Differential diagnosis

Diagnostic criteria for PLPS rely on the histologic presence of malignant adipocytes/lipoblasts in a high-grade pleomorphic sarcoma, regardless of the extent of lipogenic areas. As a consequence, any pleomorphic sarcoma enters the differential of PLPS, and adequate (extensive) sampling is crucial to pick up minute lipogenic foci. Melanoma and sarcomatoid carcinoma (renal cell carcinoma, adrenocortical carcinoma) should be ruled out. Cytoplasmic vacuolization resulting from fixation artifacts may be misleading, mimicking true lipoblasts. PLPS composed predominantly of small round cells may be confused with round cell liposarcoma (especially in the thigh). As opposed to PLPS, dedifferentiated LPS characteristically contains a juxtaposed well-differentiated liposarcomatous component and displays MDM2 and/or CDK4 nuclear reactivity.

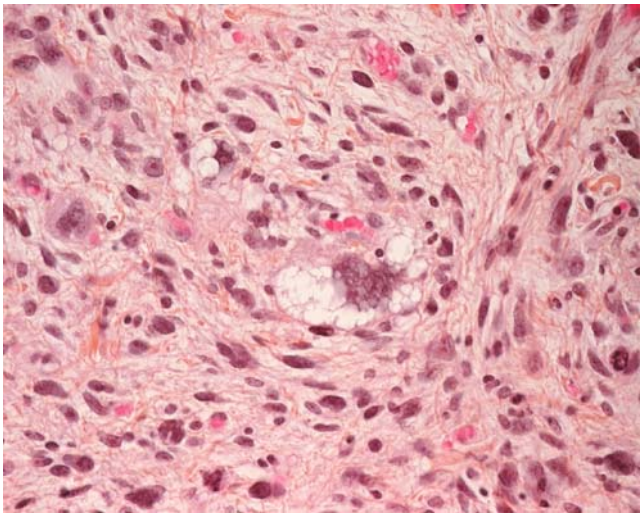

Fig. 8 Pleomorphic liposarcoma. The tumor shows the appearance of an undifferentiated pleomorphic sarcoma, except for the presence of highly pleomorphic and multivacuolated malignant adipocytes

Pleomorphic rhabdomyosarcoma

PRMS are rare neoplasms of adulthood. They account for about 5% of all adult pleomorphic soft tissue sarcomas [1, 2, 69–72].

Cytogenetics and molecular genetics

Data on the cytogenetics and molecular genetics of PRMS are scarce. They show nonspecific complex karyotypes. Numerical and unbalanced structural abnormalities are common, overlapping with those of UPS or osteosarcoma, and are different from those encountered in embryonal and alveolar rhabdomyosarcoma. Chromosomal numerical aberrations include gains of chromosomes 1, 5, 8, 14, 18, 20, and 22 and losses of chromosomes 2, 5, 6, 10, 11, 13, 14, 15, 16, 17, 18, 19, and Y, of which losses of chromosomes 2, 13, 14, 15, 16, and 19 are the most frequent [73]. Using CGH, Gordon et

al. [74] observed gains in the regions 1p22-23, 7p, 18/18q, and 20/20p, losses of 10q23 (spanning the gene PTEN), 15q21-q22, 3p, 5q32-qter, and 13, and amplicons involving the regions 1p21-p31, 1q21-q25, 3p12, 3q26-qtel, 4q28-q31, 8q21-q23/8q, and 22q. With the exception of one case [74], PRMS do not contain the t(2;13) or t(1;13) alveolar rhabdomyosarcoma reciprocal translocations.

Clinical features

PRMS usually occur in the extremities, especially the thigh, of middle-aged adults (often men) [1, 2, 69–72], although a few cases have been observed in childhood [70, 72]. They are aggressive high-grade (grade 3) tumors, prone to recurrence and metastatic dissemination (lungs) [1, 2, 69–72]. Roughly 70% of patients die of their disease within 2 years of diagnosis [69, 71, 72].

Pathologic features

PRMS are essentially composed of large, pleomorphic, epithelioid to spindle-shaped cells with abundant, deeply eosinophilic cytoplasm and vesicular nuclei with prominent nucleoli. Marked nuclear atypia and tumor necrosis are common. Monstrous, often multinucleated, giant cells resembling rhabdomyoblasts are frequently encountered (Fig. 9), but cross-striations are rarely visible.

Immunohistochemically, tumor cells are positive for desmin and fast skeletal muscle myosin but also, at least focally, for smooth muscle actin. Because of poor specificity, myoglobin is not a good marker for the diagnosis of rhabdomyosarcoma. Myogenin reactivity is usually observed in a small proportion of tumor cells. Calponin (but not h-caldesmon) is positive. Rudimentary sarcomeres and ribosome–myosin complexes are observed in tumor cells on ultrastructural examination.

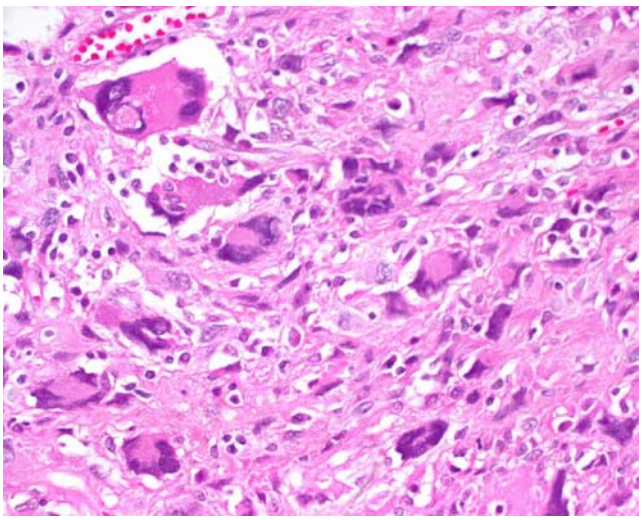

Fig. 9 Pleomorphic rhabdomyosarcoma. Intimate admixture of spindle cells and pleomorphic multinucleated giant cells corresponding to malignant rhabdomyoblasts

Differential diagnosis

The differential diagnosis for PRMS is similar to that of PLMS. Reactivity for desmin and myogenin are diagnostic clues. When faced with a tumor showing skeletal muscle differentiation, before considering the diagnosis of PRMS, other pleomorphic sarcoma subtypes that may contain foci of heterologous striated muscle differentiation should be ruled out, including dedifferentiated liposarcomas, malignant peripheral nerve sheath tumors (malignant Triton tumors), and metastases from metaplastic carcinomas (malignant mixed müllerian tumors) and Wilms' tumor.

Malignant peripheral nerve sheath tumor

MPNSTs are defined as malignant neoplasms arising from peripheral nerves or in extraneural soft tissue if it shows nerve sheath differentiation (i.e., Schwannian differentiation), excluding tumors originating from epineurial tissue or from peripheral nerve vasculature [75]. MPNSTs account for 5–8% of all soft tissue sarcomas; about 50% of them occur in the setting of NF1.

Cytogenetics and molecular genetics

Cytogenetically, MPNSTs display complex karyotypes and clonal chromosomal aberrations, regardless of clinical setting (i.e., sporadic versus NF1-associated MPNSTs). Chromosomal losses seem to be more frequent than gains [7, 76, 77]. Losses of 1p12-13, 1p21, 1p36, 3p21-pter, 9p13-21, 9p22-24, 10, 10p11-15, 11p, 11q21-25, 13q14, 15p, 16/16q24, 17/17p, 17q11-12, 17q21-25, 22, 22p, 22q13, and 22q11-12 were the most frequent abnormalities observed [7, 76, 77]. Gains mainly involved the regions 7p21-q36, 7p22, 7q, 8, 8q11-23, 1q25-44, and 5q13-35. Breakpoints are often numerous, involving many chromosomes or chromosomal regions. Regions mostly involved are: 1p, 7p22 (spanning the ETV1 gene), 11q13-23, 20q13 (spanning the SRC gene), and 22q11-13 (spanning the NF2 gene) [76, 77]. Ring chromosomes, trisomy 7, and rearrangements of 11p and 12q13-15 were also reported [7]. Amplifications are rare [77]. In the series of Fletcher et al. [7], complex rearrangements were more frequent in MPNSTs associated with von Recklinghausen's disease and in tumors showing heterologous differentiation. There were no correlations between karyotypic abnormalities and clinical parameters [7]. Large and/or high-grade tumors

frequently contain triploid or tetraploid clones, correlating with clinical aggressiveness [76]. Complex karyotypes are generally not observed in benign peripheral nerve sheath tumors (e.g., schwannoma and perineurioma), and this may help in classifying atypical peripheral nerve sheath neoplasms. Malignant Triton tumor and conventional MPNSTs lacking heterologous differentiation show similar complex karyotypes [77]. MPNSTs do not contain the t(X;18) synovial sarcoma translocation.

In CGH analyses of MPNSTs, chromosomal gains tend to outnumber losses. Most frequent minimal recurrent regions of gain included 1q24-25, 8p23-p12, 9q34, and 17q23-q25 [78]. Gain of 17q23-25 was strongly associated with poor prognosis, presence of metastases, and overexpression of some specific genes, namely topoisomerase II alpha, ETV4 (EIA), surviving/BIRC5 and HER2/neu (ERBB2) which might be involved in MPNST pathogenesis [78–81]. Gain of 7p15-p21 was also found associated with shortened survival [80]. Amplifications were also detected [82, 83].

Molecular genetics studies of MPNSTs showed that sporadic and NF1-associated MPNSTs display monoallelic or biallelic loss at the NF1 locus (localized at 17q11.2) in about 20–50% of cases [76, 83]. Germ line mutations of the NF1 gene, a tumor suppressor gene which encodes for the RasGTPase activating protein neurofibromin, have been demonstrated in families affected by von Recklinghausen disease. Loss of function of the NF1 gene (by mutation or loss of heterozygosity) is the key early step in the pathogenesis of peripheral nerve sheath tumors. It leads to neurofibromin loss and subsequent activation of the ras signaling cascade, increasing the risk of MPNST development [84]. Additional abnormalities are needed, however, to progress from benign to malignant peripheral nerve sheath tumor. TP53 (localized to 17p13) is frequently inactivated through mutations or deletions, correlating with the frequent loss of 17p [76]. The same observation applies to the regions 9p21 and 13q14 which are often rearranged or lost, resulting in an inactivation of the CDKN2A (encoding the $p16^{INK4A}$ and $p14^{ARF}$ cell cycle inhibitory proteins) and RB1 genes, respectively. The expression of $p15^{INK4B}$ and $p27^{KIP1}$, two cyclin-dependent kinase inhibitors is also altered in MPNSTs [84]. The tumor suppressor NF2 gene is located at 22q12.2, and inactivation of this gene, mostly by mutations, has been demonstrated in neurofibromatosis type 2. Since the region 22q11-13 is frequently rearranged in MPNSTs, it has been hypothesized that the NF2 gene could play some role in the tumorigenesis and/or progression of MPNST [77]. Using high-resolution DNA copy number profiling, Mantripragada et al. [83] recently reported amplifications of PDGFRA, ITGB4, MET TP73, HGF, and BIRC5/survivin and deletions of NF1, HMMR/RHAMM, MMMP13, CDKN2A, and TP53 in MPNSTs. Overexpression of BIRC5/survivin correlates with an amplicon located at distal 17q [79]. Other recently identified genes such as TRIO, IRX2, and NKD2 [10] as well as TWIST1 and TNC [83] might also be implicated in MPNST pathogenesis.

Clinical features

Conventional MPNSTs occur mostly in middle- to advanced-aged adults, without sex predilection. Fifty percent to 70% develop in preexisting neurofibroma, especially in plexiform neurofibroma associated with NF1. Sporadic MPNSTs are less frequent, presenting as deep soft tissue masses, usually in association with large nerves (e.g., sciatic). Exceptionally, they may develop within a schwannoma. Ten percent of MPNSTs occur at a site of prior irradiation. NF1-associated MPNSTs occur generally 10 years younger than sporadic forms. Pain and/or neurological symptoms (e.g., paresthesias) are the most common presenting symptoms. Predominantly affected sites include the buttock and sacral plexus, thigh, paraspinal nerves, and brachial plexus [75].

Many clinicopathologic variants of MPNSTs have been described, including epithelioid MPNST (5% of MPNSTs), MPNST with mesenchymal (osteosarcomatous, chondrosarcomatous, and/or angiosarcomatous) differentiation (10% of cases), MPNST with perineurial differentiation, MPNST with rhabdomyosarcomatous differentiation (malignant Triton tumor), and glandular MPNST. Malignant Triton tumors and glandular MPNSTs are rare and associated with NF1 in 60% and 75% of cases, respectively. Epithelioid MPNSTs, which may occur either in the subcutis or in deep soft tissues, show no relationship to NF1.

Most MPNSTs are high-grade aggressive neoplasms, especially glandular and malignant Triton tumors. Outcome in MPNSTs depends on several factors, including tumor stage, tumor size, location, histologic subtype, status of surgical margins, previous irradiation, and high (>25%) MIB-1 labeling index [75]. The prognostic value of histologic grade is limited in MPNSTs. About 60% of patients die of disease. Overall, 5- and 10-year survival rates are 34% and 23%, respectively [75]. There are no significant prognostic differences between NF1-associated and sporadic MPNSTs.

Pathologic features

Most MPNSTs measure 5 cm or more in maximal diameter. High-grade tumors frequently contain areas of necrosis and/or hemorrhage on cut section. Histologically, many MPNSTs present as monomorphic spindle cell tumors resembling adult-type fibrosarcoma or monophasic synovial sarcoma (Fig. 10). Alternating myxoid and cellular areas are frequently observed. Tumor cells tend to agglomerate

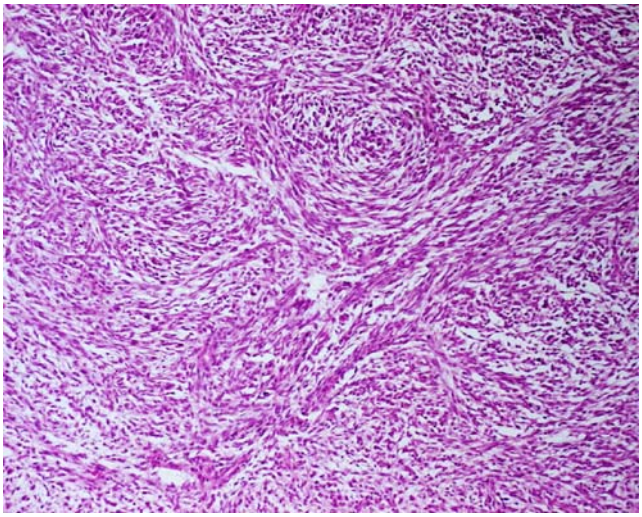

Fig. 10 Malignant peripheral nerve sheath tumor. The proliferation is composed of intersecting fascicles of monomorphic spindle cells. Some degree of whorling pattern is visible in this field

around large vessels, often infiltrating vessel walls. Tumor cell nuclei are typically buckled in well-differentiated lesions, resembling that observed in neurofibroma. Whorl structures, nuclear palisading, or reticular arrangement of tumor cells resembling perineurioma may be seen. Brisk mitotic activity and areas of geographic necrosis are common in large/high-grade neoplasms. Foci of osteosarcomatous and/or chondrosarcomatous heterologous differentiation are observed in about 10% of tumors. About 5% of MPNSTs are characterized by prominent epithelioid cytomorphology. Rarely, MPNSTs show features of perineurial differentiation or contain rhabdomyoblasts (malignant Triton tumor; Fig. 11) or glandular epithelium. In glandular MPNSTs, benign or malignant-looking glandular structures are few in number, are well demarcated from the spindle cell component, and often contain mucinous (globet) cells and chromogranin-positive endocrine cells. Squamous differentiation is very rare. Immunohistochemically, spindle cells in MPNSTs are focally reactive for S100 protein in 50% to 70% of cases. Staining is grade dependent; the higher the grade, the more patchy and less intense is the staining. They may also express CD57 and CD34, as well as EMA. EMA expression is usually taken as a sign of perineurial differentiation. MPNSTs are usually negative for cytokeratins. Most MPNSTs overexpress the P53 protein, in contrast to (non-atypical) neurofibromas. Focal reactivity for desmin and myogenin is seen in malignant Triton tumors. As opposed to conventional (e.g., spindle cell) MPNSTs, epithelioid MPNSTs are generally strongly and diffusely positive for S100 protein but negative for melanocytic and epithelial markers. Glandular structures in glandular MPNSTs express epithelial markers, CEA, and sometimes endocrine markers (chromogranin-A, CD56, synaptophysin).

Differential diagnosis

Conventional spindle cell MPNSTs should be first distinguished from monophasic synovial sarcoma and cellular schwannoma. Most spindle cell monophasic synovial sarcomas express EMA and/or cytokeratins, at least focally, and are negative for CD34. In addition, as opposed to MPNSTs, they bear the t(X;18)(p11;q11) translocation which is specific of this tumor type. In addition, to be well circumscribed, cellular schwannomas are typically strongly and diffusely positive for S100 protein. MPNSTs should also be separated from other spindle cell tumors, namely leiomyosarcoma (negativity for S100 protein, reactivity for smooth muscle actin, h-caldesmon, and desmin), spindle cell rhabdomyosarcoma (positivity for desmin and myogenin), adult-type fibrosarcoma, spindle cell carcinoma, spindle cell melanoma (diffuse reactivity for S100 protein), and spindle cell mesothelioma. Glandular MPNST should be distinguished from biphasic synovial sarcoma and epithelioid MPNST from melanoma (positivity for HMB45, Melan-A, and/or Mitf), epithelioid sarcoma, epithelioid angiosarcoma, and epithelioid-looking myoepithelioma.

Other soft tissue sarcomas with complex karyotypes

Adult-type fibrosarcoma

Twenty years ago, fibrosarcoma was a common diagnosis. With the advent of immunohistochemistry and molecular ancillary techniques, numerous entities escape the ill-defined group of fibrosarcoma (e.g., deep-seated fibromatosis, synovial sarcoma, malignant peripheral nerve sheath

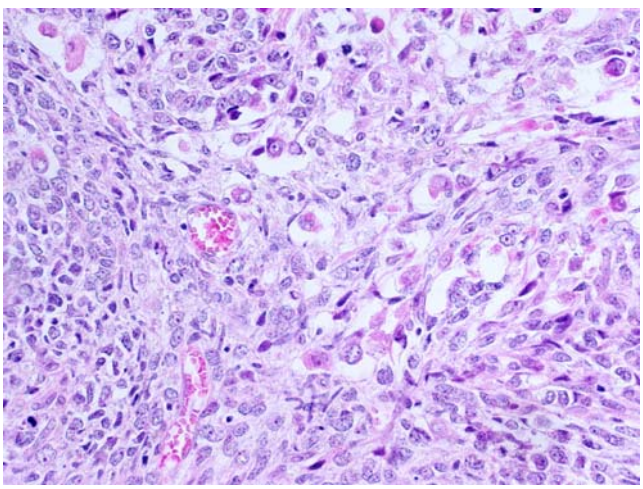

Fig. 11 Malignant Triton tumor. Small aggregates of relatively mature rhabdomyoblasts are observed, admixed with the spindle to round cell proliferation. The cytoplasm of rhabdomyoblasts is copious and markedly eosinophilic

tumor, myofibroblastic sarcomas, dedifferentiated liposarcoma, dermatofibrosarcoma with fibrosarcomatous transformation, spindle cell rhabdomyosarcoma) whereas many others were recognized as specific fibrosarcomatous entities (e.g., infantile fibrosarcoma, low-grade fibromyxoid sarcoma, sclerosing epithelioid fibrosarcoma, myxoinflammatory fibroblastic sarcoma, myxofibrosarcoma, inflammatory fibrosarcoma). Nowadays, adult-type fibrosarcoma is a diagnosis of elimination. It accounts for no more than 3–5% of adult soft tissue sarcomas, and this sarcoma category overlaps morphologically with the undifferentiated spindle cell/pleomorphic sarcoma—UPS category [1, 2].

Because of the relative uncertainty about the diagnosis of adult-type fibrosarcoma, cytogenetic data are very scarce and questionable. Cytogenetically, adult fibrosarcoma shows multiple chromosomal rearrangements. Gains of 4q, 6q, 7, and 20 and loss of chromosomes 13 and 14 have been reported [7], as well as involvement of the 2q21-qter region [1].

Angiosarcoma

Angiosarcomas are malignant neoplasms showing varying degrees of vascular differentiation. External beam radiation is an important risk factor for the development of angiosarcomas/lymphangiosarcomas of the skin, breast, and soft tissue. Other risk factors include exposure to vinyl chloride and thorium. Most angiosarcomas of soft tissue are composed by an admixture of spindle cells, epithelioid cells, and poorly formed vascular structures, although a predominantly epithelioid variant exists. Cytogenetic data are minimal for angiosarcoma. These tumors usually show complex karyotypes. The chromosomes number ranges from hypodiploid to hypertriploid. Most common chromosomal imbalances are gains of 5pter-p11, 8p12-qter, and 20pter-q12, losses of 4p, 7p15-pter, and 7p15-Y, and aberrations involving 22q [1, 2]. As opposed to Kaposi sarcoma, angiosarcomas of soft tissue are negative for HHV8. KRAS-2 and TP53 mutations were observed in thorium- and vinyl chloride-associated angiosarcomas as well as in sporadic angiosarcomas [85, 86]. An alteration of the TP53/MDM2 pathway with elevated expression of TP53 and MDM2 proteins has been documented in 60% of angiosarcomas [87]. Loss of heterozygosity at TP53, WT1, and RB1 loci was recently reported in angiosarcomas, supporting a role for these tumor suppressor genes in angiosarcoma pathogenesis [88].

Extraskeletal osteosarcoma

Extraskeletal osteosarcoma is a malignant tumor showing osteoid formation. Most are high-grade neoplasms. It accounts for less than 5% of all osteosarcomas and occurs mostly in the deep soft tissue of middle-aged adults (median age 55–65 years) [89, 90]. Many of these tumors have been reported previously as giant cell malignant fibrous histiocytomas with bone production. The most commonly affected sites included lower extremities, especially the thigh (50% of cases), thoracic wall, and internal trunk [89, 90]. Half of neoplasms measured 5 cm or more in maximal diameter. As opposed to osseous osteosarcomas, extraskeletal osteosarcomas are relatively resistant to doxorubicin-based systemic therapy, and the prognosis is poor. Metastases develop in 50% to 60% of cases [89, 90]. For patients with metastatic disease at diagnosis, median survival duration was 8 months in the series of Ahmad et al. [89]. For patients with localized disease at diagnosis, 5-year disease-specific and event-free survival rates were 46% and 47%, respectively; quite similar to that observed in high-grade soft tissue sarcomas [89]. External beam irradiation is an acknowledged risk factor for the development of extraskeletal osteosarcoma [90, 91].

Morphologically, extraskeletal osteosarcoma resembles UPS except for the presence of osteoid (and sometimes chondroid) matrix.

Data on the cytogenetics of extraskeletal osteosarcoma are very scarce. Highly complex aberrations have been reported, including gains of 1q, 2, 8, and 17p11 and losses of 1q, 2, 5, 6, 12, 13, 14, 15, 16, 18, 19, 20, 21, and Y [1, 30, 92]. These alterations parallel those observed in skeletal osteosarcoma, especially chromosomal gains and regional amplifications of chromosome arms 1q, 6p21-p12, 8q23-q24, and 17p13-p11.2 [93, 94], partial or complete loss of 6q, as well as various rearrangements of chromosomes 20 [95, 96]. TP53 (located at 17p13) and RB1 (located at 13q14) genes are consistently affected in skeletal and extraskeletal osteosarcomas (through allelic losses, rearrangements or point mutations), as well as many other genes involved in cell cycle regulation ($p14^{ARF}$, $p16^{INKa}$, MDM2, etc.) [97].

Myxoinflammatory fibroblastic sarcoma (inflammatory myxohyaline tumor)

Myxoinflammatory fibroblastic sarcoma is a low-grade neoplasm which is mostly (but not exclusively) observed in the distal extremities (50% in fingers and hands) of middle-aged adults [1, 2, 98, 99]. The lesion, which is usually small (median 3–4 cm), develops in the subcutis, in deep soft tissues, or along tendon sheaths. Histologically, it bears a striking resemblance to high-grade myxofibrosarcoma, showing alternating myxoid, cellular, inflammatory, and fibrohyalinized areas (Fig. 12). Tumor cells are either spindle-shaped or epithelioid. Epithelioid cells tend to display a copious eosinophilic cytoplasm, enlarged vesicular nuclei, and macronucleoli, thus resembling ganglion cells or virocytes (Fig. 13). Myxoid areas often contain

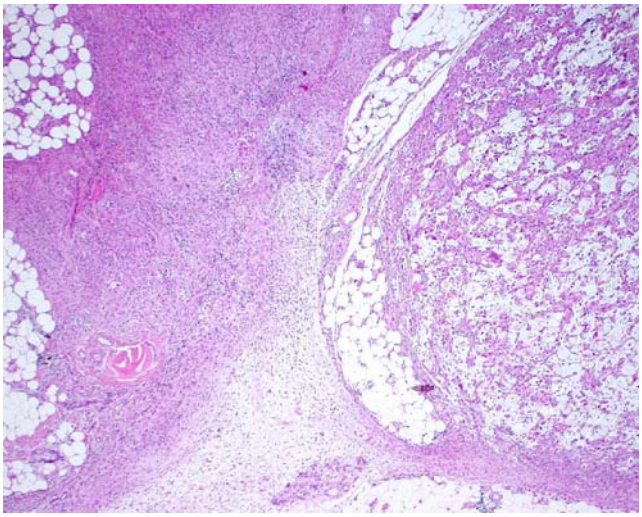

Fig. 12 Myxoinflammatory fibroblastic sarcoma (inflammatory myxohyaline tumor). An infiltrating neoplasm composed of spindle and pleomorphic cells, inflammatory elements, hypocellular to hyalinized areas, and myxoid areas containing vacuolated, lipoblast-like cells

univacuolated or multivacuolated lipoblast-like cells. Mitotic activity is usually low and tumor necrosis infrequent. Local recurrences are observed in about 20% of cases; metastases are rare (<5%).

Most myxoinflammatory fibroblastic sarcomas show complex, near-diploid, or hypotriploid karyotypes [100–103]. CGH analyses showed gains of chromosome 7 in two cases [101]. Distinctive abnormalities in myxoinflammatory fibroblastic sarcoma are the frequent presence of a balanced or unbalanced t(1;10) (p22;q24) translocation [100–102], ring chromosomes [102, 103], and amplification of the chromosomal region 3p11-12 [103]. A t(2;6)(q31;p21.3) translocation has also been described as a sole cytogenetic abnormality in this tumor type [104]. The breakpoints in the t(1;10) translocation map to TGFBR3 in 1p22 and in or near MGEA5 in 10q24, resulting in transcriptional upregulation of NPM3 and particularly FGF8, two consecutive genes located close to MGEA5 [103]. The ring chromosomes contain an amplified region in 3p11-12 which was associated with an increased expression of VGLL3 and CHMP2B. Beside typical examples of myxoinflammatory fibroblastic sarcoma, the amplicon in 3p was also detected in some inflammatory variants of undifferentiated pleomorphic sarcoma (so-called inflammatory MFH) [103]. The t(1;10) translocation was also observed in another tumor, the hemosiderotic fibrolipomatous tumor, which is likely to constitute a precursor for the myxoinflammatory fibroblastic sarcoma [103].

Radiation-associated sarcomas

Radiation-associated sarcomas are defined as sarcomas arising in a previously irradiated field after a latency period of at least 2 years [91, 105]. Occurring in about 1/1,000 patients who have undergone radiation therapy [106], it is an infrequent but well-known long-term complication of radiotherapy [91, 105–108]. They usually occur in middle-aged adults and show a more aggressive clinical course associated with shortened patient survival as compared to sporadic sarcomas [91, 105–108]. Most frequent histologic types include high-grade undifferentiated pleomorphic sarcoma (previously called malignant fibrous histiocytoma), extraskeletal osteosarcoma, fibrosarcoma, malignant peripheral nerve sheath tumor, chondrosarcoma, leiomyosarcoma, and angiosarcoma [91, 105–108].

Radiation-associated soft tissue sarcomas are typically high-grade neoplasms with complex karyotypes. Numerical and structural (mostly unbalanced) rearrangements are common, irrespective of histological type [91]. Comparing postradiation and de novo sarcomas, Mertens et al. [91] observed that loss of material from chromosome 3p (especially from the 3p21-3pter region) was most frequent in postradiation sarcomas, in addition to the varying presence of cytogenetically unrelated clones. Other frequent imbalances were losses of Xq, 3p14, 1q42-qter, and 1q23-24. CGH analyses disclosed gains of 5p, 7cen-q22, and 15cen-q15 and loss of chromosome 13 [91]. The frequency of TP53 mutations is also very high as compared to that of sporadic sarcomas (88% versus 20%) [109].

Conclusion

Sarcomas displaying complex karyotypes are much more common than those harboring relatively simple cytogenetic

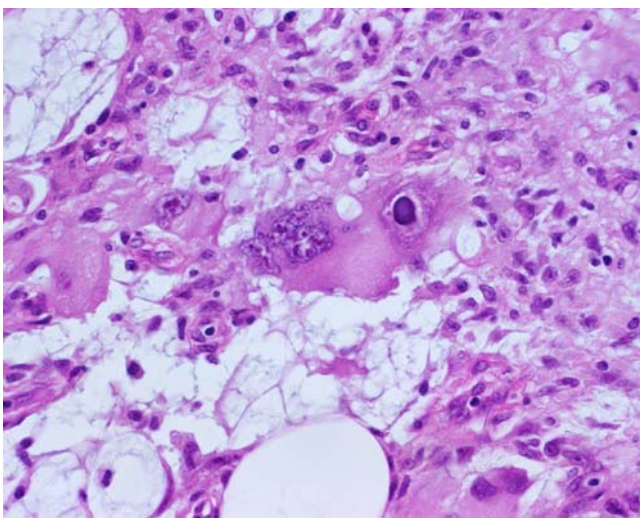

Fig. 13 Myxoinflammatory fibroblastic sarcoma (inflammatory myxohyaline tumor). Some pleomorphic cells contain viral-like intranuclear pseudoinclusions

profiles with recurrent genetic aberrations (e.g., reciprocal translocations or mutations). Within the former group, leiomyosarcomas and undifferentiated pleomorphic sarcomas predominate. Thanks to new molecular technologies such as CGH-array-based techniques and gene expression analyses, significant progresses have been accomplished regarding the identification of genes, gene products, and signaling pathways particularly involved in the pathogenesis, progression, and metastatic dissemination of sarcomas. Novel diagnostic and/or prognostic molecular markers as well as promising therapeutic targets have been gradually recognized. A new era is coming in which candidates for adjuvant therapy will be selected not only on their clinicopathologic characteristics but also on their "molecular profile".

Conflict of interest statement We declare that we have no conflict of interest.

References

1. Fletcher CDM, Unni KK, Mertens F (eds) (2002) World Health Organization classification of tumours. Pathology and genetics of tumors of soft tissue and bone. IARC Press, Lyon
2. Weiss SW, Goldblum JR (2008) In: Weiss SW, Goldblum JR (eds) Enzinger and Weiss's soft tissue tumors, 5th edn. Mosby-Elsevier, Philadelphia
3. Dei Tos AP (2006) Classification of pleomorphic sarcomas: where are we now? Histopathology 48:51–62
4. Sandberg AA (2005) Updates on the cytogenetics and molecular genetics of bone and soft tissue tumors: leiomyosarcoma. Cancer Genet Cytogenet 161:1–19
5. Mandahl N, Fletcher CDM, Dal Cin P et al (2000) Comparative cytogenetic study of spindle cell and pleomorphic leiomyosarcomas of soft tissues: a report from the CHAMP Study Group. Cancer Genet Cytogenet 116:66–73
6. Yang J, Du X, Chen K et al (2009) Genetic aberrations in soft tissue leiomyosarcoma. Cancer Lett 275:1–8
7. Fletcher CDM, Dal Cin P, De Wever I et al (1999) Correlation between clinicopathologic features and karyotype in spindle cell sarcomas. A report of 130 cases from the CHAMP Study Group. Am J Pathol 154:1841–1847
8. Wang R, Titley JC, Lu YJ et al (2003) Loss of 13q14–q21 and gain of 5p14-pter in the progression of leiomyosarcoma. Mod Pathol 16:778–785
9. Hu J, Rao UNM, Jasani S et al (2005) Loss of DNA copy number of 10q is associated with aggressive behavior of leiomyosarcomas: a comparative genomic hybridization study. Cancer Genet Cytogenet 161:20–27
10. Adamowicz M, Radlwimmer B, Rieker RJ et al (2006) Frequent amplifications and abundant expression of TRIO, NKD2, and IRX2 in soft tissue sarcomas. Genes Chromosomes Cancer 45:829–838
11. Hernando E, Charytonowicz E, Dudas ME et al (2007) The AKT-mTOR pathway plays a critical role in the development of leiomyosarcomas. Nat Med 13:748–753
12. Bjornsti MA, Houghton PJ (2004) The TOR pathway: a target for cancer therapy. Nat Med 10:594–601
13. Mita MM, Tolcher AW (2007) The role of mTOR inhibitors for treatment of sarcomas. Current Oncology Reports 9:316–322
14. Lee YF, John M, Falconer A et al (2004) A gene expression signature associated with metastatic outcome in human leiomyosarcomas. Cancer Res 64:7201–7204
15. Ren B, Yu YP, Jing L et al (2003) Gene expression analysis of human soft tissue leiomyosarcomas. Hum Pathol 34:549–558
16. Suehara Y, Kondo T, Fujii K et al (2006) Proteomic signatures corresponding to histological classification and grading of soft-tissue sarcomas. Proteomics 6:4402–4409
17. Kawaguchi K, Oda Y, Saito T et al (2003) Mechanisms of inactivation of the p16INK4a gene in leiomyosarcoma of soft tissue: decrease. J Pathol 201:487–495
18. Dei Tos AP, Maestro R, Doglioni C et al (1996) Tumor suppressor genes and related molecules in leiomyosarcoma. Am J Pathol 148:1037–1045
19. Seidel C, Bartel F, Rastetter M et al (2005) Alterations of cancer-related genes in soft tissue sarcomas: hypermethylation of RASSF1A is frequently detected in leiomyosarcoma and associated with poor prognosis in sarcoma. Int J Cancer 114:442–447
20. Kawaguchi K, Oda Y, Saito T et al (2006) DNA hypermethylation status of multiple genes in soft tissue sarcomas. Mod Pathol 19:106–114
21. Francis P, Namlos HM, Müller C et al (2007) Diagnostic and prognostic gene expression signatures in 177 soft tissue sarcomas: hypoxia-induced transcription profile signifies metastatic potential. BMC Genomics 8:73
22. Pérot G, Derré J, Coindre JM et al (2009) Strong smooth muscle differentiation is dependent on myocardin gene amplification in most human retroperitoneal leiomyosarcomas. Cancer Res 69:2269–2278
23. Deyrup AT, Lee VK, Hill CE et al (2006) Epstein–Barr virus-associated smooth muscle tumors are distinctive mesenchymal tumors reflecting multiple infection events: a clinicopathologic and molecular analysis of 29 tumors from 19 patients. Am J Surg Pathol 30:75–82
24. Kubben FJGM, Kroon FP, Hogendoorn PCW et al (1997) Absence of Epstein–Barr virus in a gastrointestinal stromal cell tumour (GIST) in an adult human immunodeficiency virus-seropositive patient with past Epstein–Barr virus (EBV) infection. Eur J Gastroent Hepatol 9:721–724
25. Moinfar F, Azodi M, Tavassoli FA (2007) Uterine sarcomas. Pathology 39:55–71
26. Quade BJ, Wang TY, Sornberger K et al (2004) Molecular pathogenesis of uterine smooth muscle tumors from transcriptional profiling. Genes Chromosomes Cancer 40:97–108
27. Miettinen M, Fetsch JF (2006) Evaluation of biological potential of smooth muscle tumours. Histopathology 48:97–105
28. Fletcher CD (1992) Pleomorphic malignant fibrous histiocytoma: fact or fiction? A critical reappraisal based on 159 tumors diagnosed as pleomorphic sarcoma. Am J Surg Pathol 16:213–228
29. Fletcher CDM (2006) The evolving classification of soft tissue tumours: an update based on the new WHO classification. Histopathology 48:3–12
30. Mertens F, Fletcher CDM, Dal Cin P et al (1998) Cytogenetic analysis of 46 pleomorphic soft tissue sarcomas and correlation with morphologic and clinical features: a report of the CHAMP Study Group. Genes Chromosomes Cancer 22:16–25
31. Derré J, Lagacé R, Nicolas A et al (2001) Leiomyosarcomas and most malignant fibrous histiocytomas share very similar comparative genomic hybridization imbalances: an analysis of a series of 27 leiomyosarcomas. Lab Invest 81:211–215
32. Carneiro A, Francis P, Bendahl PO et al (2009) Indistinguishable genomic profiles and shared prognostic markers in undifferenti-

ated pleomorphic sarcoma and leiomyosarcoma: different sides of a single coin? Lab Invest 89:668–675
33. Larramendy ML, Gentile M, Soloneski S et al (2008) Does comparative genomic hybridization reveal differences in DNA copy number sequence patterns between leiomyosarcoma and malignant fibrous histiocytoma? Cancer Genet Cytogenet 187:1–11
34. Kawai A, Kondo T, Suehara Y et al (2008) Global protein-expression analysis of bone and soft tissue sarcomas. Clin Orthop Relat Res 466:2099–2106
35. Mairal A, Terrier P, Chibon F et al (1999) Loss of chromosome 13 is the most frequent genomic imbalance in malignant fibrous histiocytomas: a comparative genomic hybridization analysis of a series of 30 cases. Cancer Genet Cytogenet 111:134–138
36. Chibon F, Mairal A, Fréneaux P et al (2000) The RB1 gene is the target of chromosome 13 deletions in malignant fibrous histiocytoma. Cancer Res 60:6339–6345
37. Nakayama R, Nemoto T, Takahashi H et al (2007) Gene expression analysis of soft tissue sarcomas: characterization and reclassification of malignant fibrous histiocytoma. Mod Pathol 20:749–759
38. Shintani K, Matsumine A, Kusuzaki K et al (2006) Expression of hypoxia-inducible factor (HIF)-I alpha as a biomarker of outcome in soft tissue sarcomas. Virchows Arch 449:673–681
39. Hunter KW (2004) Ezrin, a key component in tumor metastasis. Trends Mol Med 10:201–204
40. Kim MS, Cho WH, Song WS et al (2007) Prognostic significance of ezrin expression in pleomorphic malignant fibrous histiocytoma. Anticancer Res 27:1171–1178
41. Weng WH, Ahlén J, Aström K et al (2005) Prognostic impact of immunohistochemical expression of ezrin in highly malignant soft tissue sarcomas. Clinical Cancer Res 11:6198–6204
42. Riggi N, Cironi L, Provero P et al (2005) Development of Ewing's sarcoma from bone-marrow-derived mesenchymal progenitor cells. Cancer Res 65:11459–11468
43. Riggi N, Cironi L, Provero P et al (2006) Expression of the FUS-CHOP fusion protein in primary mesenchymal progenitor cells gives rise to a model of myxoid liposarcoma. Cancer Res 66:7016–7023
44. Matuschansky I, Hernando E, Socci ND et al (2007) Derivation of sarcomas from mesenchymal stem cells via inactivation of the Wnt pathway. J Clin Invest 117:3248–3257
45. Fletcher CD, Gustafson P, Rydholm A et al (2001) Clinicopathologic re-evaluation of 100 malignant fibrous histiocytomas: prognostic relevance of subclassification. J Clin Oncol 19:3045–3050
46. Deyrup AT, Haydon RC, Huo D et al (2003) Myoid differentiation and prognosis in adult pleomorphic sarcomas of the extremity: an analysis of 92 cases. Cancer 98:805–813
47. Bui Nguyen Binh M, Guillou L, Hostein I et al (2007) Dedifferentiated liposarcomas with divergent myosarcomatous differentiation developed in the internal trunk. A study of 27 cases and comparison to conventional dedifferentiated liposarcomas and leiomyosarcomas. Am J Surg Pathol 31:1557–1566
48. Montgomery E, Fisher C (2001) Myofibroblastic differentiation in malignant fibrous histiocytoma (pleomorphic myofibrosarcoma): a clinicopathological study. Histopathology 38:499–509
49. Fisher C (2004) Myofibrosarcoma. Virchows Arch 445:215–223
50. Merck C, Angervall L, Kindblom LG et al (1983) Myxofibrosarcoma. A malignant soft tissue tumor of fibroblastic–histiocytic origin. A clinicopathologic and prognostic study of 110 cases using multivariate analysis. Acta Pathol Microbiol Immunol Scand Suppl 282:1–40
51. Mentzel T, Calonje E, Wadden C et al (1996) Myxofibrosarcoma: clinicopathologic analysis of 75 cases with emphasis on the low grade variant. Am J Surg Pathol 20:391–405
52. Huang HY, Lal P, Qin J et al (2004) Low-grade myxofibrosarcoma: a clinicopathologic analysis of 49 cases treated at a single institution with simultaneous assessment of the efficacy of 3-tier and 4-tier grading systems. Hum Pathol 35:612–621
53. Lin CN, Chou SC, Li CF et al (2006) Prognostic factors of myxofibrosarcomas: implications of margin status, tumor necrosis, and mitotic rate on survival. J Surg Oncol 93:294–3043
54. Idbaih A, Coindre JM, Derré J et al (2005) Myxoid malignant fibrous histiocytoma and pleomorphic liposarcoma share very similar genomic imbalances. Lab Invest 85:176–181
55. Willems SM, Debiec-Rychter M, Szuhai K et al (2006) Local recurrence of myxofibrosarcoma is associated with increased in tumour grade and cytogenetic aberrations, suggesting a multistep tumour progression model. Mod Pathol 19:407–416
56. Willems SM, Mohseny AB, Balog C et al (2009) Cellular/intramuscular myxoma and grade I myxofibrosarcoma are characterized by distinct genetic alterations and specific composition of their extracellular matrix. J Cell Mol Med 13:1291–1301
57. Nascimento AF, Bertoni F, Fletcher CDM (2007) Epithelioid variant of myxofibrosarcoma: expanding the clinicomorphologic spectrum of myxofibrosarcoma in a series of 17 cases. Am J Surg Pathol 31:99–105
58. Gebhard S, Coindre JM, Michels JJ et al (2002) Pleomorphic liposarcoma: clinicopathologic, immunohistochemical, and follow-up analysis of 63 cases. A study from the French Federation of Cancer Centers Sarcoma Group. Am J Surg Pathol 26:601–616
59. Hornick JL, Bosenberg MW, Mentzel T et al (2004) Pleomorphic liposarcoma. Clinicopathologic analysis of 57 cases. Am J Surg Pathol 28:1257–1267
60. Miettinen M, Enzinger FM (1999) Epithelioid variant of pleomorphic liposarcoma: a study of 12 cases of a distinctive variant of high-grade liposarcoma. Mod Pathol 12:722–728
61. Sandberg AA (2004) Updates on the cytogenetics and molecular genetics of bone and soft tissue tumors. Liposarcoma. Cancer Genet Cytogenet 155:1–24
62. Schmidt H, Bartel F, Kappler M et al (2005) Gains of 13q are correlated with a poor prognosis in liposarcoma. Mod Pathol 18:638–644
63. Taylor BS, Barretina J, Socci ND et al (2008) Functional copy-number alterations in cancer. PLoS ONE 3:e3179
64. Rieker RJ, Joos S, Bartsch C et al (2002) Distinct chromosomal imbalances in pleomorphic and in high-grade dedifferentiated liposarcomas. Int J Cancer 99:68–73
65. Fritz B, Schubert F, Wrobel G et al (2002) Microarray-based copy number and expression profiling in dedifferentiated and pleomorphic liposarcoma. Cancer Res 62:2993–2998
66. Singer S, Socci ND, Ambrosini G et al (2007) Gene expression profiling of liposarcoma identifies distinct biological types/subtypes and potential therapeutic targets in well-differentiated and dedifferentiated liposarcoma. Cancer Res 67:6626–6636
67. Matuschansky I, Hernando E, Socci ND et al (2008) A development model of sarcomagenesis defines a differentiation-based classification for liposarcomas. Am J Pathol 172:1069–1080
68. Dei Tos AP, Mentzel T, Fletcher CDM (1998) Primary liposarcoma of the skin: a rare neoplasm with unusual high grade features. Am J Dermatopathol 20:332–338
69. Furlong MA, Mentzel T, Fanburg-Smith JC (2001) Pleomorphic rhabdomyosarcoma in adults: a clinicopathologic study of 38 cases with emphasis on morphologic variants and recent skeletal muscle-specific markers. Mod Pathol 14:595–603
70. Furlong MA, Fanburg-Smith JC (2001) Pleomorphic rhabdomyosarcoma in children: four cases in the pediatric age group. Ann Diagn Pathol 5:199–206
71. Little DJ, Ballo MT, Zagars GK et al (2002) Adult rhabdomyosarcoma. Outcome following multimodality treatment. Cancer 95:377–388
72. Parham DM, Ellison DA (2006) Rhabdomyosarcomas in adults and children. An update. Arch Pathol Lab Med 130:1454–1465

73. Li G, Ogose A, Kawashima H et al (2009) Cytogenetic and real-time quantitative reverse-transcriptase polymerase chain reaction analyses in pleomorphic rhabdomyosarcoma. Cancer Genet Cytogenet 192:1–9
74. Gordon A, McManus A, Anderson J et al (2003) Chromosomal imbalances in pleomorphic rhabdomyosarcomas and identification of the alveolar rhabdomyosarcoma-associated PAX3-FOXO1A fusion gene in one case. Cancer Genet Cytogenet 140:73–77
75. Scheithauer BW, Louis DN, Hunter S et al (2007) Malignant peripheral nerve sheath tumour (MPNST). In: Louis DN, Ohgaki H, Wiestler OD, Cavenee WK (eds) World Health Organization classification of tumours of the central nervous system. IARC, Lyon, pp 160–162
76. Mertens F, Dal Cin P, De Wever I et al (2000) Cytogenetic characterization of peripheral nerve sheath tumours: a report of the CHAMP Study Group. J Pathol 190:31–38
77. Bridge RS, Bridge JA, Neff JR et al (2004) Recurrent chromosomal imbalances and structurally abnormal breakpoints within complex karyotypes of malignant peripheral nerve sheath tumour and malignant Triton tumor: a cytogenetic and molecular cytogenetic study. J Clin Pathol 57:1172–1178
78. Kresse SH, Skarn M, Ohnstad HO et al (2008) DNA copy number changes in high-grade malignant peripheral nerve sheath tumors by array CGH. Mol Cancer 7:48
79. Storlazzi CT, Brekke HR, Mandahl N et al (2006) Identification of a novel amplicon at distal 17q containing the BIRC5/survivin gene in malignant peripheral nerve sheath tumours. J Pathol 209:492–500
80. Schmidt H, Würl P, Taubert H et al (1999) Genomic imbalances in 7p and 17q in malignant peripheral nerve sheath tumors are clinically relevant. Genes Chromosomes Cancer 25:205–211
81. Skotheim RI, Kallioniemi A, Bjerkhagen B et al (2003) Topoisomerase-II α is upregulated in malignant peripheral nerve sheath tumors and associated with clinical outcome. J Clin Oncol 21:4586–4591
82. Schmidt H, Taubert H, Würl P et al (2001) Cytogenetic characterization of six malignant peripheral nerve sheath tumors: comparison of karyotyping and comparative genomic hybridization. Cancer Genet Cytogenet 128:14–23
83. Mantripragada KK, Spurlock G, Kluwe L et al (2008) High-resolution DNA copy number profiling of malignant peripheral nerve sheath tumors using targeted microarray-based comparative genomic hybridization. Clinical Cancer Res 14:1015–1024
84. Carroll SL, Stonecypher MS (2004) Tumor suppressor mutations and growth factor signalling in the pathogenesis of NF1-associated peripheral nerve sheath tumors. I. The role of tumor suppressor mutations. J Neuropathol Exp Neurol 63:1115–1123
85. Przygodzki RM, Finkelstein SD, Keohavong P et al (1997) Sporadic and thorotrast-induced angiosarcomas of the liver manifest frequent and multiple point mutations in KRAS-2. Lab Invest 76:153–159
86. Naka N, Tomita Y, Nakanishi H et al (1997) Mutations of p53 tumor suppressor gene in angiosarcoma. Int J Cancer 71:952–955
87. Zietz C, Rossle M, Haas C et al (1998) MDM2 oncoprotein overexpression, p53 gene mutation, and VEGF upregulation in angiosarcomas. Am J Pathol 153:1425–1433
88. Domfeh AB, Fichera M, Hunt JL (2006) Allelic loss of 3 different tumor suppressor gene loci in benign and malignant endothelial tumors of the head and neck. Arch Pathol Lab Med 130:1184–1187
89. Ahmad SA, Patel SR, Ballo MT et al (2002) Extraosseous osteosarcoma: response to treatment and long-term outcome. J Clin Oncol 20:521–527
90. Jensen ML, Schumacher B, Jensen OM et al (1998) Extraskeletal osteosarcomas. A clinicopathologic study of 25 cases. Am J Surg Pathol 22:588–594
91. Mertens F, Larramendy M, Gustavsson A et al (2000) Radiation-associated sarcomas are characterized by complex karyotypes with frequent rearrangements of chromosome arm 3p. Cancer Genet Cytogenet 116:89–96
92. Mohamed AN, Zalupski MM, Ryan JR et al (1997) Cytogenetic aberrations and DNA ploidy in soft tissue sarcoma. A southwest oncology group study. Cancer Genet Cytogenet 99:45–53
93. Lau CC, Harris CP, Lu XY et al (2004) Frequent amplification and rearrangement of chromosomal bands 6p12–p21 and 17p11.2 in osteosarcoma. Genes Chromosomes Cancer 39:11–21
94. Selvarajah S, Yoshimoto M, Ludkovski O et al (2008) Genomic signatures of chromosomal instability and osteosarcoma progression detected by high resolution array CGH and interphase FISH. Cytogenet Genome Res 122:5–15
95. Bayani J, Zielenska M, Pandita A et al (2003) Spectral karyotyping identifies recurrent complex rearrangements of chromosomes 8, 17, and 20 in osteosarcomas. Genes Chromosomes Cancer 36:7–16
96. Bridge JA, Nelson M, McComb E et al (1997) Cytogenetic findings in 73 osteosarcoma specimens and a review of the literature. Cancer Genet Cytogenet 95:74–87
97. Sandberg AA, Bridge JA (2003) Updates on the cytogenetics and molecular genetics of bone and soft tissue tumors. Osteosarcoma and related tumors. Cancer Genet Cytogenet 145:1–30
98. Montgomery EA, Devaney KO, Giordano TJ et al (1998) Inflammatory myxohyaline tumor of distal extremities with virocyte or Reed-Sternberg-like cells: a distinctive lesion with features simulating inflammatory conditions, Hodgkin's disease, and various sarcomas. Mod Pathol 11:384–391
99. Meis-Kindblom JM, Kindblom LG (1998) Acral myxoinflammatory fibroblastic sarcoma: a low-grade tumor of the hands and feet. Am J Surg Pathol 22:911–924
100. Lambert I, Debiec-Rychter M, Guelinckx P et al (2001) Acral myxoinflammatory fibroblastic sarcoma with unique clonal chromosomal changes. Virchows Arch 438:509–512
101. Baumhoer D, Glatz K, Schulten H-J et al (2007) Myxoinflammatory fibroblastic sarcoma: investigations by comparative genomic hybridization of two cases and review of the literature. Virchows Arch 451:923–928
102. Mansoor A, Fidda N, Himoe E et al (2004) Myxoinflammatory fibroblastic sarcoma with complex supernumerary ring chromosomes composed of chromosome 3 segments. Cancer Genet Cytogenet 152:61–65
103. Hallor KH, Sciot R, Staaf J et al (2009) Two genetic pathways, t (1;10) and amplification of 3p11–12, in myxoinflammatory fibroblastic sarcoma, haemosiderotic fibrolipomatous tumour, and morphologically similar lesions. J Pathol 217:716–727
104. Ida CM, Rolig KA, Hulshizer RL et al (2007) Myxoinflammatory fibroblastic sarcoma showing t(2;6)(q31;p21.3) as a sole cytogenetic abnormality. Cancer Genet Cytogenet 177:139–142
105. Laskin WB, Silverman TA, Enzinger FM (1998) Postradiation soft tissue sarcomas. An analysis of 53 cases. Cancer 62:2330–2340
106. Wiklund TA, Blomqvist CP, Raty J et al (1991) Postirradiation sarcoma. Analysis of a nationwide cancer registry material. Cancer 68:524–531
107. Lagrange JL, Ramaioli A, Chateau MC et al (2000) Sarcoma after radiation therapy: retrospective multi institutional study of 80 histologically confirmed cases. Radiation therapist and pathologist groups of the Federation Nationale des Centres de Lutte Contre le Cancer. Radiology 216:197–205
108. Inoue YZ, Frassica FJ, Sim FH et al (2000) Clinicopathologic features and treatment of postirradiation sarcoma of bone and soft tissue. J Surg Oncol 75:42–50
109. Nakanishi H, Tomita Y, Myoui A et al (1998) Mutation of the p53 gene in postradiation sarcoma. Lab Invest 78:727–733

Virchows Arch (2010) 456:219–234
DOI 10.1007/s00428-009-0854-3

REVIEW AND PERSPECTIVE

Soft tissue tumors associated with *EWSR1* translocation

Salvatore Romeo · Angelo P. Dei Tos

Received: 20 August 2009 / Revised: 7 October 2009 / Accepted: 17 October 2009 / Published online: 20 November 2009
© Springer-Verlag 2009

Abstract The Ewing sarcoma breakpoint region 1 (*EWSR1*; also known as *EWS*) represents one of the most commonly involved genes in sarcoma translocations. In fact, it is involved in a broad variety of mesenchymal lesions which includes Ewing's sarcoma/peripheral neuroectodermal tumor, desmoplastic small round cell tumor, clear cell sarcoma, angiomatoid fibrous histiocytoma, extraskeletal myxoid chondrosarcoma, and a subset of myxoid liposarcoma. The fusion products between *EWSR1* and partners usually results in fusion of the N-terminal transcription-activating domain of *EWSR1* and the C-terminal DNA-binding domain of the fusion partner, eventually generating novel transcription factors. *EWSR1* rearrangement can be visualized by the means of fluorescence in situ hybridization (FISH). As soft tissue sarcomas represent a diagnostically challenging group, FISH analysis is an extremely useful confirmatory diagnostic tool. However, as in most instances a split-apart approach is used, the results of molecular genetics must be evaluated in context with morphology.

Keywords EWSR1 gene · Soft tissue tumors · Sarcoma translocations

Introduction

The Ewing sarcoma breakpoint region 1 (*EWSR1*; also known as *EWS*) represents one of the most commonly involved genes in sarcoma translocations. These structural changes result in a fusion product between *EWSR1* and several distinct partners. *EWSR1*, as implied by its name, was initially identified in Ewing sarcoma [1, 2] but it is involved in a variety of distinct clinicopathological entities. This includes Ewing's sarcoma/peripheral neuroectodermal tumour (ES/PNET), desmoplastic small round cell tumour (DSRCT), clear cell sarcoma of soft tissue (ST-CCS), angiomatoid fibrous histiocytoma (AFH), extraskeletal myxoid chondrosarcoma (EMCS), and a subset of myxoid liposarcoma (MLPS). An up-to-date list of the known translocations involving the *EWSR1* gene and the corresponding soft tissue tumor types is given in Table 1. *EWSR1* rearrangements are also described in tumors other than soft tissue tumors: i.e., cutaneous hidradenoma and mucoepidermoid carcinoma of salivary glands [3].

EWSR1 maps on 22q12, and its coding sequence includes 17 exons [4]. Related pseudogenes have been identified on chromosomes 1(annotation NC_000001.10) and 14(annotation NC_000014.8) [5]. The encoded protein is made up of 656 amino acids [4]. The N-terminal domain, transcription activation domain, is encoded by exon 1–7 and contains a repeated degenerated polypeptide of 7 to 12 residues rich in tyrosine, serine, threonine, glycine, and glutamine with consensus SYGQQSX [4]. C-terminal contains three arginine- and glycine-rich tracts (respectively encoded by exons 8–9, 14, and 16) and an RNA-binding domain (encoded by exons 11–13) [4]. The sequence of this latter allows for RNA binding and/or single-strand DNA and is common to the novel TET protein family [6]. This family includes EWSR1, FUS, TAF15, the fruit fly protein CAZ, and the zebra fish proteins EWSR1A and EWSR1B [1, 7–10] TET family has a crucial role in sarcoma genetics as also FUS and TAF15 are involved in fusion protein formation upon translocation and remarkably with the same

S. Romeo · A. P. Dei Tos (✉)
Department of Pathology, General Hospital of Treviso,
Piazza Ospedale 1,
31100 Treviso, Italy
e-mail: apdeitos@ulss.tv.it

Table 1 Chromosomal translocations involving EWSR1 in sarcomas

Tumour	Translocation	Fusion product
Angiomatoid fibrous histiocytoma	t(12;22)(q13;q12)	EWSR1–ATF1
Clear cell sarcoma	t(12;22)(q13;q12)	EWSR1–ATF1
	t(2;22)(q34;q12)	EWSR1–CREB1
Desmoplastic round cell tumor	t(11;22)(p13;q12)	EWSR1–WT1
	t(21;22)(q22;q12)	EWSR1–ERG
Extraskeletal myxoid chondrosarcoma	t(9;22)(q22;q12)	EWSR1–NR4A3
Ewing sarcoma/PNET	t(11;22)(q24;q12)	EWSR1–FLI1
	t(21;22)(q22;q12)	EWSR1–ERG
	t(20;22)(q13;q12)	EWSR1–NFATC2
	t(2;22)(q33;q12)	EWSR1–FEV
	t(7;22)(p22;q12)	EWSR1–ETV1
	t(17;22)(q12;q12)	EWSR1–E1AF
	t(2;22)(q31;q12)	EWSR1–SP3
	t(1;22)(p36.1;q12)	EWSR1–ZNF278
	t(6;22)(p21;q12)	EWSR1–POU5FI
Myxoid–round cell liposarcoma	t(12;22)(q13;q12)	EWSR1–DDIT3

partners reported for EWSR1 in an exclusive way (respectively FUS in ES, AFH, MLPS, and low grade fibromyxoid sarcoma and TAF15 in EMCS) [11].

EWSR1 messenger RNA (mRNA) is ubiquitously expressed with little variation between different tissues, its expression is stable throughout cell cycle, and the half-life is long. These three features taken together suggest that *EWSR1* is a housekeeping gene [12]. The encoded protein is mainly located in the nucleus [13] and in the C-terminal, and is present a highly positively charged nuclear localization signal, again sharing strong similarity with the respective C-terminal sequences of the TET family [13]. The role of this protein is still a matter of investigation. The processes in which it is involved are several and includes interactions with TFIID subunits and RNA polymerase II complex [14], interaction with components of the spliceosome such as splicing factor1 and the small nuclear ribonucleoprotein polypeptide C [15–17], interaction with mitotic spindle and stabilization of microtubules [9, 18], meiosis, with proposed roles in DNA pairing and recombination/repair mechanisms, and cellular senescence via its interaction with lamin A/C [19].

The formation of fusion products between *EWSR1* and partners usually results in fusion of the N-terminal transcription activating domain of *EWSR1* with removal of its RNA-binding domain and substitution with the C-terminal DNA binding of the fusion gene partner. Among the genes that fuse with *EWSR1* are often members of the erythroblastosis virus-transforming sequence (avian ETS) transcription factor family: including *FLI1*, *ERG*, *ETV1*, *ETV4*, and *FEV*. The transformation effect of fusion protein was thought to be mediated by the abnormal activation of the target genes of the fusion partner contributing the DNA-binding domain, i.e., ETS family member. However, target genes have turned out to be distinct from the expected genes [20, 21].

The most important practical outcome of the above-mentioned knowledge is that ancillary techniques have been developed for recognizing *EWSR1* rearrangement in tumors. Recent availability of *ESWR1* split-apart fluorescence in situ hybridization (FISH) probes allow diagnostic confirmation for those tumors in which this gene is rearranged. Furthermore, it is possible to amplify the mRNA transcript of the fusion product, too. As mentioned above, the presence of pseudogenes demands some extra caution in the interpretation of the results of the molecular techniques [5]. For instance, some probes for FISH might recognize also the pseudogenes sequence with subsequent presence of extra spots. For the same reason, real-time polymerase chain reaction in the absence of a DNAse treatment might end up amplifying pseudogene DNA [5]. In this review, we will discuss the feature of the soft tissue tumors harboring a translocation involving *EWSR1*.

Ewing's sarcoma/PNET

Ewing's sarcoma/PNET (also recently referred to with the somewhat misleading term “Ewing's family of tumor”) refers to a group of sarcomas made up of small blue round cells showing variable extent of neuroectodermal differentiation [22], the vast majority of which shares rearrangements of the *EWSR1* gene [22]. Soft tissue ES/PNETs are rare neoplasms accounting for about 5% of soft tissue sarcomas in adults and 10–15% in childhood. They can present at any age, however, the peak incidence is between

the first and the third decades, with no sex predilection. Most cases occur in the deep soft tissues of the paravertebral region and proximal portions of the lower and upper extremities. Visceral location, such as kidney [23], pancreas [24], and meninges [25], has been documented. The involvement of a major nerve with subsequent neurologic symptoms is reported in up to one third of cases, as in the very first example of this entity, described by Arthur Purdy Stout in 1918 [26]. Examples of ES/PNET involving the thoracopulmonary region have been eponymically indicated as Askin's tumors [27] and are currently regarded as a distinct clinical presentation of the same tumor entity.

Grossly, ES/PNET is a large multilobulated soft tissue mass with extensive necrosis and/or hemorrhage [22]. In axial tumors, frequent osseous involvement makes difficult to determine whether site of origin was in bone or soft tissue.

Microscopically, the morphologic picture shows various degree of neuroectodermal differentiation along a spectrum ranging from ES to PNET. Growth pattern is mainly lobular (Fig. 1a). At the ES end of the spectrum, the neoplastic lobules are composed of small round cells exhibiting round or ovoid vesicular nuclei, distinct nuclear membrane, small nucleoli, and poorly defined, scanty cytoplasm. At the PNET end, the neoplastic cells may have more abundant, eosinophilic cytoplasm with discernible nucleoli. Importantly, at this better differentiated end of the spectrum, a variable number of rosettes (from scarce to numerous) can be detected (Fig. 1b). Most frequently, the rosettes are of the Homer–Wright type, similar to those seen in neuroblastoma, but occasionally Flexner–Wintersteiner rosettes, resembling those ones of ependymomas, are seen. Intracytoplasmic glycogen, highlighted by periodic acid Schiff stains, is present in the majority of undifferentiated cases but only in less than half of ES/PNET-containing rosettes. The mitotic activity tends to be quite variable. Necrosis is almost always present (Fig. 1c) and can be extensive, sometimes leaving collars of viable tumor cells around the richly ramified capillary network. Occasionally, ES/PNET shows focal atypical features: i.e., presence of spindled or large anaplastic tumor cells.

Immunohistochemistry plays a major role in the differential diagnosis of ES/PNET which includes alveolar rhabdomyosarcoma (ARMS), DSRCT, poorly differentiated synovial sarcoma (SS), and Merkel cell carcinoma (MCC). CD99 (the product of the MIC2 antigen) certainly represents the most useful marker [28]. Strong CD99 membrane immunopositivity is usually seen in most ES/PNET (Fig. 1d), independently from the degree of differentiation. However, as with most differentiation markers, CD99 tends to be very sensitive but not specific. When dealing with round cell neoplasms, it has to be kept in mind that CD99 is expressed in most lymphoblastic lymphomas, in poorly differentiated SS including its round cell variant [29], in MCC, and in a small percentage of DSRCT. CD99 immunopositivity evaluated in context with morphology and along with the results of other pertinent differentiation markers helps avoiding most of the diagnostic pitfalls. However, there are still cases that may represent a true challenge.

As it has been shown recently, ES/PNET can occur as primary cutaneous neoplasm, raising the problems of the distinction from MCC [30, 31]. It is important to remember that about 20% of ES/PNET does express cytokeratins and that, on the other hand, MCC can express CD99 in approximately 30% of cases [31]. Neuroendocrine markers can be detected in both lesions (of course much more consistently in MCC). CK20 immunopositivity favors a diagnosis of MCC, as it is consistently negative in all the cases of ES/PNET tested so far [32].

The presence of neuroectodermal differentiation in ES/PNET can be demonstrated by immunopositivity for Leu7, synaptophysin, S-100 protein, neurofilaments, and chromogranin. However, all these markers exhibit high variability eventually proving of scarce diagnostic utility.

ES/PNET has been increasingly reported to occur at visceral sites. When occurring in the kidney, the main differential diagnosis is with the so-called adult variant of Wilms' tumor, particularly when undifferentiated blastemal areas predominate [23]. It has to be stressed that CD99 is usually negative in Wilms' tumor, making immunohistochemistry extremely important in the differential diagnosis. As a consequence, most adult type Wilms' tumors have been now reclassified as ES/PNET, following either immunohistochemical or molecular genetics analysis [23].

Cytogenetics and molecular genetics findings

The central karyotypic anomaly is a t(11;22) with other variants found in about 15% of cases: a t(21;22), a t(7;22), a t(17;22) a t(2;22), and a t(6;22). Rare cases of ES/PNET harbor translocation involving *FUS* in place of *EWSR1*: i.e., t(16;21)(p11;q22) with a *FUS–ERG* fusion gene [33] or t(2;16)(q35;p11) with a *FUS–FEV* fusion gene [34].

The so-called Ewing's sarcoma translocation is the best known example of sarcoma translocation as it was the first one to be identified [35] as well as the first of which the involved genes were cloned [1, 2]. Molecularly, the result of the t(11;22) is a fusion of the *EWSR1* gene with the transcription factor *FLI1* (friend leukemia virus integration site 1) on 11q24 belonging to the ETS family. This molecular aberration leads to the oncogenic conversion of the *EWSR1* gene, and the normal function of which is still poorly understood. The replacement of the RNA-binding domain of the *EWSR1* gene with the DNA-binding domain

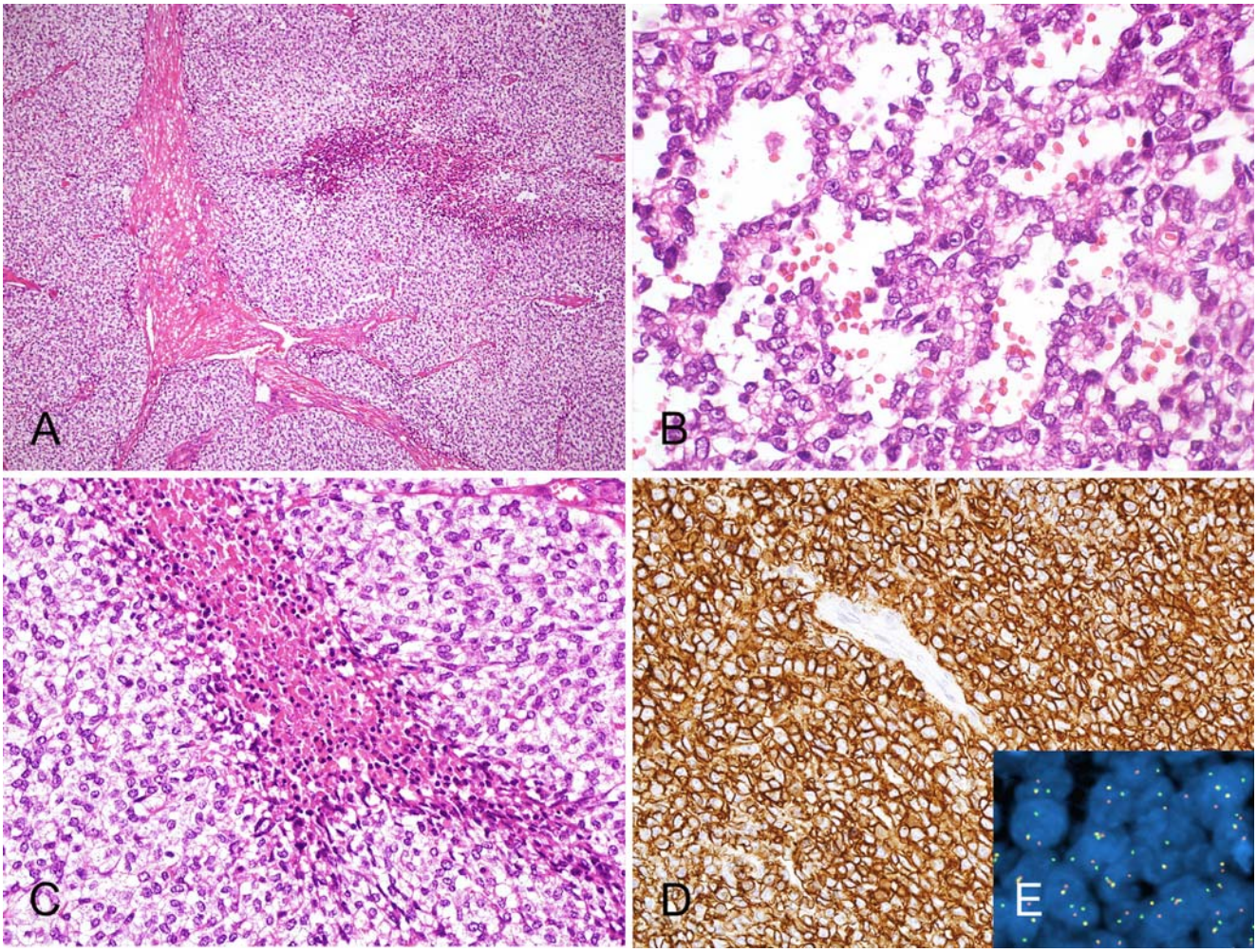

Fig. 1 ES/PNET's features: **a** Growth pattern is usually in solid sheets, **b** rosettes are often present, and **c** intratumoral necrosis is almost always observed. **d** A strong membranous positivity for CD99 immunohistochemistry is found. **e** Diagnosis is further corroborated by presence of rearrangement of *EWSR1* gene as shown by interphase FISH using split-apart probes

of the *FLI1* (or related genes) leads to the formation of a novel transcription factor whose target genes are now being elucidated. Recent in vitro and ex vivo experiments have been extremely beneficial for our understanding on the molecular effect of the fusion transcript expression. The possibility to induce expression of the fusion transcript via cell transfection has given some important clues. The main questions here were: Which is the originating cell of ESFT? Is the occurrence of the translocation and the subsequent fusion gene transcription necessary and sufficient for neoplastic transformation? Which are the key events in neoplastic transformation? Are there any secondary recurrent events? And what is their effect on the biological behavior?

In preliminary experiments, transfection of EWS–FLI1 construct in normal fibroblasts and TERT-immortalized fibroblasts was respectively inducing cell death and growth arrest (reviewed in Kovar H 2005) [36, 37]. The transfection in NIH3T3 not only augments tumorigenicity but also induces a phenotype closely resembling ESFT [37]. Taken together, these results allow concluding that the fusion transcript is indeed promoting tumorigenicity but only in the right cellular context, e.g., in NIH3T3 and not in normal fibroblasts [37]. Furthermore, transfection of fusion transcripts as for oncogenes transfection induces growth arrest unless there is already another operating mechanism, as it is happening for instance for *RAS* transfection [38]. NIH3T3 cell lines are known to be already tumorigenic [20]. In search of a cell of origin for ESFT, Riggi et al. [39] transfected murine mesenchymal stem cells with EWS–FLI1 transcript, remarkably the cells got tumorigenic, acquired a phenotype closely resembling ESFT, and more importantly, with neither apparent structural changes nor alteration in *ARF* and *TP53* pathway [39]. When the same group, Riggi et al. [40], transfected human mesenchymal stem cells with the EWSR1–FLI1 transcript, they did not get growth arrest, despite an expression profile similar to ESFT was triggered, no tumorigenicity was observed, implying that other events are necessary for transformation

[40]. These last two experiments show that mesenchymal stem cells are an attractive candidate of originating cells for ESFT: (1) they are permissive to translocation transfection with no growth arrest, (2) the expression of the fusion transcript induce a phenotype resembling ESFT, and (3) however, additional events are needed for malignant transformation. Established cell lines from ESFT allowed addressing other questions. Silencing of the fusion transcript results in a loss of the tumorigenicity [41] and a switch of phenotype toward mesenchymal stem cells [42]. These two results, on one hand, underline the importance of the fusion transcript expression for the tumorigenicity, and on the other hand, support the putative origin of ESFT from mesenchymal stem cells. Furthermore, culturing of ESFT cell lines acquired random alterations resulting in complex rearrangements [43]. Such rearrangements, although, may occur also in vivo and result in selective growth advantage of one clone with malignant progression and ultimately worse prognosis.

Recently, the fusion between *EWSR1* and a non-ETS family member has been reported. *NFATC2* is this new partner, and it functions as a T cell differentiation regulator [44]. Remarkably, *NFATC2* shares a sequence recognition with the ETS family with possible transcriptional control via activating protein complex 1 [44].

The possibility to detect these karyotypic abnormalities by the means of chromosome analysis as well as by molecular genetics on a routine basis has greatly increased diagnostic accuracy (Fig. 1e). However, even cytogenetics does not exhibit absolute specificity, as demonstrated by the existence of exceptional bonafide cases of ARMS, as well as of polyphenotipic sarcomas bearing a t(11;22) [45]. As a consequence, any result provided by molecular genetics should be evaluated in context with accurate morphological evaluation.

Several studies have claimed that molecular genetics may also prove useful in providing prognostic parameters. In particular, it seems that the presence of a type 1 EWS–FLI1 fusion (EWS exon 7 is linked in frame with exon 6 of FLI1) represents an independent positive prognostic factor [46]. However, large prospective EuroEwing trial is challenging such assumption (JCO in press).

The analysis of cell cycle regulators has also provided potentially valuable information regarding the prognosis of this important family of round cell sarcomas. Although p53 mutation and overexpression seem to delineate only a small subset of ES/PNET, they show remarkably poor clinical outcome [47, 48], and the same effect appears to be determined by deletion of the *CDKN2A* gene [49, 50]. Most likely, impairment of cell cycle/apoptosis regulation are late events in malignant progression affecting prognosis and response to therapy as shown also in other mesenchymal tumors such as gastrointestinal stromal tumors [51].

Prognosis and treatment

The prognosis of the ES/PNET family of neoplasms is poor; however, using multimodality therapy, which includes surgical resection and/or radiation therapy and chemotherapy, long-term survival has increased from less than 10% to approximately 30% to 40% [52]. It is a commonly shared opinion that lesions belonging to the less differentiated (ES) end of the spectrum are characterized by better response [53]. Unfortunately, such an assumption has not been entirely elucidated, with different studies leading to conflicting results [54, 55]. Moreover, most of cases tend to cluster in-between the extremes of the morphologic continuum making histopathologic distinction somewhat arbitrary.

The importance of the IGF1 receptor pathway in the development of ES/PNET has been recognized for some time [56, 57]. Targeting such pathway with the anti IGF1 receptor monoclonal antibody R1507 is the strategy for a single-agent clinical trial (www.clinicaltrials.gov) in patients with recurrent or refractory sarcomas including: ES/PNET, MLPS, EMCS, and DSRCT. Molecules targeting the fusion transcript are being searched, and promising results are coming from targeting the interaction of EWS–FLI1 and RNA helicase A [58]. Targeting tumor metabolism, in general, seems also an appealing alternative therapeutic strategy [59].

Desmoplastic small round cell tumor

Desmoplastic small round cell tumor is a highly malignant polyphenotipic mesenchymal neoplasm associated with a prominent fibrous stroma [60]. It mainly affects young adults with peak incidence in the second decade [60]. Male patients outnumber female patients 4 to 1 [60].

DSRCT most often arise in serous lined surfaces [60]. Originally, described as a predominantly intra-abdominal tumor, a broader distribution has emerged gradually that includes pleura [61] and tunica vaginalis [62]. Extraserous location has been occasionally reported, including parotid gland [63], posterior cranial fossa [64], central nervous system [65], bone and soft tissue [66–68], ovary [69], pancreas [70], and kidney [71, 72].

In its most frequent intra-abdominal presentation, DSRCT usually causes abdominal pain associated with ascites, abdominal distension, and/or intestinal obstruction. At surgery, the lesion usually presents as a large intra-abdominal mass associated with multiple peritoneal smaller implants and hematogenous metastases, especially to the liver [73].

Grossly, the neoplastic masses tend to be solid, firm, and multilobulated with a gray–white occasionally cystic cut

surface and most often featuring abundant coagulative necrosis. Microscopically, at low power, DSRCT is characterized by the presence of sharply demarcated clusters of small rounded cells, separated by a hypocellular desmoplastic stroma (Fig. 2a). However, desmoplasia in rare cases may be absent [74]. Cellular clusters may vary from centrally necrotic large islands to cord-like structures. In typical cases, tumor cells are usually uniform in size and shape and are characterized by small to medium size, round to oval shape, hyperchromatic nuclei, inconspicuous nucleoli, and cytoplasm varying from scanty to abundant (Fig. 2b). Mitotic figures are usually numerous, and prominent necrosis is frequently observed. More rarely, rhabdoid, spindle cell, or even signet-ring cell morphology has been reported [75, 76]. Rare cases of DSRCT exhibit a striking epithelial morphology that makes the differential diagnosis really challenging. It is also important to mention that pseudorosettes can occasionally be observed, making challenging the differential diagnosis with ES/PNET.

Immunohistochemistry plays a major role in the differential diagnosis with other small round cell tumors. The coexpression of epithelial (keratins, epithelial membrane antigen), myogenic (desmin), and neural/neuronal (neuron-specific enolase, S-100 protein, Leu 7, and synaptophysin) differentiation markers is a helpful diagnostic tool. Cytokeratin immunoreactivity is observed in the vast majority of cases (Fig. 2c); in particular when "cocktails" of different molecular weight keratins are used. It is worth noting that all DSRCTs tested so far appear to be negative for both cytokeratin 20 (usually expressed in Merkel cell carcinoma) and cytokeratin 5 (usually expressed in normal mesothelium and mesotheliomas), whereas both MOC31 and BerEP4, which are negative in mesotheliomas, are expressed in DSRCT [77]. One of the most characteristic immunohistochemical features of DSRCT is represented by the expression of desmin (Fig. 2d). A distinctive dot-like pattern of staining with tiny paranuclear globules is often observed. Of course, the expression of myogenic markers

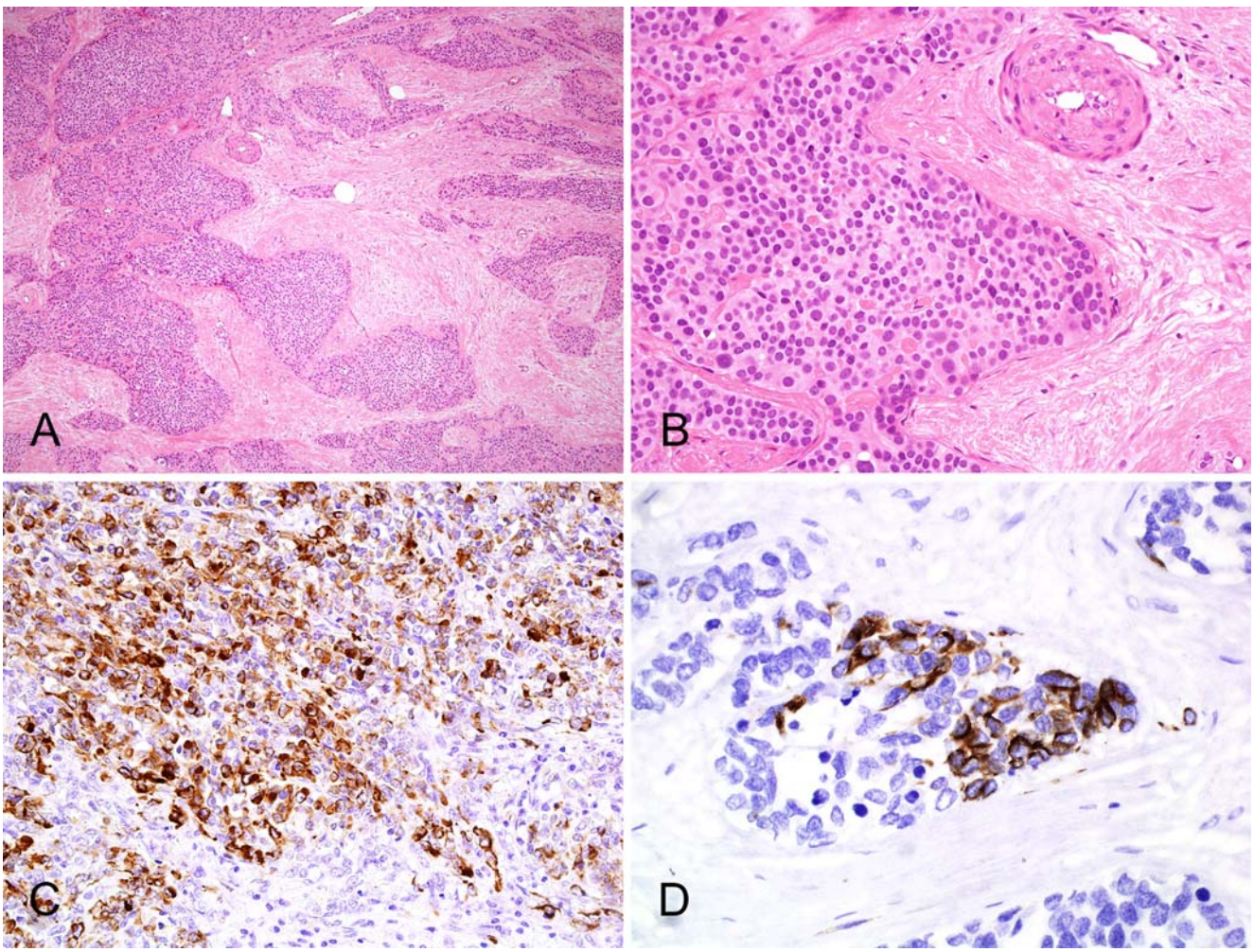

Fig. 2 DSRCT's features: **a** Solid nests of small round blue cells are surrounded by dense collagenous stroma. **b** Nuclei are hyperchromatic and cytoplasms of various size. Immunostains for cytrokeratins (**c**) and desmin (**d**) is usually positive and helpful for differential diagnosis

may mislead to a diagnosis of alveolar rhabdomyosarcoma. However, myogenin is positive in ARMS and negative in DSRCTs. Furthermore, DSRCT also tends to exhibit immunohistochemical as well as electron microscopic features of neural differentiation. The expression of neural differentiation markers is very variable [78], but both neuron-specific enolase (NSE) and CD57 have tested positive in about two thirds of cases. Unfortunately, considering the poor specificity of both markers, the presence of either NSE or CD57 immunopositivity cannot be regarded as unequivocal evidence of neural differentiation. Other more specific markers of neural/neuronal differentiation, such as synaptophysin and chromogranin, have been observed in about 20% of cases. Both MOC31 and BerEP4, which are negative in mesotheliomas, are expressed in DSRCT [77]. Interestingly, placental alkaline phosphatase, a marker for germ cell tumors, was found expressed with a paranuclear pattern of staining, similar to that of desmin expression, in 80% of the cases in a series of molecularly confirmed DSRCT [36], but its meaning has not yet been elucidated. Immunohistochemical analysis has also demonstrated overexpression of growth factors normally repressed by the wild-type WT1, as IGF-IR, PDGF-alpha, and its receptor, PDGFRbeta, latency-associated peptide of transforming growth factor beta, CCN2, a connective tissue growth factor, and IL2/15 receptor beta-chain in the neoplastic cells (the desmoplastic stroma produces IL2 and IL15). All of these molecules might contribute to the development of the typical desmoplastic stroma of this tumor [78–80].

The diagnostic use of anti-WT1 polyclonal antisera has been also suggested. However, WT1 appears to be expressed in a broad range of neoplasms including Wilms' tumors, renal cell carcinomas, mesotheliomas, and papillary serous carcinomas. As the differential diagnosis includes ES/PNET, it has to be stressed that CD99 immunopositivity is observed in less than 20% of DSRCTs. However, in contrast with the thick membrane pattern observed in ES/PNET, CD99 tends to decorate diffusely the cytoplasm of the DSRCT neoplastic cells.

Cytogenetics and molecular genetics

Cytogenetically, DSRCT is characterized by a reciprocal translocation, t(11;22)(p13;q12), that was first reported by Sawyer in 1992 [81]. At the molecular level, the Wilms' tumor gene (WT1) fuses with the EWS gene resulting in its oncogenic activation. The fusion protein functions as a novel, aberrant transcription factor that has the ability to transactivate genes that overlap with those normally regulated by WT1. One of the most interesting targets is represented by the platelet-derived growth factor alpha, a powerful fibroblast growth factor probably promoting the desmoplastic fibroblastic stroma that is typically seen in DSRCT [78]. Recently, two intra-abdominal pediatric tumors expressing EWSR1–WT1 fusion transcript and with a morphology and immunophenotype consistent with a diagnosis of leiomyosarcoma have been reported. Remarkably, both patients showed good prognosis which raises the possibility of a new entity showing the same molecular abnormality of DSRCT [82].

The existence of polyphenotypic neoplasms morphologically similar to DSRCT but containing chimeric transcripts associated with the ES/PNET category (EWS–FLI1 and EWS–ERG) underlines the importance of strict correlation between conventional morphology and genetic analysis [83].

Prognosis and treatment

DSRCT represents an extremely aggressive mesenchymal neoplasm with a dismal prognosis, despite all therapeutic efforts. Even if a modest increase of survival seems to be achieved by high-dose chemotherapy regimens, most patients die either of advanced uncontrolled local disease or of distant metastases, frequently within 24 months of diagnosis. Recent identification of ENT4, whose expression is related to clinical efficacy of a number of nucleoside analogs used in cancer chemotherapy, may represent an attractive pathway for targeting chemotherapeutic drugs into DSRCT [84].

Clear cell sarcoma of soft tissue

ST-CCS, also known as melanoma of soft parts, is a soft tissue sarcoma of young adults showing immunohistochemical as well ultrastructural features of melanocytic differentiation. It usually occurs in adolescents and young adults, with a peak incidence between the second and the fourth decades. ST-CCS is a slow-growing mass, associated with pain or tenderness in half of cases. The lower extremities are the commonest anatomic site (foot and ankle accounting for approximately 40% of cases). It is generally deep seated, most often in close proximity to tendons and aponeuroses. It has been shown that ST-CCS can involve the gastrointestinal tract wherein it tends to exhibit minimal features of melanocytic differentiation.

Grossly, ST-CCS is usually of small size, well circumscribed (Fig. 3a) but rarely encapsulated. Pigmented areas can occur. Necrosis (Fig. 3b), hemorrhage, and cystic degeneration are occasionally seen.

Microscopically, ST-CCS is composed of uniform nests and/or fascicles of polygonal to spindle cells with abundant clear or eosinophilic cytoplasm (more often, eosinophilic than clear; Fig. 3c). Nuclei are vesicular, round to ovoid,

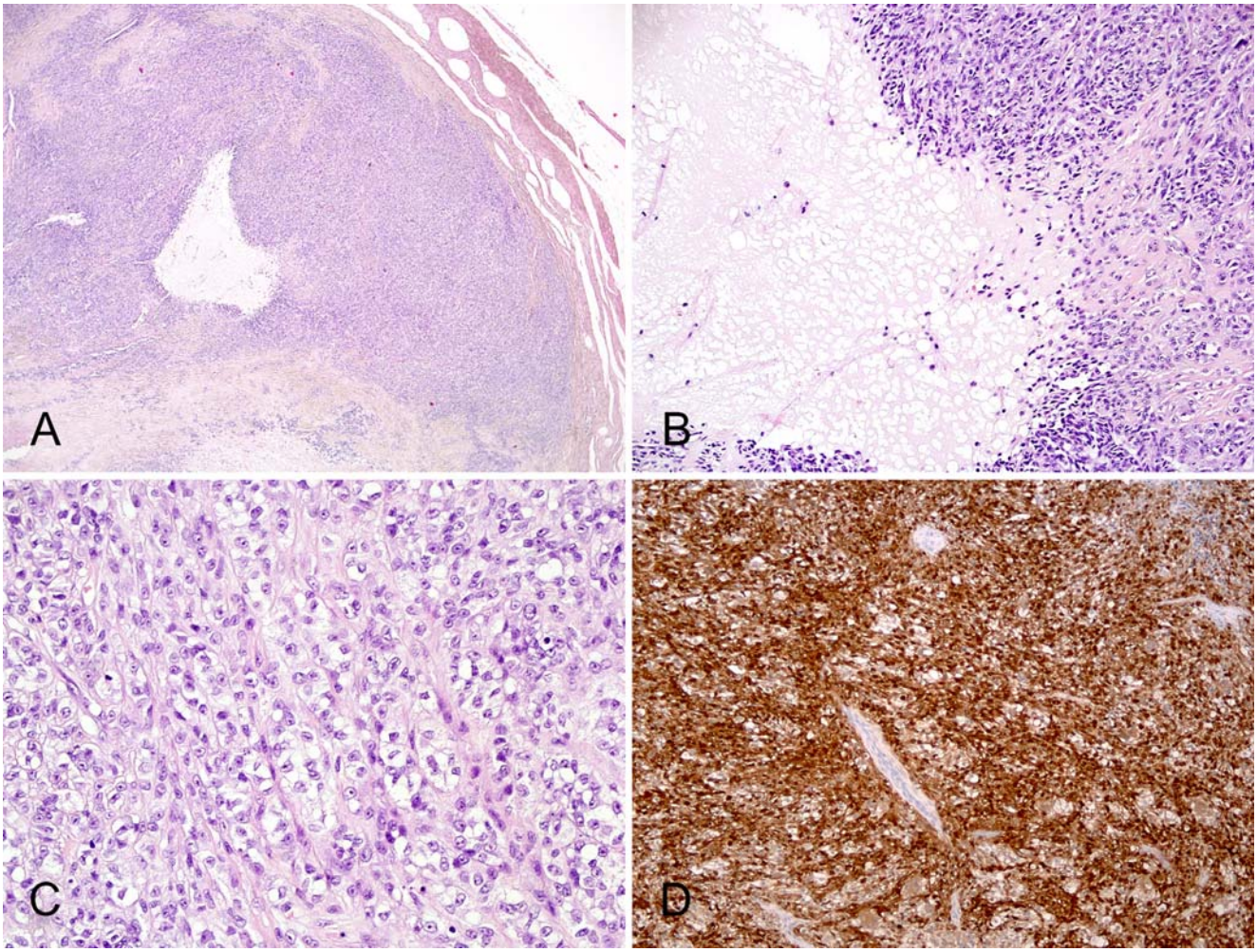

Fig. 3 ST-CCS's features: **a** Well demarcation is usually present, and **b** necrosis may occasionally be found. **c** Polygonal cells with clear cytoplasm are found, **d** almost always showing diffuse positivity for S100

with prominent nucleoli. Multinucleated giant cells are seen in half of the cases. Melanin pigment can be observed. Morphological variations are represented by presence of marked pleomorphism (associated with brisk mitotic activity) microcystic degeneration, and myxoid change of the stroma. Rare cases tend to assume a prominent spindled morphology. Pleomorphism seems to be more frequent in recurrent lesions as well as in metastases. ST-CCS shows immunoreactivity for S100 protein (Fig. 3d), HMB45, MART.1, and MITF-1 in almost all cases, with the notable exception of gastrointestinal (GI) tract cases in which only S-100 immunopositivity is most often detected [85, 86]. Expression profiling has shown consistent upregulation of avian erythroblastic leukemia viral oncogene homolog 3, and evaluation of its expression might be useful in clinical practice [87, 88].

Malignant melanoma needs to be ruled out on the basis of clinical history and absence of junctional activity [89, 90]. Metastatic melanoma can exhibits complete morphologic overlap with ST-CCS, making genetic analysis the only way to separate them [89, 90].

Cytogenetics and molecular genetics

ST-CCS is characterized by the presence of a specific translocation t(12;22)(q13;q12), fusing the *EWSR1* gene with the activating transcription factor-1 gene (*ATF1*) [91, 92]. A variant translocation t(2:22)(q34:q12) that seems to be associated with the GI tract location has been recently reported and involves the *EWSR1* gene on 22q12 and the *CREB1* gene on 2q34 [85]. Both ATF1 and cAMP-responsive element-binding protein (CREB1) belongs to the basic leucine zipper superfamily of transcription factors. Interestingly, CREB overexpression is associated with the acquisition of metastatic potential by melanoma cells [93]. Both EWSR1–ATF1 and EWSR1–CREB1 lead to the formation of chimeric transcripts in which the basic leucine zipper domain is retained. MITF upregulation is probably a

pre-existing characteristic of ST-CCS and not induced by fusion transcripts [91].

Prognosis and treatment

ST-CCS is an aggressive neoplasm, with an overall mortality ranging between 37% and 59%. Recurrences and metastases can occur even after 10 years. Nodal metastases are present in about 50% of cases. Also lung and bone metastases are frequent. Size above 5 cm, necrosis and local recurrence are unfavorable prognostic factors. The fact that multiple histone deacetylase inhibitors suppress MITF expression, it may potentially represent a novel therapeutic strategy in ST-CCS [94].

EMCS

EMCS is a rare malignant soft tissue tumor of uncertain differentiation, representing less than 3% of all soft tissue sarcomas [95]. It usually occurs in adults, with a peak incidence in the sixth decade [95]. A male predominance is reported. Despite the name, there is no convincing evidence of cartilaginous differentiation in most EMCS [96].

EMCS involves mainly the deep soft tissues of the proximal extremities and limb girdles. Thigh and popliteal fossa are the most commonly involved anatomic sites, followed by trunk, paraspinal region, foot, and head and neck regions. EMCS presents as a slow-growing soft tissue-enlarging mass, often associated with pain and tenderness. Skin ulceration and hemorrhage occur in some cases. The duration of symptoms spans from a few weeks to several years.

Grossly, EMCS is usually large and well demarcated by a fibrous pseudocapsule. It appears multinodular on cut section, with gelatinous nodules separated by fibrous septa. Hemorrhage, necrosis, and cystic degeneration can be present. Highly cellular tumors tend to be fleshy. Microscopically, EMCS can be subdivided into two types: a conventional "well differentiated" EMCS and cellular "high grade" EMCS. Low-grade forms are characterized by a multinodular architecture (Fig. 4a) with fibrous septa delimiting areas filled with strikingly hypovascular myxoid (Fig. 4b) or chondromyxoid stroma. Neoplastic cells present eosinophilic, granular to vacuolated cytoplasms, and uniform, round to oval nuclei and are organized in cords or clusters, and sometimes in a distinctive filigree or cribriform pattern. An accentuation of cellularity is typically observed at the periphery of the nodules. Ten percent of cases may contain at least focally neoplastic cells featuring an eosinophilic "rhabdoid" cytoplasm. Mitoses are usually scarce. Hemorrhage is common. True cartilage is uncommon. Cellular "high grade" EMCS shows increased cellularity associated with minimal myxoid stroma (Fig. 4c). Neoplastic cells are epithelioid and overtly atypical both in diffuse and cribriform areas (Fig. 4d). Mitotic count can be high in cellular EMCS. EMCS shows immunoreactivity for S100 protein in less than 20% of cases. Neuroendocrine differentiation, with chromogranin and synaptophysin immunoreactivity, has been reported and confirmed by gene-profiling data [97].

Mixed tumor of soft tissue/myoepithelioma/parachordoma represents the main differential diagnosis. Herein, S100 immunopositivity is generally observed as well as a relatively consistent expression of myoepithelial and epithelial differentiation markers, actin, and glial fibrillary acidic protein. Ductal differentiation can be seen focally. Chordoma exhibits a distinctive midline anatomic location, consistently coexpresses S100 and cytokeratins, and contains the characteristic physaliferous cells.

Cytogenetics and molecular genetics

The most frequent translocations observed in EMCS is t(9;22)(q22;q12) fusing *EWSR1* with *NR4A3* (also known as CHN) [98, 99]. Also, a t(9;17)(q22;q11) and a t(9;15)(q22;q21) are found, fusing the *NR4A3* gene with *RBP56* and *TAF15*, respectively. Recent data indicate that the EWSR1/NR4A3 fusion protein may activate the PPARG nuclear receptor gene that may not only play a key role in the molecular oncogenesis of EMCS but also represents a potential therapeutic target [100].

Prognosis and treatment

EMCS is associated with prolonged survival; however, local recurrences and metastases (usually to the lungs) occur in half of cases, generally more than 10 years after the diagnosis. Long survival even in the presence of metastases is reported. Large tumor size (in particular larger than 10 cm) and high-grade morphology (in particular with pleomorphic and rhabdoid cells) predict poor outcome. Response to chemotherapy is generally low, and the most effective therapeutic strategy is still represented by aggressive management of localized disease.

Angiomatoid fibrous histiocytoma

Angiomatoid fibrous histiocytoma is an intermediate, rarely metastasizing soft tissue neoplasm exhibiting a partial myoid phenotype. It should not to be confused with aneurysmal benign fibrous histiocytoma [101]. It occurs most frequently in children and young adults [101], males and females being equally affected [101]. Systemic signs such as pyrexia, anemia, or paraproteinemia are rarely

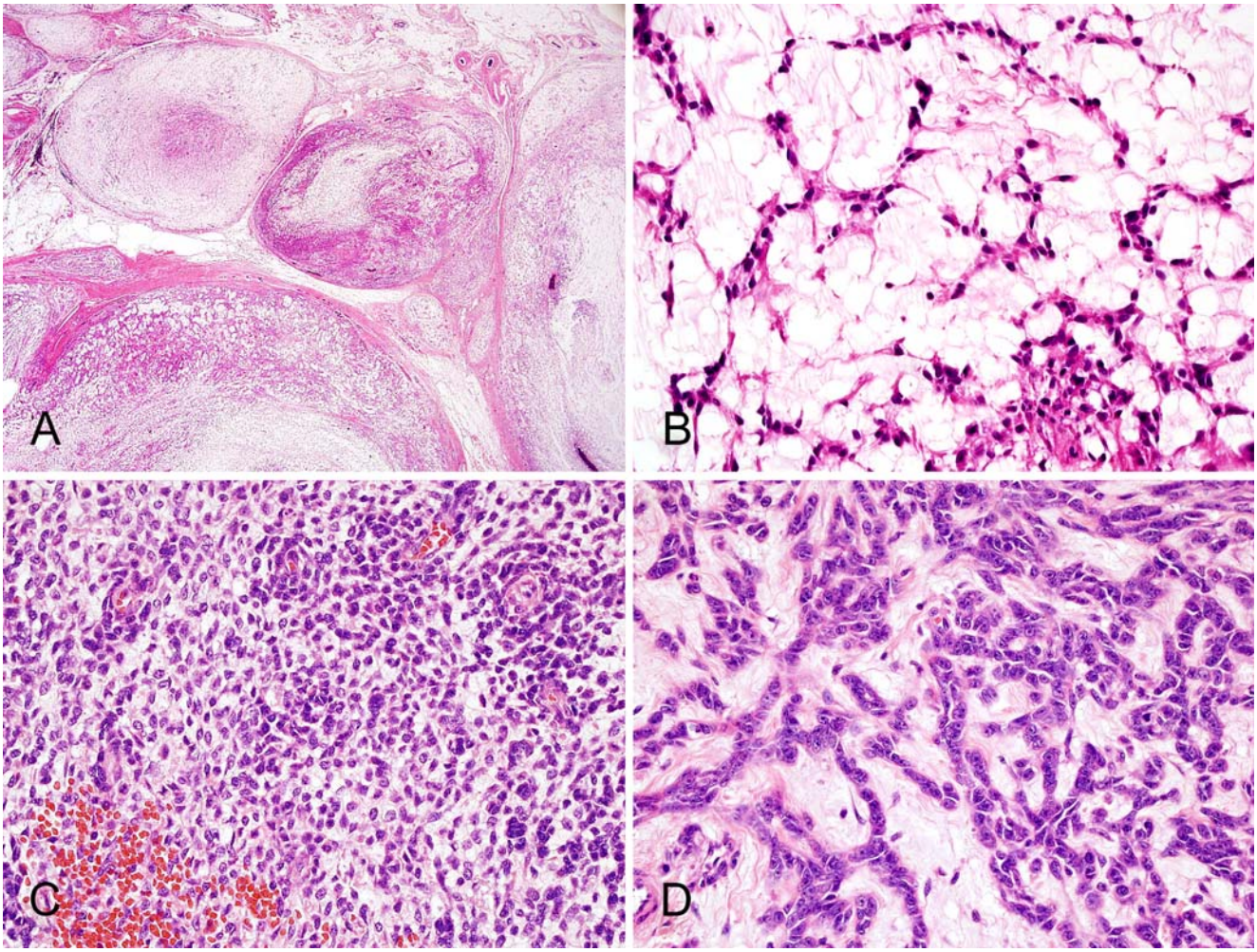

Fig. 4 EMCS's features: **a** Multinodular growth is evident, and **b** nodules are formed by hypovascular myxoid matrix mainly hypocellular. **c** More cellular, high-grade variant of EMCS with **d** epithelioid atypical cells

observed and tend to disappear following removal of the lesion.

The most frequently affected sites are represented by the superficial soft tissues of the extremities followed by the trunk and the head and neck regions [101]. Two thirds of cases occur in areas wherein lymph nodes are normally present.

Grossly, AFH is well circumscribed (Fig. 5a) and multinodular, showing cystic and hemorrhagic areas. A thick fibrous pseudocapsule is usually present at the periphery of the lesion wherein a lymphoplasmacytic infiltrate is also often observed. A multinodular proliferation of eosinophilic, "myoid" cells, featuring ovoid, uniform, plump nuclei is most often present (Fig. 5b). Hemorrhagic areas and pseudovascular spaces containing a proteinaceous material can be often observed. Stromal deposition of hemosiderin is also relatively common. Cell atypia is very rare but it can be detected occasionally (Fig. 5c). Mitotic activity is generally low. Immunohistochemically, AFH exhibits desmin positivity in approximately 40% of cases (Fig. 5d). Epithelial membrane antigen and muscle-specific actin are also positive in less than half of cases. Differential diagnosis include aneurysmal fibrous histiocytoma (more superficial, composed of a polymorphic cell population and usually desmin-negative), Intranodal Kaposi sarcoma may represent a diagnostic alternative which can be sorted out by HHSV8 immunodetection.

Cytogenetics and molecular genetics

AFH represents the first example of a mesenchymal lesion of intermediate malignancy to show a rearrangement of the *EWSR1* genes [102, 103]. Fascinatingly, AFH is characterized by the same chromosome translocation observed in ST-CCS leading to the formation of a *EWSR1–CREB1* fusion, and more rarely, of a *EWSR1–ATF1* fusion [102, 103]. Such distinctive phenotypes, in presence of the same gene rearrangement, may be explained hypothesizing that distinct differentiation programs pre-exist in two different mesenchymal progenitor cells. *EWSR1–ATF1*/*EWSR1–*

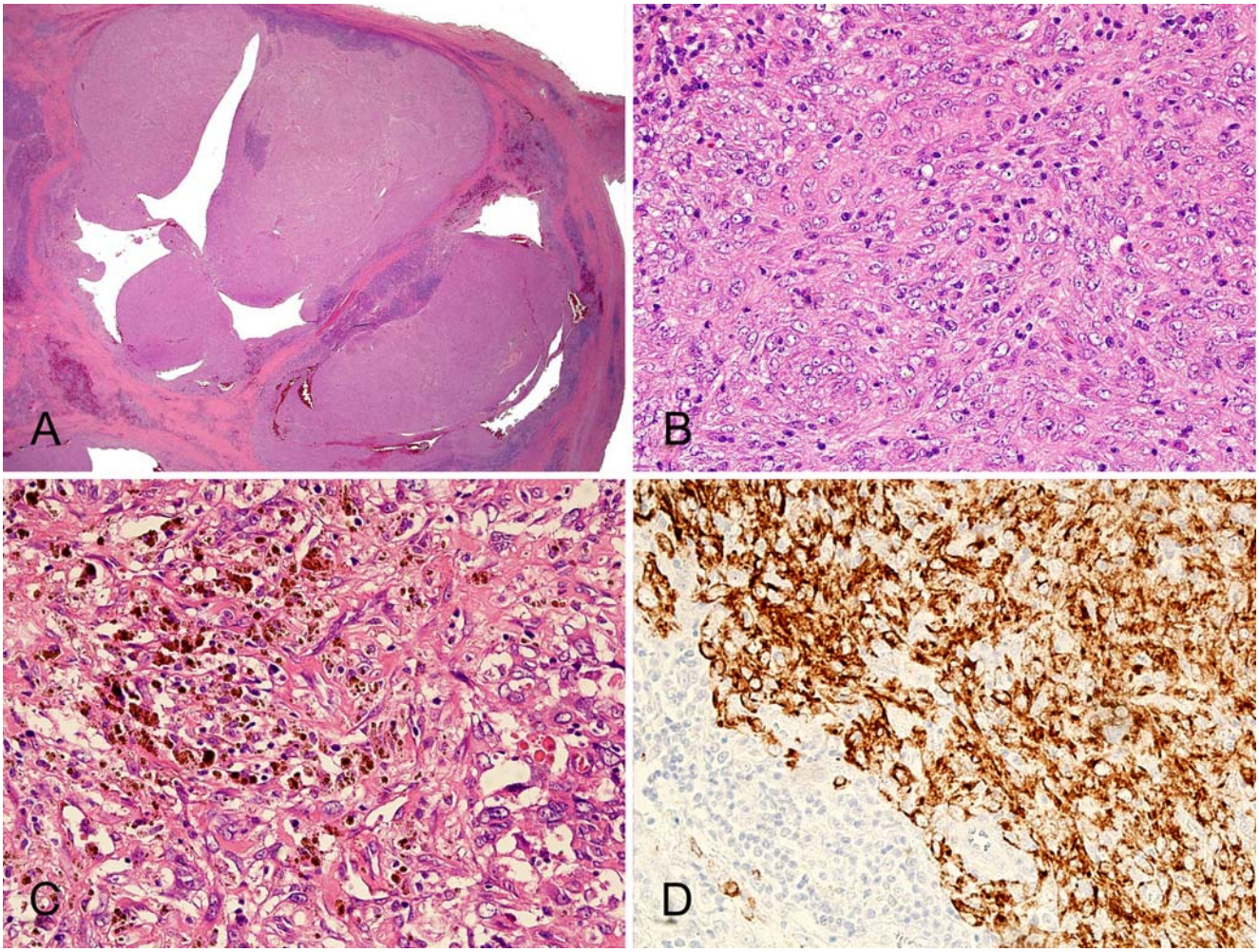

Fig. 5 AFH's features: **a** Multiple nodules with hemorrhagic changes are formed by **b** a proliferation of eosinophilic cells with plump nuclei. **c** Cell atypia may occasionally be found. **d** Neoplastic cells are often diffusely positive for desmin

CREB1 independent activation of MITF pathway in ST-CCS strongly supports this view.

Prognosis and treatment

As mentioned, current World Health Organization classification considers AFH as an intermediated malignancy soft tissue lesion, in which local recurrences are observed in less than 15% of cases, and metastatic spread to locoregional lymph nodes is being observed in less than 2% of cases. Complete local excision is considered curative.

Myxoid liposarcoma

Myxoid liposarcoma represents the second larger group of adipocytic malignancies accounting for about 30–35% of all liposarcomas [104]. Peak incidence is between the third and the fifth decade, and both sexes are equally affected [104]. Clinically, myxoid and round cell liposarcoma occur predominantly in the limbs whereas the retroperitoneal location is exceptional. Grossly, myxoid liposarcoma is most often a well-circumscribed, multinodular, gelatinous mass. The presence of hypercellular (round cell) areas may confer a fleshy appearance [104].

Microscopically, purely myxoid liposarcoma is composed by a hypocellular spindle cell proliferation set in a myxoid background, often featuring mucinous pools (Fig. 6a) [104]. Lipoblasts are most often monovacuolated, small, and tend to cluster around vessels or at the periphery of the lesion (Fig. 6b) [104]. The most distinctive morphologic clue is represented by the presence of a capillary network organized in a plexiform pattern (Fig. 6c) [104]. Myxoid/round cell liposarcoma is defined by the presence of hypercellular areas (that most frequently begins to form in a perivascular distribution) with an undifferentiated round cell component (Fig. 6d) ranging in extent between 5% and 80% [105, 106]. Pure round cell liposarcoma is a rare neoplasm in which hypercellularity or round cell differentiation account for more than 80% of tumor

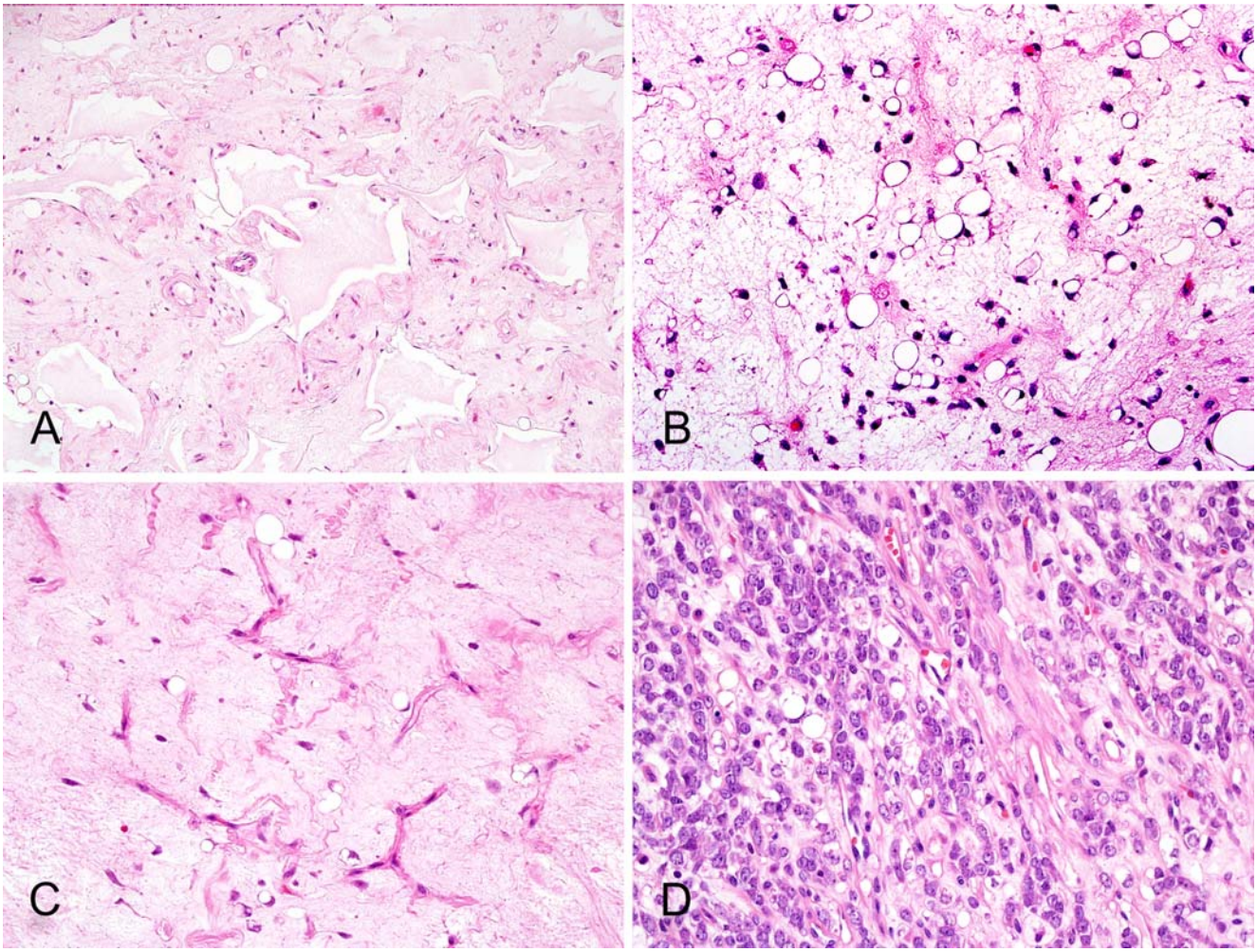

Fig. 6 MLPS's features: **a** Abundant myxoid matrix is found often deposited in mucinous pools, and **b** monovacuolated cells (lipoblasts) are encountered around vessel. **c** Typical plexiform vascular pattern resembling "crow feet" is present, and **d** a more hypercellular round cell component may be observed

tissue [104–106]. Adipocytic differentiation in pure round cell liposarcoma is hardly found, but the presence of S100 immunopositivity in the majority of the cases may be diagnostically helpful [107]. Transition to hypercellular/round cell areas is commonly observed in myxoid liposarcoma, therefore providing strong evidence in favor of the concept that myxoid and round cell liposarcoma represents a morphologic continuum of myxoid adipocytic neoplasia [108].

Well-differentiated myxoid liposarcoma must be differentiated from low-grade myxofibrosarcoma (a myxoid neoplasm composed of atypical stromal cells and pseudolipoblasts associated with distinctive archiform, capillary sized blood vessels) and EMCS (multinodular myxoid neoplasm showing oval round cells organized in strands and cords, clustering at the periphery of the nodules). Lipoblastoma can also mimic closely myxoid liposarcoma. Young age and lobular organization represent helpful clues.

Cytogenetics and molecular genetics

Myxoid liposarcoma is characterized by two main karyotypic aberrations: a t(12;16) that fuses the *DDIT3* gene on 12q13 (a member of the CCAAT/enhancer-binding protein family involved in adipocyte differentiation) [109, 110], with the *FUS* gene on 16p11. A subset is harboring a t(12;22) that fuses *DDIT3* with *EWSR1* on 22q12 [111]. The normal function of the *DDIT3* gene is to promote growth arrest, but as a consequence of the translocation, such an antiproliferative activity is lost [112]. Furthermore, both DDIT3 and FUS–DDIT3 expression in sarcoma cell lines induce adipogenesis [112].

Prognosis and treatment

The presence of hypercellularity or round cell differentiation is associated with worsening of prognosis [113]. Different

cutoff values, ranging between 5% and 25%, have been set by independent studies. A reliable assessment of the percentage of hypercellular areas is difficult to achieve as it may be hampered by inadequate sampling as well as by that degree of subjectivity that is intrinsic part of morphologic evaluation. For the time being, it appears safer to consider any amount of hypercellularity as prognostically relevant. Myxoid liposarcoma tends to recur repeatedly and tends to metastasize to both bone [114] and soft tissue locations including the retroperitoneum. Standard treatment is represented by wide surgical resection. In high-grade lesions, adjuvant therapy (radiotherapy and/or chemotherapy) may be associated. The drug trabectidin appears to be a highly promising treatment for metastatic myxoid liposarcoma [115, 116].

Conclusions

Mesenchymal tumors, in strong analogy with hematological malignancies, frequently harbor chromosome translocations. The *EWSR1* gene is one of the favorite partners as it is involved in several unrelated soft tissue lesions. Interestingly, *EWSR1* rearrangement has been recently observed in intermediate malignant tumors such as AFH. Even more, interestingly, the same alterations are observed in ST-CCS, a sarcoma phenotypically unrelated to AFH and characterized by full-blown malignant potential. This is a further example of the relative unspecificity of chromosome translocations, as also emphasized by the occurrence of ALK gene rearrangement in both inflammatory myofibroblastic tumor [117] and anaplastic large cell lymphoma [118] as well by the occurrence of the ETV6–NTRK3 fusion gene in infantile fibrosarcoma [119], mesoblastic nephroma [120], secretory carcinoma of the breast [121], and in an isolate report acute myeloid leukemia [122]. Another eloquent example is the occurrence of ASPSCR1–TEF3 fusion transcript in both alveolar soft part sarcomas as well as in pediatric forms of renal cell carcinoma [123, 124]. This does not hamper at all the diagnostic value of both cytogenetics and molecular genetics; however, it underscores the extreme importance of pairing genetic testing of tumors with proper diagnostic expertise. In particular, when using the split-apart FISH approach to *EWSR1* gene rearrangement, evaluation of the results in context with morphology becomes mandatory.

Conflict of interest statement We declare that we have no conflict of interest.

References

1. Delattre O, Zucman J, Plougastel B et al (1992) Gene fusion with an ETS DNA-binding domain caused by chromosome translocation in human tumours. Nature 359:162–165
2. Zucman J, Delattre O, Desmaze C et al (1992) Cloning and characterization of the Ewing's sarcoma and peripheral neuroepithelioma t(11;22) translocation breakpoints. Genes Chromosomes Cancer 5:271–277
3. Moller E, Stenman G, Mandahl N et al (2008) POU5F1, encoding a key regulator of stem cell pluripotency, is fused to EWSR1 in hidradenoma of the skin and mucoepidermoid carcinoma of the salivary glands. J Pathol 215:78–86
4. Plougastel B, Zucman J, Peter M et al (1993) Genomic structure of the EWS gene and its relationship to EWSR1, a site of tumor-associated chromosome translocation. Genomics 18:609–615
5. Bovée JVMG, Devilee P, Cornelisse CJ et al (1995) Identification of an EWS-pseudogene using translocation detection by RT-PCR in Ewing's sarcoma. Biochem Biophys Res Commun 213:1051–1060
6. Bertolotti A, Lutz Y, Heard DJ et al (1996) hTAF(II)68, a novel RNA/ssDNA-binding protein with homology to the proto-oncoproteins TLS/FUS and EWS is associated with both TFIID and RNA polymerase II. EMBO J 15:5022–5031
7. Crozat A, Aman P, Mandahl P et al (1993) Fusion of CHOP a novel RNA-binding protein in human myxoid liposarcoma. Nature 363:640–644
8. Morohoshi F, Arai K, Takahashi EI et al (1996) Cloning and mapping of a human RBP56 gene encoding a putative RNA binding protein similar to FUS/TLS and EWS proteins. Genomics 38:51–57
9. Azuma M, Embree LJ, Sabaawy H et al (2007) Ewing sarcoma protein ewsr1 maintains mitotic integrity and proneural cell survival in the zebrafish embryo. PLoS ONE 2:e979
10. Stolow DT, Haynes SR (1995) Cabeza, a Drosophila gene encoding a novel RNA binding protein, shares homology with EWS and TLS, two genes involved in human sarcoma formation. Nucleic Acids Res 23:835–843
11. Riggi N, Cironi L, Suva ML et al (2007) Sarcomas: genetics, signalling, and cellular origins. Part 1: the fellowship of TET. J Pathol 213:4–20
12. Aman P, Panagopoulos I, Lassen C et al (1996) Expression patterns of the human sarcoma-associated genes FUS and EWS and the genomic structure of FUS. Genomics 37:1–8
13. Zakaryan RP, Gehring H (2006) Identification and characterization of the nuclear localization/retention signal in the EWS proto-oncoprotein. J Mol Biol 363:27–38
14. Bertolotti A, Melot T, Acker J et al (1998) EWS, but not EWS-FLI-1, is associated with both TFIID and RNA polymerase II: interactions between two members of the TET family, EWS and hTAFII68, and subunits of TFIID and RNA polymerase II complexes. Mol Cell Biol 18:1489–1497
15. Zhang D, Paley AJ, Childs G (1998) The transcriptional repressor ZFM1 interacts with and modulates the ability of EWS to activate transcription. J Biol Chem 273:18086–18091
16. Knoop LL, Baker SJ (2001) EWS/FLI alters 5′-splice site selection. J Biol Chem 276:22317–22322
17. Knoop LL, Baker SJ (2000) The splicing factor U1C represses EWS/FLI-mediated transactivation. J Biol Chem 275:24865–24871
18. Leemann-Zakaryan RP, Pahlich S, Sedda MJ et al (2009) Dynamic subcellular localization of the Ewing sarcoma proto-oncoprotein and its association with and stabilization of microtubules. J Mol Biol 386:1–13
19. Li H, Watford W, Li C et al (2007) Ewing sarcoma gene EWS is essential for meiosis and B lymphocyte development. J Clin Invest 117:1314–1323
20. Thompson AD, Teitell MA, Arvand A et al (1999) Divergent Ewing's sarcoma EWS/ETS fusions confer a common tumorigenic phenotype on NIH3T3 cells. Oncogene 18:5506–5513

21. May WA, Arvand A, Thompson AD et al (1997) EWS/FLI1-induced manic fringe renders NIH 3T3 cells tumorigenic. Nat Genet 17:495–497
22. Ushigome S, Machinami R, Sorensen PH (2002) Ewing sarcoma/primitive neuroectodermal tumour (PNET). In: Fletcher CDM, Unni KK, Mertens F (eds) World Health Organization classification of tumours; pathology & genetics; tumours of soft tissue and bone. IARC Presss, Lyon, pp 298–300
23. Parham DM, Roloson GJ, Feely M et al (2001) Primary malignant neuroepithelial tumors of the kidney: a clinicopathologic analysis of 146 adult and pediatric cases from the National Wilms' Tumor Study Group Pathology Center. Am J Surg Pathol 25:133–146
24. Welsch T, Mechtersheimer G, Aulmann S et al (2006) Huge primitive neuroectodermal tumor of the pancreas: report of a case and review of the literature. World J Gastroenterol 12:6070–6073
25. Dedeurwaerdere F, Giannini C, Sciot R et al (2002) Primary peripheral PNET/Ewing's sarcoma of the dura: a clinicopathologic entity distinct from central PNET. Mod Pathol 15:673–678
26. Stout AP (1918) A tumor of the ulnar nerve. Proc N Y Pathol Soc 18:2–12
27. Askin FB, Rosai J, Sibley RK et al (1979) Malignant small cell tumor of the thoracopulmonary region in childhood: a distinctive clinicopathologic entity of uncertain histogenesis. Cancer 43:2438–2451
28. Ambros IM, Ambros PF, Strehl S et al (1991) MIC2 is a specific marker for Ewing's sarcoma and peripheral primitive neuroectodermal tumors: evidence for a common histogenesis of Ewing's sarcoma and peripheral primitive neuroectodermal tumors from MIC2 expression and specific chromosome aberration. Cancer 67:1886–1893
29. Dei Tos AP, Wadden C, Calonje E et al (1995) Immunohistochemical demonstration of glycoprotein p30/32^{mic2} (CD99) in synovial sarcoma. Appl Immunohistochem 3:168–173
30. Terrier-Lacombe MJ, Guillou L, Chibon F et al (2009) Superficial primitive Ewing's sarcoma: a clinicopathologic and molecular cytogenetic analysis of 14 cases. Mod Pathol 22:87–94
31. Hasegawa SL, Davison JM, Rutten A et al (1998) Primary cutaneous Ewing's sarcoma: immunophenotypic and molecular cytogenetic evaluation of five cases. Am J Surg Pathol 22:310–318
32. Nicholson SA, McDermott MB, Swanson PE et al (2000) CD99 and cytokeratin-20 in small-cell and basaloid tumors of the skin. Appl Immunohistochem Mol Morphol 8:37–41
33. Shing DC, McMullan DJ, Roberts P et al (2003) FUS/ERG gene fusions in Ewing's tumors. Cancer Res 63:4568–4576
34. Ng TL, O'Sullivan MJ, Pallen CJ et al (2007) Ewing sarcoma with novel translocation t(2;16) producing an in-frame fusion of FUS and FEV. J Mol Diagnostics 9:459–463
35. Aurias A, Rimbaut C, Buffe D et al (1983) Chromosomal translocations in Ewing's sarcoma. Letter to the editor. N Engl J Med 309:496–498
36. Lessnick SL, Dacwag CS, Golub TR (2002) The Ewing's sarcoma oncoprotein EWS/FLI induces a p53-dependent growth arrest in primary human fibroblasts. Cancer Cells 1:393–401
37. Kovar H (2005) Context matters: the hen or egg problem in Ewing's sarcoma. Semin Cancer Biol 15:189–196
38. Serrano M, Lin AW, McCurrach ME et al (1997) Oncogenic ras provokes premature cell senescence associated with accumulation of p53 and p16INK4a. Cell 88:593–602
39. Riggi N, Cironi L, Provero P et al (2005) Development of Ewing's sarcoma from primary bone marrow-derived mesenchymal progenitor cells. Cancer Res 65:11459–11468
40. Riggi N, Suva ML, Suva D et al (2008) EWS-FLI-1 expression triggers a Ewing's sarcoma initiation program in primary human mesenchymal stem cells. Cancer Res 68:2176–2185
41. Prieur A, Tirode F, Cohen P et al (2004) EWS/FLI-1 silencing and gene profiling of Ewing cells reveal downstream oncogenic pathways and a crucial role for repression of insulin-like growth factor binding protein 3. Mol Cell Biol 24:7275–7283
42. Tirode F, Laud-Duval K, Prieur A et al (2007) Mesenchymal stem cell features of Ewing tumors. Cancer Cells 11:421–429
43. Szuhai K, Ijszenga M, Tanke HJ et al (2006) Molecular cytogenetic characterization of four previously established and two newly established Ewing sarcoma cell lines. Cancer Genet Cytogenet 166:173–179
44. Szuhai K, Ijszenga M, De JD et al (2009) The NFATc2 gene is involved in a novel cloned translocation in a Ewing sarcoma variant that couples its function in immunology to oncology. Clin Cancer Res 15:2259–2268
45. Thorner P, Squire J, Chilton-MacNeill S et al (1996) Is the EWS/FLI-1 fusion transcript specific for Ewing sarcoma and peripheral primitive neuroectodermal tumor? A report of four cases showing this transcript in a wider range of tumor types. Am J Pathol 148:1125–1138
46. Ed A, Kawai A, Healy JH et al (1998) EWS-FL11 fusion transcript structure is an independent determinant of prognosis in Ewing's sarcoma. J Clin Oncol 16:1248–1255
47. Mangham DC, Cannon A, Li XQ et al (1995) p53 overexpression in Ewing's sarcoma/primitive neuroectodermal tumour is an uncommon event. J Clin Pathol 48M:M79–M82
48. Ueda Y, Dockhorn-Dworniczak B, Blasius S et al (1993) Analysis of mutant P53 protein in osteosarcomas and other malignant and benign lesions of bone. J Cancer Res Clin Oncol 119:172–178
49. Tsuchiya T, Sekine K, Hinohara S et al (2000) Analysis of the p16INK4, p14ARF, p15, TP53, and MDM2 genes and their prognostic implications in osteosarcoma and Ewing sarcoma. Cancer Genet Cytogenet 120:91–98
50. Wei G, Antonescu CR, de Alava E et al (2000) Prognostic impact of INK4A deletion in Ewing sarcoma. Cancer 89:793–799
51. Romeo S, Debiec-Rychter M, Van GM et al (2009) Cell cycle/apoptosis molecule expression correlates with imatinib response in patients with advanced gastrointestinal stromal tumors. Clin Cancer Res 15:4191–4198
52. Zogopoulos G, Teskey L, Sung L et al (2004) Ewing sarcoma: favourable results with combined modality therapy and conservative use of radiotherapy. Pediatr Blood Cancer 43:35–39
53. Schmidt D, Herrmann C, Jürgens H et al (1991) Malignant peripheral neuroectodermal tumor and its necessary distinction from Ewing's sarcoma. A report from the Kiel Pediatric Tumor Registry. Cancer 68:2251–2259
54. Parham DM, Hijazi Y, Steinberg SM et al (1999) Neuroectodermal differentiation in Ewing's sarcoma family of tumors does not predict tumor behavior. Hum Pathol 30:911–918
55. Terrier Ph, Henry-Amar M, Triche TJ et al (1995) Is neuroectodermal differentiation of Ewing's sarcoma of bone associated with an unfavourable prognosis? Eur J Cancer 31A:307–314
56. Toretsky JA, Kalebic T, Blakesley V et al (1997) The insulin-like growth factor-I receptor is required for EWS/FLI-1 transformation of fibroblasts. J Biol Chem 272:30822–30827
57. Toretsky JA, Steinberg SM, Thakar M et al (2001) Insulin-like growth factor type 1 (IGF-1) and IGF binding protein-3 in patients with Ewing sarcoma family of tumors. Cancer 92:2941–2947
58. Erkizan HV, Kong Y, Merchant M et al (2009) A small molecule blocking oncogenic protein EWS-FLI1 interaction with RNA helicase A inhibits growth of Ewing's sarcoma. Nat Med 15:750–756
59. Lessnick SL, Dei Tos AP, Sorensen PH et al (2009) Small round cell sarcomas. Semin Oncol 36:338–346

60. Antonescu CR, Gerald W (2002) Desmoplastic small round cell tumour. In: Fletcher CDM, Unni KK, Mertens F (eds) World Health Organisation classification of tumours, pathology and genetics, tumours of soft tissue and bone. pp 216–218
61. Parkash V, Gerald WL, Parma A et al (1995) Desmoplastic small round cell tumor of the pleura. Am J Surg Pathol 19:659–665
62. Cummings OW, Ulbright TM, Young RH et al (1997) Desmoplastic small round cell tumors of the paratesticular region. A report of six cases. Am J Surg Pathol 21:219–225
63. Wolf AN, Ladanyi M, Paull G et al (1999) The expanding clinical spectrum of desmoplastic small round-cell tumor: a report of two cases with molecular confirmation. Hum Pathol 30:430–435
64. Tison V, Cerasoli S, Morigi F et al (1996) Intracranial desmoplastic small-cell tumor. Report of a case. Am J Surg Pathol 20:112–117
65. Neder L, Scheithauer BW, Turel KE et al (2009) Desmoplastic small round cell tumor of the central nervous system: report of two cases and review of the literature. Virchows Arch 454:431–439
66. Adsay V, Cheng J, Athanasian E et al (1999) Primary desmoplastic small cell tumor of soft tissues and bone of the hand. Am J Surg Pathol 23:1408–1413
67. Hamazaki M, Okita H, Hata J et al (2006) Desmoplastic small cell tumor of soft tissue: molecular variant of EWS-WT1 chimeric fusion. Pathol Int 56:543–548
68. Murphy AJ, Bishop K, Pereira C et al (2008) A new molecular variant of desmoplastic small round cell tumor: significance of WT1 immunostaining in this entity. Hum Pathol 39:1763–1770
69. Slomovitz BM, Girotra M, Aledo A et al (2000) Desmoplastic small round cell tumor with primary ovarian involvement: case report and review. Gynecol Oncol 79:124–128
70. Bismar TA, Basturk O, Gerald WL et al (2004) Desmoplastic small cell tumor in the pancreas. Am J Surg Pathol 28:808–812
71. Su MC, Jeng YM, Chu YC (2004) Desmoplastic small round cell tumor of the kidney. Am J Surg Pathol 28:1379–1383
72. Wang LL, Perlman EJ, Vujanic GM et al (2007) Desmoplastic small round cell tumor of the kidney in childhood. Am J Surg Pathol 31:576–584
73. Stuart-Buttle CE, Smart CJ, Pritchard S et al (2008) Desmoplastic small round cell tumour: a review of literature and treatment options. Surg Oncol 17:107–112
74. Ordonez NG (1998) Desmoplastic small round cell tumor. I: a histopathologic study of 39 cases with emphasis on unusual histological patterns. Am J Surg Pathol 22:1303–1313
75. Gerald WL, Miller HK, Battifora H et al (1991) Intra-abdominal desmoplastic small round-cell tumor. Report of 19 cases of a distinctive type of high-grade polyphenotypic malignancy affecting young individuals. Am J Surg Pathol 15:499–513
76. Gerald WL, Ladanyi M, de Alava E et al (1998) Clinical, pathologic, and molecular spectrum of tumors associated with t(11;22)(p13;q12): desmoplastic small round-cell tumor and its variants. J Clin Oncol 16:3028–3036
77. Ordonez NG (1998) Desmoplastic small round cell tumor. II: an ultrastructural and immunohistochemical study with emphasis on new immunohistochemical markers. Am J Surg Pathol 22:1314–1327
78. Lee SB, Kolquist KA, Nichols K et al (1997) The EWS-WT1 translocation product induces PDGFA in desmoplastic small round-cell tumour. Na Genet 17:309–313
79. Werner H, Idelman G, Rubinstein M et al (2007) A novel EWS-WT1 gene fusion product in desmoplastic small round cell tumor is a potent transactivator of the insulin-like growth factor-I receptor (IGF-IR) gene. Cancer Lett 247:84–90
80. Wong JC, Lee SB, Bell MD et al (2002) Induction of the interleukin-2/15 receptor beta-chain by the EWS-WT1 translocation product. Oncogene 21:2009–2019
81. Sawyer JR, Tryka AF, Lewis JM (1992) A novel reciprocal chromosome translocation t(11;22)(p13;q12) in an intraabdominal desmoplastic small round-cell tumor. Am J Surg Pathol 16:411–416
82. Alaggio R, Rosolen A, Sartori F et al (2007) Spindle cell tumor with EWS-WT1 transcript and a favorable clinical course: a variant of DSCT, a variant of leiomyosarcoma, or a new entity? Report of 2 pediatric cases. Am J Surg Pathol 31:454–459
83. Katz RL, Quezado M, Senderowicz AM et al (1997) An intra-abdominal small round cell neoplasm with features of primitive neuroectodermal and desmoplastic round cell tumor and a EWS/FLI-1 fusion transcript. Hum Pathol 28:502–509
84. Li H, Smolen GA, Beers LF et al (2008) Adenosine transporter ENT4 is a direct target of EWS/WT1 translocation product and is highly expressed in desmoplastic small round cell tumor. PLoS ONE 3:e2353
85. Antonescu CR, Nafa K, Segal NH et al (2006) EWS-CREB1: a recurrent variant fusion in clear cell sarcoma association with gastrointestinal location and absence of melanocytic differentiation. Clin Cancer Res 12:5356–5362
86. Zambrano E, Reyes-Mugica M, Franchi A et al (2003) An osteoclast-rich tumor of the gastrointestinal tract with features resembling clear cell sarcoma of soft parts: reports of 6 cases of a GIST simulator. Int J Surg Pathol 11:75–81
87. Schaefer KL, Brachwitz K, Wai DH et al (2004) Expression profiling of t(12;22) positive clear cell sarcoma of soft tissue cell lines reveals characteristic up-regulation of potential new marker genes including ERBB3. Cancer Res 64:3395–3405
88. Segal NH, Pavlidis P, Noble WS et al (2003) Classification of clear-cell sarcoma as a subtype of melanoma by genomic profiling. J Clin Oncol 21:1775–1781
89. Langezaal SM, Graadt van Roggen JF, Cleton-Jansen AM et al (2001) Malignant melanoma is genetically distinct from clear cell sarcoma of tendons and aponeurosis (malignant melanoma of soft parts). Br J Cancer 84:535–538
90. Graadt van Roggen JF, Mooi WJ, Hogendoorn PCW (1998) Clear cell sarcoma of tendons and aponeuroses (malignant melanoma of soft parts) and cutaneous melanoma: exploring the histogenetic relationship between these two clinicopathological entities. J Pathol 186:3–7
91. Antonescu CR, Tschernyavsky SJ, Woodruff JM et al (2002) Molecular diagnosis of clear cell sarcoma: detection of EWS-ATF1 and MITF-M transcripts and histopathological and ultrastructural analysis of 12 cases. J Mol Diagnostics 4:44–52
92. Zucman J, Delattre O, Desmaze C et al (1993) EWS and ATF-1 gene fusion induced by t(12;22) translocation in malignant melanoma of soft parts. Nat Genet 4:341–345
93. Xie S, Price JE, Luca M et al (1997) Dominant-negative CREB inhibits tumor growth and metastasis of human melanoma cells. Oncogene 15:2069–2075
94. Yokoyama S, Feige E, Poling LL et al (2008) Pharmacologic suppression of MITF expression via HDAC inhibitors in the melanocyte lineage. Pigment Cell Melanoma Res 21:457–463
95. Lucas DR, Heim S (2002) Extraskeletal myxoid chondrosarcoma. In: Fletcher CDM, Unni KK, Mertens F (eds) Pathology & genetics. Tumours of soft tissue and bone. IARC Press, Lyon, pp 213–215
96. Aigner T, Oliveira AM, Nascimento AG (2004) Extraskeletal myxoid chondrosarcomas do not show a chondrocytic phenotype. Mod Pathol 17:214–221
97. Subramanian S, West RB, Marinelli RJ et al (2005) The gene expression profile of extraskeletal myxoid chondrosarcoma. J Pathol 206:433–444
98. Turc-Carel C, Dal Cin P, Rao U et al (1988) Recurrent breakpoints at 9q31 and 22q12.2 in extraskeletal myxoid chondrosarcoma. Cancer Genet Cytogenet 30:145–150

99. Panagopoulos I, Mertens F, Isaksson M et al (2002) Molecular genetic characterization of the EWS/CHN and RBP56/CHN fusion genes in extraskeletal myxoid chondrosarcoma. Genes Chromosomes Cancer 35:340–352
100. Filion C, Motoi T, Olshen AB et al (2009) The EWSR1/NR4A3 fusion protein of extraskeletal myxoid chondrosarcoma activates the PPARG nuclear receptor gene. J Pathol 217:83–93
101. Fanburg-Smith JC, Dal Cin P (2002) Angiomatoid fibrous histiocytoma. In: Fletcher CDM, Unni KK, Mertens F (eds) World Health Organisation classification of tumours. Pathology and genetics of tumours of soft tissue and bone. IARC Press, Lyon, pp 194–195
102. Rossi S, Szuhai K, Ijszenga M et al (2007) EWSR1-CREB1 and EWSR1-ATF1 fusion genes in angiomatoid fibrous histiocytoma. Clin Cancer Res 13:7322–7328
103. Antonescu CR, Dal CP, Nafa K et al (2007) EWSR1-CREB1 is the predominant gene fusion in angiomatoid fibrous histiocytoma. Genes Chromosomes Cancer 46:1051–1060
104. Antonescu CR, Ladanyi M (2002) Myxoid Liposarcoma. In: Fletcher CDM, Unni KK, Mertens F (eds) World Health Organisation classification of tumours. Pathology and genetics of tumours of soft tissue and bone. IARC Press, Lyon, pp 40–43
105. Kilpatrick SE, Doyon J, Choong PFM et al (1996) The clinicopathologic spectrum of myxoid and round cell liposarcoma. A study of 95 cases. Cancer 77:1450–1458
106. Smith TA, Easley KA, Goldblum JR (1996) Myxoid/round cell liposarcoma of the extremities. A clinicopathologic study of 29 cases with particular attention to extent of round cell liposarcoma. Am J Surg Pathol 20:171–180
107. Dei Tos AP, Wadden C, Fletcher CDM (1996) S-100 protein staining in liposarcoma. Its diagnostic utility in the high grade myxoid (round cell) variant. Appl Immunohistochem 4:95–101
108. Orvieto E, Furlanetto A, Laurino L et al (2001) Myxoid and round cell liposarcoma: a spectrum of myxoid adipocytic neoplasia. Semin Diagn Pathol 18:267–273
109. Tallini G, Rosai J, Fletcher CDM et al (1995) Myxoid liposarcoma represents a distinct type of liposarcoma characterised by the specific cytogenetic translocation t(12; 16)(q13; p11). Mod Pathol 8
110. Knight JC, Renwick PJ, Dal Cin P et al (1995) Translocation t (12;16)(q13;p11) in myxoid liposarcoma and round cell liposarcma: molecular and cytogenetic analysis. Cancer Res 55:24–27
111. Panagopoulos I, Hoglund M, Mertens F et al (1996) Fusion of the EWS and CHOP genes in myxoid liposarcoma. Oncogene 12:489–494
112. Engstrom K, Willen H, Kabjorn-Gustafsson C et al (2006) The myxoid/round cell liposarcoma fusion oncogene FUS-DDIT3 and the normal DDIT3 induce a liposarcoma phenotype in transfected human fibrosarcoma cells. Am J Pathol 168:1642–1653
113. Antonescu CR, Tschernyavsky SJ, Decuseara R et al (2001) Prognostic impact of P53 status, TLS-CHOP fusion transcript structure, and histological grade in myxoid liposarcoma: a molecular and clinicopathologic study of 82 cases. Clin Cancer Res 7:3977–3987
114. Schwab JH, Boland P, Guo T et al (2007) Skeletal metastases in myxoid liposarcoma: an unusual pattern of distant spread. Ann Surg Oncol 14:1507–1514
115. Grosso F, Jones RL, Demetri GD et al (2007) Efficacy of trabectedin (ecteinascidin-743) in advanced pretreated myxoid liposarcomas: a retrospective study. Lancet Oncol 8:595–602
116. Forni C, Minuzzo M, Virdis E et al (2009) Trabectedin (ET-743) promotes differentiation in myxoid liposarcoma tumors. Mol Cancer Ther
117. Lawrence B, Perez-Atayde A, Hibbard MK et al (2000) TPM3-ALK and TPM4-ALK oncogenes in inflammatory myofibroblastic tumors. Am J Pathol 157:377–384
118. Lamant L, Dastugue N, Pulford K et al (1999) A new fusion gene TPM3-ALK in anaplastic large cell lymphoma created by a (1;2)(q25;p23) translocation. Blood 93:3088–3095
119. Knezevich SR, McFadden DE, Tao W et al (1998) A novel ETV6-NTRK3 gene fusion in congenital fibrosarcoma. Nat Genet 18:184–187
120. Knezevich SR, Garnett MJ, Pysher TJ et al (1998) ETV6-NTRK3 gene fusions and trisomy 11 establish a histogenetic link between mesoblastic nephroma and congenital fibrosarcoma. Cancer Res 58:5046–5048
121. Tognon C, Knezevich SR, Huntsman D et al (2002) Expression of the ETV6-NTRK3 gene fusion as a primary event in human secretory breast carcinoma. Cancer Cells 2:367–376
122. Eguchi M, Eguchi-Ishimae M, Tojo A et al (1999) Fusion of ETV6 to neurotrophin-3 receptor TRKC in acute myeloid leukemia with t(12;15)(p13;q25). Blood 93:1355–1363
123. Argani P, Antonescu CR, Illei PB et al (2001) Primary renal neoplasms with the ASPL-TFE3 gene fusion of alveolar soft part sarcoma: a distinctive tumor entity previously included among renal cell carcinomas of children and adolescents. Am J Pathol 159:179–192
124. Ladanyi M, Lui MY, Antonescu CR et al (2001) The der(17)t (X;17)(p11;q25) of human alveolar soft part sarcoma fuses the TFE3 transcription factor gene to ASPL, a novel gene at 17q25. Oncogene 20:48–57

Virchows Arch (2010) 456:235–243
DOI 10.1007/s00428-010-0881-0

ORIGINAL ARTICLE

*PIK*ing the right isoform: the emergent role of the p110β subunit in breast cancer

Silvia Carvalho · Fernanda Milanezi · José Luís Costa · Isabel Amendoeira · Fernando Schmitt

Received: 19 October 2009 / Revised: 23 November 2009 / Accepted: 4 January 2010 / Published online: 4 February 2010
© Springer-Verlag 2010

Abstract Class IA phosphoinositide-3'-kinases (PI3Ks) regulate many cellular processes. Despite a clear implication of PI3K in cancer, the involvement of each of its isoforms namely p110α and p110β in the development of breast cancer remains elusive. Until recently, the spotlight was given to the α subunit; however, the p110β isoform has now emerged as an interesting target as well. In order to determine the importance of both these subunits in breast cancer, we aimed to study the expression of p110α and p110β in a series of invasive breast carcinomas. We constructed tissue microarrays from 315 invasive breast carcinomas and performed immunohistochemistry for p110α and β, correlating the expression patterns with clinicopathological parameters. Furthermore, overall survival was analysed through Kaplan–Meier survival curves and Cox regression. We found that p110 subunits are expressed in 23.8% of invasive breast carcinomas, of which 11.8% express p110α and 15.2% p110β. The p110α positive tumours correlated with hormone receptor (HR) expression, and were not associated with overall survival. The membrane expression of p110β was associated with worse prognosis. This was due to its link to HER2-overexpression, lower age of onset, higher grade, lymph node involvement, distant metastasis and was inversely associated with HR status. Furthermore, p110β expression was associated with worse overall survival. Importantly our results indicate a role for the beta subunit in the development/progression of HER2-overexpressing tumours, highlighting possible therapeutic associations between HER2 and p110β inhibitors.

Keywords PI3K · p110α · p110β · HER2 · Breast cancer

S. Carvalho · F. Milanezi · J. L. Costa · F. Schmitt (✉)
IPATIMUP: Institute of Molecular Pathology and Immunology of the University of Porto, University of Porto,
Rua Dr Roberto Frias s/n,
4200-465 Porto, Portugal
e-mail: fernando.schmitt@ipatimup.pt

S. Carvalho · F. Milanezi · F. Schmitt
Medical Faculty of the University of Porto, University of Porto,
Porto, Portugal

I. Amendoeira
Department of Pathology, Hospital de S. João,
Porto, Portugal

Introduction

Phosphoinositide-3-kinases (PI3K) are a family of proteins involved in the regulation of cell growth, metabolism, proliferation, glucose homeostasis and vesicle trafficking [1]. They are divided into three classes that differ in structure, substrate preference, tissue distribution, mechanism of activation and, ultimately, in function [2, 3]. In proliferation control and in tumorigenesis the most important PI3K proteins are those belonging to class I_A [4]. Class I_A PI3Ks are heterodimers comprised of a regulatory subunit (p85α, p55α, p50α, p85β and p55γ) and a catalytic subunit (p110α, p110β and p110δ) and are mainly activated downstream of cell surface receptors [1, 5]. In normal tissues, p110α and p110β are ubiquitously expressed, whereas the expression of p110δ is mainly restricted to leukocytes [6]. Uncontrolled activation of the PI3K pathway can be achieved via numerous alterations that might contribute to the development and progression of human cancer, including breast [7]. Some of these alterations may be constitutively active mutations or amplification of tyrosine kinase receptors like EGFR, HER2 or IGFR amongst others

[8]; *PI3K* gene amplification [9–11]; presence of activating mutations in the *PIK3CA* gene [4, 12]; loss or inactivating mutation of *PTEN* [1, 13–15] and constitutive recruitment and activation by *Ras* oncogene [13, 16].

In breast cancer, the *PIK3CA* gene has been a target for much scrutiny. This is due to the high mutation rate encountered (about 26%) [17], frequently found in HER2 overexpressing tumours [18, 19]. The presence of mutations in the *PIK3CA* gene is associated with p110α overexpression [18]. Thus, the α subunit has been, until quite recently, the main focus of the majority of the research related to PI3K and cancer. However, recently, the β isoform has claimed attention to its disease involvement. Although its role is not due to the occurrence of mutations [20], it was shown that mice expressing a catalytically inactive form of p110β were protected from tumour development, in an HER2-driven cancer model [21]. Furthermore, in an animal model of prostate tumour formation, induced by the loss of the *PTEN* gene, the ablation of the β subunit (but not of α), blocked tumour development [22]. Taken together, these studies show a link between p110β and cancer development either by itself or triggered by the occurrence of other cellular events. Due to the development of a great number of specific therapies directed against PI3K catalytic subunits [23], we believe that it is crucial to characterise the expression of both subunits (α and β) in invasive breast tumours to determine the importance of both isoforms in breast cancer development and/or progression.

Materials and methods

Case selection

Formalin-fixed paraffin-embedded tissues of 315 invasive breast carcinomas cases, selected from 2001 until 2006, were identified and retrieved, in a consecutive manner, from IPATIMUP and Hospital de São João, Porto, Portugal. For diagnostic purposes, all cases had information regarding clinicopathological data namely, histological type and grade, size, age, lymph node involvement, metastasis, oestrogen receptor (ER) alpha, progesterone receptor (PR) and HER2 status. The cases were once more reviewed on haematoxylin and eosin (H&E)-stained sections by the three pathologists (FM, IA and FS). The work presented is in accordance with the National regulative law of accession to tumour bank material since it is a retrospective study with solely research purpose.

Tissue microarray construction

Representative areas of different lesions were selected on H&E-stained sections and marked as described elsewhere [24]. In brief, two tissue cores (2 mm in diameter) were obtained from each selected specimen and precisely deposited into a recipient paraffin block using a tissue microarrays (TMA) workstation (TMA builder, LabVision Corporation, USA). Several TMA blocks were constructed each containing 24 tissue cores, arranged in a 4×6 sector. In each TMA block, three nonneoplastic breast tissue cores were also included as controls and one core of a histological characteristic tissue (testicular or liver tissue). After construction, 2–3 μm tissue sections were cut, and an H&E-stained section from each block was reviewed to confirm the presence of morphological representative areas of the original lesions.

Immunohistochemistry

The immunohistochemistry was performed using the Envision Detection System (DakoCytomation, Carpinteria, CA, USA). The assay conditions were as described elsewhere [24, 25]. Slides were stained for p110α, p110β, PTEN and p-AKT. Primary antibodies used, class, clone, dilutions, time and temperature of incubation, suppliers as well as antigen retrieval conditions are listed on Table 1. p110α and p-AKT were classified according to published data [18]. Briefly, immunostaining was calculated, on the basis of membrane/cytoplasmic expression (for p110α), or cytoplasmic expression (for p-AKT), by multiplying the percentage of labelled cells (ranging from 0% to 100%) by the intensity of the staining (1—weak, 2—moderate and 3—strong). Scores above 150 were considered positive. p110β was scored as negative, granular cytoplasmic or membrane staining. Regarding PTEN expression the cases were scored based on the intensity of the staining obtained in the tumour compared to internal positive controls (blood vessels). Cases were scored as negative (no tumour expression vs. normal expression in the control), reduced (low expression in the tumour vs. normal expression in the control) and normal (when the intensity was the same in both tumour and control).

Cell lines and cell culture

The epithelial breast cancer cell lines MCF7, BT474 and SKBR3 and the mesenchymal breast cancer cell line HS578T were purchased from American Type Culture Collection, and were maintained in Dulbecco's modified Eagle's medium with 10% *v*/*v* FBS and 1% *v*/*v* penicillin/streptomycin at 37°C in 5%CO_2.

Immunofluorescence

Cells were seeded at 80% confluence on 24-well plates over a 10×10 mm slide cover being afterwards fixed in

Table 1 Characteristics of the primary antibodies used

Primary antibody	Class	Clone	Dilution	Time/type of incubation	Supplier	Antigen retrieval
p110α	RM	C73F8	1:200	ON/4°C	Cell Signaling	AUS
p110β	MM	ab55593	3 μg/mL	ON/4°C	Abcam	EDTA
p-AKT	RM	736E11	1:50	ON/4°C	Cell Signaling	AUS
PTEN	MM	6H11	1:300	ON/4°C	Cascade Bioscience	AUS

p110α phosphatidylinositol 3 kinase catalytic subunit alpha, *p110β* phosphatidylinositol 3 kinase catalytic subunit beta, *p-AKT* phosphorylated AKT, *PTEN* phosphatase and tensin homolog deleted on chromosome 10, *RM* rabbit monoclonal, *MM* mouse monoclonal, *ON* overnight, *AUS* antigen unmasking solution pH6, *EDTA* ethylenediaminetetraacetic acid pH9

4% (*v*/*v*) paraformaldehyde for 20 min. All washes and incubations were performed with PBS unless stated otherwise. Next, slide covers were immersed in 50 nM NH_4Cl for 10 min and washed. Cells were permeabilized with 0.2% (*v*/*v*) Triton X-100 for 5 min, washed and incubated in 5% (*w*/*v*) bovine serum albumin (BSA) for 30 min. Incubation with primary antibody was in 5% (*w*/*v*) BSA overnight at 4°C. Cells were washed and incubated with, ALEXA 488 goat anti-rabbit (for p110α), ALEXA 594 goat anti-mouse (for p110β; Invitrogen, Paisley, UK) at 1:500 for 1 h. Specimens were mounted with VectaShield containing DAPI (Vector Laboratories Inc., Burlingame, CA, USA) and observed in a Zeiss microscope (Axio Imager Z1—fluorescent microscope) with apotome and images were taken using the Axiovision software.

Statistical analysis

The Statview software package was used for all statistical analysis. Correlations between categorical variables were performed using the chi-square test and between continuous and categorical values with analysis of variance. Overall survival (OS) was expressed as the number of months from diagnosis to the occurrence of an event (disease-related death). OS analysis was estimated using Kaplan–Meier method and compared using the log-rank test. Cox regression models were fitted to estimate hazard ratios and the corresponding 95% confidence interval for the classical prognostic factors, p110α and p110β. In all analysis, a significant level of 5% was considered.

Results

p110α and p110β expression in invasive breast carcinomas

A total of 315 cases of invasive breast carcinomas were evaluated according to their pattern of expression. In all TMAs constructed, both positive and negative cases were observed. Negative cases resulted from a staining score lower than 150 for p110α and absence or weak cytoplasmic expression for p110β. Figure 1 depicts an immunohistochemical panel showing the pattern of expression of the proteins in study. p110 subunits were expressed in 23.8% of invasive breast carcinomas (75 out of 315 cases). The positive cases for p110α presented a membrane/cytoplasmic staining whereas for p110β two patterns of expression were clearly observed: membrane staining and granular cytoplasmic staining. Strong membrane/cytoplasmic expression of p110α was observed in 11.8% (37 out of 315 cases) of the invasive breast carcinomas. Regarding p110β, 15.2% (48 out of 315 cases) of the cases were positive. Among these, strong membrane expression was observed in 66.7% and 33.3% of the cases presented a granular cytoplasmic expression (32 out of 48 and 16 out of 48, respectively; Table 2). As expected, both subunits were expressed in normal breast epithelium. To validate the use of TMA for immunoprofiling, we compared, from whole tissue sections, the expression of p110α and p110β in 15 randomly selected cases. The concordance between the expression patterns observed in TMAs and whole tissue sections was 100%.

Association between p110α and p110β and clinicopathological parameters

The importance of p110 subunits in breast cancer was further evaluated by correlating their expression with standard clinicopathological features.

Among the clinicopathological parameters studied, p110α only correlated with HR status ($p<0.0001$), with a higher percentage of p110α positive cases among the HR positive tumours—59% (22 out of 37 cases; Table 2). Regarding p110β, there was an association between its expression and age ($p=0.048$), grade ($p<0.0001$), lymph node involvement ($p=0.03$), metastasis ($p=0.044$), HR ($p<0.0001$) and HER2 ($p<0.0001$) status. The membrane positive cases had lower age of onset, higher grade, presented a higher number of lymph nodes involved and a higher rate of distant metastasis. p110β membrane expression was inversely correlated with HR status. In HER2

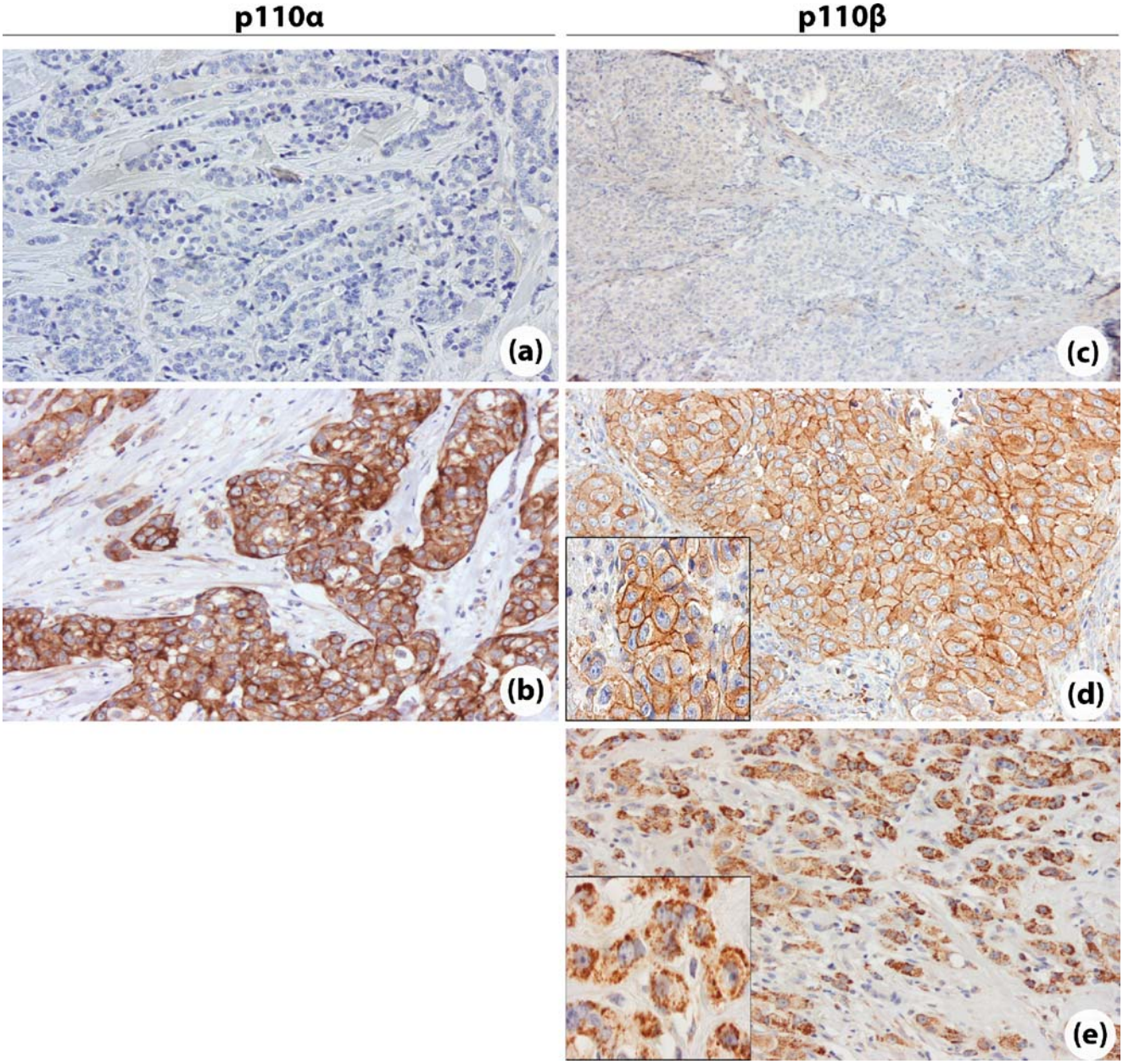

Fig. 1 p110α and p110β expression in invasive breast carcinomas. Photomicrographs of **a** invasive breast carcinoma with absence of p110α expression; **b** invasive breast carcinoma with strong membrane/cytoplasmic p110α expression; **c** invasive breast carcinoma with absence of p110β expression; **d** invasive breast carcinoma with membrane expression of p110β (better visualised in the *inset*); **e** invasive breast carcinoma with granular cytoplasmic expression (better visualised in the *inset*)

positive tumours, p110β expression was observed in 93.8% of the cases. The granular positive cases presented a similar pattern of expression as the negative cases for the clinicopathological features in analysis.

Association between p110α and p110β and PI3K pathway partners

To determine the status of activation of the PI3K pathway, the association between p110 subunits and two pathway partners—p-AKT and PTEN—was evaluated. The expression of p-AKT, a downstream target of p110, and PTEN, an antagonist of pathway activation, were assessed (Table 2). We observed an association between p-AKT and p110α, where the majority of the p110α-positive cases were also positive for p-AKT (86.49%, 32 out of 37). This association was not observed for p110β although there was a tendency for the positive cases to have a higher p-AKT expression. No association was observed between PTEN and either of the p110 subunits.

Table 2 Associations between p110α and p110β, clinicopathological parameters and PI3K-pathway partners (n=315)

Characteristic		p110α			p110β			
		Negative *n*	Positive *n*	*p* value	Negative *n*	Granular *n*	Membrane *n*	*p* value
Mean age (SD)		56.7 (13.2)	58.9 (13.0)	0.33	57.2 (13.2)	64.2 (11.0)	51.4 (11.7)	0.0048[a]
Size (cm)	≤2	137 (49.5%)	24 (64.9%)	0.08	141 (53.0%)	7 (43.8%)	13 (40.6%)	0.34
	>2	140 (50.5%)	13 (35.1%)		125 (47.0%)	9 (56.2%)	19 (59.4%)	
Grade	I	62 (22.4%)	9 (25.0%)	0.94	65 (24.4%)	4 (26.7%)	2 (6.3%)	<0.0001[a]
	II	119 (43.0%)	15 (41.7%)		124 (46.6%)	6 (40.0%)	4 (12.5%)	
	III	96 (34.6%)	12 (33.3%)		77 (29.0%)	5 (33.3%)	26 (81.2%)	
Histological type	I. Ductal carcinoma	209 (75.2%)	27 (73.0%)	0.96	199 (74.5%)	11 (68.8%)	26 (81.3%)	0.37
	I. Lobular carcinoma	14 (5.0%)	2 (5.4%)		16 (6.0%)	0 (0.0%)	0 (0.0%)	
	I. Carcinoma mixed type	30 (10.8%)	5 (13.5%)		31 (11.6%)	2 (12.5%)	2 (6.3%)	
	I. Carcinoma special type	25 (9.0%)	3 (8.1%)		21 (7.9%)	3 (18.7%)	4 (12.4%)	
LN involv. (no. nodes)	None	89 (40.8%)	15 (51.7%)	0.4	87 (42.9%)	9 (60.0%)	8 (27.6%)	0.03[a]
	Between 1 and 3	68 (31.2%)	9 (31.0%)		68 (33.5%)	2 (13.3%)	7 (24.1%)	
	More than 3	61 (28.0%)	5 (17.3%)		48 (23.6%)	4 (26.7%)	14 (48.3%)	
Metastasis	None	219 (78.7%)	32 (86.5%)	0.53	221 (82.8%)	12 (75.0%)	18 (56.2%)	0.044[a]
	Local regional	11 (4.0%)	2 (5.4%)		11 (4.1%)	0 (0.0%)	2 (6.3%)	
	Distant	37 (13.3%)	2 (5.4%)		25 (9.4%)	3 (18.8%)	11 (34.4%)	
	Both local and distant	11 (4.0%)	1 (2.7%)		10 (3.7%)	1 (6.2%)	1 (3.1%)	
HR	Negative	36 (13.0%)	15 (40.5%)	<0.0001[a]	25 (9.4%)	6 (37.5%)	20 (62.5%)	<0.0001[a]
	Positive	242 (87.0%)	22 (59.5%)		242 (90.6%)	10 (62.5%)	12 (37.5%)	
HER2	Negative	227 (81.7%)	29 (78.4%)	0.63	243 (91.0%)	11 (68.8%)	2 (6.2%)	<0.0001[a]
	Positive	51 (18.3%)	8 (21.6%)		24 (9.0%)	5 (31.2%)	30 (93.8%)	
PTEN	Negative	101 (36.9%)	10 (27.0%)	0.17	100 (38.0%)	6 (37.5%)	5 (15.6%)	0.085
	Reduced	85 (31.0%)	16 (43.3%)		83 (31.5%)	5 (31.3%)	13 (40.6%)	
	Normal	70 (25.5%)	11 (29.7%)		63 (24.0%)	4 (25.0%)	14 (43.8%)	
	Nuclear	18 (6.6%)	0 (0.0%)		17 (6.5%)	1 (6.2%)	0 (0.0%)	
p-AKT	Negative	80 (29.4%)	5 (13.5%)	0.042[a]	76 (29.1%)	5 (31.3%)	4 (12.5%)	0.13
	Positive	192 (70.6%)	32 (86.5%)		185 (70.9%)	11 (68.7%)	28 (87.5%)	
p110α	Negative				240 (89.9%)	11 (68.8%)	27 (84.4%)	0.03[a]
	Positive				27 (10.1%)	5 (31.2%)	5 (15.6%)	

I invasive, *LN Involv* lymph node involvement, *HR* hormone receptors, *HER2* human epidermal receptor 2, *PTEN* phosphatase and tensin homolog deleted on chromosome 10, *p-AKT* phosphorylated AKT, *p110α* phosphatidylinositol 3 kinase catalytic subunit alpha, *p110β* phosphatidylinositol 3 kinase catalytic subunit beta

[a] Statistically significant

Patient outcome analysis

To evaluate if p110α or β expression had an impact on overall survival we performed Kaplan–Meier survival curves. There was no difference in overall survival for p110α expression (p=0.52, Fig. 2a). However, p110β-positive breast carcinomas (either granular or membranar) had a worse outcome when compared to those without expression (p=0.021, Fig. 2b). As previously demonstrated in other studies, univariate Cox proportional hazard analysis showed that, tumour size, lymph node stage, tumour grade as well as the expression of HR and HER2 were significant predictors for overall survival. In accordance to the Kaplan–Meier curves, the expression of p110β was also a significant predictor for overall survival, showing that the membrane and the granular cytoplasm positive cases present an increased risk of death when compared to the negative cases (Table 3). However, in multivariate analysis with models including tumour size, lymph node involvement and HER2 status, p110β was not an independent factor of prediction of patient overall survival.

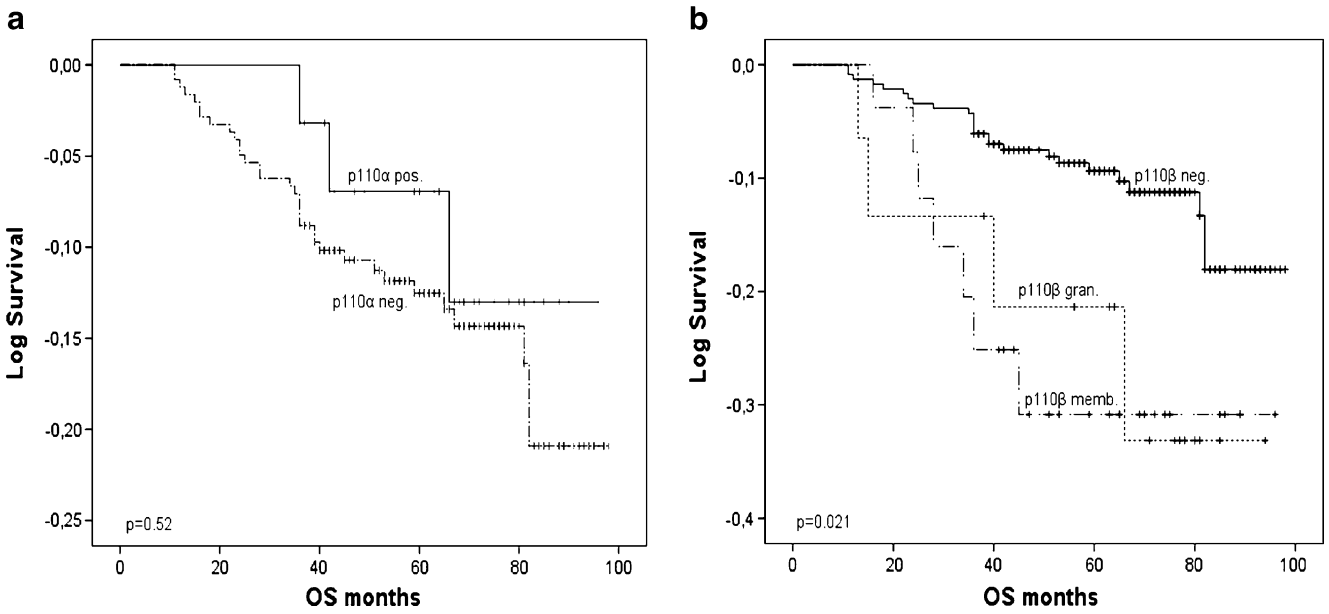

Fig. 2 Kaplan–Meier overall survival curves (derived from univariate analysis) for **a** p110α, where no association is encountered and **b** p110β where it is possible to observe that the positive cases, either membrane or granular present a worst overall survival

Analysis of p110α and p110β expression in a panel of breast cancer cell lines

After analysing p110α and β in the series of invasive breast carcinomas we assessed their expression in representative breast carcinomas cell lines in order to: (1) determine if the phenotypes observed in the invasive breast carcinomas were also observed and (2) to establish an *in vitro* model for further validation of the results observed. We selected the epithelial cell lines MCF7 (HR positive), BT474 and SKBR3 (both with HER2 overexpression) and the mesenchymal cell line HS578T. All cell lines expressed p110α with no differences in cellular localization (membrane/cytoplasmic—data not shown). Regarding p110β (Fig. 3), MCF7 lacked expression, BT474 presented a membrane/granular cytoplasmic staining, SKBR3 presented a strong membrane expression and HS578T presented a granular cytoplasmic staining.

Table 3 Univariate Cox proportional hazard analysis (overall survival) in the 315 cases of invasive breast carcinoma

Variable	Evaluation	Hazard ratio (95% confidence interval)	*p* value
Size	T1 (≤ 2 cm)	1	
	T2 (2<T≤5 cm)	3.29 (1.42 to 7.62)	0.006
	T3 (>5 cm)	11.43 (4.59 to 28.45)	<0.0001
Lymph node stage	Negative	1	
	1 to 3	3.09 (1.05 to 9.04)	0.04
	>3	5.84 (2.14 to 15.95)	0.001
Grade	I	1	
	II	1.62 (0.51 to 5.07)	0.41
	III	4.77 (1.63 to 13.92)	0.004
HR	Positive	1	
	Negative	3.14 (1.55 to 6.39)	0.002
HER2	Negative	1	
	Positive	3.44 (1.77 to 6.67)	<0.0001
p110α	Negative	1	
	Positive	0.68 (0.21 to 2.22)	0.52
p110β	Negative	1	
	Granular	2.52 (0.88 to 7.23)	0.086
	Membrane	2.68 (1.16 to 6.2)	0.021

HR hormone receptors, *HER2* human epidermal receptor 2, *p110α* phosphatidylinositol 3 kinase catalytic subunit alpha, *p110β* phosphatidylinositol 3 kinase catalytic subunit beta

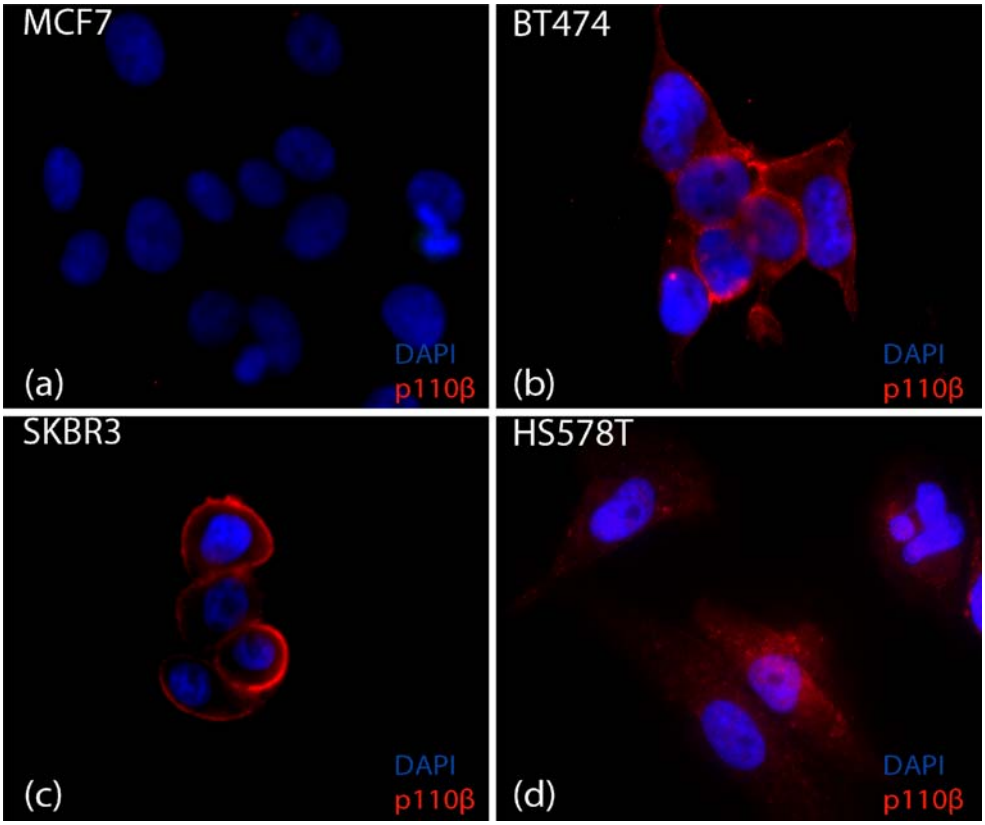

Fig. 3 p110β expression in a panel of breast cancer cell lines: (**a**–**c**)—epithelial cell lines: **a** *MCF7*—absence of expression, **b** *BT474*—membrane and granular cytoplasmic staining, **c** *SKBR3*—membrane staining, **d** mesenchymal cell line: *HS578T*—granular cytoplasmic staining

Discussion

The importance of PI3K pathway activation in breast cancer was initially highlighted by the high number of mutations in *PIK3CA* [26, 27], the gene that codifies p110α. Although the occurrence of gain of function mutations precludes the oncogenic potential of this protein, it must not mislead to the importance of other mechanisms that drive cancer development. A good example is the growing interest in p110β. Although lacking activating mutations, the β subunit has, step by step, claimed a place in the medical literature in these past few years. The absence of cancer-specific mutations associated with the β-isoform reflect its inherited oncogenic potential [28], further emphasised by the ability of the wild-type protein to induce oncogenic transformation [20, 29, 30].

In the present study, we have investigated the expression of two of the most widely expressed PI3K, catalytic subunits—p110α and p110β—in order to evaluate the possible involvement of these subunits in the development/progression of breast cancer. The data presented herein describes the emergent role of the β subunit, in breast cancer, particularly in HER2-related carcinomas. In a series of invasive breast carcinomas, p110 subunits were expressed in 23.8% of the cases: 11.8% for p110α and 15.2% for p110β. The putative relation between p110β and breast cancer was further highlighted by its association with lower age of onset of the disease, higher tumour grade, lymph node involvement and presence of metastasis in distant organs. In addition, p110β inversely correlated with HR status. Strikingly, 93.8% of the HER2 overexpressing tumours presented p110β expression. Previous studies have showed that PI3K is a preferential signalling pathway activated by HER2 [31], suggesting a link between p110α and HER2 mediated signalling [19]. However, recently, p110β was associated to HER2-related proliferation showing that this subunit has a more crucial role in this setting than p110α, as it was shown that p110β kinase activity is required for the growth of HER2-dependent mammary gland cancers [21]. Furthermore, all the cell lines studied that presented HER2 overexpression (SKBR3 and BT474), also presented high p110β expression. p110β was also associated with worst overall survival. The biological significance of the granular expression pattern observed is still unclear and requires further studies. Still, its association with worst overall survival suggests that we are not in the presence of a staining setback, but possibly p110β is engaged in other cellular functions.

Regarding p110α, the positive cases were more frequently positive for HR, and although lacking other statistically significant associations, there was a correlation between p110α expression and good prognostic markers. This is in agreement with recently published data, where *PIK3CA* mutations were associated with HR positive

tumours and favourable clinicopathological features like, older age, lower tumour grade and stage, lymph node negativity and better clinical outcome, including survival [32].

PTEN, which limits PI3K signalling by dephosphorylation of phosphatidylinositol-3-phosphate, is frequently inactivated by mutation, gene deletion or epigenetic silencing [1, 33]. Its expression study was thus justified by the need of determining if PTEN was able to counteract the overexpression of p110 subunits. We did not find an association between PTEN expression and p110 subunits. Although our results could not confirm the findings of recently published data, it is becoming increasingly clear that, p110α seems to play only a minor role as the occurrence of mutations in *PIK3CA* and PTEN loss seem to be mutually exclusive events [19]. Supporting the idea of p110β importance is the evidence, in a prostate tumour model triggered by PTEN loss, that, per se, the blockage of p110β is sufficient to inhibit tumour growth [22]. Also, in a colorectal cancer model, PTEN-deficient tumours were associated with dependency on p110β being PI3K activation, cell growth and survival due to this subunit [34].

p-AKT protein expression was observed for positive p110α cases, suggesting that whenever p110α overexpression is present, phosphorylation of AKT is more frequent, which in accordance with other published data [35, 36]. The lack of association between p-AKT and p110β can be explained by a dual function of this subunit: the positive cases for β and p-AKT might reflect a kinase-dependent function that activates the canonical PI3K/AKT pathway, or the β-positive/p-AKT negative may result from a kinase independent function that does not affect the phosphorylation status of AKT [22]. In this latter case, p110β might function as a scaffold protein required for the organisation of clathrin-coated pits or vesicles [21].

The mechanisms by which a specific PI3K isoform is preferentially recruited remains elusive. However, the expression of α and β subunits are somewhat mutually exclusive and are involved in different disease development and outcome. Our cell line model study provided the tools for future analysis of the functions of p110β, as we were able to confirm the different expression patterns observed in the invasive breast carcinomas.

The present paper is the first expression study regarding breast cancer and p110β. The β subunit was associated with a more aggressive profile of breast tumours, highly related to HER2-overexpression, higher histological grade, lymph node involvement and presence of distant metastasis. This pattern of aggressiveness was also reflected by its association, in univariate analysis, with a worse overall survival. Although this association did not hold in multivariate analysis, it can have an impact on future clinical trial designs, not only for p110β inhibitors by themselves but also in combinational HER2-related therapy schemes. As for the α subunit, the lack of association with a more aggressive phenotype should not be considered as a drawback, as its inhibitors might be applied in the hormone therapy setting as recently reported [37].

Taken together the results presented may, help to select the proper targets and populations that will benefit from the plethora of inhibitors currently in clinical trials and/or help to redirect those under development.

Acknowledgements Silvia Carvalho and José Luís Costa are the recipients of a fellowship from Fundação para a Ciência e Tecnologia (FCT), Portugal references SFRH/BD/21551/2005 and SFRH/BPD/20370/2004, respectively.

Conflict of interest The authors declare that they have no conflict of interest.

References

1. Engelman JA, Luo J, Cantley LC (2006) The evolution of phosphatidylinositol 3-kinases as regulators of growth and metabolism. Nat Rev Genet 7:606–619
2. Cantley LC (2002) The phosphoinositide 3-kinase pathway. Science 296:1655–1657
3. Wymann MP, Zvelebil M, Laffargue M (2003) Phosphoinositide 3-kinase signalling–which way to target. Trends Pharmacol Sci 24:366–376
4. Bader AG, Kang S, Zhao L et al (2005) Oncogenic PI3K deregulates transcription and translation. Nat Rev Cancer 5:921–929
5. Yuan TL, Cantley LC (2008) PI3K pathway alterations in cancer: variations on a theme. Oncogene 27:5497–5510
6. Engelman JA (2009) Targeting PI3K signalling in cancer: opportunities, challenges and limitations. Nat Rev Cancer 9:550–562
7. Di Cosimo S, Baselga J (2008) Targeted therapies in breast cancer: where are we now. Eur J Cancer 44:2781–2790
8. Klein S, Levitzki A (2009) Targeting the EGFR and the PKB pathway in cancer. Curr Opin Cell Biol 21:185–193
9. Shayesteh L, Lu Y, Kuo WL et al (1999) PIK3CA is implicated as an oncogene in ovarian cancer. Nat Genet 21:99–102
10. Racz A, Brass N, Heckel D et al (1999) Expression analysis of genes at 3q26-q27 involved in frequent amplification in squamous cell lung carcinoma. Eur J Cancer 35:641–646
11. Crowder RJ, Phommaly C, Tao Y et al (2009) PIK3CA and PIK3CB inhibition produce synthetic lethality when combined with estrogen deprivation in estrogen receptor-positive breast cancer. Cancer Res 69:3955–3962
12. Samuels Y, Ericson K (2006) Oncogenic PI3K and its role in cancer. Curr Opin Oncol 18:77–82
13. Cully M, You H, Levine AJ et al (2006) Beyond PTEN mutations: the PI3K pathway as an integrator of multiple inputs during tumorigenesis. Nat Rev Cancer 6:184–192
14. Vivanco I, Sawyers CL (2002) The phosphatidylinositol 3-Kinase AKT pathway in human cancer. Nat Rev Cancer 2:489–501
15. Wymann MP, Marone R (2005) Phosphoinositide 3-kinase in disease: timing, location, and scaffolding. Curr Opin Cell Biol 17:141–149
16. Garcia-Echeverria C, Sellers WR (2008) Drug discovery approaches targeting the PI3K/Akt pathway in cancer. Oncogene 27:5511–5526
17. Karakas B, Bachman KE, Park BH (2006) Mutation of the PIK3CA oncogene in human cancers. Br J Cancer 94:455–459

18. Lerma E, Catasus L, Gallardo A et al (2008) Exon 20 PIK3CA mutations decreases survival in aggressive (HER-2 positive) breast carcinomas. Virchows Arch 453:133–139
19. Saal LH, Holm K, Maurer M et al (2005) PIK3CA mutations correlate with hormone receptors, node metastasis, and ERBB2, and are mutually exclusive with PTEN loss in human breast carcinoma. Cancer Res 65:2554–2559
20. Zhao JJ, Liu Z, Wang L et al (2005) The oncogenic properties of mutant p110alpha and p110beta phosphatidylinositol 3-kinases in human mammary epithelial cells. Proc Natl Acad Sci U S A 102:18443–18448
21. Ciraolo E, Iezzi M, Marone R et al (2008) Phosphoinositide 3-kinase p110beta activity: key role in metabolism and mammary gland cancer but not development. Sci Signal 1:ra3
22. Jia S, Liu Z, Zhang S et al (2008) Essential roles of PI(3)K-p110beta in cell growth, metabolism and tumorigenesis. Nature 454:776–779
23. Marone R, Cmiljanovic V, Giese B et al (2008) Targeting phosphoinositide 3-kinase: moving towards therapy. Biochim Biophys Acta 1784:159–185
24. Matos I, Dufloth R, Alvarenga M et al (2005) p63, cytokeratin 5, and P-cadherin: three molecular markers to distinguish basal phenotype in breast carcinomas. Virchows Arch 447:688–694
25. Paredes J, Lopes N, Milanezi F et al (2007) P-cadherin and cytokeratin 5: useful adjunct markers to distinguish basal-like ductal carcinomas in situ. Virchows Arch 450:73–80
26. Campbell IG, Russell SE, Choong DY et al (2004) Mutation of the PIK3CA gene in ovarian and breast cancer. Cancer Res 64:7678–7681
27. Bachman KE, Argani P, Samuels Y et al (2004) The PIK3CA gene is mutated with high frequency in human breast cancers. Cancer Biol Ther 3:772–775
28. Zhao L, Vogt PK (2008) Class I PI3K in oncogenic cellular transformation. Oncogene 27:5486–5496
29. Kang S, Denley A, Vanhaesebroeck B et al (2006) Oncogenic transformation induced by the p110beta, -gamma, and -delta isoforms of class I phosphoinositide 3-kinase. Proc Natl Acad Sci U S A 103:1289–1294
30. Vogt PK, Bader AG, Kang S (2006) Phosphoinositide 3-kinase: from viral oncoprotein to drug target. Virology 344:131–138
31. Hynes NE, Lane HA (2005) ERBB receptors and cancer: the complexity of targeted inhibitors. Nat Rev Cancer 5:341–354
32. Kalinsky K, Jacks LM, Heguy A et al (2009) PIK3CA mutation associates with improved outcome in breast cancer. Clin Cancer Res 15:5049–5059
33. Hennessy BT, Smith DL, Ram PT et al (2005) Exploiting the PI3K/AKT pathway for cancer drug discovery. Nat Rev Drug Discov 4:988–1004
34. Wee S, Wiederschain D, Maira SM et al (2008) PTEN-deficient cancers depend on PIK3CB. Proc Natl Acad Sci U S A 105:13057–13062
35. Kirkegaard T, Witton CJ, McGlynn LM et al (2005) AKT activation predicts outcome in breast cancer patients treated with tamoxifen. J Pathol 207:139–146
36. Maruyama N, Miyoshi Y, Taguchi T et al (2007) Clinicopathologic analysis of breast cancers with PIK3CA mutations in Japanese women. Clin Cancer Res 13:408–414
37. Baselga J, Semiglazov V, van Dam P et al (2009) Phase II randomized study of neoadjuvant everolimus plus letrozole compared with placebo plus letrozole in patients with estrogen receptor-positive breast cancer. J Clin Oncol 27:2630–2637

Virchows Arch (2010) 456:245–250
DOI 10.1007/s00428-009-0879-7

ORIGINAL ARTICLE

Mucosal expression of claudins 2, 3 and 4 in proximal and distal part of duodenum in children with coeliac disease

Dorottya Nagy Szakál · Hajnalka Győrffy · András Arató · Áron Cseh · Kriszta Molnár · Mária Papp · Antal Dezsőfi · Gábor Veres

Received: 1 December 2009 / Revised: 18 December 2009 / Accepted: 23 December 2009 / Published online: 9 February 2010
© Springer-Verlag 2010

Abstract Duodenal biopsy is an important tool to diagnose coeliac disease (CD); however, the most reliable location of biopsy site is still questionable. Claudins (CLDNs), members of a large family of adherent junction proteins, show characteristic expression pattern in inflammatory disorders; nevertheless, CLDN expression in CD is unknown. This is a comparative study to examine the CLDN 2, 3 and 4 expressions in proximal and distal part of duodenum in children with CD and in controls. Thirty-three children with newly diagnosed CD were enrolled. Fourteen healthy children served as controls. Biopsies from proximal and distal part of duodenum were taken for routine histological analysis. Immunohistochemistry were used to detect CD3+ intraepithelial lymphocytes and CLDN 2, 3 and 4 protein expressions. Macroscopic picture, routine histology and Marsh grade depicted no differences between biopsies taken from proximal or distal part of duodenum. However, CLDN 2 expression was significantly increased in severe form of coeliac disease in bulb and in distal duodenum, and in distal part of non-severe coeliac patients, in comparison to controls. Similar association was found concerning CLDN 3 expression. Expression of CLDN 4 was similar in all groups studied. Both proximal and distal mucosal duodenal biopsies are suitable for diagnosing villous atrophy in patients with CD. Increased expressions of CLDN 2 and 3 suggest structural changes of tight junction in coeliac disease which may be, at least in part, responsible for increased permeability and proliferation observed in coeliac disease.

Keywords Claudin · Immunohistochemistry · Duodenum · Biopsy · Coeliac disease

Dorottya Nagy Szakál and Hajnalka Győrffy have equally contributed to this work.

D. Nagy Szakál · A. Arató · Á. Cseh · K. Molnár · A. Dezsőfi · G. Veres (✉)
1st Department of Pediatrics, Semmelweis University,
Bókay str. 53-54,
1083 Budapest, Hungary
e-mail: vergab@gyer1.sote.hu

H. Győrffy
2nd Department of Pathology, Semmelweis Medical University,
Budapest, Hungary

M. Papp
2nd Department of Medicine, University of Debrecen,
Debrecen, Hungary

Introduction

Coeliac disease (CD) or gluten-sensitive enteropathy is currently considered as a unique immune-mediated disorder leading to malabsorption. It is caused by the gluten fraction of cereals in susceptible people [1, 2]. The frequency of CD is constantly growing [3–5]. Through the screening examinations, the recognition of CD is higher, and the hit to find the disease in an early stage is better. High prevalence of CD was verified by Hungarian data as well (1:85) [6]. In the past, jejunal biopsies for diagnosis of CD were taken by means of suction capsule, but nowadays, biopsies are taken by upper endoscopy from the distal part of duodenum. Endoscopy is superior to suction biopsy due to the possibility of macroscopical visualisation, and several tissue samples can be collected at one time [7, 8]. However, it is still unclear, which would be the most reliable location of biopsy site: the duodenal bulb or the duodeno-jejunal junction [9–11].

Claudins (CLDNs) play a central role in the regulation of cell–cell adhesion, cell polarity and control of paracellular

Table 1 Characteristic of the patients with coeliac disease as compared to controls

Patients (*N*)	Control (14)	Coeliac disease (33)
Range, mean age (year)	1–19 (9.7)	2–17 (6.4)
Symptoms, diagnosis	Periumbilical abdominal pain (8/14), reflux symptoms (9/14)	Weight lost (12/33), chronic diarrhoea (18/33), abdominal pain (30/33)
Duodenal villous tract	Normal villous structure (14/14)	Partial villous atrophy (11/33)
		Total villous atrophy (22/33)
Coeliac serology (endomysial antibody or IgA tissue transglutaminase)	Negative (14/14)	Positive (33/33)

ion transport [12]. CLDNs are integral components of tight junction (TJ); 24 subgroups are known [13]. Recent studies have detected changes in claudin expression during cancer development and progression [14–17], but in degenerative diseases, it was not investigated yet. Earlier studies suggest that TJ has a possible role in CD pathomechanism [18–21], but no reference on published literature is known concerning claudins [22, 23]. We proposed that claudins may have a significant role in the intestinal permeability, cell to cell adhesion and the proliferation also in patients with CD.

The aim of this present study was duplex. First, we determined which part of the duodenum (the proximal or the distal region) is better for taking biopsies. Besides macroscopical view, detailed histological and CD3 immunohistochemical analysis were applied to detect subtle differences in the two duodenal regions. Moreover, the expressions of CLDNs were characterised in the proximal and distal part of duodenum in children with CD.

Materials and methods

Biopsy samples were composed of 33 newly diagnosed children with CD (20 girls and 13 boys) at the 1st Department of Pediatrics, Semmelweis University. Thirty-three children (range 2–17 years, mean age 6.4, 20 girls, 13 boys) were enrolled (Table 1). Coeliac disease was diagnosed after gastrointestinal symptoms (weight loss, failure to thrive, chronic diarrhoea, abdominal pain and fatigue), positive coeliac serology (endomysial antibody or IgA tissue transglutaminase) levels and abnormal small bowel biopsies (partial or total villous atrophy). Fourteen healthy children (11 girls, three boys) served as controls. Samples were taken from the proximal and distal part of duodenum. Biopsies were examined and analysed at the 2nd Department of Pathology, Semmelweis University.

Tissue blocks prepared from the mucosal biopsies were analysed on the basis of the morphological and the immunohistochemistrical analysis (monoclonal CD3). The villous/crypt ratio and the numbers of lymphocytes in the intraepithelial region were determined (original Marsh scoring) [24, 25]. According to the Marsh criteria, we divided our patients in two groups: Group I with less serious damages (Marsh grade up to 2) and Group II for the most serious change with villous atrophy and increased number of lymphocytes (Marsh grade 3).

Furthermore, the expression pattern of claudins in the duodenal mucosa was investigated by immunohistochemistry. The removed tissues were fixed in a 4% buffered formalin for 24 h, dehydrated and embedded in paraffin. The 3- to 4-μm thick sections were stained with haematoxylin–eosin. Paraffin sections were used for immunohistochemistry studies. The anti-CLDNs 2 and 4 antibodies were monoclonal; anti-CLDNs 3 antibodies were polyclonal purified from rabbit antiserum (Zymed, San Francisco, CA, USA). First, the slides were treated for 30 min in a target retrieval solution (Dako, Glostrup, Denmark) in a microwave oven, followed by incubation with the primary antibody at a 1:80 dilution at room temperature for 60 min and secondary antibody (biotinilated goat anti-rabbit) for 5 min in 41°C.

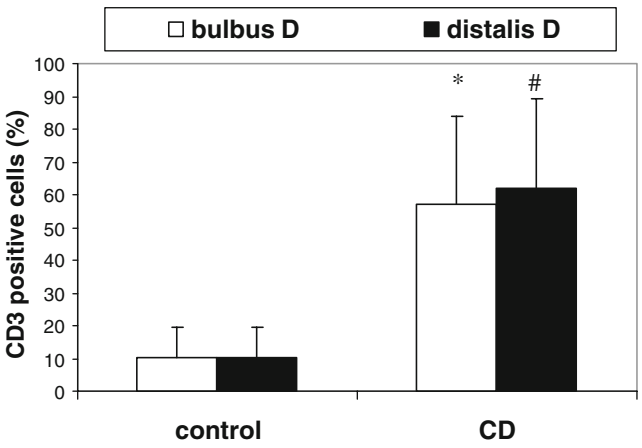

Fig. 1 The percentage of CD3 positive T cells in the intraepithelial region in biopsies of coeliac patients and controls (bulbus and distal duodenum). CD3 positive cells, taken from proximal and distal area, were significantly increased in CD patients when compared with controls (*p_1=0.026 and #p_2=0.006)

For visualisation, a standard avidin–biotin peroxidase technique (ABC system, Dako) was used with diaminobenzidine as chromogen. The sections were counterstained with haematoxylin. For each CLDN, a negative control with omission of the primary antibody was included. The reactions were carried out in a Ventana ES automatic immunostainer (Ventana Medical System Inc., Tucson, AZ, USA) using the reagents provided by the manufacturer.

The number of positive cells was calculated as follows: 10 randomly selected areas per slide were analysed using ×20 objective with 100 enterocytes counted in each field in the surface epithelium on the top of the villi. The scoring standardised for each group was as follows: 0=5%>; 1=5–20%; 2=20–40%; 3=40–60%; 4=60–80%; 5=80–100% of the cells showed positive reactions. For statistical analysis, Shapiro–Wilk test was applied to verify the normality, and the Mann–Whitney *U* test was used to compare the expression of individual CLDNs in the different groups. Results were considered to be statistically significant when $p<0.05$. The Institutional Ethical Committee approved our study; written parental informed consent was obtained.

Results

There was no significant difference between proximal and distal part of duodenum concerning macroscopical and microscopical view (Marsh scoring system) in patients with CD. Biopsies taken from proximal and distal area were shown as significant difference in the expression of CD3 positive cells compared to controls ($p_1=0.026$ and $p_2=0.006$, respectively). Increased CD3 expression was detected in biopsies from the distal region compared to the bulbus duodeni, but the difference was not significant

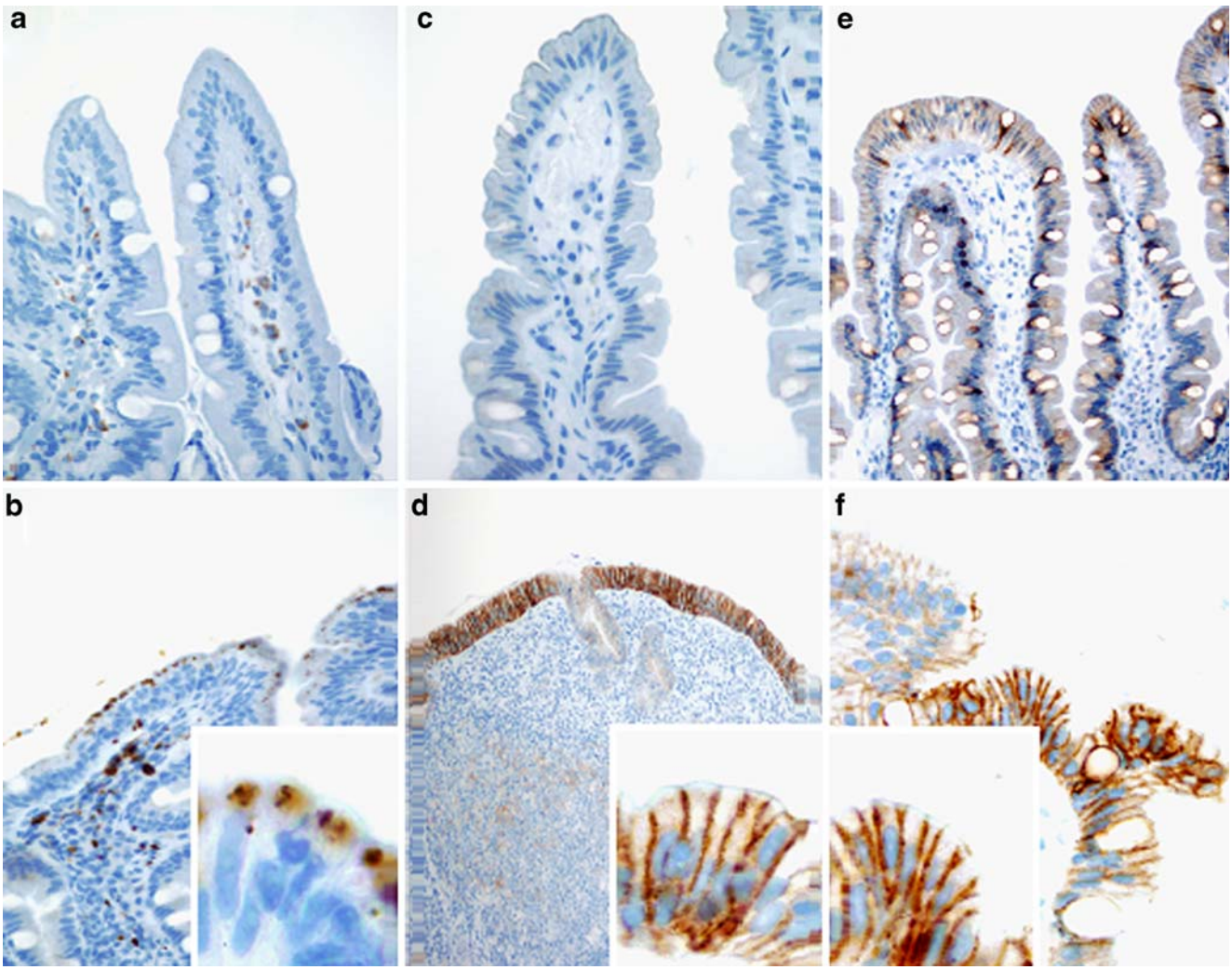

Fig. 2 Claudin expression in coeliac disease (**b**, **d**, **f**) and normal duodenal epithelium (**a**, **c**, **e**). Claudin 2 reacted in a grandular pattern, outlining the cell membrane and sometimes found inside the cytopasma. (**a** ×20, **b** ×20, **b** *insert* ×100 imm.) Claudin 3 was localised in the suprabasal layer of the epithelium showing a honeycomb appearance. (**c** ×20, **d** ×20, **d** *insert* ×100 imm.) Expression of Claudin 4 was similar. (**e** ×20, **f** ×40, **f** *insert* ×100 imm.)

(p=ns; Fig. 1). Similar tendency was observed in CLDN study; hence, elevated expression of CLDNs 2 and 3 in the distal duodenum of patients with CD was detected.

In our study, we have investigated the expression of CLDNs 2, 3 and 4 in intestinal epithelial mucosa. In CD, CLDN 2 reacted in a granular pattern, outlining the cell membrane and sometimes found inside the cytopasma. CLDNs 3 and 4 in CD were localised in the suprabasal layer of the epithelium showing a honeycomb appearance (Fig. 2).

Increased CLDNs 2 and 3 expressions in the proximal and distal part of duodenum in patients with CD compared to controls was observed Moreover, in CD patients, the expression of CLDNs was more increased in the distal region. We have found a significant difference concerning CLDN 2 in the case of mild villous atrophy (Group I) in the distal region (p=0.02) and in pronounced atrophy (Group II) in the bulb and the distal region as well (p=0.001) in CD patients when compared with controls. CLDN 2 expression was significantly increased in the proximal and distal part of CD patients with severe atrophy (Group II) in comparison to the mild atrophy (Group I; p=0.04 and p=0.03, respectively; Fig. 3). Similar changes were observed with CLDN 3, too. The expression of CLDN 3 was significantly increased in proximal and distal part of duodenum in overt atrophy (Group II) as compared to controls (p=0.01 and p=0.001, respectively). Moreover, CLDN 3 expression was significantly increased in the proximal and distal part in CD patients with pronounced atrophy (Group II) in comparison to the mild atrophy (Group I; p=0.008 and p=0.004; Fig. 4). Expression of CLDN 4 was similar in all groups studied.

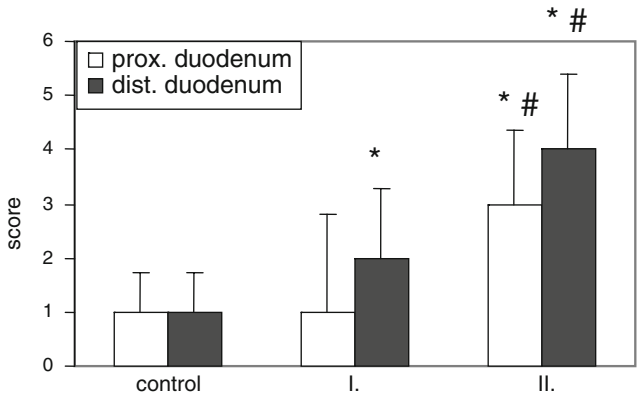

Fig. 3 CLDN 2 expression in the proximal (bulbus duodeni) and distal region of the duodenum in coeliac patients and controls (Group 1 mild, Group 2 severe villous atrophy)/*p<0.05 in CD with mild villous damage (Group 1) in the distal region and with serious damage (Group 2) in the bulb and distal region as compared to controls, #p<0.05 in CD with severe villous atrophy as compared to Group 1 in the proximal and distal part of duodenum

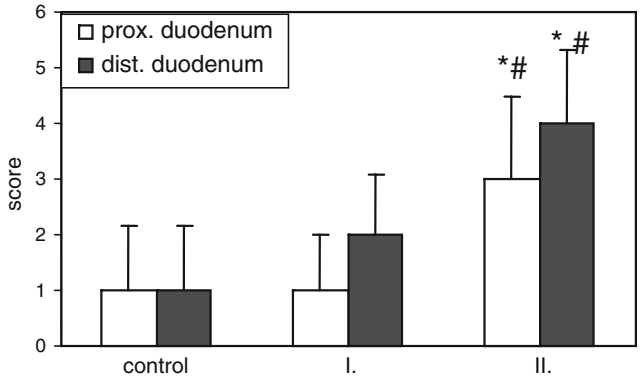

Fig. 4 CLDN 3 expression in the proximal (bulbus duodeni) and distal region of the duodenum in coeliac patients and controls. (Group 1: mild, Group 2: severe villous atrophy)/*p<0.05 in CD with serious damage (Group 2) in the bulb and distal region as compared to controls, #p<0.05 in CD with severe villous atrophy as compared to Group 1 in the proximal and distal part of duodenum

Discussion

Our results demonstrated that biopsies taken from proximal or distal part of duodenum are reliable for diagnosing CD. Nevertheless, histological scoring grade (Marsh) and the percentage of CD3 positive T cells showed slightly more severity in the distal part of duodenum. Moreover, CLDNs 2 and 3 expressions were also increased in the distal part of duodenum in comparison to the proximal part in patients with CD. These results may demonstrate that there is a slightly more serious damage in the mucosa of the distal duodenum in patients with CD. However, in everyday practice, both regions are suitable to diagnose villous atrophy in CD.

Earlier studies found a 95% concordance in the biopsies taken from the proximal duodenum and jejunum in adult population with CD [9]. Differences were found in three cases only in which there was a minor change in the proximal region (the possibility of latent CD) and more serious atrophy in the distal region. Ravelli et al. found that the total villous atrophy was significantly more frequently occurring in the distal area (distal duodenum, proximal jejunum), but when compared with the biopsies taken from one single patient, the differences were not significant [10]. As a result of their investigation, it is enough to take biopsy from one place for a trustworthy diagnosis, and this place must not necessarily be the farthest intestinal region.

As our results were compared with former investigations, we found the same results. For the correct diagnosis, it is not necessary to take the biopsy from the most distal part of the duodenum; nevertheless, the more severe damage was seen in the distal area. The difference was not significant; however, it can be important in the earlier stage of CD.

Claudins are the main components of TJ. CLDNs play an important role in the regulation of cell–cell adhesion and are responsible for maintaining cell polarity cellular arrangement, adhesion and paracellular ion transport of different tissues [26, 27]. As the damage of the cell–cell adhesion is an important role in the carcinogenesis, several recent studies have detected changes in CLDN expression during tumour diseases [28, 29]. All CLDNs were found in carcinomas, and their expression was tumour-specific [30–32]. Interestingly, in non-epithelial tumours (e.g. lymphoma), there was no expression of CLDN at all, or it was detected only in the cytoplasm. Győrffy et al. showed that the expression of CLDN 2 was increased in adenocarcinoma compared to Barrett oesophagus, while CLDN 3 and 4 were increased in both diseases compared to the foveolar epithelial cells [14].

Resnick et al. found that decreased presence of CLDN 3 was detected in normal gastric mucosa, where increased expression of CLDN 3 was associated with gastric adenocarcinomas [33]. In this paper, moderate membranous staining for CLDN 3 in intestinal metaplasia but not in normal gastric epithelium was shown similarly to our finding on duodenal mucosa. Japanese paper showed similar result, decreased CLDN 3 expression in normal gastric mucosa [34]. In a recent study, a significant increase of claudins 1 and 7 in premalignant cervical lesions and invasive cancer compared with normal cervical epithelia was shown. Moreover, CLDNs 3 and 4 were elevated in endometrial cancer in comparison to normal endometrium [35].

The possible role of CLDNs was also investigated in inflammatory bowel disease (IBD) [36, 37]. CLDN 2 expression was increased in IBD, while the expressions of CLDNs 3 and 4 were decreased in colonic epithelium [36]. This finding is contrast to our result (increased expression of CLDN 3 in CD patients); nevertheless, in human intestine, there is functional differences concerning macromolecular permeability in duodenal mucosa in comparison to colonic mucosa. Based on this knowledge, different expression of CLDN 3 in duodenal and colonic mucosa may be conceivable. It seems that proximal intestinal mucosa (gastric, duodenal) has different CLDN profile when compared with colonic mucosa. Further studies are necessary to analyse the simultaneous CLDNs expression in different part of human intestine of healthy individuals and of patients with coeliac disease or with IBD.

Increased permeability and altered cell to cell junctions in CD may correlate with the expression of TJ proteins such as CLDNs. However, the expression of CLDNs in coeliac disease was not investigated yet. Fasano et al. found that zonuline induced a pathological aggregation of tight junctions and increased the permeability of intestinal mucosa of untreated CD patients [23]. Further, studies showed that chronic gliadin exposure caused downregulation of both zonula occludens-1 (ZO-1) and occludin gene expression and activated zonulin signalling irrespective of the genetic expression of autoimmunity, leading to increased intestinal permeability [22]. Sander et al. described that the gliadin almost immediately changed the barrier function of the intestinal mucosa caused a reorganisation of actin filaments and altered expression of the TJ proteins (e.g. occludin, ZO-1, E-cadherin and claudins). Claudins 1, 3 and 4 each showed differences in their distribution and expression. After gliadin treatment of cells (human intestinal enterocytes), claudins 3 and 4 were decreased in plasma membrane staining and were increased in punctate cytosolic staining. Furthermore, the transepithelial resistance was decreased, and permeability was increased [19]. As a result of our study, there is a reference to the structural change in the TJ due to an increased CLDNs 2 and 3 expressions. In addition, our results demonstrated that the expressions of CLDNs 2 and 3 were increased in the mucosa in children with untreated CD when compared to controls. Furthermore, the expression of CLDNs and the grade of the atrophy were associated.

First and last, our study suggests that both proximal and distal part of duodenum are also reliable regions of taking biopsy sample to prove the villous atrophy in CD. However, using more sensitive methods, the distal part of duodenum depicted earlier signs of mucosal deterioration. Therefore, to diagnose slight changes of mucosal abnormality, the distal duodenum seems to be better location for intestinal biopsies. The increased expressions of CLDNs 2 and 3 suggest the structural damage of the TJs, which play a central role in the increased permeability and modified cell to cell adhesion and proliferation.

Acknowledgements This work was supported by grants NKFP-1A/0023/2002 from Hungarian Ministry of Health, National Research Development Projects; OTKA T 049559 from the National Science Research Foundation and ETT-077/2003 from the Hungarian Ministry of Health.

References

1. Dicke WK (1950) Coeliakie. MD Thesis, Utrecht
2. Marsh MN (1992) Gluten, major histocompatibility complex, and the small intestine. A molecular and immunbiologic approach to the spectrum of gluten sensitivity ('coeliac sprue'). Gastroenterology 102:330–354
3. van Heel DA, West J (2006) Recent advances in coeliac disease. Gut 55:1037–1046
4. Green PH, Cellier C (2007) Celiac disease. N Engl J Med 357:1731–1743
5. Armstrong MJ, Robins GG, Howdle PD (2009) Recent advances in coeliac disease. Curr Opin Gastroenterol 25:100–109
6. Korponay-Szabó IR, Kovács JB, Czinner A et al (1999) High prevalence of silent celiac disease in preschool children screened

with IgA/IgG antiendomysium antibodies. J Pediatr Gastroenterol Nutr 28:26–30
7. O'Loughlin EV, Dutt S, Kamath R et al (2007) Prospective peer-review audit of paediatric upper gastrointestinal endoscopy. J Paediatr Child Health 43:551–554
8. Tursi A, Brandimarte G, Giorgetti GM (2002) Endoscopic features of celiac disease in adults and their correlation with age, histological damage, and clinical form of the disease. Endoscopy 34:787–792
9. Thijs WJ, van Baarlen J, Kleibeuker JH et al (2004) Duodenal versus jejunal biopsies in suspected celiac disease. Endoscopy 36:993–996
10. Ravelli A, Bolognini S, Gambarotti M et al (2005) Variability of histologic lesions in relation to biopsy site in gluten-sensitive enteropathy. Am J Gastroenterol 100:177–185
11. Meijer JW, Wahab PJ, Mulder CJ (2003) Small intestinal biopsies in celiac disease: duodenal or jejunal? Virchows Arch 442:124–128
12. Kinugasa T, Sakaguchi T, Gu X et al (2000) Claudins regulate the intestinal barrier in response to immune mediators. Gastroenterology 118:1001–1011
13. González-Mariscal L, Betanzos A, Nava P et al (2003) Tight junction proteins. Prog Biophys Mol Biol 81:1–44
14. Győrffy H, Holczbauer A, Nagy P et al (2005) Claudin expression in Barrett's esophagus and adenocarcinoma. Virchows Arch 447:961–968
15. Aung PP, Mitani Y, Sanada Y et al (2006) Differential expression of claudin-2 in normal human tissues and gastrointestinal carcinomas. Virchows Arch 448:428–434
16. Kinugasa T, Huo Q, Higashi D et al (2007) Selective up-regulation of claudin-1 and claudin-2 in colorectal cancer. Anticancer Res 27:3729–3734
17. Soini Y, Tommola S, Helin H et al (2006) Claudins 1, 3, 4 and 5 in gastric carcinoma, loss of claudin expression associates with the diffuse subtype. Virchows Arch 448:52–58
18. Utech M, Brüwer M, Nusrat A (2006) Tight junctions and cell-cell interactions. Methods Mol Biol 341:185–195
19. Sander GR, Cummins AG, Henshall T et al (2005) Rapid disruption of intestinal barrier function by gliadin involves altered expression of apical junctional proteins. FEBS Lett 579:4851–4855
20. Visser J, Rozing J, Sapone A et al (2009) Tight junctions, intestinal permeability, and autoimmunity: celiac disease and type 1 diabetes paradigms. Ann N Y Acad Sci 1165:195–205
21. Guandalini S, Setty M (2008) Celiac disease. Curr Opin Gastroenterol 24:707–712
22. Drago S et al (2006) Gliadin, zonulin and gut permeability: effects on celiac and non-celiac intestinal mucosa and intestinal cell lines. Scand J Gastroenterol 41:408–419
23. Fasano A et al (2000) Zonulin, a newly discovered modulator of intestinal permeability, and its expression in coeliac disease. Lancet 355:1518–1519
24. Green A, Rostami B, Marsh C (2005) Diagnosis of coeliac disease. Gastroenterology 19:389–400
25. Oberhuber G, Granditsch G, Vogelsang H (1999) The histopathology of coeliac disease: time for a standardized report scheme for pathologists. Eur J Gastroenerol Hepatol 11:1185–1194
26. Furuse M (2006) Molecular mechanism behind the barrier function of tight junctions. Seikagaku 78:601–608
27. Tsukita S, Furuse M (2000) The structure and function of claudins, cell adhesion molecules at tight junctions. Ann N Y Acad Sci 915:129–135
28. Morin PJ (2005) Claudin proteins in human cancer: promising new targets for diagnosis and therapy. Cancer Res 65:9603–9606
29. Swisshelm K, Macek R, Kubbies M (2005) Role of claudins in tumorigenesis. Adv Drug Deliv Rev 57:919–928
30. Soini Y (2005) Expression of claudins 1, 2, 3, 4, 5 and 7 in various types of tumours. Histopathology 46:551–560
31. Kulka J, Tökés AM (2005) Claudin expression in breast tumors. Human Pathol 36:859
32. Tokés AM, Kulka J, Paku S et al (2005) Claudin-1, -3 and -4 proteins and mRNA expression in benign and malignant breast lesions: a research study. Breast Cancer Res 7:R296–R305
33. Resnick MB et al (2005) Claudin expression in gastric adenocarcinomas: a tissue microarray study with prognostic correlation. Human Pathol 36:886–892
34. Matsuda Y et al (2007) Gastric and intestinal claudin expression at the invasive front of gastric carcinoma. Cancer Sci 98:1014–1019
35. Szabó I et al (2009) Claudins as diagnostic and prognostic markers in gynecological cancer. Histol Histopathol 24:1607–1615
36. Prasad S, Mingrino R, Kaukinen K (2005) Inflammatory processes have differential effects on claudins 2, 3 and 4 in colonic epithelial cells. Lab Invest 85:1139–1162
37. Mankertz J, Schulzke JD (2007) Altered permeability in inflammatory bowel disease: pathophysiology and clinical implications. Curr Opin Gastroenterol 23:379–383

Virchows Arch (2010) 456:251–260
DOI 10.1007/s00428-009-0878-8

ORIGINAL ARTICLE

Microvessel density and the association with single nucleotide polymorphisms of the vascular endothelial growth factor receptor 2 in patients with colorectal cancer

Torben Frøstrup Hansen · Flemming Brandt Sørensen · Karen-Lise Garm Spindler · Dorte Aalund Olsen · Rikke Fredslund Andersen · Jan Lindebjerg · Ivan Brandslund · Anders Jakobsen

Received: 17 July 2009 / Revised: 4 November 2009 / Accepted: 22 December 2009 / Published online: 9 February 2010
© Springer-Verlag 2010

Abstract The measurement of microvessel density (MVD) is a widely accepted method for assessing the neoangiogenetic activity in neoplasia. The aim of the present study was to compare MVD with single nucleotide polymorphisms (SNPs) in the vascular endothelial growth factor receptor (*VEGFR*)*-1* and *VEGFR-2* genes and, furthermore, with quantitative measurements of the receptors in colorectal cancer (CRC) tissue. Prognosis was also assessed. Blood and tissue were collected from 110 patients surgically resected for CRC. SNPs were analysed from genomic DNA by polymerase chain reaction. MVD was assessed by immunohistochemistry using CD34 and CD105 combined with caldesmon in order to identify also immature vessels. Microvessels were counted in three fields of vision, and the mean MVD was used for statistical analysis. The VEGFR-2 1192 C/T and −604 T/C SNPs were associated with the MVD assessed by CD105. The median MVD score for the 1192 CC genotype was significantly lower compared to the CT + TT genotypes (p=0.002). The median MVD score for the −604 CC genotype was significantly higher compared to the TT + TC genotypes (p=0.009). A possible association, although non-significant, was demonstrated for the CD34-positive microvessels. The 1192 CC genotype and the −604 TT + TC genotypes correlated with improved survival. This is the first report on correlations between SNPs in the VEGF receptor genes and MVD in patients with CRC. Associations were shown between two SNPs in the VEGFR-2 gene and the CD105-positive microvessels indicating an impact on neoangiogenesis. Moreover, an association between the SNPs and survival was demonstrated. The clinical implications of these findings need further investigations.

Keywords Colorectal neoplasm · Vascular endothelial growth factor receptors · Single nucleotide polymorphisms · Microvessel density

Support: The Cancer Foundation

T. F. Hansen (✉) · K.-L. G. Spindler · A. Jakobsen
Department of Oncology, Danish Colorectal Cancer Group South, Vejle Hospital,
Kabbeltoft 25,
7100 Vejle, Denmark
e-mail: torben.hansen@slb.regionsyddanmark.dk

F. B. Sørensen · J. Lindebjerg
Department of Clinical Pathology, Danish Colorectal Cancer Group South, Vejle Hospital,
Kabbeltoft 25,
7100 Vejle, Denmark

D. A. Olsen · R. F. Andersen · I. Brandslund
Department of Biochemistry, Danish Colorectal Cancer Group South, Vejle Hospital,
Kabbeltoft 25,
7100 Vejle, Denmark

Introduction

Malignant tumours are dependent on proliferating capillaries in order to supply oxygen and nutrients for their continuous growth. This knowledge has been used to develop molecular targeted agents against the vascular endothelial growth factor (VEGF) system, which is one of the most important growth factor systems involved in the angiogenetic process.

One way of estimating the angiogenetic activity is to measure the microvessel density (MVD) in the tumour tissue. The MVD method [1], counting of microvessels in hot spots, has been the preferred method. Alternative

techniques such as the Chalkley method, the vascular grading system and interactive stereologic counting procedures using computer techniques have also been applied [2]. Visualization of endothelial cells is essential in order to count microvessels, and previously, antibodies targeting the cell markers CD31, CD34, and factor VIII were the most commonly used for this purpose. Recently, antibodies against CD105 have been introduced, and evidence suggests that this is a more specific tumour endothelial cell marker [3–6]. CD105 is a co-receptor for transforming growth factor β1 and β3 [7] and associated with proliferation of tumour endothelial cells [6]. CD105 is predominantly expressed on endothelial cells [6, 8], but a recent report suggests that it may not be specific for blood vascular endothelium only [9].

The MVD estimate seems to be higher at the invasive front compared to the central parts of epithelial tumours [6, 10]. Evidence also suggests that MVD assessed at the invasive front may have clinical relevance [6, 10, 11]. Furthermore, a differentiation between mature and immature microvessels may provide additional information [12].

The literature seems to support the use of MVD as a prognostic marker in patients with colorectal cancer (CRC) [13–15], but the prognostic value might depend on the choice of endothelial cell marker [16]. Furthermore, several studies have found a positive association between MVD and VEGF-A [10, 11, 17–19], but less is known about a possible association between MVD and the receptors in the VEGF system. These previous studies have been based on quantitative or semi-quantitative immunohistochemical (IHC) analyses, and the question on a similar association between MVD and quantitative measures of the VEGF system remains to be answered.

Genetic variations in genomic DNA, which are easily accessible through blood samples, are thought to be rather stable molecular markers compared to similar, less stable, variations in the tumour DNA. Variations in genomic DNA therefore constitute attractive candidates in relation to clinical cancer research. Also, such genetic variations in the VEGF system might change the expression of the relevant genes, but they have not previously been addressed in relation to MVD. If such associations were to be demonstrated, single nucleotide polymorphism (SNP) analysis could represent a future alternative to protein analysis and should be considered among other prognostic markers. A recent study demonstrated an association between SNPs in the VEGF-A gene and prognosis [20], but the possible associations between SNPs in the VEGF receptors and prognosis remain to be elucidated.

The aims of the present descriptive study were primarily to compare MVD with SNPs in the genes of VEGFR-1 and VEGFR-2 and to correlate MVD with quantitative measures of VEGFR-1 and VEGFR-2 in CRC tissue. Finally, we assessed the prognostic value of the MVD and the SNPs.

Materials and methods

Patients

This retrospective study consecutively included 110 patients with CRC entering the study in the period from February 2004 to July 2005, all undergoing surgical resection for histologically verified adenocarcinomas of the colon or rectum at the Department of Surgery, Vejle Hospital, Denmark. Patients who had received preoperative chemoradiation of rectal cancer were excluded. Pretreatment examinations included a chest X-ray and ultrasound or CT scan of the abdomen. Postoperatively, the tumours were histologically classified and staged according to the tumor–lymph nodes–metastases (TNM) system. The study was approved by the Regional Scientific Ethical Committee for southern Denmark according to Danish law, J.nr. S-VF-20040047, and informed consent was obtained from all patients enrolled in the study.

Tissue sampling

Immediately after surgery, the removed bowel segment was brought to the Department of Clinical Pathology and a pathologist collected samples from the tumour. Samples for protein analysis were fresh frozen and stored at −80°. All samples were stored less than 30 min after the surgical removal. Based on pathological examination, it was semi-quantitatively estimated from frozen sections that the tumour tissue used for protein analyses consisted of at least 80% tumour cells.

Analysis of single nucleotide polymorphism

Genomic DNA was isolated from whole blood by the NucleoSpin® Tissue method according to the user manual (Machery-Nagel, Germany, May 2005/Rev.04; www.bioke.com/blobs/Macherey-Nagel/GenomicDNABlood_R04.pdf). The PCR analysis was performed using the ABI PRISM 7900 HT fast real-time PCR system (Applied Biosystem, USA). Commercial assays from the same company were used for the analysis of the VEGFR-2 SNPs. Assay number and the approximate length of the amplification products (estimated by gel electrophoresis) are shown in Table 1. Primer and probes for the VEGFR-1 SNP analysis were designed according to the study by Schneider et al. [21]. Tests were optimized and a probe concentration of 250 nM and a primer concentration of 600 nM were chosen.

Table 1 Distribution of genotypes in the four SNPs analysed and the Hardy–Weinberg equilibrium test results

Parameter	Number $n=109$ (%)[e]	Hardy–Weinberg equilibrium (p)
The VEGFR-1 519 C/T SNP[a]		0.85
CC	96 (88)	
CT	13 (12)	
TT	0 (0)	
The VEGFR-2 1192 C/T SNP[b]		0.95
CC	90 (82)	
CT	18 (17)	
TT	1 (1)	
The VEGFR-2 −604 T/C SNP[c]		0.89
TT	24 (22)	
TC	51 (47)	
CC	34 (31)	
The VEGFR-2 1719 SNP[d]		0.95
TT	66 (61)	
TA	37 (34)	
AA	6 (6)	

Assay numbers of the VEGFR-2 SNPs and primer and probe sequences of the VEGFR-1 SNP are shown below. The approximate lengths of the amplification products are also shown. The sum of the percentages regarding the VEGFR-2 1719 SNP exceeds 100% due to rounding off of data

[a] The VEGFR-1 519 C/T SNP: forward primer 5′-GCA TCA ATG CGG CCG AAA A-3′, reverse primer 5′-TTT GGG AAG ACT GCG AAC CA-3′; FAM/MGP probe 6-FAM-ACG GAC ATG CTC C-NFQ-3′ and VIC/MGP probe VIC-CAC GGA CAC GCT CC-NGQ-3′; 70 bp

[b] The VEGFR-2 1192 C/T SNP; rs2305948; C__22271999_20; 70 bp

[c] The VEGFR-2 −604 T/C SNP; rs2071559; C__15869271_10; 80 bp

[d] The VEGFR-2 1719 T/A SNP; rs1870377; C__11895315_20; 120 bp

[e] Blood samples were only available for 109 patients for the SNP analysis

Extraction of proteins

Tissue samples, 10–50 mg, were homogenised by the Ultra-Turrax system (Ika, Germany), at 4°C, with 10 vol.% (*w*/*v*) buffer (20 mM Tris-HCl, 150 mM NaCl, pH 7.4, 1 mM EDTA, 10% glycerol, protease inhibitor cocktail; cat. no. P8340, Sigma-Aldrich, USA). Triton X-100 was added after homogenisation to a final sample concentration of 1% (*v*/*v*) in order to stabilize membrane bound proteins, but only under the protein extraction process, and hence did not affect the binding capacities of neither standards nor controls during the following ELISA analysis. Lysates were mixed and incubated for 30 min at 4°C followed by centrifugation at 16,000×*g* for 10 min. After supernatant recovery, protein concentration was determined using the Bicinchoninic Acid Protein Assay (Thermo Scientific, Pierce Protein Research Products, Rockford, IL, USA).

VEGFR protein analysis

The enzyme-linked immunosorbent assays, Quantikine (R&D Systems, USA; Catalog Number DVR100B and DVR200), were used to quantify VEGFR-1 and VEGFR-2 in CRC tissue. Controls were supplied from R&D Systems as well. The assay employs the quantitative sandwich enzyme immunoassay technique. Analysis was performed on a 96-well microtiter plate, pre-coated with a mouse monoclonal antibody specific for the two receptors. Samples were diluted by a factor 5 for VEGFR-1 and by a factor 10 for VEGFR-2 in sample diluents provided with the kit.

To each well was added 100 μl of Assay Diluents (RD1W, a buffered protein base) and 100 μl of protein extract, standard or control, followed by incubation for 2 h at room temperature. After four washes with wash buffer (the washing was performed on the Wellwash 4 MK2 from Thermo Electron Corporation; Thermo Fisher Scientific Inc., Waltham, MA, USA), 200 μl of VEGFR conjugate (polyclonal antibody against the two receptors conjugated to horseradish peroxidase) was added to each well and then again incubated for 2 h at room temperature. Wells were washed again and 200 μl of substrate solution (consisting of hydrogen peroxide and chromogen) was added. Then 30 min later, 50 μl of stop solution (sulphuric acid) was added, and colour change appeared. The optical density was determined using a Novo Biolabs kinetic microplate reader set to 450 nm (Molecular Devices, Sunnyvale, CA, USA). Data were analysed using Multicalc 2000 software. Wavelength correction for optical imperfections in the plates was executed automatically.

Results are presented in picograms per milligram of total protein. Tissue samples, standards and controls were assayed in duplicate and the mean was recorded. The total coefficients of variation on three levels were VEGFR1 low 12.4%, medium 12.8% and high 11.3% and VEGFR2 low 11.3%, medium 10.1% and high 8.3%.

CD34 immunostaining

The CRC specimens were fixed for 24 h in 4% buffered neutral formalin. Subsequent fixation standardized sampling was carried out followed by paraffin-embedding according to routine procedures.

Sections of 4-μm were cut and mounted on coated slides, dried for 30 min at 60°, then overnight at 37°. The tissue was deparaffinised in Estisol for 10 min at room temperature and rehydrated in graded alcohol solutions (99–70%). Hydrogen peroxide 3% was added for 5 min to

block endogenous peroxidase. Washing with water was performed before and after this blocking procedure. Heat-induced epitope retrieval was performed in order to demascade antigenes. Sections to be stained with the anti-CD34 antibody (mouse, monoclonal, Dako, code M7165, Clone QBend-10, class II) were boiled in a TEG buffer (TRIS 10 mM, EGTA 0.5 mM, Titriplex®—VI) at pH 9 for 15 min. After cooling for 15 min at room temperature, Tris-buffered saline (TBS)/Tween was added for 5 min. The anti-CD34 antibody diluted 1:100 in 1% bovine serum albumin/TBS buffer was added, and tissue sections were incubated for 30 min. After washing in TBS/Tween, final visualisation was performed using EnVision + DAB (Dako, Denmark). A solution of 0.5% copper sulphate in TBS was added for 10 min to intensify the staining pattern. The cell nuclei were stained by the addition of a Mayer haematoxylin solution. Parts of the staining procedure were performed on the Tissue-Tek Prisma, Sakura.

CD105 and caldesmon immunostaining

We also measured MVD using tissue sections stained by antibodies against CD105 and caldesmon aiming at differentiation between immature and more mature microvessels. We used a kit from Dako (code K5361, EnVision™ G│2 Doublestain System, Rabbit/Mouse, DAB+/Permanent Red) following the manufacturer's instructions with the following exceptions: antibodies, polymer/HRP and polymer/AP incubated for 30 min; incubation in DAB + working solution and permanent red for 10 min and counterstaining with hematoxylin for 1 min; no copper sulphate added. The manual procedures were used. The anti-CD105 antibody was provided from Novo Castra (endoglin NCL-CD105, Clone 4G11) and used in a 1:25 dilution. The anti-caldesmon antibody was provided from Dako (code M3557, Clone h-CD) and used in a 1:50 dilution. Heat-induced epitope retrieval in TEG buffer was performed in order to break the formalin bindings.

Microvessel counting

Initially, we compared the MVD method as described by Weidner et al. [1] and the Chalkley method as described by Fox et al. [22]. Microvessels were counted by two investigators in an independent sample of 21 tissue sections from CRC, which were not included in the study. Linear correlation analysis showed acceptable correlation between the results, MVD (r=0.80, $p<10^{-4}$) and Chalkley (r=0.60, $p<10^{-4}$). A correlation on the same level was demonstrated when the interobserver variability was analysed using difference plots. The MVD method was chosen for the later analysis because of a marginally better correlation between the two investigators. It was easier and faster to use and most of the published studies in this field also use the MVD method.

Microvessels were counted at the invasive tumour front without knowledge of patient outcome. Tumour sections were scanned for hot spots at ×40 and ×100, and counting was performed at ×200. Microvessels were counted in three hot spots, and the mean MVD was used for the later analysis. Any stained endothelial cell or endothelial cell clusters clearly separated from adjacent microvessels by tumour cells and/or stroma elements were considered a single countable microvessel. Vessel lumen was not necessary for a structure to be counted as a microvessel. Hot spots near tumour necrosis or ulcerations were not chosen, as microvessels in such areas may be associated with an inflammatory response rather than with the tumour. Also, hot spots near the section edges were avoided because of a more intense and non-specific staining in these areas. Consensus resolved any discrepancy between the observers. Regarding the CD105 (brown) and caldesmon (red) staining, only microvessels without associated red staining were counted in order to estimate the MVD of the immature vessels.

Statistical analysis

Median values were compared using the Wilcoxon's signed rank test. Chi-square statistics were used to test for Hardy–Weinberg equilibrium. Linear regression analysis was used to describe the relationship between MVD by CD34 and CD105. Prognostic associations were tested according to the Kaplan–Meier method, and the log-rank test was used to test for differences between the survival curves. Six patients with missing data were excluded from the progression-free survival (PFS) analysis. One patient had no blood sample available and hence no SNP status was analyzed, and five patients were missing survival data. All statistical calculations were carried out using the NCSS statistical software (NCSS Statistical Software, version 2007, Kaysville, UT 84037, USA). p values <0.05 were considered significant, and all tests were two-sided.

Results

Patient characteristics

Clinicopathological characteristics of the 110 included patients are listed in Table 2. The median age was 72 years (range 41–91 years). The median follow-up was 42 months (range 0.1–56.2 months), and during that period, 45 patients had either progressed or died. Five were out of reach for follow-up. PFS was defined as the time from operation until progression or death.

Table 2 Clinicopathological characteristics

	Number n=110 (%)
Gender	
Male	54 (49)
Female	56 (51)
Tumour localisation	
Colon	72 (65)
Rectum	38 (35)
pT category	
1	0 (0)
2	13 (12)
3	76 (69)
4	21 (19)
pN category	
0	60 (55)
1	20 (18)
2	30 (27)
M category	
0	89 (81)
1	21 (19)
Stage	
I	12 (11)
II	46 (42)
III	31 (28)
IV	21 (19)

Blood samples were available for 109 patients. Table 1 shows the distribution of genotypes for all four SNPs. They all followed the Hardy–Weinberg equilibrium.

No significant associations between the clinicopathological characteristics (age, gender, TNM category, stage and tumour localization) and MVD or SNPs were detected.

CD34/CD105 expression and MVD

Figure 1a, b shows sections of CRC with representative staining of CD34 and CD105 positive microvessels. In general, the anti-CD34 antibody gave a more intense staining pattern than the anti-CD105 antibody, but they were both easy to quantify. More microvessels were positive for CD34 compared to CD105: median CD34 MVD 11.67 (95% confidence interval (CI) 11.00–12.33) and median CD105 MVD 6.00 (95% CI 5.33–6.00; $p<10^{-6}$). A significant correlation was detected between the two estimates (r=0.62 and $p<10^{-4}$; Fig. 2).

MVD and SNP status

Figure 3 shows the significant association between the VEGFR-2 1192 C/T (p=0.002) and −604 T/C (p=0.009) SNPs and MVD as estimated by CD105 (n=109). A possible association, although non-significant, was found for the CD34 MVD (p=0.051 and p=0.052, respectively). MVD showed no association with the VEGFR-1 519 C/T and the VEGFR-2 1719 SNPs (data not shown).

MVD and VEGFR protein level

CRC samples from 104 patients were available for protein analysis. Table 3 shows the associations between MVD and VEGFR-1 and VEGFR-2 protein concentrations. No significant differences were found.

SNP status and VEGFR protein level

The VEGFR-2 1192 C/T SNP was significantly associated with VEGFR-2 protein concentrations in normal colorectal

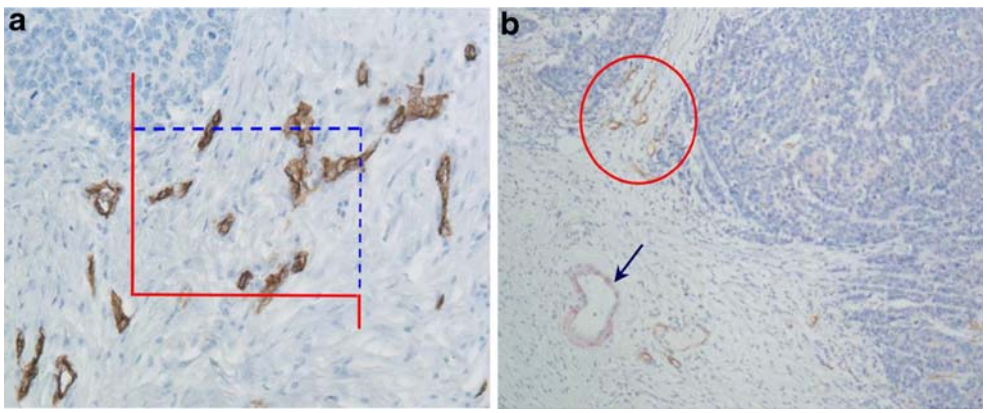

Fig. 1 **a**, **b** Immunohistochemical expression of CD34 and CD105 plus caldesmon in tumour vasculature. The two colorectal cancer sections are from different patients. **a** CD34-positive microvessels in a hot spot at the invasive tumour front. The unbiased counting frame is also illustrated. Endothelial cell-derived structures inside the frame or in contact with the *non-solid line* were counted. Structures in contact with the *solid line* were not counted. In this case, eight microvessels were counted. **b** CD105-positive microvessels in another hot spot (*circle*) at the invasive tumour front. Note the caldesmon-positive vessel indicated with the *arrow* (original magnification ×200)

tissue. The median protein concentration for the CC genotype was 68 pg/mg (95% CI 59–83 pg/mg) compared to 99 pg/mg (95% CI 79–133 pg/mg) for the CT + TT genotypes (p=0.01; n=104). No significant associations was demonstrated in CRC tissue (p=0.67). The three remaining SNPs were not associated with the protein concentrations of the relevant receptors in either normal colorectal or in CRC tissue (data not shown).

Prognosis

The prognostic importance of MVD, all SNPs and VEGFR-1 and VEGFR-2 protein concentrations were assessed (n=104). Patients were classified into two groups using median MVD as a cutoff point. In the Kaplan–Meier survival analysis, no significant effect on PFS was demonstrated using either CD34 or CD105 as illustrated in Fig. 4, which shows the survival curves in relation to the CD105 MVD (p=0.73). Similar curves were seen for the CD34 MVD (p=0.73; data not shown).

The VEGFR-2 −604 T/C SNP showed a significant correlation with PFS (p=0.03), and a marginal significant correlation was demonstrated for the VEGFR-2 1192 C/T SNP (p=0.05; Fig. 5). No significant correlations were demonstrated for the remaining two SNPs. No associations between PFS and VEGFR-1 and VEGFR-2 protein levels were demonstrated (data not shown).

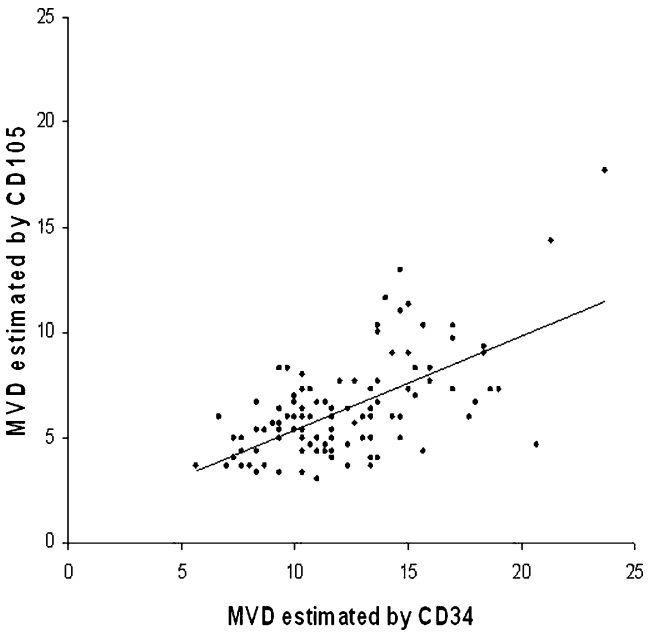

Fig. 2 Linear regression plot illustrating the correlation between MVD estimated by CD34 and CD105. The correlation was significant, r=0.62 and $p<10^{-4}$ (n=110)

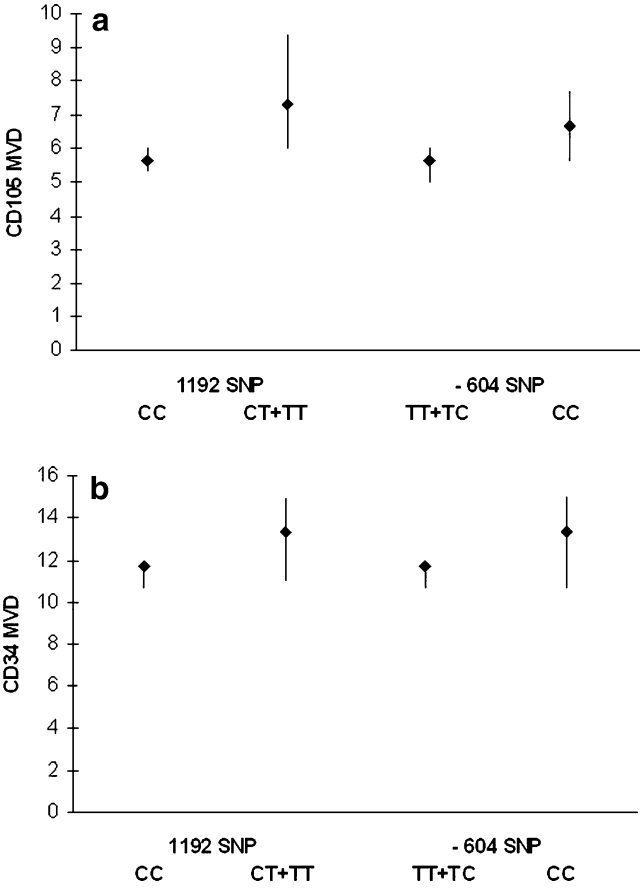

Fig. 3 **a** Median CD105 MVD scores and corresponding confidence intervals according to the genotypes for the 1192 C/T and −604 T/C VEGFR-2 SNPs. *Vertical* CD105 MVD. *Horizontal* genotypes. The differences between the median MVD score according to the genotype groups were significant, p=0.002 for the 1192 SNP and p=0.009 for the −604 SNP (n=109). **b** Median CD34 MVD scores and corresponding confidence intervals according to the genotypes for the 1192 C/T and −604 T/C VEGFR-2 SNPs. *Vertical* CD34 MVD. *Horizontal* genotypes. The differences between the median MVD score according to the genotype groups were marginally significant, p=0.051 for the 1192 SNP and p=0.052 for the −604 SNP (n=109)

Discussion

Several studies on the association between MVD and VEGF-A have been published recently [11, 17, 19, 23]. No publications on the possible correlations between the VEGF receptors and MVD exist, and there is only sparse literature on the VEGF receptors in general. These receptors may be of crucial importance to the biological function of the system. This motivated us to investigate this further in the present pilot study.

CD34 and CD105 staining was consistently present in all the cases. Microvessels were seen at a higher concentration in or around the tumour, which is in agreement with previous studies [5, 6]. Median MVD by CD105 was significantly lower than median MVD by CD34. Furthermore, CD105 seems to be preferentially expressed on small

Table 3 Association between MVD and VEGFR-1 and VEGFR-2 protein concentrations (picograms per milligram of total protein; $n=104$)

MVD	VEGFR-1		VEGFR-2	
	Median (95% CI)	*p* value	Median (95% CI)	*p* value
All patients	2534 (2131–2789)		127 (118–148)	
CD34 (median 11.67)				
>11.67	2312 (2043–2857)	0.80	140 (111–179)	0.12
<11.67	2611 (2128–3182)		123 (99–152)	
CD105 (median 6.00)				
>6.00	2570 (2121–2933)	0.84	142 (118–157)	0.85
<6.00	2461 (1772–3438)		126 (109–171)	

microvessels with a lack of smooth muscle cells in their walls. This may suggest a higher specificity of the CD105 marker for the newly formed vessels, which has also been proposed in previous studies [5–7, 24, 25]. Our results suggest a correlation between the mature and more immature microvessels as expected. When the density of immature microvessels increases, one would expect a similar increase in maturing vessels.

We tested whether genetic differences in genomic DNA were associated with differences in MVD. Genomic DNA was chosen because it is easily accessible in blood samples, and it represents a stable molecular marker compared to the genetic variations in the tumour DNA. The prognostic and predictive values of these germ line polymorphisms have recently been documented [20, 26]. In the present study, two of the SNPs, the VEGFR-2 1192 C/T and −604 T/C SNPs, had a significant relationship with MVD as estimated by CD105. A possible association, although non-significant, was found for MVD estimated by CD34. Sample size may be an explanation for the lack of significance regarding CD34. A subgroup analysis based on tumour location revealed similar associations for the patients with colon cancer only. Sample size and distribution of genotypes do not allow for meaningful statistical analyses of the patients with rectal cancer. To the best of our knowledge, this is the first report on SNPs in the VEGF system, which may have an influence on MVD in tumour tissue. These findings are interesting for several reasons. First of all, it demonstrates an association between results from a PCR-based technique and results from a technique based on visualisation of the tumour architecture and metabolism. Secondly, it gives another dimension to the term 'functional importance', which in relation to SNPs is often used to describe an influence on gene expression and protein levels. Finally, of course, it contributes to the rather limited knowledge regarding SNPs in the VEGFR genes and their possible role in CRC. One could speculate whether a SNP with an influence on the density of immature microvessels, known to depend on VEGF-A as a survival factor, could harbour predictive information regarding the response to the anti-VEGF-A antibody bevacizumab.

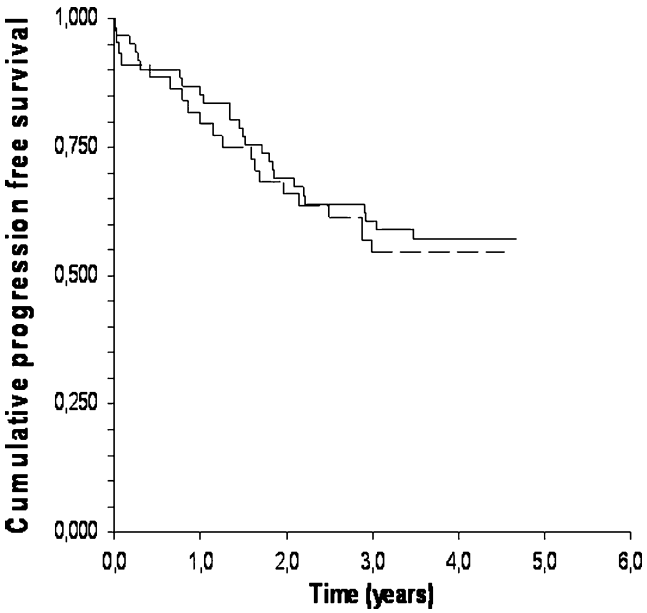

Fig. 4 Kaplan–Meier survival curves according to the CD105 MVD. The *solid line* represents patients with a low MVD score and the *hatched line* represents patients with a high MVD score, $p=0.73$ ($n=105$)

We found no association between MVD and VEGFR-1 and VEGFR-2 protein concentrations in CRC tissue. A possible explanation could be tumour heterogeneity. Although tumour cells constituted more than 80% of the cells in the tumour tissue, different amounts of non-tumour cells in the remaining fraction could still blur a possible association. Protein levels are dynamic and influenced not only by the biology of the system, and this could explain the lack of association. Searching the literature we found no reports on studies comparing MVD with quantitative protein measures of VEGFR-1 and VEGFR-2 in CRC. Further studies analysing the association between MVD and VEGF receptors are needed. A better understanding of these associations might be useful in the development of future targeted therapies.

A significant association between the VEGFR-2 1192 C/T SNP and protein concentrations of VEGFR-2 was

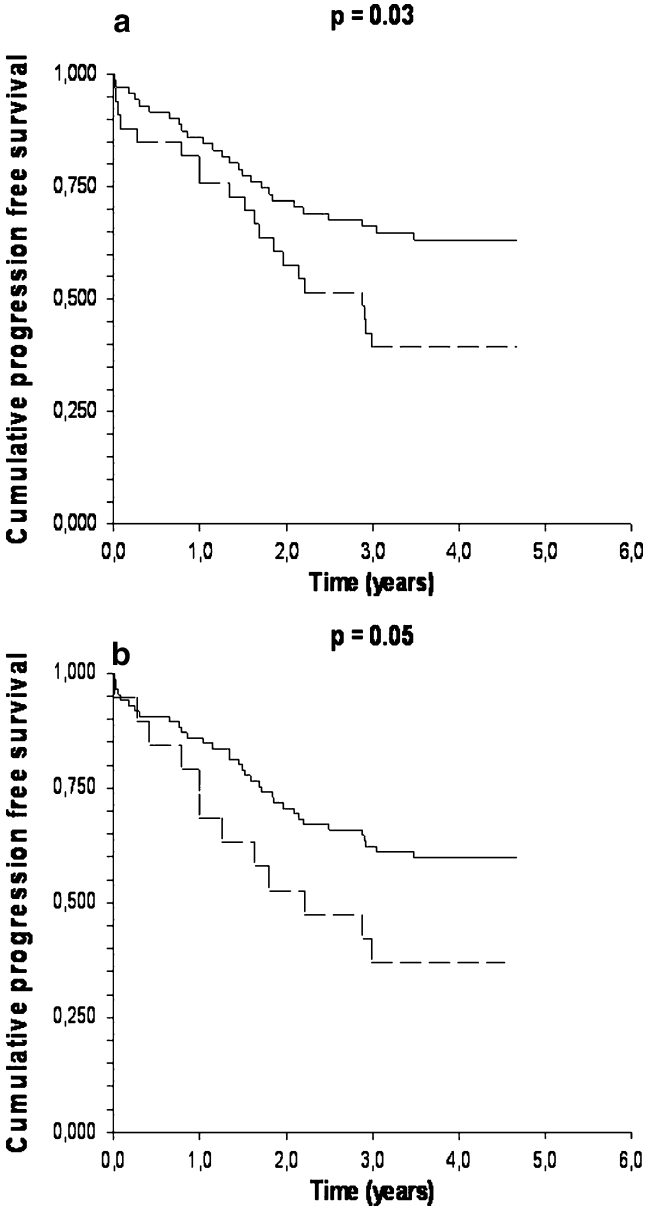

Fig. 5 **a**, **b** Kaplan–Meier survival curves according to the VEGFR-2 SNPs. **a** The survival curves according to the −604 T/C SNP. The *solid line* represents the TT + TC genotypes and the *hatched line* represents the CC genotype, $p=0.03$. **b** The survival curves according to the 1192 C/T SNP. The *solid line* represents the CC genotype and the *hatched line* represents the CT + TT genotypes, $p=0.05$ ($n=104$)

demonstrated in normal colorectal tissue, but not in CRC. This association between SNP status in genomic DNA and protein concentrations in normal tissue is not surprising, and the lack of association with protein concentrations in the neoplastic tissue may be explained by auto-regulation of the tumour cells due to mutations in the tumour DNA. The possible clinical importance of these findings is uncertain and validation is necessary.

Approximately one out of five patients had metastatic disease at time of operation. Sub-group analysis revealed no significant associations between M stage and MVD, SNPs or protein concentrations of VEGFR-1 and VEGFR-2.

In 2006, Des et al. published a meta-analysis on MVD and its prognostic importance analysing 22 studies. They concluded that using CD31 or CD34, MVD was inversely related to survival, whereas no prognostic value was demonstrated using factor VIII [14]. Romani et al. studied the prognostic role of MVD by CD105 in 125 CRC stages I–IV patients and found an increased MVD to be associated with a decreased rate of overall survival [15]. We found no association between MVD and survival, although traditional prognostic markers like the N and M stage both demonstrated a highly significant association with PFS ($p<0.001$; data not shown), indicating that our cohort of patients with CRC are representative for the disease. Other studies have also failed to show an association between MVD and survival [27, 28]. In these studies, CD31 was used as an endothelial cell marker. Based on the literature, the evidence seems to support MVD as a useful prognostic marker, although several differences in methodology may affect the results, e.g. choice of antibody, type of fixative used, use of the periphery or centre of the tumour for assessment, definition of cutoff values, observer variability in choosing hot spots etc. The lack of association between MVD and survival in our study may likewise be explained by differences in methodology or the heterogeneity in our patient material, and large scaled studies seem necessary.

We demonstrated an association between survival and the VEGFR-2 1192 C/T and −604 C/T SNPs. To our knowledge, no reports have been published regarding the prognostic value of these SNPs in patients with CRC. In a study from 2008 by Schneider et al., the association between several SNPs in the VEGF system, including the 1192 C/T and 1719 T/A SNPs and result of paclitaxel plus bevacizumab, was evaluated in 363 breast cancer patients [26]. An association between the treatment outcome and two of the VEGF-A SNPs was demonstrated, but no association with the VEGFR-2 SNPs was documented. It is worth noticing that in our study, the genotypes associated with low MVD, the 1192 CC genotype and the −604 TT + TC genotypes, where the same genotypes associated with superior survival. This association needs to be validated in another cohort of patients, but if an association indeed exists between these polymorphisms and prognosis, then it would be another argument for testing their possible predictive role in relation to anti-VEGF-A therapy in a randomised prospective trial.

A few patients in this study died within a week after their operation. Running the survival analysis with or without these patients did not change any of the conclusions. Dividing the patient material in patients with colon cancer and rectum cancer did not change the results either.

Regarding the future potential of MVD as a predictive marker, it is of some concern that MVD is not sufficient to reveal the angiogenic status of tumour neovasculature and that it offers no indication as to which patients might best respond to anti-angiogenic therapy. Assessing the maturation state of the microvessels, however, might give a better characterization of the vasculature and could prove useful in guiding anti-angiogenic treatment [29, 30]. Results from prospective randomized trials will hopefully clarify the possible predictive role of MVD in patients with CRC.

This study has the standard limitations related to retrospective studies and studies dealing with IHC. The results should be considered preliminary, and validation in another cohort of patients is of course necessary for further evidence.

In conclusion, this study showed that the VEGFR-2 1192 C/T and −604 T/C SNPs, assessed in germ line DNA, may have a functional influence on neoangiogenesis in CRC, especially indicating an impact on immature microvessels. Furthermore, an association between the same SNPs and survival was demonstrated. The clinical implications of these findings, especially the potential role of the VEGFR-2 SNPs in relation to angiogenesis in general, need further investigation.

Acknowledgements We are very thankful for the technical assistance provided by Lone Frischknecht, Lone Hartmann Hansen, Sara Egsgaard, Birgit Roed Sørensen and Karin Larsen. The study was supported by The Cancer Foundation.

Conflict of interest None.

References

1. Weidner N, Semple JP, Welch WR et al (1991) Tumor angiogenesis and metastasis—correlation in invasive breast carcinoma. N Engl J Med 324:1–8
2. Hansen S, Grabau DA, Rose C et al (1998) Angiogenesis in breast cancer: a comparative study of the observer variability of methods for determining microvessel density. Lab Invest 78: 1563–1573
3. Saad RS, Liu YL, Nathan G et al (2004) Endoglin (CD105) and vascular endothelial growth factor as prognostic markers in colorectal cancer. Mod Path 17:197–203
4. Akagi K, Ikeda Y, Sumiyoshi Y et al (2002) Estimation of angiogenesis with anti-CD105 immunostaining in the process of colorectal cancer development. Surgery 131:S109–S113
5. Minhajat R, Mori D, Yamasaki F et al (2006) Endoglin (CD105) expression in angiogenesis of colon cancer: analysis using tissue microarrays and comparison with other endothelial markers. Virchows Arch 448:127–134
6. Miller DW, Graulich W, Karges B et al (1999) Elevated expression of endoglin, a component of the TGF-beta-receptor complex, correlates with proliferation of tumor endothelial cells. Int J Cancer 81:568–572
7. Fonsatti E, Del VL, Altomonte M et al (2001) Endoglin: an accessory component of the TGF-beta-binding receptor-complex with diagnostic, prognostic, and bioimmunotherapeutic potential in human malignancies. J Cell Physiol 188:1–7
8. Fonsatti E, Sigalotti L, Arslan P et al (2003) Emerging role of endoglin (CD105) as a marker of angiogenesis with clinical potential in human malignancies. Curr Cancer Drug Targets 3:427–432
9. Royston D, Jackson DG (2009) Mechanisms of lymphatic metastasis in human colorectal adenocarcinoma. J Pathol 217:608–619
10. Takahashi Y, Kitadai Y, Bucana CD et al (1995) Expression of vascular endothelial growth factor and its receptor, KDR, correlates with vascularity, metastasis, and proliferation of human colon cancer. Cancer Res 55:3964–3968
11. Kaio E, Tanaka S, Kitadai Y et al (2003) Clinical significance of angiogenic factor expression at the deepest invasive site of advanced colorectal carcinoma. Oncology 64:61–73
12. Yonenaga Y, Mori A, Onodera H et al (2003) Absence of smooth muscle actin-positive pericyte coverage of tumor vessels correlates with hematogenous metastasis and prognosis of colorectal cancer patients. Oncology 69:159–166
13. Rajaganeshan R, Prasad R, Guillou PJ et al (2007) The influence of invasive growth pattern and microvessel density on prognosis in colorectal cancer and colorectal liver metastases. Br J Cancer 96:1112–1117
14. Des GG, Uzzan B, Nicolas P et al (2006) Microvessel density and VEGF expression are prognostic factors in colorectal cancer. Meta-analysis of the literature. Br J Cancer 94:1823–1832
15. Romani AA, Borghetti AF, Del RP et al (2006) The risk of developing metastatic disease in colorectal cancer is related to CD105-positive vessel count. J Surg Oncol 93:446–455
16. Li C, Gardy R, Seon BK et al (2003) Both high intratumoral microvessel density determined using CD105 antibody and elevated plasma levels of CD105 in colorectal cancer patients correlate with poor prognosis. Br J Cancer 88:1424–1431
17. Xiong B, Sun TJ, Yuan HY et al (2003) Cyclooxygenase-2 expression and angiogenesis in colorectal cancer. World J Gastroenterol 9:1237–1240
18. Cheng J, Slavin RE, Gallagher JA et al (2004) Expression of vascular endothelial growth factor and receptor flk-1 in colon cancer liver metastases. J Hepatobiliary Pancreat Surg 11: 164–170
19. Nakasaki T, Wada H, Shigemori C et al (2002) Expression of tissue factor and vascular endothelial growth factor is associated with angiogenesis in colorectal cancer. Am J Hematol 69:247–254
20. Kim JG, Chae YS, Sohn SK et al (2008) Vascular endothelial growth factor gene polymorphisms associated with prognosis for patients with colorectal cancer. Clin Cancer Res 14:62–66
21. Schneider BP, Radovich M, Sledge GW et al (2008) Association of polymorphisms of angiogenesis genes with breast cancer. Breast Cancer Res Treat 111:157–163
22. Fox SB, Leek RD, Smith K et al (1994) Tumor angiogenesis in node-negative breast carcinomas—relationship with epidermal growth factor receptor, estrogen receptor, and survival. Breast Cancer Res Treat 29:109–116
23. Perrone G, Vincenzi B, Santini D et al (2004) Correlation of p53 and bcl-2 expression with vascular endothelial growth factor (VEGF), microvessel density (MVD) and clinico-pathological features in colon cancer. Cancer Lett 208:227–234
24. Yu JX, Cui L, Zhang QY et al (2006) Expression of NOS and HIF-1alpha in human colorectal carcinoma and implication in tumor angiogenesis. World J Gastroenterol 12:4660–4664
25. Yu JX, Zhang XT, Liao YQ et al (2003) Relationship between expression of CD105 and growth factors in malignant tumors of

gastrointestinal tract and its significance. World J Gastroenterol 9:2866–2869
26. Schneider BP, Wang M, Radovich M et al (2008) Association of vascular endothelial growth factor and vascular endothelial growth factor receptor-2 genetic polymorphisms with outcome in a trial of paclitaxel compared with paclitaxel plus bevacizumab in advanced breast cancer: ECOG 2100. J Clin Oncol 26:4672–4678
27. Bossi P, Viale G, Lee AK et al (1995) Angiogenesis in colorectal tumors: microvessel quantitation in adenomas and carcinomas with clinicopathological correlations. Cancer Res 55:5049–5053
28. Gonzalez FJ, Vicioso L, Alvarez M et al (2007) Association between VEGF expression in tumour-associated macrophages and elevated serum VEGF levels in primary colorectal cancer patients. Cancer Biomark 3:325–333
29. Hlatky L, Hahnfeldt P, Folkman J (2002) Clinical application of antiangiogenic therapy: microvessel density, what it does and doesn't tell us. J Natl Cancer Inst 94:883–893
30. Vermeulen PB, Gasparini G, Fox SB et al (2002) Second international consensus on the methodology and criteria of evaluation of angiogenesis quantification in solid human tumours. Eur J Cancer 38:1564–1579

Virchows Arch (2010) 456:261–268
DOI 10.1007/s00428-009-0866-z

ORIGINAL ARTICLE

Tumor expression of Integrin-linked kinase (ILK) correlates with the expression of the E-cadherin repressor Snail: an immunohistochemical study in ductal pancreatic adenocarcinoma

David F. Schaeffer · Kiran Assi · Katie Chan · Andrzej K. Buczkowski · Stephen W. Chung · Charles H. Scudamore · Alan Weiss · Bill Salh · David A. Owen

Received: 2 June 2009 / Revised: 11 November 2009 / Accepted: 18 November 2009 / Published online: 21 January 2010
© Springer-Verlag 2010

Abstract Integrin-linked kinase (ILK) is a key molecule involved in mediating several biological functions including cell-matrix interactions, angiogenesis, and invasion, as well as playing a role in epithelial to mesenchymal transition (EMT) in cancer cells. In ductal pancreatic adenocarcinoma, increased expression of ILK has been linked to tumor prognosis and correlated with increased chemoresistance to drugs, such as gemcitabine. However, the precise relationship between ILK, Snail, E-cadherin, and N-cadherin expression on the stepwise development of pancreatic cancer is unknown. Hence, the purpose of this work was to investigate levels of expression of ILK, Snail, and the cadherins in pancreatic intraepithelial neoplasia (*PanIN*), and cancer. Resection specimens of 25 randomly selected patients, who underwent a pyloric preserving pancreatoduodenectomy for ductal pancreatic adenocarcinoma, were utilized for this study. Formalin-fixed paraffin embedded pancreatic tissue was immunostained for ILK, E-cadherin, N-cadherin, and Snail by standard techniques. The extent of staining positivity was scored and the results correlated with clinicopathological parameters. In 23 of 25 cases, ILK expression showed extensive positivity (>50%), while two cases did not demonstrate any ILK staining. PanIN grades 1 (n=16), 2 (n=11), and 3 (n=19) lesions demonstrated only focal positivity (<10%) for ILK. E-cadherin showed a reciprocal staining pattern to ILK in 21 of 25 cases, with only focal expression of the marker in pancreatic adenocarcinoma. Interestingly, 15 of 19 PanIN-3 lesions expressed extensive E-cadherin staining. N-cadherin, however, was moderately expressed in the majority of cases (n=18). Snail expression (n=22) correlated with ILK expression in ductal pancreatic adenocarcinoma (ρ=0.8168, p=0.02), but only minimal Snail staining activity was detected in PanIN lesions. The increase in expression of the E-cadherin repressor Snail, as well as the related increase in the ILK expression, may point towards an ILK-mediated induction, opening possible avenues for targeted drug therapy.

Keywords Pancreas · Cancer · Integrin-linked kinase (ILK) · PanIN · Snail

This paper was originally presented as a poster at the 97th Annual Meeting of the US and Canadian Academy of Pathology, March 1–7, 2008, Denver, Colorado.

D. F. Schaeffer (✉) · D. A. Owen
Department of Pathology, The University of British Columbia,
855 West 12th Avenue,
Vancouver, BC V5Z 1M9, Canada
e-mail: david.schaeffer@web.de

K. Assi · K. Chan · A. Weiss · B. Salh
Department of Medicine, The University of British Columbia,
Vancouver, BC, Canada

A. K. Buczkowski · S. W. Chung · C. H. Scudamore
Department of Surgery, The University of British Columbia,
Vancouver, BC, Canada

Introduction

Despite chemotherapy and surgical resection, the 5-year survival rate of pancreatic adenocarcinoma is dismal at 4% [1]. Rapid local spread of tumor and metastatic dissemination [2] are present in more than 80% of patients 6 months after surgery. The biological characteristics of usual ductal-type pancreatic adenocarcinoma and its propensity to

invade adjacent structures and metastasize early in the disease process are poorly understood. There have been recent advances in our understanding of the molecular mechanisms of aberrant signal transduction in cancer; inhibition of which has been exploited for the treatment of several cancer subtypes.

Integrins compromise a large family of cell-surface receptors and act as a bridge between extracellular matrix (ECM) proteins. Furthermore, they are considered to be an important mediator of tumor invasion and metastasis formation through interaction with ECM proteins [3] and their alteration has been associated with aggressive growth and metastatic capacity of several different tumor types [4–7].

Integrin-linked kinase (ILK), a 59-kDa serine/threonine protein kinase, is known to interact via the cytoplasmic domains of integrin β1 and β3 subunits [8] to regulate integrin-mediated cell adhesion and invasion, E-cadherin expression and ECM assembly [9–13]. Overexpression of ILK promotes oncogenic transformation [14, 15] and promotes tumor invasion partially due to the inhibition of E-cadherin [16, 17]. The transcription factor Snail has been shown to directly regulate expression of E-cadherin via the ILK pathway, as overexpression of ILK causes a stimulation of expression of Snail [13]. Furthermore, our group has recently shown that genetic knockdown of ILK in intestinal cells is associated with a reduction in Snail expression in colitis-associated cancer [18].

Using a pancreatic adenocarcinoma cell line level Sawai et al. [19] have demonstrated that overexpression of ILK enhances IL-1α-induced p38 MAPK phosphorylation and subsequently induces AP-1 activation, promoting aggressive capabilities of pancreatic cancer cells. They also showed that strong expression of ILK in pancreatic cancer was associated with poor patient outcome.

The aim of this study was to determine the relationship between ILK and other integral players involved in epithelial to mesenchymal transition (EMT), specifically E-cadherin, N-cadherin, and Snail in pancreatic cancer tissue, as well as in neoplastic precursor lesions (*PanIN*).

Materials and methods

Patients and paraffin-embedded tissue sample

Twenty-five consecutive pancreatic ductal adenocarcinoma patients, who underwent surgical resection at our institution, were included in this study. Inclusion criteria were based on the availability of adequate tissue for immunohistochemical analysis. A retrospective analysis of the available clinical data was performed. Ethical approval was obtained from the University of British Columbia Ethical Review Board. Basic demographic information, including age, gender, concomitant illnesses, previous surgeries, and survival data was collected for each individual patient, using the tumor registry database.

Furthermore, if applicable, the duration and regimen of adjuvant chemotherapy was recorded. Mean follow-up time of patients was 18 months. Pathological staging, determination of histological tumor grade and the presence of PanIN lesions were obtained from the original H&E slides. Mean patient age was 66.5 years (range, 47–87 years) with an even gender distribution of 14:11 (M/F). American Joint Committee on Cancer stage distribution was as follows: stage I (n=4), stage II (n=7), stage III (n=12), and stage IVB (n=2). Histological grade based on the World Health Organization (WHO) grading system was 1 (n=3), 2 (n=13), and 3 (n=9). Postoperative adjuvant therapy was administered to 12 patients, including chemoradiotherapy (n=4), radiotherapy (n=1), and chemotherapy (n=7). The administered chemotherapy was either gemcitabine (n=7) or 5-fluorouracil concurrently with radiotherapy (n=5; Table 1). Clinical and morphological data are summarized in Table 1.

Immunohistochemistry

Sections were cut at 4 micron thickness, mounted on positively charged glass slides, and baked at 60°C for a minimum of 60 min. Sections were then immersed in xylene, followed by gradated alcohols, at 10 min per solution. Antigen retrieval involved heating slides in a citrate (pH 6.0) buffer in either a microwave or a pressure cooker. Staining was achieved using biotin-free techniques including EnVision+ Kit (Dako, Carpenteria, Ca) automated and manual methods for ILK, E-cadherin, N-cadherin, and Snail. Dilutions were as follows: ILK, 1:200 (Santa Cruz Biotechnology, Santa Cruz, CA); E-cadherin, 1:200 (Upstate/Millipore, Billerica, MA); N-cadherin, 1:200 (Abcam, Cambridge, MA); and Snail, 1:100, staining was enhanced using nickel chloride, (Abcam, Cambridge, MA). Myocardium was used as a positive control tissue for ILK and N-cadherin, while mammary epithelium served as a positive control for E-cadherin. Sections of archival placental tissues served as a positive control for Snail immunoreactivity. The negative control was omission of the primary antibody (Table 2).

Evaluation of immunostaining

All staining with the ILK antiserum was cytoplasmic. E-cadherin and N-cadherin decorated cells in a membranous staining pattern; only nuclear reactivity was considered positive staining for antibody to Snail. Two investigators (DFS and DAO) assessed the results of immunostaining without the knowledge of the patients' clinicopathological

Table 1 Clinical and morphological data of the 25 patients with pancreatic adenocarcinoma analyzed

Case	Age (year)	Gender	pTNM	Stage	Grade	PanIN[a]	F/U at 18 mo	Ad Chem tx.[b]
1	75	M	pT2, N0, Mx	I	3	II-III	Alive	None
2	72	M	pT3, N1a, Mx	III	3	I	Alive	None
3	69	M	pT3, N1a, M1	IVB	2	None	Alive	Gemcitabine
4	75	F	pT3, N1a, Mx	III	2	II	Alive	None
5	67	M	pT1, N1a, Mx	III	2	IA	Alive	None
6	65	M	pT3, N0, Mx	II	2	II-III	Alive	Gemcitabine
7	81	F	pT2, N0, Mx	II	2	III	Alive	None
8	47	F	pT3, N0, Mx	II	2	II-III	Alive	5FU/Leucoverin
9	58	M	pT2, N0, Mx	I	2	I	Alive	None
10	57	F	pT3, N1a, Mx	III	1	II	Died at 14	Gemcitabine
11	71	M	pT3, N1a, M1	IVB	3	I-III	Alive	Gemcitabine
12	51	M	pT2, N1a, Mx	III	3	I-III	Died at 12	5FU/Folinic
13	74	F	pT3, N0, Mx	II	2	None	Alive	None
14	74	F	pT3, N0, Mx	II	3	I-III	Alive	Gemcitabine
15	57	M	pT3, N1a, Mx	III	3	None	Died at 13	None
16	87	F	pT3, N1a, Mx	III	2	II	Alive	Gemcitabine
17	75	F	pT2, N1a, Mx	III	1	III	Died at 13	None
18	69	M	pT2, N0, Mx	I	3	I-III	Died at 4	Gemcitabine
19	66	F	pT1, N1a, Mx	III	2	IB	Alive	5FU/Leucoverin
20	73	M	pT3, N0, Mx	II	3	IA	Died at 2	None
21	52	M	pT2, N1a, Mx	III	2	I-III	Alive	5FU/Leucoverin
22	58	F	pT3, N1a, Mx	III	1	III	Alive	5FU/Folinic
23	57	M	pT2, N1a, Mx	III	3	II	Died at 7	None
24	67	F	pT3, N0, Mx	II	3	III	Alive	None
25	75	M	pT2, N0, Mx	I	1	IB	Alive	None

[a] Multiple PanIN lesions were identified in single cases

[b] All, except patient 12 (two cycles), received adjuvant Chemotherapy for five cycles

details. Expression of all markers in the tumors was graded according to the proportion of positive cells: focal (<10% of tumor cells positive), moderate (10–50%), or extensive (>50%). For statistical analysis, the "positivity cut-off" included only moderate and high positivity cases.

Statistical analysis

Relationships between staining of ILK, Snail, E-cadherin, and N-cadherin were examined with the nonparametric Spearman's rank correlation test (ρ). Data values were expressed as means±SD.

Results

Overexpression of ILK and Snail in pancreatic cancer tissue and reduced expression in pancreatic intraepithelial neoplasm

The staining for ILK in primary pancreatic cancer tissue was mainly identified in the cytoplasm of cancer cells and infiltrating cells (Fig. 1d, g, j, and m). In noncancerous tissues, acinar, ductal, and islet cells, no staining of ILK was recorded (Fig. 1a). Twenty-three of 25 pancreatic cancers (92%) were positive for extensive (>50%) ILK

Table 2 Antibody information

Antibody	Clone	Manufacturer	Retrieval	Dilution	Positive control
ILK	65.1	Santa Cruz	Citrate, pH 6.0	1:200	Myocardium
E-cadherin	C20820	Upstate/Millipore	Citrate, pH 6.0	1:200	Mammary epithelium
N-cadherin	ab12221	Abcam	Citrate, pH 6.0	1:200	Myocardium
Snail	Ab17732	Abcam	Citrate, pH 6.0	1:100	Placenta

Santa Cuz Biotechnology, Santa Cruz, CA; Upstate/Millipore, Billerica, MA; Abcam Inc, Cambridge, MA

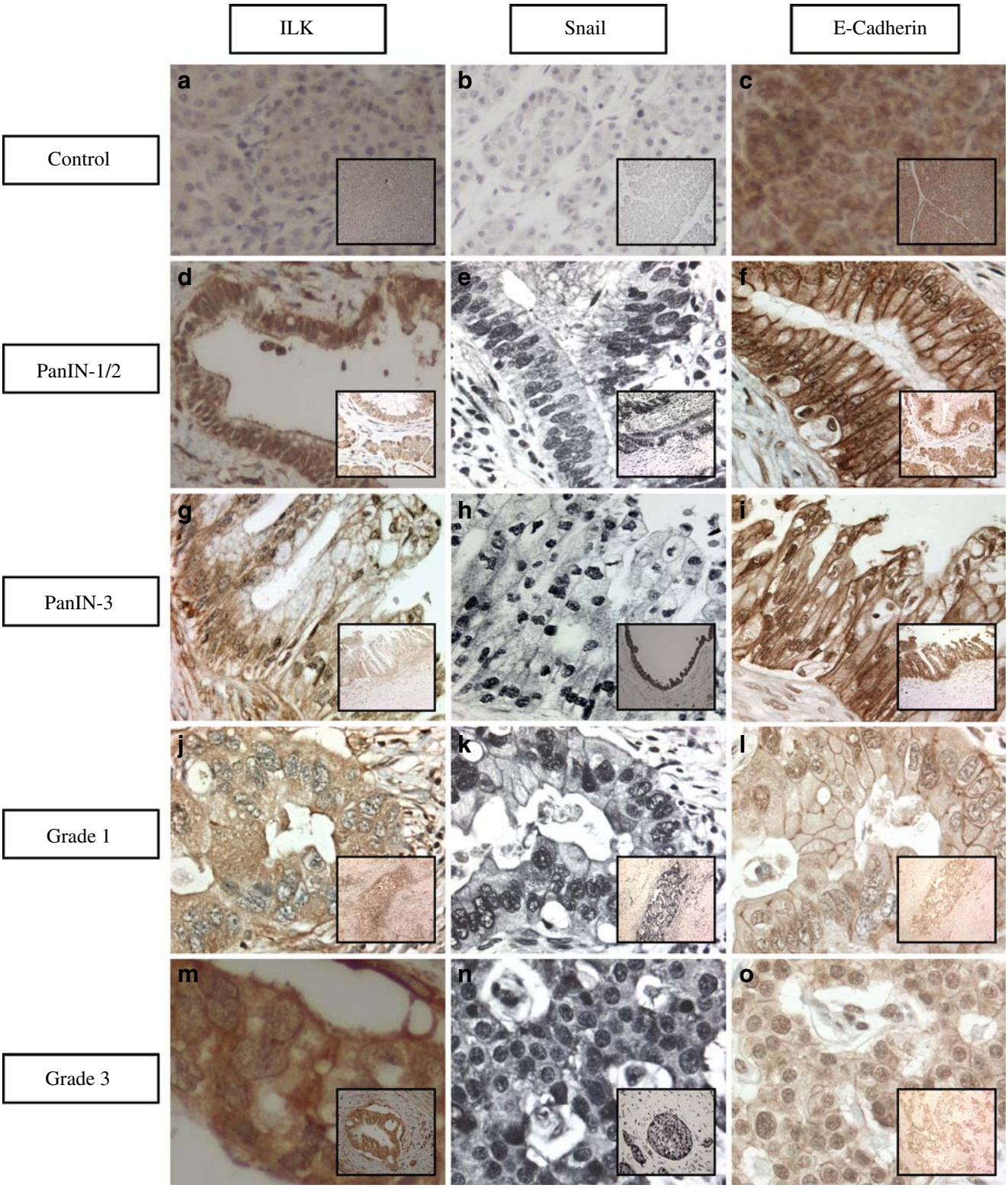

Fig. 1 Noncancerous tissue showed no staining for ILK (**a**), Snail (**b**), and E-cadherin (**c**). These pictures demonstrated ILK (**d**, **g**) and Snail (**e**, **h**) immunostaining, based on histological grading of PanIN grades 1/2 and 3 lesions and ILK (**j**, **m**) and Snail (**k**, **n**) immunoreactivity in tumors of WHO grades 1 and 3 differentiation, at ×40 magnification and ×2 magnification (inset). While there is expression of ILK and Snail, there is an increase in intensity between PanIN-1 to PanIN-3, a trend which is continued in the actual invasive component of the tumor (**j**, **k**, **m**, **n**), respectively. Note the cytoplasmic staining of the ILK patterns, while Snail shows a corresponding nuclear pattern. This staining pattern in this histological grade stands in sharp contrast to the expression profile of E-cadherin, which was absent in the majority of cases in grades 2 and 3 lesions (**l**, **o**), while positivity in staining was observed in PanIN-1/2 and PanIN-3 tumors (**f**, **i**)

staining. Only two cases, both stage II, did not display any ILK activity. A key observation was that if the tumor grade was variable within a given specimen, poorly differentiated areas of the cancer showed higher expression than well-differentiated portions (Spearman's rank correlation, ρ= 0.8972, p=0.003; Fig. 2a).

In precursor lesions of pancreatic cancer, PanIN, the expression profile of ILK was different (Fig. 1d, g). Only two of the 16 (13%) grade 1 PanIN lesions, one of the 11 (10%) grade 2 lesions, and five of the 19 (20%) grade 3 lesions exhibited ILK staining (Table 3).

The expression of Snail corresponded with the staining pattern displayed by ILK, in primary cancer tissues (Fig. 1e, h, k, and n). Twenty-two of 25 tumors (88%) showed extensive nuclear staining with Snail. The same variability of Snail staining was apparent within the tumor, dependent on differentiation, as was observed for ILK staining. Again, similar to the ILK staining pattern was the paucity of Snail expression in PanIN lesions; it was proportionally greatest in the PanIN grade 1 lesion with four of 16 (25%) being positive (Fig. 1e). Only one of 11(10%) grade 2, and two of 19 (10%) grade 3 PanIN foci showed Snail immunoreactivity (Fig. 1h and Table 3).

Reduced expression of E-cadherin and overexpression of N-cadherin in pancreatic cancer tissue

In pancreatic cancer tissues, E-cadherin expression in cancer cells was heterogenous or negative compared with that in normal epithelial tissues (Fig. 1c). This resulted in a reciprocal staining pattern as compared with ILK and Snail (Fig. 1f, i, l, and o). Twenty-one of 25 cases (84%) were found to have reduced or absent expression of E-cadherin. Only four cases showed E-cadherin staining, all of which were well or moderately differentiated tumors. Grade 3 tumors, however, demonstrated complete absence of E-cadherin (Fig. 1o). This trend was opposite in PanIN foci, with 11 of the 16 (68%) grade 1 PanIN lesions (Fig. 1f), eight of the 11 (72%) grade 2 lesions, and 15 of the 19 (79%) grade 3 lesions exhibiting E-cadherin (Fig. 1i; Table 3).

N-cadherin in pancreatic cancer tissue showed a membranous staining of the cancer cells (Fig. 3), while noncancerous tissue did not stain with N-cadherin. Eighteen of the 25 pancreatic (72%) cancers were positive for N-cadherin expression. In PanIN lesions, N-cadherin positivity was minimal, with six of the 16 (37%) grade 1 PanIN lesions, seven of the 11 (63%) grade 2 lesions, and five of the 19 (26%) grade 3 lesions exhibiting N-cadherin (Table 3). No co-expression between E-cadherin and N-cadherin was observed.

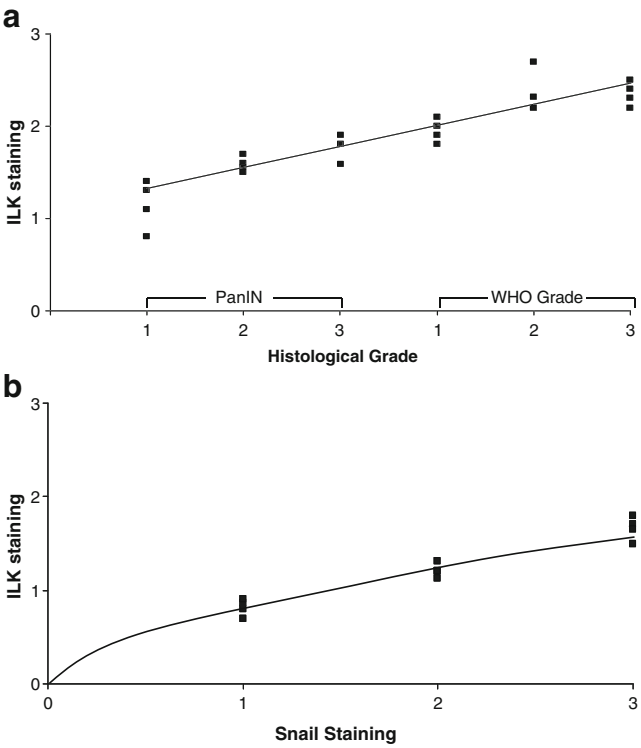

Fig. 2 Graphic representation (**a**) of the significant correlation between pathological grade and ILK expression. (Spearman's rank correlation, ρ=0.8972, p=0.003) and graphic representation (**b**) of the correlation between ILK and Snail staining (Spearman's rank correlation, ρ= 0.8168, p=0.02)

Correlation between ILK, Snail, N-cadherin, and E-Cadherin expression in PanIN and pancreatic cancer tissues

The relationship between the expression of ILK, Snail, and E-cadherin staining was analyzed on the basis of expressions only in cancer cells. In primary tumors, there was a significant correlation between ILK and Snail expression: tumors with a higher expression of ILK also showed higher expression of Snail (Spearman's rank correlation, ρ= 0.8168, p=0.02; Fig. 2b). Cells expressing ILK were found to express Snail as well. This correlation was also observed in PanIN foci: where ILK and Snail expression were significantly lower as compared with primary cancerous lesions.

There was a significant inverse correlation between the expressions of ILK and Snail to staining of E-cadherin: tumors with a higher expression of ILK and Snail showed low levels of E-cadherin. This trend was reversed in PanIN lesions, where higher expression of E-cadherin stood opposite to lower expression of ILK and Snail (Spearman's rank correlation, ρ=−0.4713, p=0.04).

No direct correlation could be established between overexpression of N-cadherin and reduced expression of E-cadherin in pancreatic cancer. Neither ILK, Snail, E-cadherin nor N-cadherin expression correlated with the pTNM stage in our cohort.

Table 3 Summary of ILK, Snail, E-cadherin, and N-cadherin IHC, by histological grade

	Number	ILK		Snail		E-cadherin		N-cadherin	
		Positive[a] (%)	Negative (%)	Positive[a] (%)	Negative (%)	Positive[a] (%)	Negative (%)	Positive[a] (%)	Negative (%)
PanIN-1	16	2 (13%)	14 (87%)	4 (25%)	12 (75%)	11 (68%)	4 (25%)	6 (37%)	10 (62%)
PanIN-2	11	1 (10%)	10 (90%)	1 (10%)	10 (90%)	8 (72%)	3 (27%)	7 (63%)	4 (36%)
PanIN-3	19	5 (26%)	14 (73%)	2 (10%)	17 (89%)	15 (79%)	4 (21%)	5 (26%)	14 (73%)
Grade 1	3	3 (100%)	0	3 (100%)	0	1 (33%)	2 (67%)	2 (67%)	1 (33%)
Grade 2	13	11 (84%)	2 (16%)	11 (84%)	2 (15%)	3 (24%)	10 (76%)	10 (76%)	3 (24%)
Grade 3	9	9 (100%)	0	8 (89%)	1 (11%)	0	9 (100%)	6 (67%)	3 (33%)

Histological grade, based on WHO classification

[a] The "positivity cut-off" included only moderate and high positivity cases

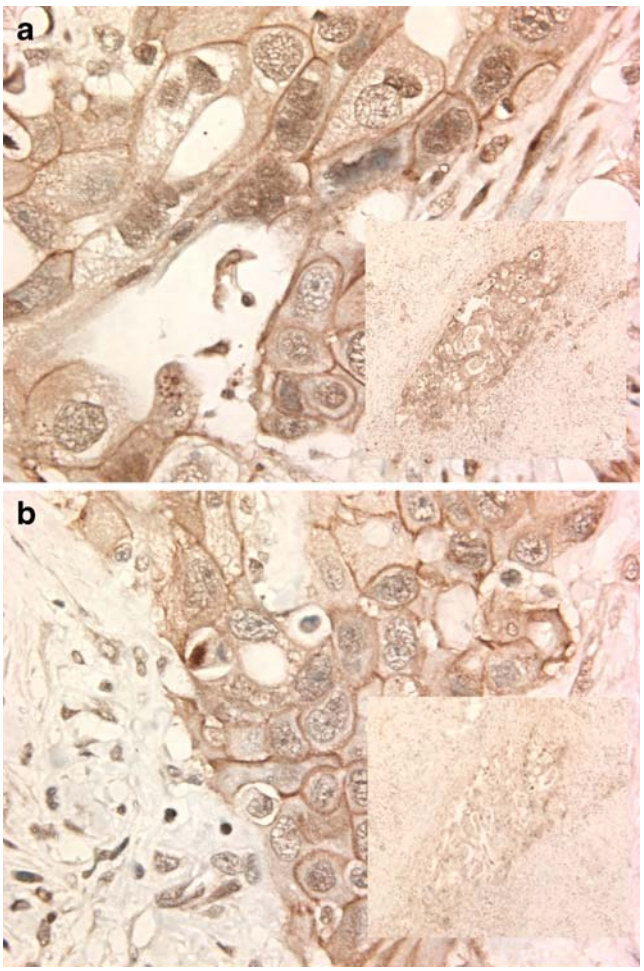

Fig. 3 Immunohistochemical staining of E-cadherin (**a**) in a grade 1 lesion and N-cadherin (**b**) in a grade 2 lesion, at ×60 magnification and ×2 magnification (*inset*). Note the typical membranous staining outlining the regions of cell–cell contact

Discussion

The present study demonstrates, to the best of our knowledge, for the first time, the relationship between tumor grade-dependent ILK and Snail protein expression in pancreatic cancer. This data may have important biological and clinical implications as strong expression of ILK in cancers has been shown to be associated with poor survival prognosis [19].

Overexpression of ILK has been reported to be correlated with tumor progression [20, 21]. Furthermore, ILK overexpression has been found to be associated with chemoresistance in pancreatic cancer [22]. In our immunohistochemical analysis, we could demonstrate that ILK expression seems to be dependent on the tumor grade with low to zero expression in the neoplastic precursor lesions PanIN and extensive expression in typical invasive adenocarcinoma. Several authors have compared the loss of epithelial characteristics at late stages of tumorigenesis to the epithelial-to-mesenchymal transitions that occur during development [23, 24]. A clear example of this correlation is provided by the downregulation of E-cadherin in pancreatic adenocarcinoma. Previous experiments have demonstrated that the transcription factor Snail, which is expressed by fibroblasts and some epithelial tumor cells, represses E-cadherin gene expression by binding directly to the E-boxes present in the proximal E-cadherin promotor region [25]. This is important as other experiments have shown that decreased expression of E-cadherin is directly associated with increased oncogenic invasion potential [16, 17]. In addition, Tan et al. [26] demonstrated that ILK directly regulates the transcription of Snail which in turn represses the expression of E-cadherin.

Epithelial-mesenchymal transition, conversion of epithelial to mesenchymal phenotype, is indicated by the loss of E-cadherin and the appearance of N-cadherin. In colorectal, breast, gastric, and salivary gland, tumors EMT has been

associated with an aggressive cancer phenotype [27–30]. A previous paper has investigated the expression of E-cadherin and N-cadherin, as well as vimentin in resected pancreatic cancers [31]. They demonstrated decrease in E-cadherin and upregulation of N-cadherin. The authors in this report hypothesized that a cadherin switch occurs in these cases, from E-cadherin to N-cadherin with EMT and attributed prognostic significance to N-cadherin expression alone. A more recent report [32] concluded that EMT in pancreatic adenocarcinoma is associated with poor survival. However, this group focused on one pathway only, examining the association of E-cadherin, fibronectin, and vimentin with P-Erk.

The findings presented here raise the possibility that the activation of ILK plays an important role in the early onset and progression of pancreatic ductal adenocarcinoma. Confirmation of this hypothesis would require a specific mechanistic study.

In conclusion, we could demonstrate tumor grade dependent increased expression of Snail and ILK within pancreatic adenocarcinoma. In light of the assumed importance of E-cadherin and N-cadherin in EMT within this cancer subtype, the expression patterns of Snail and ILK warrant further investigation to determine the possibility for targeted drug therapy.

Conflicts of interest statement We declare that we have no conflicts of interest.

References

1. Li D, Xie K, Wolff R et al (2004) Pancreatic cancer. Lancet 363:1049–1057
2. Chua YJ, Cunningham D (2005) Adjuvant treatment for resectable pancreatic cancer. J Clin Oncol 23:4532–4537
3. Giancotti FG, Ruoslahti E (1999) Integrin signaling. Science 285:1028–1032
4. Vogelmann R, Kreuser ED, Adler G et al (1999) Integrin alpha6beta1 role in metastatic behavior of human pancreatic carcinoma cells. Int J Cancer 80:791–795
5. Sawai H, Funahashi H, Matsuo Y et al (2003) Expression and prognostic roles of integrins and interleukin-1 receptor type I in patients with ductal adenocarcinoma of the pancreas. Dig Dis Sci 48:1241–1250
6. Mayoral R, Fernández-Martínez A, Boscá L et al (2005) Prostaglandin E2 promotes migration and adhesion in hepatocellular carcinoma cells. Carcinogenesis 26:753–761
7. Menendez JA, Vellon L, Mehmi I et al (2005) A novel CYR61-triggered 'CYR61-alphavbeta3 integrin loop' regulates breast cancer cell survival and chemosensitivity through activation of ERK1/ERK2 MAPK signaling pathway. Oncogene 24:761–779
8. Hannigan G, Troussard AA, Dedhar S (2005) Integrin-linked kinase: a cancer therapeutic target unique among its ILK. Nat Rev Cancer 5:51–63
9. Delcommenne M, Tan C, Gray V et al (1998) Phosphoinositide-3-OH kinase-dependent regulation of glycogen synthase kinase 3 and protein kinase B/AKT by the integrin-linked kinase. Proc Natl Acad Sci USA 95(19):11211–11216
10. Chen P, Shen WZ, Karnik P (2004) Suppression of malignant growth of human breast cancer cells by ectopic expression of integrin-linked kinase. Int J Cancer 111:881–891
11. Edwards LA, Thiessen B, Dragowska WH et al (2005) Inhibition of ILK in PTEN-mutant human glioblastomas inhibits PKB/Akt activation, induces apoptosis, and delays tumor growth. Oncogene 24:3596–3605
12. Filipenko NR, Attwell S, Roskelley C et al (2005) Integrin-linked kinase activity regulates Rac- and Cdc42-mediated actin cytoskeleton reorganization via alpha-PIX. Oncogene 24:5837–5849
13. Tan C, Cruet-Hennequart S, Troussard A et al (2004) Regulation of tumor angiogenesis by integrin-linked kinase (ILK). Cancer Cell 5:79–90
14. Janji B, Melchior C, Vallar L et al (2000) Cloning of an isoform of integrin-linked kinase (ILK) that is upregulated in HT-144 melanoma cells following TGF-beta1 stimulation. Oncogene 19: 3069–3077
15. Wu C, Keightley SY, Leung-Hagesteijn C et al (1998) Integrin-linked protein kinase regulates fibronectin matrix assembly, E-cadherin expression, and tumorigenicity. J Biol Chem 273:528–536
16. Novak A, Hsu SC, Leung-Hagesteijn C et al (1998) Cell adhesion and the integrin-linked kinase regulate the LEF-1 and beta-catenin signaling pathways. Proc Natl Acad Sci USA 95:4374–4379
17. Janji B, Melchior C, Gouon V et al (1999) Autocrine TGF-beta-regulated expression of adhesion receptors and integrin-linked kinase in HT-144 melanoma cells correlates with their metastatic phenotype. Int J Cancer 83:255–262
18. Assi K, Mills J, Owen D et al (2008) ILK regulates cell proliferation and tumor growth in murine colitis associated carcinogenesis. Gut 57:931–940
19. Sawai H, Okada Y, Funahashi H et al (2006) Integrin-linked kinase activity is associated with interleukin-1 alpha-induced progressive behavior of pancreatic cancer and poor patient survival. Oncogene 25:3237–3246
20. Dai DL, Makretsov N, Campos EI et al (2003) Increased expression of integrin-linked kinase is correlated with melanoma progression and poor patient survival. Clin Cancer Res 9:4409–4414
21. Ahmed N, Oliva K, Rice GE et al (2004) Cell-free 59 kDa immunoreactive integrin-linked kinase: a novel marker for ovarian carcinoma. Clin Cancer Res 10:2415–2420
22. Duxbury MS, Ito H, Benoit E et al (2005) RNA interference demonstrates a novel role for integrin-linked kinase as a determinant of pancreatic adenocarcinoma cell gemcitabine chemoresistance. Clin Cancer Res 11:3433–3438
23. Birchmeier C, Birchmeier W, Brand-Saberi B (1996) Epithelial-mesenchymal transitions in cancer progression. Acta Anat (Basel) 156:217–226
24. Birchmeier W, Behrens J, Weidner KM et al (1996) Epithelial differentiation and the control of metastasis in carcinomas. Curr Top Microbiol Immunol 213:117–135
25. Batlle E, Sancho E, Francí C et al (2000) The transcription factor snail is a repressor of E-cadherin gene expression in epithelial tumour cells. Nat Cell Biol 2:84–89
26. Tan C, Costello P, Sanghera J et al (2001) Inhibition of integrin linked kinase (ILK) suppresses beta-catenin-Lef/Tcf-dependent transcription and expression of the E-cadherin repressor, snail, in APC-/- human colon carcinoma cells. Oncogene 20:133– 140
27. Bates RC, Pursell BM, Mercurio AM (2007) Epithelial-mesenchymal transition and colorectal cancer: gaining insights into tumor progression using LIM 1863 cells. Cells Tissues Organs 185:29–39

28. Cheng GZ, Chan J, Wang Q et al (2007) Twist transcriptionally up-regulates AKT2 in breast cancer cells leading to increased migration, invasion, and resistance to paclitaxel. Cancer Res 67:1979–1987
29. Vasko V, Espinosa AV, Scouten W et al (2007) Gene expression and functional evidence of epithelial-to-mesenchymal transition in papillary thyroid carcinoma invasion. Proc Natl Acad Sci USA 104:2803–2808
30. Yang MH, Chang SY, Chiou SH et al (2007) Overexpression of NBS1 induces epithelial-mesenchymal transition and co-expression of NBS1 and Snail predicts metastasis of head and neck cancer. Oncogene 26:1459–1467
31. Nakajima S, Doi R, Toyoda E et al (2004) N-cadherin expression and epithelial-mesenchymal transition in pancreatic carcinoma. Clin Cancer Res 10:4125–4133
32. Javle MM, Gibbs JF, Iwata KK et al (2007) Epithelial-mesenchymal transition (EMT) and activated extracellular signal-regulated kinase (*p*-Erk) in surgically resected pancreatic cancer. Ann Surg Oncol 14:3527–3533

Virchows Arch (2010) 456:269–276
DOI 10.1007/s00428-010-0880-1

ORIGINAL ARTICLE

Polymorphous lymphoproliferative disorder: a clinicopathological analysis

Naoto Nakamichi · Naoki Wada · Masaharu Kohara · Shirou Fukuhara · Haruo Sugiyama · Hiroyasu Ogawa · Masayuki Hino · Akihisa Kanamaru · Yuzuru Kanakura · Eiichi Morii · Katsuyuki Aozasa

Received: 7 October 2009 / Revised: 2 December 2009 / Accepted: 3 January 2010 / Published online: 29 January 2010
© Springer-Verlag 2010

Abstract Lymphoproliferative disorder (LPD) with polymorphous composition of proliferation (polymorphous LPD), containing large lymphoid cells together with small lymphocytes, plasma cells, macrophages, and/or eosinophils, is found in individuals with immunodeficiency conditions. Clinicopathological findings in 19 cases of polymorphous LPD registered with the Osaka Lymphoma Study Group, Osaka, Japan, were analyzed; they represented 0.4% of the registered cases. In six cases, there was a history of rheumatoid arthritis; five of them had received immunosuppressive agents. There were no acquired immunodeficiency syndrome cases or organ transplant recipients. Southern blotting and/or polymerase chain reaction (PCR)-based clonality analysis revealed monoclonal B cell and T cell proliferation in eight and six cases (B- and T-LPD), respectively, and polyclonality in one. In B-LPD, there was polymorphous proliferation, containing large B-lymphoid cells, while medium-to-large T lymphoid cells with occasional eosinophilic infiltration were seen in T-LPD. Epstein–Barr virus (EBV) was detected in three of eight B-LPD, four of six T-LPD, and one of one polyclonal LPD. The prognosis was not favorable; the 3-year overall survival rate was 49.7± 17.3%. Thus, polymorphous LPD is relatively rare in Japan and is a heterogeneous disease with monoclonal proliferation of B or T cells; additionally, it is occasionally EBV-associated, and behaves as an aggressive lymphoma.

Supported in part by a grant (20014012) from the Ministry of Education, Science, Culture, and Sports, Japan.

N. Nakamichi · N. Wada · M. Kohara · E. Morii · K. Aozasa (✉)
Department of Pathology (C3),
Osaka University Graduate School of Medicine,
2-2 Yamadaoka,
Suita, Osaka 565-0871, Japan
e-mail: aozasa@molpath.med.osaka-u.ac.jp

N. Nakamichi · S. Fukuhara
First Department of Internal Medicine,
Kansai Medical University,
Osaka, Japan

H. Sugiyama
Department of Functional Diagnostic Science,
Osaka University Graduate School of Medicine,
Osaka, Japan

H. Ogawa
Division of Hematology, Department of Internal Medicine,
Hyogo College of Medicine,
Nishinomiya, Hyogo, Japan

M. Hino
Department of Clinical Hematology and Clinical Diagnostics,
Graduate School of Medicine, Osaka City University,
Osaka, Japan

A. Kanamaru
Division of Hematology, Department of Internal Medicine,
Kinki University School of Medicine,
Osaka, Japan

Y. Kanakura
Department of Hematology and Oncology,
Osaka University Graduate School of Medicine,
Osaka, Japan

Keywords Lymphoproliferative disorder · Polymorphous · T cell · B cell · Clonality · EBV

Introduction

Polymorphous composition of proliferation containing large lymphoid cells together with small lymphocytes, plasma cells, macrophages, and/or eosinophils is a complex issue in diagnosis: the possible spectrum ranges from reactive changes, including infectious diseases, to neoplastic diseases, such as peripheral T cell lymphoma (PTCL), and Hodgkin lymphoma (HL). In PTCL, tumor cells secrete various cytokines that induce infiltration of inflammatory cells, resulting in polymorphous composition of proliferation. The neoplastic nature of PTCL can be judged based on the presence of medium-to-large T cells showing nuclear hyperchromasia and pleomorphism, with the appearance of bizarre cells, and can be confirmed by the presence of clonal T cells [1].

Polymorphous composition of proliferation devoid of neoplastic-looking T lymphoid cells is usually found in individuals with immunodeficiency conditions, including acquired immunodeficiency syndrome (AIDS) and transplant recipients receiving immunosuppressive drugs, and is referred to as polymorphous lymphoproliferative disorder (LPD) [2]. It is well known that polymorphous LPD can also develop in patients with rheumatoid arthritis (RA) receiving methotrexate (MTX; i.e., MTX-associated LPD, MTX-LPD) [1]. Among the newly listed categories in the updated World Health Organization (WHO) classification (2008), some cases of Epstein–Barr virus (EBV)-positive diffuse large B cell lymphoma (DLBCL) in the elderly, and also show a histological picture resembling polymorphous LPD [1]. EBV-positive DLBCL of the elderly (EBV + DLBCL-E) is defined as a lymphoma that occurs in patients >50 years with no known immunodeficiency.

Polymorphous LPD is occasionally encountered in routine clinical practice: some patients have a history of organ transplantation or RA treated with MTX, but others have no sign of immunological abnormality. These findings suggest that polymorphous LPD actually comprises a heterogeneous disease with differing etiologies. A previous immunophenotypic study suggested that the predominant proliferating cells were B cells in most polymorphous LPD cases, with T cells being much less frequent [2]. In the present study, we reviewed cases of polymorphous LPD registered with the Osaka Lymphoma Study Group (OLSG). Clinicopathological findings and the presence or absence of B or T cell clones, together with any association with EBV, were analyzed to clarify which diseases are included in "polymorphous LPD" encountered in routine practice in Japan.

Materials and methods

Patients

Between November 1999 and November 2008, in total, 4,422 cases of malignant lymphomas and related conditions were registered with the OLSG. Histological specimens, obtained by biopsy, were fixed in 10% formalin, and routinely processed for paraffin embedding. Histological sections cut at 4 μm were stained with hematoxylin and eosin, and immunoperoxidase procedures. All histological sections were reviewed by one author (KA). Of these 4,422 cases, 19 (0.4%) were diagnosed as polymorphous LPD after careful differential diagnosis from PTCL-not otherwise specified (NOS), HL, and reactive conditions, through evaluation of histological specimens, flow cytometry data, and molecular analyses. The polymorphous populations included neither diagnostic Reed-Sternberg (RS) cells nor a substantial number of medium-to-large T cells with nuclear hyperchromasia, and variable numbers of bizarre cells with multilobed nuclei, indicating that diagnoses of HL or PTCL were unlikely in these cases. Adequate clinical information was available for 18 patients.

The follow-up period for survivors ranged from 1 to 60 (median, 18) months. Information for therapeutic modalities was available in 17 cases: anthracycline-based chemotherapy in nine patients (53%), rituximab with or without combination chemotherapy, mostly cyclophosphamide, doxorubicin, vincristine, and prednisolone (CHOP), in six, and allogeneic bone marrow transplantation after four cycles of chemotherapy in one. One case with RA showed spontaneous partial remission of LPD after withdrawal of MTX, and another case died before the start of therapy.

Evaluation of clonality for B and T cells

DNA was extracted from paraffin-embedded samples in 17 cases, as described previously [3]. PCR-based assessment of rearrangement in the immunoglobulin, T-cell receptor (TCR), *BCL1-IGH*, and *BCL2-IGH* genes was performed using the BIOMED-2 PCR protocol, as described previously [4]. Amplified products were electrophoresed in 6% polyacrylamide gels. A PCR mixture with no DNA was used as a negative control, and a case of lymphoid hyperplasia or peripheral mononuclear cells as a polyclonal control. Clonality analyses were not performed in two cases because no paraffin-embedded samples were available.

Immunohistochemistry

An immunohistochemical study on the paraffin sections was conducted using the Envision+ system (DAKO, Carpinteria, CA, USA). Monoclonal antibodies used and

their dilutions were CD20 (1:400), CD3 (1:50), CD8 (1:100), CD30 (1:50; DakoCytomation, Glostrup, Denmark), and CD4 (1:40; NovoCastra, Newcastle, UK).

Classification of cases, according to the WHO scheme (2008)

Based on clinical, histological, immunohistochemical, and molecular data, the present cases were classified according to the WHO scheme (2008) [1]. Briefly, cases with monoclonal rearrangement of the TCR gene, but without specific characteristics, such as positive anti-human T-lymphotropic virus type I (HTLV-I) antibody and/or monoclonal integration of HTLV-1 proviral DNA in the tumor cells, and appearance of clusters of "clear cells," were classified as PTCL-NOS. Cases showing diffuse proliferation of large B-lymphoid cells with a prominent polymorphous cellular background containing small lymphoid cells, plasma cells, histiocytes, and/or eosinophils that appeared neoplastic were classified as DLBCL-NOS, and cases in individuals >50 years, with the EBV genome in the nuclei of proliferating cells, with no known immunodeficiency or prior lymphoma, were classified as EBV^+ DLBCL-E. LPD that arose in patients treated with immunosuppressive drugs for autoimmune diseases or conditions other than an allograft/autograft transplant setting were classified as other iatrogenic immunodeficiency-associated LPD.

In situ hybridization

RNA in situ hybridization using an EBV-encoded RNA (EBER)-1 probe was performed as described previously [5], with some modifications. Briefly, a 30-base oligonucleotide probe, 5′-AGACACCGTCCTCACCACCCGGGACTTGTA-3′, corresponding to the sense and antisense sequences of a portion of the EBER-1 gene, a region of the EBV genome that is actively transcribed in latently infected cells, was synthesized. The Raji cell line was used as a positive control. As negative controls, hybridizing mixtures containing sense or antisense probes after RNase treatment were used.

Results

Clinical findings

Clinical findings from 19 patients with polymorphous LPD are summarized in Table 1. Patient ages ranged from 28 to 80 (median, 65) years, with a male:female ratio of 7:12. All but one case presented with nodal disease. One case presented with a skin lesion. Three cases had stage I disease, three stage II, five stage III, seven stage IV, and one unknown. No case had a leukemic blood picture or a bulky mass at presentation or during the course. Six cases had histories of RA; five of them received immunosuppressive agents, such as methotrexate, predonisolone, or anti-tumor necrosis factor (TNF)α agents. No patient had a history of AIDS or organ transplantation. Hepatomegaly and/or splenomegaly were found in about half the patients. B symptoms were found in 42% of patients. Serum levels of lactate dehydrogenase were high in 14 of 18 (78%) cases. All patients showed elevated levels of serum soluble IL-2 receptor (the highest value was 29,300 U/mL).

Clonality analysis

DNA was extracted from paraffin-embedded samples and used for PCR-based clonality analysis; DNA was fragmented and unsuitable for analysis in six cases. As a result, clonality analysis on the paraffin-embedded samples was performed in 11 cases (cases 3, 6, 8, 9, 13, 14, 15, 16, 17, 18, and 19; Table 2). Frozen samples were available and used for Southern blot analysis for IgH and TCRβ chain gene rearrangement in 11 cases. In total, clonality analysis was possible in 15 cases: monoclonal proliferation of B and T cells was found in eight and six cases, respectively (Fig. 1a, b); one case (case 14) showed polyclonal proliferation of both the IgH and TCRβ genes. t(14;18)(q32;q21) with the *BCL2-IGH* rearrangement was detected in one case (case 16; Fig. 1c); no case showed t(11;14)(q13;q32) with the *BCL1-IGH* rearrangement. Identical results for clonality were observed in all but one case (case 8), in which Southern blot analysis showed a germline configuration, but the PCR-based method confirmed the presence of a T cell clone.

Pathological findings

Common histological findings in these 19 cases were diffuse, polymorphous cellular proliferation, principally occupying the interfollicular areas, with preservation of lymph follicles in a few cases. Varying numbers of large lymphoid cells were scattered in the polymorphous areas, but their nuclei were neither hyperchromatic nor multilobed, unlike the pleomorphic appearances typically found in the neoplastic proliferation of B and T cells. Mitotic figures were seen occasionally. Vascular proliferation was not marked in any case (Fig. 2).

The WHO classification (2008) was applied to 15 cases for which clonality data were available (Table 2). In the eight cases with monoclonal proliferation of B cells, a mild degree of fibrosis was found in two cases and necrosis in one. Plasma cells were few in number and eosinophils were rarely found. Macrophages were frequently found in three cases, with formation of epithelioid cell clusters in one. Immunohistochemistry revealed diffuse proliferation of

Table 1 Clinical features of 19 patients with polymorphous lymphoproliferative disorder

No.	Age	Sex	Immune abnormalities	Immunosupressive agents	Hepatosplenomegaly	BM involvement	B symptoms	IPI	LDH	PS	Stage	Extranodal disease	sIL2R (U/ml)	Follow-up (months)
1	66	F	No	No	No	No	No	L	na	0	1	0	na	60 A
2	59	F	No	No	Yes	No	Yes	na	High	0	3	na	na	32 DT
3	53	F	No	No	Yes	No	Yes	LI	High	0	4	1	3,550	7 DT
4	41	F	No	No	na	Yes	No	HI	WNL	2	4	2	1,750	60 A(PR)
5	80	F	No	No	No	No	No	na	WNL	na	na	na	1,010	46 DID
6	75	F	RA	MTX	Yes	No	Yes	H	High	4	4	1	5,150	11 A(PR)
7	28	M	No	No	Yes	Yes	No	HI	High	1	4	5	1,690	25 A
8	72	F	RA	No	No	No	No	HI	High	0	1	0	2,510	15 DT
9	61	M	No	No	No	Yes	No	LI	High	0	4	1	2,140	20 A(CR)
10	78	F	No	No	Yes	No	Yes	H	High	3	3	na	29,300	3 DT
11	68	F	RA	MTX and PSL	Yes	Yes	Yes	H	High	4	4	1	10,200	24 A
12	76	F	RA	PSL	Yes	na	No	HI	WNL	1	4	2	3,690	1 DT
13	70	M	No	No	na	No	Yes	na	High	na	3	na	4440	3 DT
14	72	F	RA	MTX and anti-TNF α	No	na	No	L	High	1	1	1	573	7 A(CR)
15	78	M	No	No	No	No	No	L	WNL	1	2	0	3,460	5 A(CR)
16	60	M	No	No	No	na	No	na	High	1	2	na	914	na
17	74	M	No	No	Yes	No	Yes	HI	High	1	3	na	4,870	10 A
18	76	M	No	No	No	No	Yes	HI	High	2	2	na	785	1 A
19	49	F	RA	MTX	No	No	No	LI	High	0	3	na	460	5 A(PR)

Abbreviations: *BM* bone marrow, *IPI* international prognostic index, *L* low, *LI* low intermediate, *HI* high intermediate, *H* high, *LDH* lactate dehydrogenase, *PS* performance status, *sIL2R* soluble IL-2 receptor, *F* female, *M* male, *RA* rheumatoid arthritis, *MTX* methotrexate, *PSL* predonisolone, *TNF* tumor necrosis factor, *na* data not available, *WNL* within normal limit, *A* alive, *DT* death due to tumor, *DID* death with intercurrent disease, *PR* partial remission, *CR* complete remission

Table 2 Pathological findings and follow-up data of 15 cases undergoing clonality analysis

Clonality analysis			T cell				Therapy	Complication at presentation	Follow-up (months)	Categorization in WHO classification (2008)
No.	Paraffin	Frozen	EBV	CD4		CD8				
3	T	T	+	+	=	+	CHOP, auto-PBSCT		7 DT	PTCL-NOS
6	T	T	+	+	>	−	MTX withdrawal + mPSL	CAEBV	11 A(PR)	PTCL-NOS
7	nd	T	+	+	=	+	CHOP + allo-BMT	HPS, CAEBV	25 A	PTCL-NOS
8	T	Polyclonal	+	+	>	+	THP-COP, other		15 DT	PTCL-NOS
9	T	nd	−	+	=	+	na		20 A(CR)	PTCL-NOS
19	T	T	−	+	>	+	MTX withdrawal		5 A(PR)	PTCL-NOS
5	nd	B	−	−	<	+	THP-COP, other	Chronic HBV hepatitis	46 DID	DLBCL-NOS
13	B	B	−	+	>	+	R-THP-COP	HPS	3 DT	DLBCL-NOS
15	B	nd	−	+	=	+	R-THP-COP	Type 2 DM	5 A(CR)	DLBCL-NOS
16	B with t(14:18)	B	−	+	=	+	na	Chronic HBV hepatitis	na	DLBCL-NOS
18	B	nd	−	+	>	+	R-THP-COP		1 A	DLBCL-NOS
10	nd	B	+	na		na	R+mPSL+CY	HPS	3 DT	EBV^+ DLBCL of the elderly
17	B	B	+	+	=	+	PSL+CyA	Pure red cell aplasia	10 A	EBV^+ DLBCL of the elderly
11	nd	B	+	+	>	+	mPSL, R+THP+CY		24 A	Other iatrogenic LPD
14	Polyclonal	nd	+	+	=	+	MTX and anti-TNFα withdrawal		7 A(CR)	Other iatrogenic LPD

Abbreviations: *EBV* Epstein–Barr virus, *nd* not done due to no samples available or severe DNA fragmentation, *na* data not available, *CHOP* cyclophosphamide, doxorubicin, vincristine, and prednisolone, *auto-PBSCT* autologous peripheral blood stem cell transplantation, *R* Rituximab, *THP* pirarubicin, *COP* cyclophosphamide, vincristine, and prednisone, *MTX* methotrexate, *allo-BMT* allogeneic bone marrow transplantation, *mPSL* methylprednisolone, *CY* cyclophosphamide, *PSL* predonisolone, *CyA* cyclosporine A, *A* alive, *DT* death due to tumor, *DID* death with intercurrent disease, *PR* partial remission, *CR* complete remission, *HBV* hepatitis B virus, *CAEBV* chronic active EBV infection, *HPS* hemophagocytic syndrome, *PTCL* peripheral T cell lymphoma, *DLBCL* diffuse large B cell lymphoma, *NOS* not otherwise specified, *LPD* lymphoproliferative disorders

$CD20^+$ large lymphoid cells admixed with $CD3^+$ small lymphoid cells (Fig. 3).

In six cases with monoclonal proliferation of T cells, eosinophil infiltration was marked in three. Plasma cells were occasionally seen in all cases. Macrophages were numerous in three cases, with epithelioid cell clusters in one. Immunohistochemically, $CD3^+$ cells were small-to-medium in size, indistinguishable from reactive lymphoid

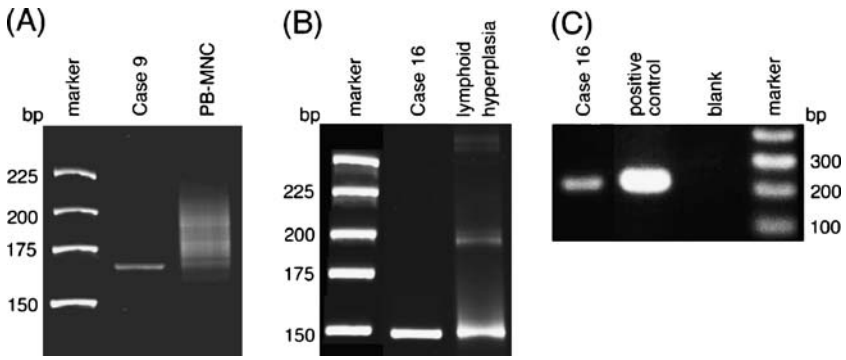

Fig. 1 Clonality analysis using the BIOMED-2 primer set. **a** Case 9 showed T cell monoclonality with the BIOMED-2 TCRG Tube A primer set. **b** Case 16 showed B cell monoclonality with the BIOMED-2 IGK Tube A primer set. **c** t(14;18)(q32;q21) with *BCL2-IGH* rearrangement was also detected in case 16 with the BIOMED-2 t(14;18)(q32;q21) tube A primer set. *PB-MNC* peripheral blood mononuclear cells

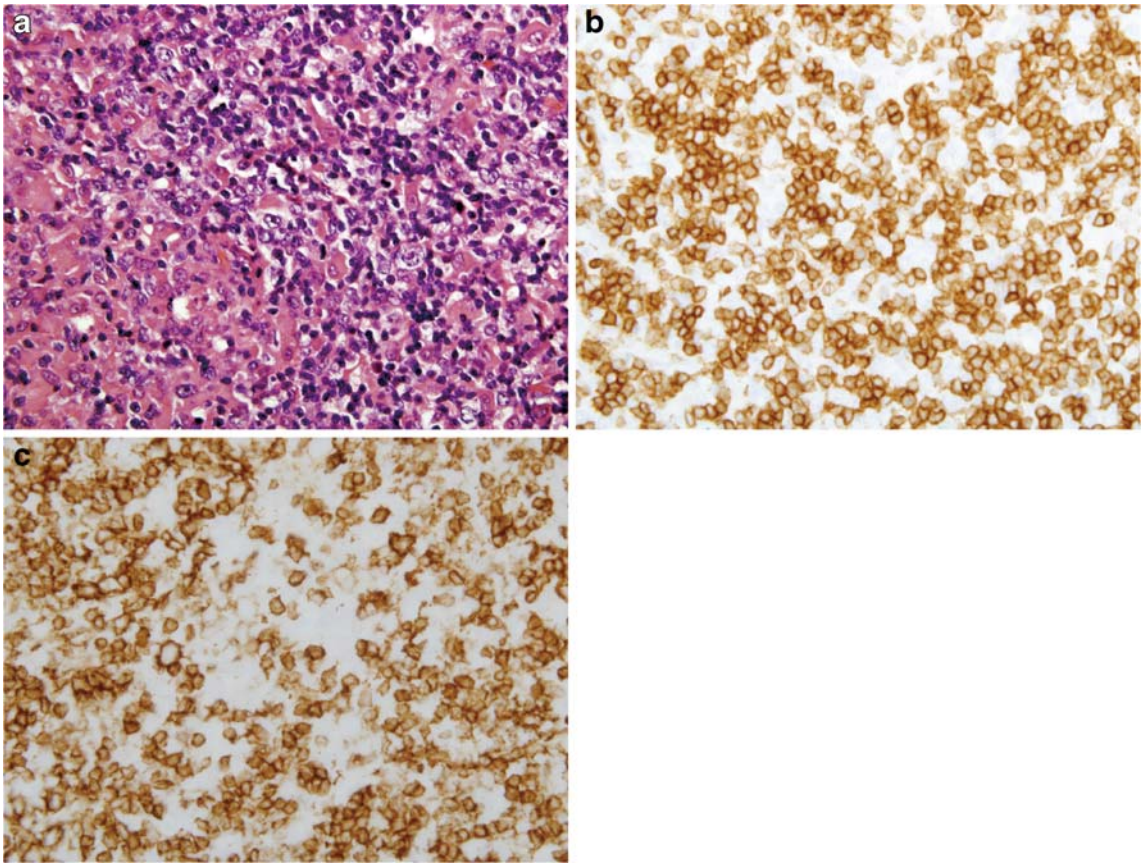

Fig. 2 Diffuse polymorphous proliferation containing large lymphoid cells with prominent nucleoli admixed with small lymphocytes and macrophages in B-LPD (case 18; **a**). An epithelioid cell cluster is seen in the lower left corner. Mitotic figures were seen occasionally (H&E, ×400). Small lymphoid cells were positive for CD3 (**b**), whereas large lymphoid cells were CD20-positive (**c**). This case was classified as diffuse large B cell lymphoma, not otherwise specified, by the WHO classification (2008)

cells. These $CD3^+$ cells were exclusively $CD4^+CD8^-$ in one case, and $CD4^+$ cells predominated or were about equal in number to $CD8^+$ cells in five. $CD20^+$ large lymphoid cells were scattered in four cases.

In one case (case 14) showing polyclonality for B and T cells, large lymphoid cells expressed CD30, but there were no diagnostic RS cells. This case was diagnosed as Hodgkin-like LPD.

Clinicopathological findings in the remaining four cases, in which clonality analysis was not performed, were quite similar to the 15 cases in which it was; thus, it was supposed that these four cases may be neoplastic in nature. Indeed, two of the four patients died due to tumors.

In situ hybridization

RNA in situ hybridization using the EBER-1 probe was performed in all 19 cases. EBV-positive lymphoid cells were detected in eight cases: three of eight cases, four of six cases, and one of one case with monoclonal B, T cell, and polyclonal proliferation. A diagnosis of chronic, active EBV infection was made in two (cases 6 and 7) of these cases at the onset of their LPD. The EBV-positive rate was higher in cases with RA than those without, but not statistically significantly so (p=0.117; Fisher's exact test).

Prognosis

The 3-year overall survival (OS) rate was 49.7±17.3%. Univariate analysis revealed that EBV positivity, history of RA, and B or T cell monoclonality were not prognostic factors. Patients with age ≥70 years showed a worse prognosis than those <70 (33.8±25.1% vs. 57.1±24.9%), but the difference was not statically significant (p=0.091).

Discussion

Through review of clinical and pathological features in more than 4,000 cases of malignant lymphomas and related conditions registered with OLSG, 19 cases (0.43%) were judged to be polymorphous LPD after careful exclusion of reactive changes, PTCL, and HL. Thus, polymorphous LPD is rather rare in Japan. Use of immunosuppressive

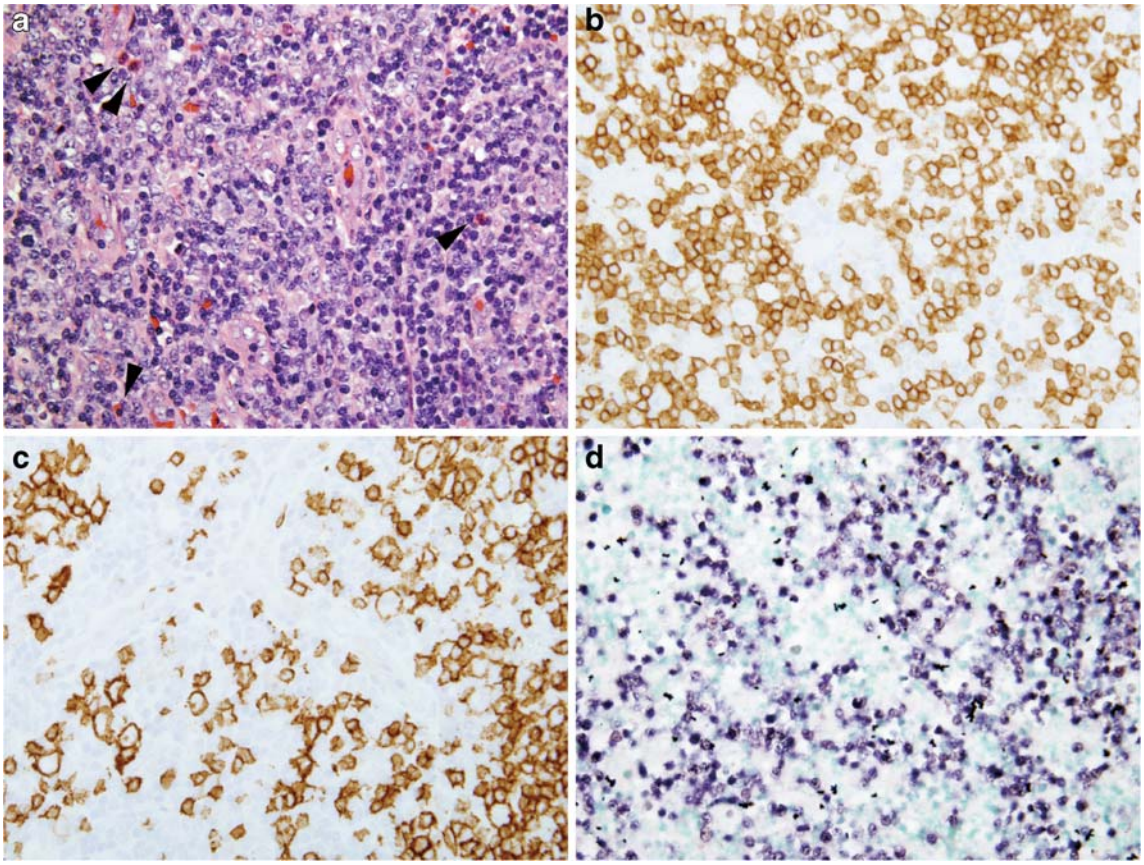

Fig. 3 Diffuse polymorphous cellular proliferation containing medium-to-large lymphoid cells without pleomorphic appearance, small lymphocytes, and eosinophils (*arrowhead*) in T-LPD (case 19; **a**) (H&E, ×400). Small lymphoid cells were CD3-positive (**b**) and medium-to-large lymphoid cells were CD20-positive (**c**). Because PCR clonality analysis by T cell receptor rearrangement revealed T cell clonality, this case was judged to be one of peripheral T cell lymphoma, not otherwise specified, based on the WHO classification (2008). T-LPD and B-LPD could not be distinguished by histological or immunohistochemical features, except for the prominence of eosinophils in the former. In situ hybridization with the EBER-1 probe revealed positive signals in the nucleolus of large lymphoid cells (case 17; **d**)

agents in connection with organ transplantation and AIDS are major causes of polymorphous LPD in Western countries [6–8], but these are less common in Japan [9–11]. This was reflected in the present results: no patient was a transplant recipient or had AIDS.

Molecular analyses revealed that polymorphous LPD was actually a monoclonal proliferation of B (eight cases) or T cells (six cases), intermingled with numerous inflammatory cells. Among 11 cases examined in frozen materials, B or T cell clonality was detected in 10; PCR-based clonality analyses revealed the clonal proliferation of T cells in the remaining case. Except for this case, identical results were obtained between the Southern blot- and PCR-based analyses. Our previous study on MTX-LPD in Japan showed that approximately 80% of cases were B cell in nature [12]. However, the four cases here with MTX-LPD consisted of heterogeneous diseases: T cell LPD with or without EBV, B cell LPD with EBV, and LPD of polyclonal nature with EBV.

The present cases were selected from cases registered with OLSG, based on histological findings of polymorphous composition of proliferation occupying the whole lymph nodal architecture, but devoid of diagnostic RS cells, to exclude HL or medium-to-large T cells with nuclear hyperchromasia and pleomorphic appearances, consisting of multilobed cells, to exclude PTCL-NOS. The proliferating cells were large B-lymphoid cells in the present B cell-proven LPD and medium-to-large T lymphoid cells in T cell-proven LPD. Eosinophils were marked in about half of T-LPD cases, in contrast to the scarcity of eosinophils in the B-LPD cases. One case (case 14) had polyclonal LPD, and the histological picture was HL-like LPD, based on the criteria of Kamel et al. [13].

When the WHO classification (2008) was used, the present 15 cases who underwent clonality analysis were categorized as PTCL-NOS in six cases, DLBCL-NOS in five, EBV^+ DLBCL-E in two, and other iatrogenic LPD in two (Table 2). A possible diagnosis of follicular lymphoma was suggested

in one case of B cell LPD with the BCL2-IGH rearrangement; however, careful observation did not reveal a follicular pattern of proliferation, but showed diffuse proliferation of large B cells, admixed with small T lymphocytes ($CD4^+$= $CD8^+$). This case was tentatively classified as DLBCL-NOS.

Polymorphous LPD is occasionally found in individuals with immunodeficiency conditions. Indeed, six (32%) of the 19 cases had suffered from RA, and two had received MTX (cases 6 and 19), and one each had received MTX and anti-TNFα agents (case 14), MTX and prednisolone (case 11), and prednisolone (case 12; Table 1). Because RA predominantly affects females, inclusion of RA patients resulted in female predominance in the present series.

EBV was detected in eight of 19 (42%) cases: three of four patients with MTX-LPD and five of 15 (33%) non-MTX-LPD cases were EBV-positive. Since Ellman et al.'s first report on lymphoma in a patient with RA who received low-dose MTX [14], a relationship between MTX medication and development of LPD has been discussed [15]. Approximately 50% of MTX-LPD cases are reported to be EBV-positive in the literature [15], and all but one of the present MTX-LPD cases were EBV-positive. MTX may promote the development of EBV-positive lymphomas in RA patients because of its immunosuppressive properties as well as by reactivating latent EBV infection [16]. Previous studies revealed that anti-EBV antibody titers were higher in RA patients, regardless of MTX medication, than in healthy individuals, although proof of a direct causal link between RA and high EBV titer has not been made [17].

The 3-year OS rate in the present series was approximately 50%, which is similar to aggressive non-Hodgkin's lymphoma, where the 5-year OS was reported to be 52% [18]. The four cases with MTX-LPD, including polyclonal LPD (case 14), showed more favorable prognoses. Indeed, when these MTX-LPD cases were excluded, the prognosis in the remaining cases of polymorphous LPD was much worse. Thus, polymorphous LPD should be treated as an aggressive lymphoma. The four cases with no data on clonality of the proliferating cells also tended to show aggressive courses.

In conclusion, the present study showed that polymorphous LPD is (1) quite a rare disease in Japan, (2) MTX-related in some cases, (3) heterogeneous in nature, with mostly monoclonal proliferation of B or T cells, (4) occasionally EBV-associated, and (5) behaves as an aggressive lymphoma. MTX-LPD is a condition closely related to EBV and immunosuppression, and shows a better clinical course than LPD in immunocompetent patients. Polymorphous LPD in the context of immunocompetent patients is biologically and clinically heterogeneous, mostly corresponding to DLBCL or PTCL.

Acknowledgments This study was supported in part by a grant (20014012) from the Ministry of Education, Science, Culture, and Sports, Japan.

Conflict of interest statement We declare that we have no conflict of interest.

References

1. Swerdlow SH, Campo E, Harris NL et al (2008) WHO classification of tumours of haematopoietic and lymphoid tissues. IARC, Lyon
2. Knowles DM (1999) Immunodeficiency-associated lymphoproliferative disorders. Mod Pathol 12:200–217
3. Greer CE, Wheeler CM, Manos MM (1995) PCR amplification from paraffin-embedded tissues: sample preparation and the effects of fixation. In: Dieffenbach CW, Dveksler GS (eds) PCR primer: a laboratory manual. Cold Spring Harbor Laboratory, New York, pp 99–112
4. van Dongen JJ, Langerak AW, Bruggemann M et al (2003) Design and standardization of PCR primers and protocols for detection of clonal immunoglobulin and T-cell receptor gene recombinations in suspect lymphoproliferations: report of the BIOMED-2 Concerted Action BMH4-CT98-3936. Leukemia 17:2257–2317
5. Weiss LM, Jaffe ES, Liu XF et al (1992) Detection and localization of Epstein-Barr viral genomes in angioimmunoblastic lymphadenopathy and angioimmunoblastic lymphadenopathy-like lymphoma. Blood 79:1789–1795
6. Lewin KJ (1997) Post-transplant lymphoproliferative disorders. Pathol Oncol Res 3:177–182
7. Little RF (2003) AIDS-related non-Hodgkin's lymphoma: etiology, epidemiology, and impact of highly active antiretroviral therapy. Leuk Lymphoma 44(Suppl 3):S63–68
8. Martin-Gomez MA, Pena M, Cabello M et al (2006) Posttransplant lymphoproliferative disease: a series of 23 cases. Transplant Proc 38:2448–2450
9. Bando T, Date H, Minami M et al (2008) First registry report: lung transplantation in Japan: The Japanese Society of Lung and Heart-Lung Transplantation. Gen Thorac Cardiovasc Surg 56:17–21
10. Bowman KW, Richard SA (2003) Culture, brain death, and transplantation. Prog Transplant 13:211–215
11. UNAIDS (2007) AIDS epidemic update: December 2007. Joint United Nations Programme on HIV/AIDS (UNAIDS) and the World Health Organization (WHO), Geneva
12. Hoshida Y, Xu JX, Fujita S et al (2007) Lymphoproliferative disorders in rheumatoid arthritis: clinicopathological analysis of 76 cases in relation to methotrexate medication. J Rheumatol 34:322–331
13. Kamel OW, Weiss LM, van de Rijn M et al (1996) Hodgkin's disease and lymphoproliferations resembling Hodgkin's disease in patients receiving long-term low-dose methotrexate therapy. Am J Surg Pathol 20:1279–1287
14. Ellman MH, Hurwitz H, Thomas C et al (1991) Lymphoma developing in a patient with rheumatoid arthritis taking low dose weekly methotrexate. J Rheumatol 18:1741–1743
15. Salloum E, Cooper DL, Howe G et al (1996) Spontaneous regression of lymphoproliferative disorders in patients treated with methotrexate for rheumatoid arthritis and other rheumatic diseases. J Clin Oncol 14:1943–1949
16. Feng WH, Cohen JI, Fischer S et al (2004) Reactivation of latent Epstein-Barr virus by methotrexate: a potential contributor to methotrexate-associated lymphomas. J Natl Cancer Inst 96:1691–1702
17. Toussirot E, Roudier J (2007) Pathophysiological links between rheumatoid arthritis and the Epstein-Barr virus: an update. Joint Bone Spine 74:418–426
18. The International Non-Hodgkin's Lymphoma Prognostic Factors Project (1993) A predictive model for aggressive non-Hodgkin's lymphoma. N Engl J Med 329:987–994

Virchows Arch (2010) 456:277–285
DOI 10.1007/s00428-009-0869-9

ORIGINAL ARTICLE

Genomic profiling reveals subsets of dedifferentiated liposarcoma to follow separate molecular pathways

Ralf J. Rieker · Juergen Weitz · Burkhard Lehner · Gerlinde Egerer · Andrea Mueller · Bernd Kasper · Peter Schirmacher · Stefan Joos · Gunhild Mechtersheimer

Received: 17 September 2009 / Revised: 20 November 2009 / Accepted: 24 November 2009 / Published online: 29 December 2009
© Springer-Verlag 2009

Abstract With the aim to provide more insight into their biology, a series of 79 liposarcomas (LS) representative of all main subtypes was analysed for chromosomal imbalances using comparative genomic hybridization. Based on the genetic data, unsupervised hierarchical clustering unveiled two main LS clusters, each with two subclusters, one comprising three subsets. The first main cluster consisted of one larger subcluster, being characterised by gains/high-level amplifications of chromosomal subregions 12q13–q15, and exclusively included well-differentiated and dedifferentiated LS. A smaller subcluster was set apart on the basis of recurrent gains of 20q13 and 8q24, and mainly comprised pleomorphic and myxoid/round cell LS. The larger subcluster was subdivided into three subsets, one with nearly exclusive overrepresentations of 12q13–q15, the second with additional frequent gains of 1q21–q24, and the third with further recurrent overrepresentations of 6q22–q24, 20q13, and 12q24 and frequent losses of 13q14–q21 and 11q22–q23. While the first subset comprised both well-differentiated and dedifferentiated LS, the second and third subsets entirely included dedifferentiated LS. The second main cluster was characterised by recurrent overrepresentations of 5p13–p15, 1q21–q24, 1p12–p21, and 17p11.2–p12 and essentially comprised pleomorphic and myxoid/round cell LS. A separation of this second main cluster into two subclusters was based on additional gains on 22q13 and losses on 1q42–q43. Genomic profiling reveals genetically distinct subsets of dedifferentiated LS, which are clearly different from pleomorphic, myxoid/round cell, and, for some subsets, from well-differentiated LS. These data indicate that dedifferentiated LS follow separate tumourigenic pathways and that genetic analysis is important to unravel these differences.

Keywords Liposarcoma · Comparative genomic hybridization · Genomic profiling · Cluster analysis

Electronic supplementary material The online version of this article (doi:10.1007/s00428-009-0869-9) contains supplementary material, which is available to authorized users.

R. J. Rieker · A. Mueller · P. Schirmacher · G. Mechtersheimer
Institute of Pathology, University Hospital,
INF 220/221,
69120 Heidelberg, Germany

R. J. Rieker (✉)
Department of Pathology, Medical University Innsbruck,
Muellerstrasse 44,
6020 Innsbruck, Austria
e-mail: ralf.rieker@i-med.ac.at

J. Weitz
Department of Surgery, University Hospital,
INF 110,
69120 Heidelberg, Germany

B. Lehner
Department of Orthopedic Surgery, University Hospital,
Schlierbacher Landstrasse 220,
69118 Heidelberg, Germany

G. Egerer · B. Kasper
Department of Internal Medicine, University Hospital,
INF 410,
69120 Heidelberg, Germany

S. Joos
German Cancer Research Center,
INF 280,
69120 Heidelberg, Germany

Introduction

Liposarcomas (LS) are the most common soft tissue sarcomas in adults and comprise approximately 20% of all

sarcomas. According to the World Health Organization, four main subtypes are distinguished: well-differentiated, dedifferentiated, myxoid/round cell, and pleomorphic LS [1]. The morphological diversity of LS reflects their great variation in biological behaviour ranging from non-metastasizing neoplasms like well-differentiated LS (WDLS) to lipogenic sarcomas with overt metastatic potential like round cell LS or pleomorphic LS (PLLS) [1].

WDLS represent the largest group of lipogenic malignancies and account for about 40–45% of all LS. Cytogenetically, WDLS show characteristic ring and giant marker chromosomes that contain amplified genetic material derived from chromosomal subregions 12q13–q15, as was shown by fluorescence in situ hybridization and comparative genomic hybridization (CGH) [2]. In a number of cases, co-amplification of 1q21–q22 and/or 12q21–q22 is detected [3, 4]. By Southern blot analysis, amplifications of *MDM2*, *CDK4*, *HMGI-C*, and *SAS*, which are located within 12q13–q15, have been identified in WDLS [2, 5].

Dedifferentiated LS (DDLS), originally defined by Evans in 1979 [6], consists of WDLS combined either with a high-grade component resembling high-grade malignant fibrous histiocytoma (MFH) or fibrosarcoma or with a low-grade component having the appearance of fibromatosis or low-grade myxofibrosarcoma [6–10]. About 90% of DDLS contain a dedifferentiated component at primary diagnosis, whereas 10% represent recurrences of WDLS [1, 5, 8]. The behaviour of DDLS is more aggressive than that of pure WDLS, with a local recurrence rate of 41–75%, a distant metastasis rate of 9–20%, and a disease-related mortality rate of 30–50% [8–10]. With respect to the site of origin, patients with retroperitoneal tumours display a significantly worse survival than those with tumours in other sites [9]. Neither low-grade dedifferentiation nor a low percentage of dedifferentiation was associated with an improved outcome in this tumour series comprising 155 DDLS [9]. Yet, it was demonstrated that all seven cases with metastases of a series of 354 retroperitoneal WDLS/DDLS contained more than 50% dedifferentiated elements in their primaries, were exclusively de novo lesions and showed a predominant myxofibrosarcoma-like morphology in most (five out of seven) cases [11]. Similarly to WDLS, however, DDLS most often have ring and marker chromosomes, and also double minutes containing amplified material from 12q13–q15 with *MDM2* and *CDK4* as the main target genes, indicative of a kinship to or even derivation of these tumours from WDLS [2, 5, 12, 13].

Myxoid/round cell LS (MRLS) is the second most common subtype of LS, accounting for more than one-third of LS, and representing about 10% of all adult soft tissue sarcomas. In contrast to other subtypes of LS or other myxoid sarcomas, MRLS tends to metastasize to soft tissues or bone before it spreads to the lungs [14]. MRLS typically shows the reciprocal translocation t(12;16)(q13;p11) or, in a minority of cases, the reciprocal translocation t(12;22)(q13;q12) [13]. Trisomy 8, isochromosome 7q, 6q deletions, and a der(16)t(1;16) have been detected as secondary aberrations in MRLS [13].

PLLS represents the rarest type of LS comprising approximately 5% of all lipogenic sarcomas. Except for the presence of definite evidence of lipoblastic differentiation, the predominant histological pattern of PLLS is often MFH-like, epithelioid/carcinoma-like, or myxofibrosarcoma-like [15, 16]. In general, PLLS is an aggressive mesenchymal neoplasm showing a metastasis rate of 32–43%, particularly to lungs, and an overall tumour-associated mortality of 32–50% [15–17]. In PLLS, complex chromosomal changes without specific rearrangements have been detected in karyotypic analyses [13, 18]. Yet, in previous comparative CGH studies we and others identified distinct and recurrent chromosomal imbalances in PLLS [19–22].

The aim of this study was to compare the patterns of chromosomal copy number changes as detected by CGH in a series of 79 LS comprising representative numbers of all main subtypes. An unsupervised hierarchical clustering was performed in order to unravel genetically separate subgroups of LS. Our data show, that (1) the different subtypes of LS are characterised by sets of distinct and recurrent chromosomal aberrations, and (2) DDLS comprise genetically distinct subsets. We conclude from these data that DDLS follow separate tumourigenic pathways and that genetic analysis is important to unravel these differences.

Materials and methods

Tumour samples

Seventy-nine LS samples from 79 patients obtained between 1989 and 2002 were retrieved from the archives of the Institute of Pathology, University of Heidelberg, Germany. Tumour diagnoses were based on standard histopathological criteria in conjunction with immunohistochemical analysis according to the World Health Organization classification [1]. The histological slides from all cases were reviewed by two independent pathologists (GM and RJR) to confirm the diagnosis and the histological LS subtype. The clinicopathological data of the eight WDLS, the dedifferentiated components of the 37 DDLS, the 14 MRLS, and the 20 PLLS analysed are given in Supplementary Table 1. The dedifferentiated component of the DDLS was MFH-like in 28, fibrosarcoma-like in six, and myxofibrosarcoma-like in three cases. The PLLS were of the undifferentiated pleomorphic high-grade/MFH-like variant with definite evidence of at least focal lipoblastic differentiation in 16, of the epithelioid/carcinoma-like variant in two, and of the myxofibrosarcoma-

like variant in two cases. The CGH results of 23 of the 79 cases have been reported previously [19].

Comparative genomic hybridization

Tumour DNA was isolated from 23 frozen and 56 paraffin-embedded samples. For frozen tissues, tumour sampling for DNA extraction was performed as described previously [19]. For formalin-fixed and paraffin-embedded (FFPE) tissue samples, tumour tissue for DNA extraction was marked on hematoxylin and eosin-stained paraffin tissue slides and manually microdissected from serial paraffin sections (8–10 μm). In DDLS, only the dedifferentiated tumour components were selected for CGH analysis. Extraction of genomic DNA was performed by proteinase K digestion (2 mg/ml in 50 mM Tris-HCl, 1 mM EDTA, 0.5% Tween 20) followed by ethanol precipitation. The reference DNA was isolated from the peripheral blood of healthy individuals or from paraffin-embedded normal placenta tissue.

CGH was performed with minor modifications as reported originally [23]. Briefly, tumour DNA was labelled with biotin-16-dUTP (Roche, Mannheim, Germany), and control DNA was labelled with digoxigenin-11-dUTP (Roche) using nick translation according to the manufacturer´s instructions. Then, 1 μg of biotin-labelled tumour DNA, 1 μg of digoxigenin-labelled control DNA, and 50 μg cot-1-DNA (Gibco/BRL, Gaithersburg, MD, USA) were co-denatured with normal metaphase spreads (Vysis, Downers Grove, IL, USA) in a heat block at 75°C for 7 min, followed by 37°C for 20 min, and hybridised in a humid chamber at 37°C for 48 h. After post-hybridization washes up to a stringency of 0.1 × SSC at 42°C, tumour and control DNA were detected via rhodamin-conjugated anti-digoxigenin and fluorescein-conjugated avidin (Roche), respectively. Chromosomes were counterstained with 4,6-diamino-2-phenylindole (Sigma, München, Germany). Image analysis was performed using an epifluorescence microscope (Axiovert S100, Zeiss, Wetzlar, Germany) with a charged-couple device camera, and the CytoVision 3.52 software package (Applied Imaging, Sunderland, UK) or the ISIS CGH software package (MetaSystems, Altlußheim, Germany). A minimum of ten metaphases was photographed per case, yielding an average of 15 individual specimen of each chromosome used for comparative fluorescence analysis. Pericentromeric subregions 1q11–q12, 9q11–q12, and 16q11.1–q11.2, chromosome subregions 1p32-pter, as well as chromosome 19 and Y were not scored due to a high number of false positive results [23]. The X chromosome was excluded from the analyses since imbalances could not be investigated for all patients because of use of control DNA that did not match the patient´s sex in every case. Fluorescence ratios were determined using both fixed cutoff values (0.75 for losses, 1.25 for gains, and 2.0 for amplifications) and cutoff values with a twofold SD. Only chromosomal aberrations that were detected with both evalution approaches were scored.

Unsupervised hierarchical cluster analysis

Imbalances of 278 chromosomal subbands of a total of 73 LS with chromosomal alterations were analysed by unsupervised hierarchical cluster analysis [24] using the Cluster and TreeView software (version 2.11, http://rana.stanford.edu/software) for uncentered complete linkage clustering. For this purpose, the status of chromosomal subbands from each tumour sample was converted to a score of 1 (gain), 3 (high-level amplification), 0 (balanced), or −1 (loss). Gains/high-level amplifications, losses, and balanced chromosomal subregions were represented in the final map as green, red, and black, respectively.

Statistical analysis

Differences between patient subgroups concerning chromosomal gains and losses, histological tumour subtype, stage, grade, tumour site, and age distribution were assessed using test procedures for categorical data (Chi-square test) or non-parametric test procedures (Kruskal–Wallis test). A test result with a p value less or equal 5% ($p \leq 0.05$) was denoted as significant. No adjustment for multiple testing was applied; therefore, the test results should be interpreted in an exploratory way.

Results

Clinico-pathological data of the liposarcomas

The clinico-pathological data of the LS are given in Supplementary Table 1. The 79 tumour samples analysed comprised eight WDLS, the dedifferentiated components of 37 DDLS, 14 MRLS, and 20 PLLS from 79 patients. Of these tumours, 50 were primary and 29 were recurrent lesions. The patients included 52 men and 27 women with an average age of 58.5 years (range: 29–84 years). The sites of origin of the LS were the retroperitoneum (42 cases), the lower extremity (31 cases), the upper extremity (five cases), and the thoracic wall (one case). WDLS and DDLS were primarily located in the retroperitoneum (5/8 and 31/37 cases), whereas PLLS and MRLS were mainly located in the lower extremity (15/20 and 10/14 cases, respectively; $p<0.0001$). With regard to the French Federation of Cancer Centers (FNCLCC) grading scheme [25], 11 cases were well differentiated (G1), 19 tumours were moderately differentiated (G2), and 49 LS were poorly differentiated (G3). According to the UICC, most tumours were classified as pT2b (45 cases), followed

by rpT2b (25 cases), pT2a and rpT1a (three cases each), pT1b (two cases), and rpT1b (one case). Within the series of DDLS and WDLS, recurrent tumours were significantly more common (24/45 primary vs. 21/45 recurrent cases) as compared to the series of PLLS and MRLS, which comprised mainly primary lesions (26/34 primary vs. 8/34 recurrent cases; $p=0.0358$).

Recurrent numerical chromosomal copy number gains and losses in LS

The DNA copy number changes of the individual tumours are detailed in Supplementary Table 1 and the most recurrent chromosomal imbalances of the different subtypes of LS are given in Table 1.

Except for six MRLS, in all the tumours analysed (i.e., 73/79 cases), at least one chromosomal alteration was found. Within the series of 73 LS with chromosomal aberrations, the number of detected changes varied from 1 to 26/case (average: 9.9/case). Gains of chromosomal material (average: 7.4/case) were found strikingly more frequent than losses (average: 2.5/case; $p=0.0001$). Moreover, the total numbers of detectable chromosomal gains and losses were significantly different between the individual subtypes of LS, being highest in PLLS (average: 15.8 imbalances/case, range: 5–24), followed by DDLS (average: 9.1 imbalances/case, range: 1–26), MRLS (average: 7 imbalances/case, range 2–13), and WDLS (average: 1.8 imbalances/case, range: 1–3; $p<0.0001$).

Within the series of WDLS, the minimal common chromosomal subregions most frequently affected by overrepresentations were on 12q13–q15 (6/8, 75%).

In DDLS, the most recurrent common overrepresentations were identified on 12q13–q15 (36/37, 97%), 12q24 (17/37, 46%), 20q13 (15/37, 41%), as well as 6q22–q24 and 9q33–q34 (each 9/37, 24%). Losses predominantly affected chromosomal subbands 13q14–q21 (13/37, 35%) and 11q22–q23 (8/37, 22%).

Within the series of PLLS, the most frequent common overrepresentations were on 5p13–p15 (13/20, 65%), 20q13 (12/20; 60%), 6p21 and 17p11.2–p12 (each 9/20, 45%), 9q33–q34 (8/20, 40%), 1p12–p21, 1q21–q24, and 22q13 (each 7/20, 35%), as well as 1p31, 12q24, 13q33–q34, and 21q21–q22 (each 6/20, 30% each). Losses mainly affected chromosomal subbands 1q42–q43 and 11q22–q23 (6/20, 30% each), as well as 2q33–q36 and 13q14–q21 (5/20, 25% each).

MRLS displayed recurrent gains of 8q24 and 20q13 (4/14, 29% each), and on 1q21–q24 (3/14, 21%).

Comparing PLLS and DDLS, chromosomal imbalances detected significantly more frequently in PLLS than in DDLS included overrepresentations of 5p13–p15 ($p=0.00017$), 17p11.2–p12 ($p<0.0007$), 13q33–q34 ($p=0.0057$), and 1p12–p21 ($p<0.0003$). Vice versa, overrepresentations of 12q13–q15 were detected significantly more frequent in DDLS than in PLLS ($p<0.0001$).

A total of 99 high level amplifications were identified in 54 tumours ranging from 1 to 5 amplicons per case (Supplementary Table 1). Most commonly involved sub-

Table 1 Recurrent chromosomal imbalances identified by CGH in different subtypes of liposarcoma

WDLS ($n=8$)	DDLS ($n=37$)	PLLS ($n=20$)	MRLS ($n=14$)
Gains			
12q13–q15 (75%)	12q13–q15 (97%)	5p13–p15 (65%)	8q24 (29%)
	12q24 (46%)	20q13 (60%)	20q13 (29%)
	20q13 (41%)	6p21 (45%)	1q21–q24 (21%)
	6q22–q24 (24%)	17p11.2–p12 (45%)	
	9q33–q34 (24%)	9q33–q34 (40%)	
		1p12–p21 (35%)	
		1q21–q24 (35%)	
		22q13 (35%)	
		1p31 (30%)	
		12q24 (30%)	
		13q33–q34 (30%)	
		21q21–q22 (30%)	
Losses			
	13q14–q21 (35%)	11q22–q23 (30%)	
	11q22–q23 (22%)	1q42–q43 (30%)	
		2q33–q36 (25%)	
		13q14–q21 (25%)	

WDLS well-differentiated liposarcoma, *DDLS* dedifferentiated liposarcoma, *PLLS* pleomorphic liposarcoma, *MRLS* myxoid/round cell liposarcoma

regions were detected within chromosomal subbands 12q12–q21 (37 cases), next within 5p13–p15 (ten cases), 6q22–q25 (nine cases), 20q12–q13 (seven cases), 1q21–q25 (six cases), and 12q23–q24 (five cases). High level amplifications were most often observed in DDLS (average: 1.9/case), followed by PLLS (average 1.1/case), and WDLS (average: 0.75/case). MRLS were devoid of any detectable amplicons.

Unsupervised hierarchical cluster analysis

The dendrogram of the 73 clustered tumours with detectable chromosomal imbalances is shown in Fig. 1. Tumours with the highest degree of similarity were grouped in short-branched clusters and further connected to related cases generating higher order clusters of decreasing similarity as indicated by longer branches. The recurrent chromosomal imbalances and the histological subtypes of the LS in the different clusters, subclusters, subgroups, and subsets are given in Table 2.

Hierarchical cluster analysis revealed two main clusters, one (CL1) being characterised by recurrent overrepresentations of 12q13–q15 (39/51 vs. 2/22 cases, $p<0.0001$), the other (CL2) by frequent overrepresentations of 5p13–p15 (13/22 vs. 6/51, $p<0.0001$), 1q21–q24 (11/22 vs. 5/51, $p<0.0001$), 1p12–p21 (8/22 vs. 1/51, $p<0.0001$), and 17p11.2–p12 (8/22 vs. 5/51, $p=0.0069$), as well as recurrent losses of 2q33–q36 (6/22 vs. 0/51, $p=0.0001$) and 1q42–q43 (6/22 vs. 3/51, $p=0.0113$). The number of chromosomal imbalances was much lower in CL1 tumours (average: 7.6/case) than in CL2 cases (average: 14.4/case; $p=0.0002$). CL1 primarily comprised WDLS and DDLS (43/51 cases), while CL2 was essentially composed of PLLS and MRLS (20/22 cases; $p<0.0001$). Regarding the FNCLCC grading scheme, CL1 tumours were significantly associated with low grade malignancy, whereas CL2 tumours were significantly associated with high-grade malignancy ($p=0.0041$). The majority of CL1 cases arose in the retroperitoneum (36/51 cases) while the majority of CL2 cases were located in the lower extremity (14/22; $p=0.0004$).

Within CL1 two main subclusters emerged, the first (CL1a) harbouring recurrent gains/high-level amplifications of 12q13–q15 (36/41 vs. 3/10 cases, $p=0.0001$), and the second (CL1b) frequent overrepresentations of 20q13 (7/10 vs. 11/41, $p=0.0020$) and 8q24 (5/10 vs. 2/41, $p=0.0002$). While CL1a was exclusively composed of WDLS and DDLS (41/41 cases), CL1b mostly included PLLS and MRLS (8/10; $p=0.0006$). The CL1a subcluster was further divided into two subgroups (CL1a1 and CL1a2). CL1a2 tumours differed from CL1a1 cases by recurrent gains of 6q22–q24 (5/9 vs. 4/32 cases, $p=0.0065$), 20q13 (7/9 vs. 4/32, $p=0.0001$), and 12q24 (6/9 vs. 9/32, $p=0.0362$), as well as by frequent losses of 13q14–q21 (6/9 vs. 5/32, $p=0.0026$), and 11q22–q23 (4/9 vs. 3/32, $p=0.0147$). The number of chromosomal imbalances was much lower in CL1a1 tumours (average: 5.3/case) than in CL1a2 cases (average: 12.9/case; $p=0.0025$). CL1a1 comprised both WDLS (8/41 cases) and DDLS (33/41 cases), while CL1a2 was exclusively composed of nine DDLS. Finally, subcluster CL1a1 was split in two subsets (CL1a1-1 and CL1a1-2) based on additional gains of 1q21–q24 in tumours of the second subset (4/10 vs. 1/22 cases, $p=0.0241$). The second subset comprised solely DDLS, which were significantly associated with high-grade malignancy (10/10 vs. 14/22; $p=0.0352$), and which showed a trend to more frequent chromosomal gains (average: 5.9 gains/case), as compared to tumours of the first subset (average: 3.3 gains/case; $p=0.0508$).

The second main cluster, which was characterised by recurrent gains/high-level amplifications of 5p13–p15, 1q21–q24, 1p12–p21, and 17p11.2–p12, primarily included PLLS and a number of MRLS. This cluster was split into two subclusters (CL2a and CL2b) based on additional recurrent gains of 22q13 and losses of 1q42–q43 in the first subcluster (7/14 vs. 0/8 cases, $p=0.0180$ and 6/14 vs. 0/8, $p=0.0339$, respectively).

Overall, with regard to stage (primary vs. recurrent tumour), age, and gender of the patients, there were no significant differences between the genetically distinct tumour clusters, subclusters, subgroups, and subsets.

Discussion

Using CGH and unsupervised hierarchical clustering, we have analysed the patterns of chromosomal imbalances in a comprehensive series of the main subtypes of LS. Our data show, that (1) the different subtypes of LS are characterised by sets of distinct and recurrent chromosomal aberrations, and (2) subsets of DDLS follow different molecular pathways. Therefore, genetic discrimination is a useful complement to conventional pathological evaluation in discriminating histomorphologically similar components of different subtypes or subgroups of LS and improves the insight into the molecular events that drive their biology.

For now, the phenomenon of dedifferentiation in DDLS is essentially considered to be time-dependent. However, progression of dedifferentiation is greatly variable, and thus the prognosis is unpredictable in individual cases. Moreover, about 90% of DDLS exhibit areas of dedifferentiation at the time of primary diagnosis, whereas only roughly 10% are recurrences of WDLS [1, 5, 7]. Therefore, the process of dedifferentiation in LS is presumed to be dependent on additional parameters that are not described by established clinico-pathological features. Several reports have sug-

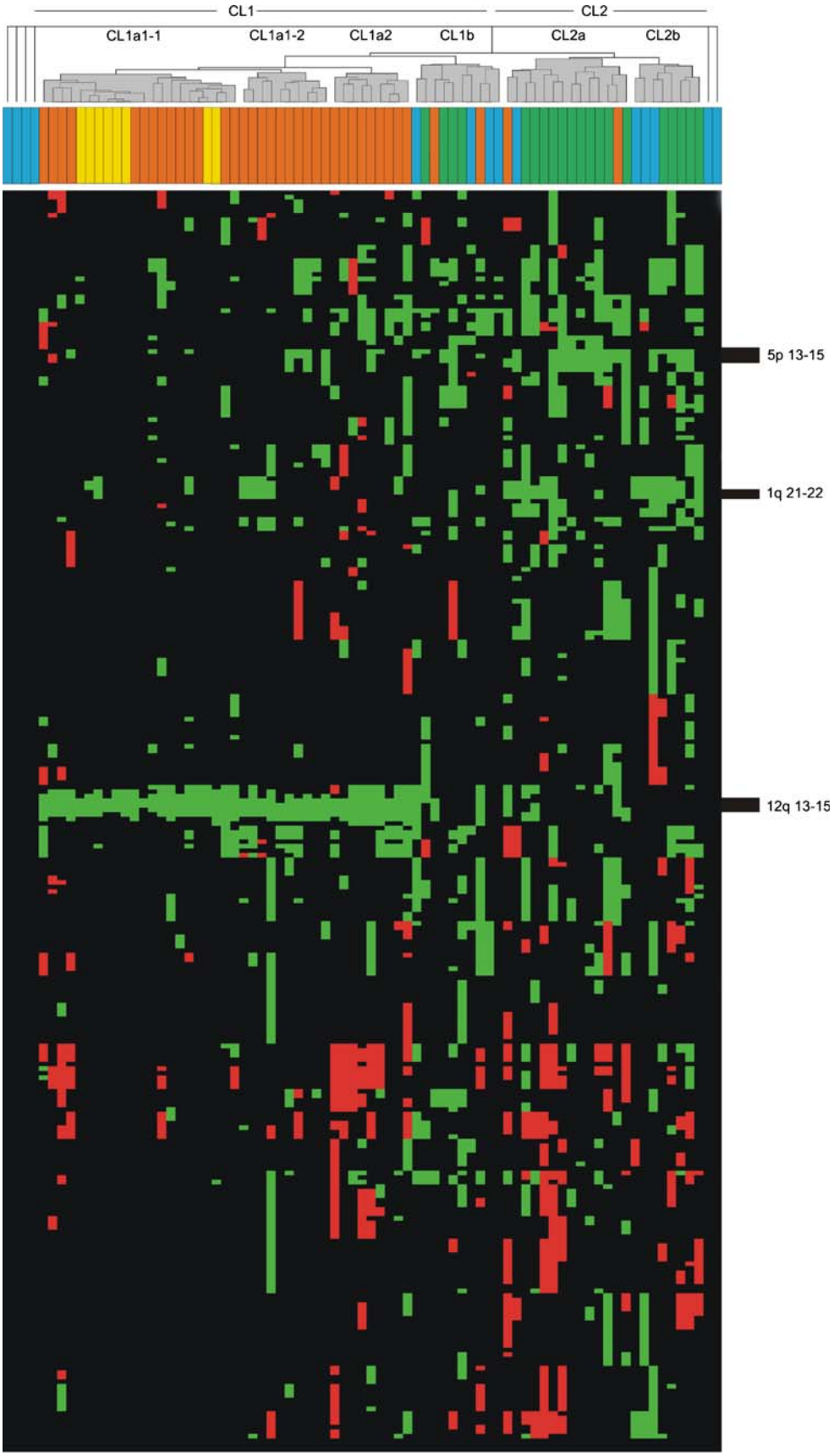

Fig. 1 Unsupervised hierarchical cluster analysis of chromosomal imbalances as identified by CGH in 73 out of 79 liposarcoma samples. The dendogramm shows two main clusters (CL1 and CL2) yielding finally six subsets (CL1a1-1, CL1a1-2, CL1a2, CL1b, CL2a, and CL2b). The liposarcoma subtypes are indicated by *separately coloured bars*: WDLS *yellow*; DDLS *orange*; PLLS *green*; MRLS *blue*. Gains and high-level amplifications (*green squares*) and losses (*red squares*) of 278 chromosomal subregions are displayed below the dendrogram. Each row represents a single chromosomal subregion, each column shows the chromosomal status for a single tumour sample. Selected, cluster-associated chromosomal subregions are indicated on the *right*

Table 2 Characteristics of the separate genomic clusters, subclusters, subgroups, and subsets of liposarcoma

Main clusters	C1 (*n*=51)				C2 (*n*=22)	
					+5p13–p15, +1q21–q24, +1p12–p21, +17p11.2–p12, −2q33–q36	
	WDLS (*n*=8), DDLS (*n*=35), PLLS (*n*=4), MRLS (*n*=4)				DDLS (*n*=2), PLLS (*n*=16), MRLS (*n*=4)	
Sub-clusters	C1a (*n*=41) +12q13–q15			C1b (*n*=10)	C2a (*n*=14)	C2b (*n*=8)
	WDLS (*n*=8), DDLS (*n*=33)					
Sub-groups	C1a1 (*n*=32) +12q13–q15		C1a2 (*n*=9)			
	WDLS (*n*=8), DDLS (*n*=24)					
Subsets	C1a1-1 (*n*=22)	C1a1-2 (*n*=10)				
	+12q13–q15	+12q13–q15	+12q13–q15	+20q13, +8q24	+5p13–p15, +1q21–q24, +1p12–p21, +17p11.2–p12, −2q33–q36	+5p13–p15, +1q21–q24, +1p12–p21, +17p11.2–p12, −2q33–q36
		+1q21–q24	+6q22–q24, +20q13, +12q24, −13q14–q21, −11q22–q23		+22q13, −1q42–q43	
	WDLS (*n*=8), DDLS (*n*=14)	DDLS (*n*=10)	DDLS (*n*=9)	DDLS (*n*=2), PLLS (*n*=4), MRLS (*n*=4)	DDLS (*n*=2), PLLS (*n*=11), MRLS (*n*=1)	PLLS (*n*=5), MRLS (*n*=3)

WDLS well-differentiated liposarcoma, *DDLS* dedifferentiated liposarcoma, *PLLS* pleomorphic liposarcoma, *MRLS* myxoid/round cell liposarcoma

gested an association between dedifferentiation and the altered expression of specific proteins such as MDM2, p53, H-ras, β-catenin, and retinoblastoma protein [12, 26–29]. Also, chromosomal imbalances additionally to overrepresent 12q13–q15 were more frequent in DDLS than in WDLS [19]. Thus far, however, there are only very few studies naming molecular features, which might define separate subsets of DDLS. These include differences in terms of MDM2 and p53 involvement in retroperitoneal vs. non-retroperitoneal WDLS/DDLS [12], and differences with respect to gene expression profiles in subsets of DDLS within a comprehensive series of all subtypes of LS analysed by use of a human genome oligonucleotide array [30].

Notably, within our series of DDLS, three genetically distinct subsets emerged, which were not only different from each other but also from PLLS and MRLS. One subset shared in common with WDLS frequent gains and high-level amplifications of chromsomal subregions 12q13–q15 in the absence of further recurrent chromosomal aberrations. These data corroborate the view that overrepresentations of 12q13–q15 with *MDM2* and *CDK4* as pathogenetically relevant genes are central in the initiation of both WDLS and DDLS [2, 5, 12, 13]. In addition to overrepresentations of 12q13–q15, the second and third tumour subsets, which were each exclusively composed of DDLS and thus separated from WDLS, harboured also gains of 1q21–q24 and gains of 6q22–q24, 20q13, and 12q14 as well as losses of 13q14–q21 and 11q22–q23, respectively. We deduce from these data that different molecular pathways are followed by subsets of DDLS, which, additionally to *MDM2* on 12q14.3–q15 and *CDK4* on 12q14 involve particular genes on chromosome arms 1q, 6q, 11q, 12q, 13q, and 20q.

The second subset of DDLS, which was characterised by recurrent overrepresentations of 1q21–q24 additionally to gains/high level amplifications of 12q13–q15, was associated with high-grade malignancy as compared to the DDLS included in the first subset. Interestingly, overrepresentations of 1q21–q24 were also frequently observed in our series of PLLS and MRLS and in other types of sarcoma such as leiomyosarcoma and MFH [3]. Moreover, the occurrence of 1q22–q24 overrepresentation was shown to be associated with the dedifferentiation of a WDLS to a highly malignant metastatic osteosarcoma [31]. Yet, contrasting to our data on infrequent gains of 1q21–q24 in WDLS, overrepresentations of 1q21–q22 were also described in subsets of WDLS of other series [3, 21].

Regarding the third subset of DDLS, one of the discriminating genetic features of the tumours included in this subset was a frequent overrepresentation of 6q22–q24. Within this chromosomal subregions, *ASK1*, a member of the JNK–MAPK pathway, also known as *MAPK5K,* is a promising target gene. *ASK1*, which inhibits adipocyte

differentiation, has been identified as a target gene of 6q23 amplifications in retroperitoneal MFH, which also harboured amplifications of 12q14–q15 and were suggested to correspond to undifferentiated LS [32]. Treatment of a cell line derived from one of these retroperitoneal MFH/undifferentiated LS cases with thioredoxin, a well-known inhibitor of *ASK1*, led to dramatic modifications of morphology and progressive accumulation of lipid droplets [32]. With respect to the recurrent losses of chromosomal subbands 13q14–q21, which were also characteristic of the third subset of DDLS, one of the promising candidate genes included in this region is the *retinoblastoma-1 (RB1)* gene located at 13q14. *RB1* was found to show more prominent loss of heterozygosity (LOH) in DDLS as compared to WDLS [28]. Furthermore, in an independent study, dedifferentiated components of DDLS showed LOH of *RB1* and abnormal retinoblastoma protein expression more frequently than noted in the well-differentiated components and the dedifferentiated components of some cases harboured mutations and promoter methylation, whereas none of these alterations were seen in the well-differentiated components [29]. Overrepresentation of 12q24, which was a recurrent finding in the third subset of DDLS as well has also been frequently observed in another type of high grade sarcoma, namely malignant peripheral nerve sheath tumour (MPNST) [32], while being mostly absent in WDLS [2–4, 21]. Unlike differences relating to the tumour grade, there were no differences with respect to the site of origin and stage (primary vs. recurrent) between the DDLS forming the genetically different tumour subsets in our series of LS.

In contrast to the complex chromosomal changes with nonrandom rearrangements found in karyotypic analysis of PLLS, we and others identified recurrent chromosomal imbalances in PLLS by use of CGH [19–22]. In corroboration of our previous data on a smaller tumour series, a number of recurrent chromosomal imbalances, namely overrepresentations of 5p13–p15, 17p11.2–p12, 1p12–p21, and also 13q33–q34, correlated significantly with PLLS as compared to DDLS. Based on these and further recurrent chromosomal imbalances, the vast majority of PLLS supplemented by a number of MRLS were included in the second main cluster of our series of LS, and thus separated from the majority of DDLS.

Recurrent gains and high level amplifications of chromosomal subregion 5p13–p15, one of the distinguishing genetic features of the second main cluster of LS, which was significantly associated with high grade malignancy, are also known from other high grade sarcomas such as leiomyosarcomas (LMS), MFH, and MPNST [33–36]. Using a DNA microarray including 418 BAC clones representing 99% of chromosome arm 5p, we found *TRIO*, *IRX2*, and *NKD2* to be frequently affected by high-level amplifications as well upregulated in a gene–dosage dependent manner in a series of high grade sarcomas which comprised PLLS, DDLS, MFH, and MPNST [36]. Therefore, these genes represent candidate targets of 5p amplifications in soft tissue sarcomas and might play a crucial role during the progression of these tumours. Interestingly, gains of 5p were found to be associated with an unfavourable clinical course in LMS [36]. Overrepresentations on 17p11.2–p12 were shown to be a recurrent feature of other high-grade sarcomas such as LMS [34, 35, 37] and osteosarcomas as well [38]. Given the recurrent overrepresentations of 5p13–p15 and 17p11.2–p12 in PLLS and in other non-lipogenic high-grade sarcomas, but not in DDLS, these chromosomal subregions might contain genes contributing to the recognised more aggressive behaviour of PLLS as compared to DDLS [8–10, 15–17].

We are not aware of a specific bias introduced in our collective, but the power for statistical comparison was reduced by the lower number of WDLS compared to DDLS and by the partial use of FFPE tissues, for which a lower sensitivity for genomic imbalances cannot be excluded.

In conclusion, our study shows that PLLS display recurrent chromosomal alterations, some of which are shared by a subset of MRLS, but which are significantly different from those characteristically found in DDLS and WDLS. Furthermore, based on their genomic profiles, DDLS are divided in distinct subsets, which are partly associated to grade and different from WDLS. Thus, subsets of DDLS appear to follow separate tumourigenic pathways and genetic analysis is important to unravel these differences.

Acknowledgements The skilful technical and photographic assistance of Marion Moock and John Moyers is gratefully acknowledged. This study was supported by the Tumorzentrum Heidelberg/Mannheim, Germany (FSPI.1) and the Deutsche Krebshilfe.

Conflict of interest The authors declare that they have no conflict of interest.

References

1. Fletcher CDM, Unni K, Mertens K (2002) WHO classification of tumours. Pathology and genetics of tumours of soft tissue and bone. IARC Press, Lyon
2. Pedeutour F, Forus A, Coindre J-M et al (1999) Structure of supernumerary ring and giant rod chromosomes in adipose tissue tumors. Genes Chromosomes Cancer 24:30–41
3. Forus A, Weghuis DO, Smeets D et al (1995) Comparative genomic hybridization analysis of human sarcomas: I. occurrence of genomic imbalances and identification of a novel major amplicon at 1q21–q22 in soft tissue sarcomas. Genes Chromosomes Cancer 14:8–14
4. Szymanska J, Virolainen M, Tarkkanen M et al (1997) Overrepresentation of 1q21–23 and 12q13–21 in lipoma-like liposarcomas but not in benign lipomas: a comparative genomic hybridization study. Cancer Genet Cytogenet 99:14–18

5. Dei Tos AP, Doglioni C, Piccinin S et al (2000) Coordinated expression and amplification of the MDM2, CDK4, and HMGI-C genes in atypical lipomatous tumours. J Pathol 190:531–536
6. Evans HL (1997) Liposarcoma: a study of 55 cases with a reassessment of its classification. Am J Surg Pathol 3:507–523
7. Weiss SW, Rao VK (1992) Well-differentiated liposarcoma (atypical lipoma) of deep soft tissue of the extremities, retroperitoneum, and miscellaneous sites. A follow-up study of 92 cases with analysis of the incidence of "dedifferentiation". Am J Surg Pathol 16:1051–1058
8. McCormick D, Mentzel T, Beham A, Fletcher CDM (1994) Dedifferentiated liposarcoma. Clinicopathologic analysis of 32 cases suggesting a better prognostic subgroup among pleomorphic sarcomas. Am J Surg Pathol 18:1213–1223
9. Henricks WH, Chu Y-C, Goldblum JR, Weiss SW (1997) Dedifferentiated liposarcoma: a clinicopathological analysis of 155 cases with a proposal for an expanded definition of dedifferentiation. Am J Surg Pathol 21:271–281
10. Hasegawa T, Seki K, Hasegawa F et al (2000) Dedifferentiated liposarcoma of retroperitoneum and mesentery: varied growth patterns and histological grades: a clinicopathologic study of 32 cases. Hum Pathol 31:717–727
11. Huang H-Y, Brennan MF, Singer S, Antonescu CR (2005) Distant metastasis in retroperitoneal dedifferentiated liposarcoma is rare and rapidly fatal: a clinicopathological study with emphasis on the low-grade myxofibrosarcoma-like pattern as an early sign of dedifferentiation. Mod Pathol 18:976–984
12. Pilotti S, Della Torre G, Lavarino C et al (1997) Distinct mdm2/p53 expression patterns in liposarcoma subgroups: implications for different pathogenetic mechanisms. J Pathol 181:14–24
13. Sandberg AA (2004) Updates on the cytogenetics and molecular genetics of bone and soft tissue tumors: liposarcoma. Cancer Genet Cytogenet 155:1–24
14. Kilpatrick SE, Doyon J, Choong PFM, Sim FH, Nascimento AG (1996) The clinicopathologic spectrum of myxoid and round cell liposarcoma. A study of 95 cases. Cancer 77:1450–1458
15. Gebhard S, Coindre J-M, Michels J-J et al (2002) Pleomorphic liposarcoma: clinicopathologic, immunohistochemical, and follow-up analysis of 63 cases. Am J Surg Pathol 26:601–616
16. Hornick JL, Bosenberg MW, Mentzel T et al (2004) Pleomorphic liposarcoma. Clinicopathologic analysis of 57 cases. Am J Surg Pathol 28:1257–1267
17. Downes KA, Goldblum JR, Montgomery EA, Fisher C (2001) Pleomorphic liposarcoma. A clinicopathologic analysis of 19 cases. Mod Pathol 14:179–184
18. Mertens F, Fletcher CDM, Dal Cin P et al (1998) Cytogenetic analysis of 46 pleomorphic soft tissue sarcomas and correlation with morphologic and clinical features: a report of the CHAMP study group. Genes Chromosomes Cancer 22:16–25
19. Rieker RJ, Joos S, Bartsch C et al (2002) Distinct chromosomal imbalances in pleomorphic and in high-grade dedifferentiated liposarcomas. Int J Cancer 99:68–73
20. Fritz B, Schubert F, Wrobel G et al (2002) Microarray-based copy number and expression profiling in dedifferentiated and pleomorphic liposarcoma. Cancer Res 62:2993–2998
21. Schmidt H, Bartel F, Kappler M et al (2005) Gains of 13q are correlated with a poor prognosis in liposarcoma. Mod Pathol 18:638–644
22. Ibdaih A, Coindre J-M, Derré J et al (2005) Myxoid malignant fibrous histiocytoma and pleomorphic liposarcoma share very similar genomic imbalances. Lab Invest 85:176–181
23. Kallioniemi OP, Kallioniemi A, Piper J et al (1994) Optimizing comparative genomic hybridization for analysis of DNA sequence copy number changes in solid tumors. Genes Chromosomes Cancer 10:231–243
24. Eisen MB, Spellman ST, Brown PO, Botstein D (1998) Cluster analysis and display of genome-wide expression patterns. Proc Natl Acad Sci USA 95:14863–14868
25. Guillou L, Coindre JM, Bonichon F et al (1997) Comparative study of the National Cancer Institute and French Federation of Cancer Centers Sarcoma Group grading systems in a population of 410 adult patients with soft tissue sarcoma. J Clin Oncol 15:350–362
26. Sakamoto A, Oda Y, Adachi T et al (2001) H-ras oncogene mutation in dedifferentiated liposarcoma. Polymerase chain reaction-restriction fragment length polymorphism analysis. Am J Clin Pathol 115:235–242
27. Sakamoto A, Oda Y, Adachi T et al (2002) Beta-catenin accumulation and gene mutation in exon 3 in dedifferentiated liposarcoma and malignant fibrous histiocytoma. Arch Pathol Lab Med 126:1071–1078
28. Schneider-Stock R, Boltze C, Jaeger V et al (2002) Significance of loss of heterozygosity of the RB1 gene during tumour progressin in well-differentiated liposarcomas. J Pathol 197:654–660
29. Takahira T, Oda Y, Tamiya S et al (2005) Alterations of the RB1 gene in dedifferentiated liposarcoma. Mod Pathol 18:1461–1470
30. Singer S, Socci ND, Ambrosini G et al (2007) Gene expression profiling of liposarcoma identifies distinct biological types/subtypes and potential therapeutic targets in well-differentiated and dedifferentiated liposarcoma. Cancer Res 67:6626–6636
31. Forus A, Larramendy ML, Meza-Zepeda LA et al (2001) Dedifferentiation of a well-differentiated liposarcoma to a highly malignant metastatic osteosarcoma: amplification of 12q14 at all stages and gain of 1q22–q24 associated with metastases. Cancer Genet Cytogenet 125:100–111
32. Chibon F, Martiani O, Derrė J et al (2004) ASK1 (MAP3K5) as a potential therapeutic target in malignant fibrous histiocytoma with 12q14–q15 and 6q23 amplifications. Genes Chromosomes Cancer 40:32–37
33. Mechtersheimer G, Otaňo-Joos M, Ohl S et al (1999) Analysis of chromosomal imbalances in sporadic and NF1-associated peripheral nerve sheath tumors by comparative genomic hybridization. Genes Chromosomes Cancer 25:362–369
34. El-Rifai W, Sarlomo-Rikala M, Knuutila S, Miettinen M (1998) DNA copy number changes in development and progression of leiomyosarcomas of soft tissues. Am J Pathol 153:985–990
35. Otaňo-Joos M, Mechtersheimer G, Ohl S et al (2000) Detection of chromosomal imbalances in leiomyosarcoma by comparative genomic hybridization and interphase cytogenetics. Cytogenet Cell Genet 90:86–92
36. Adamowicz M, Radlwimmer B, Rieker RJ et al (2006) Frequent amplifications and abundant expression of TRIO, NKD2, and IRX2 in soft tissue sarcomas. Genes Chromosomes Cancer 45:829–838
37. Wang R, Titley JC, Lu Y-J et al (2003) Loss of 13q14–q21 and gain of 5p14-pter in the progression of leiomyosarcoma. Mod Pathol 16:778–785
38. Lau CC, Harris CP, Lu X-Y et al (2004) Frequent amplification and rearrangement of chromosomal bands 6p12–p21 and 17p11.2 in osteosarcoma. Genes Chromosomes Cancer 79:11–21

Virchows Arch (2010) 456:287–300
DOI 10.1007/s00428-009-0873-0

ORIGINAL ARTICLE

A tumor-specific cellular environment at the brain invasion border of adamantinomatous craniopharyngiomas

Stefanie Burghaus · Annett Hölsken · Michael Buchfelder · Rudolf Fahlbusch · Beat M. Riederer · Volkmar Hans · Ingmar Blümcke · Rolf Buslei

Received: 31 August 2009 / Revised: 20 November 2009 / Accepted: 6 December 2009 / Published online: 13 January 2010
© Springer-Verlag 2010

Abstract Craniopharyngiomas (CP) are benign epithelial tumors of the sellar region and can be clinicopathologically distinguished into adamantinomatous (adaCP) and papillary (papCP) variants. Both subtypes are classified according to the World Health Organization grade I, but their irregular digitate brain infiltration makes any complete surgical resection difficult to obtain. Herein, we characterized the cellular interface between the tumor and the surrounding brain tissue in 48 CP (41 adaCP and seven papCP) compared to non-neuroepithelial tumors, i.e., 12 cavernous hemangiomas, 10 meningiomas, and 14 metastases using antibodies directed against glial fibrillary acid protein (GFAP), vimentin, nestin, microtubule-associated protein 2 (MAP2) splice variants, and tenascin-C. We identified a specific cell population characterized by the coexpression of nestin, MAP2, and GFAP within the invasion niche of the adamantinomatous subtype. This was especially prominent along the finger-like protrusions. A similar population of presumably astroglial precursors was not visible in other lesions under study, which characterize them as distinct histopathological feature of adaCP. Furthermore, the outer tumor cell layer of adaCP showed a distinct expression of MAP2, a novel finding helpful in the differential diagnosis of epithelial tumors in the sellar region. Our data support the hypothesis that adaCP, unlike other non-neuroepithelial tumors of the central nervous system, create a tumor-specific cellular environment at the tumor–brain junction. Whether this facilitates the characteristic infiltrative growth pattern or is the consequence of an activated Wnt signaling pathway, detectable in 90% of these tumors, will need further consideration.

Keywords Craniopharyngioma boundary · Neuropathology · Immunohistochemistry · Immunofluorescence · Precursor cells · MAP2

S. Burghaus · A. Hölsken · I. Blümcke · R. Buslei (✉)
Department of Neuropathology, University Hospital of Erlangen,
Schwabachanlage 6,
91054 Erlangen, Germany
e-mail: rolf.buslei@uk-erlangen.de

M. Buchfelder
Department of Neurosurgery, University Hospital of Erlangen,
Erlangen, Germany

R. Fahlbusch
International Neuroscience Institute,
Hannover, Germany

B. M. Riederer
Institut de Biologie Cellulaire/Morphologie, Université Lausanne,
Lausanne, Switzerland

V. Hans
Department of Neuropathology,
Evangelisches Krankenhaus Bielefeld,
Bielefeld, Germany

Introduction

Craniopharyngiomas (CP) are rare epithelial tumors with an incidence of 0.13 cases per 100,000 persons per year [1]. Although occurring at any age, they are the most common non-neuroepithelial CNS neoplasms in children, accounting for 5–10% of intracranial tumors in this age group [2, 3]. Two different forms have to be distinguished histologically and clinically: a more frequent adamantinomatous (adaCP) from a papillary subtype (papCP). Activating β-catenin mutations as well as aberrant nuclear β-catenin accumulation are hallmarks of adaCP, setting them apart from other cystic lesions of the sellar region [4–7]. CP are thought to derive from remnants of Rathke's pouch epithelium which explains their usual location in close relation to the

pituitary, the pituitary stalk, and the hypothalamus. Although benign in histological appearance, these tumors are often associated with unfavorable and occasionally disastrous sequelae which still cause controversy in treatment strategies and management [8–12]. A major challenge are finger-like tumor protrusions into the surrounding brain parenchyma which makes gross total removal difficult to obtain and accounts for tumor relapse [13]. Brain invasion of adaCP also affects the hypothalamus, which is one of the major players in food intake control. Endocrinological deficits including fatal obesity have been reported following radical surgery. Proved prognostic factors for the risk of recurrence/regrowth include a small tumor size (<4 cm), a favorable localization, complete surgical resection, patients' age (>5 years), and the absence of severe hypothalamic involvement [11, 14–17]. Even though the growth pattern is so important for treatment and outcome of these tumors, the tumor–brain interface of CP has not been explored in detail. In the present study, we have characterized the transition zone of CP and compared the findings with that of various other non-neuroepithelial tumors including cavernous hemangiomas, meningiomas, as well as metastases. All these lesions are sharply delineated from surrounding brain tissue, invade for only short distances, and form cellular aggregates. Depending on the tumor type, they exhibit a varying amount of gliosis, hemosiderin deposits and hypoxic cell damage in the extracellular matrix (ECM) of the central nervous system (CNS) surrounding the lesion. To determine possible similarities and differences in the cellular response of the affected brain parenchyma, we analyzed the area up to 500 μm surrounding the tumor boundary using immunohistochemistry and double immunofluorescence. Thereby, we focused on the expression patterns of glial fibrillary acid protein (GFAP), microtubule-associated protein 2 (MAP2), nestin, vimentin, and tenascin-C (TN-C).

Nestin, GFAP, and vimentin are intermediate filament proteins, the latter being well-established diagnostic markers for reactive astrocytes (both), astroglial tumors (GFAP), as well as a broad spectrum of mesenchymal cell types and lesions (vimentin). Nestin is a major component of the developing cytoskeleton in radial glia cells, germinal matrix cells [18], as well as adult neural precursors [19]. Nestin is considered as neuroepithelial stem/progenitor cell marker but can be observed also in endothelial cells [20, 21].

TN-C is a multifunctional ECM glycoprotein often expressed at locations of mesenchymal–epithelial interaction during development as well as in the neovasculature and stroma of undifferentiated tumors [22]. The expression of tenascin is associated with development and growth under normal and pathological conditions, whereas the distribution in normal adult tissue is restricted. Tenascin is almost absent in the mature brain [23–25], but ubiquitously expressed by malignant gliomas [26] and plays a major role in shaping axonal guidance during CNS development [27].

The MAP2 epitope is a well-established marker for ganglion cells in the CNS, the spinal cord, the autonomous nervous system, and the vegetative nervous system. It binds to and stabilizes microtubules and is involved in cell proliferation as well as neuronal differentiation [28–30]. Each MAP2 transcript is the result of alternative splicing of a single gene located on human chromosome 2 [31–33]. The cellular expression of MAP2 and its splice forms are precisely regulated during brain development as well as in mature nervous tissue [28]. The embryonic splice variant MAP2e can be detected also in neuroepithelial tumors, thus serving as a useful diagnostic tool [34]. Since a specific antibody detecting only the embryonal form is not available, we applied an antibody against the adult transcript of MAP2 (MAP2a+b) as well as an antibody detecting both the adult and the embryonic form (MAP2c).

In this study, we microscopically investigated the specific cellular pattern within the borderzone of CP and other non-neuroepithelial tumors to better characterize the interplay between solid tumor parts and the adjacent brain parenchyma. This data will be an important basis for further experimental strategies addressing molecular signaling pathways of epithelial tumor formation and infiltration into the CNS.

Materials and methods

Surgical and biopsy specimens from 180 patients with CP were reviewed from the archives of the Department of Neuropathology at the University Hospital of Erlangen, the International Neuroscience Institute Hannover, and the Evangelic Hospital in Bielefeld. Only those 48 specimens were included into this study (with time of surgery [TOS], 1993–2008) in which sufficient amount of central nervous tissue along the tumor boundary could by microscopically identified. The same applied for meningiomas (n=10; TOS, 2003–2007), cavernous hemangiomas (n=12; TOS, 2004–2007), and metastatic tumors (n=14; TOS, 2003–2007). Each specimen was classified according to World Health Organization (WHO) guidelines using hematoxylin and eosin staining as well as a panel of well-established immunohistochemical markers in the differential diagnosis of tumors of the CNS, whenever needed [35].

Neuropathological examination and immunohistochemistry

An immunohistochemical examination of all surgical specimens was performed using the following panel of antibodies and respective dilutions: GFAP (1:800, monoclonal, clone 6F2; Dako, Glostrup, Denmark), nestin (1:5,000, polyclonal; Chemicon, Billerica, USA), TN-C (1:50, monoclonal, clone

Table 1 Summary of clinical data in patients with adaCP (n=41), papCP (n=7), cavernous hemangiomas (n=12), meningiomas (n=10), and metastases (n=14)

Case no.	Diagnosis	Sex	Age [years]	TOS [year]
1	adaCP	f	2	1996
2	adaCP	f	3	2002
3	adaCP	f	4	2007
4	adaCP	f	4	2008
5	adaCP	m	8	2000
6	adaCP	m	9	2000
7	adaCP	f	9	2004
8	adaCP	m	10	2005
9	adaCP	m	10	2005
10	adaCP	f	12	2006
11	adaCP	f	12	2006
12	adaCP	m	13	2007
13	adaCP	f	14	1999
14	adaCP	m	15	2006
15	adaCP	f	16	2002
16	adaCP	f	17	2001
17	adaCP	m	19	2001
18	adaCP	m	20	2004
19	adaCP	m	22	2001
20	adaCP	m	24	2006
21	adaCP	f	26	2003
22	adaCP	m	27	2004
23	adaCP	m	28	2000
24	adaCP	m	29	2006
25	adaCP	f	29	2004
26	adaCP	m	32	1999
27	adaCP	f	33	1994
28	adaCP	m	35	2006
29	adaCP	f	35	2006
30	adaCP	m	42	1995
31	adaCP	f	43	2003
32	adaCP	m	49	2007
33	adaCP	f	54	2007
34	adaCP	f	55	2001
35	adaCP	m	56	2005
36	adaCP	m	58	1993
37	adaCP	f	60	1997
38	adaCP	f	67	1994
39	adaCP	f	68	2002
40	adaCP	m	70	2006
41	adaCP	m	70	2003
		f=20, m=21	Mean=29.5	
42	papCP	m	19	2005
43	papCP	m	28	2004
44	papCP	f	42	2004
45	papCP	f	49	2005
46	papCP	f	56	2006
47	papCP	m	57	2006

Table 1 (continued)

Case no.	Diagnosis	Sex	Age [years]	TOS [year]
48	papCP	m	60	2004
		f=3, m=4	Mean=44.4	
49	Cavernous hemangioma	m	20	2007
50	Cavernous hemangioma	m	22	2007
51	Cavernous hemangioma	m	24	2007
52	Cavernous hemangioma	m	25	2006
53	Cavernous hemangioma	f	28	2006
54	Cavernous hemangioma	f	31	2004
55	Cavernous hemangioma	f	37	2007
56	Cavernous hemangioma	m	41	2005
57	Cavernous hemangioma	m	42	2005
58	Cavernous hemangioma	f	55	2007
59	Cavernous hemangioma	m	63	2006
60	Cavernous hemangioma	m	64	2004
		f=4, m=8	Mean=37.7	
61	Meningioma (WHO grade I)	f	48	2004
62	Meningioma (WHO grade I)	f	56	2004
63	Meningioma (WHO grade I)	m	63	2004
64	Meningioma (WHO grade I)	f	68	2004
65	Atypical meningioma (WHO grade II)	f	22	2005
66	Atypical meningioma (WHO grade II)	m	50	2005
67	Atypical meningioma (WHO grade II)	m	68	2006
68	Atypical meningioma (WHO grade II)	m	80	2003
69	Clear cell meningioma (WHO grade II)	f	69	2007
70	Anaplastic meningioma (WHO grade III)	f	73	2003
		f=6, m=4	Mean=59.7	
71	Adenocarcinoma (breast carcinoma)	f	49	2007
72	Adenocarcinoma (breast carcinoma)	f	52	2007
73	Adenocarcinoma (lung carcinoma)	f	59	2007
74	Adenocarcinoma (lung carcinoma)	f	65	2004
75	Adenocarcinoma (lung carcinoma)	m	68	2003
76	Adenocarcinoma (colorectal carcinoma)	m	73	2007
77	Clear cell carcinoma (renal carcinoma/hypernephroma)	f	73	2007
78	Low differentiated carcinoma (breast carcinoma)	f	38	2003
79	Malignant melanoma	m	65	2007
80	Squamous cell carcinoma (cervix carcinoma)	f	48	2004
81	Squamous cell carcinoma (oropharynx carcinoma)	m	65	2007
82	Squamous cell carcinoma (hypopharynx carcinoma)	f	68	2005
83	Squamous cell carcinoma (lung carcinoma)	m	72	2006
84	Squamous cell tumor/adenocarcinoma (ovarian/lung carcinoma)	f	71	2005
		f=9, m=5	Mean=61.9	

Grading was based concerning the revised WHO classification system of tumors of the nervous system

Case no. case number, *f* female, *m* male, *TOS* time of surgery

49; Novocastra, Newcastle upon Tyne, UK), and vimentin (1:500, monoclonal, clone Vim 3B4; Dako, Glostrup, Denmark). We used two antibodies that recognize different isoforms of MAP2. A monoclonal antibody clone C (MAP2C, 1:100, monoclonal; supplied by Dr. B. Riederer, Lausanne) directed against the adult and the embryonic form, whereas MAP2a+b (1:500, monoclonal, clone AP-20; Sigma, Saint Louis, USA) detects exclusively the adult variant. Both

antibodies have been characterized previously in several studies and in different species [30–34, 36, 37]. All biopsy samples were fixed overnight in 4% formalin and routinely processed into liquid paraffin. Sections were cut at 4 µm with a microtome (Microm, Heidelberg), stretched in hot water (60°C), and mounted on positively charged slides (Superfrost + Menzel). The slides were air-dried in an incubator at 37°C overnight. Staining procedure with antibodies against GFAP, vimentin, MAP2a+b, and MAP2c was performed using a semiautomated benchmark apparatus (Nexes, Ventana, Illkirch, France) and the Ventana DAB staining system following the manufacturer's recommendations and as described previously [38]. Microwave pretreatment was used for all immunohistochemical reactions (0.01 M citrate buffer pH 6.0, 3 min 900 W, and afterwards 2×10 min 250 W). For nestin and TN-C staining, tissue slides were exposed to the primary antibody for 1 h, respectively, overnight in each case at 4°C. Pronase pretreatment was performed when recommended. All slides were counterstained with hematoxylin. Grading was based on the WHO classification system of tumors of the nervous system [35].

Evaluation of immunohistochemical staining

Immunohistological staining patterns of GFAP, MAP2, nestin, TN-C, and vimentin expression were analyzed independently by three observers (S.B., R.B., and I.B.) in an area up to 500 µm surrounding the tumor boundary. Results were assessed semiquantitatively as follows: grade 0, no immunopositivity; +, individual positive CNS cells at the boundary (<10%); ++, moderate fraction of positive CNS cells at the boundary (10–50%); +++, high fraction of positive CNS cells at the boundary (>50%). Thereafter, a quotient for every group and marker was calculated, setting 0=0, +=1, ++=2, and +++=3 divided by the number of samples [39, 40]. For statistical analysis, we used the Mann–Whitney test and the paired *t* test (GraphPad Software Inc., CA, USA). Statistical significance was attributed to *p* values lower than 0.05.

Double immunofluorescence staining

Selected tissue sections were incubated overnight with primary antibodies directed against nestin (1:4,000, polyclonal, rabbit; Chemicon, Billerica, USA), GFAP (1:500, monoclonal, clone 6F2, mouse; Dako, Glostrup, Denmark), as well as MAP2c (1:80, monoclonal, mouse; supplied by Dr. B. Riederer) at 4°C and subsequently with fluorescence labeled secondary antirabbit antibodies conjugated with carbocyanine (Cy) 2 (diluted 1:200, green; Jackson ImmunoResearch/Dianova, Hamburg, Germany), or antimouse Cy 3 (diluted 1:50, red; Jackson ImmunoResearch/Dianova, Hamburg, Germany). Immunohistochemical staining procedure of cell nuclei was performed using Hoechst 33342 (Sigma-Aldrich, Schnelldorf, Germany) for 5 min at room temperature. Slides were analyzed using an Olympus BX-51 fluorescent microscope (Olympus, Hamburg, Germany) equipped with an F-View II CCD camera (Soft Imaging System, Stuttgart, Germany).

Results

We examined the expression patterns of GFAP, vimentin, nestin, TN-C, and MAP2 at the tumor–brain boundary in 84 surgical brain specimens. Additionally, we studied MAP2 immunoreactivity in 48 CP using antibodies directed against adult and embryonic MAP2 isoforms. All samples showed specific histomorphological and immunohistochemical hallmarks of the respective entities. Thus, a total of 41 patients suffering from adaCP (21 males and 20 females; male to female ratio, 1.1/1) and seven papCP (four males and three females; male to female ratio, 1.3/1) were histologically confirmed. The age of patients at TOS ranged between 2 and 70 years (median, 29.5 years) in the adaCP group and between 19 and 60 years (median, 44.4 years) in the papCP group. The cavernous hemangioma cohort contained eight male and four female patients (male to female ratio, 2/1) with a median of 37.7 years. Meningiomas were distributed to different WHO grades as follows: four meningiomas corresponds to WHO grade I (one male and three female patients; male to female ratio, 0.7/1; median, 58.8 years), five atypical meningiomas (WHO grade II; three male and two female patients; male to female ratio, 1.5/1; median, 57.8 years), and one anaplastic meningiomas (WHO grade III; female; 73 years old).

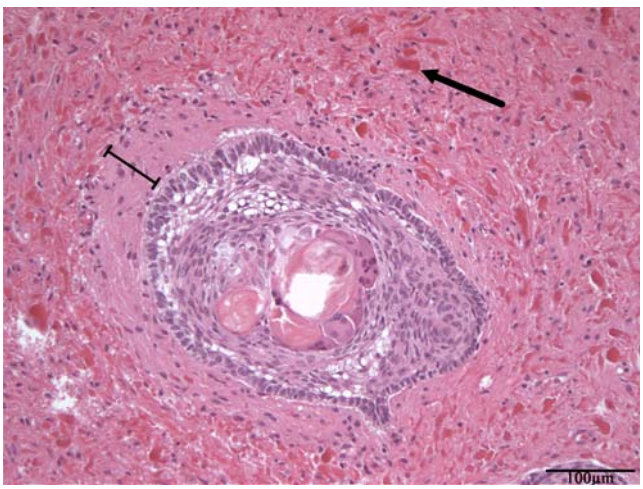

Fig. 1 Hematoxylin and eosin staining of an adaCP showing a typical tumor cell protrusion into the surrounding brain tissue. The tumor is characterized by whorl-like cell clusters, a palisaded basal cell layer, calcifications, and wet keratin. Gliotic reaction rich in Rosenthal fibers (*arrow*) in the surrounding brain parenchyma. Between the tumor zone and the gliosis, there is a small rim (*bar*) without gliotic changes (case no. 10; scale bar, 100 µm)

Metastases were diagnosed as six adenocarcinomas, four squamous cell carcinomas, one malignant melanoma, two poorly differentiated carcinomas, and one renal clear cell carcinoma (five males and nine females; male to female ratio, 0.6/1; median, 61.9 years). The clinical data of included patients is summarized in Table 1. All samples showed a sharp demarcation without diffuse single tumor cell infiltrations into the CNS. Mainly adaCP and metastases frequently exhibited small invading tumor cell groups and finger-like protrusions, pushing aside rather than infiltrating the surrounding brain parenchyma (Fig. 1).

For statistical comparisons of staining results between the various tumor entities, individual staining scores were obtained for each antibody, as described above.

GFAP staining scores at the tumor–brain interface

Formation of a gliotic rim around the lesion was detectable in all patients, although to a varying extent. GFAP immunoreactivity was seen in the cell bodies of reactive astrocytes but also within fibrillary processes. The calculated staining quotients for GFAP were 2.5 for meningiomas, 2.9 for adaCP, and 3.0 for papCP, cavernous hemangiomas, and metastases. Statistical analysis revealed only a slight significant difference comparing adaCP and meningiomas ($p<0.038$; Table 2). While GFAP was not detectable in the respective tumor cells, parts resembling fibrotic degeneration within adaCP displayed strong GFAP expression and, therefore, may represent remnants of enclosed gliotic brain tissue.

Table 2 Amount of the various immunohistological staining patterns collected in an area up to 500 μm surrounding the tumor boundary

IHC staining/tumor group	Cases (*n*)	Results				Quotient
		0	+	++	+++	
GFAP/						
adaCP	41			3	38	2.9
papCP	7				7	3.0
Cavernous hemangiomas	12				12	3.0
Meningiomas	10			5	5	2.5[a]
Metastases	14				14	3.0
Map2c/						
adaCP	41	3	4	27	7	1.9
papCP	7	1	4	2		1.1[a]
Cavernous hemangiomas	12	12				0.0[a]
Meningiomas	10	10				0.0[a]
Metastases	14	11	1	2		0.4[a]
Map2a+b/						
adaCP	23	1	7	14	1	1.7[b]
papCP	6	4	2			0.3[b]
Nestin/						
adaCP	41			19	22	2.5
papCP	7	1	1	3	2	1.9
Cavernous hemangiomas	12		2	4	6	2.3
Meningiomas	10	2	3	3	2	1.5[a]
Metastases	14			7	7	2.5
TN-C/						
adaCP	41			1	40	3.0
papCP	7		1	2	4	2.4
Cavernous hemangiomas	12		1	11		1.9[a]
Meningiomas	10		1	9		1.9[a]
Metastases	14		1	8	5	2.3[a]
Vimentin/						
adaCP	41			10	31	2.8
papCP	7			1	6	2.9
Cavernous hemangiomas	12		3	8	1	1.8[a]
Meningiomas	10	5	4	1		0.6[a]
Metastases	14	5		5	4	1.6[a]

Results were assessed semi-quantitatively for each protein as follows: grade 0, no immunopositivity; +, individual positive CNS cells at the boundary (<10%); ++, moderate fraction of positive CNS cells at the boundary (10–50%); and +++, high fraction of positive CNS cells at the boundary (>50%). Thereafter, a quotient for every group and marker was calculated, setting 0=0, +=1, ++=2, and +++=3 divided by the number of samples

IHC immunohistochemistry

[a] Statistical significance was attributed to *p* values lower than 0.05 with the Mann–Whitney test in relation to adaCP of the respective immunohistological staining

[b] Statistical significance was attributed to *p* values lower than 0.05 with the paired *t* test in relation to the staining with MAP2c of the respective tumor group

MAP2 expressing cells at the tumor–brain boundary and the basal tumor cell layer of adaCP

Only mature neurons were found to label with MAP2c antibodies in the surrounding brain tissue of cavernous hemangiomas and meningiomas. In contrast, a peculiar MAP2c-expressing cell population was detectable at the interface between the brain and three metastases (quotient, 0.4) as well as six papCP (quotient, 1.1). These cells showed ramifying processes and small nuclei, but no ganglion cell morphology. This cell population was particularly abundant next to adaCP with a quotient of 1.9. In addition, a staining gradient was always detectable, emerging from the finger-like protrusions towards the adjacent brain parenchyma (Fig. 2). The staining scores reached significant differences ($p=0.0186$ for adaCP compared to papCP as well as $p<0.0001$ for adaCP versus cavernous hemangiomas, meningiomas, and metastases; Table 2).

Representative CP samples with a significant amount of MAP2c-positive cells in the tumor–brain junction (23 adaCP and six papCP) were selected for additional analysis using a specific antibody directed against the adult isoform of MAP2 (MAP2a+b). Compared to MAP2c (quotients of the selected tumor samples: adaCP, 2.1 and papCP, 1.1), both groups exhibited lower numbers of MAP2a+b-expressing cells surrounding the tumor (quotients: adaCP, 1.7 and papCP, 0.3). The statistical analysis using a paired t test reached significance in both adaCP ($p=0.0005$) as well as papCP ($p=0.0250$). Detailed results are shown in Table 2.

Interestingly, there was a consistent MAP2c expression in the outer basal epithelial tumor cell layer of all adaCP, which was never observed in papCP, cavernous hemangiomas, and meningiomas. In line with the literature, several

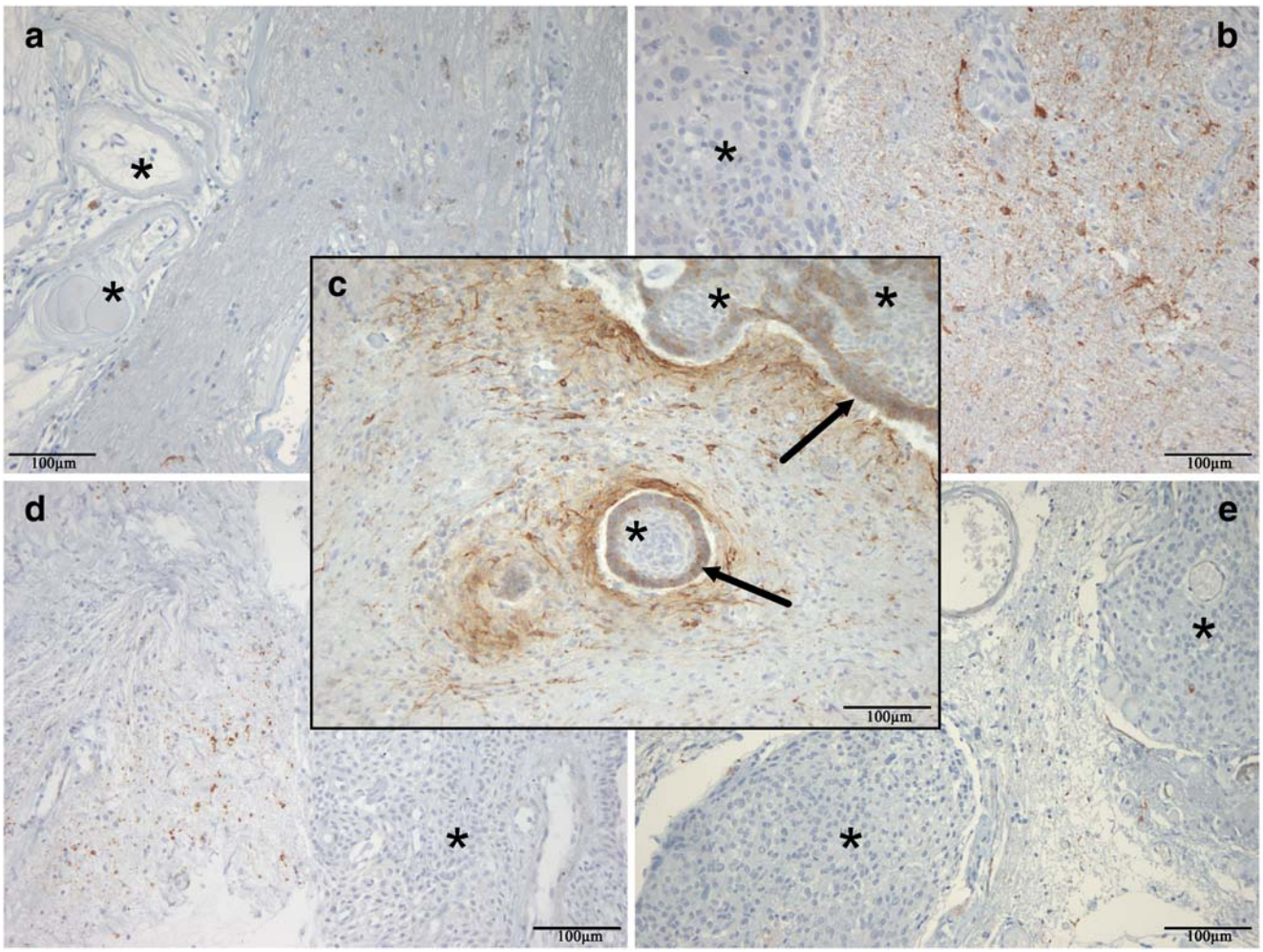

Fig. 2 Immunohistochemical staining patterns using an antibody directed against Map2c. **a** Grading of cavernous hemangiomas=0 (case no. 51). **b** Grading of metastases=2 (case no. 82). **c** Grading of adaCP=2. **d** Grading of papCP=2 (case no. 43). **e** Grading of meningiomas=0 (case no. 60). Beside the detected cell clusters in the tumor environment, there was a consistent MAP2c expression in the outer basal epithelial tumor cell layer of adaCP (*arrow*; case no. 28). Adamantinomatous craniopharyngiomas (*adaCP*), papillary craniopharyngiomas (*papCP*), cavernous hemangiomas, meningiomas, and metastases. Scale bar in **a**–**e**, 100 µm. The *asterisk* indicates a lesion

metastases (eight out of 14, 57%) offered a significant MAP2c expression. This was not restricted to the outer cell layer but diffusely distributed throughout the tumor (data not shown). Comparing the staining results of the antibodies directed against different MAP2 isoforms, expression of adult MAP2a+b was negative in five out of 23 adaCP (21.7%), whereas the intensity and distribution of MAP2a+b was diminished in the remaining samples, compared to MAP2c (Fig. 3).

Nestin-expressing cell clusters in close association with non-neuroepithelial lesions invading the brain

An antibody directed against nestin revealed immunoreactive cells at the invasion border of all tumors and lesions under study. The staining scores showed higher values in the brain parenchyma adjacent to adaCP (quotient, 2.5) compared to meningiomas (quotient, 1.5; $p=0.0059$), without a significant difference comparing adaCP and papCP. However, cavernous hemangiomas (quotient, 2.3) and metastases (quotient, 2.5) exhibited nearly the same scores like adaCP (Table 2), but a distinct gradient with clusters of nestin-expressing cells next to finger-like protrusions was exclusively found in adaCP (Fig. 4).

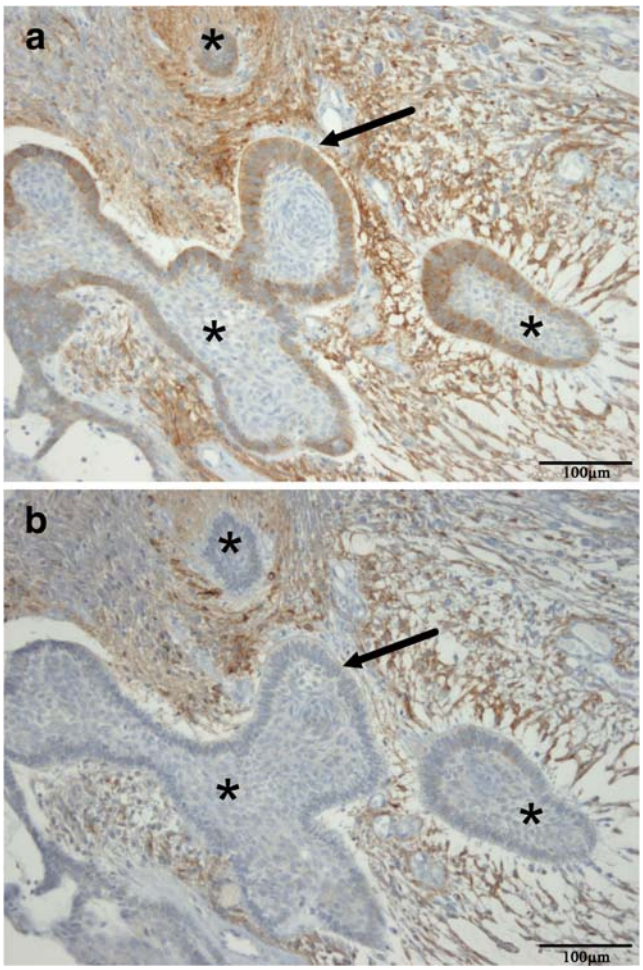

Fig. 3 Immunohistochemical staining pattern using antibodies directed against different MAP2 isoforms in a serial section of an adaCP. adaCP (case no. 34) exhibited a significantly stronger expression of MAP2c (**a**), representing the adult and embryonal variant compared to MAP2a+b (**b**), specifically directed against the adult isoform. This observation was not restricted to cells in the tumor environment but also detectable in the outer basal tumor cell layer of adaCP (*arrow*). Scale bar in **a** and **b**, 100 µm. The *asterisk* indicates a lesion

TN-C staining patterns at the tumor–brain boundary of CP and other non-neuroepithelial tumors

We detected a variable amount of TN-C expression at the brain parenchyma bordering all entities under study, whereas the cells in the lesion appeared negative. Parts resembling fibrotic degeneration within adaCP displayed variable amounts of TN-C. Statistical evaluation revealed the following staining scores: 1.9 for cavernous hemangiomas and meningiomas, 2.3 for metastases, 2.4 for papCP, and 3.0 for adaCP. The correlation between both CP variants and other entities under study reached significance with $p \leq 0.0022$ (Table 2). Interestingly, in some tumors, varying staining patterns were simultaneously observed surrounding adaCP. An increasing staining gradient with the highest values of TN-C expression at the tumor rim was present, as well as small margins of low immunoreactivity, in particular next to small finger-like protrusions without reactive astrocytes (Fig. 5).

Vimentin staining scores in the brain adjacent to CP and other non-neuroepithelial lesions

The amount of vimentin-expressing cells in the brain parenchyma adjacent to the lesions displayed obvious differences. The immunohistochemical staining quotients were as following: metastases=1.6, meningiomas=0.6, cavernous hemangiomas=1.8, adaCP=2.8, and papCP=2.9. Statistical analysis revealed significant differences between CP, cavernous hemangiomas, meningiomas, and metastases with $p \leq 0.002$ (Table 2). Areas surrounding finger-like protrusions in adaCP exhibited the strongest immunoreactivity (data not shown). Furthermore, macrophages and endothelial cells within the tumors as well as fibrotic degenerations and gliotic brain tissue inside adaCP also displayed variable amounts of vimentin.

Double immunofluorescence analysis

To further characterize the MAP2-expressing cell population at the tumor–brain interface of adaCP, we performed double immunofluorescence staining with antibodies directed against MAP2c, nestin, and GFAP. Coexpression of nestin and MAP2c as well as GFAP was detected close to finger-like protrusions into adjacent brain structures.

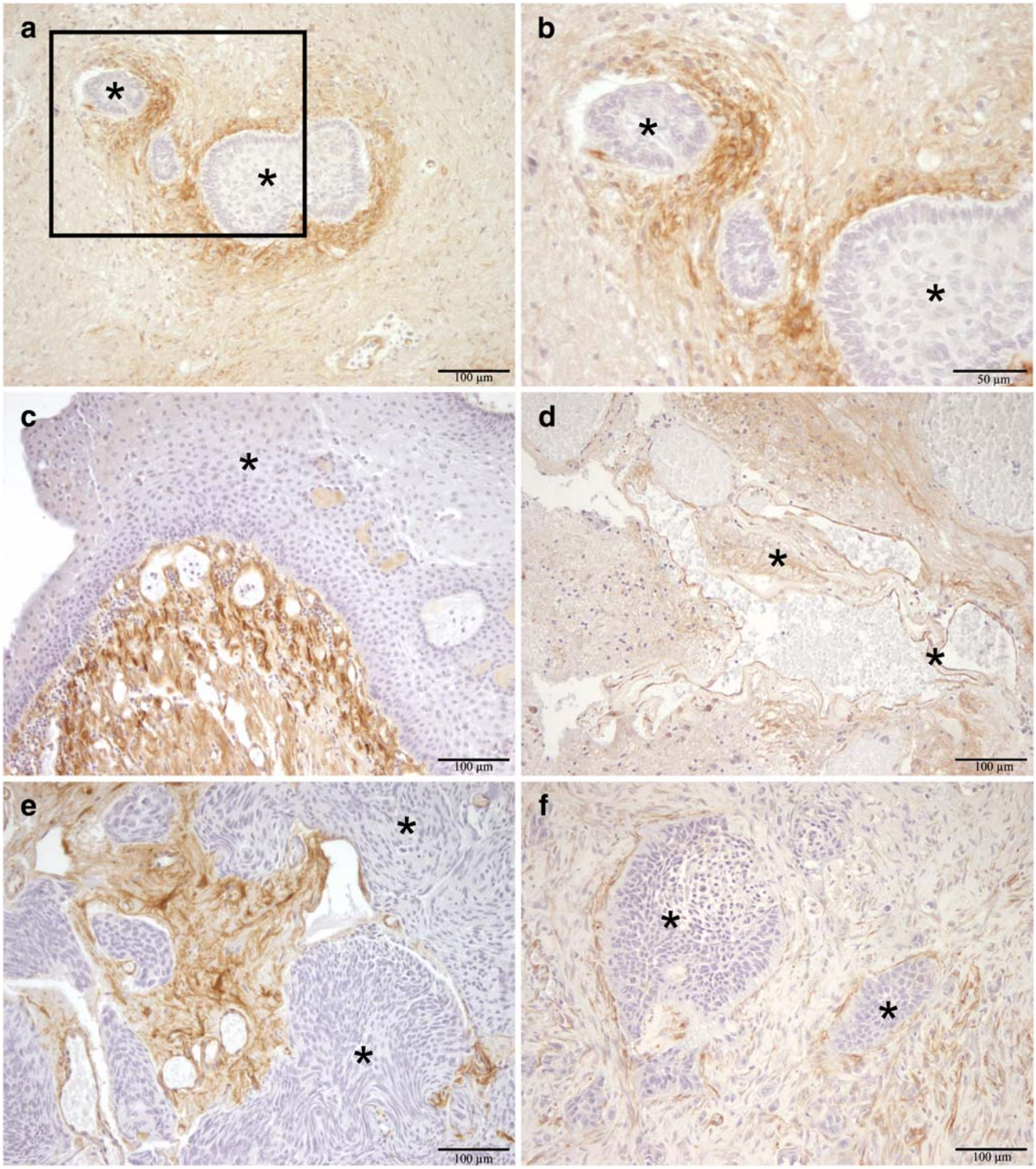

Fig. 4 Immunohistochemical staining patterns using an antibody directed against nestin. **a** and **b** The ECM next to adaCP displayed compactly packed clusters of nestin-expressing cells. Grading of adaCP=3 (case no. 30). **c** Grading of papCP=3 (case no. 42). **d** Grading of cavernous hemangiomas=3 (case no. 51). **e** Grading of meningiomas=3 (case no. 65). **f** Grading of metastases=2 (case no. 83). Scale bar in **a**, **c**–**e**, 100 µm and in **b**, 50 µm. The *asterisk* indicates a lesion

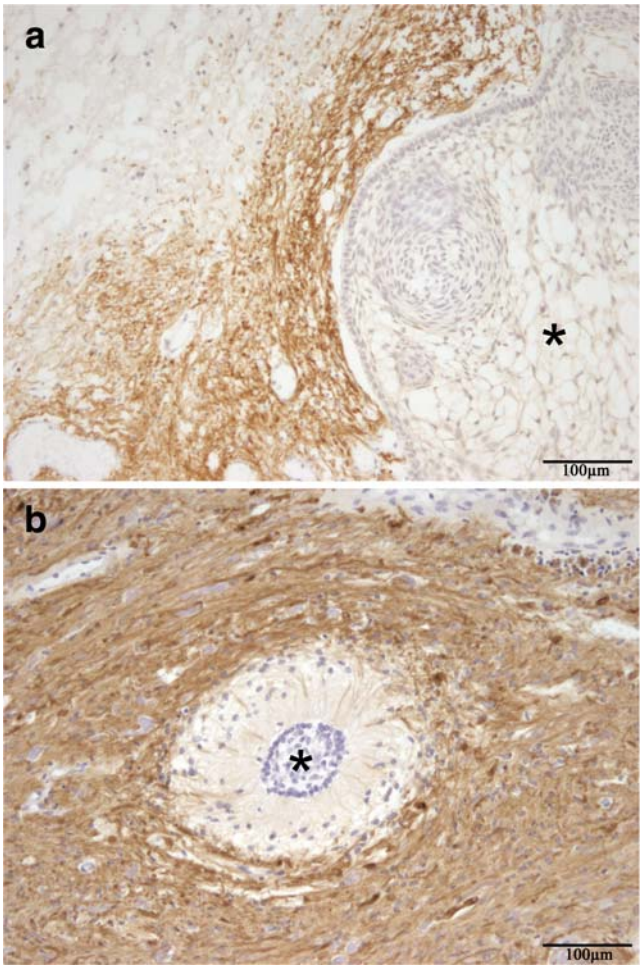

Fig. 5 Immunohistochemical staining patterns of adaCP using an antibody directed against TN-C. **a** In adaCP, there is an increasing gradient with highest amounts of TN-C expression in close relation to the tumor rim (case no. 2, grading=3). **b** A small margin of low immunoreactivity was observed at transverse sections of finger-like protrusions (case no. 34, grading=3). Scale bar in **a** and **b**, 100 µm. The *asterisk* indicates a lesion

Whereas GFAP expression was detectable in reactive astrocytes throughout the brain parenchyma, MAP2c and nestin immunoreactivities were restricted to the peculiar cell population located at the brain–parenchymal rim next to tumor excrescences (Fig. 6). A similar population of presumably astroglial precursors was not visible within the tumor mass.

Discussion

CP are benign tumors without histopathological or clinical signs of malignancy, such as nuclear atypia, dedifferentiation, significant mitotic activity, or metastases [35]. Regardless, CNS invasion is a frequent finding in adaCP compared to papCP [41, 42] and other non-neuroepithelial lesions like meningiomas, metastases, and cavernous hemangiomas. In contrast to the macroscopically distinct tumor capsule along adaCP, the tumor borders are irregular at the microscopic level with digitate infiltrations into adjacent brain structures [43], i.e., the hypothalamus and the basal ganglia [44]. This distinct growth pattern renders gross total tumor resection difficult to obtain and leads to frequent recurrence and serious neuroendocrine symptoms, including obesity, endocrine dysfunction, and visual impairment. Biochemical mechanisms for CP cell migration, predisposing this conspicuous growth pattern, remain poorly understood [9, 45]. A requisite for tumor cell migration is adhesion to the surrounding matrix and several studies have shown that the ECM is changed by invading tumors [46, 47]. We, therefore, performed an immunohistochemical study to characterize the cellular composition at the tumor–brain interface of CP, in particular the adaCP subtype, in comparison to other non-neuroepithelial tumors of the CNS, i.e., papCP, meningiomas, cavernous hemangiomas, and metastases. In contrast to these other lesions, we were able to characterize a specific cellular environment with the formation of a peculiar niche around finger-like protrusions of adaCP. This border zone is characterized by the appearance of a cell population of probably astroglial precursors in a TN-C and vimentin-enriched ECM. These cells show a distinct coexpression of MAP2, nestin, and GFAP (Fig. 6). Notwithstanding, the occurrence of MAP2 is precisely regulated during brain development and the complete lack of glial MAP2 expression in non-neoplastic lesions of the adult brain has been repeatedly demonstrated [34, 36]. To our knowledge, the only exceptions are MAP2c-expressing oligodendroglial progenitors occurring in multiple sclerosis plaques [48] or in HIV encephalitis [49]. In contrast to adult CNS in which MAP2a, MAP2b, and MAP2c are confined to neurons, glial precursor cells transiently express an alternatively spliced embryonic transcript including exon 13 (MAP2e) [33, 36]. We uncovered a peculiar cell population offering a glial phenotype with a distinct expression of both the embryonic and the adult transcript of MAP2. These cells occurred especially in the vicinity of adaCP. The coexpression of GFAP suggests their astrocytic origin, whereas colocalization with nestin is compatible with an immature developmental stage. Nestin is an established marker for stem/progenitor cells [50, 51]. Its expression in the adult human brain is strictly regulated and restricted to the subependymal zone as well as the hippocampus [23]. A transient expression of nestin in astroglial cells following neural grafting or brain lesions as well as in proliferative endothelium was described [21, 52]. We were able to identify nestin-expressing cells in the brain parenchyma adjacent to various lesions, which were most common along digitate brain protrusions of adaCP (Fig. 4). Here, they are embedded into a vimentin- and TN-C-enriched

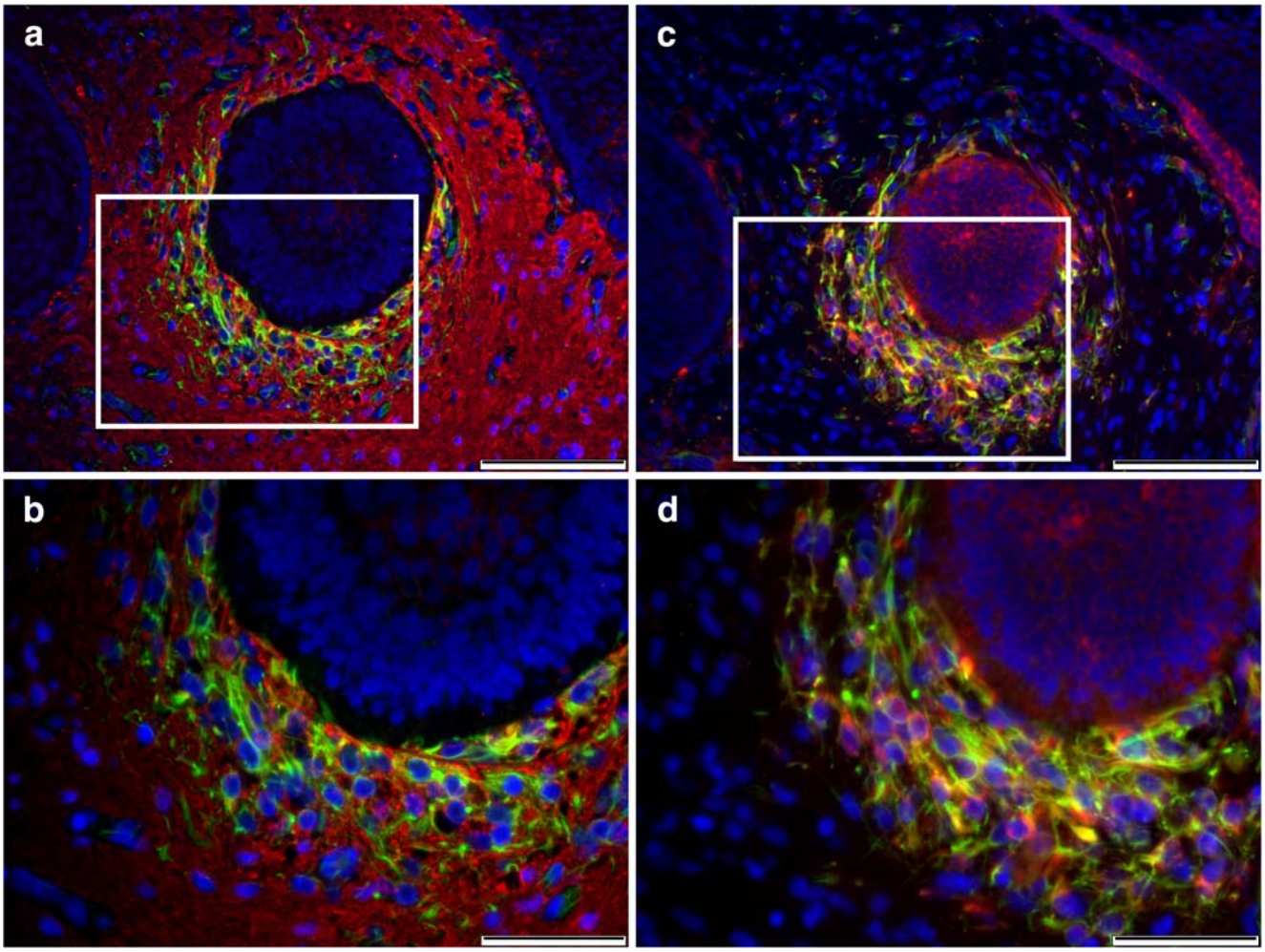

Fig. 6 Double immunofluorescence of adaCP was performed using antibodies against GFAP (*red color* in **a** and **b**) and MAP2c (*red color* in **c** and **d**) as well as against nestin (*green color* in **a**–**d**). In opposite to the vast majority of GFAP-positive reactive astrocytes surrounding the tumor, MAP2 expression was restricted to the outer basal tumor cell layer and several cell clusters around finger-like tumor protrusions. These cell clusters showing an intense coexpression of MAP2c/nestin and of GFAP/nestin represent presumably astroglial precursors (case no.4). Scale bar in **a** and **c**, 200 μm and in **b** and **d**, 100 μm

glial matrix. TN-C is an extracellular protein mainly secreted by immature as well as reactive astrocytes [24] and upregulated during embryogenesis [26, 53]. It plays an important role in shaping axonal guidance and is associated with mesenchymal–epithelial interactions [22]. Furthermore, TN-C is ubiquitously expressed in malignant gliomas where it stimulates tumor cell invasion [54]. TN-C expression in CP was already described as being restricted to fibrotic degenerations amid solid tumor parts [53]. We confirm these findings in our CP cohort, but found a simultaneous coexpression of vimentin and GFAP in these areas, which may represent rather remnants of enclosed brain tissue. Significantly enhanced TN-C expression along most of the finger-like protrusions of adaCP and the apical sites of papCP also support the hypothesis that TN-C is implicated in CP migration and invasion. In line with this assumption, Lefranc and colleagues were able to detect TN-C expression in both the optical chiasm and the pituitary stalk next to invading CP [39]. Furthermore, expression of various integrin subunits supports an interaction between CP tumor cells and ECM to provide adhesiveness, a precondition for tumor cell invasion. TN-C expression is known to be especially high at sites of epithelial mesenchymal transformation (EMT), and one remarkable feature of the resulting patterns is the development of a boundary-like appearance, which correlates with functional and molecular subdivisions of different compartments, i.e., at the invasion front of colorectal adenocarcinomas [55] and developing neuroanatomical structures [56, 57]. In this context, the confirmation of specific cell clusters in the TN-C-rich tumor–brain interface of adaCP allows several hypotheses. (1) These cells could represent primary adult glial cells, especially reactive astrocytes building a gliotic border. However, reactive astrocytes

normally lack MAP2 and nestin expression, which was exclusively restricted to these cell clusters in our specimens. (2) The re-expression of immature molecular markers may be indicative for the occurrence or recruitment of astroglial precursors and, therefore, a reversion to an immature phenotype which might be less susceptible to attendant hypoxia, as described elsewhere [52]. Such a process, to the best of our knowledge, has never been described so far in the tumor–brain junction of adaCP. Further studies will have to clarify the functional significance of such cells in the tumor–brain interface.

The development of a surrounding gliosis is well-known for many types of tumors and thought to be the response of the brain parenchyma to hypoxia and inflammation [58]. Our results show that the formation of the ECM surrounding non-neuroepithelial lesions in the brain is not always the same but depends on the tumor entity. It also suggests that specific tumor–brain interactions affect ECM modulation and might have influence on the growth pattern. Activating β-catenin mutations as well as aberrant nuclear β-catenin accumulation are hallmarks of adaCP, setting them apart from other lesions in the sellar region [4–7]. β-Catenin is a major component of the Wnt signaling pathway and nuclear protein accumulation is associated with target gene activation, decreased proliferation, and epithelial morphogenesis [38, 59]. The pathogenic impact of altered Wnt signaling in adaCP remains to be specified. β-Catenin is known to regulate the expression of TN-C in the ECM of colorectal tumors, especially at the invasion front where it is involved in the process of EMT, tumor cell migration, and invasion [55]. Thus, by regulating TN-C gene expression, β-catenin could be actively involved in the modification of the ECM, which in turn regulates the migration and invasiveness of adaCP into surrounding brain structures. These results require further experimental in vitro data addressing the impact of an activated Wnt signaling pathway on the migration capacity of adaCP tumor cells.

To the best of our knowledge, MAP2 expression in CP has not yet been reported. We, therefore, focused our analysis onto MAP2 and studied the expression patterns of both the embryonic and adult isoforms in various non-neuroepithelial lesions. Surprisingly, all adaCP showed a distinct and consistent MAP2 expression (Fig. 2). Furthermore, there was a statistically significant difference in the staining patterns of both MAP2 antibodies, indicating abundant expression of the embryonic isoform. Interestingly, neoplastic cells with MAP2 expression were not equally distributed throughout the tumor, rather than clustered at the outer epithelial margin bordering either brain parenchyma or mesenchymal scarring (Fig. 3). The MAP2 epitope is a well-established marker in the differential diagnosis of low-grade neuroepithelial tumors. With the exception of melanomas and small cell lung cancer, MAP2 expression is rare in metastatic and non-neuroepithelial neoplasms [34]. It can be concluded from our presented data that MAP2 serves also as a useful marker in the differential diagnosis of tumors in the sellar region, even in small tissue specimens. This is particularly helpful when adaCP and papCP are difficult to differentiate. Moreover, the circumscribed staining pattern is clearly different from the more diffused expression described for pituitary adenomas, whereas Rathke's cleft cysts remain always negative irrespective of squamous epithelial metaplasia (own observations and [40]).

In conclusion, our data support the hypotheses that adaCP induce a tumor-specific cellular environment at the brain invasion border. This includes the occurrence of a peculiar cell population of presumably astroglial precursors in close relation to the characteristic finger-like protrusions of adaCP. Further studies will have to clarify whether this specific environment supports tumor cell migration and is the consequence of increased Wnt signaling detectable in 90% of adaCP. Furthermore, MAP2 is a novel histopathological marker in the differential diagnosis of epithelial tumors of the sellar region.

Acknowledgements We kindly thank T. Jungbauer, K. Kalus, B. Rings, S. Sterner, and especially V. Schmidt for the expert technical support. We thank Dr. R. Coras and Dipl. Biochem. K. Kobow for the helpful discussions. This work was supported by the ELAN Foundation from the University Hospital of Erlangen, School of Medicine.

Conflict of interest statement The authors declare that they have no conflict of interest.

References

1. Bunin GR, Surawicz TS, Witman PA et al (1998) The descriptive epidemiology of craniopharyngioma. J Neurosurg 89:547–551
2. Kuratsu J, Ushio Y (1996) Epidemiological study of primary intracranial tumors in childhood. A population-based survey in Kumamoto Prefecture, Japan. Pediatr Neurosurg 25:240–246, discussion 247
3. Adamson TE, Wiestler OD, Kleihues P et al (1990) Correlation of clinical and pathological features in surgically treated craniopharyngiomas. J Neurosurg 73:12–17
4. Sekine S, Shibata T, Kokubu A et al (2002) Craniopharyngiomas of adamantinomatous type harbor beta-catenin gene mutations. Am J Pathol 161:1997–2001
5. Kato K, Nakatani Y, Kanno H et al (2004) Possible linkage between specific histological structures and aberrant reactivation of the Wnt pathway in adamantinomatous craniopharyngioma. J Pathol 203:814–821
6. Buslei R, Nolde M, Hofmann B et al (2005) Common mutations of beta-catenin in adamantinomatous craniopharyngiomas but not in other tumours originating from the sellar region. Acta Neuropathol (Berl) 109:589–597
7. Hofmann BM, Kreutzer J, Saeger W et al (2006) Nuclear beta-catenin accumulation as reliable marker for the differentiation

between cystic craniopharyngiomas and rathke cleft cysts: a clinico-pathologic approach. Am J Surg Pathol 30:1595–1603
8. Kendall-Taylor P, Jonsson PJ, Abs R et al (2005) The clinical, metabolic and endocrine features and the quality of life in adults with childhood-onset craniopharyngioma compared with adult-onset craniopharyngioma. Eur J Endocrinol 152:557–567
9. Karavitaki N, Cudlip S, Adams CB et al (2006) Craniopharyngiomas. Endocr Rev 27:371–397
10. Gleeson H, Amin R, Maghnie M (2008) 'Do no harm': management of craniopharyngioma. Eur J Endocrinol 159(Suppl 1):S95–S99
11. Muller HL (2008) Childhood craniopharyngioma. Recent advances in diagnosis, treatment and follow-up. Horm Res 69:193–202
12. Fahlbusch R, Hofmann BM (2008) Surgical management of giant craniopharyngiomas. Acta Neurochir (Wien) 150:1213–1226
13. Kawamata T, Kubo O, Hori T (2005) Histological findings at the boundary of craniopharyngiomas. Brain Tumor Pathol 22:75–78
14. Fahlbusch R, Honegger J, Paulus W et al (1999) Surgical treatment of craniopharyngiomas: experience with 168 patients. J Neurosurg 90:237–250
15. Muller HL, Albanese A, Calaminus G et al (2006) Consensus and perspectives on treatment strategies in childhood craniopharyngioma: results of a meeting of the Craniopharyngioma Study Group (SIOP), Genova, 2004. J Pediatr Endocrinol Metab 19(Suppl 1):453–454
16. Garre ML, Cama A (2007) Craniopharyngioma: modern concepts in pathogenesis and treatment. Curr Opin Pediatr 19:471–479
17. Puget S, Garnett M, Wray A et al (2007) Pediatric craniopharyngiomas: classification and treatment according to the degree of hypothalamic involvement. J Neurosurg 106:3–12
18. Lendahl U, Zimmerman LB, McKay RD (1990) CNS stem cells express a new class of intermediate filament protein. Cell 60:585–595
19. Wei LC, Shi M, Chen LW et al (2002) Nestin-containing cells express glial fibrillary acidic protein in the proliferative regions of central nervous system of postnatal developing and adult mice. Brain Res Dev Brain Res 139:9–17
20. Messam CA, Hou J, Berman JW et al (2002) Analysis of the temporal expression of nestin in human fetal brain derived neuronal and glial progenitor cells. Brain Res Dev Brain Res 134:87–92
21. Sugawara K, Kurihara H, Negishi M et al (2002) Nestin as a marker for proliferative endothelium in gliomas. Lab Invest 82:345–351
22. Erickson HP, Bourdon MA (1989) Tenascin: an extracellular matrix protein prominent in specialized embryonic tissues and tumors. Annu Rev Cell Biol 5:71–92
23. Gu H, Wang S, Messam CA et al (2002) Distribution of nestin immunoreactivity in the normal adult human forebrain. Brain Res 943:174–180
24. Joester A, Faissner A (2001) The structure and function of tenascins in the nervous system. Matrix Biol 20:13–22
25. Scheffler B, Faissner A, Beck H et al (1997) Hippocampal loss of tenascin boundaries in Ammon's horn sclerosis. Glia 19:35–46
26. Reardon DA, Zalutsky MR, Bigner DD (2007) Antitenascin-C monoclonal antibody radioimmunotherapy for malignant glioma patients. Expert Rev Anticancer Ther 7:675–687
27. Liu HY, Nur EKA, Schachner M et al (2005) Neurite guidance by the FnC repeat of human tenascin-C: neurite attraction vs. neurite retention. Eur J Neurosci 22:1863–1872
28. Riederer B, Matus A (1985) Differential expression of distinct microtubule-associated proteins during brain development. Proc Natl Acad Sci U S A 82:6006–6009
29. Riederer BM, Barakat-Walter I (1992) Differential distribution of two microtubule-associated proteins, MAP2 and MAP5, during chick dorsal root ganglion development in situ and in culture. Brain Res Dev Brain Res 68:111–123
30. Ferralli J, Doll T, Matus A (1994) Sequence analysis of MAP2 function in living cells. J Cell Sci 107(Pt 11):3115–3125
31. Kindler S, Schulz B, Goedert M et al (1990) Molecular structure of microtubule-associated protein 2b and 2c from rat brain. J Biol Chem 265:19679–19684
32. Kalcheva N, Albala J, O'Guin K et al (1995) Genomic structure of human microtubule-associated protein 2 (MAP-2) and characterization of additional MAP-2 isoforms. Proc Natl Acad Sci U S A 92:10894–10898
33. Shafit-Zagardo B, Davies P, Rockwood J et al (2000) Novel microtubule-associated protein-2 isoform is expressed early in human oligodendrocyte maturation. Glia 29:233–245
34. Blumcke I, Muller S, Buslei R et al (2004) Microtubule-associated protein-2 immunoreactivity: a useful tool in the differential diagnosis of low-grade neuroepithelial tumors. Acta Neuropathol (Berl) 108:89–96
35. Louis DN, Ohgaki H, Wiestler OD et al (2007) The 2007 WHO classification of tumours of the central nervous system. Acta Neuropathol 114:97–109
36. Blumcke I, Becker AJ, Normann S et al (2001) Distinct expression pattern of microtubule-associated protein-2 in human oligodendrogliomas and glial precursor cells. J Neuropathol Exp Neurol 60:984–993
37. Yasuda Y, Fujita S (2003) Distribution of MAP1A, MAP1B, and MAP2A&B during layer formation in the optic tectum of developing chick embryos. Cell Tissue Res 314:315–324
38. Buslei R, Holsken A, Hofmann B et al (2007) Nuclear beta-catenin accumulation associates with epithelial morphogenesis in craniopharyngiomas. Acta Neuropathol (Berl) 113:585–590
39. Lefranc F, Mijatovic T, Decaestecker C et al (2005) Monitoring the expression profiles of integrins and adhesion/growth-regulatory galectins in adamantinomatous craniopharyngiomas: their ability to regulate tumor adhesiveness to urrounding tissue and their contribution to prognosis. Neurosurgery 56:763–776
40. Rotondo F, Oniya K, Kovacs K et al (2005) MAP-2 expression in the human adenohypophysis and in pituitary adenomas. An immunohistochemical study. Pituitary 8:75–79
41. Weiner HL, Wisoff JH, Rosenberg ME et al (1994) Craniopharyngiomas: a clinicopathological analysis of factors predictive of recurrence and functional outcome. Neurosurgery 35:1001–1010, discussion 1010–1011
42. Crotty TB, Scheithauer BW, Young WF Jr (1995) Papillary craniopharyngioma: a clinicopathological study of 48 cases. J Neurosurg 83:206–214
43. Hirano A, Wate R (2007) Diagnostic clues and more from photographs. Neuropathology 27:1–9
44. Liszczak T, Richardson EP Jr, Phillips JP et al (1978) Morphological, biochemical, ultrastructural, tissue culture and clinical observations of typical and aggressive craniopharyngiomas. Acta Neuropathol 43:191–203
45. Karavitaki N, Brufani C, Warner JT et al (2005) Craniopharyngiomas in children and adults: systematic analysis of 121 cases with long-term follow-up. Clin Endocrinol (Oxf) 62:397–409
46. Rutka JT, Apodaca G, Stern R et al (1988) The extracellular matrix of the central and peripheral nervous systems: structure and function. J Neurosurg 69:155–170
47. Giese A, Rief MD, Loo MA et al (1994) Determinants of human astrocytoma migration. Cancer Res 54:3897–3904
48. Shafit-Zagardo B, Kress Y, Zhao ML et al (1999) A novel microtubule-associated protein-2 expressed in oligodendrocytes in multiple sclerosis lesions. J Neurochem 73:2531–2537
49. Cosenza MA, Zhao ML, Shankar SL et al (2002) Up-regulation of MAP2e-expressing oligodendrocytes in the white matter of patients with HIV-1 encephalitis. Neuropathol Appl Neurobiol 28:480–488
50. Toma JG, Akhavan M, Fernandes KJ et al (2001) Isolation of multipotent adult stem cells from the dermis of mammalian skin. Nat Cell Biol 3:778–784

51. Kim SY, Lee SH, Kim BM et al (2004) Activation of nestin-positive duct stem (NPDS) cells in pancreas upon neogenic motivation and possible cytodifferentiation into insulin-secreting cells from NPDS cells. Dev Dyn 230:1–11
52. Krum JM, Rosenstein JM (1999) Transient coexpression of nestin, GFAP, and vascular endothelial growth factor in mature reactive astroglia following neural grafting or brain wounds. Exp Neurol 160:348–360
53. Leins A, Riva P, Lindstedt R et al (2003) Expression of tenascin-C in various human brain tumors and its relevance for survival in patients with astrocytoma. Cancer 98:2430–2439
54. Sarkar S, Nuttall RK, Liu S et al (2006) Tenascin-C stimulates glioma cell invasion through matrix metalloproteinase-12. Cancer Res 66:11771–11780
55. Beiter K, Hiendlmeyer E, Brabletz T et al (2005) beta-Catenin regulates the expression of tenascin-C in human colorectal tumors. Oncogene 24:8200–8204
56. Faissner A, Steindler D (1995) Boundaries and inhibitory molecules in developing neural tissues. Glia 13:233–254
57. O'Brien TF, Faissner A, Schachner M et al (1992) Afferent-boundary interactions in the developing neostriatal mosaic. Brain Res Dev Brain Res 65:259–267
58. Freeman RS, Barone MC (2005) Targeting hypoxia-inducible factor (HIF) as a therapeutic strategy for CNS disorders. Curr Drug Targets CNS Neurol Disord 4:85–92
59. Holsken A, Kreutzer J, Hofmann BM et al (2009) Target gene activation of the Wnt signaling pathway in nuclear beta-catenin accumulating cells of adamantinomatous craniopharyngiomas. Brain Pathol 19(3):357–364

Virchows Arch (2010) 456:301–308
DOI 10.1007/s00428-009-0877-9

ORIGINAL ARTICLE

Lethal epiphyseal stippling in the foetus and neonate; pathological implications

Helen Wainwright · Peter Beighton

Received: 14 October 2009 / Revised: 21 November 2009 / Accepted: 18 December 2009 / Published online: 19 January 2010
© Springer-Verlag 2010

Abstract Autopsy reports accumulated since 1991 contained 30 cases in which routine radiological investigation had demonstrated radio-dense stippling of the epiphyses. The case histories, pregnancy progress, clinical manifestations, cytogenetic investigations, and autopsy findings have been tabulated and analysed for the purpose of diagnostic discrimination. Firm diagnoses were obtained in eight instances: warfarin embryopathy—three, trisomy 18—three, lethal multiple pterygium syndrome—one. Other possible but unconfirmed diagnoses were chromosomal aneuploidy—three, sonic hedgehog phenotype—one, CHARGE association—one, intrauterine infection—one. The value of autopsy in foetuses and neonates with lethal epiphyseal stippling syndromes is exemplified by the detection of multiple visceral abnormalities in ten instances.

Keywords Autopsy · Chondrodysplasia · Embryopathy · Genetics · Skeletal

Introduction

The term "Stippled Epiphyses" pertains to the radiological appearance of small calcific foci in the axial skeleton and spine. This abnormality is a major but non-specific diagnostic feature of a number of genetic, cytogenetic and acquired disorders. Stippling is present in the foetus and neonate, but usually disappears by the age of 2 years.

In pathological practice, stippling may be detected by routine radiographic imaging of a deceased foetus or neonate, prior to autopsy. The question of differential diagnosis then arises. A variety of visceral manifestations may also be found at autopsy; these may represent established diagnostic markers, components of existing syndromes or concomitants of undelineated entities. In order to achieve diagnostic precision, cytogenetic studies, metabolic investigations for peroxysomal and lysosomal disorders, plasma sterol estimation and mutation analysis may also be indicated.

We have analysed the clinical, radiological and autopsy findings in 30 deceased foetuses and neonates with stippled epiphyses. Our observations are presented, depicted and discussed in this article.

Methods and materials

Foetuses and deceased neonates are routinely sent for autopsy to HW in the Division of Anatomical Pathology, Faculty of Health Sciences, UCT. A clinical, family and pregnancy history, together with relevant laboratory findings form part of the referral. Full body antero-posterior and lateral radiographs are routinely obtained prior to autopsy. Thereafter, any necessary histological and biochemical investigations are undertaken. For logistical reasons, cytogenetic studies are not always feasible. The routine Venereal Disease Research Laboratory test for maternal syphilis had been undertaken in the majority of the pregnancies and two positive results were obtained. Most

H. Wainwright
Division of Pathology, Faculty of Health Sciences,
University of Cape Town,
Observatory,
7925 Cape Town, South Africa

P. Beighton (✉)
Division of Human Genetics, Faculty of Health Sciences,
University of Cape Town,
Observatory,
7925 Cape Town, South Africa
e-mail: Peter.Beighton@uct.ac.za

of the pregnancies in this series had taken place before routine human immunodeficiency virus testing was established. Similarly, studies of sterol metabolism and molecular investigation were not undertaken. High ethical standards are maintained and appropriate consent forms are explained and signed prior to autopsy. All records and data are carefully archived and indexed.

Since 1991, HW has conducted more than 3,047 autopsies in accordance with this protocol. Of these, epiphyseal stippling was detected radiologically in 30. Analysis of the archived material pertaining to these cases forms the subject of this communication.

Results

Analysis of the 30 cases revealed that there were 15 males and 15 females. Foetal age ranged from 17 weeks gestation to a term infant aged 2 days. Maternal age ranged from 17 to 43 years. A firm history of maternal anticoagulant therapy facilitated a diagnosis of warfarin embryopathy in three of the foetuses with stippling. Autopsy findings and relevant factors in the 30 cases are presented in Table 1. In view of the importance of warfarin embryopathy, the three cases are grouped together at the end of the table.

Seven cases had features suggestive of aneuploidy, which was confirmed cytogenetically in four by full karyotype prenatal amniocentesis (trisomy 18, three cases; trisomy 13, one case). In three, the chromosomes were normal. One foetus had features of CHARGE association and one had the lethal multiple pterygium syndrome with hydrops fetalis. Intrauterine infection was incriminated in one instance. In the remaining 16 cases, it was not possible to reach a firm diagnosis. In particular, no instances of the Conradi-Hünermann category of conditions were diagnosed. Autopsy revealed extensive visceral malformation in ten foetuses, but it was not possible to diagnose any specific genetic or developmental syndromes.

One case was suggestive of a non-specific familial disorder with a dysmorphic infant and mother, and mental retardation in both parents. This infant also had congenital heart disease, cystic hygroma of the neck and hypoplastic genitalia. In another family, a previous pregnancy had resulted in an abnormal foetus. Four cases had facial clefting: one had aneuploidy; one had severe facial clefting and clinical features suggestive of abnormality of the sonic hedgehog gene; one had a cleft lip and trisomy 18; and one had a cleft lip which had fused in utero, together with macrocephaly due to intracerebral haemorrhage. Eleven cases had congenital heart disease including the four with proven aneuploidy. One had cardiomyopathy.

Cerebral pathology was a frequent finding at autopsy. Three cases had neural tube defects ranging from craniorachischisis to spina bifida occulta with spinal lipoma. Three cases had polymicrogyria and one had holoprosencephaly. There were three cases with brain haemorrhage; one causing hydrocephalus, one with intraventricular haemorrhage and white matter necrosis, and one with associated asymmetric intrauterine growth restriction. Minor cerebral pathology included intracerebral calcification and microglial nodules in the foetus with congenital infection. There were two cases with abnormal gyral pattern. Skeletal dysplasia of uncertain type was suspected in one case with extensive stippling, abnormal lumbar vertebrae and tubular bones, together with severe hydrocephalus and associated porencephalic cysts.

Stippling confined to the calcanei was the most frequent finding in 15 cases. Three had stippling only of the talus. Single instances of stippling confined to the sacrum and to the tibia were also found. Cases with multiple sites of stippling included four with four involved sites, two of which had warfarin exposure; three with three sites; and four with two sites. The extent of epiphyseal stippling did not appear to correlate with the duration of pregnancy or to the magnitude and severity of visceral involvement. Equally, apart from warfarin embryopathy, the anatomical distribution of the stippling was apparently unrelated to any specific diagnosis in the majority of cases.

Discussion

There is semantic and taxonomic confusion concerning the term “stippled epiphyses”. This designation was initially employed to describe non-specific radiographic abnormalities which were likened to the punctate opaque appearance produced by flicking paint onto a glass plate. Thereafter, “stippled epiphyses” became an alternative designation for the heterogeneous Conradi-Hünermann group of disorders, which were also known as “chondrodysplasia punctata”. The term “chondrodysplasia punctata” (CDP) is currently used as a generic synonym for all forms of stippling. Despite the foregoing, it is now apparent that epiphyseal stippling is a feature of a wide range of genetic, chromosomal and acquired conditions. An updated classification has been promulgated, in which the causes of stippling are categorised into metabolic abnormalities, disruption of vitamin K metabolism and chromosomal abnormalities [1].

In the foetus or neonate with epiphyseal stippling, diagnostic precision is crucial for accurate genetic counselling, prognostication and appropriate management of neonates. In the South African context, warfarin is widely used in the prophylaxis of mitral valvular disease, which reaches a high prevalence in this country. Indeed, the observation that stippling occurred in three of the 30 cases in the series

Table 1 Autopsy findings and relevant factors in 30 cases of lethal epiphyseal stippling

	Case no	Mat age	Maternal factors	Gest age (weeks)	Sex	BW (gms) Status	Clinical features	Prenatal U/S or amniocentesis	X-ray	Autopsy	Diagnosis
1	73/91	32	Mental retardation, both parents	40	M	2,846	Dysmorphic	Amniocentesis normal	Stippled femora, calcaneus	L.superior vena cava	
				C/S			Cystic hygroma of neck		11 pairs ribs	Atrioventricular septal defect	
				Live birth			Hypoplastic genitals			Hypoplastic left ventricle	
			Dysmorphic mother	Died at 2 days						Coarctation central caecum	
2	80/91	37	Vdrl−	22 termination	M	350 fresh	Neural tube defect (thoraco-lumbar)	Spina bifida	Stippled vertebrae, calcaneus	Neural tube defect	
							Hydrocephalus	Hydrocephalus	11 pairs ribs		
							Recessed upper jaw				
3	30/91	17	Vdrl−	26 intrauterine death	F	840	Abnormal pinnae		Stippled proximal and distal femora, proximal tibia	Pulmonary hypoplasia	
							Protruberant eyes		Short tubular bones	Pelviureteric junction obstruction	
							Skeletal dysplasia			Abnormal arch vessel	
										Laryngeal stenosis	
4	52/92	25		24 termination	F	650 survived 1 h	Dysmorphic	Conical skull	Stippled calcaneus	Single atrium	T18
							Overlapping fingers	Exomphalos	Thin ribs	Atrio-ventricular septal defect	
							Exomphalos	Amniocentesis—T18		Ventricular septal defect	
							Short neck			Tubular hypoplasia of aorta	
										Central caecum	
										R lobe liver in sac	
										Horseshoe kidney	
										Bicornuate bicollis uterus	
5	61/92	24	Vdrl−	36	M	1,800 stillbirth	Multiple pterygia	Polyhydramnios	Stippled R calcaneus	Pulmonary hypoplasia	Lethal multiple pterygium syndrome
							L club foot	Hydrops	Scoliosis	Central caecum	
							Micropenis		Thin ribs		
6	15/93	22	Vdrl−	26	M	1,190 macerated stillbirth	Hydrops	Intrauterine death	Stippled calcaneus, vertebrae, sacrum	Pulmonary hypoplasia	
								Hydrops			
7	26/94	19	Vdrl− smoker	36 normal delivery	F	1,740 survived 15 h	Dysmorphic	Polyhydramnios	Brachydactyly	3 teeth lower jaw	CHARGE association
							Proptosis	Amniocentesis normal	Stippled calcaneus	Pulmonary hypoplasia	
							Choanal atresia			Renal hypoplasia	
							Cleft palate			Polymicrogyria	
										Atrial septal defect	
										Dilated cardiomyopathy	

Table 1 (continued)

	Case no	Mat age	Maternal factors	Gest age (weeks)	Sex	BW (gms) Status	Clinical features	Prenatal U/S or amniocentesis	X-ray	Autopsy	Diagnosis
8	80/94	27	Smoker Vdrl−	27	F	1,249 macerated stillbirth	Camptodactyly		Stippled calcaneus	Atrial septal defect	Chromosomal?
			Pyelo-nephritis (treated)				Simian crease		Bell-shaped chest	Ventricular septal defect	
										Hypoplastic left ventricle	
										Atretic aortic valve	
										Single umbilical artery	
										Foetal thrombotic vasculopathy	
										Trophoblast inclusions	
										Sacral lipoma	
										Neural tube defect, occult	
9	18/95	36	Vdrl−	30 spontaneous delivery	M	940	Dysmorphic	Polyhydramnios Encephalocoele	Stippled calcaneus	Scalp oedema Posterior nuchal cyst	
										Microstomia	
										Fixed tongue	
										Diaphragmatic hernia	
										L superior vena cava	
										Tubular hypoplasia of aortic isthmus	
										Stenosis oesophago-gastric junction	
										Microophthalmia	
										Periventricular calcification in brain	
										Cerebellar heterotopia	
										Microscopic renal dysplasia	
10	72/95			28 termination	F	1,112 fresh	Dysmorphic	Amniocentesis T13	Stippled R calcaneus 10 pairs of ribs	Exomphalos L superior vena cava	T13
										Ventricular septal defect	
										Double outlet right ventricle	
										Aortopulmonary window	
										Bilateral hydronephrosis	
										Bicornuate bicollis uterus	
										Retinal dysplasia	
11	110/96			26 breech delivery	F	722 survived 1 h	Large head	Hydranencephaly	Stippled L calcaneus	Single umbilical artery Hydrocephalus	
										Haemorrhage in brain	

12	127/97	26	G3P0 Previous abnormal foetus	17 termination	M	150 macerated stillbirth	Large head	Short femurs Abnormal heart Small chin Amniocentesis normal	Stippled calcaneus and hyoid bone 11 pairs ribs	Single umbilical artery Atrial septal defect Ventricular septal defect Abnormal cerebral gyral pattern Adrenal cytomegaly	
13	192/97	38	Vdrl-	35 normal delivery	F	2,159 survived 3 days	Dysmorphic Absent L radius and thumb Overlapping fingers Club feet Exomphalos	Amniocentesis T18	Stippled proximal and distal tibia	Ventricular septal defect Hypoplastic ascending aorta Polymicrogyria Meckel diverticulum	T18
14	201/97	27	Gestational proteinuric hypertension	25	M	565 macerated stillbirth			Stippled calcaneus	Severe asymmetric intrauterine growth retardation	
15	153/98	29	Vdrl+ Smoker Alcohol abuse	22	M	450 macerated stillbirth	Flat nose		Stippled calcaneus, sacrum, vertebra, elbow region	Asymmetric intrauterine growth retardation Brain haemorrhage	
16	15/99	23	Vdrl+ Gestational proteinuric hypertension	27	M	1,160 macerated stillbirth			Stippled talus	Placental infarct	
17	40/99	28	Vdrl−	33 C/S	M	2,015 fresh	Hydrops Large head Fused cleft lip		Stippled R talus	Brain haemorrhage Intraventricular haemorrhage White matter necrosis	
18	76/01	24	Vdrl-	32 C/S	F	1,990/hrs	Hydrops	Polyhydramnios	11 pairs ribs Stippled R calcaneus	Splenomegaly Hepatomegaly Microglial nodule Portal fibrosis Pulmonary hypoplasia	Congenital infection
19	78/01	26	Vdrl-	30	F	1,130 macerated stillbirth	Cleft lip	Atrioventricular septal defect Cleft lip Absent forearm	Absent ulna Flexed hands Absent thumb, index finger Scoliosis Stippled sacrum	Atrioventricular septal defect Tubular hypoplasia of aortic isthmus Oesophageal atresia Tracheoesophageal fistula Holoprosencephaly Liver fibrosis	T18
20	62/02	-	Extrauterine pregnancy Ruptured uterus	38	M	1,653 macerated stillbirth	Foetal compression	Iniencephaly scoliosis	Stippled talus		

Table 1 (continued)

	Case no	Mat age	Maternal factors	Gest age (weeks)	Sex	BW (gms) Status	Clinical features	Prenatal U/S or amniocentesis	X-ray	Autopsy	Diagnosis
21	65/02	20	Gestational proteinuria Hypertension	26	F	1,000 stillbirth	Swollen arm		Stippled hips, vertebrae, calcaneus Scoliosis	Microscopic renal dysplasia	
22	96/02	22	smoker	22 miscarriage	F	410		Anencephaly	Stippled calcaneus Absent R 12th rib	Craniorachischisis Hypoplastic adrenals Chorioamnionitis Microscopic renal dysplasia	
23	100/03	-	Twin foetal reduction 16 wks	27	M	890 macerated stillbirth	Small chin		Stippled calcaneus 11pairs ribs	Diamniotic dichorionic twins	
24	35/04	28	Vdrl−	40 normal delivery	M	2,550 Survived 6 hrs	Dysmorphic Microophthalmia Ectrodactyly Polydactyly Syndactyly		Stippled calcaneus 11 pairs ribs	L superior vena cava Bicuspid Aortic valve Ventricular septal defect Single coronary artery Cleft spleen Abnormal gyri Retinal dysplasia Ciliary body coloboma	
25	114/04	43		20	F	110 macerated stillbirth		Cystic hygroma Ascites Pleural effusion	Stippled calcaneus 11pairs ribs	Pulmonary hypoplasia Asymmetric Intrauterine growth retardation	Chromosomal?
26	211/07	30		30	M	731/macerated stillbirth	Macrocephaly Overlapping Fingers Intrauterine growth retardation		Stippled calcaneus	Pulmonary hypoplasia Ventricular septal defect Tubular hypoplasia of aortic isthmus Haemorrhage in brain	Chromosomal?
27	136/03	31	Polycystic kidney disease	24	F			Dandy-Walker cyst Facial cleft	Stippled vertebra, calcaneus Absent clavicle Absent mandible 11 pairs ribs	Cutis aplasia Anopthalmia Sinus tag Short humerus 2 toes L foot Posterior fossa cyst Dilated lateral ventricle Single umbilical artery No uterus Renal agenesis Short bowel blind ending Symmetrical phocomelia	Shh deficiency (Sonic Hedgehog phenotype)

28	54/91	Warfarin therapy	28	F	1,065 fresh stillbirth	Hydrocephaly	Stippled vertebra, long bones, scapula 11 ribs	Subdural haemorrhage	Warfarin embryopathy
		Cardiac valvular disease				Flat nasal bridge		Hydrocephalus	
								Premature closure of the ductus arteriosus	
								Abnormal position of bile duct	
29	156/00	Warfarin therapy	29	M	2,100 macerated stillbirth	Flat nasal bridge	Dot calcification of the talus	Cerebellar maturation 32-33 weeks	Warfarin embrypoathy
		DVT						Pelvi-ureteric junction obstruction	
		Polyhydrammios							
30	7/04	Warfarin therapy	18 termination	F	180 fresh	Flat nasal bridge	Stippled calcaneum, tibia, humeri, femora	Optic nerve neuroma	Warfarin embryopathy
		Thrombocytosis				Macroglossia		Myocardial calcification	
						Hypoplastic extremities		Pelvi-ureteric junction obstruction	

reflects this situation. The fact that stippling was recognised in a foetus after 18 weeks gestation in 2004 indicates that warfarin was still in use in early pregnancy in the period of maximum teratogenicity at this time. It is also relevant that in the authors' experience, stippling is not an inevitable consequence of warfarin embryopathy.

The foetal alcohol syndrome is another environmentally determined disorder which is very common in South Africa; foetal stippling has been attributed to this condition, and it is possible that some of the cases of unknown cause resulted from this factor. In the absence of a positive pregnancy history, however, firm diagnosis was not feasible.

Chromosomal abnormalities were detected by amniocentesis and full karyotyping in four of the cases, and the manifestations in another three were also compatible with aneuploidy. If cytogenetic investigations on the foetuses or neonates could have been undertaken as a routine in the series, especially where multiple malformations were present, it seems likely that further instances of chromosomal aberrations would have been detected. It is noteworthy that no instances of Down syndrome (trisomy 21) featured in the series as this relatively common condition is an inconsistent cause of stippling [2].

The various forms of the Conradi-Hünermann syndrome feature in the differential diagnosis of epiphyseal stippling, and the presence of dermal and ocular abnormalities is suggestive of this condition. Nevertheless, no dermal lesions such as alopecia, whorls, or ichthyosis were seen in the cases in this series. It may be relevant, however, that 11 were macerated, and it is possible that skin lesions could have been missed due to advanced maceration. Ocular lesions were present in five cases. Two had protuberant/proptosed eyes. Two had micro-ophthalmia; one associated with multiple malformations including diaphragmatic hernia and congenital heart disease; the other was associated with ciliary body coloboma and retinal dysplasia, ectrodactyly and polysyndactyly, dysplastic nails and coarse hair. None of the cases had obvious cataracts, which are a characteristic feature of the Conradi-Hünermann syndrome.

The sonic hedgehog phenotype which features in this series had previously been proposed as the diagnosis in a foetus with extensive stippling, severe craniofacial and limb dysmorphism, together with extensive cardiac, intestinal and genito-urinary malformations [3]. This disorder may represent yet another potentially lethal cause of extensive stippling.

Some skeletal dysplasias and other conditions associated with epiphysial stippling have been shown to result from defects in the biosynthesis of cholesterol [4, 5]. Cholesterol is crucial for modification of embryonic signalling proteins. [6]. Impairment of this process leads to abnormal endochondral bone formation with resultant foci of calcification within the cartilage which is radiographically visible as stippling [7].

One case was the third consecutive foetus to be lost at 17 weeks. This macerated male foetus had macrocephaly with an abnormal gyral pattern, congenital heart disease, short femurs and stippled calcaneii and hyoid bone. There was a single umbilical artery, adrenal cytomegaly and normal chromosomes. Early intrauterine death raises the possibility of chromosomal or genetic disorder or of severe metabolic disease. This foetus had severe asymmetric intrauterine restriction and a placenta with chorionic villi showing evidence of ischaemia, so maternal vascular disease may have played a role. In this context, maternal lupus erythematosus has been implicated as a cause of stippling [8–10], as have other forms of autoimmune disease [11, 12], but we were unable to obtain a history of conditions in these categories in the mother of this foetus.

The X-linked dominant form of chondrodysplasia punctata (CDPX2) is the consequence of mutations in the emopamil binding protein (EBP) gene at Xp11.2-p11.23 [13]. Abnormal sterols are present in the plasma of affected persons but not in individuals with other forms of CDP [14]. Other epiphyseal stippling conditions in which enzyme defects occur in post-squalene cholesterol biosynthesis include Smith-Lemli-Opitz syndrome, desmosterolosis, congenital hemidysplasia with ichthyosiform erythroderma and limb defects syndrome, lathosterolosis and hydrops-ectopic calcification-moth-eaten skeletal dysplasia.

We suggest that a routine pathological approach to a foetus, stillbirth or deceased neonate should include a full maternal and pregnancy history, antero-posterior and lateral radiographic babygrams and full cytogenetic karyotyping. Fibroblast culture and DNA banking are additional options which are worthwhile. If stippling is radiographically evident, fibroblast culture for possible metabolic abnormalities including both lysosomal and peroxisomal disorders, sterol analysis on plasma samples and mutation analysis of Xp11-11p.23 for EBP may assist in making a definitive diagnosis [15]. It must be emphasised, however, that EBP mutations make only a small contribution to the overall causes of stippling.

Comment

Analysis of a postmortem series of 30 cases with epiphyseal stippling which was evident on babygrams revealed a minority of cases in which a definite cause/association for the stippling was identified. These included aneuploidy and maternal warfarin exposure. In many instances, a definitive cause was not found. The demonstration of extensive visceral malformations in ten of the undiagnosed cases emphasises the importance of autopsy in the investigation of lethal epiphyseal stippling.

Acknowledgments We are grateful for support from the South African Medical Research Foundation and the National Research Foundation.

Conflict of interest The authors declare that they have no conflict of interest.

References

1. Irving MD, Chitty LS, Mansour S, Hall CM (2008) Chondrodysplasia punctata: a clinical diagnostic and radiological review. Clin Dysmorphol 17(4):229–241
2. Hernandez J, Salas S, Pastor I, Quero J, Collado F, Omenaca F (1988) Chondrodysplasia punctata associated with Down syndrome. Presentation of a case and review of the literature. An Esp Pediatr 28:145–147
3. Wainwright H, Beighton P (2009) Multiple malformations: a possible sonic hedgehog phenotype. Virchows Arch 454:3345–3347
4. Kelly RI, Wilcox WG, Smith M et al (1999) Abnormal sterol metabolism in patients with Conradi-Hünermann-Happle syndrome and sporadic lethal chondrodysplasia punctata. Am J Med Genet 83(3):213–219
5. Opitz JM, Zanni G, Reynolds JF et al (2002) Defects of blastogenesis. Am J Med Genet 115(4):269–286
6. Porter FD (2003) Human malformation syndromes due to inborn errors of cholesterol synthesis. Curr Opin Pediatr 15(6):607–613
7. Pazzaglia UE, Zarattini G, Donzelli C, Benetti A, Bondioni MP, Groli C (2008) The nature of cartilage stippling in chondrodysplasia punctata: histopathological study of Conradi-Hünermann syndrome. Fetal Pediatr Pathol 27(2):71–81
8. Costa T, Tiller G, Chitayat D, Silverman E (1993) Maternal systemic lupus erythematosus (SLE) and chondrodysplasia punctata in two infants; coincidence or association? First Meeting of Bone Dysplasia Society, Chicago
9. Toriello HV (1998) Chondrodysplasia punctata and maternal systemic lupus erythematosus. J Med Genet 35(8):698–699
10. Kozlowski K, Basel D, Beighton P (2004) Chondrodysplasia punctata and maternal lupus erythemtosus. Clin Genet 66(6):545–549
11. Shanske AL, Bernstein L, Herzog R (2007) Chondrodysplasia punctata and maternal autoimmune disease: a new case and review of the literature. Pediatrics 120(2):436–441
12. Chitayat D, Keating S, Zand DJ, Costa T, Zackie EH, Silverman E, Tiller G, Unger S, Miller S, Kingdom J, Toi A, Curry CJ (2008) Chondrodysplasia punctata associated with maternal autoimmune diseases: expanding the spectrum from systemic lupus erythematosus (SLE) to mixed connective tissue disease (MCTD) and scleroderma report of eight cases. Am J Med Genet 146A (23):3038–3053
13. Ikegawa S, Ohashi H, Ogata T et al (2000) Novel and recurrent EBP mutations in x-linked dominant chondrodysplasia punctata. Am J Med Genet 94:300–305
14. Kolb-Mäurer A, Grzeschik KH, Haas D, Bröcker EB, Hamm H (2008) Conradi-Hünermann-Happle syndrome (X-linked dominant chondrodysplasia punctata) confirmed by plasma sterol and mutation analysis. Acta Derm Venereol 88(1):47–51
15. Tysoe C, Law CJ, Caswell R, Clayton P, Ellard S (2008) Prenatal testing for a novel EBP missense mutation causing X-linked dominant chondrodysplasia punctata. Prenat Diagn 28(5):384–388

Virchows Arch (2010) 456:309–315
DOI 10.1007/s00428-009-0876-x

ORIGINAL ARTICLE

Localization of HSP47 mRNA in murine bleomycin-induced pulmonary fibrosis

Tomoyuki Kakugawa · Hiroshi Mukae · Yoshitaka Hishikawa · Hiroshi Ishii · Noriho Sakamoto · Yuji Ishimatsu · Takeshi Fujii · Takehiko Koji · Shigeru Kohno

Received: 2 November 2009 / Accepted: 16 December 2009 / Published online: 22 January 2010
© Springer-Verlag 2010

Abstract Heat shock protein 47 (HSP47) is a collagen-specific molecular chaperone that has been shown to play a major role in the processing and/or secretion of procollagen. However, the knowledge on which cells are actually synthesizing HSP47 in the lung parenchyma in pulmonary fibrosis was only limited. The aim of the present study was to investigate the localization of HSP47 messenger ribonucleic acid (mRNA) in normal lung and in the lungs of mice in bleomycin-induced pulmonary fibrosis, using in situ hybridization. For the purpose, ICR mice were intravenously injected with 10 mg/kg per day of bleomycin for five consecutive days. The lung cells expressing HSP47 mRNA were identified in control (saline alone) and bleomycin-treated mice by in situ hybridization. The signal for HSP47 mRNA was markedly increased in bleomycin-treated lungs compared with that of controls. HSP47 mRNA was localized in α-smooth-muscle-actin-positive myofibroblasts, surfactant-protein-A-positive type II pneumocytes, and F4/80-positive macrophages in the active fibrotic areas. These results suggest that these cells may synthesize procollagen in the fibrotic process of bleomycin-treated lungs through upregulation of HSP47 mRNA and play an important role in fibrogenesis.

Keywords Pulmonary fibrosis · Heat shock protein 47 · In situ hybridization

This study was supported in part by a research grant from the Ministry of Education, Science, Sports, and Culture of Japan.

T. Kakugawa · N. Sakamoto · Y. Ishimatsu · S. Kohno
Second Department of Internal Medicine,
Nagasaki University School of Medicine,
Nagasaki, Japan

H. Mukae (✉)
Division of Respiratory Disease,
University of Occupational and Environmental Health,
Kitakyushu, Japan
e-mail: hmukae@med.uoeh-u.ac.jp

Y. Hishikawa · T. Koji
Department of Histology and Cell Biology,
Nagasaki University Graduate School of Biomedical Sciences,
Nagasaki, Japan

H. Ishii
Internal Medicine II, Oita University Faculty of Medicine,
Yufu, Japan

T. Fujii
Department of Infectious Disease and Applied Immunology,
Institute of Medical Science, University of Tokyo,
Tokyo, Japan

Introduction

Idiopathic pulmonary fibrosis (IPF) is a devastating disorder characterized by excess deposition of extracellular matrix [1]. Increased synthesis and deposition of extracellular matrix is considered to be an important cause of fibrosis in experimental and human lung diseases [2, 3]. However, the molecular mechanisms underlying the excessive deposition of collagen in the fibrotic lesions are not fully understood.

It is of interest to know which cells principally contribute to fibrogenesis in the lung. Although several studies in experimental models emphasized the important role of the alveolar epithelium in normal repair [4, 5], the prevailing hypothesis regarding the pathogenesis of interstitial pulmonary fibrosis has revealed that the disease is due to a chronic unsolved inflammatory response, and in

this context, roles of the epithelium have been largely neglected. However, there is increasing evidence supporting the notion that epithelial injury in the absence of ongoing inflammation is sufficient to cause the development of pulmonary fibrosis [4–6] and that alveolar epithelial cells may be the primary source of cytokines and growth factors involved in fibroblast migration and proliferation [6]. In addition, many studies have demonstrated that macrophages are also a source of mediators capable of regulating fibroblast proliferation and other functions that are responsible for the fibrogenic outcome [7, 8]. In spite of these findings, the precise biological link among alveolar epithelial injury, macrophage activation, and fibrosis represents a challenging puzzle in which several pieces remain to be assembled.

Heat shock protein 47 (HSP47) is a collagen-binding, stress-inducible protein localized in the endoplasmic reticulum. HSP47 has a specific role in the intracellular processing of procollagen production as a collagen-specific molecular chaperone [9–12]. HSP47 expression was upregulated in experimental animal models of fibrosis, including murine bleomycin-induced pulmonary fibrosis [13, 14], rat peritoneal sclerosis [15], and carbon tetrachloride-induced rat liver cirrhosis [16]. In addition, we previously reported that the expression of human HSP47 was increased in the fibrotic lesions of IPF [17, 18], fibrotic transplanted kidney [19], and peritoneal sclerosis [20]. These findings suggest that HSP47 may play an important role in collagen synthesis in various fibrotic disorders.

We have recently shown in rodent bleomycin-induced pulmonary fibrosis model that type II pneumocytes in addition to myofibroblasts express HSP47 with the progression of fibrosis, while these cells did not express HSP47 in the control lungs [13, 14]. We also previously reported that regenerated type II pneumocytes in usual interstitial pneumonia express HSP47 [17, 18]. These findings suggest that type II pneumocytes in addition to myofibroblasts become synthesizing procollagen through the induction of HSP47 and play an important role in the development of fibrosis. However, the previous reports have not shown direct evidence that type II pneumocytes actually synthesize HSP47 in pulmonary fibrosis because all the previous findings were based on only protein level using immunohistochemistry.

Hence, this study was undertaken to investigate whether type II pneumocytes actually synthesize HSP47 in fibrotic lung. For this purpose, we employed the technique of nonradioactive in situ hybridization with a high resolution to localize the cells and tissue areas expressing HSP47 at mRNA level in normal and bleomycin-induced fibrotic lungs of mice.

Methods

Treatment of animals

Male 10-week-old ICR mice weighing 36–39 g were purchased from Charles River Japan, Inc. (Yokohama, Japan). The animals were specific pathogen free and maintained under standard conditions with free access to drinking water and pelleted food at the Animal Center of Biomedical Research, Nagasaki University. The mice were randomly divided into two experimental groups, bleomycin-treated (n=4) and control (n=4) groups. The mice were intravenously injected with 10 mg/kg per day of bleomycin (Nippon Kayaku, Tokyo, Japan) dissolved (2 mg/ml) in saline for five consecutive days. For controls, age-matched mice received an identical volume of saline alone. At 49 days after the commencement of bleomycin or saline treatment, mice were sacrificed and evaluated in the following manner.

The experimental protocol was approved by the Ethics Review Committees for Animal Experimentation of Nagasaki University.

Biochemicals and chemicals

Paraformaldehyde was purchased from Merck (Darmstadt, Germany), and 3,3′-diaminobenzidine-4HCl (DAB) was purchased from Dojin Laboratories (Kumamoto, Japan). A mixed bed resin (AG501-X8(D) resin) was purchased from Bio-Rad Laboratories (Tokyo, Japan). 3-Aminopropyltriethoxysilane, proteinase K, bovine serum albumin (BSA, minimum 98%, electrophoresis), yeast transfer RNA (type X-SA), salmon testis DNA, dextran sulfate, polyadenylic acid, heparin, and Briji 35 were purchased from Sigma Chemical (St. Louis, MO, USA). Formamide (nuclease and protease free) was purchased from Nacalai Tesque (Kyoto, Japan). All other reagents used in this study were purchased from Wako Pure Chemicals (Osaka, Japan) and were of analytical grade.

Antibodies

Primary antibodies used for the immunohistochemical studies included anti-α-smooth muscle actin (SMA; Neomarkers, Fremont, CA, USA), anti-F4/80 (Serotic, Oxford, UK), anti-surfactant protein (SP)-A (Santa Cruz Biotechnology, Santa Cruz, CA, USA). α-SMA, F4/80, and SP-A were used as markers for myofibroblasts, macrophages, and type II pneumocytes, respectively. Negative control studies were performed with irrelevant immunoglobulin G with the same subclass of the first antibodies instead of the primary antibodies.

Tissue preparation

At 49 days after the commencement of bleomycin or saline injection, mice from each group were sacrificed by exsanguination under deep anesthesia (sodium pentobarbital, 50 mg/kg, intraperitoneally). Lungs were then removed from each mouse via a midline incision and were fixed in 10% neutral-buffered formalin, embedded in paraffin, and processed to obtain 4-μm sections for staining with hematoxylin–eosin and Azan-Mallory staining. Sequential lung sections were placed on silane-coated glass slides for in situ hybridization and immunohistochemical analyses. In the mirror sections, two consecutive sections were mounted on glass slides with the common cut surface facing upward, so that the same surface of cut cells was compared in different staining ways.

Probes and labeling

Sense and antisense oligo-DNA sequences corresponding to nucleotides no. 564–608 of the murine HSP47 cDNA sequence [21] were synthesized. These 45-base oligo-DNAs were added with two repeats of adenine–thymine–thymine at 5′ ends and three repeats of it at 3′ ends, respectively, for thymine–thymine (T–T) dimers [22]. We conducted a computer-assisted search (GenBank nucleic acid sequence database Release 129) of the above HSP47 oligo-DNA sequences (without adenine–thymine–thymine repeats) and found appropriate homology only with mouse HSP47 or related mRNA sequences. These HSP47 oligo-DNAs were haptenized by introducing T–T dimers by 12,000 Jm^{-2} UV irradiation, as described previously [22]. We performed immunodetection and dot-blot hybridization using HSP47 probes described previously in detail [22, 23], and these results indicated that antisense probes were specific and had adequate sensitivity to be useful for in situ hybridization.

In situ hybridization

In situ hybridization was performed as described previously [24]. Briefly, lung paraffin sections were deparaffinized with toluene and rehydrated by serially graded ethanol solutions. The slides were treated with 0.2 N HCl for 20 min and proteinase K (50 μg/ml, 37°C for 15 min), successively. After the slides were postfixed with 4% paraformaldehyde in phosphate-buffered saline (PBS), the slides were immersed twice with 2 mg/ml glycine in PBS for 15 min. Hybridization was carried out at 37°C for HSP47 overnight in a medium containing 10 mM Tris–HCl (pH 7.4), 1 mM EDTA, 0.6 M NaCl, 1× Denhardt's solution, 250 μg/ml yeast transfer RNA, 125μg/ml salmon testis DNA, 10% dextran sulfate, 200 U/ml heparin, 10 μg/ml polyadenylic acid (potassium salt), 40% deionized formamide, and 2.0 μg/ml T-T dimerized HSP47 probe. After hybridization, the slides were washed five times with 2× saline sodium citrate (SSC; 0.15 M NaCl, 0.015 M Na citrate, pH 7.0)/50% formamide at 37°C for 1 h each and finally washed twice with 2× SSC at room temperature for 15 min. After successive treatment with ethanol and acetone to dilapidate the sections, the slides were subjected to enzyme immunohistochemistry. After incubation with blocking solution (5% BSA, 100 μg/ml salmon testis DNA, 100 μg/ml yeast transfer RNA, and 500 μg/ml mouse IgG in PBS) for 1 h at room temperature, the slides were reacted overnight with horse radish peroxidase (HRP) mouse anti-T–T antibody (1:80) at room temperature. After washing with 0.075% Brij 35 in PBS, the visualization of HRP sites was performed with DAB, Ni, Co, and H_2O_2 according to the method of Adams [25]. To confirm the specificity of mRNA signals, a variety of control experiments were conducted. In every experimental run, sense probe was used as a negative control. To evaluate the level of hybridizable RNAs in tissue sections, a 28S rRNA probe was used as a positive control in every case [23].

Immunohistochemistry

To confirm the localization of HSP47 mRNA, immunohistochemistry was performed with the conventional avidin–biotin peroxidase histochemical technique using Histomouse™-Plus Kits (Zymed Laboratories, South San Francisco, CA, USA) for α-SMA and the Vectastain Elite ABC Kit (Vector Laboratories, Burlingame, CA, USA) for F4/80 and SP-A. Briefly, sequential paraffin sections (4 μm thick) were deparaffinized with toluene and were rinsed thoroughly with ethanol. Sections were then soaked in 0.3% H_2O_2 with absolute methanol for 20 min at room temperature to inactivate the endogenous peroxidase activity. They were incubated with blocking serum for 30 min and then covered with primary antibodies and incubated for 1 h. After washing in phosphate-buffered saline, sections were processed further using kits according to the instructions provided by the manufacturer and then developed with 3,3′-DAB and H_2O_2. Finally, the sections were counterstained with methyl green and mounted.

Results

Histological findings

As shown in Fig. 1, marked interstitial pneumonitis and fibrosis was noted in the lungs of bleomycin-treated mice

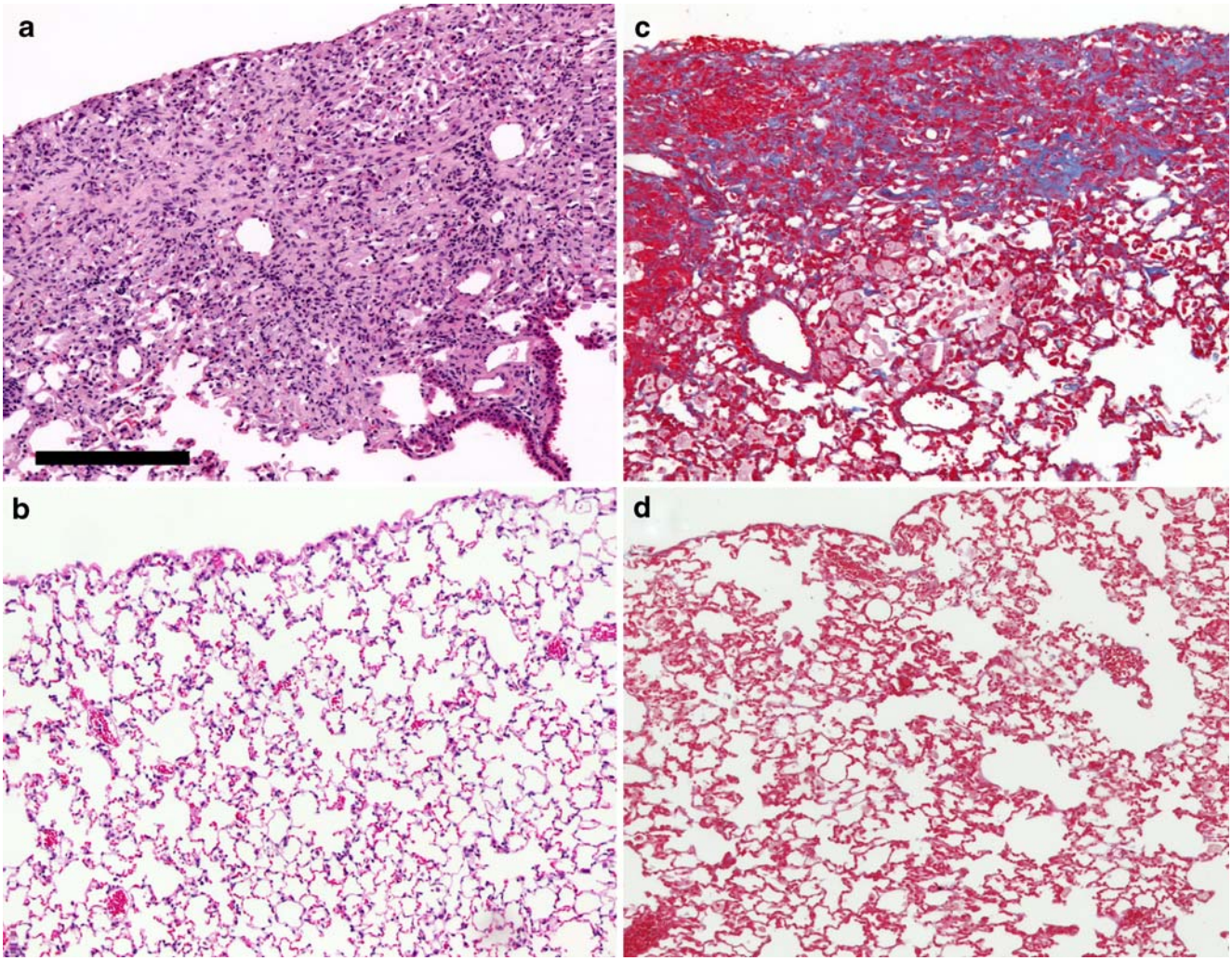

Fig. 1 Photomicrographs of representative lung specimens in bleomycin-treated (**a**, **c**) and control (**b**, **d**) groups. **a**, **b** Hematoxylin and eosin staining and **c**, **d** Azan-Mallory staining. Calibration bar=200 μm

(Fig. 1a), while no significant change was noted in the lungs of control mice (Fig. 1b). The pneumonitis and fibrosis were found mainly in the subpleural regions. With the Azan-Mallory staining, collagen deposition was seen in the lung of bleomycin-treated mice (Fig. 1c), while almost no collagen deposition was seen in the lung of control mice (Fig. 1d).

In situ hybridization for HSP47 mRNA

HSP47 mRNA was not found in control lung (Fig. 2a). However, there was a significant increase in the number of cells expressing HSP47 mRNA in the lungs of bleomycin-treated mice (Fig. 2b). When an adjacent section was hybridized with HSP47 sense probes, the staining intensity was markedly reduced compared to that with HSP47 antisense probe (Fig. 2c).

Localization of HSP47 mRNA

To determine the type of cells that expressed HSP47 mRNA, we performed hematoxylin and eosin staining and immunohistochemistry for α-SMA, SP-A, and F4/80, in addition to in situ hybridization for HSP47 mRNA using adjacent sections and mirror sections in the bleomycin-treated mice. The majority of HSP47-mRNA-positive interstitial spindle-shaped cells (Fig. 3a and b) were also positive for α-SMA (Fig. 3c), indicating that these cells were myofibroblasts. And most of the HSP47-mRNA-positive cuboidal cells located in alveolar walls (Fig. 3d and e) were also positive for SP-A (Fig. 3f), indicating that these cells were type II pneumocytes. Furthermore, HSP47-mRNA-positive intra-alveolar mononuclear cells (Fig. 3g, h) were identified similarly as macrophages, based upon the F4/80 costaining (Fig. 3i).

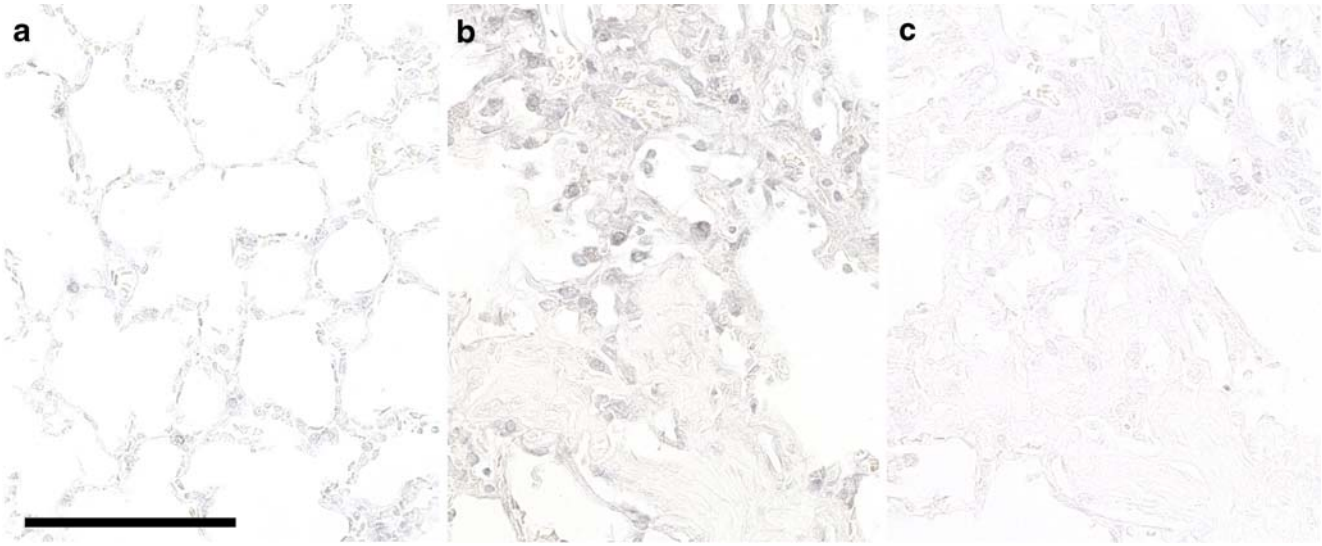

Fig. 2 In situ detection of HSP47 mRNA in lung specimens of bleomycin-treated and control mice. HSP47 mRNA was not found in control lung (**a**). There was a significant increase in the number of cells expressing HSP47 mRNA in the lungs of bleomycin-treated mice (**b**). When an adjacent section was hybridized with HSP47 sense probe, the staining intensity was markedly reduced compared to that with HSP47 antisense probe (**c**). Calibration bar=100 μm

Discussion

The present study confirmed the expression and localization of HSP47 at mRNA levels in bleomycin-treated lungs. HSP47 mRNA was localized in SP-A-positive type II pneumocytes, F4/80-positive macrophages, and α-SMA-positive myofibroblasts. HSP47 binds to the nascent types I–V procollagen immediately after procollagen is translated into the endoplasmic reticulum [9, 26]. HSP47 is thought to prevent the incorrect unfolding and aggregation of nascent procollagen polypeptide chains until the correct carboxy-terminal association has been made [27]. Recent reports have demonstrated that HSP47 expression is restricted to phenotypically altered collagen-producing cells, and its expression correlates well with that of collagen [15, 17, 19, 20]. Clarke et al. [28] demonstrated that cell lines that did not produce collagen mRNA lacked the capacity to produce HSP47 mRNA. The present findings together with these previous studies imply that type II pneumocytes and macrophages in addition to myofibroblasts might become synthesizing collagen in the process of pulmonary fibrosis. However, the exact mechanism of intracellular processing of HSP47 and procollagen in these cells remains unclear.

While many neoteric cell lineages migrate during embryogenesis to new locations using a fate pathway that involves epithelial–mesenchymal transition [29, 30]; such transitions in mature tissues are less well appreciated. However, transitions do occur, particularly during oncogenesis [31] and fibrogenesis [32, 33]. This process has been particularly studied in renal fibrosis. It has been hypothesized that, when basement membrane is injured by matrix metaroproteinase, epithelial cells that detach from their basement membrane may enter into epithelial–mesenchymal transition, express HSP47 and other mesenchymal markers, and divide as fibroblasts [33–35]. Whether this process takes place in the lung in IPF or in other forms of pulmonary fibrosis is largely unknown, but urgent evaluation in vitro and in vivo would be necessary. The present findings that type II pneumocytes express HSP47 mRNA imply that the similar process might take place in pulmonary fibrosis. Further studies are warranted in order to elucidate the precise mechanism(s) involved in this process.

We previously reported that the treatment with pirfenidone, an antifibrotic agent, decreased the expression of HSP47 at protein level in bleomycin-induced pulmonary fibrosis in mice [14]. Furthermore, it was demonstrated that inhibition of HSP47 by antisense oligodeoxynucleotides markedly suppressed the production of collagen in 3T6 cells [12], in experimental proliferative glomerulonephritis [36] and in experimental peritoneal fibrosis [15]. These findings suggest that HSP47 might be a promising target for the treatment of pulmonary fibrosis. Further studies using an antisense oligonucleotide against HSP47 are underway in our laboratories to examine whether this antisense suppresses collagen accumulation in an experimental pulmonary fibrosis induced by bleomycin.

In summary, we have successfully identified the localization of HSP47 mRNA in pulmonary fibrosis in bleomycin-treated lungs. Our results suggest that type II pneumocytes and macrophages, in addition to myofibroblasts, might synthesize procollagen in the fibrotic process

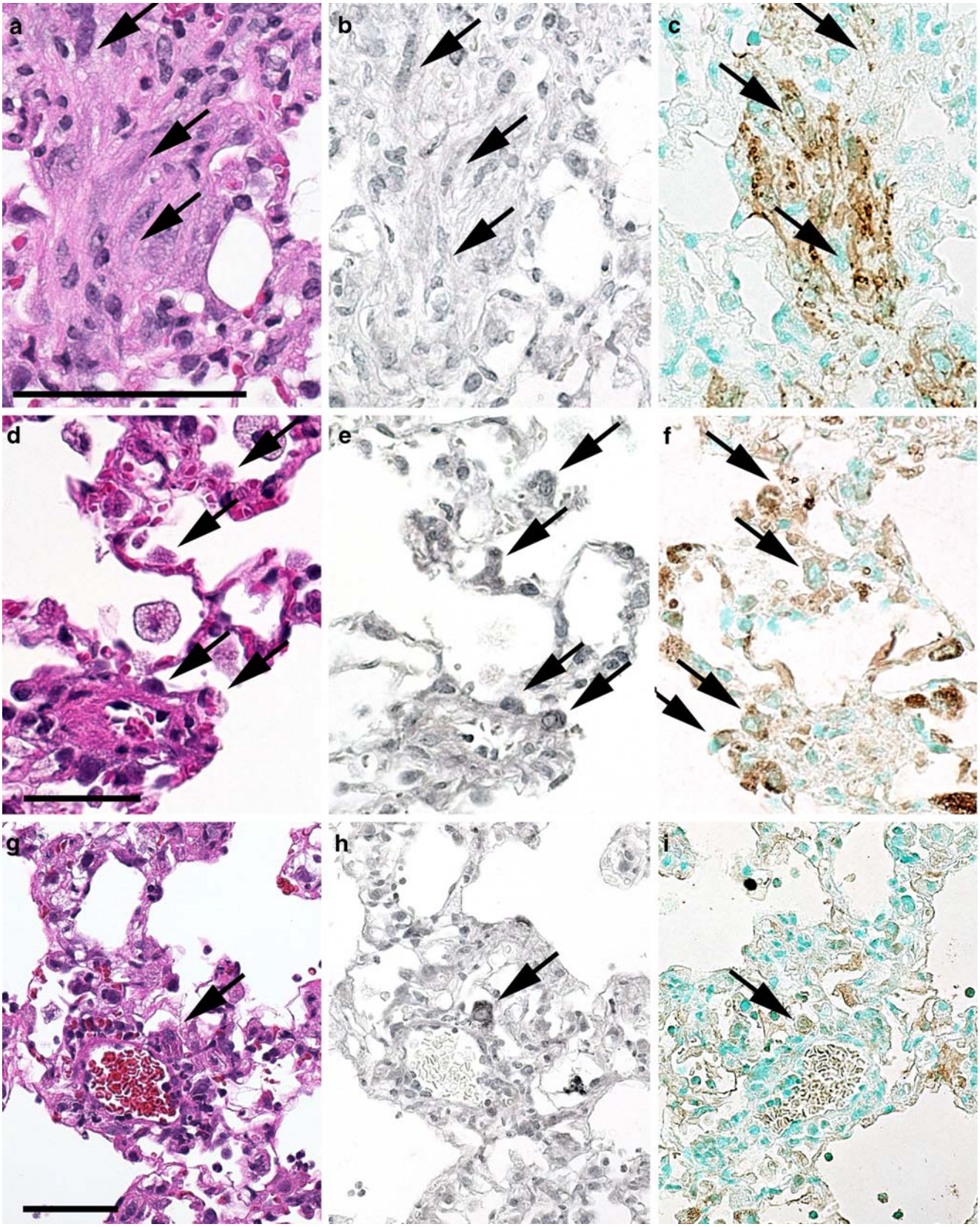

Fig. 3 Identification of cell types of HSP47-mRNA-positive cells in the lung tissues of bleomycin-treated mice. **a**, **d**, **g** Hematoxylin and eosin staining. **b**, **e**, **h** HSP47 mRNA staining by in situ hybridization. **c**, **f**, **i** Immunohistochemistry for α-SMA, SP-A, and F4/80, respectively. Each set of photos (**a**–**c**, **d**–**f**, and **g**–**i**) was taken from adjacent and mirror sections. Calibration bar=50 μm

of bleomycin-treated lungs, through upregulation of HSP47 mRNA. Further studies are required to investigate the exact mechanism of intracellular processing of HSP47 and procollagen in these cells.

Acknowledgments The authors thank Mr. Atsushi Yokoyama for the excellent technical support.

Conflict of interest statement We declare that we have no conflict of interest.

References

1. Crouch E (1990) Pathobiology of pulmonary fibrosis. Am J Physiol 259:L159–L184
2. Specks U, Nerlich A, Colby TV et al (1995) Increased expression of type VI collagen in lung fibrosis. Am J Respir Crit Care Med 151:1956–1964
3. Zhang K, Gharaee-Kermani M, McGarry B et al (1994) In situ hybridization analysis of rat lung alpha 1(I) and alpha 2(I) collagen gene expression in pulmonary fibrosis induced by endotracheal bleomycin injection. Lab Invest 70:192–202
4. Adamson IY, Young L, Bowden DH (1988) Relationship of alveolar epithelial injury and repair to the induction of pulmonary fibrosis. Am J Pathol 130:377–383
5. Haschek WM, Witschi H (1979) Pulmonary fibrosis—a possible mechanism. Toxicol Appl Pharmacol 51:475–487
6. Selman M, King TE, Pardo A (2001) Idiopathic pulmonary fibrosis: prevailing and evolving hypotheses about its pathogenesis and implications for therapy. Ann Intern Med 134:136–151
7. Khalil N, Bereznay O, Sporn M et al (1989) Macrophage production of transforming growth factor beta and fibroblast collagen synthesis in chronic pulmonary inflammation. J Exp Med 170:727–737
8. Martinet Y, Rom WN, Grotendorst GR et al (1987) Exaggerated spontaneous release of platelet-derived growth factor by alveolar macrophages from patients with idiopathic pulmonary fibrosis. N Engl J Med 317:202–209
9. Nakai A, Satoh M, Hirayoshi K et al (1992) Involvement of the stress protein HSP47 in procollagen processing in the endoplasmic reticulum. J Cell Biol 117:903–914
10. Nagata K, Saga S, Yamada KM (1986) A major collagen-binding protein of chick embryo fibroblasts is a novel heat shock protein. J Cell Biol 103:223–229
11. Saga S, Nagata K, Chen WT et al (1987) pH-dependent function, purification, and intracellular location of a major collagen-binding glycoprotein. J Cell Biol 105:517–527
12. Sauk JJ, Smith T, Norris K et al (1994) HSP47 and the translation–translocation machinery cooperate in the production of alpha 1(I) chains of type I procollagen. J Biol Chem 269:3941–3946
13. Ishii H, Mukae H, Kakugawa T et al (2003) Increased expression of collagen-binding heat shock protein 47 in murine bleomycin-induced pneumopathy. Am J Physiol Lung Cell Mol Physiol 285: L957–L963
14. Kakugawa T, Mukae H, Hayashi T et al (2004) Pirfenidone attenuates expression of HSP47 in murine bleomycin-induced pulmonary fibrosis. Eur Respir J 24:57–65
15. Nishino T, Miyazaki M, Abe K et al (2003) Antisense oligonucleotides against collagen-binding stress protein HSP47 suppress peritoneal fibrosis in rats. Kidney Int 64:887–896
16. Masuda H, Fukumoto M, Hirayoshi K et al (1994) Coexpression of the collagen-binding stress protein HSP47 gene and the alpha 1 (I) and alpha 1(III) collagen genes in carbon tetrachloride-induced rat liver fibrosis. J Clin Invest 94:2481–2488
17. Iwashita T, Kadota J, Naito S et al (2000) Involvement of collagen-binding heat shock protein 47 and procollagen type I synthesis in idiopathic pulmonary fibrosis: contribution of type II pneumocytes to fibrosis. Hum Pathol 31:1498–1505
18. Kakugawa T, Mukae H, Hayashi T et al (2005) Expression of HSP47 in usual interstitial pneumonia and nonspecific interstitial pneumonia. Respir Res 6:57
19. Abe K, Ozono Y, Miyazaki M et al (2000) Interstitial expression of heat shock protein 47 and alpha-smooth muscle actin in renal allograft failure. Nephrol Dial Transplant 15:529–535
20. Shioshita K, Miyazaki M, Ozono Y et al (2000) Expression of heat shock proteins 47 and 70 in the peritoneum of patients on continuous ambulatory peritoneal dialysis. Kidney Int 57:619–631
21. Takechi H, Hirayoshi K, Nakai A et al (1992) Molecular cloning of a mouse 47-kda heat-shock protein (HSP47), a collagen-binding stress protein, and its expression during the differentiation of F9 teratocarcinoma cells. Eur J Biochem 206:323–329
22. Koji T, Nakane PK (1996) Recent advances in molecular histochemical techniques: in situ hybridization and southwestern histochemistry. J Electron Microsc (Tokyo) 45:119–127
23. Yoshii A, Koji T, Ohsawa N et al (1995) In situ localization of ribosomal RNAs is a reliable reference for hybridizable RNA in tissue sections. J Histochem Cytochem 43:321–327
24. Koji T, Chedid M, Rubin JS et al (1994) Progesterone-dependent expression of keratinocyte growth factor mRNA in stromal cells of the primate endometrium: keratinocyte growth factor as a progestomedin. J Cell Biol 125:393–401
25. Adams JC (1981) Heavy metal intensification of DAB-based HRP reaction product. J Histochem Cytochem 29:775
26. Natsume T, Koide T, Yokota S et al (1994) Interactions between collagen-binding stress protein HSP47 and collagen. Analysis of kinetic parameters by surface plasmon resonance biosensor. J Biol Chem 269:31224–31228
27. Thomson CA, Ananthanarayanan VS (2000) Structure–function studies on HSP47: pH-dependent inhibition of collagen fibril formation in vitro. Biochem J 349(Pt 3):877–883
28. Clarke EP, Jain N, Brickenden A et al (1993) Parallel regulation of procollagen I and colligin, a collagen-binding protein and a member of the serine protease inhibitor family. J Cell Biol 121:193–199
29. Tam PP, Behringer RR (1997) Mouse gastrulation: the formation of a mammalian body plan. Mech Dev 68:3–25
30. Hay ED, Zuk A (1995) Transformations between epithelium and mesenchyme: normal, pathological, and experimentally induced. Am J Kidney Dis 26:678–690
31. Boyer B, Valles AM, Edme N (2000) Induction and regulation of epithelial–mesenchymal transitions. Biochem Pharmacol 60: 1091–1099
32. Strutz F, Okada H, Lo CW et al (1995) Identification and characterization of a fibroblast marker: FSP1. J Cell Biol 130: 393–405
33. Ng YY, Huang TP, Yang WC et al (1998) Tubular epithelial–myofibroblast transdifferentiation in progressive tubulointerstitial fibrosis in 5/6 nephrectomized rats. Kidney Int 54:864–876
34. Iwano M, Plieth D, Danoff TM et al (2002) Evidence that fibroblasts derive from epithelium during tissue fibrosis. J Clin Invest 110:341–350
35. Zeisberg M, Bonner G, Maeshima Y et al (2001) Renal fibrosis: collagen composition and assembly regulates epithelial-mesenchymal transdifferentiation. Am J Pathol 159:1313–1321
36. Sunamoto M, Kuze K, Tsuji H et al (1998) Antisense oligonucleotides against collagen-binding stress protein HSP47 suppress collagen accumulation in experimental glomerulonephritis. Lab Invest 78:967–972

Virchows Arch (2010) 456:317–323
DOI 10.1007/s00428-010-0882-z

ORIGINAL ARTICLE

Osteoclast-like cells in soft tissue leiomyosarcomas

C. L. M. H. Gibbons · S. G. Sun · M. Vlychou · K. Kliskey · Y. S. Lau · A. Sabokbar · N. A. Athanasou

Received: 22 October 2009 / Revised: 17 December 2009 / Accepted: 6 January 2010 / Published online: 2 February 2010
© Springer-Verlag 2010

Abstract Giant cell-rich leiomyosarcoma of soft tissues is an unusual variant of malignant smooth muscle tumor characterized by the presence of numerous multinucleated giant cells (MNGCs). The nature of MNGCs and the cellular mechanisms underlying their accumulation in this tumor are poorly understood. Analysis of the expression of osteoclast, macrophage, and smooth muscle markers in two cases of giant cell-rich leiomyosarcoma revealed that the MNGCs in giant cell-rich leiomyosarcoma were negative for smooth muscle markers and that these cells expressed an osteoclast-like phenotype, being positive for CD45, CD68, tartrate-resistant acid phosphatase, and CD51 but negative for CD14 and HLA-DR. Scattered tumor-associated macrophages (TAMs) also expressed this phenotype. Leiomyosarcoma tumor cells strongly reacted for CD51 but were negative for CD14, CD45, and CD68. An analysis of 25 conventional (nongiant cell-containing) leiomyosarcomas found isolated $CD68^{+}$ MNGCs in three cases (12%), all of which were grade II/III leiomyosarcomas containing a prominent TAM infiltrate. Leiomyosarcoma-derived TAMs in the presence of receptor activator for nuclear factor kappa B ligand (RANKL) and macrophage colony-stimulating factor were capable of differentiating into osteoclast-like cells capable of resorbing bone. Reverse transcription polymerase chain reaction studies showed that RANKL, osteoprotegerin, and TNF-related apoptosis-inducing ligand were expressed by leiomyosarcoma cells. Our findings indicate that the giant cells found in leiomyosarcomas are osteoclast-like and that they are formed from TAMs by a RANKL-dependent mechanism.

Keywords Osteoclasts · Leiomyosarcoma · RANKL · Bone resorption · Giant cells

C. L. M. H. Gibbons · S. G. Sun · M. Vlychou · K. Kliskey · Y. S. Lau · A. Sabokbar · N. A. Athanasou (✉)
Department of Pathology, Nuffield Dept of Orthopaedics, Rheumatology and Musculoskeletal Science, University of Oxford, Nuffield Orthopaedic Centre, Headington, Oxford OX3 7LD, UK
e-mail: nick.athanasou@noc.anglox.nhs.uk

Introduction

Leiomyosarcoma of soft tissues is a relatively rare malignant tumor composed of spindle-shaped cells that exhibit smooth muscle differentiation. Leiomyosarcomas arise most commonly in the retroperitoneum but have a wide anatomic distribution in the body, accounting for approximately 10% of all soft tissue sarcomas of the extremities [1, 2]. The diagnosis of leiomyosarcoma is confirmed by demonstrating tumor cell expression of smooth muscle antigens including smooth muscle actin (SMA), desmin, and H-caldesmon.

Leiomyosarcomas exhibit a variable degree of differentiation and a number of morphological variants have been described. One unusual variant of leiomyosarcoma contains numerous multinucleated giant cells (MNGCs); this giant cell-rich leiomyosarcoma has been reported in a variety of locations including the uterus, adrenal gland, bowel, spermatic cord, heart, and soft tissues of the extremities [3–10]. Unlike tumor giant cells, which are often found in poorly differentiated leiomyosarcomas, the MNGCs in giant cell-rich leiomyosarcomas do not express smooth muscle markers and are thought to represent an unusual host response to the tumor. These MNGCs have been shown to express CD68 and are commonly described as osteoclast-like, but it is not certain whether they are true osteoclasts as CD68 expression is also a feature of macrophages and macrophage polykaryons [11, 12]. MNGCs in giant cell-rich leiomyosarcomas have not been shown to

exhibit specific features of osteoclasts, such as lacunar resorption or the expression of tartrate-resistant acid phosphatase (TRAP) and CD51/vitronectin receptor (VNR) [13].

Osteoclasts are highly specialized members of the mononuclear phagocyte system [13, 14]. Osteoclast precursors circulate in the monocyte fraction [15, 16], and osteoclasts can be formed from monocytes and macrophages when these cells are cultured in the presence of receptor activator for nuclear factor kappa B ligand (RANKL) and macrophage colony-stimulating factor (M-CSF) [17]. Osteoprotegerin (OPG) is a decoy receptor for RANKL and acts to inhibit osteoclast differentiation. MNGCs are found in a number of benign and malignant soft tissue tumors. In giant cell tumor of tendon sheath and giant cell-rich malignant fibrous histiocytoma, these MNGCs have been shown to express some of the phenotypic characteristics of mature osteoclasts [18–20]. It has also been shown that osteoclasts can be formed from tumor-associated macrophages (TAMs) in mesenchymal tumors and that this involves an interaction with RANKL-expressing stromal cells [21], but whether this mechanism accounts for the accumulation of MNGCs in leiomyosarcoma and other giant cell-containing soft tissue tumors is not known.

In this study, our aim has been to determine the cellular and molecular mechanisms underlying the accumulation of MNGCs in giant cell-rich leiomyosarcoma. We have analyzed the cytochemical and antigenic phenotype of MNGCs in these tumors using a number of osteoclast-specific markers. In addition, we have examined whether TAMs derived from soft tissue leiomyosarcomas are capable of osteoclast differentiation and sought to determine whether this occurs by a RANKL-dependent mechanism.

Materials and methods

Clinical and radiological features of tumor specimens analyzed in this study

This study was approved by the Oxford Clinical Research Ethics Committee. Twenty-seven leiomyosarcomas of soft tissue were obtained from the files of the Nuffield Orthopaedic Centre, Oxford. Two of these cases were diagnosed as giant cell-rich leiomyosarcomas containing numerous osteoclast-like MNGCs. The first of these cases was a deep soft tissue tumor of the thigh (8.5 cm maximum) which arose in a 69-year-old female. Radiological appearances of this giant cell-rich leiomyosarcoma are shown in Fig. 1. The second tumor (4.5 cm maximum) arose in the gluteus maximus of the left buttock of a 25-year-old male.

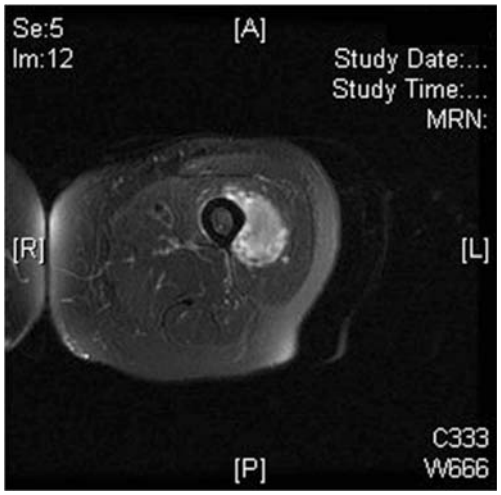

Fig. 1 Axial T2-weighted magnetic resonance image with fat saturation of a giant cell-rich leiomyosarcoma shows a heterogeneous intermediate signal intensity, well-circumscribed soft tissue tumor abutting the left femur

Immunohistochemistry

Immunohistochemical staining was carried out by an indirect immunoperoxidase technique (ChemMate Envision, Dako, UK). Tissue sections were dewaxed and rehydrated by successive immersion in xylene, graded ethanol, and water. Antigen retrieval was performed by microwave treatment (700 W, 2×4 min) in Target Retrieval Solution (Dako, UK). Endogenous peroxidase was blocked by 0.2% (*v*/*v*) hydrogen peroxide in 80% ethanol and protein block serum prior to 30 min incubation with mouse monoclonal antibodies 1A4, D33, anticaldesmon h-CD, PD7/26, CR3/43, and KPI (Dakopatts, UK) directed against SMA, desmin, H-caldesmon, CD45, HLA-DR, and CD68, respectively, and with NCL-CD51 and NCL-L-CD14-223 (Novocastra, UK) directed against VNR (CD51) and CD14, respectively. Antigens were detected by incubation with labeled polymer and diaminobenzidine. The sections were then counterstained with hematoxylin, dehydrated, cleared, and mounted. Sections of normal skin, lymph node, and bone marrow were used as positive control tissue.

Isolation of leiomyosarcoma tumor-associated macrophages and osteoclast formation assays

In order to determine whether leiomyosarcoma TAMs were capable of differentiating into multinucleated cells expressing features of the osteoclast phenotype, TAMs were isolated from two cases of leiomyosarcoma of the extremities, one a tumor of the thigh arising in a 34-year-old female, the other a tumor of the calf arising in a 27-year-old female. Both tumors did not contain giant cells. The tumor tissue was washed in sterile phosphate-buffered saline. Fragments of

the tumor were then placed in 1 mg/ml of collagenase type 1 (Sigma-Aldrich, Dorset, UK) and incubated for 1 h. The digested tissue suspension was passed through a 70-μm pore size cell strainer (Falcon®, Becton Dickinson, Oxford, UK). The filtrate was centrifuged at 1,800 rpm for 10 min and the cell pellet suspended in 2 ml of minimal essential medium (MEM) containing 10% heat-inactivated fetal bovine serum (FBS) supplemented with 100 U/ml penicillin and 10 μg/ml streptomycin (MEM/FBS). The cell yield was counted in a hemocytometer after lysis of red blood cells with 5% (*v*/*v*) acetic acid; 1×10^5 cells per well were added to dentine slices and glass coverslips in a 96-well tissue culture plate. After 3 h of incubation, the dentine slices and glass coverslips were washed in MEM/FBS to remove any non-adherent cells and were then transferred into 24-well tissue culture plates. All cultures were maintained in 1 ml MEM/FBS for up to 21 days in the presence of 25 ng/ml human M-CSF (R&D Systems Europe, UK) and 30 ng/ml soluble human RANKL (PeproTech, UK); culture medium and factors were replenished every 3–4 days. Negative cultures were maintained in MEM/FBS with M-CSF alone.

Cytochemical and functional assessment of osteoclast formation

Following incubation for 24 h and 21 days, cultures on glass coverslips were fixed and stained cytochemically for the osteoclast-associated enzyme TRAP and immunocytochemically for the presence of CD14 and VNR as previously described [18, 21–23]. Functional evidence of TAM–osteoclast differentiation was determined by a lacunar resorption assay system using cell cultures on dentine slices [14, 16, 19, 21]. After 21 days incubation, the cells were removed from the dentine slices by treatment with 0.1 M ammonium hydroxide. The dentine slices were washed in distilled water and ultrasonicated to remove adherent cells; the slices were examined by light microscopy after staining with 0.5% (*v*/*v*) toluidine blue to reveal areas of lacunar resorption.

Leiomyosarcoma—monocyte cocultures and messenger RNA expression of osteoclastogenic factors

After collagenase digestion of the two leiomyosarcomas, mononuclear cells isolated from the tumors were resuspended in MEM/FBS and placed in a 25-cm^2 tissue culture flask. The medium was changed after 24 h of incubation and then at 5- to 7-day intervals. These cultures, containing mononuclear spindle-shaped cells, were passaged when confluent and recultured twice.

To determine whether these mononuclear cells could induce osteoclast formation, $CD14^+$ human peripheral blood monocytes were cocultured with leiomyosarcoma-derived stromal cells for 21 days in the presence of M-CSF on both glass coverslips and dentine slices. Osteoclast formation was assessed by expression of TRAP and VNR and evidence of lacunar resorption as described above.

To determine whether the leiomyosarcoma-derived cells cocultured with monocytes expressed the messenger RNA (mRNA) for RANKL, OPG and TNF-related apoptosis-inducing ligand (TRAIL), these cells were isolated as described above and then treated with trypsin (0.25%)/ethylenediaminetetraacetic acid (1 mM). Total RNA extraction was carried out using the RNeasy® mini kit (QIAGEN, Hombrechtikon, Switzerland), according to the manufacturer's instructions. Single-strand complementary DNA (cDNA) was synthesized from 2.0 μg of total RNA using the SuperScript® First-Strand Synthesis System for semi-quantitative reverse transcription polymerase chain reaction (RT-PCR; Invitrogen, Paisley, UK). cDNA was amplified by PCR using specific primers to RANKL, OPG, and TRAIL with GAPDH control as previously described [24, 25]. PCR products were fractionated on 1% agarose gels, and gel pictures were scanned with Alpha-Imager 2200 (Alpha Innotech Corporation, USA). Positive controls were normal human bone stromal cells, which are known to express RANKL, OPG, and TRAIL.

Results

Morphological and immunophenotypic characteristics of giant cell-rich leiomyosarcoma

The two tumors which were diagnosed as giant cell-rich leiomyosarcomas were both high-grade (grade III) sarcomas that contained interlacing bundles of plump, mainly spindle-shaped tumor cells with elongated or ovoid vesicular, blunt-ended nuclei (Fig. 2). Some tumor cells showed perinuclear vacuolation. Tumor cells exhibited a high mitotic rate (more than five mitotic figures high-power field) and showed prominent cellular and nuclear pleomorphism; many of the tumor cells had large hyperchromatic or vesicular nuclei and there were numerous tumor giant cells. Scattered throughout the tumor were areas of necrosis and numerous large osteoclast-like MNGCs which had abundant pale-staining cytoplasm and multiple round, vesicular nuclei with prominent nucleoli; these cells did not show nuclear atypia or mitotic activity.

Immunohistochemistry showed that the spindle-shaped and pleomorphic tumor cells expressed SMA, caldesmon, desmin, and VNR but did not react for CD45, CD68, or CD14. The osteoclast-like MNGCs strongly reacted for CD45, CD68, and VNR but not CD14, HLA-DR or muscle actin/SMA, caldesmon, or desmin (Fig. 3a, b). A heavy macrophage infiltrate was seen throughout the tumor; most

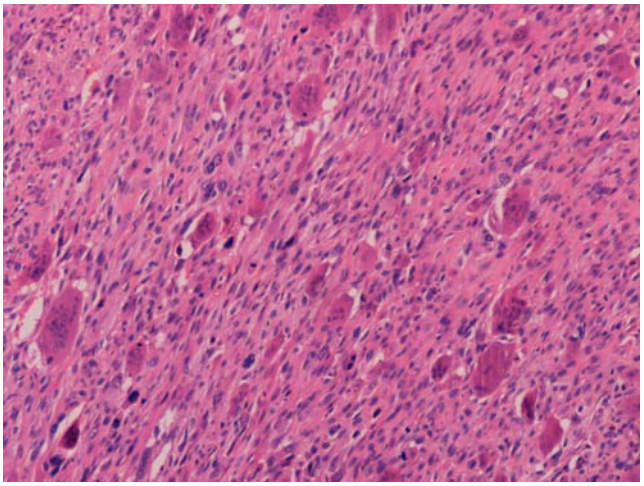

Fig. 2 Giant cell-rich leiomyosarcoma containing numerous osteoclast-like MNGCs and spindle-shaped tumor cells (H&E staining, ×100 magnification)

of these cells expressed CD68, CD14, and HLA-DR; on serial sections, it was noted that a minority of $CD68^+$ macrophages also expressed VNR.

Expression of macrophage and osteoclast markers in conventional leiomyosarcomas

In order to characterize the TAM infiltrate in leiomyosarcomas, representative sections of 25 conventional (i.e., nongiant cell-containing) leiomyosarcomas of soft tissue of the extremities were stained for CD68, VNR, CD14, and HLA-DR. TAMs expressing CD68, CD14, and HLA-DR but not VNR were noted in all tumors, three of which also contained a few discrete $CD68^+/VNR^+$ MNGCs (Fig. 3c). These three cases were all grade III leiomyosarcomas that contained a heavy TAM infiltrate as assessed by CD68 staining.

Leiomyosarcoma TAM–osteoclast differentiation

After 24 h of incubation on glass coverslips, both in the presence and absence of RANKL and M-CSF, adherent mononuclear cells isolated from two conventional leiomyosarcomas were found to be entirely negative for the osteoclast markers TRAP and VNR. These cells strongly expressed CD14, a macrophage antigen which is known not to be present on osteoclasts [11]. The adherent mononuclear cells isolated from the tumors were thus TAMs that expressed the phenotypic characteristics of macrophages and not osteoclasts. In 21-day cultures incubated with RANKL and M-CSF, osteoclast-like MNGCs that expressed TRAP and VNR were noted in TAM cultures (Fig. 4a). No $TRAP^+$ or VNR^+ MNGCs were formed when RANKL or M-CSF was omitted from the cultures.

Cultures of TAMs isolated from both cases of leiomyosarcoma were incubated on dentine slices for up to 21 days in the presence M-CSF and RANKL. After 24 h of incubation, these cultures showed no evidence of lacunar

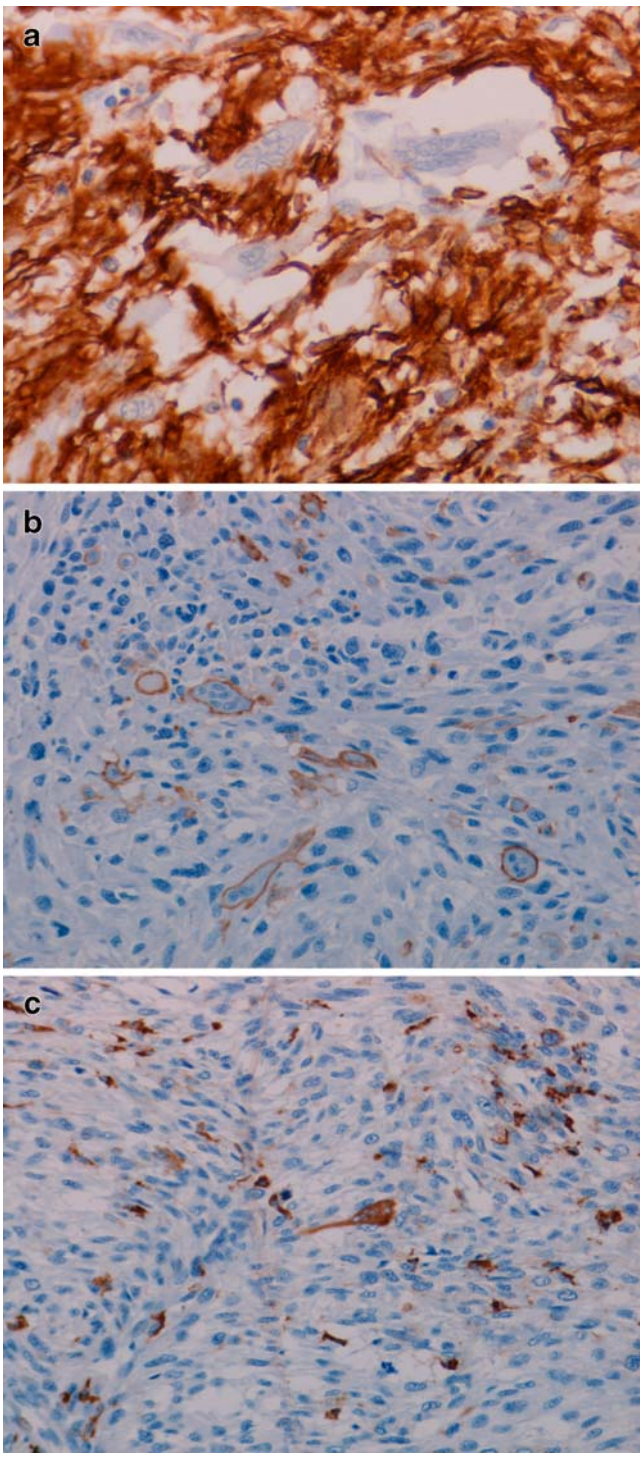

Fig. 3 Immunohistochemistry shows the absence of SMA expression (**a**) and the expression of VNR (**b**) by MNGCs in a giant cell-rich leiomyosarcoma. **c** CD68 expression by TAMs and a single MNGC found in a conventional leiomyosarcoma (×200 magnification)

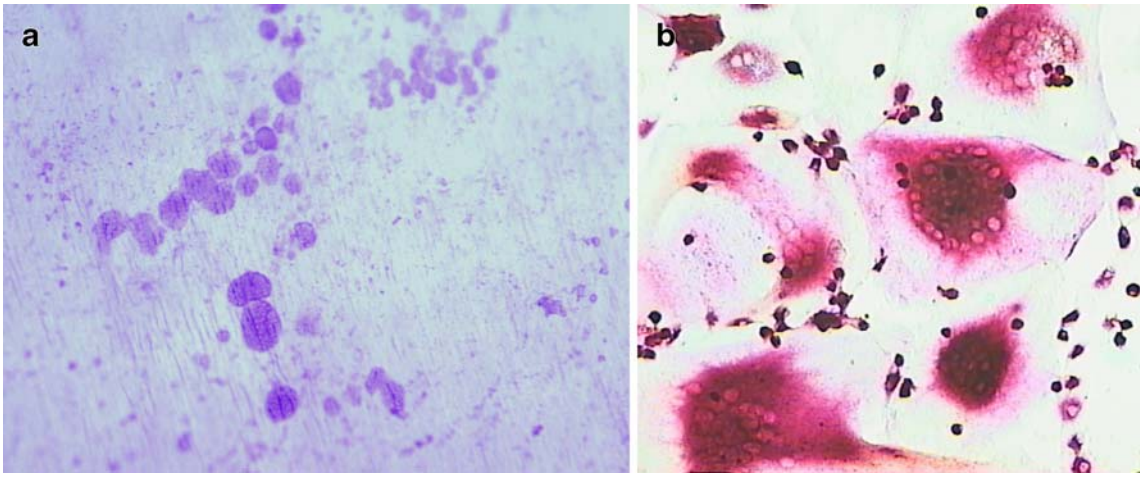

Fig. 4 The 21-day culture of leiomyosarcoma-derived TAMs in the presence of RANKL and M-CSF showing **a** formation of $TRAP^+$ MNGCs (×200 magnification) and **b** lacunar resorption pit formation on a dentine slice stained with toluidine blue (×100 magnification)

resorption on dentine slices. However, in 21-day cultures, there was functional evidence of osteoclast differentiation with the formation of several areas of lacunar resorption on dentine slices (Fig. 4b). Resorption was evident as discrete areas of osteolysis composed of single or compound resorption pits on the surface of the dentine slice. The mean number (± standard error of the mean [SEM]) of pits formed on the dentine slices in the presence of RANKL and M-CSF was 16.8±1.8.

Leiomyosarcoma cells support osteoclastogenesis and express RANKL, OPG, and TRAIL

After three passages, cultures of cells isolated from both cases of soft tissue leiomyosarcoma were composed entirely of spindle-shaped mononuclear cells which expressed SMA but not CD14, CD68, or TRAP. No MNGCs were present in these cultures. These cells, when cocultured with monocytes, resulted in the formation of MNGCs that expressed TRAP and VNR. Cocultures on dentine slices resulted in the formation of resorption pits similar to those seen in TAM cultures incubated with M-CSF and RANKL. The mean number (± SEM) of pits formed on the dentine slices was 28±1.6. These results indicate that the leiomyosarcoma mononuclear cells are capable of supporting the differentiation of monocytes into osteoclasts. RT-PCR studies on these cultured leiomyosarcoma-derived mononuclear cells showed that these cells exhibited expression of mRNA for RANKL, OPG, and TRAIL (Fig. 5).

Discussion

Previous studies of giant cell-rich leiomyosarcomas have noted that these tumors contain MNGCs that express CD68 [4, 5, 8, 9], an antigen which is strongly expressed by all cells of the mononuclear phagocyte series including monocytes, macrophages, macrophage polykaryons, and osteoclasts [11, 12]. Osteoclasts are distinguished from macrophage polykaryons immunophenotypically by the expression of VNR (CD51) and the absence of CD14 and HLA-DR [11]. In this study, we have shown that the MNGCs in giant cell-rich leiomyosarcomas exhibit the specific antigenic phenotype of osteoclasts and that they are distinct from smooth muscle tumor cells, being negative for SMA, desmin, and caldesmon.

To determine the mechanism whereby osteoclastic MNGCs form in soft tissue leiomyosarcoma, we isolated TAMs from two cases of conventional leiomyosarcoma and cultured them for 21 days in the presence of the osteoclastogenic factors, RANKL and M-CSF. Under these conditions, $CD14^+$ TAMs differentiated into multinucleated $CD14^-/TRAP^+/VNR^+$ osteoclasts that were capable of lacunar resorption. Osteoclast precursors have been shown to lose and acquire macrophage and osteoclast markers respectively in the process of osteoclast differentiation [26]; in the same way, leiomyosarcoma $CD14^+/TRAP^-/VNR^-$

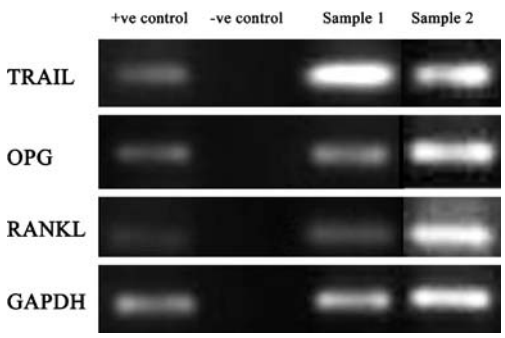

Fig. 5 Expression of RANKL, OPG, and TRAIL mRNA by SMA^+ leiomyosarcoma cells. RT-PCR products were fractionated on agarose gel. *Lane 1*, positive control, *lane 2* negative control, *lanes 3 and 4* leiomyosarcoma-derived cells from two different patients

TAMs differentiated into $CD14^-/TRAP^+/VNR^+$ osteoclastic MNGCs after 21 days in culture; moreover, these cells also acquired the ability to carry out lacunar resorption, a unique functional feature of osteoclasts. Our findings thus indicate that the formation of osteoclast-like MNGCs in leiomyosarcomas is likely to occur by TAM–osteoclast differentiation.

To investigate further the mechanism whereby osteoclastic MNGCs form in leiomyosarcomas, we isolated SMA^+ mononuclear cells from two cases of conventional leiomyosarcoma and incubated them with monocytes in the absence of RANKL. Osteoclast formation, as evidenced by the formation of $TRAP^+/VNR^+$ MNGCs, occurred under these conditions, indicating that these leiomyosarcoma-derived cells were likely to express RANKL. This was confirmed by RT-PCR studies which showed that these SMA^+ mononuclear cells expressed the mRNA for RANKL. These findings suggest that osteoclast differentiation in leiomyosarcomas occurs by a RANKL-dependent mechanism in which mononuclear phagocyte osteoclast precursors in the TAM population interact with RANKL-expressing SMA^+ leiomyosarcoma cells. Leiomyosarcoma cells are known to produce a number of factors that promote RANKL-induced osteoclast formation including vascular endothelial growth factor (VEGF), insulin-like growth factor (IGF), and interleukin-6 (IL-6) [27–29]. VEGF regulates the expression of RANK, the receptor for RANKL, and can substitute for M-CSF to induce osteoclast formation [30, 31]. IGF-1 also regulates RANKL and OPG expression in osteoclastogenesis [32, 33]. IL-6 is thought to play a role in osteoclast formation and pathological bone resorption in a number of osteoclast-rich conditions including Paget's disease and giant cell tumor of bone [34, 35]; IL-6 not only influences RANKL-dependent osteoclastogenesis but can also substitute for RANKL to induce osteoclast formation [36, 37].

TAMs are derived from circulating blood monocytes, and tumor cells have been shown to secrete chemoattractant factors for monocytes [38, 39]. We found that leiomyosarcoma tumor cells strongly expressed the $\alpha v\beta_3$ integrin, VNR; this is of interest as $\alpha v\beta_3$ expression by tumor cells, such as breast cancer cells, has been shown to enhance the recruitment of osteoclast precursors [40]. Whether VNR is expressed by mononuclear cells in other benign and malignant giant cell-containing mesenchymal soft tissue tumors, e.g., giant cell of tendon sheath and giant cell-rich malignant fibrous histiocytoma/giant cell tumor of soft parts [18–20], is not certain. It is known, however, that mesenchymal cells grown from giant cell tumor of bone and giant cell tumor of soft parts, like leiomyosarcoma cells, express the mRNA for RANKL, OPG, and TRAIL, three factors which play a major role in regulating osteoclast formation. RANKL is required for the differentiation of monocytes and macrophages into osteoclasts, while OPG, which also binds TRAIL, acts as a decoy receptor for RANKL to inhibit macrophage–osteoclast differentiation [41].

We have shown in this study that giant cell accumulation in leiomyosarcoma occurs by TAM–osteoclast differentiation via a RANKL-dependent mechanism. Both the cases of giant cell-rich leiomyosarcoma, as well as the cases of conventional leiomyosarcoma which contained a few giant cells, were high-grade sarcomas that had a heavy TAM infiltrate. On the basis of our findings, it could be argued that MNGC formation in leiomyosarcomas occurs when there is either reduced OPG or increased RANKL and TRAIL expression, TAM–osteoclast differentiation being a function of the differential expression of RANKL, TRAIL, and OPG by SMA^+ leiomyosarcoma cells. Analysis of the factors which modulate RANKL, OPG, and TRAIL expression and play a part in determining whether MNGCs are formed in leiomyosarcomas (and possibly other benign and malignant soft tissue tumors) may merit further investigation.

Acknowledgements We would like to thank Mrs. C. Lowe for typing the manuscript. This study was supported by the BOA Wishbone Trust, Jenny Mays-Smith Skin Cancer Research Fund, Oxfordshire Health Service Research Committee and the Rosetrees Charitable Trust. NAA is part of the European Network of Excellence EuroBoNeT (LSHC-CT-2006-018814).

Conflict of interest statement We declare that we have no conflict of interest.

References

1. Evans HL, Shipley J (2002) Leiomyosarcoma. In: Fletcher DCM, Ummi KK, Merters F (eds) Pathology and genetics of tumours of soft tissue and bone. IARC, Lyon, pp 131–134
2. Weiss SW, Goldblum JR (2001) Leiomyosarcoma. In: Weiss SW, Goldblum JR (eds) Enzinger and Weiss's soft tissue tumours, 4th edn. Mosby, St. Louis, pp 727–748
3. Darby AJ, Papadaki L, Beilby JO (1975) An unusual leiomyosarcoma of the uterus containing osteoclast like giant cells. Cancer 360:495–504
4. Matthews TJ, Fisher C (1994) Leiomyosarcoma of soft tissue and pulmonary metastasis, both with osteoclast like giant cells. J Clin Pathol 47:370–371
5. Mentzel T, Calonie E, Fletcher DC (1994) Leiomyosarcoma with prominent osteoclast like giant cells: analysis of eight cases closely mimicking the so-called giant cell variant of malignant fibrous histiocytoma. Am J Surg Pathol 18:258–265
6. Watanabe K, Hiraki H, Ohishi M et al (1996) Uterine leiomyosarcoma with osteoclast like giant cells: histopathological and cytological observations. Pathol Int 46:656–660
7. Konety BR, Singh J, Lyne JC et al (1996) Leiomyosarcoma with osteoclast like giant cells of the spermatic cord. A case report and review of the literature. Urol Int 56:259–262
8. Katoh M, Shigematsu H (1999) Leiomyosarcoma of the heart and its pulmonary metastasis, both with prominent osteoclast like multinucleated giant cells expressing tartrate resistant acid phosphatase activity. Pathol Int 49:74–78

9. Terada T, Endo K, Maeta H et al (2000) Epithelioid leiomyosarcoma with osteoclast like giant cells in the rectum. Arch Pathol Lab Med 124:438–440
10. Candanedo-Gonzalez FA, Vela Chavez T, Cerbulo Vazquez A (2005) Pleomorphic leiomyosarcoma of the adrenal gland with osteoclast like giant cells. Endocr Pathol 16:75–81
11. Pulford KA, Rigney EM, Micklem KJ et al (1989) KPI: a new monoclonal antibody that detects a monocytes/macrophage associated antigen in routinely processed tissue sections. J Clin Pathol 42:414–421
12. Athanasou NA, Quinn J (1990) Immunophenotypic difference between osteoclasts and macrophage polykaryons: immunohistological distinction and implications for osteoclast ontogeny and function. J Clin Pathol 43:997–1004
13. Athanasou NA (1996) The cellular biology of bone resorbing cells. J Bone Joint Surg 78A:1096–1112
14. Quinn J, Sabokbar A, Athanasou NA (1996) Cells of the mononuclear phagocyte series differentiate into osteoclastic lacunar bone resorbing cells. J Pathol 179:106–111
15. Udagawa N, Takahashi N, Akatsu T et al (1990) Origin of osteoclasts: mature monocytes and macrophages are capable of differentiating into osteoclasts under a suitable microenvironment prepared by bone marrow derived stromal cells. Proc Natl Acad Sci USA 87:7260–7264
16. Fujikawa Y, Quinn JMW, Sabokbar A et al (1996) The human mononuclear osteoclast precursor circulates in the monocyte fraction. Endocrinology 139:4058–4060
17. Quinn JM, Elliott J, Gillespie MT et al (1998) A combination of osteoclast differentiation factor and macrophage colony stimulating factor is sufficient for both human and mouse osteoclast formation in vitro. Endocrinology 139:4424–4427
18. Athanasou NA, Quinn J, Ferguson D et al (1991) Bone resorption by macrophage polykaryons of a giant cell tumour of tendon sheath. Br J Cancer 63:527–553
19. Flanagan AM, Chambers TJ (1989) Osteoclasts are present in the giant cell variant of malignant fibrous histiocytoma. J Pathol 159:53–57
20. Lau YS, Sabokbar A, Gibbons CLMH et al (2005) Phenotypic and molecular studies on giant cell tumours of bone and soft tissues. Hum Pathol 36:945–954
21. Yang TT, Sabokbar GCML et al (2002) Human mesenchymal tumour associated macrophages differentiate into osteoclastic bone resorbing cells. J Bone Joint Surg 84B:452–456
22. Minkin C (1982) Bone acid phosphatase tartrate resistant acid phosphatase as a marker of osteoclast function. Calcif Tissue Int 34:285–290
23. Horton MA, Lewis D, McNulty K et al (1985) Monoclonal antibodies to osteoclastoma (giant cell bone tumours): definition of osteoclast specific cellular antigens. Cancer Res 45:5663–5669
24. Lau YS, Danks L, Sun SG, Sabokbar A et al (2007) RANKL-dependent and RANKL-independent molecular mechanisms of macrophage-osteoclast differentiation in breast cancer. Breast Cancer Res Treat 96:1716–1722
25. Lau YS, Sun SG, Gibbons CMLH et al (2007) Cellular and humoral mechanisms of osteoclast formation in Ewing's sarcoma. Br J Cancer 89:928–932
26. Faust J, Lacey DL, Hunt P et al (1999) Osteoclast markers accumulate on cells developing from human peripheral blood mononuclear precursors. J Cell Biochem 72:67–80
27. Potti A, Ganti AK, Tendulkar K et al (2004) Determination of vascular endothelial growth factor (VEGF) overexpression in soft tissue sarcomas and the role of overexpression in leiomyosarcoma. J Cancer Res Clin Oncol 130:52–56
28. Van der Ven LT, Roholl PJ, Gloudemans T et al (1997) Expression of insulin like growth factors (IGFs), their receptors and IGF binding protein3 in normal, benign and malignant smooth muscle tissues. Br J Cancer 75:1631–1640
29. Tabibzadeh SS, Poubouridis D, May LT et al (1989) Interleukin 6 immunoreactivity in human tumours. Am J Pathol 135:427–433
30. Min JK, Kim YM, Kim EC et al (2003) Vascular endothelial growth factor up regulates expression of receptor activator of NF kappa B (RANK) in endothelial cells. Concomitant increase of angiogenic responses to RANK ligand. J Biol Chem 278:39548–39557
31. Aldridge SE, Lennard TW, Williams JR et al (2005) Vascular endothelial growth factor receptors in osteoclast differentiation and function. Biochem Biophys Res Commun 335:793–798
32. Wang Y, Nishida S, Elalieh HZ et al (2006) Role of IGF1 signaling in regulating osteoclastogenesis. J Bone Miner Res 21:1350–1358
33. Rubin J, Ackert Bicknell CL, Zhu L et al (2002) IGF1 regulates osteoprotegerin (OPG) and receptor activator of nuclear factor kappaB ligand in vitro and OPG in vivo. J Clin Endocrinol Metab 87:4273–4279
34. Atkins GJ, Haynes DR, Graves SE et al (2000) Expression of osteoclast differentiation signals by stromal elements of giant cell tumours. J Bone Miner Res 15:640–649
35. Ehrlich LA, Roodman GD (2005) The role of immune cells and inflammatory cytokines in Paget's disease and multiple myeloma. Immunol Rev 208:252–266
36. Devlin RD, Reddy SV, Savino R et al (1998) IL6 mediates the effects of 1L1 or TNF, but not PTHrP or 1, 25(OH)2D3, on osteoclast like cell formation in normal bone marrow cultures. J Bone Miner Res 13:393–399
37. Kudo O, Sabokbar A, Pocock A et al (1998) Interleukin-6 and interleukin-11 support human osteoclast formation by a RANKL independent mechanism. Bone 32:1–7
38. Mantovani A, Botiazzi B, Coloth F et al (1992) The origin and function of tumour associated macrophages. Immunol Today 13:265–276
39. Yamashiro S, Takaya M, Nishi T et al (1994) Tumour derived monocyte chemoattractant protein induces intratumoral infiltration of monocyte derived macrophage subpopulation in transplanted rat tumour. Am J Pathol 145:856–867
40. Sloan EK, Pouliot N, Stanley KL et al (2006) Tumour specific expression of alphavbeta3 integrin promotes spontaneous metastasis of breast cancer to bone. Breast Cancer Res 8:R20
41. Blair HC, Athanasou NA (2004) Recent advances in osteoclast biology and pathological bone resorption. Histol Histopathol 19:189–199

Virchows Arch (2010) 456:325–337
DOI 10.1007/s00428-009-0840-9

ORIGINAL ARTICLE

Transgenic mice expressing nitroreductase gene under the control of the podocin promoter: a new murine model of inductible glomerular injury

Guillaume Macary · Jérome Rossert · Patrick Bruneval · Chantal Mandet · Marie-France Bélair · Pascal Houillier · Jean-Paul Duong Van Huyen

Received: 16 June 2009 / Revised: 8 September 2009 / Accepted: 18 September 2009 / Published online: 6 October 2009
© Springer-Verlag 2009

Abstract The present work identifies a new mouse model of inductible acute glomerular injury leading to focal segmental glomerulonephritis. We take advantage of the suicide gene/prodrug nitroreductase/CB1954 combination, in which nitroreductase converts CB1954, a monofunctional alkylating agent, into its toxic form. We generate two lines of transgenic mice in which the nitroreductase gene was placed under the control of the podocyte-specific gene podocin. The functional analysis of transgenic mice lines showed that CB1954 treatment induced a severe but transitory proteinuria. Sequential histopathological analysis was performed on serial kidney biopsies. Injured glomeruli showed acute lesions with early podocyte vacuolization and detachment, podocyte apoptosis, and cellular proliferation leading to a marked hypercellularity of the urinary space that was associated with collapsing of the glomerular tuft. After 1 month, progressive scarring lead to focal segmental glomerulosclerosis with fibrous capsular adhesion, hyalinosis, and podocytosis associated with interstitial fibrosis. The phenotype of podocytes was changed exhibiting dedifferentiation characterized by the loss of podocyte specific proteins/transcription factor and the expression of injury markers. Bowman's capsule cells were also involved in the cellular changes in a manner suggesting epithelial to mesenchymal transition. This model of podocyte injury in transgenic mice provides new insights into the cellular mechanisms of podocytopathies and their progression to scarring.

Keywords Podocytes · Focal segmental glomerulosclerosis · Nitroreductase · Transgenic models · Proteinuria · Kidney disease progression

Pascal Houillier and Jean-Paul Duong Van Huyen contributed equally to this work.

G. Macary · P. Bruneval · C. Mandet · M.-F. Bélair · P. Houillier · J.-P. D. Van Huyen
INSERM UMRS 872, Centre de recherche des Cordeliers,
Equipe 3,
75006 Paris, France

P. Bruneval · P. Houillier · J.-P. D. Van Huyen
Assistance Publique-Hôpitaux de Paris,
Hôpital Européen Georges Pompidou,
75015 Paris, France

P. Bruneval · P. Houillier · J.-P. D. Van Huyen
Université Paris Descartes,
75006 Paris, France

J. Rossert
AMGEN Global Regulatory Affairs & Safety,
Thousand Oaks, CA, USA

J.-P. D. Van Huyen (✉)
Service d'anatomie pathologique,
Hôpital Européen Georges Pompidou,
20-40 rue Leblanc,
Paris 75015, France
e-mail: jp.dvh@wanadoo.fr

Introduction

In humans, the majority of kidney diseases which progress to chronic renal failure are initiated by glomerular injury [1]. Therefore, the understanding of the mechanisms implicated in the progression of glomerular injury to

complete nephron loss is crucial to elaborate new therapeutic strategies. This will be possible when one will be able to delineate the pathways controlling glomerular recovery and scarring, or governing the transfer of glomerular injury onto the tubulointerstitial compartment. In addition to the well-established but somewhat limited models of glomerular lesions such as puromycin-induced nephrosis in the rat or Thy-1 mesangioproliferative glomerulonephritis, several knockout or transgenic murine models of specific glomerular injury recently brought new insights in glomerular pathophysiology [2–6]. Indeed, these latter models aimed to target a specific glomerular cell type among the complex cellular background engaged in glomerular diseases. The podocytes are considered now as the major cell population in glomeruli not only because of their crucial role in glomerular filtration control, but also because of their recently discovered remodeling properties in glomerulogenesis and in many glomerulopathies. The knowledge about podocyte shifted from a terminally differentiated cell only able to control filtration to a cell exhibiting plasticity characteristics, namely dedifferentiation [7–10], transdifferentiation [10, 11], and proliferation [9, 12]. This resulted in the concept of dysregulated podocyte involved mainly in focal segmental glomerulosclerosis (FSGS) and human HIV-associated nephropathy (HIVAN) [7, 8, 10]. This also supported the reality that podocytes could contribute to the formation of the crescents in proliferative glomerulonephritis [13, 14].

A property of experimental models is the ability to perform sequential renal tissue analysis to better assess the natural history kidney diseases. Therefore, the aim of this work was to develop a model of glomerular injury by specifically targeting the podocytes using a suicide transgene model and to follow the natural history of the disease from the specific podocyte insult to the progression to scarring FSGS lesions and tubular and interstitial changes. We take advantage of the suicide gene/prodrug nitroreductase (NTR)/CB1954 ([5-aziridin-1-yl]-2,4 dinitrobenzamide) combination, in which NTR converts CB1954, a monofunctional alkylating agent, into its toxic form. To date, this strategy has been validated in the field of cancer research [15, 16]. Interestingly, in vitro studies have shown that this approach is effective in poorly or nonproliferating cells. In vivo, the expression of the NTR gene under the control of tissue-specific promoters in transgenic mice was followed by selective elimination of the cell type in which NTR was expressed in the presence of systemic CB1954 administration [17–19]. We generate transgenic mice in which the gene of the bacterial enzyme NTR was placed under the control of the podocyte-specific gene podocin. Systemic administration of CB1954 induced an acute glomerular injury leading to chronic kidney lesions with focal segmental glomerulosclerosis, interstitial fibrosis, and tubular atrophy. This is the first study to validate the effectiveness of the suicide gene/prodrug strategy in the field of renal pathophysiology.

Materials and methods

Plasmid construction

A 4.4-kb fragment of the podocin promoter cloned into pGL3 (Promega) was kindly provided by Dr L. Heidet. The minimal 2.5-kb fragment of this promoter was amplified by polymerase chain reaction (PCR) according to Moeller et al. [20], and subcloned into pCRII vector (TOPO TA Cloning® Kit, Invitrogen). The NotI site was suppressed by digesting and fill-in, and this ΔNot 2.5-kb podocin promoter was subcloned by Acc65i/ApaI restriction enzyme digestion and ligation into a modified pCI (called pGCj) in which PCMV has been replaced by a multicloning site containing Acc65i and ApaI, to obtain the pGCJ-ΔN2.5P plasmid.

Nitroreductase gene into pCM vector was kindly provided by Dr D. Drabek [17]. NotI fragment was subcloned into our plasmid to obtain pGCj-ΔN2.5P-NTR. At the same time, LacZ reporter gene was cloned under the control of the same fragment of podocin promoter (pGCj-ΔN2.5P-LacZ; Fig. 1a).

Generation of transgenic mice

The podocin promoter/NTR and podocin promoter/LacZ transgenic constructs were isolated from these plasmids by PvuI restriction enzyme digestion and gel purification. They were co-injected into pronuclei from fertilized C57Bl/6×CBA strain mouse eggs using standard techniques. Four lines which had integrated the NTR transgene were characterized by PCR amplifying a 210pb fragment from NTR gene (forward: ttaacgctacgctgccgaaatct; reverse: tgaa gatttagcgggtattgag) and confirmed by Southern blot. X-gal coloration of transgenic kidney was then performed as previously described [13]. F1 transgenic mice were bred with wild-type C57Bl/6 mice to obtain heterozygous and WT littermates, which were screened by NTR PCR on tail DNA samples.

Experimental protocol

Animals and protocol of treatment

All animals used in this study were heterozygous females aged 2 to 3 months and weighing 20–25 g. Transgenic mice (CB1954/podoNTR-Tg) received two intraperitoneal injections of CB1954 of 80 mg/kg, diluted at 4 mg/ml in PBS

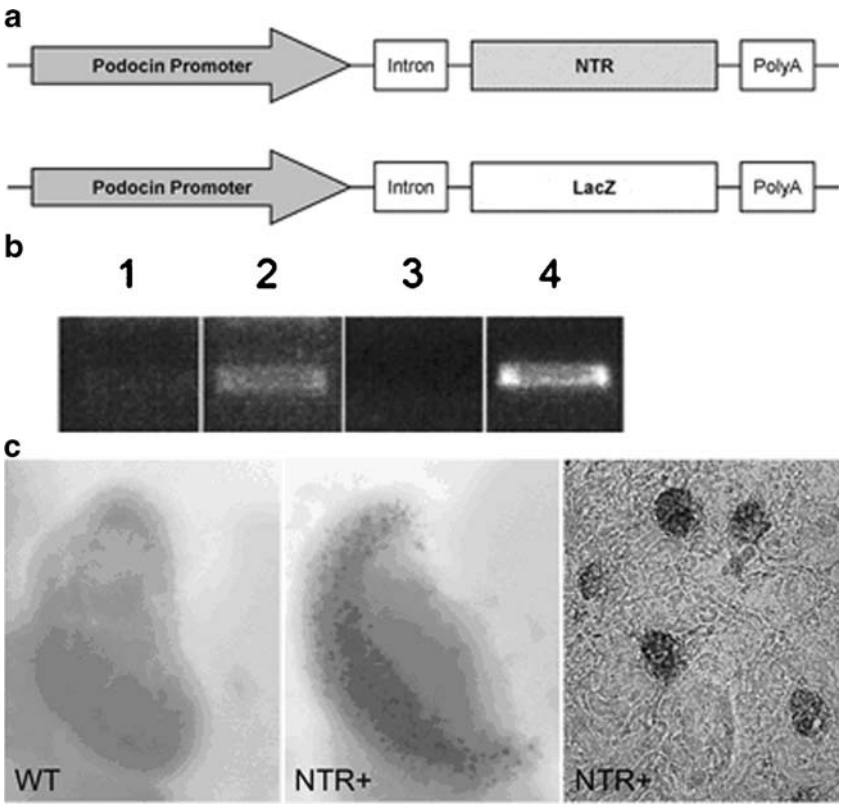

Fig. 1 Elaboration and validation of the model. **a** Schematic representation of microinjected fragments: gene of interest (nitroreductase) and reporter gene (LacZ) are driven by podocin promoter. Intron and polyA sequences have been added to allow a high expression level of transgenes. **b** RT-PCR assays confirm specific kidney expression of nitroreductase. Lane 1 is negative control (water), lane 2 is kidney sample, lane 3 is negative control of reverse transcription (RT-), and lane 4 is positive control (plasmid). **c** Half kidneys of WT and NTR positive mice identified by PCR have been X-gal-stained in order to estimate the expression of the reporter gene: LacZ is expressed only in NTR positive mice within the cortex and more precisely within the glomeruli

20% DMSO. The first injection was done at day 0 (d0) and the second at day 2 (d2). Wild type mice injected with CB1954 (CB1954/WT mice) following the same protocol and heterozygous transgenic mice injected with the vehicle alone (vehicle/podoNTR-Tg mice) were used as controls. Animal groups were as follows: transgenic mice (n=15, from three independent experiments) and wild-type (n=3) mice littermates; an additional control group of transgenic mice (n=3) was injected with the vehicle alone. The experiments were performed in accordance with regulations of French Ministry of Agriculture. Mice had free access to tap water and normal chow.

Protocol of analysis

Both biological and histological parameters in the same individuals issued from both groups of CB1954/podoNTR-Tg and CB1954/WT mice were assessed prospectively in the study.

For physiological analysis, animals were placed in metabolic cages (one animal per cage) from d−4 to d0 for acclimatizing. Twenty-four hour urine was collected at d−1–d0, d7–d8, d14–d15, and at d29–d30, in order to assess renal function and urinary protein excretion. Body weights were also measured. Blood samples were obtained by puncture of the retro-orbital sinus.

For microscopic analysis, renal biopsies were performed in mice at d8 and d15. Under anesthesia (mixture of xylazine and ketamine), the lateral abdominal wall was opened under the last rib and kidney was extracted. A thin sample of renal cortex was removed with a razor blade. Bleeding was controlled thanks to hemostatic wick (Coalgan®, Brothier Laboratories, Nanterre, France) before kidney was reintroduced and the wall sutured. In our study design, one kidney was biopsied at d8 and the other at d15. The entire kidneys were removed at sacrifice at d30. Figure 2 shows the Masson's trichrome-stained sections on d8 and d15 kidney biopsies and on d30 nephrectomies for a single animal. A mean number of 50±3 glomeruli per kidney biopsy section (n=25 from 13 mice) was available for histopathology. On d30 nephrectomies, a limited cortical fibrous scar, measuring less than 1/5 of the cortex surface, was excluded from microscopic analysis.

Biological parameters analysis

Urine samples were analyzed with an automat Konelab 20 (Thermo). Urinary protein concentration was measured by photometric method, urinary creatinine concentration by enzymatic reaction. Blood samples were centrifuged to obtain plasma. Plasma creatinine concentration was mea-

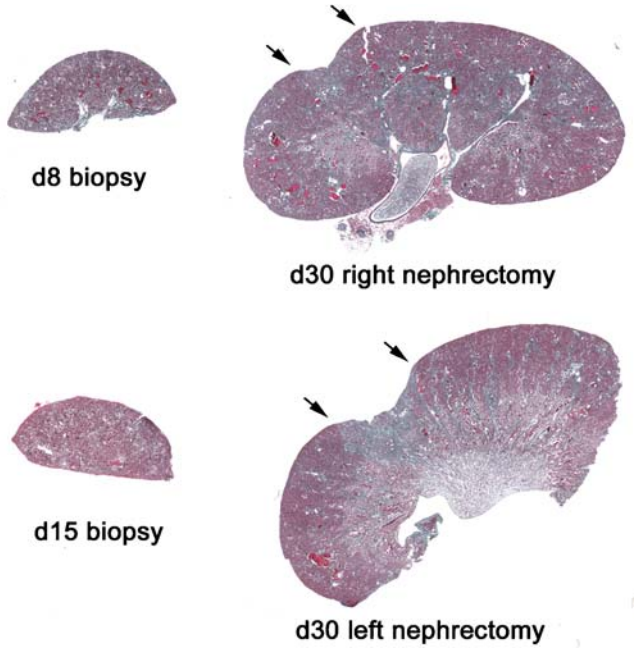

Fig. 2 Masson's trichrome-stained sections of d8 and d15 kidney biopsies and of d30 right and left nephrectomies, obtained from the same animal during the longitudinal follow-up of kidney histopathology. Tissue samples obtained by the kidney biopsies were appropriate for light microscopy analysis. In d30 nephrectomy, a fibrous scar (between the two arrows) measuring less than 1/5 of the kidney surface area was excluded from further analysis

sured by high-performance liquid chromatography method (Dionex).

Tissue sample and histopathology

All kidney tissues were fixed in alcoholic Bouin' solution, formalin, or in glutaraldehyde. For histopathology, four µm-thick sections were stained with hematein-eosin, silver stain, and Masson's trichrome stain. The glomeruli were assessed for both acute lesions including cell vacuolization, cellular proliferation, and chronic lesions including glomerulosclerosis, tuft-to-capsule adhesion, hyalin material deposition, cellular droplets. Vascular injury was addressed in interlobulary arteries and arterioles. The tubular-interstitial compartment was evaluated for tubular atrophy, dilatation, or casts, and for interstitial inflammation and fibrosis.

A semi-quantitative evaluation of glomerular lesions, interstitial fibrosis, and tubular atrophy was performed in a blinded fashion in the kidney samples (d8 and d15 biopsies, and d30 nephrectomies) along the follow-up study. For glomerular histopathology, an average of 50 and 100 glomeruli per sample was assessed in biopsies and nephrectomy specimens, respectively. For the d30 kidneys, counts were performed in areas distant from the scar of the previous biopsy. The number of injured glomeruli, with both acute and chronic lesions, was expressed as a percentage of the total number of counted glomeruli. Interstitial fibrosis and tubular atrophy were assessed semi-quantitatively as previously described [21].

Immunohistochemistry

Immunohistochemistry was performed on 4-µm thick kidney sections with the following primary antibodies: rabbit polyclonal anti-human WT1 (Santa Cruz Biotechnology, Santa Cruz, California, USA), rat monoclonal anti-mouse Ki67 (DAKO, Trappes, France), mouse monoclonal anti-human synaptopodin (Progen, Biotechnik, Heidelberg, Germany), goat polyclonal anti-human nephrin (Santa Cruz Biotechnology), mouse monoclonal anti-human α-smooth muscle actin (NeoMarkers, Fremont, CA, USA), mouse monoclonal anti-human desmin (DAKO). A three step streptavidin-biotin technique with prior antigen retrieval procedure was used with secondary anti-rabbit (1/400), anti-mouse (1/200), anti-rat (1/300), and anti-goat (1/200) biotinylated antibodies and streptavidin-peroxidase amplification ELITE and ABC-phosphatase kits (all from Vector laboratories, Burlingame, USA) [11, 22]. Diaminobenzidine (DAKO) and Fast Red (DAKO) were used as chromogens.

Results of immunohistochemistry were semi-quantitatively assessed in a blind fashion at d30. The number of glomeruli with abnormal expression of desmin and of α-smooth muscle actin and the number of glomeruli with impaired synaptopodin labeling were expressed as a percentage of total glomeruli. For cell proliferation, the Ki-67 labeling index was calculated as the mean of the number of Ki-67-positive nuclei/glomerulus, in 50 glomeruli.

TUNEL technique

Apoptosis was detected by the in situ DNA nick end-labeling technique (TUNEL). Sections were incubated first with proteinase K (Sigma, Saint Quentin Falavier, France), at 20 µg/ml and for 15 min at room temperature. A TUNEL kit (ApopTag peroxidase kit, Chemicon-Millipore, Molsheim, France) was then used as previously described [10].

Transmission electron microscopy

Tissues were fixed in 2% glutaraldehyde in PBS. Samples from the cortex were submitted to standard technique as previously described [23].

Statistical analysis

All results are expressed as the mean±SEM. Statistical analysis was performed by analysis of variance followed by

unpaired student's *t* test or Mann–Whitney nonparametric test when appropriate. Statistical significance was defined as $p<0.05$ (*). Statistical analysis performed between the two types of controls: Wild-type mice injected with CB1954 (CB1954/WT mice) and transgenic mice injected with the vehicle alone (vehicle/podoNTR-Tg mice) showed similar results (data not shown). Thus, these animals were pooled into a single control group.

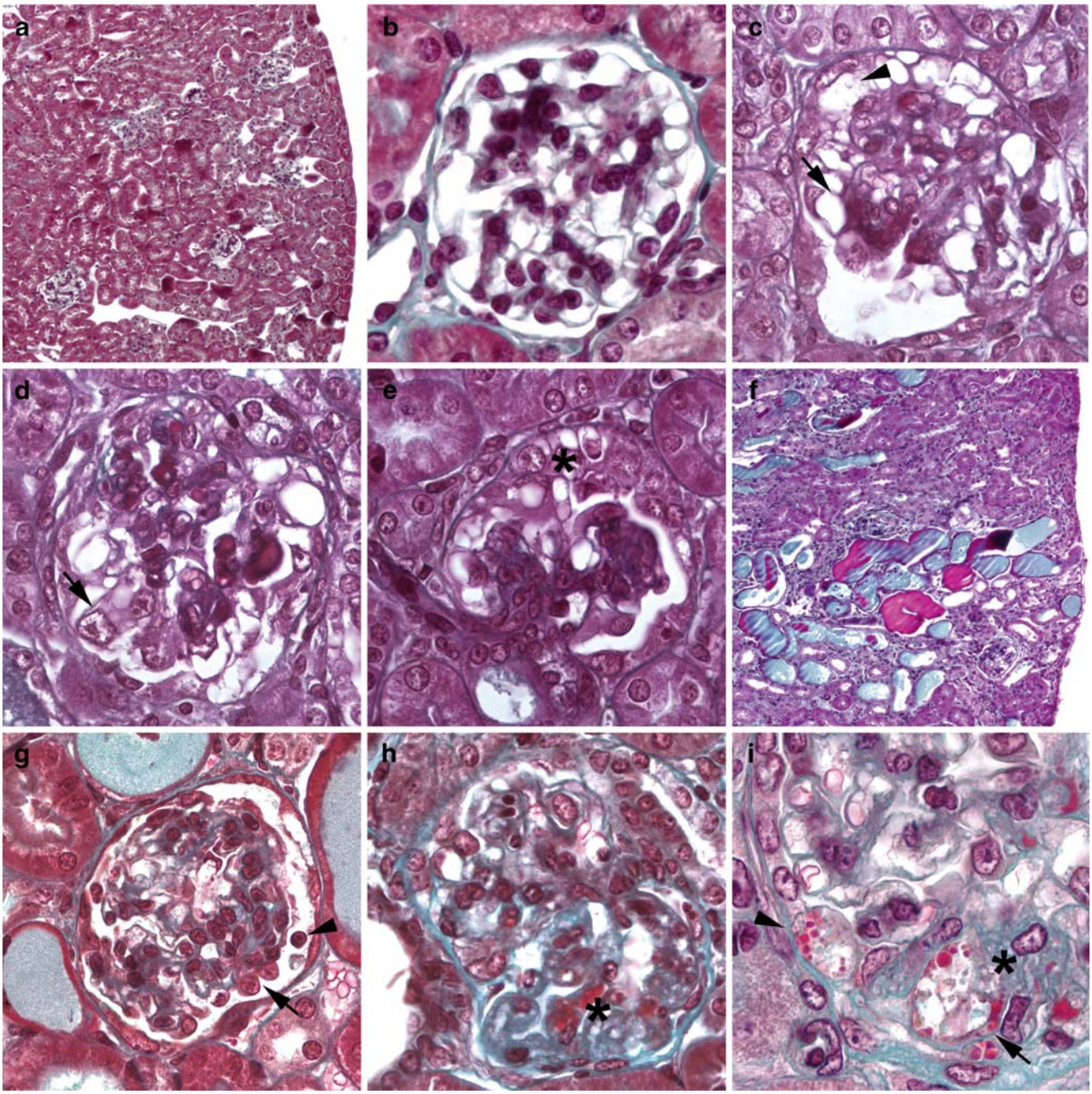

Fig. 3 Light microscopy in podocin-NTR transgenic mice treated with the vehicle alone (control mice, **a**–**b**) or with CB1954 (**c**–**i**), in d8 biopsies (**a**–**e**), and in d30 nephrectomies (**f**–**i**). Control mice remain normal (**a** and **b**). Acute lesions were mainly observed at d8 and included: cytoplasmic vacuolization of podocytes (**c**) and of parietal cells (**c**, *arrowhead*) with podocyte hypertrophy (**d**). The most severely injured glomeruli showed marked hypercellularity in the urinary space (*) with collapsing of the capillary loops. D30 nephrectomies were characterized by areas of interstitial fibrosis and tubular dilatation (**f**). The chronic changes of glomeruli were characterized by hypertrophic podocytes (**g**, *arrow*), detachment of the podocytes in the urinary space (**g**, *arrowhead*) and by fibrous adhesions of the glomerular tuft to the Bowman's capsule with hyalinosis (**h**, **i**, *). The podocytes (**i**, *arrow*) and the parietal cells of the Bowman's capsule (**g**, *arrowhead*) appeared swollen with cytoplasmic hyalin droplets. Trichrome stain (**a**, **f**: ×50; **b**–**e**, **g**–**h**: ×600; **i**: ×1,000)

Results

Transgenic mouse glomeruli express nitroreductase gene and have a normal structure

Kidney-specific expression of NTR was confirmed by RT-PCR (Fig. 1b). LacZ reporter gene expression was detectable in glomeruli of transgenic but not wild-type mice by X-gal staining (Fig. 1c). We examined the structure of transgenic mouse glomeruli at light microscopic and ultrastructural levels to determine whether the expression of the transgene changed glomerular structure. There were no detectable structural abnormalities in transgenic mice (Fig. 3a-b). In particular, podocytes were present with normal distribution and structure, and transmission electron microscopy showed that podocyte foot processes were normal (not shown). Urine from transgenic mice had no increase in protein. Therefore, nitroreductase was expressed in podocytes of transgenic mice and its expression by itself did not change the structure of mouse glomeruli.

CB1954 injection increases the mortality in transgenic mice

CB1954 treatment was associated with an early over-mortality in podoNTR-Tg mice: 47% (7/15 animals) of treated transgenic mice died within the first 3 days. Necropsy was not performed in these animals. One additional mouse died after the d15 biopsy from anesthesic side effects. Both wild-type mice injected with CB1954 and transgenic mice injected with the vehicle alone remained healthy during the 30 day-follow-up. Thus, seven CB1954/podoNTR-Tg, three CB1954/WT, and three vehicle/podoNTR-Tg mice completed the entire longitudinal 30 days protocol and were further completely evaluated in terms of renal function and histopathology.

CB1954 injection induces transient proteinuria in transgenic mice

The results of the longitudinal physiological study are given in Table 1. Body weight, urinary volume, and urinary

Table 1 Urinary parameters

		Time (days)				ANOVA		
		0	8	15	30	Time	Group	Interaction
Body Weight (g)	Control	22.99±1.1 n=6	23.2±1.0 n=6	22.7±0.9 n=6	21.4±1.2 n=6	p=0.787	p=0.237	p=0.267
	CB1954/podonNTR-Tg	22.3±0.9 n=7	21.2±0.3 n=7	22±0.3 n=7	22.3±0.4 n=7			
Plasma creatinine concentration (μmol/L)	Control	5.7±0.2 n=5	6.4±0.4 n=5	4.2±0.2 n=5	5.6±0.7 n=5	p=0.126	p=0.206	p=0.431
	CB1954/podonNTR-Tg	5.2±0.7 n=7	5.1±0.4 n=4	4.7±0.2 n=4	5.1±0.3 n=7			
Urinary volume (μl/24 h)	Control	878±108 n=6	730±124 n=6	690±220 n=6	650±190 n=5	p=0.655	p=0.644	p=0.821
	CB1954/podonNTR-Tg	741±98 n=7	691±101 n=7	790±136 n=7	814±173 n=7			
Urinary creatinine excretion (μmol/24 h)	Control	1.78±0.16 n=6	1.69±0.11 n=6	1.68±0.21 n=6	1.87±0.69 n=5	p=0.065	p=0.662	p=0.8
	CB1954/podonNTR-Tg	1.49±0.31 n=7	1.13±0.07 n=7	1.58±0.24 n=6	1.52±0.2 n=6			
Urinary protein excretion (mg/24 h)	Control	0.76±0.12 n=6	0.43±0.04 n=6	0.39±0.06 n=6	0.34±0.06 n=4	p=0.102	p=0.02	p=0.055
	CB1954/podonNTR-Tg	0.47±0.06 n=7	4.26±1.63 n=7	2.31±0.94* n=6	0.74±0.98* n=5			
Urinary Protein/creatinine ratio (mg/μmol cratinine)	Control	0.44±0.1 n=6	0.26±0.03 n=6	0.25±0.05 n=6	0.18±0.05 n=4	p=0.113	p=0.019	p=0.084
	CB1954/podonNTR-Tg	0.35±0.05 n=7	3.86±1.58* n=7	1.79±1.02* n=6	0.59±0.18* n=5			

Control: as described in the "Material and method" section, vehicle/podoNTR-Tg (n=3) and CB1954/WT n=3 mice were pooled; CB1954/podoNTR-Tg: podoNTR transgenic mice treated with CB1954 (n=7). Data expressed as mean±SEM for n animals. Two-way ANOVA with time- and group-effects. Comparisons between groups are made at different time-point

*p<0.05, Mann–Whitney non parametric test

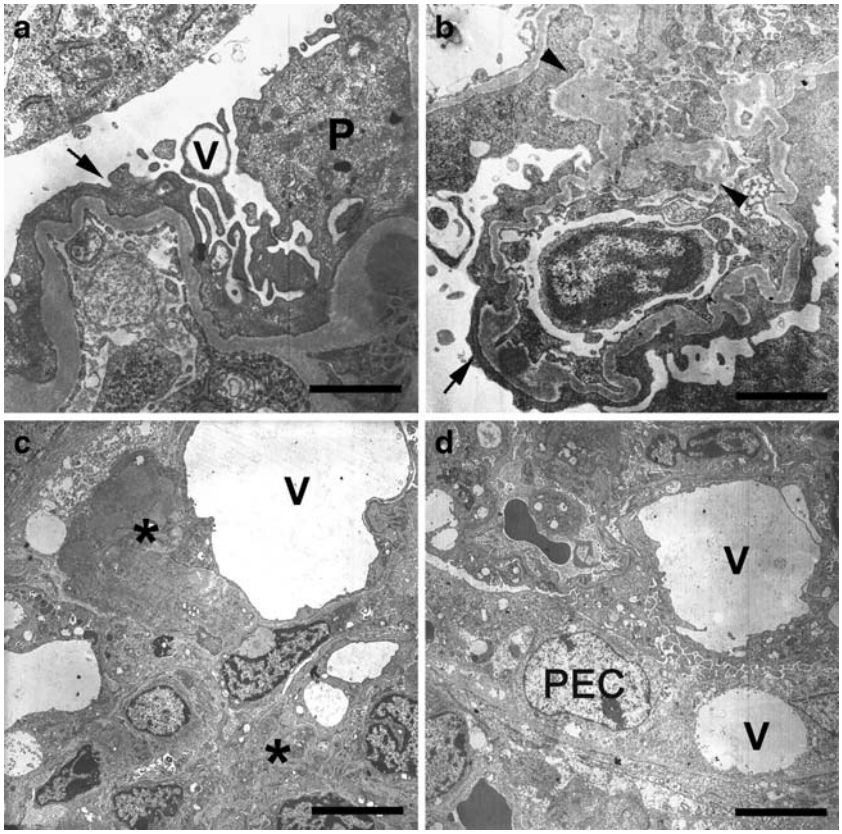

Fig. 4 Ultrastructural analysis of podocin-NTR transgenic mice treated with CB1954 at d8. **a** Podocytes (*P*) with foot process disappearance (*arrow*) and a small cytoplasmic vacuolization (*V*). **b** Excessive folding of the GBM (*arrowheads*) was present in area of podocyte injury (*arrow*). **c** Completely collapsed capillary loops with folded GBM (*) with adjacent podocyte vacuolization (*V*). **d** Cellular vacuoles (*V*) in parietal epithelial cell (PEC), (**a**: bar 3 μm; **b**–c: bar 5 μm)

creatinine excretion remained constant throughout the study and similar in CB1954/podoNTR-Tg and in control groups. In PodoNTR-Tg mice, CB1954 treatment induced proteinuria (assessed by both 24-h total urinary protein excretion and urinary protein/creatinine ratio) that peaked at d8 and progressively decreased at d15 and d30, while remaining significantly higher than in controls.

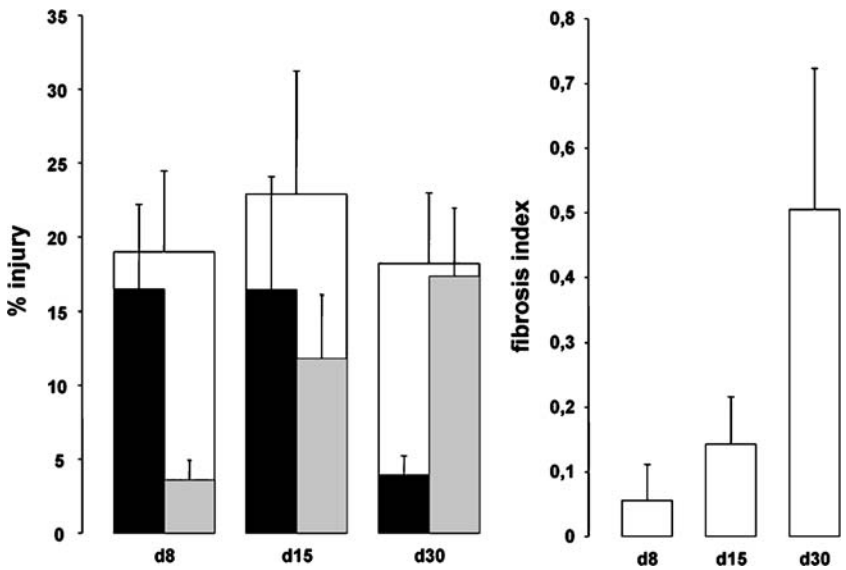

Fig. 5 Evolution of the glomerular lesions (**a**) and the interstitial fibrosis (**b**) from d8 to d30. The percentage of impaired glomeruli is figured in *open bars* and is the ratio of the number of glomeruli with one or more lesions to the total number of observed glomeruli. In *black bars* is figured the ratio of glomeruli showing acute injuries to the total impaired glomeruli, and in grey bars the ratio of glomeruli exhibiting chronic lesions to the total impaired glomeruli. Acute glomerular lesions decrease with time and chronic lesions increase with time whereas the percentage of injured glomeruli did not vary. The index of interstitial fibrosis (*open bars*) increases from d8 to d30. The results are presented as mean±SEM

CB1954 injection induces an acute glomerular injury in transgenic mice leading to focal segmental glomerulosclerosis

Histopathology is shown in Fig. 3 and the quantification of the lesions are summarized in Fig. 5. Both control animal groups, CB1954/WT and vehicle/podoNTR-Tg, had no significant kidney lesions at d8, d15, and d30 (Fig. 3a-b, data not shown). In transgenic mice treated with CB1954, d8 kidney biopsies were characterized by acute lesions affecting an average of 1/6 of the glomeruli, while the remaining glomeruli were normal by light microscopy. Glomerular injury (Fig. 3c-e) was characterized by vacuolated and hypertrophic podocytes and parietal epithelial cells (PEC) of the Bowman's capsule that crowded the urinary space and by global or segmental collapsed of the glomerular tuft. No mesangial hypercellularity nor cellular proliferation or leukocyte infiltration within the capillary loops were observed. Only mild tubular abnormalities such as tubular dilatation with flattening of the tubular epithelia were observed at this stage. Interstitial fibrosis was absent. Similar lesions were still observed in the same extent in d15 biopsies, but were significantly reduced in d30 nephrectomies. Electron microscopy findings are illustrated in Fig. 4. Ultrastructural analysis of the glomeruli at d8 showed that altered podocytes showed foot process disappearance and cytoplasmic vacuolization. Below these injured podocytes, the glomerular basement membrane was folded and completely packed in the more severely collapsed loops. PEC also showed cytoplasmic vacuolization.

D30 nephrectomies were characterized by focal segmental glomerulosclerosis affecting 18±4% of the glomeruli associated with severe tubular and interstitial injury (Fig. 3f–i). The involved glomeruli were characterized by fibrous scars with adhesions to Bowman's capsule and hypertrophic podocytes covered sclerotic tuft loops. Hyalinosis, i.e., the accumulation of amorphous glassy material beneath the glomerular basement membrane was observed

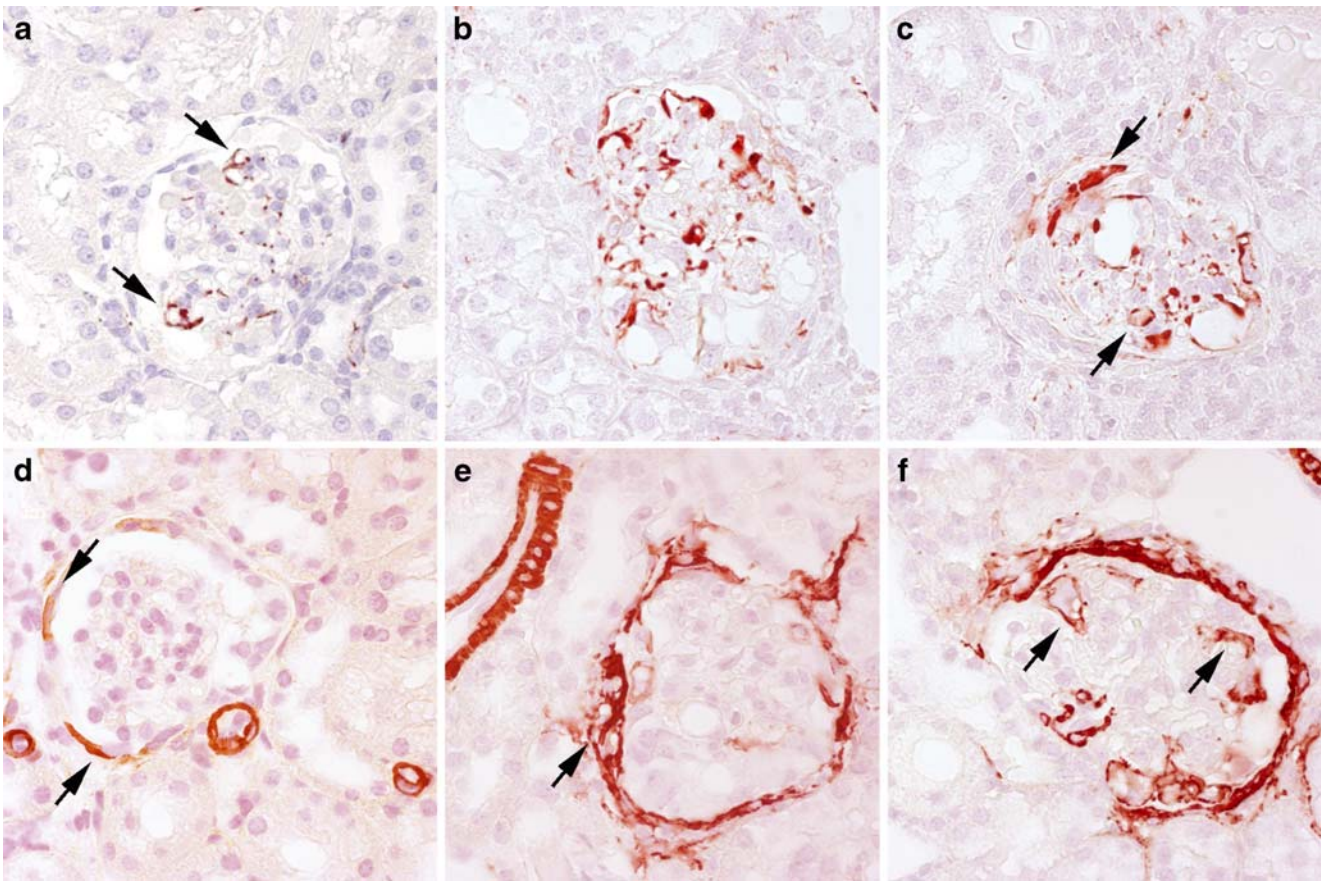

Fig. 6 Immunohistochemical markers of glomerular injury: desmin (**a**–**c**) and α-smooth muscle actin (**d**–**f**) in d8 kidney biopsies of podocin-NTR transgenic mice treated with CB1954. The intensity of glomerular injury increases from left to right panels. Mild alterations were characterized by a scarce podocyte expression of desmin (**a**, *arrows*) and by a limited expression of α-smooth muscle actin by PEC lining the Bowman's capsule (**d**, *arrows*). No mesangial cell was labeled with α-smooth muscle actin. Desmin immunoreactivity increased in more severely injured glomeruli (**b**) as α-smooth muscle actin staining extended to the entire Bowman's capsule (**e**). In severe lesions, both desmin (**c**, *arrows*) and α-smooth muscle actin (**f**, *arrows*) labeled cells in the urinary space. (**a**–**f**: ×600)

in sclerotic lesions. The podocytes and more rarely the PEC of the Bowman's capsule appeared swollen with vacuolated and hyaline droplets. In some glomeruli, the podocytes were detached and floated in the urinary space. Tubular atrophy and dilatation with interstitial fibrosis was associated with the severity of glomerular sclerosis and their distribution followed that of the glomerular sclerosis.

Figure 5 depicts the evolution of the quantification of glomerular lesions and interstitial fibrosis index from d8 to d30. The percentage of injured glomeruli did not vary over time (19±5% at d8, 23±8% at d15, and 18±4% at d30; n=7). The type of glomerular damage was variable over time, with some glomeruli exhibiting both acute and chronic lesions, particularly at d15. Acute glomerular lesions were similarly observed at d8 and d15 but were strongly reduced at d30 (16±5% at d8, 16±7% at d15, and 4±1% at d30; n=7) while the percentage of glomeruli exhibiting chronic lesions constantly increased with time (4±1% at d8, 12±4% at d15, 17±4% at d30; n=7). Interstitial fibrosis score significantly increased with time (0.06±0.05 at d8, 0.14±0.07 at d15, 0.5±0.21 at d30; n=7).

Glomerular cell phenotypes were changed. Figure 6 illustrates the results of immunohistochemistry showing markers of glomerular injury: desmin and α-smooth muscle actin. As early as d8, the markers of glomerular injury were expressed in glomeruli. Desmin was strongly expressed in podocytes in injured glomeruli whereas it was negative in normal glomeruli (Fig. 6a-c). Desmin expression was observed in podocytes still attached to the glomerular tuft and in cells filling the urinary space. Interestingly α-smooth muscle actin, usually considered as a marker of mesangial cell activation, was expressed with an unconventional pattern. Mesangial cells were negative whereas PEC along the Bowman's capsule and occasional cells in the urinary space strongly expressed α-smooth muscle actin (Fig. 6d–f). The markers of podocytes differentiation, synaptopodin (Fig. 7a–d), nephrin (Fig. 7b–e), and WT1 (Fig. 7c–f) were also lost in a segmental pattern in affected glomeruli as early

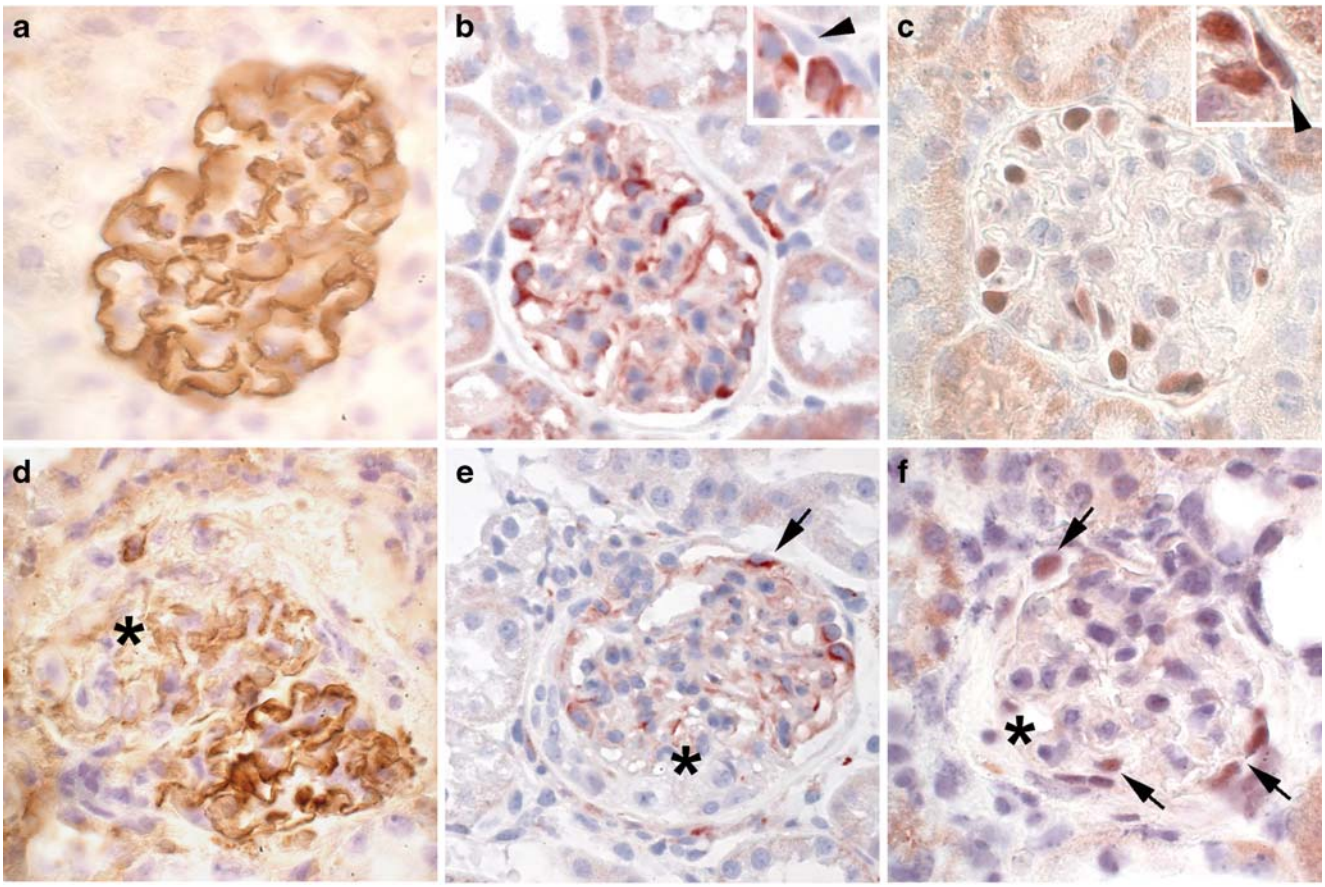

Fig. 7 Immunohistochemical markers of podocyte differentiation: synaptopodin (**a**, **d**), nephrin (**b**, **e**), and WT-1 (**c**–**f**) in d8 kidney biopsies from podocin-NTR transgenic mice treated with CB1954 (**d**–**f**) or with the vehicle alone (control mice, **a**–**c**). In control mice, synaptopodin (**a**), nephrin (**b**), and WT-1 (**c**) labeled all the podocytes covering the glomerular tuft. Parietal cells rarely expressed WT-1 (**c**, *inset*, *arrowhead*), were negative for nephrin (**b**, *inset*, *arrowhead*). In injured glomeruli, all three markers were lost within the segmental lesions (*) and were expressed in the podocytes in remnants of the glomerular tuft (*arrows*), (**a**–**f**: ×600)

as d8. None of these podocyte markers labeled any cells within urinary space. The proliferation marker Ki-67 was strongly expressed in injured glomeruli from d8 biopsies to d30 nephrectomies (Fig. 8a–c). The TUNEL technique showed rare apoptotic cells, both podocytes and PEC, in injured glomeruli (Fig. 8d–e). Interestingly, injury, dedifferentiation, and cell proliferation markers displayed a sustained altered expression in glomeruli undergoing glomerulosclerosis as illustrated by glomerular counts performed at d30 (Fig. 9).

Correlations between proteinuria, histopathology, and immunohistochemistry

The relationship between histopathology at d8 and at d30 was first evaluated. The percentage of glomeruli with acute lesions at d8 significantly correlated with the percentage of glomeruli with chronic lesions at d30 (R2=0.76, p=0.011, n=7) and with the extent of interstitial fibrosis as assessed by fibrosis index at d30 (R2=0.7, p=0.019, n=7). Concerning the relationship between physiological parameters and histopathology, proteinuria at d8 significantly correlated with the extent of acute histological lesions at d8 (R2=0.77, p=0.01, n=7), with the extent of chronic lesions at d30 (R2=0.92, p=0.001, n=7), and with the fibrosis index at d30 (R2=0.85, p=0.003, n=7). Furthermore, proteinuria at d8 also correlated with the loss of synaptopodin expression at d30 (R2=0.50, p=0.04, n=7) and with glomerular Ki-67 index at d30 (R2=0.79, p=0.007, n=7), while no correlation was observed with desmin and α-smooth muscle actin glomerular expression at d30.

Discussion

The present work describes a new mouse conditional model of glomerular injury leading focal segmental glomerulosclerosis in its collapsing variant. We generated several lines of transgenic mice in which the suicide gene/prodrug

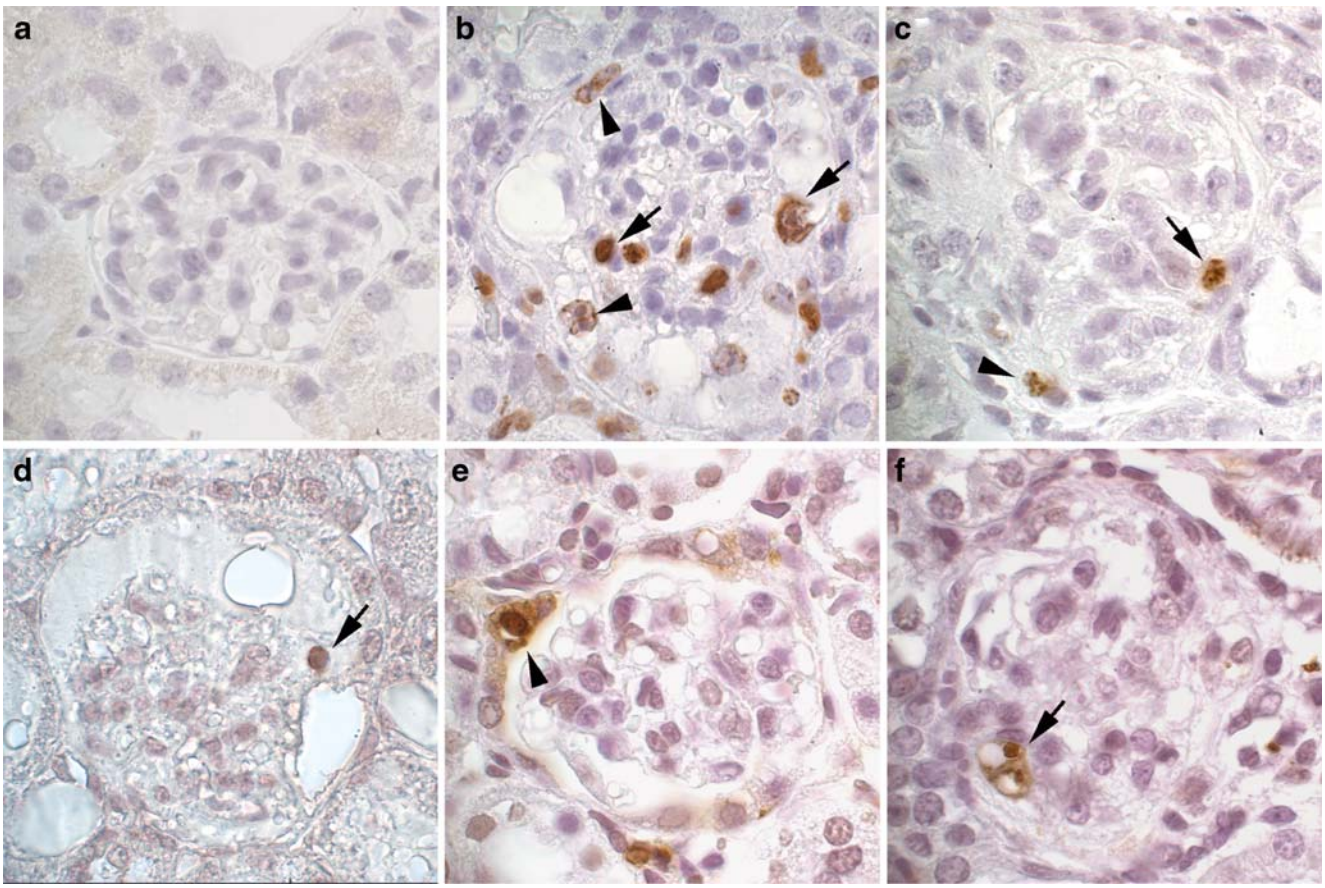

Fig. 8 Cell proliferation and apoptosis in kidney biopsies from podocin-NTR transgenic mice treated with CB1954. Ki67 labeling in transgenic mice treated with vehicle alone (**a**) and with CB1954 (**b**–**c**) at d8 (**a**–**b**) and d30 (**c**). In control mice, no cell proliferation was observed. In severely injured glomeruli at d8, Ki67 labeled numerous cells within the glomerular tuft and in the urinary space (*arrows*) and cells along the Bowman capsule (*arrowhead*). The number of Ki67 glomerular positive cells decreased at day 30 (**c**). TUNEL technique showed rare apoptotic cells at d8 (**d**), d15 (**e**) and, at d30 (**f**), floating in the urinary space (**d**, *arrow*), lining the Bowman's capsule (**e**, *arrowhead*), and in a segmental scar lesion (**f**, *arrow*), (**a**–**f**: ×600)

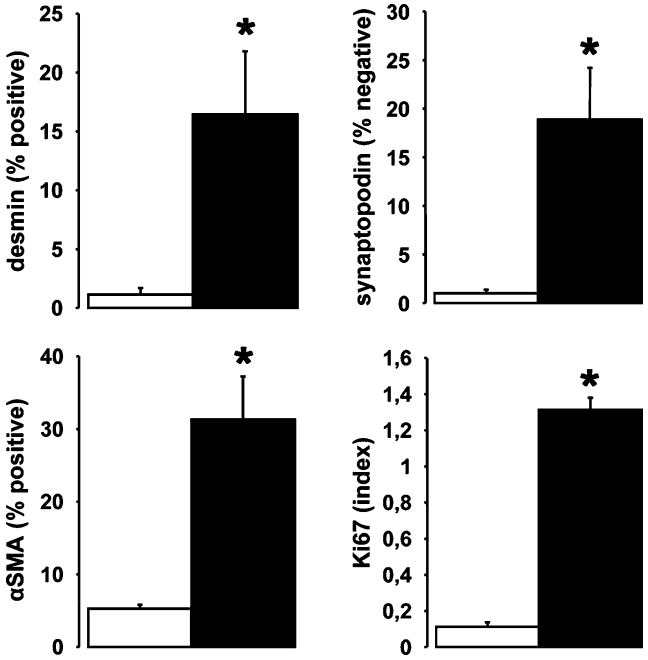

Fig. 9 Semi-quantitative assessment of glomerular markers: desmin (**a**), synaptopodin (**b**), α-smooth muscle actin (**c**), and cell proliferation Ki67 (**d**) at d30, in control mice (*open bars*) and in treated podo-NTR transgenic mice (*black bars*). The results are presented as mean± SEM; *$p<0.05$

nitroreductase was placed under the control of the podocyte-specific gene podocin. Two intraperitoneal administrations of CB1954, a monofunctional alkylating agent which is in vivo converted by nitroreductase into its toxic form, lead to an acute glomerular disease characterized by proteinuria, vacuolization of the podocytes and parietal cells. For the histological follow-up of these animals, we established a new protocol of serial kidney biopsies in mice that allowed us to circumvent the variability of response due to the heterogenous genetic background in these first transgenic lines and to the individual biological reactivity.

Our study, like other recently published murine models, clearly identified the podocyte injury as a crucial event in the pathophysiology of FSGS [13, 24]. Herein, podocyte injury is evidenced by both electron microscopy and immunohistochemistry. Ultrastructural analysis shows an early foot process flattening followed by cytoplasmic vacuolization. Moreover, EM shows area of abnormal folding of the GBM located below the injured podocytes. It is now well established that such GBM lesions may be secondary to the detachment of injured or dysregulated podocytes and is considered as the hallmark of the collapsing variant of FSGS [25–27]. The glomerular expression of desmin, an established marker of podocyte damage in rodents, the loss of podocyte differentiation markers, synaptopodin, nephrin and WT1, and cell proliferation demonstrate podocyte damage. Absence of podocyte markers may reflect podocyte de-differentiation and/or podocyte loss, both resulting from CB1954-cytotoxicity. Podocyte apoptosis could contribute to podocyte loss.

In our model, it is likely that injured and detached proliferating podocytes participate to the hypercellularity of the urinary space. Histopathology clearly identifies hypertrophic podocytes in close contact with PEC (see Fig. 4c and d). Like others, we fail to demonstrate podocyte differentiation markers in these cells. This is not a surprise since we and others have previously observed that injured podocytes loose their differentiation markers and may undergo transdifferentiation in the urinary space [24]. Interestingly, desmin, regarded as a classical marker of podocyte injury, labels cells that display various morphologic type, from hypertrophic podocytes to fibroblast-like PEC lining the Bowman's capsule. However, desmin labeling of cells in the urinary space is not a proof per se of podocytes migration because one cannot exclude an abnormal expression of desmin by the damaged PEC. Indeed, early glomerular injury involved not only visceral podocytes but also PEC that displayed vacuolization and apoptosis. Podocytes and PEC share a common embryonic origin and parietal podocytes have been documented in several species, including rat, rabbits, and humans [28]. Parietal podocytes are lining the Bowman capsule in mature glomeruli and are defined by the expression of markers of the podocyte lineage. In our model, one cannot rule out that such parietal podocytes express the NTR transgene and are sensitive to its direct toxicity of CB1954. However, parietal podocytes have not been unambiguously demonstrated in mice. In the present study, while very rare WT1 positive cells are observed lining the Bowman capsule (see Fig. 8c), no expression of other podocytes markers such as synaptopodin, podocalyxin, and nephrin is found in cells in parietal position in either wild-type or transgenic CB1954-treated mice. Another possible explanation of early injury of PEC is the bystander property of NTR/CB1954 combination that has been underlined by cancer studies [29, 30]. In bystander effect, the toxic form of CB1954 that is generated in the NTR-expressing podocytes could be released in the Bowman urinary space and induce parietal cell injury. Interestingly, no mesangial cell myofibroblastic activation and proliferation, as assessed by the absence of expression of α-smooth muscle actin and Ki67 respectively, was observed in our model. This suggests that the toxic effect of NTR/CB1954 combination is limited to the extracapillary compartment, may be because of a "clearing" effect of the urinary ultrafiltration flux that would have preserved the endocapillary cells from cell toxicity. One original aspect of our model is the expression of α-smooth muscle actin by PEC as soon as d8 in still apparently normal glomeruli (see Fig. 7d). In more severe lesions, we found a widespread expression of α-smooth muscle actin both in PEC lining the Bowman's capsule (see Fig. 7e) and in cells

located within the crescents (see Fig. 7f). This strongly suggests that epithelial to mesenchymal transition in PEC could play an important role in initiation and progression of glomerular injury [31]. Finally, as expected, the proliferation marker Ki-67 is strongly expressed in damaged glomeruli, and again labeled both podocytes and PEC.

In our model, acute and chronic glomerular lesions are morphologically close to human focal and segmental glomerulosclerosis, mainly in its collapsing variant and in its non otherwise specified variant, respectively. Our model shares several features of human HIVAN, mainly podocyte dysregulation and tubular lesions. Our follow-up protocol clearly demonstrates a shift from acute to chronic lesions with time, while the total percentage of injured glomeruli remains constant. This indicates that acute injury progressively leads to scarring of the damaged glomeruli. In this line, both cell proliferation and apoptosis are still ongoing at d30 (see Fig. 9) suggesting an active process of glomerular cell turnover. However, urinary protein content that is strongly increased at day 8 progressively returns to baseline at d30. The mechanisms responsible of such normalization of proteinuria over time are not elucidated and may involve some glomerular recovery which has been correlated with the extent of podocyte loss [3]. Interestingly, serial kidney biopsies allowed us to make correlations between d8 proteinuria and histopathology. Thus, in our model, not only d8 proteinuria is clearly associated with acute lesions, but it also predicts the intensity of d30 glomerular and interstitial chronic lesions. Moreover, d8 proteinuria is also closely linked with the markers of podocyte loss/dedifferentiation and of cell proliferation within the glomeruli at d30.

In conclusion, we have established here a new and suitable model of conditional mouse acute glomerular injury leading to focal segmental glomerulosclerosis. Interestingly, while this transgenic mouse model was designed to induce selective podocyte injury, toxicity seems to affect other cells of the extracapillary compartment, namely Bowman's capsule cells. The podo-NTR transgenic line that could be combined with other recent transgenic model [32] is a valuable tool to investigate in the mechanisms of glomerular injury and recovery and in the pathways of progression to glomerular fibrosis.

Conflict of interest statement We declare that we have no conflict of interest.

References

1. Kriz W, LeHir M (2005) Pathways to nephron loss starting from glomerular diseases-insights from animal models. Kidney Int 67:404–419
2. Eremina V, Wong MA, Cui S et al (2002) Glomerular-specific gene excision in vivo. J Am Soc Nephrol 13:788–793
3. Wharram BL, Goyal M, Wiggins JE et al (2005) Podocyte depletion causes glomerulosclerosis: diphtheria toxin-induced podocyte depletion in rats expressing human diphtheria toxin receptor transgene. J Am Soc Nephrol 16:2941–2952
4. Roselli S, Heidet L, Sich M et al (2004) Early glomerular filtration defect and severe renal disease in podocin-deficient mice. Mol Cell Biol 24:550–560
5. Juhila J, Roozendaal R, Lassila M et al (2006) Podocyte cell-specific expression of doxycycline inducible Cre recombinase in mice. J Am Soc Nephrol 17:648–654
6. Asano T, Niimura F, Pastan I et al (2005) Permanent genetic tagging of podocytes: fate of injured podocytes in a mouse model of glomerular sclerosis. J Am Soc Nephrol 16:2257–2262
7. Bariety J, Nochy D, Mandet C et al (1998) Podocytes undergo phenotypic changes and express macrophagic-associated markers in idiopathic collapsing glomerulopathy. Kidney Int 53:918–925
8. Barisoni L, Kriz W, Mundel P et al (1999) The dysregulated podocyte phenotype: a novel concept in the pathogenesis of collapsing idiopathic focal segmental glomerulosclerosis and HIV-associated nephropathy. J Am Soc Nephrol 10:51–61
9. Barisoni L, Bruggeman LA, Mundel P et al (2000) HIV-1 induces renal epithelial dedifferentiation in a transgenic model of HIV-associated nephropathy. Kidney Int 58:173–181
10. Bariety J, Bruneval P, Hill G et al (2001) Posttransplantation relapse of FSGS is characterized by glomerular epithelial cell transdifferentiation. J Am Soc Nephrol 12:261–274
11. Bariety J, Hill GS, Mandet C et al (2003) Glomerular epithelial-mesenchymal transdifferentiation in pauci-immune crescentic glomerulonephritis. Nephrol Dial Transplant 18:1777–1784
12. Shankland SJ, Eitner F, Hudkins KL et al (2000) Differential expression of cyclin-dependent kinase inhibitors in human glomerular disease: role in podocyte proliferation and maturation. Kidney Int 58:674–683
13. Moeller MJ, Soofi A, Hartmann I et al (2004) Podocytes populate cellular crescents in a murine model of inflammatory glomerulonephritis. J Am Soc Nephrol 15:61–67
14. Bariety J, Bruneval P, Meyrier A et al (2005) Podocyte involvement in human immune crescentic glomerulonephritis. Kidney Int 68:1109–1119
15. Bridgewater JA, Springer CJ, Knox RJ et al (1995) Expression of the bacterial nitroreductase enzyme in mammalian cells renders them selectively sensitive to killing by the prodrug CB1954. Eur J Cancer 31A:2362–2370
16. Benouchan M, Do Nascimento F, Perret GY et al (2006) Delivery of the bacterial nitroreductase gene into endothelial cells prolongs the survival of tumour-bearing mice by bystander mechanisms. Int J Oncol 28:457–462
17. Drabek D, Guy J, Craig R et al (1997) The expression of bacterial nitroreductase in transgenic mice results in specific cell killing by the prodrug CB1954. Gene Ther 4:93–100
18. Isles AR, Ma D, Milsom C et al (2001) Conditional ablation of neurones in transgenic mice. J Neurobiol 47:183–193
19. Felmer R, Cui W, Clark AJ (2002) Inducible ablation of adipocytes in adult transgenic mice expressing the E. coli nitroreductase gene. J Endocrinol 175:487–498
20. Moeller MJ, Sanden SK, Soofi A et al (2002) Two gene fragments that direct podocyte-specific expression in transgenic mice. J Am Soc Nephrol 13:1561–1567
21. Ménard J, Karam H, Véniant M et al (1997) Effects of calcium blockade on end-organ damage in experimental hypertension. J Hypertens 15(suppl 3):S19–S30
22. Van Huyen JP, Cheval L, Bloch-Faure M et al (2008) GDF15 triggers homeostatic proliferation of acid-secreting collecting duct cells. J Am Soc Nephrol 19:1965–1974

23. Van Huyen JP, Batisse D, Heudes D et al (2006) Alteration of cytochrome oxidase subunit I labeling is associated with severe mitochondriopathy in NRTI-related hepatotoxicity in HIV patients. Mod Pathol 19:1277–1288
24. Matsusaka T, Xin J, Niwa S et al (2005) Genetic engineering of glomerular sclerosis in the mouse via control of onset and severity of podocyte-specific injury. J Am Soc Nephrol 16:1013–1023
25. Barisoni L, Madaio MP, Eraso M et al (2005) The kd/kd mouse is a model of collapsing glomerulopathy. J Am Soc Nephrol 16:2847–2851
26. D'Agati VD (2008) Podocyte injury in focal segmental glomerulosclerosis: lessons from animal models (a play in five acts). Kidney Int 73:399–406
27. D'Agati VD, Fogo AB, Bruijn JA et al (2004) Pathologic classification of focal segmental glomerulosclerosis: a working proposal. Am J Kidney Dis 43:368–382
28. Bariety J, Mandet C, Hill GS et al (2006) Parietal podocytes in normal human glomeruli. J Am Soc Nephrol 17:2770–2780
29. Westphal EM, Ge J, Catchpole JR et al (2000) The nitroreductase/CB1954 combination in Epstein-Barr virus-positive B-cell lines: induction of bystander killing in vitro and in vivo. Cancer Gene Ther 7:97–106
30. Wilson WR, Pullen SM, Hogg A et al (2002) Quantitation of bystander effects in nitroreductase suicide gene therapy using three-dimensional cell cultures. Cancer Res 62:1425–1432
31. Smeets B, Dijkman HB, te Loeke NA et al (2003) Podocyte changes upon induction of albuminuria in Thy-1.1 transgenic mice. Nephrol Dial Transplant 18:2524–33
32. Appel D, Kershaw DB, Smeets B et al (2009) Recruitment of podocytes from glomerular parietal epithelial cells. J Am Soc Nephrol 20:333–343

Virchows Arch (2010) 456:339–342
DOI 10.1007/s00428-009-0874-z

CASE REPORT

Intrahepatic cholangiocarcinoma resembling a thyroid follicular neoplasm

Adele Fornelli · Arrigo Bondi · Elio Jovine · Vincenzo Eusebi

Received: 12 October 2009 / Revised: 24 November 2009 / Accepted: 6 December 2009 / Published online: 15 January 2010
© Springer-Verlag 2010

Abstract The first case of well-differentiated intrahepatic cholangiocarcinoma with remarkable follicular architecture resembling a follicular neoplasm of thyroid is described in a 52-year-old man. The follicles contained homogenous eosinophilic material akin to colloid and were lined by benign-looking cuboidal cells. Immunohistochemically, thyroid transcription factor-1 (TTF-1) and thyroglobulin were negative and the patient had no evidence of a previous or concomitant thyroid tumour. This case can be added to the list of extrathyroid primary tumours that resemble thyroid neoplasms.

Keywords Cholangiocarcinoma · Thyroid-like tumour · Liver

Introduction

The vast majority of intrahepatic well-differentiated cholangiocarcinomas are mucous-producing malignant neoplasms that show cord-like, tubular and papillary patterns [1].

V. Eusebi
Sezione Anatomia, Istologia e Citologia Patologica "M. Malpighi", University of Bologna,
Bologna, Italy

A. Fornelli · A. Bondi
U.O. Anatomia Patologica, Ospedale Maggiore,
Bologna, Italy

E. Jovine
U.O. Chirurgia Generale A, Ospedale Maggiore,
Bologna, Italy

V. Eusebi (✉)
Anatomia Patologica, Ospedale Bellaria,
Via Altura 3, 40139 Bologna, Italy
e-mail: Vincenzo.eusebi@unibo.it

The purpose of this work was to report a case of well-differentiated intrahepatic cholangiocarcinoma with remarkable follicular architecture resembling a thyroid neoplasm, a novel histological variant which, to the best of our knowledge, has never been described.

It appears that this new histological type has to be added to the list of those neoplastic lesions, so far reported in the breast and kidney [2–6], that show thyroid-like features.

Case report

A 52-year-old male suffering from abdominal pain for several months was admitted to hospital. Family history was not relevant. Computerized tomography (CT) scan of the abdomen revealed a homogeneous enhancing lesion of the right hepatic lobe of 18 cm in greatest axis. No other lesions were found. Laboratory data, including thyroid function tests, were within normal range. There was no evidence of lesions in the thyroid gland nor in the laterocervical lymph nodes at ultrasonography and CT scan. A core biopsy of the liver mass was obtained and the patient underwent right hepatic lobectomy following the pre-operative diagnosis of cholangiocarcinoma.

Thirteen months after surgery, the patient is alive with no evidence of recurrent or metastatic disease.

Materials and methods

Tissues both from pre-operative core biopsy and surgically resected specimens were fixed in 10% neutral buffered formalin, processed and stained with haematoxylin and eosin (H&E) as routine and also with alcian blue pH 2.5 and periodic acid Schiff (PAS) with diastase pre-digestion.

Immunohistochemistry was performed with automated immunostainer (Ventana, Benchmark), using pre-diluted antisera for TTF-1, thyroglobulin, hepatic specific antigen, CK7, CK20, CK19, CAM 5.2, CEA, chromogranin, CD56 and synaptophysin.

Results

The core biopsy consisted of three small cylinders of tissue.

The surgical specimen consisted of a right hepatic lobe weighing 1,200 g and showing a well-demarcated mass that measured 18 cm in greatest axis. The liver parenchyma appeared compressed, and a thin fibrous capsule was present. The cut surface was brownish in colour with numerous cystic cavities throughout that imparted a spongy appearance (Fig. 1). Occasional cysts were filled with blood.

Histology from the core biopsy as well as the surgical specimen was superimposable and therefore will be described together (Fig. 2a).

At low power, the lesion was circumscribed by a thin fibrous capsule and showed a remarkable follicular architecture (Fig. 2b). Follicles were of various sizes, ranging from small to large. The content of follicles closely resembled colloid being pale eosinophilic with occasional vacuoles at the interface with the epithelium (Fig. 3). Some follicles were empty and occasionally contained fresh haemorrhage. The stroma between follicles was constituted by thin bands of collagen.

The neoplastic cells were mostly cuboidal with granular eosinophilic cytoplasm. Nuclei were round to ovoid in shape with scanty chromatin and inconspicuous nucleoli. Some nuclei were clear and showed neat membrane that was occasionally grooved (Fig. 3). Mitoses were 1/10 hpf (×400). No vascular nor capsular invasion was seen. Liver

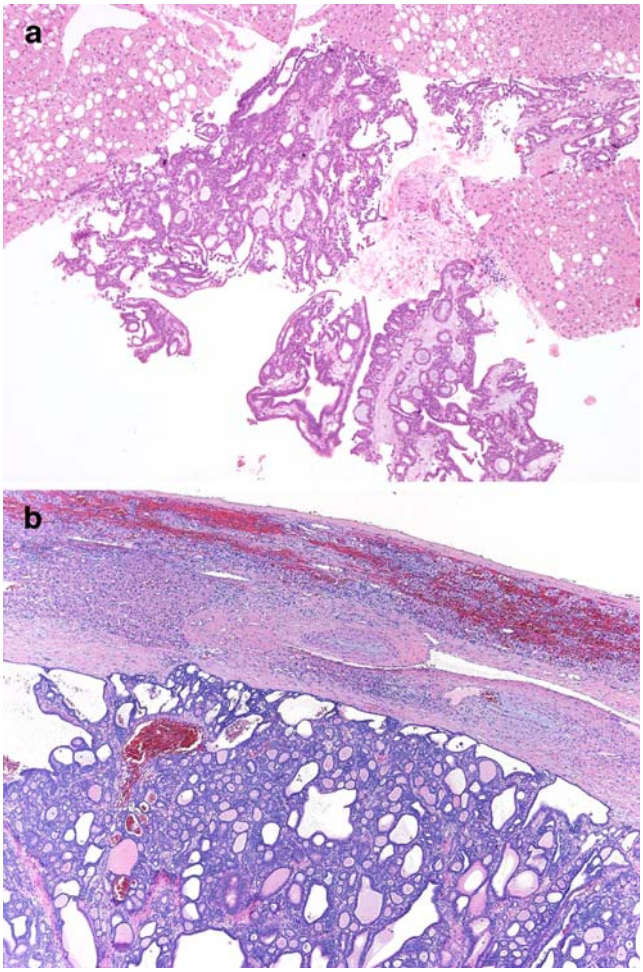

Fig. 2 **a** Core biopsy. **b** Surgical resection: the neoplasm is sharply demarcated from the surrounding liver parenchyma, and a follicular pattern is clearly evident

Fig. 1 Spongy appearance with many cystic spaces ranging from minute to various millimetres in greatest axis

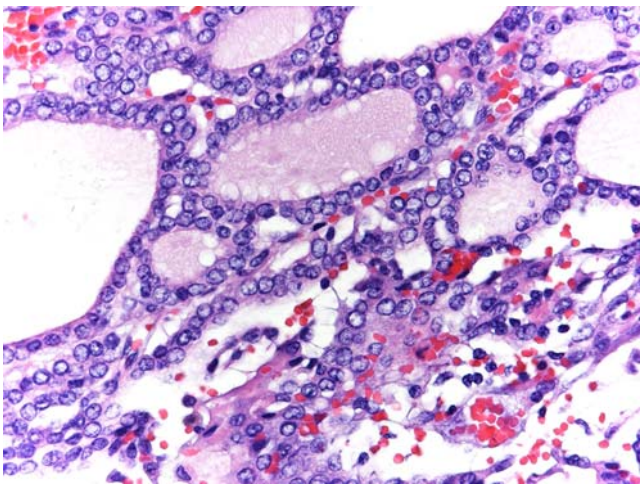

Fig. 3 Nuclei are vescicular, slightly atypical and clear

tissue adjacent to the tumour appeared compressed. Mild steatosis was also present. Dysplastic nuclei were not seen.

The eosinophilic luminal content of follicles was rich in mucosubstances as evidenced by positivity for alcian blue pH 2.5 and PAS after diastase digestion (Fig. 4). Neoplastic cells were positive for CK7 (Fig. 5), CK19, CAM 5.2 and CK AE1 and consistently negative for CEA, CK20, CD56, hepatic specific antigen, thyroglobulin, TTF-1, CD56, synaptophysin and chromogranin.

Discussion

The case here reported was a large hepatic tumour showing spongy cut surface with occasional blood-filled cystic spaces. Histologically, a remarkable follicular architecture was evident. Neoplastic cells were mostly cuboidal with regular nuclei showing grooves and clearing of the chromatin.

The macroscopic and histological features were so similar to a follicular variant of papillary carcinoma of the thyroid that the final diagnosis was established with great difficulty in spite of extensive clinical, radiological and pathological investigations.

Metastasis to the liver from well-differentiated carcinomas of the thyroid is a well-known, although rare phenomenon [7]. An additional remote possibility would be that of ectopic normal thyroid tissue in the liver as the case reported by Strohschneider et al. [8]. Nevertheless, in the present patient, the neoplastic cells were all negative for thyroglobulin and TTF-1 at the variance with well-differentiated thyroid neoplasms and ectopic normal thyroid tissues wherever they are found. Finally, no evidence of a thyroid lesion of any kind was found by clinical investigations, ultrasonography, CT scan and laboratory tests.

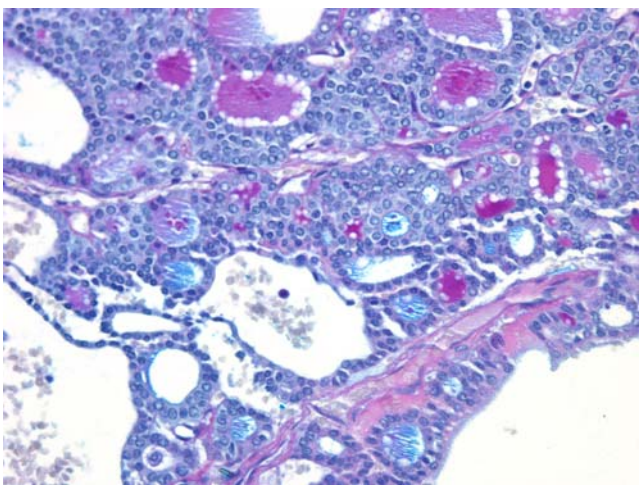

Fig. 4 The "follicular" content stains either for PAS after diastase or alcian blue pH 2.5 indicating presence of mucosubstances

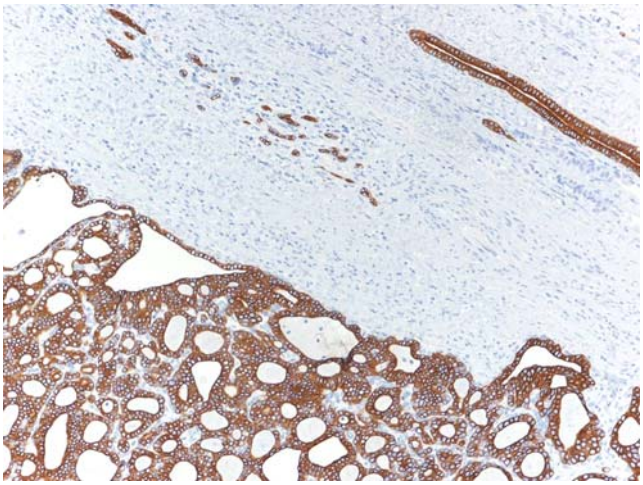

Fig. 5 Neoplastic cells and normal bile ducts stain for keratin 7

As no other primary was found after 13 months, including breast, kidney and pancreas, the cholangiocellular nature of the hepatic neoplasm was then favoured for the presence of mucosubstances and further supported by immunohistochemistry that evidenced CK7, CK19 and CAM 5.2 positivity along with CK20 and hepatic-specific antigen negativity. The mild atypical changes of nuclei together with the low mitotic count prompted us to exclude bile duct adenoma. The latter nearly always does not exceed 1 cm in greatest axis, it is discovered as an incidental finding and histologically is composed of bland glandular structures within a fibrous stroma [1]. Biliary cystoadenomas of the serous variant are different from the present case as they have abundant cellular fibrous stroma and large cystic spaces [9].

Foucar et al [10] described an unusual variant of peripheral well-differentiated cholangiocarcinoma in a 27-year-old pregnant patient with histological features very similar to the present case. As stated in their paper, the authors like us underwent great diagnostic difficulties in establishing the diagnosis. The tumour was considered unresectable as it involved the entire right and part of the left lobes. The mass enlarged progressively along 14 years up to 8.600 g and led to the patient's death for inferior vena cava occlusion by neoplastic thrombosis. Therefore, it seems that the present case shares with many histological similarities of Foucar et al. for what seems to be a low grade malignancy cholangiocarcinoma [10].

Neoplastic lesions having thyroid-like features have been reported in the breast and in the kidney [2–6]. In the breast, the several cases described were superimposable to the tall cell variant of papillary carcinoma of thyroid [2, 3]. The cases reported in kidney were very similar to follicular carcinoma of thyroid [4–6]. Therefore, it seems that

thyroid-like features can occur in tumours located in different organs, and liver has to be added to the list.

Diagnostic erroneous interpretation can be avoided by being aware of the existence of tumours in the liver that histologically mimic follicular carcinomas of thyroid, and more cases are needed to establish the biological behaviour.

Acknowledgments Professor Juan Rosai is thanked for having reviewed the case.

Conflict of interest statement We declare that we have no conflict of interest.

References

1. Ferrel L, Kakar S (2007) Tumors of the liver, gallbladder and biliary tree. In: Fletcher CDM (ed) Diagnostic histopathology of tumors, 3rd edn. Elsevier Limited
2. Eusebi V, Damiani S, Ellis IO et al (2003) Breast tumor resembling the tall cell variant of papillary thyroid carcinoma. Am J Surg Pathol 27:1114–1118
3. Tosi AL, Ragazzi M, Asioli S et al (2007) Breast tumor resembling the tall cell variant of papillary thyroid carcinoma: report of 4 cases with evidence of malignant potential. Int J Surg Pathol 5:14–19
4. Jung SJ, Chung JI, Park SH et al (2006) Thyroid follicular carcinoma-like tumor of the kidney: a case report with morphologic, immunohistochemical and genetic analysis. Am J Surg Pathol 30:411–415
5. Sterlacci W, Verdofer I, Gabriel M et al (2008) Thyroid follicular carcinoma-like renale tumor: a case report with morphologic, immunophenotypic, cytogenetic and scintigraphic studies. Virchows Arch 452:91–95
6. Amin MB, Gupta R, Ondrej H et al (2009) Primary thyroid like follicular carcinoma of the kidney: report of six cases of a histologically distinct adult renal epithelial neoplasm. Am J Surg Pathol 33:393–400
7. Rosai J, Carcangiu ML, De Lellis R (1992) Tumors of the thyroid gland, Atlas of Tumor Pathology, third series, fascicle 5, Armed Forces Institute of Pathology
8. Strohschneider T, Timm D, Worbes C (1993) Ectopic thyroid gland tissue in the liver. Der Chirurg 64:751–753
9. Manouras A, Markogiannakis H, Lagoudianakis E et al (2006) Biliary cystoadenoma with mesenchymal stroma: report of a case and review of the literature. World J Gastroenterlo 12:6062–6069
10. Foucar E, Kaplan LR, Gold JH et al (1979) Well differentiated peripheral cholangiocarcinoma with unusual clinical course. Gastroenterlogy 77:347–353

Virchows Arch (2010) 456:343–354
DOI 10.1007/s00428-010-0888-6

ORIGINAL ARTICLE

Meningeal hemangiopericytomas and hemangiopericytoma/solitary fibrous tumors of extracranial soft tissues: a comparison

Andrea Ambrosini-Spaltro · Vincenzo Eusebi

Received: 7 October 2009 / Revised: 15 January 2010 / Accepted: 21 January 2010 / Published online: 18 February 2010
© Springer-Verlag 2010

Abstract The current World Health Organization (WHO) classification of central nervous system tumors lists meningeal hemangiopericytomas (HPC) and meningeal solitary fibrous tumors (SFT) as separate entities. On the contrary, SFT and HPC of soft tissues are regarded in the WHO soft tissue fascicle as features of the same entity. The clinical data, histology, and immunohistochemistry of 18 cases of meningeal HPC and 12 cases of peripheral soft tissue HPC–SFT were compared. Both intracranial and soft tissue lesions had significant similarities that included staghorn vasculature, necrotic areas, cytologic atypia, and positivities for CD99, collagen IV, and reticulin. Nevertheless, intracranial tumors were more cellular than HPC–SFT of soft tissues and had fewer collagen bands. Meningeal HPC in addition had more mitoses, higher Ki67 index, stained less intensely for CD34 and B-cell lymphoma 2 (BCL2) than HPC–SFT of soft tissues. Meningeal HPCs recurred in 13 out of 14 cases (92.9%). One of the patients died in the postoperative period for a recurrent lesion 5 years after the diagnosis, and another patient developed an extracranial metastasis 13 years after surgery. None of the six cases of HPC–SFT of soft tissues available for follow-up recurred. Both meningeal and soft tissue tumors appear to represent different features of the same entity. A more aggressive phenotype of the tumor together with incomplete surgical resection of intracranial lesions might explain the noticeable clinical difference between HPC of the meninges and HPC–SFT of soft tissues.

Keywords Hemangiopericytoma · Solitary fibrous tumor · Meninges · Soft tissue

A. Ambrosini-Spaltro · V. Eusebi
Section of Anatomic Pathology "Marcello Malpighi",
Department of Oncology and Haematology,
University of Bologna, Bellaria Hospital,
Bologna, Italy

V. Eusebi (✉)
Section of Anatomic Pathology "Marcello Malpighi",
Bellaria Hospital,
via Altura 3,
40139 Bologna, Italy
e-mail: vincenzo.eusebi@unibo.it

Introduction

The term hemangiopericytoma (HPC) was introduced by Stout and Murray in 1942 for tumors located in the retroperitoneum, buttock, and thigh [1]. They proposed an origin from "pericytic"-modified smooth muscle cells located around blood vessels, a cell described by Zimmermann in 1923 [2]. The first cases of meningeal HPC were reported in 1938 by Cushing and Eisenhardt under the term "angioblastic meningioma" [3] and subsequently, in 1954, by Begg and Garret, as "cranial meningeal hemangiopericytoma" [4]. The latter stated that both lesions were identical, and that these tumors were very similar to the HPCs described by Stout and Murray in soft tissues [1].

Solitary fibrous tumors (SFTs), described in the pleura by Klemperer and Rabin in 1931 [5], were originally regarded as mesotheliomas [6]. Subsequently, SFTs have been observed in a number of extrapleural sites [7–9], including soft tissues and meninges [10].

In the 2006 World Health Organization (WHO) fascicle of soft tissue tumors, it is stated that the histological appearances and clinical behavior of HPC and solitary fibrous tumor are similar, a view also shared by others [11]. Accordingly, the unifying term "hemangiopericytoma/solitary fibrous tumor" (HPC–SFT) was proposed [12]. In spite of this view, in the 2007 WHO fascicle of central

nervous system tumors, it was stated that HPC and SFT of meninges are histologically and clinically different entities, being HPC of meninges a frequently recurring tumor [13].

The aim of this paper was to study the morphological, immunohistochemical, and clinical differences and similarities between meningeal HPC and HPC–SFT of soft tissues.

Materials and methods

From the files of the Section of Anatomic Pathology "Marcello Malpighi" of the University of Bologna, all intracranial and intraspinal lesions diagnosed as HPC and SFT from 1993 to 2009 were retrieved and reviewed by both of us. We collected a total of 31 specimens from 18 patients (eight of them showed multiple recurrences). Three cases were excluded for the lack of agreement on the diagnosis. The only case labeled meningeal SFT (patient 14, specimen 26) appeared to be a recurrence of HPC and was regarded as such. When different specimens from the same patient were available in our files, we counted them separately for statistical purposes, as they exhibited morphological and immunohistochemical differences in various parameters. Sizes of the lesions were obtained radiologically in three cases and macroscopically in the remaining cases. Extent and radicality of the surgical excision were obtained either in the primary or in the recurrent lesions. Clinical follow-up was available in 14 out of 18 patients. It ranged from 1 to 16 years (mean, 9.0; SD, 4.8 years).

In addition, 12 consecutive tumors from 12 patients of HPC–SFT arising in extracranial soft tissues were studied. The major axis of the lesions was determined by gross macroscopic examination.

Follow-up of these cases was obtained in 6 out of 12 patients. It ranged from 4 to 11 years (mean, 8.0; SD, 2.7 years).

All cases were studied histologically for the presence of cellularity, "staghorn vasculature," necrosis, cytological atypia, collagen bundles, and number of mitoses in ten high power fields (HPF), which were the classical criteria for the diagnosis of HPC and SFT adopted by Enzinger and Weiss [14]. Cellularity was low, moderate, and high (Fig. 1a, b, d, e). Staghorn vasculature was semiquantitatively classified as absent/rare, moderate, and diffuse (Fig. 2a, b, d, e). Necrosis and collagen bands were quantified as absent, focal, and diffuse. Cytological atypia was mild, moderate, and severe, according to the shape and size of the nuclei. Mitoses were evaluated in ten HPF. From representative blocks, immunohistochemical stains were obtained for Ki67, CD34, B-cell lymphoma 2 (BCL2), CD99, CD31, epithelial membrane antigen (EMA), smooth muscle actin (SMA), D2-40, collagen IV, and progesterone receptors (PgR).

Reticulin stain (Gomori) was also obtained, since the rich network of reticulin fibers is considered typical of the meningeal HPC [15]. In collagen IV and reticulin-stained sections, we evaluated the staining distribution in a three-scale grading as follows: 1+, only around blood vessels; 2+, around blood vessels and nests of neoplastic cells; and 3+, around blood vessels and decorating individual neoplastic cells in a diffuse pattern. For all the other immunohistochemical markers, a semiquantitative score was used, determining the percentage of positive neoplastic cells in comparison to the total number of neoplastic cells detected in the same slide. CD34 positivity was also scored as either patchy or diffuse, which are distributions believed to be more typical of HPC and SFT, respectively [16]. The list of primary antibodies with the respective dilutions is summarized in Table 1. A standard procedure with secondary antibodies and avidin/biotin method was used.

Statistical analysis

From the numerical variables of all parameters, we compared the mean and standard deviation (SD) in the two groups of lesions. The variables shown by the meningeal tumors were compared with their corresponding counterparts shown by the extracranial neoplasms by calculating the non-parametric Mann–Whitney U test. The null hypothesis stated the presence of significant differences between the two lesions. Two-tailed tests and statistical significance with p less than 0.05 were considered. GraphPad Prism 5.0 for Windows (GraphPad Software, Inc., La Jolla, CA, USA) was used.

Results

Meningeal HPC

Clinical data from 18 patients are summarized in Table 2, pathological features in Table 3, and immunohistochemical and histochemical results in Table 4.

Clinical features There was female predominance (12 patients) with age ranging from 17 to 74 years (mean, 51.9; SD, 15.1 years). All patients were treated with surgery. In each patient, the excision of the lesion was described radical by the surgeon, with the exception of two cases where the surgeon incompletely removed the lesions for preserving neurological functionality. Seven patients received radiation therapy, and two of them were also treated with chemotherapy.

In four patients, follow-up information was not available. In 13 out of 14 (92.9%) patients, recurrences were observed. In eight of such patients, the number of tumor recurrences ranged from 1 to 4 (mean, 1.6), in a length of time ranging

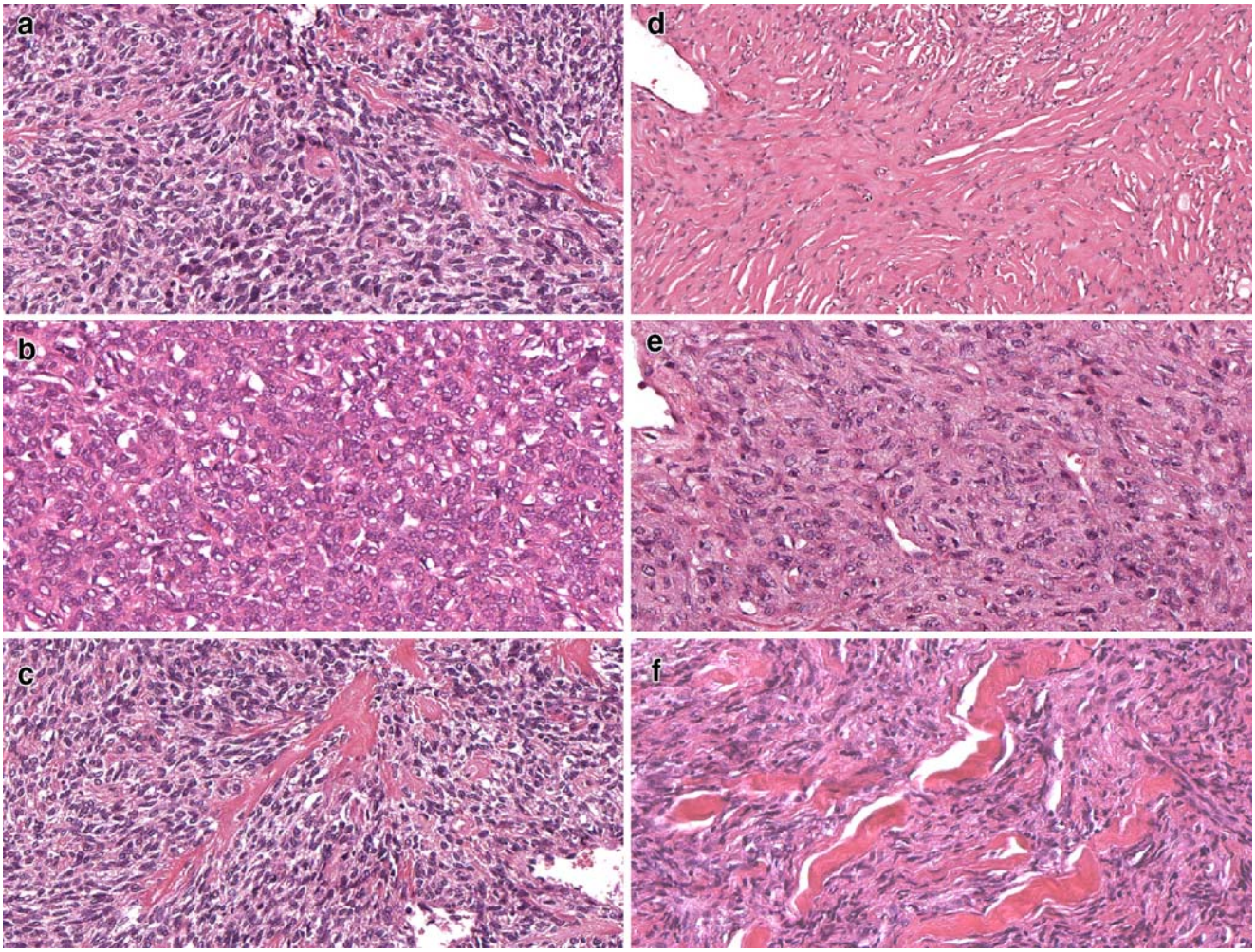

Fig. 1 Cellularity and collagen bundles. In hemangiopericytoma (HPC) of the meninges, cellularity is predominantly moderate (**a**, specimen N. 1, Pt. N. 1), sometimes high (**b**, specimen N. 29, Pt. N. 16), and associated with focal amount of collagen bundles (**c**, specimen N. 2, Pt. N. 2). In HPC–solitary fibrous tumor of peripheral soft tissues, cellularity is predominantly low (**d**, N. 7), sometimes moderate (**e**, N. 12), with diffuse collagen bundles (**f**, N.8)

from 1 to 13 years (mean, 8.9 years). In two patients, the recurrent lesions only were available for the study, as the primary tumors had been removed in other institutions. In three patients, a well-documented clinical and radiological recurrence was observed, but further treatment was refused by the patients. In one case, only no recurrence was observed. In case 8, a metastasis to the hip manifested after 13 years from the first surgery. One case (patient 17) died of postoperative bleeding right after the removal of a recurrent tumor and 5 years after the first surgery. All other patients are alive (range, 1–16 years; mean, 8.5 years).

Pathological features The size of lesions ranged from 1 to 10 cm in greatest axis (mean, 4.7; SD, 3.1 cm). Histologically, cellularity was low in 1, moderate in 27, and high in 3 specimens (Fig. 1a, b). Typical "staghorn" vessels were observed in 28 out of 31 specimens (9 numerous, 16 moderate, and 3 rare; Fig. 2a, b). Areas of necrosis were identified in five specimens from two patients (Fig. 2c); focal necrosis was also detected in another specimen, which was a recurrent lesion (n. 26 from patient 14). Cytologic atypia was mild in 7 specimens, moderate in 22 specimens, and severe in 2 specimens. Collagen bands were diffuse in 12 specimens and focal (Fig. 1c) in other 12 specimens; in seven specimens, no collagen bands were detected. Mitoses per ten HPF varied in different specimens from 1 to 25 (mean, 4.8; SD, 5.4).

Immunohistochemical and histochemical features Unstained sections were not available for all specimens studied. Ki67 index ranged from 0.5% to 30% (mean, 7%; SD, 8%) in all the specimens. CD34 was positive in 24 out of 31 specimens, ranging from 5% to 80% of the total neoplastic population (mean, 48% of cells; SD, 31%) and was completely negative in seven specimens from two patients (patients 7 and 8). CD34 staining pattern was patchy in 20

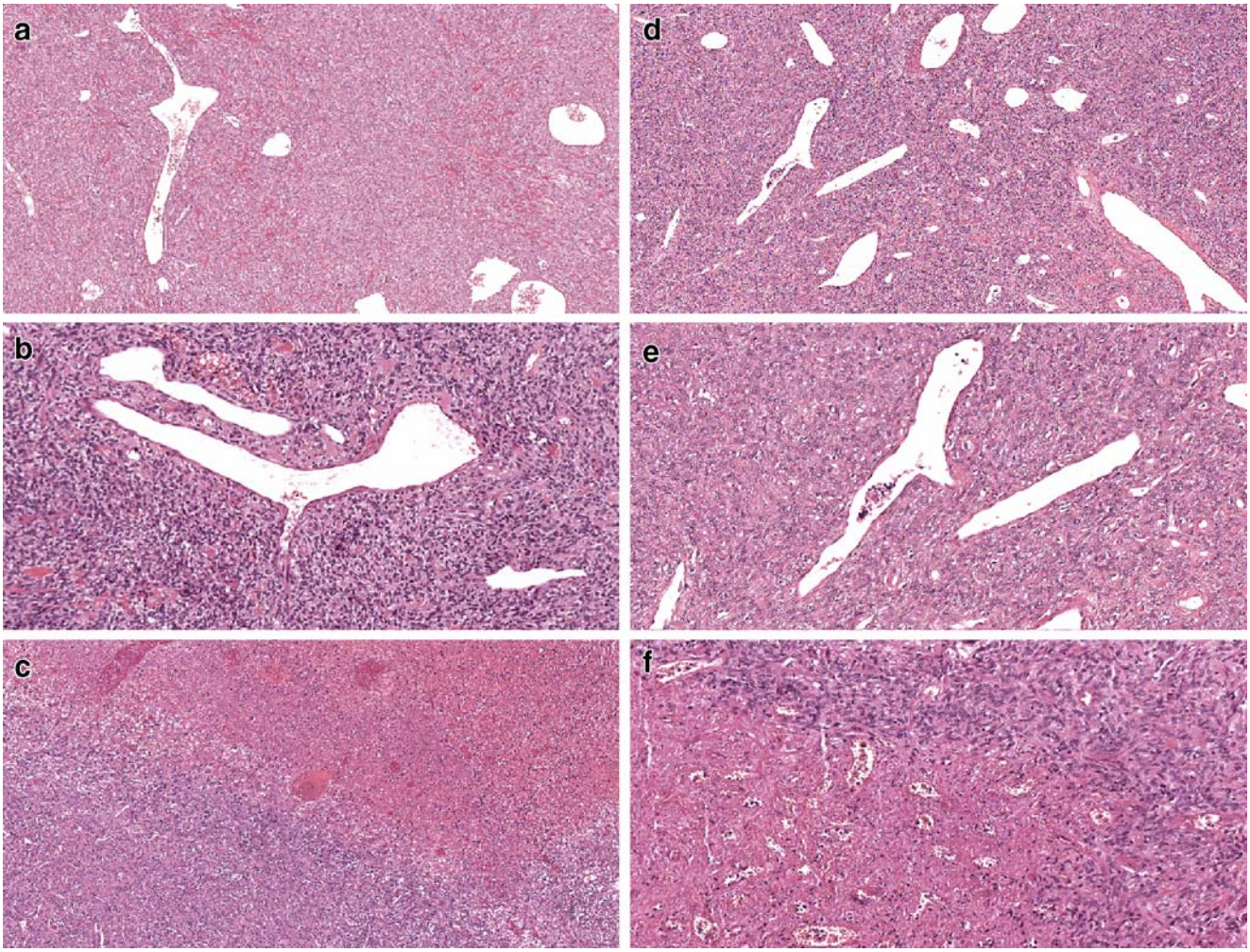

Fig. 2 Staghorn vasculature and necrosis. In meningeal hemangiopericytoma (HPC), typical staghorn vasculature (**a**, **b**, specimen 7, Pt. N. 7) and necrosis (**c**, specimen N. 12, Pt. N. 8) are observed. Peripheral soft tissue HPC–solitary fibrous tumor exhibits staghorn vessels (**d**, **e**, N. 1) and necrotic areas (**f**, N. 7) as well

specimens (Fig. 3a) and diffuse in four specimens. BCL2 was positive in 13 out of 29 specimens (mean, 40% of the cells; SD, 27%), and CD99 was positive in seven out 21 specimens (mean, 15% of the cells; SD, 30%; Fig. 3c).

In all specimens from all cases studied, CD31, EMA, and SMA were consistently negative in the neoplastic cells. Only three out of 27 specimens exhibited focal positivity for D2-40 (less than 5% of neoplastic cells).

Table 1 List of antibodies used

Antigen	Source	Clone	Dilution	Antigen retrieval
Ki67	Dako	MIB-1	1:200	Wcap buffer
CD34	Neomarkers	QB-END/10	1:400	Wcap buffer
BCL2	Dako	124	1:25	Wcap buffer
CD99	Dako	12E7	1:50	Wcap buffer
CD31	Dako	yc70A	1:20	Wcap buffer
EMA	Dako	E29	1:100	Wcap buffer
SMA	Dako	1A4	1:100	Wcap buffer
D2-40	Signet	D240	1:50	Wcap buffer
Collagen IV	Dako	CIV 22	1:100	Wcap buffer
PgR	Dako	PgR 636	1:50	Wcap buffer

BCL2 B-cell lymphoma 2, *EMA* epithelial membrane antigen, *SMA* smooth muscle actin, *PgR* progesterone receptor, *Wcap* wax capture

Table 2 Clinical data in meningeal hemangiopericytoma

Pt N	Specimen N	Sex	Age	Site	Treatment	FU
1	1	F	74	Falx cerebri	S, RT	A&W 4 years
2	2	M	70	Occipital	S	NA
3	3	M	17	Occipital	S	NA
4	4	F	49	Occipital	S	NA
5	5	F	59	Spinal L3-L4	S	NA
6	6	F	55	Parieto-occipital	S	Recurrent lesion after 16 years (primary lesion treated in other institution); A: 16 years
7	7 8 9 10	M	47	Torcular Herophili and sinus transversus	S, RT	Primary and three recurrent lesions after 1, 4, and 8 years; A: 8 years
8	11 12 13	F	51	Longitudinal sinus	S	Primary and two recurrent lesions after 5 and 7 years, metastasis in the hip after 13 years; A: 13 years
9	14 15	M	61	Right cavernous sinus	S	Primary and one recurrent lesion after 1 year; A: 1 year
10	16 17	F	44	Petrous pyramid	S, RT, CT	Two recurrent lesions after 12 and 14 years (primary lesion treated in other institution); A: 14 years
11	18 19 20	F	60	Wall of fourth ventricle	S	Primary and two recurrent lesions after 1 and 7 years, clinical control after 8 years; A: 8 years
12	21	F	64	Spinal D3-D4	S	One recurrent lesion after 9 years and documented radiological and clinical recurrence after 10 years (primary lesion treated in other institution); A: 10 years
13	22 23 24	F	60	Falx cerebri	S, RT, CT	Primary and two recurrent lesions after 1 and 3 years; A: 3 years
14	25 26	M	32	Spinal D3-D5	S	Primary and one recurrent lesion after 7 years; A: 7 years
15	27	F	52	Occipitocervical	S, RT, CT	Primary lesion, documented radiological recurrence after 8 years; A: 8 years
16	28 29	F	30	Right optical nerve	S	Primary and one recurrent lesion after 16 years; A: 16 years
17	30	F	40	Frontotemporal, right	S, RT	Primary lesion, documented clinical recurrence after 5 years, postoperative death; DOD: 5 years
18	31	M	69	Temporal, left	S	Second recurrent lesion after 12 years (primary lesion and first recurrence after 11 years, both treated in other institution); A: 12 years

Pt patient, *N* number, *FU* follow-up, *S* surgical treatment, *RT* radiotherapy, *CT* chemotherapy, *A&W* alive and well with no recurrences, *A* alive, *DOD* died of disease, *NA* not assessed

A network of reticulin fibers was detected in all specimens from all cases. Reticulin stain showed that 20 out of 31 specimens had 3+ score; nine out of 31 specimens, 2+ score; and two out of 31 specimens, 1+ score (Fig. 4a–c). Collagen IV showed 17 out of 27 specimens having 3+ score; nine out of 27 specimens, 2+ score; and one out of 27 specimens, 1+ score (Fig. 4d–f).

Positivity for PgR was detected in four out of 18 specimens from 18 cases, with values ranging from 3% to 70% of the cells (mean, 26% of the cells; SD, 17%). In six out 18 specimens, only scattered cells were positive for PgR, and eight specimens were completely negative for PgR.

Soft tissue HPC–SFT

Clinical data of the 12 patients of SFT of peripheral soft tissues are summarized in Table 5, histological features in Table 6, and related immunohistochemical and histochemical data in Table 7.

Table 3 Morphological data in meningeal hemangiopericytoma

Pt N	Specimen N	Major axis (cm)	Staghorn vasculature	Collagen bundles	Necrosis	Cellularity	Cytologic atypia	Mitoses[a]
1	1	3	Moderate	Diffuse	Absent	Moderate	Moderate	4
2	2	6	Numerous	Focal	Absent	Moderate	Moderate	3
3	3	3	Moderate	Focal	Absent	Moderate	Moderate	4
4	4	3	Moderate	Diffuse	Absent	Moderate	Mild	1
5	5	4	Moderate	Diffuse	Absent	Moderate	Mild	1
6	6	5	Numerous	Absent	Absent	Moderate	Moderate	10
7	7	3	Moderate	Diffuse	Absent	Moderate	Moderate	2
	8	4	Numerous	Diffuse	Absent	Moderate	Moderate	2
	9	3	Moderate	Absent	Absent	Moderate	Moderate	1
	10	10	Rare	Focal	Absent	Moderate	Moderate	5
8	11	4.5	Numerous	Focal	Absent	Moderate	Mild	2
	12	3	Moderate	Focal	Diffuse	Moderate	Moderate	4
	13	4.5	Moderate	Focal	Diffuse	Moderate	Moderate	3
9	14	7	Numerous	Focal	Absent	Moderate	Mild	2
	15	3	Numerous	Absent	Absent	Moderate	Moderate	1
10	16	10	Absent	Focal	Absent	Moderate	severe	25
	17	6	Absent	Focal	Absent	Moderate	Moderate	18
11	18	1.6	Moderate	Absent	Absent	Moderate	Mild	2
	19	3	Rare	Focal	Absent	Moderate	Moderate	5
	20	2	Moderate	Absent	Absent	High	Moderate	3
12	21	6	Numerous	Focal	Absent	Moderate	Moderate	2
13	22	6	Moderate	Absent	Diffuse	Moderate	Moderate	10
	23	4	Moderate	Absent	Diffuse	Moderate	Moderate	5
	24	15	Numerous	Diffuse	Diffuse	Moderate	Moderate	8
14	25	2	Absent	Diffuse	Absent	Moderate	Moderate	2
	26	3	Moderate	Diffuse	Focal	Moderate	Moderate	2
15	27	1	Rare	Diffuse	Absent	Moderate	Moderate	1
16	28	0.7	Moderate	Diffuse	Absent	Moderate	Mild	1
	29	3	Moderate	Focal	Absent	High	Severe	12
17	30	10	Numerous	Diffuse	Absent	High	Moderate	6
18	31	7.5	Moderate	Diffuse	Absent	low	Mild	3

Pt patient, *N* number

[a] Mitoses were counted per ten high power fields

Clinical features Patients were six males and six females, with age ranging from 36 to 88 years (mean, 60.7 years, SD, 17). Lesions were located in the pleura (five cases), orbital region (two cases), limbs (two cases), abdominal cavity (two cases), and one case in the pelvic cavity. Surgery was the only treatment in all cases. Resection was radical in ten cases. In two cases located in the orbit, the tumors were removed incompletely. Follow-up was available in six patients only. None of these patients exhibited a recurrence. Specifically, five patients are alive and well; one patient died of a metastatic colonic carcinoma.

Pathological features The lesions ranged from 1.4 to 21.5 cm in greatest axis (mean, 5.4 cm; SD, 5.7). Cellularity was low in seven and moderate in five specimens (Fig. 1d, e). Typical "staghorn" vessels were found in all the 12 cases (four numerous, eight moderate; Fig. 2d, e). Necrosis was focally observed in one case (Fig. 2f). Cytologic atypia was mild in four and moderate in eight tumors. Collagen bands were numerous in 11 cases (Fig. 1f) and focal in one case. Mitoses ranged from 1 to 4 (mean, 1.6; SD, 1.0) per ten HPF.

Immunohistochemical and histochemical features Ki67 index ranged from 0.5% to 3% of the total neoplastic population (mean, 2% of the cells; SD, 1%) in all the patients. In all 12 patients, CD34 was positive, being the staining pattern, patchy in five, and diffuse in seven patients (Fig. 3b). BCL2 was positive in ten out of 12 patients

Table 4 Immunohistochemical and histochemical data in meningeal hemangiopericytoma

Pt N	Specimen N	Ki67	CD34	CD34 pattern	BCL2	CD99	CD31	EMA	SMA	D2-40	Collagen IV	Reticulin	PgR
1	1	0.5%	80%	Diffuse	70%	30%	neg	neg	neg	neg	3+	3+	neg
2	2	5%	60%	Patchy	20%	30%	neg	neg	neg	neg	3+	3+	<1%
3	3	0.5%	50%	Patchy	neg	neg	neg	neg	NA	NA	3+	3+	20%
4	4	5%	70%	Patchy	20%	10%	neg	neg	NA	neg	3+	3+	neg
5	5	1%	20%	Patchy	20%	NA	NA	neg	NA	NA	NA	3+	3%
6	6	7%	10%	Patchy	20%	neg	neg	neg	neg	neg	3+	3+	70%
7	7	0.5%	neg	neg	15%	30%	neg	neg	neg	neg	3+	3+	<1%
	8	0.5%	neg	neg	5%	70%	neg	neg	neg	neg	3+	3+	NA
	9	10%	neg	neg	5%	80%	neg	neg	neg	neg	3+	3+	NA
	10	7%	neg	neg	10%	70%	neg	neg	neg	neg	3+	3+	NA
8	11	0.5%	neg	neg	5%	neg	neg	neg	neg	neg	3+	1+	10%
	12	25%	neg	neg	30%	neg	neg	neg	neg	neg	3+	3+	NA
	13	20%	neg	neg	5%	neg	neg	neg	neg	neg	3+	3+	NA
9	14	7%	60%	Patchy	50%	neg	neg	neg	neg	neg	2+	3+	<1%
	15	3%	30%	Patchy	50%	neg	neg	neg	neg	neg	3+	3+	NA
10	16	30%	20%	Patchy	NA	neg	neg	neg	60%	neg	2+	2+	<1%
	17	NA	40%	Patchy	80%	neg	neg	neg	60%	neg	2+	2+	NA
11	18	5%	50%	Patchy	30%	neg	neg	neg	neg	neg	3+	2+	neg
	19	2%	5%	Patchy	50%	neg	neg	neg	neg	neg	3+	3+	NA
	20	4%	10%	Patchy	80%	40%	neg	neg	neg	neg	3+	3+	NA
12	21	1%	40%	Patchy	70%	neg	neg	neg	neg	neg	2+	2+	neg
13	22	5%	70%	Patchy	neg	neg	neg	neg	neg	<5%	2+	1+	neg
	23	10%	70%	Patchy	20%	10%	neg	neg	neg	<5%	2+	2+	NA
	24	15%	70%	Patchy	20%	5%	neg	neg	neg	<5%	2+	3+	NA
14	25	3%	50%	Patchy	50%	neg	neg	neg	neg	neg	2+	2+	<1%
	26	0.5%	80%	Diffuse	neg	neg	neg	neg	neg	neg	1+	2+	NA
15	27	0.5%	80%	Diffuse	neg	neg	neg	neg	neg	NA	2+	3+	neg
16	28	1%	90%	Diffuse	40%	30%	NA	neg	NA	NA	NA	3+	neg
	29	20%	10%	Patchy	80%	90%	NA	neg	NA	NA	NA	2+	NA
17	30	10%	30%	Patchy	70%	20%	neg	neg	neg	neg	3+	2+	neg
18	31	20%	60%	Patchy	NA	NA	NA	neg	NA	NA	NA	3+	<1%

Pt patient, *N* case number, *NA* not assessed, *neg* negative, *EMA* epithelial membrane antigen, *SMA* smooth muscle actin, *PgR* progesterone receptor

(mean, 69% of the cells; SD, 29%); CD99 was positive in six out of 12 lesions (mean, 28% of the cells; SD, 18%; Fig. 3d). In all 12 patients studied, CD31, EMA, SMA, and D2-40 were negative in the neoplastic cells.

The network composed of reticulin fibers was detected in all patients. Reticulin stain was positive in 9/12 cases with 3+, 1/12 cases with 2+, and 2/12 cases with 1+. Collagen IV showed five out of 12 lesions with 3+ score, six out of 12 cases with 2+ score, and one out of 12 cases with 1+ score.

Positivity for PgR was detected in nine out of 12 patients with values variable from 5% to 60% of the total neoplastic proliferation (mean, 24% of the cells; SD, 22%). In 2/12 cases, only scattered cells were positive for PgR, and one case was completely negative for PgR.

Statistical analysis

On the basis of Mann–Whitney *U* test, *significant similarities* were detected between meningeal HPC and soft tissue HPC–SFT by examining the presence of staghorn vasculature ($U=154.0$; $p=0.3398$), necrosis ($U=163.0$, $p=0.3424$), cytologic atypia ($U=158.0$, $p=0.3535$), CD99 ($U=86.50$, $p=0.2539$), collagen IV ($U=126.0$, $p=0.2165$), and reticulin ($U=174.5$, $p=0.7180$). *Significant differences* were found between meningeal HPC and soft tissue HPC–SFT: cellularity ($U=76.00$, $p=0.0001$), mitoses ($U=79.50$, $p=0.0032$), and Ki67 ($U=104.5$, $p=0.0345$) were higher in meningeal tumors. On the contrary, collagen bundles ($U=84.00$, $p=0.0023$), CD34 ($U=83.50$, $p=0.0053$), and BCL2

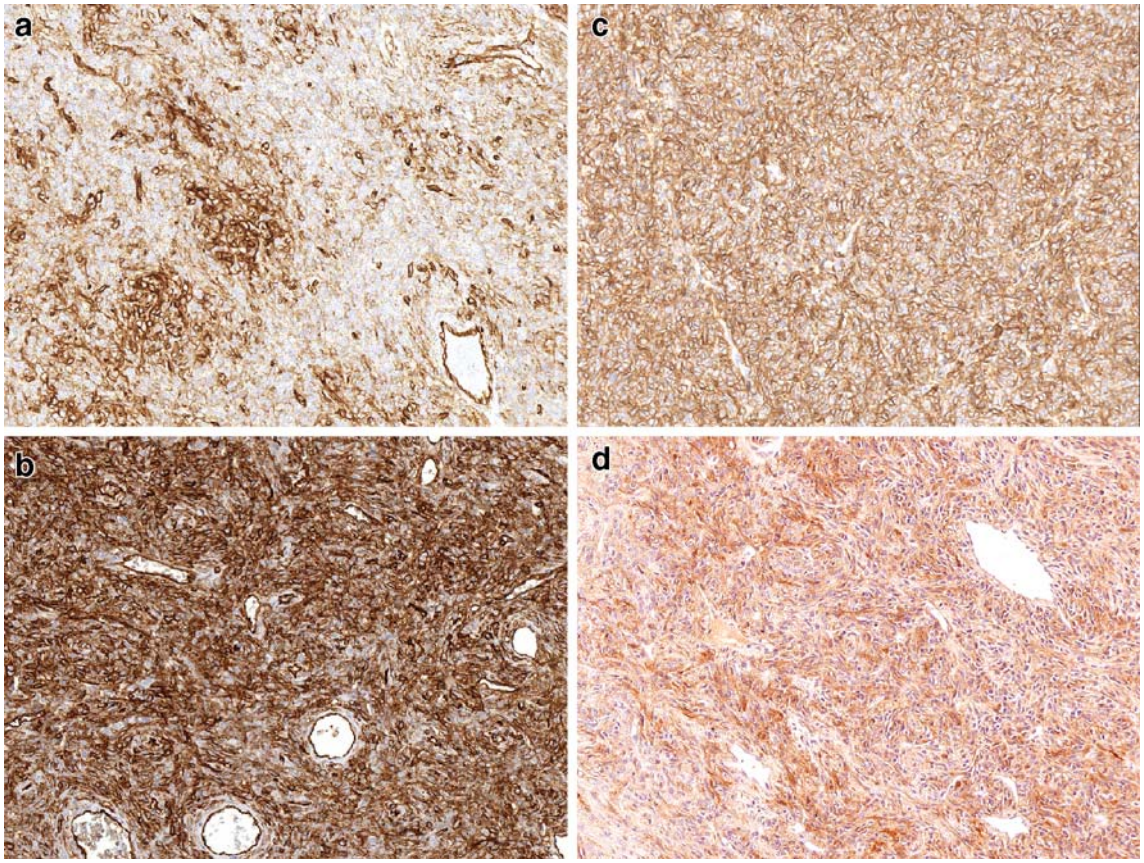

Fig. 3 Immunohistochemical features. Meningeal hemangiopericytoma (HPC) usually exhibits CD34 immunoreactivity with a patchy distribution (**a**, specimen 31, Pt. N. 18), while soft tissue solitary fibrous tumor predominantly shows diffuse immunoreactivity for CD34 (**b**, N.1). Nevertheless, CD99 is consistently expressed by both meningeal (**c**, specimen 29, Pt. N. 16) and soft tissue (**d**, N.1) lesions

(U=70.50, p=0.0068) were all parameters more frequently encountered in peripheral soft tissue lesions.

Discussion

In the meninges, HPC is considered a separate entity from SFT, while in peripheral soft tissues, HPC and SFT are regarded as features of the same condition (HPC–SFT). In order to assess similarities and differences between these lesions, we studied 31 meningeal HPCs from 18 patients and 12 soft tissue HPC–SFTs from 12 patients.

In the present series, meningeal HPC and soft tissue HPC–SFT showed several statistically significant differences. Higher cellularity, higher number of mitoses, and higher Ki67 labeling index were detected in meningeal HPC in comparison to HPC–SFT of soft tissues. On the contrary, diffuse collagen bands, high CD34, and BCL2 positivities were more frequently detected in HPC–SFT of soft tissues than in meningeal HPC.

Consistent similar features were also present between the two groups of lesions. The typical "staghorn" vasculature has been characteristically found in 90.3% specimens (88.8% of the patients) of meningeal HPC and in 100% of soft tissue HPC–SFT (U=154.0; p=0.3398). Necrosis was identified in 19.4% specimens (5.6% of the patients) of meningeal HPC and in 8.3% of soft tissue HPC–SFT (U=163.0, p=0.3424); cytological atypia was moderate in 70.9% specimens (55.6% of the patients) of meningeal HPC and in 66.6% of cases of soft tissue HPC–SFT (U=158.0, p=0.3535). CD99 was positive in 33.3% of specimens (27.8% of the patients) in meningeal lesions and in 50% of patients in soft tissue lesions (U=86.50, p=0.2539). All lesions from both groups exhibited similar reticulin network, as evaluated both by collagen IV antibody and by Gomori's and same pattern of staining for PgR.

D'Amore et al. comparing soft tissue and meningeal HPCs found same results as in the present series and concluded that similarities outnumber the differences and that both tumors are almost indistinguishable from one another on the basis of morphology, immunohistochemistry, and ultrastructural analyses [17].

In the present series, meningeal HPC recurred in 13 out 14 (92.9%) of the patients, and one case presented a metastasis to the subcutaneous tissue in the right hip, while neither recurrences nor metastases were observed in soft

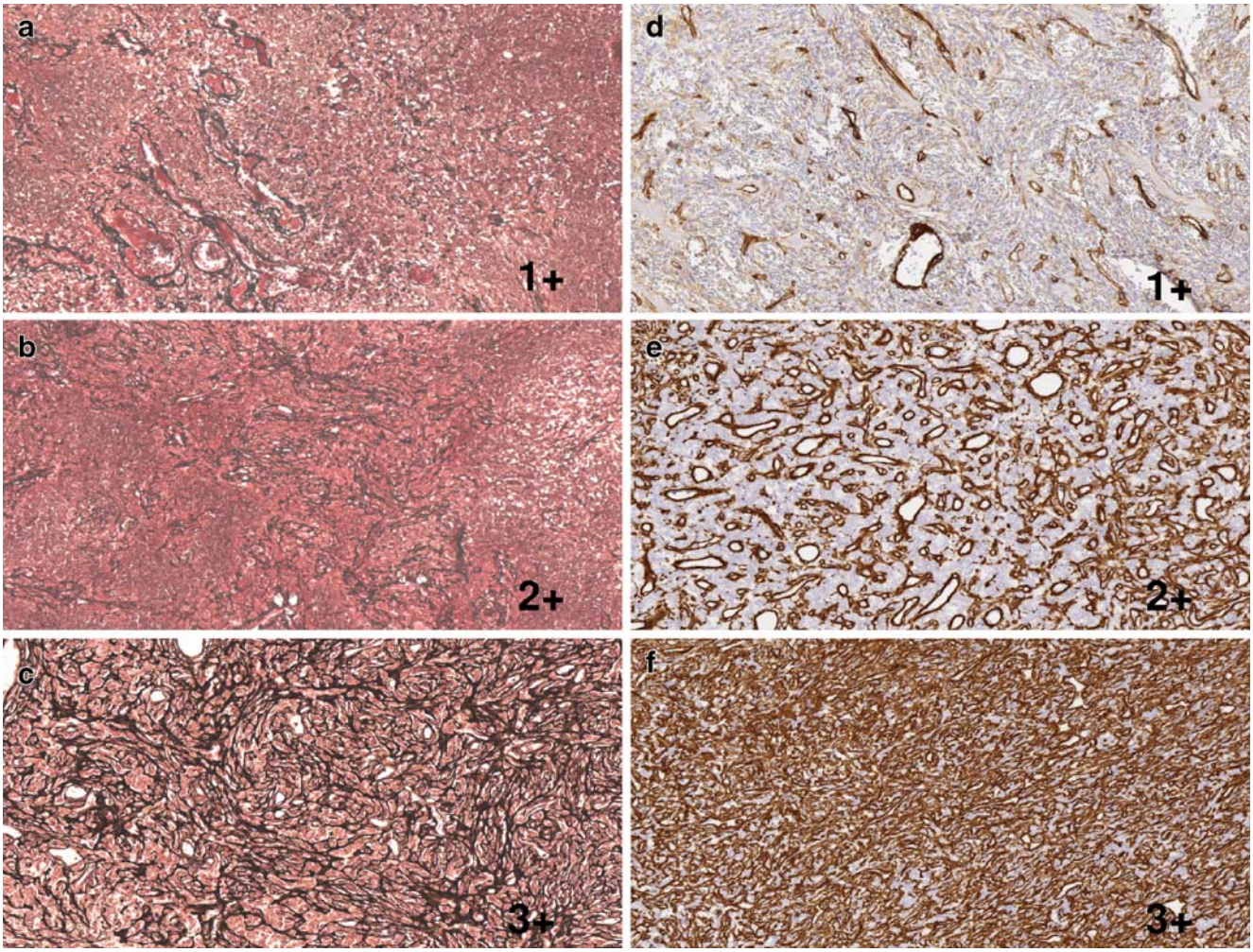

Fig. 4 Three-scale grading adopted for evaluating reticulin fibers both by histochemistry (Gomori, **a**–**c**) and by immunohistochemistry (collagen IV, **d**–**f**). 1+: the reticulin fibers are present only around blood vessels (**a**: Gomori, **d**: collagen IV); 2+: the reticulin fibers are distributed around blood vessels and around nests of neoplastic cells (**b**: Gomori, **e**: collagen IV); 3+: the reticulin fibers are distributed around blood vessels and individually decorate neoplastic cells in a diffuse pattern (**c**: Gomori, **f**: collagen IV)

Table 5 Clinical data in hemangiopericytoma–solitary fibrous tumor of soft tissues

N	Sex	Age	Site	Surgical procedure	FU
1	F	51	Thigh	Resection	A&W 7 years
2	M	44	Orbit	NA	A&W 11 years
3	F	88	Abdomen	Resection	NA
4	M	82	Mesentery	NA	A&W 4 years
5	F	72	Pleura	NA	A&W 8 years
6	F	67	Orbit	NA	A&W 10 years
7	F	82	Pleura	Nodulectomy, inferior lobe of the left lung	NA
8	M	53	Arm	NA	NA
9	M	56	Pleura	Atypical resection, superior lobe of the right lung	NA
10	F	46	Pleura	Nodulectomy, superior lobe of the right lung	NA
11	M	36	Pleura	Pulmonary nodulectomy	NA
12	M	51	Retroperitoneum	Resection of retroperitoneal neoplasia and ileostomy	DOC

N case number, *FU* follow-up, *A&W* alive and well with no recurrences, *A* alive, *DOC* died of other causes, *NA* not assessed

Table 6 Morphological data in hemangiopericytoma–solitary fibrous tumor of soft tissues

N	Major axis (cm)	Staghorn vasculature	Collagen bundles	Necrosis	Cellularity	Cytologic atypia	Mitoses[a]
1	6	Numerous	Diffuse	Absent	Moderate	Moderate	2
2	3	Numerous	Diffuse	Absent	Moderate	Mild	1
3	10.5	Moderate	Diffuse	Focal	Moderate	Moderate	3
4	5	Moderate	Focal	Absent	Low	Moderate	2
5	4.5	Moderate	Diffuse	Absent	Low	Mild	1
6	2.5	Moderate	Diffuse	Absent	Low	Mild	1
7	2	Moderate	Diffuse	Absent	Low	Mild	1
8	2	Moderate	Diffuse	Absent	Moderate	Moderate	1
9	2.9	Moderate	Diffuse	Absent	Low	Moderate	1
10	1.4	Numerous	Diffuse	Absent	Low	Moderate	1
11	3	Moderate	Diffuse	Absent	Low	Moderate	1
12	21.5	Numerous	Diffuse	Absent	Moderate	Moderate	4

N case number

[a] Mitoses were counted per ten high power fields

tissue HPC–SFT. These data are comparable to two series with long-lasting (15 years) follow-up, where meningeal HPC exhibited recurrences in 91% [18] and 85% [19] of the cases, respectively. On the contrary, soft tissue HPC–SFTs show occasional recurrences with much more favorable outcome [20].

Multiple recurrences have led to regard meningeal HPC as a distinct entity from intracranial SFT. Nevertheless, in spite of the several statements that intracranial SFTs have a benign clinical behavior [10, 21], there are many cases of intracranial SFT that have recurred and even manifested distant metastases [9, 22–26], as to indicate that the two conditions are clinically very similar.

When cases of SFT of pleura recur or metastasize, they frequently show high cellularity, high number of mitotic figures, necrosis, and nuclear pleomorphism [27] or signs of dedifferentiation such as abrupt transition to high-grade areas, loss of CD34 expression, and overexpression of p53 and p16 [28]. In our series, meningeal tumors were typically associated with low expression of CD34, high cellularity, high number of mitoses, and high Ki67 labeling index, which are all features similar to those seen in malignant or dedifferentiated SFTs.

Meningeal HPC is classified as a WHO grade II lesion. An anaplastic variant (grade III) of meningeal HPC has been described by Mena et al. in cases showing necrosis, more than five mitoses per ten microscopic fields (×400), and at least two of the following microscopic features: moderate to high nuclear atypia and moderate to high cellularity [29]. In our series, on the basis of these criteria,

Table 7 Immunohistochemical and histochemical data in hemangiopericytoma–solitary fibrous tumor of soft tissues

N	Ki67	CD34	CD34 pattern	BCL2	CD99	CD31	EMA	SMA	D2-40	Collagen IV	Reticulin	PgR
1	1%	40%	Patchy	80%	30%	neg	neg	neg	neg	3+	3+	neg
2	3%	40%	Patchy	70%	neg	neg	neg	neg	neg	3+	3+	60%
3	1%	70%	Diffuse	0%	10%	neg	neg	neg	neg	3+	3+	5%
4	3%	80%	Diffuse	70%	neg	neg	neg	neg	neg	2+	3+	neg
5	0.5%	30%	Patchy	70%	neg	neg	neg	neg	neg	2+	1+	20%
6	1%	70%	Patchy	40%	10%	neg	neg	neg	neg	2+	3+	8%
7	3%	80%	Diffuse	70%	40%	neg	neg	neg	neg	2+	3+	5%
8	3%	70%	Diffuse	80%	neg	neg	neg	neg	neg	2+	3+	20%
9	1%	80%	Diffuse	60%	30%	neg	neg	NA	neg	3+	3+	5%
10	0.5%	80%	Diffuse	70%	0%	neg	neg	NA	neg	2+	1+	30%
11	0.5%	80%	Diffuse	80%	0%	neg	neg	neg	neg	1+	2+	60%
12	3%	70%	Patchy	neg	50%	neg	neg	neg	neg	3+	3+	neg

N case number, *NA* not assessed, *neg* negative, *EMA* epithelial membrane antigen, *SMA* smooth muscle actin, *PgR* progesterone receptor

seven patients with meningeal HPC exhibited anaplastic (grade III) features along the Mena et al. criteria. All these patients had recurrences. Nevertheless, with the exception of one, all the other cases of the present series that showed grade II recurred, and one metastasized. This probably would indicate that grade cannot be considered the only parameter useful to predict prognosis in meningeal HPC. It is possible that high recurrence rate of meningeal HPC is also linked to incomplete resection of the lesion, as stated by the surgeons in three cases of the present series.

It is pertinent to remember that meningiomas (WHO grade II) may recur despite their low grade because of incomplete resection [30].

If incomplete resection due to neurosurgical procedures is among the reasons responsible for the frequent recurrences in HPC, it is reasonable to accept that HPC–SFTs of the peripheral soft tissues seldom recur due to the fact that these tumors are more amenable to complete surgical excision. In keeping with this view, tumors located in the orbit, mediastinum, abdomen, pelvis, and retroperitoneum, where the radical excision is probably difficult to achieve, tend to recur more frequently, in comparison to those located in the limbs [8, 31–33].

It seems that in the meninges, HPC and SFT represent, by analogy with the extracranial soft tissue compartment, a morphological spectrum of same lesion. The remarkable differences observed in prognosis between meningeal lesions and their soft tissue counterparts can be explained by the high incidence of "dedifferentiated" meningeal HPC–SFT coupled with incomplete surgical resection.

Acknowledgements Work partly financed by University of Bologna (ex 60%) and PERNO (Project of Emilia-Romagna region on Neuro-Oncology). Dr. Samanta Manoni, MD and Dr. Deborah Malvi, MD have helped us with the clinical information retrieval.

References

1. Stout AP, Murray MR (1942) Hemangiopericytoma: a vascular tumor featuring Zimmermann's pericytes. Ann Surg 116:26–33
2. Zimmermann K (1923) Der feinere Bau der Blutcapillaren. Z Anat Entwicklungsgesch 68:29–109
3. Cushing H, Eisenhardt L (1938) Meningiomas, their classification, regional behaviour, life history, and end surgical results. Charles C. Thomas, Springfield
4. Begg CF, Garret R (1954) Hemangiopericytoma occurring in the meninges: case report. Cancer 7:602–606
5. Klemperer P, Rabin CB (1931) Primary neoplasms of the pleura: a report of five cases. Arch Pathol 11:385–412
6. Stout AP, Murray MR (1942) Localized pleural mesothelioma. Arch Pathol 34:951–964
7. Brunnemann RB, Ro JY, Ordonez NG et al (1999) Extrapleural solitary fibrous tumor: a clinicopathologic study of 24 cases. Mod Pathol 12:1034–1042
8. Fukunaga M, Naganuma H, Nikaido T et al (1997) Extrapleural solitary fibrous tumor: a report of seven cases. Mod Pathol 10:443–450
9. Hasegawa T, Matsuno Y, Shimoda T et al (1999) Extrathoracic solitary fibrous tumors: their histological variability and potentially aggressive behavior. Hum Pathol 30:1464–1473
10. Carneiro SS, Scheithauer BW, Nascimento AG et al (1996) Solitary fibrous tumor of the meninges: a lesion distinct from fibrous meningioma. A clinicopathologic and immunohistochemical study. Am J Clin Pathol 106:217–224
11. Tavassoli FA, Eusebi V (2009) Benign soft tissue lesions. In: Tavassoli FA, Eusebi V (eds) AFIP Atlas of tumor pathology. Tumors of the mammary gland, fourth series. Fascicle 10. American Registry of Pathology, Washington, pp 263–290
12. Guillou L, Fletcher JA, Fletcher CD et al (2002) Extrapleural solitary fibrous tumour and haemangiopericytoma. In: Unni KK, Mertens F, Fletcher CD (eds) WHO classification of tumours of soft tissue and bone. IARC Press, Lyon, pp 86–90
13. Giannini C, Rushing EJ, Hainfellner JA (2007) Haemangiopericytoma. In: Louis DN, Ohgaki H, Wiestler OD, Cavenee WK (eds) WHO classification of tumours of the central nervous system, 4th edn. IARC Press, Lyon, pp 178–180
14. Weiss S, Goldblum J (2008) Soft tissue tumors of intermediate malignancy of uncertain type. In: Weiss S, Golblum J (eds) Enzinger and Weiss's soft tissue tumors, 5th edn. Mosby, Elsevier, Philadelphia, pp 1093–1160
15. Hayashi Y, Uchiyama N, Hayashi Y et al (2009) A reevaluation of the primary diagnosis of hemangiopericytoma and the clinical importance of differential diagnosis from solitary fibrous tumor of the central nervous system. Clin Neurol Neurosurg 111:34–38
16. Perry A, Scheithauer BW, Nascimento AG (1997) The immunophenotypic spectrum of meningeal hemangiopericytoma: a comparison with fibrous meningioma and solitary fibrous tumor of meninges. Am J Surg Pathol 21:1354–1360
17. D'Amore ES, Manivel JC, Sung JH (1990) Soft-tissue and meningeal hemangiopericytomas: an immunohistochemical and ultrastructural study. Hum Pathol 21:414–423
18. Vuorinen V, Sallinen P, Haapasalo H et al (1996) Outcome of 31 intracranial haemangiopericytomas: poor predictive value of cell proliferation indices. Acta Neurochir (Wien) 138:1399–1408
19. Guthrie BL, Ebersold MJ, Scheithauer BW et al (1989) Meningeal hemangiopericytoma: histopathological features, treatment, and long-term follow-up of 44 cases. Neurosurgery 25:514–522
20. Espat NJ, Lewis JJ, Leung D et al (2002) Conventional hemangiopericytoma: modern analysis of outcome. Cancer 95:1746–1751
21. Tihan T, Viglione M, Rosenblum MK et al (2003) Solitary fibrous tumors in the central nervous system. A clinicopathologic review of 18 cases and comparison to meningeal hemangiopericytomas. Arch Pathol Lab Med 127:432–439
22. Ogawa K, Tada T, Takahashi S et al (2004) Malignant solitary fibrous tumor of the meninges. Virchows Arch 444:459–464
23. Ng HK, Choi PC, Wong CW et al (2000) Metastatic solitary fibrous tumor of the meninges. Case report. J Neurosurg 93:490–493
24. Ritz R, Roser F, Bornemann A et al (2005) Recurrence and increased proliferation rate of a solitary fibrous tumor in the central nervous system—case report and review of the literature. Clin Neuropathol 24:252–256
25. Miyashita K, Hayashi Y, Fujisawa H et al (2004) Recurrent intracranial solitary fibrous tumor with cerebrospinal fluid dissemination. Case report. J Neurosurg 101:1045–1048
26. Martin AJ, Fisher C, Igbaseimokumo U et al (2001) Solitary fibrous tumours of the meninges: case series and literature review. J Neurooncol 54:57–69
27. England DM, Hochholzer L, McCarthy MJ (1989) Localized benign and malignant fibrous tumors of the pleura. A

clinicopathologic review of 223 cases. Am J Surg Pathol 13:640–658
28. Mosquera JM, Fletcher CD (2009) Expanding the spectrum of malignant progression in solitary fibrous tumors: a study of 8 cases with a discrete anaplastic component—is this dedifferentiated SFT? Am J Surg Pathol 33:1314–1321
29. Mena H, Ribas JL, Pezeshkpour GH et al (1991) Hemangiopericytoma of the central nervous system: a review of 94 cases. Hum Pathol 22:84–91
30. Borovich B, Doron Y, Braun J et al (1986) Recurrence of intracranial meningiomas: the role played by regional multicentricity. Part 2: clinical and radiological aspects. J Neurosurg 65:168–171
31. Dorfman DM, To K, Dickersin GR et al (1994) Solitary fibrous tumor of the orbit. Am J Surg Pathol 18:281–287
32. Fukunaga M, Naganuma H, Ushigome S et al (1996) Malignant solitary fibrous tumour of the peritoneum. Histopathology 28:463–466
33. Vallat-Decouvelaere AV, Dry SM, Fletcher CD (1998) Atypical and malignant solitary fibrous tumors in extrathoracic locations: evidence of their comparability to intra-thoracic tumors. Am J Surg Pathol 22:1501–1511

Virchows Arch (2010) 456:355–365
DOI 10.1007/s00428-010-0898-4

ORIGINAL ARTICLE

Sporadic hybrid oncocytic/chromophobe tumor of the kidney: a clinicopathologic, histomorphologic, immunohistochemical, ultrastructural, and molecular cytogenetic study of 14 cases

Fredrik Petersson · Zoran Gatalica · Petr Grossmann · Maria Delia Perez Montiel · Isabel Alvarado Cabrero · Stela Bulimbasic · Anthony Swatek · Lubomir Straka · Tomas Tichy · Milan Hora · Naoto Kuroda · Ben Legendre · Michal Michal · Ondrej Hes

Received: 7 January 2010 / Revised: 9 February 2010 / Accepted: 16 February 2010 / Published online: 19 March 2010
© Springer-Verlag 2010

Abstract Hybrid oncocytic/chromophobe tumors (HOCT) of the kidney have been described in patients with Birt–Hogg–Dubé syndrome (BHD) and in association with renal oncocytosis without BHD. HOCT in patients without evidence of BHD or renal oncocytosis is exceedingly rare, and these cases have been poorly characterized. We have identified and studied 14 cases of HOCT from previously diagnosed renal oncocytomas (398 cases) and chromophobe renal cell carcinomas (351 cases) without evidence of BHD or renal oncocytosis. Immunohistochemical, ultrastructural, and molecular genetic studies analyzing numerical chromosomal changes, loss of heterozygosity for chromosome 3p, and mutation status of *VHL*, *c-kit*, *PDGFR*, and folliculin (*FLCN*) genes were performed.

F. Petersson
Department of Pathology,
National University Hospital System,
Singapore, Singapore

Z. Gatalica
Department of Pathology,
Creighton University School of Medicine,
Omaha, NE, USA

F. Petersson · P. Grossmann · M. Michal · O. Hes (✉)
Department of Pathology, Charles University,
Medical Faculty and Charles University Hospital Plzen,
Alej Svobody 80,
304 60 Plzen, Czech Republic
e-mail: hes@medima.cz

M. D. Perez Montiel
Department of Pathology, Institute Nacional de Cancerologia,
Mexico City, Mexico

I. Alvarado Cabrero
Department of Pathology, Centro Medico,
Mexico City, Mexico

S. Bulimbasic
Department of Pathology, University Hospital Dubrava,
Zagreb, Croatia

A. Swatek
Department of Pathology, University of Kansas,
Kansas City, MO, USA

L. Straka
Department of Pathology, Regional Hospital Presov,
Prešov, Slovakia

T. Tichy
Department of Pathology,
Palacky's University Hospital Olomouc,
Olomouc, Czech Republic

M. Hora
Department of Urology, Charles University,
Medical Faculty and Charles University Hospital Plzen,
Plzen, Czech Republic

N. Kuroda
Department of Pathology, Red Cross Hospital Kochi,
Kochi, Japan

B. Legendre
Transgenomic, Inc.,
Omaha, NE, USA

HOCTs were identified in nine men and five women (age range 40–79 years). The size of tumors ranged from 2 to 11 cm. All tumors displayed a solid alveolar architecture and were composed of cells with abundant granular eosinophilic oncocytic cytoplasm with perinuclear halos. Occasional binucleated neoplastic cells were present, but irregular, hyperchromatic, wrinkled (raisinoid) nuclei were absent. The cytoplasm contained numerous mitochondria of varying sizes, but only sparse microvesicles with amorphic lamellar content were found. Tumors were positive for CK7 (12/14), AE1-AE3 (14/14), anti-mitochondrial antigen (14/14), E-cadherin (11/13), parvalbumin (12/14), and epithelial membrane antigen (14/14). Tumors were generally negative for racemase, CK20, CD10, and carboanhydrase IX. Interphase fluorescence *in situ* hybridization revealed multiple chromosomal losses and gains with a median of four (range 1–9) chromosomal aberrations per case. Monosomy of chromosome 20 was common and found in 7 of 14 cases. Monosomy of chromosomes 6 and 9 was present in 4 of 14 cases each, of which two cases displayed monosomy for both chromosomes 6 and 9. Polysomy of chromosomes 10, 21, and 22 was found in 4/14 cases each, of which one case displayed polysomy for all these three chromosomes. No pathogenic mutations were found in the *VHL*, *c-kit*, *PDGFR*, and folliculin (*FLCN*) genes. (1) We have shown that hybrid oncocytic/chromophobe tumors of the kidney do occur, albeit rarely, outside the Birt–Hogg–Dubé syndrome and without associated renal oncocytosis. (2) These tumors constitute a relatively homogenous group with histomorphologic features of both chromophobe renal cell carcinoma and renal oncocytoma. (3) Sporadic hybrid oncocytic/chromophobe renal tumors are characterized by multiple numerical aberrations (both mono- and polysomies) of chromosomes 1, 2, 6, 9, 10, 13, 17, 21, and 22 and lack of mutations in the *VHL*, c-*kit*, *PDGFRA*, and *FLCN* genes. (4) The tumors seem to behave indolently as no evidence of malignant behavior was documented in our series, although admittedly, the follow-up was too short to fully elucidate the biological nature of this rare neoplasm. At worst, these tumors could have a low malignant potential, which only can be found out with longer follow-up.

Keywords Kidney · Birt–Hogg–Dube syndrome · Hybrid renal cell tumor · Sporadic · Oncocytoma · Chromophobe renal cell carcinoma · Molecular genetics

Introduction

Hybrid oncocytic/chromophobe tumors (HOCT) of the kidney have been recognized for years. HOCT are defined as tumors having a mixture of cells with the morphological features of those seen in chromophobe renal cell carcinoma (CHRCC) and renal oncocytoma (RO). Most frequently, these tumors have been described in patients with Birt–Hogg–Dubé syndrome (BHD) [1–3] or in association with renal oncocytosis [4–7] without evidence of BHD. In the present study, we describe the clinicopathologic, immunohistochemical, genetic, and ultrastructural features of HOCT in a cohort of 14 patients without evidence of BHD or renal oncocytosis.

Materials and methods

A review of 398 RO and 351 CHRCC from the routine and consultation files of the University Hospital Plzen, University Hospital Dubrava Zagreb, University Hospital Kansas City, Institute Nacional de Cancerologia, and Centro Medico in Mexico City revealed 24 patients with renal tumors having the histological features of HOCT. Additional investigation resulted in the final identification of 14 cases without any clinical evidence of BHD. These cases were further studied. Tissue for light microscopy had been fixed in 10% buffered formalin and embedded in paraffin using routine procedures. Five-micrometer-thin sections were cut and stained with hematoxylin and eosin and Hale's colloidal iron stain.

Immunohistochemistry The following primary antibodies were employed: epithelial membrane antigen (EMA; E29, monoclonal, DakoCytomation, Glostrup, Denmark, 1:1,000); pan-cytokeratins (CAM 5,2, monoclonal, Becton-Dickinson, San Jose, CA, USA, 1:200; and AE1-AE3, monoclonal, Biogenex, San Ramon, CA, 1:1,000), CD10 (56C6, Novocastra, Burlingame, CA, USA, 1:20), cytokeratin 7 (OV-TL12/30, monoclonal, DakoCytomation, 1:200), cytokeratin 20 (M7019, monoclonal, DakoCytomation, 1:100), racemase (P504S, monoclonal, Zeta, Sierra Madre, CA, USA, 1:50), vimentin (D9, monoclonal, Neomarkers, Westinghouse, CA, USA, 1:1,000), parvalbumin (PA-235, Sigma Chemical Company, St. Luis, MO, USA, 1:500), anti-mitochondrial antigen (113-1, monoclonal, Biogenex, 1:800), and Ki 67 (MIB1, monoclonal, DakoCytomation, 1:1,000), c-kit (CD 117, polyclonal, DakoCytomation), E-cadherin (12H6, monoclonal, Zymed, San Francisco, CA, USA, 1:200), and carbonic anhydrase IX (rhCA9, monoclonal, RD systems, Abingdon, GB, 1:100). The primary antibodies were visualized using the supersensitive streptavidin–biotin–peroxidase complex (Biogenex). Appropriate positive controls were employed.

Ultrastructural examination Small pieces of the formaldehyde-fixed wet tissue of two cases were post-fixed in glutaraldehyde and routinely processed by electron microscopy.

Neoplastic, paraffin-embedded tissue was deparaffinized in three additional cases and was further processed for the ultrastructural study.

Molecular genetics

Fluorescence *in situ* hybridization methods

A 4-μm-thick tissue section was placed onto a positively charged slide. Hematoxylin and eosin-stained slides were examined for the identification of areas for cell counting. The unstained slide was routinely deparaffinized and incubated in the 1× Target Retrieval Solution Citrate, pH 6 (DAKO, Glostrup, Denmark) for 40 min at 95°C and subsequently cooled for 20 min at room temperature (RT) in the same solution. The slide was washed in deionized water for 5 min and the tissue was treated with proteinase K (20 mg/ml; SERVA, Heidelberg, Germany) for 4 min at RT. The slide was then placed into deionized water for 5 min, dehydrated in a series of ethanol solution (70%, 85%, and 96% for 2 min each), and air-dried. Probes for detection of aneuploidy of chromosomes 1, 2, 6, 7, 9, 10, 13, 17, 20, 21, and 22 (VYSIS/Abbott Molecular, Abbott Park, IL, USA; Table 1) were mixed with water and LSI/WCP hybridization buffer (VYSIS/Abbott Molecular) in a 1:2:7 ratio. An appropriate amount of probe mix was applied on sections, covered with a glass coverslip, and sealed with rubber cement. Slides were incubated in the ThermoBrite™ instrument (StatSpin/Iris Sample Processing, Westwood, MA, USA) with co-denaturation parameters 85°C for 8 min and hybridization parameters 37°C for 16 h. The coverslip was then removed and the slides were placed in post-hybridization wash solution (2× SSC/0.3% NP-40) at 72°C for 2 min. Slides were air-dried in the dark, counterstained with DAPI II (VYSIS/Abbott Molecular), coverslipped, and immediately examined.

Table 1 Probes for aneuploidy detection of chromosomes 1, 2, 6, 7, 9, 10, 13, 17, 20, 21, and 22

Chromosome	Probe
1	CEP 1 Satellite III
2	CEP 2 (D2Z1)
6	CEP 6 (D6Z1)
7	CEP 7 (D7Z1)
9	CEP 9
10	CEP 10
13	LSI 13 (RB1)
17	CEP 17 (D17Z1)
20	CEP 20 (D20Z1)
21	LSI 21
22	LSI 22 (BCR)

FISH interpretation

The sections were examined with an Olympus BX51 fluorescence microscope using a ×100 objective and either a triple bandpass filter set (DAPI/SpectrumGreen™/SpectrumOrange™) or single bandpass filters (SpectrumGreen or SpectrumOrange). Scoring of aneuploidy was performed by counting the number of fluorescent signals in >100 randomly selected non-overlapping tumor cell nuclei. The slides were independently counted by two observers (PG and OH). Cutoff values were evaluated in at least 100 non-overlapping cell nuclei in five normal non-neoplastic control tissues of kidney for each analyzed probe, i.e., 55 negative control fluorescence in situ hybridization (FISH) were performed. For monosomy, the average number of single signal was 28.1 and standard deviation 5.5. For polysomy, the average number of three or more signals were 4.0 and standard deviation 1.9. The monosomy and polysomy for the studied chromosomes was defined as the presence of one signal per cell in >45% and three or more signals in >10% (mean ± 3 standard deviations in normal tissue, both rounded up), respectively.

c-kit, *PDGFRA*, and *VHL* mutation analysis

DNA for molecular genetic investigation was extracted from formalin-fixed, paraffin-embedded tissue. Several 5-μm-thick sections were placed on the slides. Hematoxylin and eosin-stained slides were examined for the identification of neoplastic tissue. Subsequently, neoplastic tumor and non-neoplastic tissue from unstained slides was scraped and DNA was isolated by the NucleoSpin® Tissue Kit (MACHEREY-NAGEL, Düren, Germany) according to the manufacturer's protocol. In several cases, where quality or amount of extracted DNA was low, genomic DNA concentration was performed with the Microcon 100 (Millipore, Billerica, MA, USA) according to the manufacturer's protocol.

Mutation analysis of exons 9, 11, 13, and 17 of the *c-kit* gene, exons 12, 14, and 18 of the *PDGFRA* gene, and exons 1, 2, and 3 of the *VHL* gene was performed using PCR and direct sequencing. PCR was carried out using primers shown in Table 2. The reaction conditions were as follows: 12.5 μl of HotStart Taq PCR Master Mix (QIAgen, Hilden, Germany), 10 pmol of each primer, 100 ng of template DNA, and distilled water up to 25 μl. The amplification program consisted of denaturation at 95°C for 15 min and then 40 cycles of denaturation at 95°C for 1 min, annealing at 55°C for 1 min, and extension at 72°C for 1.5 min for all amplicons. The program was finished by 72°C incubation for 7 min.

Table 2 PCR primers used in mutation analysis

Gene and exons	Name	Primers (sequence 5′→3′)
c-kit exon 9a[a]	c-kit e9aNF	GAGTAAGCCAGGGCTTTTGTT
	c-kit e9aNR	CGTGCCATTGTGCTTGAAT
c-kit exon 9b[b]	c-kit e9bNF	CCGTTTGGAAAGCTAGTGGT
	c-kit e9bNR	CAGAGCCTAAACATCCCCTTA
c-kit exon 11	c-kit e11NF	TGTTCTCTCTCCAGAGTGCTCTAA
	c-kit e11NR	ACCCAAAAAGGTGACATGGA
c-kit exon 13	c-kit e13fN	GCCAGTTGTGCTTTTTGCTA
	c-kit e13rN	TTGATAACCTGACAGACAATAAAAGG
c-kit exon 17[1]	c-kit e17WF	ATGGTTTTCTTTTCTCCTCC
	c-kit e17WR	TACATTATGAAAGTCACAGG
PDGFRA exon 12[1]	PDG e12F	CTCTGGTGCACTGGGACTTT
	PDG e12R	GGAGGTTACCCCATGGAACT
PDGFRA exon 14	PDG e14fN	TGGACTGATATGTGATTTATTCTTTCA
	PDG e14rN	AATCCTCACTCCAGGTCAGTG
PDGFRA exon 18[1]	PDG e18F	GCTACAGATGGCTTGATCCTG
	PDG e18R	GACCAGTGAGGGAAGTGAGG
VHL exon 1	VHL e1-1	CGCGAAGACTACGGAGGT
	VHL e1-2	GTCTTCTTCAGGGCCGTA
VHL exon 1	VHL e1-3	GAGGCAGGCGTCGAAGAG
	VHL e1-4	GCGATTGCAGAAGATGACCT
VHL exon 1	VHL e1-5	GCCGAGGAGGAGATGGAG
	VHL e1-6	CCCGTACCTCGGTAGCTGT
VHL exon 1	VHL e1-7	CCGTATGGCTCAACTTCGAC
	VHL e1-8	GCTTCAGACCGTGCTATCGT
VHL exon 2	VHL e2-1	ACCGGTGTGGCTCTTTAACA
	VHL e2-2	TCCTGTACTTACCACAACAACCTT
VHL exon 3	VHL e3-1	GCAAAGCCTCTTGTTCGTTC
	VHL e3-2	ACATTTGGGTGGTCTTCCAG
VHL exon 3	VHL e3-3	CAGGAGACTGGACATCGTCA
	VHL e3-4C	CCATCAAAAGCTGAGATGAAAC

[a] 5′ end of exon 9

[b] 3′ end of exon 9

The successfully amplified PCR products were then purified using the Agencourt AMPure System (Agencourt Bioscience Corporation, Beverly, MA, USA) to remove unincorporated dNTPs, primers, and salts. The purified products were then bidirectionally sequenced using the Big Dye Terminator Sequencing kit (Applied Biosystems, Foster City, CA, USA). Unincorporated dye terminators were then removed from the sequencing reaction by the Agencourt CleanSEQ system and subsequently run on an ABI Prism® 3130xl sequencer (Applied Biosystems) at a constant voltage of 13.2 kV for 20 min.

For loss of heterozygosity (LOH) analysis of neoplastic tissue DNA, STR markers D3S1768, D3S1300, D3S1317, and D3S666 located on the short arm of chromosome 3

Table 3 PCR primers used in LOH analysis of chromosome 3p

Marker	Name	Primers (sequence 5′→3′)
D3S1768	D3S1768SF	GGTTGCTGCCAAAGATTAGA
	D3S1768A	CACTGTGATTTGCTGTTGGA
D3S1300	D3S1300SF	AGCTCACATTCTAGTCAGCCT
	D3S1300A	GCCAATTCCCCAGATG
D3S1317	D3S1317-1.1	TACAAGTTCAGTGGAGAACC
	D3S1317-1.2	CCTCCAGGCCATACACAGTCA
D3S666	D3S666-SK#15	CAAGGCATTAAAGTGGCCACGC
	D3S666-SK#16	GTTTGAACCAGTTTCCTACTGAG

(3p) were chosen from the database (Gene Bank UniSTS). The primers are listed in Table 3. PCR conditions were the same as mentioned above. PCR products were mixed with Gene Scan-500LIZ Size Standard (Applied Biosystems) and run on an ABI Prism 3130xl sequencer at a constant voltage of 15 kV for 20 min. A sample was considered LOH-positive if the ratio of non-tumor DNA to tumor DNA was >2 or <0.5.

FLCN mutation analysis

Tumor DNA was extracted from five cases and used as the genomic template for PCR amplification of exons 1–14 of the FLCN gene as recently described [8] with commercially available K562 cell line genomic DNA as a reference (Promega, Madison, WI, USA). In short, amplicons included both the coding sequence as well as 50 bp of intronic sequence to allow for the detection of mutations residing in/near splice junction regions. Primer selection was performed with MutationDiscovery.com, a web-based software (Transgenomic, Inc., Omaha, NE, USA) which incorporates Primer 3 oligonucleotide selection and design criteria. All primers were then checked to ensure that they were specific for the for PCR target sequence using the NCBI BLAST website (http://blast.ncbi.nlm.nih.gov/Blast.cgi). Specificity and yield of each PCR product was routinely assessed by gel electrophoresis (Invitrogen, Carlsbad, CA, USA). Ten microliters of each heteroduplexed PCR products was treated with Surveyor® Nuclease and its associated reagents (Transgenomic, Inc.). The digestion reaction was incubated at 42°C for 60 min. A stop solution was then added to the digestion reaction to halt enzyme activity. Eight microliters of the resulting mixture was then injected onto the WAVE® HS System on a sizing gradient predicted by Transgenomic Navigator™ Software. Bidirectional sequencing was performed following internal protocols developed and validated by Transgenomic.

Results

Basic clinicopathologic data are summarized in Table 4. All patients were admitted to hospital for a renal mass. No other tumors had been detected preoperatively. All but one patient underwent simple nephrectomy. No evidence of BHD was found in any of the patients on review of available clinical and pathology data. No additional information was available in two cases; however, these two cases were tested for FLCN gene mutations and no germline mutations were detected. Follow-up (range 2–7 years, median 3 years) was available for seven patients. Of these patients, nine were men and five women. The age ranged from 40 to 79 years (median 63.5 years).

Gross features All tumors were well circumscribed and non-encapsulated with homogenous tan to brown cut surfaces. Necrosis was not seen. Fibrotic strands resembling central scar in oncocytoma were seen in case no. 1 (Fig. 1). The size of tumors ranged from 2 to 11 cm (mean 5.2 cm). All cases were confined to the kidney with no infiltration of the perirenal or sinusoidal fatty tissue or renal veins.

All tumors were composed of neoplastic cells with nuclei displaying mild nuclear pleomorphism and abundant granular eosinophilic cytoplasm predominantly arranged in a solid alveolar pattern (Fig. 2). Frequently, neoplastic cells had a perinuclear halo, and occasional binucleated cells were identified (Fig. 3a, b). No raisinoid nuclei as seen in classic chromophobe renal carcinomas were identified. Mostly, tumor cells resembled cells of renal oncocytoma with

Table 4 Basic clinicopathologic data

Case no.	Sex/age (years)	TNM (WHO 2004)	Size (cm)	BHD sy	Follow- up
1	M/40	T1, N0, M0	3	0	2 years AW
2	M/78	T1,N0, M0	2	0	4 years AW
3	F/74	T1, N0, M0	5	0	7 years AW
4	M/69	T1, N0, M0	2	0	4 years AW
5	M/62	T1, N0, MX	6	?[a]	NA
6	M/56	T1, N0, M0	10	0[a]	NA
7	F/64	T1, N0, M0	3.5	0	2 years AW
8	M/75	T1, N0, M0	6	0	2 years AW
9	F/46	T1, N0, M0	4	0[a]	NA
10	M/74	T1, N0, M0	4	0	4 years AW,
11	M/63	T1, NX, MX	6.8	0[a]	NA
12	F/48	T2, N0, M0	11	0	NA
13	F/79	T1,N0,M0	4	0	NA
14	M/62	T1,N0,M0	6	?[a]	NA

F female, *M* male, *A/W* alive and well, *BHD sy* clinical signs for Birt–Hogg–Dube syndrome, *NA* not available, , 0 = no clinical signs of BHD sy, ? = no information about BHD sy status available

[a] No evidence of FLCN gene mutation

Fig. 1 Photomicrograph of a gross surgical specimen of a hybrid oncocytic/chromophobe renal tumor showing a well-circumscribed tan to brown lobulated tumor with central fibrotic strands resembling renal oncocytoma

perinuclear cytoplasmic clearing. Occasional small tubules were present. Small amounts of lipofuscin were present in the cytoplasm of occasional cells (Fig. 4).

Five tumors showed areas composed of neoplastic tissue with the morphologic features of RO and CHRCC, respectively. However, no typical raisinoid nuclei were present in chromophobe-like areas (Fig. 5). In between these areas, there was a gradual transition from RO-like and CHRCC-like areas. No distinct separation of both components was noted.

Hale's colloidal iron stain was positive only focally in the apical portion of scattered cells. The pattern of positivity resembled more renal oncocytoma than CHRCC. No diffuse cytoplasmic positivity was discerned.

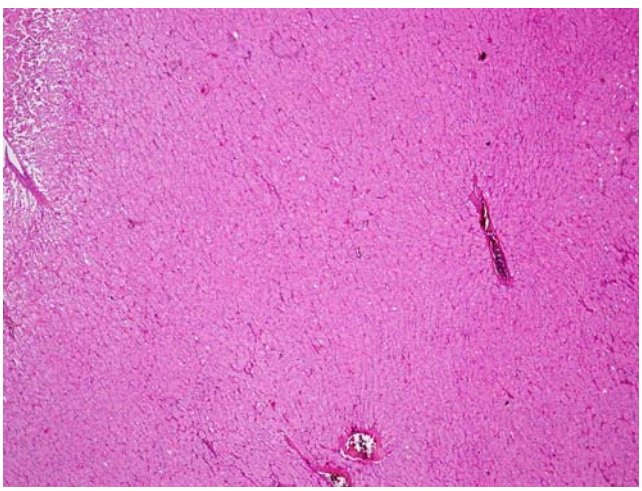

Fig. 2 Photomicrograph of a histological section (hematoxylin and eosin, original magnification ×25) of a hybrid oncocytic/chromophobe renal tumor. The tumor shows a homogenous, solid alveolar architecture

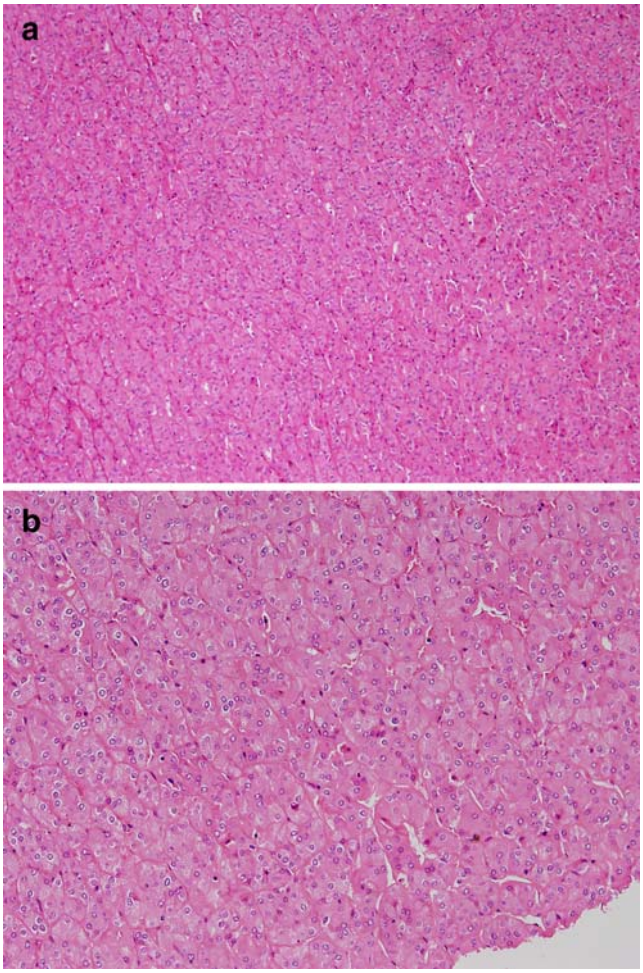

Fig. 3 **a** Photomicrograph of a histological section (hematoxylin and eosin, original magnification ×40) of a hybrid oncocytic/chromophobe renal tumor. The tumor was composed of eosinophilic cells with abundant eosinophilic granular cytoplasm. **b** Photomicrograph of a histological section (hematoxylin and eosin, original magnification ×100) of a hybrid oncocytic/chromophobe renal tumor. Neoplastic cells have round nuclei with no wrinkled edges ie no raisinoid nuclei were seen. There was a weak cytoplasmic clearing of the cytoplasm around the nucleus (perinuclear halo)

Immunohistochemistry

The immunohistochemical findings are summarized in Table 5. All tumors tested were positive for low-molecular-weight cytokeratins: AE1-AE3 (14/14), EMA (14/14), and anti-mitochondrial antigen (14/14; Fig. 6).

Most tumors were positive for CK7 (12/14; Fig. 7), E-cadherin (11/13), and parvalbumin (12/14), whereas there was a lack of reactivity for racemase (only focal positivity in one case), CK20 (0/14), CD10 (focal positivity in 3/14), and carboanhydrase IX (focal and strong positivity in case 8 and 14). All tumors (14/14) showed focal immunoreactivity for vimentin.

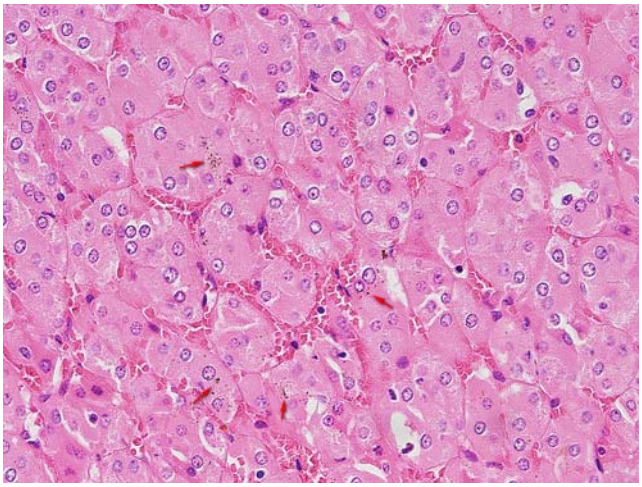

Fig. 4 Photomicrograph of a histological section (hematoxylin and eosin, original magnification ×200) of a hybrid oncocytic/chromophobe renal tumor. Small amount of lipofuscin (*arrows*) were present within the abundant granular eosinophilic cytoplasm. HE ×200

Molecular genetics

The results of the FISH study are summarized in Table 6. None of the cases were disomic for all the chromosomes tested for (1, 2, 6, 9, 10, 13, 17, 20, 21, and 22); all cases showed either mono- or polysomy for at least one of the tested centromeres. The median number of chromosomes that showed numerical aberrations per case was 4 (range 1–9). The most common numerical aberration was monosomy of chromosome 20, which was present in seven cases (Fig. 8). Monosomy of chromosomes 6 and 9 was observed in four cases each, of which two cases showed monosomy for both chromosomes 6 and 9. Polysomy of chromosomes 10, 21, or 22 was found in four cases each, of which one case (no. 14) showed polysomy for all these chromosomes.

No LOH of the short arm of chromosome 3 (3p) were discovered in any of the successfully analyzed cases. Results are summarized in Table 7.

The results of the mutation analysis for the *VHL*, *c-kit*, and *PDGFRA* genes are summarized in Table 8. No mutations were observed in any of the samples. A single nucleotide polymorphism in exon 18 in the *PDGFRA* gene was found in four cases (Table 8).

Neither amino acid changing mutations nor splice site mutations in the *FLCN* gene were observed in any of the five samples tested. Multiple exonic and intronic single nucleotide polymorphisms were detected (data not shown).

Ultrastructure

Five cases were examined by electron microscopy, and all consistently showed neoplastic cell containing numerous mitochondria of varying sizes. Only sparse microvesicles with amorphic lamellar content were present. No cells with abundant microvesicles in the cytoplasm were identified. Nuclei were mostly round, and only occasional nucleoli were detected. In one case (no. 7), small intracytoplasmatic tubuli covered by microvilli were found.

Discussion

BHD is an autosomal dominant genodermatosis characterized by multiple fibrofolliculomas in the head and neck region and upper trunk area, associated with an increased risk for the development of renal neoplasia and spontaneous pneumothorax [9]. BHD is associated with mutations in the folliculin (*FLCN*) gene which is located on chromosome 17p12q11 [1, 4]. In the renal cortex of patients with BHD, there are frequently multiple microscopic foci of aggregated oncocytic cells (oncocytomatosis/oncocytosis), and the most common renal neoplasms associated with BHD are the hybrid oncocytic/chromophobe tumors. However, conventional (and pure) clear cell carcinomas, oncocytomas, chromophobe renal cell carcinomas, and papillary renal cell carcinomas have also been reported in the setting of BHD [9, 10]. Recently, three small series of sporadic HOCT have been published [11–13], but without any chromosomal or molecular genetic studies.

Based solely on histological features, two types of HOCT could be identified in our study. One type was composed of cells with abundant eosinophilic granular cytoplasm with predominantly solid alveolar architecture. These cells frequently displayed a perinuclear halo and were occasionally binucleated. No raisionoid nuclei were present in this group. The second type was composed of mixed areas of otherwise typical RO and areas strongly

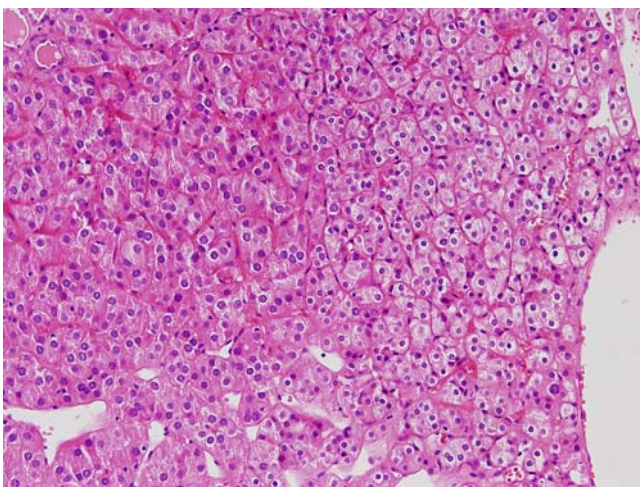

Fig. 5 Photomicrograph of a histological section (hematoxylin and eosin, original magnification ×100) of a hybrid oncocytic/chromophobe renal tumor. In some tumors, the cytoplasmic clearing was more prominent

Table 5 Immunohistochemical examination

Case no.	Racemase	CK7	CK20	CD10	CD117	PV	EMA	CANH IX	AE1-3	MIA	Cadherin	Vimentin	MIB1
1	+foc	0	0	+foc	++foc	+foc	++ +foc	0	+++	++	–	++foc	1–5/hpf
2	0	+++	0	0	+foc	+++	+++	0	+++	+++	+	++foc	2–11/ hpf
3	0	+++	0	0	+foc	+++	+++	0	+++	+	+	++foc	2–4/hpf
4	0	+++	0	0	0	0	+++	0	+++	+++	++	++foc	2–6/hpf
5	0	+++	0	0	+foc	+++	+++	0	+++	++	0	++foc	3–5/hpf
6	0	+++	0	0	+foc	+++	+++	0	+++	+++	++	++foc	0–3/hpf
7	0	++	0	0	+foc	+++	+++	0	+++	+++	+	++foc	4–6/hpf
8	0	+++	0	++foc	+	+++	+++	+foc	++	+++	+++	++foc	0–1/hpf
9	0	+++	0	0	0	+++	+++	0	+++	+++	+++	+foc	2–4/hpf
10	0	0	0	++foc	+foc	+++	+++	0	+++	+++	++	++foc	1–3/hpf
11	0	+++	0	0	+foc	+++	+++	0	+foc	++	++	++foc	1–8/hpf
12	0	++	0	0	0	+foc	+++	0	+++	+++	++	+foc	0–4/hpf
13	0	foc+	0	0	+	0	++	0	+++	+++	0	++foc	0–1/hpf
14	0	+++	0	0	+foc	+++	+++	+++	+++	++	+++	++foc	1–3/hpf

CAM5.2 cytokeratin, *AE1-AE3* cytokeratin, *CK7* cytokeratin 7, *CK20* cytokeratin 20, *EMA* epithelial membrane antigen, *MIA* antimitochondrial antigen, *PV* parvalbumin, *CANH IX* carbonic anhydrase IX, *MIB1* antibody against Ki 67 antigen, *hpf* high power field, *foc* focal

"+" = weak positivity, "++" = moderate positivity, "+++" = strong positivity

resembling CHRCC. However, no typical raisinoid nuclei or binucleation were found in these CHRCC-like areas. The histological transition zone between these two cytomorphological extremes was gradual, and the possibility of a collision tumor is therefore unlikely. Interestingly, on gross examination, these tumors were homogenous; however (except for the frequent central stellate scar in RO), no grossly visible differences between RO and CHRCC exist. Moreover, these two morphological types showed no consistent differences in either the immunohistochemical or the molecular genetic studies. The multicentricity of renal cell tumors as frequently seen in BHD was not documented in any of our patients [9, 10].

In a recently published series of sporadic HOCT [11–13], no data on numerical chromosomal anomalies have been provided. Our series showed multiple numerical chromosomal aberrations, both monosomic and polysomic. The most common numerical aberration was monosomy of

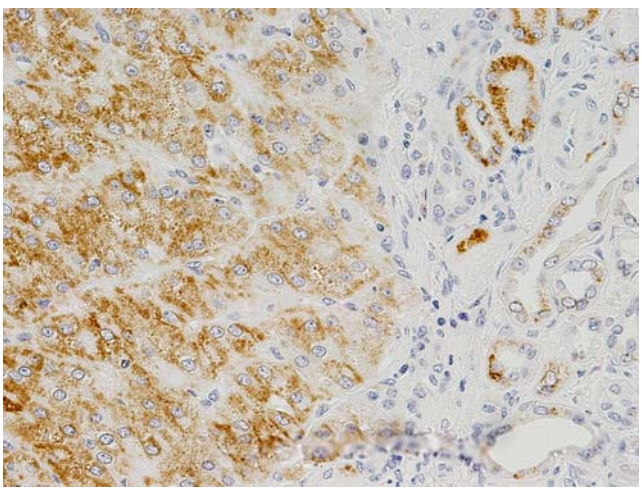

Fig. 6 Photomicrograph of a section from the immunohistochemical study (original magnification ×200) of a hybrid oncocytic/chromophobe renal tumor. Antimitochondrial antigen positivity was accentuated in the periphery of the cytoplasm in neoplastic cells. Normal kidney parenchyma is seen to the *right part* of the figure

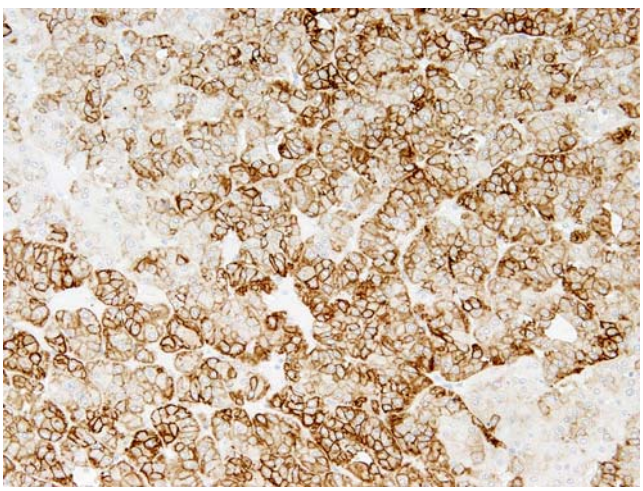

Fig. 7 Photomicrograph of a section from the immunohistochemical study (original magnification ×100) of a hybrid oncocytic/chromophobe renal tumor. There was strong cytoplasmic reactivity for cytokeratin 7 which was enhanced in the periphery of neoplastic cells

Table 6 FISH analysis of chromosomes 1, 2, 6, 7, 9, 10, 13, 17, 20, 21, and 22

Case	CEP 1	CEP 2	CEP 6	CEP 7	CEP 9	CEP 10	LSI 13	CEP 17	CEP 20	LSI 21	LSI 22
1	D	D	D	D	D	P	D	D	M	D	D
2	D	P	D	D	P	D	D	D	M	P	D
3	D	D	D	D	D	P	D	D	NA	D	D
4	D	M	M	D	M	M	D	D	M	M	D
5	D	P	D	D	M	P	P	D	NA	D	D
6	D	D	P	D	D	D	D	M	M	D	D
7	P	D	P	D	M	D	D	M	M	P	P
8	D	NA	NA	NA	NA	NA	NA	P	NA	NA	NA
9	D	M	D	M	D	D	D	D	M	D	D
10	M	D	P	D	P	D	NA	P	D	P	P
11	M	M	M	P	P	M	M	D	P	D	P
12	NA	D	M	D	M	M	NA	D	M	D	D
13	NA	NA	M	D	NA	NA	NA	D	NA	NA	NA
14	D	D	D	D	D	P	NA	D	P	P	P

D disomy, *P* polysomy, *M* monosomy, *NA* not analyzable

chromosome 20 which was present in seven cases. Monosomy of chromosome 20 is a rather unusual feature for renal cell tumors and is a highly unusual feature of chromophobe renal cell carcinoma. Two of our cases (cases 4 and 9) showed multiple monosomies only, without any detectable polysomy. In both of these cases, monosomy of chromosome 2 was present. No raisinoid nuclei, binucleation, or cytoplasmic clearing were present in these cases. Based on these chromosomal and morphologic characteristics, we do not believe that these tumors represent merely a variant of CHRCC.

Confronted with a renal tumor composed of large eosinophilic granular cells, the differential diagnostic considerations include a clear cell renal cell carcinoma with a predominance of granular cells. This is easily discriminated based on the lack of diffuse vimentin and CD10 positivity in the immunohistochemical study, absence of LOH for 3p, and no mutations observed in the *VHL* gene. Another differential diagnostic consideration is the oncocytic variant of papillary RCC. Papillary RCC show at least focal definitive fibrovascular cores (which were lacking in all our cases) and display strong positivity for racemase (not seen in any of the cases studied). Moreover, all papillary RCCs, including the oncocytic variant, display trisomy for chromosomes 7 and 17 [14, 15]. Polysomy of chromosome 7 or 17 (not in combination) was only present in two of our cases, but also in combination

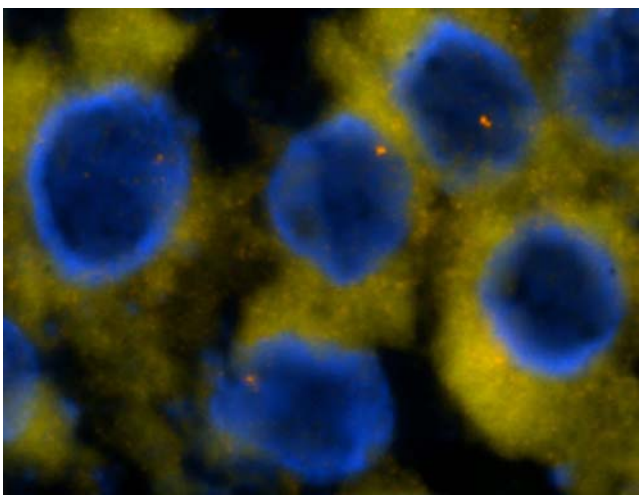

Fig. 8 Photomicrograph from the FISH study showing monosomy of chromosome 20 that was found in seven cases

Table 7 LOH status of chromosome 3p

Case no./marker	D3S666	D3S1300	D3S1768	D3S1317
1	NI	NEG	NEG	NEG
2	ND	ND	ND	ND
3	NA	NA	NEG	NEG
4	NI	NEG	NEG	NEG
5	NI	NEG	NEG	NEG
6	NEG	NA	NEG	NEG
7	NEG	NEG	NEG	NI
8	NA	NA	NA	NA
9	NEG	NEG	NEG	NEG
10	NA	NA	NA	NI
11	NI	NI	NEG	NEG
12	ND	ND	ND	ND
13	NA	NA	NA	NA
14	ND	ND	ND	ND

NI non-informative marker, *NEG* negative, *NA* not analyzable, *ND* not done

Table 8 VHL, C-kit, and PDGFRA mutation status

Case no./gene	VHL			c-KIT				PDGFRA		
	Exon 1	Exon 2	Exon 3	Exon 9	Exon 11	Exon 13	Exon 17	Exon 12	Exon 14	Exon 18
1	wt	wt	wt	wt	wt	wt	wt	wt	wt	wt[1]
2	wt	wt	wt	wt	wt	wt	wt	wt	wt	wt
3	wt	wt	wt	wt	wt	wt	wt	wt	wt	wt
4	wt	wt	wt	wt	wt	wt	wt	wt	wt	wt
5	wt	wt	wt	wt	wt	wt	wt	wt	wt	wt
6	wt	wt	wt	wt	wt	wt	wt	wt	wt	wt
7	wt	wt	wt	wt	wt	wt	wt	wt	wt	wt
8	wt	wt	wt	wt	wt	wt	wt	wt	wt	wt[1]
9	wt	wt	wt	wt	wt	wt	wt	wt	wt	wt[1]
10	wt	wt	wt	wt	wt	wt	wt	wt	wt	wt
11	wt	wt	wt	wt	wt	wt	wt	wt	wt	wt[1]
12	wt	wt	wt	wt	wt	wt	wt	wt	wt	wt
13	wt	wt	wt	wt	wt	wt	wt	wt	wt	wt
14	wt	wt	wt	wt	wt	wt	wt	wt	wt	wt

Wt wild-type sequence, *wt*[1] PDGFRA variation in exon 18 (position c.2472C>T, p.V824V)—heterozygous

with other numerical changes not characteristically seen in PRCC (Table 4). Renal oncocytomas may show a wide range of cytomorphological appearances including variants with lesional cells with voluminous cytoplasm. None of the cases presented in this study had typical stellatae central scar, although some areas in the tumors presented show definitive oncocytic features (as reflected in the preferred terminology of HOCT). Moreover, although we frequently identified an abundance of mitochondria in the cytoplasm of lesional cells, the presence of perinuclear halos in our cases is typically not seen in oncocytomas. Renal oncocytomas display variable genetic changes. Some oncocytomas are composed of mixed population of cells with normal as well as abnormal karyotypes [16, 17]. In a previous study, no numerical chromosomal changes were detected using comparative genomic hybridization in RO with renal vein extension [18]. However, loss of chromosomes 1 and 14 has been reported in RO [19, 20]. The most difficult differential diagnostic consideration of a HOCT is CHRCC. Obviously, the presence of oncocytoma-like areas is of paramount importance in correctly identifying a sporadic HOCT. However, this is a subjective matter, and if these areas are not well sampled, difficulties may ensue.

Histomorphologically, although we identified perinuclear halos and occasional binucleated neoplastic cells, we did not find any raisinoid nuclei typically present in CHRCC. Moreover, the staining pattern for Hale's colloidal iron was different from that seen in CHRCC and resembled the pattern most commonly encountered in RO.

Ultrastructurally, microvesicles with amorphic lamellar content were scarcely present. These structures are typically abundant in neoplastic cells in conventional CHRCC; however, they are frequently damaged due to improper fixation [21]. A molecular genetic study focusing on numerical chromosomal aberrations may prove very helpful. Chromosomal changes typical for CHRCC are multiple monosomies of chromosomes 1, 2, 6, 7, 10, 13, 17, and 21 [22, 23]. Hence, from a molecular point of view, CHRCC is typified by multiple monosomies and the absence of polysomies, as was frequently detected in the tumors in this study. Moreover, monosomy for chromosome 20 is highly unusual for a CHRCC, and this was the most frequently detected numerical chromosomal aberration among our cases. Based on morphology, the distinction of syndromatic (BHD) versus sporadic cases of HOCT cannot reliably be made and necessitates clinicopathologic correlation and mutation analysis of the *FLCN* gene in selected cases.

This cohort of patients was composed of two different ethnic groups.

The first group was of Caucasian origin (11 cases) and the second group of Hispanic origin (three cases). The tumors in these two groups of patients showed no differences in morphologic features or cytogenetic findings.

In conclusion, (1) we have shown that hybrid oncocytic/chromophobe tumors of the kidney do occur, albeit rarely, outside the Birt–Hogg–Dubé syndrome and without associated renal oncocytosis. (2) These tumors constitute a relatively homogenous group with histomorphologic features of both chromophobe renal cell carcinoma and renal oncocytoma. (3) Sporadic hybrid oncocytic/chromophobe renal tumors are characterized by multiple numerical

aberrations (both mono- and polysomies) of chromosomes 1, 2, 6, 9, 10, 13, 17, 21, and 22 and lack of mutations in the *VHL*, c-*kit*, *PDGFRA*, and *FLCN* genes. (4) The tumors seem to behave indolently as no evidence of malignant behavior was documented in our series, although admittedly, the follow-up was too short to fully elucidate the biological nature of this rare neoplasm. At worst, these tumors could have a low malignant potential, which only can be found out with longer follow-up.

Acknowledgment The study was supported by Czech Government grant agency: IGA 9722-4.

Conflict of interest We declare that we have no conflict of interest.

References

1. Imada K, Dainichi T, Yokomizo A et al (2009) Birt–Hogg–Dube syndrome with clear-cell and oncocytic renal tumour and trichoblastoma associated with a novel FLCN mutation. Br J Dermatol 160:1350–1353
2. Kluijt I, de Jong D, Teertstra HJ et al (2009) Early onset of renal cancer in a family with Birt–Hogg–Dube syndrome. Clin Genet 75:537–543
3. Murakami T, Sano F, Huang Y et al (2007) Identification and characterization of Birt–Hogg–Dube associated renal carcinoma. J Pathol 211:524–531
4. Adley BP, Smith ND, Nayar R et al (2006) Birt–Hogg–Dube syndrome: clinicopathologic findings and genetic alterations. Arch Pathol Lab Med 130:1865–1870
5. Cossu-Rocca P, Eble JN, Zhang S et al (2008) Interphase cytogenetic analysis with centromeric probes for chromosomes 1, 2, 6, 10, and 17 in 11 tumors from a patient with bilateral renal oncocytosis. Mod Pathol 21:498–504
6. Nagashima Y, Mitsuya T, Shioi KI et al (2005) Renal oncocytosis. Pathol Int 55:210–215
7. Tickoo SK, Reuter VE, Amin MB et al (1999) Renal oncocytosis: a morphologic study of fourteen cases. Am J Surg Pathol 23:1094–1101
8. Gatalica Z, Lilleberg SL, Vranic S et al (2009) Novel intronic germline FLCN gene mutation in a patient with multiple ipsilateral renal neoplasms. Hum Pathol 40:1813–1819
9. Pavlovich CP, Walther MM, Eyler RA et al (2002) Renal tumors in the Birt–Hogg–Dube syndrome. Am J Surg Pathol 26:1542–1552
10. Pavlovich CP, Grubb RL 3rd, Hurley K et al (2005) Evaluation and management of renal tumors in the Birt–Hogg–Dube syndrome. J Urol 173:1482–1486
11. Delongchamps NB, Galmiche L, Eiss D et al (2009) Hybrid tumour 'oncocytoma–chromophobe renal cell carcinoma' of the kidney: a report of seven sporadic cases. BJU Int 103:1381–1384
12. Mai KT, Dhamanaskar P, Belanger E et al (2005) Hybrid chromophobe renal cell neoplasm. Pathol Res Pract 201:385–389
13. Waldert M, Klatte T, Haitel A et al (2010) Hybrid renal cell carcinomas containing histopathologic features of chromophobe renal cell carcinomas and oncocytomas have excellent oncologic outcomes. Eur Urol 57:661–666. doi:10.1016/j.eururo.2009.05.009
14. Hes O, Brunelli M, Michal M et al (2006) Oncocytic papillary renal cell carcinoma: a clinicopathologic, immunohistochemical, ultrastructural, and interphase cytogenetic study of 12 cases. Ann Diagn Pathol 10:133–139
15. Lefevre M, Couturier J, Sibony M et al (2005) Adult papillary renal tumor with oncocytic cells: clinicopathologic, immunohistochemical, and cytogenetic features of 10 cases. Am J Surg Pathol 29:1576–1581
16. Kovacs G, Szucs S, Eichner W et al (1987) Renal oncocytoma. A cytogenetic and morphologic study. Cancer 59:2071–2077
17. Kovacs G, Welter C, Wilkens L et al (1989) Renal oncocytoma. A phenotypic and genotypic entity of renal parenchymal tumors. Am J Pathol 134:967–971
18. Hes O, Michal M, Sima R et al (2008) Renal oncocytoma with and without intravascular extension into the branches of renal vein have the same morphological, immunohistochemical and genetic features. Virchows Arch 452:285–293
19. Herbers J, Schullerus D, Chudek J et al (1998) Lack of genetic changes at specific genomic sites separates renal oncocytomas from renal cell carcinomas. J Pathol 184:58–62
20. Presti JC Jr, Moch H, Reuter VE et al (1996) Comparative genomic hybridization for genetic analysis of renal oncocytomas. Genes Chromosomes Cancer 17:199–204
21. Bonsib SM, Bray C, Timmerman TG (1993) Renal chromophobe cell carcinoma: limitations of paraffin-embedded tissue. Ultrastruct Pathol 17:529–536
22. Brunelli M, Eble JN, Zhang S et al (2005) Eosinophilic and classic chromophobe renal cell carcinomas have similar frequent losses of multiple chromosomes from among chromosomes 1, 2, 6, 10, and 17, and this pattern of genetic abnormality is not present in renal oncocytoma. Mod Pathol 18:161–169
23. Kuroda N, Katto K, Yamaguchi T et al (2008) Chromophobe renal cell carcinoma: useful diagnostic application of imprint cytology and fluorescence in situ hybridization of chromosomes 10 and 21 in two cases of typical and eosinophilic variants. Med Mol Morphol 41:227–232

Virchows Arch (2010) 456:367–375
DOI 10.1007/s00428-010-0894-8

ORIGINAL ARTICLE

Acute kidney injury in human leptospirosis: an immunohistochemical study with pathophysiological correlation

Eduardo Rocha Araujo · Antonio Carlos Seguro · Anne Spichler · Antonio J. Magaldi · Rildo A. Volpini · Thales De Brito

Received: 3 November 2009 / Revised: 26 January 2010 / Accepted: 11 February 2010 / Published online: 9 March 2010
© Springer-Verlag 2010

Abstract Tubulointerstitial nephritis is a common clinico-pathological finding in leptospirosis. Clinically, nonoliguric acute kidney injury (AKI), hypokalemia, sodium, and magnesium wasting frequently occur in leptospirosis. The exact mechanisms of renal involvement remain largely unclear. Immunohistochemistry to detect expression of the endogenous sodium/hydrogen exchanger isoform 3 (NHE 3), aquaporin 1 and 2, α-Na^+K^+ATPase, and sodium–potassium–chloride cotransporter in its NKCC2 isoform was performed on kidneys removed during autopsy of human leptospirosis cases and kidneys removed during autopsy of human non-leptospirosis cases with and without evidence of acute tubular necrosis (ATN). A decrease in NHE 3, aquaporin 1, and α-Na^+K^+ATPase expression occurred in proximal convoluted tubule cells. Expression of aquaporin 1 was preserved along the descending thin limb of the loop of Henle in the outer medulla. α-Na^+K^+ATpase expression was essentially preserved in the distal tubules, i.e., the thick ascending limb of the loop of Henle, macula densa, and distal convoluted tubule. Aquaporin 2 expression in the collecting tubules was enhanced compared to those of non-leptospirotic kidneys. NKCC2 cotransport isoform was expressed in the thick ascending limb of the loop of Henle and was essentially preserved in leptospirotic kidneys. Primary injury of the proximal convoluted tubules is regarded as the hallmark of the kidney in leptospirosis. Sodium and water transport are particularly affected with increased distal potassium excretion, hypokalemia, and polyuria. Enhanced expression of aquaporin 2 in medullary collecting tubules is probably an attempt to retain water during the nonoliguric phase of renal failure.

Keywords Leptospirosis · Human · Kidney · Immunohistochemistry

E. R. Araujo · T. De Brito
Department of Pathology, S. Paulo University Medical School,
Av. Dr. Enéas de Carvalho Aguiar 470,
São Paulo, Brazil

A. C. Seguro · A. Spichler · A. J. Magaldi · R. A. Volpini
Renal Disease Basic Research Laboratory-LIM 12-"Hospital das Clinicas", University of S. Paulo Medical School,
São Paulo, Brazil

E. R. Araujo · T. De Brito (✉)
Instituto de Medicina Tropical de S.Paulo,
CEP 05403-000 São Paulo, Brazil
e-mail: thalesbr@usp.br

Introduction

Leptospirosis is an acute septicemic febrile illness that affects humans and/or animals in all parts of the world. The etiological agent is *Leptospira interrogasns*, which can spread from animal reservoirs to humans. *Leptospira biflexa* is a saprophytic species usually found in surface waters and soils.

Leptospirosis is a public health problem worldwide and is epidemic in areas of Brazil, particularly during the rainy season. Worldwide, a strong occupational association has been verified, together with universal risk from rodent-carrier-mediated infection, especially prevalent in tropical countries [1, 2].

Only pathogenic leptospira adhere to renal epithelial cells and hepatocytes, and this might indicate that outer membrane proteins from virulent leptospira are important to understand the pathogenesis of the disease [3, 4].

Tubulointerstitial nephritis is the main cause of acute kidney injury (AKI) in leptospirosis, mainly manifested as polyuria and hypokalemia. Glomerular manifestations, when

present, are of a mild nonspecific reactive mesangioproliferative glomerulonephritis [5]. Tubular functional alterations precede a decrease in the glomerular filtration rate. Both humans and experimental animals show increased urinary fractional excretion of potassium and sodium, suggesting increased distal potassium excretion caused by distal sodium delivery consequent to proximal tubules damage and impairment of sodium reabsorption [1, 6, 7].

A limited number of specialized studies have focused on the molecular basis of ionic dysfunction in kidneys among patients and/or experimental animals with severe leptospirosis [8]. The aim of this work was to provide support for the main pathophysiological alterations described in AKI in human leptospirosis using immunohistochemistry. Antibodies against different electrolyte and water transport pathways were used to morphologically detect their expression in the different segments of the tubular architecture of the diseased human kidney. Differences with findings in experimental animal models are stressed [1, 8, 9]. Leptospirotic and non-leptospirotic human kidneys were compared in an attempt to detect in terms of renal transporters the differences between both forms of tubular necrosis.

Material and methods

Human samples

Kidneys from four autopsies of patients with Weil's syndrome that were part of previous publications [3, 5] were used. The main clinico-epidemiological and laboratory data are presented in Table 1. Except for patient 3, who was 67 years old, the average age was roughly 24 years old. Clinical and epidemiological information are in agreement with those observed in fatal leptospirosis. Illness duration averaged 5 days, and no laboratory diagnostic data of leptospirosis were available. The autopsies were complete and besides macro- and microscopic findings highly suggestive of leptospirosis, immunohistochemical assay, as previously described [5], was positive mainly in the liver and kidney samples. Special care was taken in selecting autopsies performed after an average of 5 to 12 h of death to obtain a more preserved histology. Kidney fragments were fixed in 10% neutral formalin, embedded in paraffin, and routinely stained with hematoxylin–eosin. In all patients, previously described findings of acute tubular necrosis and interstitial nephritis were observed [3, 5].

Immunohistochemical assay

Essential data regarding the immunohistochemical protocols are presented in Table 2. Briefly, immunohistochemistry to detect different electrolyte and water transport pathways was routinely performed on paraffin sections using the antibodies listed in Table 2 and a standard protocol [3, 5]. When necessary, heat antigen retrieval was performed in a microwave oven in ethylenediaminetetraacetate buffer (pH8.0). Peroxidase-conjugated polymer (Table 2) and diaminobenzidine were used to develop the immune and chromogen reactions.

Controls:

1. Reactions, in which primary antibody was replaced with saline or normal human serum, were performed as negative controls.
2. Antibodies were tested on kidneys of autopsies of two patients with normal kidneys. Both were male, one 38 and the other 40 years old. The first had a tumor of the spinal cord (Glioblastoma multiform) and the other was HIV positive, with pulmonary manifestations and opportunistic infections. Kidney sections showed essentially normal architecture in both patients. Again, the autopsies selected were performed an average of 6 to 12 h after death.
3. Antibodies were also tested in four biopsies of normal human kidneys donated for renal transplantation to screen organ donors.
4. Antibodies were tested on samples from four non-leptospirotic patients with ATN (Table 3).
5. For evaluation of immunoperoxidase staining of type-3 Na^+/H^+ exchanger (NHE3) and aquaporin 1 (AQP1),

Table 1 Leptospirosis: clinico-epidemiological data

Case number/ sex/age	Clinical and epidemiological information	Illness duration (days)
1/m/29y	Fever, muscular pain for the last 5 days, jaundice, bipalpebral edema, acute renal failure, pulmonary hemorrhage, abdominal pain and vomiting, low platelet count	5
2/m/20y	Contact with rats and contaminated water, fever and muscular pain for the last 8 days. Jaundice, conjunctival hemorrhage, dyspnea and hemorrhagic sputum, acute renal failure	8
3/f/67y	Contact with sewage and rats. Fever, muscular pain and respiratory failure (pulmonary hemorrhage). Jaundice. Hepatomegaly.	4
4/f/22y	Contact with sewage and rats. Fever, muscular pain and respiratory failure (pulmonary hemorrhage). Jaundice. Hepatomegaly.	4

y years

Table 2 Essential data regarding the immunohistochemical protocols

Primary antibody	Clone	Dilution	Link
NHE-3	Monoclonal	1/20	NOVOLINK-Novocastra
Aquaporin 1 (ab95660)	Monoclonal	1/10,000	NOVOLINK-Novocastra
Aquaporin 1 (ab11023)	Monoclonal	1/15,000	NOVOLINK-Novocastra
Aquaporin 2	Polyclonal	1/100	LSAB-Dako
α-Na,K ATPase	Monoclonal	1/2,000	NOVOLINK-Novocastra
NKCC2	Polyclonal	1/500	NOVOLINK-Novocastra

each tubulointerstitial grid field measuring 0.34 mm^2 was graded semiquantitatively, and the mean score for extension and intensity per kidney was calculated. Each score reflected changes in the extent and intensity of the staining and depended on the percentage of grid field showing positive staining: 0, absent or <5% of extension; I, 5–25% of extension or weak intensity; II, 25–50% of extension or mild intensity; III, 50–75% of extension or moderate to strong intensity; and IV, >75% of extension or strong intensity.

Results

The clinico-epidemiological data of the selected patients were highly suggestive of leptospirosis. The illness was of short duration, and this, usually associated with delayed clinical diagnosis, contributed to the lack of important confirmatory laboratory tests. However, at autopsy, histopathological findings and immunohistochemistry revealed tissue antigen deposits mostly in the liver and kidney, supporting the diagnosis of leptospirosis [5]. Furthermore, antibodies against a leptospiral surface adhesion protein of 21 kDa present only in pathogenic leptospira-labeled cell membrane of liver, renal-connecting tubules, and collecting ducts in all four autopsies. Adhesion protein antigenic deposits were also demonstrated in macrophages, particularly in the liver [3].

Renal pathology showed enlarged kidneys with pale cortex and focal tubulointerstitial nephritis with antigens present in macrophages of the inflammatory infiltrate. Besides macrophages, lymphocytes, plasma cells, and occasionally eosinophils constituted part of the inflammatory infiltrate. Tubular necrosis and interstitial edema were present. Kidney pathology was essentially similar in all patients but showed different intensities, such that case 2 exhibited more accentuated and case 4 less marked tubular necrosis.

Except for being more focal and not accompanied by interstitial nephritis, ATN was morphologically similar to that observed in leptospirosis.

Immunohistochemistry

NHE3 Antibodies against endogenous NHE3 were present in autopsied normal non-leptospirotic kidneys at the luminal side of proximal convoluted tubules. In leptospirosis, groups of proximal convoluted tubules with a normal NHE3 expression alternated with others with poor or absent expression (Fig. 1a and b). Those with flat lining were usually the site of absent NHE3 expression.

Expression of NHE3 was rarely observed on the parietal epithelium of the Bowman capsule and in few endothelial cells of interstitial vessels.

Non-leptospirotic ATN showed essentially similar findings but with a more focal expression.

AQP1 AQP1 is an active water-selective pore that permits osmotically driven water movement. Two different antibodies against aquaporin 1 water channel protein were used. One (ab95660), from an epitope of active channel loop (intracellular C-terminal AQP1), was expected to be expressed over the cell luminal membrane. The other (ab11023), from an epitope within the cytoplasmic domain of the water-specific channel aquaporin 1 (Table 2), was expected to be expressed in the cytoplasm. Observation revealed that both were

Table 3 Acute terminal tubular necrosis

Case number	Age and sex	Main autopsy findings	Clinicopathological findings
1	49 y f	LE. Acute respiratory syndrome. Aspergillosis. Septicemia	Septicemic shock
2	15y f	Hepatic cirrhosis (probably C hepatitis) Gastrointestinal hemorrhage	Hemorrhagic shock
3	46y f	Acute hepatic necrosis Gastrointestinal hemorrhage	Hemorrhagic shock
4	80y m	Streptococcal skin infection (Erysipela) Septicemia	Septicemic shock

y years, *f* female, *m* male

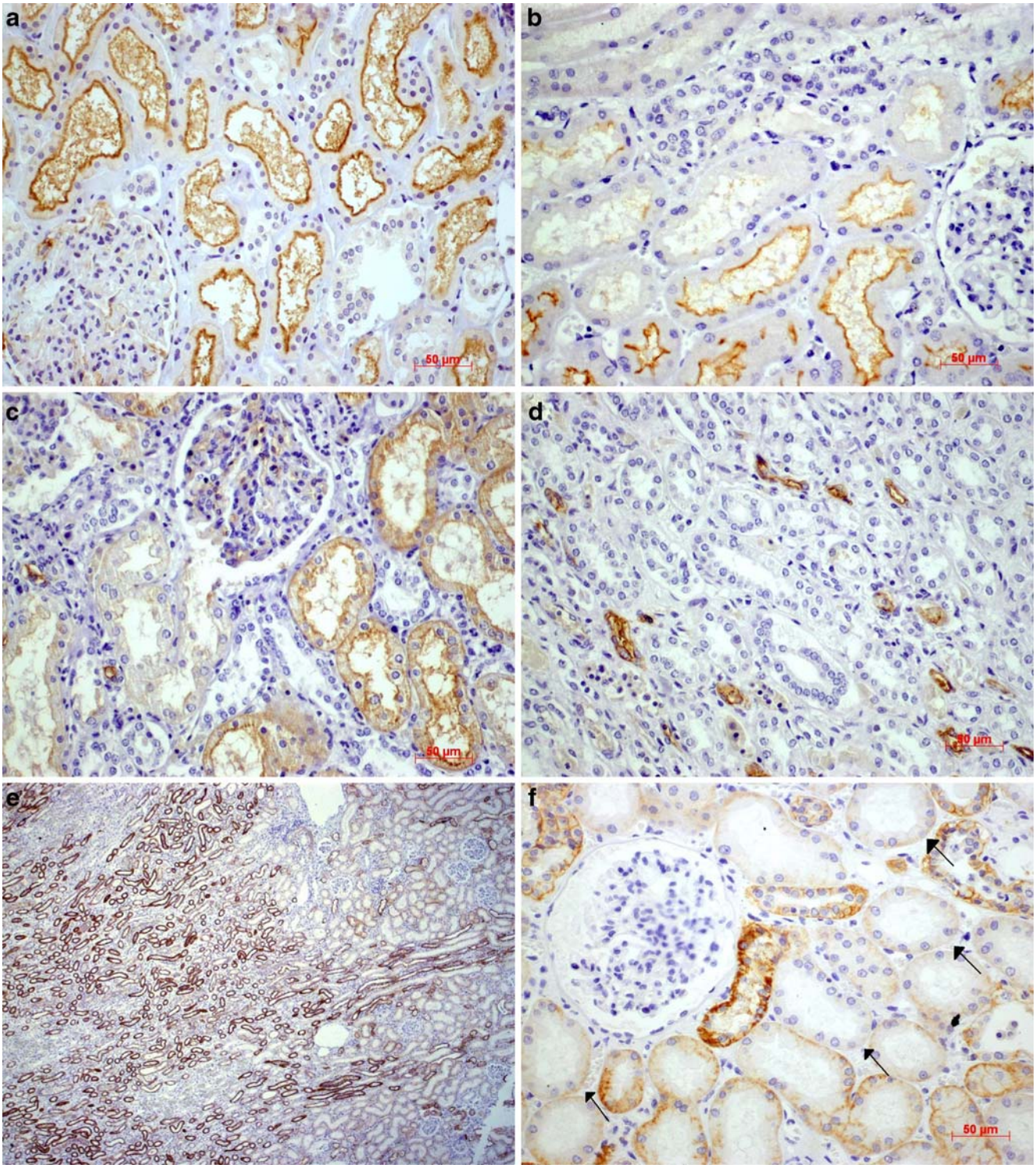

Fig. 1 **a** Expression of the endogenous NHE3 is observed on the luminal side of proximal tubular cells of a non-leptospirotic autopsy kidney without acute tubular necrosis. **b** Kidney in leptospirosis: groups of proximal convoluted tubules where NHE3 irregular expression alternates with others, usually with a flat epithelial lining, with absent expression. **c** Aquaporin 1 shows absent expression in groups of proximal convoluted tubules in leptospirosis side by side with others with preserved expression. **d** Expression of aquaporin 1 is essentially preserved in thin limbs of the loop of Henle. Collecting duct cells were unlabeled. **e** Similar to controls, the sodium potassium pump (α-Na^+K^+ATpase) was expressed in distal tubules, particularly in the thick ascending limb of the loop of Henle in leptospirosis. **f** A predominant basal linear and more diffuse granular expression of the sodium potassium pump is also present in the cytoplasm of proximal tubular cells and disappears in groups of tubular cells in leptospirosis (*arrows*). Marked expression is observed close to the glomerulus in what appears to be either a dilated thick ascending limb of the loop of Henle or a transition of the thick ascending limb to a distal convoluted tubule

expressed on the luminal side of the proximal convoluted tubules, while ab11023 was also partially expressed as a rim in the cytoplasm beneath the cell membrane.

The pattern of both aquaporin 1 expression were essentially similar and were analyzed in the autopsy of normal non-leptospirotic human kidneys showing extensive labeling of the proximal convoluted tubules that continued uninterrupted into descending thin limbs in outer medulla. However, differences occurred in the level of expression between groups of proximal convoluted tubules. A similar pattern was observed in biopsied normal kidneys. Furthermore, abrupt transitions from heavily labeled to poorly or unlabeled segments of thin limbs were observed in the inner medulla, as previously described [10, 11].

Expression of aquaporin 1 was present in endothelial cells of few glomeruli. Endothelial cells of the glomerular vascular pole and a few interstitial capillaries were also labeled, while collecting duct cells were unlabeled.

Leptospirosis groups of proximal convoluted tubules expressed aquaporin 1 side by side with tubules with poor or absent expression, with the latter also usually present in tubules lined by flat epithelium (Fig. 1c). Expression of aquaporin 1 in thin limbs (Fig. 1d) was either preserved or, apparently, even more accentuated.

The findings in ATN were essentially similar but more focal compared to those of leptospirosis.

The immunohistochemical studies showed an decreased intensity of the immunoreaction of NHE3 and AQP1 in the renal cortex of leptospirosis and ATN groups when compared to controls ($p<0.05$; Fig. 2). Extension of the immunoreaction did not show any statistical difference among the studied groups.

AQP2 Aquaporin 2 (AQP2) is expressed at the apical side of the connecting tubule and collecting principal duct cells. In the normal autopsied non-leptospirotic kidney, the expression was not uniform when various collecting ducts were compared, and the labeling was usually irregular and even absent in groups of connecting tubules (Fig. 3a) and collecting ducts close to the papilla; however, in the biopsied pretransplant normal kidney, expression of aquaporin 2 was marked in the cortical collecting ducts when they were available (Fig. 3e). Medullary collecting ducts were not present in the biopsied kidney.

When autopsied normal non-leptospirotic kidneys were compared to cases of leptospirosis, a stronger and more diffuse expression was observed in the latter (Fig. 3b and c). Increased expression of aquaporin 2 was also observed in cases of ATN (Fig. 3d) but less diffused compared to the kidney in leptospirosis. Low number of grid fields did not permit the semiquantitative evaluation of AQP2 expression.

α-Na^+K^+ATpase The sodium potassium pump, observed both in biopsied and necropsied normal kidneys, was clearly expressed in the distal tubules which consist of three distinct segments: thick ascending limb of the loop of Henle, the macula densa, and the distal convoluted tubule. Faint linear basal and granular cytoplasmatic expression was present at the proximal convoluted tubules lining cells. In leptospirosis, expression of the α-Na^+K^+ATpase was essentially preserved in the distal tubules (Fig. 1e) but was diminished and even absent in groups of proximal convoluted tubules (Fig. 1f). Expression of α-Na^+K^+ATpase was occasionally observed in groups of collecting ducts of the medulla. α-Na^+K^+ATpase expression was preserved in ATN.

NKCC2 A polyclonal antibody against rat kidney was shown to be equally specific for human kidney. The isoform NKCC2 has an anatomic location which corresponds to the thick ascending limb of the loop of Henle. NKCC2 expression was particularly evident at these locations at the luminal and initial lateral border of cells of normal biopsied kidney. However, NKCC2 expression was equally present in autopsied leptospirotic and non-leptospirotic kidneys except for one non-leptospirosis ATN, where expression of NKCC2 cotransporter was not present in isolated segments of the thick ascending limb of the loop of Henle. One aspect worth noting, different degrees of expression were focally observed in leptospirotic patients where isolated segments of the thick limb of the loop of Henle showed a faint luminal expression side by side with others with more marked expression (Fig. 3d).

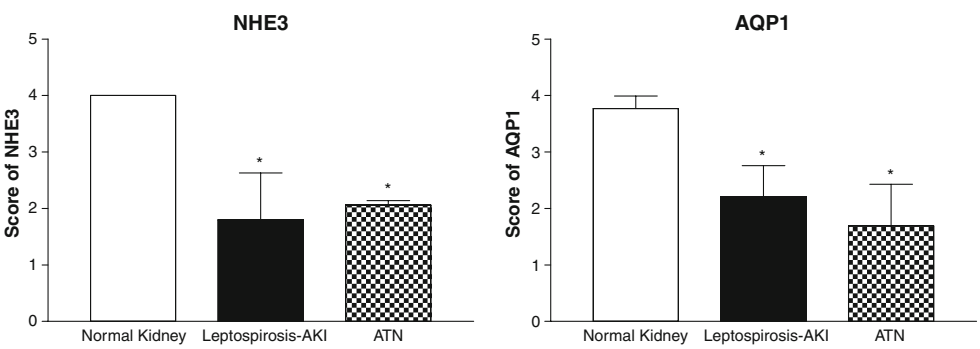

Fig. 2 Immunostaining scores of intensity for NHE3 and AQP1 in the tubulointerstitial area of the renal cortex of normal kidneys, AKI in leptospirosis and ATN. Data are expressed as mean ± SD. *$p<0.05$ (versus normal kidney)

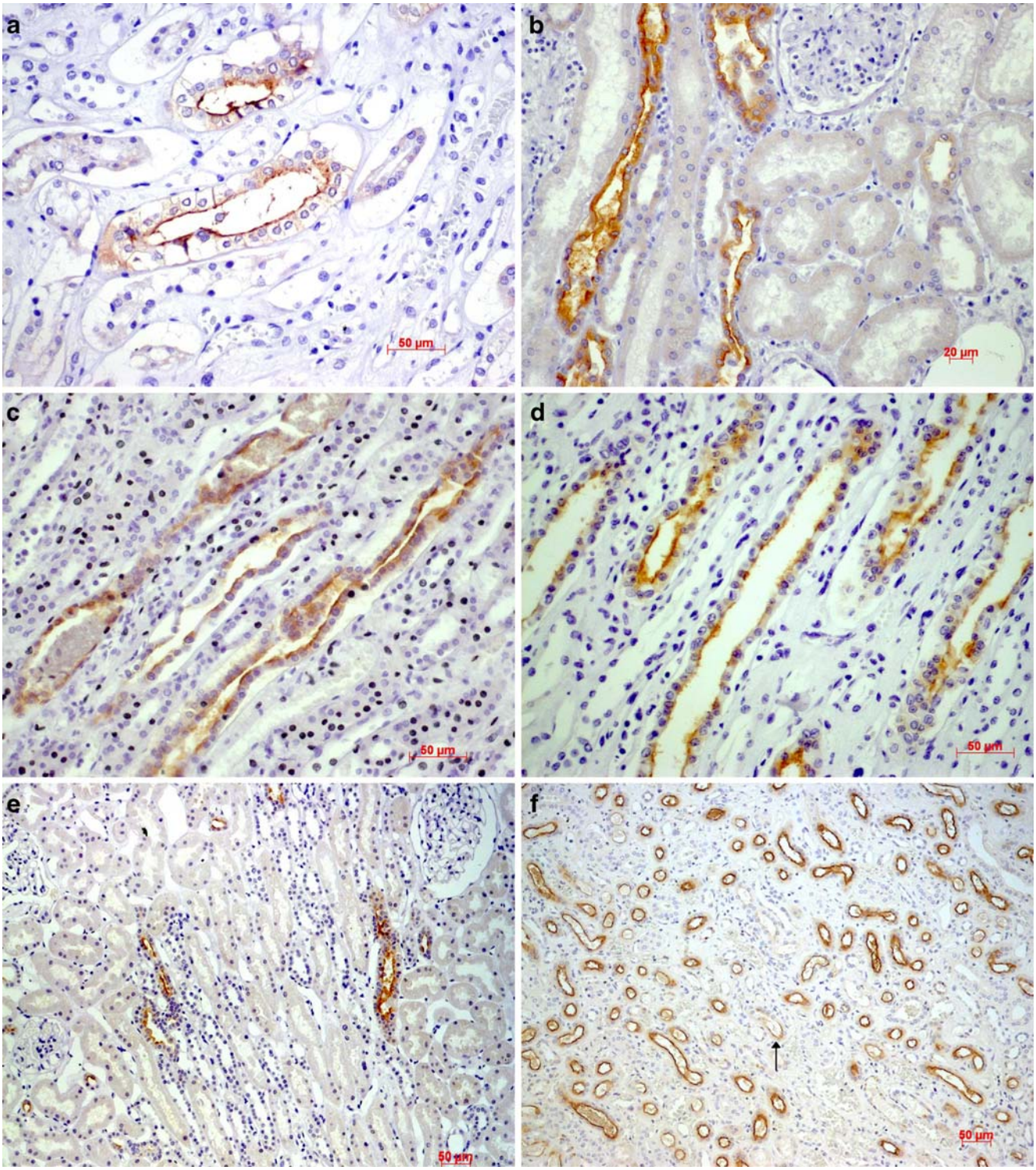

Fig. 3 **a** Aquaporin 2 expression present in the medulla of non-leptospirotic kidney is irregular in contrast with a marked expression detected in leptospirosis in cortical (**b**) and medullar collecting tubules (**c**). **d** Marked expression of aquaporin 2 is also observed in medullary collecting tubules in cases of non-leptospirotic acute tubular necrosis. **e** Marked expression of aquaporin 2 in the few assessed cortical collecting tubules in the biopsied human kidney. **f** NKCC2 is expressed in the thick ascending limb of the loop of Henle, but different degrees of expression are observed in some limbs in leptospirosis (*arrow*)

Discussion

Leptospirosis is a septicemic disease with infectious vasculitis. Pathogenesis of the AKI described in the disease is multifactorial, but hypotension, hypovolemia, and direct action of leptospires and/or their proteins are important contributors [12]. Vasculitis with hemorrhage, fever, diarrhea, and vomiting are important determinants of dehydration and hypovolemia. Direct leptospiral action has been described on tubular cells and is also responsible for the focal interstitial nephritis. Recently, several outer membrane proteins of pathogenic leptospira, among them LipL.32 [4] and the more recently described adhesion protein Lsa21 [3], were identified, located in renal tubules; these are considered important mediators in the pathogenesis of leptospirosis.

Clinically, AKI in leptospirosis is commonly associated with a special form of tubular dysfunction which precedes the decrease in glomerular function rate [6, 7]. Proximal renal tubular dysfunction is prevalent in leptospirosis, as demonstrated by hyperphosphaturia, glycosuria, and proximal renal tubular acidosis [1, 6]. The proximal renal tubular dysfunction is more clearly understood when we consider that this part of the nephron is one of the main targets for leptospiral colonization. Acute renal failure in leptospirosis is frequently associated with polyuria and hypokalemia, with an elevated urinary fractional excretion of potassium. Human and experimental studies [1, 6, 7, 13] have demonstrated that in leptospirosis, the proximal tubular injury is responsible for the decrease in sodium and water reabsorption and the increase in sodium and water delivery to the distal nephron, which may enhance potassium excretion [7, 14].

The immunohistochemical findings presented, showing diminished expression of the sodium/NHE3 and aquaporin 1 in proximal convoluted tubules are in agreement with and support the pathophysiological findings described above. The decrease in protein expression of the sodium transporter partially explains the polyuria, while directly agreeing with the high fractional excretion of sodium detected in the disease. Furthermore, because aquaporins are membrane-inserted water channel proteins [10, 15, 16], their altered expression contributes to deficient water reabsorption from the renal tubular fluid and, therefore, also contributes to the polyuria. One aspect worth mentioning is that the thin descending limb of the loop of Henle, which also plays an important role in urinary concentration, showed preserved aquaporin 1 expression in both ATN and AKI in leptospirosis, therefore, playing, up to certain point, a compensatory role in water reabsorption.

Experimental microperfusion studies [7] showed that the medullary thick ascending limb has transepithelial potential difference and relative sodium-chloride permeability preserved in leptospirosis-infected animals. However, in the inner medullary collecting ducts of infected animals, diffusional water permeability did not increase in the presence of vasopressin, indicating vasopressin resistance, a finding in agreement with the high frequency of polyuria in AKI in leptospirosis.

Recently, an outer membrane leptospiral 21-kDa protein (Lsa21) was isolated [3] exhibiting extracellular matrix-binding properties. Immunohistochemical data showed that Lsa21 is present on the apical side of cells of the human distal nephron, particularly in medullary collecting tubules from the autopsies in the present study.

The thick ascending limb of the loop of Henle is involved in Na^+, K^+, and Cl^- migration from the tubular fluid, which is responsible for the establishment of the hypertonic interstitium of the renal medulla. When NKCC2 is inhibited, a large increase in urinary flow of urine that is virtually isosmotic with plasma is observed [14]. A rise in the sodium offer, as observed in leptospirosis, would be expected to prevent subsequent local release of chloride and potassium.

Reports exist regarding NKCC2 mRNA expression inhibition in leptospirosis and evidence both in humans [17, 18] and experimental models [8] of dysfunction in the thick ascending limb of the loop of Henle. The function of this segment is also altered by ischemia and severe jaundice. However, in an animal model of leptospirosis with less severe acute kidney injury, Andrade et al. observed an increase in NKCC2 expression [1]. Moreover, Khositseth et al. [19] reported for the first time magnesium wasting in a large number of leptospirotic patients, a finding principally ascribed by the authors to dysfunction of the thick ascending limb of the loop of Henle. It is also possible, however, that magnesium wasting is related to the injury of proximal convoluted tubules present in leptospirosis.

Except for sparse immunohistochemical altered expression detected in isolated segments, the present data support the findings reported in experimental studies [1, 6] of an essentially preserved thick ascending loop of Henle, which probably acts as a regulatory mechanism for the increased offer of Na^+ and impaired reabsorption of potassium in the filtrate. No altered immunohistochemical expression of NKCC2 was observed in ATN. It is noteworthy that the expression of the α-Na^+K^+ATpase was also essentially preserved in the thick ascending limb of the loop of Henle and was compromised only in groups of proximal convoluted tubules, where, as detected in the cases studied, its expression is not marked. α-Na^+K^+ATpase expression was preserved in ATN. Taken as a whole, the current data suggest active participation of the thick ascending limb of the loop of Henle in the maintenance of renal function and injury recovery in human leptospirosis.

The expression of aquaporin 2 in the apical region of principal cells of collecting tubules confirms that these are the main target for regulation of their permeability by

vasopressin [1, 6]. However, immunohistochemical data showed preserved, or even increased, expression of the vasopressin-sensitive water channel aquaporin 2 in collecting tubules and ducts, both in ATN and AKI in leptospirosis. Moreover, recently, urine semiquantitative densitometric analysis reviewed that, in comparison with health controls, recovering leptospirosis patients presented higher urinary expression of AQP2 and NKCC2 [20]. Both findings could be interpreted as a compensatory response to increase reabsorption of the excess water delivered to the distal nephron.

Apparently, antigenic deposits of Lsa21 protein in collecting ducts do not interfere in aquaporin 2 immunohistochemical expression. The preserved aquaporin 2 in the distal nephron does not support the vasopressin resistance reported in experimental studies [1, 7]; thus, experimental and human autopsy results cannot be compared directly.

In normal biopsied kidney donated for transplantation, the occasional cortical collecting ducts assessed exhibited marked aquaporin 2 expression due probably to maneuvers preceding and during the surgical procedure which might lead to an ischemia of short duration.

Briefly, when leptospirotic AKI and ATN are compared, the data show that the immunohistochemical expression of the different electrolyte and water pathways studied had points in common, except for the fact that in ATN, the findings were focal than those detected in leptospirosis, suggesting accentuated and extensive aggression in the latter. Some differences, however, can be highlighted between ATN and leptospirotic AKI. In leptospirosis, experimental data shows a primary injury that mainly affects the proximal convoluted tubules, and this contributes to more intense tubular damage in this disease compared to ATN. The reported pathophysiological dysfunction of the thick ascending limb [17], which was not entirely supported by the immunohistochemical data, together with leptospiral antigen deposits in collecting tubules [3], are findings not observed in ATN.

Currently, autopsy findings of the kidney in human leptospirosis might be regarded, at least in some cases, as the result of an association of leptospirotic AKI and ATN. This might explain the more accentuated and diffuse findings observed in leptospirosis, with points in common when the two entities are compared. In this respect, clinical [21, 22] and experimental reports [23] are more elucidative concerning the segments of the nephron initially injured.

It seems that in leptospirosis, pathogenetic factors, such as more intense and persistent hypovolemia caused principally by the accentuated and diffuse infectious vascular injury, presence of the agent and/or its antigens, possible toxins and interstitial nephritis, are essential determinants to understanding the degree of injury detected and the patterns seen both in leptospirotic and non-leptospirotic acute tubular injury [12].

Acknowledgements Work supported by grants from LIM 06 and 12 (S. Paulo Medical School, University of S. Paulo and "Hospital das Clinicas," S. Paulo Brazil).

Dr. Mark Knepper and Dr. Carolyn Ecelbarger from the NHI (USA) kindly donated to us the anti-NHE3 and α-Na^+K^+Atpase antibodies used in this work.

Conflict of interest statement We declare that we have no conflict of interest.

References

1. Andrade L, Rodrigues AC Jr, Sanches TRC et al (2007) Leptospirosis leads to dysregulation of sodium transporters in the kidney and lung. Am J Physiol Renal Physiol 292:F586–F592
2. Faine S, Adler B, Bolin C et al (1999) Leptospira and leptospirosis, 2nd edn. MediSci, Melbourne
3. Atzingen MV, Barbosa AS, De Brito T et al (2008) Lsa21, a novel leptospiral protein binding adhesive matrix molecules and present during human infection. BMC Microbiol 8:70. doi:10.1186/1471-2180-8-70
4. Haake DA, Chao G, Zuerner RL, Barnett JK et al (2000) The leptospiral outer membrane protein LipL32 is a lipoprotein expressed during mammalian infection. Infect Immunol 68:2276–2285
5. De Brito T, Menezes LF, Lima DMC et al (2006) Immunohistochemical and in situ hybridization studies of the liver and kidney in human leptospirosis. Virchows Arch 448:576–583
6. Andrade L, Daher EF, Seguro AC (2008) Leptospiral nephropathy. Semin Nephrol 28:383–394
7. Magaldi AJ, Yasuda PH, Kudo LH et al (1992) Renal involvement in leptospirosis: a pathophysiologic study. Nephron 62:332–339
8. Spichler A, Ko AI, Fagonde Silva E et al (2007) Reversal of renal tubule transporter downregulation during severe leptospirosis with antimicrobial therapy. Am J Trop Med Hyg 77:1111–1119
9. Olesen ET, de Seigneux S, Wang G et al (2009) Rapid and segmental specific dysregulation of AQP2, S256-pAQP2 and renal sodium transporters in rats with LPS-induced endotoxaemia. Nephrol Dial Transplant 24(8):2338–2349
10. Agre P, Bonhivers M, Borgnia MJ (1998) Minireview—the aquaporins, blueprints for cellular plumbing systems. J Biol Chem 273(24):14659–14662
11. Maunsbach AB, Marples D, Chin E et al (1997) Aquaporin 1 water channel expression in human kidney. J Am Soc Nephrol 8:1–14
12. Abdulkader RCRM, Silva MV (2008) The kidney in leptospirosis. Pediatr Nephrol 23:2111–2120. doi:10.1007/s00467-008-0811 -4
13. Davila de Arriaga AJ, Rocha AS, Yasuda PH et al (1982) Morpho-functional patterns of kidney injury in the experimental leptospirosis of the guinea-pig(*l.icterohaemorrhagiae*). J Pathol 138:145–161
14. Russell JM (2000) Sodium-Potassium-Chloride cotransport. Physiol Rev 80:211–276
15. Nielsen S, Frokler J, Marples D et al (2002) Aquaporins in the kidneys: from molecules to medicine. Physiol Rev 82:205–244
16. Bedford JJ, Leader JP, Walker RJ (2003) Aquaporin expression in normal human kidney and in renal disease. J Am Soc Nephrol 14:2581–2587
17. Lin Chun-Liang, Wu Mai-Szu, Yang Chih-Wei et al (1999) Leptospirosis associated with hypokalemia and thick ascending limb dysfunction. Nephrol Dial Transplant 14:193–195
18. Wu MS, Yang CW, Pan MJ et al (2004) Reduced renal NA+-K+-Cl^- co-transporter activity and inhibited NKCC2 mRNA expression by

Leptospira shermani :from bed-side to bench. Nephrol Dial Transplant 19:2472–2479
19. Khositseth S, Sudjaritja N, Tananchai P et al (2008) Renal magnesium wasting and tubular dysfunction in leptospirosis. Nephrol Dial Transplant 23:952–958
20. Sanches TR, Santos PM, Seguro AC et al (2009) NKCC2 and AQP2 protein expression is upregulated in the recovering phase of leptospirosis-induced acute kidney injury (AKI). J Am Soc Nephrol 20:362A
21. Liamis G, Rizos E, Elisaf MS (2000) Reversible proximal tubular disfunction in a patient with acute febrile illness and normal renal function: an evidence towards leptospirosis. Clin Nephrol 53(4):316
22. Liberopoulos E, Bairaktari E, Elisaf M (2002) Reversible proximal tubular disfunction in a patient with acute febrile illness, marked hyperbilirubinemia and normal renal function: evidence of leptospirosis. Nephron 91:532–533
23. Yang C-W, Wu M-S, Pan M-J (2001) Leptospirosis renal disease. Nephrol Dial Transplant 16(suppl 5):73–77

Virchows Arch (2010) 456:377–386
DOI 10.1007/s00428-010-0892-x

ORIGINAL ARTICLE

Distinguishing between primary endocervical and endometrial adenocarcinomas: is a 2-marker (Vim/CEA) panel enough?

Chiung-Ling Liao · Jeng-Dong Hsu · Ming-Yung Lee · Lai-Fong Kok · Yi-Ju Li · Po-Hui Wang · Chung-Chin Yao · Chih-Ping Han

Received: 23 November 2009 / Revised: 20 January 2010 / Accepted: 4 February 2010 / Published online: 11 March 2010
© Springer-Verlag 2010

Abstract Gynecological pathologists are used to operating many panels of various markers in combination for the diagnostic distinction between primary endocervical and endometrial adenocarcinomas. The conventional 3-marker (ER/Vim/CEA) panel is the most promising tool. In this study, our aim is to investigate whether a 2-marker panel is enough to distinguish between these two gynecologic malignancies. Additionally, we wish to determine which one is the most favorable among eight panels tested, including six 2-marker (ER/CEA, PR/CEA, Vim/CEA, ER/p16^{INK4a}, PR/p16^{INK4a}, Vim/p16^{INK4a}) and two 3-marker (ER/Vim/CEA, ER/Vim/p16^{INK}) panels. A tissue microarray was constructed using paraffin-embedded, formalin-fixed tissues from 35 hysterectomy specimens, including 14 primary endocervical adenocarcinomas and 21 primary endometrial adenocarcinomas. Utilizing the avidin-biotin complex (ABC) method, tissue array sections were immunostained with five commercially available antibodies (ER, Vim, CEA, PR, and p16^{INK4a}) to evaluate their individual frequencies of expression. We found that all eight aforementioned panels showed an encouraging range of overall accuracy (69.2% to 78.3%). However, one panel

Chiung-Ling Liao, Jeng-Dong Hsu, and Ming-Yung Lee have equally contributed to this article.

C.-L. Liao · P.-H. Wang · C.-P. Han (✉)
Department of Obstetrics and Gynecology,
Chung-Shan Medical University Hospital,
Taichung, Taiwan, Republic of China
e-mail: hanhaly@gmail.com

C.-L. Liao · C.-P. Han
Institute of Medicine, Chung-Shan Medical University,
Taichung, Taiwan, Republic of China

J.-D. Hsu
Department of Pathology,
Chung Shan Medical University Hospital,
Taichung, Taiwan, Republic of China

J.-D. Hsu · Y.-J. Li
Department of Pathology, School of Medicine,
Chung Shan Medical University,
Taichung, Taiwan, Republic of China

M.-Y. Lee
Department of Statistics and Informatics Science,
Providence University,
Taichung, Taiwan, Republic of China

L.-F. Kok
Department of Pathology, China Medical University Hospital,
Taichung, Taiwan, Republic of China

P.-H. Wang
Department of Obstetrics and Gynecology, School of Medicine,
Chung-Shan Medical University,
Taichung, Taiwan, Republic of China

C.-C. Yao (✉)
Department of Surgery, Chung-Shan Medical University Hospital,
Taichung, Taiwan, Republic of China
e-mail: hanhaly@gmail.com

C.-C. Yao
Department of Surgery, School of Medicine,
Chung-Shan Medical University Hospital,
Taichung, Taiwan, Republic of China

C.-P. Han
Clinical Trial Center, Chung-Shan Medical University Hospital,
Taichung, Taiwan, Republic of China

of 2-markers (Vim, CEA) exhibited the most efficiency (78.3%) in the diagnostic distinction between primary endocervical and endometrial adenocarcinomas. Based on the analyzed data, we conclude that the 2-marker (Vim/CEA) panel seems adequate to be an appropriate, convenient, and efficient means to distinguish between primary endocervical and endometrial adenocarcinomas. Even though there were a limited number of cases, this study still provides valuable references to help avoid wasting resources and unnecessary marker testing.

Keywords Endocervical · Endometrial · Adenocarcinomas · Tissue microarray · Immunohistochemistry (IHC) · Estrogen · Progesterone · Vimentin · Carcinoembryonic antigen · $p16^{INK4a}$ (P16)

ECA	Endocervical adenocarcinomas
EMA	Endometrial adenocarcinomas
TMA	Tissue microarray
IHC	Immunohistochemistry
ER	Estrogen receptor
PR	Progesterone receptor
Vim	Vimentin
CEA	Carcinoembryonic antigen
H&E	Hematoxylin and eosin
NPV	Negative predictive value
PPV	Positive predictive value

Introduction

Although careful morphologic examination usually results in a confident diagnosis, the distinction between a primary endocervical adenocarcinoma (ECA) and endometrial adenocarcinoma (EMA) may be difficult in small biopsies or curetted tissue specimens. In some cases, tumors may be present in both endometrial and endocervical sites. Therefore, preoperative imaging does not help to establish the site of origin. Difficulties may also arise in the pathological examination of a large surgically resected specimen for a tumor that involves both the lower uterine segment and upper endocervix. Since the choice of initial therapy may differ substantially, it is important to ascertain the site of origin of the cancer. For EMA, staging is surgical; while for primary ECA, staging is clinical. Treatment plans and adjuvant therapies are different for primary ECA and EMA [1, 2].

No single antibody is totally specific for any one neoplasm. At present, panels with a variety of combinations of ER, PR, Vim, CEA, and $p16^{INK4a}$-marker were commonly used in distinguishing between ECA and EMA. Previously, we compared the performances of 3-marker (ER/Vim/CEA), 4-marker (ER/Vim/CEA/PR), and 5-marker (ER/Vim/CEA/PR/$p16^{INK4a}$) panels and found that the 3-marker (ER/Vim/CEA) panel seems to be the most favorable tool in distinguishing these two gynecologic malignancies. In this study, we wish to evaluate the performances of six 2-marker (Vim/CEA, ER/CEA, PR/CEA, ER/$p16^{INK4a}$, PR/$p16^{INK4a}$, and Vim/$p16^{INK4a}$) and two 3-marker (ER/Vim/CEA and ER/Vim/$p16^{INK}$) panels, in order to determine the most economical and useful panel which can be used as an appropriate comprehensive tool in distinguishing between primary ECA and EMA [3–6].

Materials and methods

The study material consisted of specimens of primary endocervical adenocarcinomas of the endocervical type, (n=14), and primary endometrial adenocarcinomas of the endometroid type (n=21). Their differentiation levels or grades were classified systematically, based on the criteria from Association of Directors of Anatomic and Surgical Pathology, the WHO/ISGP classification, and FIGO histological grading system (Table 1). The characteristics of the commercialized antibodies, TMA slide construction, immu-

Table 1 Samples used in the tissue microarray

Endometrial carcinoma		Endocervical carcinoma	
Type/grade	No. of cases	Type/grade	No. of cases
Endometroid type	21	Endocervical type	14
Grade I	10	Well differentiated	1
Grade II	6	Moderately differentiated	11
Grade III	5	Poorly differentiated	2
Total	21	Total	14

Endometrial adenocarcinomas (endometroid type) were classified by the WHO/ISGP classification and FIGO histological grading system. Endocervical adenocarcinomas (endocervical type) were architecturally graded by the recommendations of the Association of Directors of Anatomic and Surgical Pathology (ADASP) with architectural (the percentage of solid growth, excluding squamous) and cytologic (nuclear) criteria

nohistochemical (IHC) stainings, and their scoring mechanisms have been described in our previous report [3–6]. Briefly, formalin-fixed and paraffin-embedded tissue array specimens with 1.5-mm, 5 μm individual cores, were deparaffinized in xylene, rehydrated through serial dilutions of alcohol, and washed in PBS (pH 7.2), the buffer which was used for all subsequent washes. Slides were stained with five monoclonal antibodies (ER, Vim, CEA, PR, $p16^{INK4a}$). The TMA slides were simultaneously reviewed and scored by the two aforementioned board-certified pathologists (CP Han and LF Kok), using a two-headed microscope.

Since IHC scoring algorithms have not been optimized and standardized, a variety of scoring systems such as H-score, the Quick score, and the Allred score have been employed. Several methods are known [e.g., immunoreactive score, H-score, the Quick score, and the Allred score] for reporting various marker results. In this report, the marker expressions were interpreted using the German semi-quantitative scoring system as usual in considering the intensity and extent of staining. The final IHC scores were determined by multiplying the positive intensity (score: 0–3) and the positive area of extent (score: 0–4), yielding a range from 0 to 12. The threshold for differentiating between final positive and negative immunostaining was set at 4 for interpretation. This optimal cut-off value for this study was determined by using the receiver operating characteristic (ROC) curve analysis and Youden index [7, 8]. This method of assessment has been widely accepted and used in previous studies [3–6, 9–13]. To distinguish between primary ECA and EMA, the sensitivity and specificity of EC-type and EM-type immunoprofiles were compared. Sensitivity was defined as the ratio of accurate expression of a typical EC-type or EM-type immunoprofile among the primary endocervical or endometrial adenocarcinoma in origin. Specificity was defined as the number of tissues that lack typical EC-type or EM-type immunoprofile expressions over the number of tissues that were actually not the primary endocervical or endometrial adenocarcinoma originally. Overall accuracy of a test is the measure of "true" findings (i.e., true positive plus true negative results) divided by all test results. It combines the sensitivity and specificity into a single measure of the percentage of cases (positive and negative) for which the assay result agrees with the true status [3–6, 13]. Analyses were performed using SPSS statistical software (SPSS, Inc., Chicago, IL, USA). All tests were 2-sided and a p value <0.05 was considered statistically significant.

Results

In ECA, a typical EC-type immunoprofile exhibited (1) Vim-/CEA+, ER-/CEA+, PR-/CEA+, ER-/$p16^{INK4a}$+, PR-/$p16^{INK4a}$ + and Vim-/$p16^{INK4a}$+ in the 2-marker panels and (2) ER-/Vim-/CEA+ and ER-/Vim-/$p16^{INK}$+ in the 3-marker panels. In EMA, a typical EM-type immunoprofile exhibited (1) Vim+/CEA-, ER+/CEA-, PR+/CEA-, ER+/$p16^{INK4a}$-, PR+/$p16^{INK4a}$-, and Vim+/$p16^{INK4a}$- in the 2-marker panels and (2) ER+/Vim+/CEA- and ER+/Vim+/$p16^{INK}$- in the 3-marker panels. However, a non-typical immunoprofile is defined as marker expressions other than typical EC-type and typical EM-type expression patterns [3–6, 13–20].

Table 2 shows the panel expression patterns in primary ECA. Of the 14 ECA cases, there were (1) nine cases with a typical EC-type immunoprofile and five cases with several non-typical type immunoprofiles in the ER/CEA panel, (2) nine cases with a typical EC-type immunoprofile and five cases with several non-typical type immunoprofiles in the ER/$p16^{INK4a}$ panel, (3) nine cases with a typical EC-type immunoprofile and five cases with several non-typical type immunoprofiles in the Vim/CEA panel, (4) ten cases with a typical EC-type immunoprofile and four cases with several non-typical type immunoprofiles in the Vim/$p16^{INK4a}$ panel, (5) nine cases with a typical EC-type immunoprofile and five cases with several non-typical type immunoprofiles in the PR/CEA panel, (6) eight cases with a typical EC-type immunoprofile and six cases with several non-typical type immunoprofiles in the PR/$p16^{INK4a}$ panel, (7) eight cases with a typical EC-type immunoprofile and six cases with several non-typical type immunoprofiles in the ER/Vim/CEA panel, and (8) eight cases with a typical EC-type immunoprofile and six cases with several non-typical type immunoprofiles in the ER/Vim/$p16^{INK4a}$ panel.

Table 3 shows the panel expression patterns in primary EMA. Of the 21 EMA cases, there were (1) 12 cases with a typical EM-type immunoprofile and nine cases with several non-typical type immunoprofiles in the ER/CEA panel, (2) nine cases with a typical EM-type immunoprofile and 12 cases with several non-typical type immunoprofiles in the ER/$p16^{INK4a}$ panel, (3) 13 cases with a typical EM-type immunoprofile and eight cases with several non-typical type immunoprofiles in the Vim/CEA panel, (4) nine cases with a typical EM-type immunoprofile and 12 cases with several non-typical type immunoprofiles in the Vim/$p16^{INK4a}$ panel, (5) ten cases with a typical EM-type immunoprofile and 11 cases with several non-typical type immunoprofiles in the PR/CEA panel, (6) seven cases with a typical EM-type immunoprofile and 14 cases with several non-typical type immunoprofiles in the PR/$p16^{INK4a}$ panel, (7) ten cases with a typical EM-type immunoprofile and 11 cases with several non-typical type immunoprofiles in the ER/Vim/CEA panel, and (8) seven cases with a typical EM-type immunoprofile and 14 cases with several non-typical type immunoprofiles in the ER/Vim/$p16^{INK4a}$ panel.

Table 4 displayed the typical and non-typical immunoprofile performances of six 2-marker and two 3-marker panels in diagnostic distinction between 14 ECA and 21

Table 2 Panel performance for the diagnosis of ECA (sample size 14)

ER>3	Vim>3	PR>3	CEA>3	$p16^{INK4a}$>3	Number	With this panel (%)
Two-marker panel						
ER, CEA-marker panel						
−			−		3	21.43%
−			+		***9***	***64.29%***
+			−		1	7.14%
+			+		1	7.14%
ER, $p16^{INK4a}$-marker panel						
−				−	3	21.43%
−				+	***9***	***64.29%***
+				−	0	0.00%
+				+	2	14.29%
VIM, CEA-marker panel						
	−		−		4	28.57%
	−		+		***9***	***64.29%***
	+		−		0	0.00%
	+		+		1	7.14%
VIM, $p16^{INK4a}$-marker panel						
	−			−	3	21.43%
	−			+	***10***	***71.43%***
	+			−	0	0.00%
	+			+	1	7.14%
PR, CEA-marker panel						
		−	−		2	14.29%
		−	+		***9***	***64.29%***
		+	−		2	14.29%
		+	+		1	7.14%
PR, $p16^{INK4a}$-marker panel						
		−		−	3	21.43%
		−		+	***8***	***57.14%***
		+		−	0	0.00%
		+		+	3	21.43%
Three-marker panel						
ER, Vim, CEA-marker panel						
−	−		−		3	21.42%
−	−		+		***8***	***57.14%***
−	+		+		1	7.14%
+	−		+		1	7.14%
+	−		−		1	7.14%
ER, Vim, $p16^{INK4a}$-marker panel						
−	−			−	3	21.43%
−	−			+	***8***	***57.14%***
−	+			+	1	7.14%
+	−			+	2	14.29%

The row in italic bolds is defined as typical EC-type immunoprofile. Other rows are defined as non-typical immunoprofile

− score negative, + score positive

EMA. (1) Of the 2-marker panel (ER/CEA), the typical EC-type immunoprofile (ER-/CEA+) was present in nine out of 14 (64.3%) of the ECA tumors, as well as in one out of 21 (4.76%) of the EMA tumors ($p<0.001$). The typical EM-type immunoprofile (ER+/CEA-) was present in one out of 14 (7.4%) of the ECA tumors, but was present in 12 out of 21 (57.1%) of the EMA tumors ($p=0.004$). The non-typical type immunoprofile panel was present in four out of 14 (28.2%) of the ECA tumors, as well as in eight out of 21 (48.1%) of the EMA tumors. (2) Of the 2-marker panel

Table 3 Panel performance for the diagnosis of EMA (sample size 21)

ER> 3	Vim> 3	PR> 3	CEA> 3	$p16^{INK4a}$> 3	Number	With this panel (%)
Two-marker panel						
ER, CEA-marker panel						
−			−		5	23.81%
−			+		1	4.76%
+			−		***12***	***57.14%***
+			+		3	14.29%
ER, $p16^{INK4a}$-marker panel						
−				−	5	23.81%
−				+	1	4.76%
+				−	***9***	***42.86%***
+				+	6	28.57%
VIM, CEA-marker panel						
	−		−		4	19.05%
	−		+		2	9.52%
	+		−		***13***	***61.90%***
	+		+		2	9.52%
VIM, $p16^{INK4a}$-marker panel						
	−			−	5	23.81%
	−			+	1	4.76%
	+			−	***9***	***42.86%***
	+			+	6	28.57%
PR, CEA-marker panel						
		−	−		7	33.33%
		−	+		1	4.76%
		+	−		***10***	***47.62%***
		+	+		3	14.29%
PR, $p16^{INK4a}$-marker panel						
		−		−	7	33.33%
		−		+	1	4.76%
		+		−	***7***	***33.33%***
		+		+	6	28.57%
3-marker panel						
ER/Vim/CEA						
−	−		−		2	9.52%
−	−		+		1	4.76%
−	+		−		3	14.85%
+	−		−		2	9.52%
+	−		+		1	4.76%
+	+		−		***10***	***47.62%***
+	+		+		2	9.52%
ER/Vim/$p16^{INK4a}$						
−	−			−	3	14.29%
−	+			−	2	9.52%
−	+			+	1	4.76%
+	−			−	3	14.29%
+	+			−	***7***	***33.33%***
+	+			+	5	23.81%

The row in italic bolds is defined as typical EM-type immunoprofile. Other rows are defined as non-typical immunoprofile

− score negative, + score positive

Table 4 The typical and non-typical immunoprofile performances of six 2-marker and two 3-marker panels in diagnostic distinction between ECA and EMA

Panel	Immunoprofile	ECA	EMA	*p* value
ER/CEA	Typical EC-type	9/14 (64.3%)	1/21 (4.8%)	<0.001
	Typical EM-type	1/14 (7.1%)	12/21 (57.1%)	0.004
	Non-typical	4/14 (28.6%)	8/21 (48.1%)	
ER/$p16^{INK4}$	Typical EC-type	9/14 (64.3%)	1/21 (4.8%)	<0.001
	Typical EM-type	0/14 (0%)	9/21 (42.9%)	0.005
	Non-typical	5/14 (35.7%)	11/21 (52.3%)	
VIM/CEA	Typical EC-type	9/14 (64.3%)	2/21 (9.5%)	0.001
	Typical EM-type	0/14 (0%)	13/21 (61.9%)	<0.001
	Non-typical	5/14 (35.7%)	6/21 (28.6%)	
VIM/$p16^{INK4}$	Typical EC-type	10/14 (71.4%)	1/21 (4.8%)	<0.001
	Typical EM-type	0/14 (0%)	9/21 (42.9%)	0.005
	Non-typical	4/14 (28.6%)	11/21 (52.3%)	
PR/CEA	Typical EC-type	9/14 (64.3%)	1/21 (4.8%)	<0.001
	Typical EM-type	2/14 (14.3%)	10/21 (47.6%)	0.07
	Non-typical	3/14 (21.4%)	10/21 (47.6%)	
PR/$p16^{INK4}$	Typical EC-type	8/14 (57.1%)	1/21 (4.8%)	0.001
	Typical EM-type	0/14 (0%)	7/21 (33.3%)	0.027
	Non-typical	6/14 (42.9%)	13/21 (61.9%)	
ER/Vim/CEA	Typical EC-type	8/14 (57.1%)	1/21 (4.8%)	0.001
	Typical EM-type	0/14 (0%)	10/21 (47.6%)	0.002
	Non-typical	6/14 (42.9%)	10/21 (47.6%)	
ER/Vim/$p16^{INK4a}$	Typical EC-type	8/14 (57.1%)	0/21 (0.0%)	<.001
	Typical EM-type	0/14 (0.0%)	7/21 (33.3%)	0.027
	Non-typical	6/14 (42.9%)	14/21 (66.7%)	

A typical EC-type immunoprofile reveals (1) Vim-/CEA+, ER-/CEA+, PR-/CEA+, ER-/$p16^{INK4}$+, PR-/$p16^{INK4}$+, and Vim-/$p16^{INK4}$+ in the 2-marker panels; as well as (2) ER-/Vim-/CEA + and ER-/Vim-/$p16^{INK}$ + in the 3-marker panels. A typical EM-type immunoprofile reveals (1) Vim+/CEA-, ER+/CEA-, PR+/CEA-, ER+/$p16^{INK4}$-, PR+/$p16^{INK4}$- and Vim+/$p16^{INK4}$- in the 2-marker panels; as well as (2) ER+/Vim+/CEA- and ER+/Vim+/$p16^{INK}$- in the 3-marker panels. A non-typical immunoprofile is defined as marker expressions other than typical EC-type and typical EM-type expression patterns

($ER/p16^{INK4a}$), the typical EC-type immunoprofile (ER-/$p16^{INK4a}$+) was present in nine out of 14 (64.3%) of the ECA tumors, as well as in one out of 21 (4.76%) of the EMA tumors ($p<0.001$). The typical EM-type immunoprofile (ER+/$p16^{INK4a}$-) was present in zero out of 14 (0%) of the ECA tumors, but was present in nine out of 21 (42.9%) of the EMA tumors ($p=0.005$). The non-typical type immunoprofile panel was present in five out of 14 (35.7%) of the ECA tumors, as well as in 11 out of 21 (52.3%) of the EMA tumors. (3) Of the 2-marker panel (Vim/CEA), the typical EC-type immunoprofile (Vim-/CEA+) was present in nine out of 14 (64.3%) of the ECA tumors, as well as in two out of 21 (9.5%) of the EMA tumors ($p=0.001$). The typical EM-type immunoprofile (Vim+/CEA-) was present in zero out of 14 (0%) of the ECA tumors, but was present in 13 out of 21 (61.9%) of the EMA tumors ($p<0.001$). The non-typical type immunoprofile panel was present in five out of 14 (35.7%) of the ECA tumors, as well as in six out of 21 (28.6%) of the EMA tumors. (4) Of the 2-marker panel ($Vim/p16^{INK4a}$), the typical EC-type immunoprofile (Vim-/$p16^{INK4a}$+) was present in ten out of 14 (71.4%) of the ECA tumors, as well as in one out of 21 (4.8%) of the EMA tumors ($p<0.001$). The typical EM-type immunoprofile (Vim+/$p16^{INK4a}$-) was present in zero out of 14 (0%) of the ECA tumors, but was present in nine out of 21 (42.9%) of the EMA tumors ($p=0.005$). The non-typical type immunoprofile panel was present in four out of 14 (28.6%) of the ECA tumors, as well as in 11 out of 21 (52.3%) of the EMA tumors. (5) Of the 2-marker panel (PR/CEA), the typical EC-type immunoprofile (PR-/CEA+) was present in nine out of 14 (64.3%) of the ECA tumors, as well as in one out of 21 (4.8%) of the EMA tumors ($p<0.001$). The typical EM-type immunoprofile (PR+/CEA-) was present in two out of 14 (14.3%) of the ECA tumors, but was present in ten out of 21 (47.6%) of the EMA tumors ($p=0.07$). The non-typical type immunoprofile panel was present in three out of 14 (21.4%) of the ECA tumors, as well as in ten out of 21 (47.6%) of the EMA tumors. (6) Of the 2-marker panel ($PR/p16^{INK4a}$), the typical EC-type immunoprofile (PR-/$p16^{INK4a}$+) was present in eight out of 14 (57.1%) of the ECA tumors, as well as in one out of 21 (4.8%) of the EMA tumors ($p=0.001$). The typical EM-type immunoprofile (PR+/$p16^{INK4a}$-) was present in zero out of 14 (0%) of the ECA tumors, but was present in four out of 21 (33.3%) of the EMA tumors ($p=0.027$). The non-typical type immunoprofile panel was present in six out of 14 (42.9%) of the ECA tumors, as well as in 16 out of 21 (61.9%) of the EMA tumors. (7) Of the 3-marker panel (ER/Vim/CEA), the typical EC-type immunoprofile (ER-/Vim-/CEA+) was pres-

ent in eight out of 14 (57.1%) of the ECA tumors, as well as in one out of 21 (4.8%) of the EMA tumors (p=0.001). The typical EM-type immunoprofile (ER+/Vim+/CEA-) was present in none out of 14 (0%) of the ECA tumors, but was present in ten out of 21 (47.6%) of the EMA tumors (p=0.002). The non-typical type immunoprofile panel was present in six out of 14 (42.9%) of the ECA tumors, as well as in ten out of 21 (47.6%) of the EMA tumors. (8) Of the 3-marker (ER/Vim/p16^{INK4a}) panel containing p16^{INK4a}, the typical EC-type immunoprofile (ER-/Vim-/p16^{INK4a}+) was present in eight out of 14 (57.1%) ECA tumors, as well as zero out of 21 (0.0%) EMA tumors (p<0.001). The typical EM-type immunoprofile (ER+/Vim+/p16^{INK4a}-) was present in 0 out of 14 (0%) ECA tumors, as well as in 7 out of 21 (33.3%) EMA tumors (p=0.027). The non-typical type immunoprofile panel was present in six out of 14 (42.9%) ECA tumors, as well as in 14 out of 21 (66.7%) EMA tumors.

Table 5 displayed the comparisons of the test effectiveness and performance of typical EC-type or typical EM-type immunoprofiles of the six 2-marker panels (Vim/CEA, ER/CEA, PR/CEA, ER/p16^{INK4a}, PR/p16^{INK4a}, and Vim/p16^{INK4a}) and two 3-marker panels (ER/Vim/CEA and ER/Vim/p16^{INK}) in diagnostic distinctions between primary ECA and EMA. The results showed that all eight panels revealed an encouraging range of overall accuracy from 69.2% to 78.3%. The 2-markers (Vim, CEA) panel exhibited the most efficiency (78.3%) in the diagnostic distinction between primary endocervical and endometrial adenocarcinomas.

Discussion

Distinguishing between primary ECA and EMA before planning a patient's treatment is clinically important. Although careful morphologic examination usually allows for a practical distinction between a primary ECA and EMA, the histopathologic differentiations may be difficult in small biopsy or curetting specimens using H&E stain alone. Difficulties may also occur in the examination of a large surgically resected specimen when the tumor involves both the lower uterine segment and upper endocervix. When there is doubt and indistinguishable primaries, immunohistochemistry may assist. Although we have investigated that each one of the five immunomarkers (ER, Vim, CEA, PR, and p16^{INK4a}) can significantly distinguish ECA tumors from EMA tumors [3–6], no study has identified a single marker and/or a single panel of markers that clearly and consistently makes this distinction in all cases. We have reported that ER/Vim/CEA panel offers a good performance. Extra PR-marker and/or p16^{INK4a}-marker adds no supplemental benefit to the 3-marker panel (ER/Vim/CEA) in the diagnostic distinction between these two gynecologic malignancies (ECA vs. EMA) [3–6]. At this point, we wish to determine whether a 2-marker panel is enough to provide the convenient, efficient and cost-effective means in confidently distinguishing preoperatively between a primary ECA and EMA. In this report, we not only investigate the performance and test effectiveness of the eight panels tested, including ER/CEA, PR/CEA, Vim/CEA, ER/p16^{INK4a}, PR/p16^{INK4a}, Vim/p16^{INK4a}, ER/Vim/CEA, and ER/Vim/p16^{INK4a}; but also scientifically determine the most appropriate panel in distinguishing between these two gynecologic malignancies (ECA vs. EMA). Our data will help in the referral and management of ECA and EMA cases worldwide.

Of the six 2-markers panels (ER/CEA, PR/CEA, Vim/CEA, ER/p16^{INK4a}, PR/p16^{INK4a}, and Vim/p16^{INK4a}), ECA tends to be of the typical EC-type (ER-/CEA+, PR-/CEA+, Vim-/CEA+, ER-/p16^{INK4a}+, PR-/p16^{INK4a}+, and Vim-/p16^{INK4a}+) immunoprofiles; as well as EMA tends to be of the typical EM-type (ER+/CEA-, PR+/CEA-, Vim+/CEA-, ER+/p16^{INK4a}-, PR+/p16^{INK4a}-, and Vim+/p16^{INK4a}-) immunoprofiles. Additionally, of the two 3-marker panels (ER/Vim/CEA and ER/Vim/p16^{INK}), ECA tends to be of the typical EC-type (ER-/Vim-/CEA+ and ER-/Vim-/p16^{INK}+) immunoprofiles; as well as EMA tends to be of the typical EM-type (ER+/Vim+/CEA- and ER+/Vim+/p16^{INK}-) immunoprofiles [3–6, 14–24]. In this analysis, all eight panels showed statistically significant differences (p<0.05) in typical immunoprofile expression frequencies between ECA and EMA (Table 4). However, immunohistochemical overlaps may exist, and unexpected "aberrant" expressions can occur. There have been many non-typical EC-type and EM-type panel expressions, which makes this diagnostic dilemma unresolved as of yet.

Regarding the typical EC-type or EM-type immunoprofile expression in its respective 2- or 3-marker panel, Table 5 shows that (1) the sensitivity and negative predictive value (NPV) were 64.3% and 80.0% in 14 of the ECA tumors, as well as 57.1% and 59.1% in 21 of the EMA tumors in the ER/CEA panel; (2) the sensitivity and NPV were 64.3% and 80.0% in 14 of the ECA tumors, as well as 42.9% and 53.8% in 21 of the EMA tumors in the ER/p16^{INK4a} panel; (3) the sensitivity and NPV were 64.3% and 79.2% in 14 of the ECA tumors, as well as 61.9% and 63.6% in 21 of the EMA tumors in the Vim/CEA panel; (4) the sensitivity and NPV were 71.4% and 83.3% in 14 of the ECA tumors, as well as 42.9% and 53.8% in 21 of the EMA tumors in the Vim/p16^{INK4a} panel; (5) the sensitivity and NPV were 64.3% and 80.0% in 14 of the ECA tumors, as well as 50.0% and 50.0% in 21 of the EMA tumors in the PR/CEA panel; (6) the sensitivity and NPV were 57.1% and 76.9% in 14 of the ECA tumors, as well as 33.3% and 50.0% in 21 of the EMA tumors in the PR/p16^{INK4a} panel; (7) the sensitivity and NPV were 57.1% and 76.9% in 14 of the

Table 5 Comparisons of the test effectiveness and performance among the six 2-marker and two 3-marker panels with typical EC-type or typical EM-type immunoprofiles for diagnostically distinguishing between ECA and EMA

		ER, CEA	ER $p16^{INK4a}$	Vim, CEA	Vim, $p16^{INK4a}$	PR, CEA	PR, $p16^{INK4a}$	ER, Vim, CEA	ER/Vim/$p16^{INK4a}$
Sensitivity (95% CI)	Typical EC-type	0.643	0.643	0.643	0.714	0.643	0.571	0.571	0.571
	(*N*=14)	(0.484, 0.802)	(0.484, 0.802)	(0.484, 0.802)	(0.565, 0.864)	(0.484, 0.802)	(0.407, 0.735)	(0.407, 0.735)	(0.407, 0.735)
	Typical Em-type	0.571	0.429	0.619	0.429	0.500	0.333	0.476	0.333
	(*N*=21)	(0.410, 0733)	(0.267, 0.590)	(0.460, 0.778)	(0.267, 0.590)	(0.337. 0.663)	(0.179, 0.487)	(0.331, 0.642)	(0.177, 0.490)
Specificity (95% CI)	Typical EC-type	0.952	0.952	0.905	0.952	0.952	0.952	0.952	1.000
	(*N*=14)	(0.882, 1.000)	(0.882, 1.000)	(0.808, 1.000)	(0.882, 1.00)	(0.882, 1.023)	(0.882, 1.023)	(0.882, 1.000)	(1.000, 1.000)
	Typical EM-type	0.929	1.000	1.000	1.000	0.500	1.000	1.000	1.000
	(*N*=21)	(0.844, 1.000)	(1.000, 1.000)	(1.000, 1.000)	(1.000, 1.000)	(0.337, 0.663)	(1.000, 1.000)	(1.000, 1.000)	(1.000, 1.000)
Positive predictive value (95% CI)	Typical EC-type	0.900	0.900	0.818	0.909	0.900	0.889	0.889	1.000
	(*N*=14)	(0.801, 0.999)	(0.801, 0.999)	(0.690, 0.946)	(0.814, 1.000)	(0.801, 0.999)	(0.785, 0.993)	(0.785, 0.993)	(1.000, 1.000)
	Typical EM-type	0.923	1.000	1.000	1.000	0.500	1.000	1.000	1.000
	(*N*=21)	(0.836, 1.000)	(1.000, 1.000)	(1.000, 1.000)	(1.000, 1.000)	(0.337, 0.663)	(1.000, 1.000)	(1.000, 1.000)	(1.000, 1.000)
Negative predictive value (95% CI)	Typical EC-type	0.800	0.800	0.792	0.833	0.800	0.769	0.769	0.778
	(*N*=14)	(0.667, 0.933)	(0.667, 0.933)	(0.657, 0.926)	(0.710, 0.957)	(0.667, 0.933)	(0.630, 0.909)	(0.630, 0.909)	(0.640, 0.916)
	Typical EM-type	0.591	0.538	0.636	0.538	0.500	0.500	0.560	0.500
	(*N*=21)	(0.430, 0752)	(0.376, 0.701)	(0.479, 0.794)	(0.376, 0.701)	(0.337, 0.663)	(0.337, 0.663)	(0.396, 0.724)	(0.334, 0.666)
Accuracy (95% CI)	Typical EC-type	0.829	0.829	0.800	0.857	0.829	0.800	0.800	0.829
	(*N*=14)	(0.704, 0.953)	(0.704, 0.953)	(0.667, 0.933)	(0.741, 0.973)	(0.704, 0.953)	(0.667, 0.933)	(0.667, 0.933)	(0.704, 0.953)
	Typical EM-type	0.714	0.657	0.771	0.657	0.500	0.600	0.686	0.6
	(*N*=21)	(0.567, 0.862)	(0.502, 0.812)	(0.634, 0.909)	(0.502, 0.812)	(0.337, 0.663)	(0.440, 0.760)	(0.532, 0.840)	(0.438, 0.762)
Overall accuracy (95% CI)	*N*=35	0.76	0.726	0.783	0.737	0.631	0.68	0.732	0.692
		(0.620, 0.900)	(0.580, 0.872)	(0.648, 0.917)	(0.593, 0.881)	(0.474, 0.789)	(0.528, 0.832)	(0.587, 0.876)	(0.541, 0.842)

ECA tumors, as well as 47.6% and 56.0% in 21 of the EMA tumors in the ER/Vim/CEA panel; and (8) the sensitivity and NPV were 57.1% and 77.8% in 14 of the ECA tumors, as well as 33.3% and 50.0% in 21 of the EMA tumors in the ER/Vim/p16^{INK4a} panel. Generally, all indicated a high false-negative rate. If the staining results are not in agreement with the typical EC-type or EM-type immunoprofile, despite which one of the 2-marker or 3-marker panels is used, there would be a high probability that the corresponding ECA or EMA tumor diagnosis would be doubtful and inconclusive. The low sensitivity and NPV are the limiting factors for the application of any 2- or 3-marker panel immunoprofiles as an efficient screening tool for ECA and EMA.

On the other hand, (1) the specificity and positive predictive value (PPV) were 95.2% and 90.0% in 14 of the ECA tumors, as well as 92.9% and 92.3% in 21 of the EMA tumors in the ER/CEA panel; (2) the specificity and PPV were 95.2% and 90.0% in 14 of the ECA tumors, as well as 100% and 100% in 21 of the EMA tumors in the ER/p16^{INK4a} panel; (3) the specificity and PPV were 90.5% and 81.8% in 14 of the ECA tumors, as well as 100% and 100% in 21 of the EMA tumors in the Vim/CEA panel; (4) the specificity and PPV were 95.2% and 90.9% in 14 of the ECA tumors, as well as 100% and 100% in 21 of the EMA tumors in the Vim/p16^{INK4a} panel; (5) the specificity and PPV were 95.2% and 90.0% in 14 of the ECA tumors, as well as 50% and 50% in 21 of the EMA tumors in the PR/CEA panel; (6) the specificity and PPV were 95.2% and 88.9% in 14 of the ECA tumors, as well as 100% and 100% in 21 of the EMA tumors in the PR/p16^{INK4a} panel; (7) the specificity and PPV were 95.2% and 88.9% in 14 of the ECA tumors, as well as 100% and 100% in 21 of the EMA tumors in the ER/Vim/CEA panel; and (8) the specificity and PPV were 100% and 100% in 14 of the ECA tumors, as well as 100% and 100% in 21 of the EMA tumors in the ER/Vim/p16^{INK4a} panel. Except for PR/CEA panel in EMA tumors, all the other panels in this report indicated a low false-positive rate. If the staining result matches up with the typical EC-type or EM-type immunoprofile, despite which one of the remaining 2-marker or 3-marker panels is used, there is a high probability that the corresponding ECA or EMA tumor diagnosis will be accurate and conclusive. Accordingly, with the exception of PR/CEA panel, the high specificity and PPV are the promising factors for the application of any of the 2- or 3-marker panel immunoprofiles as a confident confirmatory tool for ECA and EMA.

The accuracy means the degree of veracity. The 2-marker (Vim/p16^{INK4a}) panel deserves the highest accuracy rate of 85.7% of all panels tested when using a typical EC-type immunoprofile to make a definitively exact diagnosis of 14 primary ECAs; while the 2-marker (Vim/CEA) panel deserves the highest accuracy rate of 77.1% of all panels tested when using a typical EM-type immunoprofile to make a definitively exact diagnosis of 21 primary EMAs.

The data in this study showed that the overall accuracies among the eight testing panels (ER/CEA, PR/CEA, Vim/CEA, ER/p16^{INK4a}, PR/p16^{INK4a}, Vim/p16^{INK4a}, ER/Vim/CEA, and ER/Vim/p16^{INK}) had an encouraging range from 69.2% to 78.3%. With the highest overall accuracy (78.3%), the 2-marker panel (Vim/CEA) may act as the most comprehensive and appropriate panel in distinguishing between primary ECA and EMA. Although the number of cases available is limited (N=35), this study still can provide approximately 70% power for detecting a 15% difference. This article is a continuing report on the topic "IHC markers in distinguishing between ECA and EMA" within our research series. Based on the data presented, we are confident that a 2-marker (Vim/CEA) panel would be sufficient in making a diagnostic distinction between primary ECA and EMA.

In addition, if the panel of 2 markers (Vim/CEA) fails to help distinguish between these two tumor types (i.e., equivocal immunoprofile of Vim+/CEA+ or Vim-/CEA-), we suggest that the first choice of additional marker is ER because ER (+) favors the site of endometrial origin [25]. On the other hand, most ECA contain high-risk human papillomavirus (HPV) DNA, whereas EMA rarely do. The p16^{INK4a} marker appears to be a sensitive surrogate for the presence of HPV infection. Hence, p16^{INK4a} staining can be regarded as the second choice because p16^{INK4a} (+) favors the site of endocervical origin [26–28].

In summary, the results of immunohistochemistry should always be interpreted in the context of morphology, and in general, panels of antibodies should be used rather than relying on a single antibody. We have reappraised each of the five most commonly used monoclonal antibodies, ER, Vim, CEA, PR, and p16^{INK4a} as well as their respective eight panels including ER/CEA, PR/CEA, Vim/CEA, ER/p16^{INK4a}, PR/p16^{INK4a}, Vim/p16^{INK4a}, ER/Vim/CEA, and ER/Vim/p16^{INK4a}, in distinguishing between primary ECA and EMA. After assessing the parameters of each panel performance and test effectiveness, such as sensitivity, specificity, NPV, PPV, and the overall accuracy of all 2- and 3-marker panels tested, this study analysis has showed that a panel of 2-markers (Vim/CEA) seems to be the most comprehensive. Although the PR-, ER-, or p16^{INK4a}-marker alone appears to be useful, they do not add any meaningful benefits to the performance of the 2-marker (Vim/CEA) panel. Despite the limited number of cases, the data looks like that Vim/CEA panel would be enough to definitively distinguish between primary ECA and EMA.

Conclusions

Distinguishing between primary ECA and EMA can often be accomplished by routine gross and histological exami-

nations, but some cases uncover tumors with undetermined origins or overlapping histomorphologic features. An accurate diagnosis may require the use of ancillary IHC stains. Although data from this study were obtained from a limited number of cases, our results can still provide valuable references for selecting a convenient and economical panel of markers. Based on this study analysis of the efficiency and overall accuracy of all eight panels tested, we propose that the 2-marker (Vim/CEA) panel seems to be sufficient to provide a simple and fast way for appropriately distinguishing between ECA and EMA.

Acknowledgment This work was supported in parts by grants from Department of Health (DOH99-FDA-43002-H), Chung Shan Medical University (G098N0013) and Chung Shan Medical University Hospital (CSH-2010-C-016), Taiwan, Republic of China. I am extremely grateful to Prof. Ou ST, Ph.D. and Kung MF, Ph.D. for their guidance in statistical analysis as well as her helpful comments.

Conflict of interest statement We declare that we have no conflict of interest.

References

1. Lurain JR, Bidus MA, Elkas JC (2007) Uterine cancer, cervical and vaginal cancer. In: Berek RS (ed) Novak's gynecology, 14th edn. Lippincott Williams & Wilkins (LWW), Philadelphia, pp 1343–1402
2. Schorge JO, Knowles LM, Lea JS (2004) Adenocarcinoma of the cervix. Curr Treat Options in Oncol 5:119–127
3. Han CP, Lee MY, Kok LF, et al (2010) A reappraisal of three-marker (ER/Vim/CEA), four-marker (ER/Vim/CEA/PR), and five-marker (ER/Vim/CEA/PR/p16INK4a) panels in the diagnostic distinction between primary endocervical and endometrial adenocarcinomas in a tissue microarray study. Arch Gynecol Obstet in press, doi:10.1007/s00404-009-1151-8
4. Han CP, Kok LF, Wang PW et al (2010) Scoring $p16^{INK4a}$ immunohistochemistry based on independent nucleic staining alone can sufficiently distinguish between endocervical and endometrial adenocarcinomas in a tissue microarray study. Mod Path 22:797–806
5. Yao CC, Kok LF, Lee MY et al (2009) Ancillary p16(INK4a) adds no meaningful value to the performance of ER/PR/Vim/CEA panel in distinguishing between primary endocervical and endometrial adenocarcinomas in a tissue microarray study. Arch Gynecol Obstet 280(3):405–413
6. Han CP, Lee MY, Kok LF et al (2009) Adding the p16INK4a-marker to the traditional 3-marker (ER/Vim/CEA) panel engenders no supplemental benefit in distinguishing between primary endocervical and endometrial adenocarcinomas in a tissue microarray study. Int J Gynecol Pathol 28(5):489–496
7. Zweig MH, Campbell G (1993) Receiver-operating characteristic (ROC) plots: a fundamental evaluation tool in clinical medicine. Clin Chem 39:561–577
8. Metz CE (1978) Basic principles of ROC analysis. Semin Nucl Med 8:283–298
9. Kamoi S, AlJuboury MI, Akin MR et al (2002) Immunohistochemical staining in the distinction between primary endometrial and endocervical adenocarcinomas: another viewpoint. Int J Gynecol Pathol 21:217–223
10. Khoury T, Tan D, Wang J et al (2006) Inclusion of MUC1 (Ma695) in a panel of immunohistochemical markers is useful for distinguishing between endocervical and endometrial mucinous adenocarcinoma. BMC Clin Pathol 6:1
11. Han CP, Lee MY, Tzeng SL et al (2008) Nuclear receptor interaction protein (NRIP) expression assay using human tissue microarray and immunohistochemistry technology confirming nuclear localization. J Exp Clin Cancer Res 27:25
12. Hanley B (2007) Variance in multiplex suspension array assays: carryover of microspheres between sample wells. J Negat Results Biomed 6:6
13. Bodner G, Schocke MF, Rachbauer F et al (2002) Differentiation of malignant and benign musculoskeletal tumors: combined color and power Doppler US and spectral wave analysis. Radiology 223:410–416
14. Mhawech-Fauceglia P, Herrmann F, Bshara W et al (2008) Intraobserver and interobserver variability in distinguishing between endocervical and endometrial adenocarcinoma on problematic cases of cervical curettings. Int J Gynecol Pathol 27:431–436
15. McCluggage WG, Sumathi VP, McBride HA et al (2002) A panel of immunohistochemical stains, including carcinoembryonic antigen, vimentin, and estrogen receptor, aids the distinction between primary endometrial and endocervical adenocarcinomas. Int J Gynecol Pathol 21:11–15
16. Wehling M (2008) Translational medicine: science or wishful thinking? J Transl Med 6:31
17. Dabbs DJ, Sturtz K, Zaino RJ (1996) Distinguishing endometrial from endocervical adenocarcinoma. Hum Pathol 27:172–177
18. Castrillon DH, Lee KR, Nucci MR (2002) Distinction between endometrial and endocervical adenocarcinoma: an immunohistochemical study. Int J Gynecol Pathol 21:4–10
19. Alkushi A, Irving J, Hsu F et al (2003) Immunoprofile of cervical and endometrial adenocarcinomas using a tissue microarray. Virchows Arch 442:271–277
20. Miller RT (2002) Endocervical *vs.* endometrial adenocarcinoma, *THE FOCUS – Immunohistochemistry* Jan; 1–2
21. Miller RT (2003) Endocervical *vs.* endometrial adenocarcinoma: update on useful immunohistochemical markers, *THE FOCUS – Immunohistochemistry* Apr; 1–2
22. Reid-Nicholson M, Iyengar P, Hummer AJ (2006) Immunophenotypic diversity of endometrial adenocarcinomas: implications for differential diagnosis. Mod Pathol 8:1091–1100
23. McCluggage WG, Jenkins D (2003) p16 immunoreactivity may assist in the distinction between endometrial and endocervical adenocarcinoma. Int J Gynecol Pathol 22:231–235
24. Mittal K, Soslow R, McCluggage WG (2008) Application of immunohistochemistry to Gynecologic Pathology. Arch Pathol Lab Med 132:402–423
25. McCluggage WG (2004) A critical appraisal of the value of immunohistochemistry in diagnosis of uterine neoplasms. Adv Anat Pathol 11:162–171
26. Ansari-Lari MA, Staebler A, Zaino RJ et al (2004) Distinction of endocervical and endometrial adenocarcinomas: immunohistochemical p16 expression correlated with human papillomavirus (HPV) DNA detection. Am J Surg Pathol 28:160–167
27. McCluggage WG (2004) Re: distinction of endocervical and endometrial adenocarcinomas: immunohistochemical p16 expression correlated with human papilloma virus (HPV) DNA detection. Am J Surg Pathol 28:974
28. Han CP, Lee MY, Tyan YS (2009) p16(INK4) and CEA can be mutually exchanged with confidence between both relevant three-marker panels (ER/Vim/CEA and ER/Vim/p16(INK4)) in distinguishing primary endometrial adenocarcinomas from endocervical adenocarcinomas in a tissue microarray study. Virchows Arch 455:353–361

Virchows Arch (2010) 456:395–401
DOI 10.1007/s00428-010-0900-1

ORIGINAL ARTICLE

p63 short isoforms are found in invasive carcinomas only and not in benign breast conditions

Dario de Biase · Luca Morandi · Roberta Degli Esposti · Claudia Ligorio · Annalisa Pession · Maria P. Foschini · Vincenzo Eusebi

Received: 8 October 2009 / Revised: 10 February 2010 / Accepted: 21 February 2010 / Published online: 12 March 2010
© Springer-Verlag 2010

Abstract Two N-terminal isoforms characterize the p63 protein: the transactivating isoform TAp63 and the amino-terminal truncated isoform ΔNp63. Two further N-terminal isoforms lacking exon 4 (d4TAp63 and ΔNp73L) have been reported. Purpose of the study was to investigate the molecular expression of N-terminal p63 isoforms in benign and malignant breast tissues. Eighteen randomly selected cases of invasive breast carcinoma (IBC) of luminal type, two cases of in situ duct carcinoma (DCIS/DIN), and 20 specimens of normal and benign breast tissues were studied. All cases were immunostained for p63. Reverse polymerase chain reaction and nested PCR were performed to evaluate p63 N-terminal expression patterns. These isoforms whenever present were validated by sequencing. All cases of normal breast, benign lesions, and the two cases of DCIS/DIN expressed ΔNp63 and TAp63 isoforms only. The two variants lacking exon 4 (ΔNp73L and d4TAp63) were not found. All invasive carcinomas expressed the ΔNp63 and TAp63 isoforms as well as the two short isoforms lacking exon 4 which were found in 11 (d4TAp63) and four (ΔNp73L) cases. The present cases of luminal-type IBC showed p63 isoforms together with short variants lacking exon 4. These isoforms were not observed in non-neoplastic breast tissue. Presence of p63 in invasive breast carcinomas of luminal type, as seen at molecular level, suggests caution to include p63 as a marker of basal-like carcinomas.

Keywords Breast carcinoma · p63 · Molecular characterization · Alternative isoforms

D. de Biase · L. Morandi · C. Ligorio · M. P. Foschini (✉) · V. Eusebi
Department of Haematology and Oncological Sciences "L. and A. Seragnoli", Section of Anatomic Pathology at Bellaria Hospital, University of Bologna,
Via Altura 3,
40139 Bologna, Italy
e-mail: mariapia.foschini@unibo.it

R. Degli Esposti
Unit of Medical Oncology, Department of Oncology, Bellaria Hospital,
Bologna, Italy

A. Pession
Department of Experimental Pathology, University of Bologna,
Bologna, Italy

Introduction

p63 is a sequence-specific DNA-binding factor, homologue of the tumor suppressor and transcription factor p53, located on chromosome 3q27–29. Both family members, p53 and p63, have several protein domains in common: an N-terminal transactivation (TA) domain, a central DNA-binding domain, and an oligomerization domain. The human p63 gene is composed of 15 exons that can be expressed in three alternatively spliced C-terminal isoforms (α, β, and γ) and transcribed from an alternative promoter located in intron 3. The transactivating isoforms (TAp63) are generated by a promoter upstream of exon 1, while the alternative promoter located in intron 3 leads to the expression of N-terminal truncated isoforms (ΔNp63) [1, 2].

TAp63 isoforms induce cell cycle arrest, play an important role in cell differentiation and also regulate independent sets of genes that are not transcriptional targets of p53 [3]. In contrast, ΔNp63 proteins act as dominant-negative inhibitors of the p53 family [4, 5], leading to the hypothesis that these isoforms may exhibit proto-oncogenic function.

In normal epithelium, balance between these proteins maintains correct cell proliferation and differentiation. Probably an anomalous regulation of the expression of ΔN and TA proteins increases the proliferation rate of epithelia, generating the background for neoplastic transformation; moreover, in transforming cells, the imbalance between TA and ΔN might cause the characteristic aggressive phenotype, inhibiting the cell cycle control by p53. Previous studies have demonstrated that ΔNp63 is the predominant isoform expressed in squamous cell carcinomas of oral cavity [6], and anomalous p63 expression was associated with progression to metastasis and correlated with poor prognosis in urothelial carcinomas [7].

In addition, two new isoforms have been described with the same sequence as TAp63 and ΔNp63 but lacking exon 4: d4TAp63 and ΔNp73L, respectively. ΔNp73L has been found only in squamous cell carcinoma of the oral cavity but not in normal oral mucosa and normal salivary gland tissues [6, 8, 9].

Therefore, it seems that an altered expression of p63 gene has an important role in neoplastic development.

As revealed by immunohistochemistry, p63 is expressed by basal and parabasal cells of non-neoplastic stratified epithelia and by myoepithelial cells and basal cells of non-neoplastic exocrine glands such as the prostate, bronchi, and breast [10–14].

Immunohistochemical detection of p63 in breast is of practical value as it is helpful in the distinction between in situ and invasive carcinomas at light microscopy [12, 13]. Furthermore, p63 is expressed in tumors showing myoepithelial cell differentiation and in some of the so-called basal-like triple negative carcinomas [15].

Unfortunately, the antibodies anti-p63 presently available recognize only ΔNp63 or TAp63 isoforms but not those lacking exon 4.

Furthermore, no data are available on the molecular expression patterns of p63 N-terminal isoforms in normal and neoplastic breast tissues.

The purpose of the present study was to evaluate the molecular expression of p63 N-terminal isoforms in normal and neoplastic breast tissues.

Materials and methods

Selection of cases

Forty randomly selected samples of breast tissue, from 32 patients, were collected.

Criteria for inclusion in the study were the following:

1. Frozen tissue available for molecular study
2. No treatment with any form of adjuvant therapy

Tissues were received fresh. Before proceeding with molecular analyses, a frozen 5-μm section in each case was obtained and stained with hematoxylin and eosin. After morphological evaluation, the remnant of the sample was collected in RNAlater (Qiagen, Hilden, Germany) and then snap-frozen in liquid nitrogen and stored at -80°C.

The rest of lesional tissue was fixed in 10% buffered formalin and processed as routine for diagnosis.

Eighteen cases of invasive breast carcinoma (IBC) and two of duct in situ carcinoma (DIN/DCIS) led to obtain 20 frozen specimens. There were also 12 cases of non-neoplastic breast tissues that led to an equal number of specimens. Finally, from tissues of quadrantectomies not involved by the related tumor, eight specimens of benign tissue were taken. Therefore, in carcinomas, each case corresponded to a specimen. In non-neoplastic tissue, the number of specimens was higher than the number of cases.

Criteria for histological diagnoses were those of WHO [16]. Grading for invasive carcinomas was that of Elston and Ellis [17]. Pleomorphic variant of invasive lobular carcinomas was defined according to the criteria described by Eusebi et al. [18]. Rakha et al.'s criteria [19] were employed to subdivide the luminal and basaloid phenotypes.

Immunohistochemistry

Immunohistochemistry was performed on 5-μm-thick sections cut from selected paraffin blocks. All specimens were stained with monoclonal 4A4 antibody (Labvision/NeoMarkers, Fremont CA, USA, 1:200), that recognizes all p63 isoforms. Additional antibodies reported in Table 1 were employed only in cases of IBC. An automatic immunostainer (Ventana-Benchmark, Tucson, AZ, USA) was used. Semiquantitative evaluation was performed

Table 1 Antibodies employed for immunohistochemistry

Antibody	Dilution	Source	Antigen retrieval/detection system
Ki67	1:200	Dako[a]	CC1[b,d]
Estrogen	Prediluted	Ventana-Benchmark[b]	CC1[b,d]
Progesterone	Prediluted	Ventana-Benchmark[b]	CC1[b,d]
c-erb-B2	1:50	Labvision/NeoMarkers[c]	CC1[b,e]
CK14	1:400	Labvision/NeoMarkers[c]	CC1[b,e]

[a] Dako, Denmark

[b] Ventana-Benchmark, Tucson, AZ, USA

[c] Labvision/NeoMarkers, Fremont CA, USA

[d] Detected by "Universal alkaline phosphatase red detection system" (Ventana-Benchmark)

[e] Detected by "Ultraview universal DAB detection system" (Ventana-Benchmark)

Table 2 Primers used for PCR and nested PCR analysis

Name and exon	Sequence (5′-3′)
ΔNp63ex3′ (sense)	ACCTggAAAACAATgCCCAgAC
ΔNp63ex7out (antisense)	TTCATCCCTCCAACACAACTgC
TAp63ex2 (sense)	ACCCCAgCTCATTTCTCTTggA
TAp63ex5out (antisense)	ggTggggTCATCACCTTgATCT
ΔNp63ex6nst (antisense)	gCATggCTgTTCCCCTCTACTC
TAp63ex5nst (antisense)	ATggggCATgTCTTTgCAATTT
ActBfw (sense)	TTgCCgACAggATgCAgAAggA
ActBrv (antisense)	AggTggACAgCGAggCCAggAT

counting the percentage of positive neoplastic cells in ten different fields at ×40 magnification.

RNA extraction and RT-PCR

Each sample (20–80 μg) of frozen tissue was treated according to the RNeasy Protect Mini Kit protocol (QIAGEN, Hilden, Germany). RNA concentration was measured using the Quant-iT™ RNA kit (Invitrogen, Carlsbad, CA). The sample concentration was normalized to obtain a total quantity of RNA of about 500 ng of each sample. cDNA synthesis was carried out using 9 μl of total RNA previously denatured at 65°C. Retrotranscription was performed at 37°C for 1 h in a total volume of 20 μl in the presence of 300 ng of random primers (Invitrogen, Milan), 5 U of RNase inhibitor (GE Healthcare, Milan), 0.5 mM dNTPs (SIGMA, Milan), 10 mM DTT, and 200 U of MMLV (Invitrogen, Milan), followed by a denaturing step at 65°C for 15 min to inactivate the reverse transcriptase.

PCR and nested PCR

The first PCR was performed using the primers reported in Table 2. ΔNp63ex3′ and ΔNp63ex7out were used to identify the ΔNp73L, TAp63ex2, and TAp63ex5out for TAp63 isoforms; 200 μM dNTPs (Sigma-Aldrich SRL, Italy), 1× buffer green (Roche, Manheim, Germany), 0.2 μM each primer, 1 U FastStart *Taq* polymerase (Roche, Manheim, Germany), and 2 μl of cDNA were put in a total reaction volume of 25 μl. After a first denaturation step at 95°C for 4 min, the reaction continued for 38 cycles of 95°C for 30 s, 58°C for 1 min, and 72°C for 1 min. The final extension was 72°C for 10 min. The second PCR was carried out changing the two antisense primers: ΔNp63ex6nst for ΔNp63 and TAp63ex5nst for TAp63. The reaction contained the same reagents of first PCR with the addition of only 1 μl of the first PCR product. The steps of reaction were the same as of the first PCR but not for the number of cycles (33 instead of 38). The PCR products were run in a 3% agarose gel. A PCR for β-actin analysis was performed as a reference control with the same conditions specified for p63 using the primers reported in Table 2 (ActBfw and ActBrv).

Band purification and sequence analysis

To be sure that the bands visualized in the agarose gel correspond to isoforms under study, we cut them off from the gel and sequenced them. The bands were cut off and treated following the protocol of the MinElute Gel Extraction kit (QIAGEN, Hilden, Germany). Preparations of the DNA sequencing reactions were performed in agreement with the CEQ2000 Dye Terminator Cycle Sequencing with Quick Start Kit (Beckman Coulter, Fullerton, CA, USA). After purification with the Agencourt CleanSEQ kit (Agencourt, Beverly, MA), the products were loaded on the CEQ2000 (Beckman Coulter, Fullerton, CA, USA).

Results

All the patients were female, ranging in age from 37 to 83 years (mean, 59.1 years). The samples under study included 15 normal breasts, one cystic disease with apocrine cyst, two fibroadenomas, two specimens containing predominantly epitheliosis (usual duct hyperplasia), and 20 carcinomas: 12 invasive duct carcinomas (IDC; six grade II, six grade III), two DIN/DCIS, six invasive lobular carcinomas (ILC), of which three were of the pleomorphic variant. All

Table 3 Immunocytochemical and molecular findings in normal tissues and benign breast tissues

Tissue	Number of specimen	p63 IHC[a]	p63 isoforms (nested PCR)			
			ΔNp63	*ΔNp73L*	*TAp63*	*d4TAp63*
Normal	15	+	15/15	0/15	12/15	0/15
Apocrine cyst	1	+	1/1	0/1	0/1	0/1
Fibroadenoma	2	+	2/2	0/2	2/2	0/2
Epitheliosis	2	+	2/2	0/2	1/2	0/2

[a] Positivity is limited to myoepithelial cells located around ducts and lobules

Table 4 Histological, immunohistochemical, and molecular findings in carcinomas

Case	Sex/age	Diagnosis	Grade	pT	pN	IHC						p63 isoforms (nested PCR)			
						Er%	Pr%	Ki67%	c-erb-B2	CK14	p63%[a]	ΔNp63	ΔNp73L	TAp63	d4TAp63
1	68	PILC	III	2	2A	80	70	12	2+	−	−	+	+	+	+
2	51	PILC	III	3	1A	70	−	15	−	−	−	+	+	+	−
3	66	PILC	III	1c	3	90	50	15	−	−	Rare[b]	+	−	+	−
4	75	ILC	II	2	0	80	−	15	3+	−	−	+	−	+	−
5	73	ILC	III	1c	1A	30	−	20	2+	−	−	+	−	+	+
6	50	ILC	II	1c	0	60	90	5	−	−	−	+	−	+	−
7	72	IDC	III	2	0	90	90	40	−	−	−	+	−	+	+
8	52	IDC	III	2	1A	60	50	25	3+	−	10%	+	+	+	+
9	56	IDC	II	2	2A	90	−	6	3+	−	Rare[b]	+	−	+	−
10	67	IDC	II	1c	2A	90	90	5	2+	−	−	+	−	−	−
11	37	IDC	II	1a	0	90	70	30	−	−	−	+	−	+	+
12	80	IDC	II	2	0	90	90	10	−	−	−	+	−	+	−
13	75	IDC	III	2	3A	80	15	20	3+	−	5%	+	−	+	+
14	74	IDC	III	1c	0	90	80	30	2+	−	Rare[b]	+	−	+	+
15	58	IDC	II	1b	0	90	50	15	1+	−	Rare[b]	+	+	+	+
16	53	IDC	III	2	3A	90	40	25	3+	−	−	+	−	+	+
17	49	IDC	III	2	1A	90	60	25	1+	−	−	+	−	+	+
18	53	IDC	II	1c	0	90	30	5	−	−	−	+	−	+	+
19	66	DCIS	III	Tis	0	90	5	18	1+	−	−	+	−	−	−
20	58	DCIS	II	Tis	0	95	80	12	−	−	−	+	−	+	−

ILC invasive lobular carcinoma, *IDC* invasive duct carcinoma, *DCIS* duct carcinoma in situ, *PILC* pleomorphic ILC, *T* tumor, *N* lymph nodes, (+) positive, (−) negative, *Er* estrogen receptors, *Pr* progesterone receptors, *CK* cytokeratin

[a] Percentage evaluated in neoplastic cells (excluding normal myoepithelial cells present)

[b] Up to 1% of cell positivity

carcinomas showed a "luminal" phenotype (Tables 3 and 4). Specifically, all cases were positive for estrogen and progesterone receptors and negative for keratin 14.

Immunohistochemical results

Normal breast and benign lesions The p63 and CK14 antibodies stained the nuclei and cytoplasm, respectively of the myoepithelial cells that were present in the ducts and acini (Table 3). No staining was observed in the luminal cells (Fig. 1).

Carcinomas In four cases, p63 antibody stained the nuclei of rare (no more than 1%) neoplastic cells scattered through the invasive carcinoma (Table 4). In two additional cases, p63 antibody stained 5% (case 13) and 10% (case 8) of the neoplastic cells (Fig. 2). In this latter case, p63-positive neoplastic cells were detected also in the related lymph node metastasis. No p63-positive cells were detected in the remaining 14 carcinomas. Myoepithelial cells of residual normal ducts, when present in the different sections, constituted internal positive controls.

Nested PCR

Normal breast and benign lesions All samples expressed ΔNp63, TAp63, or both isoforms at the same time. ΔNp63 was expressed in all samples, while TAp63 was expressed in 15 out of 20 (75%) samples (Table 3). The short variants, ΔNp73L and d4TAp63, were never expressed.

Carcinomas All cases of in situ and invasive carcinomas expressed ΔNp63, TAp63, or both isoforms at the same time (Table 4). ΔNp63 was expressed in all cases, while TAp63 in 18 out of 20 (90%) cases. The short isoforms appeared only in cases of invasive carcinomas, while these were absent in the two DIN/DCIS. Specifically, ΔNp73L was expressed in four out of 18 (22%) cases and d4TAp63 in 11 out of 18 (61%) cases of IBC.

Fig. 1 Case 1: Pleomorphic invasive lobular carcinoma. Myoepithelial cells only stain for p63 in one entrapped non-neoplastic small duct

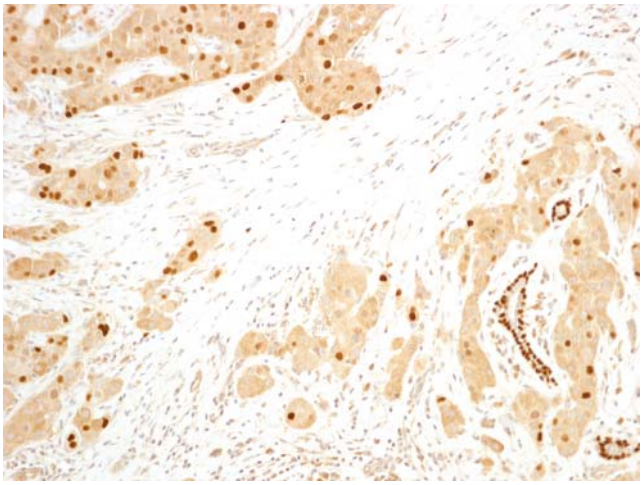

Fig. 2 Case 8: IDC grade III. p63 stains myoepithelial cells of one entrapped non-neoplastic small duct as well as 10% of nuclei of neoplastic elements

Sequencing

In all cases, the sequences obtained from "normal band" (normal isoforms, ΔNp63, and TAp63) revealed the last amino acid of exon 3 (tryptophan) linked to the complete sequence of exon 4. Vice versa, in IBC, the electropherogram obtained from a lower band, revealed the last amino acid of exon 3 linked to the complete sequence of exon 5, indicating that exon 4 was spliced out (Figs. 3 and 4).

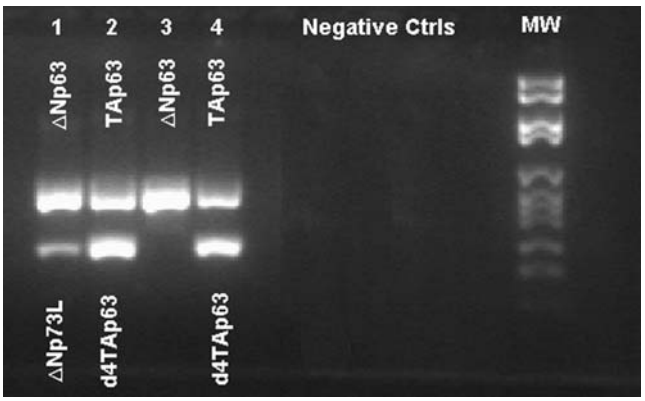

Fig. 3 Gel of p63 isoforms. *Lower bands* represent the short isoforms (lacking exon 4), while *upper bands* represent the full-length isoforms. *Lanes 1–2*: samples 1 (Table 3); *lanes 3–4*: sample 7 (Table 3); *Ctrls* controls, *MW* molecular weight marker (DNA molecular weight marker VI, Roche Diagnostics Corporation, IN, USA)

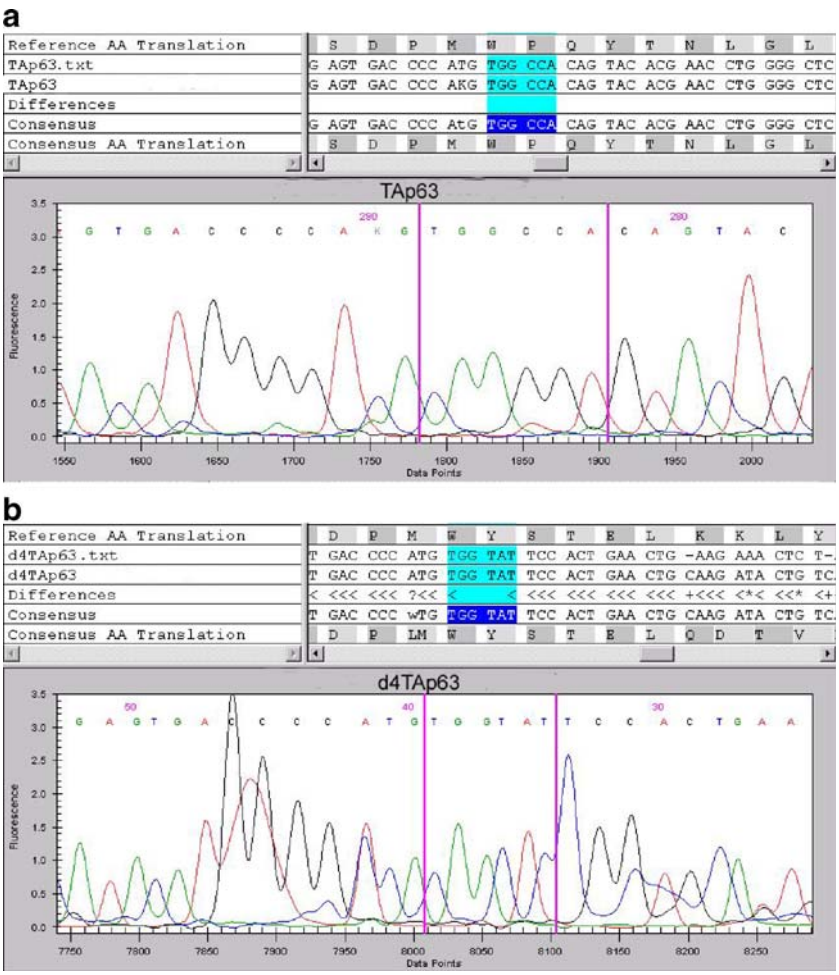

Fig. 4 Electropherogram of bands obtained after nested PCR. **a** Sequences of full-length (*TAp63*) and **b** shorter isoform (*d4TAp63*). In shorter isoform sequence, it is possible to observe as tryptophan (last amino acid of exon 3) is followed by the sequence of exon 5 (starting with a tyrosine) and not by a proline (first amino acid of exon 4)

Relation between nested PCR results and clinical, morphological, and immunohistochemical data

The four invasive carcinomas presenting the ΔNp73L isoform were histologically diagnosed as IDC in two cases (grades III and II, respectively) and ILC, pleomorphic type (grade III) in the remaining two. Three out of these four (75%) cases that expressed ΔNp73L had lymph node metastases at presentation (Table 4).

It is pertinent to emphasize that immunohistochemistry was less sensitive as p63 positivity was detected in the two cases of IDC only (Table 4, cases 8 and 15).

d4TAp63 (Table 4) isoform was observed in 11 out of 18 (61%) cases of invasive carcinoma which were two ILC (cases 1 and 5) and nine IDC (cases 7, 8, 11, 13, and 14–18). Six cases (55%) had lymph node metastases.

Discussion

In the present study, 40 specimens from normal breast, benign lesions, DIN/DCIS, and invasive carcinomas were analyzed by immunohistochemistry and RT-PCR in order to disclose the patterns of p63 expression.

Immunopositivity for p63 in invasive carcinomas of the breast has been described in myoepithelial, metaplastic, and some salivary gland-like carcinomas [12, 13, 20, 21]. p63 was found to be positive in 55.5% of basal-like carcinoma of the breast [15], while a much lower positivity that ranged from 0.6% to 19.5% was observed in "ordinary" luminal-type invasive carcinomas [14, 15, 20]. The present cases were all luminal-type invasive carcinomas [19, 21], negative for CK14. With the exception of four cases that contained rare positive cells and two in which p63 positivity was found in 5% and 10% of the neoplastic cells, the remaining invasive carcinomas were devoid of p63 immunostaining.

In normal breast, in benign lesions, and in the two cases of DIN/DCIS, immunohistochemistry for p63 stained myoepithelial cells only. In addition, in these same cases, the full-length isoforms ΔNp63 and TAp63 (with exon 4) were detected by PCR, suggesting that these same isoforms were most probably expressed by normal myoepithelial cells.

On the contrary, PCR consistently revealed the full-length p63 isoforms in all invasive carcinomas at variance with

immunohistochemistry that stained only occasional p63-positive cells in no fewer than six cases. These discrepant data between molecular and immunohistochemical techniques are probably due to the fact that PCR is a sensitive technique that reveals isoforms even if expressed in small quantity.

Invasive carcinomas, in addition, showed in 12 cases one of the two or both short isoforms (ΔNp73L and d4TAp63, lacking exon 4) paralleling the results obtained in salivary gland carcinomas [9] and squamous cell carcinomas of oral cavity [6, 9, 22] where ΔNp73L isoform was not found in normal salivary gland tissue [9] and in non-neoplastic squamous oral mucosa [6]. Moreover, the expression of ΔNp73L has been found to be associated to low expression of E-cadherin, an association predictive of development of lymph node metastases in oral squamous cell carcinomas [22].

Therefore, it seems from the present data that IBC with luminal phenotype can express p63, especially in its altered isoforms.

In conclusion, it appears that:

1. Presence of p63 in invasive carcinomas of luminal type as seen at molecular level suggests caution to include p63 as a specific marker of basal-like carcinomas.
2. The short isoforms that lack exon 4 are only present in the neoplastic cells of invasive carcinomas.

Acknowledgments This paper was financed with funds from the Ministry of University and Research (MIUR) of Italy and University of Bologna (M. P. F. and V. E.).

Conflict of interest statement We declare that we have no conflict of interest.

References

1. Levrero M, Laurenzi VD, Costanzo A et al (2000) The p53/p63/p73 family of transcription factors: overlapping and distinct functions. J Cell Sci 113:1661–1670
2. Strano S, Rossi M, Fontemaggi G et al (2001) From p63 to p53 across p73. FEBS Lett 490:163–170
3. Barbieri CE, Pietenpol JA (2006) p63 and epithelial biology. Exp Cell Res 312:695–706
4. Yang A, Kaghad M, Wang Y et al (1998) p63, a p53 homolog at 3q27–29, encodes multiple products with transactivating, death-inducing, and dominant-negative activities. Mol Cell 2:305–316
5. Lee HO, Lee JH, Choi E et al (2006) A dominant negative form of p63 inhibits apoptosis in a p53-independent manner. Biochem Biophys Res Commun 344:166–172
6. Foschini MP, Gaiba A, Cocchi R et al (2004) Pattern of p63 expression in squamous cell carcinoma of the oral cavity. Virchows Arch 444:332–339
7. Urist MJ, Di Como CJ, Lu ML et al (2002) Loss of p63 expression is associated with tumour progression in bladder cancer. Am J Pathol 161:1199–1206
8. Senoo M, Tsuchiya I, Matsumura Y et al (2001) Transcriptional dysregulation of the p73L/p63/p51/p40/KET gene in human squamous cell carcinomas: expression of Delta Np73L, a novel dominant-negative isoform, and loss of expression of the potential tumour suppressor p51. Br J Cancer 84:1235–1241
9. Foschini MP, Gaiba A, Cocchi R et al (2005) p63 expression in salivary gland tumours: role of DeltaNp73L in neoplastic transformation. Int J Surg Pathol 13:329–335
10. Di Como CJ, Urist MJ, Babayan I et al (2002) p63 expression profiles in human normal and tumour tissues. Clin Cancer Res 8:494–501
11. Wang X, Mori I, Tang W et al (2002) p63 expression in normal, hyperplastic and malignant breast tissues. Breast Cancer 9:216–219
12. Reis-Filho JS, Milanezi F, Amendoeira I et al (2003) Distribution of p63, a novel myoepithelial marker, in fine-needle aspiration biopsies of the breast: an analysis of 82 samples. Cancer 99:172–179
13. Barbareschi M, Pecciarini L, Cangi MG et al (2001) p63, a p53 homologue, is a selective nuclear marker of myoepithelial cells of the human breast. Am J Surg Pathol 25:1054–1060
14. Reis-Filho JS, Simpson PT, Martins A et al (2003) Distribution of p63, cytokeratins 5/6 and cytokeratin 14 in 51 normal and 400 neoplastic human tissue samples using TARP-4 multi-tumour tissue microarray. Virchows Arch 443:122–132
15. Matos I, Dufloth R, Alvarenga M et al (2005) p63, cytokeratin 5, and P-cadherin: three molecular markers to distinguish basal phenotype in breast carcinomas. Virchows Arch 447:688–694
16. Tavassoli FA, Devilee P (2003) WHO. Pathology and genetics of tumours of the breast and female genital organs. IARC Press, Lyon
17. Elston CW, Ellis IO (2002) Pathological prognostic factors in breast cancer. I. The value of histological grade in breast cancer: experience from a large study with long-term follow-up. Histopathology 41:154–161
18. Eusebi V, Magalhanes F, Azzopardi JG (1992) Pleomorphic lobular carcinoma of the breast: an aggressive tumour showing apocrine differentiation. Hum Pathol 23:655–662
19. Rakha EA, Putti TC, Abd El-Rehim DM et al (2006) Morphological and immunophenotypic analysis of breast carcinomas with basal and myoepithelial differentiation. J Pathol 208:495–506
20. Koker MM, Kleer CG (2004) p63 expression in breast cancer: a highly sensitive and specific marker of metaplastic carcinoma. Am J Surg Pathol 28:1506–1512
21. Tavassoli FA, Eusebi V (2009) Tumors of mammary gland. AFIP Atlas of Tumor Pathology. American Registry of Pathology, Washington
22. Foschini MP, Cocchi R, Morandi L et al (2008) E-cadherin loss and Delta Np73L expression in oral squamous cell carcinomas showing aggressive behavior. Head Neck 30:1475–1482

Virchows Arch (2010) 456:403–409
DOI 10.1007/s00428-010-0897-5

ORIGINAL ARTICLE

Co-expression of CD173 (H2) and CD174 (Lewis Y) with CD44 suggests that fucosylated histo-blood group antigens are markers of breast cancer-initiating cells

Wei-Ming Lin · Uwe Karsten · Steffen Goletz · Ruo-Chuan Cheng · Yi Cao

Received: 8 November 2009 / Revised: 10 February 2010 / Accepted: 16 February 2010 / Published online: 19 March 2010
© Springer-Verlag 2010

Abstract Histo-blood group antigens CD173 (H2) and CD174 (Lewis Y) are known to be developmentally regulated carbohydrate antigens which are expressed to a varying degree on many human carcinomas. We hypothesized that they might represent markers of cancer-initiating cells (or cancer stem cells, CSC). In order to test this hypothesis, we examined the co-expression of CD173 and CD174 with stem cell markers CD44 and CD133 by flow cytometry analysis, immunocytochemistry, and immunohistochemistry on cell lines and tissue sections from breast cancer. In three breast cancer cell lines, the percentage of $CD173^{+}/CD44^{+}$ cells ranged from 17% to >60% and of $CD174^{+}/CD44^{+}$ from 21% to 57%. In breast cancer tissue sections from 15 patients, up to 50% of tumor cells simultaneously expressed CD173, CD174, and CD44 antigens. Co-expression of CD173 and CD174 with CD133 was also observed, but to a lesser percentage. Co-immunoprecipitation and sandwich ELISA experiments on breast cancer cell lines suggested that CD173 and CD174 are carried on the CD44 molecule. The results show that in these tissues CD173 (H2) and CD174 (LeY) are associated with CD44 expression, suggesting that these carbohydrate antigens are markers of cancer-initiating cells or of early progenitors of breast carcinomas.

Keywords Breast cancer-initiating cells · Co-expression · CD44 · CD173 (H2) · CD174 (LeY)

W.-M. Lin · Y. Cao (✉)
Laboratory of Molecular and Experimental Pathology,
Key Laboratory of Animal Models and Human Disease Mechanisms of CAS and Yunnan Province,
Kunming Institute of Zoology, Chinese Academy of Sciences,
32 Jiaochang Donglu,
Kunming, Yunnan 650223, China
e-mail: caoy@mail.kiz.ac.cn

U. Karsten · S. Goletz
Glycotope GmbH,
Berlin-Buch, Germany

R.-C. Cheng
Department of General Surgery, First Affiliated Hospital of Kunming Medical College,
Kunming, China

W.-M. Lin
College of Life Sciences, Longyan University,
Longyan, China

Introduction

Cancer-initiating cells have been defined as a unique subpopulation in tumors that possess the ability to initiate tumor growth and sustain tumor self-renewal [1]. A great number of more or less specific markers of cancer-initiating cells have been described during recent years. Among the markers most widely accepted is CD44. CD44 is a cell surface type I transmembrane glycoprotein involved in cell–cell interactions, cell adhesion, and migration. It is a receptor for hyaluronic acid, but can also interact with other ligands [2]. CD44 was found to be expressed on cancer-initiating cells in gastric cancer [3]. Together with another membrane glycoprotein, CD133, it has been proposed to be capable of identifying a cancer-initiating population in the brain, in the colon, and in other solid tumors [4].

ABH and Lewis (Le) blood group antigens are cell surface carbohydrate structures. Besides their expression on erythrocytes, they are also widely distributed in body fluids

and normal tissues, especially on epithelia of glandular tissues. CD173 (H2, Fucα1-2Gal-β1-4GlcNAcβ1-) and CD174 (LeY, Fucα1-2Gal-β1-4[Fucα1-3]GlcNAcβ1-) are fucosylated derivatives of the same type 2 precursor carbohydrate chain found on glycoproteins. CD173 is synthesized by the addition of a fucose to the type 2 precursor chain mediated by the α1-2 fucosyltransferase encoded by the H gene. CD174 results from the additional action of the α1-3 fucosyltransferase encoded by the LeX gene.

A number of studies have shown that abnormal expression of CD173 and CD174 occurs in epithelial malignancies [5, 6]. In a previous study, we have found that CD173 and CD174 were expressed on $CD34^+$ hematopoietic progenitors [7]. Moreover, fucosylated histo-blood group antigens increase the tumorigenicity of rat colon adenocarcinoma cells [8]. We hypothesized that CD173 and CD174 might be specifically expressed on cancer-initiating cells. The expression of CD173 and CD174 on cancer-initiating cells has not been investigated up to now. In this study, we have examined whether and to what extent CD173 and CD174 are co-expressed with the stem cell marker CD44 in breast carcinoma. Since it was found that tamoxifen increases the number of $CD44^+/CD24^-$ breast cancer-initiating cells [9], we also used flow cytometry analysis to evaluate whether the expression of CD173 and CD174 was affected by treatment of 4-OHT in cultured breast cancer cells. Moreover, since H blood group antigens were found to be carried on CD44 in the rat PRO cell line [10], we also investigated whether CD44 is a carrier of CD173 and CD174 in human breast carcinoma cells in vitro.

Materials and methods

Cell lines and cell culture

The breast adenocarcinoma cell lines MDA-MB-231, MDA-MB-435, and MCF-7 were used in this study. These cell lines were routinely cultured in Dulbecco's modified Eagle's medium containing 10% fetal calf serum. The cells were grown at 37°C in an atmosphere of 5% CO_2/95% air and close to 100% relative humidity.

Immunocytochemistry

The cells were plated onto polylysine (Sigma, Saint Louis, MO, USA)-coated slides in culture medium overnight. Thereafter, the medium was carefully aspirated and the slides were air-dried. Wrapped slides could be stored at −80°C until use. For immunocytochemistry, cells were fixed with cold (−20°C) acetone for 15 min, blocked with 2% bovine serum albumin (BSA) for 30 min, and incubated with CD44 mAb (G44-26, mouse IgG2b, BD Biosciences, Franklin Lakes, NJ, USA) together with mAbs CD173 (A46-B/B10, mouse IgM) [11] or CD174 (A70-C/C8, mouse IgM), both from Glycotope GmbH (Berlin, Germany) for 60 min. The slides were subsequently incubated with a mixture of fluorescein isothiocyanate (FITC)-conjugated anti-mouse IgM (μ chain-specific; F9259, Sigma) and Cy3-conjugated goat anti-mouse IgG (γ chain-specific; #69732, Jackson Laboratories, West Grove, PA, USA). Counterstaining was performed with 4′,6-diamidino-2-phenylindole dihydrochloride (DAPI; Beyotime Biotechnology, Jiangsu, China). Negative controls were incubated with mouse serum instead of the specific mAb. The slides were mounted with glycerol and analyzed by fluorescence microscopy.

Flow cytometry analysis

Cell suspensions from established cell lines were prepared at a density of 1×10^6 cells/100 μl. They were washed twice with phosphate-buffered saline (PBS) containing 2% BSA and incubated with primary antibodies at 4°C for 20 min, followed by anti IgG-Cy3 (γ chain-specific) and anti IgM-FITC (μ chain-specific) in appropriate concentrations at 4°C for 20 min. Flow cytometry was performed on a FACScan (BD Biosciences). Collected data from 10,000 cells and WinMDI software were used for the analysis of FACS data files.

For 4-hydroxytamoxifen (4-OHT) treatment, MDA-MB-231, MDA-MB-435, and MCF-7 breast adenocarcinoma cell lines were exposed to 4-OHT (#H6278, Sigma) at a final concentration of 20 nM for 24 h. Then, flow cytometry analysis was performed as described above.

Immunoprecipitation

One million cells were treated with 1 ml of 1% Triton X-100 in 50 mM Tris–HCl, pH8.0, 150 mM NaCl containing a mixture of protease inhibitors (#539134, Calbiochem, Darmstadt, Germany), and homogenized with oscillation at 4°C for 30 min. After centrifugation for 10 min at 15,000×*g*, supernatants were taken. Protein G-agarose beads (#P-4691, Sigma) were incubated for 4 h with anti-CD44 antibody at 4°C on a shaker. The protein G-agarose beads were added to the supernatants and incubated on an end-over-end mixer overnight at 4°C. The beads were collected by centrifugation and washed. The pellets were resuspended in sodium dodecyl sulfate polyacrylamide gel electrophoresis (SDS-PAGE) sample buffer and boiled for 5 min. The immunoprecipitates were subsequently separated on polyacrylamide gels (8%) and probed using anti-CD173 and anti-CD174 antibodies in Western blotting.

Sandwich ELISA

Ninety-six-well polystyrene microplates were coated with a capture antibody against CD44 at 1 μg/ml in coating buffer at 4°C for 14 h. After blocking with 5% BSA, 100 μl of the supernatants prepared as described above was added to the wells and incubated at room temperature for 2 h. Then, the plates were incubated with CD173 or CD174 mAb followed by peroxidase-labeled goat anti-mouse IgM antibody (μ chain-specific; Southern Biotech, Birmingham, AL, USA). Color reaction was developed with *o*-phenylenediamine dihydrochloride solution at room temperature. The reaction was stopped with 2.5 M sulfuric acid. Negative controls were performed with 2% BSA instead of the mAbs. The optical density of each well was determined within 30 min using a microplate reader (Bio-Rad, Hercules, CA, USA) at 492 nm.

Tissues and immunohistochemistry

Fifteen breast carcinoma specimens were obtained from patients who had undergone initial surgery. The samples were fully encoded to protect patient confidentiality, and the study and study protocols were approved by the local research ethics committees at all participating sites.

The fresh tissues were embedded carefully at −20°C with OCT compound (optimal cutting temperature) in plastic mold, cut into 4- to 8-μm sections after equilibration in the cryostat chamber, and fixed with cold (−20°C) acetone for 15 min. Then, immunofluorescence double staining was performed as described above. In addition, the CD133 antibody (ANC9C5, mouse IgG1, Ancell, Bayport, MN, USA) was also used for the double staining on the tissues. Cell numbers were counted at ×100 magnification with a Nikon microscope. The percentage of double-positive cells was estimated in digital pictures.

In three additional cases of breast intraductal carcinoma, we also performed immunoperoxidase staining. The tissue sections were treated with 3% H_2O_2 for 30 min to suppress endogenous peroxidases, washed three times with PBS, and blocked with 2% BSA. They were incubated with CD173 antibody then treated with peroxidase-labeled goat ant-mouse immunoglobulin antiserum (DAKO, Copenhagen, Denmark). Negative controls were performed with 2% BSA instead of the CD173 antibody. Color was developed with diaminobenzidine. Counterstaining was performed with hematoxylin.

Statistical analysis

The statistical analyses were performed using unpaired *t* test, Fisher's exact test, or the Spearman correlation test. Data were expressed as means ± SEM. A value of $P<0.05$ was considered statistically significant.

Results

Expression of CD173 and CD174 on breast cancer cell lines

Flow cytometric analysis and immunohistological staining revealed that CD173 and CD174 were localized at the cellular surface (Fig. 1a). The breast cell lines showed frequent CD173 and CD174 expression: MDA-MB-231, MDA-MB-435, and MCF-7 contained about 27%, 92%, and 80% of CD173 positive cells, as well as about 44%, 57%, and 72% of CD174-positive cells, respectively.

Co-expression of CD44 with CD173 or CD174 in breast cancer cell lines

Immunocytological staining experiments were performed to investigate the co-expression of CD173 or CD174 with CD44 on breast cancer cells. We observed in many cells an overlay of CD44 staining with CD173 and CD174; an example is given in Fig. 1a–c. Semiquantitative data from flow cytometry experiments are shown in Fig. 2a and summarized in Table 1.

To assess whether CD44, CD173, and CD174 expression is simultaneously affected after exogenous treatment, we treated the breast cancer culture cells with 4-OHT. In semiquantitative flow cytometric analysis, 4-OHT treatment increased the percentage of $CD44^+CD173^+$ and $CD44^+CD174^+$ cells in MDA231 ($P<0.05$, Fig. 2b), but not in MDA-MB-435 and MCF-7 cells ($P>0.05$, data not shown).

Co-expression of CD44 or CD133 with CD173 or CD174 in breast carcinoma tissues

Among the examined 15 breast carcinoma tissues, CD44, CD173, and CD174 staining was also predominantly observed at the cell membrane. CD44-, CD173-, and CD174-positive cells were present in a scattered or clustered pattern, which varied among individuals. CD173- and CD174-positive cells were found in most cases. The mean percentage of CD173- and CD174-positive cells was 51% and 52% of the total cancer cells, respectively. CD44 showed strong immunoreactivity (positively stained carcinoma cells amounted to 53%) in all cases. Interestingly, cases with increased CD173 and CD174 expression correlated with raised CD44 expression ($P<0.05$). Most importantly, more than 95% of CD173- and CD174-positive cells, respectively, co-expressed the CD44 antigen (Fig. 1d–i).

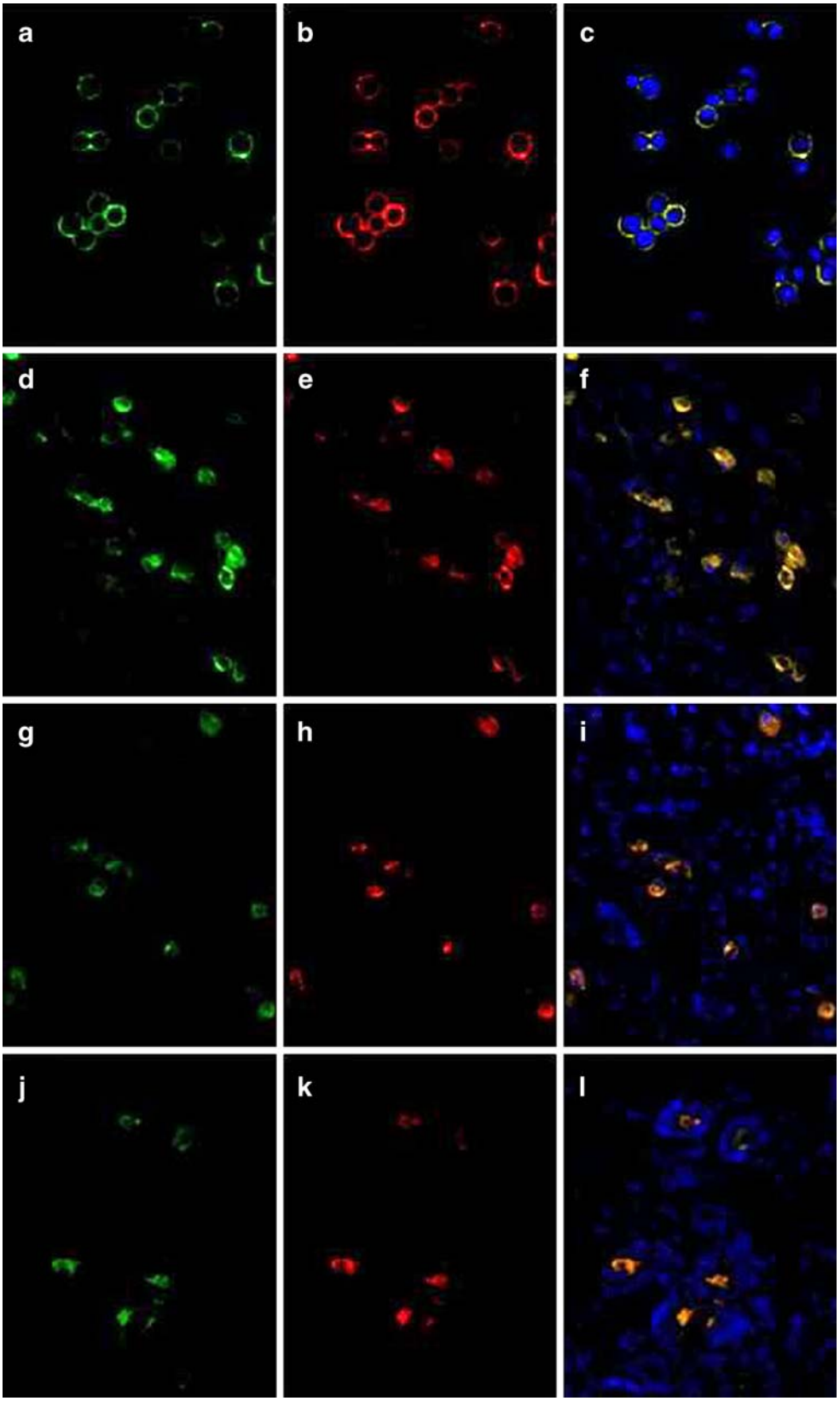

Fig. 1 Double immunofluorescence staining of breast cancer cells. **a**–**c** Cell line MCF-7. **d**–**l** Breast cancer tissue sections. Cells were stained with monoclonal antibodies G44-26 (CD44, IgG2b) or ANC9C5 (CD133, IgG.1) and with A70-C/C8 (CD174, IgM) or A46-B/B10 (CD173, IgM), followed by incubation with anti-IgG-Cy3 (γ chain-specific, *red*) and anti-IgM-FITC (μ chain-specific, *green*). **c**, **f**, **i**, **l** are merged pictures; nuclei are counterstained with DAPI (*blue*). CD 173 (**a**, **d**) is in many cases co-expressed with CD44 (**b**, **e**). CD174 (**g**, **j**) shows co-expression with CD44 (**h**) as well as with CD133 (**k**). Magnification, ×200

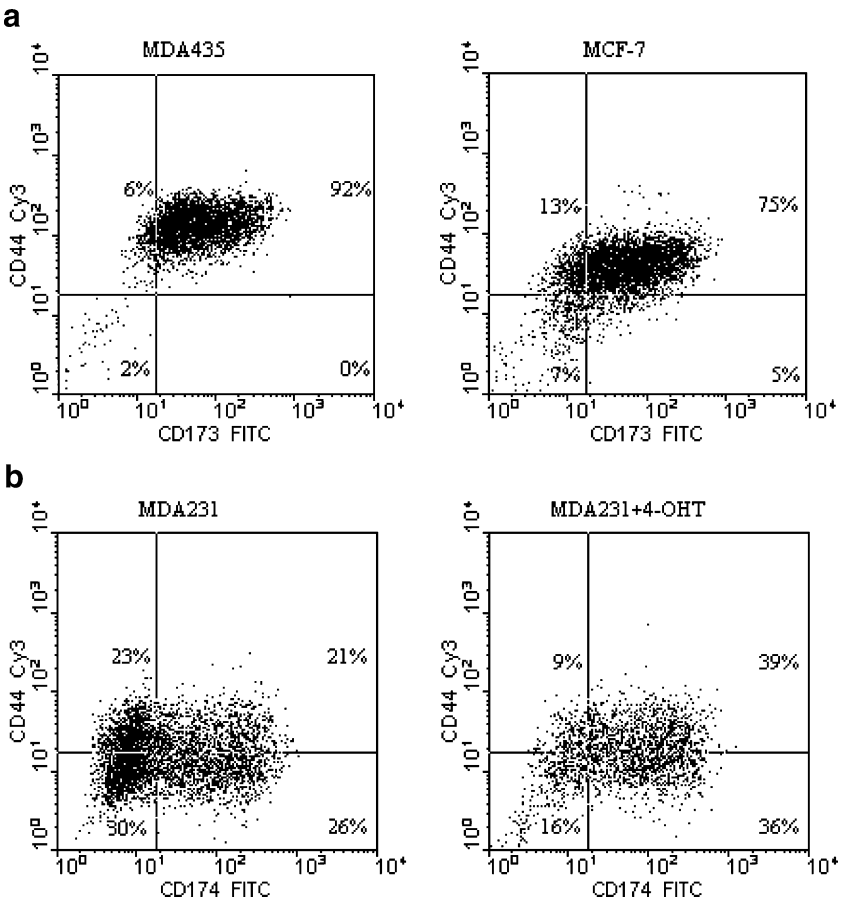

Fig. 2 **a** Flow cytometric analysis of $CD44^+/CD173^+$ expression in the breast adenocarcinoma cell lines MDA-MB-435 and MCF-7. Cancer cells were incubated with anti-CD44 (IgG2b) and anti-CD174 (IgM) antibodies, respectively, followed by incubation with anti-IgG-Cy3 (γ chain-specific) and anti-IgM-FITC (μ chain-specific). Values are taken from one of three similar experiments. Large proportions of both cell lines are positive for both markers (CD44 and H2). **b** Flow cytometric analysis of $CD44^+/CD174^+$ expression on MDA-MB-231 cells before and after 4-OHT treatment. 4-OHT treatment results in an increase in the proportion of cells expressing both CD44 and CD174 (LeY). Values are taken from one of three similar experiments

CD133 is also a marker of cancer-initiating cells. Therefore, we asked whether CD173 or CD174 was co-expressed with this marker in breast carcinoma tissues. We found that CD133 was indeed co-expressed with CD173 and CD174, although at a lower percentage (<5% of the total cancer cells, Fig. 1j–l). The manifestation of the lower co-expressed percentage was due to only a small subpopulation of cancer cells (<5%) possessing CD133. In addition, we found that cases with increased CD173 and CD174 expression correlated with raised CD133 expression ($P<0.05$, data not shown).

Expression of CD173 on basal cells of intraductal breast carcinomas

In three cases of intraductal breast carcinomas, CD173 mAb stained the basal cells of the remaining duct walls. In normal ducts of transitional tissues of the same sections, the basal cell layer was only occasionally positive for CD173. The expression of CD173 in these cells was independent of the ABH blood group type and of the secretor status of the individual (data not shown).

Evidence for CD44 carrying CD173 or CD174

Potential glycoproteins carrying CD173 or CD174 were analyzed in three breast carcinoma cell lines by immunoprecipitation and in a sandwich ELISA. The CD44 immunoprecipitate from the lysates of the three cell lines was subjected to immunoblot analysis using mAbs CD173 and CD174. Both antibodies stained the CD44 band (Fig. 3).

In a sandwich ELISA with anti-CD44 as capture antibody followed by mAbs CD173 and CD174, both antibodies scored positive in all three cell lines examined,

Table 1 Flow cytometric analysis of CD44, CD173, and CD174 expression in breast carcinoma cell lines

Cell lines	$CD44^+$ (%)	$CD173^+$ (%)	$CD174^+$ (%)	$CD44^+/CD173^+$ (%)	$CD44^+/CD174^+$ (%)
MDA-MB-435	>60	>60	~57	>60	~57
MDA-MB-231	~44	~27	~44	~17	~21
MCF-7	>60	>60	>60	>60	~46

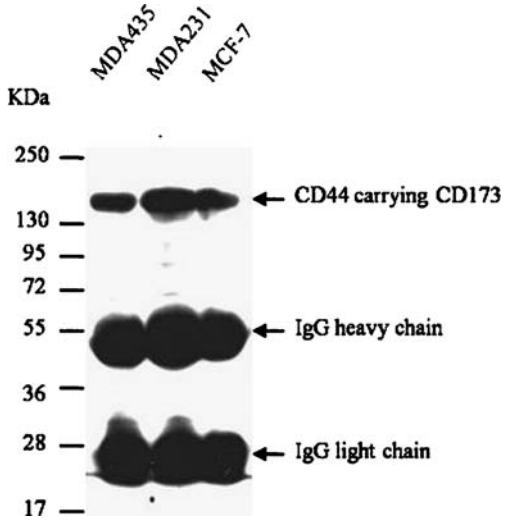

Fig. 3 Immunoprecipitation of lysates from breast adenocarcinoma cell lines MDA-MB-231, MDA-MB-435, and MCF. The CD44-immunoprecipitated material was resolved by SDS-PAGE and analyzed by immunoblotting using mAb CD173. The data show that in breast carcinomas. CD44 is a carrier of CD173 (H2)

indicating that CD173 and CD174 epitopes are expressed on the CD44 molecule (Table 2).

Discussion

The existence of cancer-initiating cells is well documented in brain, lung, and breast cancers [1, 3]. They are functionally defined as self-renewing, quiescent, and multi-potent cells that are able to multi-lineage differentiation. According to the cancer stem cell theory, recurrences and metastases of cancer depend on cancer-initiating cells [12]. Since cancer-initiating cells or cancer stem cells clearly differ from the majority of cells of the tumor mass, studying the expression and function of surface molecules on cancer-initiating cells is an important aspect of tumor biology.

In previous studies, we found that CD173 and CD174 were expressed on $CD34^+$ hematopoietic progenitors [7]. Moreover, fucosylated histo-blood group antigens (H antigens) were co-expressed on CD44v6 after transfection of α(1-2)fucosyltransferase concomitant with an enhanced tumorigenicity in rat colon adenocarcinoma cells [8]. In this study, we examined whether CD173 and/or CD174 are co-expressed with the cancer-initiating cell marker CD44 in human breast carcinoma cells and tissues.

The results indicate that CD44 together with CD173 or CD174 are located at the cell surface and exhibit co-expression in a significant proportion of cultured breast cancer cells and in tissue specimens taken from breast cancer. Tamoxifen was reported to increase the number of mammary cancer stem cells [9]. In this study, the number of $CD44^+/CD173^+$ or $CD44^+/CD174^+$ breast cancer cells could be enhanced in cultured cells after tamoxifen (4-OHT) treatment. Therefore, we conclude that CD44 is co-expressed with CD173 and CD174 in breast cancer.

An interesting observation was the strong staining for CD173 of myoepithelial/basal cells in cases of intraductal breast carcinomas similar to our earlier study [13]. At present, we cannot explain the cause and significance of this observation. Since H and LeY antigens are developmentally regulated antigens, this phenomenon might also be indicative of an ongoing epithelial–mesenchymal transition of these cells. This will, however, be addressed in further studies.

Type 2-based ABH oligosaccharides are carried on several different glycoproteins and glycolipids [14]. In epithelial ovarian cancer, the major carrier proteins of CD174 are CA125 and MUC1 [15]. In $CD34^+$ hematopoietic stem cells, the major carrier of CD173 and CD174 is a 170-kDa glycoprotein [7]. CD44 is also a carrier of H antigens [10]. Here, we have used a sandwich ELISA and immunoprecipitation to demonstrate that CD44 is a major carrier of CD173 and CD174 in breast cancer cells.

It is believed that CD173 and CD174 structures on glycoprotein expressed by carcinomas contribute to adhesion, cell aggregation, invasion, and metastasis. CD174 is involved in early cell–cell contacts during tumor-associated angiogenesis [16]. Histochemistry alone cannot decide what the function and significance of the expression of CD173 and CD174 on cancer-initiating cells is. However, a pathophysiological significance of the expression of CD173 and CD174 in carcinomas has been demonstrated. CD173 and CD174 are apparent markers of the degree of malignancy in cancer patients [5, 17]. Higher expression of CD173 and CD174 was more often found in patients

Table 2 Binding of CD173 and CD174 antibodies in a sandwich ELISA with CD44 as catcher antibody in three breast cancer cell lines

Tissue derivation	Cell lines	$CD44^+/CD173^+$	$CD44^+/CD174^+$
Adenocarcinoma	MDA-MB-435	+	(+)
Adenocarcinoma	MDA-MB-231	+	+
Adenocarcinoma	MCF-7	+	(+)

Score according to OD_{490} values minus blank as follows: ++, >0.5; +, 0.1–0.5; (+), 0.05–0.1; −, <0.05

with high grade and poor prognosis compared to those with better prognosis [6]. In lymph node negative breast carcinomas, over-expression of CD174 was associated with significantly decreased patient survival [18]. Increased tumorigenicity mediated by α1-2 fucosylation is associated with increased resistance to apoptosis and escape from immune control [10, 19]. These phenomena observed in previous studies may be associated with the expression of CD173 and CD174 on the cancer-initiating cells. Hitherto, the pathophysiological functions of CD173 and CD174 on cancer-initiating cells have not been known. They have to be determined in future work.

Failure of current cancer therapies may be ascribed to the inefficacy of drugs on potentially quiescent cancer-initiating cells. Treatment strategies therefore need to consider the presence of cancer-initiating cells. The high expression of CD173 and especially of CD174 on the surface of cancer-initiating cells in breast carcinomas suggests that these antigens could be potential targets for antibody-mediated diagnosis and therapy. Anti-LeY antibodies have already been tried in adjuvant cancer therapy [20]. More recent studies have demonstrated that the administration of low doses of anti-CD174 mAb may lead to an effective anti-tumor response, even without induction of TNF-α release [21], and anti-CD174 antibody conjugated with doxorubicin is presently under evaluation in the therapy of epithelial tumors [22]. The fact that up to half of the population of cancer cells are of the $CD173^+/CD44^+$ or of the $CD174^+/CD44^+$ phenotype is not a general argument against the CSC hypothesis [23].

In summary, the identification of CD173 and CD174 on cancer-initiating cells may offer new opportunities in the design of therapies that target cancer-initiating cells in the prevention of relapse.

Acknowledgments We thank the First Affiliated Hospital of Kunming Medical College for providing patient samples and gratefully acknowledge the technical assistance of Ms. Fan Xiao-Na. This research was supported by a grant from Yunnan Province Science and Technology Department (2008CCO15).

Conflict of interest statement UK and SG are employees of Glycotope GmbH.

References

1. Boman BM, Wicha MS (2008) Cancer stem cells: a step toward the cure. J Clin Oncol 26:2795–2799
2. Marhaba R, Zöller M (2004) CD44 in cancer progression: adhesion, migration and growth regulation. J Mol Histol 35:211–231
3. Takaishi S, Okumura T, Tu S et al (2009) Identification of gastric cancer stem cells using the cell surface marker CD44. Stem Cells 27:1006–1020
4. Tirino V, Desiderio V, d'Aquino R et al (2008) Detection and characterization of $CD133^+$ cancer stem cells in human solid tumours. PloS One 3:e3469
5. Fujitani N, Liu Y, Toda S et al (2000) Expression of H type 1 antigen of ABO histo-blood group in normal colon and aberrant expressions of H type 2 and H type 3/4 antigens in colon cancer. Glycoconj J 17:331–338
6. Baldus SE, Mönig SP, Zirbes TK et al (2006) Lewis(y) antigen (CD174) and apoptosis in gastric and colorectal carcinomas: correlations with clinical and prognostic parameters. Histol Histopathol 21:503–510
7. Cao Y, Merling A, Karsten U et al (2001) The fucosylated histo-blood group antigens H type 2 (blood group O, CD173) and Lewis Y (CD174) are expressed on $CD34^+$ hematopoietic progenitors but absent on mature lymphocytes. Glycobiology 11:677–683
8. Goupille C, Hallouin F, Meflah K et al (1997) Increase of rat colon carcinoma cells tumorigenicity by α(1-2) fucosyltransferase gene transfection. Glycobiology 7:221–229
9. Mani SA, Guo W, Liao MJ et al (2008) The epithelial–mesenchymal transition generates cells with properties of stem cells. Cell 133:704–715
10. Rapoport E, Pendu JL (1999) Glycosylation alterations of cells in late phase apoptosis from colon carcinomas. Glycobiology 9:1337–1345
11. Karsten U, Pilgrim G, Hanisch F-G et al (1988) A new monoclonal antibody (A46-B/B10) highly specific for the blood group H type 2 epitope: generation, epitope analysis, serological and histological evaluation. Br J Cancer 58:176–181
12. Gilbert CA, Ross AH (2009) Cancer stem cells: cell culture, markers, and targets for new therapies. J Cell Biochem 108:1031–1038
13. Karsten U, Papsdorf G, Pauly A et al (1993) Subtypes of non-transformed human mammary epithelial cells cultured in vitro: histo-blood group antigen H type 2 defines basal cell-derived cells. Differentiation 54:55–66
14. Hakomori S (1981) Blood group ABH and Ii antigens of human erythrocytes: chemistry, polymorphism, and their developmental change. Semin Hematol 18:39–62
15. Yin BW, Finstad CL, Kitamura K et al (1996) Serological and immunochemical analysis of Lewis y (Ley) blood group antigen expression in epithelial ovarian cancer. Int J Cancer 65:406–412
16. Moehler TM, Sauer S, Witzel M et al (2008) Involvement of alpha 1-2-fucosyltransferase I (FUT1) and surface-expressed Lewis(y) (CD174) in first endothelial cell–cell contacts during angiogenesis. J Cell Physiol 215:27–36
17. Steplewska-Mazur K, Gabriel A, Zaje W et al (2000) Breast cancer progression and expression of blood group-related tumor-associated antigens. Hybridoma 19:129–133
18. Madjd Z, Parsons T, Watson NF et al (2005) High expression of Lewis y/b antigens is associated with decreased survival in lymph node negative breast carcinomas. Breast Cancer Res 7:R780–R787
19. Goupille C, Marionneau S, Bureau V et al (2000) α1-2 Fucosyltransferase increases resistance to apoptosis of rat colon carcinoma cells. Glycobiology 10:375–382
20. Stahel RA, Lacroix H, Sculier JP et al (1992) Phase I/II study of monoclonal antibody against Lewis Y hapten in relapsed small-cell lung cancer. Ann Oncol 3:319–320
21. Dettke M, Pálfi G, Loibner H (2000) Activation-dependent expression of the blood group-related lewis Y antigen on peripheral blood granulocytes. J Leukoc Biol 68:511–514
22. Tolcher AW, Suqarman S, Gelmon KA et al (1999) Randomized phase II study of BR96-doxorubicin conjugate in patients with metastatic breast cancer. J Clin Oncol 17:478–484
23. Gupta PB, Chaffer CL, Weinberg RA (2009) Cancer stem cells: mirage or reality? Nat Med 15:1010–1012

Virchows Arch (2010) 456:411–422
DOI 10.1007/s00428-010-0886-8

ORIGINAL ARTICLE

Peripheral nerve sheath tumors of the gastrointestinal tract: a multicenter study of 58 patients including NF1-associated gastric schwannoma and unusual morphologic variants

Abbas Agaimy · Bruno Märkl · Julia Kitz · Peter H. Wünsch · Hans Arnholdt · Laszlo Füzesi · Arndt Hartmann · Runjan Chetty

Received: 29 December 2009 / Revised: 13 January 2010 / Accepted: 13 January 2010 / Published online: 13 February 2010
© Springer-Verlag 2010

Abstract The frequency and morphological spectrum of gastrointestinal peripheral nerve sheath tumors (PNSTs) from consecutive case material has not been studied in the c-KIT era. We reviewed all mesenchymal gastrointestinal (GI) lesions at our departments according to current diagnostic criteria. PNSTs formed the third commonest group of mesenchymal GI tumors with a lower frequency (≤5%) compared to gastrointestinal stromal tumors (GISTs; ~50%) and smooth muscle neoplasms (~30%). Granular cell tumors (GCTs; n=31) and schwannomas (n=22) were the most common types of PNSTs encountered. Rare tumors included neurofibromatosis 1 (NF1)-associated PNSTs (n=5) and gastric perineurioma (n=1). Thirteen schwannomas (including also some recent cases) were initially diagnosed as GIST, leiomyoma, or neurofibroma. Unusual histological variants included sigmoid GCT with prominent lipomatous component (n=1), reticular–microcystic schwannoma of small (n=1) and large (n=1) bowel, NF1-associated gastric schwannoma (the first case to date), and psammomatous melanotic colonic schwannoma unrelated to Carney complex (n=1). PNSTs coexisted with GIST in four patients (three had definite NF1). In conclusion, PNSTs of the GI tract are rare uniformly benign neoplasms that may show schwannian, perineurial, fibroblastic, or mixed differentiation. Most of them (92%) occurred sporadically unassociated with NF1 or NF2. Gastrointestinal PNSTs are still underrecognized by general pathologists. Awareness of their diverse morphology will help to avoid confusing them with smooth muscle neoplasms and GIST that they may closely mimic.

Keywords GIST · PNST · Schwannoma · Granular cell tumor · NF1 · Perineurioma

B. Märkl · H. Arnholdt
Institute of Pathology, Klinikum Augsburg
Augsburg, Germany

J. Kitz · L. Füzesi
Institute of Pathology, University Hospital
Göttingen, Germany

P. H. Wünsch
Institute of Pathology, Klinikum Nürnberg
Nürnberg, Germany

R. Chetty
Department of Pathology, University Health Network,
and Department of Laboratory Medicine and Pathobiology,
University of Toronto
Toronto, Canada

A. Agaimy (✉) · A. Hartmann
Pathologisches Institut, Universitätsklinikum Erlangen
Krankenhausstraße 12,
91054 Erlangen, Germany
e-mail: abbas.agaimy@uk-erlangen.de

Introduction

Following the seminal discovery of activating *KIT* mutations in mesenchymal gastrointestinal tumors formerly classified as "smooth muscle" or "neurogenic neoplasms," the term "gastrointestinal stromal tumor" (GIST) has been redefined as a specific clinicopathologic and molecular diagnostic entity with implications for therapy and prognosis [1]. According to current diagnostic criteria, a majority

of primary mesenchymal neoplasms of the gastrointestinal tract (GI tract) represent GISTs [1]. Although the existence of GI neoplasms with true neural differentiation has been long recognized [2, 3], only a few selective series describing the clinicopathologic characteristics of one tumor type of peripheral nerve sheath tumors (PNSTs) from specific GI site have been published in the c-KIT era [4–8]. Thus, the frequency and full spectrum of gastrointestinal PNSTs from a consecutive case material has not been covered in a single study. In our experience, gastrointestinal PNSTs are still underrecognized by general pathologists and may be the source of diagnostic confusion as many of them may be mistaken for smooth muscle neoplasms and GISTs. Because of the completely different therapeutic options and biological potentials of the different categories of mesenchymal GI neoplasms, a precise histological diagnosis is mandatory.

The aim of this study was to analyze the frequency and morphologic diversity of PNSTs in the GI tract, thereby looking for unusual and possibly underrecognized variants that might represent a diagnostic challenge.

Material and method

All mesenchymal lesions of the GI tract from the esophagus to the anorectum at our departments (1997–2009) were retrieved by a computerized search for tumors classified as "neurofibroma, schwannoma, neurinoma, spindle cell tumor, peripheral nerve sheath tumor, neurofibromatosis, GIST, stromal tumor, leiomyoma, leiomyoblastoma, or leiomyosarcoma." Hematoxylin and Eosin (H&E)-stained slides have been reviewed by two experienced pathologists (A.A. & R.C.). One case has been reported previously [9], but more extended follow-up was obtained. Immunohistochemistry (IHC) was performed on 5-μm sections using a polymer Kit purchased from Zytomed systems Ltd., Berlin, Germany according to the manufacturer's instructions and the following antibodies: protein S100 (polyclonal, 1:2,500, DakoCytomation, Glostrup, Denmark), CD56 (1:100, Novocastra), desmin (1:250, DakoCytomation), α-smooth muscle actin (α-SMA; 1:200, DakoCytomation), CD34 (1:200, DakoCytomation), CD117 (polyclonal, 1:200, DakoCytomation), glial fibrillary acidic protein (GFAP; 1:50, DakoCytomation), calretinin (1:2, Zytomed), and α-inhibin (1:100, Serotec, UK). Schwannomas were also stained with a monoclonal antibody recognizing the antigen DOG-1 (1:200, Novocastra). In addition, further markers were applied selectively in some cases, based on relevant differential diagnoses (antibody sources and protocols are available upon request). Follow-up data were obtained from clinical records, from pathology reports, and from treating doctors.

Results

Frequency and distribution of gastrointestinal PNSTs

A total of 58 patients were recovered. PNSTs represented 5% of all mesenchymal tumors of the GI tract in our case material contrasting a percentage of ~50% for GISTs and ~30% for smooth muscle neoplasms. Five patients (8%) were known to have neurofibromatosis 1 (NF1), but none had features of NF2 or other tumor syndrome. Patients were 34 women and 24 men with a mean age of 52 years (range, 17–87). Histologically, tumors were classified as granular cell tumor (n=31), gastrointestinal schwannoma (n=22), gastric perineurioma (n=1), and NF1-associated PNSTs (n=5). Several fibroblastic colorectal polyps were seen but excluded from further analysis due to the controversy regarding their neoplastic nature and relationship to peripheral nerve sheath tumors. No case of sporadic solitary neurofibroma, "epithelioid Schwann cell hamartoma," or conventional malignant PNST (MPNST) was found. The clinicopathologic features of the individual tumor types are discussed in detail below.

Granular cell tumors (Table 1)

These affected 19 women and 12 men aged 17–87 years (mean, 50 years). All were incidental findings during endoscopic investigation for other diseases or for nonspecific upper GI symptoms. Three tumors were ulcerated. Most tumors originated in the distal esophagus/gastroesophageal junction (n=24). Two involved the mid-esophagus. One tumor each originated in the cardia, body, cecum, sigmoid colon, and rectum. Treatment was endoscopic biopsy or marginal polypectomy in almost all cases. In five of ten patients who underwent a control endoscopic biopsy at 8–52 months (mean, 21 months), tumor cells were detected, probably indicating residual tumor, but none showed progressive growth or metastasis. However, most patients were lost to follow-up due to the benign nature of the lesion. Size of the tumors ranged from 2 to 20 mm (mean, 6 mm). Multiple tumors were not observed. Pseudoepitheliomatous squamous hyperplasia of overlying mucosa was a common feature of esophageal lesions (Fig. 1a). All but one tumor were centered in the lamina propria mucosae/submucosa. Tumors revealed typical sheets of large polyhedral cells having granular PAS-positive cytoplasm with hyaline droplets and small centrally located nuclei. All tumors but one showed infiltrating borders, and three have infiltrated into the muscularis propria (Fig. 1b). Focal spindling was seen in two cases (Fig. 1c). One tumor from the sigmoid colon combined features of granular cell tumors (GCT) and submucosal lipoma with a peculiar nodule-in-nodule pattern and predominance of fatty component (Fig. 1d, e). The largest tumor (20 mm) originated in the muscularis propria of the rectum and presented clinically as a

Table 1 Clinicopathologic features of gastrointestinal granular cell tumors (n=31)

No.	Age sex	Histology	Site	Size (mm)	Symptoms/other associated diseases	Treatment	IHC S100	Outcome
1	44 F	Conventional	Esophagus	3	Nonspecific	Biopsied	NA	NA
2	l17 F	Conventional	Esophagus ora serrata	2	Ulcerated + fungi papilloma-like HP	Biopsied	+ve	NA
3	73 M	Conventional	Esophagus distal	10	Nonspecific, ulcerated	Polypectomy (R0)	+ve	NA
4	68 M	Conventional	GEJ	<5 mm	Polyp		+ve	NA
5	42 F	Conventional	GEJ	<5 mm	Polyp		+ve	NA
6	55 M	Conventional	Esophagus	5	Nonspecific	Biopsy, then excised (R0)	NA	NA
7	54 F	Conventional	Esophagus	<5 mm	NA	Biopsied	NA	NA
8	32 F	Conventional	Mid-esophagus	<5 mm	NA	Biopsied	NA	NA
9	36 F	Conventional	Esophagus	2	Nonspecific, polyp	Polypectomy (R0)	+ve	No recurrence at 14 months
10	45 F	Conventional	Esophagus	8	Nonspecific, polyp	Polypectomy (R1)	+ve	Positive biopsy at 8 months
11	41 M	Conventional	Esophagus	4	Nonspecific	Biopsied	+ve	NA
12	62 F	Conventional	Esophagus 19 cm		NA	Biopsied	+ve	Positive biopsy at 52 months (during investigation for AML)
13	39 F	Conventional	Esophagus	2	Nonspecific	Biopsied	+ve	NED at 4 months
14	87 F	Conventional	Esophagus	5	Nonspecific	biopsied	+ve	NA
15	44 F	Conventional	Esophagus 36 cm	2	NA	biopsied	+ve	NED at 18 months
16	56 F	Conventional	Esophagus	5	Reflux	Biopsied	+ve	Alive and well
17	51 M	Conventional	Esophagus	5	Discomfort swallowing	Biopsied	+ve	Alive and well
18	43 M	Conventional	Esophagus	7	Epigastic pain incidental	Biopsied	+ve	Alive and well
19	57 M	Conventional	Esophagus	5	Reflux/Barrett's incidental	Biopsied	+ve	Alive and well
20	64 F	Conventional	Esophagus	6	Incidental asymptomatic	Biopsied	+ve	Alive and well
21	67 M	Conventional	Esophagus	5	Incidental asymptomatic	Biopsied	+ve	Alive and well
22	50 F	Conventional	Esophagus	5	Incidental asymptomatic	Biopsied	+ve	Positive biopsy at 15 months
23	44 M	Conventional	Esophagus	<5 mm	Incidental asymptomatic	Biopsied	+ve	NED at 5 months
24	48 M	Conventional	Esophagus	<5 mm	Incidental asymptomatic	Biopsied	+ve	NA
25	55 F	Conventional	Esophagus	<5 mm	Incidental asymptomatic	Biopsied	+ve	Positive biopsy at 15 months
26	51 F	Conventional	Esophagus	<5 mm	Incidental asymptomatic	Biopsied	+ve	Positive biopsy at 17 and 32` months
27	48 F	Conventional	Cardia	12	Nonspecific	Polypectomy (R1)	+ve	NA
28	58 M	Conventional	Body, residual stomach	13	Ulcerated	Wedge excision	+ve	NED at 2 months
29	58 F	Conventional	Rectum intramural	20	Incidental "as tumor between rectum and vagina"	Complete excision	+ve	Recent case. 5 mm polypoid leiomyoma of M. mucosae of esophagus simultaneously
30	32 F	Conventional focal spindling	Cecum	5	Per anal bleeding, incidental coloscopic finding	Polypectomy (R0)	+ve	NA
31	44 M	Submucosal lipoma-GCT	Sigmoid	5	Perforated diverticulitis	Incidental in diverticular specimen	+ve	NA

GCT granular cell tumor, *NA* not available, *NED* no evidence of disease, *AML* acute myeloid leukemia

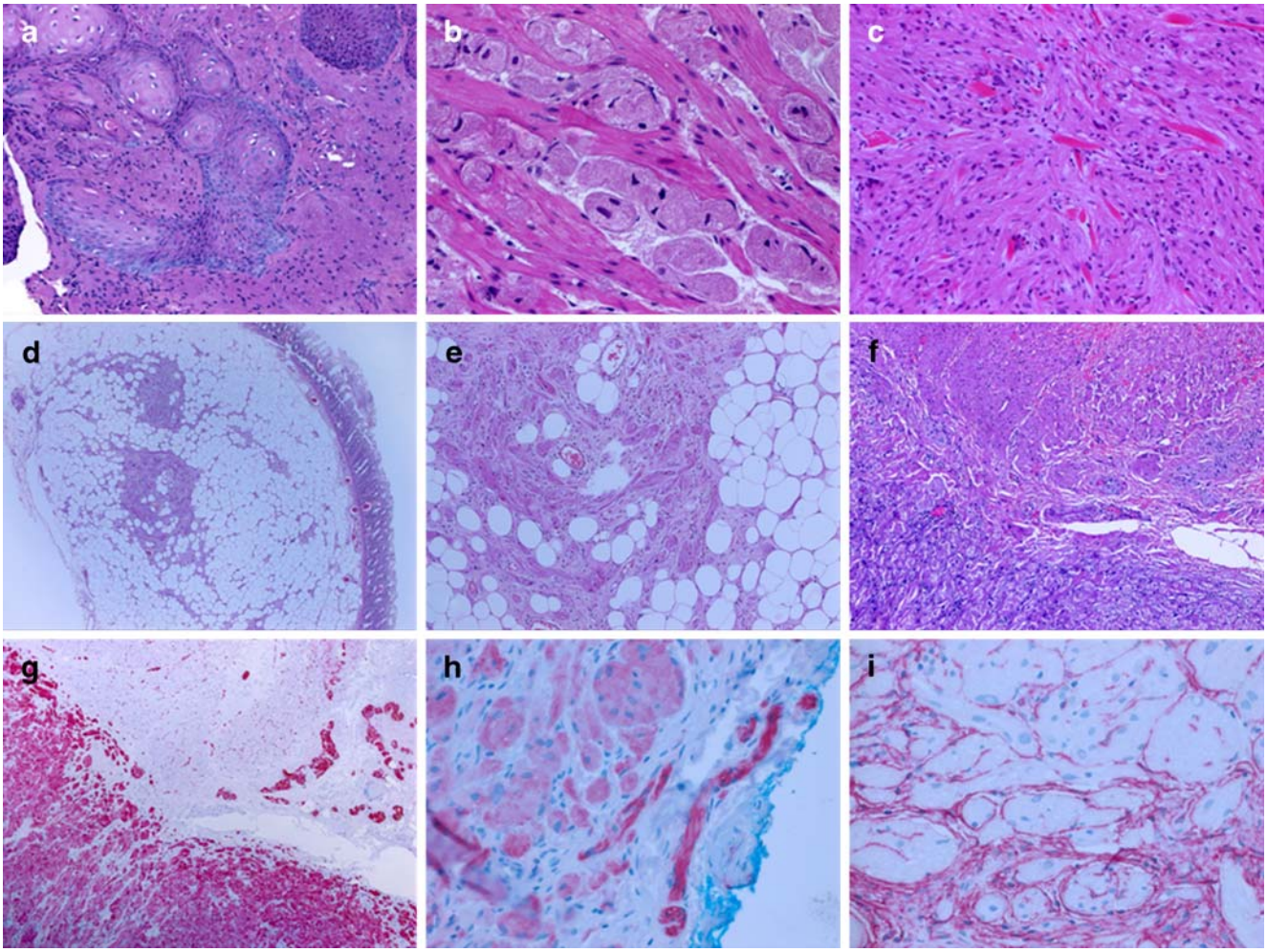

Fig. 1 Representative images of GCTs in the GI tract with subepithelial growth in the esophagus associated with pseudoepitheliomatous hyperplasia (**b**) and infiltration of the muscularis propria (**b**). Prominent spindling mimicking GIST was seen in two cases (**c**). Whole-mount section of lipomatous cecal GCT with nodule-in-nodule pattern (**d**), paucity of tumor cells toward the mucosa contrasts with conventional GCT. Almost equal proportions of fat cells and granular cells were seen at higher magnification (**e**). Rectal GCT (**f**, *lower left*) arising from Auerbach plexus (*upper right*) highlighted with protein S100 immunostaining in **g**. α-Inhibin showed a moderate staining that was less intense than in adjacent nerve on the right (**h**). CD34 reactivity was more prominent at the tumor periphery (**i**, *lower field*)

"rectovaginal septum mass." This tumor blended with the Auerbach plexus in a manner reminiscent of GIST (Fig. 1f, g) and showed focal peritumoral lymphoid cuffs. In tumors with available paraffin blocks or unstained slides, IHC revealed strong expression of protein S100 (17/17; Fig. 1g), CD56 (17/17), and variable expression of calretinin (11/14) and α-inhibin (11/14; Fig. 1h). Four cases stained variably with CD34 in the granular tumor cells as well as in slender bipolar mesenchymal cells scattered between them. CD34 was more prominent toward infiltrating tumor borders (Fig. 1i). All tumors were negative for CD117, desmin, and α-SMA.

Gastrointestinal schwannomas (Table 2)

Patients were 14 women and 8 men aged 38–86 (mean age, 63 years). Sixteen tumors (73%) originated in the stomach, four (18%) in the large bowel (one each in cecum, descendosigmoidal junction, sigmoid colon, and rectum), one in the mid-jejunum, and one at an unspecified intestinal site. Symptoms were nonspecific upper abdominal symptoms or epigastric mass for symptomatic gastric tumors, but many were incidental findings during investigation or at surgery for other diseases. One patient had definite NF1 (see also Table 3). Three patients had one or more other tumors unrelated to NF1: colorectal adenoma/cancer (n=2), breast cancer (n=2), papillary thyroid carcinoma (n=1), and small lymphocytic lymphoma/chronic lymphocytic leukemia (CLL; n=1). Clinical diagnosis was uniformly "gastric wall tumor, most probably GIST." Gastric tumors involved predominantly the body (n=12), two originated in the antrum, and two at unspecified gastric sites. Tumor size ranged from 0.7 to 15.5 cm (mean, 3.5 cm). Ten patients

Table 2 Clinicopathologic features of gastrointestinal schwannomas (n=22)

No.	Age sex	Definite diagnosis	Initial diagnosis	Site	Size (cm)	Symptoms/other disease	NF1	Outcome
1	66 F	Schwannoma	FS: schwannoma	Body small curvature	2.8	Heartburn, intermittent epigastric pain	No	NA
2	86 F	Schwannoma	H&E: sclerosing GIST, IHC: schwannoma	Body/fundus	5.0	Nonspecific	No	45 M ANED
3	59 M	Schwannoma	FS: schwannoma	Body	3.8	Nonspecific	No	43 M ANED
4	62 F	Schwannoma	H&E: leiomyoma, IHC: schwannoma	Antrum	2.0	Nonspecific	No	38 M ANED
5	60 F	Schwannoma	H&E probable leiomyoma, IHC: neurinoma	Body	6.0	Nonspecific, gastric wall tumor	No	NA
6	38 M	Schwannoma	H&E core biopsy: schwannoma, IHC: schwannoma	Body anterior wall	15.5	Nonspecific, gastric wall tumor	No	Recent case
7	67 F	Schwannoma	FS: GIST, neurofibroma	Gastric body anterior wall	5.5	Incidental on CT for retroperitoneal abscess, history of BRCA, PTC, and CLL	No	12 M ANED
8	75 M	Schwannoma	H&E: neurofibroma, IHC: Neurofibroma	Body distal third	3.0	1-mm gastric GIST, diffuse neurofibroma, and carcinoid of appendix, cutaneous neurofibromas	Yes	Died of unrelated disease postoperatively
9	71 M	Schwannoma	Neurofibroma, exclude NF1	Body posterior wall	2.7	Nonspecific	No	77 M ANED
10	73 F	Schwannoma	Neurinoma/PNST	Body	2.5	Duodenal ulcer, nonspecific	No	NA
11	53 M	Schwannoma	GIST	Lesser curve, antrum	2.5	Epigastric pain and bleeding	No	36 M ANED
12	57 F	Schwannoma	Schwannoma	Stomach	1.1	Nonspecific	No	7 M ANED
13	50 M	Schwannoma	Schwannoma	Stomach	3.5	Nonspecific	No	NA
14	66 M	Schwannoma	Schwannoma	Stomach body	4.0	Nonspecific	No	NA
15	58 F	Schwannoma	H&E core biopsy: schwannoma, IHC: schwannoma	Stomach body	4.5	Epigastric mass	No	NA
16	57 F	Schwannoma	GIST	Stomach body large curvature	3.0	Nonspecific	No	Recent case
17	71 F	Schwannoma	GIST	Intestine, unspecified	0.7	Incidental to colorectal adenoma, history of BRCA	No	NA
18	71 M	Schwannoma	Schwannoma	Rectum	0.7	Nonspecific	No	NA
19	66 F	Schwannoma	FS: probable GIST, IHC: schwannoma	Sigmoid-descending colon junction	4.7	Stenosis with increasing constipation, endoscopy, and CT suspicious of GIST	No	Recent case
20	67 F	Reticular schwannoma	BMT; neurinoma	Cecum	1.0	As polyp on follow-up colonoscopy after sigmoid cancer 15 years ago	No	12 M ANED
21	67 F	Reticular schwannoma	GIST, 2nd opinion: unusual GIST, 3rd opinion: unusual PNST	Mid-jejunum	2.2	Incidental to 10.5-cm omental–gastric GIST	No	2 M ANED
22	43 F	Psammomatous melanotic	Neuroendocrine tumor versus GIST	Sigmoid colon	0.5–0.8 each	Incidental on routine endoscopy, no Carney's complex	No	48 M ANED

ANED alive with no evidence of disease, *BMT* benign mesenchymal tumor, *BRCA* breast cancer, *CLL* chronic lymphocytic leukemia/lymphoma, *DD* differential diagnosis, *FS* frozen section, *H&E* hematoxylin and eosin stain, *IHC* immunohistochemistry, *M* month, *NA* not available, *NF1* neurofibromatosis 1, *PNST* peripheral nerve sheath tumor, *PTC* papillary thyroid carcinoma

Table 3 Clinicopathologic features of non-GIST manifestations of NF1 (n=5)

No.	Age sex	Diagnosis	Site	Size (cm)	Symptoms	Other NF1-associated tumors?	GIST?	Follow-up/outcome
1	20 F	Diffuse mucosal neurofibromatosis	Rectosigmoidal junction + small bowel	Diffuse	Nonspecific abdominal symptoms	Cutaneous neurofibromas	No GIST	32 M/ alive and well
2	23 M	Neurofibromatosis Plexiform neurofibroma	Ileum Ileum + mesentery	Diffuse 8	Appendicitis-like symptoms, tumor incidental to appendectomy	Plexiform cutaneous neurofibroma	No GIST	NA
3	36 M	Plexiform neurofibroma	Stomach + small bowel	Multiple, largest 4×4×2	Epigastric pain	Cutaneous neurofibroma, duodenal somatostatinoma	Gastric GIST	24 M/alive and well
4	45 M	3 minute neurofibromas 2 minute neurofibromas	Appendix Stomach	0.3 each multiple	All tumors autopsy findings	Cutaneous neurofibroma. mediastinal MPNST	2 minute gastric GISTs	Died of mediastinal MPNST
5	75 M	Diffuse neurofibroma Schwannoma	Appendix/mesoappendix Gastric body	2 3	Appendicitis-like symptoms Abdominal pain	Diffuse cutaneous neurofibromas, carcinoid of appendix simultaneously	1-mm gastric GIST	Died of unrelated disease postoperatively

NA not available, *NF1* neurofibromatosis 1, *MPNST* malignant peripheral nerve sheath tumor, *M* month

had a mean follow-up of 31.7 months (range, 2–77 months); none had evidence of progressive disease or new tumors. Extended follow-up was obtained for the previously reported patient with melanotic psammomatous schwannoma (48 months); there was no evidence of recurrence or development of new tumors.

Grossly, the majority showed a homogenous tan-yellow or whitish cut surface with strikingly firm to hard consistency so that diagnosis was suspected in some cases upon bisecting the tumor (Fig. 2a). Only nine tumors were initially correctly diagnosed histologically. Initial diagnoses included GIST/sclerosing GIST (n=9), neurofibroma (n=3), and involuted leiomyoma (n=1). Two recent gastric tumors were correctly diagnosed by core needle biopsy. The jejunal tumor (reticular variant) was coincidental to a huge extramural gastric GIST leading to misinterpretation of the large GIST as peritoneal metastasis of the small mural jejunal tumor. All gastric tumors were moderately cellular throughout with abundant wavy collagen fibers. Prominent lymphoid cuffs were seen in all cases (Fig. 2b) but were less prominent in the reticular variant. Of interest, one patient with a gastric schwannoma had a history of small lymphocytic lymphoma/CLL. His tumor displayed extensive lymphoid cuffing that turned out to be neoplastic on IHC and molecular analysis (Fig. 2c). He also had perigastric lymph nodes involved by the CLL. Most tumors showed a variable mixture of microtrabecular, macrotrabecular, nested, storiform, and cellular patterns (Fig. 2d–h). Antoni A and B areas were lacking in all cases as well as true nuclear palisading. However, three tumors including the NF1 associated one had foci of nuclear crowding reminiscent of palisading. Three tumors showed areas of sclerosis and confluent dystrophic calcification superficially reminiscent of calcifying fibrous tumors, but these were usually focal findings in otherwise typical schwannomas. One multifocal sigmoid schwannoma showed sheets of plump to spindled cells, scattered psammoma bodies, and occasional pigmentation consistent with psammomatous melanotic schwannoma. The histologic features of this tumor have been reported in more details previously [9]. One cecal tumor and one jejunal tumor revealed a reticular–microcystic pattern that is reminiscent of perineurioma of soft tissue. The cecal tumor showed slender bipolar cells infiltrating between the mucosal crypts with scattered eosinophils and prominent CD34 reactivity superficially mimicking inflammatory fibroid polyp (Fig. 2i). However, the deeper portion of the tumor within the submucosa showed typical reticular–microcystic pattern (Fig. 2j) with prominent protein S100 expression in all tumor cells (Fig. 2k). IHC revealed a strong expression of protein S100 in all schwannomas (Fig. 2l) and variable usually focal expression of CD56 (11/11) and GFAP (9/9). CD34 was detectable in the stromal cells in areas of sclerosis, but not in tumor cells,

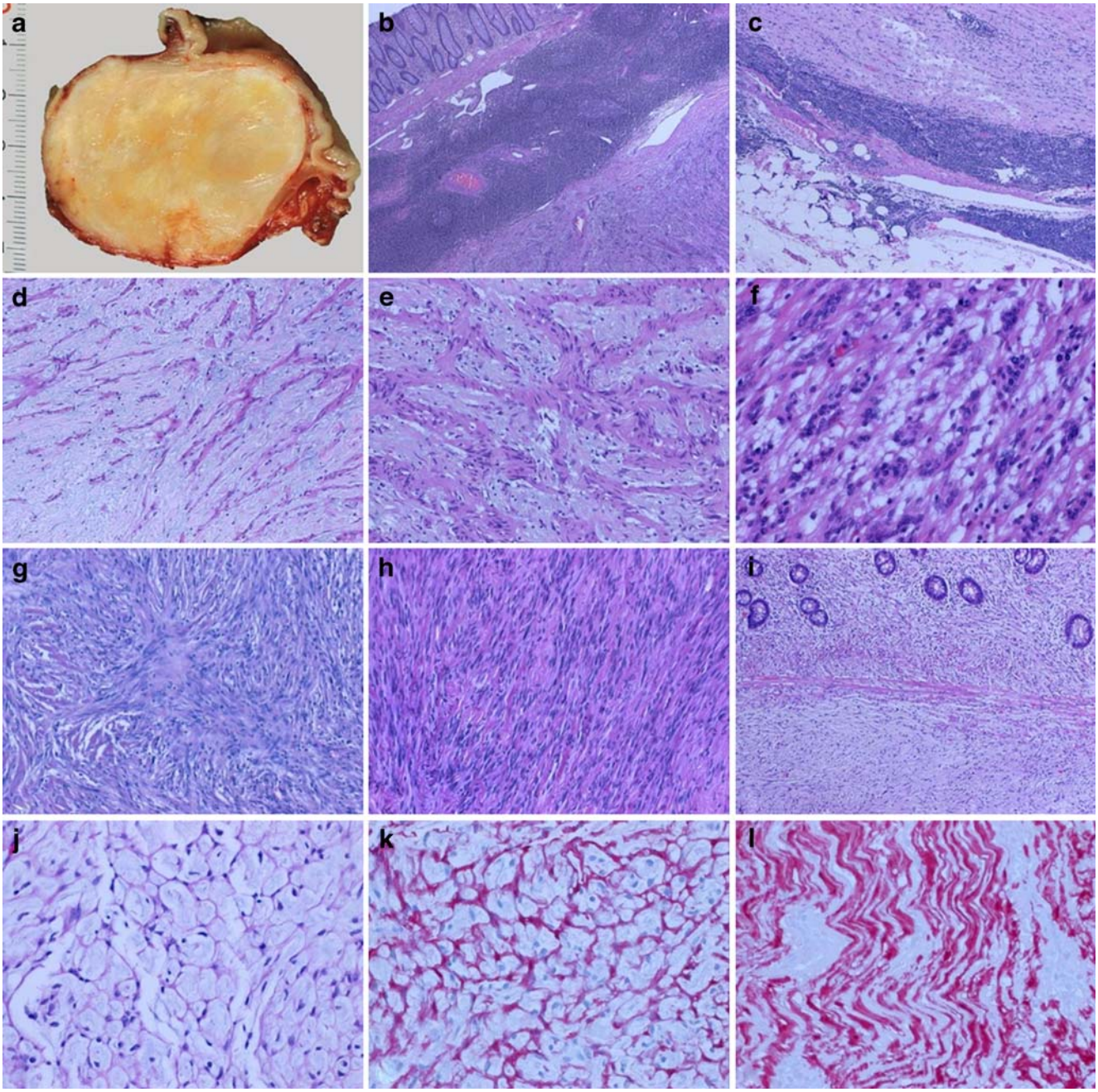

Fig. 2 Gross and microscopic features of gastrointestinal schwannomas: Gastric schwannomas were well circumscribed intramural masses with homogeneous tan-yellow cut surface (**a**). Prominent submucosal lymphoid cuffs were seen in sigmoid schwannoma (**b**). Neoplastic (CLL) lymphoid cuffs in gastric schwannoma showed irregular infiltration into subserosal fat. Microtrabecular (**d**), macrotrabecular (**e**), nested (**f**), storiform (**g**), and cellular (**h**) histologic patterns. Cecal reticular schwannoma infiltrated into both mucosa and submucosa (**i**) with prominent reticular–microcystic pattern in deeper portion of the tumor (**j**) and diffuse S100 expression (**k**). S100 expression in gastric schwannoma was typically diffuse and strong with wavy pattern (**l**)

except for the cecal reticular schwannoma. Scattered epithelial membrane antigen (EMA)-positive perineurial cells were seen in several cases. All six cases examined were negative for calretinin and α-inhibin. All of the schwannomas have been stained with CD117, and 12 cases were also stained with the antibody DOG-1 and were found completely negative for both markers.

Gastric perineurioma

The patient was a 58-year-old man who presented with epigastric pain without relevant clinical history or signs of NF1 or NF2. A 5×3×2 cm measuring mass was excised from the stomach. The patient was alive and well 5 years after surgery. The tumor was well circumscribed but

nonencapsulated and was centered in the submucosa (Fig. 3a). It was composed of slender cells with wavy nuclei and long bipolar cytoplasmic extensions arranged in diffuse pattern with intervening thin capillaries (Fig. 3b). Onion skin pattern and eosinophil-rich infiltrate typically seen in inflammatory fibroid polyp were lacking. Tumor cells expressed diffusely EMA (Fig 3c) and variably CD34, but were negative for S100, CD117, desmin, α-SMA, and h-caldesmon. This tumor lacked the organoid biphasic pattern of the recently described hybrid schwannoma/perineurioma [10].

Gastrointestinal manifestation of NF1 (Table 3)

Five patients presented with GI manifestations of NF1 (other than GIST) at a mean age of 39 years. All had clinical features of NF1. One patient had multiple minute neurofibromas in the gastric fundus and in the vermiform appendix associated with multiple minute gastric fundus GISTs, all diagnosed at autopsy (Fig. 4a, b). He died of locally advanced mediastinal MPNST. Another had a plexiform neurofibroma of ileum/mesentery accompanied by diffuse mucosal neurofibromatosis in the ileum (Fig. 4c–e). One patient had multiple plexiform neurofibromas in stomach and small bowel, in addition to a large gastric GIST and a duodenal somatostatinoma. Another patient presented with stenosing diffuse mucosal neurofibromatosis in the rectosigmoid colon and small bowel at ages 11 and 14 years, respectively. She had no circumscribed tumors. Histologically, GI neurofibromatosis manifested either as diffuse spindle cell proliferation displacing mucosal crypts apart or as a ganglioneuromatous proliferation involving the submucosa (Fig. 4f). The fifth patient, a 75-year-old man, presented with concurrent gastric schwannoma (Fig. 4g–i) and a diffuse neurofibroma in the appendix/mesoappendix in addition to microscopic appendiceal carcinoid. He had a 1-mm microscopic GIST detected incidentally in the gastric specimen intimately associated with the gastric schwannoma (Fig. 4j–l). This patient had multiple cutaneous neurofibromas in the whole body. He died postoperatively of nontumor-related cause.

Discussion

In this study, we reviewed the spectrum of PNSTs of the GI tract in a consecutive case material, demonstrating that PNSTs encompass a heterogeneous group of rare uniformly benign GI tumors that may differentiate along any of the cellular components of the peripheral nerves. PNSTs with schwannian differentiation (GCTs and schwannomas) comprised 91% of all GI PNSTs. The majority occurred sporadically unrelated to NF1 or NF2.

A neurogenic derivation of GCTs has been demonstrated in several studies, and a schwannian line of differentiation is currently widely accepted [11]. GCTs have been documented in the setting of NF1 [12] and as a novel component in hybrid PNSTs of soft tissue [13]. However, their distinct histology warrants their separation from neurofibroma and schwannoma. GCTs of the GI tract comprised ≤5% of all GCTs [11]. The esophagus (80%) and large bowel (10%) are predilection sites in our study

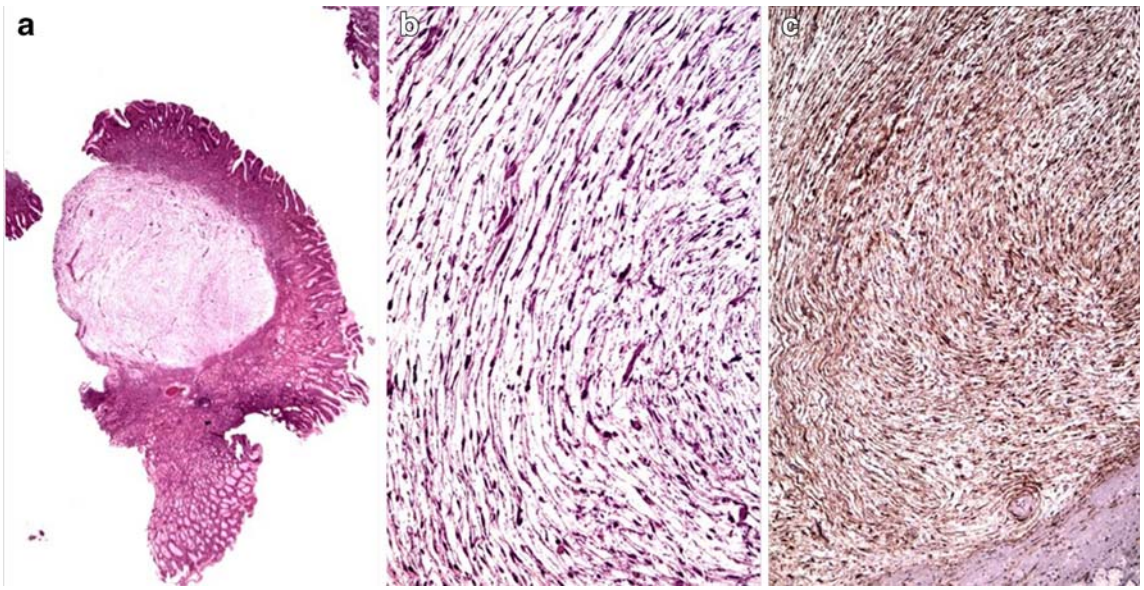

Fig. 3 Histological features of gastric perineurioma. The tumor formed a circumscribed nodular mass occupying the submucosa (**a**). Long slender cells with bipolar cytoplasm were seen at higher magnification (**b**). The tumor cells stained diffusely with epithelial membrane antigen (**c**)

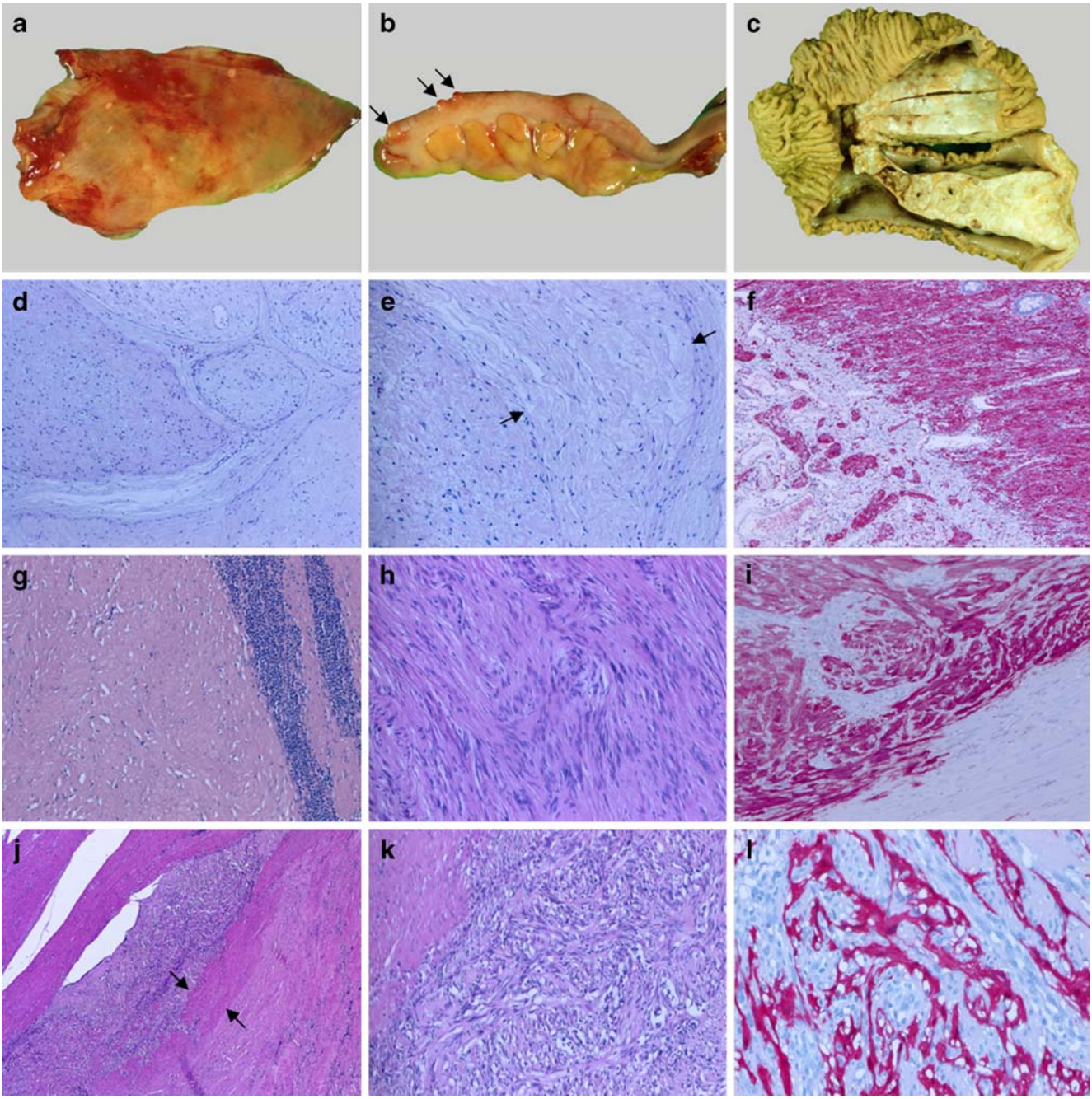

Fig. 4 Spectrum of NF1-associated peripheral nerve sheath tumors of the GI tract. Autopsy specimen showed multiple minute plaque-like nodules on the gastric serosa that turned out to be either minute GISTs or neurofibromas (**a**). Three minute neurofibromas in the appendix from same patient protruded from the serosa (**b**). Large plexiform neurofibroma in the ileal wall/mesentery from another patient formed multiple nodules (**c**, **d**). Reticular perineurioma-like component (*between arrows*) was a common finding at the periphery of neurofibromatous nodules (**e**). Diffuse neurofibromatosis was composed of dense S100-positive spindle cell proliferation separating mucosal crypts (*right*) associated with submucosal ganglioneuromatous hyperplasia (*left*; **f**). NF1-associated sclerosing gastric schwannoma with prominent lymphoid cuffs (**g**), occasional fascicular growth (**h**), and strong diffuse S100 staining (**i**). Microscopic GIST in the midfield separated from sclerosing schwannoma (*lower right*) by muscle bundles (*between arrows*) from same patient (**j**). Higher magnification of the GIST is shown in **k**. Protein S100 staining highlighted prominent neural hyperplasia accompanying the GIST (**l**). The GIST coexpressed CD117 and CD34 (not shown)

and in previous series [14, 15]. Diagnosis of GCTs is usually not problematic. Rare GCTs with prominent spindling may mimic GIST [15, 16], but more typical diagnostic areas are usually present. GCTs are negative for CD117, desmin, α-SMA, and h-caldesmon. They are uniformly S100-positive, and they stain variably with CD56, calretinin, α-inhibin, and CD34 [17, 18]. Infiltration of the muscularis propria may be seen and does not indicate

malignancy. Two GCTs in our series displayed unusual features. The sigmoid colon tumor showed a prominent lipomatous component similar to a recently described cecal tumor [19]. The nature of the adipocytic component (pre-existing submucosal lipoma versus adipocytic differentiation) remains obscure. The uniform distribution of adipocytes and absence of stromal reaction suggested a dual differentiation, but this remains speculative. Adipocytic differentiation has been rarely documented in PNSTs of the soft tissue [20]. Furthermore, rare GCTs have shown hyalinization/calcification [21] and osseous metaplasia [22]. The largest GCT in this study originated from the rectal Auerbach plexus as a rectovaginal septum mass. This unusual intramural variant should be distinguished from GIST, in particular from epithelioid GIST with granular cytoplasmic change [23].

Schwannomas comprise 2–7% of mesenchymal GI neoplasms. To date, less than 200 cases have been reported [3–8, 24]. The stomach was the most common site involved followed by the large bowel. The esophagus and the small bowel are only rarely affected. The age distribution, origin in the muscularis propria, and predilection for gastric body are features shared with GISTs. Grossly, schwannomas lack cystic changes and hemorrhages commonly seen in GISTs. A thin marginal halo (corresponding to lymphoid cuffs) seen on endoscopic ultrasound is a helpful feature in their preoperative evaluation [25]. Schwannomas show a mixture of diverse histological patterns. Their separation from GISTs and smooth muscle tumors is facilitated by the typical histology of the latter and by lower cellularity and the prominent lymphoid cuffs in schwannomas. By IHC, schwannomas are uniformly S100-positive, and they do not stain with CD117 [5, 8] and DOG-1 [26], features that help to separate them from GISTs.

Reticular–microcystic schwannoma is a recently defined rare variant with a predilection for visceral sites [27]. Including our two cases, a total of eight cases of this rare variant were reported in the GI tract; three from the large bowel, three from the small bowel, and two from the stomach [27, 28]. The striking predilection of this variant for the intestine contrasts with its rarity in the stomach where most GI schwannomas occur. Compared to usual GI schwannomas, the reticular–microcystic variant presented at higher mean age (75.8 versus 63 years) and showed higher female predilection (3:1 versus 1.5:1). Seven of the eight patients had a median follow-up of 13 months; none developed progressive disease or recurrence.

In this study, we documented the first NF1-associated GI schwannoma. Although it is possible that this might represent a mere coincidence, the occurrence of a neurogenic neoplasm in an NF1-patient is most likely to be considered a manifestation of the disorder. Given the overlapping features of gastric schwannoma with neurofibroma, the fact that many schwannomas in the current study were initially considered neurofibromas, and the high suspicion of neurofibroma in NF1 patients, it is possible that some GI schwannomas in NF1 patients might have been interpreted as neurofibroma [29, 30]. Of interest, intratumoral axons and perineurial cells were detected in GI schwannomas, supporting a neurofibroma-like histogenesis [31]. Moreover, the study by Lasota et al [32] has shown that loss of heterozygosity (LOH) at *NF2* was rare in GI schwannomas (5%), and no *NF2* mutations could be detected in 13 cases analyzed. Instead, LOH on 17q involving *NF1* occurred frequently in GI schwannomas (50%), suggesting a distinct molecular pathogenesis that is more akin to that of plexiform neurofibroma [32]. However, a recent case of gastric schwannoma harbored a mutation in *NF2* [33], suggesting that the molecular pathogenesis of GI schwannoma is probably heterogeneous. The absence of calretinin and α-inhibin as additional markers of schwannian differentiation [18, 34] in six of our GI schwannomas represents a further argument for a neurofibroma-like histogenesis.

Although ~25% of digestive schwannomas were associated with coincidental GI malignancies [3], the concurrence of GI PNSTs with clinically meaningful GISTs seems to be rare with only two previously reported cases [5, 35] and two other cases in the current study including one patient with NF1. However, coexistence of minute incidental gastric GISTs with PNSTs in two of our NF1 patients might represent a mere coincidence, given the high prevalence of incidental gastric GISTs in the general population [36].

Conventional (soft tissue type) perineurioma is rare in the GI tract. Including our case, five GI neoplasms with features of soft tissue perineuriomas [37] have been reported: two in stomach and one each in jejunum, colon, and esophagus [38–40]. Two cases with follow-up (54 and 60 months) showed a benign course [39]. Two further cases with hybrid features of schwannoma–perineurioma were reported from the colon [10, 41]. However, a group of small polypoid mucosal lesions presumed to show peripheral nerve sheath differentiation was the subject of controversy in several recent reports in the literature. They have been reported as mucosal perineurioma [39], fibroblastic polyps [42], mucosal epithelioid nerve sheath tumor [43], and mucosal Schwann cell hamartoma [44]. The nature and the pathogenesis of these lesions and their relationship, if any, to perineurioma remain currently controversial.

MPNST are quite rare in the GI tract, but their real frequency is unknown. We encountered no MPNST in our cases. Recent case reports (~10 cases) contained no detailed histologic descriptions or microphotographs, making it difficult to rule out sarcomatoid carcinoma and other spindle cell neoplasms [45]. Moreover, it is appreciated that most malignant GI schwannomas preceding the c-KIT era probably represented GIST.

In summary, we reported on a series of PNSTs of the GI tract demonstrating a wider variation in their clinicopatho-

logic profiles and histology including the first NF1-associated GI schwannoma and other unusual histological variants that posed diagnostic challenge. Awareness of the diverse histologic appearance of these mostly benign rare tumors should facilitate their recognition and separation from the more common GI stromal tumors and smooth muscle neoplasms that they may closely mimic both grossly and histologically.

Conflict of interest None.

References

1. Miettinen M, Lasota J (2006) Gastrointestinal stromal tumors: pathology and prognosis at different sites. Semin Diagn Pathol 23:70–83
2. Yagihashi S, Kimura M, Kurotaki H et al (1987) Gastric submucosal tumours of neurogenic origin with neuroaxonal and Schwann cell elements. J Pathol 153:41–50
3. Daimaru Y, Kido H, Hashimoto H et al (1988) Benign schwannoma of the gastrointestinal tract: a clinicopathologic and immunohistochemical study. Hum Pathol 19:257–264
4. Sarlomo-Rikala M, Miettinen M (1995) Gastric schwannoma—a clinicopathological analysis of six cases. Histopathology 27:355–360
5. Miettinen M, Shekitka KM, Sobin LH (2001) Schwannomas in the colon and rectum: a clinicopathologic and immunohistochemical study of 20 cases. Am J Surg Pathol 25:846–855
6. Kwon MS, Lee SS, Ahn GH (2002) Schwannomas of the gastrointestinal tract: clinicopathological features of 12 cases including a case of esophageal tumor compared with those of gastrointestinal stromal tumors and leiomyomas of the gastrointestinal tract. Pathol Res Pract 198:605–613
7. Goh BK, Chow PK, Kesavan S et al (2008) Intraabdominal schwannomas: a single institution experience. J Gastrointest Surg 12:756–760
8. Hou YY, Tan YS, Xu JF et al (2006) Schwannoma of the gastrointestinal tract: a clinicopathological, immunohistochemical and ultrastructural study of 33 cases. Histopathology 48:536–545
9. Chetty R, Vajpeyi R, Penwick JL (2007) Psammomatous melanotic schwannoma presenting as colonic polyps. Virchows Arch 451:717–720
10. Hornick JL, Bundock EA, Fletcher CD (2009) Hybrid schwannoma/perineurioma: clinicopathologic analysis of 42 distinctive benign nerve sheath tumors. Am J Surg Pathol 33:1554–1561
11. Scheithauer BW, Woodruff JM, Erlandson RA (1999) Tumors of the peripheral nervous system. In: Rosai J, Sobin LH (eds) Atlas of tumor pathology, 3rd series, fascicle 24. Armed Forces Institute of Pathology, Washington DC
12. Finkel G, Lane B (1982) Granular cell variant of neurofibromatosis: ultrastructure of benign and malignant tumors. Hum Pathol 13:959–963
13. Zarineh A, Costa ME, Rabkin MS (2008) Multiple hybrid granular cell tumor-perineuriomas. Am J Surg Pathol 32:1572–1577
14. Johnston MJ, Helwig EB (1981) Granular cell tumors of the gastrointestinal tract and perianal region: a study of 74 cases. Dig Dis Sci 26:807–816
15. Parfitt JR, McLean CA, Joseph MG et al (2006) Granular cell tumours of the gastrointestinal tract: expression of nestin and clinicopathological evaluation of 11 patients. Histopathology 48:424–430
16. Prematilleke IV, Sujendran V, Warren BF et al (2004) Granular cell tumour of the oesophagus mimicking a gastrointestinal stromal tumour on frozen section. Histopathology 44:502–503
17. Maiorano E, Favia G, Napoli A et al (2000) Cellular heterogeneity of granular cell tumours: a clue to their nature? J Oral Pathol & Med 29:284–290
18. Fine SW, Li M (2003) Expression of calretinin and the alpha-subunit of inhibin in granular cell tumors. Am J Clin Pathol 119:259–264
19. Mori T, Orikasa H, Shigematsu T et al (2006) An Ultrastructural and immunohistochemical study of a combined submucosal granular cell tumor and lipoma of the colon showing a unique nodule-in-nodule structure: putative implication of CD34 or prominin-2-positive stromal cells in its histopathogenesis. Virchows Arch 449:137–139
20. Plaza JA, Wakely PE Jr, Suster S (2006) Lipoblastic nerve sheath tumors: report of a distinctive variant of neural soft tissue neoplasm with adipocytic differentiation. Am J Surg Pathol 30:337–344
21. Hong R, Lim SC (2009) Granular cell tumor of the cecum with extensive hyalinization and calcification: a case report. World J Gastroenterol 15:3315–3318
22. Lee KH, Cho JH, Han YW et al (2006) A rare case of ossifying granular cell (Abrikossoff) tumour. Acta Derm Venereol 86:548–549
23. Adamiak A, Lee CH, Nielsen TO et al (2009) Duodenal epithelioid gastrointestinal stromal tumor with prominent granular cell features. Hum Pathol 40:599–602
24. Hirasaki S, Kanzaki H, Fujita K et al (2008) Ileal schwannoma developing into ileocolic intussusception. World J Gastroenterol 14:638–640
25. Jung MK, Jeon SW, Cho CM et al (2008) Gastric schwannomas: endosonographic characteristics. Abdom Imaging 33:388–390
26. Miettinen M, Wang ZF, Lasota J (2009) DOG1 antibody in the differential diagnosis of gastrointestinal stromal tumors: a study of 1840 cases. Am J Surg Pathol 33:1401–1408
27. Liegl B, Bennett MW, Fletcher CD (2008) Microcystic/reticular schwannoma: a distinct variant with predilection for visceral locations. Am J Surg Pathol 32:1080–1087
28. Tozbikian G, Shen R, Suster S (2008) Signet ring cell gastric schwannoma: report of a new distinctive morphological variant. Ann Diagn Pathol 12:146–152
29. Fuller CE, Williams GT (1991) Gastrointestinal manifestations of type 1 neurofibromatosis (von Recklinghausen's disease). Histopathology 19:1–11
30. Basile U, Cavallaro G, Polistena A et al (2010) Gastrointestinal and retroperitoneal manifestations of type 1 neurofibromatosis. J Gastrointest Surg 14:186–194
31. Zámecník M, Mukensnabl P, Sokol L et al (2004) Perineurial cells and nerve axons in gastrointestinal schwannomas: a similarity with neurofibromas. An immunohistochemical study of eight cases. Cesk Patol 40:150–153
32. Lasota J, Wasag B, Dansonka-Mieszkowska A et al (2003) Evaluation of NF2 and NF1 tumor suppressor genes in distinctive gastrointestinal nerve sheath tumors traditionally diagnosed as benign schwannomas: a study of 20 cases. Lab Invest 83:1361–1371
33. Ogasawara N, Sasaki M, Ishiguro H et al (2009) Gastric schwannoma with adjacent external progression harbored aberrant NF2 gene. Dig Endosc 21:192–195
34. Fine SW, McClain SA, Li M (2004) Immunohistochemical staining for calretinin is useful for differentiating schwannomas from neurofibromas. Am J Clin Pathol 122:552–559
35. Ince AT, Yavuzer D, Kiliç G et al (2008) Coincidental occurrence of granular cell tumor and gastrointestinal stromal tumor in a patient. Turk J Gastroenterol 19:135–136
36. Agaimy A, Wünsch PH, Hofstaedter F et al (2007) Minute gastric sclerosing stromal tumors (GIST tumorlets) are common in adults and frequently show c-KIT mutations. Am J Surg Pathol 31:113–120
37. Hornick JL, Fletcher CD (2005) Soft tissue perineurioma: clinicopathologic analysis of 81 cases including those with atypical histologic features. Am J Surg Pathol 29:845–858

38. Agaimy A, Wünsch PH (2005) Perineurioma of the stomach: a rare spindle cell neoplasm that should be distinguished from gastrointestinal stromal tumor. Pathol Res Pract 201:463–467
39. Hornick JL, Fletcher CD (2005) Intestinal perineuriomas: clinicopathologic definition of a new anatomic subset in a series of 10 cases. Am J Surg Pathol 29:859–865
40. Kelesidis T, Tarbox A, Lopez M et al (2009) Perineurioma of esophagus: a first case report. Am J Med Sci 338:230–232
41. Emanuel P, Pertsemlidis DS, Gordon R et al (2006) Benign hybrid perineurioma-schwannoma in the colon. A case report. Ann Diagn Pathol 10:367–370
42. Groisman GM, Polak-Charcon S (2008) Fibroblastic polyp of the colon and colonic perineurioma: 2 names for a single entity? Am J Surg Pathol 32:1088–1094
43. Lewin MR, Dilworth HP, Abu Alfa AK et al (2005) Mucosal benign epithelioid nerve sheath tumors. Am J Surg Pathol 29:1310–1315
44. Gibson JA, Hornick JL (2009) Mucosal Schwann cell "hamartoma": clinicopathologic study of 26 neural colorectal polyps distinct from neurofibromas and mucosal neuromas. Am J Surg Pathol 33:781–787
45. Telem DA, Pertsemlidis D (2008) Malignant peripheral nerve sheath tumor: an unusual cause of intussusception. J Gastrointest Surg 12:1609–1611

Virchows Arch (2010) 456:423–431
DOI 10.1007/s00428-009-0872-1

ORIGINAL ARTICLE

Striking LD_{50} variation associated with fluctuations of CYP2E1-positive cells in hepatic lobule during chronic CCl_4 exposure in mice

Hiroshi Irie · Anshin Asano-Hoshino · Yoshihisa Sekino · Makoto Nogami · Tomoyuki Kitagawa · Hiroaki Kanda

Received: 6 September 2009 / Revised: 1 December 2009 / Accepted: 6 December 2009 / Published online: 13 February 2010
© Springer-Verlag 2010

Abstract Intraperitoneal injection of serially diluted carbon tetrachloride (CCl_4) from 0.2 to 2.0 ml/kg produced an LD_{50} value of 0.46 ml/kg in the normal mouse. Following repeated administration of 0.2 ml/kg CCl_4 twice a week for 1 and 3 months, the LD_{50} values were over 2.0 and 0.72 ml/kg, respectively. A single administration of 0.2 ml/kg CCl_4 induced, within 24 h, apoptotic death of liver cells in the centrilobular zone 3 that were observed positive in cytochrome P450 2E1 (CYP2E1). However, after repeated exposure to 0.2 ml/kg twice a week for 1 month, cells in the centrilobular area were almost completely replaced with CYP2E1-negative cells. These cells were tolerant to CCl_4. After 3 months of exposure, a considerable number of CYP2E1-positive hepatocytes were observed throughout the periportal zone 1 and intermediate zone 2. Thus, fluctuations in CYP2E1-positive cells during chronic exposure to low doses of CCl_4 induced tolerance, which can be partially lost after prolonged CCl_4 exposure.

H. Irie (✉) · A. Asano-Hoshino · Y. Sekino
Departments of Anatomy,
Teikyo University School of Medicine,
Kaga2-11-1, Itabash-Ku,
Tokyo 173-8605, Japan
e-mail: iriehiro@med.teikyo.u-ac.jp

M. Nogami
Department of Legal Medicine,
Teikyo University School of Medicine,
Kaga2-11-1, Itabash-Ku,
Tokyo 173-8605, Japan

T. Kitagawa · H. Kanda
Department of Pathology, Cancer Research Institute,
Ariake, Koutou-Ku, 3-10-6,
Tokyo 135-8550, Japan

Keywords Carbon tetrachloride · Centrilobule · CYP2E1 · Apoptosis

Introduction

Carbon tetrachloride (CCl_4) induces hepatic injury in humans and experimental animals [1–4]. It is the most extensively studied among hepatotoxins. Centrilobular liver necrosis is observed in human cases of accidental acute CCl_4 poisoning as well as in exposure in experimental animals. In rodents, a single dose of CCl_4 causes extensive centrizonal necrosis followed by complete histological reconstitution in a couple of weeks [4]. It is also known that repeated administration of CCl_4 leads to liver fibrosis extending from the portal triad to parenchyma, the reasons for which remain to be understood.

What is clear so far is that pre-treatment with small doses of CCl_4 renders the rat liver resistant to subsequent large doses [5–12]. This induced tolerance was thought to be somehow related to alterations in CCl_4 metabolites. It is known that this phenomenon is an example of the autoprotection from toxic substances. The accepted mechanism for CCl_4 autoprotection is based on the destruction CCl_4 bioactivation system by the low (protective) dose of CCl_4. But the precise mechanism for this phenomenon remained to be further studied.

Cytochrome P450 (CYP) is involved in the metabolism of CCl_4 and is known to be related to liver injury. Of the multiple CYP forms present in the liver endoplasmic reticulum, CYP2E1 has been identified as a key-metabolizing enzyme for CCl_4. CYP2E is a xenobiotic-metabolizing enzyme that produces highly toxic radicals from CCl_4 causing the liver injury [1–3, 13–17]. In fact, as reported recently in support of this notion, the hepatic

damage by CCl_4 was not observed once CYP2E1 was knocked out in mice [18–20]. Furthermore it is of considerable interest that this enzyme is also related to the metabolism of alcohol and acetaminophen [2, 3, 21, 22]. CYP2E1 is induced by ethanol and produces reactive oxygen species in ethanol metabolism [23]. There are conflicting reports of the direct involvement of these reactive oxygen species in causing liver damage in alcohol consumption. It should be pointed out here, however, that in prior exposure to alcohol in animals or in human cases of alcohol abuse, CCl_4-induced hepatotoxicity is enhanced [24–27].

The present study was carried out in an attempt to elucidate the mechanisms of tolerance to CCl_4. We report here a striking variation of LD_{50} values in mice following repeated administration of small doses of CCl_4 and that this variation was associated with zonal fluctuations of CYP2E1-positive cells in the exposed liver. Morphological features in acute and chronic CCl_4 exposure-induced liver lesions were correlated with the distribution of CYP2E1.

Materials and methods

Materials

CCl_4 of a 99.8% purity and olive oil were purchased from Kanto Chemical Co. (Tokyo) and Miyazawa Chemicals Co. (Tokyo), respectively. BALB/c male mice were obtained from Charles River Laboratories and used at 6–8 weeks of age (weighing approximately 25 g). All animal experiments were performed in compliance with the principles of laboratory animal care (NIH publication No. 86–23, revised 1985) and with Teikyo University School of Medicine Committee guidelines.

Development of tolerance to CCl_4 and CCl_4 LD_{50} after chronic exposure

The experimental schedule used for the development of tolerance to CCl_4 was similar to the method normally used for the induction of liver cirrhosis [4]. One hundred and fifty mice were injected i.p. twice a week with 0.2 ml/kg CCl_4, which is below the LD_{50} dosage. Body weights were determined once every 2 weeks, and corresponding volumes of CCl_4 doses equivalent to 0.2 ml/kg were used. At either 1 or 3 months, six groups that consisted of 10 mice in each were injected i.p. with serial dilutions (*v*/*v*) of 0.2, 0.4, 0.6, 0.8, and 1.0 ml/kg, and 2.0 ml/kg CCl_4 was diluted with olive oil. The mice were carefully observed for clinical signs of CCl_4 exposure and monitored for survival. In the control, 140 mice were injected i.p. with 0.2 ml/kg of olive oil twice a week. At both 1 and 3 months, six groups of 10 control mice were challenged with serially diluted CCl_4 for LD_{50} examination in the same way as the mice with chronic exposure to CCl_4.

Effects of 0.2 ml/kg CCl_4 injection

Thirty mice were injected i.p. with a single administration of 0.2 ml/kg CCl_4. Five mice for each of six time points were killed at 0, 6, 12, 24, 48, and 72 h. In addition, five mice with chronic exposure to CCl_4 were killed at both 1 and 3 months. Mouse livers were removed, fixed with 10% neutral buffer formalin, and embedded in paraffin. Paraffin blocks were sectioned by a microtome and stained with hematoxylin and eosin. Body weight and liver weight were measured at autopsies performed at 0 h, 1 month, and 3 months. Unfixed liver tissue fragments were saved simultaneously for western blots and kept at −80°C.

Liver enzyme assays

Blood samples were collected at each time point of 12, 24, 48, or 72 h after single i.p. injection of 0.2 ml/kg CCl_4. In either 1- or 3-month experiment, mice were injected twice a week with 0.2 ml/kg CCl_4, and blood samples were collected before each injection for the enzyme assay. Alanine aminotransferse (ALT) and aspartate aminotransferse (AST) were measured in sera using conventional methods [28].

Apoptosis (TUNEL) staining

TUNEL (terminal deoxynucleotidyl transferase biotin-dUTP nick end labeling) staining was performed using an In Situ Cell Death Detection Kit, POD (Boehringer-Mannheim, Mannheim, Germany) as instructed in the manual. Deparaffinized sections were dehydrated by an alcohol series and incubated with proteinase K (20 μg/ml in 10 mM Tris–HCl, pH7.4) at 37°C for 15 min. After blocking with 3% bovine serum albumin in phosphate-buffered saline (PBS) for 20 min, the sections were exposed to the TUNEL reaction mixture, including fluorescein-labeled nucleotide and terminal deoxynucleotidyl transferase, at 37°C for 60 min. Subsequently, peroxidase-labeled goat anti-fluorescein antibody was mixed at 37°C for 30 min, followed by incubation with DAB (3,3′-diaminobenzidine tetrahydrochloride) substrate at a room temperature for 10 min. Counterstaining was done with Meyer's hematoxylin solution for 5 s.

Immunohistochemistry

For CYP2E1 staining, DAKO universal kit (DAKO, Denmark) was used. The specimens from specific time

points were prepared by the microtome cutting of paraffin blocks into 4-μm-thick sections. Specimens were incubated in 0.1% hydrogen peroxidase for 5 min and washed in PBS. After blocking the non-specific antibody binding, specimen sections were incubated with 100 μl aliquots of anti-rat CYP2E1 rabbit antibody (Chemicon International, Inc., USA) diluted 500 times in PBS containing 1% BSA (Sigma Chemical Co., Germany) at 4°C, washed three times with PBS, and incubated in anti-rabbit immunoglobulin goat antibody for 30 min. Immunoreactivity was visualized by incubating the specimens with DAB.

Morphometric analysis of P450 2E1 in the liver tissue

Olympus life science edition software (FLVFS-LS) was used for the morphometric analysis of change in the P450 2E1 area of the mouse liver after administration of CCl_4. Briefly, the liver tissues of three mice from each time point after administration of CCl_4 were stained for P450 2E1 immunohistochemically. The positive area was measured in a 100-times-magnified visual field of the light microscope, and a ratio of the positive area to the overall area of visual field was calculated.

Western blot

Lysis buffer (0.1 M Tris, 1% 2-mercaptoethanol, 5% SDS, and 0.002% bromophenol blue) was added to liver tissues (approximately 0.1 g) at the time points indicated, and the mixture was boiled for 5 min. Ten-microgram protein-equivalent liver tissue homogenates were applied in each well. Proteins were separated by electrophoresis on polyacrylamide gels in a 5–15% continuous gradient (Mini-PROTEAN II Ready Gels, Bio-Rad Laboratories) in the presence of 0.1% SDS. Separated proteins were transferred electrophoretically to nitrocellulose membranes (Bio-Rad Laboratories). Non-specific protein binding was blocked by treating the membranes with Tris-buffered saline (TBS; 25 mM Tris–HCl, 150 mM NaCl, pH7.4) containing 0.05% Tween 20 (TBS-T) and 3% skim milk (Wako Pure Chemical Industries, Tokyo) at 37°C for 1 h. Next, the membranes were incubated overnight with 10 μl of anti-rat CYP2E1 rabbit antibody (Chemicon International, Inc., USA) and rabbit polyclonal to beta actin antibody (abcam plc, Cambridge, UK) in 5 ml of TBS-T containing 1% skim milk at 4°C. After washing with TBS-T, the membranes were incubated at 37°C for 1 h with peroxidase-conjugated anti-rabbit goat serum (DAKO, Denmark), washed three times with TBS-T and once with TBS. DAB and hydrogen peroxide were added for staining.

Statistical analysis

Student's paired *t* test was used to determine the significance of differences in mouse body weights and liver weights in the mice administered with CCl_4 twice a week for 1 and 3 months, and in the non-treated control. The Cochran–Mantel–Haenszel test was used to analyze the significance of CCl_4 LD_{50} values in the mice administered with CCl_4 twice a week for 1 and 3 months and in the non-treated control [29]. Statistical analysis was performed using SAS statistical software (version 8.2; SAS Institute, Japan).

Results

Toxicity profile in mice with and without repeated administration of 0.2 ml/kg

The mice without prior exposure to CCl_4 became immobile in 1 h after injection of 2 ml/kg of undiluted CCl_4, and all died within 12 h. Ten mice challenged with 0.8 ml/kg died within 2 or 3 days. One half of mice challenged with 0.4 ml/kg recovered and survived to give an LD_{50} value of 0.46 ml/kg (Fig. 1a). In the group with prior administration of 0.2 ml/kg CCl_4 twice a week for 1 month, over 50% of mice survived the challenge of undiluted CCl_4 (Fig. 1b). The LD_{50} of mice exposed to 0.2 ml/kg CCl_4 twice weekly for 1 month prior to the serial dilution challenge was over 2 ml/kg. In the mice exposed to 0.2 ml/kg CCl_4 twice a week for 3 months, the LD_{50} value was 0.72 ml/kg (Fig. 1c). Evidently, the longer pre-treatment period rendered the animals less tolerant to CCl_4. In the Cochran–Mantel–Haenszel test, the LD_{50} values obtained in the serial dilution challenge for three groups of mice with and without prior treatment with 0.2 ml/kg CCl_4 were statistically significant ($P<0.001$). The LD_{50} in the mice given olive oil only was similar to that of the non-treated mice. Therefore, the mice with prior exposure to 0.2 ml/kg CCl_4 appeared to develop tolerance to CCl_4, and the tolerance once developed decreased in the course of prolonged exposure.

Clinicals

The mice bristled, became increasingly inactive in 12 to 24 h after the first 0.2 ml/kg CCl_4 injection, and were completely immobile by 24 h; a month after this initial and repeated challenge, the mice recovered to appear normal and not particularly different from the untreated control; in 2 months, the mice behaved abnormally in that they ran around wildly and jumped to avoid injection; in 3 months, this excited behavior disappeared even upon repeated

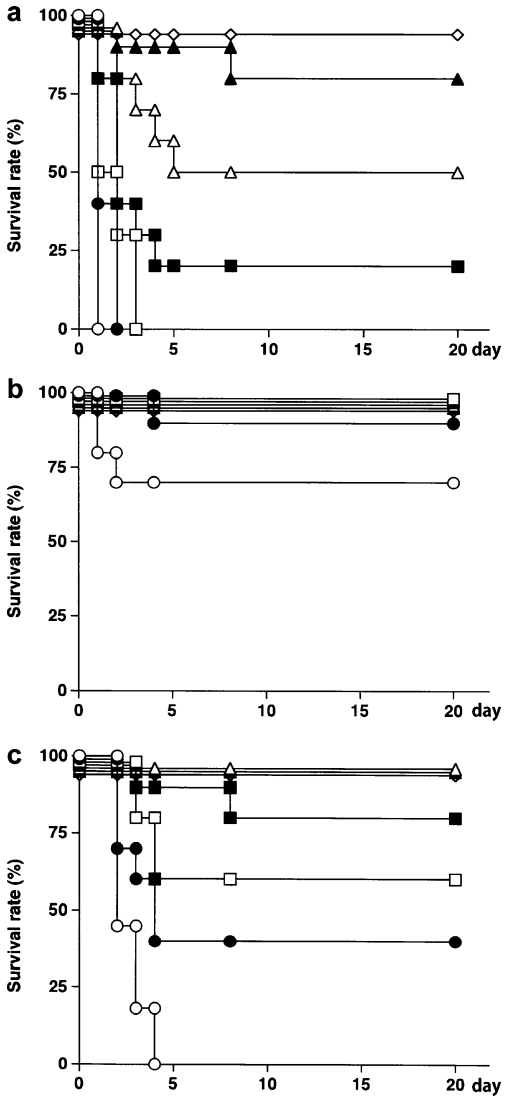

Fig. 1 Fluctuation of LD_{50} in BALB/c mice challenged with serially graded CCl_4. **a** Non-treated mice; **b** 0.2 ml/kg CCl_4, twice a week, repeatedly for 1 month; **c** 0.2 ml/kg CCl_4, twice a week, repeatedly for 3 months. *Empty circles* undiluted 2 ml/kg CCl_4, *filled circles* 1 ml/kg diluted CCl_4, *empty squares* 0.8 ml/kg diluted CCl_4, *filled squares* 0.6 ml/kg diluted CCl_4, *empty diamonds* 0.4 ml/kg diluted CCl_4, *filled triangles* 0.2 ml/kg diluted CCl_4, and *empty triangles* 0.05 ml of olive oil only. The Cochran–Mantel–Haenszel test was used to analyze the significance of the LD_{50} values in mice injected with 0.2 ml/kg CCl_4 twice a week for 1 and 3 months and in the non-treated control. Mortality rate (dead mice/total mice) of non-treated group versus 1-month group was 56.2% versus 5.0%. The rate of non-treated group versus 3-month group was 56.2% versus 27.5%. The rate of 1-month group versus 3-month group was 5.0% versus 27.5%. The confidence interval of 95% in the difference of rate between the two groups did not include 0%. In **b** and **c**, long-term experiments, only one mouse died 2 days after the third administration of 0.2 ml/kg in the 3-month experiment

injections, and the mice became less mobile than the control. The abnormal behavior observed in 2 months after the hepatotoxin exposure may derive from portal systemic encephalopathy caused by chronic liver damage.

Serum ALT and AST levels

Serum levels of ALT and AST in mice administered with 0.2 ml/kg CCl_4 are shown in Table 1. All mice survived the injection of 0.2 ml/kg CCl_4. At 24 h, the levels of these enzymes were 20,000 and 18,900 units/l, respectively, indicating marked impairment of the liver function or so-called fulminant hepatic failure. These enzymatic levels decreased in the mice that survived 1-month exposure to 0.2 ml/kg CCl_4 but increased again to 2,928 and 2,235 units/l, respectively, in the mice with 3-month exposure. In either 1- or 3-month experiment, mice were injected twice a week with 0.2 ml/kg CCl_4, and blood samples were collected before each injection for the enzyme assay. Therefore, the enzyme levels were those in 2–3 days after the last injection. These data of serum enzyme levels indicated increasing chronic liver dysfunction that occurred in the mice with prolonged 3-month exposure to 0.2 ml/kg CCl_4. The control mice administered with olive oil alone did not show liver dysfunction.

Mouse body weight and liver weight

No significant difference was observed in body weight between non-treated mice, olive oil-administered mice and CCl_4-treated mice at 1 and 3 months. However, there was a significant difference between the liver weights of CCl_4-treated mice and non-treated or oil-administered mice as shown in Table 2. The body weights and liver weights of oil-administration were similar to those of untreated mice.

Gross and microscopic appearances of 0.2 ml/kg CCl_4-treated mouse liver

The liver shrunk and changed grayish to a grayish-brown color 12 to 24 h after 0.2 ml/kg CCl_4 administration (Fig. 2b) but recovered to be a brownish color in 96 h. After 1 month of repeated exposure to 0.2 ml/kg CCl_4, the liver was swollen, with an uneven nodular surface (Fig. 2c). After 3 months, the liver was more swollen than after 1 month, and the overall appearance was similar to liver cirrhosis. Several large nodules were observed in the livers of these mice (Fig. 2d, arrows).

Histologically, a few acidophilic liver cells died with leukocyte infiltration within 6 h of 0.2 ml/kg CCl_4 administration (Fig. 3b), and centrilobular liver cells died increasingly over the next 12 h. Compared with the liver of a non-treated mouse (Fig. 3a), the liver cells close to the central veins appeared homogenous, stainable by eosin and frequently contained pyknotic or completely degenerated nuclei. The centrilobular lesion corresponded to so-called zone 3 and was observed expanded (Fig. 3c). Furthermore, lytic necrosis occurred at the center of the lobule. The dead

Table 1 Serum ALT and AST of mice with i.p. injection of 0.2 ml/kg CCl_4

	0	12h	24h	48h	72h	1m	3m
ALT (U)	19±3[a]	20,000±253	13,625±364	2,691±103	696±23	1,240±33	2,938±119
AST (U)	17±1.3[b]	18,900±435	12,500±126	2,480±93	500±24	1,038±23	2,235±203

[a] Mean±SE value of serum ALT of three mice

[b] Mean±SE value of serum AST of three mice

h hours, *m* month

area was clearly demarcated from the intact area. Approximately 72 h after 0.2 ml/kg CCl_4 injection, liver cells began to regenerate in the periportal area of zones 1 and 2 with concomitant shrinkage of the centrilobular lesion. The centrilobular area (zone 3) was observed reconstituted thereafter even in the course of 1 month repeated 0.2 ml/kg CCl_4 administration (Fig. 3d), though pericellular fibrosis appeared in a few cases.

After 3 months of repeated exposure to 0.2 ml/kg CCl_4, apoptotic cells and calcified cells were observed scattered around the periportal zone 1 areas (Fig. 3e). Zone 3 was preserved intact but the periportal area appeared inflamed. Strands of fibrous tissue radiated from the portal tracts and broke up the lobule into small irregular masses of liver cells that looked like irregular fibrosis or marked periportal fibrosis. The fibrosis appeared similar to the liver cirrhosis observed after 6 month of repeated exposure to 0.2 ml/kg CCl_4 (data not shown).

TUNEL-positive cells

The distribution of TUNEL-positive cells during chronic exposure to CCl_4 was examined (Fig. 3f–j). In 24 h after 0.2 ml/kg CCl_4 injection, the center of the positive area became amorphous. DNA was fragmented extensively at the center of the lesion. The DNA fragmentation was observed to be surrounded by hepatocytes with TUNEL-positive nuclei, as early as 6 h after 0.2 ml/kg CCl_4 injection. A few hepatocytes with TUNEL-positive nuclei were contiguous to zone 3 (Fig. 3g). As shown in Fig. 3h, DNA fragmentation reached a peak in 24 h and decreased thereafter. A small number of TUNEL-positive cells appeared scattered in zone 1 or zone 2 in the livers of mice administered with 0.2 ml/kg CCl_4 twice a week for 1 and 3 months (Fig. 3i, j). Apoptotic cells in zone 1 at 1 month were very few and were more frequent at 3 months. DNA fragmentation did not occur in the liver tissues of the control group.

Table 2 The body weight and liver weight of mouse with non-treatment, oil i.p., and CCl_4 i.p. repeated administration

	Treatments	0	1	3 months
Body weight	None	26.2±0.94[a]	27.0±1.5	32.9±0.23
	Oil i.p.	26.5±1.05	28.0±1.05	32.1±0.34
	CCl_4 i.p.	26.5±1.38	27.1±1.05	34.4±1.13
Liver weight	None	1.23±0.05[b]	1.70±0.05	2.18±0.10
	Oil i.p.	NT[c]	1.69±0.12	2.03±075
	CCl_4 i.p.	NT	2.08±0.19[d]	2.74±0.22[d]

i.p. intraperitoneal

[a] Mean±SD of body weight of five mice

[b] Mean±SD of liver weight of five mice

[c] Not tested

[d] $P<0.05$

Location of CYP2E1-positive cells

The locations of CYP2E1-positive cells were stained in the liver immunohistochemically after 0.2 ml/kg CCl_4 injection (Fig. 3k–o). In non-treated mice, CYP2E1-positive cells were largely present at the centrilobular zone 3 region of the hepatic lobule (Fig. 3k). At 6 h after 0.2 ml/kg CCl_4 injection, the P450 2E1 area began to disappear from the periphery of zone 3 with leukocyte infiltration. At 24 h after injection, most of the CYP2E1-positive cells had disappeared from the region with concurrent death of a large number of hepatic cells there (Fig. 3m). A small number of CYP2E1-positive cells that still remained disappeared later. After 1 month of repeated CCl_4 exposure twice weekly, CYP2E1-positive cells were observed to be negligible in the centrilobular region, whereas a small number of such cells appeared in the periportal zone 1 area (Fig. 3n). After 3 months of repeated CCl_4 exposure, CYP2E1-positive cells increased in number in zones 1 and 2 (Fig. 3o). In the control group with olive oil-only injection, CYP2E1-positive cells were located in zone 3 similar to those in the non-treated mice. Figure 4a shows the morphometrical change in the P450 2E1 area after a single and repeated administration of CCl_4. P450 2E1 decreased after CCl_4 injection and was an almost unobservable level after 1 month, but a considerable number of positive cells reappeared in 3 months. In the Western blot (Fig. 4c), CYP2E1 was barely visible as a band of 56,000 Da at 12 to 24 h after 0.2 ml/kg CCl_4 injection. In the single injection schedule, CYP2E1 recovered around 96 h and later (data not shown), whereas it remained minimally synthesized

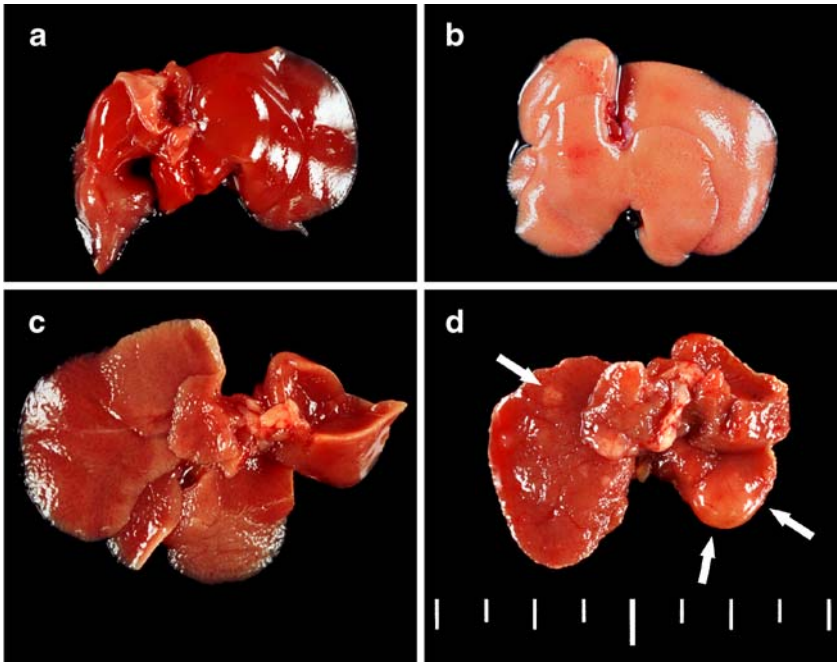

Fig. 2 Gross findings of mouse livers. **a** Normal liver from a non-treated mouse; **b** 12 h after i.p. injection of 0.2 ml/kg CCl_4, shrunken and grayish to grayish-brown in color; **c** 1 month of 0.2 ml/kg CCl_4 injection repeated twice a week, swollen and uneven surface; **d** 6 months of similarly repeated injection, slightly shrunken and uneven surface with several large nodules (*arrows*), measures 5 mm

where the injection was repeated twice a week for 3 months.

Discussion

Hepatotoxic damage by CCl_4 is mainly attributed to its toxic metabolite, trichloromethyl radical ($CCl_3\cdot$), which is formed by the action of CYP2E1. This radical reacts with oxygen to generate a highly reactive species, trichloromethyl peroxy radical ($CCl_3OO\cdot$) that initiates chain reactions of lipid peroxidation, causing subsequent cellular damage. CYP2E1 is the key enzyme in CCl_4 metabolism and is considered to be significantly involved in liver damage and mortality. On the other hand, tolerance to CCl_4 through exposure to small doses of CCl_4 has been documented in rodents [5–11]. The development of tolerance was thought to be achieved by depressing the liver's microsomal drug-metabolizing system [6]. Mice treated with a small dose of CCl_4 acquired a prolonged sleeping time when treated with hexobarbital metabolized in the same system as CCl_4 [6]. Rechnagal et al. proposed a lipid peroxidation theory for this tolerance development in which a small dose of CCl_4 depressed cytochrome P450 activity in such a way as to suppress lipid peroxidation in rats [8]. According to this concept, the destruction of liver cytochrome P450 by the protective dose presumably causes decreased bioactivation of subsequently administered CCl_4, which results in decreased toxicity.

The present study has shown a remarkable fluctuation of LD_{50} in mice following repeated administration of 0.2 ml/kg CCl_4. The animals injected with 0.2 ml/kg CCl_4 twice weekly for 1 and 3 months became five and 1.5 times more tolerant to CCl_4, respectively, compared to the non-treated ones. This change in tolerance to CCl_4 was found to be associated with the disappearance of CYP2E1-positive hepatocytes from the centrilobular zone 3 after 1 month, while an appreciable number of these cells reappeared in the periportal zone 1 and intermediate zone 2 after 3 months. The amount of CCl_4 used in the present study was similar to the dosage in the literature with only minor variations in medication methods for different animal species [5–8, 25].

Carbre et al. have already reported that early hepatic cell death due to CCl_4 is apoptotic [30]. Our histological and immunohistochemical observations clearly showed that CCl_4 caused apoptotic death of the liver cells and the apoptosis occurred at the sites where CYP2E1-positive cells were present as shown in Fig. 3g, h, j, l, m, and o. It is well known that CYP2E1 is present in zone 3 in the proposed metabolic zoning of the liver lobule [31]. In liver regeneration, there is apparently a migration of new hepatocytes from zones 1 and 2 to zone 3 [32, 33]. In the present investigation, it has also been shown that during twice weekly administration of 0.2 ml/kg CCl_4, the regenerated zone 3 hepatocytes were CYP2E1 negative at 1 and 3 months, as they originally arose from CYP2E1-negative hepatocytes in zones 1 and 2. These regenerated cells should be resistant to CCl_4 from being observed lacking apoptotic morphology in the zone 3 (Fig. 3i). Although the death of the mice may be attributed to multiple factors, it is suggested here that the number and distribution of CYP2E1-positive hepatocytes in their zonal presence is an important determining factor for sensitivity

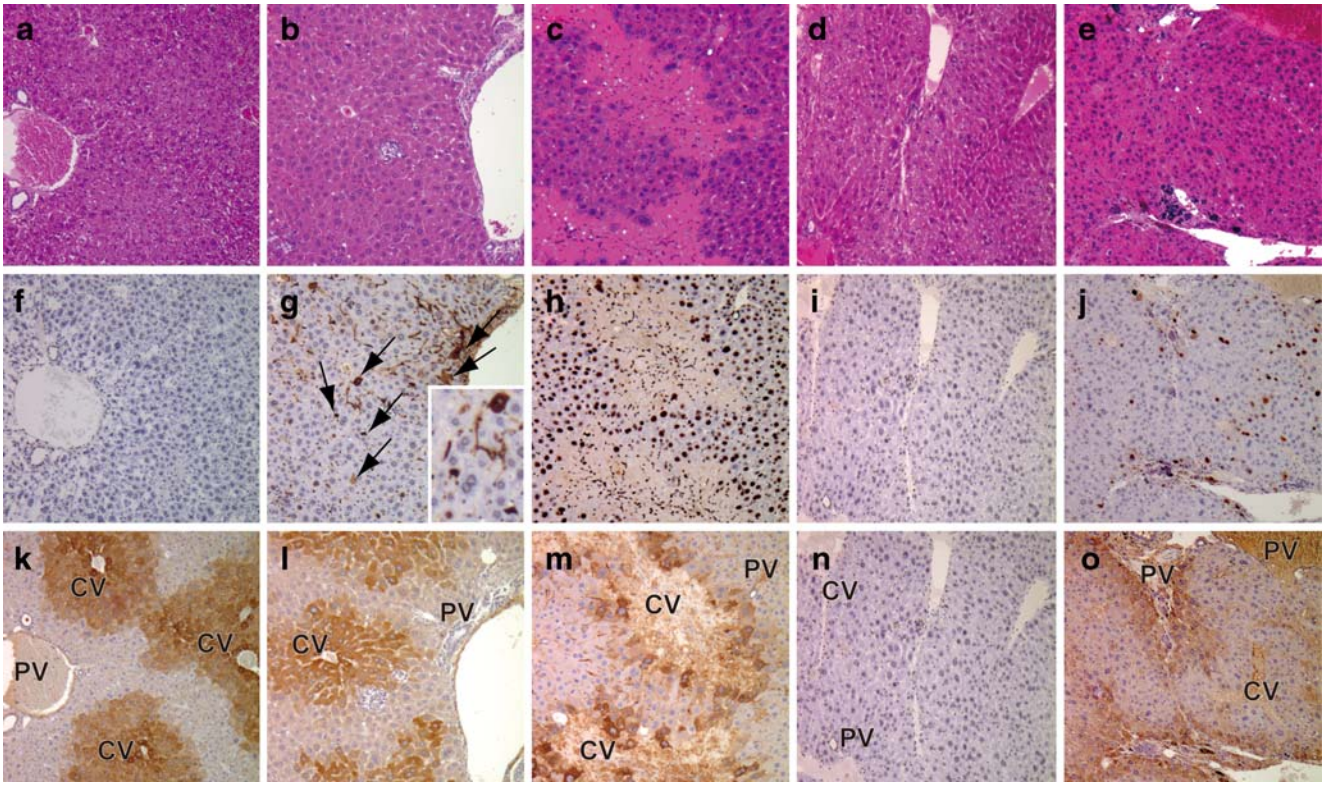

Fig. 3 Liver histology. **a** Non-treated control (hematoxylin eosin, ×100); **b** 6 h after injection of 0.2 ml/kg CCl_4 (hematoxylin eosin, ×100); **c** 24 h after injection of 0.2 ml/kg CCl_4 (hematoxylin eosin, ×100), confluent and zonal hepatic cell death lesions are conspicuous; **d** 1 month after repeated administration of 0.2 ml/kg CCl_4 twice a week (hematoxylin eosin, ×100); centrilobules (zone 3) are almost completely reconstituted; **e** 3 months after similarly repeated administration of 0.2 ml/kg CCl_4; centrilobular area is preserved but periportal area is inflamed (hematoxylin eosin, ×100); sequential changes of TUNEL-positive cells in the liver after 0.2 ml/kg CCl_4 administration (**f**–**j**). **f** Non-treated control (×100), **g** 6 h after injection of 0.2 ml/kg CCl_4 (×100). The *inset* shows higher magnification of same visual field (×400); **h** 24 h after injection of 0.2 ml/kg CCl_4 (×100), confluent, and zonal hepatic cell death lesions are conspicuous; **i** 1 month after repeated administration of 0.2 ml/kg CCl_4 twice a week (×100); **j** 3 months after similar repeated administration of 0.2 ml/kg CCl_4 (×100). Sequential changes in the location of CYP2E1-positive cells in the liver after 0.2 ml/kg CCl_4 administration (**k**–**o**). **k** Non-treated control (×100), strongly CYP2E1-positive cells in the centrilobular zone 3; **l** 6 h after injection of 0.2 ml/kg CCl_4 (×100); **m** 24 h after injection of 0.2 ml/kg CCl_4 (×100), confluent, and zonal hepatic cell death lesion are conspicuous; **n** 1 month after repeated administration of 0.2 ml/kg CCl_4 twice a week (×100), CYP2E1-positive cells disappeared; **o** 3 months after similar repeated administration of 0.2 ml/kg CCl_4 (×100), a few strongly CYP2E1-positive cells appeared in the periportal area. *c* central vein, *p* portal triad

to CCl_4. This notion is strongly supported by reports that mice with knocked out CYP2E1 were highly resistant to CCl_4, with neither noticeable histological liver damage nor abnormal serum levels of ALT and AST upon CCl_4 administration [18–20]. This notion is strongly supported by reports that mice with knocked out CYP2E1 were highly resistant to CCl_4, with neither noticeable histological liver damage nor abnormal serum levels of ALT and AST upon CCl_4 administration [18–20]. The serum levels of these enzymes likely reflect liver damage, or the extent of tolerance to the toxin. Here, in our study, the serum levels of ALT and AST in 2–3 days after the last CCl_4 injection in the prolonged 3-month exposure protocol indicated increasing liver damage or partial loss of tolerance to the toxin as CYP2E1-positive cells reappeared in periportal zone 1 and intermediate zone 2. It would be a direct indication of tolerance level, in the prolonged exposure protocol, to assay the enzymes immediately, that is several hours, after the last toxin administration using a sufficiently larger number of mice than in the present study. This approach remains to be taken in the future study.

There are a few reports that CCl_4 autoprotection may not be related to the decreased microsomal cytochrome P450 content in the liver that was caused by the bioactivation of protective doses [9, 10]. In this concept, hepatocellular regeneration stimulated by low doses of CCl_4 may augment and sustain tissue repair processes to permit tissue restoration even from severe liver injury caused by a subsequent large dose of CCl_4. Recently there is also the report assumed that the augmentation of innate immunity by low dose of CCl_4 treatment takes part of this protection [11]. However, circumstantial evidence cannot completely

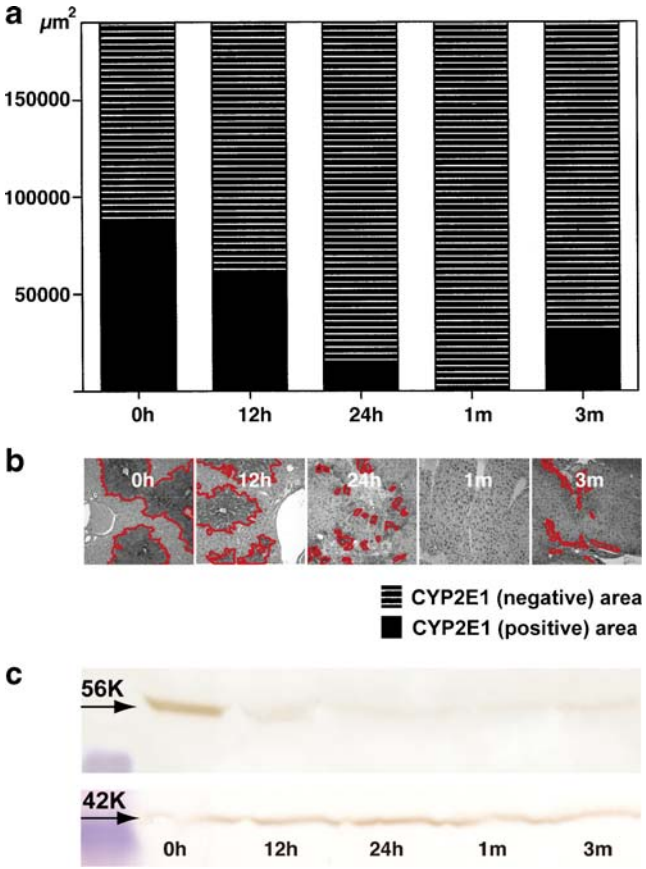

Fig. 4 **a** Sequential changes of ratio between CYP2E1-positive and CYP2E1-negative areas with time. All area of the ×100-magnified visual field by the light microscope is 189,767 μm^2. **b** One example of the image used, and it is same figures shown in Fig. 3 **k**, **l**, **m**, **n**, and **o**. The CYP2E1-positive area was measured in areas *enclosed by red lines*. Each positive and negative columns were mean of five visual-field areas of three mice specimens. **c** One representative picture from three Western blot analyses of CYP2E1 expression in the liver. CYP2E1 bands (*upper*) and β-actin bands (*lower*) show its production at 0, 12, and 24 h after a single administration of 0.2 ml/kg CCl_4 and at 1 and 3 months after repeated administration of CCl_4, twice a week. *Left side lane* shows molecular weight marker, carbonic anhydrase (41.5 kDa, *violet*)

explain the phenomenon of autoprotection. Rather, the primary cause might be CYP2E1, and this xenobiotic enzyme could be a more important factor in CCl_4 toxicity based on the evidence of the lack of CCl_4-induced hepatotoxicity in the CCl_4 knockout mice [18–20]. It is known that glutathione is involved in the tolerance to poisonous substances such as anti-cancer drugs. It remains of interest whether or not glutathione is also involved in the tolerance development to CCl_4 [34, 35].

CYP2E1-positive cells appeared again not in zone 3 but in zones 1 and 2 following the repeated administration of 0.2 ml/kg CCl_4. Centrilobular hepatocytes could regenerate from cells in zones 1 and 2 that remained viable in the course of CCl_4 exposure, thus not expressing CYP2E1. It has been reported that donor hepatocytes acquired position-specific enzyme expression while proliferating in the liver parenchyma of a recipient rat with prior treatment of retrosine and partial hepatectomy. This finding indicates that hepatocytes are subject to microenvironmental change in their plasticity of gene expression [36]. Taken together, it is highly likely that CCl_4 damages the microenvironment of zone 3.

As shown in Tables 1 and 2, liver dysfunction increased and liver weight increased more after 3 months than after 1 month of CCl_4 treatment. The increase of the liver weight after 3 months can be attributed to the increase in liver fibrous tissue. However, the critical factor in increased liver dysfunction and susceptibility to CCl_4 is thought to be the re-appearance of CYP2E1-positive cells, followed by the apoptosis of the CYP2E1-positive cells, and by fibrosis and inflammatory cell infiltration in zone 1 and zone 2 during chronic exposure to CCl_4. Microscopic findings in the liver exposed to 3 months of repeated CCl_4 administration looked like chronic hepatitis. These features were different from those in the acute phase and might reflect increased toxicity after the prolonged exposure, although other factors such as cytokines and stelle cells may also be involved [37, 38]. It is proposed here that zonal fluctuations of CYP2E1-positive cells are responsible for CCl_4 susceptibility and for structural remodeling of the pre-exposed liver to repeatedly exposed liver. This notion accounts for the variation of CCl_4 LD_{50} in repeatedly exposed mice. It remains to be further studied why and how CYP2E1-positive cells reappear at the peripheral zone. It is likely that prolonged exposure to CCl_4 induces similar tolerance in humans. To the best of our knowledge, however, there has been no such report on induced tolerance in humans. Incidentally, it is well known that CYP2E1 increases in chronic alcoholism and that these alcoholics are abnormally sensitive to CCl_4 [21, 22]. Alcohol is also metabolized by microsomal ethanol oxidizing system in addition to alcohol dehydrogenase. CYP2E1 has a high affinity for alcohol. It is said that this enzyme dramatically increases in chronic alcohol consumption, and it accounts for resistance for alcohol. In humans there are many cases of acute CCl_4 poisoning reported in literature, mostly occupational exposure to the solvent and accidental inhalation of CCl_4. Besides the workers in isopropyl alcohol packing plant were reported to become severely ill after accidental exposure to CCl_4 [25, 26]. In other words, this accounts for the susceptibility of the alcoholic to drugs that are hepatotoxic on account of metabolites and which when given normal doses can cause serious liver injury. Taking into account our experimental results, the above phenomenon may be attributed to the increase of CYP2E1-positive target cells to CCl_4 in heavy alcoholic abuse.

Acknowledgments The authors thank A H Koyama, Professor, Department of Virology, Wakayama Medical University, Graduate, for constructive comments.

Funding This study was supported in part by a research grant from Teikyo University School of Medicine.

Conflict of interest statement We declare that we have no conflict of interest.

References

1. Wiliams AT, Burk RF (1990) Carbon tetrachloride hepatotoxicity: example of free radical-mediated injury. Semin Liver Dis 10:279–284
2. Zimmerman HJ (1982) Chemical hepatic injury and its detection. In: Gabriel PW (ed) Toxicology of the liver. Raven, New York, pp 1–46
3. Sherlock S (1993) Drug and the liver. In: Sherlock S, Dooley J (eds) Disease of the liver and biliary system. Blackwell Scientific, London, pp 332–356, Sherlock S: Alcohol and the Liver. ibid., pp 370–389
4. Cameron GR, Karnaratne WAE (1933) Carbon tetrachloride cirrhosis in relation to liver regeneration. J Pathol Bacteriol 42:1–21
5. Dambrauskas T, Cornish HH (1970) Effect of pretreatment of rats with carbon tetrachloride on tolerance development. Toxicol Appl Pharmacol 17:83–97
6. Ugazio G, Koch RR, Recknagel RO (1972) Mechanism of protection against carbon tetrachloride by prior carbon tetrachloride administration. Exp Mol Pathol 16:281–285
7. Pound AW, Lawson TA (1975) Reduction of carbon tetrachloride toxicity by prior administration of a single small dose in mice and rats. Br J Exp Pathol 56:172–179
8. Recknagel RO, Glende EA Jr, Ugazio G et al (1974) New data in support of the lipoperoxidation theory for carbon tetrachloride liver injury. Israel J Med Sci 10:301–311
9. Thakore KN, Mehendale HM (1991) Role of hepatocellular regeneration in CCl_4 autoprotection. Toxicol Pathol 19:47–58
10. Rao YC, Mehendale HM (1991) Colchicine antibiotics CCl_4 autoprotection. Toxicol Pathol 19:597–606
11. Taira Z, Yabe K, Miyake S et al (2002) Intracellular Ca^{2+} mediating biodefense signal on CCl_4-induced autoprotection. Nippon Yakurigaku Zasshi 120:119–121
12. Wu Q, Gang D, Tian N et al (2009) Protection of regenerating liver partial hepatectomy from carbon tetrachloride hepatotoxicity in rats: roles of mitochondrial uncoupling protein 2 and ATP stores. Dig Dis Sci 54:1918–1925
13. McCay PB, Lai EK, Poyer JL et al (1984) Oxygen- and carbon-centered free radical formation during carbon tetrachloride metabolism: observation of lipid radicals in vivo and in vitro. J Biol Chem 259:2135–2143
14. Armbrust T, Batusic D, Ringe B et al (1997) Mast cells distribution in human liver disease and experimental rat liver fibrosis. Indication for mast cell participation in development of liver fibrosis. J Hepatol 26:1042–1054
15. Guengerich FP, Kim DH, Iwasaki M (1991) Role of human cytochrome P450 2E1 in the oxidation of many low molecular weight cancer suspects. Chem Res Toxicol 4:168–179
16. Healy LN, Pluta LJ, Recio L (1999) Expression and distribution of cytochrome p450 2E1 in B6C3f1 mouse liver and testes. Chem Biol Interact 121:199–207
17. Rao PS, Mangipudy RS, Mehendale HM (1990) Tissue injury and repair as parallel and opposing responses to CCl_4 hepatotoxicity: a novel dose-response. Toxicology 118(1):181–193
18. Ghanayem BI, Wang H, Sumner SCJ (2000) Using cytochrome p-450 gene knock-out mice to study chemical metabolism, toxicity, and carcinogenicity. Toxicol Pathol 28:839–850
19. Gonzalez FJ (2001) The use of gene knockout mice to unravel the mechanisms of toxicity and chemical carcinogenesis. Toxicol Lett 120:199–208
20. Wong FWY, Chan WY, Lee SST (1998) Resistance to carbon tetrachloride-induced hepatotoxicology in mice which lack CYP2E1 expression. Toxicol Appl Pharmacol 253:109–118
21. Lieber CS (1991) Hepatic, metabolic and toxic effects of ethanol; 1991 uptake. Alcohol Clin Exp Res 15:573–592
22. Lieber CS (1997) Ethanol metabolism, cirrhosis and alcoholism. Clin Chem Acta 257:57–84
23. Zimmermann HJ, Maddrey WC (1995) Actaminophen (paracetamol) hepatotoxicity with regular intake of alcohol: analysis of instances of therapeutic misadventure. Hepatology 22:767–773, 37
24. Williams AT, Burk RF (1990) Carbon tetrachloride hepatotoxicity; example of free radical-mediated injury. Semin Liver Dis 10:279–284
25. Gadeholt G (1984) Ethanol-inducible cytochrome P450 is more susceptible to in vitro carbontetrachloride-mediated destruction than phenobarbital inducible and β-naphthoflavone-inducible cytochrome P-450. Acta Pharmacol Toxicol 55:216–223
26. Manno M, Rezzadore M, Grossi M, Sbrana C (1966) Potentiation of occupational carbon tetrachloride toxicity by ethanol abuse. Hum Environ Toxicol 15:294–300
27. Folland DS, Schaffner W, Ginn HE et al (1976) Carbon tetrachloride toxicity potentiated by isopropyl alcohol. JAMA 236:1853–1856
28. Bergmyer HU (1984) Enzymes: transferases. In: Berger HU (ed) Methods of enzyme analysis, 3rd edn. Verlag Chemie, Weinhem, pp 416–457
29. Lindis RJ, Heyman ER, Koch CC (1978) Average of partial association in three way contingency tables. Int Stat Rev 46:237–254
30. Cabre M, Ferre N, Folch J et al (1999) Inhibition of hepatic cell nuclear DNA fragmentation by zinc in carbon tetrachloride-treated rats. J Hepatol 31:228–234
31. Jungermann K (1988) Metabolic zonation of liver parenchyma. Semin Liver Dis 8:329–341
32. Zajicek G, Oren R, Weinreb M Jr (1985) The streaming liver. Liver 5:293–300
33. Crisham JW (1962) A morphologic study of deoxyribonucleic acid synthesis and Cell proliferation in regenerating rat liver; autoradiography with thymidine H^3. Cancer Res 22:842–849
34. Ishikawa T, Ali-Osman F (1993) Glutathione-associated cis-diamminedichloroplatinum (II) metabolism and ATP-dependent efflux from leukemia cells. J Biol Chem 268:20116–20125
35. Siemann DW, Beyers KL (1993) In vivo therapeutic potential of combination thiol depletion and alkylating. Chemotherapy 68:1071–1079
36. Koenig S, Aurich H, Schneider C et al (2007) Zonal expression of hepatocytic marked enzymes during liver population. Histochem Cell Biol 128:105–114
37. Du Duffiled JS, Forbes SJ, Constandinow CM et al (2005) Selective depletion of macrophages reveals distinct, opposing roles during liver injury and repair. J Clin Invest 15:56–65
38. Jeong W-I, Park O, Radaeva S et al (2006) Stat 1 inhibits liver fibrosis in mice by inhibiting stellate cell proliferation and stimulating NK cell cytotoxicity. Hepatology 44(172):1441–1451

Virchows Arch (2010) 456:433–441
DOI 10.1007/s00428-010-0884-x

ORIGINAL ARTICLE

Immunohistochemical detection of steroid receptor cofactors in ovarian endometriosis: involvement of down-regulated SRC-1 expression in the limited growth activity of the endometriotic epithelium

Akihisa Suzuki · Akiko Horiuchi · Kenji Oka · Tsutomu Miyamoto · Hiroyasu Kashima · Tanri Shiozawa

Received: 9 December 2009 / Revised: 6 January 2010 / Accepted: 8 January 2010 / Published online: 13 February 2010
© Springer-Verlag 2010

Abstract To study the steroid hormone-induced growth mechanisms of endometriosis, the immunohistochemical expression of steroid hormone receptor cofactors was investigated in 37 cases of endometriotic epithelia and was compared with that of eutopic endometria of identical patients. The expression of steroid receptor coactivators (p300/CBP and SRC-1) and corepressors (NCoR and SMRT) was examined in relation to the estrogen receptor (ER), the progesterone receptor (PR), and Ki-67. Results of immunostaining were indicated as a "positivity index" (PI, full score; 100). The expression of ER and PR in endometriotic epithelia largely resembled that in eutopic endometria, however, the expression of Ki-67 in the proliferative phase (PI 13.8±2.4, mean±SD) was significantly lower than that in eutopic endometria (32.6±10.6). The expression of SRC-1 in eutopic endometria was increased in the proliferative phase (56.5±16.8) and decreased in the secretory phase (14.8±6.9). In endometriosis, however, the PI for SRC-1 did not show apparent cyclic changes during the menstrual cycle. Moreover, the expression of SRC-1 in endometriotic epithelia in the proliferative phase was significantly lower than that in eutopic endometria. These findings suggested the reduced proliferative activity in endometriotic epithelia to be related to the reduced expression of SRC-1.

A. Suzuki · A. Horiuchi · K. Oka · T. Miyamoto · H. Kashima · T. Shiozawa (✉)
Department of Obstetrics and Gynecology,
Shinshu University School of Medicine,
3-1-1 Asahi,
Matsumoto 390-8621, Japan
e-mail: tanri@shinshu-u.ac.jp

Keywords Endometriosis · SRC-1 · Steroid receptor cofactor

Introduction

Endometriosis is characterized histologically by the presence of endometrial tissue at ectopic loci. The endometriotic epithelial cells, as observed in normal eutopic endometria, also express estrogen receptors (ERs) and progesterone receptors (PRs). The growth of endometriotic tissue is considered to be controlled by sex steroid hormones [1, 2], and the hormone-dependent growth mechanisms of normal endometrial epithelia have been investigated with respect to the cyclic expression of estrogen receptor/progesterone receptor (ER/PR) and steroid-synthesizing enzymes [3] and the involvement of growth factors or cytokines [4]. In addition, we previously demonstrated the cyclic expression of cell cycle regulators in normal endometria [5], as well as the estrogen-induced expression of cyclins in normal and malignant endometrial epithelia [6, 7]. However, the regulation of steroid hormone-mediated growth in endometriosis has not fully been investigated.

Recent studies of steroid receptor signaling identified a group termed steroid receptor cofactors [8, 9]. These proteins bind to steroid receptors in a ligand-dependent fashion, and the receptor-bound forms then bind to the basal transcriptional machinery of the target genes, resulting in transcription. They are now divided functionally into two subclasses, i.e., coactivators and corepressors. The former stimulate and the latter suppress transcription. Therefore, steroid receptor cofactors play an important role in steroid receptor signaling. We previously reported a cyclic change in the expression of

steroid receptor coactivator 1 (SRC-1) and p300/CREB binding protein (p300/CBP), as well as the actual binding of these coactivators to ERs in the normal human endometrium, indicating the functional involvement of coactivators in estrogen-regulated growth [10]. In addition, we reported an aberrant expression of cofactors in endometrial carcinoma, which may explain the relative hormone-independency of this tumor [11]. However, the expression of these cofactors has not been investigated in endometriotic tissues. Therefore, in the present study, we examined the expression of two coactivators (p300/CBP and SRC-1) and two corepressors [nuclear receptor corepressor (NCoR) and silencing mediator for retinoid and thyroid hormone receptors (SMRT)]: p300/CBP and SRC-1 are considered crucial to the first step of transcription [12], and NCOR and SMRT recruit ERs/PRs [13, 14]. The expression of these cofactors was examined immunohistochemically in endometriotic (ectopic) epithelia and compared with levels in normal endometrial (eutopic) epithelia of the same patients with ovarian endometriosis. In addition, their association with the expression of ER, PR, and Ki-67 (a marker for cell proliferation) was also studied to elucidate the significance of the expression of cofactors in the endometriotic epithelium.

Materials and methods

Patients

Both samples from eutopic and ectopic (ovarian) endometria were obtained from a total of 37 patients with ovarian endometriosis who underwent a total abdominal hysterectomy and salpingo-oophorectomy or ovarian cystectomy at Shinshu University Hospital, Japan. The age of the patients ranged from 36 to 51 years (mean, 42.9 years). The patients had a regular menstrual cycle and no history of hormonal treatment with GnRH analogs, danazol, contraceptive pills, etc. within 6 months preceding the surgery. Patients with signs of any endometrial or ovarian malignancies demonstrated by the histopathological diagnosis were excluded. The study was approved by the hospital ethics committee, and all patients gave informed consent before surgery. Of the 37 patients, 20 were in the proliferative phase, and 17 were in the secretory phase.

Immunohistochemistry

Indirect immunostaining was performed using specific antibodies against SRC-1, p300/CBP, NCoR, and SMRT. The antibody for p300/CBP was purchased from NeoMarkers (Fremont, CA). The antibodies for SRC-1 and NCoR were from Upstate Biotechnology (Lake Placid, NY), and the anti-SMRT antibody was from Santa Cruz Biotechnology (Santa Cruz, CA). An anti-Ki-67, anti-ER antibody that specifically recognizes ER-α, and an anti-PR antibody that recognizes both PR-A and PR-B, were obtained from Immunotech (Marseille, France). Each immunohistochemical staining procedure was performed using the avidin–biotin–peroxidase complex method with a Histofine Max-PO detector kit (Nichirei, Tokyo, Japan). Briefly, after routine deparaffinization and rehydration, sections were microwaved in a 0.01 M citrate buffer, pH 6.0, for 15 min. After the blocking of endogenous peroxidase activity, the sections were incubated with the specific primary antibodies (diluted 1:100 with phosphate-buffered saline (PBS)/bovine serum albumin) or control non-immunized mouse or rabbit serum at 4°C overnight. After a wash with PBS, biotinylated antimouse or rabbit immunoglobulin G (IgG) was applied for 30 min at room temperature. As a negative control of the secondary antibody, biotinylated anti-rabbit or mouse IgG was used for mouse and rabbit primary antibodies, respectively. After washing with PBS, each sample was visualized with 0.05% 3′,3′-diaminobenzidine. Counterstaining was performed lightly with hematoxylin.

Interpretation of immunohistochemical staining

The staining was also described in terms of a positivity index (PI), which indicates the percentage of positive cells among 200 arbitrarily selected cells from three high-power fields in each section. Each PI was determined by averaging results from two reviewers (A. S. and T. S.). The PI of the eutopic endometrium was assessed in the functional layer. Statistical analyses for the comparison between eutopic and ectopic endometria and between the proliferative and secretory phases were done with the Mann–Whitney *U* test. A P value<0.05 was considered significant. These analyses were done using the StatView software package (Abacus, Berkeley, CA).

Results

The specific staining of each antibody was identified in the nucleus. All control slides yielded negative staining. The PIs for the cofactors, the steroid receptors, and Ki-67 both in eutopic and in ectopic endometrial epithelial cells are described as the mean±standard deviation (SD) and listed in Table 1. Representative immunostaining of the cofactors is shown in Figs. 1 and 2, while that of steroid receptors and Ki-67 is shown in Fig. 3.

Expression of ER, PR, and Ki-67

The expression of both ER and PR in eutopic endometrial epithelia was significantly higher in the proliferative phase (PI for ER, 87.6±8.7 and for PR, 80.8±16.8, Figs. 1a, e and

Table 1 Results of immunostaining for coactivators, corepressors, ER, PR, and Ki-67 in the eutopic and the ectopic endometrial epithelial cells

	Proliferative $N=20$	Secretory (total) $N=17$	Early secretory $N=5$	Mid-secretory $N=7$	Late secretory $N=5$
CBP					
Eutopic	95.1±2.5	90.6±9.5	95.2±2.5	90.4±7.2	86.4±1.4
Ectopic	91.5±2.4	91.3±3.8	93±3.0	89.9±5.6	91.5±1.4
SRC-1					
Eutopic	56.5±16.8	14.8±6.9[b]	24.1±9.1	10.4±12.2	11.9±14.3
Ectopic	30.9±16.5[a]	23.9±10.8	18.6±6.4	24.4±14.8	28.5±21.4
NCoR					
Eutopic	14.9±6.8	4.3±3.4[b]	9.7±5.6	1.9±3.2	2.1±1.6
Ectopic	15.3±10.6	20.6±11.1	9.3±11.1	23.1±10.0[a]	28.4±12.6[a]
SMRT					
Eutopic	0.96±1.8	0.97±1.1	2.1±1.1	0.5±1.2	0.5±0.8
Ectopic	2.6±3.2	3.3±4.6	3.9±3.5	3.2±7.1	2.7±2.2
ER					
Eutopic	87.6±8.7	23.8±9.5[b]	59.4±16.1	9.2±4.9	8.7±9.2
Ectopic	63.7±2.4	35.1±3.6[b]	59.9±3	23.7±5.6	26.3±1.4
PR					
Eutopic	80.8±16.8	32.6±23.8[b]	70.4±18.1	20.4±24.4	11.9±28.5
Ectopic	61.1±16.5	32.6±16.1	48.3±12.7	24.4±14.8	28.5±21.4
Ki-67					
Eutopic	32.6±2.5	4.8±4.1[b]	13.8±2.4	1.1±7.2	0.9±1.4
Ectopic	13.8±2.4[a]	2.8±3.6	5.4±3.0	1.9±4.8	1.4±2.5

[a] PI significantly different from that in the eutopic endometrium ($P<0.05$)

[b] PI significantly different from that in the proliferative phase

2) than secretory phase (PI for ER, 23.8±9.5 and for PR 32.6±23.8, Fig. 1b, f). In ectopic endometrial epithelia, the expression of ER and PR also showed a cyclic change during the menstrual cycle, however, differences in PIs between the proliferative and secretory phases were smaller than in eutopic endometria (Fig. 2). The expression of Ki-67 in the eutopic endometrial gland was predominant in the proliferative phase (PI 32.6±2.5, Fig. 1i) and significantly reduced in the secretory phase (PI 4.8±4.1, $P<0.05$, Fig. 1j). In contrast, there was no significant difference in PIs for Ki-67 in ectopic endometria (Fig. 1k, l) between the proliferative and the secretory phases (PI 13.8±2.4 vs. 2.8±3.6, Fig. 2). Notably, the PI for Ki-67 during the proliferative phase was significantly lower ($P<0.05$) in ectopic than eutopic endometria (Fig. 2).

Expression of steroid receptor coactivators

p300/CBP was distributed diffusely in eutopic endometrial epithelia irrespective of menstrual phase (PI 95.1±2.5 in the proliferative phase, PI 90.6±9.5 in the secretory phase, Fig. 3a, b). In ectopic epithelia, again, p300/CBP was expressed diffusely throughout the menstrual cycle; PIs for p300/CBP in the proliferative and the secretory phase were 91.5±2.4 and 91.3±3.8, respectively (Fig. 3c, d). There was no significant difference in the expression of p300/CBP between eutopic and ectopic endometria in either menstrual phase (Fig. 3i, left). SRC-1-positive cells were also spread diffusely in eutopic endometria in the proliferative phase (PI 56.5±16.8, Fig. 3e, f), but decreased in number in the secretory phase (Fig. 3i, right), with a lowest PI in the mid-secretory phase (PI 10.4±12.2). There was a significant difference in PIs between the proliferative and secretory phases ($P<0.05$). In contrast, the expression of SRC-1 in ectopic epithelia was persistently observed during the menstrual cycle (Fig. 3g–i, right), with no significant difference between the proliferative and secretory phases (Fig. 3i, right). In addition, the PI was significantly lower (PI 30.9±16.5) in ectopic epithelia than eutopic endometria (PI 56.5±16.8) in the proliferative phase. There was no significant difference in PIs between the eutopic (PI 14.8±6.9) and ectopic (PI 23.9±10.8) endometria in the secretory phase.

Expression of steroid receptor corepressors

In eutopic endometrial epithelia, NCoR-positive cells were sporadically observed in the proliferative phase (Fig. 4a, PI 14.9±6.8) and negligible in the secretory phase (PI 4.3±3.4, Fig. 4b, i, left). In contrast, the NCoR-positive cells in endometriotic epithelia were observed throughout the menstrual cycle (Fig. 4c, d, and i, left), with PIs in the mid (PI 23.1±10.0) and late (PI 28.4±12.6) secretory phases being significantly higher in ectopic epithelia than

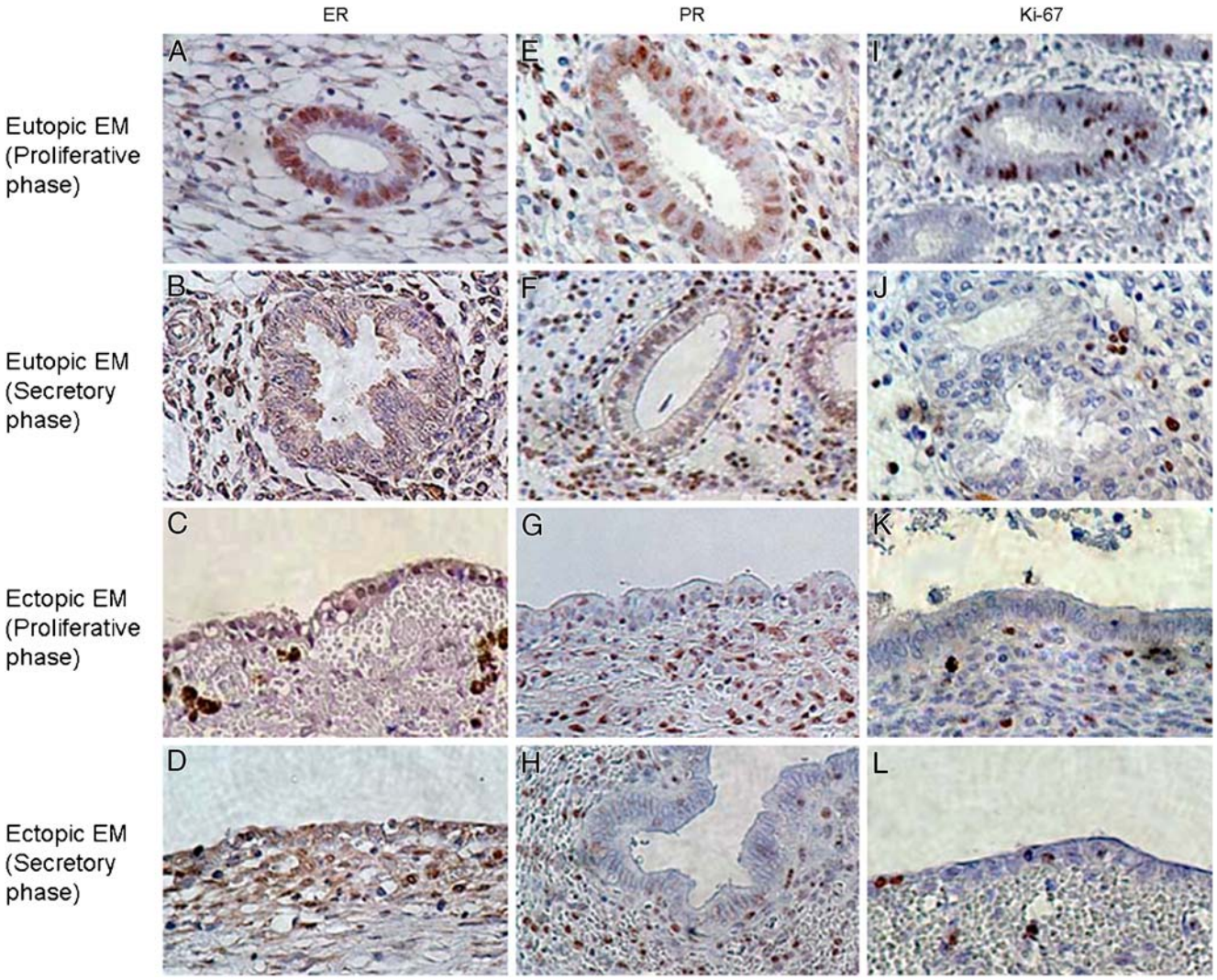

Fig. 1 Immunostaining of ER, PR, and Ki-67 in eutopic and ectopic endometria. In eutopic endometrial glands, ER and PR were expressed diffusely in the proliferative phase (**a** and **e**, respectively) and down-regulated in the secretory phase (**b** and **f**, respectively). The expression of Ki-67 was observed predominantly in the proliferative phase (**i**) and rarely observed in the secretory phase (**j**). The expression of ER and PR in ectopic endometrium was less evident in the ectopic endometrial gland in the proliferative (**c** and **g**, respectively) and secretory (**d** and **h**, respectively) phases. The expression of Ki-67 was rarely observed in ectopic endometrium (**k** and **l**), while staining was observed in the secretory phase (**l**). (A-L, ×175)

eutopic endometria. The number of SMRT-positive cells was limited in both the eutopic (Fig. 4e, f) and ectopic (Fig. 4g, h) endometrial epithelia. There was no significant difference in the PIs between eutopic and ectopic endometria in the proliferative or secretory phase (Fig. 4i, right).

Discussion

The expression of steroid receptors (ER and PR) in eutopic endometrial epithelia showed a cyclic change during the menstrual cycle, being predominant in the proliferative phase and down-regulated in the secretory phase. The expression of Ki-67, a marker of proliferation, also showed a cyclic change. This expression pattern was consistent with our previous report [5] and others [15, 16]. The expression of ER/PR and Ki-67 in endometriotic epithelial cells also showed cyclic changes during the menstrual cycle, however, the changes were less dynamic than those in the eutopic endometrium. These findings were in line with previous reports [16, 17]. In addition, Ki-67 labeling was significantly lower in endometriotic epithelia than eutopic endometrial tissue in the proliferative phase despite the similar levels of ER and PR. Jones et al. also reported that the expression of Ki-67 was constant during the menstrual cycle and reduced in ectopic epithelia compared with eutopic endometria, though the expression of ER/PR in both epithelia was similar [16]. Our results were consistent

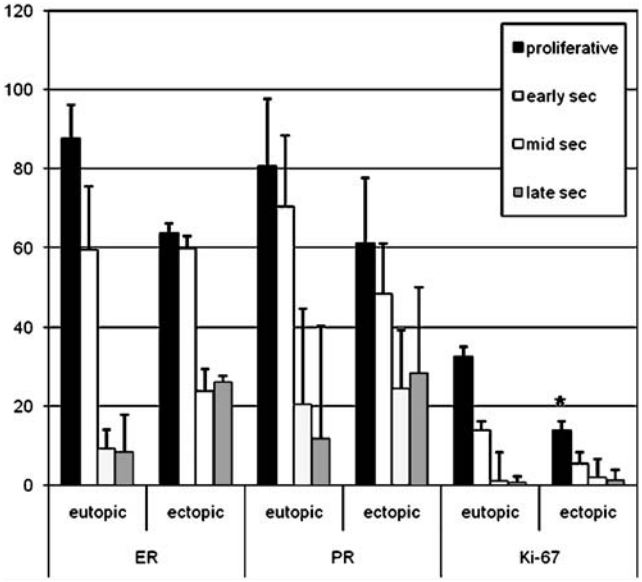

Fig. 2 Graphic demonstration of the immunostainings of ER, PR, and Ki-67. The expression of ER was highest in the proliferative phase and declined through the secretory phase in eutopic endometrium (*leftmost*, *left*). In ectopic endometrium, ER expression was reduced in the proliferative phase and slightly increased in the secretory phase (*leftmost*, *right*). The expression of PR was also predominant in the proliferative phase and decreased in the secretory phase in eutopic endometrium (*mid*, *left*). The same pattern of expression was observed in ectopic endometrium (*mid*, *right*). The PI for Ki-67 in the eutopic endometrial gland was highest in the proliferative phase and negligible after the mid-secretory phase (*rightmost*, *left*). The PI for Ki-67 in the proliferative phase was significantly lower in the ectopic endometrial gland. The PI for Ki-67 was higher in the ectopic than eutopic endometrial gland in the secretory phase (*rightmost*, *right*)*$P<0.05$

with these reports. These findings indicate a dysfunctional estrogen-induced growth mechanism in the ectopic epithelium. ER has two isoforms, ER-α, and ER-β [18], indicating that the actions of estrogen were regulated by the ratio of ER-α/ER-β. Reportedly, the mRNA ratio for ER isoforms in ovarian endometriosis was different from that in the eutopic endometrium [19], however, another study found the opposite [20]. Thus, it is difficult to explain the reduced proliferative potential of endometriotic epithelia only in terms of the quality or quantity of ERs. More recent studies showed steroid receptor cofactors to be important regulators of ER function [21] and that estrogen-activated transcription was not governed solely by the ER–ERE interaction [22]. These reports supported the possible involvement of steroid receptor cofactors in reduced ER-mediated growth in ectopic epithelia.

More importantly, the present study showed a reduction in the expression of SRC-1 in ectopic epithelia, especially during the proliferative phase. The expression of SRC-1 in eutopic endometrial epithelia showed a cyclic change during the menstrual cycle, i.e., SRC-1 was expressed in more than 50% of the epithelial cells in the proliferative phase but just 15% during the secretory phase. This expression pattern was consistent with our previous observation [10]. In addition, we demonstrated that SRC-1 was directly associated with ER-α [10], suggesting a crucial role for SRC-1 in the ER-mediated proliferation of endometrial epithelial cells. These findings strongly suggested the involvement of the reduced SRC-1 expression in the limited growth activity in ectopic epithelia. SRC-1 belongs to the p160 family and is characterized by a basic helix–loop–helix /Per–AhR–Arnt–Sim domain at the N terminus and by a p300/CBP-binding site in the midportion [23]. SRC-1 has histone acetyl transferase activities, which actualize the gene transcription [24] and is known to bind with ER. The ER/SRC-1 complex was reportedly important for estrogen-induced gene transcription in breast cancer cells [25]. In addition, we also revealed that the expression of SRC-1 was reduced in endometrial carcinoma compared with normal endometrium, suggesting that loss of SRC-1 is one of the mechanisms leading to the loss of steroid hormone-dependency during the carcinogenesis [11]. To our knowledge, this is the first report to demonstrate the involvement of SRC-1 in the reduced growth activity of ectopic endometrial epithelia.

Regulatory mechanisms for the expression of SRC-1 are not fully understood, however, estrogen up-regulated SRC-1 expression in breast cancer cells [26], while it did not affect SRC-1 expression in the rat uterus [27] or human endometrial carcinoma [26]. Previous studies suggested that ectopic endometrial glands might exist in a different hormonal micro-milieu from eutopic endometria due to their ovarian localization and induction of estrogen-catalyzing hormones toward increasing the estrogen concentration [3, 28, 29], however, no study has directly determined estrogen concentrations in endometriotic lesions for technical reasons. In addition, Leite et al. revealed that SRC-1, unlike other cofactors, was subject to repression by tumor necrosis factor alpha (TNF-α) in uterine smooth muscle cells [30]. TNF-α levels in peritoneal fluids were reported to be increased in patients with endometriosis [31]. Therefore, SRC-1 may be a target of cytokines because endometriotic lesions are often characterized by the infiltration of leukocytes and macrophages.

In the current study, we also demonstrated the diffuse expression of p300/CBP throughout the menstrual cycle in both eutopic and ectopic endometrial epithelia. p300/CBP has been reported to be associated with various nuclear receptors including the retinoid receptor, the thyroid hormone receptor, and also steroid receptors [32]. p300/CBP interacts with TFIIB via its binding domain and has histone acetylase activity which is essential for histone remodeling and enables the promoter to initiate transcription [33]. More recently, p300/CBP was found to be involved in other cellular signaling pathways such as the epidermal growth factor

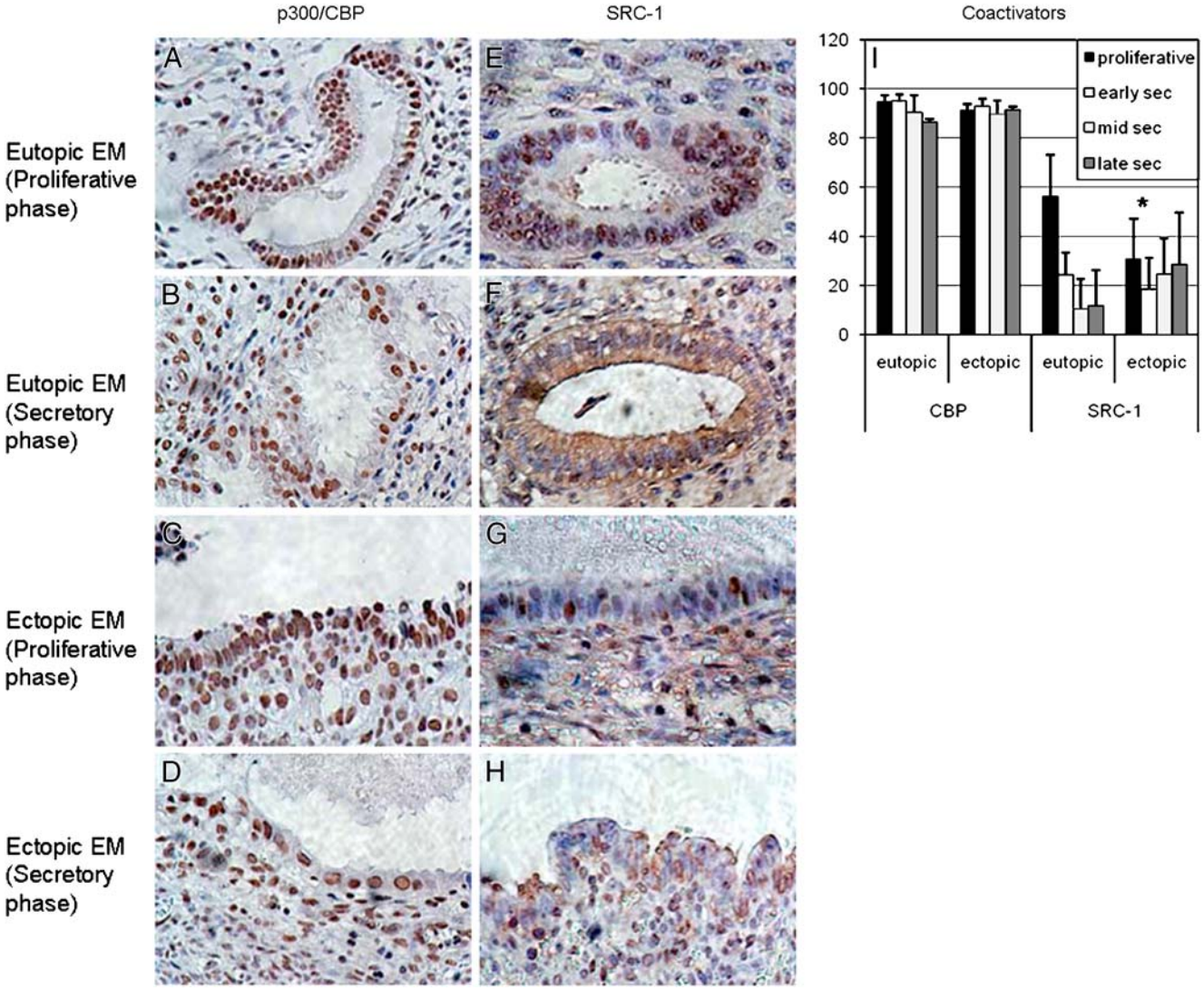

Fig. 3 Results of immunostaining for coactivators in eutopic and ectopic endometria. In eutopic endometrium, p300/CBP was diffusely expressed both in the proliferative (**a**) and in the secretory phase (**b**). The expression of p300/CBP was also diffuse throughout the menstrual cycle (**c** and **d**). In eutopic endometrium, SRC-1 was diffusely expressed in the proliferative phase (**e**), but rarely detected in the secretory phase (**f**). The expression of SRC-1 in the proliferative phase was lower in ectopic endometrium (**g**) than eutopic (**e**) endometria. Staining for SRC-1 was observed even in the secretory phase in the ectopic endometrium. (A-H, ×200) *I*: A graphic representation of the immunostaining for steroid receptor coactivators. The expression of p300/CBP was constant throughout the menstrual period in both eutopic and ectopic endometria. The expression of SRC-1 in eutopic endometrium showed a cyclic change during the menstrual period. The cyclic pattern was less evident in ectopic endometrium due to a significant reduction in the proliferative ectopic endometrium*$P<0.05$

pathway [34] and nuclear factor kappa pathway [35]. In the normal endometrium, p300/CBP was constantly expressed throughout the menstrual cycle in both stromal and glandular cells and formed a complex with ER or PR [10]. The present study also suggested its house-keeping role and involvement in numerous signaling pathways in endometrial glandular cells.

Our study also demonstrated that the expression of NCoR in eutopic endometria was higher in the proliferative phase than secretory phase. This was consistent with previous reports determining NCoR mRNA levels [36] and protein expression [10] in normal endometria. Its expression was significantly higher in endometriotic epithelia than in eutopic endometria in the mid- and late secretory phases where progesterone functions to induce the differentiation of endometrium. We previously reported the up-regulation of NCoR expression in endometrial hyperplasia [11]. In addition, we reported that the expression of NCoR in endometrial hyperplasia was enhanced by progestin treatment [7]. These studies suggested the involvement of NCoR in progestin-induced growth suppression in pathologic endometrial tissues, and the results

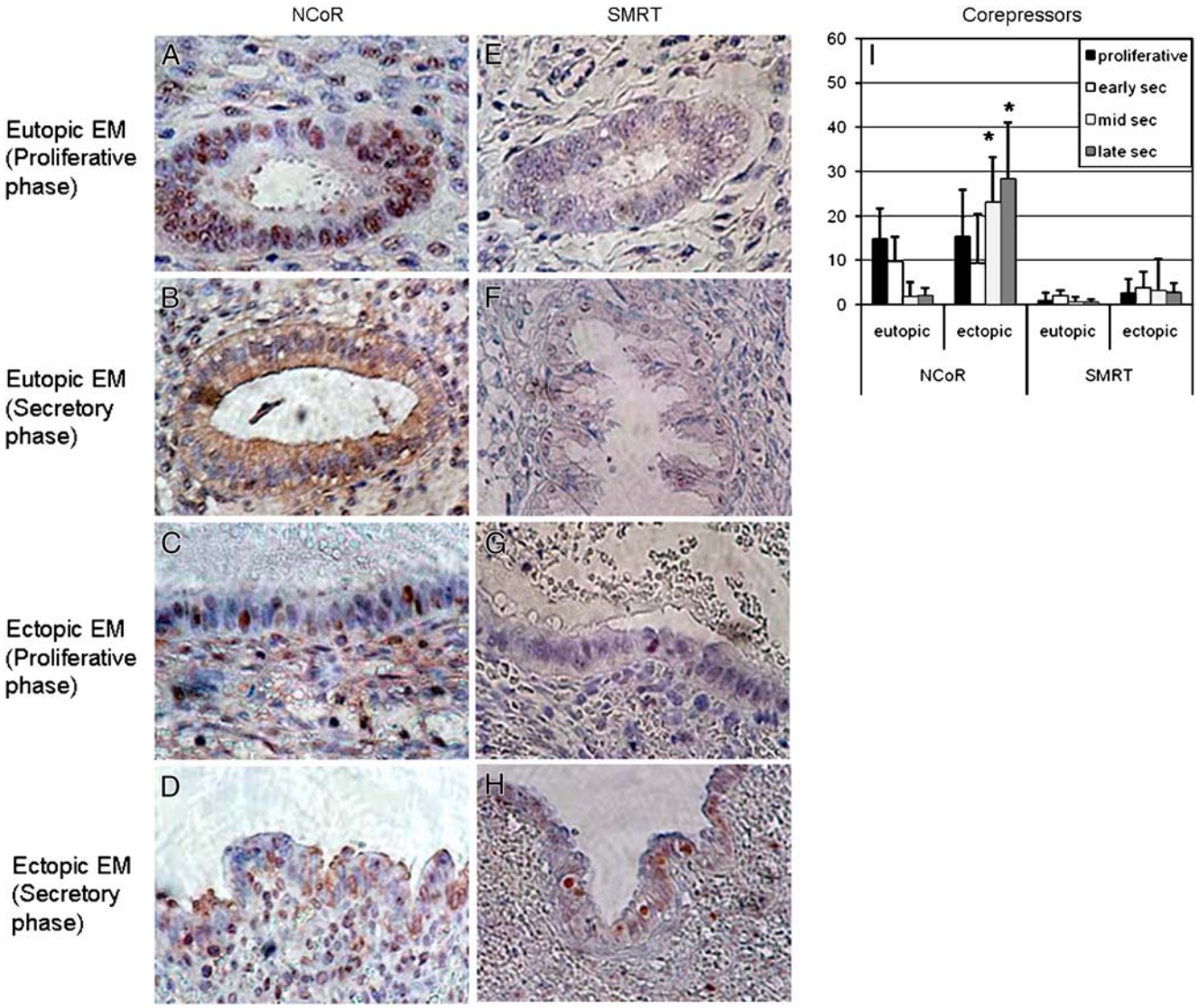

Fig. 4 Immunostaining of corepressors in eutopic and ectopic endometria. In the eutopic endometrium, NCoR staining was predominant in the proliferative phase (**a**) and almost absent in the secretory phase (**b**). In contrast, NCoR staining was sporadic and constant in the ectopic endometrium (**c** and **d**). Immunostaining of SMRT was almost absent throughout the menstrual cycle (**e** and **f**). In the ectopic endometrium, SMRT staining was absent in the proliferative phase (**g**) and focally distributed in the secretory phase (**h**). (A-H, ×200) *I*: Graphic representation of the immunostainings of steroid receptor corepressors. PIs were lower for corepressors and were lower than those for coactivators. NCoR was predominantly expressed in the proliferative phase in the eutopic endometrium and in the secretory phase in the ectopic endometrium (*left*). The expression of SMRT was negligible in both eutopic and ectopic endometria (*right*)*$P<0.05$

of the present study were in line with those studies. The functional involvement of NCoR in endometriotic epithelia remains unclear. However, typical morphological changes in the secretory phase as observed in eutopic endometrial epithelia were not observed in endometriotic epithelial cells [37]. In addition, a recent study suggested that progesterone responsiveness was modulated in endometriotic epithelia via impaired progesterone signaling, which resulted in reduced differentiation and apoptosis [38]. NCoR reportedly was able to form a complex with PR [39] and recruited to a PR-responsive element in the presence of progestins [40], thus, it is likely that NCoR is involved in the down-regulation of genes targeted by progesterone.

With regard to SMRT, involvement in the suppression of sex steroid-mediated signaling has also been suggested, however, its expression was negligible in eutopic and ectopic endometria. This result was consistent with previous findings in normal endometria [10], and the functional significance of SMRT in endometriotic epithelia also remains to be elucidated.

In conclusion, we demonstrated the expression of cofactors in endometriosis and revealed a significant

decrease in the expression of SRC-1 in endometriotic epithelia, suggesting ER-mediated growth to be regulated by a reduction in SRC-1/ER-α expression in endometriotic lesions. Further study of sex steroid hormone signaling in endometriosis is warranted.

Acknowledgment

Conflict of interest statement We declare that we have no conflict of interest.

References

1. Strauss J III, Coutifaris C (1999) The endometrium and myometrium: regulation and dysfunction. In: Yen SSC, Jaffe RB, Barbieri R (eds) Reproductive endocrinology, 4th edn. WB Saunders, Philadelphia, pp 218–256
2. Giudice LC, Kao LC (2004) Endometriosis. Lancet 364:1789–1799
3. Matsuzaki S, Fukaya T, Suzuki T et al (1999) Oestrogen receptor alpha and beta mRNA expression in human endometrium throughout the menstrual cycle. Mol Hum Reprod 5:559–564
4. Giudice LC (1994) Growth factors and growth modulators in human uterine endometrium: their potential relevance to reproductive medicine. Fertil Steril 61:1–17
5. Shiozawa T, Li SF, Nakayama K et al (1996) Relationship between the expression of cyclins/cyclin-dependent kinases and sex-steroid receptors/Ki67 in normal human endometrial glands and stroma during the menstrual cycle. Mol Hum Reprod 2:745–752
6. Shiozawa T, Miyamoto T, Kashima H et al (2004) Estrogen-induced proliferation of normal endometrial glandular cells is initiated by transcriptional activation of cyclin D1 via binding of c-Jun to an AP-1 sequence. Oncogene 23:8603–8610
7. Kashima H, Horiuchi A, Uchikawa J et al (2009) Up-regulation of nuclear receptor corepressor (NCoR) in progestin-induced growth suppression of endometrial hyperplasia and carcinoma. Anticancer Res 29:1023–1029
8. McKenna NJ, Lanz RB, O'Malley BW (1999) Nuclear receptor coregulators: cellular and molecular biology. Endocr Rev 20:321–344
9. McKenna NJ, O'Malley BW (2000) From ligand to response: generating diversity in nuclear receptor coregulator function. J Steroid Biochem Mol Biol 74:351–356
10. Shiozawa T, Shih HC, Miyamoto T et al (2003) Cyclic changes in the expression of steroid receptor coactivators and corepressors in the normal human endometrium. J Clin Endocrinol Metab 88:871–878
11. Uchikawa J, Shiozawa T, Shih HC et al (2003) Expression of steroid receptor coactivators and corepressors in human endometrial hyperplasia and carcinoma with relevance to steroid receptors and Ki-67 expression. Cancer 98:2207–2213
12. Freedman LP (1999) Increasing the complexity of coactivation in nuclear receptor signaling. Cell 97:5–8
13. Huang HJ, Norris JD, McDonnell DP (2002) Identification of a negative regulatory surface within estrogen receptor alpha provides evidence in support of a role for corepressors in regulating cellular responses to agonists and antagonists. Mol Endocrinol 16:1778–1792
14. Pickartz H, Beckmann R, Fleige B et al (1990) Steroid receptors and proliferative activity in non-neoplastic and neoplastic endometria. Virchows Arch A Pathol Anat Histopathol 417:163–171
15. Jones RK, Bulmer JN, Searle RF (1995) Immunohistochemical characterization of proliferation, oestrogen receptor and progesterone receptor expression in endometriosis: comparison of eutopic and ectopic endometrium with normal cycling endometrium. Hum Reprod 10:3272–3279
16. Nisolle M, Casanas-Roux F, Donnez J (1997) Immunohistochemical analysis of proliferative activity and steroid receptor expression in peritoneal and ovarian endometriosis. Fertil Steril 68:912–919
17. Mosselman S, Polman J, Dijkema R (1996) ER beta: identification and characterization of a novel human estrogen receptor. FEBS Lett 392:49–53
18. Fujimoto J, Hirose R, Sakaguchi H et al (1999) Expression of oestrogen receptor-alpha and -beta in ovarian endometriomata. Mol Hum Reprod 5:742–747
19. Brandenberger AW, Lebovic DI, Tee MK et al (1999) Oestrogen receptor (ER)-alpha and ER-beta isoforms in normal endometrial and endometriosis-derived stromal cells. Mol Hum Reprod 5:651–655
20. Misiti S, Schomburg L, Yen PM et al (1998) Expression and hormonal regulation of coactivator and corepressor genes. Endocrinology 139:2493–2500
21. Klinge CM, Jernigan SC, Mattingly KA et al (2004) Estrogen response element-dependent regulation of transcriptional activation of estrogen receptors alpha and beta by coactivators and corepressors. J Mol Endocrinol 33:387–410
22. Leo C, Chen JD (2000) The SRC family of nuclear receptor coactivators. Gene 245:1–11
23. Spencer TE, Jenster G, Burcin MM et al (1997) Steroid receptor coactivator-1 is a histone acetyltransferase. Nature 389:194–198
24. Tai H, Kubota N, Kato S (2000) Involvement of nuclear receptor coactivator SRC-1 in estrogen-dependent cell growth of MCF-7 cells. Biochem Biophys Res Commun 267:311–316
25. Thenot S, Charpin M, Bonnet S et al (1999) Estrogen receptor cofactors expression in breast and endometrial human cancer cells. Mol Cell Endocrinol 156:85–93
26. Nephew KP, Ray S, Hlaing M et al (2000) Expression of estrogen receptor coactivators in the rat uterus. Biol Reprod 63:361–367
27. Noble LS, Simpson ER, Johns A et al (1996) Aromatase expression in endometriosis. J Clin Endocrinol Metab 81:174–179
28. Zeitoun K, Takayama K, Sasano H et al (1998) Deficient 17beta-hydroxysteroid dehydrogenase type 2 expression in endometriosis: failure to metabolize 17beta-estradiol. J Clin Endocrinol Metab 83:4474–4480
29. Leite RS, Brown AG, Strauss JF III (2004) Tumor necrosis factor-alpha suppresses the expression of steroid receptor coactivator-1 and -2: a possible mechanism contributing to changes in steroid hormone responsiveness. FASEB J 18:1418–1420
30. Eisermann J, Gast MJ, Pineda J et al (1988) Tumor necrosis factor in peritoneal fluid of women undergoing laparoscopic surgery. Fertil Steril 50:573–579
31. Shibata H, Spencer TE, Onate SA et al (1997) Role of co-activators and co-repressors in the mechanism of steroid/thyroid receptor action. Recent Prog Horm Res 52:141–164, discussion 16
32. Kwok RP, Lundblad JR, Chrivia JC et al (1994) Nuclear protein CBP is a coactivator for the transcription factor CREB. Nature 370:223–226
33. Zhang X, Jeyakumar M, Petukhov S et al (1998) A nuclear receptor corepressor modulates transcriptional activity of antagonist-occupied steroid hormone receptor. Mol Endocrinol 12:513–524
34. Zanger K, Radovick S, Wondisford FE (2001) CREB binding protein recruitment to the transcription complex requires growth factor-dependent phosphorylation of its GF box. Mol Cell 7:551–558
35. Zhong H, May MJ, Jimi E et al (2002) The phosphorylation status of nuclear NF-kappa B determines its association with CBP/p300 or HDAC-1. Mol Cell 9:625–636
36. Wieser F, Schneeberger C, Hudelist G et al (2002) Endometrial nuclear receptor co-factors SRC-1 and N-CoR are increased in

human endometrium during menstruation. Mol Hum Reprod 8:644–650
37. Metzger DA, Olive DL, Haney AF (1988) Limited hormonal responsiveness of ectopic endometrium: histologic correlation with intrauterine endometrium. Hum Pathol 19:1417–1424
38. Bulun SE, Cheng YH, Yin P et al (2006) Progesterone resistance in endometriosis: link to failure to metabolize estradiol. Mol Cell Endocrinol 248:94–103
39. Wagner BL, Norris JD, Knotts TA et al (1998) The nuclear corepressors NCoR and SMRT are key regulators of both ligand- and 8-bromo-cyclic AMP-dependent transcriptional activity of the human progesterone receptor. Mol Cell Biol 18:1369–1378
40. Wang D, Wang Q, Awasthi S et al (2007) Amino-terminal domain of TIF2 is involved in competing for corepressor binding to glucocorticoid and progesterone receptors. Biochemistry 46:8036–8049

Virchows Arch (2010) 456:443–447
DOI 10.1007/s00428-010-0889-5

ORIGINAL ARTICLE

Imprint cytology in tumor tissue bank quality control: an efficient method to evaluate tumor necrosis and to detect samples without tumor cells

Pascaline Boudou-Rouquette · Noura Touibi · Pierre-Yves Boëlle · Emmanuel Tiret · Jean-François Fléjou · Dominique Wendum

Received: 12 November 2009 / Revised: 6 January 2010 / Accepted: 31 January 2010 / Published online: 27 February 2010
© Springer-Verlag 2010

Abstract Quality assessment of the tissue stored in a tumor biobank is crucial because it is estimated that approximately 10% of the frozen samples are unsuitable for a molecular analysis mainly because of sampling problems in the tissue. We studied the value of imprint cytology (IC) versus frozen section to quantify necrosis and tumor cells in the tissue. The amount of tumor cells and necrosis was assessed by one pathologist on the frozen sections and ICs independently on 100 consecutive tumor samples. It was expressed as a percentage on frozen sections and on a four-level semiquantitative scale for IC (0 to 3+). Overall agreement between the quantity of tumor cells on IC and on frozen section was fair (K=0.23). Sensitivity and specificity of IC to detect the absence of tumor cell on the frozen section were 57% (4/7) and 98% (91/93), respectively. Overall agreement between necrosis quantification on IC and on frozen section was substantial (K=0.66).Sensitivity and specificity of IC to detect significant necrosis (defined as more than 30% necrosis) were 100% (3/3) and 98% (95/97), respectively. We show that IC is efficient to semiquantify necrosis in a tumor sample and to detect significant necrosis. IC seems to be less efficient to quantify tumor cells.

Keywords Imprint cytology · Frozen sections · Tissue banking · Quality control

P. Boudou-Rouquette · N. Touibi · J.-F. Fléjou · D. Wendum (✉)
Service d'Anatomie et Cytologie Pathologiques, AP-HP,
Hôpital Saint-Antoine,
184 rue du faubourg St Antoine,
75571 Paris Cedex 12, France
e-mail: dominique.wendum@sat.aphp.fr

N. Touibi · J.-F. Fléjou · D. Wendum
Tumorothèque Cancer-Est,
Paris, France

P.-Y. Boëlle
Unité de Santé Publique, AP-HP, Hôpital Saint-Antoine,
184 rue du faubourg St Antoine,
75571 Paris Cedex 12, France

P.-Y. Boëlle · E. Tiret · J.-F. Fléjou · D. Wendum
UPMC, Univ Paris 06,
Paris, France

E. Tiret
Service de Chirurgie générale et digestive, AP-HP,
Hôpital Saint-Antoine,
184 rue du faubourg St Antoine,
75571 Paris Cedex 12, France

Introduction

"Molecular pathology" expands dramatically in Anatomic Pathology. Indeed, molecular analyses of tissues are more and more often essential for diagnosis, prognosis, and/or treatment indication particularly in cancer (e.g., targeted therapies) [1–3]. Although formalin-fixed paraffin-embedded tissues can be used for some molecular analyses, frozen tumor tissues are still necessary in many cases. Moreover, frozen tumor tissues are one of the most essential resources for oncological research programs [4]. Knowing the pathological diagnosis or the histological composition of the stored tissue is essential before its use. Indeed, it is estimated that approximately 10% of the samples are unsuitable for a molecular analysis mainly because of sampling problems in

the tissue (no tumor, insufficient tumor cells, and insufficient viable tumor cells) [5]. Quality assessment of the stored tissue is therefore crucial. Three different techniques can be used to perform a morphological control: the frozen section, the mirror image, and the imprint cytology. Frozen section represents the reference in term of morphological control because it analyzes the frozen tissue itself, but it is time consuming. Performed at −20°C, it may favor nucleic acid degradation. It also consumes tissue, and this can sometimes be problematic when the tissue sample is very small. The mirror image consists in sampling a tissue just nearby the frozen tissue and to perform a conventional histological analysis on it. This technique gives a very good morphological aspect of the tissue; however it analyzes the tissue next to the frozen one and not the frozen tissue itself. Several studies have validated intraoperative imprint cytology (IC) as an alternative to frozen section for diagnosis [6, 7]. IC has advantages in terms of rapidity, cost, and tissue preservation. Therefore, IC could be an interesting technique for quality assessment of the frozen stored tissue. In this study, we evaluated the accuracy (specificity, sensitivity, positive predictive value, and negative predictive value) of IC versus frozen section to quantify necrosis and the percentage of tumor cells in the tissue.

Materials and methods

Surgical specimens with tumors were transported immediately from the surgical ward to the Department of Pathology. Several pathologists of the laboratory (n=10) performed the macroscopic examination, sampling, and touch imprints. After macroscopic examination, tumor tissue and normal tissue were sampled from each surgical specimen by a pathologist assisted by a technician. The samples were snap frozen in liquid nitrogen and stored in 2 ml cryovials in an –80°C freezer. A morphological control was performed on the tumor sample using two techniques: IC and frozen section. To avoid any delay in freezing, IC was performed as follows: The sample was gently pressured on a glass slide and then immediately snap-frozen; the slide was then air dried and stained with a rapid variation of May–Grünwald–Giemsa staining. Frozen sections were performed in a second time: The frozen tumor sample on which imprint cytology had been performed was removed from the freezer and put into the cooling chamber of a cryostat. A 5-μm frozen section was performed and stained with hematoxylin, phloxin, and saffron.

One hundred consecutive tumors samples were reviewed by one pathologist (DW, senior pathologist specialized in liver and gastrointestinal pathology with a moderate cytological practice). The amount of tumor cells and necrosis was assessed by the pathologist on the frozen sections and on IC independently. On IC, necrosis and the amount of tumor cells were assessed semiquantitatively as follows: 0, no necrosis or no tumor cells on the imprint; 1+, mild necrosis or tumor cells; 2+, moderate amount of necrosis or tumors cells; 3+, marked amount of necrosis or tumor cells. On frozen sections, quantification was expressed by percentage of necrosis on the slide and percentage of tumor cells among all cells. We defined a significant necrosis on frozen sections as more than 30% of the sample, leading specimen unsuitable for research. In order to assess the kappa coefficient, percentages were divided into four categories: 0 corresponded to 0–5%, 1 to 6–30%, 2 to 31–60%, and 3 to 61–100%.

All the procedures satisfied the requirements of ethical rules.

Statistical analysis

Sensitivity and specificity were calculated to determine the accuracy of IC for quality control, compared to frozen sections which were considered as the reference.

Sensitivity to detect the absence of tumor cells on the frozen section was defined as the number of negative IC results (0, no tumor cell on IC) among those with negative frozen section samples (no tumor cell on frozen section). Specificity was defined as the percentage of positive IC results (IC with tumor cells) among those with positive frozen section samples (tumor cells on frozen section). Negative predictive value was defined as the probability to have tumor cells on frozen section, when IC showed tumor cells. Positive predictive value defined as the probability to have indeed frozen section without tumor cells, when IC showed no tumor cells, was also calculated.

We evaluated in the same manner the presence of necrosis. Sensitivity to detect significant necrosis (>30%) on frozen sections was defined as the percentage of positive IC results (moderate or marked amount of necrosis on IC (2+ or 3+)) among those with positive frozen section samples (>30% of necrosis on frozen sections). Specificity was defined as the percentage of negative IC results (no or mild necrosis, 0 or 1+ on IC) among those with negative frozen sections (less than 30% necrosis on frozen section). Negative predictive value was defined as the probability to have frozen sections without significant necrosis (less than 30% necrosis on frozen section), when IC showed no necrosis or mild necrosis (0 or 1+). Positive predictive value, the probability to have indeed significant necrosis on frozen sections (>30%) when IC showed moderate or marked necrosis (2+ or 3+), was also calculated.

In addition, we used the K (kappa) statistic with linear weighting to measure the agreement between IC in frozen

section and the amount of tumor cells or necrosis [8]. The interpretation of the agreement's value was based on the Landis and Koch Scale (0–0.19 slight, 0.2–0.39 fair, 0.4–0.59 moderate, 0.6–0.79 substantial, and ≥0.8 almost perfect) [9].

Results

The distribution of the tissue samples is summarized in Table 1. Colon, rectum, and liver represented 70% of the processed tissues.

In seven cases out of 100, there were no tumor cells on frozen section. In four cases out of these seven, there were no tumor cells on IC (Table 2). Therefore, the observed sensitivity of IC to detect the absence of tumor cells on the frozen section was 57% (4/7, CI 95%: 25–84%). In the three remaining cases, there were tumor cells on IC, although on the frozen sections, we observed normal tissue: In these cases, the samples labeled "normal tissue" and "tumor tissue" had been switched. In two cases out of 100, there were no tumor cells on IC, whereas there was tumoral tissue on the frozen section (Table 2). The observed specificity of IC to detect the absence of tumor cells on frozen section was 98% (91/93, CI 95%: 93–99%). The positive predictive value of IC to detect the absence of tumor cells in the frozen tissue was 67% (4/6, CI 95%: 30–90%), and the negative predictive value was 97% (91/94, CI 95%: 91–99%; Table 3).

Overall agreement between the quantity of tumor cells on IC and the percentage of tumor cellularity on frozen section was fair (K=0.23). Concerning necrosis, in three cases, there was significant necrosis on frozen section (>30%) and also on the corresponding imprint cytology (Fig. 1, Table 4): Sensitivity of IC to detect necrosis was 100% (3/3, CI 95%: 44–100%). Specificity of IC to detect significant necrosis was 98% (95/97, CI 95%: 93–99%). The positive predictive value of IC to detect significant necrosis was 60% (3/5, CI 95%: 23–88%), and the negative predictive value was 100% (95/95, CI 95%: 96–100%; Table 5). Overall agreement between quantity of necrosis on IC and the percentage of necrosis on frozen section was substantial (K=0.66; Table 4).

Table 1 Distribution of the tissue samples

	Number		Number
Colon	27	Small bowel	2
Rectum	17	Anus	1
Liver	15	Pancreas	1
Lymph nodes	12	Fallopian Tube	1
Breast	9	Myometrium	1
Stomach	5	Bladder	1
Peritoneum	3	Lower limb	1
Ovary	2		
Esophagus	2	Total	100

Table 2 Correlation between amount of tumor cells on IC and on frozen section

Tumor cells on IC	Tumor cells on frozen section (categories)				
	0 (0–5%)	1 (6–30%)	2 (31–60%)	3 (61–100%)	
0	4	0	0	2	6
1+	0	3	2	6	11
2+	1	4	6	24	35
3+	2	3	8	35	48
	7	10	16	67	100

Discussion

In this study, we evaluated IC for quality control of tumor tissue samples in biobanks. We compared IC to frozen sections for quantifying the amount of tumor cells and necrosis in the sample.

We have shown that IC was easy to perform with only two failures (no tumor cells on IC and tumor cells present on frozen sections). IC does not seem to be efficient to assess the amount of tumor cells as we found only a fair correlation (K=0.23) between the amount of tumor cells on IC and on frozen sections evaluated semiquantitatively. This is in contradiction with a previous study that showed a substantial correlation between tumor cellularity on imprints and the sample [10]. However, in this study, IC was evaluated only in breast tumor samples, whereas we evaluated IC in a variety of tumors: breast cancer but also colon, rectum, liver, and lymphomas. Indeed, the tumor characteristics may influence the performance of IC. Moreover, IC was performed and analyzed in a different way. Mangia et al. performed several IC slides, and the area with the highest cellular density was analyzed by two pathologists who counted the tumor cells in ten high power fields. This method is very different compared to ours

Table 3 Comparison of results of imprint cytology (IC) and frozen section to detect the absence of tumor cells (n=100)

	Absence of tumor cells on frozen section	Tumor cells on frozen section
Absence of tumor cells on IC	4	2
Tumor cells on IC	3	91

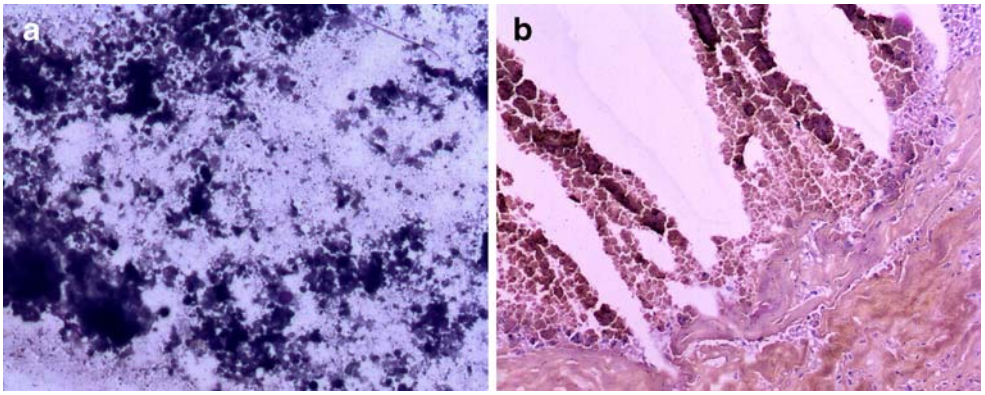

Fig. 1 **a** Imprint cytology with marked necrosis (3+) (rapid May–Grunwald–Giemsa staining) and **b** the corresponding frozen section (hematoxylin–phloxin–saffron staining) showing more than 61% necrosis on the tissue sample

where one IC slide is performed and assessed rapidly by one pathologist with an easy semiquantitative scale.

In addition, the lack of correlation between IC and frozen section may be related to the pathologists who performed IC. Indeed, in our study, nearly all the pathologists of the department (n=10) have performed the sampling and IC slides, and this could lead to a significant difference in cellularity. In accordance with that hypothesis, the two imprints without tumor cells but with tumor cells present on frozen sections were performed by the same pathologist. Although imprints do not seem to be efficient to assess the amount of tumor cells in the tissue sample, it appears to be efficient to identify samples without tumor cells. Indeed, when excluding the three samples with an erroneous labeling, IC detected all the four samples with no tumor cells in the tissue. We were very surprised to see that there were three errors. Consequently, we immediately changed the manner the vials were labeled. IC cannot detect errors in cryovial labeling but quality control by mirror image neither. Detecting such mistakes necessitates a morphological control when the sample is taken out of the vial just before its use or the use of a different technique that allows frozen sections and storage in the same time [11].

IC seems to be efficient to evaluate the amount of tumor necrosis in the samples. Indeed, we found a substantial agreement between the amount of necrosis evaluated on IC and on frozen sections (K=0.66). This is the first study to show the validity of IC to assess tumor necrosis. Sampling was performed after macroscopic examination by a pathologist; therefore, IC can detect necrosis in samples erroneously considered suitable for banking after this macroscopic examination. Moreover, IC was efficient to detect significant necrosis defined as more than 30% necrosis on the frozen sections (100% sensitivity for IC with more than mild necrosis). The positive predictive value of moderate or marked necrosis on IC to detect significant necrosis in the sample appears to be low (60%), but this is because the absolute number of samples with significant necrosis was low (n=3). In fact, only two samples showed a moderate or marked necrosis on IC with less than 30% necrosis in the frozen sections (Table 5). Since the cutting area on the frozen sections may not be exactly the imprinted area, this could lead to a small difference.

Consequently to this study, we decided to perform systematically a frozen section control on the samples with a moderate or marked necrosis on IC. To conclude, in this study we showed that IC is efficient to evaluate the amount of necrosis in a tumor sample and that it can be used to detect the samples with significant necrosis which have to be eliminated. IC seems to be less efficient to evaluate the abundance of tumor cells but can be used to detect the samples without tumor cells. However, IC cannot identify labeling errors of the cryovials that might occur.

Table 4 Correlation between amount of necrosis on IC and on frozen section

Necrosis on IC	Necrosis on frozen section (categories)				
	0 (0–5%)	1 (6–30%)	2 (31–60%)	3 (61–100%)	
0	85	6	0	0	91
1+	0	4	0	0	4
2+	0	1	1	1	3
3+	0	1	0	1	2
	85	12	1	2	100

Table 5 Comparison of results of imprint cytology (IC) and frozen section to detect the presence of necrosis (n=100)

	Significant necrosis (>30%) on frozen section	Absence of significant necrosis on frozen section
Necrosis 2+ or 3+ on IC	3	2
Absence or mild of necrosis (0 or 1+) on IC	0	95

Conflict of interest All the authors declare that they have no conflict of interest.

References

1. Hill DA, O'Sullivan MJ, Zhu X et al (2002) Practical application of molecular genetic testing as an aid to the surgical pathologic diagnosis of sarcomas: a prospective study. Am J Surg Pathol 26:965–977
2. Lievre A, Bachet JB, Le Corre D et al (2006) KRAS mutation status is predictive of response to cetuximab therapy in colorectal cancer. Cancer Res 66:3992–3995
3. Bachet JB, Hostein I, Le Cesne A et al (2009) Prognosis and predictive value of KIT exon 11 deletion in GISTs. Br J Cancer 101:7–11
4. Oosterhuis JW, Coebergh JW, van Veen EB (2003) Tumour banks: well-guarded treasures in the interest of patients. Nat Rev Cancer 3:73–77
5. Qualman SJ, France M, Grizzle WE et al (2004) Establishing a tumour bank: banking, informatics and ethics. Br J Cancer 90:1115–1119
6. Motomura K, Nagumo S, Komoike Y et al (2008) Accuracy of imprint cytology for intraoperative diagnosis of sentinel node metastases in breast cancer. Ann Surg 247:839–842
7. Soo V, Shen P, Pichardo R et al (2007) Intraoperative evaluation of sentinel lymph nodes for metastatic melanoma by imprint cytology. Ann Surg Oncol 14:1612–1617
8. Fleiss J, Cohen J (1973) The equivalence of weighted kappa and the interclass correlation coefficient as measures of reliability. Educ Psychol Meas 33:613–619
9. Landis JR, Koch GG (1977) The measurement of observer agreement for categorical data. Biometrics 33:159–174
10. Mangia A, Chiriatti A, Chiarappa P et al (2008) Touch imprint cytology in tumor tissue banks for the confirmation of neoplastic cellularity and for DNA extraction. Arch Pathol Lab Med 132:974–978
11. Steu S, Baucamp M, von Dach G et al (2008) A procedure for tissue freezing and processing applicable to both intra-operative frozen section diagnosis and tissue banking in surgical pathology. Virchows Arch 452:305–312

Virchows Arch (2010) 456:449–454
DOI 10.1007/s00428-010-0887-7

MEETING REPORT

The role of the pathologist in tissue banking: European Consensus Expert Group Report

Generoso Bevilacqua · Fred Bosman · Thibaut Dassesse · Heinz Höfler · Anne Janin · Rupert Langer · Denis Larsimont · Manuel M. Morente · Peter Riegman · Peter Schirmacher · Giorgio Stanta · Kurt Zatloukal · Elodie Caboux · Pierre Hainaut

Received: 14 January 2010 / Accepted: 15 January 2010 / Published online: 16 February 2010
© The Author(s) 2010. This article is published with open access at Springerlink.com

Abstract Human tissue biobanking encompasses a wide range of activities and study designs and is critical for application of a wide range of new technologies (-"omics") to the discovery of molecular patterns of disease and for implementation of novel biomarkers into clinical trials. Pathology is the cornerstone of hospital-based tissue biobanking. Pathologists not only provide essential information identifying the specimen but also make decisions on what should be biobanked, making sure that the timing of all operations is consistent with both the requirements of clinical diagnosis and the optimal preservation of biological products. This document summarizes the conclusions of a Pathology Expert Group Meeting within the European Biological and Biomolecular Research Infrastructure (BBMRI) Program. These recommendations are aimed at providing guidance for pathologists as well as for institutions hosting biobanks on

This paper reflects the consensus of an expert working group of the Biobank and Biomolecular Research Infrastructure program that met in Munich on 17–18 December 2008. Authors are listed in alphabetical order and participated equally to this working group. The last two authors, EC and PH (IARC) convened the meeting and organized the manuscript.

G. Bevilacqua
Division of Surgical, Molecular and Ultrastructural Pathology,
University of Pisa and Pisa University Hospital, Medical School,
via Roma 57,
56126 Pisa, Italy
e-mail: g.bevilacqua@med.unipi.it

F. Bosman
Institut de Pathologie, CHUV,
Rue du bugnon 25,
1011 Lausanne, Switzerland
e-mail: Fred.Bosman@chuv.ch

T. Dassesse
European Organisation for Research and Treatment (EORTC),
Translational Research Unit,
Avenue E. Mounier, 83 b11,
1200 Brussels, Belgium
e-mail: thibaut.dassesse@gmail.com

H. Höfler
Institut für Allgemeine Pathologie und Pathologische Anatomie,
Der Technischen Universität München,
Ismaninger Str. 22,
81675 Munich, Germany
e-mail: hoefler@helmholtz-muenchen.de

A. Janin
Pathological Anatomy and Cytology, Saint Louis Hospital,
1 avenue Claude Vellefaux,
75475 Paris, France
e-mail: anne_janin@yahoo.com

R. Langer
Institute of Pathology, Klinikum Rechts der Isar,
Technische Universität München,
Trogerstrasse 18,
Munich 81675, Germany
e-mail: Rupert.Langer@lrz.tu-muenchen.de

D. Larsimont
Institut Jules Bordet, Service of Pathological Anatomy,
Cytology and Cytogenetics, Tumors Centre,
Rue Héger-Bordet 1,
1000 Brussels, Belgium
e-mail: denis.larsimont@bordet.be

M. M. Morente
Tumor Bank Unit, Molecular Pathology Program,
Spanish National Cancer Centre—CNIO,
Melchor Fernandez Almegro 3,
28029 Madrid, Spain
e-mail: mmorente@cnio.es

how to better integrate and support pathological activities within the framework of biobanks that fulfill international standards.

Keywords Pathology · Biobanks · Biomarkers · Harmonization · Standards · Translational research

Introduction

Over the past 20 years, biobanking of human specimens has become a central activity underpinning all aspects of biomedical research as well as the development of personalized medicine [1–4]. Biobanking encompasses a wide range of specimen types and sample collection designs, ranging from population-based biobanking of specimens from healthy subjects in large, epidemiological cohorts to specific biobanking of diseased tissues obtained in the course of clinical interventions [2, 5–7]. Human tissue biobanking is of particular importance for implementation of novel biomarkers into clinical trials, as well as for the application of a wide range of new technologies (-"omics") to the discovery and validation of new, molecular patterns of disease [8–12].

Heterogeneity and variability of pre-analytical practices is a major source of error in analyzing biobanked specimens. In recent years, large international efforts have converged towards the harmonization of standard operating procedures for biobanking, providing a basis for improving reproducibility and comparability of molecular data as well as for designing large, multicentric studies involving specimen exchanges among different centers [4, 13–17].

The most critical steps in the workflow of biospecimen acquisition and annotation for biobanking involve hospital pathologists. Pathology is the cornerstone of tissue biobanking. The most basic minimal standard for any biobanking operation is to identify and define the nature and origin of the tissues to be kept in the biobank. This requires specialized pathology expertise. Furthermore, pathologists also make decisions on what should be biobanked, making sure that the timing of all operations is consistent with both the requirements of clinical diagnosis and the optimal preservation of biological products. Pathologists also play a central role in the design of studies involving banked biospecimens and in the dialogue between clinicians and researchers. The rapid development of biobanking as an essential process in translational research and personalized medicine places strong demands on the work of the pathologist.

This document summarizes the conclusions of a Pathology Expert Group Meeting that took place in Munich in December 2008 within the European Biological and Biomolecular Research Infrastructure (BBMRI) Program [4, 18]. The experts have considered all aspects of the involvement of the pathologist in the biobanking process. They also discussed the impact of biobanking on pathology practice. The recommendations developed in the document are aimed at providing guidance for pathologists as well as for institutions hosting biobanks on how to better integrate and support pathological activities within the framework of biobanks that fulfill international standards.

Scope and definition

1. The focus of the working group is the banking for research of human tissues in a clinical context. This activity is hereby defined as "tissue banking". It includes, but is not limited to, the banking of residual specimens obtained in the course of clinical procedures as well as of "post-mortem material."
2. Tissue banking is a chain of operations that includes informing patients and obtaining the proper consent (depending on local requirements), data acquisition, tissue procurement, annotation, preservation, storage, quality control, cataloguing, managing of access, processing and distribution. Pathology expertise is required at several steps. Tissue banking also requires expertise in cryobiology, quality management, legal/ethical aspects, project management, staff management, administration and networking.

P. Riegman
Department of Pathology, Josephine Nefkens Institute,
Erasmus Medical Center,
Be 235b Dr Molwaterplein 50,
3015 GE Rotterdam, The Netherlands
e-mail: p.riegman@erasmusmc.nl

P. Schirmacher
Institute for Pathology, Heidelberg University Hospital,
Im Neuenheimer Feld 220,
69120 Heidelberg, Germany
e-mail: Peter.Schirmacher@med.uni-heidelberg.de

G. Stanta
Department of Clinical,
Morphological and Technological Sciences, Cattinara Hospital,
Surgical Pathology Bldg, Strada di Fiume 447,
Trieste 34149, Italy
e-mail: stanta@icgeb.org

K. Zatloukal
Institute of Pathology, Medical University of Graz,
Auenbruggerplatz 25,
8036 Graz, Austria
e-mail: kurt.zatloukal@meduni-graz.at

E. Caboux · P. Hainaut (✉)
International Agency for Research on Cancer (IARC),
150, cours Albert Thomas,
69008 Lyon, France
e-mail: hainaut@iarc.fr

3. "Pathology archives" represent a special type of tissue repository that may support tissue banking, provided that they fulfill required standards with respect to (1) documentation of variations; (2) cataloguing; (3) rules of access; (4) fulfillment of legal requirements for use as research resource. The primary role of these archives is to document diagnosis and to support later/metachronous diagnostic analyses but they should be developed in a way that allows them to fulfill roles in research as well.

Recommendations

R1: The working group recommends developing a published reference framework for "organizing and managing a tissue bank" in clinical practice, defining standards that distinguish "archive" from 'tissue bank".

R2: In the accreditation process of a pathology laboratory, the quality and compliance to standard of the tissue archive/tissue banks must be taken into consideration.

Tissue banking: critical role in articulating translational research and personalized medicine

1. Tissue banking in a clinical context is essential for the procurement of high quality samples for translational research aimed at biomarker discovery and validation as well as identification of new targets for therapy. It is therefore a strategic activity for research and innovation in biomedicine.
2. Tissue banking is critical for implementing and applying biomarkers in clinical practice. It lays the foundations for the discovery of new targets for therapy and for drug discovery. It sets conditions and procedures allowing patients to benefit from new developments in biomarkers as well as personalized medicine and is therefore beneficial for future diagnosis and treatment and for public health. In this vision, each patient contributes to the care that will be provided to the future patients.
3. Translational research on biomarkers encompasses three overlapping phases: discovery, validation, and implementation. Each phase has different requirements in terms of tissue banking.
4. Discovery phase is aimed at identifying biomarkers and molecular targets for therapy, establishing their prevalence and formulating hypotheses on their biological and medical significance in ex vivo analyses. This requires access to well annotated and pathologically reviewed case series, either based on specimens collected and processed in the course of clinical diagnostic activities or in specific tissue collection protocols.
5. Validation phase is aimed at demonstrating the effect and significance of a potential biomarker. This requires applying ex vivo analyses within study designs with adequate epidemiological and statistical power. Such designs may be comparable to those of clinical trials except that they do not necessarily imply de novo specimen collection using invasive procedures. In a number of cases, these studies can be constructed using retrospective or prospective collections.
6. Implementation phase is aimed at translating biomarkers into clinical practice in affordable, cost-effective conditions and at integrating new biomarkers into diagnostic practice. This requires applying biomarkers to a large series of specimens collected using standard operating clinical protocols.

Recommendations

R3: Contributing to medical progress through participation in tissue banking should be offered to the largest possible number of patients.

R4: Tissue banking should take into consideration the need for collecting appropriate reference samples. Whenever possible and appropriate, the reference sample may consist of corresponding tissue not affected by the disease process.

R5: Clinical practice should evolve to take into account the most effective way to exploit new molecular validated biomarkers and therapeutic targets. This requires technical innovation on evidence-based protocols for tissue procurement, preservation and processing. Innovation should also aim at better using archived collections.

R6: Given that specimens collected in clinical practice are critical for research, rules of patient information and consent should be compatible with the broad use of such specimens in conditions fulfilling strict criteria of protection of persons and data. The working group recommends that further work is developed to increase awareness on these issues and to develop ethical and legal procedures at the national and European level.

Role of the pathologist

1. The pathologist has an essential role in tissue banking. His medical and scientific expertise is required at two distinct phases in the process of tissue banking: (1) in making diagnostic decisions, providing specific annotations and overseeing specimen procurement and preservation, and (2) in reviewing specimens and providing information prior to specimen processing and distribution to research laboratories.
2. Through his role in tissue banking, the pathologist is a key actor in the continuity between research and medical care.
3. The pathologist adds value and expertise to the definition of the banked tissue and is a critical scientific contributor to research carried out on the specimen.
4. The pathologist validates the appropriateness of the banked tissue specimen and its use for a particular research purpose, excluding conflicts with diagnostic purposes.

5. The pathologist has a key role as custodian of the banked specimens. Tissue collections are best developed in the context of a pathology department or pathology service.

Recommendations

R7: No tissue banking for research should take place without proper pathology documentation. All specimens used within research programs must have been reviewed and assessed by a pathologist.

R8: The standard for tissue banking is a tissue sample and not derived products or isolated molecules.

R9: The pathologist should have an active participation in decisions of access to banked specimens.

R10: Efforts should be made to better communicate the role of pathology in tissue banking.

Role of institutions

1. Tissue banking is not the exclusive responsibility of pathology departments. It should be run in the context of institutions (mainly hospitals or universities) that are responsible for providing the whole chain of expertise and the organizational frame required for tissue banking.
2. Institutions are responsible for the maintenance, sustainability, and accessibility of tissue banks, adequate level of training of the staff and the protection of patient rights. Full cost calculation is an essential step in guaranteeing the sustainability of the tissue bank.

Recommendations

R11: Institutions should commit adequate resources and staff dedicated to acquisition, processing and proper distribution of both data and specimens and assisting the pathologist in all tasks that do not require a qualification in pathology. The basic requirements are (1) daily and technical management, (2) data and specimen collection management and (3) expertise in biobanking ethics and law, and (4) networking biobanks. Biobank staff, depending on the size of the pathology department should include at least a tissue bank manager and a technician in addition to the pathologist. The institution should commit adequate resources for pathologists to be involved, in addition to their clinical task, in tissue-banking activities.

R12: Technical and pathology expertise should be provided by the pathology department; the added scientific value should be recognized.

R13: Institutional commitment and appropriateness of the level of resources dedicated to tissue banks should be considered as critical elements in the process of tissue bank accreditation, which could be part of a general hospital or pathology accreditation.

R14: The institution should be responsible for setting and publicizing the rules of access to tissue banks.

R15: The rights of the patients should be taken into account in the procedures and rules for access and use of the tissue bank.

R16: In granting access to tissue-banked specimens, a general principle of "minimal sample amount of tissue necessary for the project" is recommended.

R17: Each procurement of banked tissue for research should be formalized through a Material Transfer Agreement (the scope and content of this MTA is a matter for further elaboration at the European level).

R18: Funding agencies should be aware of the requirements of tissue banking before granting funds for a research project. Projects using banked specimens should specifically (1) provide assurance of the participation and support of the tissue banks; (2) consider the costs of specimen procurement and processing in relation with their specific research application.

R19: A European framework for the professionalization of tissue banking should be developed, e.g., through a teaching program at master level.

Tissue banking in clinical trials

1. Clinical trials offer a wide range of designs with added value for the discovery, validation and implementation of potential new biomarkers
2. Using biomarkers is critical for the interpretation of many therapeutic trials in particular for defining the characteristics of responders vs. non-responders.
3. In future medical care, biomarkers will become mandatory for allocating patients to appropriate therapeutic protocols.
4. The participation of a biobank into a clinical trial should obey to the same strict technical, legal, and ethical standards independently of the type of promoter, academic, or industrial.

Recommendations

R20: As a rule, tissue banking should be considered as an option in every clinical trial.

R21: The need for biomarker application and the possibility of using trials for biomarker validation should be taken into account in the statistical and logistical design of the trial.

R22: Pathologists should be involved in trial design.

R23: There should be a comprehensive registry in the tissue bank (ideally coupled to an institutional clinical trial registry system) of the tissue samples collected in the context of clinical trials.

Improving standards for tissue banking within clinical practice

1. There are technical differences in current standards for tissue processing in pathology practice and in tissue banking.
2. Many protocols used in tissue banking, e.g., for duration of fixation, optimal time for preservation and duration of storage, are mainly based on experience rather than evidence.
3. There is a need for more adequate markers of quality for the tissue-banking process for the qualification of banked tissue specimens for specific research applications.

4. Discovery, validation, and implementation of biomarkers and therapeutic targets in the clinics require a very large series of specimens with inter-laboratory comparison. Such studies need strong networking between dedicated platforms using harmonized, comparable protocols.

R24: Innovation in tissue banking should focus on reducing gaps between standards for clinical practice and for research, and on the development of biomarkers for the quality control of tissue-banking procedures

R25: The development of evidence-based protocols supported by published data should be a priority. Journal editors should be made aware of this priority and should solicit contributions to support this effort. Scientific journals should develop proper expert reviewing for the correct collection, handling and processing of human tissues forming the basis of published data.

R26: It is recommended that current European initiatives and programs that develop technical platforms for large-scale specimen analysis are duly reviewed, assessed, and "harvested" for developing models for future network development.

Incentives for increasing the participation of pathologists

1. Tissue banking is an important mechanism by which pathologists participate in generating and increasing knowledge in biomedicine.
2. In many instances, the involvement of the pathologist adds scientific value to the banked specimens beyond the requirements of routine diagnosis. This added value corresponds to an intellectual property.
3. Tissue-banking activities entail considerable costs and demands on pathology staff time.

R27: Efforts should be made to increase the awareness of the pathology community that (1) participating in research through tissue banking is part of their professional duties; (2) tissue banking is an instrument for managing the evolution of pathology work towards integration of biomarker analysis in clinical practice.

R28: Pathologists should be involved as scientists in developing the design of studies using banked specimens and in interpreting their results.

R29: The scientific involvement of pathologists should be acknowledged in publication authorship. This involvement may consist of specific diagnostic procedures and annotations at the time of specimen acquisition and/or pathology review before specimen processing for specific research purposes.

R30: Contributing to tissue banking should not compete with the performance of clinical pathology duties; therefore, sufficient time and resources should be committed by institutions to the performance of tissue-banking activities.

R31: In developing research on banked specimens, researchers should take into account the costs of the tissue-banking operation and should include these costs in grant applications.

Conclusions and perspectives: a strategic vision for tissue banking in Europe

Today, tissue banks have a key role in the process of biomarker and drug target discovery through the procurement of annotated specimens to innovative research programs. In addition to this research role, the use of cellular and molecular biomarkers is rapidly becoming a standard part of hospital pathology practice and of therapeutic decision schemes. Tissue banking is the key mechanism for pathologists to get involved in translating newly discovered biomarkers into clinical practice [3]. Furthermore, tissue banking will rapidly become an intrinsic part of pathology requirements in the context of standard clinical care.

Given its strong linkage with clinical activities, tissue banking is best performed at the local level, and its sustainability requires investment in infrastructure at the local and/or regional and national levels, to avoid duplication of effort and achieve critical mass necessary to address major academic research programs, as well as to secure a strong position in addressing the needs of industry. Therefore, tissue banks must be organized in operational networks [18].

Implementation of biomarkers will require large networks interconnecting tissue banks, analysis and distribution platforms and several other data resources such as databases of clinical information and population-based disease registries. Biobank networks should have fully documented standard operating procedures, share tissue bank catalogues, and clear rules for access [19–21]. They should also be able to run research projects based on collections developed in several tissue banks. Such projects may be retrospective (using previously banked specimens) or prospective. Running the same, hypothesis-driven collection protocol through a large network of tissue banks that adhere to the same standards will allow assembling large case series addressing a wide range of clinical conditions. In developing such protocols, the diversity of European populations and ecological contexts is an asset for the design of sophisticated case–case comparison studies [22].

To achieve this vision, it is essential to perform innovative research on improving all aspects of specimen processing, including the development of quality controls applicable to retrospective collections. This requires a dedicated effort from funding agencies and from the scientific and medical publication community. Training of highly qualified tissue-banking professionals will increase the standards of tissue banking as well as the recognition of tissue banking as an integral part of biomedicine. This will also facilitate the development and dissemination of a corpus of harmonized, evidence-based tissue-banking procedures.

Conflict of interest statement We declare that we have no conflict of interest.

Open Access This article is distributed under the terms of the Creative Commons Attribution Noncommercial License which permits any noncommercial use, distribution, and reproduction in any medium, provided the original author(s) and source are credited.

References

1. Riegman PH, Dinjens WN, Oosterhuis JW (2007) Biobanking for interdisciplinary clinical research. Pathobiology 74:239–244
2. Riegman PH, Morente MM, Betsou F et al (2008) Biobanking for better healthcare. Mol Oncol 2:213–222
3. Morente MM, Fernandez PL, de Alava E (2008) Biobanking: old activity or young discipline? Semin Diagn Pathol 25:317–322
4. Asslaber M, Zatloukal K (2007) Biobanks: transnational, European and global networks. Brief Funct Genomic Proteomic 6:193–201
5. Pukkala E, Andersen A, Berglund G et al (2007) Nordic biological specimen banks as basis for studies of cancer causes and control–more than 2 million sample donors, 25 million person years and 100,000 prospective cancers. Acta Oncol 46:286–307
6. Ioannidis JP, Adami HO (2008) Nested randomized trials in large cohorts and biobanks: studying the health effects of lifestyle factors. Epidemiology 19:75–82
7. Brand AM, Probst-Hensch NM (2007) Biobanking for epidemiological research and public health. Pathobiology 74:227–238
8. Srivastava S, Gopal-Srivastava R (2002) Biomarkers in cancer screening: a public health perspective. J Nutr 132:2471S–2475S
9. Srinivas PR, Kramer BS, Srivastava S (2001) Trends in biomarker research for cancer detection. Lancet Oncol 2:698–704
10. Scheel JR, Kuo MD (2006) Exploring the human genome in cancer with genomic approaches. J Vasc Interv Radiol 17:1225–1233
11. Rai AJ (2007) Biomarkers in translational research: focus on discovery, development and translation of protein biomarkers to clinical immunoassays. Expert Rev Mol Diagn 7:545–553
12. Maruvada P, Wang W, Wagner PD et al (2005) Biomarkers in molecular medicine: cancer detection and diagnosis. Biotechniques Suppl:9–15
13. Caboux E, Plymoth A, Hainaut P (2007) Common minimal technical standards and protocols for Biological Resource Centers dedicated to Cancer Research. IARC Working Group Reports 2:1–38
14. Betsou F, Barnes R, Burke T et al (2009) Human biospecimen research: experimental protocol and quality control tools. Cancer Epidemiol Biomarkers Prev 18:1017–1025
15. Knoppers BM, Fortier I, Legault D et al (2008) The Public Population Project in Genomics (P3G): a proof of concept? Eur J Hum Genet 16:664–665
16. Moore HM, Compton CC, Lim MD et al (2009) 2009 Biospecimen research network symposium: advancing cancer research through biospecimen science. Cancer Res 69:6770–6772
17. Riegman PH, Dinjens WN, Oomen MH et al (2006) TuBaFrost 1: uniting local frozen tumour banks into a European network: an overview. Eur J Cancer 42:2678–2683
18. Yuille M, van Ommen GJ, Brechot C et al (2008) Biobanking for Europe. Brief Bioinform 9:14–24
19. Vaught JB, Lockhart N, Thiel KS et al (2007) Ethical, legal, and policy issues: dominating the biospecimen discussion. Cancer Epidemiol Biomarkers Prev 16:2521–2523
20. Lemrow SM, Colditz GA, Vaught JB et al (2007) Key elements of access policies for biorepositories associated with population science research. Cancer Epidemiol Biomarkers Prev 16:1533–1535
21. Van Veen EB, Riegman PH, Dinjens WN et al (2006) TuBaFrost 3: regulatory and ethical issues on the exchange of residual tissue for research across Europe. Eur J Cancer 42:2914–2923
22. Riboli E (2001) The European Prospective Investigation into Cancer and Nutrition (EPIC): plans and progress. J Nutr 131:170S–175S

Virchows Arch (2010) 456:455–461
DOI 10.1007/s00428-010-0885-9

CASE REPORT

Localized intrapancreatic malignant mesothelioma: a rare entity that may be confused with other pancreatic neoplasms

Rosanny Espinal-Witter · Elliot L. Servais · David S. Klimstra · Michael D. Lieberman · Rhonda K. Yantiss

Received: 29 October 2009 / Revised: 22 December 2009 / Accepted: 11 January 2010 / Published online: 11 February 2010
© Springer-Verlag 2010

Abstract Malignant mesothelioma usually presents with diffuse involvement of the pleura or peritoneum. Circumscribed or localized malignant mesothelioma has been described in these locations, as well as the viscera, in which case it may cause diagnostic confusion with other, more common entities. Herein, we describe the first well-documented case of primary intrapancreatic malignant mesothelioma in the English literature. The patient was an otherwise healthy 39-year-old woman who presented with a symptomatic mass in the head of the pancreas that was completely resected via pancreaticoduodenectomy. The tumor was composed of cysts, papillae, and tubules lined by cells with abundant eosinophilic cytoplasm and immunohistochemically expressed CA-125, calretinin, and D2-40. Follow-up revealed no evidence of residual or recurrent disease 32 months after surgery. This report also describes the clinical and pathologic characteristics of an intrapancreatic mesothelioma and provides a review of the literature regarding entities that may be considered in the differential diagnosis of this tumor.

Keywords Epithelioid · Pancreatic tumor · Immunohistochemistry

R. Espinal-Witter (✉) · R. K. Yantiss
Department of Pathology and Laboratory Medicine,
Weill Medical College of Cornell University,
525 East 68th Street,
New York, NY 10021, USA
e-mail: roe2005@nyp.org

R. K. Yantiss
e-mail: rhy2001@med.cornell.edu

E. L. Servais · M. D. Lieberman
Department of Surgery,
Weill Medical College of Cornell University,
525 East 68th Street,
New York, NY 10021, USA

E. L. Servais
e-mail: els9066@nyp.org

M. D. Lieberman
e-mail: mdlieber@med.cornell.edu

D. S. Klimstra
Department of Pathology,
Memorial Sloan Kettering Cancer Center,
1275 York Avenue,
New York, NY 10021, USA
e-mail: klimstrd@mskcc.org

Introduction

Most solid tumors of the pancreas are primary epithelial neoplasms, and approximately 80% of symptomatic neoplasms are ductal adenocarcinomas [1]. The true incidence of pancreatic endocrine neoplasms is unknown, although these lesions account for 5–8% of clinically relevant pancreatic neoplasms, followed in frequency by acinar cell carcinoma and solid pseudopapillary neoplasm [2–5]. In contrast to primary ductal carcinomas, metastases to the pancreas are relatively infrequent, accounting for only 3–12% of all pancreatic malignancies [6, 7]. Metastases to the pancreas typically originate from the kidney, lung, breast, gastrointestinal tract, skin, and prostate and often manifest within a year of diagnosis of the primary malignancy [6]. However, mesenchymal neoplasms that originate in the pancreas are distinctly uncommon, and primary tumors of other cell lineages are quite rare. In this report, we describe the clinical, histologic, and immunohistochemical features of a malignant mesothelioma that developed in the pancreas of a young woman. To our knowledge, this is the first documented case of a primary intrapancreatic mesothelioma in the English literature.

Clinical history

A 39-year-old female presented with a 1-month history of right-sided abdominal pain and intermittent nausea without vomiting or weight loss. There was no history of asbestos exposure or jaundice, and liver function tests were within normal limits [alanine transaminase, 14 U/L (normal, 3–40 U/L); aspartate transaminase, 18 U/L (normal, 3–35 U/L); alkaline phosphatase, 76 U/L (normal, 20–125 U/L); total bilirubin, 0.7 mg/dl (normal, 0.2–1.3 mg/dl); direct bilirubin, 0.1 mg/dl (normal, 0.1–0.4 mg/dl)]. The patient's serum carcinoembryonic antigen (CEA) level was normal (0.9 ng/ml; normal, 0.0–2.5 ng/ml) and the CA19-9 level was slightly elevated (56 U/ml; normal, 0–37 U/ml). An abdominal ultrasound revealed a heterogeneous mass in the head of the pancreas, and this finding was confirmed by a subsequent computerized tomography (CT) study that demonstrated a 4-cm mass in the pancreatic head without lymphadenopathy or vascular invasion (Fig. 1a). A fine-needle aspiration was not performed. Given the clinical concern for a pancreatic malignancy, a pancreaticoduodenectomy was performed.

Material and methods

The surgical resection specimen consisted of the head of the pancreas, distal stomach, duodenum, proximal jejunum, and distal common bile duct. Routinely processed (10% buffered formalin), paraffin-embedded tissue sections were examined and the tumor was evaluated using a panel of immunohistochemical markers at the dilutions enumerated in Table 1. Immunohistochemical stains were performed using standard techniques. A sample of the tumor was also submitted for electron microscopy, however, prior formalin fixation resulted in artifactual distortion that precluded ultrastructural evaluation.

Results

Intraoperative exploration revealed an isolated mass in the head of the pancreas. The ovaries were normal and there were no other intra-abdominal masses or nodules. The pancreas contained a 4.5×4.0×3.9-cm well-circumscribed, solid, and cystic yellow tumor (Fig. 1b). The tumor did not involve the pancreatic duct, common bile duct, ampulla, or duodenum. Tissue sections demonstrated a heterogeneous neoplasm composed of cysts, papillary excrescences, nests, and cords of epithelioid cells enmeshed within a collagenous stroma (Fig. 2). Most of the neoplastic cells contained abundant eosinophilic or vacuolated cytoplasm and displayed mild to moderate cytologic atypia. The nuclei were round to ovoid with irregular contours, peripherally condensed chromatin, and inconspicuous nucleoli. Mitotic figures were relatively infrequent (<1/×400 magnification fields). Although grossly circumscribed, the tumor was unencapsulated and infiltrated the pancreatic parenchyma. Lymphovascular invasion was present, and 13 regional lymph nodes were negative for metastatic tumor deposits.

Immunohistochemical studies demonstrated strong and diffuse staining of tumor cells for keratins (CK AE1/AE3, CAM 5.2, and CK7), epithelial membrane antigen (EMA), and several markers typically expressed by mesothelial cells [CA-125, calretinin (cytoplasm and nucleus), and D2-40]. Weak, patchy staining for CK5/6 was also present. The tumor cells displayed only cytoplasmic β-catenin staining

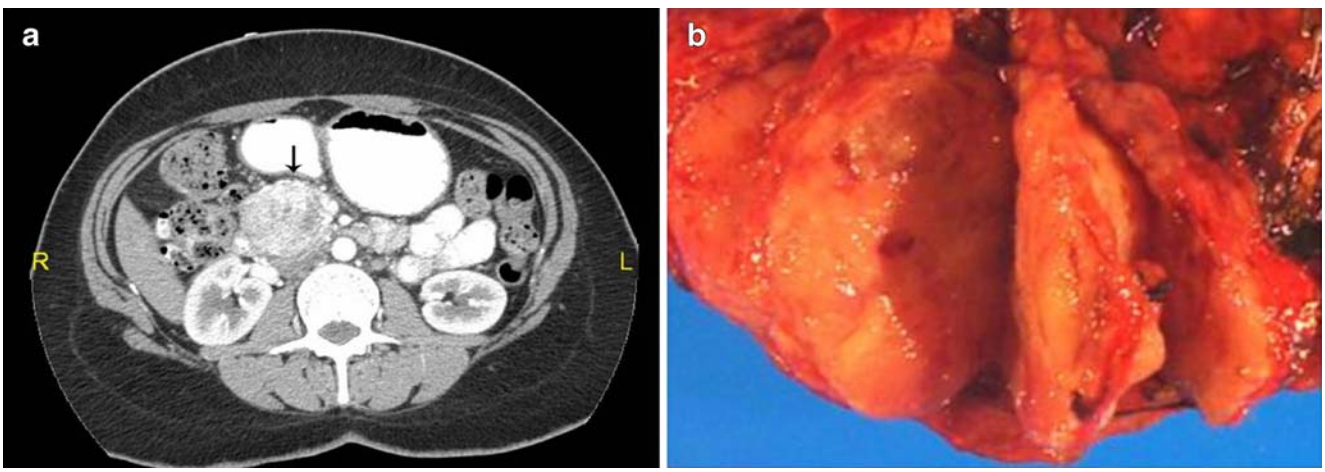

Fig. 1 A CT scan of the abdomen revealed a heterogeneous enhancing mass (*arrow*) within the head of the pancreas (**a**), corresponding to a well-circumscribed, solid, and cystic tumor in the surgical resection specimen (**b**)

Table 1 Immunohistochemical stains used in case evaluation

	Dilution	Manufacturer
Epithelial markers		
Cam 5.2	1:200	Becton Dickinson; San Jose, CA
AE1/AE3	1:6,000	Chemicon; Temecula, CA
Cytokeratin 7	1:800	DakoCytomation; Carpinteria, CA
Cytokeratin 20	1:100	DakoCytomation; Carpinteria, CA
EMA	1:100	Becton Dickinson; San Jose, CA
CA-125	1:1,000	Signet; Emeryville, CA
CEA	1:250	BioGenex; San Ramon, CA
Mesothelial markers		
B72.3	1:200	BioGenex; San Ramon, CA
D2-40	1:50	Novacastra; Newcastle, UK
Calretinin	1:80	Zymed; South San Francisco, CA
WT-1	1:50	Novacastra; Newcastle, UK
BerEP4	1:200	DakoCytomation; Carpinteria, CA
CD15	1:50	Becton Dickinson; San Jose, CA
Cytokeratin 5/6	1:75	DakoCytomation; Carpinteria, CA
Endocrine markers		
Chromogranin	1:400	BioGenex; San Ramon, CA
Synaptophysin	1:100	Neomarkers; Fremont, CA
Other markers		
α-1-antichymotrypsin	1:500	DakoCytomation; Carpinteria, CA
α-1-antitrypsin	1:10,000	Novacastra; Newcastle, UK
Vimentin	1:20	Becton Dickinson; San Jose, CA
β-Catenin	1:200	Becton Dickinson; San Jose, CA
α-Fetoprotein	1:25	Vision Novacastra; Newcastle, UK
Inhibin	1:80	Serotec; Kidlington, UK
P63	1:100	BioGenex; San Ramon, CA

and were negative for CEA, vimentin, α-1-antitrypsin, α-1-antichymotypsin, α-fetoprotein, B72.3, CK20, inhibin, p63, WT-1, chromogranin, and synaptophysin (Fig. 3). Overall, the combined morphologic and immunohistochemical features were most compatible with a diagnosis of localized epithelioid malignant mesothelioma.

The patient had an uneventful postoperative course and was discharged in stable condition. She received no adjuvant therapy and remained well and disease-free 32 months after resection of the tumor.

Discussion

In this report, we describe a case of primary epithelioid malignant mesothelioma that developed in the pancreas of a 39-year-old woman with no history of asbestos exposure. The tumor appeared as a solitary solid and cystic lesion in the head of the pancreas, unassociated with any evidence of other abdominal disease. It displayed a combination of solid, tubular, and papillary cellular growth patterns characteristic of mesothelioma and showed strong immunohistochemical staining for CA-125, calretinin, and D2-40, supporting the diagnosis [8]. The tumor also lacked immunoexpression of several other markers that would have suggested alternative diagnoses.

Malignant mesothelioma usually develops in the pleural cavities, followed in frequency by the peritoneal, and rarely, the pericardial surfaces [9–12]. Primary peritoneal malignant mesothelioma diffusely involves the peritoneum, producing a variety of symptoms, including an abdominal mass, ascites, distention, pain, and weight loss [12]. Similar to pleural malignant mesothelioma, most peritoneal tumors affect older males (mean age, 60 years; male/female ratio, 3/1), are associated with a history of asbestos exposure, and pursue an aggressive clinical course [11, 12]. However, a second incidence peak occurs among young adult females (mean age, 47 years) as shown by Baker et al. in the largest series of such cases reported to date [13]. Malignant mesotheliomas that develop in this group are not clearly related to asbestos exposure and show limited organ invasion [14, 15]. Tumors from young women also pursue a relatively indolent clinical course with a mean survival of 56 months (range, 1 month to 15 years), indicating that peritoneal malignant mesotheliomas that develop among

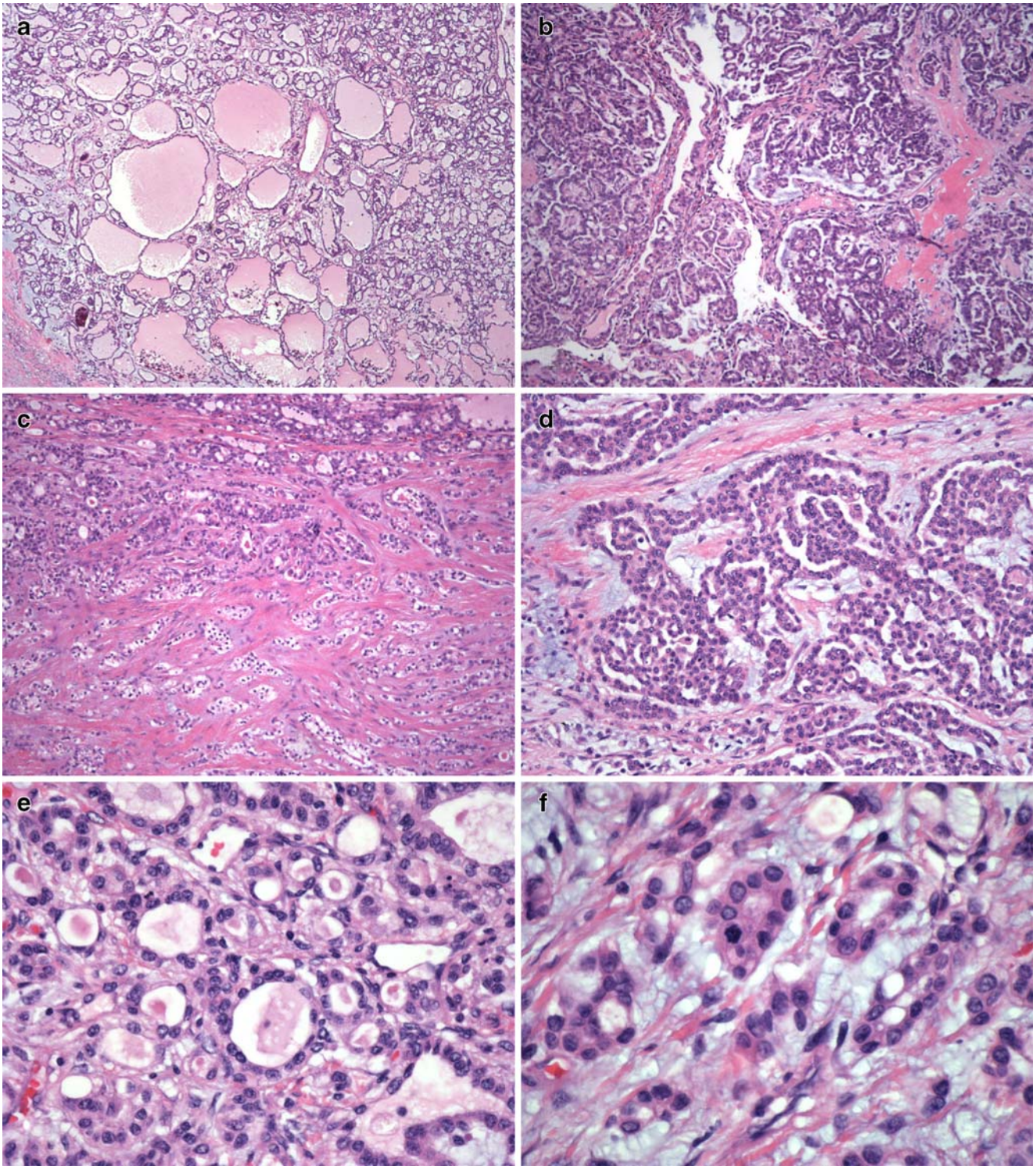

Fig. 2 The tumor displayed histologic heterogeneity. In some areas, it displayed multiple cysts of variable size that contained proteinaceous material (**a**), whereas papillary structures (**b**) and infiltrating nests and tubules of tumor cells were noted in other areas (**c**). Papillary areas contained tufts of epithelial cells (**d**) and small tubules that were lined by cuboidal cells with eosinophilic cytoplasm. The tumor cells showed mild cytologic atypia with round nuclei, inconspicuous nucleoli, and infrequent mitotic figures (**e**, **f**). Occasional cells contained cytoplasmic vacuoles reminiscent of signet ring cells (**f**, *upper right*). Metaplastic ossification was also noted (**b**, *right*)

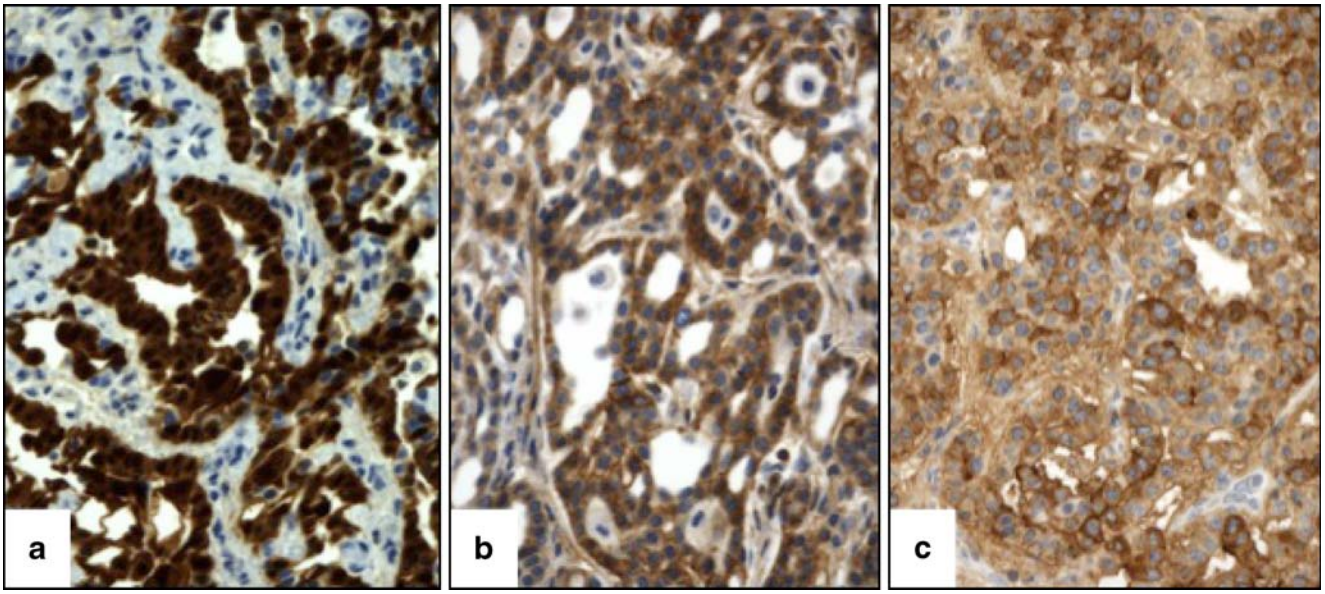

Fig. 3 Tumor cells displayed strong cytoplasmic staining for calretinin (**a**) and D2-40 (**b**). Although cytoplasmic staining for β-catenin was noted, nuclear staining was absent (**c**)

young women may be biologically distinct from those affecting older men [15].

Localized malignant mesotheliomas are much less common than diffuse neoplasms, and most involve the pleura or peritoneal surfaces [16, 17]. In the largest series to date, Allen and Cagle described 23 cases of localized malignant mesothelioma, all of which presented as well-circumscribed tumors [17]. In that series, localized malignant mesotheliomas more commonly developed in older males, but only four (17%) were associated with a history of asbestos exposure. In contrast to diffuse malignant mesothelioma, 50% of patients were alive after several years of follow-up [17].

Primary malignant mesothelioma rarely develops in solid organs in the absence of pleural, peritoneal, or pericardial involvement, but cases have been reported to occur in the lung, gonads, and liver [9]. Two intrapulmonary malignant mesotheliomas have been described to date. The diagnosis in both cases was confirmed by tissue culture and electron microscopy, although it was unknown whether either patient had a history of asbestos exposure [18]. Gonadal malignant mesotheliomas account for fewer than 1% of all mesotheliomas, as described in a series of four ovarian and three testicular tumors reported by Attanoos and Gibbs [19]. Gutgemann and Standop reported a case of intrahepatic mesothelioma that developed in a 62-year-old patient who lacked any known history of asbestos exposure. That patient was treated with hepatic segmentectomy, but developed metastatic mesothelioma in periaortic lymph nodes 5 months later [20]. Three other intrahepatic mesotheliomas have been reported to develop in older patients (mean age, 62.6 years) who lacked a documented history of asbestos exposure, but, in contrast to the previously described case, all were disease-free upon limited follow-up (mean, 22 months) [10, 21–23]. Sasaki et al. also reported a case of localized hepatic malignant biphasic mesothelioma in a patient with known asbestosis [24]. Two other studies have documented the occurrence of primary pancreatic malignant mesothelioma, but only one exists in the English literature [25]. That report described a 10-cm solid mass in the pancreatic tail, but the authors provided no information regarding the disease distribution or the morphologic, immunohistochemical, or ultrastructural features of that tumor [26].

The differential diagnosis of intrapancreatic malignant mesothelioma includes several biologically distinct entities, namely, secondary involvement of the pancreas by a peritoneal malignant mesothelioma, primary pancreatic neoplasms, and metastases. The former may be distinguished from intrapancreatic mesothelioma only after careful evaluation of the peritoneal and pleural cavities. Solid pseudopapillary neoplasms of the pancreas may mimic the clinical and morphologic features of intrapancreatic mesothelioma. These lesions typically develop in the second or third decades of life and show a predilection to affect females [27]. Similar to the tumor described in this case, solid pseudopapillary neoplasms are grossly well-circumscribed, variably solid, and cystic intrapancreatic lesions that are composed of sheets and nests of epithelioid cells with eosinophilic cytoplasm. Features that may suggest the diagnosis of solid pseudopapillary neoplasm include the dyshesive appearance of the neoplastic cells, the presence of convoluted and irregular nuclear membranes, a paucity of mitotic figures, and the presence of intracellular and extracel-

lular hyaline globules. Moreover, solid pseudopapillary neoplasms never exhibit true lumen formation, as were noted in the current case. Solid pseudopapillary neoplasms also show characteristic immunohistochemical features that distinguish them from malignant mesotheliomas. They typically express vimentin and nuclear β-catenin, as well as synaptophysin, α-1-antitrypsin, and α-1-antichymotrypsin, all of which were negative in this case [28].

The solid variant of pancreatic serous adenoma may be considered in the differential diagnosis of intrapancreatic malignant mesothelioma since it typically appears as a solid, well-circumscribed pancreatic mass with thick fibrous bands and may contain epithelioid cells with faintly eosinophilic or clear cytoplasm arranged in nests, cords, and cysts [29, 30]. Since its original description, 10 cases of solid serous adenoma have been described in the literature. These tumors tend to occur among older patients (mean, 60 years) and there is no gender predilection [31]. They may occur throughout the pancreas, and their cytologic and immunohistochemical features are identical to those of serous cystadenomas. The neoplastic cells are uniform and polygonal and contain glycogen, which is PAS-positive and diastase-sensitive [30]. In contrast to the current case, serous adenomas lack morphologic heterogeneity, show minimal cytologic atypia, and display virtually no mitotic activity. Serous cells express cytokeratin 7, EMA, and neuron-specific enolase, but are negative for mesothelial markers.

Well-differentiated pancreatic endocrine neoplasms may also show secondary cystic degeneration and contain cells with abundant eosinophilic cytoplasm, potentially mimicking the features of intrapancreatic malignant mesothelioma. However, endocrine neoplasms show bland nuclear features with stippled chromatin, typically lack true lumen formation, and express endocrine markers, such as chromogranin and synaptophysin [3]. Pancreatic acinar cell carcinomas may share some morphologic features with mesothelioma, including a relatively cellular proliferation of neoplastic cells arranged in solid nests that show a variable amount of gland formation. Acinar cell carcinomas commonly display a monotonous cytologic appearance and contain cells with abundant eosinophilic cytoplasm. In contrast to mesothelioma, however, acinar cell carcinomas lack a tubulopapillary growth pattern. They produce pancreatic enzymes and stain immunohistochemically for trypsin, chymotrypsin, and lipase [28].

Secondary malignant tumors of the pancreas may show morphologic features that overlap with those observed in malignant mesothelioma. Patients with metastatic melanoma involving the pancreas usually have evidence of metastatic disease in other organs, although the pancreas may be the only site of metastases in some cases [32]. Metastatic melanoma to solid organs may display solid and cystic areas lined by cells with abundant eosinophilic cytoplasm; although they generally show marked nuclear pleomorphism and cellular necrosis, both of which were lacking in the current case [33]. Moreover, the immunohistochemical profile of melanoma is distinct from that of malignant mesothelioma in that the former strongly expresses S-100 and HMB-45, but is negative for cytokeratins [33]. Metastatic renal cell carcinoma accounts for 62% of all metastases to the pancreas, which may be the sole site of metastatic disease [4]. Metastatic renal cell carcinoma may display a microcystic growth pattern that simulates the appearance of intrapancreatic malignant mesothelioma, particularly if the tumor cells contain abundant eosinophilic cytoplasm. Fortunately, most renal cell carcinomas that metastasize to the pancreas show a clear cell phenotype and a characteristic vascular pattern, both of which are lacking in malignant mesothelioma. Renal cell carcinomas also coexpress cytokeratins and vimentin, as well as CD10, EMA, CA-IX, MUC1, and MUC3 [34]. Finally, peritoneal serous papillary carcinoma may be considered in the histologic differential diagnosis of malignant mesothelioma, but it has not been described as a primary pancreatic malignancy, and most patients with pancreatic involvement would also be expected to have considerable tumor burden in the peritoneal cavity [35, 36].

In summary, malignant mesothelioma may rarely occur as an intrapancreatic neoplasm that mimics the clinical and pathologic features of pancreatic solid pseudopapillary neoplasms, pancreatic endocrine neoplasms, and metastases to this organ. Similar to malignant mesotheliomas that develop in other solid organs, the case reported herein was unassociated with a history of asbestos exposure. Although clinical follow-up is limited, the biologic behavior of this tumor has been favorable, suggesting that pancreatic malignant mesothelioma may be less aggressive than similar tumors of the pleural and peritoneal surfaces.

Acknowledgement The authors would like to sincerely thank Dr. Juan Rosai, member of the Centro Diagnostico Italiano (CDI, Milano, Italy) for reviewing this case and contributing to the final diagnosis.

Conflict of interest statement We declare that we have no conflict of interest.

References

1. Schima W, Ba-Ssalamah A, Kolblinger C et al (2007) Pancreatic adenocarcinoma. Eur Radiol 17:638–649
2. O'Grady HL, Conlon KC (2008) Pancreatic neuroendocrine tumours. Eur J Surg Oncol 34:324–332
3. Lack E (2003) Pathology of the pancreas, gallbladder, extrahepatic biliary tract, and ampullary region. Oxford University Press, New York
4. Mulkeen AL, Yoo PS, Cha C (2006) Less common neoplasms of the pancreas. World J Gastroenterol 12:3180–3185

5. Adams AL, Siegal GP, Jhala NC (2008) Solid pseudopapillary tumor of the pancreas: a review of salient clinical and pathologic features. Adv Anat Pathol 15:39–45
6. Merkle EM, Boaz T, Kolokythas O et al (1998) Metastases to the pancreas. Br J Radiol 71:1208–1214
7. Crippa S, Angelini C, Mussi C et al (2006) Surgical treatment of metastatic tumors to the pancreas: a single center experience and review of the literature. World J Surg 30:1536–1542
8. Ordonez NG (2005) Immunohistochemical diagnosis of epithelioid mesothelioma: an update. Arch Pathol Lab Med 129:1407–1414
9. Liu YC, Kuo YL, Yu CP et al (2004) Primary malignant mesothelioma of the greater omentum: report of a case. Surg Today 34:780–783
10. Leonardou P, Semelka RC, Kanematsu M et al (2003) Primary malignant mesothelioma of the liver: MR imaging findings. Magn Reson Imaging 21:1091–1093
11. Bani-Hani KE, Gharaibeh KA (2005) Malignant peritoneal mesothelioma. J Surg Oncol 91:17–25
12. Taub RN, Keohan ML, Chabot JC et al (2000) Peritoneal mesothelioma. Curr Treat Options Oncol 1:303–312
13. Baker PM, Clement PB, Young RH (2005) Malignant peritoneal mesothelioma in women: a study of 75 cases with emphasis on their morphologic spectrum and differential diagnosis. Am J Clin Pathol 123:724–737
14. Goldblum J, Hart WR (1995) Localized and diffuse mesotheliomas of the genital tract and peritoneum in women. A clinicopathologic study of nineteen true mesothelial neoplasms, other than adenomatoid tumors, multicystic mesotheliomas, and localized fibrous tumors. Am J Surg Pathol 19:1124–1137
15. Kerrigan SA, Turnnir RT, Clement PB et al (2002) Diffuse malignant epithelial mesotheliomas of the peritoneum in women: a clinicopathologic study of 25 patients. Cancer 94:378–385
16. Crotty TB, Myers JL, Katzenstein AL et al (1994) Localized malignant mesothelioma. A clinicopathologic and flow cytometric study. Am J Surg Pathol 18:357–363
17. Allen TC, Cagle PT, Churg AM et al (2005) Localized malignant mesothelioma. Am J Surg Pathol 29:866–873
18. Alvarez-Fernandez E, Escalona-Zapata J (1982) Intrapulmonary mesotheliomas: their identification by tissue culture. Virchows Arch A Pathol Anat Histol 395:331–343
19. Attanoos RL, Gibbs AR (2000) Primary malignant gonadal mesotheliomas and asbestos. Histopathology 37:150–159
20. Gutgemann I, Standop J, Fischer HP (2006) Primary intrahepatic malignant mesothelioma of epithelioid type. Virchows Arch 448:655–658
21. Imura J, Ichikawa K, Takeda J et al (2002) Localized malignant mesothelioma of the epithelial type occurring as a primary hepatic neoplasm: a case report with review of the literature. APMIS 110:789–794
22. Rout P, Rameshkumar K, Srikrishna NV (1999) Hepatic mesothelioma. Indian J Gastroenterol 18:176–177
23. Marubayashi S, Ohdan H, Asahara T et al (1998) Malignant mesothelioma originating in the hepatic falciform ligament: report of a case. Surg Today 28:929–931
24. Sasaki M, Araki I, Yasui T et al (2009) Primary localized malignant biphasic mesothelioma of the liver in a patient with asbestosis. World J Gastroenterol 15:615–621
25. Luttges J, Pierre E, Zamboni G et al (1997) [Malignant non-epithelial tumors of the pancreas]. Pathologe 18:233–237 (in German)
26. De Jong SA, Pickleman J, Rainsford K (1993) Nonductal tumors of the pancreas. The importance of laparotomy. Arch Surg 128:730–734 (discussion 734–736)
27. Geers C, Moulin P, Gigot JF et al (2006) Solid and pseudopapillary tumor of the pancreas—review and new insights into pathogenesis. Am J Surg Pathol 30:1243–1249
28. Klimstra DS (2007) Nonductal neoplasms of the pancreas. Mod Pathol 20(Suppl 1):S94–S112
29. Choi JY, Kim MJ, Lee JY et al (2009) Typical and atypical manifestations of serous cystadenoma of the pancreas: imaging findings with pathologic correlation. AJR Am J Roentgenol 193:136–142
30. Stern JR, Frankel WL, Ellison EC et al (2007) Solid serous microcystic adenoma of the pancreas. World J Surg Oncol 5:26
31. Machado MC, Machado MA (2008) Solid serous adenoma of the pancreas: an uncommon but important entity. Eur J Surg Oncol 34:730–733
32. Nikfarjam M, Evans P, Christophi C (2003) Pancreatic resection for metastatic melanoma. HPB (Oxford) 5:174–179
33. Piura B, Kedar I, Ariad S et al (1998) Malignant melanoma metastatic to the ovary. Gynecol Oncol 68:201–205
34. Zhao B, Kimura W, Futakawa N et al (1997) Renal cell carcinoma of the spindle cell type with metastasis to the pancreas: a case report. Jpn J Clin Oncol 27:58–61
35. Bhuyan P, Mahapatra S, Sethy S et al (2009) Extraovarian primary peritoneal papillary serous carcinoma. Arch Gynecol Obstet (in press)
36. Dalrymple JC, Bannatyne P, Russell P et al (1989) Extraovarian peritoneal serous papillary carcinoma. A clinicopathologic study of 31 cases. Cancer 64:110–115

Virchows Arch (2010) 456:463–472
DOI 10.1007/s00428-010-0913-9

ORIGINAL ARTICLE

Detection and clinical significance of bone marrow involvement in patients with rhabdomyosarcoma

Lenka Krsková · Marcela Mrhalová · Irena Hilská · David Sumerauer · Eva Drahokoupilová · Peter Múdry · Roman Kodet

Received: 23 September 2009 / Revised: 11 February 2010 / Accepted: 25 March 2010 / Published online: 20 April 2010
© Springer-Verlag 2010

Abstract Childhood rhabdomyosarcoma (RMS) has two major histological subtypes: alveolar (aRMS) and embryonal. The aim of the study was to monitor minimal disseminated disease (MDD) using real-time quantitative reverse-transcription PCR (RQ-RT-PCR) of the *PAX3-FKHR*, *PAX7-FKHR* fusion genes and *myoD1* gene. We prepared an assay using RQ-RT-PCR for a quantitative assessment of MDD in aRMS by using hydrolysis probe for quantification of *PAX3-FKHR*, *PAX7-FKHR* and *myoD1* genes and *beta-2-microglobulin* housekeeping gene. Primary tumor samples (44), samples of local recurrences (26) from 48 patients with aRMS were examined by nested RT-PCR and RQ-RT-PCR techniques. Additionally, bone marrow samples (115), peripheral blood progenitor cell samples (27), and peripheral blood samples (25) from 33 aRMS patients were tested. *PAX3/7-FKHR* and *myoD1* transcripts proved to be a sensitive tool for detection of MDD in RMS. We were able to identify 15/25 patients with bone marrow (BM) involvement at the time of presentation using RQ-RT-PCR. We analyzed *PAX3-FKHR* or *PAX7-FKHR* expression during the course of the disease. The RQ-RT-PCR results correlated well with nested RT-PCR results ($p<0.0001$). The presence of metastases is the most adverse prognostic factor in RMS, and bone marrow is a frequent site of the tumor dissemination in RMS, especially in aRMS. Our results detecting the fusion transcripts or *myoD1* transcript in the BM or peripheral blood suggest that patients with positive findings are at high risk of the tumor progression.

Keywords Bone marrow · Minimal disseminated disease · Real-time PCR · Alveolar rhabdomyosarcoma

L. Krsková (✉) · M. Mrhalová · I. Hilská · R. Kodet
Department of Pathology and Molecular Medicine,
2nd Faculty of Medicine,
Charles University and Faculty Hospital in Motol,
Prague, Czech Republic
e-mail: lkrskova@email.cz

D. Sumerauer · E. Drahokoupilová
Department of Pediatric Hematology and Oncology,
2nd Faculty of Medicine,
Charles University and Faculty Hospital in Motol,
Prague, Czech Republic

P. Múdry
Faculty Hospital in Brno, Clinic of Pediatric Oncology,
Brno, Czech Republic

Introduction

Rhabdomyosarcoma (RMS) is the most common pediatric soft tissue sarcoma. On the basis of histopathological criteria, RMS in childhood is classified into two main subtypes: embryonal RMS (eRMS) and alveolar RMS (aRMS) [1]. Alveolar variant portend an unfavorable prognosis [1, 2]. The majority of aRMS (about 80 %) are characterized by a reciprocal chromosomal translocation t(2;13)(q35;q14) or by its variant t(1;13)(p36;q14), involving the *PAX3* and *FKHR* or *PAX7* and *FKHR* genes, respectively.

Approximately in 20% of patients RMS presents as disseminated disease at the time of diagnosis. Lungs, lymph nodes, and bone marrow are frequently involved. Patients with metastatic disease continue to have a very poor prognosis. Local recurrences are also common in advanced local disease.

Molecular detection of minimal disseminated disease (MDD) by a sensitive molecular method could contribute to a better treatment stratification of these patients. For gene fusion-positive aRMS, the possibility of detecting tumor specific chimeric transcripts in peripheral blood (PB), bone marrow (BM), or peripheral blood progenitor cells (PBPC)

by RT-PCR has been demonstrated [3, 4]. For fusion-negative aRMS, the analysis relies on expression of tissue-specific genes—for example *myoD1* or *myogenin*.

In the current study, we analyzed mRNA level of fusion genes or the tissue-specific marker *myoD1* in a group of 48 patients with aRMS. The presence of minimal disseminated disease in PB, BM, or PBPC was analyzed by real-time RT-PCR (RQ-RT-PCR) in 33 children with aRMS at the time of the disease diagnosis and during and/or after therapy.

Materials and methods

Patients and samples

There were 20 boys and 28 girls in the study group (Table 1). Thirty-two patients with alveolar RMS had chimeric products identified (26 PAX3-FKHR and six PAX7-FKHR). Sixteen cases with alveolar morphology were fusion gene negative aRMS (Fig. 1). Twenty-six patients had localized aRMS, and 22 had metastatic disease at the time of presentation. Eighty-seven BM samples (bilateral iliac BM trephines) and 19 PB samples from 24 fusion-positive aRMS patients, 28 BM, and six PB samples from nine fusion-negative aRMSs were analyzed.

To determine the specificity of *myoD1* for RMS at the molecular level, we analyzed a group of non-RMS neoplasms (Table 2).

RNA extraction and preparation of complementary DNA

Total RNA was isolated from fresh frozen (67 cases) or paraffin-embedded sections (12 cases) and from both cryosections and paraffin-embedded sections (four cases) using extraction with Trizol Reagent (Life Technologies, Merelbeke, Belgium) or High Pure RNA Paraffin Kit from Roche (Roche, Mannheim, Germany), both according to the manufacturer's instructions. Also, 41 fresh frozen samples obtained from various neoplasms were extracted using the same protocol.

Complementary DNA (cDNA) was prepared from 11 μl of RNA in 20 μl of reaction volume. The reaction mixture contained Tris–HCl 50 mM, pH 8.3; KCl 75 mM; $MgCl_2$ 3 mM; dithiotreitol 10 mM; dNTP 0.5 mM each; random hexamers 12.5 mM; and 50 units of MMLV reverse Transcriptase (Gibco BRL, Carlsbad, TX, USA) according to the manufacturer's instructions. Reverse-transcription included an incubation period of 60 min at 37°C.

Qualitative RT-PCR for fusion gene *PAX3-FKHR*, *PAX7-FKHR* and for *MyoD1* was performed with primers which are listed in the Table 3. Each PCR reaction was carried out with an initial denaturation step at 95°C for 5 min, annealing for 30 s and extension at 72°C for 30 s, followed

Table 1 aRMS patients

Case	Sex	Age	FusionGene	Follow-up
1	F	14	PAX3-FKHR	DD
2	F	19	PAX3-FKHR	DD
3	F	15	PAX3-FKHR	DD
4	M	12.5	PAX3-FKHR	DD
5	F	6.5	PAX3-FKHR	AW
6	F	15	PAX3-FKHR	DD
7	F	5.5	PAX3-FKHR	DD
8	F	13	PAX3-FKHR	DD
9	F	13.5	PAX3-FKHR	DD
10	M	15	PAX3-FKHR	DD
11	F	0.25	PAX3-FKHR	DD
12	M	13	PAX3-FKHR	DD
13	M	18.5	PAX3-FKHR	DD
14	F	44	PAX3-FKHR	LOST
15	F	9	PAX3-FKHR	DD
16	M	6	PAX3-FKHR	DD
17	F	7	PAX3-FKHR	DD
18	F	9	PAX3-FKHR	DD
19	F	17.5	PAX3-FKHR	AW
20	F	14	PAX3-FKHR	AW
21	F	7	PAX3-FKHR	AW
22	F	3.5	PAX3-FKHR	AW
23	F	10	PAX3-FKHR	DD
24	M	11.5	PAX3-FKHR	DD
25	M	16	PAX3-FKHR	DD
26	M	1	PAX7-FKHR	AW
27	M	1.5	PAX7-FKHR	AW
28	M	5.5	PAX7-FKHR	AW
29	F	6	PAX7-FKHR	AW
30	F	10	PAX7-FKHR	LOST
31	F	2	PAX7-FKHR	DD
32	M	8	NEG	AW
33	M	10	NEG	AW
34	M	0.1	NEG	DD
35	M	5	NEG	AD
36	M	6.5	NEG	DD
37	F	2.5	NEG	DD
38	F	7	NEG	DD
39	M	79	NEG	DD
40	F	2	NEG	DD
41	M	5	NEG	AW
42	M	7	NEG	AW
43	F	14	NEG	DD
44	F	4	NEG	DD
45	M	20	NEG	DD
46	M	9	NEG	AW
47	F	1.5	NEG	AW
48	M	15.5	NEG	AW

M man, *F* female, *AW* alive well, *DD* died of disease, *AD* alive with disease

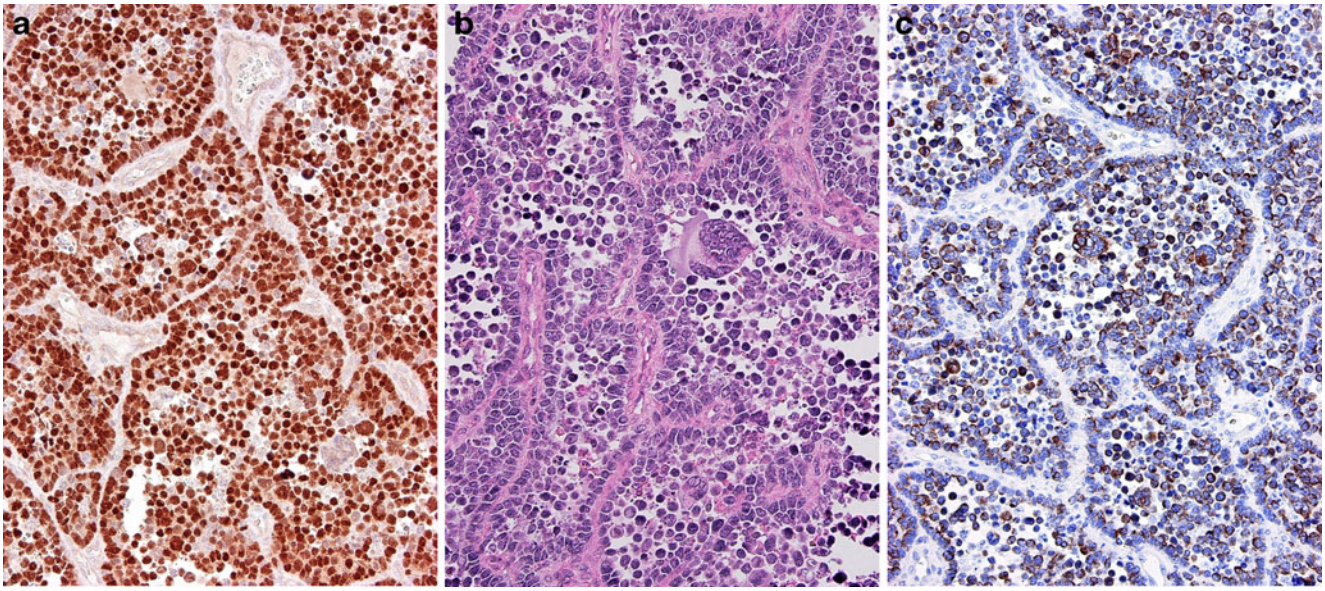

Fig. 1 **a** Alveolar RMS of the left face in a 2-year-old girl displaying a typical pseudoalveolar pattern, stained with HE. **b** The same tumor with immunohistochemical demonstration of desmin (DAKO), counterstained with hematoxylin. **c** Immunohistochemical nuclear staining of myogenin (DAKO) in all tumor cells (still the same case).This case represents aRMS with negative finding of PAX3,7-FKHR fusion genes

by 30 cycles of denaturation at 95°C for 15 s, annealing for 5 s and extension at 72°C for 5 s. One microliter of undiluted PCR product was added to the semi-nested reaction mix for the second round of 30 cycles. The quality of the isolated RNA was assayed with the A2 and A3 oligonucleotide primers to detect the ubiquitously expressed cABL kinase. Negative controls lacking either RNA or RT were routinely included. Products were identified by 1.5% agarose gel electrophoresis and ethidium bromide staining.

Quantitative RT-PCR for fusion gene *PAX3-7/FKHR* and for *myoD1* was performed on LightCycler (Roche), using TaqMan technology. Primers and probes are listed in the Table 3. PAX3/FKHR and PAX7/FKHR primers and probes for RQ-RT-PCR were designed by TipMolBiol; *myoD1* primers and probe were obtained from Applied Biosystems. Human *beta* 2 *microglibulin* was used as a housekeeping gene [5].

β2-microglobulin and PAX3/7-FKHR, myoD1 plasmid DNA calibrators

The *β2-microglobulin*, fusion genes, and *myoD1* sequences were cloned into a PCR 2.1 TOPO cloning vector and were transformed into *E. coli* recipient culture, using the TOPO TA Cloning Kit (Invitrogen). The selected clones were screened using Miniprep method and quantified by spectrophotometer.

Normalization of β2-microglobulin and fuse genes or myoD1 expression

The expression of fusion genes or *myoD1* was calculated using absolute quantification. Plasmids with the insert were diluted in decimal steps into Salmon Sperm DNA. A diluting line of plasmids was used for preparation of standard curves. Normalized expression ($myoD1_N$ or $PAX3/7\text{-}FKHR_N$) was determined as a ratio between *myoD1* or fusion transcript and *β2-microglobulin* levels.

Each PCR run was performed in duplicate, and the mean value of results was calculated.

The sensitivity of the assay for *myoD1* was 18 copies of *myoD1* transcript, for *PAX3-FKHR* 33–330 copies and for *PAX7-FKHR* 440 copies.

Results

Specificity of *myoD1*

In agreement with Gallego et al. [6], we found a higher sensitivity of $myoD1_N$ compared with $PAX3/7\text{-}FKHR_N$ expression, but it has to be cautioned that very low levels of *myoD1* expression were detected in two of 15 healthy bone marrows (the median of $myoD1_N$ mRNA level was 0, mean value was 1.24×10^0, the cutoff limit for BM positivity in RMS patients was determined as $myoD1_N$

Table 2 Non-RMS samples

Type	Number	$myoD1_N$ median $myoD1_N$ mean value
BM from healthy donors	15	0.0×10^0 1.24×10^0
BM from NHL patients	6	0.0×10^0 2.02×10^0
Adult muscle	6	1.64×10^5 1.90×10^5
Non-RMS tumors	18	1.56×10^2 3.43×10^4
Teratoma	2	
Synovial sarcoma	1	
EWS	1	
Alveolar sarcoma of soft tissues	3	
Liposarcoma	1	
Nephroblastoma	1	
Infantile fibromatosis	2	
Infantile myofibroblastic tumor	1	
Leiomyocellular sarcoma	1	
Malignant mixed müllerian tumor	1	
Rhabdomyoma	2	
Extraskeletal myxoid chondrosarcoma	1	
Epitheloid sarcoma	1	
Rhabdoid tumors	4	
Rhabdoid tumor kidney	3	3.03×10^4
Rhabdoid tumor brain)	1	4.8×10^0
Non-Hodgkin lymphomas	19	5.45×10^0 1.16×10^1
Mucosa-associated lymphoid tissue lymph.	3	
PTCL	2	
Burkitt lymphoma	2	
Follicular lymphoma	6	
Mantle cell lymphoma	3	
Diffuse large B cell lymphoma	3	
Ductal breast carcinoma	10	0.0×10^0 7.51×10^0

8.9×10^0). Also a weak positivity of *myoD1* expression was detected in one of six BMs from the patients with hematological malignancies (BM with a massive infiltration by mantle cell lymphoma).

Extending our previous observations [4] we observed that *myoD1* transcript is not fully specific for RMS. Of the 18 non-RMS tumors, only one case (a leiomyosarcoma) was negative; median of the mRNA level of positive cases was 1.56×10^2; mean value was 3.43×10^4 with a strong positivity in tumor samples with a clear rhabdomyoblastic differentiation (teratoma with muscle differentiation, nephroblastoma with rhabdomyoblastic differentiation, and malignant mixed müllerian tumor with rhabdomyoblastic differentiation). Additionally, four rhabdoid tumors were analyzed; the median of mRNA level for rhabdoid tumor of the kidney was 3.03×10^4 in contrast to the rhabdoid tumor of the brain (median 4.8×10^0). In 19 patients with non-Hodgkin lymphomas, the median of $myoD1_N$ mRNA level was 5.45×10^0, mean value 1.16×10^1. The median of $myoD1_N$ mRNA for adult muscle was 1.64×10^5, and the result was very similar to the level observed in both aRMS (median 1.5×10^5) and eRMS (median 1.13×10^5; data not shown).

The utility of *myoD1* as a marker was confirmed by RQ-RT-PCR negativity of a majority of BM samples obtained

Table 3 List of primers for qualitative and quantitative RT-PCR

MyoD1	
F-MyoD1:	5′AGC ACT ACA GCG GCG ACT 3′
R-MyoD1:	5′GCG ACT CAG AAG GCA CGT C 3′
PAX–FKHR and PAX7–FKHR	
PAX3:	5′AGC TAT ACA GAC AGC TTT GT 3′
PAX7:	5′ GCT TCT CCA GCT ACT CTG AC 3′
FKHR-A:	5′ CTC TGG ATT GAG CAT CCA CC 3′
FKHR-B:	5′ TCC AGT TCC TTC ATT CTG CA 3′
cABL	
A2:	5′ TTC AGC GGC CAG TAG CAT CTG ACT T 3′
A3:	5′ TGT GAT TAT AGC CTA AGA CCC GGA GCT TTT 3′
B-2-microglobulin	
B2M-F	5′ TGA CTT TGT CAC AGC CCA AGA TA-3′
B2M-R	5′ AAT CCA AAT GCG GCA TCT TC-3′
B2M probe	5′ TGA TGC TGC TTA CAT GTC TCG ATC CCA-3′
MyoD1 (mix of primers and probe obtained from Applied Biosystem)	
PAX3/FKHR	
PAX3-S	5′ CCC CAT GAA CCC CAC CA-3′
FKHR-A	5′ GAA TGA ACT TGC TGT GTA GGG ACA 3′
PAX3/FKHR probe	5′ TGG CCT CTC ACC TCA GAA TTC AAT TCG T 3′
PAX7/FKHR	
PAX7-F	5′GCG CCC TCC AAC CAC AT-3′
FKHR-A	5′ GAA TGA ACT TGC TGT GTA GGG ACA 3′
PAX7/FKHR probe	5′ ACG GCC TGT CTC CTC AGA ATT CAQA TTC GT 3′

from RMS patients or from other patients with both malignant (alveolar soft part sarcoma and leiomyosarcoma) and non-malignant diseases (infantile fibromatosis).

The level of myoD1 mRNA in aRMS

We did not observe any statistical difference in the level of $myoD1_N$ mRNA in aRMS. The median of $myoD1_N$ mRNA for fusion-positive aRMS was 1.17×10^5, mean value 3.29×10^5; the median of $myoD1_N$ mRNA for fusion-negative aRMS was 2.2×10^5, mean value 4.78×10^5.

Specificity of *PAX3/7-FKHR* fusion gene for *aRMS*

PAX3-FKHR or *PAX7-FKHR* transcripts were found specific for aRMS. We did not find PAX3/7-FKHR positivity in any of non-RMS tumors. The median of $PAX3\text{-}FKHR_N$ mRNA for aRMS was 1.18×10^5, mean value 6.11×10^5, and median of $PAX7\text{-}FKHR_N$ mRNA for aRMS was 2.75×10^3, mean value 6.26×10^3.

PAX3/7-FKHR and myoD1 in RMS and main risk factors—age, generalization of the disease

The relation between age and generalization of the disease at diagnosis (the two principal risk factors of RMS) and *myoD1* or *PAX3-FKHR* expression in the primary tumor samples was analyzed. In children at different age groups (≤1, 1–10, and ≥10) no major difference in *myoD1* or *PAX3-FKHR* expression was observed ($p>0.05$). A similar finding was observed for groups of localized and metastatic aRMSs ($p>0.05$) but with a trend of a higher $myoD1_N$ and a higher $PAX3\text{-}FKHR_N$ mRNA level ($p=0.23$) in the group with metastatic disease.

PAX3/7-FKHR and myoD1 at the time of diagnosis and the follow-up of patients

PAX3-FKHR and *myoD1* expression in primary tumors were analyzed at the time of presentation. There was no significant difference in $myoD1_N$ and $PAX3\text{-}FKHR_N$ expression levels between patients in complete remission and patients with the progression of RMS. In poor-outcome patients, we observed a tendency for a higher mRNA level of $PAX3\text{-}FKHR_N$ at diagnosis ($p=0.13$).

Detection of MDD in microscopically tumor-free resection borders

In two patients with alveolar RMS and the presence of *PAX3-FKHR*, fused gene RT-PCR and RQ-RT-PCR was used to identify malignant cells in resection margins of the

tumor at the time of the tumor recurrence. RNA was extracted from 10×5-μm thick sections of the tumor tissue; the first and last sections were verified by light microscopy. In the first case, one of nine samples taken from the tumor margin, which were shown to be microscopically free of tumor or uncertain whether they contain tumor cells or not on frozen section histology, revealed the fusion transcript *PAX3-FKHR* (normalized 8.4×10^{1} copies) and *myoD1* (normalized 5.76×10^{3} copies) in comparison with the primary tumor sample (*PAX3-FKHR*$_N$ 2.5×10^{5} copies, *myoD1*$_N$ 1.57×10^{5}) and recurrent tumor sample (*PAX3-FKHR*$_N$ 1.18×10^{5} copies, *myoD1*$_N$ 5.52×10^{4} copies). In the second case, a resection border revealed the fusion transcript *PAX3-FKHR* (normalized 2.35×10^{4} copies) and *myoD1* (normalized 2.39×10^{4} copies) in comparison with the primary tumor sample (*PAX3-FKHR*$_N$ 8.35×10^{4} copies, *myoD1*$_N$ 9.89×10^{4}). In one patient with aRMS the presence of *PAX3-FKHR* fused gene and *myoD1* were detected in pleural effusion (*PAX3-FKHR*$_N$ 3.32×10^{2} copies, *myoD1*$_N$ 3.17×10^{4}), and this finding helped to confirm relapse of the disease in this patient without any further surgical intervention.

Bone marrow involvement at diagnosis–RQ-RT-PCR

Table 4 shows the results of BM involvement in patients with aRMS.

Of the 33 BM samples from 18 fusion-positive aRMS patients, 19 were positive by RQ-RT-PCR. Of the 12 children in whom BM infiltration was detected by RQ-RT-PCR technique nine relapsed and died of the disease. Three of six children with negative BM at the time of presentation died. In PBPC samples, we were able to identify infiltration by the tumor cells in ten of 26 (38.5%).

Of the 11 BM samples from seven fusion-negative aRMSs, four were *myoD1*-positive by RQ-RT-PCR. Of the three children in whom BM infiltration was detected, one died of progressive disease, compared with one of four children with negative BM at the time of diagnosis. We were able to identify an infiltration by aRMS cells in one of four PBPC samples.

We detected BM involvement at the time of diagnosis in 11 of 14 patients with metastatic RMS in comparison with the patients with localized disease, in whom the positivity was detected in three of nine, who were tested.

Quantitative evaluation of MDD by RQ-RT-PCR identified a very low level of *myoD1* and/or *PAX3-FKHR* in three patients who were negative by qualitative nested RT-PCR, all of them are alive. For bone marrow involvement in particular, the survival probability was different between the groups with or without the nested RT-PCR positive bone marrow infiltration at diagnosis ($p=0.04$), but the RQ-RT-PCR results did not reach statistical significance ($p=0.21$; Fig. 2a, b).

Marrow disease at the presentation was not associated significantly with any variable, although there was a trend for disseminated tumor cells in the BM to be found more frequently in association with unfavorable primary sites (parameningeal and genitourinary, bladder or prostate) or with metastatic tumor.

Table 4 Results of BM involvement in patients with aRMS

Case	BM at the time of Dg(RQ-RT-PCR/ Q-RT-PCR)	BM during follow-up (RQ-RT-PCR)	BM during follow-up(qualitative RT-PCR)
1	+/+	3/5	2/5
2	−/−	1/2	1/2
3	NA	2/2	2/2
4	−/−	1/3	1/3
5	+/−	NA	NA
6	+/+	3/4	4/4
7	+/+	2/4	1/4
8	+/+	NA	NA
9	NA	1/3	1/3
10	+/+	2/2	1/2
11	NA	1/1	0/1
12	+/+	1/1	1/1
13	+/+	2/3	2/3
14	−/−	NA	NA
15	NA	4/5	4/5
16	NA	0/3	1/3
17	+/+	0/1	0/1
19	+/+	0/1	0/1
21	+/−	NA	NA
24	+/+	3/6	2/6
25	−/−	0/1	0/1
27	−/−	NA	NA
28	−/−	NA	NA
29	NA	0/1	0/1
33	+/−	NA	NA
34	−/−	NA	NA
35	+/+	NA	NA
36	NA	1/1	0/1
37	NA	1/3	1/3
41	−/−	NA	NA
42	+/+	3/6	2/6
47	−/−	NA	NA
48	−/−	NA	NA

NA not available, +/+ positive result using RQ-RT-PCR and nested RT-PCR, −/− negative result using both methods, +/− positive result using RQ-RT-PCR, negative with nested RT-PCR, 3/6 number of positive BM from BM aspirates tested (left and/or right iliac BM trephines)

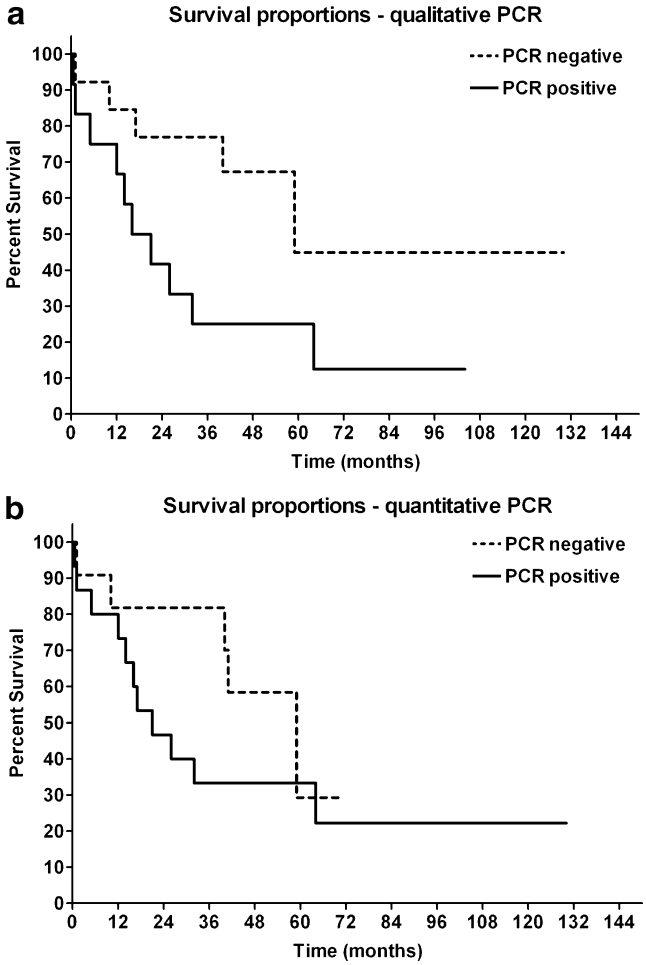

Fig. 2 **a** Kaplan–Meier survival analysis for patients with (1) or without (0) BM involvement at diagnosis, $p=0.04$ Patients with zero $myod1_N$ and/or *fusion gene*$_N$ at presentation (number of patients=14) retained their significantly better prognosis compared with those with detectable level of $myod1_N$ and/or *fusion gene*$_N$ (number of patients=12)–nested RT-PCR results. **b** Kaplan–Meier survival analysis for patients with (number of patients=15) or without BM involvement at diagnosis (number of patients=12), $p=0.21$ (RQ-RT-PCR results)

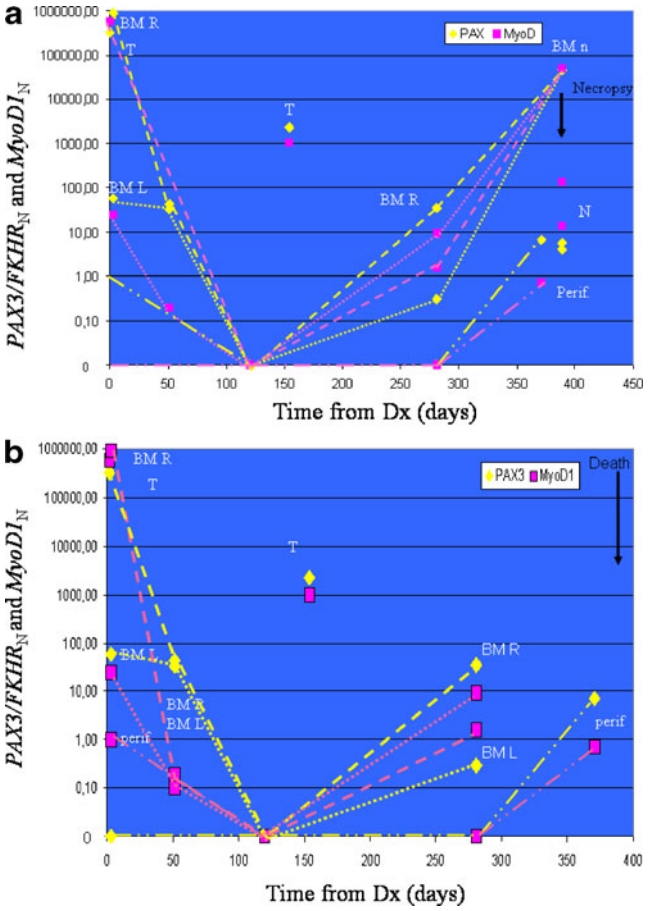

Fig. 3 **a**, **b** Correlation among $PAX3/FKHR_N$ and $myoD1_N$ dynamics and the course of disease in two illustrative patients. Both patients suffered from aRMS and had massive content of rhabdomyoblasts in bone marrow aspirates at the time of diagnosis. Values on *left vertical axis* represent $PAX3/FKHR_N$ and $myoD1_N$ on logarithmic scale and length of the follow-up in days is on *horizontal axis*. *BM* bone marrow aspirate, *BM R* right iliac BM trephine, *BM L* left iliac BM trephine, *perif.* peripheral blood, *T* tumor, *LN* lymph node at the time of necropsy

Bone marrow involvement during the disease course

We analyzed $PAX3/7\text{-}FKHR_N$ and/or $myoD1_N$ expression levels during the course of the disease in 66 sequential BM samples obtained from 18 fusion-positive aRMS patients. BM investigation was performed in case of a previous positivity, in case of a suspected relapse of the disease, and occasionally at the time of the last therapy administration. Thirteen of the 18 patients had a detectable BM involvement in at least one BM sample. A majority of BM samples from relapsed patients and/or closely before a clinical relapse revealed $PAX3/7\text{-}FKHR_N$ or $myoD1_N$ in at least one of the iliac BM trephines. Thirteen of these patients died for disease progression. Figure 3 shows an example of monitoring dynamics of $PAX3/7\text{-}FKHR_N$ and $myoD1_N$ levels during the treatment.

Microcirculating disease

We analyzed only five PB samples at the time of diagnosis obtained from the patients with aRMS. In three circulating tumor cells were found by PAX–FKHR positivity. Of them, one relapsed and lives with the disease progression; the other two positive and two negative patients fare well in complete remission. All patients with positive PB at the time of diagnosis had tumors diagnosed at advanced stages (III and IV).

Discussion

Data on specificity of *myoD1* expression are contradictory. Frascella et al. considered *myoD1* a sensitive and a specific

marker for the molecular diagnosis of RMS [7]. In our study, in accordance with observations published by Gattenloehner et al., we found that *myoD1* transcript is not entirely specific for RMS [8]. We found *myoD1* transcripts (median 1.64×10^5) in a normal skeletal muscle, a result similar to that seen in aRMS (median 1.5×10^5) and eRMS (median 1.13×10^5). Furthermore, other mesenchymal neoplasms used as a control tissue revealed $myoD1_N$ expression (median 1.56×10^2, mean value 3.43×10^4). The positivity of *myoD1* in these tumors may be caused by a mesenchymal origin of these tumors similarly as is the case with RMS. Additionally, four rhabdoid tumors revealed *myoD1* expression, but with a different expression level between rhabdoid tumors of the kidney (median 3.03×10^4) and rhabdoid tumor of the brain (median 4.8×10^0). Some non-Hodgkin's lymphomas (NHLs) show also $myoD1_N$ expression, though weak (median 5.45×10^0, mean value 1.16×10^1). An exception of the tested NHLs was mucosa-associated lymphoid tissue lymphomas. The positivity of *myoD1* in NHLs is difficult to explain. All these results diminish the usefulness of *myoD1* as a single molecular marker in molecular diagnosis of RMS. From the same reason *myoD1* detection is not applicable as a marker of minimal disseminated disease in microscopically tumor-free resection borders.

Davicioni et al. published that *myoD1* is a PAX–FKHR target gene, and it was expressed twofold higher in PAX–FKHR transduced embryonal cell line RD compared with vector control [9]. In contrast to this finding, we did not observe any significant difference between expression levels of *myoD1* in all subgroups of RMS (both the chimeric gene-positive and negative).

The potential clinical value of determining minimal (submicroscopical) residual disease in situ by detection of fusion transcripts *PAX3/FKHR* was confirmed by our findings showing fusion transcripts in microscopically tumor-free resection borders. This approach also helps to distinguish the residual tumor cells with advanced differentiation (post-therapy changes) from atrophic and regenerating muscle cells at the site of the tumor removal.

The presence of metastases is one of the most significant negative prognostic factors in RMS [10], and bone marrow is a frequent site of distant tumor dissemination, particularly in aRMS. Morphologically detectable tumor cells in BM are present at the time of presentation in about 30% of patients with metastatic disease[11]. Thus, we established an assay for a sensitive detection of bone marrow involvement in RMS aimed at the assessment of whether MDD may be associated with specific clinical and biological features and whether it may be of a prognostic value. We were able to find only a limited number of reports investigating the presence of disseminated tumor cells in morphologically negative BM obtained from patients with RMS at the time of diagnosis. Some of these studies used RT-PCR methods evaluating the expression of *PAX3/7-FKHR* [3, 12] or *myoD1* and *myogenin* [13] or immunohistochemistry of MyoD1 and myogenin on BM cytospins [14]. Despite a lower specificity of *myoD1* transcript for RMS and a discrete positivity in a limited number of separated PBPC samples obtained from healthy donors, a good correlation was found between the expression of PAX3-*7/FKHR* and *myoD1* in our study. The strategy for the study of MDD in RMS patients lays in the analysis of multiple markers (fusion genes, *myoD1*, *myogenin*, etc.) by RQ-RT-PCR method which increases the reliability of such an investigation, diminishing false-positive results. In the present study, a real-time RQ-RT-PCR assay was used for the detection of *PAX3/7-FKHR* and *myoD1* transcripts in BM and/or PB in a group of aRMS patients. Using *myoD1* and fusion gene transcripts, we detected tumor infiltration in all microscopically positive bone marrows. In addition, we found RQ-RT-PCR positivity in morphologically negative bone marrow samples. Using RQ-RT-PCR, we found a higher sensitivity of *myoD1* compared with *PAX3/7-FKHR* expression, but the result must be evaluated with a great caution as already discussed. Using the *myoD1* molecular marker, we were able to demonstrate BM infiltration by the tumor cells in a patient with malignant teratoma and rhabdomyoblastic differentiation, in a patient with poorly differentiated soft tissue sarcoma (normalized *myoD1* transcript in primary tumor sample, 1.45×10^5 and 1.9×10^2, respectively). From that reason, we may conclude that *myoD1* transcript is very sensitive but lacks specificity for RMS. Nevertheless, with some caution using cutoff limit for BM positivity and in a combination with other molecular markers of RMS, *myoD1* molecular detection may be applicable for detection of MDD.

There is another point to be considered and it is the relation between MDD and histology and a role of the bone marrow involvement detected using RT-PCR methods in predicting an outcome of the disease. The prognostic impact of micrometastatic disease on RMS is still unclear. Kelly at al. described two patients who died of progressive disease and with BM involvement detected by RT-PCR alone [3]. Our previous study also showed the prognostic impact of BM infiltration and the patient's outcome [4]. In the study published by Gallego et al., the authors did not find a correlation between microcirculating disease detected at the presentation of the disease and the outcome [6]. Their findings confirmed a previous study by Thomson et al. (1999), which reported that patients with overt metastatic disease had circulating tumor cells at the time of diagnosis (67%) and that this finding was without any prognostic significance [15]. We found a significant difference in overall survival probability between the groups with or

without BM infiltration detected by nested RT-PCR alone at the time of diagnosis (p=0.04), but not detected by RQ-RT-PCR technique (p=0.22). We are convinced of this finding that the limited number of patients did not allow us to draw significant difference of prognostic value using RQ-RT-PCR. The results of nested RT-PCR and RQ-RT-PCR were different only in three patients.

We found only a limited number of reports investigating the presence of disseminated tumor cells in BM from RMS patients at the time of presentation [3, 6, 13, 16] using RT-PCR method or immunostaining [14]. In the study by Kelly et al. [3], BM involvement detected by RT-PCR was detected in 14% of RMS patients, Michelagnoli et al. found the BM infiltration in 22 % of samples [13] and McDowell in 27 % of BM samples [14]. The proportion of BM positivity at the time of diagnosis by RMS cells in our group of patients with localized aRMS (33.3%) was even higher. This frequency seems also comparable to the frequency reported in other localized childhood solid tumors such as neuroblastoma (34 %) [17] and Ewing's sarcoma (19 %) [18]. In localized RMS, an analysis of previous studies has also allowed a prediction of failure patterns leading to modifications in the treatment strategy [19]. In the current study, the bone marrow involvement was detected in a significant proportion of patients with metastatic aRMS (78.5%). We were able to demonstrate that BM involvement at the time of diagnosis is associated with the disease progression and a poor clinical outcome in patients with aRMS. These findings suggest that patients with localized aRMS but BM involvement represent a subset of patients at high risk of progression who might benefit from intensification of the therapy and from a more frequent molecular monitoring.

It is reported that the prevalence of minimal BM infiltration by RT-PCR and RQ-RT-PCR of *PAX3,7-FKHR* or *myoD1* at diagnosis is a common event in aRMS. It would be of interest to assess whether the fusion genes or *myoD1* expression levels in BM at diagnosis correlate with BM infiltration response kinetics and whether the expression levels at different time points of the disease course may predict a risk of relapse in patients in a complete clinical remission. In the majority of the patients, we detected a significant increase in $PAX3/FKHR_N$ or $myoD1_N$ levels accompanying the relapse. Analysis of whether or not the increase in fusion genes or *myoD1* mRNA levels really predict the relapse was hampered by the fact that some crucial samples necessary to verify our preliminary data were not available (they were not taken from ethical reasons and because a regular BM sampling at certain points of the disease treatment and following it is not a part of a standard procedure).

In conclusion, analysis of multiple markers by sensitive methods such as RT-PCR and especially RQ-RT-PCR in patients with aRMS argue for the sensitivity of the results. We expect that using such sensitive methods for molecular detection of MDD might contribute to a better understanding of the disease biology and development, and it may enable more individualized specific treatment stratification. It may also lead to the initiation of efforts to explore therapeutic strategies based on the improved understanding of the MDD kinetics.

Acknowledgement The study was supported by the Grant *GAČR 304/07/0532*, the Research Project of the Ministry of Education, Youth and Sports of the Czech Republic No. 0021620813 and by the Research Project of the Ministry of Health MZOFNM2005.

All experiments comply with the current laws of Czech Republic.

Conflict of interest The authors declared no conflict of interest.

References

1. Newton WA Jr (1995) Classification of rhabdomyosarcoma. Curr Top Pathol 89:241–59
2. Tobar A, Avigad S, Zoldan M et al (2000) Clinical relevance of molecular diagnosis in childhood rhabdomyosarcoma. Diagn Mol Pathol 9(1):9–13
3. Kelly KM, Womer RB, Barr FG (1996) Minimal disease detection in patients with alveolar rhabdomyosarcoma using a reverse transcriptase-polymerase chain reaction method. Cancer 78 (6):1320–7
4. Krskova L, Mrhalova M, Sumerauer D et al (2006) Rhabdomyosarcoma: molecular diagnostics of patients classified by morphology and immunohistochemistry with emphasis on bone marrow and purged peripheral blood progenitor cells involvement. Virchows Arch 448(4):449–58
5. Bijwaard KE, Aguilera NS, Monczak Y et al (2001) Quantitative real-time reverse transcription-PCR assay for cyclin D1 expression: utility in the diagnosis of mantle cell lymphoma. Clin Chem 47(2):195–201
6. Gallego S, Llort A, Roma J et al (2006) Detection of bone marrow micrometastasis and microcirculating disease in rhabdomyosarcoma by a real-time RT-PCR assay. J Cancer Res Clin Oncol 132 (6):356–62
7. Frascella E, Rosolen A (1998) Detection of the MyoD1 transcript in rhabdomyosarcoma cell lines and tumor samples by reverse transcription polymerase chain reaction. Am J Pathol 152(2):577–83
8. Gattenloehner S, Dockhorn-Dworniczak B, Leuschner I et al (1999) A comparison of MyoD1 and fetal acetylcholine receptor expression in childhood tumors and normal tissues: implications for the molecular diagnosis of minimal disease in rhabdomyosarcomas. J Mol Diagn 1(1):23–31
9. Davicioni E, Finckenstein FG, Shahbazian V et al (2006) Identification of a PAX-FKHR gene expression signature that defines molecular classes and determines the prognosis of alveolar rhabdomyosarcomas. Cancer Res 66(14):6936–46
10. Maurer HM, Gehan EA, Beltangady M et al (1993) The Intergroup Rhabdomyosarcoma Study-II. Cancer 71(5):1904–22
11. Ruymann FB, Newton WA Jr, Ragab AH et al (1984) Bone marrow metastases at diagnosis in children and adolescents with rhabdomyosarcoma. A report from the intergroup rhabdomyosarcoma study. Cancer 53(2):368–73

12. Athale UH, Shurtleff SA, Jenkins JJ et al (2001) Use of reverse transcriptase polymerase chain reaction for diagnosis and staging of alveolar rhabdomyosarcoma, Ewing sarcoma family of tumors, and desmoplastic small round cell tumor. J Pediatr Hematol Oncol 23(2):99–104
13. Michelagnoli MP, Burchill SA, Cullinane C et al (2003) Myogenin-a more specific target for RT-PCR detection of rhabdomyosarcoma than MyoD1. Med Pediatr Oncol 40 (1):1–8
14. McDowell HP, Donfrancesco A, Milano GM et al (2005) Detection and clinical significance of disseminated tumour cells at diagnosis in bone marrow of children with localised rhabdomyosarcoma. Eur J Cancer 41(15):2288–96
15. Thomson B, Hawkins D, Felgenhauer J et al (1999) RT-PCR evaluation of peripheral blood, bone marrow and peripheral blood stem cells in children and adolescents undergoing VACIME chemotherapy for Ewing's sarcoma and alveolar rhabdomyosarcoma. Bone Marrow Transplant 24 (5):527–33
16. Sartori F, Alaggio R, Zanazzo G et al (2006) Results of a prospective minimal disseminated disease study in human rhabdomyosarcoma using three different molecular markers. Cancer 106(8):1766–75
17. Moss TJ, Law YM, Slamon DJ et al (1988) N-myc protein expression by neuroblastoma cells that have metastasized to bone marrow. Prog Clin Biol Res 271:91–101
18. Schleiermacher G, Peter M, Oberlin O et al (2003) Increased risk of systemic relapses associated with bone marrow micrometastasis and circulating tumor cells in localized Ewing tumor. J Clin Oncol 21(1):85–91
19. Wharam MD, Meza J, Anderson J et al (2004) Failure pattern and factors predictive of local failure in rhabdomyosarcoma: a report of group III patients on the third Intergroup Rhabdomyosarcoma Study. J Clin Oncol 22(10):1902–8

Virchows Arch (2010) 456:473–482
DOI 10.1007/s00428-010-0915-7

ORIGINAL ARTICLE

Impact of podoplanin expression in oral squamous cell carcinoma: clinical and histopathologic correlations

Matthias Kreppel · Martin Scheer · Uta Drebber · Lutz Ritter · Joachim E. Zöller

Received: 4 January 2010 / Revised: 2 March 2010 / Accepted: 29 March 2010 / Published online: 15 April 2010
© Springer-Verlag 2010

Abstract Cervical lymph node metastases reduce the overall survival of patients with oral squamous cell carcinoma (OSCC) and require a neck dissection. However, elective management of a clinical N0 neck remains a controversial topic, as there are no reliable factors available predicting cervical lymph node metastases. Recent studies suggest an impact of podoplanin expression on metastatic spread to the cervical lymph nodes. Our aim was to investigate the influence of podoplanin expression on prognosis and metastatic lymphatic spread. In our retrospective study, podoplanin expression was examined in a set of 80 patients with OSCC by immunhistochemistry. We analysed associations between the level of podoplanin expression and various clinicopathologic parameters. In 67 patients (84%), podoplanin was expressed on the tumour cells. Nineteen patients (24%) showed high levels of expression. The 5-year overall survival (31%) for patients with high levels of podoplanin expression was significantly lower ($p<0.001$) than for patients with low and moderate expression of podoplanin (93% and 65%, respectively). There was an association between podoplanin expression and the frequency of cervical lymph node metastases. Cervical lymph node metastases were found in 79% of the patients with high podoplanin expression, while patients with weak podoplanin expression had metastases in only 22% ($p<0.001$). None of the 13 patients without podoplanin expression had cervical lymph node metastases. We concluded that podoplanin is expressed frequently in OSCC and that podoplanin expression correlates with cervical lymph node metastases and clinical outcome.

Keywords Podoplanin · Immunhistochemistry · Oral cancer · Prognosis · Cervical lymph node metastases

M. Kreppel (✉) · M. Scheer · L. Ritter · J. E. Zöller
Department for Oral and Cranio-maxillo and Facial Plastic Surgery, University of Cologne,
Kerpener Strasse 62,
50931 Cologne, Germany
e-mail: mattheskreppel@yahoo.de

U. Drebber
Department of Pathology, University of Cologne,
Cologne, Germany

M. Kreppel · M. Scheer · U. Drebber · L. Ritter · J. E. Zöller
Centre of Integrated Oncology (CIO) Cologne-Bonn,
Cologne, Germany

Introduction

Carcinoma of the oral cavity is the sixth most common cancer worldwide with an annual incidence of more than 500,000 cases [1]. The incidence is influenced by lifestyle, habits, demographic and genetic factors [2]. In 2009, the estimated incidence of oral and oropharyngeal cancer in the USA was 35,000, representing 2.4% of all newly diagnosed cancers and resulting in 1.4% of cancer-related deaths [3].

Despite improved therapeutic procedures, the prognosis remains poor [4, 5] yielding 5-year overall survival rates from 45% to 58% [6, 7]. This fact can be attributed to several factors: Failure to respond to available chemotherapy, late presentation of the lesions and lack of suitable markers for early detection [8, 9]. Even in the earliest stages of disease, oral squamous cell carcinoma (OSCC) may vary dramatically in treatment response and recurrence. Consequently, a significant number of patients with early stage oral cancer die of the disease. Thus, there is a strong need to understand the development of OSCC and to identify new and additional prognostic factors that can improve the

clinical staging system and establish appropriate treatment modalities [10, 11].

Cervical lymph node metastases are widely accepted as the strongest independent prognostic factor in patients with OSCC [12–16]. There is a positive correlation between the size of the primary tumour and the appearance of lymph node metastases, although some patients with small tumours have lymph node metastases, whereas patients with large tumours do not develop lymph node metastases [17]. A strong positive correlation was also reported between tumour thickness and survival [18, 19]. Study results suggest that molecular features of the tumour play an essential role in determining the aggressiveness of the tumour [20–24].

Recent studies identified podoplanin as a potential predictor of lymphatic dissemination in OSCC [1, 23, 25, 26]. Podoplanin is a mucin-type transmembrane glycoprotein that is specifically expressed in lymphatic endothelial cells but not in blood endothelial cells [27, 28]. Podoplanin knockout mice have lymphatic defects associated with diminished lymphatic transport, congenital lymphedema and dilation of lymphatic vessels [29], suggesting that, under physiological conditions, podoplanin plays an important role in regulating peripheral lung cell proliferation and lymphatic vascular development. Apart from head and neck squamous cell carcinoma, particularly in oral cancer [23, 30], podoplanin is expressed in carcinoma of the skin [31], lung [32], uterus [33], colon [34], oesophagus [35, 36], in mesothelioma [37] in astrocytoma [38, 39]. Investigations have shown that podoplanin, the oncofetal protein M2A recognised by the D2-40 antibody and the type I alveolar cell marker hT1ά-2 are identical proteins [25].

In the past, podoplanin has been used frequently to assess intra- and peritumoural lymphatic vessel density in oral squamous cell carcinoma, which is correlated with metastatic spread to the lymph nodes and a poor prognosis [28, 40, 41]. Recent studies have shown that podoplanin is also expressed in oral dysplastic and hyperplastic lesions with a risk of cancer development raising the question whether podoplanin may have further biological functions in premalignant oral lesions [23, 25, 30]. It has been reported that podoplanin acts as a mediator of tumour cell invasion in the absence of epithelial cell dedifferentiation [42].

In this study, we used the monoclonal antibody D2-40, which specifically stains podoplanin to assess the expression of podoplanin in OSCC cells and to determine potential associations between the expression patterns and clinicopathologic characteristics, especially overall survival, disease-specific survival and the occurrence of cervical lymph node metastases. So far, no reliable parameters have been found to assess the risk of lymph node metastases in a clinically N0-situation of the neck [43–45].

Materials and methods

Patients and specimens

The retrospective study included 80 treatment-naive patients with a biopsy proven primary squamous cell carcinoma of the oral cavity of stages I–IV who were treated at the Department of Cranio-maxillo-facial Surgery at the University of Cologne between October 2002 and June 2005. All patients underwent primary surgery including a neck dissection. Histopathologic

Table 1 Patient and tumour characteristics

Patients' characteristics, *N* (%)	
Patients	80
Male	51 (63.7%)
Female	29 (36.3%
Age (years)	
Mean ± SD	61.5±
Median	61.8
Smoking	
Yes	63 (78.8%)
No	17 (21.2%)
Alcohol	
Yes	53 (66.2%)
No	27 (33.8%)
Tumour site	
Floor of mouth	35 (43.8%)
Tongue	18 (22.5%)
Upper and lower gingiva	14 (17.5%)
Hard palate	5 (7.5%)
Cheek	8 (10.0%)
pT Stage	
T1	24 (30.0%)
T2	27 (33.8%)
T3	6 (7.5%)
T4	23 (28.7%)
pN Stage	
N0	49 (61.3%)
N1	9 (11.3%)
N2	22 (27.5%)
pUICC Stage	
I	23 (28.7%)
II	13 (16.3%)
III	8 (10.0%)
IV	36 (45.0%)
Podoplanin Expression	
No Podoplanin	13 (16.3%)
Weak	18 (22.5%)
Moderate	30 (37.5%)
High	19 (23.8%)

staging (pTNM) was performed according to the 6th edition of the UICC [46]. All patients with stage II, III, and IV additionally received an adjuvant concurrent chemoradiation with carboplatin AUC 5 in weeks 1 and 5 and a radiation dose of 61–65 Gy. Patients who did not receive the adjuvant scheme were excluded from this study. The patients' clinical characteristics are listed in Table 1.

Tissue processing and immunohistochemical analysis

Formalin-fixed, paraffin-embedded specimens were obtained from the operation theatre and handled in the Department of Pathology, at the University of Cologne for further processing. The tissue samples were obtained from the peripheral invasion front of the tumour. Clinicopathologic parameters were obtained from the medical charts including the histopathologic and surgical reports. Follow-up data were gathered from a combination of chart review and the local government office for registration of residents. The average follow-up time was 42.9 months.

Immunhistochemistry was performed using the avidin–biotin–peroxidase complex technique (ABC-technique) [30, 47]. Paraffin sections measuring 4 μm in thickness of the excised tumours were placed on positively charged glass sides. The slides were deparaffinised and rehydrated in descending concentrations of ethanol. For antigen unmasking, the slides were steamed with 10 mmol/L citrate buffer, pH6.0 (Dako Cytomation, Carpinteria, CA) for 20 min. After cooling down for 45 min the slides were blocked against endogenous peroxidase by incubation in 3% hydrogen peroxide for 10 min, followed by incubation with 10% horse serum for 30 min at room temperature. The slides were then incubated with the monoclonal antibody D2-40 diluted 1:100 (Vector Laboratories, Burlingame, CA) at 4°C overnight followed by signal development processes according to the manufacturer's protocol (Vectastatin Elite ABC kit, Vector Laboratories, Burlingame, CA). Counterstaining of the slides was achieved with Mayer's haematoxylin (Dako Cytomation). Expression of podoplanin in lymphatic endothelial cells in the stroma served as a positive internal control. Only one slide for each case was analysed.

In consideration of a previously published scheme to evaluate immunohistochemical samples [48], the epithelial podoplanin staining was quantified on a scale from 0

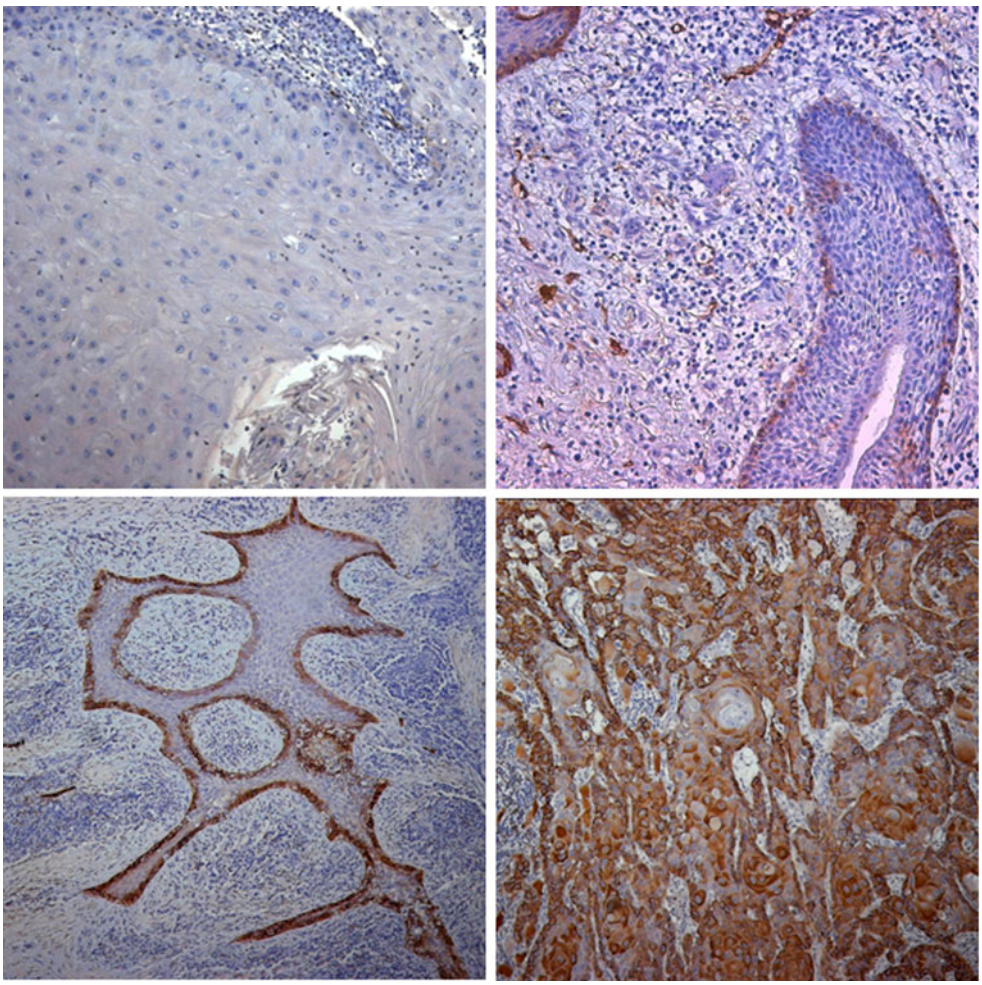

Fig. 1 Patterns of podoplanin expression: *Top left*: tumour without podoplanin expression at 200× (score 0), *top right*: tumour with weak podoplanin expression at 200× (score 1), *bottom left*: moderate expression of podoplanin 100× (score 2), bottom right: high podoplanin expression at 200× (score 3)

(negative) to 3 (strong staining) in consensus of two investigators (U.D. and M.S.) without knowledge of the patient's clinical history. The final score took into account both the intensity of the staining and the amount of positive cells according to the following scheme: both were classified from 0 to 3 (0=no podoplanin, 1=weak expression, 2=moderate expression, 3=high expression), added up and divided by 2. If the final score was not an even number, it was assigned to the lower group, for example a score of 1.5 was regarded as weak expression.

Statistical analysis

Associations between podoplanin expression and clinicopathologic variables were assessed using the Wilcoxon rank sum test for continuously distributed variables and the χ^2-test and Fisher exact test for categorical variables.

The Kaplan–Meier survival analysis method was used to estimate the events of interest for overall survival (time interval from beginning of primary therapy until death. Patients who did not die were censored at their last date of follow-up) and disease-specific survival (time interval from beginning of primary therapy until death through OSCC. Patients who died of other reasons or did not die were censored at their last date of follow-up) [49]. The log rank test was used to compare survival times among patients with different characteristics. P values of less than 0.05 were considered as significant and printed in bold. A Cox proportional hazard model was calculated to estimate the prognostic impact of patient and tumour-related factors in a multivariate analysis on survival, which were significant in univariate analysis [50].

All calculations were conducted using SPSS 17.0

Results

In OSCC, two different patterns of podoplanin expression emerged (Fig. 1): the first type showed a diffuse expression of podoplanin in the tumour cells. The membrane of the tumour cells showed a stronger staining than the cytoplasm. In the second type, focal expression of

Table 2 Associations of podoplanin and patient characteristics

Associations of podoplanin and patient characteristics

	No podoplanin	Weak expression	Moderate expression	High expression	*P*
Age (years)					0.420
Mean ± SD	64.7±12.1	61.6±13.4	61.9±10.1	58.8±13.8	
Median (min, max)	64 (44, 86)	59 (37, 91)	63 (38, 82)	62 (30, 85)	
Gender (%)					0.832
Male	9 (17.6%)	10 (19.6%)	19 (37.3%)	13 (25.5%)	
Female	4 (13.8%)	8 (27.8%)	11 (37.9%)	6 (20.5%)	
Smoking					0.161
No	1 (5.9%)	2 (11.8%)	10 (58.8%)	4 (23.5%)	
Yes	12 (19.1%)	16 (25.4%)	20 (31.7%)	15 (23.8%)	
Alcohol					0.434
No	2 (7.5%)	7 (25.9%)	12 (44.4%)	6 (22.2%)	
Yes	11 (20.8%)	11 (20.8%)	18 (33.9%)	13 (24.5%)	
pT stage (%)					0.016
T1 & T2	12 (23.1%)	14 (26.9%)	18 (34.6%)	8 (15.4%)	
T3 & T4	1 (3.6%)	4 (14.3%)	12 (42.8%)	11 (39.3%)	
pN Stage (%)					<0.001
N0	13 (26.5%)	14 (28.6%)	18 (36.7%)	4 (8.2%)	
N1 & N2	0	4 (12.9%)	12 (38.7%)	15 (48.4%)	
EPS					0.231
EPS-negative	13 (19.4%)	16 (23.9%)	23 (34.3%)	15 (22.4%)	
EPS-positive	0	2 (15.4%)	7 (53.8%)	4 (30.8%)	
pUICC Stage					<0.001
UICC I & II	12 (32.4%)	11 (29.7%)	11 (29.7%)	3 (8.2%)	
UICC III & IV	1 (2.3%)	7 (16.3%)	19 (44.2%)	16 (37.2%)	

podoplanin in the peripheral layer of the tumour proliferation area was found.

Thirteen tumours did not express podoplanin at all.

Podoplanin expression and associations with clinicopathologic parameters in patients with primary OSCC

In 13 tumours (16.3%), no sign of podoplanin expression was observed; weak expression was found in 18 patients (22.5%). A moderate expression was visualised in 30 patients (37.5%), while, in 19 cases (23.8%), the tumours exhibited a high level of podoplanin expression. As shown in Table 2, age (p=0.420) and gender (p=0.832) did not show an association with podoplanin expression.

The χ^2 test revealed a strong association between T stage and podoplanin expression (p=0.016). In 50.0% of the patients with stage T1 and T2 the tumour cells had no or weak podoplanin expression, while only five patients (17.9%) with an advanced primary tumour of stage T3 and T4 showed no or weak podoplanin expression. Our analyses showed that 39.3% patients with locally advanced tumours of stage T3 and T4 had a strong podoplanin expression, which was only diagnosed, in 15.4% of the patients with tumours of stage T1 and T2.

The presence of lymph node metastases had the strongest association with podoplanin expression (p< 0.001). Among the 31 patients with lymph node metastases, 15 (48.4%) had high levels of podoplanin expression in the primary tumour compared with 8.2% of the patients with no detectable cervical lymph node metastases. Extra-capsular spread (ECS) of the tumour in patients with cervical lymph node metastases tended to be associated with podoplanin expression in the primary tumour. In 11 out of 13 patients with ECS, a moderate or high level of podoplanin expression was observed; however, the association was not significant (p=0.231).

In addition, podoplanin expression was significantly associated with a higher UICC stage (p<0.001). In 81.4% of the patients who presented with stage III and IV, a moderate or high level of podoplanin expression was found in the primary tumour, while only 37.9% patients with UICC stage I and II showed moderate or high levels of podoplanin expression.

Table 3 Identification of prognostic factors by univariate analysis (log rank test)

Univariate analysis of prognostic factors				
Parameter	5-year OS	*P* value	5-year DSS	*P* value
Age		0.067		0.116
≤61 years (lower half of median)	72.2%		84.8%	
>61 years (upper half of median)	50.9%		55.2%	
Gender		0.750		0.567
Male	64.8%		69.5%	
Female	67.4%		69.3%	
Tumour site		0.669		0.865
T stage		0.059		0.072
T1 & T2	75.6%		78.8%	
T3 & T4	50.7%		54.8%	
N stage		0.032		0.089
N0	76.2%		77.6%	
N1 & N2	50.6%		56.3%	
UICC stage		0.023		0.032
I & II	82.1%		84.1%	
III & IV	49.8%		59.3%	
Margin status	0.113		0.116	
R0	67.4%		71.0%	
R1	58.3%		61.9%	
Podoplanin expression		<0.001		0.001
No podoplanin	90.9%		100%	
Weak	93.3%		93.3%	
Moderate	64.8%		69.7%	
High	31.1%		37.2%	

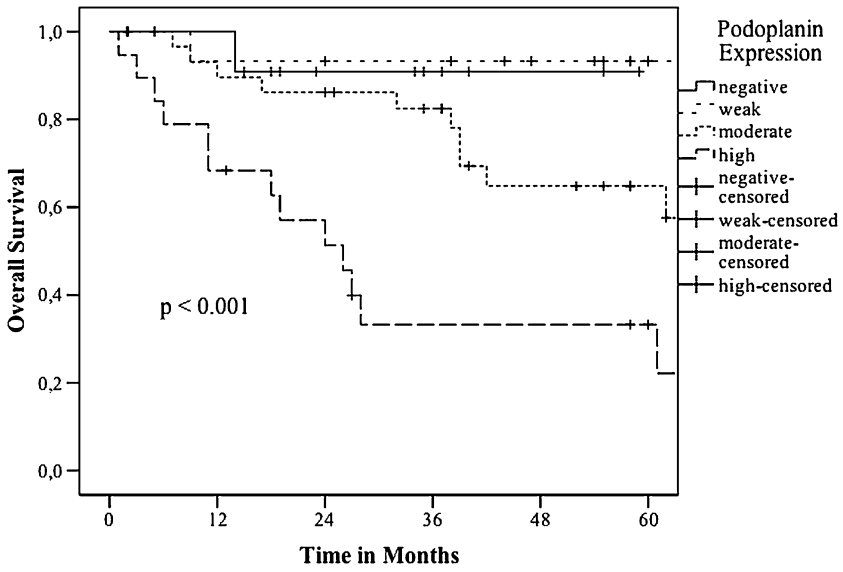

Fig. 2 Overall survival according to the different levels of podoplanin expression (log rank test, $p<0.001$)

Smoking ($p=0.161$) and alcohol consumption ($p=0.434$) did not have a significant association with the level of podoplanin expression in the tumour cells.

Parameters predicting overall survival and disease-specific survival in patients with OSCC

One of our main aims was determine whether podoplanin expression in primary tumours of OSCC is a feasible parameter to predict the patients' outcome with respect to survival. Using the Kaplan–Meier product limit method we calculated the 5-year survival rates for overall survival and disease-specific survival with regard to the podoplanin expression. Table 3 presents the 5-year survival rates for overall survival and disease-specific survival.

In univariate analysis, the level of podoplanin expression had a strong impact on the overall survival ($p<0.001$) and on disease-specific survival ($p=0.001$). A continuous decrease of the 5-year overall survival rate was found from 93.3% for patients with weak expression to 64.8% for patients with moderate expression and to 31.1% for patients with high expression of podoplanin (Fig. 2). Patients with podoplanin-negative primary tumours had a slightly lower overall survival after 5 years (90.7%) than patients with weak podoplanin expression. A similar trend can be observed for disease-specific survival (Fig. 3).

N stage and UICC stage reached the 95% significance level for overall survival in univariate analysis ($p<0.05$), too. However, T stage, age, gender, tumour site and status of the resection margins did not have a significant impact

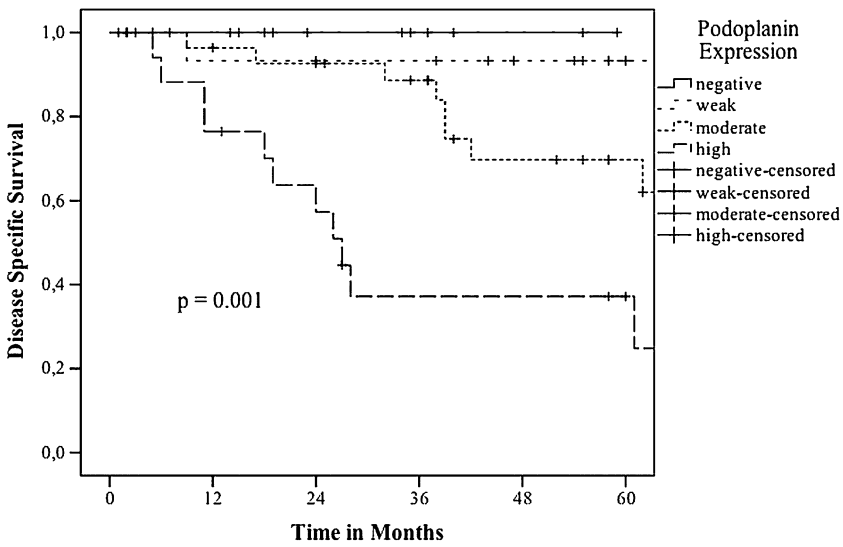

Fig. 3 Disease-specific survival according to the different levels of podoplanin expression (log rank test, $p=0.001$)

Table 4 Identification of prognostic factors by multivariate analysis for overall survival (Cox proportional hazard regression model)

Multivariate analysis of prognostic factors		
Parameter	Hazard ratio (95% confidence interval)	*P* value
Podoplanin expression		0.019
Negative vs. weak	0.134 (0.015–1.182)	0.070
Negative vs. moderate	0.062 (0.008–0.509)	0.010
Negative vs. high	0.389 (0.161–0.939)	0.036
N stage (N0 vs. N1&N2)	0.913 (0.364–2.292)	0.846

on the overall survival of our patients. For disease-specific survival, N stage did not quite reach the 95% significance level ($p=0.089$).

The results of multivariate analysis are displayed in Tables 4 and 5. Multivariate analysis was performed with parameters that were significant in univariate analysis (podoplanin expression, nodal status for both survival parameters and additionally UICC stage for overall survival) to determine whether the effect of podoplanin expression on overall survival and disease-specific survival is dependent on other risk factors. For overall survival, a multivariate analysis was conducted with a model including podoplanin expression and N stage. N stage did not have significant impact on overall survival ($p=0.846$) in multivariate analysis, whereas podoplanin expression was significantly associated with overall survival ($p=0.019$). For overall survival, a second model using UICC stage and instead of N stage and podoplanin expression was created. The patients' prognosis was significantly influenced by the level of podoplanin expression ($p=0.021$), whereas UICC stage did not have a significant impact on overall survival ($p=0.377$).

For disease-specific survival podoplanin expression was found to be the only significant prognostic factor in multivariate analysis ($p=0.049$), too. UICC stage did not significantly influence disease-specific survival in multivariate analysis ($p=0.300$).

Discussion

The specific staining of the lymphatic endothelial cells and the tumour cells is consistent with findings in previous studies [23, 51]. Most of the studies tried to show an association between lymphovascular density in OSCC and cervical lymph node metastases [20, 52, 53]. Longatto-Filho et al. [53] reported a correlation between peritumoural lymphovascular density and survival, Franchi et al. [20] showed an association between peritumoural lymphovascular density and cervical lymph node metastases; Kyzas et al., however, pointed out that only intratumoural lymphovascular density and not peritumoural lymphovascular density had an impact on the clinical outcome [54]. However, assessing lymphovascular density takes up a great deal of time and is therefore not suitable as a prognostic parameter in daily routine. In this study, we focused on the level of podoplanin expression on the tumour cells themselves to investigate the impact of podoplanin as a prognostic marker for lymph node metastases and overall survival.

The reported incidence of occult regional lymph node metastases in clinical N0 necks of patients with OSCC varies from 6% to 46%. Occult regional metastases may be found even in cases with small primary T1 tumours [55]. A reliable marker, which is able to predict the chance of regional lymph node metastases, could be a great asset in decision of an elective treatment of a clinical N0 neck. The χ^2 test revealed a very strong association between podoplanin expression in the primary tumour and cervical lymph node metastases ($p<0.001$), which suggests that the level of podoplanin expression in tumour cells is a reliable parameter to predict the appearance of cervical lymph node metastases. Recently, Yuan et al. described this association at the same significance level [23].

Univariate analysis showed a strong impact of podoplanin expression ($p<0.001$) and cervical lymph node status

Table 5 Identification of prognostic factors by multivariate analysis for disease-specific survival (Cox proportional hazard regression model)

Multivariate analysis of prognostic factors		
Parameter	Hazard ratio (95% confidence interval)	*P* value
Podoplanin expression		0.049
Negative vs. weak	0.189 (0.000–infinite)	0.971
Negative vs. moderate	0.083 (0.010–0.673)	0.020
Negative vs. high	0.394 (0.162–0.956)	0.037
UICC stage (I&II vs. III&IV)	0.511 (0.144–1.817)	0.300

(p=0.032) on overall survival. Multivariate analysis confirmed our findings. In fact, podoplanin was the only parameter that exhibited a significant prognostic impact on overall survival and disease-specific survival in univariate and multivariate analysis.

Our results confirm the assumption that high levels of podoplanin expression in the primary tumour of OSCC are associated with advanced T stage, lymphatic spread to the cervical region and poor clinical outcome. Yuan et al. described similar findings, except they could not find an association between T stage and podoplanin expression. However, their observations were limited to a set of 60 patients with tongue cancer [23].

The results suggest that podoplanin might play a role in lymphatic spread and in tumour invasion and progression.

The biological function of podoplanin is not yet fully understood, but it has been proposed that podoplanin is able to enhance tumour invasion by promoting the tumour cell mobility [25]. Cancer cell migration and invasion involves active remodelling of the actin cytoskeleton [56]. However, podoplanin does not interact directly with actin but via ERM proteins such as ezrin radixin and moesin [57]. It has been shown that overexpression of podoplanin leads to an increased phosphorylation of ezrin which links podoplanin to the observed rearrangement of the actin cytoskeleton [57]. Apart from that, podoplanin increases the activities of Rho-family GTPases, mainly RhoA [42], which is also linked to tumour cell mobility.

Dumoff et al. reported a strong correlation between low expression of podoplanin and both lymphatic invasion and nodal metastasis in uterine cervical cancer [33]. These findings indicate that the biological function of podoplanin may vary between different types of cancer. A recent study, however, showed similar correlations between the level of podoplanin expression in esophageal squamous cell carcinoma (ESCC) and OSCC, suggesting the role of podoplanin may be common in ESCC and OSCC [23, 36]. The results indicate that podoplanin may be a marker for cancer stem cells of ESCC. Knockdown of podoplanin expression in ESCC cell lines resulted in reduction of in vitro colony formation and in vivo tumourigenic activity. Podoplanin knockdown cells also showed decreased invasive ability and were more vulnerable to cisplatin and 5-FU, two anticancer drugs frequently used in chemotherapy for ESCC and OSCC [36, 58, 59]. These results support the assumption that there is an important role for podoplanin in tumourigenesis and progression in ESCC and in OSCC.

Although we were able to show significant associations between the level of podoplanin expression, T stage, N stage and the significant impact of the level of podoplanin expression on overall survival and disease-specific survival in univariate and multivariate analysis, prospective studies with larger cohorts are needed to clarify the role podoplanin in precancerous lesions and invasive carcinoma. Exploring the function of biomarkers like podoplanin offers the opportunity to move from a tumour model of temporal determinism to one of biological determinism as carcinogenesis is not defined by what stage the patient is in at detection but rather by molecular and characteristics of the tumour and the host.

Conflict of interest The authors declare that they have no potential or actual conflict of interest.

References

1. Vormittag L, Thurnher D, Geleff S et al (2009) Co-expression of Bmi-1 and podoplanin predicts overall survival in patients with squamous cell carcinoma of the head and neck treated with radio(chemo)therapy. Int J Radiat Oncol Biol Phys 73:913–918
2. Shah JP, Gil Z (2008) Current concepts in management of oral cancer—surgery. Oral Oncol 45:394–401
3. Jemal A, Siegel R, Ward E et al (2009) Cancer statistics, 2009. CA Cancer J Clin 59:225–249
4. Bernier J, Domenge C, Ozsahin M et al (2004) Postoperative irradiation with or without concomitant chemotherapy for locally advanced head and neck cancer. N Engl J Med 350:1945–1952
5. Neville BW, Day TA (2002) Oral cancer and precancerous lesions. CA Cancer J Clin 52:195–215
6. Eich HT, Löschke M, Scheer M et al (2008) Neoadjuvant radiochemotherapy and radical resection for advanced squamous cell carcinoma of the oral cavity. Outcome of 134 patients. Strahlenther Onkol 184:23–29
7. Klug C, Wutzl A, Kermer C et al (2005) Preoperative radiochemotherapy and radical resection for stages II to IV oral and oropharyngeal cancer: grade of regression as crucial prognostic factor. Int J Oral Maxillofac Surg 34:262–267
8. Martin-Villar E, Scholl F, Gamallo C et al (2005) Characterization of human PA2.26 antigen (T1alpha-2, podoplanin), a small membrane mucin induced in oral squamous cell carcinomas. Int J Cancer 113:899–910
9. Patel V, Leethanakul C, Gutkind J (2001) New approaches to the understanding of the molecular basis of oral cancer. Crit Rev Oral Biol Med 12:55–63
10. Nagpal J, Das B (2003) Oral cancer: reviewing the present understanding of its molecular mechanism and exploring the future directions for its effective management. Oral Oncol 39:213–221
11. Shah N, Trivedi T, Tankshali R et al (2009) Prognostic significance of molecular markers in oral squamous cell carcinoma: a multivariate analysis. Head Neck 31:1544–1556
12. Greenberg J, El Naggar K, Mo V et al (2003) Disparity in pathologic and clinical lymph node staging in oral tongue carcinoma. Implications for therapeutic decision making. Cancer 98:508–515
13. Shaw J, Lowe D, Woolgar J et al (2009) Extracapsular spread in oral squamous cell carcinoma. Head Neck (in press)

14. Shingaki S, Takada M, Sasai K et al (2003) Impact of lymph node metastasis on the pattern of failure and survival in oral carcinomas. Am J Surg 185:278–284
15. Woolgar J, Hall G (2009) Determinants of outcome following surgery for oral squamous cell carcinoma. Future Oncol 5:51–61
16. Iype E, Sebastian P, Mathew A et al (2008) The role of selective neck dissection (I-III) in the treatment of node negative (N0) neck in oral cancer. Oral Oncol 44:1134–1138
17. Arduino PG, Carrozzo M, Chiecchio A et al (2008) Clinical and histopathologic independent prognostic factors in oral squamous cell carcinoma: a retrospective study of 334 cases. J Oral Maxillofac Surg 66:1570–1579
18. Scheer M, Kübler AC, Manawi NN et al (2005) Endosonographic imaging of tumor thickness in oral squamous cell cancer and its effect on the incidence of lymph node metastases. Mund Kiefer GesichtsChir 9:282–289
19. Yuen A, Ng R, Lam P, Ho A (2008) Preoperative measurement of tumor thickness of oral tongue carcinoma with intraoral ultrasonography. Head Neck 30:230–234
20. Franchi A, Gallo O, Massi D et al (2004) Tumor lymphangiogenesis in head and neck squamous cell carcinoma: a morphometric study with clinical correlations. Cancer 101:973–978
21. Miyahara M, Tanuma J, Sugihara K, Semba I et al (2007) Tumor lymphangiogenesis correlates with lymph node metastasis and clinicopathologic parameters in oral squamous cell carcinoma. Cancer 110:1287–1294
22. Sedivy R, Beck-Mannagetta J, Haverkampf C et al (2003) Expression of vascular endothelial growth factor-C correlates with the lymphatic microvessel density and the nodal status in oral squamous cell cancer. J Oral Pathol Med 32:455–460
23. Yuan P, Temam S, El-Naggar A et al (2006) Overexpression of podoplanin in oral cancer and its association with poor clinical outcome. Cancer 107:563–569
24. Wang L, Liu T, Wang Y et al (2007) Altered expression of desmocollin 3, desmoglein 3, and beta-catenin in oral squamous cell carcinoma: correlation with lymph node metastasis and cell proliferation. Virchows Arch 451:959–966
25. Raica M, Cimpean A, Ribatti D (2008) The role of podoplanin in tumor progression and metastasis. Anticancer Res 28:2997–3006
26. Völker H, Scheich M, Nowack I et al (2009) Lymphangiosis carcinomatosa in squamous cell carcinomas of larynx and hypopharynx—value of conventional evaluation and additional immunohistochemical staining of D2–40. World J Surg Oncol 7:25
27. Kahn H, Marks A (2002) A new monoclonal antibody, D2-40, for detection of lymphatic invasion in primary tumors. Lab Invest 82:1255–1257
28. Schacht V, Dadras S, Johnson L et al (2005) Up-regulation of the lymphatic marker podoplanin, a mucin-type transmembrane glycoprotein, in human squamous cell carcinomas and germ cell tumors. Am J Pathol 166:913–921
29. Breitender-Geleff S, Soleiman A, Kowalski H et al (1999) Angiosarcomas express mixed endothelial phenotypes of blood and lymphatic capillaries: podoplanin as a specific marker for lymphatic endothelium. Am J Pathol 154:385–394
30. Kawaguchi H, El-Naggar A, Papadimitrakopoulou V et al (2008) Podoplanin: a novel marker for oral cancer risk in patients with oral premalignancy. J Clin Oncol 26:354–360
31. Durchdewald M, Guinea-Viniegra J, Haag D et al (2008) Podoplanin is a novel fos target gene in skin carcinogenesis. Cancer Res 68:6877–6883
32. Shimada Y, Ishii G, Atsumi N et al (2009) Expression of podoplanin, CD44, and p63 in squamous cell carcinoma of the lung. Cancer Sci 100:2054–2059
33. Dumoff K, Chu C, Harris E et al (2006) Low podoplanin expression in pretreatment biopsy material predicts poor prognosis in advanced-stage squamous cell carcinoma of the uterine cervix treated by primary radiation. Mod Pathol 19:708–716
34. Liang P, Hong J, Ubukata H et al (2006) Increased density and diameter of lymphatic microvessels correlate with lymph node metastasis in early stage invasive colorectal carcinoma. Virchows Arch 448:470–475
35. Chuang W, Yeh C, Wu Y et al (2009) Tumor cell expression of podoplanin correlates with nodal metastasis in esophageal squamous cell carcinoma. Histol Histopathol 24:1021–1027
36. Rahadiani N, Ikeda J, Makino T et al (2010) Tumorigenic role of podoplanin in esophageal squamous-cell carcinoma. Ann Surg Oncol. doi:10.1245/s10434-009-0895-5
37. Padgett D, Cathro H, Wick M, Mills S (2008) Podoplanin is a better immunohistochemical marker for sarcomatoid mesothelioma than calretinin. Am J Surg Pathol 32:123–127
38. Mishima K, Kato Y, Kaneko M et al (2006) Increased expression of podoplanin in malignant astrocytic tumors as a novel molecular marker of malignant progression. Acta Neuropathol 115:483–488
39. Shibahara J, Kashima T, Kikuchi Y et al (2006) Podoplanin is expressed in subsets of tumors of the central nervous system. Virchows Arch 448:493–499
40. Erovic B, Neuchrist C, Kandutsch S et al (2003) CD9 expression on lymphatic vessels in head and neck mucosa. Mod Pathol 16:1028–1034
41. Ji R (2006) Lymphatic endothelial cells, tumor lymphangiogenesis and metastasis: new insights into intratumoral and peritumoral lymphatics. Cancer Metastasis Rev 25:677–694
42. Wicki A, Lehembre F, Wick N et al (2006) Tumor invasion in the absence of epithelial–mesenchymal transition: podoplanin-mediated remodeling of the actin cytoskeleton. Cancer Cell 9:261–272
43. Ferlito A, Silver C, Rinaldo A (2009) Elective management of the neck in oral cavity squamous carcinoma: current concepts supported by prospective studies. Br J Oral Maxillofac Surg 47:5–9
44. Yuen A, Ho C, Chow T et al (2009) Prospective randomized study of selective neck dissection versus observation for N0 neck of early tongue carcinoma. Head Neck 31:765–772
45. D'Cruz A, Siddachari R, Walvekar R et al (2009) Elective neck dissection for the management of the N0 neck in early cancer of the oral tongue: need for a randomized controlled trial. Head Neck 31:618–624
46. O'Sullivan B, Shap J (2003) New TNM staging criteria for head and neck tumors. Semin Surg Oncol 21:30–42
47. Bhalang K, Kafrawy A, Miles D (1999) Immunohistochemical study of the expression of human chorionic gonadotropin-beta in oral squamous cell carcinoma. Cancer 85:757–762
48. Renkonen J, Wolff H, Paavonen T (2002) Expression of cyclooxygenase-2 in human tongue carcinoma and its precursor lesions. Virchows Arch 440:594–587
49. Kaplan EL, Meier P (1958) Non-parametric estimation from incomplete observations. J Am Statist Assoc 53:457–481
50. Cox D (1972) Regression modell and life-tables. J R Stat Soc 34:187–220
51. Atsumi N, Ishii G, Kojima M et al (2008) Podoplanin, a novel marker of tumor-initiating cells in human squamous cell carcinoma A431. Biochem Biophys Res Commun 373:31–36
52. Chung M, Min J, So Y et al (2009) Correlation between lymphatic vessel density and regional metastasis in squamous cell carcinoma of the tongue. Head Neck epub ahead of print
53. Longatto-Filho A, Oliveira T, Pinheiro C et al (2007) How useful is the assessment of lymphatic vascular density in oral carcinoma prognosis? World J Surg Oncol 5:140

54. Kyzas P, Geleff S, Batistatou A et al (2005) Evidence for lymphangiogenesis and its prognostic implications in head and neck squamous cell carcinoma. J Pathol 206:170–177
55. Capote A, Escorial V, Muòoz-Guerram M et al (2007) Elective neck dissection in early-stage oral squamous cell carcinoma–does it influence recurrence and survival? Head Neck 29:3–11
56. Madan R, Brandwein-Gensler M, Schlecht N et al (2006) Differential tissue and subcellular expression of ERM proteins in normal and malignant tissues: cytoplasmic ezrin expression has prognostic signficance for head and neck squamous cell carcinoma. Head Neck 28:1018–1027
57. Martin-Villar E, Megias D, Castel S et al (2006) Podoplanin binds ERM proteins to activate RhoA and promote epithelial–mesenchymal transition. J Cell Sci 119:4541–4553
58. Fan K, Lin C, Kang C et al (2007) Combined-modality treatment for advanced oral tongue squamous cell carcinoma. Int J Radiat Oncol Biol Phys 67:453–461
59. Bernier J (2009) Current state-of-the-art for concurrent chemoradiation. Semin Radiat Oncol 19:3–10

Virchows Arch (2010) 456:483–490
DOI 10.1007/s00428-010-0905-9

ORIGINAL ARTICLE

Overexpression of carbonic anhydrase IX (CAIX) in vulvar cancer is associated with tumor progression and development of locoregional lymph node metastases

Matthias Choschzick · Linn Woelber · Stephan Hess · Christine zu Eulenburg · Jörg Schwarz · Ronald Simon · Sven Mahner · Fritz Jaenicke · Volkmar Müller

Received: 15 December 2009 / Revised: 31 January 2010 / Accepted: 12 March 2010 / Published online: 1 April 2010
© Springer-Verlag 2010

Abstract Carbonic anhydrase IX (CAIX) is a strictly membranous expressed metalloenzyme involved in cell adhesion, pH homeostasis, and cancer progression. The protein is specifically overexpressed in a wide variety of malignant tumors. This study was designed to assess the role of CAIX in primary vulvar cancer. One hundred forty-two well-characterized primary vulvar carcinomas were analyzed on a tissue microarray (TMA). Three tissue cores were sampled from each tumor. CAIX expression was determined by immunohistochemistry, using a four-step scoring system. To determine CAIX expression in benign vulvar tissue, we constructed a TMA with 120 samples of normal mucosa and non-neoplastic diseases. CAIX expression was found in 77/135 (57%) of all assessable vulvar cancer specimens and 48 (35.5%) exhibited a moderate or strong expression. CAIX expression in vulvar carcinomas was significantly stronger compared to non-neoplastic vulvar tissue ($p<0.001$). High levels of CAIX expression were related to pT stage ($p<0.01$), tumor size ($p<0.01$), depth of invasion ($p<0.05$), as well as inguinal lymph node metastases ($p<0.05$). There was also a trend towards shorter recurrence-free patient survival in CAIX-positive compared to CAIX-negative vulvar cancers. CAIX staining results in different tissue cores from the same tumor were homogeneous, raising the possibility of a hypoxia-independent expression. In conclusion, CAIX is overexpressed in the majority of vulvar carcinomas with relationships to advanced tumor stages and development of lymph node metastases. Our data support the potential therapeutic benefit of newly developed targeting antibodies in advanced vulvar cancer.

Keywords Carbonic anhydrase · Vulvar cancer · Metastasis · Prognosis

Matthias Choschzick and Linn Woelber contributed equally to this study.

M. Choschzick · S. Hess · R. Simon
Institute of Pathology,
University Medical Centre Hamburg-Eppendorf,
Hamburg, Germany

L. Woelber · J. Schwarz · S. Mahner · F. Jaenicke · V. Müller
Department of Gynecology,
University Medical Centre Hamburg-Eppendorf,
Hamburg, Germany

C. zu Eulenburg
Department of Medical Biometry and Epidemiology,
University Medical Centre Hamburg-Eppendorf,
Hamburg, Germany

M. Choschzick (✉)
Department of Pathology,
University Medical Centre Hamburg-Eppendorf,
Martinistr. 52,
20246 Hamburg, Germany
e-mail: mchoschz@uke.uni-hamburg.de

Present Address:
J. Schwarz
Department of Gynecology, Asklepios Clinic Nord,
Hamburg, Germany

Introduction

In recent years, aerobic glycolysis (*Warburg effect)* has been recognized as an important metabolic feature of cancer [1]. The glycolytic phenotype has major biochemical consequences for the microenviroment of tumor cells. The intracellular lactate excess results in acidification of the extracellular space and upregulation of acid-regulating

proteins like carbonic anhydrases [2]. This enzyme family catalyzes the reversible hydration of CO_2 to HCO_3 and plays a pivotal role in tissue pH homeostasis. Currently, there are 16 known different α-carbonic anhydrases in mammalians [3, 4]. The isoenzymes differ substantial in their subcellular localization and catalytic activity.

Carbonic anhydrase IX (CAIX) is a transmembrane zinc metalloenzyme, first detected in the HeLA cancer cell cell line [5]. Apart from its role in the regulation of pH, CAIX has a function in cell adhesion and is important for growth and survival of tumor cells under normoxia and hypoxia [6, 7]. CAIX expression is strongly induced by hypoxia through stabilization of the transcription factor HIF-1α [8]. In non-neoplastic tissues, CAIX shows a very limited expression pattern. Low levels of CAIX have been reported to be immunohistochemically detectable in mesothelial cells, gland epithelium of stomach, biliary tract, and small intestine as well as choroid plexus [9]. Despite its sparse expression in normal tissues, CAIX is overexpressed in a wide variety of malignant cell lines and tumors. High levels of CAIX were found to be associated with unfavorable patient outcome in breast carcinomas, bladder cancer, advanced cervical carcinomas, and lung cancer [10–13]. The CAIX expression pattern in vulvar carcinoma is not yet determined. To gain more insight into the potential role of CAIX expression in vulvar cancer, a tissue microarray containing 142 tumor samples with clinical follow-up data was constructed. Our data suggest that CAIX overexpression may be linked to initiation and progression of vulvar carcinomas with potential therapeutic implications.

Material and methods

Vulvar cancer tissue microarray

A total of 142 formalin-fixed (buffered neutral aqueous 4% solution), paraffin-embedded squamous cell vulvar carcinomas were available from the Institute of Pathology, University Medical Centre Hamburg-Eppendorf in Hamburg between 1993 and 2008. The median patient age was 63.4 (range 26–95)years. Data were retrieved from patients' records, the tumor registry and death certificates. Clinicopathologic factors were evaluated by reviewing medical charts and pathologic reports. Clinical outcome was followed from the date of primary surgery to the date of death or October 2008. Written informed consent was obtained from all included subjects to review their medical records when they attended the clinic according to our investigational review board and ethics committee guidelines.

TMA construction was as described previously [14]. Briefly, tissue cylinders with a diameter of 1.3 mm were punched from representative tumor areas of a "donor" tissue block using a homemade semiautomatic robotic precision instrument and brought into different recipient

Table 1 Association between CAIX expression and clinicopathological tumor characteristics

				Carbonic anhydrase IX		
		On array (*n*)	Analyzable (*n*)	Score 0 and 1 (%)	Score 2 and 3 (%)	*p* value
All samples		142	135	64.5	35.5	
Histologic tumor type	Keratinizing	83	79	67.1	32.9	0.37
	Non-keratinizing	22	19	73.6	26.4	
	Basaloid	24	24	62.5	37.5	
	Others[a]	13	13	38.4	61.6	
Tumor stage	pT1a	2	1	100.0	0	
	pT1b	51	47	80.8	19.2	<0.01
	pT2	72	70	52.8	47.2	
	pT3	14	14	64.3	35.7	
	pT4	1	1	0.0	100	
Nodal stage	pN0	79	75	68.0	32	0.65
	pN1	33	32	59.4	40.6	
	pN2	7	6	16.7	83.3	
Grading	G1	11	11	63.6	36.4	0.36
	G2	66	62	71.0	29	
	G3	28	25	64.0	36	
HPV	Negative	82	76	68.4	31.6	0.58
	Positive[b]	38	37	67.5	32.5	

[a] Seven mixed, fourt warty, two verrucous

[b] 25xHPV16, 5xHPV33, 8xHPV others

paraffin blocks each containing 142 individual samples. Three different tissue cores were sampled from each tumor. Additionally, we constructed a TMA with one tissue core each from 120 benign specimens to determine CAIX expression in non-neoplastic vulvar tissue. This array contained 78 samples with matched normal mucosa remote from tumor, 15 samples with lichen sclerosus, 19 samples with lichen simplex, and nine specimens with labial hypertrophy.

Immunohistochemistry

Four micrometer sections of the multitumor TMA blocks were transferred to an adhesive coated slide system (Instrumedics, Hackensack, NJ, USA). Standard indirect immunoperoxidase procedures were used for the detection of Ki67 protein (DAKO, Glostrup, Denmark). The Ki67 labeling index (Ki67 LI) was defined as the fraction of tumor cells showing any nuclear Ki67 immunoreactivity. Tumor cells (100) were counted per tissue spot to determine the Ki67 LI. A Carbonic Anhydrase IX IHC Kit (Siemens Healthcare Diagnostics, Tarrytown, NY, USA, cat. number CAIXOS) utilizing monoclonal mouse anti-human CAIX, clone M75 was applied to detect CAIX. Immunohistochemical staining of CAIX was performed according the recommendations of the manufacturer. CAIX expression level was determined by using a four-step scoring system as proposed by the kit supplier. In brief, the CAIX staining intensity and the fraction of stained tumor cells were recorded for each tissue spot. Only membranous staining pattern was considered positive. The staining intensity was estimated in a four-step scale (none, weak, moderate, strong). The final staining pattern was scored according to the following criteria: Negative=score 0 (no

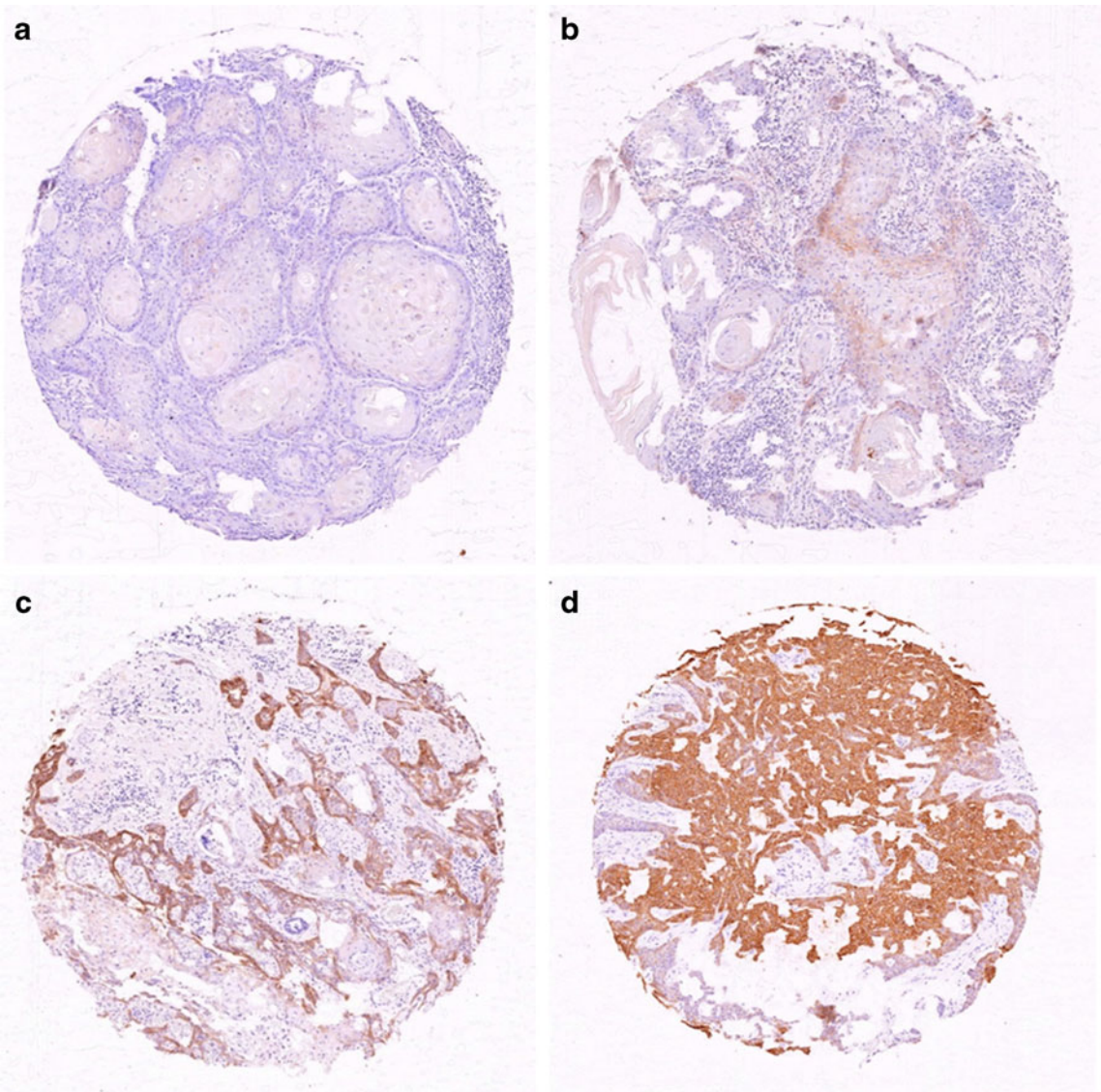

Fig. 1 Examples of CAIX immunohistochemistry results in vulvar carcinomas: negative (**a**), weak (**b**), moderate (**c**), and strong (**d**) staining

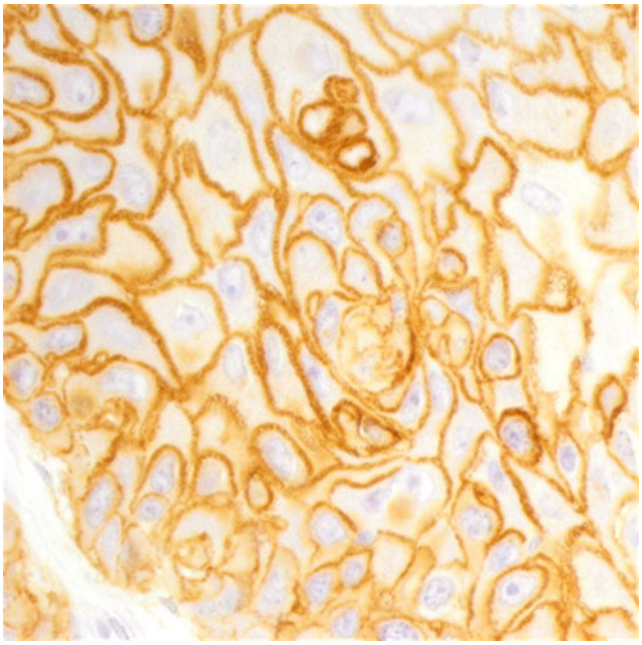

Fig. 2 CAIX immunostaining in a case of vulvar carcinoma with strong expression: the CAIX expression is completely restricted to the cell membrane (×400)

staining or membrane staining <10% of tumor cells), weak= score 1 (partial membrane staining or weak complete membrane staining >10% of tumor cells), moderate=score 2 (weak to moderate complete membrane staining >10% of tumor cells), strong=score 3 (strong and complete membrane staining in >10% of tumor cells). A final cumulative score for assessment of tissue CAIX expression was made from all interpretable core biopsies. Only tumors with at least two assessable tissue cores are enclosed in our study. For further statistical analysis, we established a two-tier scoring system: score 0 and score 1 as well as score 2 and 3, corresponding with low and high expression levels, were put together, respectively. For the two-tier scoring system, kappa-type statistic revealed a substantial strength of agreement (κ=0.66) in CAIX assessment between different core biopsies of one tumor and moderate agreement (κ=0.48) for the four-tier scoring system. Therefore, it was reasonable to use the two-step scoring system in this study.

HPV detection

Analysis of the tumor HPV status was done with conventional PCR and standard MY09/11 consensus primers as described elsewhere [15]. PCR products were sequenced on a 377 ABI Prism Sequencer (PE Applied Biosystems).

Statistics

Pearson's chi-squared test and student's *t* test were used to study the relationship between CAIX and clinicopathological parameters. The kappa statistics were applied to measure agreement between different tissue core series on the TMA's. Agreement was considered slight if κ <0.2, fair if κ 0.21-0.40, moderate if κ 0.41-0.60, substantial if κ 0.61-0.80 and perfect if κ >0.80 [16]. Survival effect of CAIX was assessed by Kaplan-Meier curves and log-rank tests. Analysis was performed using *R* statistical software package for Windows (version 2.7.2, *R* Foundation for statistical computing).

Results

CAIX immunohistochemistry

A total of 135 cancerous samples were informative for determination of the CAIX expression. CAIX was detectable in 77/135 (57%) of all interpretable specimens. 48 (35.5%) samples exhibited a moderate or strong staining result (Table 1). Representative tumor examples are shown in Fig. 1. CAIX protein expression was always membranous (Fig. 2). Weak cytoplasmic signals occurred sometimes in cases with low CAIX expression (score 0 and 1). Tumor-associated stromal cells as well as inflammatory cells stained negative for CAIX.

CAIX expression, concordance analysis

CAIX is a hypoxia associated protein with potentially heterogeneous tissue distribution. Therefore, in our study, we arrayed triplicate tissue cores from each tumor. To test the reliability of our analysis, we performed a correlation

Table 2 Distribution of CAIX expression in triplicate tissue cores from different representative tumor areas

CAIX expression[a]	Core 1	Core 2	Core 3	*p* value
Score 0	76 (53.5%)	63 (44.4%)	61 (43.0%)	0.77
Score 1	19 (13.4%)	25 (17.6%)	20 (14.1%)	
Score 2	20 (14.1%)	18 (12.7%)	21 (14.8%)	
Score 3	22 (15.5%)	27 (19.0%)	25 (17.6%)	
Not assessable	5 (3.5%)	9 (6.3%)	15 (10.6%)	

[a] Four-tier scoring system for more detailed data description

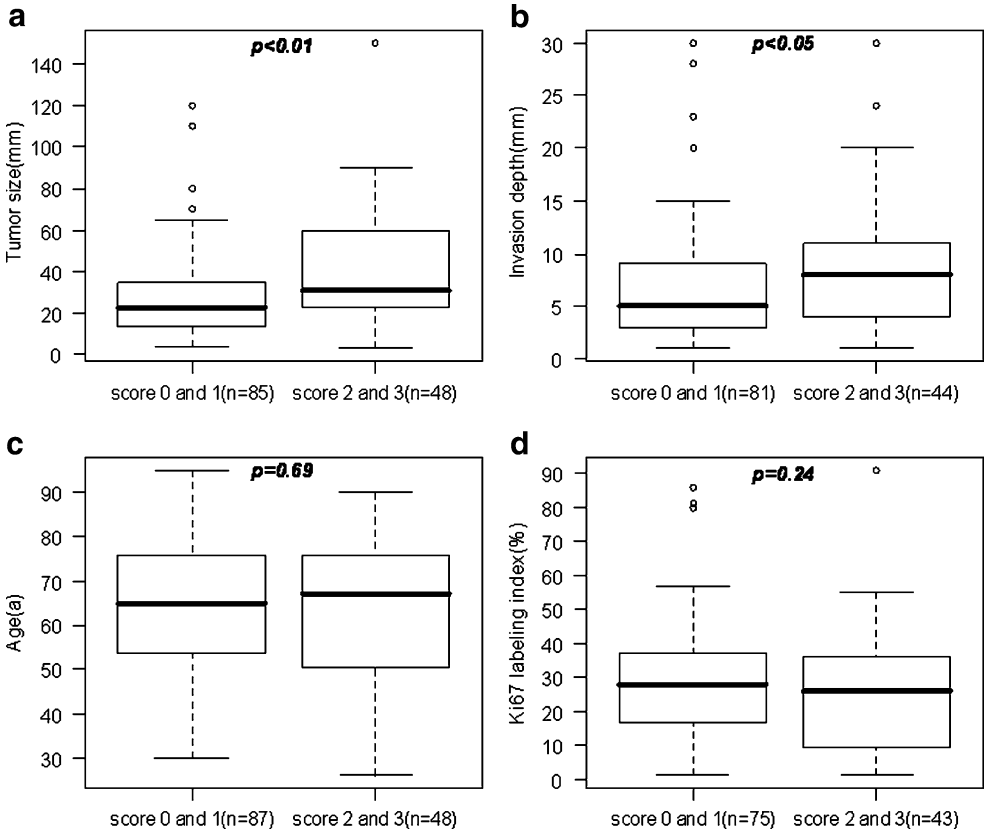

Fig. 3 CAIX expression in dependence of tumor size (**a**), depth of invasion (**b**), patient age (**c**), and tumor proliferation (**d**)

analysis between CAIX expression results of corresponding cores. There were no significant differences in the distribution of CAIX levels between the three core biopsies (Table 2). For concordance analysis, we used only specimens with three assessable tissue cores. Of the specimens, 76.9% showed a complete match of all three core biopsies, each of them from a different representative tumor area.

CAIX and clinicopathological parameters

Table 1 summarizes the association of CAIX expression in vulvar carcinomas to clinicopathological parameters. Increased levels of CAIX were significantly associated with advanced pT stage ($p<0.01$, pT1b vs. pT2) and tumor size ($p<0.01$; Fig. 3a), respectively. Furthermore, CAIX expression was significantly correlated to depth of invasion ($p<0.05$; Fig. 3b). No relation of CAIX level and patient age as well as Ki67 tumor proliferation index could be found ($p<0.05$, each; Fig. 3c and d).There was no association between CAIX expression and histological tumor typing, pN category, tumor grade, and HPV status of vulvar carcinomas. The number of positive regional lymph nodes was associated with high CAIX expression levels ($p<0.05$; Fig. 4). 23.8% of tumor specimens with high CAIX expression showed three or more lymph node metastases whereas in only two cases (2.7%) with no or weak CAIX expression three positive lymph nodes were diagnosed.

CAIX in non-neoplastic vulvar tissue

A total of 120 non-neoplastic vulvar tissue specimens were arrayed for comparative analyses (Table 3). The expression

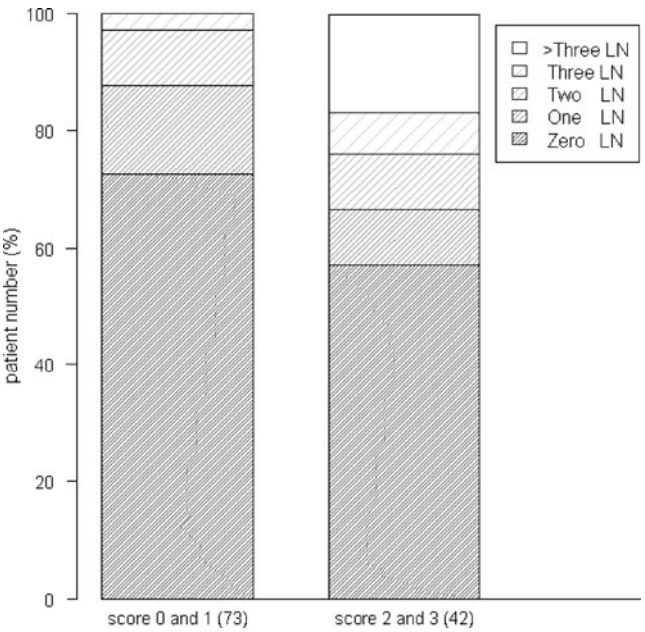

Fig. 4 CAIX expression in relation to number of positive regional lymph nodes in vulvar carcinoma: CAIX expression was significantly higher in patients with more than three lymph node metastases ($p<0.05$)

Table 3 CAIX expression in matched normal mucosa remote from tumor and in non-neoplastic vulvar diseases

	On array (*n*)	Analyzable (*n*)	Carbonic anhydrase IX		*p* value
			Score 0 and 1(%)	Score 2 and 3 (%)	
Normal mucosa	78	69	98.6	1.4	<0.001
Lichen sclerosus	15	14	92.9	7.1	
Lichen simplex	18	15	100.0	-	
Hypertrophy labia	9	9	100.0	-	

level was generally much lower than in tumor tissues ($p<0.001$). 89.7% of all assessable non-neoplastic specimens were completely negative for CAIX. In positive samples, the expression was restricted to basal cells of the overlying squamous epithelium. Stromal tissue was always negative. There were no differences in CAIX expression between normal mucosa remote from tumor and cases with lichen simplex or hypertrophy of labia. Squamous epithelium in lichen sclerosus showed significantly elevated CAIX levels. However, the expression was patchy and only one specimen showed a moderate staining intensity.

CAIX and patient survival

All previously established associations between vulvar cancer prognosis and clinicopathological parameters were retained in the subset of 100 tumors at our TMA with survival data [17].

Tumor size ($p<0.006$), pN ($p<0.002$), depth of invasion ($p=0.002$), and patient age ($p=0.002$) were strongly associated with poor prognosis in univariate analysis. There was also a trend towards shortened disease-free patient survival in tumors with elevated CAIX expression but this result failed to reach statistical significance. The proportion of patients alive and without recurrence after 5 years was 58% with moderate/strong expression and 74% with none/low expression of CAIX with a median 5 years disease-free survival of 26 versus 28 months; $p=0.15$, Fig. 5).

Discussion

The comparatively high number of analyzed vulvar cancer samples in this study in combination with survival data collected during previous studies enabled a comprehensive survey of CAIX expression with multiple clinicopathological parameters and cell proliferation. More than 50% of vulvar cancers showed various levels of detectable CAIX expression. Despite the high levels in carcinomas, we found no or only weak CAIX staining in matched normal squamous epithelium and non-neoplastic vulvar diseases. These observations are completely in line with results already achieved in other tumors including squamous cell carcinomas and precursor lesions of cervix, head and neck and esophagus [18–20]. Taken together, enhanced expression of CAIX is an important key feature of cancerogenesis in vulvar carcinoma.

Numerous studies had previously demonstrated that TMA's are reliable tools for immuno-histochemical examination of protein expression [21, 22]. As clearly shown in comparative experiments, analysis of a single high-density tissue microarray section is representative for the whole tumor and may be superior to large section data for some biomarkers [23]. However, in studies with only limited sample numbers, three tissue cores per case may be more valid for accurate assessment of protein expression in tumors [24–26]. Recently, Fons et al. found a good agreement of staining results between TMA and whole sections in an expression study of six different nuclear, cytoplasmic, and membranous antigens in vulvar cancer [27]. These observations are not markedly different from results in our analysis and confirm our methodological

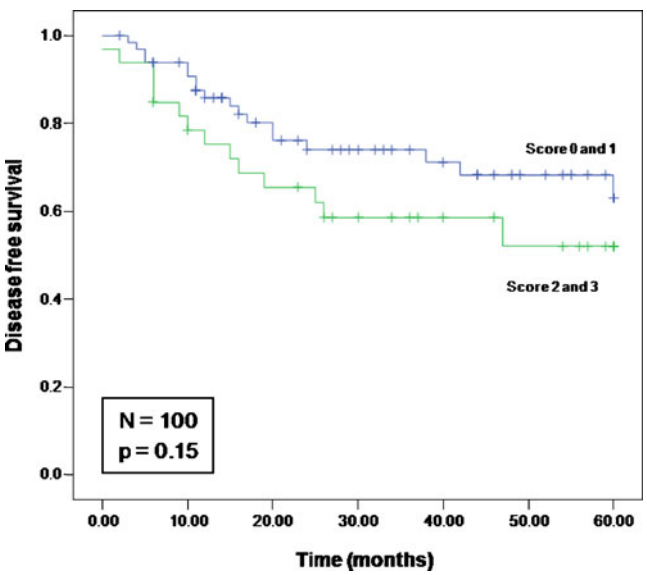

Fig. 5 Prognostic relevance of CAIX expression in vulvar carcinoma

approach. Thus, the CAIX expression data in the present study can be regarded as representative for the whole tumor. In our data set, there were no differences in distribution of CAIX levels in three different analyzed tissue core series. Moreover, independent from the used scoring systems, there was a significant correlation between CAIX results in tissue cores from the same tumor. Because tissue cores are obtained from different representative tumor areas, this result suggests that the distribution of CAIX expression is relatively homogeneous in vulvar carcinomas. Tumor hypoxia plays a critical role in CAIX expression in the majority of malignant tumors [28]. Strong correlation of CAIX expression to pT stage and depth of invasion in vulvar carcinomas also underscores the important role of a hypoxic microenvironment. Up-regulation of CAIX via the phosphatidylinositol-3-kinase or the mitogen-activated protein kinase pathways could be an alternative explanation for homogeneous expression [29, 30].

Interestingly, we found clearly elevated CAIX expression levels in lichen sclerosus. The coincidence of lichen sclerosus and vulvar cancer is well known and lichen sclerosus is usually regarded as a potential preneoplastic condition. The histological hallmark of this disease is a thick hyalinized collagen band in the papillary and the upper reticular dermis. This microscopic feature may be causative for diminished oxygen diffusion with increase of CAIX expression. Hypoxia is an important trigger for CAIX expression via stabilization of the transcription factor HIF1α [31]. Therefore, in contrast to our results in advanced tumors, it can be hypothesized that latent tissue hypoxia plays a role in early stages of a subset of vulvar carcinomas.

In our study, we did not find any influence of HPV status and tumor proliferation on CAIX expression level. No link between HPV detection or HPV subtype and CAIX expression was found by others in head and neck squamous cell carcinomas and cervical intraepithelial neoplasia [32, 33]. Independence of CAIX expression from patient age in the present examination also points in this direction because the known connection of younger age and higher incidence of HPV-related vulvar cancers. In contrast to Ki67, CAIX staining showed no relation to dysplasia grade in cervical epithelium or in ductal carcinoma in situ of the breast [33, 34]. Thus, CAIX expression is likely not driven by cell cycle or viral oncogenes.

CAIX expression showed numerous associations to various clinicopathological features like pT stage, tumor size, depth of invasion, and lymph node metastases. All of these features are well known to be related with unfavorable clinical outcome [17, 35]. The adverse prognostic impact of CAIX expression was already shown in a range of other tumor entities. In our study, we found also a tendency to shortened disease-free survival in CAIX positive cases. The effect was not significant, probably because low patient numbers. However, in our cohort, there was a strong correlation of CAIX expression to the number of positive regional lymph nodes and advanced pT stage. Up-regulation of CAIX is probably an adaptation to aerobic glycolysis in tumor cells for maintenance of intracellular pH in advanced carcinomas. Acidification of extracellular space by this mechanism may contribute to tumor cell invasion and development of metastases as shown in several studies [36, 37]. Therefore, high levels of CAIX may promote the development of locoregional lymph node metastases in vulvar carcinomas. Advanced vulvar carcinomas without CAIX overexpression might be able to overcome tissue hypoxia by activation of other metabolic pathways. However, expression of CAIX seems to be one step towards worse prognosis.

In summary, CAIX is overexpressed in a substantial proportion of advanced vulvar carcinomas and is potentially related to adverse clinicopathological parameters and unfavorable patient outcome. The exclusive expression of CAIX in cancerous tissues makes the enzyme a suitable target for therapeutic interventions. Currently developed CAIX-targeting antibodies (G250) achieved anti-tumor activity in mouse xenograft tumor models and phase II clinical trials [38, 39]. Our data further support the concept of CAIX representing a suitable therapeutic target in human cancer including advanced vulvar carcinomas.

Conflict of interest statement We declare that we have no conflict of interest.

References

1. Vander Heiden MG, Cantley LC, Thompson CB (2009) Understanding the Warburg effect: the metabolic requirements of cell proliferation. Science 324:1029–1033
2. Fang JS, Gillies RD, Gatenby RA (2008) Adaptation to hypoxia and acidosis in carcinogenesis and tumor progression. Semin Cancer Biol 18:330–337
3. Potter CP, Harris AL (2003) Diagnostic, prognostic and therapeutic implications of carbonic anhydrases in cancer. Br J Cancer 89:2–7
4. Winum JY, Poulsen SA, Supuran CT (2009) Therapeutic applications of glycosidic carbonic anhydrase inhibitors. Med Res Rev 29:419–435
5. Zavada J, Zavadova Z, Pastorekova S et al (1993) Expression of MaTu-MN protein in human tumor cultures and in clinical specimens. Int J Cancer 54:268–274
6. Potter C, Harris Al (2004) Hypoxia inducible carbonic anhydrase IX, marker of tumour hypoxia, survival pathway and therapy target. Cell Cycle 3:164–167
7. Robertson N, Potter C, Harris AL (2004) Role of carbonic anhydrase IX in human tumor cell growth, survival, and invasion. Cancer Res 64:6160–6165

8. Kaluz S, Kaluzova M, Liao SY et al (2009) Transcriptional control of the tumor- and hypoxia-marker carbonic anhydrase 9: a one transcription factor (HIF-1) show? Biochim Biophys Acta 1795:162–172
9. Ivanov S, Liao SY, Ivanova A et al (2001) Expression of hypoxia-inducible cell-surface transmembrane carbonic anhydrases in human cancer. Am J Pathol 158:905–919
10. Hussain SA, Ganesan R, Reynolds G et al (2007) Hypoxia-regulated carbonic anhydrase IX expression is associated with poor survival in patients with invasive breast cancer. Br J Cancer 96:104–109
11. Klatte T, Seligson DB, Rao JY (2009) Carbonic anhydrase IX in bladder cancer: a diagnostic, prognostic, and therapeutic molecular marker. Cancer 115:1448–1458
12. Loncaster JA, Harris AL, Davidson SE et al (2001) Carbonic anhydrase (CA IX) expression, a potential new intrinsic marker of hypoxia: correlations with tumor oxygen measurements and prognosis in locally advanced carcinoma of the cervix. Cancer Res 61:6394–6399
13. Swinson DE, Jones JL, Richardson D (2003) Carbonic anhydrase IX expression, a novel surrogate marker of tumor hypoxia, is associated with a poor prognosis in non-small-cell lung cancer. J Clin Oncol 21:473–482
14. Simon R, Mirlacher M, Sauter G (2004) Tissue microarrays. Biotechniques 36:98–105
15. Petersen I, Schewe C, Schluns K et al (2007) Inter-laboratory validation of PCR-based HPV detection in pathology specimens. Virchows Arch 451:701–716
16. Landis JR, Koch GG (1977) The measurement of observer agreement for categorical data. Biometrics 33:159–174
17. Woelber L, Mahner S, Voelker K et al (2009) Clinicopathological prognostic factors and patterns of recurrence in vulvar cancer. Anticancer Res 29:545–552
18. Lee WY, Huang SC, Hsu KF et al (2008) Roles for hypoxia-regulated genes during cervical carcinogenesis: somatic evolution during the hypoxia-glycolysis-acidosis sequence. Gynecol Oncol 108:377–384
19. Choi SW, Kim JY, Park JY et al (2008) Expression of carbonic anhydrase IX is associated with postoperative recurrence and poor prognosis in surgically treated oral squamous cell carcinoma. Hum Pathol 39:1317–1322
20. Tanaka N, Kato H, Inose T et al (2008) Expression of carbonic anhydrase 9, a potential intrinsic marker of hypoxia, is associated with poor prognosis in oesophageal squamous cell carcinoma. Br J Cancer 99:1468–1475
21. Bubendorf L, Nocito A, Moch H et al (2001) Tissue microarray (TMA) technology: miniaturized pathology archives for high-throughput in situ studies. J Pathol 195:72–79
22. Ruiz C, Seibt S, Al Kuraya K (2006) Tissue microarrays for comparing molecular features with proliferation activity in breast cancer. Int J Cancer 118:2190–2194
23. Torhorst J, Bucher C, Kononen J et al (2001) Tissue microarrays for rapid linking of molecular changes to clinical endpoints. Am J Pathol 159:2249–2256
24. Fons G, Hasibuan SM, van der Velden J et al (2007) Validation of tissue microarray technology in endometrioid cancer of the endometrium. J Clin Pathol 60:500–503
25. Gulmann C, Butler D, Kay E et al (2003) Biopsy of a biopsy: validation of immunoprofiling in gastric cancer biopsy tissue microarrays. Histopathology 42:70–76
26. Rubin MA, Dunn R, Strawderman M et al (2002) Tissue microarray sampling strategy for prostate cancer biomarker analysis. Am J Surg Pathol 26:312–319
27. Fons G, van der Velden J, Burger M et al (2009) Validation of tissue microarray technology in vulvar cancer. Int J Gynecol Pathol 28:76–82
28. Ruan K, Song G, Ouyang G (2009) Role of hypoxia in the hallmarks of human cancer. J Cell Biochem 107:1053–1062
29. Kaluz S, Kaluzova M, Chrastina A et al (2002) Lowered oxygen tension induces expression of the hypoxia marker MN/carbonic anhydrase IX in the absence of hypoxia-inducible factor 1 alpha stabilization: a role for phosphatidylinositol 3'-kinase. Cancer Res 62:4469–4477
30. Kopacek J, Barathova M, Dequiedt F et al (2005) MAPK pathway contributes to density- and hypoxia-induced expression of the tumor-associated carbonic anhydrase IX. Biochim Biophys Acta 1729:41–49
31. Denko NC (2008) Hypoxia, HIF1 and glucose metabolism in the solid tumour. Nat Rev Cancer 8:705–713
32. Kong CS (2009) The relationship between human papillomavirus status and other molecular prognostic markers in head and neck squamous cell carcinomas. Int J Radiat Oncol Biol Phys 74:553–561
33. Resnick M (1996) Viral and histopathologic correlates of MN and MIB-1 expression in cervical intraepithelial neoplasia. Hum Pathol 27:234–239
34. Wykoff CC, Beasley N, Watson PH et al (2001) Expression of the hypoxia-inducible and tumor-associated carbonic anhydrases in ductal carcinoma in situ of the breast. Am J Pathol 158:1011–1019
35. Drew PA, al-Abbadi MA, Orlando CA (1996) Prognostic factors in carcinoma of the vulva: a clinicopathologic and DNA flow cytometric study. Int J Gynecol Pathol 15:235–241
36. Svastova E, Hulikova A, Rafajova M et al (2004) Hypoxia activates the capacity of tumor-associated carbonic anhydrase IX to acidify extracellular pH. FEBS Lett 577:439–445
37. Swietach P, Patiar S, Supuran CT et al (2009) The role of carbonic anhydrase 9 in regulating extracellular and intracellular pH in 3-D tumor-cell growths. J Biol Chem 284:20299–20310
38. Mulders P, Bleumer I, Debruyne F, et al. (2004) Specific monoclonal antibody-based immunotherapy by targeting the RCC-associated antigen carbonic anhydrase-IX(G250/MN) Urologe A 43 Suppl 3:S146-147: 146-147
39. Bauer S, Oosterwijk-Wakka JC, Adrian N et al (2009) Targeted therapy of renal cell carcinoma: synergistic activity of cG250-TNF and IFNg. Int J Cancer 125:115–123

Virchows Arch (2010) 456:491–497
DOI 10.1007/s00428-010-0914-8

ORIGINAL ARTICLE

Comparison of morphological, immunohistochemical, and molecular genetic features of inflammatory fibroid polyps (Vanek´s tumors)

Ondrej Daum · Jana Hatlova · Vaclav Mandys · Petr Grossmann · Petr Mukensnabl · Zdenek Benes · Michal Michal

Received: 19 January 2010 / Revised: 26 February 2010 / Accepted: 25 March 2010 / Published online: 15 April 2010
© Springer-Verlag 2010

Abstract Vanek´s tumor (inflammatory fibroid polyp) is a rare benign lesion occurring throughout the digestive tract. Histologically, two patterns can be recognized. Classical Vanek´s tumor contains concentric formations of proliferating spindle cells which are CD34 positive. Atypical, inflammatory pseudotumor-like Vanek´s tumor lacks concentric formations and is CD34 negative. Recently, mutations in platelet-derived growth factor receptor alpha (*PDGFRA*) were reported in gastric and small intestinal Vanek´s tumors. In this study, *KIT* exons 9, 11, 13, and 17, *PDGFRA* exons 12, 14, and 18, and a part of exon 15 *BRAF* for point mutation V600E were screened in 23 cases of Vanek´s tumor, both classical (n=16) and inflammatory pseudotumor-like (n=7). No mutations in all analyzed exons of *KIT* and *BRAF* and in exon 14 of *PDGFRA* were detected. Six Vanek´s tumors harbored activating mutations in *PDGFRA* exons 12 (n=5) and 18 (n=1), respectively: S566_E571delinsK (n=1), S566_E571delinsR (n=4), and D842 del (n=1). The mutations were detected in the classical (n=5), as well as inflammatory pseudotumor-like (n=1) Vanek´s tumors. The results of this study suggest that the two morphological patterns of Vanek´s tumor more probably represent only variants of one type of tumor than two different lesions. Furthermore, *BRAF* mutations were not shown to drive growth of *PDGFRA* wild-type Vanek´s tumors.

Keywords GIT · Inflammatory fibroid polyp · Vanek´s tumor · *PDGFRA* · *BRAF* · CD34

O. Daum (✉) · P. Mukensnabl · M. Michal
Department of Pathology, Medical Faculty Hospital,,
Charles University in Prague, Medical Faculty in Plzen,
Edvarda Benese 13,
Plzen 305 99, Czech Republic
e-mail: DAUM@fnplzen.cz

J. Hatlova
Department of Pathology, Charles University Medicine Faculty,
Teaching Hospital in Hradec Kralove,
Hradec Kralove, Czech Republic

V. Mandys
Department of Pathology,
Medical Faculty Hospital Kralovske Vinohrady,
Charles University in Prague, Third Faculty of Medicine,
Prague, Czech Republic

P. Grossmann
Biopticka laborator s.r.o.,
Plzen, Czech Republic

Z. Benes
Department of Hepatogastroenterology,
Medical Faculty Thomayer Hospital,
Prague, Czech Republic

Introduction

Vanek's tumor (inflammatory fibroid polyp, IFP) is a rare mesenchymal lesion of the gastrointestinal tract first described by Vanek in 1949 [1]. Histologically, it is distinguished as a localized proliferation of spindle, stellate, or epithelioid cells centered in the submucosa, accompanied by an inflammatory reaction predominantly composed of lymphocytes and eosinophilic granulocytes, with lymphatic vessels, capillaries, and vascular channels in the stroma having propensity for fibroproduction and edema. Most investigators considered this lesion to be of non-neoplastic, benign, and reactive origin. However, recently, mutations in platelet-derived growth factor receptor alpha (*PDGFRA*) were reported in IFPs of the stomach [2] and small intestine

[3], raising suspicion of a possible neoplastic origin and relationship between *PDGFRA*-mutated gastrointestinal stromal tumors (GISTs) and IFPs.

In our previous article, we reported on the association of presence of onion skin-like concentric formations (CF) of spindle cells with immunoexpression of CD34 in these cells and discussed the possibility of existence of two different lesions commonly designated as Vanek´s tumor and the hypothesis of various evolutional stages of one type of disease [4]. To further elucidate the relationship between CD34 positive and negative Vanek´s tumors, we collected 24 cases to compare their molecular genetic profile with the presence of concentric formations and immunoexpression of CD34.

Furthermore, because activating V600E *BRAF* mutation was recently suggested to represent a possible alternative early molecular event in some *KIT* and *PDGFRA* wild-type GISTs [5, 6], we also performed molecular genetic analysis of a part of exon 15 of *BRAF* to clarify its potential role in development of Vanek´s tumors.

Material and methods

Twenty-four specimens of Vanek's tumor were retrieved from the files of the Sikl's Department of Pathology in Pilsen, the consultation files of one of the authors (MM), and archives of the Fingerland's Department of Pathology in Hradec Kralove and Department of Pathology of Medical Faculty Hospital Kralovske Vinohrady in Prague. Tissue for light microscopy was fixed in 4% formaldehyde and embedded in paraffin using routine procedures. Five-micrometer-thick sections were cut from the tissue blocks and stained with hematoxylin–eosin.

For immunohistochemical investigations, the following primary antibodies were used: CD117, c-kit (polyclonal, 1:150, Dako, Glostrup, Denmark), CD34 Ab-1 (QBEnd/10, 1:800, NeoMarkers, Fremont, CA). No special pretreatment was used. The primary antibodies were visualized using the supersensitive streptavidin–biotin–peroxidase complex (Biogenex, San Ramon, CA). Appropriate positive and negative control slides were employed.

DNA for molecular genetic investigation was extracted from formalin-fixed, paraffin-embedded tissues. Several 5-μm-thick sections were placed on the slides. Hematoxylin- and eosin-stained slides were examined for determination of area of tumor tissue. Then, tumor tissue from unstained slides was scraped, and DNA was isolated by the NucleoSpin® Tissue Kit (MACHEREY-NAGEL GmbH & Co. KG, Düren, Germany) according to the manufacturer's protocol.

Mutational analysis of exons 9, 11, 13, and 17 of the *KIT* gene (accession number U63834), exons 12, 14, and 18 of the *PDGFRA* gene (accession number D50017), and a part of exon 15 of the *BRAF* gene for point mutation V600E was performed using PCR and direct sequencing.

PCR was carried out using primers shown in Table 1. The reaction conditions were as follows: 12.5 μl of HotStart Taq PCR Master Mix (QIAgen, Hilden, Germany), 10 pmol of each primer, 100 ng of template DNA, and distilled water up to 25 μl. The amplification program consisted of denaturation at 95°C for 15 min and then 40 cycles of denaturation at 95°C for 1 min, annealing at 55°C for 1 min, and extension at 72°C for 1.5 min for all amplicons. The program was finished by 72°C incubation for 7 min.

Successfully amplified PCR products were purified with magnetic particles Agencourt® AMPure® (Agencourt Bioscince Corporation, A Beckman Coulter Company, Beverly, MA, USA), both side sequenced using Big Dye Terminator Sequencing kit (PE/Applied Biosystems, Foster City, CA, USA) and purified with magnetic particles Agencourt® CleanSEQ® (Agencourt Bioscince Corporation, A Beckman Coulter Company, Beverly, MA, USA) all according to the manufacturer's protocol, then run on an automated sequencer ABI Prism 3130xl (Applied Biosystems, Foster City, CA, USA) at a constant voltage of 13.2 kV for 20 min.

Results

Clinical findings

Clinical findings are summarized in Table 2. The patients included 9 men and 15 women with a mean age of 64 years (range, 43–82 years). However, the male to female ratio suffers from selection bias, as the cases from Prague and Hradec Kralove were originally retrieved for the purpose of HUMARA study. Eighteen cases were located in the stomach and six in the small intestine. The size was known in 23 cases, and it varied from 0.3 to 6 cm (mean, 2.5 cm)

Histological and immunohistochemical findings

Microscopically, all lesions were composed of spindle and stellate to epithelioid cells. The nuclei were smooth-contoured, oval, or spindle-shaped, with finely granular chromatin and small nucleoli. The cytoplasm was scanty and amphophilic. The cells were uniform and devoid of mitoses. The inflammatory component of the lesions consisted predominantly of lymphocytes and eosinophilic granulocytes, but plasma cells and histiocytes were also present. The loose stroma showed various grades of edema and collagenization and was rich in capillaries and small-caliber vessels. Seventeen cases (cases 2, 3, 5, 6, 7, 8, 9, 10,

Table 1 PCR primers used in the study

Gene/exons	Name	Primers
KIT exon 9a[ac]	c-kit e9aNF	GAGTAAGCCAGGGCTTTTGTT
	c-kit e9aNR	CGTGCCATTGTGCTTGAAT
KIT exon 9b[bc]	c-kit e9bNF	CCGTTTGGAAAGCTAGTGGT
	c-kit e9bNR	CAGAGCCTAAACATCCCCTTA
KIT exon 11	c-kit e11NF	TGTTCTCTCTCCAGAGTGCTCTAA
	c-kit e11NR	ACCCAAAAAGGTGACATGGA
KIT exon 13	c-kit e13fN	GCCAGTTGTGCTTTTTGCTA
	c-kit e13rN	TTGATAACCTGACAGACAATAAAAGG
KIT exon 17[c]	c-kit e17WF	ATGGTTTTCTTTTCTCCTCC
	c-kit e17WR	TACATTATGAAAGTCACAGG
PDGFRA exon 12[c]	PDG e12F	CTCTGGTGCACTGGGACTTT
	PDG e12R	GGAGGTTACCCCATGGAACT
PDGFRA exon 14	PDG e14fN	TGGACTGATATGTGATTTATTCTTTCA
	PDG e14rN	AATCCTCACTCCAGGTCAGTG
PDGFRA exon 18[c]	PDG e18F	GCTACAGATGGCTTGATCCTG
	PDG e18R	GACCAGTGAGGGAAGTGAGG
BRAF exon 15	BRAF-V600E-F	TGAAGACCTCACAGTAAAAATAGGTG
	BRAF-V600E-R	TTAATCAGTGGAAAAATAGCCTCAA

[a] 5′ end of exon 9

[b] 3′ end of exon 9

[c] see Reference [14]

Table 2 Clinical, histological, and molecular genetic findings

Case	Sex	Age	Localization	Diameter (cm)	CF	CD34	Exon 12 *PDGFRA*	Exon 18 *PDGFRA*
1	F	50	Small intestine	Unknown	−	−	wt	wt
2	F	59	Ileum	3	+	+	mut[1]	wt
3	F	67	Stomach	5	+	+	mut[2]	wt
4	M	61	Stomach	2.5	−	−	wt	wt
5	F	71	Stomach	1	+	+	wt	wt
6	M	74	Stomach	2	+	+	wt	wt
7	F	45	Stomach	4	+	+	wt	wt
8	M	79	Stomach	2	+	+	NA	NA
9	M	51	Stomach	1.8	+	+	wt	wt
10	F	46	Small intestine	5	+	+	mut[2]	wt
11	F	74	Stomach	1	+	+	wt	wt
12	M	73	Stomach	4	+	+	wt	wt
13	M	58	Stomach	0.8	+	+	wt	wt
14	F	82	Stomach	0.5	+	+	wt	wt
15	M	68	Stomach	0.8	–	–	wt	wt
16	F	66	Stomach	1.2	+	+	wt	wt
17	F	76	Ileum	4	–	–	wt	wt
18	F	67	Stomach	2.2	–	–	wt	wt
19	F	67	Stomach	6	–	–	wt	wt
20	F	43	Stomach	1.7	–	–	mut[2]	wt
21	F	64	Duodenum	3	+	+	wt	mut[3]
22	F	57	Small intestine	5	+	+	mut[2]	wt
23	M	74	Stomach	0.4	+	+	wt	wt
24	M	63	Stomach	0.3	+	+	wt	wt

CF concentric formations

mut[1] p.S566_E571delinsK, c.1697_1711del

mut[2] p.S566_E571delinsR, c.1698_1712del

mut[3] p.D842del, c.2524_2526delGAC (deletion in frame)

11, 12, 13, 14, 16, 21, 22, 23, 24) showed apparent concentric formations composed of spindle-shaped cells with long slender cytoplasmic processes arranged in an onion skin-like pattern around vessels and mucosal glands (Fig. 1). The residual seven cases (cases 1, 4, 15, 17, 18, 19, 20) represented the subtype of Vanek´s tumor devoid of concentric formations (Fig. 2).

All cases were negative in staining with antibody against KIT protein (CD117). Results of immunoexpression of CD34 antigen in the spindle cells are shown in Table 2. Briefly, the seventeen cases showing concentric formations were also CD34 immunopositive. On the contrary, the cases lacking concentric formations were CD34 negative.

Molecular genetic findings

One sample (case 8) was non-analyzable. No mutations were detected in exons 9, 11, 13, and 17 of *KIT* gene. Likewise, the V600E substitution or any other mutation in exon 15 of *BRAF* gene was not present in any of the studied cases. As for *PDGFRA*, no case showed mutations in exon 14.

The results of mutational analysis of exons 12 and 18 of the *PDGFRA* gene are shown in Table 2. Briefly, five cases showed deletion mutations in exon 12 and one case in exon 18. More accurately, case 2 showed S566_E571delinsK; four cases (cases 3, 10, 20, 22) showed S566_E571delinsR. The polyp mutated in exon 18 (case 21) harbored D842 deletion. Five of the 6 mutated cases belonged to the group of Vanek´s tumor with concentric formations and CD34 immunoexpression (cases 2, 3, 10, 21, 22). Case 20, although showing the same type of mutation as cases 3, 10, and 22, lacked concentric formations and CD34 immunoexpression (Fig. 3).

Discussion

In 1949, Vanek presented six tumoriform lesions of the stomach originating in the submucosa and elevating mucosa, histologically consisting of cells reminiscent of fibroblasts, inflammatory infiltrate rich in lymphocytes and eosinophilic leukocytes, edema, collagenous fibrils, and abundant vasculature. He described the affection as submucosal granuloma with eosinophilic infiltration and interpreted it as a reactive process, probably of inflammatory origin [1]. In 1953, the supposed fibroblastic origin of proliferating spindle and stellate cells was confirmed by Helwig and Ranier who defined the lesion as a peculiar type of granulation tissue, naming it inflammatory fibroid polyp [7].

Proliferating spindle cells are arranged in onion skin-like pattern (CF) around vessels and mucosal glands in a substantial proportion of cases. In this study, these concentric formations were recognizable in 17 cases (cases 2, 3, 5, 6, 7, 8, 9, 10, 11, 12, 13, 14, 16, 21, 22, 23, 24).

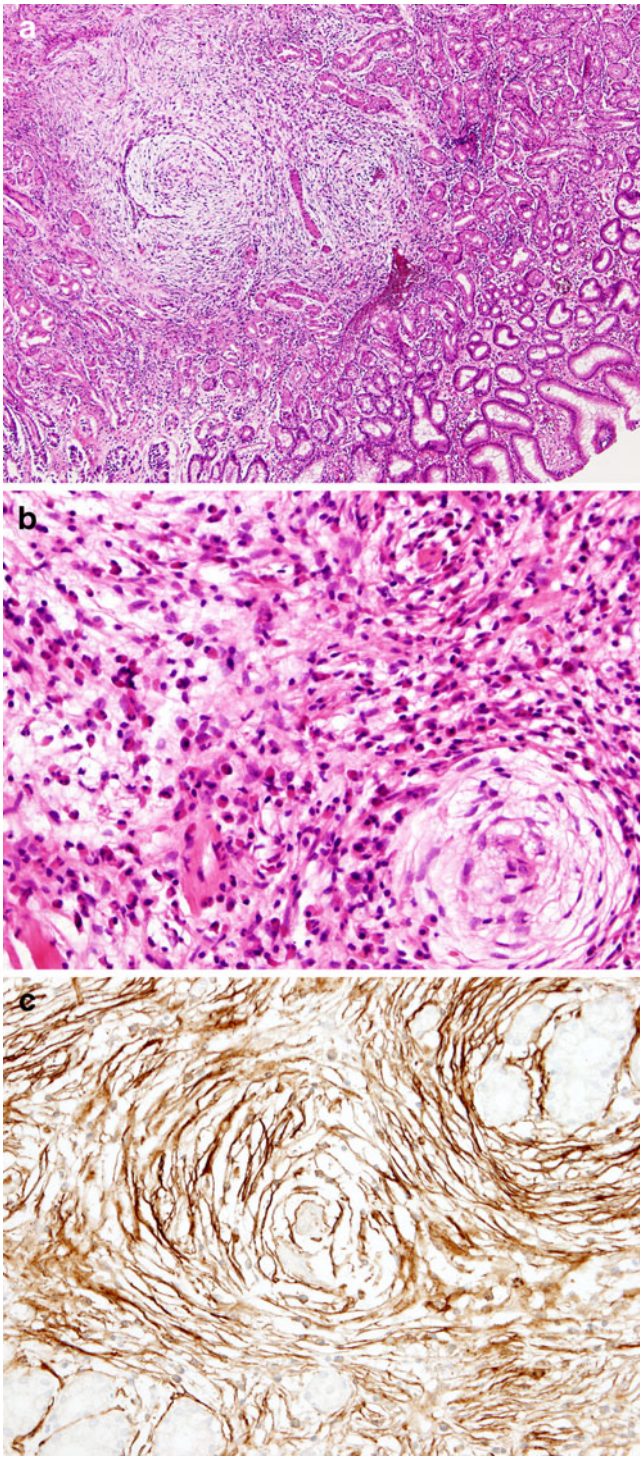

Fig. 1 Classical type of Vanek´s tumor (case 3) shows prominent onion skin-like concentric formations of spindle cells (**a**). Higher magnification reveals accompanying inflammatory infiltrate-rich in eosinophilic leukocytes (**b**). The spindle cells are readily CD34 positive (**c**)

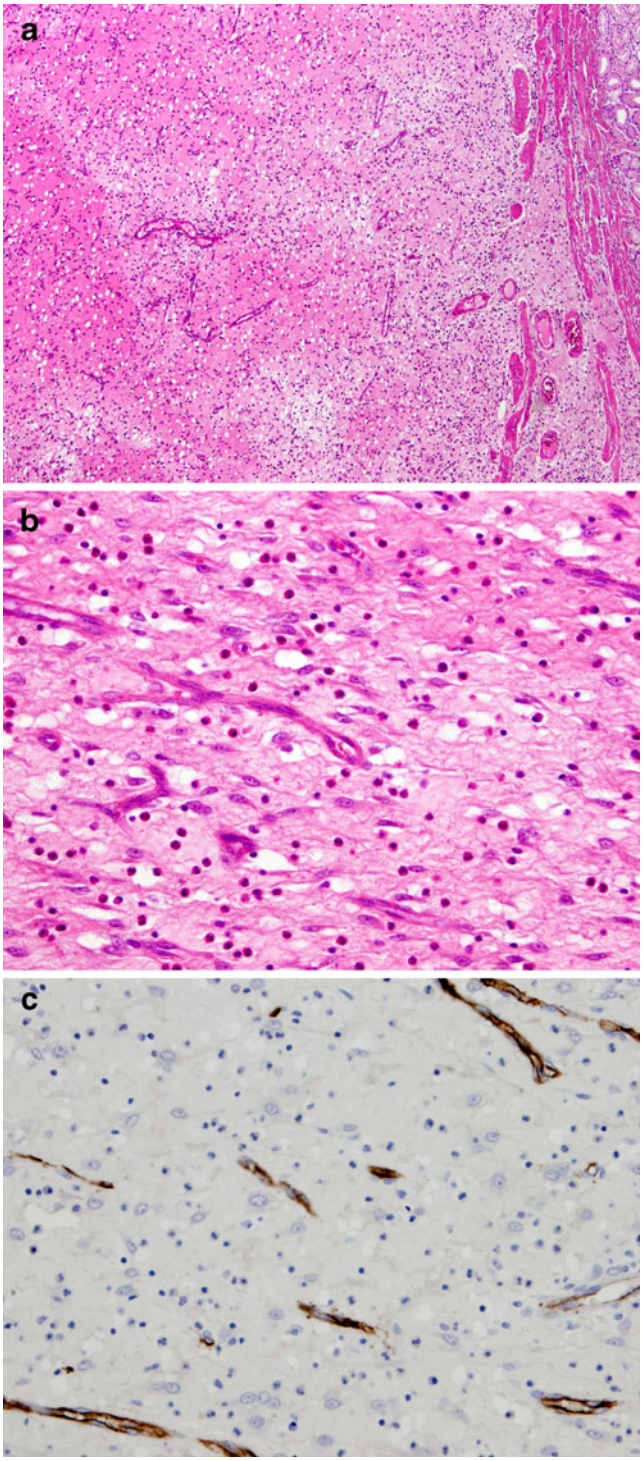

Fig. 2 Inflammatory pseudotumor-like Vanek´s tumor (case 18) is devoid of concentric formations (**a**), and the spindle to epithelioid cells dispersed in edematous stroma with inflammatory infiltrate rich in eosinophilic leukocytes (**b**) are apparently CD34 negative (**c**)

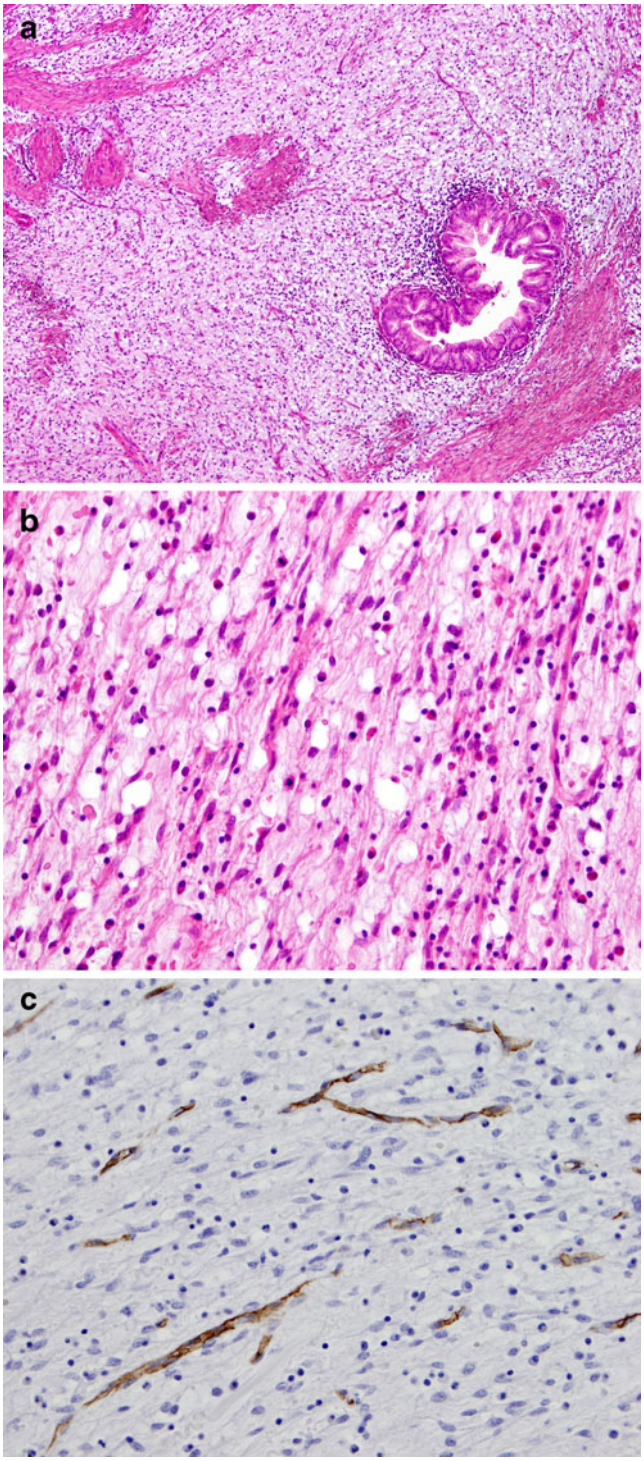

Fig. 3 Although case 20 is histologically similar to case 18 regarding its architectural pattern (**a**), cellular composition (**b**), and absence of staining with antibody against CD34 (**c**); it harbored a mutation of *PDGFRA*

Similarly, positive immunohistochemical staining of spindle and stellate cells with antibody against CD34 became one of the diagnostic criteria of Vanek's tumor [8, 9].

However, in our previous study of 18 lesions diagnosed as Vanek's tumor, we found three cases to be negative for the antibody against CD34 [4]. These lesions also lacked

concentric onion skin-like formations of spindle cells. We noticed only one study of Kim et al. describing similar results in the literature [10]. The authors presented two Vanek's tumors of the small intestine and one localized in the stomach, each of them lacking concentric formations and being CD34 negative. They suggested that existence of two histogenetically different lesions commonly diagnosed as Vanek's tumor could explain these results. Makhlouf and Sobin compared a series of Vanek's tumors with inflammatory pseudotumors (inflammatory myofibroblastic tumors) of the gastrointestinal tract and found many overlapping features including a presence of onion skin-like pattern in both lesions. In the gastric location, the concentric formations were much less pronounced in inflammatory pseudotumors than in Vanek's tumors [11], and in this location, they could help in differential diagnosis between Vanek's tumor and inflammatory pseudotumor [12]. In contrast, intestinal Vanek's tumors had less apparent onion skin-like pattern, thus showing strong overlap with inflammatory pseudotumors. Simultaneously, the intestinal lesions tend to show CD34-negativity that is more typical of inflammatory pseudotumors. Those results supported the Kim et al. suggestion that CD34 negative Vanek's tumor without onion skin-like pattern could represent a distinctive lesion different from conventional Vanek's tumor. An alternative explanation for the lack of onion skin-like pattern and CD34 negativity was offered by Kim and Kim [13]. They suggested that some atypical features in Vanek's tumor represented evolutional changes of the lesion. They demonstrated different histologic patterns in relation to the size of the lesion, distinguishing four stages, the first two stages (nodular and fibrovascular) showing concentric formations of immature and mature fibroblasts, marked inflammatory infiltration and early collagenization. The latter two stages (sclerotic and edematous) thought to represent variants of one "organized stage" are devoid of concentric formations of fibroblast-like cells [13].

Although traditionally regarded as a non-neoplastic reactive lesion, recent identification of *PDGFRA*-activating mutations has provided strong evidence of clonal proliferation and suggests a neoplastic nature of IFP [2, 3]. Unfortunately, none of these two studies correlated the presence of *PDGFRA* mutation with morphological features of Vanek´s tumors. Hence, we performed morphological–molecular genetic correlation of 24 IFPs. Analyzable DNA was extracted from 23 cases, 16 of the conventional type (i.e., CD34 and CF positive), 7 devoid of CF, and CD34 negative, thus more akin to inflammatory pseudotumor. To fully investigate their relationship with gastrointestinal stromal tumor, we analyzed not only hot spots of the *PDGFRA* and *KIT* genes, but also of exon 15 of *BRAF* gene to exclude V600E mutation which was recently shown to represent a possible alternative early molecular event in some *KIT* and *PDGFRA* wild-type GISTs [5, 6].

In total, six cases showed a mutation of the *PDGFRA* gene, whereas no mutations were detected in analyzed exons of *KIT* and *BRAF* genes. The frequency of mutated cases was considerably lower than in previous studies [2, 3]. It might be a consequence of the low number of cases that may be responsible for statistically unexpected findings, or it may result from differences in sensitivities between laboratories (the cellularity of these lesions is very low which makes the molecular genetic analysis more difficult than in usual cellular tumors). Five of these cases were classical Vanek´s tumors (i.e., CD34 and CF positive). Three types of mutations were detected in these five tumors, more specifically one small intestinal case harbored S566_E571delinsK in exon 12, one gastric and two intestinal ones S566_E571delinsR in the same exon, and one duodenal case showed D842del in exon 18. The *PDGFRA*-mutated CD34 and CF negative gastric tumor harbored the same S566_E571delinsR mutation in exon 12 as three conventional Vanek´s tumors. Although the small number of cases does not allow reliable statistical analysis, we suggest that our results are more in accord with the theory of etiopathogenetical unity of various morphological subtypes of so-called IFP as described in the original Vanek´s article [1], than with the theory of two different lesions.

In summary, we have shown that both classical (CD34 and CF positive) and inflammatory pseudotumor-like (CD34 and CF negative) IFPs may be driven by activating *PDGFRA* mutations. Then, this study has been the first to investigate possible oncogenic role of *BRAF* mutations in *PDGFRA* wild-type Vanek´s tumors. In the scope of current knowledge, the term inflammatory fibroid polyp seems misleading. Therefore, Lasota et al. [3] has recently coined the term "inflammatory fibroid tumor" for this lesion; however, we prefer using the traditional and widely spread designation of "Vanek´s tumor" in creating new terminology.

Conflict of interest statement We declare that we have no conflict of interest.

References

1. Vanek J (1949) Gastric submucosal granuloma with eosinophilic infiltration. Am J Pathol 25:397–411
2. Schildhaus HU, Cavlar T, Binot E, Buttner R, Wardelmann E, Merkelbach-Bruse S (2008) Inflammatory fibroid polyps harbour mutations in the platelet-derived growth factor receptor alpha (PDGFRA) gene. J Pathol 216:176–182

3. Lasota J, Wang ZF, Sobin LH, Miettinen M (2009) Gain-of-function PDGFRA mutations, earlier reported in gastrointestinal stromal tumors, are common in small intestinal inflammatory fibroid polyps. A study of 60 cases. Mod Pathol 22:1049–1056
4. Daum O, Hes O, Vanecek T et al (2003) Vanek's tumor (inflammatory fibroid polyp). Report of 18 cases and comparison with three cases of original Vanek's series. Ann Diagn Pathol 7:337–347
5. Agaram NP, Wong GC, Guo T et al (2008) Novel V600E BRAF mutations in imatinib-naive and imatinib-resistant gastrointestinal stromal tumors. Genes Chromosomes Cancer 47:853–859
6. Agaimy A, Terracciano LM, Dirnhofer S, Tornillo L, Foerster A, Hartmann A, Bihl MP (2009) V600E BRAF mutations are alternative early molecular events in a subset of KIT/PDGFRA wild-type gastrointestinal stromal tumours. J Clin Pathol 62:613–616
7. Helwig EB, Ranier A (1953) Inflammatory fibroid polyps of the stomach. Surg Gynecol Obstet 96:335–367
8. Hasegawa T, Yang P, Kagawa N, Hirose T, Sano T (1997) CD34 expression by inflammatory fibroid polyps of the stomach. Mod Pathol 10:451–456
9. Wille P, Borchard F (1998) Fibroid polyps of intestinal tract are inflammatory-reactive proliferations of CD34-positive perivascular cells. Histopathology 32:498–502
10. Kim MK, Higgins J, Cho EY, Ko YH, Oh YL (2000) Expression of CD34, bcl-2, and kit in inflammatory fibroid polyps of the gastrointestinal tract. Appl Immunohistochem Mol Morphol 8:147–153
11. Makhlouf HR, Sobin LH (2002) Inflammatory myofibroblastic tumors (inflammatory pseudotumors) of the gastrointestinal tract: how closely are they related to inflammatory fibroid polyps? Hum Pathol 33:307–315
12. Zamecnik M (2002) Onionskin-like pattern in inflammatory lesions of the gastrointestinal tract. Hum Pathol 33:1241, author reply 1241-1242
13. Kim YI, Kim WH (1988) Inflammatory fibroid polyps of gastrointestinal tract. Evolution of histologic patterns. Am J Clin Pathol 89:721–727
14. Michal M, Vanecek T, Sima R et al (2006) Mixed germ cell sex cord-stromal tumors of the testis and ovary. Morphological, immunohistochemical, and molecular genetic study of seven cases. Virchows Arch 448:612–622

Virchows Arch (2010) 456:499–505
DOI 10.1007/s00428-010-0912-x

ORIGINAL ARTICLE

Mitochondrion-rich differentiated adenocarcinomas of the stomach: clinicopathological, immunohistochemical and electron microscopy study of nine cases

Rosario A. Caruso · Patrizia Napoli · Alberto Nania · Antonino Parisi · Francesco Fedele · Valeria Zuccalà

Received: 18 December 2009 / Revised: 16 March 2010 / Accepted: 18 March 2010 / Published online: 15 April 2010
© Springer-Verlag 2010

Abstract Pathologic and prognostic data of nine patients with mitochondrion-rich carcinomas (MRC) were compared retrospectively to data of 101 patients with conventional gastric adenocarcinomas. MRC was defined as a tumour composed predominantly, or entirely, of columnar adenocarcinoma cells with eosinophilic cytoplasm and a strong supranuclear immunoreactivity for antimitocondrial antibody. Electron microscopy confirmed supranuclear distribution of mitochondria in MRC while immunostaining pattern was irregular or absent in the remaining 101 cases. MRC exhibited a tubulopapillary or cribriform growth pattern with focal infiltration of neutrophils in the tumour stroma. Prominent necrosis was present including segmental and intraluminal "dirty necrosis", while mitotic and ki-67 proliferative rates were low. MRC showed immunohistochemical findings compatible with gastric differentiation ($CK7^+/CK20^-/CDX^-$).When MRC were compared with non-MRC carcinomas, tumour size (<4 cm vs >4 cm, $P<0.01$), frequency of lymph node metastases (11% vs. 80%, $P<0.01$), low stage (I, II) at diagnosis (100% vs. 56%, $P<0.01$), Goseki's group I (100% vs. 6%, $P<0.01$), and better survival (0% vs. 70%, $P<0.01$) differed significantly. Our results suggest that MRC of the stomach may be considered a low-grade malignancy with an excellent prognosis.

Keywords Stomach · Mitochondrion-rich carcinoma · Immunohistochemistry · Electron microscopy

R. A. Caruso (✉) · A. Nania · F. Fedele
Dipartimento di Patologia Umana, Policlinico Universitario,
98168 Messina, Italy
e-mail: rosariocaruso@tin.it

A. Parisi
Dipartimento di Scienze Chirurgiche Generali e Speciali,
Policlinico Universitario,
98168 Messina, Italy

P. Napoli
Servizio di Anatomia Patologica, Ospedale Piemonte,
Messina, Italy

V. Zuccalà
Istituto di Anatomia Patologica,
Università degli Studi "Magna Grecia",
Catanzaro, Italy

Introduction

Gastric adenocarcinomas are histopathologically divided into two types, differentiated and undifferentiated type [1] or intestinal and diffuse type [2], based on tendency to form glands. Other classifications include World Health Organization (WHO) [3] and Goseki's classifications [4], which are based on the identification of the major component of the tumour regardless of the various minor components.

Oncocytic adenocarcinoma of the stomach is a newly described entity, with only very few cases reported in literature [5–7]. Oncocyte is a descriptive term for a neoplastic or non-neoplastic cell packed with mitochondria that give a granular eosinophilic appearance to its large cytoplasm in haematoxylin and eosin (H&E)-stained sections [8]. However, cells with eosinophilic cytoplasm are commonly seen in adenocarcinomas of the gastrointestinal tract and must be distinguished from oncocytic neoplasms [9]. Moreover, cytoplasmic eosinophilia relates not only to the presence of mitochondria but also to other non-ribosomal intracellular organelles such as lysosomes, neuroendocrine granules, secretory (exocrine) granules, cytoplasmic filaments, and smooth endoplasmic reticulum [8]. However, rare cases of mixed mucus-secreting and oncocytic carcinomas have been described in various organs such as thyroid [10],

pancreas [11], and liver [12]. Ultrastructurally, the common characteristics of these cases were numerous mitochondria and mucus droplets in the cytoplasm of tumour cells. Recently, a distinction between true oncocytic neoplasms and mitochondrion-rich carcinomas (MRC) of the thyroid has been suggested as the two histological types exhibit relevant clinicopathologic differences [13].

By reviewing the histological characteristics of 110 gastric carcinomas and by utilising histochemistry and immunohistochemical techniques for mitochondria, we retrospectively identified nine MRC of the stomach and studied them clinicopathologically. In addition, we focused on the ultrastructural features of MRC and, in particular, on the correlation between immunostaining pattern with antimitochondrial antibody and the mitochondrial localization at ultrastructural level. Finally, we investigated expression patterns of cytokeratin (CK7/CK20) and CDX2, a transcriptional factor associated with the intestinal phenotype of gastric carcinoma [14].

Materials and methods

The Department of Human Pathology (University Hospital; Messina, Italy) holds files of a total of 110 cases of surgically resected stomach in which gastric tumours were routinely processed for both light and electron microscopic observations from 1995 to 2001. Age, gender, tumour location and size, lymphatic and vascular invasion, as well as pTNM stage [15] were evaluated by reviewing medical charts and pathologic records. Each gastric carcinoma was classified according to WHO [3] and Goseki's [4] classification. These classifications are based on the identification and classification of the major component of the tumour on H&E coloration. Goseki's classification was realised on an adjacent tumour slide with Periodic Acid Schiff and Alcian Blue (pH 2.5) combined coloration. Four groups were defined: group I, high tubular differentiation and poor mucin content; group II, high tubular differentiation and high mucin content; group III, poor tubular differentiation and poor mucin content; and group IV, poor tubular differentiation and high mucin content [4].

Mitochondrial phenotypical analysis and classification

Representative sections from paraffin blocks were examined for phenotypical analysis. H & E staining and immunostain of mitochondria antigen (Clone DO-7, Dako, Denmark) were used as markers for MRC. MRC included any case composed predominantly, or entirely, of tumour cells with eosinophil cytoplasm and a strongly positive immunostaining pattern in the supranuclear cytoplasm. Care was taken not to confuse oncocytic carcinomas with MRC. They are characterised by voluminous eosinophilic cytoplasm, large vesicular nuclei, and prominent nucleoli. Furthermore, antimitochondrial immunostaining pattern is strong and diffuse in the cytoplasm. Using these procedures, nine examples of MRC were identified.

Immunohistochemistry

To evaluate the tumour phenotype of 9 MRC, the following immunohistochemical panel was used: chromogranin A (clone DAK-A3; dilution 1:1800; Dako), synaptophysin (clone SY38; dilution 1:200, Dako), lysozyme (code A0099; dilution 1:200; Dako), Ki-67 (Clone MIB-1; dilution 1/100, Dako), CK7 (Clone OV-TL 12/30,dilution 1/250, Dako) CK20 (clone KS20.8; dilution 1:100, Dako), and CDX2 (Clone CDX2-88; dilution 1/50; BioGenex, San Ramon, CA, USA). As controls, known positive tissue sections and negative controls devoid of primary antibody were used.

Mitotic figures were counted in 10 high-power fields (HPF, ×400), while the percentages of ki67-positive nuclei were established at ×250 enlargement by counting at least 1,000 cells in the area showing higher reactivity.

Electron microscopy

Small pieces of fresh tumour tissue from the nine cases were immediately fixed in 3% phosphate-buffered glutaraldeyde pH 7.4 and post-fixed in 1% osmium tetroxide. Semi-thin araldite-embedded sections were stained with Giemsa's reagent. From the selected blocks, sections of 80 nm thickness were double-stained with uranyl acetate and lead citrate. They were then examined and photographed with a Philips EM 300 electron microscope.

Statistical analysis

Data distribution was expressed as counts and percentages for categorical variables and was compared by means of the Fisher's exact test. Clinical outcome of the patients was followed from date of surgery to date of death or December 1, 2006. The follow-up period ranged from 1 month to approximately 90 months (median 42 months).Patients dying from other causes were censored at the date of their death. Survival differences were analysed by Kaplan-Meier curve and log-rank test. Significance level was 0.05.

Results

Expression of antimitochondrial antibody in gastric carcinomas

Expression of antimitochondrial antibody was heterogeneous in many tumours. Of the 110 positive tumours, nine were

composed predominantly, or entirely, by adenocarcinoma cells showing a strongly positive pattern. Immunoreactivity for mitochondria was concentrated in the supranuclear cytoplasm and does not involve the apical cytoplasm (Fig. 1). Strong, diffuse cytoplasmic immunoreactivity, similar to that described in oncocytic carcinomas, was not found. In the remaining 101 cases, the antimitochondrial staining pattern was irregular or absent (Fig. 2). In 30 out of 101 cases, only a portion displayed a MRC with a characteristically strong supranuclear antimitochondrial positivity. The proportion of MRC component ranged from 5% to 30% of total tumour volume.

Correlation between MRC phenotype and clinicopathologic factors

Comparisons of the nine MRC with the remaining 101 tumours showed significantly improved survival in the former group (log rank 8.44; $P<0.01$). Distinctive histological features were noticed in MRC when compared with worse cases. In particular, MRC were observed significantly ($P<0.01$) more frequently in patients with a tumour size <4 cm than in those with tumours >4 cm. Group I (Goseki's classification) was more frequently observed in MRC than in conventional tumours ($P<0.01$). Lack of angioinvasion and no or only sporadic lymph vessel invasion differed significantly between MRC and conventional tumours ($P<0.01$). According to the nodal status, the percentage of MRC with lymph node metastases was lower than that of conventional tumours ($P<0.01$). Stages I and II were observed more frequently in MRC ($P<0.01$) (Table 1).There were no significant differences with regard to other factors such as sex ratio and age, localization, and depth of invasion.

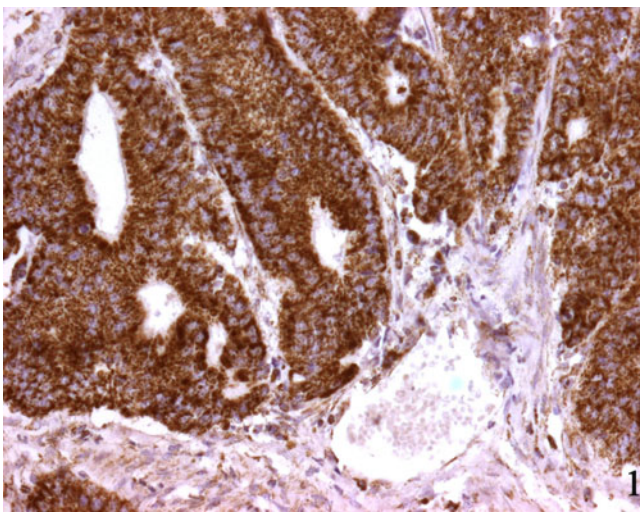

Fig. 1 Antimitochondria antibody is positive in the supranuclear cytoplasm of adenocarcinoma cells, ×200

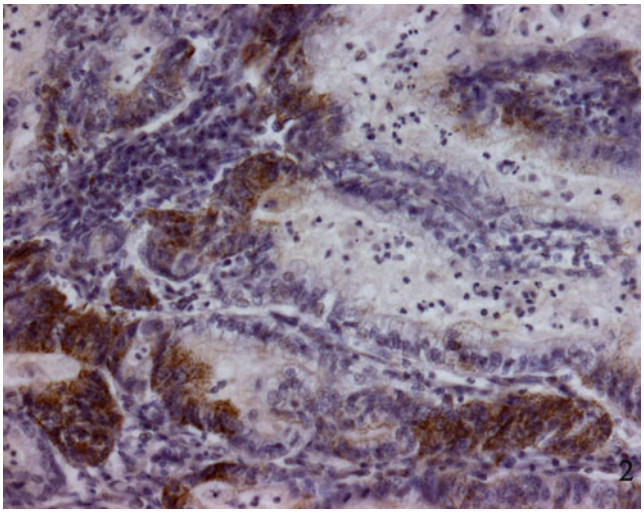

Fig. 2 Gastric adenocarcinoma with antimitochondrial immunostaining pattern irregular or absent, ×200

Morphologic findings of nine MRC

The analyses of most other immunohistochemical markers and electron microscopic features were restricted to the series of nine MRC (Table 2). On microscopic examination, tumours exhibited a tubulopapillary growth pattern with a focal intratumoural neutrophil infiltrate (Fig. 3). Cribriform pattern was also seen (Fig. 4). Cytologically, tumour cells showed stratified, oval-to-round nuclei with prominent nucleoli, simulating an oncocytic appearance. However, cytoplasm was eosinophilic mainly in the supranuclear portion (Fig. 3). All cases were associated with segmental and intraluminal "dirty necrosis" (Fig. 4). Typically, dirty necrosis consisted of densely eosinophilic, coarsely granular, necrotic debris containing neutrophils and abundant karyorrhectic material of sloughed carcinoma cells (Fig. 4). When stained with periodic acid Schiff and Alcian blue, tumour cells were shown to have mucin positivity on the luminal surface. A trace of mucins was sometimes discernible in the apical portion of the cytoplasm. In patient 2, micrometastatic adenocarcinoma cells were present in the marginal sinuses of two out of 15 lymph nodes. All tumours expressed low proliferative rates (median mitoses 5/10 HPFs, range 3-10 and median Ki67 index 10%, 7-20%). Strong immunoreactivity for CK7 was found in all nine cases of MRC. There were no cases that exhibited immunoreactivity for chromogranin A, synaptophysin, lysozyme, CK20, or CDX2 (Table 2).

Electron microscopy

Electron microscopy, performed in nine MRC, showed highly differentiated adenocarcinomas (Fig. 5). Close intercellular contacts between tumour cells were by

Table 1 Clinicopathological findings of the patients

Patients	MRC *N*=9 (%)	Non-MRC *N*=101 (%)	*P* value
Age, years			
Median, range	68, 55-80	64, 37-84	NS
Gender			
Male	6 (67)	68 (67)	NS
Female	3 (33)	33 (33)	
Location			
Upper third	0 (0)	19 (19)	NS
Middle third	2 (22)	36 (36)	
Lower third	7 (78)	56 (55)	
Tumour size, cm			
<4	8 (89)	3 (3)	<0.01
>4	1 (11)	98 (97)	
Goseki system			
Type I	9 (100)	6 (6)	<0.01
Type II	0	20 (20)	
Type III	0	55 (54)	
Type IV	0	20 (20)	
Lymphatic permeation			
Absent	8 (89)	19 (19)	<0.01
Present	1 (11)	82 (81)	
Vascular permeation			
Absent	9 (100)	81 (80)	<0.01
Present	0	20 (20)	
Depth of invasion			
T1	1 (11)	4 (4)	NS
T2	6 (67)	73 (72)	
T3	2 (22)	19 (19)	
T4	0	5 (5)	
Lymph node metastasis			
Negative	8 (89)	20 (20)	<0.01
Positive	1 (11)	81 (80)	
Stage of disease			
Ia, b	7 (78)	18 (18)	<0.01
II	2 (22)	38 (38)	
III	0	33 (33)	
IV	0	12 (11)	
Outcome			
Alive	9 (100)	26 (26)	<0.01
Died of other disease	0	4 (4)	
Died of recurrence	0	71 (70)	

junctional complexes and small desmosomes. Cell nuclei of the tumour cells were round to oval and contained prominent nucleoli. The apical plasma membrane projected long irregular microvilli into the lumen. The mitochondria were concentrated in the supranuclear cytoplasm (Fig. 5). In three out of nine cases of MRC, a variable quantity of dense secretory granules could be found in the supranuclear cytoplasm (Fig. 6). In the remaining six cases, there were not intracytoplasmic secretory granules (Fig. 7). Tumour cell cytoplasm also showed many free ribosomes, few strands of rough endoplasmic reticulum, scattered lysosomes, and lipid bodies. Intracellular canaliculi, tubulovesicles, and neurosecretory granules were not seen. Some adenocarcinoma cells showed ultrastructural signs of necrosis-like cell death including brush border disorganisation, dilatation of nuclear envelope, and condensed chromatin in small patches (Fig. 7). Neutrophil migration across the neoplastic glands was associated with tumour cell death (Fig. 7).

Discussion

In this study, we describe the clinicopathological characteristics encountered in a group of nine patients with a variant of gastric adenocarcinoma for which we are suggesting the term MRC. We chose the term MRC as this tumour is the gastric counterpart of the mitochondrion-rich follicular carcinoma of the thyroid [13]. MRC of the stomach are composed predominantly, or entirely, of tumour cells with eosinophilic cytoplasm and supranuclear immunoreactivity for antimitocondrial antibody. Electron microscopy confirmed the supranuclear distribution of mitochondria in these MRC. Although the predominant cytoplasmic organelle in these neoplasms is the mitochondrion, none of the lesions had densely packed mitochondria as is characteristically found in oncocytomas [16]. A few small dense secretory granules could be found under electron microscope in the apical cytoplasm in three out of nine cases of MRC. Therefore, the nine cases of MRC constitute a subset of Goseki's group I tumours (well-differentiated tubules, poor intracellular mucus) [4]. Gastric adenocarcinomas containing neuroendocrine cells [17] may exhibit granular eosinophilic cytoplasm. However, in our cases there was neither immunohistochemical nor ultrastructural evidence of neuroendocrine differentiation.

The disease entity of extremely well-differentiated adenocarcinoma of the stomach has often been a clinicopathological subject of discussion, as its biological behaviour is possibly highly malignant, in spite of the difficulty of making endoscopic and histopathological diagnoses [18]. Endoh et al. [19] reported eight cases of extremely well-differentiated adenocarcinomas mimicking complete-type intestinal metaplasia confirmed by phenotypic investigation using immunohistochemical methods. The histological pattern of extremely well-differentiated adenocarcinoma is unlike the pattern observed in MRC where there is no histochemical or ultrastructural evidence of goblet-like cells in adenocarcinoma glands. Furthermore, in our cases of MRC, there was neither lysozyme immunoreactivity nor ultrastructural evidence of Paneth cell differentiation. The homeoprotein CDX2 is important for the early differentiation

Table 2 Clinicopathological findings of MRC

Case	Sex	Age	Site	pTNM stage	Histology	Size	Mitoses 10 HPF	Ki67	CK7	CK20	CDX2	Outcome
1	M	68	Antrum	T2N0M0	Cribriform	3.5	5	10	Positive	Negative	Negative	Alive
2	F	55	Antrum	T1N1M0	Tubulopapillary	3	4	10	Positive	Negative	Negative	Alive
3	M	80	Antrum	T2N0M0	Cribriform	2.5	4	7	Positive	Negative	Negative	Alive
4	M	67	Antrum	T3N0M0	Tubulopapillary	6	7	10	Positive	Negative	Negative	Alive
5	F	65	Body	T2N0M0	Tubulopapillary	3	5	7	Positive	Negative	Negative	Alive
6	M	69	Antrum	T2N0M0	Cribriform	4.5	10	20	Positive	Negative	Negative	Alive
7	F	70	Body	T2N0M0	Tubulopapillary	2.5	3	7	Positive	Negative	Negative	Alive
8	M	75	Antrum	T3N0M0	Tubulopapillary	4	6	10	Positive	Negative	Negative	Alive
9	M	65	Antrum	T2N0M0	Tubulopapillary	2	3	8	Positive	Negative	Negative	Alive

M male, *F* female, *NED* no evidence of disease

and maintenance of intestinal epithelial cells [14]. Although CDX2 is not expressed in normal epithelium of the stomach, it is expressed in nearly all intestinal metaplasia and in a subset of gastric carcinomas [14]. However, CDX2 was not expressed in our cases of MRC, thus ruling out their intestinal differentiation. In addition, the cytokeratin profile of MRC (CK 7 positive; CK20 negative) was not compatible with an intestinal phenotype. In fact, gastric-type carcinomas show a tendency toward positive staining for CK7 and negative staining for CK20, whereas intestinal-type carcinomas tended to be positive for CK20 regardless of the result for CK7 [20]. Other cases of extremely well-differentiated adenocarcinomas mimicking normal gastric mucosa have also been reported [18]. Again, the histological pattern observed in MRC is unlike that observed in gastric-type well-differentiated adenocarcinoma where neoplastic glands consist of cuboidal to tall columnar cells with clear mucinous cytoplasm showing foveolar or mucous-neck/pyloric gland phenotype. According to Karam [21, 22], three out of nine MRC exhibited ultrastructural features similar to normal pre-pit cells where a few secretory granules are present within the apical cytoplasm. However, these ultrastructural observations need to be supported in further immunohistochemical studies using markers of foveolar cells (MUC5AC and human gastric mucin), mucous neck cell and pyloric gland cells (MUC6), chief cells (Pepsinogen II and RUNX3), and parietal cells (proton pump alpha subunit).

MRC share some histological features of stromal reaction with ordinary colorectal adenocarcinomas. These include dirty necrosis and prominent neutrophil infiltration that have also been reported in the oncocytic variant of colorectal carcinoma [9]. Dirty necrosis has traditionally been regarded as a characteristic feature of colorectal cancer [23]. However, the presence of dirty necrosis is not a specific morphologic marker of colorectal adenocarcinoma

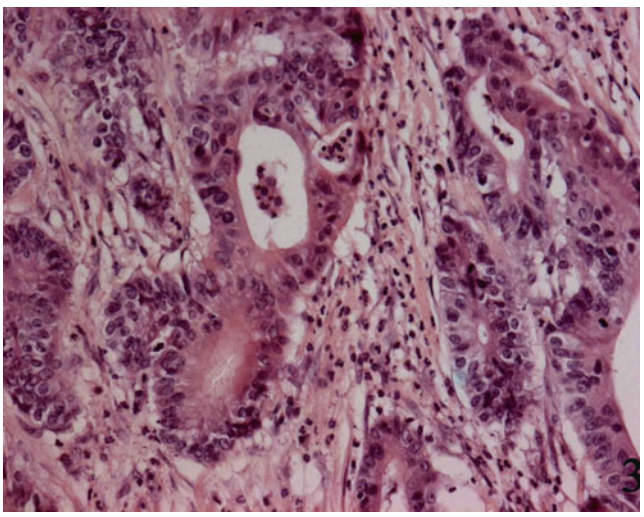

Fig. 3 Adenocarcinoma glands lined with columnar cells with eosinophilic cytoplasm, particularly in the supranuclear portion. Neutrophils are seen both in the tumour stroma and within the neoplastic glands; H&E ×200

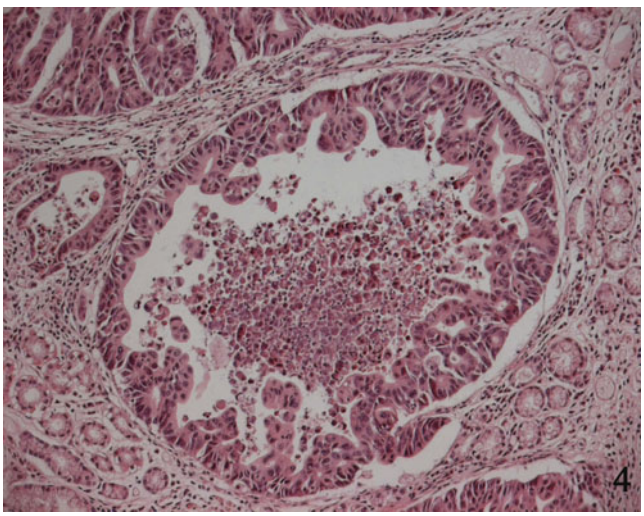

Fig. 4 Example of MRC with a cribriform pattern. Note the presence of intraluminal dirty necrosis resembling what is commonly seen in colorectal adenocarcinoma; H&E ×100

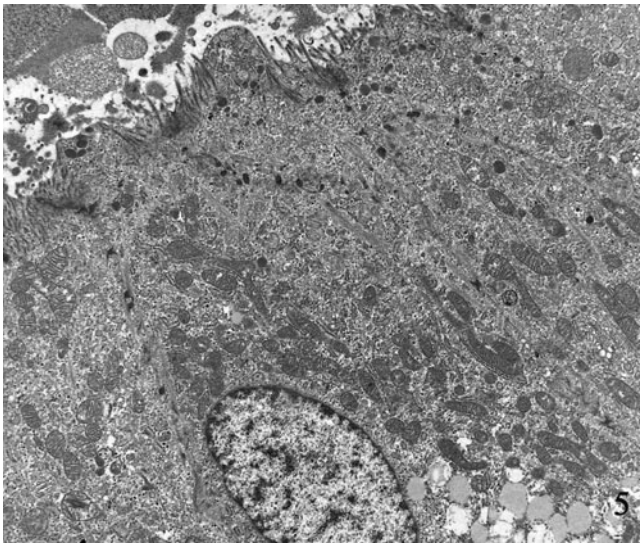

Fig. 5 Ultrastructural examination of tumour cells confirmed the characteristic supranuclear localization of mitochondria; ×6,000

when examining tissues from liver metastases [23]. In fact, dirty necrosis may be present not only in MRC but also in extremely well-differentiated gastric adenocarcinomas [19] as well as in ovarian metastases of gastric adenocarcinoma [24].

According to Maximo et al. [25], mitochondria can accumulate only in cells of tumours that are not actively dividing (i.e. in relatively slow-growing neoplasms); in rapidly growing neoplasms the division of neoplastic cell cytoplasm prevents the accumulation of the mitochondria.

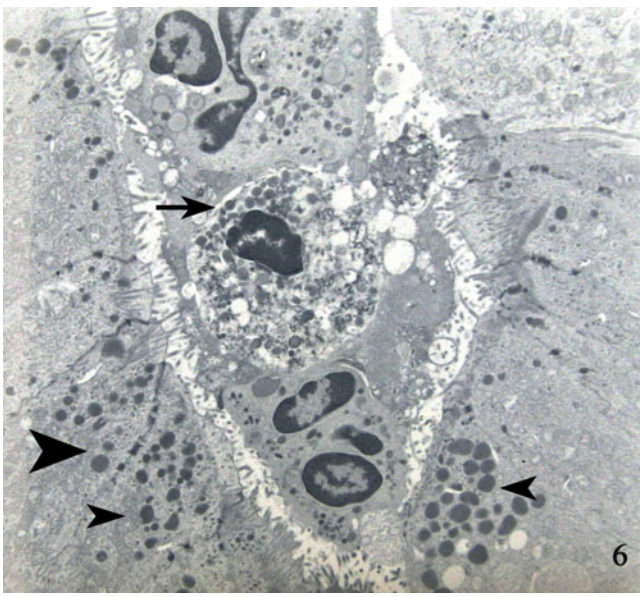

Fig. 6 Ultrastructural features of adenocarcinoma gland with dirty necrosis consisting of cell debris, viable neutrophils, and apoptotic neutrophil (*arrow*). Columnar adenocarcinoma cells show a variable quantity of spherical or oval dense secretory granules in the apical cytoplasm (*arrowheads*); ×6,000

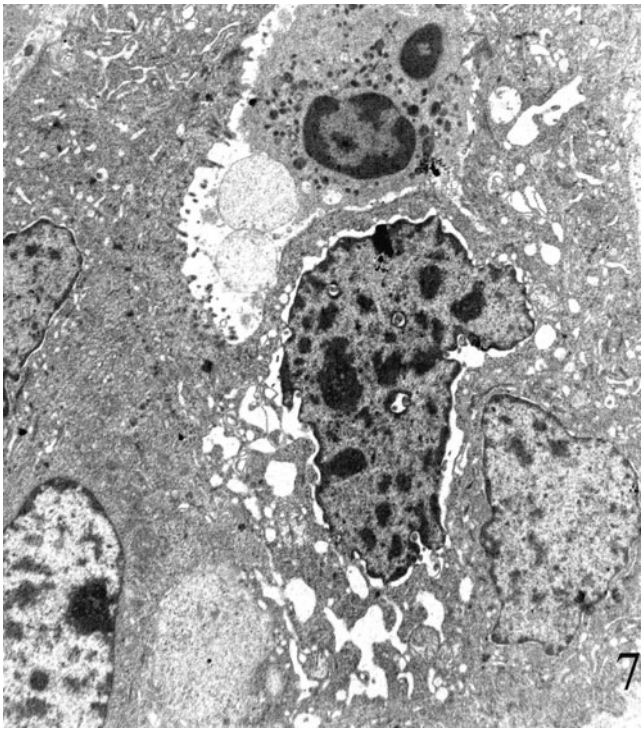

Fig. 7 Intraluminal neutrophil associated with necrosis-like tumour cell death such as dilatation of nuclear envelope, brush border disorganisation, and condensed chromatin in small patches. Note the absence of intracytoplasmic secretory granules; ×6,000

In other words, the accumulation of mitochondria in neoplastic lesions indicates a low proliferative turnover and is thus associated, in many instances, with benign neoplasms or malignant tumours of low malignancy [25]. In the same way, the cases examined in our study with MRC were characterised by small size, rare lymph node metastases, and a low stage at diagnosis. The low malignancy of these tumours was also suggested by microscopic features such as low proliferative rates, lack of angioinvasion, none or only sporadic lymph vessel invasion. Finally, all nine patients underwent curative gastric resection and are still alive without any evidence of recurrence (Table 1).

Mitochondria contained in cancer cells exhibit two major alterations. First, cancer cell mitochondria often exhibit a reduced oxidative phosphorylation, whereby ATP is generated through the conversion of glucose to pyruvate and excess pyruvate is then eliminated as the waste product lactate (Warburg effect) [26]. Second, they are often relatively resistant to the induction of mitochondrial membrane permeabilization, which is the rate-limiting step of the intrinsic pathway of apoptosis [27]. The mechanisms of mitochondrial membrane permeabilization resistance have come under close scrutiny as apoptosis resistance constitutes one of the essential hallmarks of cancer. Our light and electron microscopic data are in keeping with this

observation, since a non-apoptotic necrosis-like tumour cell death was found in our cases of MRC. In contrast to classical apoptosis, the chromatin was not condensed into compact and almost geometric figures under the nuclear membrane, but small patches of condensed chromatin were spread throughout the nucleus, as described in necrosis-like cell death [28]. Defect in the execution of apoptosis enable neoplastic cells to survive beyond their intended life span, allowing them to accumulate DNA alterations that deregulate cell proliferation and increase cell motility and other changes that play important roles in the progression of tumours. Gastric cancers constitute a highly heterogeneous group of tumours with respect to epidemiology, genetics, histopathology and biological behaviour. Focal areas of MRC were observed in 30 out of 101 cases of gastric carcinoma. They represent residual tumour subclones that are probably correlated with the progression of these tumours. Extensive morphologic and biomolecular studies are warranted for elucidation of the role of mitochondria in carcinogenesis and/or cancer progression of gastric carcinoma.

In conclusion, the nine cases reported here show a mitochondrion-rich phenotype confirmed immunohistochemically and ultrastructurally, with features which have not previously been reported in literature. MRC have paucity of lymph node metastasis, low proliferative activity, and a low stage at diagnosis. This tumour behaves biologically as a low-grade malignancy associated with a good prognosis and should be distinguished from other more aggressive tumours of the stomach.

Conflict of interest The authors declare that they have no conflict of interest.

References

1. Nakamura K, Sugano H, Takagi K (1968) Carcinoma of the stomach in incipient phase: its histogenesis and histological appearances. GANN 59:251–258
2. Laurén P (1965) The two histological main types of gastric carcinoma: diffuse and so-called intestinal type carcinoma. Acta Pathol Microbiol Scand 64:31–49
3. Hamilton SR, Aaltonen LA (2000) Pathology and genetics of tumours of the digestive system. World Health Organization Classification of Tumours Vol 2. IARC Press, Lyon
4. Goseki N, Takizawa T, Koike M (1992) Differences in the mode of extension of gastric cancer classified by histological types: new histological classification of gastric carcinoma. Gut 33:606–612
5. Takubo K, Honma N, Sawabe M, Arai T, Izumiyama-Shimomura N, Kammori M, Sasajima K, Esaki Y (2002) Oncocytic adenocarcinoma of the stomach: parietal cell carcinoma. Am J Surg Pathol 26:458–465
6. Batistatou A, Doukas M, Baltogiannis G, Panelos J, Kamina S, Charalabopoulos K, Agnantis NJ (2007) Early gastric carcinoma with oncocytic features and extensive metastases. Pathol Res Pract 203:539–541
7. Motta MP, Athanazio DA, Motta A, Studart E, Athanazio PR (2008) Parietal cell (oncocytic) adenocarcinoma of the stomach in a female patient: superficial spreading and extensive nodal involvement. Int J Surg Pathol 16:447–449
8. Nappi O, Ferrara G, Wick MR (1999) Neoplasms composed of eosinophilic polygonal cells: an overview with consideration of different cytomorphologic patterns. Semin Diagn Pathol 16:82–90
9. Chetty R, Serra S, Kennedy E, Govender D (2009) Oncocytic rectal adenocarcinomas. Hum Pathol 40:478–483
10. Uccella S, La Rosa S, Finzi G, Erba S, Sessa F (2000) Mixed mucus-secreting and oncocytic carcinoma of the thyroid: pathologic, histochemical, immunohistochemical, and ultrastructural study of a case. Arch Pathol Lab Med 124:1547–1552
11. Adsay NV, Adair CF, Heffess CS, Klimstra DS (1996) Intraductal oncocytic papillary neoplasms of the pancreas. Am J Surg Pathol 20:980–994
12. Terada T, Taniguchi M (2004) Intraductal oncocytic papillary neoplasm of the liver. Pathol Int 54:116–123
13. Tsybrovskyy O, Rößmann-Tsybrovskyy M (2009) Oncocytic versus mitochondrion-rich follicular thyroid tumours: should we make a difference? Histopathology 55:665–682
14. Werling RW, Yazij H, Bacchi G et al (2003) CDX2, a highly sensitive and specific marker of adenocarcinomas of intestinal origin: an immunohistochemical survey of 476 primary and metastatic carcinomas. Am J Surg Pathol 27:303–310
15. Sobin LH, Wittekind C (1997) TNM classification of malignant tumors, 5th edn. Wiley, New York, pp 59–62
16. Tallini G (1998) Oncocytic tumours. Virchows Arch 433:5–12
17. Jiang SX, Mikami T, Umezawa A, Saegusa M, Kameya T, Okayasu I (2006) Gastric large cell neuroendocrine carcinomas: a distinct clinicopathologic entity. Am J Surg Pathol 30:945–953
18. Kushima R, Vieth M, Borchard F, Stolte M, Mukaisho K, Hattori T (2006) Gastric-type well-differentiated adenocarcinoma and pyloric gland adenoma of the stomach. Gastric Cancer 9:177–184
19. Endoh Y, Tamura G, Motoyama T, Kjioka Y, Watanabe H (1999) Well-differentiated adenocarcinoma mimicking complete-type intestinal metaplasia in the stomach. Hum Pathol 30:826–832
20. Kim MA, Lee HS, Yang HK, Kim WH (2004) Cytokeratin expression profile in gastric carcinomas. Hum Pathol 35:576–581
21. Karam SM, Leblond CP (1993) Dynamics of epithelial cells in the corpus of the mouse stomach. I. Identification of proliferative cell types and pinpointing of the stem cell. Anat Rec 236:259–279
22. Karam SM (2010) Mouse models demonstrating the role of stem/progenitor cells in gastric carcinogenesis. Front Biosci 15:595–603
23. Wong NA, Neville LP (2007) Specificity of intra-acinar necrosis as a marker of colorectal liver metastasis. Histopathology 51:725–727
24. Lerwill MF, Young RH (2006) Ovarian metastases of intestinal-type gastric carcinoma: a clinicopathologic study of 4 cases with contrasting features to those of the Krukenberg tumor. Am J Surg Pathol 30:1382–1388
25. Máximo V, Lima J, Soares P, Sobrinho-Simões M (2009) Mitochondria and cancer. Virchows Arch 454:481–495
26. Warburg O (1956) On respiratory impairment in cancer cells. Science 124:269–270
27. Kroemer G, Galluzzi L, Vandenabeele P et al (2009) Classification of cell death: recommendations of the Nomenclature Committee on Cell Death 2009. Cell Death Differ 16:3–11
28. Leist M, Jäättelä M (2001) Four deaths and a funeral: from caspases to alternative mechanisms. Nat Rev Mol Cell Biol 2:589–598

Virchows Arch (2010) 456:507–514
DOI 10.1007/s00428-010-0908-6

ORIGINAL ARTICLE

Role of E-cadherin gene in gall bladder cancer and its precursor lesions

T. Padma Priya · V. K. Kapoor · N. Krishnani · Vinita Agrawal · Suraksha Agrawal

Received: 2 February 2010 / Revised: 3 March 2010 / Accepted: 13 March 2010 / Published online: 8 April 2010
© Springer-Verlag 2010

Abstract The aim was to investigate the genomic instability in the E-cadherin (*CDH1*) gene and to correlate it with its protein expression in gall bladder cancer (GBC) and in other gall bladder (GB) diseases viz. chronic cholecystitis (CC), xantho-granulomatous cholecystitis (XGC), and normal GB to explicate its role in GBC tumorigenesis. Microsatellite instability (MSI) and loss of heterozygosity (LOH) in *CDH1* were studied using D16S421, D16S496, D16S503, D16S512, D16S2624, and D16S3021 microsatellite markers and D2S123 (2p16), D2S382 (2q24), D6S292 (6q21–23), D7S480 (7q31), and D17S796 (17p13.1–3) were used to investigate genomic instability at 2p, 2q, 6q, 7q, and 17p loci in 40 GBC, 50 CC, 34 XGC, and 15 normal GB cases. Immunohistochemistry was carried out to analyze the E-cadherin and p53 protein expression. Overall LOH in *CDH1* and other markers was high in GBC and XGC as compared to CC; however, it did not correlate with its protein expression in GBC cases. Loss of E-cadherin expression was high in GBC (67%), while majority of the CC (94%) and XGC (91%) cases retained positive E-cadherin expression. Overexpression of p53 was high in GBC (43%) whereas CC, XGC, normal GB cases were negative for p53 overexpression. None of the normal GB cases showed genomic instability at any of the markers. High LOH in *CDH1* and other chromosomal loci in GBC indicated that the genomic instability followed a GBC>XGC>CC trend during the process of neoplastic transformation in GB, highlighting the fact that CC might act as a precursor lesion of GBC.

Keywords Gall bladder cancer (GBC) · Chronic cholecystitis (CC) · Xantho-granulomatous cholecystitis (XGC) · *CDH1* · Genomic instability

T. P. Priya (✉) · S. Agrawal
Department of Medical Genetics, Sanjay Gandhi Post Graduate Institute of Medical Sciences,
Raebareli Road,
Lucknow, UP 226014, India
e-mail: padma_29@rediffmail.com

V. K. Kapoor
Department of Surgical Gastroenterology, Sanjay Gandhi Post Graduate Institute of Medical Sciences,
Raebareli Road,
Lucknow, UP, India

N. Krishnani · V. Agrawal
Department of Pathology, Sanjay Gandhi Post Graduate Institute of Medical Sciences,
Raebareli Road,
Lucknow, UP 226014, India

Introduction

Gall bladder cancer (GBC) has been described as the fourth most common (after breast, cervix, and ovary) cancer in women in various states of India viz. Uttar Pradesh, Bihar, Orissa, West Bengal, and Assam [1, 2]. Incidence rate of GBC in the northern part of India, i.e., 2.5–8.9/100,000 female and 1.6–3.7/100,000 male is comparable with that of Chile, which has the highest incidence of GBC in the world [2]. Poor prognosis and very high incidence rates in North India warrant effective screening and better diagnostic procedures.

Invasive GBC is often preceded by preneoplastic lesions, including dysplastic changes of the gallbladder epithelium. Majority of the patients with GBC have gall stones (GS) and a history suggestive of chronic cholecystitis (CC), which is characterized with repeated attacks of acute cholecystitis [3]. Xantho-granulomatous cholecystitis

(XGC) is a rare presentation of CC, characterized by xantho-granuloma, severe fibrosis, and foam cells; XGC is often misdiagnosed pre-operatively and intra-operatively as GBC. Hence identification of premalignant conditions in the morphologic background of CC and XGC might help in understanding the hyperplasia–metaplasia–dysplasia–neoplasia sequence of GBC progression, facilitating its early diagnosis and hence, better prognosis.

Molecular pathogenesis of GBC is, however, poorly understood. The genetic changes in several epithelial malignancies are associated with activation of oncogenes and inactivation of tumor suppressor genes. E-cadherin (*CDH1*) is a tumor suppressor gene located on chromosome 16q22.1, which is critical for the development and maintenance of Ca^{2+}-dependent cell adhesion, polarity, and differentiation of epithelial cells [4]. Significant differences in the protein expression of E-cadherin between normal, inflamed, and cancerous gall bladder tissues have been reported [5]. p53, regarded as the guardian of the genome, regulates the maintenance of the genomic integrity, loss of function of which leads to accelerated mutagenesis, further driving genomic instability.

Owing to the high incidence of GBC in north India and the dearth of reports on molecular pathophysiology of GBC, the current study was designed to investigate genomic instability in *CDH1* and to compare it with the E-cadherin and p53 protein expression in GBC, along with non-malignant CC, XGC, and normal GB cases. As investigation of genomic instability at various other chromosomal regions harboring important target genes might unveil other putative tumor suppressor genes involved in GBC, we further aimed to examine MSI and LOH at chromosomal regions 2p, 2q, 6q, 7q, and 17p.

Methods

Sample collection

Paired blood and tissue samples were collected from patients who underwent surgery for GBC, CC, and XGC in the Department of Surgical Gastroenterology, Sanjay Gandhi Postgraduate Institute of Medical Sciences (SGPGIMS), Lucknow in northern India during the years 2004–2006. Normal GB tissues were obtained from patients operated for diseases such as choledochal cyst, periampullary carcinoma, jaundice, etc. All the tissue samples were histopathologically confirmed at the Department of Pathology, SGPGIMS. The TNM staging of the GBC tumors was assessed according to the American Joint Committee on Cancer (AJCC) guidelines [6]. Clinical and pathological data of GBC cases were obtained from the hospital information system (HIS) of SGPGIMS (Table 1).

Table 1 Primer sequences and PCR conditions

Marker		Primer sequence	Product size
D16S421	F	ACATGAACCGATTGGACTGA	206–216
	R	CCGTTCCCTATATTTCCTGG	
D16S496	F	GAAAGGCTACTTCATAGATGGCAAT	217
	R	ATAAGCCACTGCGCCCAT	
D16S503	F	AGTGCTCTGGAATGATGTG	206–216
	R	TTGCTAGGTAGTTGTCTCCC	
D16S512	F	TGAGAGCCAAATAAATAAATGG	232
	R	TCACGTTGTGAATGCAAGT	
D16S2624	F	TGAGGCAATTTGTTACAGAGC	206
	R	TAATGTACCTGGTACCAAAAACA	
D16S3021	F	TGTGGATGTCATCACAAGG	143
	R	CACAGATATGTTTCATCTAGGGAG	
D2S123	F	AAACAGGATGCCTGCCTTTA	156–174
	R	GGACTTTCCACCTATGGGAC	
D2S382	F	ATGCTAAATCTCAAAGCCAGTCT	144–174
	R	CTAATCTCAATTCAGTGCTCCT	
D6S292	F	AATTCACAAGACACAATCTCAG	197–227
	R	AGAACTAAAGTTGCCTGTTCNTGTA	
D7S480	F	CTTGGGGACTGAACCATCTT	160
	R	AGCTACCATAGGGCTGGAGG	
D17S796	F	CAATGGAACCAAATGTGGTC	141–161
	R	AGTCCGATAATGCCAGGATG	

The study was approved by the Ethics Committee of the institute.

DNA extraction and genomic instability (MSI and LOH) analysis

Genomic DNA from both blood and frozen tissue (100 mg) samples was extracted by using salting out and Proteinase K methods. Blood and minced tissue samples were treated with red cell and tissue lysis buffer, respectively. To the pellet obtained after centrifugation, proteinase K buffer and 10% SDS (sodium dodecyl sulphate) were added and mixed properly. After phenol:chloroform (5:1) treatment and followed by centrifugation, genomic DNA was obtained by ethanol precipitation. A panel of six dinucle-

Table 2 PCR conditions of all the 16 microsatellite markers

PCR conditions	Temperature (°C)	Time
Initial denaturation	95	5 min
Denaturation	94	40 s
Annealing	48.5–60	40 s
Extension	72	30 s
Additional cycles	29 cycles	
Final extension	72	10 min

Table 3 Comparison of MSI and LOH in *CDH1* in GBC, CC, XGC, and normal GB groups

Group	MSI-H (%)	MSI-S (%)	*p* value	LOH (%)	No LOH (%)	*p* value
CC (*n*=50)	07 (14.0)	26 (52.0)	1.0	09 (18.0)	41 (82.0)	0.01
GBC (*n*=40)	09 (22.5)	26 (65.0)		17 (42.5)	23 (57.5)	
XGC (*n*=34)	07 (20.6)	13 (38.2)	1.0	13 (38.2)	21 (61.8)	0.7
GBC (*n*=40)	09 (22.5)	26 (65.0)		17 (42.5)	23 (57.5)	
CC (*n*=50)	07 (14.0)	26 (52.0)	0.5	09 (18.0)	41 (82.0)	0.04
XGC (*n*=34)	07 (20.6)	13 (38.2)		13 (38.2)	21 (61.8)	
Normal GB (*n*=15)	00 (00.0)	15 (100.0)	1.0	00 (00.0)	15 (100.0)	0.004
XGC (*n*=34)	07 (20.6)	13 (38.2)		13 (38.2)	21 (61.8)	
Normal GB (*n*=15)	00 (00.0)	15 (100.0)	0.04	00 (00.0)	15 (100.0)	0.002
GBC (*n*=40)	09 (22.5)	26 (65.0)		17 (42.5)	23 (57.5)	
Normal GB (*n*=15)	00 (00.0)	15 (100.0)	0.08	00 (00.0)	15 (100.0)	0.1
CC (*n*=50)	07 (14.0)	26 (52.0)		09 (18.0)	41 (82.0)	

otide microsatellite markers viz. D16S421 (16q21.1), D16S496 (16q21.1), D16S503 (16q13), D16S512 (16q21–22), D16S2624 (16q21–22), and D16S3021 (16q22–23) were selected for the study of MSI and LOH in *CDH1*, and D2S123 (2p16), D2S382 (2q24), D6S292 (6q21–23), D7S480 (7q31), and D17S796 (17p13.1–3) were selected to study the genomic instability at 2p, 2q, 6q, 7q and 17p loci in GBC, CC, XGC, and normal GB cases. The forward primers were fluorescently labeled and sequences of both forward and reverse primers of all the 11 microsatellite markers were obtained from the Human Genome Database (Table 1). PCR was carried out for 30 cycles and the annealing conditions of all the 11 microsatellite markers ranged between 48.5 and 60 °C (Table 2). PCR products were run on an automated ABI 3130 genetic analyzer, and analysis of MSI and LOH was carried out using GENESCAN™ and GENEMAPPER™ software (version 4.0). For the reproducibility and confirmation of the results for MSI and LOH, each run was repeated for four times on the ABI 3130 genetic analyzer.

Appearance of one or more novel peaks or shift in the peaks in the tumor sample as compared to the blood DNA sample suggested microsatellite instability (MSI). MSI was classified into three groups: MSI-H (instability in >=30% of the markers) (MSI high), MSI-L (instability in <30% of the markers) (MSI low), and MSI-S (no MSI) (MSI stable). Loss of heterozygosity (LOH) was assigned when there was a significant reduction (>50%) in the intensity of the peak in tumor DNA as compared to the blood DNA [7].

Immunohistochemistry

Immunohistochemistry was performed by using streptavidin–biotin immunoperoxidase-based detection method [8]. Primary antibodies used were mouse anti-human E-cadherin monoclonal antibody, specific for E-cadherin (clone NCH-38, Dako Corporation, Denmark) and mouse anti-human monoclonal antibody, recognizing both wild and mutant type p53 (clone DO-7, Dako corporation, Denmark). Positive controls for p53 study were prepared from known p53 positive cases of colon mucosa. Negative controls were prepared by incubation of sections with only non-immune rabbit serum instead of the primary antibodies. Estimated percentage of positively stained tumor cells and the intensity of the staining were taken into consideration for scoring the p53 expression (0 to 6). A score of less than 3 was considered as negative, while a score of >=3 was considered as overexpression [9]. E-cadherin expression was scored in the range of 1–4 viz. 1, negative; 2, weak staining; 3, moderate staining, and 4, intense staining [10].

Statistical analysis

Continuous variables like age were represented as mean ± SD, and differences in the age of the patients among different groups were compared using Student's *t* test. Categorical variables were analyzed by chi-square and Fisher's exact test with Yates correction using 5% level of significance. Odds Ratio and Confidence Interval were calculated using Graph Pad Instat version 3.06. Binary logistic analysis was done using SPSS 15.

Table 4 Logistic regression analysis results of LOH in *CDH1* (GBC and CC as dependent variables)

Parameter	*B*	S.E.	*p* value	Exp (*B*)	95% C.I. for Exp (*B*)	
					Lower	Upper
LOH	1.204	0.516	0.02	3.334	1.214	9.159
Age	−0.050	0.019	0.008	0.951	0.917	0.987
Gender (female)	0.554	0.486	0.25	1.740	0.671	4.509
Constant	1.676	1.023	0.10	5.344		

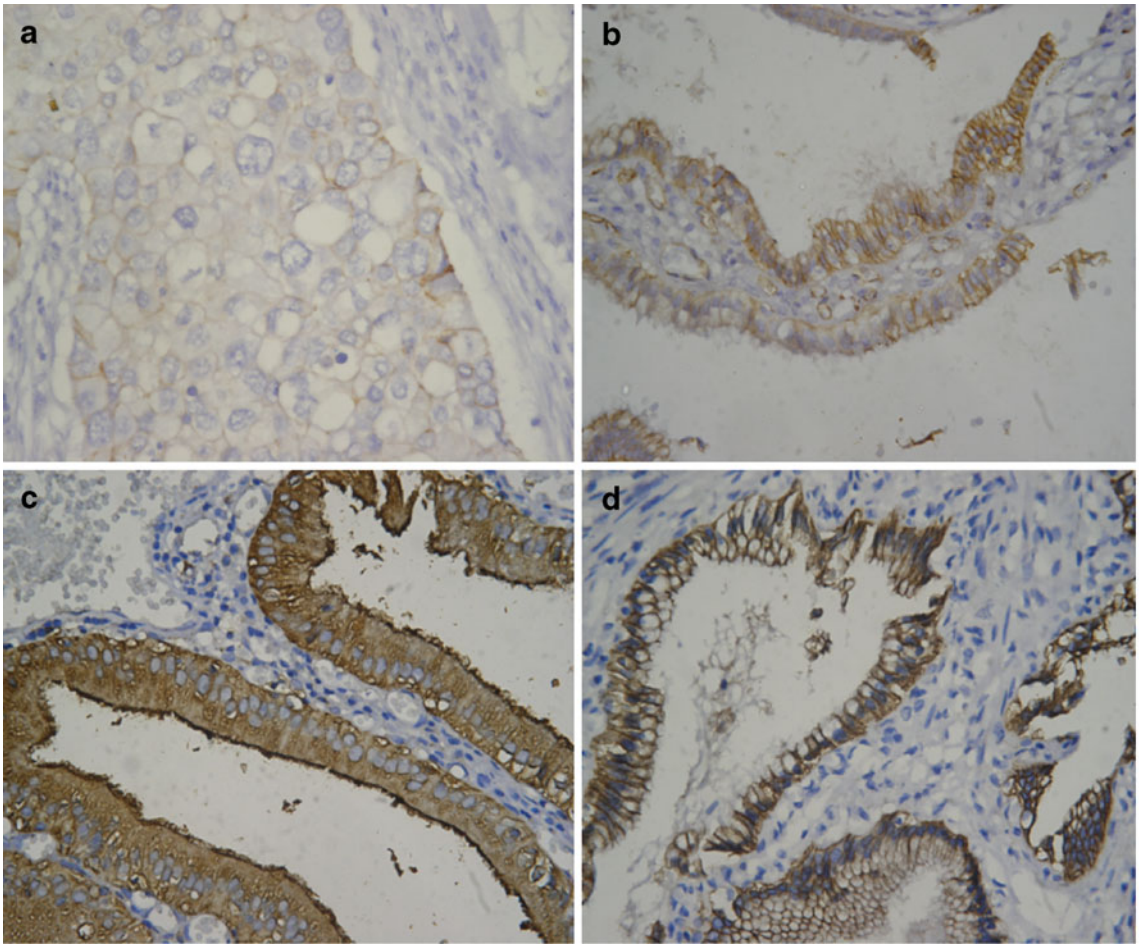

Fig. 1 Representation of E-cadherin expression in a GBC sample **a** negative (score 1) **b** weak positive (score 2) **c** moderate (score 3), and **d** strong positive expressions (score 4)

Results

MSI and LOH in *CDH1*

Frequency of MSI did not differ significantly between the GBC, CC, and XGC groups. However, LOH was significantly different when GBC vs. CC, GBC vs. normal GB, XGC vs. CC, and XGC vs. normal GB groups were compared (Table 3). No significant association was observed when MSI in *CDH1* was compared with the clinical and pathological features of the GBC cases such as age, gender, tumor location, depth of tumor invasion, nodal spread, distant organ metastasis, stage and grade of the tumor, and the presence/absence of gall stones. LOH in *CDH1* showed a significant association with only stage of the tumors. It was seen that a high frequency (n=9/17, 53%) of LOH positive cases was in stage III (p=0.04) (data not shown).

Binary logistic regression analysis revealed that LOH, but not MSI, in *CDH1* (p=0.02, Exp (B)=3.334) and age (p=0.008, Exp (B)=0.951) of the patients had a role as significant predictors of the GBC when compared with CC cases (Table 4). No such correlation was observed between GBC and XGC groups.

Table 5 Comparison of E-cadherin protein expression profile in GBC, CC, XGC, and normal GB groups

Groups	E-cadherin (+) (%)	E-cadherin (−) (%)	p value
GBC (n=36)	12 (33.3)	24 (66.6)	0.001
CC (n=46)	43 (93.5)	03 (06.5)	
GBC (n=36)	12 (33.3)	24 (66.6)	0.001
XGC (n=33)	30 (90.1)	03 (09.1)	
CC (n=46)	43 (93.5)	03 (06.5)	0.7
XGC (n=33)	30 (90.1)	03 (09.1)	
GBC (n=36)	12 (33.3)	24 (66.6)	0.01
Normal GB (n=15)	15 (100.0)	00 (00.0)	
CC (n=46)	43 (93.5)	03 (06.5)	0.0001
Normal GB (n=15)	15 (100.0)	00 (00.0)	
XGC (n=33)	30 (90.1)	03 (09.1)	0.0001
Normal GB (n=15)	15 (100.0)	00 (00.0)	

Table 6 Frequency of MSI and LOH at other markers in GBC, CC, and XGC cases

Chromosomal locus and marker		GBC (n=40)			CC (n=50)			XGC (n=34)		
		MSI%)	LOH (%)	NI[a]	MSI (%)	LOH (%)	NI[a]	MSI (%)	LOH (%)	NI[a]
2p	D2S123	05/40 (12.5)	02/36 (05.6)	04 (10.0)	04/50 (08.0)	02/50 (04.0)	00 (00.0)	03/34 (08.8)	02/34 (05.8)	0
	D2S382	05/40 (12.5)	01/31 (03.2)	09 (22.5)	03/50 (6.0)	00/50 (00.0)	00 (00.0)	03/34 (8.8)	00/34 (00.0)	0
6q	D6S292	03/40 (07.5)	01/33 (03.0)	07 (17.5)	02/50 (04.0)	02/44 (04.5)	06 (12.0)	01/34 (02.9)	02/26 (07.7)	08
7q	D7S480	02/40 (05.0)	02/26 (07.7)	14 (35.0)	02/50 (04.0)	00/50 (00.0)	00 (00.0)	01/34 (02.9)	00/34 (00.0)	0
17p	D17S796	01/40 (02.5)	02/21 (9.5)	19 (47.5)	02/50 (04.0)	01/35 (02.8)	15 (30.0)	02/34 (05.9)	00/34 (00.0)	0

[a] NI=Non informative

E-cadherin protein expression

It was observed that out of 40 GBC cases, only 36 cases showed evaluable lining epithelium. Among the 36 cases, absence of E-cadherin protein expression (score=1) was observed in 15 (42%) cases, 9 (25%) cases showed weak E-cadherin protein expression (score=2), while 12 (33%) cases showed moderate to strong E-cadherin protein expression (score=3–4) (Fig. 1). Out of the 50 CC cases, 4 cases had an absence of evaluable lining epithelium. Out of the remaining 46 cases, 2 cases (4%) showed absence of E-cadherin protein expression (score=1), 1 case (2%) revealed weak expression (score=2), strong E-cadherin protein expression was observed in 43 (94%) (score=3–4). In the XGC cases, 1 out of 34 cases revealed absence of evaluable epithelial lining, and absence of E-cadherin protein expression was observed in 3/33 (9%) cases. The rest of the 30 cases (91%) showed strong (score=4) E-cadherin protein expression. A significant difference existed in the E-cadherin protein expression pattern among GBC vs. CC, GBC vs. XGC, and GBC vs. normal GB groups (p=0.001, p=0.001, and p=0.01, respectively) (Table 5). Significant correlation was not observed between E-cadherin protein expression and genomic instability in *CDH1* locus.

MSI and LOH at the all the chromosomal loci

We observed that in the GBC, CC, and XGC cases, the highest frequency of MSI and LOH was observed at 16q locus i.e., *CDH1* region as compared to other loci. A high frequency of instability in the 3p chromosomal region (*FHIT* gene) was also found in our study [11]. Interestingly, none of the normal GB cases showed any MSI or LOH. Incidence of MSI and LOH in 2p, 2q, 6q, 7q, and 17p was quite low as compared to instability in *CDH1* (Table 6).

When overall MSI at all the markers (six markers in 16q and five markers located at other chromosomal loci) were compared among GBC, CC, and XGC, it was found that 2/40 (5%) and 1/34 (3%) MSI-H was observed in GBC and XGC, respectively, whereas, no MSI-H was observed in CC. When incidence of overall LOH at all the loci was compared among GBC, CC, and XGC, it was observed that 21/40 (53%) LOH was observed in GBC, 10/50 (20%) in CC, and 17/34 (50%) in XGC. LOH in GBC differed significantly from that of CC (p=0.001). A significant difference was also observed in the frequency of LOH among XGC vs. CC, (p 0.004) (Table 7).

We found that none of the clinical parameters of GBC cases had a significant association with the overall LOH or MSI at all the loci (data not shown).

Comparison of p53 expression and genomic instability in *CDH1* and at the other chromosomal loci

It was observed that out of the 40 GBC cases, 17 (43%) showed p53 overexpression while 23 cases were negative for p53 expression. All the CC (n=50), XGC (n=34), and normal GB (n=15) cases were negative for p53 expression (Fig. 2). A borderline association was observed between p53 overexpression and the overall LOH at all the six loci in GBC cases (p=0.06), while it showed no significant

Table 7 Comparison of overall LOH at all markers among GBC, CC, and XGC cases

Group	LOH (%)	No LOH (%)	p value
GBC (n=40) CC (n=50)	21 (52.5) 10 (20.0)	19 (37.5) 40 (80.0)	p=0.001, OR=2.62; 95% CI=1.40–4.91
GBC (n=40) XGC (n=34)	21 (52.5) 17 (50.0)	19 (37.5) 17 (50.0)	1.0
CC (n=50) XGC (n=34)	10 (20.0) 17 (50.0)	40 (80.0) 17 (50.0)	p=0.004, OR=0.4; 95% CI=0.20–0.76

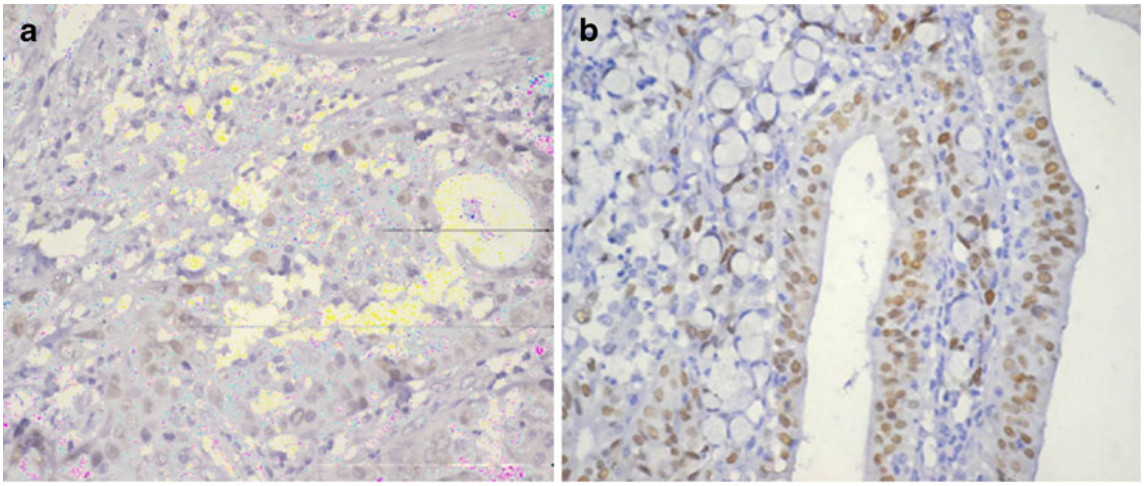

Fig. 2 Representation of p53 expression in a GBC sample **a** negative (score 2) **b** positive expressions (score 4)

association with MSI (Table 8). Genomic instability in the *CDH1* region (16q) did not show a significant correlation with the p53 overxpression and also no correlation was observed between p53 overexpression and E-cadherin expression in GBC. Further, we did not observe any significant association between p53 overexpression and the genomic instability in D17S796 in GBC, CC, and XGC.

Discussion

GBC is the most common malignancy in the biliary tract, associated with late diagnosis and poor prognosis with an overall 5-year survival rate ranging from 5 to 13% [12]. As the incidence of GBC in northern and central India is very high, identification of reliable molecular prognostic markers is imperative for its early diagnosis and improved prognosis.

A high frequency of LOH at CDH1 has been reported in several other malignancies [13, 14]. A significantly high LOH in XGC than in CC and absence in normal GB in our study might suggest that LOH may be the major genetic alteration occurring in the severely inflamed epithelial mucosa of XGC cases.

We found that loss of E-cadherin expression was a more prominent event in GBC as compared to CC, XGC, and normal GB. Several reports suggest that the expression of E-cadherin diminishes as the tumor progresses [5, 15]. Expression of E-cadherin and β-catenin has been reported to be significantly different between normal, inflamed, and cancerous gall bladder tissues, and the change of the protein expression with the associated loss of adhesive mechanisms may lead to a cancerous pathway in GBC [15]. LOH in *CDH1* has been shown to be associated with a trend towards reduced E-cadherin expression [16]; we, however, did not observe this correlation.

As a significant association was not observed between loss of E-cadherin expression and genomic instability in *CDH1*, it may be hypothesized that loss of its expression might be due to the transcriptional or post-translational modifications or due to modifications caused by the alterations in the other genes of the wnt signaling pathway, which may occur even in the absence of somatic and germline alterations in *CDH1* [17, 18]. Promoter methylation and germline mutation studies on *CDH1* may further confirm the mechanism behind its inactivation. Further *CDH1* has been reportedly involved in diverse mechanisms, and loss of which is beneficial for tumor cells to invade and trigger metastasis. Also *CDH1* reportedly has a role in the regulation of apoptosis. Hence, either control of gene expression at the transcriptional level or retaining an intact allele subsequent to LOH might be important for *CDH1* and other tumor-suppressor genes possessing diverse functions [19].

The second hypothesis may suggest that *CDH1* may not be the main target of LOH at 16q and some other tumor suppressor genes on 16q may be responsible in the causation of GBC. Hence, further functional studies on *CDH1* and components of the wnt signalling pathway would elucidate the role of *CDH1* in GBC, XGC and CC pathogenesis.

In contrast to a report in breast cancer, we did not find a significant association between genomic instability in

Table 8 Comparison of p53 expression and genomic instability at the six chromosomal loci in GBC cases

Overall genomic instability at all the 6 chromosomal loci			
p53 expression	LOH (21/40)	No LOH (19/40)	*p* value
Positive	12 (70.6)	05 (29.4)	0.06
Negative	09 (39.1)	14 (60.9)	

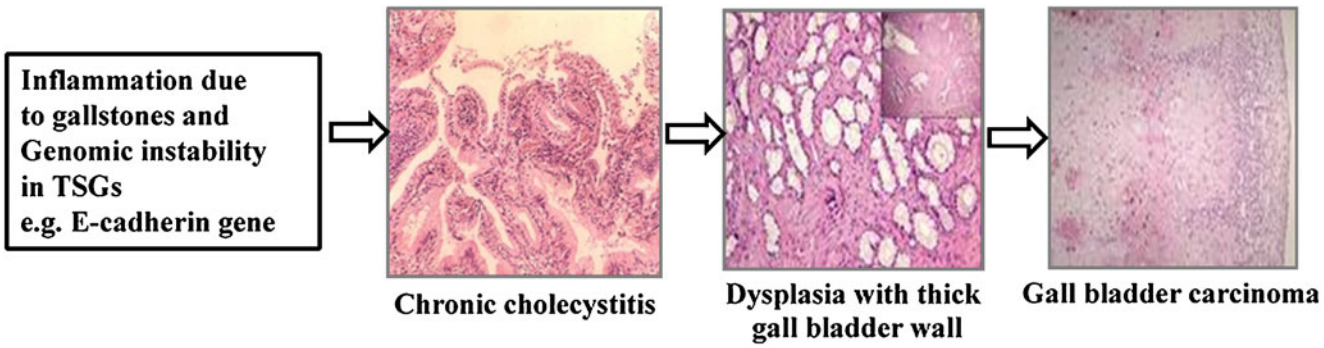

Fig. 3 Illustration of the trend of genetic instability and progressive changes in the gall bladder epithelium TSG (Tumor suppressor gene)

CDH1 and p53 overexpression, and in addition, we did not observe a significant association between E-cadherin expression and p53 overexpression [20]. These results indicate that p53 protein might not be involved in the regulation of the E-cadherin expression in GBC. A significant correlation between LOH at D17S796 and p53 overexpression was not found in the present study. In several solid tumors, frequent LOH or DNA methylation changes occur in the telomeric region at 17p13.3 with the absence of any p53 genetic alterations. These results suggest that one or more tumor suppressor genes located at 17p13.3 could be involved in tumorigenesis [21].

A significant difference in the incidence of LOH among GBC, CC, and XGC cases might suggest that LOH might play an important role in accelerating the genetic alterations during the progression of GBC. Occurrence of LOH in CC and XGC cases may suggest that they can act as early lesions with preneoplastic changes of the gallbladder epithelium. A significantly low LOH in CC cases as compared to XGC may be suggestive of the fact that XGC is an advanced and destructive variant of CC [22]. In accordance to our results, there are some reports showing a positive correlation of MSI in non-neoplastic, chronically inflamed tissues from patients with ulcerative colitis, rheumatoid arthritis, and colorectal cancer [23]. Further as a significant difference in the incidence of LOH and in the p53 expression was observed among CC and GBC cases, we may hypothesize that CC may be a preneoplastic stage in the pathway towards progression of GBC [24].

It has been observed that GBC arises usually as a consequence of chronic inflammation in association with gall stones [25]. Elevated risk of GBC in American Indians, as in Pima Indians in the south-western US, is positively correlated with the increased incidence of cholelithiasis and chronic cholecystitis [26]. From the presence of genomic instability in CC and XGC and its absence in normal GB cases, it can be hypothesized that chronic irritation in the gall bladder epithelium due to inflammation might accelerate the process of genetic alterations in genes regulating various cellular processes in CC, and XGC cases which is evident from the progressive hyperplastic, metaplastic, and dysplastic changes in gallbladder epithelium resulting in carcinoma in situ and subsequently GBC (Fig. 3). Hence, identification of genetic alterations in these precursor stages of GBC might strengthen their role in the pathogenesis, as well as in the early diagnosis of GBC.

Conclusions

Our results show that the mechanism of pathogenesis of GBC, XGC, and CC may be different but might still follow some common molecular pathway whereby, the genetic alterations in CC and XGC might be the early events in the process of gall bladder tumorigenesis. High frequency of LOH at all the chromosomal loci might indicate that LOH, but not MSI, could play a role in the pathogenesis of GBC. Further studies on promoter methylation and germline mutations in *CDH1* may highlight its role in gall bladder tumorigenesis.

Acknowledgments This work was undertaken with the grant from the Department of Biotechnology (DBT), Government of India. T. Padma Priya received a fellowship from the Council of Scientific and Industrial Research (CSIR), Government of India for carrying out this study. We are thankful to Shraddha Srivastava and Sanjay Kumar Johari for the technical help. We are also grateful to all the patients for their participation in the study and informed consent was obtained from all of them.

Conflict of interest statement We declare that we have no conflict of interest.

References

1. Kapoor VK, McMichael AJ (2003) Gallbladder cancer: an 'Indian' disease. Natl Med J India 16:209–213
2. Dhir V, Mohandas KM (1999) Epidemiology of digestive tract cancers in India IV. Gall bladder and pancreas. Indian J Gastroenterol 18:24–28

3. Silk YN, Douglass HO Jr, Nava HR et al (1989) Carcinoma of the gallbladder. The Roswell Park experience. Ann Surg 210:751–757
4. Berx G, Staes K, van Hengel J et al (1995) Cloning and characterization of the human invasion suppressor gene E-cadherin (E-cadherin). Genomics 26:281–289
5. Puhalla H, Herberger B, Soleiman A et al (2005) E-cadherin and β-catenin expression in normal, inflamed and cancerous gallbladder tissue. Anticancer Res 6:4249–4254
6. Fleming ID, Phillips JL, Menck HR et al (1997) The National Cancer Data Base report on recent hospital cancer program progress toward complete American Joint Committee on Cancer/TNM staging. Cancer 80:2305–2310
7. Boland CR, Thibodeau SN, Hamilton SR et al (1998) A National Cancer Institute Workshop on Microsatellite Instability for cancer detection and familial predisposition: development of international criteria for the determination of microsatellite instability in colorectal cancer. Cancer Res 58:5248–5257
8. Chaube A, Tewari M, Garbyal RS et al (2006) Preliminary study of p53 and c-erbB-2 expression in gallbladder cancer in Indian patients. BMC Cancer 6:126
9. Misra S, Chaturvedi A, Goel MM et al (2000) Overexpression of p53 protein in gallbladder carcinoma in North India. Eur J Surg Oncol 26:164–167
10. Balaram P, Alex S, Panikkar B et al (2004) Adhesion-related proteins E-cadherin, P-cadherin, CD44, and CD44v6, and antimetastatic protein nm23H1 in complete hydatidiform moles in relation to invasion potential. Int J Gynecol Cancer 14:532–539
11. Priya TP, Kapoor VK, Krishnani N et al (2009) Fragile histidine triad (FHIT) gene and its association with p53 protein expression in the progression of gall bladder cancer. Cancer Invest 27:764–773
12. Ito H, Matros E, Brooks DC et al (2004) Treatment outcomes associated with surgery for gallbladder cancer: a 20-year experience. J Gastrointest Surg 8:183–190
13. Zhang SH, Cong WM, Xian ZH et al (2005) Clinicopathological significance of loss of heterozygosity and microsatellite instability in hepatocellular carcinoma in China. World J Gastroenterol 11:3034–3039
14. Pecina-Slaus N, Kljaic M, Nikuseva-Martic T (2005) Loss of heterozygosity of APC and CDH1 genes in laryngeal squamous cell carcinoma. Pathol Res Pract 201:557–563
15. Wei Y, Van Nhieu JT, Prigent S et al (2002) Altered expression of E-cadherin in hepatocellular carcinoma: correlations with genetic alterations, beta-catenin expression, and clinical features. Hepatology 36:692–701
16. Moreno-Bueno G, Hardisson D, Sarrio D et al (2003) Abnormalities of E- and P-cadherin and catenin (beta-, gamma-catenin, and p120ctn) expression in endometrial cancer and endometrial atypical hyperplasia. J Pathol 199:471–478
17. Grady WM, Willis J, Guilford PJ et al (2000) Methylation of the promoter as the second genetic hit in hereditary diffuse gastric cancer. Nat Genet 26:16–17
18. Soares P, Berx G, van Roy F et al (1997) E-cadherin gene alterations are rare events in thyroid tumors. Int J Cancer 70:32–38
19. Cheng CW, Wu PE, Yu JC et al (2001) Mechanisms of inactivation of E-cadherin in breast carcinoma: modification of the two-hit hypothesis of tumor suppressor gene. Oncogene 20:3814–3823
20. Bukholm IK, Nesland JM, Karesen R et al (1997) Expression of E-cadherin and its relation to the p53 protein status in human breast carcinomas. Virchows Arch 431:317–321
21. Stocklein H, Smardova J, Macak J et al (2008) Detailed mapping of chromosome 17p deletions reveals HIC1 as a novel tumor suppressor gene candidate telomeric to TP53 in diffuse large B-cell lymphoma. Oncogene 27:2613–2625
22. Karabulut Z, Besim H, Hamamci O et al (2003) Xanthogranulomatous cholecystitis. Retrospective analysis of 12 cases. Acta Chir Belg 103:297–299
23. Hofseth LJ, Khan MA, Ambrose M et al (2003) The adaptive imbalance in base excision-repair enzymes generates microsatellite instability in chronic inflammation. J Clin Invest 112:1887–1894
24. Yanagisawa N, Mikami T, Yamashita K et al (2003) Microsatellite instability in chronic cholecystitis is indicative of an early stage in gallbladder carcinogenesis. Am J Clin Pathol 120:413–417
25. Schottenfeld D, Beebe-Dimmer J (2006) Chronic inflammation: a common and important factor in the pathogenesis of neoplasia. CA Cancer J Clin 56:69–83
26. Tazuma S, Kajiyama G (2001) Carcinogenesis of malignant lesions of the gallbladder. The impact of chronic inflammation and gallstones. Langenbeck's Arch Surg 386:224–229

Virchows Arch (2010) 456:515–521
DOI 10.1007/s00428-010-0901-0

ORIGINAL ARTICLE

Anti-CD10 (56C6) is expressed variably in adrenocortical tumors and cannot be used to discriminate clear cell renal cell carcinomas

Özgür Mete · Yersu Kapran · Mine G. Güllüoğlu · Işın Kılıçaslan · Yeşim Erbil · Yasemin Giles Şenyürek · Ferhunde Dizdaroğlu

Received: 26 December 2009 / Revised: 18 February 2010 / Accepted: 20 February 2010 / Published online: 14 April 2010
© Springer-Verlag 2010

Abstract In the evaluation of retroperitoneal masses, the practicing pathologist faces a dilemma when making a diagnosis based on histology given the often overlapping morphologic appearances of the adrenocortical carcinoma, renal cell carcinoma (RCC), and hepatocellular carcinoma (HCC). CD10 is expressed in a membranous fashion in the vast majority of clear cell RCCs; therefore, it is widely used for distinction from its mimics. However, its expression is not well-investigated in adrenal cortical tumors. We examined CD10 expression in 47 surgically resected adrenocortical tumors (26 adenomas and 21 carcinomas) and compared with 20 clear cell RCCs and 25 HCCs. Twenty HCCs (80%), 18 RCCs (90%), 11 adrenocortical carcinomas (52%), and 18 adrenocortical adenomas (69%) were positive for CD10. HCCs were characterized by a canalicular staining, and clear cell RCCs exhibited membranous or mixed membranous-cytoplasmic staining. Adrenocortical tumors displayed mainly cytoplasmic staining. Four adrenocortical carcinomas and one adenoma also displayed the membranous staining pattern. Despite the relatively small number of samples, our preliminary results revealed that adrenocortical tumors may express CD10 (Clone: 56C6). The most important point from this paper is the fact that anti-CD10 expression has not been previously reported in adrenocortical carcinomas. This suggests that CD10 does not seem to be a useful marker for discriminating clear cell RCCs from adrenocortical tumors since CD10 expression does not rule out the possibility of adrenocortical tumors. This feature should be kept in mind when constructing an antibody panel for an epithelial tumor that involves the adrenal gland and kidney, especially in small biopsy specimens.

Keywords CD10 · Adrenocortical carcinoma · Adrenocortical adenoma · Hepatocellular carcinoma · Renal cell carcinoma

Ö. Mete (✉) · Y. Kapran · M. G. Güllüoğlu · I. Kılıçaslan · F. Dizdaroğlu
Department of Pathology, Istanbul Faculty of Medicine, Istanbul University,
Capa,
34800 Istanbul, Turkey
e-mail: ozgurmete77@gmail.com

Y. Erbil · Y. Giles Şenyürek
Department of General Surgery, Istanbul Faculty of Medicine, Istanbul University,
Istanbul, Turkey

Introduction

Although imaging studies provide important information for detection and localization of adrenocortical tumors, the definitive diagnosis must be established by pathological examination. Even at the time of the surgery, a clear determination of the exact origin of a particular tumor cannot always be confirmed, especially for large lesions. The differential diagnosis between metastatic renal cell carcinoma (RCC), hepatocellular carcinoma, and primary adrenocortical carcinoma, which may share some morphological similarities, can be challenging, especially in the setting of limited tissue (e.g., core biopsies).

CD10, or the common acute lymphoblastic leukemia antigen, is a cell-surface neutral endopeptidase that inactivates bioactive peptides [1, 2]. After its initial description in neoplastic and nonneoplastic hematolymphoid tissue (lymphoid precursor cells, some myeloid cells, and germinal center B cells), an increased number of human non-hematolymphoid neoplasms were shown to express CD10

Table 1 Clinical and gross findings of adrenocortical tumors

Parameters	Adenomas, *n* (%)	Carcinomas, *n* (%)
Total	26 (100)	21 (100)
Female	20 (77)	12 (57)
Male	6 (23)	9 (43)
Age (mean±std[a]) (years)	42.57±14.38	42.81±16.05
Size (mean±std[a]) (cm)	3.48±1.05	10.55±4.60
Weight (mean±std[a]) (g)	20.07±9.47	490.47±441.11
Right/left side	9/17	14/7
Macroscopic necrosis	0 (0)	20 (95)
Cystic degeneration	3 (12)	1 (5)
Hemorrhage	3 (12)	15 (71)

[a] *std* Standard deviation

antigen [1–6]. Since CD10 is expressed in a membranous fashion in the vast majority of clear cell RCCs, it is widely used for the distinction of RCC [2–4, 7]. However, its expression has not been well-investigated in adrenocortical adenomas and carcinomas. For this reason, we examined the expression pattern of CD10 in adrenocortical tumors, and compared its expression profile with hepatocellular carcinomas and clear cell RCCs.

Materials and methods

Tissue samples

We collected 47 surgically resected adrenocortical tumors (26 adrenal cortical adenomas and 21 adrenal cortical carcinomas), 25 hepatocellular carcinomas, and 20 clear cell RCCs, from the archives of the Department of Pathology, Istanbul Faculty of Medicine, Istanbul University. All cases were classified according to the standard diagnostic criteria including modified Weiss criteria for adrenocortical carcinomas. Patient age, gender information, and the gross pathologic features (size, weight, necrosis, cystic degeneration, and hemorrhage) of the adrenocortical tumors were reviewed. Radiologically, all adrenocortical tumors were characterized by unilateral mass. The gross and microscopic presence of non-tumorous adrenal tissue adjacent to the tumors helped us to ensure that these were primary adrenal tumors. Moreover, in the evaluation of adrenocortical carcinomas, the presence of positive immunostaining for synaptophysin, α-inhibin and Melan-A (Clone: A103) helped us to verify the adrenal cortical differentiation.

Immunohistochemistry

One paraffin block having the most representative area was selected for the immunohistochemical study for each tumor. Routine immunohistochemical staining was performed manually on formalin-fixed, paraffin-embedded tissues using the streptavidin–biotin-complex method (Lab Vision Corp., Fremont, CA, USA) after a pretreatment with heat-induced antigen unmasking by incubating the sections in 10 mmol/l of citrate buffer solution (pH: 6) using a domestic pressure cooker (25 min, 1 atm). The entire procedure was carried out in room temperature. Immunohistochemistry was performed using anti-CD10 antibody (Monoclonal, mouse anti-human, Clone: 56C6, 1:10, 120 min, Novocastra Laboratories, UK). Representative paraffin blocks that contain normal renal cortical parenchyma and non-tumorous liver except bile canaliculi were used as positive and negative controls, respectively. Moreover, the heat-induced antigen retrieval was also paralleled by serial sections run without primary antibody incubation. The results of immunohistochemical staining were recorded as positive (>10% of tumors cells staining) and the staining patterns (cytoplasmic, membranous, mixed cytoplasmic-membranous, and canalicular), and immunostaining area percentages (10–25, 25–50, 50–75, and 75–100%) were noted.

Results

Clinical and gross pathological findings

The main clinical and gross findings of adrenocortical tumors are summarized in Table 1. A female predominance

Table 2 The immunoreactivity patterns and rates

Patterns and rates	ACC *n* (%) 21 (100)	ACA *n* (%) 26 (100)	HCC *n* (%) 25 (100)	Clear cell RCC *n* (%) 20 (100)
Positivity rates	11 (52)	18 (69)	20 (80)	18 (90)
No staining	10 (48)	8 (31)	5 (20)	2 (10)
Membranous	3 (14)	0 (0)	0 (0)	15 (75)
Cytoplasmic	7 (33)	17 (65)	0 (0)	0 (0)
Canalicular	0 (0)	0 (0)	20 (80)	0 (0)
Membranous and cytoplasmic	1 (5)	1 (4)	0 (0)	3 (15)

ACC adrenocortical carcinoma, *ACA* adrenocortical adenoma, *HCC* hepatocellular carcinoma, *Clear cell RCC* clear cell renal cell carcinoma

Table 3 The distribution of CD10 immunostaining area percentages

CD10 immunostaining area percentages (%)	ACC *n* (%) 21 (100)	ACA *n* (%) 26 (100)	HCC *n* (%) 25 (100)	Clear cell RCC *n* (%) 20 (100)
0–10	10 (48)	7 (27)	5 (20)	2 (10)
10–25	5 (24)	17 (65)	5 (20)	3 (15)
25–50	3 (14)	2 (8)	1 (4)	3 (15)
50–75	2 (9)	0 (0)	4 (16)	8 (40)
75–100	1 (5)	0 (0)	10 (40)	4 (20)

ACC adrenocortical carcinoma, *ACA* adrenocortical adenoma, *HCC* hepatocellular carcinoma, *Clear cell RCC* clear cell renal cell carcinoma

is observed in tumor groups. Female/male ratios in adenomas and carcinomas were 3.2 and 1.3, respectively. The mean weight of the cortical carcinomas (490.47± 441.11 g) is greater than that of adenomas (20.07±9.47 g). Carcinomas were located predominantly in the right adrenal gland (right/left: 2) and adenomas were located more in the left adrenal gland (right/left: 0.53). No necrosis was found in adenomas, and nearly all carcinomas (95%) exhibited varying proportions of necrosis.

Immunohistochemical findings

The immunoreactivity patterns, rates, and percentages of immunostained areas are summarized in Tables 2 and 3. Nonneoplastic renal cortical parenchyma revealed positive immunostaining in the proximal tubular epithelium and glomerular cells. Normal liver parenchyma exhibited CD10 expression in bile canaliculi. Non-tumorous adrenal cortex revealed focal and weak cytoplasmic staining in two cases.

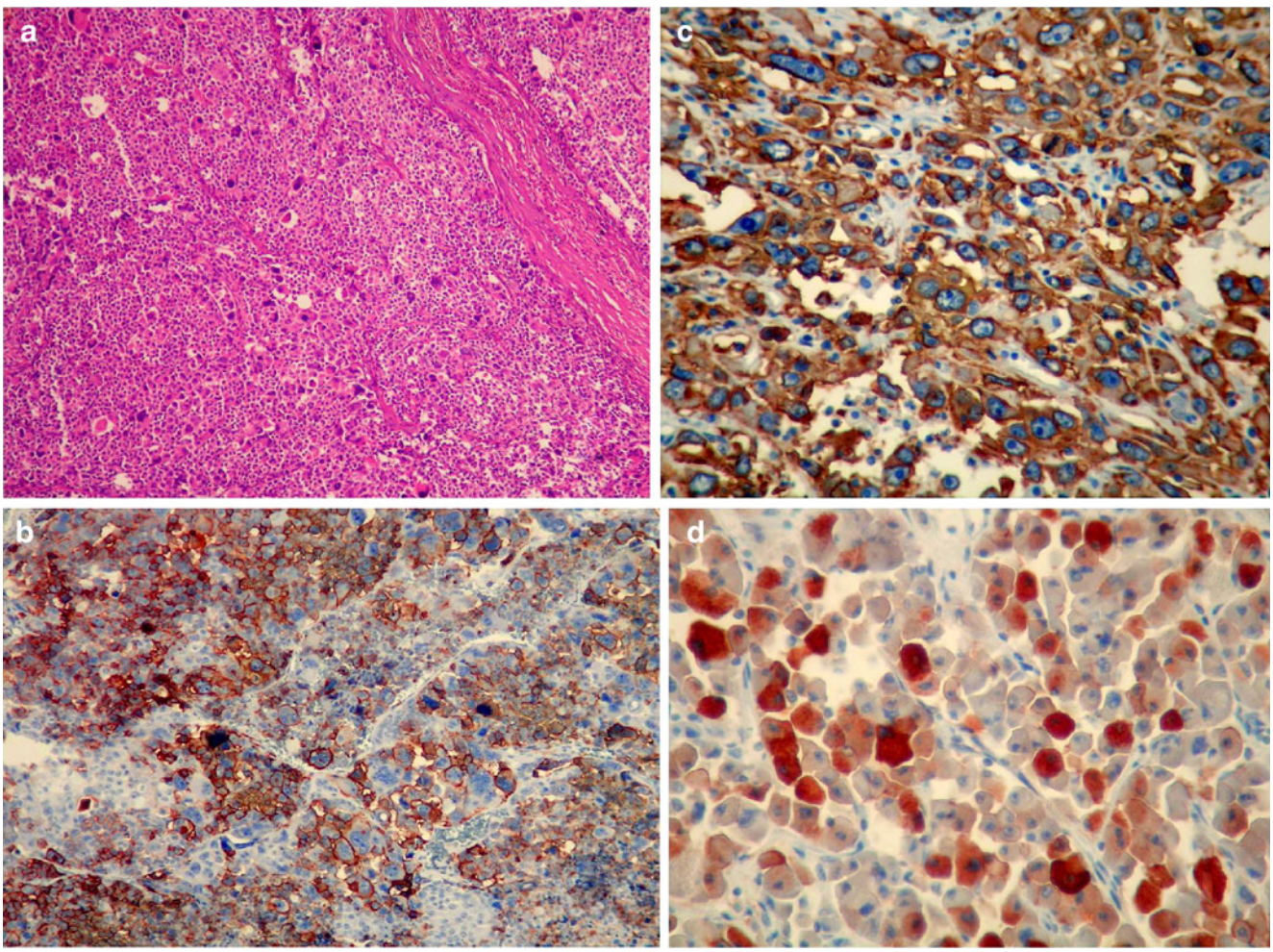

Fig. 1 **a** Adrenocortical carcinoma (H&E), **b** membranous immunostaining (Anti-CD10), **c** mixed membranous-cytoplasmic immunostaining (Anti-CD10), **d** diffuse cytoplasmic immunostaining (Anti-CD10)

Adrenocortical carcinomas

Eleven cases (52%) were positive for CD10 (Fig. 1). Membranous staining was present in three cases (14%). One case (5%) showed mixed membranous-cytoplasmic staining, while in seven cases (33%) cytoplasmic staining was present with accentuation in the paranuclear region. Cytoplasmic immunoreactivity was generally weak, and the staining percentage ranged from 20 to 50%. However, the staining percentage of the case that exhibited mixed membranous-cytoplasmic pattern was categorized as 75–100%, and other three cases, which exhibited membranous staining pattern, revealed a staining percentage of 25–50, 50–75, and 50–75%, respectively.

Adrenocortical adenomas

Eighteen cases (69%) were positive for CD10 (Fig. 2). Membranous and cytoplasmic staining was present in 1 case (4%) and 17 cases (65%) showed cytoplasmic staining. The majority of cytoplasmic staining was weak, and the staining percentage ranged from 10 to 30%.

Hepatocellular carcinomas

Twenty cases (80%) were positive for anti-CD10 with a canalicular pattern, which is characterized by a branching or short linear positivity between two cells rather than within them (Fig. 3a). The staining percentage ranged from 20 to 100%.

Clear cell RCCs

Eighteen cases (90%) were positive for CD10 (Fig. 3b). Pure membranous staining was present in 15 cases (75%), and 3 cases (15%) showed mixed membranous-cytoplasmic staining. The majority of cytoplasmic staining was moderate to strong, and the staining percentage ranged from 20 to 100%.

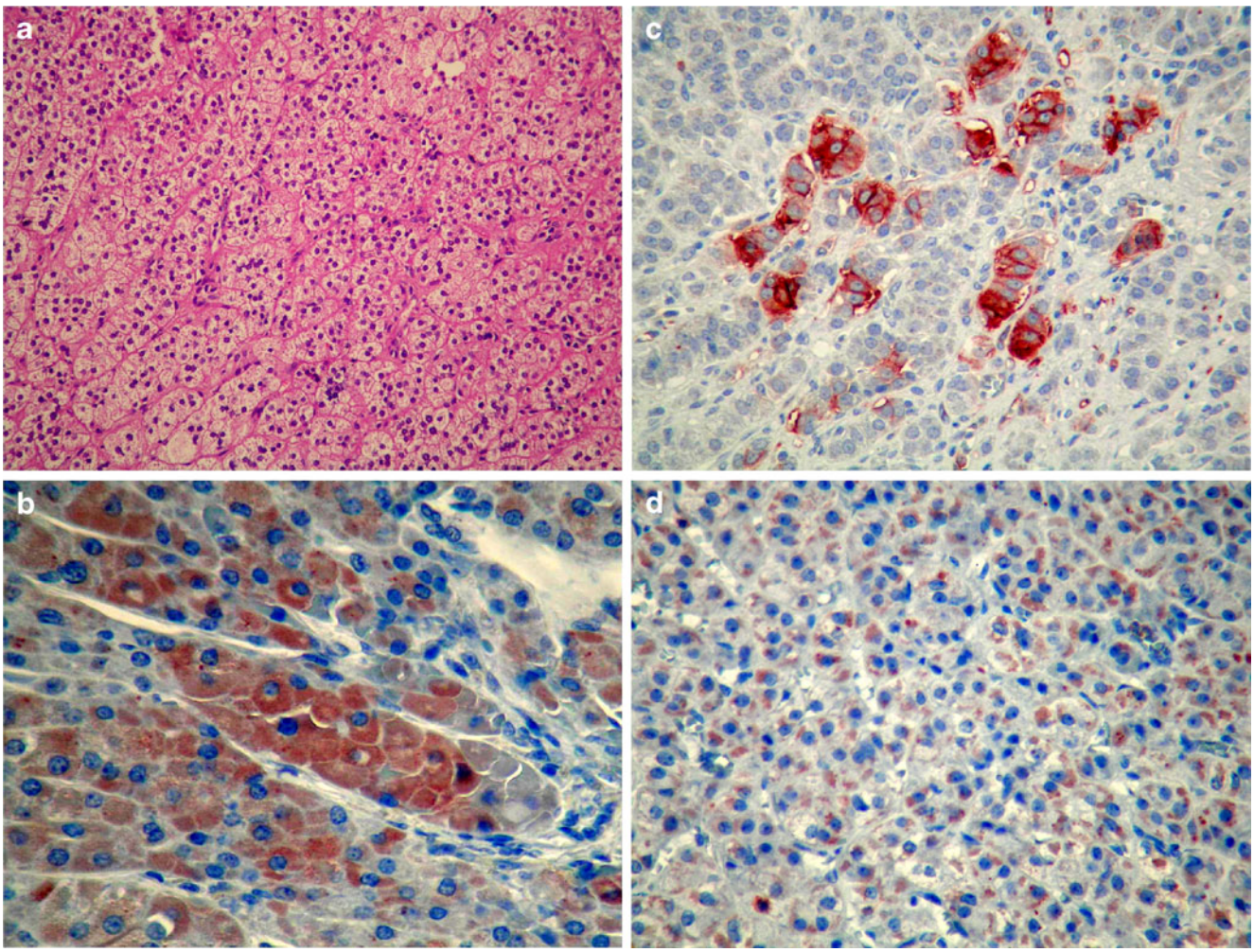

Fig. 2 **a** Adrenocortical adenoma (H&E), **b** cytoplasmic immunostaining (Anti-CD10), **c** mixed membranous-cytoplasmic immunostaining (Anti-CD10), **d** cytoplasmic paranuclear (Golgi type) immunostaining (Anti-CD10)

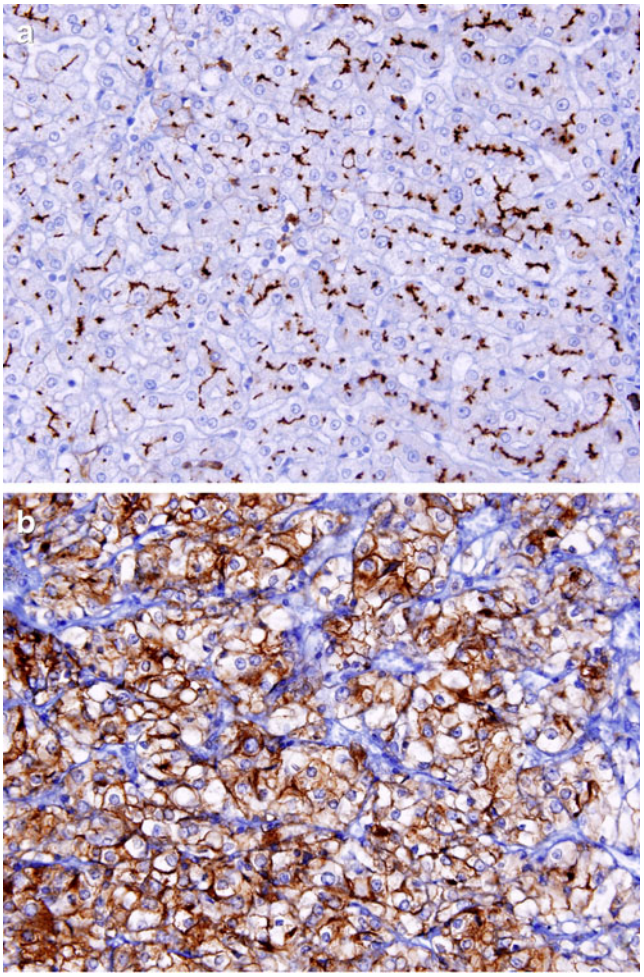

Fig. 3 **a** Canalicular immunostaining in hepatocellular carcinoma (Anti-CD10), **b** membranous and focal cytoplasmic immunostaining in clear cell renal cell carcinoma (Anti-CD10)

Discussion

In the evaluation of retroperitoneal masses, adrenocortical carcinomas, RCCs, hepatocellular carcinomas, angiomyolipomas, gastrointestinal stromal tumors, soft tissue tumors, lymphoid malignancies, and metastatic tumors should be considered in the differential diagnosis. Because of the close anatomical relation of the adrenal gland with kidney and surrounding retroperitoneal fat, adrenal neoplasm may pose clinical and pathological diagnostic challenges. In this context, the distinction of adrenocortical carcinomas from renal cell carcinomas and hepatocellular carcinomas has been recognized as particularly difficult especially in core biopsies [5–8]. The practicing pathologist may not be confident enough to make a definitive diagnosis based only on histology, given the often overlapping morphologic appearances of these tumors.

CD10 has been considered a useful marker of RCC, because of its high level of expression in clear cell and papillary RCCs [2–4, 7]. On the other hand, a number of recent studies have shown that cytoplasmic CD10 is variably expressed in renal oncocytomas and in other eosinophilic variants of RCC [6]. Moreover, the membranous CD10 expression pattern, which is reported to range from 82 to 100% in clear cell renal cell carcinomas, is commonly accepted to distinguish renal carcinomas from adrenocortical carcinomas [2–5, 7]. Chu and Arber [2] studied CD10 (clone: 56C6) expression in 505 non-hematopoietic tumors, including ten adrenocortical carcinomas; in that analysis, all ten adrenocortical carcinomas were negative for CD10, whereas 41 of 46 cases (89%) of RCC were positive. According to their results, CD10 immunohistochemistry is extremely helpful in the differential diagnosis of RCC and adrenocortical carcinoma [2]. Subsequently, Pan et al. [5] investigated 15 markers in a tissue microarray study of 895 different tumors including 40 adrenocortical carcinomas and 62 adrenocortical adenomas. Among the antibodies studied, anti-CD10 (clone: 270) revealed cytoplasmic and membranous staining in only one adrenocortical adenoma, and no CD10 positivity was demonstrated in adrenocortical carcinomas [5]. The present study revealed that adrenocortical tumors may display

Table 4 Comparison of the methods used in previous series

Study	Pan et al. [5]	Chu and Arber [2]	Present study (Mete et al.)
Antigen	CD10	CD10	CD10
Clone	270	56C6	56C6
Source	Novocastra, Newcastle, UK	Novocastra, Burlingame, CA	Novocastra Laboratories, UK
Pretreatment	Microwave, citrate (pH: 6)	Food steamer, EDTA (pH:8)	Pressure cooker, citrate (pH:6)
Dilution	1/40	1/20	1/10
Incubation time	Not available	25 min	120 min
Application method	High density tissue array slides	Automated immunostainer, whole section slides	Non-automated staining, whole section slides
Detection system	Biotin-free DAKO Envision-plus system	Streptavidin–biotin-complex technique	Streptavidin–biotin-complex technique

variable immunoreactions with anti-CD10 antibody (clone: 56C6). Furthermore, four adrenocortical carcinomas and one adrenocortical adenoma revealed a membranous staining pattern, which is regarded typical of clear cell RCCs.

It is of interest that previous studies used different methods in terms of antibody clone, incubation time, dilution ratio, pretreatment, detection system, and application (Table 4). Our study highlighted that CD10 expression (clone: 56C6) was heterogeneous in adrenocortical tumors (Table 3). Therefore, the use of it in limited tissue samples such as tissue microarrays may not reflect this heterogeneity well enough. Furthermore, we observed that the heat-induced antigen retrieval process with EDTA (pH: 8) revealed weaker staining in some of the positive control tissues, when compared with the staining in tissues processed with citrate (pH: 6). Therefore, the use of different antibody clones, antigen retrieval methods, incubation time, and concentration may explain possible discrepancies between the results of different studies.

On the other hand, CD10 is developmentally regulated in precursor epithelial cells, and CD10 loss from methylation leads to increased cell migration, cell growth, and cell survival in epithelial cell, contributing to neoplastic development and progression [9]. It is clear that CD10 possesses multiple biological effects; therefore CD10 may be more than just a marker for discrimination of some tumors [9]. However, the latter requires further investigations in larger series in order to illuminate whether the loss or presence of CD10 is of clinical significance in adrenocortical tumors.

Pan et al. highlighted that polyclonal-CEA and CD10 were valuable because of their high specificity for hepatocellular carcinomas, which share some overlapping morphological features with adrenocortical tumors [5]. However, only the canalicular pattern, the thick, waxy, branching, or short linear, dot-like positivity between cells rather than within them, was regarded as specific for hepatocellular carcinomas [5]. This pattern is regarded to have a diagnostic importance, as the membranous and/or cytoplasmic CD10 staining pattern is not observed in hepatocellular carcinomas. In comparison with HCCs, we did not observe any canalicular staining in adrenocortical tumors.

Melan-A (A103) and α-inhibin immunoreactivities have been advocated as being useful in distinguishing adrenocortical tumors [5, 10]. However, certain types of non-epithelial tumors including sex cord stromal tumors and some soft tissue tumors have been reported to express α-inhibin and Melan-A (A103) [11–14]. Soft tissue tumors with epithelioid differentiation, may also mimic the morphology of primary adrenocortical carcinomas, and are usually both negative for epithelial markers such as pankeratin and epithelial membrane antigen in the majority of cases. Furthermore, it is of interest that RCCs, particularly those associated with t(6;11) and t(X;1p11)/TFE3 translocations may be negative for keratins and may exhibit Melan-A [13]. Another diagnostic challenge in the adrenal region is the distinction of adrenocortical carcinomas from metastatic or primary melanoma and pure epithelioid angiomyolipoma (EAML), which may show Melan-A (A103) positivity [12, 15]. However, this distinction can be usually made by the demonstration of the absence of pan-melanocytic antigens (S100 protein, HMB-45, Melan-A (A103 and other clones), CD63, tyrosinase and microphthalmia-associated transcription factor), and muscle markers. In this context, it is worth stressing that CAM5.2 and S-100 protein may occasionally be positive, albeit focal, in EAMLs [12]. In special situations, the distinction of an adrenocortical carcinoma may require the use of other markers such as SF-1 (steroidogenic factor-1) and DAX-1 (dosage-sensitive sex reversal adrenal hypoplasia congenital critical region on the X chromosome gene 1) [16–18]. Recently, Kaneko et al. [18] showed that DAX-1 and SF-1 can be used to diagnose the site of origin of metastatic adrenocortical carcinoma in patients clinically presenting with widespread metastasis and bulky retroperitoneal masses.

In conclusion, our preliminary results revealed that adrenocortical tumors may also express CD10. Despite the relatively small number of samples, the most important point from this paper is the fact that anti-CD10 expression has not been previously reported in adrenocortical carcinomas. This suggests that anti-CD10 (56C6) does not seem to be a useful marker for the distinction of renal cell carcinomas from adrenocortical tumors; since its expression does not rule out the possibility of adrenocortical tumors. Therefore, it is important to remember this feature when constructing an antibody panel for a retroperitoneal epithelial neoplasm that involves the adrenal gland and kidney; especially in the setting of limited tissue sample (e.g. core biopsies or FNA specimens).

Acknowledgements This study was supported by the research fund of Istanbul University (Project number: UDP-2768/23072008). The preliminary results of this study were partially presented during the poster session of the XXVII. Congress of the International Academy of Pathology in Athens (October, 12–17, 2008).

Conflict of interest statement We declare that we have no conflict of interest.

References

1. McIntosh GG, Lodge AJ, Watson P et al (1999) NCL-CD10-270: a new monoclonal antibody recognizing CD10 in paraffin-embedded tissue. Am J Pathol 154:77–82

2. Chu P, Arber DA (2000) Paraffin-section detection of CD10 in 505 non-hematopoietic neoplasms: frequent expression in renal cell carcinoma and endometrial stromal sarcoma. Am J Clin Pathol 113:373–382
3. Langner C, Ratschek M, Rehak P et al (2004) CD10 is a diagnostic and prognostic marker in renal malignancies. Histopathol 45:460–467
4. Avery AK, Beckstead J, Renshaw AA et al (2000) Use of antibodies to RCC and CD10 in the differential diagnosis of renal neoplasms. Am J Surg Pathol 24:203–210
5. Pan CC, Chen PC, Tsay SH et al (2005) Differential immunoprofiles of hepatocellular carcinoma, renal cell carcinoma, and adrenocortical carcinoma: a systemic immunohistochemical survey using tissue array technique. Appl Immunohistochem Mol Morphol 13:347–352
6. Mete O, Kilicaslan I, Uysal V (2009) Does CD10 immunoexpression have a diagnostic utility in the differential diagnosis of renal oncocytomas and eosinophilic variants of chromophobe renal cell carcinomas? Pathol 41:191–193
7. Pan CC, Chen PCH, Ho DMT (2004) The diagnostic utility of MOC31, BerEP4, RCC marker and CD10 in the classification of renal cell carcinoma and renal oncocytoma: an immunohistochemical analysis of 328 cases. Histopathol 45:452–459
8. Kato I, Inayama Y, Yamanaka S et al (2009) Epithelioid angiomyolipoma of the kidney. Pathol Int 59:38–43
9. Papandreou CN, Nanus DM (2010) Is methylation the key to CD10 loss? J Pediatr Hematol Oncol 32:2–3
10. DeLellis RA, Lloyd RV, Heitz PU, Eng C (2004) World Health Organization classification of tumours. Pathology and genetics of tumours of endocrine organs. IARC, Lyon
11. Stewart CJ, Nandini CL, Richmond JA (2000) Value of A103 (Melan-A) immunostaining in the differential diagnosis of ovarian sex cord stromal tumours. J Clin Pathol 53:206–211
12. Aydin H, Magi-Galluzzi C, Lane BR et al (2009) Renal angiomyolipoma: clinicopathologic study of 194 cases with emphasis on the epithelioid histology and tuberous sclerosis association. Am J Surg Pathol 33:289–297
13. Zamecnik M, Michal M, Mukensnabl P (2003) Reactivity of granular cell tumors for inhibin and other markers of sex cord and steroid cell differentiation. Am J Surg Pathol 27:413–414
14. Schraith DF, Hahm GK, Niemann TH et al (2003) Alpha-inhibin immunoreactivity in soft-tissue neoplasia. Mod Pathol 16:1205–1209
15. Banerjee SS, Eyden B (2008) Divergent differentiation in malignant melanomas: a review. Histopathol 52:119–129
16. Doghman M, Cazareth J, Douguet D et al (2009) Inhibition of adrenocortical carcinoma cells proliferation by SF-1 inverse agonists. J Clin Endocrinol Metab 94:2178–2183
17. Bakke M, Zhao L, Hanley NA et al (2001) SF-1: a critical mediator of steroidogenesis. Mol Cell Endocrinol 171:5–7
18. Kaneko T, Kojima Y, Umemoto Y et al (2008) Usefulness of transcription factors Ad4BP/SF-1 and DAX-1 as immunohistologic markers for diagnosis of advanced adrenocortical carcinoma. Horm Res 70:294–299

Virchows Arch (2010) 456:523–532
DOI 10.1007/s00428-010-0909-5

ORIGINAL ARTICLE

Amyloid in endomyocardial biopsies

Barbara Kieninger · Magdalena Eriksson · Reinhard Kandolf · Philipp A. Schnabel · Stefan Schönland · Arnt V. Kristen · Ute Hegenbart · Peter Lohse · Christoph Röcken

Received: 4 February 2010 / Revised: 11 March 2010 / Accepted: 15 March 2010 / Published online: 8 April 2010
© Springer-Verlag 2010

Abstract The prognosis of cardiac amyloidosis depends on the nature and origin of the amyloid protein deposited. However, little is known about the prevalence and origin of amyloid in heart muscle biopsies. We therefore examined retrospectively the distribution and origin of amyloid in a consecutive series of endomyocardial biopsies. Endomyocardial biopsies with verified presence of amyloid from 101 patients were included. Amyloid was classified immunohistochemically in each of them. Our collective comprised 63 men and 38 women, with a mean age of 66 years (range 37–85 years). Cardiac amyloidosis was the most common of the AL (54 patients) or ATTR type (42 patients). In five individuals, amyloid remained unclassified. AL amyloidosis was subdivided into ALλ (45 patients) and ALκ amyloid (nine patients). AA amyloid was not found in any individual. The amount of amyloid was higher in AL than in ATTR amyloidosis. Genomic DNA was extracted and examined by DNA sequencing in 19 patients with ATTR amyloidosis. Five (26%) individuals carried *TTR* mutations (p.Val20Ile, p.Val30Met (twice), p.Asp39Val and p.Glu54Asp) and were classified as suffering from hereditary ATTR amyloidosis. Amyloid in endomyocardial biopsies is most commonly of immunoglobulin light chain origin, followed by non-hereditary and hereditary-type ATTR amyloid.

Keywords Amyloid · Endomyocardial biopsy · AL · ATTR

B. Kieninger · M. Eriksson · C. Röcken
Department of Pathology, Charité University Hospital,
Berlin, Germany

R. Kandolf
Department of Molecular Pathology, Eberhard Karls University,
Tübingen, Germany

P. A. Schnabel
Department of Pathology, University of Heidelberg,
Heidelberg, Germany

S. Schönland · U. Hegenbart
Medical Department V, Amyloidosis Clinic, Hematology,
University of Heidelberg,
Heidelberg, Germany

A. V. Kristen
Department of Cardiology, Angiology, and Respiratory Medicine,
University of Heidelberg,
Heidelberg, Germany

P. Lohse
Department of Clinical Chemistry—Grosshadern,
Ludwig-Maximilians University,
Munich, Germany

C. Röcken (✉)
Department of Pathology, Christian-Albrechts-University,
Arnold-Heller-Str. 3/14,
24105 Kiel, Germany
e-mail: christoph.roecken@uk-sh.de

Introduction

Amyloidosis is a conformational disease characterized by the deposition of insoluble fibrillar protein aggregates with antiparallel β-pleated sheet conformation. It presents either as a systemic disease with deposits in multiple organs and tissues, or as a localized disorder affecting a single anatomic site [1]. More than 26 different autologous, physiological peptides and proteins have been identified to be able to form amyloid in humans [2].

While amyloidosis can affect virtually every organ and often presents first with proteinuria or renal failure, cardiac involvement often determines the patient's prognosis. It is the most serious complication in patients with systemic amyloidosis and the cause of death in more than half of all cases [3, 4]. The heart is affected in approximately 50% of

immunoglobulin light chain-derived AL amyloidosis cases [5]. As this is a very aggressive form, affected individuals have a mean survival of 1.08 years after diagnosis [6, 7]. Cardiac involvement is less frequent in transthyretin-derived ATTR amyloidosis, and the prognosis is often more favorable because of a slower progression rate and a lack of toxic effects on the heart [8]. In serum amyloid A-derived AA amyloidosis, heart involvement, in contrast, is quite unusual [3, 6].

Patients with cardiac amyloidosis suffer from a restrictive cardiomyopathy, arrhythmias, conduction disturbances and congestive heart failure [9]. In fact, 10% of all noncoronary cardiomyopathies turn out to be cardiac amyloidoses [10]. There are some findings in non-invasive examinations that should arouse suspicion of amyloidosis. The ECG might show a pseudoinfarction pattern, and, as pathognomonic sign, a low voltage in spite of increased ventricular wall thickness which can be confirmed in the echocardiogram. Moreover, one might find an abnormal texture with a patchy increased myocardial echogenity, called granular sparkling [3, 11]. Furthermore, there are promising developments concerning cardiovascular magnetic resonance imaging: cardiac amyloidosis can be identified by a distinct pattern of late gadolinium enhancement with good sensitivity and excellent specificity [12]. However, histological examination of an amyloid-bearing biopsy is mandatory to reach a correct diagnosis [4]. It is also necessary to classify the amyloid protein, e.g. by immunohistochemistry, in order to assess patient prognosis and treatment. When it comes to severe cardiac amyloidosis, radical therapeutical approaches are sometimes performed. Patients with AL amyloidosis might undergo heart transplantation followed by chemotherapy and stem cell transplantation; in case of ATTR amyloidosis, a combined heart and liver transplantation is available in a few specialized centers [9, 13].

The management of patients with amyloidosis depends on the accurate histological diagnosis and classification of the amyloid deposits. In order to achieve this goal, surgical pathologists may wish to rely on data obtained from larger biopsy series, providing information about the expected prevalence and likelihood of a diagnosis in a biopsy specimen. During the last 3 years, the Amyloid Registry of the Charité Hospital in Berlin has collected significant numbers of amyloid-containing biopsies from various tissue sites (>500 cases in the last 3 years). We noticed that the prevalence of the different amyloid types was not uniform, and we hypothesized that the dissimilar distribution of different amyloid types in various organ biopsies may depend on the clinical course of an amyloid disease and its symptoms. Two recent retrospective investigations on kidney and liver biopsies supported our hypothesis [14, 15]. We were able to show that AA amyloidosis is very common in kidney biopsies and a rarity in liver biopsies [14, 15]. However, it is well-known from autopsy studies that AA amyloidosis is a systemic disease that can affect the kidney and liver with equal prevalences. However, we were unaware of the prevalences of the different amyloid types in heart biopsies and whether the immunohistochemical classification of cardiac amyloidosis is different from the classification of amyloid in other biopsy samples. The contractile activity of the heart may promote diffusion of serum proteins into the amyloid deposits thereby prohibiting accurate classification.

In order to fill this gap of knowledge, we reviewed all amyloid-containing endomyocardial biopsy specimens submitted to three different Departments of Pathology within the last 2 years, assessed the suitability of immunohistochemistry for the classification of cardiac amyloid and elucidated which types of amyloid are most common in endomyocardial biopsies.

Material and methods

Patients

All consecutive amyloid-containing endomyocardial biopsies from 101 patients were retrieved from the Amyloid Registry of the University of Berlin, which receives referrals throughout Germany for the immunohistochemical classification of amyloid as well as from the Departments of Pathology at the Universities of Heidelberg and Tübingen between January 2006 and October 2008. The selection of these biopsies was based on the histological identification of amyloid by Congo red staining and polarization microscopy. Immunohistochemical staining of serial sections was done in all 101 cases. For the DNA analysis, biological material such as blood samples or formalin-fixed and paraffin-embedded (FFPE) tissue was used. Blood samples were drawn after the patient had given written informed consent. Tissue samples were obtained for diagnostic purposes only. The study was conducted after the pathological investigations had been completed. Following the identification of cases with ATTR amyloidosis, all specimens were anonymized prior to the genetic analyses. The study was carried out in accordance with the guidelines set out by the German government and the local Ethics Committee of the University of Berlin.

Histology and immunohistochemistry

The tissue biopsies were fixed in buffered formalin and embedded in paraffin. Serial sections were stained with hematoxylin and eosin. Amyloid was detected in Congo red stained sections viewed under cross-polarized light. Immu-

nohistochemistry was performed with commercially available monoclonal antibodies directed against AA amyloid (1:600) and polyclonal antibodies directed against amyloid P component (1:5,000), fibrinogen (1:2,000), lysozyme (1:3,000), transthyretin (1:4,000), λ-light chain (1:160,000) and k-light chain (1:160,000; all DAKO, Hamburg, Germany). Non-commercially available polyclonal antibodies were directed against apolipoprotein AI (1:1,000), λ-light chain-derived amyloid proteins (AL1, 1:3,000) and anti-λ-light chain peptide (AL3, 1:250; AL7, 1:500). Immunostaining was done with the BenchMark® XT immunostainer using the ultraView™ Universal Alkaline Phosphatase Red Detection Kit (both Ventana Medical Systems, Inc., Tucson, Arizona, USA). Prior to incubation with AL7 and the antibodies directed against amyloid P component, λ- and κ-light chains as well as transthyretin, sections were pretreated with Cell Conditioning 1 according to the manufacturer's instructions (CC1, Ventana). Prior to incubation with anti-apoAI, sections were treated with citrate buffer (32 min, 95°C). The specificity of immunostaining was verified using specimens containing known classes of amyloid (AA amyloid, apolipoprotein AI, transthyretin and λ-light chain), using positive controls recommended by the manufacturers (remaining antibodies) as well as omitting the primary antibodies as a negative control.

The stained serial sections were examined twice by two different observers (BK and CR) in a blinded manner. Identification of the amyloid protein was considered to be positive when there was strong homogeneous immunostaining of the entire amyloid deposits. Uneven and weak staining of some deposits, in contrast, was classified as a negative result. Strong, even and homogeneous staining of the entire amyloid deposits with more than one antibody directed against different amyloid precursor proteins was categorized as unclassifiable.

The evaluation of the degree of deposition was done by visual judgement. At grade I, less than 25% of the myocardial area consisted of amyloid; at grade II, 25–50%; and at grade III, more than 50% (Fig. 1).

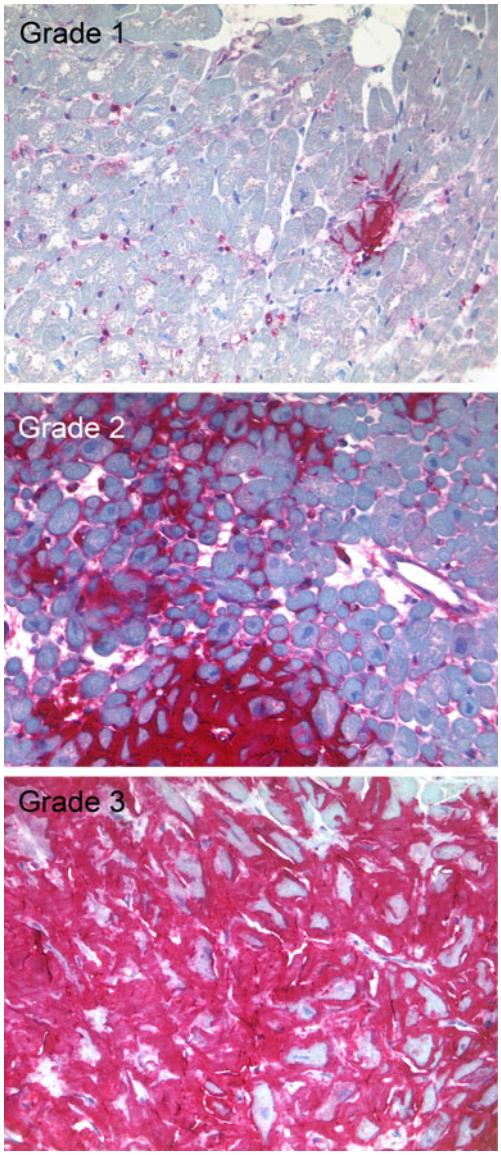

Fig. 1 Illustration of degrees of amyloid deposition. At grade I, up to 25% of the endomyocardial biopsy consists of amyloid. Grade II shows involvement of 25% to 50% of the myocardium while at grade III more than 50% of the biopsy is affected. Original magnification 200×

DNA extraction

Of the 42 patients diagnosed with ATTR, biological samples were available from 19. FFPE tissue biopsies with a sufficient amount of myocardial tissue were available from 11 and blood from nine of these 19 patients. In one case, both FFPE tissue and blood could be examined. Total genomic DNA was extracted using kits from Qiagen (Hilden, Germany).

DNA amplification and sequencing

Amplification of the *TTR* exons 1, 2, 3 and 4 was done by the polymerase chain reaction (PCR) with the following specific primer pairs: exon 1 (246 bp) forward: 5′-tcagattggcaggga taagc-3′ and reverse 5′-gcaaagctggaaggagtcac-3′; exon 2 (250 bp) forward 5′-ttcgctccagatttctaatacca-3′ and reverse 5′-agtcctgtgggagggttctt-3′; exon 3 (203 bp) forward 5′-gctc tggtggaaatggatct-3′ and reverse 5′-gaatgccaaaagcaaaaacc-3′; exon 4 (244 bp) forward 5′-gctctggtggaaatggatct-3′ and reverse 5′-gcatatgaggtgaaaacactgct-3′. A 50-µl reaction mixture contained 400–600 ng DNA, 0.2–1 µM of the exon-specific primer pairs, 1× PCR buffer, 1.5 U Taq polymerase, 0.2 µM dNTPs and eventually also Q-solution or $MgCl_2$ as recommended by the manufacturer (Qiagen, Hilden, Germany). The following thermocycling conditions were

used: initial denaturation at 94°C for 3 min, 40 cycles of 94°C for 1 min, 56–58°C for 1.5 min and 72°C for 1 min, followed by a final elongation step at 72°C for 7 min. A negative control with water instead of DNA was included in each PCR run, and blood isolated from an individual with wild-type TTR was used as a positive control. Quality and size of PCR products were analyzed by agarose gel electrophoresis.

Direct sequencing was either performed by Invitek (Berlin, Germany) or with the use of ABI BigDye Terminator reagents (Applied Biosystems, Foster City, USA) on ABI PRISM 310 Genetic Analyzers v1.1 or v.1.3. In some cases, only exons 2, 3 and 4 were sequenced since no mutations have been reported in the three N-terminal amino acids encoded by exon 1. The same set of primers as for the first PCR was used. To avoid detection of genomic artifacts due to errors of Taq polymerase, a second independent PCR and cycle sequencing reaction was carried out with DNA samples revealing a mutation.

Results

Histology and immunohistochemistry

One hundred and one endomyocardial biopsies were available from 101 patients including 63 (62%) men and 38 (38%) women. The age of the patients ranged from 37 to 85 years (mean 66 years). AL amyloid was found in 54 (53%) patients and ATTR amyloid in 42 (42%). The amyloid deposits remained unclassifiable in five (5%) patients. There was no case of AA-, AApoAI-, AFib- or ALys amyloidosis in our series (Table 1).

AL amyloidosis

The 54 patients with AL amyloidosis were further subdivided into 45 (83%) patients with AL amyloid of λ-light chain origin and 9 (17%) patients with AL amyloid of κ-light chain origin. The λ- to κ-light chain ratio was 5:1 (Fig. 2).

The ALλ group consisted of 29 (64%) men and 16 (36%) women, with a mean age of 61 years (range 41 to 81 years). The amount of amyloid deposited was mild (grade I) in seven (16%) cases, moderate (grade II) in 20 (44%) and extensive (grade III) in 18 (40%). Amyloid was deposited exclusively in the interstitium in 11 (24%) patients and in the vessel walls in two (5%) patients. The majority of the patients had both interstitial and vascular amyloid deposits [32 (71%)]. The morphology of the interstitial deposits was mostly of reticular, pericellular appearance [22 (51%)]. In 13 (30%) patients, there were additionally micronodular amyloid deposits and 8 (19%) specimens showed only the latter.

Nine patients were found to suffer from AL amyloidosis of κ-light chain origin. The three (33%) men and six (67%) women had a mean age of 67 years at the time of diagnosis (range 52 to 80 years). The amount of ALκ amyloid was categorized as grade II in four (44%) patients and grade III in five (56%). No case had grade I amyloid deposits. Seven (78%) patients showed mixed interstitial and vascular deposits, while two (22%) presented only with interstitial deposits. These interstitial deposits were mostly reticular in four (45%) cases, micronodular in three (33%) and a combination of both in another two (22%).

ATTR amyloidosis

The 42 patients with cardiac ATTR amyloid had a mean age of 70 years, ranging from 37 to 85 years. This group comprised 28 (67%) men and 14 (33%) women. The amount of amyloid was mild in nine cases (21%), moderate in 21 (50%) and extensive in 12 (29%). Pure interstitial deposits occurred in 35 of the 42 (83%) specimens. In addition, another seven biopsies (17%) showed vascular involvement. The interstitial amyloid deposits had a reticular aspect in nine (21%) cases, looked more micronodular in 20 (48%) and showed both patterns in 13 (31%) (Fig. 3).

Unclassifiable amyloid deposits

Amyloid remained unclassifiable in the biopsies of three men and two women. The patient age ranged from 55 to

Table 1 Correlation of amyloid proteins with patient age and gender

		Age [*n* (%)]						Gender	
	No. (%)	30 to 39	40 to 49	50 to 59	60 to 69	70 to 79	80 to 89	Women	Men
AL (λ)	45 (44)	–	7 (16)	13 (29)	16 (36)	8 (18)	1 (2)	16 (36)	29 (64)
AL (κ)	9 (9)	–	–	2 (25)	3 (38)	2 (25)	1 (12)	6 (67)	3 (33)
ATTR	42 (42)	1 (2)	–	3 (7)	11 (26)	21 (50)	6 (14)	14 (33)	28 (67)
Amyloid n.o.s.	5 (5)	–	–	1 (20)	–	4 (80)	–	2 (40)	3 (60)
Total	101 (100)	1 (1)	7 (7)	19 (19)	30 (30)	35 (35)	8 (8)	38 (38)	63 (62)

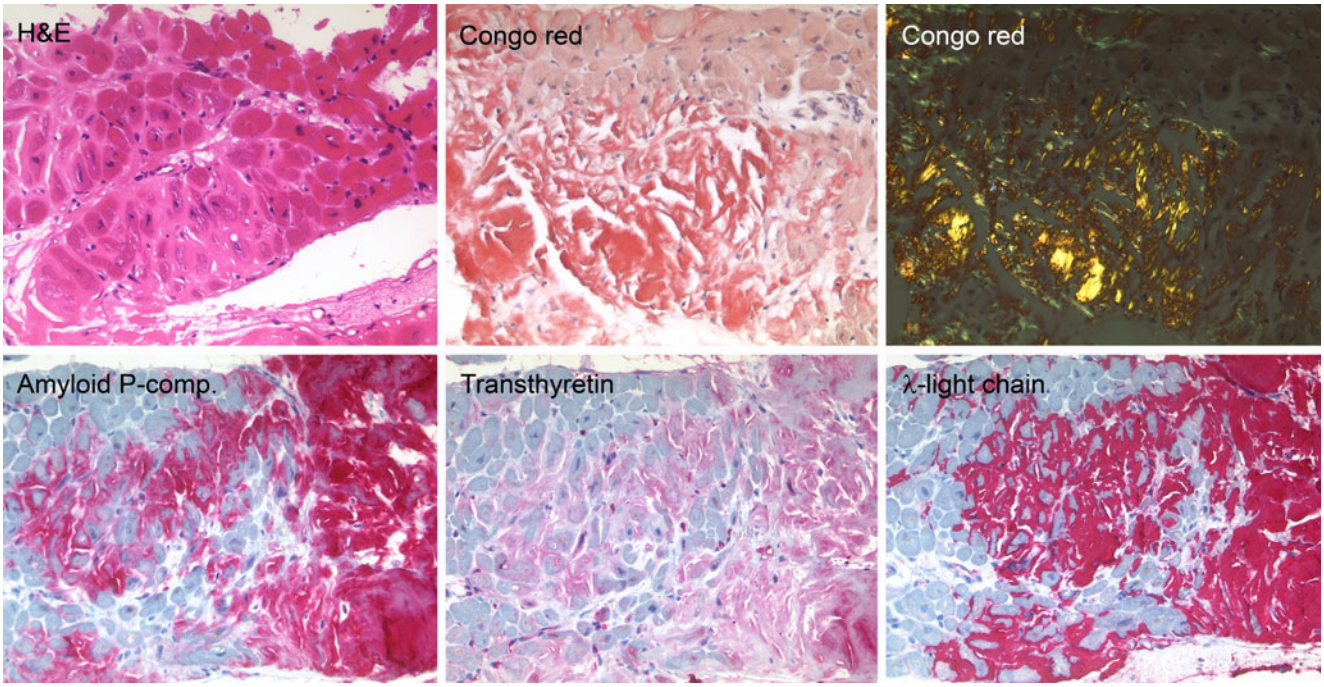

Fig. 2 AL λ amyloidosis in endomyocardial biopsy. A fine mesh work of intersitital amyloid deposits in the myocard was noted in H&E-stained sections, which stained bright red in Congo red and showed a characteristic apple green birefringence in polarized light (Congo red, *upper middle* and *right* panels). The amyloid deposits were strongly and homogeneously immunoreactive for amyloid P component (*amyloid P-comp.*) and λ-light chain. The antibody directed against transthyretin showed only weak reactions at the edge of the amyloid deposits and no staining in the center and was interpreted as contamination of the interstitium and amyloid by serum proteins. Original magnification 200×

76 years (mean age 70 years). All five patients (100%) had moderate amounts (grade II) of amyloid, with both vascular and interstitial deposits in four (80%) and interstitial deposition in only one (20%) patient. All five biopsies were of reticular appearance, and three of them showed micronodular deposits in addition.

DNA analysis

In 19 of the 42 patients with cardiac ATTR amyloidosis, genomic DNA was available for molecular analysis. In five (26%) patients, TTR mutations were found, including p.Asp39Val, p.Glu54Asp and p.Val20Ile each in a single patient, as well as p.Val30Met in two. The mutations were found in three men and two women. Their mean age was 57.2 years (range 37–70 years) compared with 72.5 years (range 63–84 years) of the 14 wild-type TTR patients.

Clinical information

Only little clinical information was available from the 101 patients in our collective. Eleven of them (11%) had been reported to suffer from heart insufficiency caused by restrictive cardiomyopathy as well as by HOCM and HNOCM. Among the 54 patients with AL amyloidosis, an underlying plasma cell dyscrasia like multiple myeloma was reported in five cases (9%). Moreover, three patients (3%) were also affected with renal insufficiency.

Discussion

To the best of our knowledge, this is the largest analysis of a consecutive series of amyloid-bearing endomyocardial biopsies applying 11 different antibodies directed against a large variety of amyloid proteins on every case. Collins et al. [16] studied only 17 biopsies and Crotty et al. [17] applied only five antibodies. In addition, our study is also the first that investigated the prevalence and type of *TTR*-gene mutations among individuals with biopsy-proven cardiac ATTR amyloidosis.

Prevalences of amyloid types in the heart and in unselected autopsy series

Our retrospective analysis of 101 endomyocardial biopsies from patients with cardiac amyloidosis showed that 95% of the patients suffered from either AL or ATTR amyloidosis. The high prevalence of AL amyloidosis in endomyocardial biopsies is in agreement with observations made by

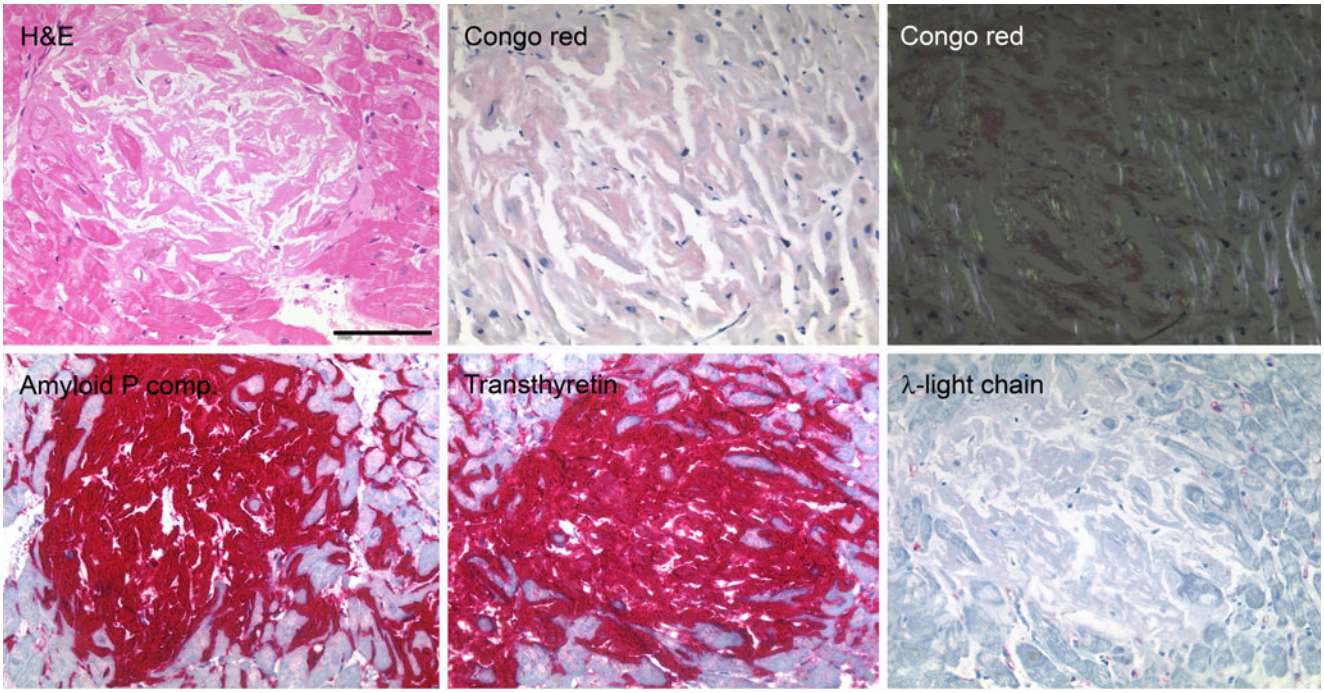

Fig. 3 ATTR amyloidosis in endomyocardial biopsy. Confluent micronodular and interstitial amyloid deposits were found in this case in H&E-stained sections. The amyloid deposits stained red with Congo red and showed typical green birefringence in polarized light (Congo red, *upper middle* and *right* panels). A homogeneous immunostaining was observed with antibodies directed against amyloid P component and transthyretin. There was no reaction with the antibody directed against λ-light chain. Original magnification 200×

Benson, who described amyloid of light chain origin as the most common cause of amyloid cardiomyopathy [18]. Similar to Shah et al. [9], we found a predominance of λ-light chain-derived AL amyloid. However, in contrast to other series, we found ATTR amyloid to be three times more common in the exclusive series of endomyocardial biopsies than in an unselected series of pathology specimens of diverse anatomical origin [19]. The divergent prevalences of ATTR amyloid in different study populations are probably due to the heterogeneous anatomical distribution and clinical presentation of systemic amyloidoses. While AL amyloid may affect virtually every organ, other types of systemic amyloidosis show a more distinct anatomical distribution and clinical presentation. In addition, a study bias may exist in our collective since the Amyloid Registry of the Charité is a referral center for complicated cases and the Department of Pathology of the University of Heidelberg also receives selected cases of amyloid-containing endomyocardial biopsies. Nevertheless, the prevalences in our collective differ enormously from the distribution of amyloid types found in two recent studies from our group focussing on renal [14] and hepatic amyloidoses [15], respectively (Fig. 4). The kidney was mainly affected by AL and AA amyloidoses in almost equal parts, while amyloidosis in the liver was caused by light chains in most of the cases. In both organs, ATTR amyloidosis seemed to be a rare finding. Although these varieties might be influenced by the potential study bias, they give us a useful lead which types of amyloidosis should be initially expected in a biopsy specimen of a certain organ (Fig. 4).

ATTR—senile and hereditary pathogenesis

ATTR amyloid occurs as senile systemic variant without a *TTR*-gene mutation and predominantly affects the heart and blood vessels [20]. In this respect, it is not surprising that senile systemic ATTR amyloidosis was the second most prevalent type of amyloid in our current patient series. Interestingly, only 26% of the genetically tested patients with cardiac ATTR amyloid were identified as hereditary type. In a recent systemic analysis of all patients with ATTR amyloidosis, including biopsies of diverse anatomical sites, we identified 40% as carriers of *TTR*-gene mutations [21]. The different prevalences of non-hereditary and hereditary ATTR amyloidosis in surgical pathology specimens are probably simply a reflection of the different clinical courses and histoanatomical distributions of the two variants. The different natures and pathologies of non-hereditary and hereditary ATTR amyloidosis are further supported by findings made by Westermark et al., who reported different staining characteristics and differences in the primary structure of the deposited amyloid proteins [17, 22, 23].

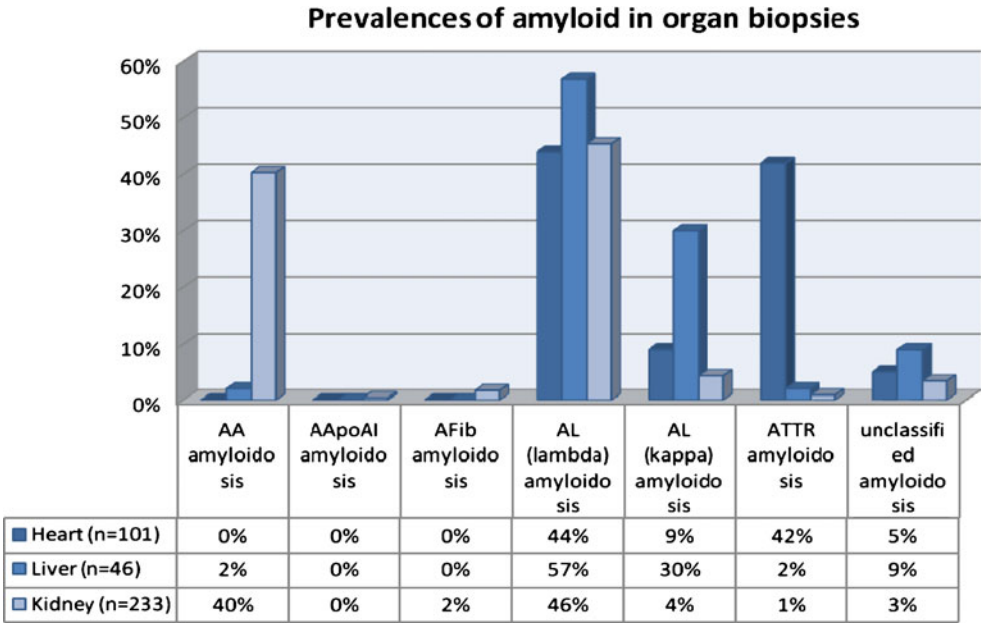

Fig. 4 Prevalences of amyloid types in different organs

Lack of AA amyloidosis in the heart

None of our patients were found to suffer from AA-, ApoAI-, AFib- or ALys amyloidosis. While the latter three belong to the group of rare hereditary amyloidoses which primarily affect the kidneys, AA amyloidosis is the second most common type of systemic amyloidosis, which was found in 24–49% of the patients in three unselected autopsy series [20, 24, 25]. However, with regard to cardiac involvement, two studies on endomyocardial biopsies showed either a total lack of AA amyloidosis [17] or a few cases with negligible amounts of amyloid [10]. This is due to the fact that systemic AA amyloidosis rarely involves the heart [6, 25] and if it does, it remains clinically insignificant in most of the cases [3, 17]. Clinically, AA amyloidosis mainly presents with renal involvement [9]. As these patients develop a nephrotic syndrome quickly, they undergo a conventional biopsy of the kidney [24]. In fact, AA amyloidosis is the second most common type of systemic amyloidosis in our large series of more than 200 amyloid-containing kidney biopsies, reaching 40% compared with 2% ATTR amyloid [14]. Even if cardiac involvement is suspected in AA amyloidosis, the diagnosis is often already reached by kidney or rectal biopsy, making an endomyocardial biopsy unnecessary. Thus, cardiac involvement is likely more common than encountered in endomyocardial biopsies.

Unclassified cases

In five of our patients, the amyloid deposits remained unclassifiable. The reason for this was homogeneous staining of the amyloid deposits with more than a single antibody. Unfortunately, we were unable to discriminate, if this was due to co-deposition of more than one amyloid protein, as some authors have described [17, 25] or just a contamination of the amyloid deposits with other serum proteins (especially immunoglobulins) [26, 27]. The contractile activity of the heart and the disturbance of the normal architecture by amyloid support the diffusion of serum proteins into the amyloid deposits, which are then detected by immunohistochemistry. However, the overall prevalence of unclassifiable cases did not differ significantly from that one observed in kidney biopsies [14], and the contractile activity of the heart does not seem to increase the risk of a "background staining". However, immunohistochemistry is fraught with intrinsic problems. Amyloid consists of tightly packed protein aggregates, which may be poorly accessible to antibodies. This degrades the quality and signal-to-noise ratios of immunohistochemical stains. Amyloid deposits also often trap ancillary molecules including immunoglobulins, which can interact with the anti-immunoglobulin antibodies. These phenomena can cause considerable difficulties in the interpretation of immunohistochemical results and can even lead to misclassification of amyloid subtypes [19]. Laser microdissection and mass-spectrometry based proteomic analysis [28] or luminescent-conjugated polymer spectroscopy [29] bear the potential to compensate the shortcomings of immunohistochemistry.

Patients' age and gender (Table 2)

In our series of amyloid-containing endomyocardial biopsies, male patients predominated with 62%. Similar

Table 2 Summary of previous and present studies

Reference	Year	Classification/antibodies	Study populations *n* m:f	AL *n* (%) m:f Mean age (range)	Results ATTR *n* (%) m:f Mean age (range)	n.o.s. *n* (%) m:f Mean age (range)
Smith et al. [10]	1984	Underlying diseases, clinical findings, monoclonal protein, distribution of organ involvement, no immunostaining	47 35:12	21 (45) 22:4 57.6 years (35–83)	26 (55) 13:8 83 years (70–89)	–
Crotty et al. [17]	1994	AA amyloid, amyloid P component, λ-light chain, κ-light chain, transthyretin	100 81:19	74 (74) – 61 years	26 (26) – 73 years	–
Collins et al. [16]	2009	AA amyloid, apolipoprotein AI, β2-microglobulin, fibrinogen, IgA, IgG, IgM, λ-light chain, κ-light chain, transthyretin	17 12:5	14 (82%) 9:5 56 years (37–75)	–	3 (18) 3:0 70 years (67–77)
Current series	2010	AA amyloid, amyloid P component, apolipoprotein AI, fibrinogen, lysozyme, λ-light chain (four separate antibodies), κ-light chain, transthyretin	101 63:38	54 (53) 32:22	42 (42) 28:14 70 years (37–85)	5 (5) 3:2 70 years (55–76)

observations have been made by others, including a large series of surgical pathology specimens with amyloid [19], previous studies of the heart [10, 17, 30] and unselected autopsy series [24, 25]. A putative explanation might be that AL amyloid, the most common type of systemic amyloidosis, is due to a plasma cell dyscrasias such as multiple myeloma, which predominantly affect men. However, in ATTR amyloidosis, where male prevalence ranges from 63% to 82% [10, 24, 25, 31], the underlying cause remains unknown.

Another interesting but expected observation was the age distribution of our patients. Only 22% of the individuals with AL amyloidosis were 70 years and older, while 64% of the patients with ATTR amyloidosis were in their eighth and ninth decades of life. In this respect, amyloid in endomyocardial biopsies is not much different from amyloid at other anatomical sites [14, 15, 19].

Deposition pattern

Regarding the distribution of the amyloid deposits, it was interesting to note that 83% of the biopsies with ATTR amyloid showed mostly a solely interstitial without a vascular deposition pattern. 72% of the patients with AL amyloidosis had deposits at both sites. These results are similar to those reported by Smith et al. [10] and Crotty et al. [17]. Furthermore, patients with AL amyloidosis were found to suffer from more extensive deposits (grade III in 43% of the cases) compared with ATTR amyloidosis (grade III in 29% of the specimens). Both observations, i.e. the pattern and extent of deposition, might explain the much better prognosis of patients with cardiac ATTR amyloidosis compared with those suffering from AL amyloidosis [3, 6]. However, as the size of the endomyocardial biopsies was highly variable and often very small, the risk of a sampling error has to be taken into account. Furthermore, no detailed clinical information was available from our patients. Hence, it is difficult or even impossible to draw firm conclusions with regard to the affection of the whole heart and the patient's prognosis. For this purpose, it is advisable to use clinical parameters like ventricular wall thickness, ejection fraction or NT-proBNP levels, which are also used to monitor therapeutic response in AL patients [32]. More reliable information concerning the distribution in the whole organ may be obtained from heart explants of autopsy specimens and is the focus of recent and future investigations [13, 33].

Hereditary ATTR amyloidosis

Our DNA analysis of 19 patients with ATTR amyloidosis identified five carriers of point mutations in the *TTR* gene. These cases were categorized as hereditary ATTR amyloidosis, which is the most common hereditary type. More than 90 amyloid-associated mutations of the *TTR* gene have been reported until today. Many of the encoded TTR variants show a regional accumulation, such as the p. Val30Met with a high prevalence in distinct parts of Portugal, Sweden and Japan [2, 34]. Furthermore, they show differences concerning their affinity to organs. While

some TTR variants predominantly cause familial amyloidotic polyneuropathy (FAP), there are also mutations that result in a cardiomyopathy in nearly 100% of the cases such as p.Val30Met, p.Thr60Ala, p.Ile84Ser and p.Val122Ile [6, 9, 18]. In our series, the p.Val30Met substitution was found in two patients, which is in agreement with earlier studies describing it as one of the most common mutations [7, 34]. Furthermore, this variant is known to nearly always involve the heart [9]. As expected, carriers of *TTR*-gene mutations were on average 15 years younger than carriers of two wild-type alleles. However, the patient age of hereditary and non-hereditary ATTR amyloidosis overlapped in our series in the seventh decade of life: the youngest patient suffering from senile systemic ATTR amyloidosis was 63 years and the oldest patient with hereditary ATTR amyloidosis was 70 years, being a carrier of the p.Glu54Asp exchange. Several cases of hereditary ATTR amyloidosis have now been reported with a late disease onset [18], e.g. the p.Val20Ile mutation is thought to be associated with a late-onset cardiac amyloidosis [35]. Thus, it is important to emphasize that patient age does not exclude heredity [19] and that genetic counseling should be considered independent from patient age.

Conflict of interest The authors have no conflict of interest to declare.

References

1. Merlini G, Bellotti V (2003) Molecular mechanisms of amyloidosis. N Engl J Med 349(6):583–596
2. Picken MM (2007) New insights into systemic amyloidosis: the importance of diagnosis of specific type. Curr Opin Nephrol Hypertens 16(3):196–203
3. Hoyer C, Angermann CE, Knop S et al (2008) Cardiac amyloidosis. Med Klin (Munich) 103(3):153–160
4. Röcken C, Sletten K (2003) Amyloid in surgical pathology. Virchows Arch 443(1):3–16
5. Eshaghian S, Kaul S, Shah PK (2007) Cardiac amyloidosis: new insights into diagnosis and management. Rev Cardiovasc Med 8 (4):189–199
6. Hassan W, Al-Sergani H, Mourad W et al (2005) Amyloid heart disease. New frontiers and insights in pathophysiology, diagnosis, and management. Tex Heart Inst J 32(2):178–184
7. Ikeda S (2004) Cardiac amyloidosis: heterogenous pathogenic backgrounds. Intern Med 43(12):1107–1114
8. Falk RH (2005) Diagnosis and management of the cardiac amyloidoses. Circulation 112(13):2047–2060
9. Shah KB, Inoue Y, Mehra MR (2006) Amyloidosis and the heart: a comprehensive review. Arch Intern Med 166(17):1805–1813
10. Smith TJ, Kyle RA, Lie JT (1984) Clinical significance of histopathologic patterns of cardiac amyloidosis. Mayo Clin Proc 59:547–555
11. Rahman JE, Helou EF, Gelzer-Bell R et al (2004) Noninvasive diagnosis of biopsy-proven cardiac amyloidosis. J Am Coll Cardiol 43(3):410–415
12. Vogelsberg H, Mahrholdt H, Deluigi CC et al (2008) Cardiovascular magnetic resonance in clinically suspected cardiac amyloidosis: noninvasive imaging compared to endomyocardial biopsy. J Am Coll Cardiol 51(10):1022–1030
13. Sack FU, Kristen A, Goldschmidt H et al (2008) Treatment options for severe cardiac amyloidosis: heart transplantation combined with chemotherapy and stem cell transplantation for patients with AL-amyloidosis and heart and liver transplantation for patients with ATTR-amyloidosis. Eur J Cardiothorac Surg 33 (2):257–262
14. Hv H, Mihatsch M, Lobeck H et al (2009) Prevalence and origin of amyloid in kidney biopsies. Am J Surg Pathol 33(8):1198–1205
15. Gioeva Z, Kieninger B, Röcken C (2009) Amyloidosis in liver biopsies. Pathologe 30(3):240–245
16. Collins AB, Smith RN, Stone JR (2009) Classification of amyloid deposits in diagnostic cardiac specimens by immunofluorescence. Cardiovasc Pathol 18(4):205–216
17. Crotty TB, Li CY, Edwards WD et al (1995) Amyloidosis and endomyocardial biopsy: correlation of extent and pattern of deposition with amyloid immunophenotype in 100 cases. Cardiovasc Pathol 4:39–42
18. Benson MD (1992) Hereditary amyloidosis and cardiomyopathy. Am J Med 93(1):1–2
19. Kebbel A, Röcken C (2006) Immunohistochemical classification of amyloid in surgical pathology revisited. Am J Surg Pathol 30 (6):673–683
20. Strege RJ, Saeger W, Linke RP (1998) Diagnosis and immunohistochemical classification of systemic amyloidoses. Report of 43 cases in an unselected autopsy series. Virchows Arch 433:19–27
21. Eriksson M, Büttner J, Todorov T et al (2009) Prevalence of germline mutations in the TTR gene in a consecutive series of surgical pathology specimens with ATTR amyloid. Am J Surg Pathol 33(1):58–65
22. Bergstrom J, Gustavsson A, Hellman U et al (2005) Amyloid deposits in transthyretin-derived amyloidosis: cleaved transthyretin is associated with distinct amyloid morphology. J Pathol 206 (2):224–232
23. Ihse E, Ybo A, Suhr O et al (2008) Amyloid fibril composition is related to the phenotype of hereditary transthyretin V30M amyloidosis. J Pathol 216(2):253–261
24. Baretton G, Linke RP, Löhrs U (1990) Systemische Amyloidosen. Immunhistochemische Typisierung an Autopsien mit Hilfe zahlreicher spezifischer Antikörper. Pathologe 11:71–79
25. Chastonay P, Hurlimann J (1986) Characterization of different amyloids with immunological techniques. Path Res Pract 181:657–663
26. Röcken C, Schwotzer E, Linke RP et al (1996) The classification of amyloid deposits in clinicopathological practice. Histopathology 29:325–335
27. van de Kaa CA, Hol PR, Huber J et al (1986) Diagnosis of the type of amyloid in paraffin wax embedded tissue sections using antisera against human and animal amyloid proteins. Virchows Archiv [A] 408:649–664
28. Vrana JA, Gamez JD, Madden BJ et al (2009) Classification of amyloidosis by laser microdissection and mass spectrometry-based proteomic analysis in clinical biopsy specimens. Blood 114 (24):4957–4959
29. Nilsson KP, Ikenberg K, Aslund A et al (2010) Structural typing of systemic amyloidoses by luminescent-conjugated polymer spectroscopy. Am J Pathol 176(2):563–574
30. Pellikka PA, Holmes DR Jr, Edwards WD et al (1988) Endomyocardial biopsy in 30 patients with primary amyloidosis and suspected cardiac involvement. Arch Intern Med 148(3):662–666
31. Rapezzi C, Riva L, Quarta CC et al (2008) Gender-related risk of myocardial involvement in systemic amyloidosis. Amyloid 15 (1):40–48

32. Palladini G, Campana C, Klersy C et al (2003) Serum N-terminal pro-brain natriuretic peptide is a sensitive marker of myocardial dysfunction in AL amyloidosis. Circulation 107(19):2440–2445
33. Hosch W, Kristen AV, Libicher M et al (2008) Late enhancement in cardiac amyloidosis: correlation of MRI enhancement pattern with histopathological findings. Amyloid 15(3):196–204
34. Suhr OB, Svendsen IH, Andersson R et al (2003) Hereditary transthyretin amyloidosis from a Scandinavian perspective. J Intern Med 254(3):225–235
35. Jacobson DR, Pan T, Kyle RA et al (1997) Transthyretin ILE20, a new variant associated with late-onset cardiac amyloidosis. Hum Mutat 9:83–85

Virchows Arch (2010) 456:533–541
DOI 10.1007/s00428-010-0896-6

ORIGINAL ARTICLE

Microsatellite instability of the colorectal carcinoma can be predicted in the conventional pathologic examination. A prospective multicentric study and the statistical analysis of 615 cases consolidate our previously proposed logistic regression model

Ruth Román · Montse Verdú · Miquel Calvo · August Vidal · Xavier Sanjuan · Mireya Jimeno · Antonio Salas · Josefina Autonell · Isabel Trias · Marta González · Beatriz García · Natalia Rodón · Xavier Puig

Received: 21 October 2009 / Revised: 11 February 2010 / Accepted: 17 February 2010 / Published online: 15 April 2010
© Springer-Verlag 2010

Abstract High microsatellite instability (MSI-H) allows the identification of a subset of colorectal carcinomas associated with good prognosis and a higher incidence of Lynch syndrome. The aim of this work was to assess the interobserver variability and optimize our MSI-H prediction model previously published based on phenotypic features. The validation series collected from five different hospitals included 265 primary colorectal carcinomas from the same number of patients. The eight clinicopathological parameters that integrate our original model were evaluated in the corresponding centers. Homogeneity assessment revealed significant differences between hospitals in the estimation of the growth pattern, presence of Crohn-like reaction, percentage of cribriform structures, and Ki-67 positivity. Despite this observation, our model was globally able to predict MSI-H with a negative predictive value of 97.0%. The optimization studies were carried out with 615 cases and resulted in a new prediction model RERtest8, which includes the presence of tumor infiltrating lymphocytes at the expense of the percentage of cribriform structures. This refined model achieves a negative predictive value of 97.9% that is maintained even when the immunohistochemical parameters are left out, RERtest6. The high negative predictive value achieved by our models allows the reduction of the cases to be tested for MSI to less than 10%. Furthermore, the easy evaluation of the parameters included in the model renders it a useful tool for the routine practice and can reinforce other published models and the current clinical protocols to detect the subset of colorectal

R. Román (✉) · M. Verdú · M. González · B. García · N. Rodón · X. Puig
BIOPAT. Biopatologia Molecular, SL, Grup Assistència,
Avda. Diagonal 660, planta-1,
08034 Barcelona, Spain
e-mail: rroman@biopat.es

X. Puig
Hospital de Barcelona-SCIAS,
Grup Assistència,
Barcelona, Spain

M. Verdú · A. Vidal · X. Puig
Histopat Laboratoris,
Barcelona, Spain

M. Calvo
Statistics Department, Universitat de Barcelona,
Barcelona, Spain

A. Vidal · X. Sanjuan
Department of Pathology, Hospital Universitari de Bellvitge,
Barcelona, Spain

M. Jimeno
Department of Pathology, Hospital del Mar,
Barcelona, Spain

A. Salas
Department of Pathology, Hospital Mútua de Terrassa,
Terrassa, Spain

J. Autonell
Department of Pathology, Hospital General de Vic,
Vic, Spain

I. Trias
Department of Pathology, Hospital Plató,
Barcelona, Spain

cancer patients bearing hereditary nonpolyposis colorectal cancers risk and/or MSI-H phenotype.

Keywords Microsatellite instability · Prediction model · Colorectal cancer · Pathological parameters · Hereditary nonpolyposis colorectal cancer

Introduction

The study of global genomic and epigenomic changes occurring during colorectal carcinogenesis, mainly chromosomal instability (CIN), microsatellite instability (MSI), and CpG island methylation phenotype, is allowing the classification of colorectal tumors according to their molecular status [1] and the establishment of correlations between such status and key parameters like patient's outcome and treatment response [2]. Two main alternative carcinogenic mechanisms have been proposed, the CIN and the microsatellite instability (MIN) pathways.

The most common CIN pathway, involving approximately 90% of sporadic colorectal tumors and all cases of familial adenomatous polyposis, follows the adenoma carcinoma sequence through sequential accumulation of a series of mutations at crucial regulatory genes showing frequent chromosomal gains and losses [3]. On the contrary, tumors developing through the MIN pathway show a high degree of MSI (MSI-H) [4] which is due to alterations in the mismatch repair genes (MMR), mainly MLH1, MSH2, and MSH6 [5]. These alterations can be caused by germline mutations, which give rise to hereditary nonpolyposis colorectal cancers (HNPCC) [6] or by epigenetic silencing through hypermethylation of the MLH1 promoter [7]. Patients carrying both sporadic and hereditary MIN colorectal cancers exhibit a better prognosis and a poor response to 5-fluorouracil-based chemotherapy compared to those with CIN tumors [8, 9]. It is therefore essential to distinguish between these two main types of carcinomas.

Testing for MSI or for loss of MMR in all colorectal cancer cases would be a very expensive and time-consuming task to identify only the approximately 10% of tumors following the MIN pathway. It has become clear during the last years that these tumors display common morphological characteristics such as proximal location, mucinous differentiation, solid growth pattern, presence of intraepithelial lymphocytes and Crohn's-like lymphocytic reaction which can make them distinguishable from CIN tumors [10-12].

Several studies have been reported in the literature in an effort to identify MIN status of colorectal tumors. Recently, Jenkins and colleagues [13] used pathology features described in the Bethesda guidelines to predict MSI in a group of patients diagnosed with colorectal carcinomas before age 60 with the primary aim of identifying HNPCC candidates. Also lately another model has been published by Greenson and colleagues [14] which classifies MSI-H tumors with an 85% accuracy looking at pathologic features. The objective of our work was to validate and improve with a multicentric study a logistic model based on clinicopathological features previously designed in our laboratories to predict microsatellite instability [15]. We used a nonselected population of 615 colorectal carcinomas to provide pathologists with an easy to use tool to identify a large subset of carcinomas which do not present a MSI-H status and would need no MIN analysis. The major aim of our study was to achieve a high negative predictive value which would reduce greatly the number of cases to be tested for MSI.

Materials and methods

Validation series

For our validation series, a total of 265 unselected primary colorectal cancer cases were prospectively collected from five different centers in the area of Catalonia, Spain.

Cases were evaluated by the corresponding pathologist following standard published criteria without previous specific training. Immunohistochemical analysis was also carried out at each participating center according to their own routine protocols in order to preserve interobserver heterogeneity. Histopathologic features were recorded as previously described [15]. Briefly such features included categorical and numerical variables. Categorical variables recorded were gender, tumor location, tumor configuration, extent of invasion, intramural and extramural thin-walled vessel invasion (TWVI), venous vessel invasion (VVI), perineural invasion (PNI), growth pattern, peritumoral Crohn-like reactivity which was considered positive when at least three nodular aggregates of lymphocytes were present within a single low power field (4× magnification), presence of tumor infiltrating lymphocytes (TIL) characterized by the finding of at least four intraepithelial lymphocytes in a high power field (40× magnification) [16], and presence of residual adenomas. Numerical variables evaluated were age, tumor size, number of affected lymph nodes, percentage of solid [17], mucinous, cribriform, micropapillary and microglandular patterns, as well as expression of Ki-67 and p53 by immunohistochemistry. Representative formalin-fixed paraffin-embedded blocks of paired tumor and normal tissue were then sent to our center for MSI-H prediction and MSI-H molecular analysis.

Simultaneously a prospective series of 148 cases was collected and identically assessed in our institution; this added interobserver variability and also serve to increase the global validation series.

Optimization series

The global series employed for the improvement of our prediction model included the 265 external cases from our validation series, another 146 from the prospective series evaluated in our institution, plus the 204 cases from our first study [15]. A summary of the histopathological variables of our global series is displayed on Table 1.

Microsatellite instability analysis

Genomic DNA was extracted from ten 5-μm-thick sections of paired normal and tumor samples by macrodissection of selected areas followed by a proteinase K-phenol/chloroform protocol. DNA (200 ng) were used for each specific PCR reaction after the assessment of DNA quality.

MSI status was evaluated as described previously [15], using a panel of 11 microsatellites composed by the five microsatellites from the NCI panel (BAT25, BAT26, D5S346, D2S123, and D17S250) [18] in a multiplex PCR reaction, five additional microsatellites originally aimed at detecting the LOH status of chromosome 18q (D18S55, D18S58, D18S61, D18S64, and D18S69) [19] also amplified in a multiplex reaction and a microsatellite at the TP53 locus on 17p (P53CA) [20]. Fluorescent amplicons were analyzed on an automated ABI PRISM® 310 Genetic Analyzer using the GeneScan software (PE Applied Biosystems). According to the consensus definitions of the US NCI, tumors were classified as exhibiting MSI-H when 30% or more of the tested loci resulted unstable and non-MSI-H when they were less than 30%. Tumors exhibiting low microsatellite instability (up to three unstable markers out of 11) were considered together with stable tumors.

Immunohistochemical analysis

Immunohistochemical analysis in our institution was performed by ABC immunoperoxidase staining method, using mouse monoclonal antibodies DO-7 and MIB-1 (DakoCytomation, Denmark A/S) detecting p53 and Ki-67 proteins, respectively. Positive and negative controls were included in each experiment. Immunohistochemical evaluation was conducted double-blind by scoring the estimated percentage of tumor cells showing nuclear staining.

Statistical analysis

Our previous experience with the logistic regression model [15] capable to predict very accurately MSI instability impels us to assay again this modeling approach with the multicenter data set. Our purpose is to obtain a mathematical expression in order to estimate the probability of a tumor exhibiting MSI-H according to the following equation:

$$P = 1 - \frac{1}{1 + e^{x}} \qquad (*)$$

Where P is the expected probability of MSI-H and

$$x = \beta_0 + \beta_1 x_1 + \beta_2 x_2 + \ldots + \beta_n x_n$$

is the development of the linear component of (*). β_0 is the independent term of the regression equation, β_i is the regression coefficient for the i-th explanatory variable, and x_i is the value of the i-th variable for any individual tumor. Notice that for dichotomous variables, x_i assumes value 1 or 0.

Instead of the classical stepwise regression used in our previous publication [15] we follow here a different strategy to select the variables included in the model and to estimate their coefficients. In a first stage of our current approach, we use an automatic selection procedure of the variables based on the recent developments of the statistical topic known as *shrinkage methods* for model selection. More precisely, we use the methodology *Regularization Paths for Generalized Linear Models via Coordinate Descent* described in Friedman et al. [21, 22] implemented by these authors in the glmnet package running on the R statistical environment [23]. The glmnet package does not currently provide any stopping criteria to the user, we employ in our R script the Schwartz criteria combined with the tenfold cross-validation technique. For each of the ten validation sets, where it is successively excluded 10% of the full data set, the glmnet package with the Schwartz criteria [24] select the subset of variables that must be introduced in the logistic equation among our set of 30 maximum possible explanatory candidates. Therefore, a table with the frequency of each of the possible explanatory variable included in the ten final models, one for each validation data set, can be obtained.

These results are used in the second stage of our approach, which discards, if any, variables included in less than 70% of the final models. In order to configure the final form of the equation, we take into account in this step the clinicopathological knowledge of the variables.

When the variables in the right side of the equation are definitively established, we proceed to estimate the coefficients in the logistic model and validate its predictive capability. In this third stage, we use a huge resampling approach, where the basic element consists on a random split of the full data set in two subsets. The first subset, the training set, is used to compute the coefficients of the logistic model. They are obtained also via glmnet package, with the shrinkage parameter equal to 0. Then, the predictive capability is computed on the second subset, the validation set. We repeat 1,000 times this basic procedure of random split and predictive computations on the resulting validation set in order to avoid potential biases on the results due to the random selection. We compute the average value of

Table 1 Clinicopathological variables of the global optimization series

Categorical variable	MSS (%) $n=563$	MSI-H (%) $n=52$
Gender		
Male	336 (59.7)	22 (42.3)
Female	227 (40.3)	30 (57.7)
Location		
Proximal	177 (31.4)	45 (86.5)
Distal	386 (68.6)	7 (13.5)
Configuration		
Exophytic	244 (43.3)	23 (44.2)
Ulcerated	230 (40.9)	23 (44.2)
Stenosing	89 (15.8)	6 (11.5)
Extent of invasion (pT)		
pT1	37 (6.6)	1 (1.9)
pT2	83 (14.7)	7 (13.5)
pT3	271 (48.1)	33 (63.5)
pT4	172 (30.6)	11 (21.2)
Intramural TWVI		
Present	172 (30.6)	16 (30.7)
Absent	391 (69.4)	36 (69.2)
Extramural TWVI		
Present	141 (25.0)	11 (21.2)
Absent	422 (75.0)	41 (78.9)
Intramural VVI		
Present	40 (7.1)	2 (3.8)
Absent	522 (92.7)	50 (96.2)
Extramural VVI		
Present	113 (20.1)	8 (15.4)
Absent	450 (79.9)	44 (84.6)
Intramural PNI		
Present	54 (9.6)	2 (3.8)
Absent	509 (90.4)	50 (96.2)
Extramural PNI		
Present	76 (13.5)	3 (5.8)
Absent	487 (86.5)	49 (94.2)
Growth pattern		
Expansive	193 (34.3)	32 (61.5)
Infiltrative	370 (65.7)	20 (38.5)
Crohn-like lymphoid reaction		
Present	190 (33.7)	41 (78.8)
Absent	373 (66.3)	11 (21.2)
TIL		
Present	86 (15.3)	29 (55.8)
Absent	477 (84.7)	23 (44.2)
Residual adenoma		
Present	176 (31.3)	15 (28.8)
Absent	387 (68.7)	37 (71.2)

Table 1 (continued)

Numerical variable	Mean±SD	Mean±SD
Age	69.1±11.6	69.8±12.9
Tumor size (mm)	43.2±21.1	57.5±17.1
Solid pattern (%)	5.0±12.9	23.7±35.2
Mucinous pattern (%)	9.2±20.7	32.3±32.5
Cribriform pattern (%)	4.3±10.1	12.3±19.7
Micropapillary pattern (%)	2.0±6.9	0.3±1.5
Microglandular pattern (%)	3.2±9.8	0.6±2.2
Nodal involvement (*n*)	2.0±3.7	2.2±5.7
Ki67 proliferative index (%)	62.4±21.7	72.6±17.0
p53 overexpression (%)	43.3±38.5	17.9±24.1

the coefficients and the average prediction capability of the new proposed model over the random 1,000 data sets. We compare its results to the obtained with our previous prediction model [15] using the same 1,000 validation data sets.

Results

Validation studies

The first approach to test the robustness of our original prediction model was the assessment of the homogeneity between the participating hospitals, following the model's equation:

$$P = 1 - \frac{1}{1 + e^{x}}$$

$$x = -2.648 - a \times 1.6 - b \times 1.884 - c \times 2.401 + d \times 0.045 + e \times 0.021 - f \times 0.118 + g \times 0.05 - h \times 0.029$$

Cases were assigned as MSI-H when $P>0.29$. The coefficients of the linear component (x) corresponded to: (a) location (0=proximal, 1=distal), (b) growth pattern (0=expansive, 1=infiltrative), (c) Crohn-like response (0=present, 1=absent), (d) solid pattern%, (e) mucinous pattern%, (f) cribriform pattern, (g) Ki-67%, and (h) p53 accumulation%.

Significant differences were revealed in the estimation of the expansive growth, presence of Crohn-like inflammatory response, percentage of cribriform structures, and Ki-67 expression (Table 2). Despite this interobserver discrepancies, our original model was globally able to predict MSI-H with a negative predictive value of 97.0%, reducing the number of cases to be tested for MSI to just 11%. The results obtained with our own prospective series were equivalent, achieving a negative predictive value of 97.8% and did not differ from those obtained in the initial study where the negative predictive value was 97.8%. Accuracy, sensitivity, specificity, positive, and negative predicted values of the three series are shown in Table 3.

Optimization studies

Out of the 615 colorectal carcinomas included in our global series, 52 (8.5%) exhibited MSI-H. The clinicopathological variables of this series are illustrated in Table 1. The *glmnet* cross-validation analysis carried out with the global series, involving a total of 1,000 random data sets, found that tumor location, percentage of solid and mucinous components, presence of Crohn-like response and TIL were strongly associated with the MSI status being present in 976 to 1,000 of the generated models. The growth pattern included in 715 models and the expression of Ki-67 (in 592) and p53 (in 651) were also considered to be predictive of the MSI status and thus included in our optimized model, named RERtest8:

$$P = 1 - \frac{1}{1 + e^{x}}$$

$$x = 2.925 + a \times 1.563 + b \times 1.034 + c \times 1.426 + d \times 0.588 - e \times 0.046 - f \times 0.028 - g \times 0.031 + h \times 0.021$$

The coefficients of the linear component (x) corresponded to: (a) location (0=proximal, 1=distal), (b) growth pattern (0=expansive, 1=infiltrative), (c) Crohn-like response (0=present, 1=absent), (d) TIL%, (e) solid pattern%, (f) mucinous pattern%, (g) Ki-67%, and (h) p53 accumulation%.

Comparing these data with our original model, it should be noted that TIL has been included in the equation at the expense of the proportion of cribriform pattern which has been left out of the optimized model. Table 4 shows the accuracy,

Table 2 Homogeneity assessment between the five participating hospitals

	Center 1	Center 2	Center 3	Center 4	Center 5	*p* value
Proximal	6	12	18	42	26	0.33
Distal	4	15	42	58	42	
Infiltrative	6	4	37	44	26	**<0.001**
Expansive	4	23	23	56	50	
Crohn-like						
Present	1	11	15	69	17	**<0.001**
Absent	9	16	45	31	51	
Solid pattern (%)	–	5.7	1.2	1.2	6.5	0.20
Mucinous pattern (%)	–	11	10	10	6.5	0.81
Cribriform pattern (%)	–	25	17	11	18	**<0.001**
Ki-67 proliferative index (%)	–	68	69	67	78	**0.004**
p53 expression (%)	–	40	55	43	47	0.32

Significant differences are highlighted in bold

sensitivity, specificity, positive, and negative predicted values achieved by the optimized model. Considering that the expression of Ki-67 and p53 by immunohistochemistry were the variables with a weaker relation to the MSI status and were also the only parameters that could not be determined just by morphology assessment, a second alternative model was constructed that excluded these two variables, RERtest6:

$$P = 1 - \frac{1}{1 + e^{x}}$$

$$x = 1.114 + a \times 1.523 + b \times 1.046 + c \times 1.591 + d \times 0.893 - e \times 0.042 - f \times 0.031$$

The coefficients of the linear component (x) corresponded to: (a) location (0=proximal, 1=distal), (b) growth pattern (0=expansive, 1=infiltrative), (c) Crohn-like response (0=present, 1=absent), (d) TIL%, (e) solid pattern%, (f) mucinous pattern%.

The statistical parameters of this alternative model are also shown in Table 4. A probability value of a tumor being MSS lower than 80% ($P<0.8$) was empirically set as a cutoff point to discriminate between MSI-H and MSS tumors with both models. Figure 1 shows representative pictures of the histological parameters finally included in our optimized model RERtest6, and Fig. 2 shows the ROC curves of the optimized models RERtest8 and RERtest6 compared to that of our original model.

Discussion

The complexity and cost of the MSI study added to the increasing availability of tailored therapies, and screening programs has triggered the development of models based on pathological features to predict instability status. The model that we had published [15] and has now been further validated, focus on a non-selected population of patients with colorectal cancer aiming at identifying not only possible Lynch syndrome candidates, but any carcinomas exhibiting an MSI-H phenotype and thus a better prognosis.

The multicenter validation carried out with samples from five different centers has proved that our original model was robust enough to overcome not only interobserver variability but also differences between the immunohistochemistry methods employed.

The optimization studies with a global series of 615 colorectal carcinomas gave rise to an improved model, RERtest8, in which the percentage of cribriform structures was left out of the equation while the presence of TIL was included. This new model is in closer concordance with other recently published models where proximal tumor location, presence of TIL, Crohn-like reaction, mucinous component, and poor differentiation were assigned as predictors of MSI status [13, 14]. Nevertheless, there are important differences to be pointed out. The MsPath score published by Jenkins and colleagues [13] looks at the pathology features high-

Table 3 Statistical parameters achieved in our initial study, validation set, and prospective set

	Initial study	Validation set	Our Prospective set
Accuracy	95.10	91.32	91.41
Sensitivity	77.78	66.67	83.33
Specificity	96.77	93.44	92.41
Positive predictive value	70.00	46.67	57.69
Negative predictive value	97.83	97.02	97.81
Total (n)	204	265	148

Table 4 Statistical parameters achieved with our optimized models, with and without including immunohistochemistry parameters

	RERTest8	RERTest6
Accuracy	92.48	92.09
Sensitivity	78.14	78.01
Specificity	93.80	93.39
Positive predictive value	53.45	51.78
Negative predictive value	97.93	97.91
Total (n)	615	615

lighted by Bethesda guidelines in a series of colorectal carcinomas diagnosed before age 60 with the main aim of identifying Lynch syndrome candidates. The study published by Greenson and colleagues [14], even though it does not restrict its series by the patient's age, finds age under 50 to be the only independent predictor of MSI-H status and includes this parameter as the second most influencing after TIL in the equation of their Pathscore. In contrast, we have not found age to be predictive of the MSI status neither in our initial multivariate logistic analysis nor in our current optimized model. This may be due to the high mean age of patients in our series 69.2. This high mean age could also be an explanation for the low percentage of MSI-H cases found in our study (8.5%), compared to other series described in literature (10–15%), [1] since HNPCC patients typically have an early onset of the illness.

The impact of each of the parameters included also varies between models. Proximal tumor location and presence of peritumoral Crohn-like inflammatory response are the strongest predictive parameters in our RERtest8 model followed by expansive growth pattern and TIL. The expansive growth pattern was not included in the other above-mentioned models, although it was found to be a MSI predictor by univariate analysis in the study of

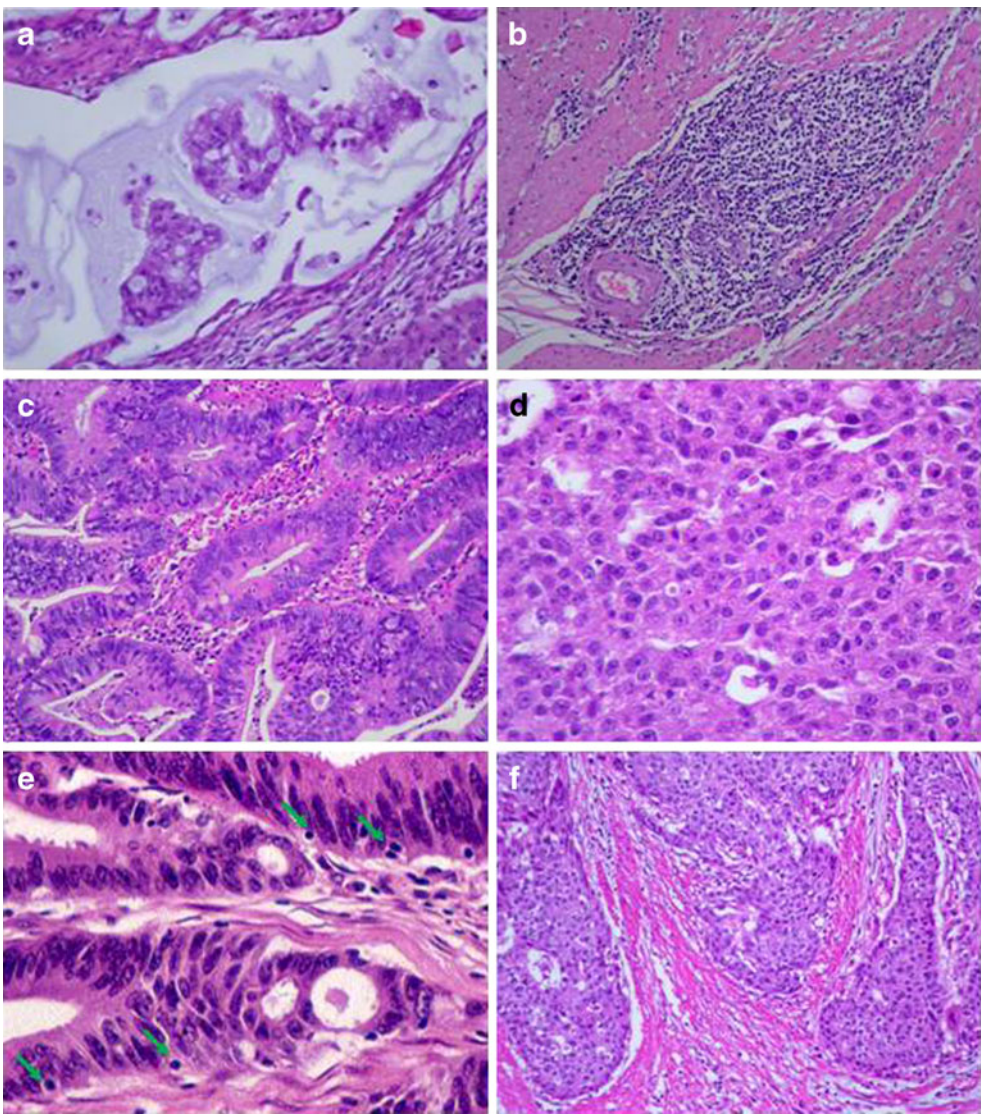

Fig. 1 Histological parameters included in our optimized model RERtest6. **a** Adenocarcinoma with extracellular mucinous pattern (H&E, 400x). **b** "Crohn like" inflammatory response (H&E, 200x). **c** Adenocarcinoma without solid pattern (H&E, 200x). **d** 100% solid pattern (H&E, 400x). **e** Tumor infiltrating lymphocytes (TIL) (H&E, 400x). **f** Expansive growth in tumoral margin (H&E, 200x)

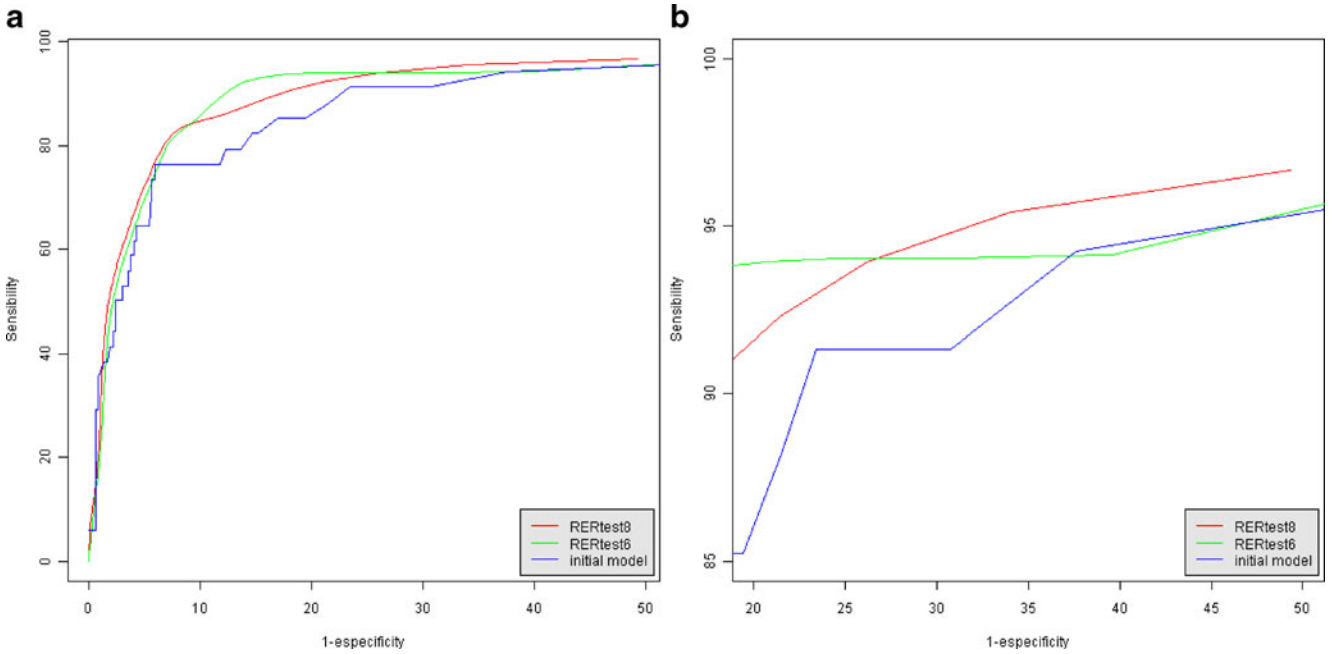

Fig. 2 **a** ROC curves of the optimized and original models and **b** *enlarged view* of the area of interest

Greenson. The grade of differentiation was assessed and integrated in our model by looking at the percentage of solid component (Fig. 1c, d). The presence of mucinous pattern was also measured as a percentage in order to better adjust its influence, since the mean of the mucinous pattern found in our MSI-H group was as low as 32.3%. The two immunohistochemistry parameters, p53 expression and Ki-67 proliferative index, were the weakest factors incorporated in our RERtest8, this together with the fact that they are the only parameters that are not morphological allowed us to reconstruct our model excluding them, the RERtest6 model.

The general approach of our optimization studies was to maximize the negative predictive value of our models in order to construct a tool that would allow the reduction of cases to be

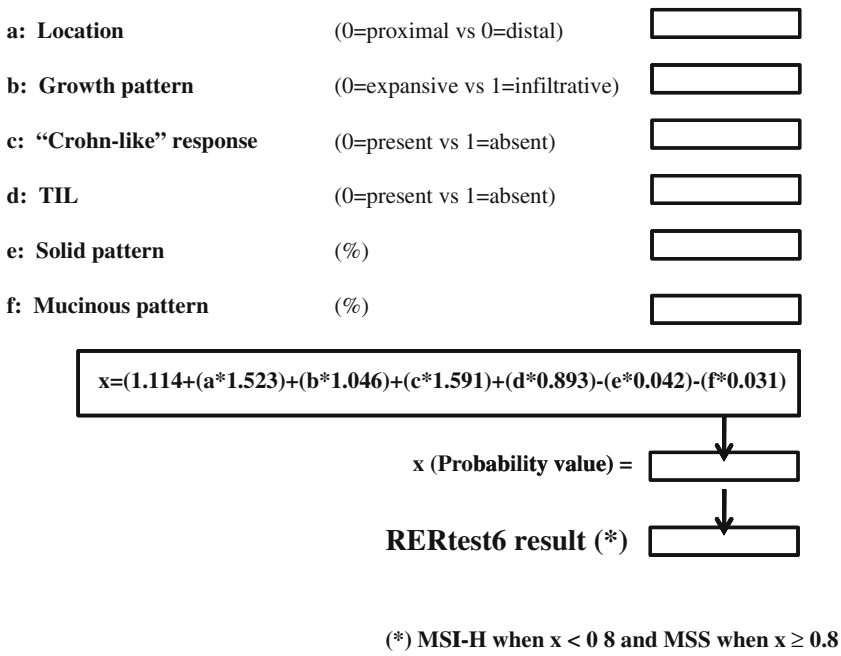

Fig. 3 RERtest6 Model in Microsoft's Excel format. As shown, the pathologist assessing the case should include either *0* or *1* in the cells corresponding to categorical variables (**a–d**) and the percentage of solid or mucinous component in cells **e** and **f**. The model's formula result is calculated in a separate cell, and in the last cell the case is classified as MSS or MSI-H depending on the *x* value

tested for MSI and could be easily implemented in an Excel document for daily use (Fig. 3). In this way, we present two models RERtest8 and RERtest6, with and without immunohistochemistry parameters, with negative predictive values of 97.9% that allow the reduction of the cases to be tested for MSI to approximately 10%; we proposed that only those cases predicted as MSI-H should be confirmed as such. Furthermore, the easy evaluation of the parameters included in the models, the fact that it is not influenced by interobserver variability and the possibility of excluding immunohistochemistry parameters, renders it a very useful tool for the routine practice and can reinforce the current clinical protocols to detect the subset of colorectal cancer patients bearing MSI-H phenotype, and thus a better prognosis, and HNPCC risk.

Acknowledgment The authors thank Eva Torija from BIOPAT for her secretarial assistance in data collection.

Conflict of interest statement We declare that we have no conflict of interest.

References

1. Ogino S, Goel A (2008) Molecular classification and correlates in colorectal cancer. J Mol Diagnostics 10:13–27, s.l
2. Gryfe RH, Kim H, Hsieh ET (2000) Tumor microsatellite instability and clinical outcome in young patients with colorectal cancer. N Engl J Med 342:69–77, s.l
3. Fearon ER, Volgestein B (1990) A generic model for colorectal tumorigenesis. Cell 61:759–767
4. Thibodeau SN, Bren G, Schaid D (1993) Microsatellite instability in cancer of proximal colon. Science 260:816–819, s.l
5. Jass JR, Do KA, Simms LA (1998) Morphology of sporadic colorectal cancer with DNA replication errors. Gut 42:673–679, s.l
6. Fujiwara T, Stolker JM, Watanabe T et al (1998) Accumulated clonal genetic alterations in familial and sporadic colorectal carcinomas with widespread instability in microsatellite sequences. Am J Pathol 153:1063–1078, s.l
7. Herman JG, Umar A, Polyak K et al (1998) Incidence and functional consequences of hMLH1 promoter hypermethylation in colorectal carcinoma. Proc Natl Acad Sci 95:6870–6875, s.l
8. Arnold CN, Goel A, Boland CR (2003) Role of hMLH1 promoter hypermethylation in drug resistance to 5-fluorouracil in colorectal cancer cell lines. Int J Cancer 106:66–73, s.l
9. Ribic CM, Sargent DJ, Moore MJ et al (2003) Tumor microsatellite-instability status as a predictor of benefit from fluorouracil-based adjuvant chemotherapy for colon cancer. N Engl J Med 349:247–257
10. Jass JR (2004) HNPCC and sporadic MSI-H colorectal cancer: a review of the morphological similarities and differences. Familial Cancer 3:93–100, s.l
11. Kakar S, Aksoy S, Burgart LJ, Smyrk TC (2004) Mucinous carcinoma of the colon: correlation of loss of mismatch repair enzymes with clinicopathologic features and survival. Mod Pathol 17:696–700
12. Ogino S, Brahmandam M, Cantor M et al (2006) Distinct molecular features of colorectal carcinoma with signet ring cell component and colorectal carcinoma with mucinous component. Mod Pathol 19:59–68, s.l
13. Jenkins MA, Hayashi S, O'Shea et al (2007) Pathology features in Bethesda guidelines predict colorectal cancer microsatellite instability: a population-based study. Gastroenterology 133:48–56
14. Greenson JK, Huang S, Herron C et al (2009) Pathologic predictors of mirosatellite instability in colorectal cancer. Am J Surg Pathol 33:126–133
15. Colomer A, Erill N, Vidal A et al (2005) A novel logistic model based on clinicopathological features predicts microsatellite instability in colorectal carcinomas. Diagn Mol Pathol 14:213–223
16. Michael-Robinson JM, Biemer-Huttmann A, Purdie DM et al (2001) Tumour infiltrating lymphocytes and apoptosis are independent features in colorectal cancer stratified according to microsatellite instability status. Gut 48:360–366
17. Hamilton SR, Aaltonen LA (2000) Pathology and genetics of tumours of the digestive system. eds World Health Organization Classification of Tumors, IARC Press, Lyon, pp 103–143
18. Boland CR, Thibodeau SN, Hamilton SR et al (1998) A National Cancer Institute Workshop on microsatellite instability for cancer detection and familial predisposition: development of international criteria for the determination of microsatellite instability in colorectal cancer. Cancer Res 58:5248–5257
19. Jen J, Kim H, Piantadosi S et al (1994) Allelic loss of chromosome 18q and prognosis in colorectal cancer. N Engl J Med 331:213–221
20. Jones MH, Nakamura Y (1992) Detection of loss of heterozygosity at the human TP53 locus using a dinucleotide repeat polymorphism. Genes Chromosom Cancer 5:89–90
21. Friedman J, Hastie T, Tibshirani R (2008) Glmnet: Lasso and elastic-net regularized generalized linear models: http://www-stat.stanford.edu/~hastie/Papers/glmnet.pdf
22. Friedman J, Hastie T, Höfling H, Tibshirani R (2007) Pathwise coordinate optimization. Ann Appl Stat 1(2):302–332
23. R Development Core Team. R (2008) A language and environment for statistical computing. s.l.: R Foundation for Statistical Computing, Vienna, Austria. ISBN 3-900051-07-0, URL http://www.R-project.org
24. Schwarz G (1978) Estimating the dimension of a model. Ann Stat 6:461–464

Virchows Arch (2010) 456:543–560
DOI 10.1007/s00428-010-0883-y

ORIGINAL ARTICLE

Decidual vascular patterns in first-trimester abortions

Yuri Musizzano · Ezio Fulcheri

Received: 12 May 2009 / Revised: 11 January 2010 / Accepted: 11 January 2010 / Published online: 16 February 2010
© Springer-Verlag 2010

Abstract In many cases of early spontaneous abortion (ESA), no reasonable etiology can be documented. However, some of these cases show abnormal decidual vessels that could be overlooked when examined on hematoxylin and eosin (H&E) slides alone. Diagnostic accuracy could be improved by the use of a limited histochemical (HC) and immunohistochemical (IHC) panel. We reviewed 1,095 ESAs, selecting 176 cases with abnormal decidual vessels and subclassifying them into three groups on the basis of decidual vascular pattern. Various HC and IHC stainings were performed in order to assess their use in improving diagnostic sensitivity. Histological findings on H&E were recorded and compared to the results obtained with HC and IHC. A variable role in the improvement of morphologic details was demonstrated for all three tested HC stainings (periodic acid–Schiff, Masson's trichrome, Weigert's stain for fibrin) and for two of the IHC markers (smooth muscle actin, human placental lactogen). In many cases of ESA, only compatibility diagnoses can be formulated. However, using a limited panel of HC and IHC stainings, some significant findings can be more reliably reported, allowing the pathologist to acquire confidence in his routine diagnostic work.

Keywords Abortion · Luteal defect · Autoimmune diseases · Histopathological diagnosis

Y. Musizzano · E. Fulcheri
Anatomic Pathology, University of Genoa,
Genoa, Italy

E. Fulcheri (✉)
Istituto di Anatomia Patologica,
Via De Toni, 14,
16132 Genoa, Italy
e-mail: ezio.fulcheri@unige.it

Background

Early spontaneous abortion (ESA) is defined as the premature expulsion of the conceptus, occurring during the embryonic period, up to the end of the eighth developmental week (corresponding to ten gestational weeks) [1]. However, for practical purposes, it seems useful to consider as ESAs all miscarriages occurring in the first trimester of pregnancy, i.e., those presenting until the 90th day (12 weeks and 6 days) of pregnancy. According to this definition, ESA is the outcome of up to 14% of pregnancies [2], and in up to 2% of pregnant women, at least three consecutive miscarriages have occurred, leading to a diagnosis of recurrent abortion [3].

Unfortunately, in the ESA pathology, inconclusive diagnoses are still made, and too many reports are actually nondiagnostic, since they merely describe the presence of decidua and chorionic structures following miscarriage. Obviously, this reality is heterogeneous, and the quality of the reports depends on the competence of any given laboratory or pathologist; usually, even the institutions most accurately reporting ESA specimens tend to readily reach a reliable diagnosis in cases showing morphological features known to be the expression of well-defined pathologies, such as maternal infections, detachments, hemorrhages, and frank chromosomal abnormalities (seen in roughly 50% of ESAs). Pathologic findings in genetic ESAs are seen mainly in the chorionic plate—even in absence of cytogenetic tests—while infections usually manifest as significant inflammatory infiltrate in the ovum (villitis, intervillitis, chorioamnionitis, funisitis) as well as in the decidua (endometritis).

Unfortunately, a gray zone remains where the level of diagnostic accuracy results very low if compared to the international standards accepted in the investigation of

other organs of systems, so that in a large amount of abortion cases no obvious cause can be identified.

In some instances, this happens because diagnostic features, although standardized, need a specialist approach; in other cases, findings are subtle, inapparent, or ambiguous, so that even an expert embryopathologist is unable to reach a reliable diagnosis. Moreover, different pathologies show similar and frequently overlapping morphologies, thus affecting a histopathological report's feasibility and objectivity.

In our opinion, a number of ESAs could be explained by accurate histopathological investigation of decidual vessels. Recent investigations about the implantation process have pointed out the role of extravillous trophoblast cells (EVTs) invading the decidua [4–9]: in choriodecidual specimens from normal pregnancies (e.g., in specimens from voluntary termination of pregnancy), three different EVT cell populations may be seen [10], namely: (1) cell islands covering the villi, (2) cell columns migrating through the decidual stroma toward the spiral arteries, and (3) scattered cells in the lumen of converted decidual arteries (Fig. 1). Any modification in this equilibrium can be considered to be pathologic. In normal decidual specimens, spiral arteries in the basal decidua appear dilated, with thin walls and EVTs around and inside the lumen: this is the so-called physiologic conversion of decidual vessels. The stroma, in turn, shows characteristic features of decidual transformation, i.e., large eosinophilic, glycogen-rich endometrial stromal cells.

Conversely, some ESA specimens show unconverted decidual vessels (UDVs), lacking intravascular EVTs. These cases are probably caused by insufficient progestinic support [11, 12], and in the present work we will call them Group 1 ESAs. Otherwise, decidual vascular walls appear thickened owing to a number of physiopathologic factors; in the 2004 edition of the AFIP Atlas of Placental Pathology [13], the chapter "Decidual vasculopathy" (DV) lists two different histopathologic pictures, namely, acute atherosis (AA) and hypertrophic decidual vasculopathy (HDV). Briefly, the former roughly resembles atherosclerosis, its histopathologic hallmarks being infarct, fibrinoid necrosis, and thrombosis, while the latter essentially is represented by concentric hypertrophy of arterial walls. AA and HDV may be responsible for pregnancy wastage linked to a wide range of pathophysiologic abnormalities, such as persistent responsiveness to vasospasm owing to preserved muscularis, villous infarct arising in thrombosed vessels, and post-ischemic rupture of the necrotic vascular wall [14]. HDV is more likely caused by hypertensive or dismetabolic pathogenesis (so much so that it is often compared to atherosclerotic lesions, as confirmed by ultrastructural investigations [15]), while AA is believed to underlie the decidual vascular pathology which may be seen in autoimmune diseases. Indeed, AA is sometimes compared to acute vascular rejection in transplanted kidney [16].

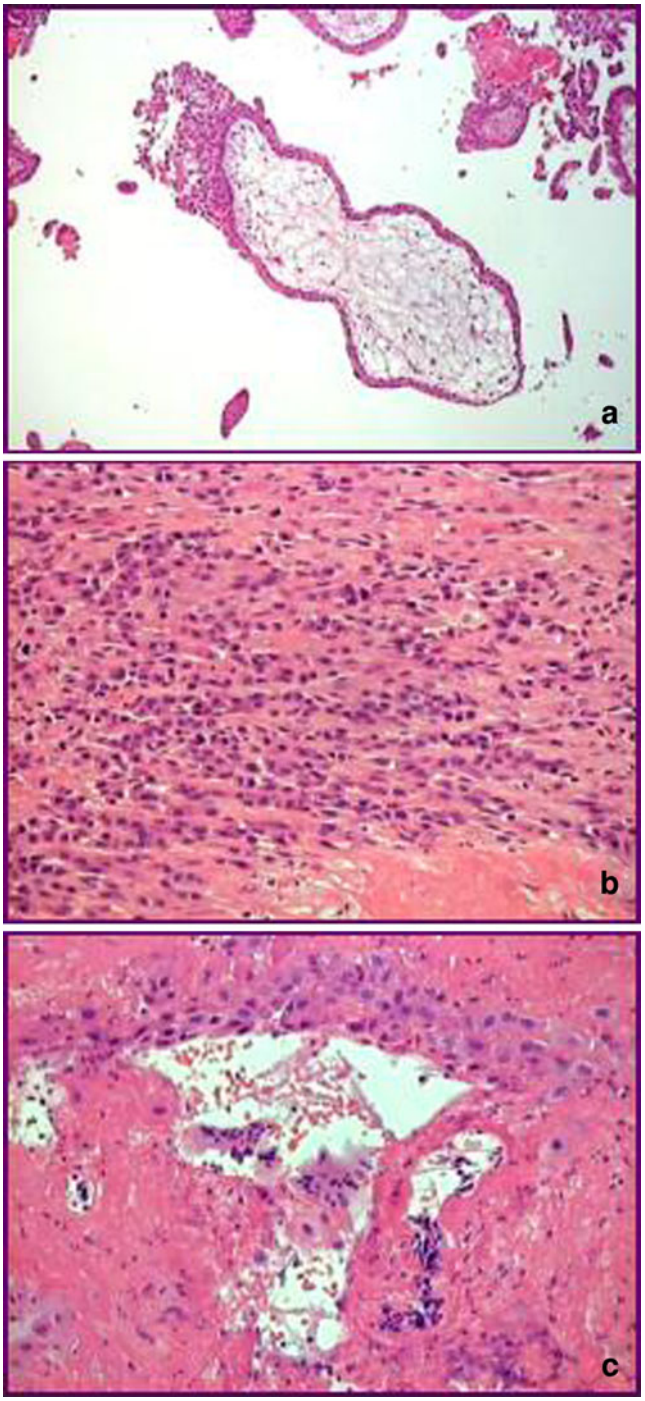

Fig. 1 Extravillous trophoblast (EVT) cell populations: cells islands covering the villi (**a**), cell columns migrating through the decidua (**b**), and cells invading maternal vascular endothelium (**c**); (modified from Prada et al. [10])

On the basis of histopathological findings alone, a group of ESAs (Group 2A in our study) could be assumed to more probably depend on autoimmune maternal diseases [17,

18], while those histologically showing decidual vasculopathy (Group 2B) could be assumed to relate to other pathophysiologic processes, e.g., hypertension. However, the distinction between these two entities, if any, is very fuzzy and nothing more than a probable diagnosis can be made. Hence, for the purposes of this work, while we analyzed them separately, in the end we preferred to include both conditions in a larger group of cases sharing histopathological features of vascular damage (Group 2).

In a routine pathology setting, differential diagnosis between decidual vessels, which are unconverted ab initio, and spiral arteries, which underwent physiologic conversion prior to be damaged, can be difficult for at least three reasons. Firstly, in hematoxylin–eosin (H&E) slides, at low magnification, both conditions seem to share abnormally thickened vascular walls in the basal decidua, near to the maternal–fetal interface marked by the Nitabuch's stria (normally thick and well defined). Secondly, Group 2 ESAs (both 2A and 2B) often show aspecific or misunderstood histopathologic lesions. Thirdly, diagnosis of "histopathological picture suggestive of luteal defect," when feasible, is still made on the basis of ill-defined criteria, such as "inadequate endometrial decidualization."

In this work, we have attempted to list those findings which could be used as differential diagnostic features in the investigation of ESAs characterized by abnormal decidual vessels. Subsequently, we have reviewed different common histopathologic and immunohistochemical stainings that could be useful in the diagnosis of ESA, evaluating the applicability of any method. Our results could be of value in routine diagnostics, making examinations easier with the employment of common and easy stainings and by contributing to the formulation of a diagnostic flow chart.

Materials and methods

We reviewed all specimens from ESAs which occurred in the University Obstetrics and Gynaecology Unit and subsequently underwent histopathological examination in our Anatomic Pathology Institute from January 2005 to December 2008.

Gestational age was never higher than 90 days (13th gestational week, i.e., 12 weeks and 6 days), and ESAs occurring earlier than 7 gestational weeks were not considered in this study. Endometrial curettages following incomplete expulsion and prolonged retention of the products of the conception were rejected from this series in order to select only cases of recent abortion caused by detachment/hemorrhage leading to the death of the conceptus during the 24–48 h preceding the extraction. This was made to minimize the risk of artifacts due to prolonged exposition to the uterine microenvironment (i.e., autolysis, secondary inflammation of the retained conceptus).

Treatment of the material

ESA specimens were received fresh or fixed in formalin (e.g., "weekend miscarriages"), and a gross description was given, following the protocol used in our institution. All cases featuring a readily recognizable gestational sac and/or embryo or fetus were immediately investigated with a dissection stereomicroscope: features of the gestational sac (including villous morphology) and the embryo or fetus (including fetal adnexa) were described and encoded following the above-mentioned protocol [19, 20]. Whenever embryonic material was received in small fragments, careful examination of the specimen was performed, looking for parts of embryo and picking them up. Recognizable parts of decidua were cut in large strips, and parts of the chorionic plate were sampled by unfolding the fragments without cutting them. Specimens were routinely fully sampled or, alternatively, until four biocassettes were filled; additional samples were taken from embryo or gestational sac when detected.

Curettage samples were fixed for 12–24 h in 10% buffered formalin, processed, and paraffin embedded. From each block, 4-μm-thick histologic sections were obtained and routinely stained with H&E.

Histochemistry and immunohistochemistry

All non-chromosomic, noninfectious cases diagnosed as suggestive of luteal defect (Group 1), of autoimmune diseases (Group 2A), or consistent with decidual vasculopathy (Group 2B) were reviewed, performing histochemistry and immunohistochemistry to investigate the histochemical and immunohistochemical phenotype of decidual vessels in normal and pathologic conditions (Table 1).

Basic histochemical stainings

Periodic acid–Schiff (PAS) was performed in order to evaluate decidual stromal cells, which in normal pregnancies appear large, eosinophilic, and glycogen-rich; therefore, well-decidualized stromal cells were expected to show strongly PAS-positive cytoplasm.

Masson's trichrome stain (MT), which selectively makes fibrous tissues go green, was expected to give more accurate morphologic details about the mesenchymal component of vascular walls, thus highlighting fibrosis or sclerosis, if any.

Weigert's stain for fibrin (WF) stains the areas of fibrin deposition blue, and it is useful in cases of suspected acute atherosis due to the presence of fibrinoid necrosis of the vessels. Therefore, it was expected to provide evidence of

Table 1 Histochemical and immunohistochemical stainings performed (left) and their expected targets in the investigation of ESA specimens (right)

Basic histochemical stainings	
Periodic acid–Schiff	Stromal decidualization of the endometrium
Masson's trichrome stain	Fibrosis and status of vascular walls
Weigert's stain for fibrin	Fibrinoid deposition in vascular walls
Basic immunohistochemical stainings	
Vimentin	Fibroblasts
α-Smooth muscle actin	Smooth muscle cells, myofibroblasts
Desmin	Fibroblasts, myofibroblasts
CD31	Endothelial vascular cells (lymphatic and blood vessels)
CD34	Endothelial vascular cells (blood vessels)
β-hCG	(Extravilllous) trophoblast
Placental lactogen	(Extravilllous) trophoblast

atherosis or, otherwise, to rule it out in cases with amorphous vascular wall thickening.

Basic immunohistochemical stainings

A broad immunohistochemical panel was performed on formalin-fixed, paraffin-embedded, 4-μm-thick slides. A standard avidin–biotin complex (ABC) technique was employed for all immunostains; antibodies were optimized for use on an automated slide stainer in combination with Ventana detection kits; hence, no reconstitution, mixing, dilution, or titration was required, except for human placental lactogen (hPL). Pretreatment (enzymatic or in microwave) was performed for vimentin, desmin, CD31, and CD34 as well as endogenous biotin blocking for vimentin, CD31, CD34, and hPL. Signal amplification was required for CD31 alone. Finally, all slides were counterstained with hematoxylin for 4 min. Antibodies and their technical details are listed in Table 2.

Vimentin is largely expressed by mesenchymal-derived cells; hence, appropriate immunohistochemistry was performed to point out the structure of vascular walls and the fibroblastic component [21]; it was believed to provide an easily evaluable overview of both vascular and stromal architecture of the decidua.

α-Smooth muscle actin (α-SMA) is expressed mainly by smooth muscle cells and myofibroblasts. Anti-α-SMA immunohistochemistry was performed in order to evaluate the status of the muscularis propria in vascular walls [21, 22]; physiologically converted decidual vessels normally show thinned and fragmented muscular wall or lack it at all. Moreover, α-SMA is expressed by human decidual stromal cells (DSCs), which appear as myofibroblast-like cells. Based on recent studies, IL-10 relaxes DSCs by reducing α-SMA inclusion into their stress fibers and therefore by decreasing its expression. This relaxing activity may be of relevance for the maintenance of pregnancy; [23] however, this aspect was not covered by our study, which focused on decidual vascular findings.

Desmin [24] is usually expressed by smooth muscle cells, mesothelial cells, myoblasts, myofibroblasts (showing variable reactivity) [21], and by the endometrium (focally reactive). Anti-desmin antibodies, together with anti-smooth muscle actin, were expected to improve the evaluation of the muscularis and to be of help in recognizing myofibroblasts [25]. The latter are fibroblasts expressing features of smooth muscle differentiation and taking part in the growth, development, and repair of normal tissues as well as in diseases of many different organs. Even in decidual vessels, myofibroblasts may be seen as a consequence of adaptive modification of fibroblasts, which acquire α-SMA; it is a ubiquitous cellular tissue repair mechanism, since myofibroblasts are involved in adventitia remodeling (e.g., in coronaries, they may contribute to neointima growth after balloon-induced injury [26]).

Endothelial vascular markers, antibodies directed against two molecules expressed by endothelial vascular cells, namely *CD31* (marking both blood and lymphatic vessels) and *CD34* (specific for blood vessels), were used to more accurately identify decidual microvessels and capillaries and to assess the status of vascular endothelia.

Human placental lactogen is routinely employed in our institute during the investigation of miscarriage/abortion specimens [27]. It is a sensitive and specific trophoblast marker, which usually identifies all three EVT cell populations; hence, it allows assessment of whether physiologic conversion has taken place. In this study, we employed NCL-PLp, a rabbit polyclonal antibody specific for hPL, obtained from placental lactogen isolated from human placenta. It stains the membrane and cytoplasm of syncytiotrophoblast cells, and it is useful for hPL detection in the placenta and in cells showing trophoblastic differentiation. NCL-PLp was incubated for 60 min at 25°C at 1:200 dilution, performing standard ABC technique in a Benchmark automatic immunostainer.

Human chorionic gonadotropin-beta (β-hCG) is selectively expressed in trophoblast cells, and anti-hCG immu-

Table 2 Immunohistochemical panel including technical data for any staining

Immunostain	Primary Ab (clone)	Source	Code	Dilution	Pretreatment	Incubation	Biotin blocking	Amplification
Vimentin	Confirm™ anti-vimentin (V9)	Ventana®	790-2917	RTU	EDTA buffer (pH8.0) for 30 min at 100°C	16 min at 37°C	Yes	No
α-SMA	Anti-smooth muscle actin (1A4)	Ventana®	760-2833	RTU	No	60 min at room temperature	No	No
Desmin	Confirm™ anti-desmin (NCL-DE-R11)	Ventana®	760-2513	RTU	Protease 1 for 4 min	32 min at 37°C	No	No
CD31	Anti-CD31 (JC/70A)	Ventana®	760-2619	RTU	EDTA buffer (pH8.0) for 60 min at 100°C	32 min at 37°C	Yes	Yes
CD34	Confirm™ anti-CD34 (QBEnd/10)	Ventana®	790-2927	RTU	EDTA buffer (pH8.0) for 30 min at 100°C	28 min at 37°C	Yes	No
hPL	NCL-PLp	Novocastra™	–	1:500	EDTA buffer (pH8.0) for 30 min at 100°C	60 min at 25°C	Yes	No
β-hCG	Anti-hCG	Ventana®	760-2650	RTU	No	8 min	No	No

α-SMA alpha-smooth muscle actin, *hPL* human placental lactogen, *β-hCG* human chorionic gonadotropin-beta, *RTU* ready-to-use formulation, *EDTA* ethylenediaminetetraacetic acid

nohistochemistry was performed, in combination and for comparison with anti-hPL. It was not expected to mark EVTs.

Data processing

Patient's age, ethnic group, and main clinical data provided by our Obstetrics and Gynaecology Unit were recorded, focusing on amenorrhea dating and obstetric clinical history. In the heterogeneous group of ESA specimens featuring abnormal decidual vessels, we compared clinical and histopathological data of cases attributed to luteal defect (Group 1) on the basis of morphological evaluation to those of ESAs showing truly vasculopathic decidual lesions (Groups 2A and 2B).

All histological elementary lesions were described using the microscopic examination protocol in use in our institute (Fig. 2). In particular, adequacy was assessed, based on the presence of basal and parietal decidua [28, 29] and on the presence of significant chorionic plate portions. Cases lacking basal decidua or with very small chorionic plate portions (e.g., limited to only a few villi) were considered inadequate. The most common histopathological features were recorded with regard to gestational age; clinical and histological data were recorded and analyzed using Microsoft® Excel software.

Histochemical and immunohistochemical results were assessed in terms of usefulness in routine diagnostics, by considering the role of these stainings in increasing sensitivity and specificity. Diagnostic usefulness of each staining was then discussed.

Two quantitatively different but qualitatively similar control populations were selected. In order to compare clinical data, all cases already diagnosed as primarily caused by infectious/inflammatory processes ("I-ESAs" in this study) were selected and clinically re-evaluated. Among the latter, 72 cases were drawn using a series of casual numbers generated in Microsoft® Excel, histopathologically reviewed and used for morphological comparison ("Controls"). This population was designed to provide a group roughly as large as the two largest groups of cases (Group 1—71 patients and Group 2A—74 patients).

Results

Prevalence of decidual vascular abnormalities

We retrospectively reviewed 1,095 ESAs that occurred in 14- to 56-year-old women (mean age, 34.3 years), in 16.1% of cases showing decidual vascular abnormalities. Among the latter, 71 cases morphologically suggestive of inadequate progestinic support were included in Group 1 (6.5%

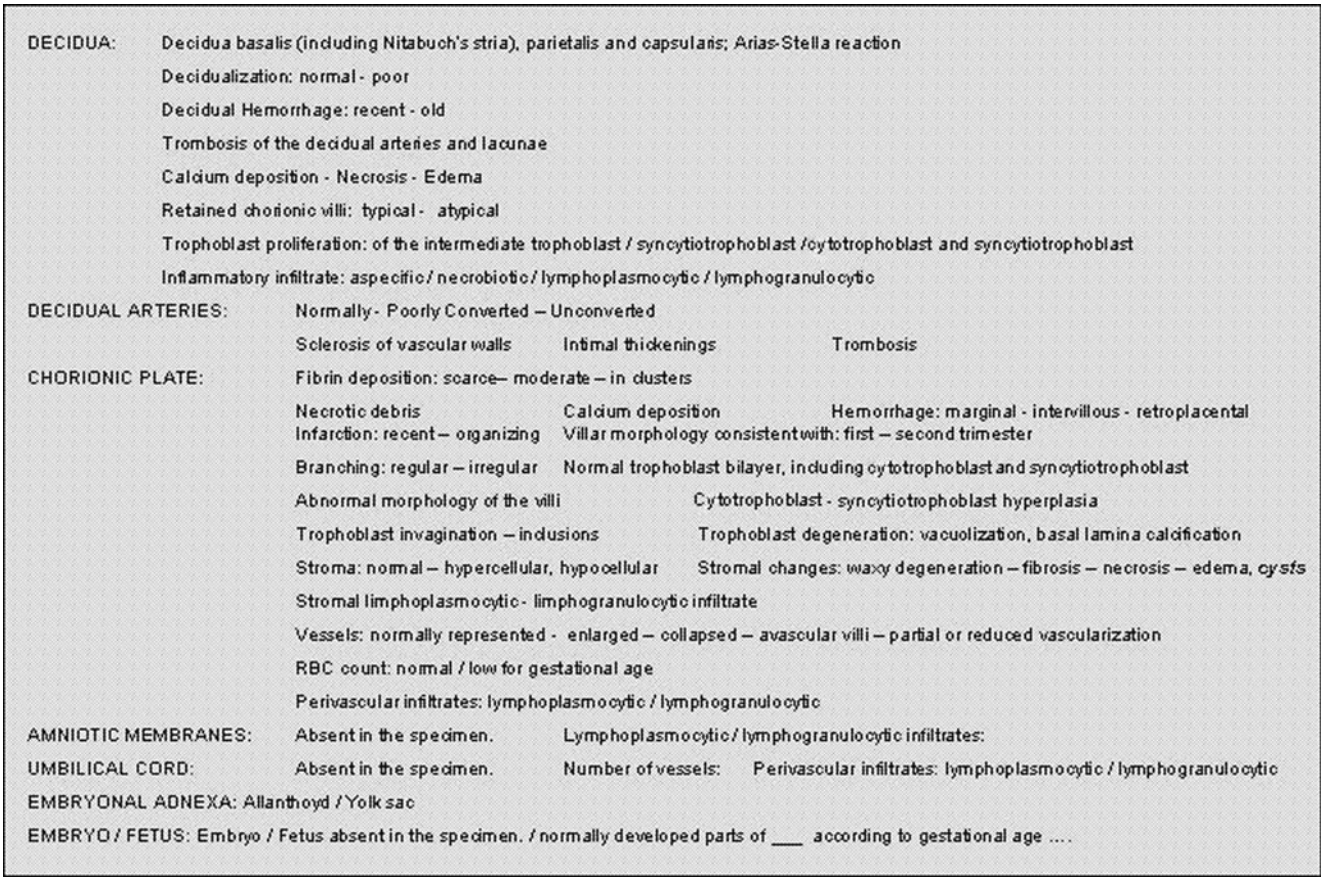

Fig. 2 Checklist for the microscopic examination of abortion specimens (May 22, 2007—according to UNI EN ISO 9001-2000 norm, no. 9122. AO10)

of the whole case series), 74 cases previously diagnosed as suggestive of autoimmune diseases in Group 2A (6.8%), and 31 showing classic decidual vasculopathy in Group 2B (2.8%).

By comparison, 373 cases (34.1%) were attributed to karyotype abnormalities, 187 (17.1%) to inflammatory–infectious diseases (I-ESAs), and 150 (13.7%) to abruption due to massive retroplacental hemorrhage, owing to the lack of significant amounts of chorionic plate or implantation decidua. For 91 ESA specimens (8.3% of all cases), it was not possible to assess the cause of miscarriage; different *noxae* accounted for the remaining 118 cases (10.8%).

Age

The overwhelming majority of patients (1,020 women, 93.2%) were 25 to 44 years old at the time of miscarriage, the majority of them clustering in the 35- to 39-year-old group (378 women, 34.5%). Only 15 patients were teenagers (1.37%), and 13 (1.2%) were 45 or older. Age did not significantly differ between Group 1 (34.1 years; range, 17–45), Group 2A (33.5 years; range, 15–47), Group 2B (34.7 years; range, 18–44), Controls (34.4 years; range, 20–44), and the larger I-ESA group (34.1 years; range, 14–45). However, the age peak of the patients in Group 1 was slightly anticipated: 36.6% of women were 30 to 34 years old, while among the others the peak occurred later, in the 35–39 years age bracket (31.1% in Group 2A, 35.5% in Group 2B, 34.7% in the selected Controls, and 36.9% among all I-ESAs); moreover, 54.9% of Group 1 patients were younger than 35, while 51.9% of women in the whole series were 35 or older.

Gestational age

Overall mean gestational age at the time of miscarriage was 9.8 weeks (range, 7–13 weeks). Cases in which gestational age was not provided by clinicians or was irretrievable were not included in the study. Mean gestational age was lower in Group 1 (9.2 weeks; range, 7–13) than in Group 2A (9.6 weeks; range, 7–13) or Group 2B (10.0 weeks; range, 8–13). Mean gestational age was 9.6 in Controls and 9.8 in the whole I-ESA group (range, 7–13 for both), in line with the whole case series. Despite our cases showing variable gestational age, none of them occurred earlier than 7 nor

later than 13 weeks. By correlating the distribution of gestational age with decidual vascular patterns, we found no particular difference between the three groups (Fig. 3). Anyway, some fluctuations should be noted:

- The largest proportion of cases in Group 1 occurred in the first 9 weeks (71.2% vs. 50.7% in Group 2A, 48.4% in Group 2B, and 49.9% in Controls).
- Gestational age distribution of Group 2A closely followed that of Controls, with a regular distribution from 8 to 10 weeks (around 20% of patients for each week).
- Group 2B cases clustered around nine gestational weeks, while none of them occurred before 8 weeks.

Clinical records

The overall prevalence of *repeated or recurrent miscarriage* did not significantly differ between the groups, being slightly higher in Group 2 (24.8%)—and particularly in Group 2A (29.7%)—than in Group 1 (22.5%) patients. Repeated or recurrent aborters were 17.6% among I-ESAs and 16.7% among Controls, in line with the overall prevalence of 18.3% registered for the whole series of 1,095 women.

Patients were considered to have a history of *infertility* when they referred assisted fertilization, anovulatory cycles, or low progesterone levels. Group 2 patients referred such a history of infertility more frequently (14.3%) than Group 1 (5.6%) or Controls (2.5%), the prevalence in the whole series being 5.3%. Similarly, patients in Group 2 had more frequently undergone previous *pathologic pregnancies* (8.6% vs. 2.8% in Group 1, 1.4% in Controls, and 1.6% overall) and *operative delivery* (6.7% vs. 2.8%, 2.7%, and 4.4%, respectively).

Not surprisingly, a history of *endocrine disease* other than progesterone defect was more frequent (4.2%) in Group 1 than in the other patients (1.9% in Group 2, 1.4% in Controls, and 1.6% overall).

Autoimmune diseases were referred in 1.4% of all the ESA mothers, while their prevalence rose to 4.2% among Group 1 women and to 6.7% in Group 2, with an expected peak of 8.1% in the subgroup of cases histopathologically suggestive of autoimmune disease (Group 2A). Conversely, among Controls no maternal autoimmune disease was observed. All the above-mentioned clinical features are summarized in Table 3.

It should be pointed out that, given the usually sudden onset of miscarriage, in many cases clinical history was not collected nor referred. For similar reasons, in the majority of cases progesterone levels were not tested nor followed up.

Histological representativeness and adequacy of the specimens

We evaluated and compared the structures observed in each ESA specimen to rule out any cause of anatomic discrepancy between the groups eventually caused by incomplete

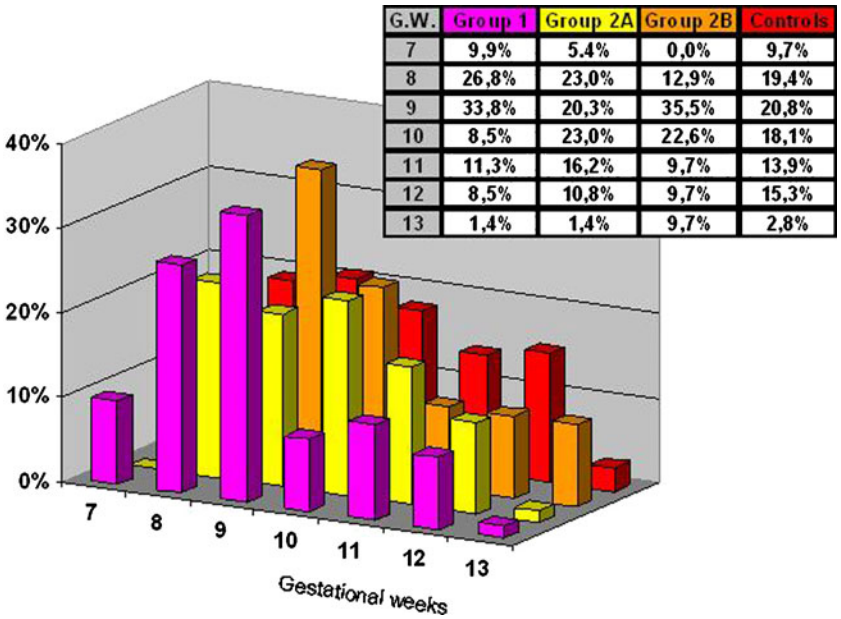

Fig. 3 Gestational age distribution in different ESA groups considered in the present study. No significant difference was found; anyway, Group 1 cases seemed to occur a little earlier, with a larger proportion of abortions seen before the end of the ninth week. Age distribution in Controls was particularly regular (*G.W.* gestational week)

abortion in the Obstetrics and Gynaecology Unit or by wrong sampling in our institute. Specimens from different groups showed similar composition, as summarized in Table 4. In particular, *basal decidua* was present in all samples, while *parietal decidua* was seen in the overwhelming majority, ranging from 96.8% in Group 2B to 90.3% in Controls. Conversely, *capsular decidua* was seen only in 25.4% of Group 1 cases, in 20.3 of Group 2A, in 19.4% of Group 2B, and in 20.8% of Controls.

The presence of *chorionic structures* slightly decreased from 100% in Group 2B specimens to 95.9% in Group 2A, 90.1% in Group 1 and 87.5% in Controls, while parts of *embryo/fetus* were macroscopically seen and histologically confirmed in 9.9% of Group 1, 8.1% of Group 2A, 16.1% of Group 2B, and 12.5% of Controls.

Free *amniotic membranes* were seen only in 5.6% of Group 1 and in 5.4% of Group 2A specimens, while they were described in 9.7% of Group 2B cases and in 11.1% of Controls. The higher prevalence of amniotic membranes in Controls could imply a greater sensitivity by the pathologist in the recognition of amniotic membranes in ESA specimens when they show chorioamnionitis or when an infectious cause of miscarriage is suspected. The *umbilical cord*, another target in inflammatory conditions, was seen only in 1.4% of Group 2A specimens and in 2.8% of Controls, while in Groups 1 and 2B no parts of it were ever described.

Three structures—basal and parietal decidua and chorionic plate—were almost always present, allowing us to perform adequate histological examinations, write a detailed report, and suggest some diagnosis.

Our results confirmed an excellent uniformity of the specimens, and this is thought to depend on standardized clinical procedures for endometrial curetting, as well as on the standard protocol used in our institute.

Moreover, we looked for histological features of prolonged retention in utero in order to assess the state of conservation of the specimens. Apart from some mild to moderate inflammatory infiltrate, which actually does not give reliable informations on this issue, we never found

Table 3 Main clinical features of ESAs, according to their decidual vascular patterns on histological examination

Clinical history	Group 1 (*N*=71)		Group 2A (*N*=74)		Group 2B (*N*=31)		Group 2 (*N*=105)		Controls (*N*=72)		I-ESA (*N*=187)		All (*N*=1,095)	
Age (years)														
Mean	34.1	(17–45)	35.5	(15–47)	34.7	(18–44)	33.8	(15–47)	34.4	(20–44)	34.1	(14–45)	34.3	(14–56)
Median	34.0		34.0		35.0		35.0		35.0		35.0		35.0	
Gestational weeks														
Mean	9.2	(7–13)	9.6	(7–13)	10.0	(8–13)	9.7	(7–13)	9.6	(7–13)	9.8	(7–13)	9.8	(7–13)
Median	9.0		10.0		10.0		10.0		9.5		10.0		10.0	
Spontaneous miscarriage	16	22.5%	22	29.7%	4	12.9%	26	24.8%	12	16.7%	33	17.6%	200	18.3%
Spontaneous delivery	6	8.5%	14	18.9%	2	6.5%	16	15.2%	9	12.5%	22	11.8%	89	8.1%
Voluntary abortion	3	4.2%	4	5.4%	1	3.2%	5	4.8%	8	11.1%	14	7.5%	62	5.7%
Operative delivery	2	2.8%	7	9.5%	–	–	7	6.7%	4	5.6%	5	2.7%	48	4.4%
Assisted fertilization	3	4.2%	4	5.4%	4	12.9%	8	7.6%	3	4.2%	5	2.7%	34	3.1%
History of diabetes	3	4.2%	2	2.7%	2	6.5%	4	3.8%	1	1.4%	2	1.1%	23	2.1%
Other endocrine diseases	3	4.2%	2	2.7%	–	–	2	1.9%	1	1.4%	3	1.6%	18	1.6%
Anovulatory cicles	1	1.4%	6	8.1%	–	–	6	5.7%	–	–	–	–	17	1.6%
Autoimmune diseases	3	4.2%	6	8.1%	1	3.2%	7	6.7%	–	–	–	–	15	1.4%
History of hypertension	1	1.4%	3	4.1%	–	–	3	2.9%	–	–	1	0.5%	15	1.4%
Chronic infection	–	–	–	–	–	–	–	–	1	1.4%	3	1.6%	13	1.2%
Ectopic pregnancy	–	–	–	–	–	–	–	–	2	2.8%	2	1.1%	11	1.0%
Luteal defect	–	–	1	1.4%	–	–	1	1.0%	–	–	–	–	7	0.6%
Therapeutic abortion	–	–	–	–	–	–	–	–	1	1.4%	2	1.1%	5	0.5%
Genetic diseases/ abnormalities	–	–	2	2.7%	1	3.2%	3	2.9%	1	1.4%	1	0.5%	7	0.6%
Pathologic pregnancy (other)	2	2.8%	5	6.8%	4	12.9%	9	8.6%	1	1.4%	2	1.1%	18	1.6%
Infertility (AF + LD + AN)	4	5.6%	11	14.9%	4	12.9%	15	14.3%	3	4.2%	5	2.7%	58	5.3%

Specimens selected for histopathological comparison ("Controls," 72 patients) should not be confused with the larger group from which they were drawn ("I-ESA," 187 patients), the latter including all cases previously diagnosed as primarily caused by infection/inflammation

AF assisted fertilization, *LD* luteal defect, *AN* anovulatory cycles

Table 4 Composition of ESA specimens according to their decidual vascular patterns on histological examination: basal decidua was always present, while other structures showed minimal prevalence variations between the groups

Structures	Group 1 (*N*=71) (%)	Group 2A (*N*=74) (%)	Group 2B (*N*=31) (%)	Controls (*N*=72) (%)
Basal decidua	100.0	100.0	100.0	100.0
Parietal decidua	94.4	93.2	96.8	90.3
Capsular decidua	25.4	20.3	19.4	20.8
Chorionic plate	90.1	95.9	100.0	87.5
Amniotic membranes	5.6	5.4	9.7	11.1
Umbilical cord	–	1.4	–	2.8
Embryo/fetus	9.9	8.1	16.1	12.5
Fetal adnexa	–	4.1	–	–

important necro-inflammatory or degenerative alterations (autolysis of the embryo, mineralization of villous stroma, massive fibrosis, intravascular karyorrhexis, and fibrous obliteration or septation of villous vessels) indicating prolonged retention. Some degree of endothelial lesion was sometimes observed, but this can be seen following very brief retentions not exceeding 48 h; similarly, vascular fibrosis or sclerosis never associated with septation or obliteration.

Morphological features in routine H&E slides

In all three groups of cases (1, 2A, and 2B), arteries of the basal decidua had thick walls in H&E; however, in Group 1, this was due to the persistence of unconverted intima and muscularis, while in Group 2, an eosinophilic, amorphous matter and, frequently, intimal thickening were observed in vascular walls. Those features were seen also in vessels far from the implantation site, which, in normal pregnancies, remain physiologically unconverted (Fig. 4). The main morphological features in each group are listed and compared in Table 5 (decidua) and Table 6 (chorionic plate).

Group 1 Failure of decidual vessels to convert was one major histopathological criterion allowing us to suggest a suspect of inadequate progesterone supply. UDVs were present in 93% of the 71 Group 1 cases. Theoretically, even *inadequate stromal decidualization (ISD)* of the endometrium would indicate luteal defect, but it is poorly defined, and its recognition tends to be somewhat subjective. Moreover, in our case series, true ISD was seen only in six cases (8.5%), where it was always seen together with UDVs. In all the remaining cases (7%) in which the finding of UDVs was not reported, it could be assessed by immunohistochemistry (see below) which in these patients showed that there were no EVTs invading maternal vessels nor any true decidual vascular lesions (characteristic of Group 2). Hence, those cases were diagnosed as "suggestive of inadequate progestinic support."

Conversely, when UDVs are observed but vascular lesions are difficult to rule out due to the presence of confounding factors, minor histopathologic criteria can help if both decidual and chorionic structures are evaluable in the specimen. Such minor criteria could be ISD, normal lumen size of decidual vessels, absence of vascular fibrosis/sclerosis in the decidua, and no fibrin deposition and villous fibrosis in the chorionic plate.

Group 2 These cases showed a spectrum of histopathological lesions, but none of them appeared to be as specific as UDVs for Group 1. However, by comparing both groups, a number of different features could be found, since several lesions were seen three to 14 times more frequently than in Group 1. It is the case of *intimal thickening*, a hallmark of immune vascular lesion, which was nearly 12 times more common in Group 2 (48.6%) and, in particular, nearly 14 times more common in Group 2A (56.8%) than in Group 1 (4.2%). Conversely, some minor lesions such as ISD, observed in 8.5% of Group 1 cases, were never found here. In this group, it is really difficult to differentiate cases suggestive of autoimmune disease from those more probably consistent with decidual vasculopathy, owing to the partial overlapping of these conditions. For this reason, we preferred to join 2A and 2B subgroups together into the more uniform Group 2. In general, however, *chronic mild villitis/intervillitis* (45.9% vs. 12.9%), *intimal thickening of decidual vessels* (56.8% vs. 29.0%), *perivascular infiltrate* (16.2% vs. 3.2%), and the presence of *granulocytic infiltrate in the decidua* (32.4% in Group 2A and 19.4% in Group 2B) accounted for the most significant differences between these subgroups.

Controls As expected in this group, *inflammatory infiltrate of the decidua* was really frequent, showing granulocytes in 56.9% of cases (11.3% in Group 1 and 28.6% in Group 2) and lymphocytes alone in 68.1% (38.0% in Group 1 and 44.8% in Group 2). Interestingly, *fibrosis and/or sclerosis of the vascular walls* were seen only in 1.4% of Controls (21.1% in Group 1 and 59.0% in Group 2). When Groups 1

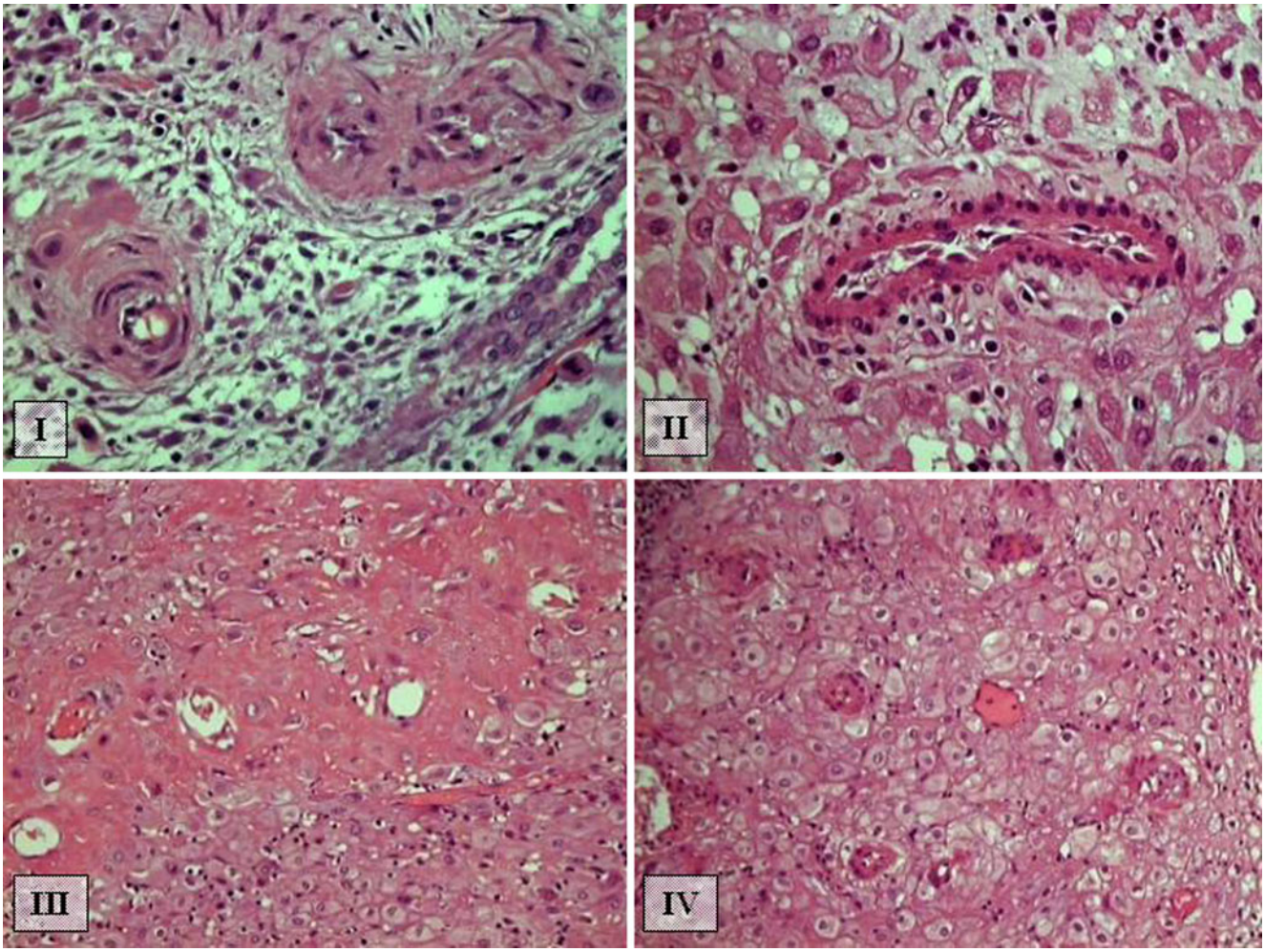

Fig. 4 Comparison between decidual walls in Groups 1 and 2 decidual vascular patterns (H&E): unconverted vessels in the basal decidua (*I*) and far from the implantation site (*II*) in Group 1; sclerotic appearance of vessels of the basal decidua (*III*) and at distance (*IV*) in Group 2. The Group 2 case here depicted was diagnosed as suggestive of maternal autoimmune disease (Group 2A) due to the presence of intimal thickening and granulocytic infiltrate in the decidua (mainly in perivascular spaces) and villitis in the chorionic plate

Table 5 Comparison of the most common histopathological findings in the decidua in the three groups of cases (1, 2A, 2B) and the Controls

Decidual findings	Group 1 (*N*=71) (%)	Group 2A (*N*=74) (%)	Group 2B (*N*=31) (%)	Controls (*N*=72) (%)
UDVs	93.0	12.2	6.5	–
Edema	52.1	48.6	51.6	48.6
Hemorrhage	52.1	74.3	74.2	79.2
Thrombosis	49.3	62.2	64.5	55.6
Lymphoplasmocytic infiltrate	43.7	45.9	41.9	68.1
Aspecific/necrobiotic infiltrate	23.9	36.5	35.5	13.9
Fibrosis/sclerosis of vascular walls	21.1	55.4	67.7	1.4
Thickening of vascular walls	12.7	14.9	16.1	–
Lymphogranulocytic infiltrate	11.3	32.4	19.4	56.9
Intimal thickening	4.2	56.8	29.0	1.4
Vascular stenosis	1.4	10.8	12.9	–
Perivascular inflammatory infiltrate	2.8	16.2	3.2	–
ISD	8.5	–	–	–

UDVs unconverted decidual vessels, *ISD* inadequate stromal decidualization

Table 6 Comparison of the most common histopathological findings in the chorionic plate in the three groups of cases (1, 2A, 2B) and the Controls

Chorionic plate findings	Group 1 (*N*=71) (%)	Group 2A (*N*=74) (%)	Group 2B (*N*=31) (%)	Controls (*N*=72) (%)
Edema	36.6	43.2	38.7	22.2
Fibrin deposition	32.4	83.8	61.3	36.1
Waxy degeneration	31.0	41.9	48.4	26.4
Collapsed vessels	26.8	36.5	22.6	15.3
Fibrosis of the villi	16.9	41.9	48.4	16.7
Syncytiotrophoblast hyperplasia	12.7	28.4	29.0	15.3
Villitis/intervillitis	11.3	45.9	12.9	36.1
Reduced vascularization	9.9	9.5	6.5	5.6
Hypocellular stroma	7.0	14.9	9.7	11.1
Retroplacental hemorrhage	5.6	16.2	16.1	15.3
Irregularly branching villi	5.6	10.8	12.9	1.4

and 2 were considered together to build a series including all ESAs with pathologic decidual vessels ("Cases"), the above-mentioned differences seemed even stronger, granulocytic infiltrate being observed in 21.6% of cases (vs. 56.9% in Controls), lymphoplasmocytic infiltrate in 42.0% vs. 68.1%, and, particularly, fibrosis or sclerosis of vascular walls in 43.8% vs.1.4%.

The prevalence of major histopathological findings in decidual vessels was fairly constant for each group regardless of gestational week, and no significant difference was found when the patients were grouped by gestational age: to give an example, UDVs were found both in "earlier" (until 9 weeks) and "later" abortions (12–13 weeks). This analysis of morphological vascular features depending on gestational age is provided in Table 7.

Histological differential criteria in ESAs showing decidual vascular abnormalities are summarized in Table 8.

Histochemical and immunohistochemical findings

It is virtually impossible to assess how much specific stainings contribute to diagnostic accuracy. The latter was then assessed for each staining on a descriptive basis by two expert embryopathologists and then expressed in a semi-quantitative scale for each histopathological finding previously seen in H&E:

(−) was attributed when a histopathological finding seen on routine H&E slides was not modified by the staining.
(+) was assigned to those findings for which histological details were more evident following histochemistry or immunohistochemistry.
(++) was assigned to those findings that were frequently missed on routine H&E slides and then reliably seen on histochemistry or immunohistochemistry alone.

The efficacy of each staining in increasing diagnostic accuracy is summarized in Table 9, while Table 10 is intended to represent our opinion about the usefulness of each staining for the different pathological pictures; in this context, we added a further category (−/+), which indicates the usefulness of histochemistry (HC) or immunohistochemistry (IHC) in a minority of cases (i.e., for WF and desmin).

Periodic acid–Schiff PAS stain helped us evaluate the level of decidualization of endometrial stromal cells; properly decidualized cells are characterized by large, pale, glycogen-rich cytoplasm. As already mentioned, the absence of these features appears to be aspecific, and frank ISD was observed only in a minority of Group 1 cases, were there was also no physiologic conversion of decidual vessels. However, PAS staining proved to be very specific for glycogen-rich cytoplasm of decidual stromal cells; hence, it was very useful in assessing decidualization together with UDV recognition and investigation.

Masson's trichrome stain MT was of great diagnostic use, since it allowed us to more precisely assess vascular wall conditions. In Group 1, we found normally thick decidual vessels, while in Group 2 marked vessel wall fibrosis and a slight thickening of the intima were observed. In both cases, arteries far from the implantation site showed features similar to those seen in basal decidua (i.e., thickened fibrotic walls).

Weigert's stain for fibrin Finally, WF, when negative, allowed us to rule out fibrinoid necrosis in several suspected cases of acute atherosis. In standard cases of decidual vasculopathy, fibrinoid necrosis can be recognized as an acellular, brilliantly eosinophilic, and glassy transformation of the vascular wall, while atherosis, often accom-

Table 7 Most common decidual vascular findings depending on gestational age; no significant difference was found in any single group

Decidual vascular findings	GW	Group 1 (*N*=71) (%)	Group 2A (*N*=74) (%)	Group 2B (*N*=31) (%)
Thrombosis	8–9	41.9	46.9	66.7
	10–11	64.3	72.4	60.0
	12–13	42.9	77.8	66.7
Fibrosis/sclerosis of vascular walls	8–9	18.6	59.4	73.3
	10–11	28.6	58.6	80.0
	12–13	28.6	33.3	33.3
Thickening of vascular walls	8–9	9.3	15.6	13.3
	10–11	28.6	13.8	10.0
	12–13	–	22.2	33.3
UDVs	8–9	90.7	9.4	6.7
	10–11	92.9	13.8	10.0
	12–13	100.0	22.2	–
Stenosis	8–9	–	12.5	6.7
	10–11	7.1	6.9	20.0
	12–13	–	22.2	16.7
Intimal thickenings	8–9	2.3	65.6	26.7
	10–11	7.1	55.2	50.0
	12–13	14.3	22.2	–
Vasculitis	8–9	–	9.4	6.7
	10–11	–	–	–
	12–13	–	–	–
Perivascular inflammatory infiltrate	8–9	–	12.5	–
	10–11	14.3	24.1	–
	12–13	–	11.1	–

GW gestational week

panying fibrinoid necrosis, manifests as intramural accumulation of foamy macrophages, resembling cells seen in atherosclerosis. These changes may occur in converted or unconverted vessels. Therefore, we had to rule out fibrinoid necrosis as the root cause of the amorphous matter seen in vascular walls. With WF, fibrinoid necrosis usually appears as a blue-stained fibrin band in the vascular wall, which actually was never observed. However, since only some decidual vasculopathy cases feature acute atherosis and no convincing evidence of WF-positivity was obtained in any of the acute atherosis cases, WF proved to be only partially useful in decidual vasculopathy investigations. Figure 5 illustrates the conditions of a sclerotic vascular wall in a specimen from Group 2, as seen with PAS, MT, and WF.

Table 8 Morphological differential criteria in ESAs showing decidual vascular abnormalities in routine H&E slides

	Group 1	Group 2A	Group 2B
Appearance of decidual vessels	UDVs with normally contracting vascular walls	Sclerosis, usually lacking fibrinoid necrosis	Hypertrophy, fibrinoid necrosis-
Intima	Normal	Intimal thickenings (+++)	Intimal thickenings (+)
Muscularis	Normal	Diminished or absent s.m.c.	Hypertrophic or diminished s.m.c.
Vascular/perivascular inflammatory infiltrate	Usually absent	Frequent	Usually absent
Stromal decidualization	ISD in ~10%	Normal	Normal
Intervillous fibrin	+	+++	++
Villitis	Rare (~10%)	Very frequent (~50%)	Rare (~10%)

s.m.c. smooth muscle cells, *UDVs* unconverted decidual vessels, *ISD* inadequate stromal decidualization

Table 9 Usefulness of histochemistry (HC) and immunohistochemistry (IHC) for any of the most frequent histopathological findings in the decidua of ESAs with abnormal decidual vessels; frequencies in Groups 1 and 2 relate to the prevalence of any finding on H&E routine slides, while the increase of diagnostic sensitivity is reported in a semiquantitive scale for each stain

Histopathological findings	*H&E*		*HC*			*IHC*						
	Group 1	Group 2	PAS	MT	WF	Vim	Des	α-SMA	CD31	CD34	hPL	βhCG
UDVs	93.0%	10.5%	-	+	-	-	-	++	-	-	++	-
Edema	54.9%	49.5%	+	-	-	-	-	-	-	-	-	-
Hemorrhage	52.1%	74.3%	-	-	-	-	-	-	-	-	-	-
Thrombosis	49.3%	62.9%	-	+	+	-	-	-	-	-	-	-
Lymphocytic infiltrate	38.0%	44.8%	+	-	-	-	-	-	-	-	-	-
Aspecific infiltrate	29.6%	36.2%	+	-	-	-	-	-	-	-	-	-
Fibrosis/sclerosis of vascular walls	21.1%	59.0%	-	++	++	+	+	++	-	-	-	-
Thickening of vascular walls	12.7%	15.2%	-	++	-	+	+	++	-	-	-	-
Granulocytic infiltrate	11.3%	28.6%	-	-	-	-	-	-	-	-	-	-
Intimal thickening	4.2%	48.6%	+	+	-	-	-	+	-	-	-	-
Perivascular Infiltrate	2.8%	12.4%	+	-	-	-	-	-	-	-	-	-
ISD	8.5%	-	++	-	-	-	-	-	-	-	-	-

Columns in yellow indicate the most useful stains

PAS periodic acid–Schiff, *MT* Masson's trichrome stain, *WF* Weigert's stain for fibrin, *Vim* vimentin, *Des* desmin, *α-SMA* alpha-smooth muscle actin, *hPL* human placental lactogen, *βhCG* human chorionic gonadotropin-beta, *UDVs* unconverted decidual vessels, *ISD* inadequate stromal decidualization

Vimentin Anti-vimentin immunostaining did not show any peculiar feature in spiral arteries of Group 1 specimens, whereas in some other cases—particularly in Group 2B—it revealed the lack of fibroblasts, hence confirming the amorphous nature of the substance in the thickened walls. However, these and other findings were more easily and more specifically assessed by using anti-smooth muscle actin antibodies, so that anti-vimentin immunostaining was found to be of very little usefulness in decidual vessel investigation.

α-Smooth muscle actin The presence or absence of smooth muscle cells was confirmed by performing immunohistochemistry for α-SMA: in Group 1, the muscularis was preserved with normal smooth muscle cells. This is the morphologic background of responsiveness to vasospasm. More importantly, it prevents the physiologic drop of systemic blood pressure occurring in spiral arteries during normal pregnancies. Conversely, vessels in Group 2, although usually lacking smooth muscle cells, remained thick and firm, owing to the amorphous substance deposition (Fig. 6).

Desmin Together with smooth muscle actin, desmin helped us evaluate the muscular component of vascular walls. It also allowed recognizing myofibroblasts, which may be an adaptive modification of fibroblasts following modifications of blood pressure or circulation. However, anti-desmin immunostaining failed to provide any additional information to the previously performed α-SMA, which proved to be more specific and accurate in detecting vascular smooth muscle cells. Hence, the usefulness of anti-desmin immunohistochemistry in decidual vessel investigations seems arguable.

Human placental lactogen The presence of hPL-positive invasive EVTs in Group 2 specimens confirmed that in autoimmune or hypertensive diseases maternal vessels, following earlier intermediate trophoblast colonization, may then have undergone immunologic damage. Conversely, in Group 1 they remained unconverted, without any significant intravascular EVTs (Fig. 7). Despite the occasional finding of scattered hPL-positive EVTs in some lumens, classical UDVs appeared as thick vessels, without normal EVTs around and inside the vascular wall.

Endothelial vascular markers Immunostaining for CD31 and CD34 surface endothelial molecules proved to be very reliable in the identification of vascular structures, showing intense and diffuse reactivity in both cases. However, by comparing routine H&E slides with immunolabeled ones, only a very low number of vessels not readily identified on routine histological examination could be recognized. Moreover, all these vessels detected by immunohistochem-

Table 10 Usefulness of histochemistry (HC) and immunohistochemistry (IHC) in ESAs featuring abnormal decidual vessels, depending on their decidual vascular patterns

	Group 1	Group 2A	Group 2B
PAS	++	++	++
MT	++	++	++
WF	-	-/+	-/+
Vim	-	-	-
Des	-/+	-	-/+
α-SMA	++	++	++
CD31	-	-	-
CD34	-	-	-
hPL	++	+	+
β-hCG	-	-	-

Estimated usefulness:
- very limited
-/+ useful in a minority of cases
+ useful in the majority of cases
++ very useful / diagnostic

Lines in yellow indicate the most useful stains. Estimated usefulness: − very limited, −/+ useful in a minority of cases, + useful in the majority of cases, ++ very useful/diagnostic

PAS periodic acid–Schiff, *MT* Masson's trichrome stain, *WF* Weigert's stain for fibrin, *Vim* vimentin, *Des* desmin, *α-SMA* alpha-smooth muscle actin, *hPL* human placental lactogen, *βhCG* human chorionic gonadotropin-beta

istry showed small-caliber thin walls and stretched and collapsed lumens; hence, they provided no additional information about decidual vascular pathology. Moreover, in cases with subintimal thickenings characteristic of Group 2A, CD34 added no significant information, since this finding was usually easily seen with H&E.

In conclusion, CD31 and CD34 did not seem to increase diagnostic accuracy.

Human chorionic gonadotropin beta Anti-β-hCG immunostaining, although positive in the villous trophoblast seen in parts of the chorionic plate, resulted negative in EVTs. Therefore, there is no reason for using anti-β-hCG in association with hPL, which, instead, should be preferred.

Finally, in order to improve diagnostic accuracy in the investigation of decidual vessels, a panel including PAS, MT, WF, and immunohistochemical markers for α-SMA and hPL was deemed to be sufficient.

Two particular circumstances, where the above listed panel resulted to be very useful, are the following:

1. Vessels with mild fibrosis and no intravascular EVTs detected by H&E examination: in these cases, hPL increased diagnostic sensitivity in detecting any invasive EVT; when normally represented, hPL-positive EVTs allowed us to rule inadequate progestinic support and to assign the case to Group 2. This feature usually paired up with α-SMA-positive vascular walls.
2. Thickened vessels with variable fibrosis/sclerosis and uncertain persistence of smooth muscle cells on H&E examination: in these cases, the use of anti-α-SMA, unnecessarily together with desmin and vimentin, contributed to assessing whether the muscularis structure—which, in some cases, showed no smooth muscle cells or myofibroblasts—was preserved (in Group 1) or damaged (in Group 2).

Conclusions

From a pathogenetic point of view, in Group 1 decidualized endometrium is very likely to get no progestinic support, whereas Group 2A shows histopathologic features similar to those observed in autoimmune damage of term pregnancy placenta; in Group 2B, hypertrophy or necrosis may arise on a background systemic vasculopathy. However, it should be pointed out that, especially when clinical investigations are missing or inaccurate, diagnoses in terms of "suggestive of..." are the only possible ones in our pathology reports. As a matter of fact, in this study, as well as in routine diagnostics, we could not correlate all pathologic features to a well-defined pathogenetic pathway, but we could only assume it on the basis of clinical correlations—when feasible—and by comparing our findings to physiopathologic investigation results already demonstrated in other organs. Similarly, histopathologic diagnosis is often difficult and inconclusive even in late spontaneous abortion (LSA): in LSA, actually, diagnosis is based only on the placenta, given the fact that the specimens very rarely include the decidua.

However, it seems that an appropriate histochemical and immunohistochemical panel could increase diagnostic sensitivity in ESAs, thus making morphological diagnosis more reliable and reducing the "gray zone" in the difficult diagnostics of abortion. More interestingly, such improvement could be achieved using a very limited panel, including no more than two immunohistochemical markers (α-SMA, hPL) and two or three less expensive histochemical stainings (PAS, MT, WF). The risk of unreliable immunohistochemical results (i.e., false positive and false negative) caused by altered antigens would be dramatically reduced by performing immunohistochemistry on tissues

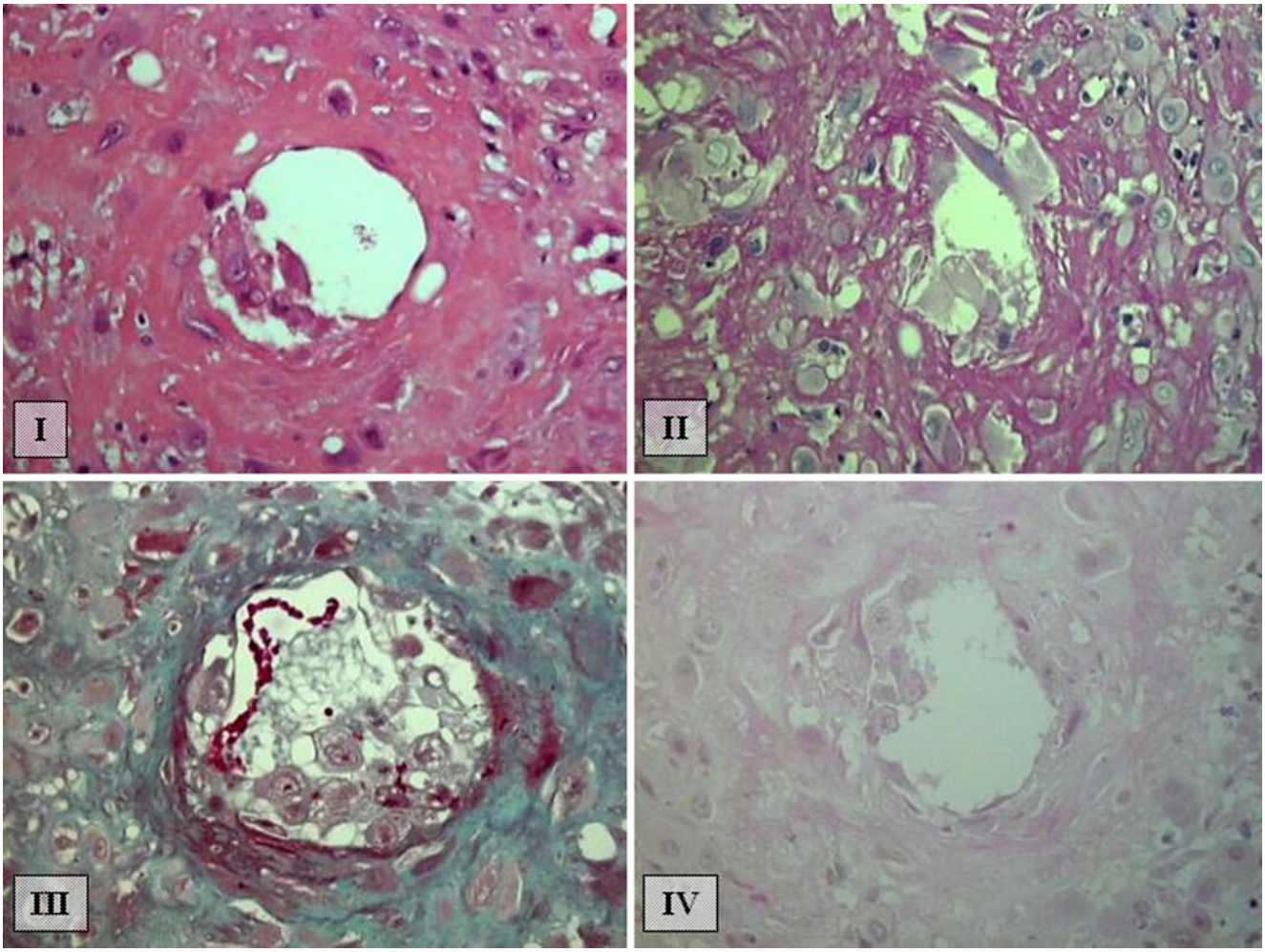

Fig. 5 Vascular thickening in a Group 2A case (H&E, PAS, MT, WF): sclerotic appearance of vessels of the decidua basalis in this case diagnosed as suggestive of autoimmune maternal disease as seen with H&E (*I*), PAS (*II*), and Masson's trichrome stain (*III*) does not consist of fibrinoid necrosis, as illustrated by negative Weigert's staining for fibrin (*IV*)

which proved on H&E slides to be devoid of alterations consistent with prolonged retention in utero. Moreover, for the most important antibodies (e.g., α-SMA), internal control is frequently available.

In the majority of Group 1 cases, we found only unconverted decidual vessels, with no significant vascular lesion: when UDVs are detected and *hPL*-positive invasive EVTs are strongly reduced or absent, inadequate progestinic support can reasonably be suspected. Moreover, although rarely evident, ISD is an additional feature associated with UDVs and the lack of intravascular EVTs; therefore, an easy-to-use *PAS* stain could be included in the panel. The proposal of a pathologic diagnosis of consistency with inadequate progestinic support could allow the clinician to approach future pregnancies by monitoring the likely luteal defect and providing more targeted treatments.

The assessment of vascular wall conditions—a milestone in the ESA investigation—seems of great diagnostic use when made by anti-*α-SMA* staining rather than by desmin and/or vimentin. In Group 1, the former usually reveals normal smooth muscle cells in the muscularis of vessels near the Nitabuch's stria. Conversely, in Group 2, vascular walls usually appeared diffusely damaged, both in the basal and parietal decidua; true histopathologic lesions were observed, particularly in the 2A subgroup. In these cases, histochemistry and immunohistochemistry were proved to be very useful in demonstrating fibrosis (*MT*), residual damaged smooth muscle cells (anti-α-SMA), and when present, fibrinoid necrosis (*WF*). This panel also allowed us to observe conditions that were somewhat different and complementary to those usually seen in DV or AA (wall hypertrophy, thrombosis, fibrinoid necrosis, and/or macrophage infiltration) and probably representing a different kind of vascular damage.

In the heterogeneous Group 2, further distinction between 2A and 2B patterns can be attempted on the basis of histopathological criteria, such as the presence or absence of intimal thickening, fibrinoid necrosis, and inflammatory infiltrate in the decidua. Other findings in the chorionic

plate—such as villitis or abundant fibrin deposition—can suggest autoimmune processes rather than true decidual vasculopathy. It should be pointed out that for such differential diagnosis no particular staining is necessary apart from WF, which is required in order to confirm fibrinoid necrosis.

In conclusion, we believe that, whenever obvious morphological findings are observed indicating well-known causes of abortion, the histological examination could be based on H&E slides alone; to name a few, this is the case of infections (massive lymphocytic and/or granulocytic infiltrate, bacterial or fungal colonies) or massive infarction (large thrombi and hemorrhage). In this context, histochemistry or immunohistochemistry could eventually play a role in rare cases, when a specific etiologic agent is suspected and confirmation by specific HC stainings (e.g., PAS, Grocott, Ziehl-Nielsen) or antibodies (e.g., anti-Cytomegalovirus) is required for diagnosis.

Conversely, we suggest that, when no reasonable cause of abortion can be documented and thickened vessels are present in the decidua basalis, an appropriate histochemical and immunohistochemical panel should be performed. The application of a few stainings (PAS, MT, WF, hPL, and α-SMA) helps improve morphologic details and can confirm or rule out initial diagnostic suspicions. Moreover, although some overlapping pictures persist, in general, this panel provides a limited number of staining patterns. Hence, on the basis of morphological, histochemical, and immunohistochemical findings, an easy diagnostic algorithm could be proposed in the investigation of ESA specimens showing abnormal decidual arteries (Fig. 8).

Once more, it should be stressed that, when facing ESAs in routine diagnostics, the pathologist usually has only limited

Fig. 7 Invasive EVTs in Groups 1 and 2 decidual vascular patterns (hPL): in Group 1, unconverted vessels of the basal decidua lack invasive intermediate trophoblast (*I*), while in Group 2 cases, hPL-positive EVTs are evident in and around the lumen (*II*). Arteries far from the implantation site lack trophoblast in both groups (*III*, *IV*), as observed in physiologic pregnancy

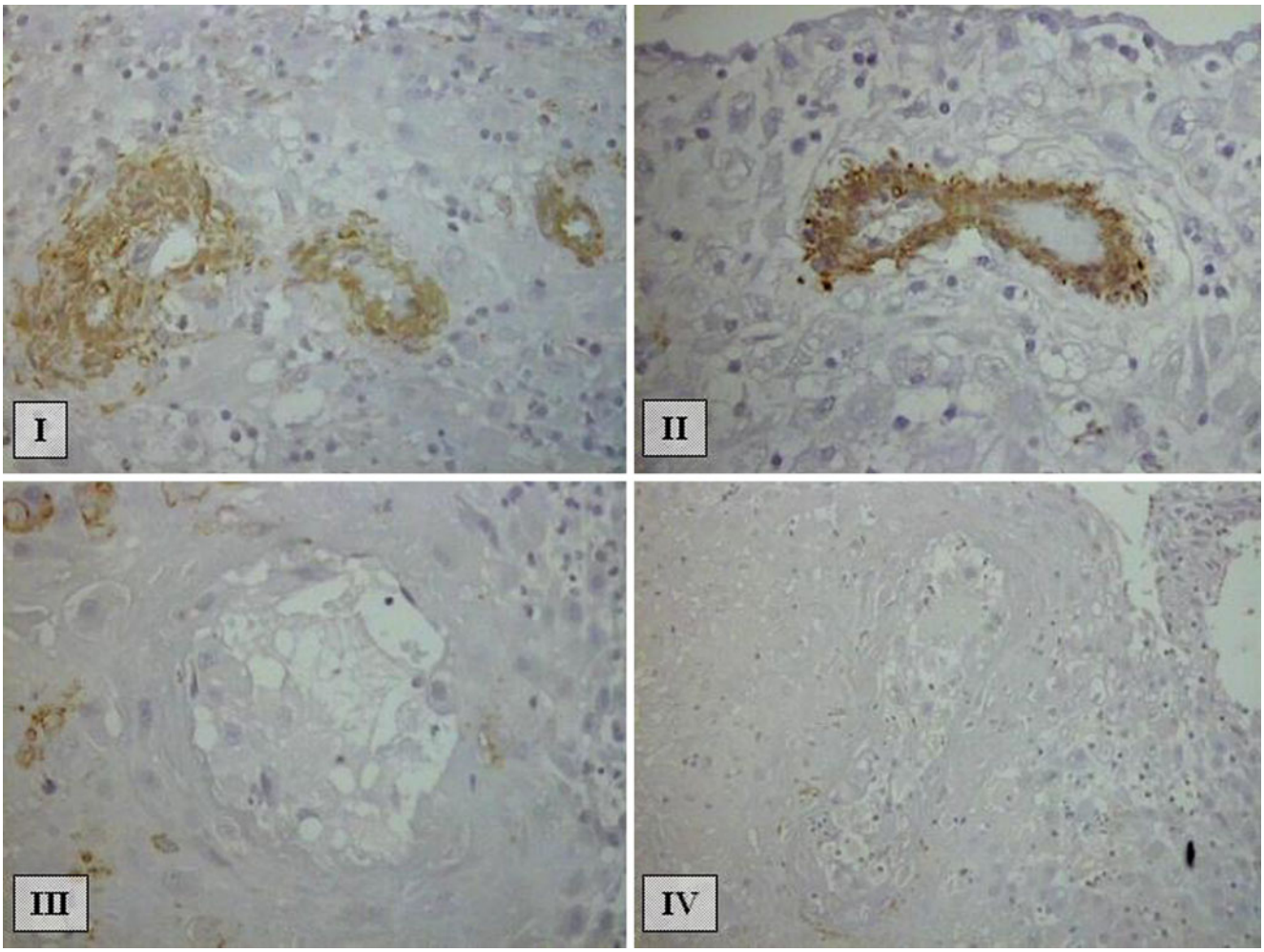

Fig. 6 Status of the muscularis in Groups 1 and 2 decidual vascular patterns (α-SMA): in Group 1, unconverted vessels in the basal decidua (*I*) and far from the implantation site (*II*) show preserved muscularis with actin-positive smooth muscle cells; conversely, arteries from Group 2 are diffusely damaged by fibrosclerosis and lack normal muscular walls (*III*, *IV*)

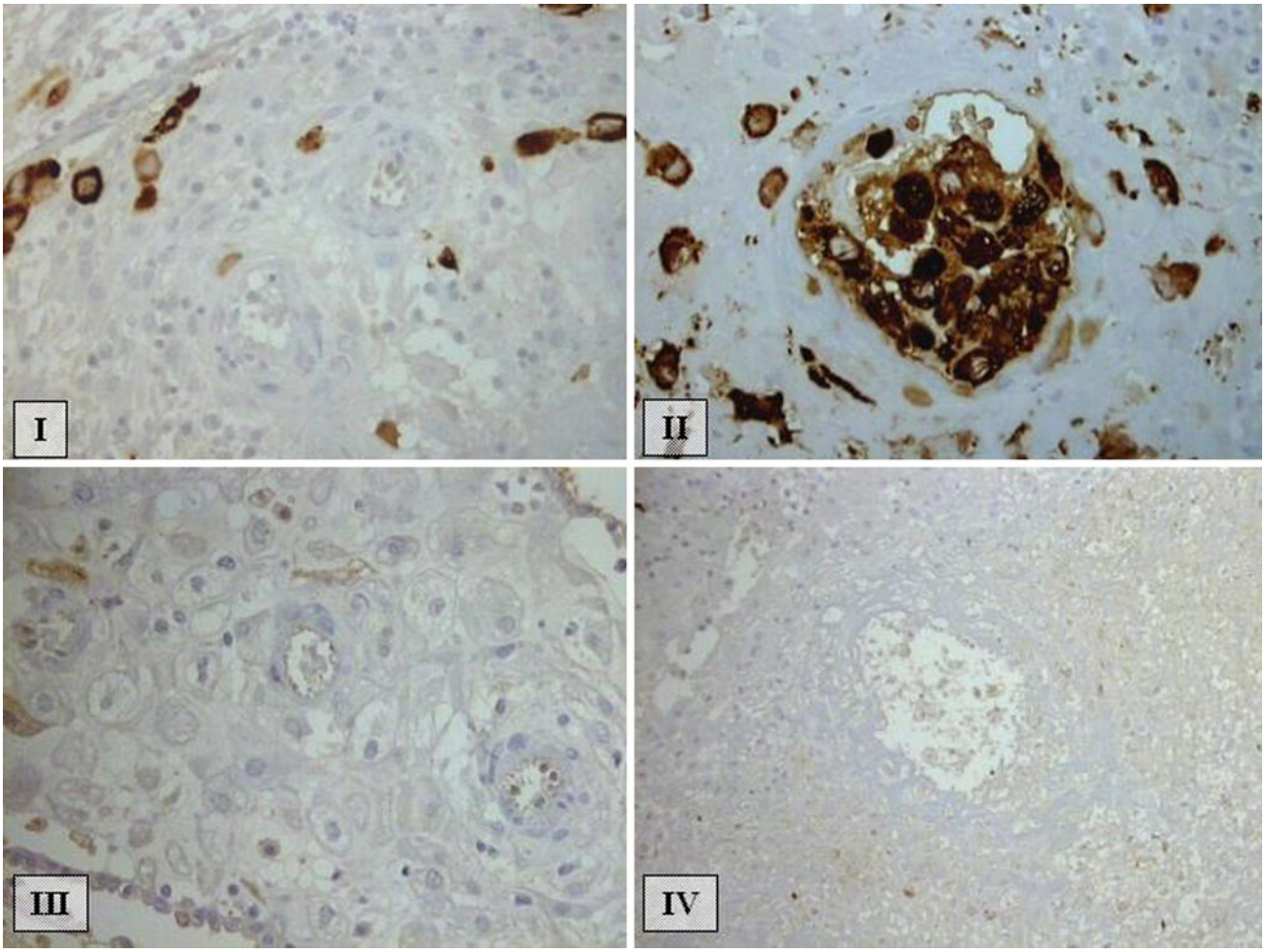

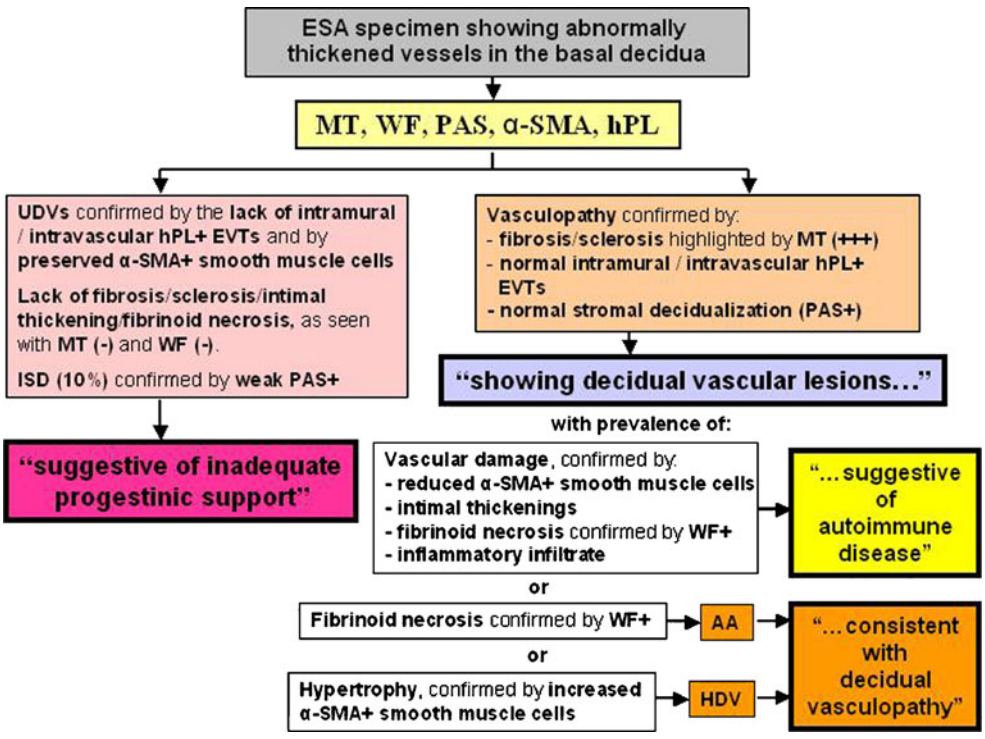

Fig. 8 Proposal of a diagnostic flow chart for the evaluation of ESAs showing abnormal decidual vessels on routine histological examination (*MT* Masson's trichrome stain, *WF* Weigert's stain for fibrin, *PAS* periodic acid–Schiff, *α-SMA* alpha-smooth muscle actin, *hPL* human placental lactogen, *UDVs* unconverted decidual vessels, *EVTs* extravillous trophoblast cells, *ISD* inadequate stromal decidualization)

clinical history available and can formulate his/her presumptive diagnosis on morphological findings alone. Moreover, due to limited clinical data, many of the above discussed decidual vascular pictures cannot be related to a well-defined clinical condition of the patient. It is then clear that the only diagnoses we can formulate are: "…suggestive of inadequate progestinic support/luteal defect" or "...suggestive of maternal autoimmune disease (also subclinical)" or "...showing histopathological features consistent with decidual vasculopathy". However, in our opinion, using the above discussed histochemical and immunohistochemical panel, some significant findings can be more reliably reported, helping the pathologist become more confident in everyday diagnostics.

In our experience, the proposal to clinicians of morphological diagnoses suggesting underlying pathologic conditions has indeed involved a different management of the patient in following pregnancies. Unfortunately, our casuistry is too recent to permit an extensive retrospective review, but we personally verify the value of our diagnostic hypotheses when we are requested to give a second opinion on repeated abortion specimens, as well as when we are involved in interdisciplinary audits for the planning of the patient's clinical management.

In conclusion, our work does not aim at a new classification of spontaneous abortion; rather, we attempted to provide some criteria for the evaluation and interpretation of specimens that routinely the pathologist is requested to investigate, often in absence of adequate clinical information.

Acknowledgments The authors would like to thank Mrs. Anna Scandale and Ms. Simona Pigozzi for performing histochemical and immunohistochemical stainings discussed in the present work, and for providing technical data listed in the text.

Conflict of interest statement We declare that we have no conflict of interest.

References

1. Kalousek DK, Lau AE (1992) Pathology of spontaneous abortion. In: Dimmick JE, Kalousek DK (eds) Developmental pathology of the embryo and fetus. Lippincott, Philadelphia, p 55
2. Wang X, Chen C, Wang L et al (2003) Conception, early pregnancy loss, and time to clinical pregnancy: a population-based prospective study. Fertil Steril 79:577–584
3. Lejeune V (2006) Early recurrent spontaneous abortion: how to take care in 2006? Gynecol Obstet Fertil 34:927–937
4. Georgiades P, Ferguson-Smith AC, Burton GJ (2002) Comparative developmental anatomy of the murine and human definitive placentae. Placenta 23:3–19
5. Pijnenborg R, Bland JM, Robertson WB et al (1983) Uteroplacental arterial changes related to interstitial trophoblast migration in early human pregnancy. Placenta 4:397–413
6. Naicker T, Khedun SM, Moodley J et al (2003) Quantitative analysis of trophoblast invasion in preeclampsia. Acta Obstet Gynecol Scand 82:722–729
7. Espinoza J, Romero R, Mee Kim Y et al (2006) Normal and abnormal transformation of the spiral arteries during pregnancy. J Perinat Med 34:447–458
8. Kim YM, Bujold E, Chaiworapongsa T et al (2003) Failure of physiologic transformation of the spiral arteries in patients with preterm labor and intact membranes. Am J Obstet Gynecol 189:1063–1069
9. Kalkunte S, Lai Z, Tewari N et al (2008) In vitro and in vivo evidence for lack of endovascular remodeling by third trimester trophoblasts. Placenta 29:871–878
10. Prada V, Musizzano Y, Mora M et al (2010) Immunohistochemical evidence of HLA-G expression in extravillous trophoblast invading decidual tissues. J Biol Res (in press)
11. Potdar N, Konje JC (2005) The endocrinological basis of recurrent miscarriages. Curr Opin Obstet Gynecol 17:424–428
12. Christensen B, Schindler AE (1997) Luteal defect in pregnancy as the cause of habitual abortion. Zentralbl Gynakol 119:462–466
13. Kraus FT, Redline RW, Gersen DJ et al (2004) AFIP Atlas of nontumor pathology no. 3—Placental pathology. Armed Forces Institute of Pathology
14. Benirschke K, Kaufmann P (2006) Pathology of the human placenta, 5th edn. Springer, New York
15. Katabuchi H, Yih S, Ohba T et al (2003) Characterization of macrophages in the decidual atherotic spiral artery with special reference to the cytology of foam cells. Med Electron Microsc 36:253–262
16. Nayar R, Lage JM (1996) Placental changes in a first trimester missed abortion in maternal systemic lupus erythematosus with antiphospholipid syndrome; a case report and review of the literature. Hum Pathol 27:201–206
17. Sherer Y, Tartakover-Matalon S, Blank M et al (2003) Multiple autoantibodies associated with autoimmune reproductive failure. J Assist Reprod Genet 20:53–57
18. Shoenfeldt Y, Blank M (2004) Autoantibodies associated with reproductive failure. Lupus 13:643–648
19. Poland BJ, Miller JR, Harris M et al (1981) Spontaneous abortion. A study of 1, 961 women and their conceptuses. Acta Obstet Gynecol Scand Suppl 102:1–32
20. O'Rahilly R, Bossy J, Müller F (1981) Introduction to the study of embryonic stages in man. Bull Assoc Anat (Nancy) 65:141–236
21. De Lellis RA (1984) Advances in immunohistochemistry. Mosby-Year Book, Saint Louis
22. Bussolati G, Gugliotta P, Fulcheri E (1984) Immunohistochemistry of actin in normal and neoplastic tissues, Chapter 19. In: DeLellis RA (ed) Masson monographs in diagnostic pathology no.7—Advances in immunohistochemistry. Masson Publishing USA, New York
23. Kimatrai M, Blanco O, Muñoz-Fernández R et al (2005) Contractile activity of human decidual stromal cells. II. Effect of Interleukin-10. J Clin Endocrinol Metab 90:6126–6130
24. Ceccarelli C, Eusebi V, Bussolati G (1988) Desmin and sarcomeric myosins in the diagnosis of rhabdomyosarcomas, Chapter 9. In: DeLellis RA (ed) Advances in immunohistochemistry. Raven, New York
25. Powell DW, Mifflin RC, Valentich JD et al (1999) Myofibroblasts. I. Paracrine cells important in health and disease. Am J Physiol 277:C1–C19
26. Zalewski A, Shi Y (1997) Vascular myofibroblasts. Lessons from coronary repair and remodeling. Arterioscler Thromb Vasc Biol 17:417–422
27. Musizzano Y, Fulcheri E (2007) Peculiar features of intermediate trophoblast proliferation in decidual vascular walls in autoimmune diseases and luteal defects. Exp Biol Rep 1(1)
28. Collins P (ed) (1995) Embriology and development, in: Gray's anatomy, 38th edn. Churchill Livingstone, New York, p 166
29. Fulcheri E, Mariuzzi GM (2007) Patologia della gravidanza, Chapter 12.8. In: Mariuzzi GM (ed) Anatomia Patologica e correlazioni anatomo-cliniche. Piccin Nuova Libraria, Padova, pp 1946–1948

Virchows Arch (2010) 456:561–569
DOI 10.1007/s00428-010-0890-z

ORIGINAL ARTICLE

Immunohistochemical characterization of reparative tissue present in human osteoarthritic tissue

Randall D. C. Barley · Adetola B. Adesida · Keith M. Bagnall · Nadr M. Jomha

Received: 14 May 2009 / Revised: 23 January 2010 / Accepted: 2 February 2010 / Published online: 25 February 2010
© Springer-Verlag 2010

Abstract Studies involving disease progression in osteoarthritis (OA) have typically focused on the deterioration of native articular cartilage (AC) rather than the de novo cartilage which is frequently present. In general, there are two categories of de novo tissue observed in OA: (1) a pannus-like fibrocartilage that overlays native AC and (2) osteophytes. In this study, 30 AC samples representing a range of disease stages consistent with early to intermediate OA were examined for the occurrence of pannus-like tissue. All AC samples were examined immunohistochemically and compared with cartilage from three mature-looking osteophytes. To accomplish this, serial cartilage sections, derived from total knee arthroplasty specimens, were stained with hematoxylin and eosin and probed with antibodies raised against collagen type I, collagen type II, and aggrecan. Pannus-like tissue ranging from fibrous tissue to fibrocartilage was observed in 3 out of 30 AC samples. The appearance of this tissue was restricted to cartilage displaying signs of intermediate deterioration consistent with Outerbridge grade 2. Collagen type I, collagen type II, and aggrecan were abundant in both pannus-like tissue and osteophyte cartilage. In OA, the intrinsic repair process can yield a range of tissue types between fibrous tissue and fibrocartilage that is well integrated with the underlying, eroded AC. The absence of repair tissue from osteoarthritic samples representing the early stages of AC deterioration indicated that a relationship exists between macroscopic damage and a localized cellular repair response. Several histological and immunohistochemical similarities were also observed between the pannus-like tissue and osteophyte-derived cartilage, suggesting a common developmental process.

Keywords Osteoarthritis · Fibrocartilage · Osteophyte · Intrinsic repair · Collagen · Aggrecan

R. D. C. Barley · A. B. Adesida · K. M. Bagnall · N. M. Jomha (✉)
Department of Surgery, University of Alberta,
2D2.28 W.C. Mackenzie Health Sciences Centre,
Edmonton, AB, Canada T6G 2B7
e-mail: njomha@ualberta.ca

Introduction

Osteoarthritis (OA) is a common, degenerative joint disease characterized by pain, joint stiffness, and dysfunction which represents a major cause of disability [1]. Although traditionally viewed as a continuously progressive degenerative disease [2], evidence continues to emerge which details the non-linearity of OA progression. For example, 23% of OA patients report periods of symptomatic improvement [3] suggesting that interludes in disease progression may be a common occurrence. The complexity of OA progression appears to extend beyond mere interludes between periods of active cartilage erosion because physical evidence indicates that 16% of patients with OA of the knee demonstrate radiographic increases in their joint space [4]. While the precise type of tissue responsible for the above-mentioned increases remains unclear, a more recent study by Shibakawa et al. [5] histologically characterized the soft tissue or reparative tissue covering OA articular surfaces and found the tissue to closely resemble fibrocartilage based on positive staining for type I collagen and no staining for proteoglycans and type II collagen. When taken together, these reports suggest that interludes exist during OA progression in which the production of repair-like fibrocartilage may be a common feature. To date, there are two main types of tissues that have been described in association with advanced OA:

fibrocartilage [6] and osteophytes [7]. According to one study, fibrocartilage occurs in over 90% of total knee arthroplasty (TKA) specimens; thus, indicating the ubiquitous intrinsic repair capacity of AC [8]. This abundant repair tissue, which typically overlays damaged articular cartilage (AC) in OA joints, was termed pannus-like by Shibakawa et al. in order to distinguish it from true pannus tissue observed in rheumatoid arthritis [5]. In contrast to the expression profile seen in hyaline AC, Shibakawa et al. reported that the pannus-like tissue was high in collagen type I and low in both aggrecan and collagen type II. Despite the prevalence of fibrocartilage in OA, its composition and lack of durability seems to foster little scientific interest as evidenced by the limited number of publications on the tissues' characteristics and biological relevance. In contrast to the pannus-like fibrocartilage, osteophytes are cartilage-covered nodules of bone that characteristically appear around the margins of osteoarthritic joints (reviewed in [9]). Although being a hallmark of advanced OA, osteophytes also have received little scientific attention. However, one study conducted by Gelse and co-workers found that osteophytes emerge as fibrous tissue and mature through a series of steps ultimately resulting in cartilage with a distinctly hyaline-like appearance [10]. They discovered that juvenile osteophytes are high in collagen type I and low in aggrecan and collagen type II (i.e., similar to fibrocartilage), whereas mature osteophytes were low in collagen type I and high in aggrecan and collagen type II (i.e., similar to hyaline cartilage). Given the similarities between juvenile osteophytes and the pannus-like tissue reported by Shibakawa et al., a direct immunohistological comparison is merited to determine the extent of the similarities and whether there is also evidence for maturation among samples of pannus-like tissue.

Given that the soft tissue or reparative covering articular surface of OA tissues are a common yet frequently overlooked feature of OA, this study was designed to ascertain (1) whether de novo fibrocartilagenous tissue was present in minimally damaged AC, (2) the extent to which fibrocartilagenous tissues share immunohistochemical (IHC) features in common with osteophytes, and (3) whether tissues associated with early AC deterioration displayed the typical pattern of extracellular matrix (ECM) expression for fibrocartilage. This study provides a descriptive histological and immunohistochemical analysis and comparison of the soft tissue associated with OA.

Materials and methods

Tissue collection and processing

OA tissue from femoral condyles was obtained during surgery for TKA. The tissue was immediately placed in saline solution and stored at 4°C for up to 24 h. One-centimeter-diameter cylindrical cores of AC and underlying bone (dowels) were obtained from load-bearing regions using a stainless steel coring tool. Cartilage was removed from the underlying bone at the cartilage–bone junction, and the AC was fixed in 4% formalin. Dowels representing only Outerbridge (OB) grades 0, 1, and 2 [11] were collected for analysis. A total of 10 dowels were collected for each of the 3 OB grades for a total of 30 dowels. The 30 dowels were collected from 17 OA patients (7 males and 10 females) that ranged in age from 58 to 84 years (mean age of 67.4±7.4 years). The second experimental group consisted of three fully developed, mature looking osteophytes that were harvested from a single joint. The osteophyte-furnished cartilage was removed from the underlying bone and was treated in parallel with the cartilage from the dowels.

Histology

Formalin-fixed AC was embedded in paraffin, sectioned at 5-μm intervals and mounted on Superfrost Plus glass slides. Immediately prior to staining, sections were deparaffinized using ProPar (Anatech Ltd) and rehydrated in a graded series of ethanol washes. Deparaffinized sections were subjected to routine hematoxylin and eosin (H&E) staining to show overall tissue morphology. All sections were dehydrated through a series of graded ethanol washes for 20 s each, mounted, and visualized at ×50 magnification on a Leica DM/RE microscope. Photomicrographs of representative regions within the sections were taken using a CoolSnap CCD camera (Fig. 1). All sections were visually examined and the presence of any fibrous tissue or fibrocartilage was noted.

Immunohistochemistry

AC sections were deparaffinized and subjected to an optimized antigen retrieval step consisting of a 60-min digestion in 5 mg/ml pepsin, pH 2.0 (Sigma Cat # P-7000). The pepsin digest was optimized to avoid saturation staining and thus yield the greatest amount of information regarding relative staining levels within a section. Following digestion, sections were rinsed thoroughly in water to remove the pepsin, and endogenous peroxidase activity was quenched using a 30-min incubation in 3% H_2O_2 in methanol. All immunohistochemistry was performed using Vectastain Elite ABC kits (Vector Laboratories, Cat. # 6102 and 6105) according to the manufacturer's directions. Primary antibodies [mouse anti-collagen type I (MAB 3391, Chemicon) or mouse anti-collagen type II (MAB 8887, Chemicon) or rabbit anti-aggrecan (AF 1220, R&D Systems] were applied to separate AC sections from each

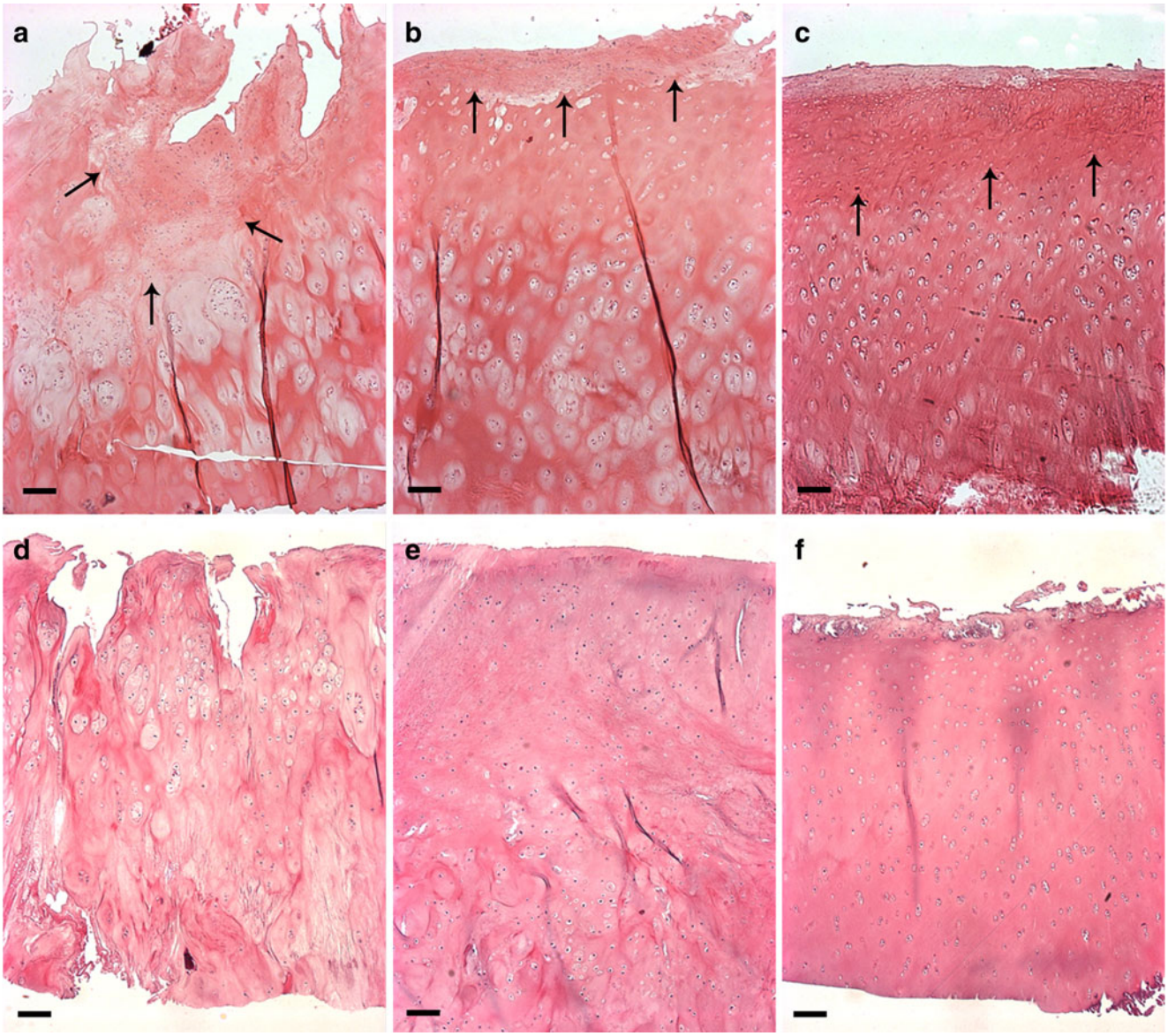

Fig. 1 Micrographs showing the range of pannus-like tissue (**a**–**c**) and osteophyte cartilage (**d**–**f**) found in osteoarthritis specimens. Hematoxylin and eosin stained sections showing a well-integrated fibrous repair tissue (**a**), a poorly integrated fibrocartilagenous lamination (**b**), and a fibrocartilagenous restoration of an articulating surface (**c**), a mixture of fibrous tissue and fibrocartilage (**d**), predominantly fibrocartilage (**e**), and predominantly hyaline-like tissue (**f**). Tissue below the *arrows* represents native articular cartilage while tissue above the *arrows* represents de novo tissue synthesis. Notice the morphological variation within both the pannus-like tissue and osteophyte cartilage. *Bar*=100 μm

sample at a 1:100 dilution in phosphate-buffered saline (PBS), then incubated for 30 min in a humidified chamber. Sections were washed in PBS, and biotinylated secondary antibodies were applied for 30 min. Following the secondary antibody incubation, AC sections were washed in PBS and incubated for 30 min in VectaStain ABC reagent. After a final rinse in PBS, color development was achieved by incubating the sections for 5 min in metal-enhanced 3,3'-diaminobenzidine (DAB) (Pierce Cat # 1856090). Stained tissue sections were dehydrated using a series of graded ethanol washes, mounted, and visualized at ×50 magnification on a Leica DM/RE microscope. Photomicrographs of representative regions within the sections were taken using a CoolSnap CCD camera (Figs. 2 and 3). Confirmation of antibody specificity to collagen type I and collagen type II was performed using 5-μm thick sections of normal human AC and human anterior cruciate ligament (ACL). No significant cross-reactivity was observed with either MAB 3391 or MAB 8887. Sections in which primary antibodies were omitted showed no significant non-specific staining.

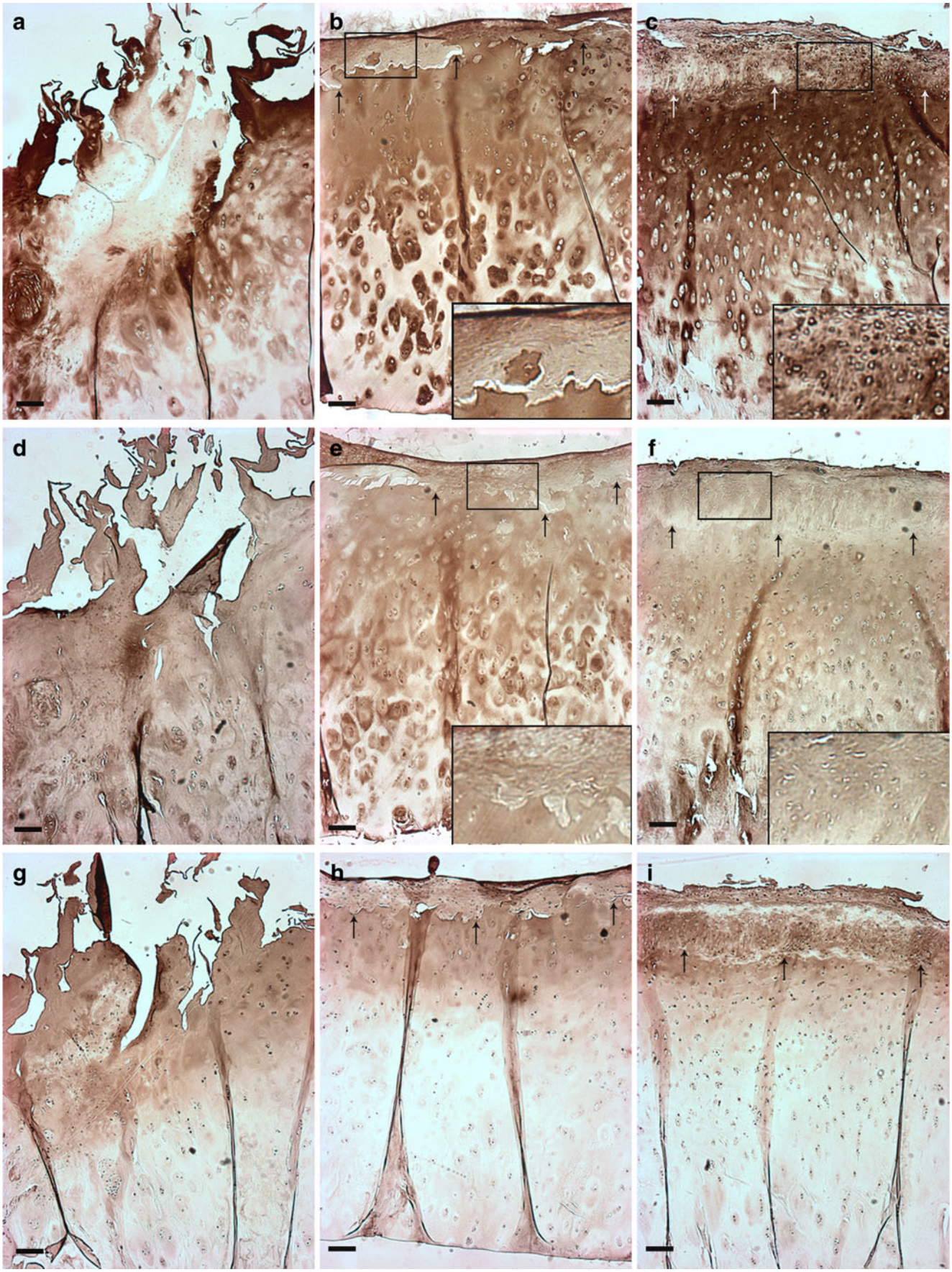
a
b
c
d
e
f
g
h
i

◀ **Fig. 2** Micrographs showing pannus-like tissue sections stained for collagen type II (**a**–**c**), aggrecan (**d**–**f**), and collagen type I (**g**–**i**). Notice the abundance of collagen type II and aggrecan in the pannus-like tissue. Also note the strong similarities in the intensity of collagen type II and aggrecan staining between the pannus-like tissue and the native articular cartilage that underlies it. *Arrows* indicate de novo tissue boundary. *Box* indicates the location of the inset. *Bar*=100 μm

Results

Histology

Three of the thirty samples displayed morphology atypical for either normal AC or degraded OA cartilage. This atypical tissue ranged in appearance from fibrous tissue (a high density of elongated fibroblast-like cells in a matrix displaying the typical wavy pattern of collagen fibril staining) to fibrocartilage (round, sparsely distributed chondrocyte-like cells in a more homogeneously staining matrix). In all three cases, the de novo tissue was associated with AC samples showing some of the most advanced signs of deterioration in the study (i.e., Outerbridge 2). Figure 1a shows an example of characteristic fibrous tissue in-filling a large, deep fissure in the native AC. Integration of the fibrous tissue appeared to be very good; however, the defect was not completely filled and an irregular surface remained. Figure 1b shows an example of tissue more closely resembling fibrocartilage

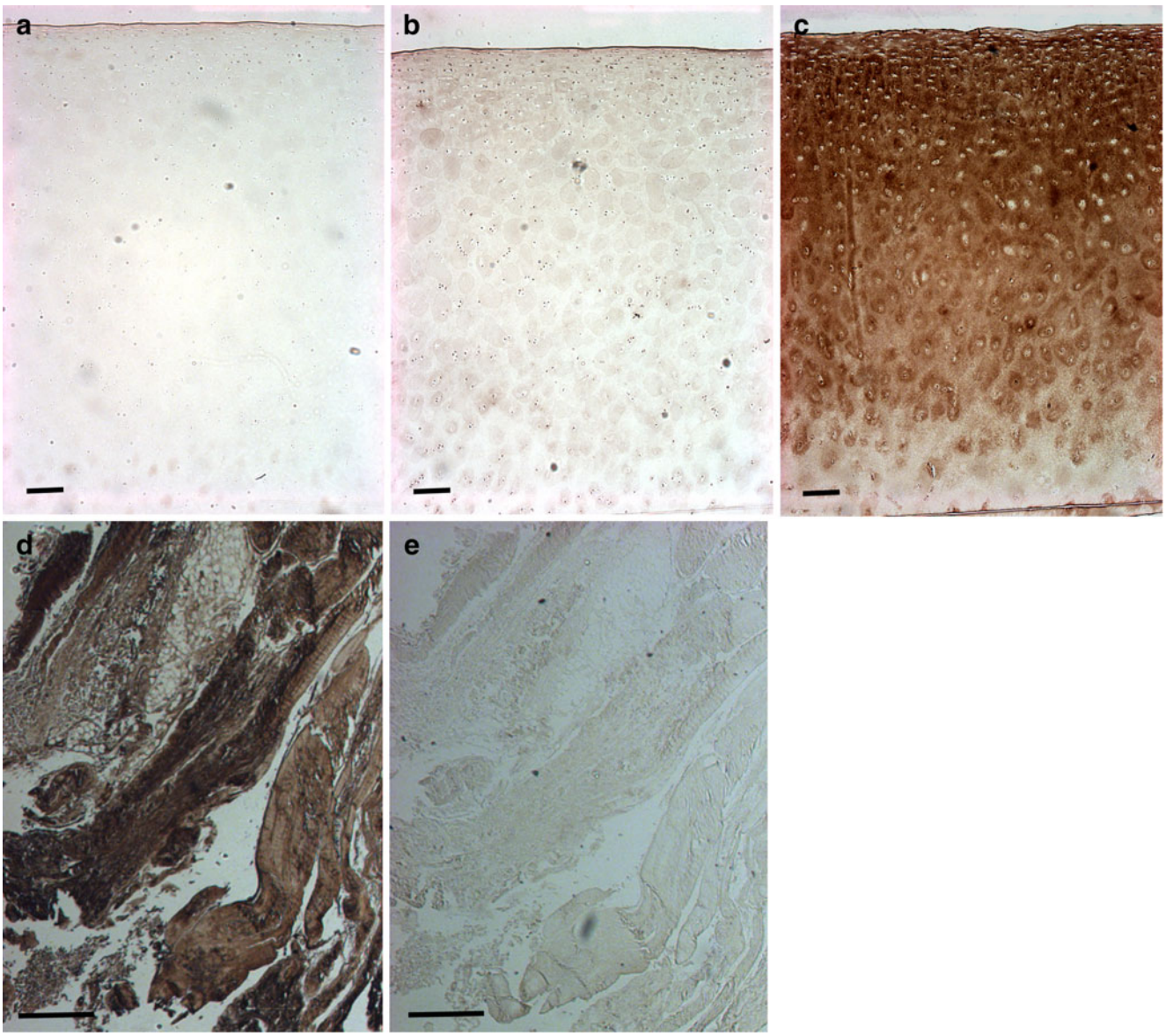

Fig. 3 Micrographs showing the relative differences in staining intensity within 5-μm tissue sections. Normal human articular cartilage stained with either no primary antibodies (**a**) or primary antibodies raised against collagen I (**b**) or collagen II (**c**). Notice the intense staining with anti-collagen II antibodies and the relative absence of staining with anti-collagen I antibodies. Human anterior cruciate ligament stained with antibodies against collagen I (**d**) or collagen II (**e**). *Bar*=100 μm

which had resurfaced an area larger than the dowel itself. The incompletely integrated pannus-like tissue loosely overlaid the previously eroded native AC. In contrast to the irregular surface associated with the fibrous tissue, the sample in Fig. 1b yielded a relatively smooth surface. Finally, Fig. 1c provided an example of fibrocartilage greater than 0.5 mm thick that was observed covering a region larger than 1 cm in diameter. This fibrocartilage tissue was completely integrated with the underlying native AC below as evidenced by the sharply delineated, yet congruent boundary between the upper fibrocartilage and lower AC. Unlike the vascular features of the fibrocartilagenous pannus-like tissue reported by Shibakawa and co-workers, the fibrocartilage featured here, lacked vascularity as evidenced by the absence of the vascular lumen.

Similar to the pannus-like tissue, the histology of osteophyte cartilage also displayed a broad range of tissue types. Osteophyte cartilage ranged from a heterogeneous mixture of fibrous tissue (Fig. 1d) to tissue closely resembling hyaline cartilage (Fig. 1f). The overall level of tissue organization differed considerably both within and between samples. Histologically, the surface of the osteophytes varied from relatively smooth (Fig. 1e) to moderately fibrillated (Fig. 1d). The average depth of osteophyte cartilage (1.84±0.10) was consistent with the depth of observed in normal AC [12].

Immunohistochemistry

Abundant collagen type II staining was detected in fibrocartilagenous tissue regardless of the degree of tissue integration. When compared to the underlying native AC, intermediate to high levels of collagen type II staining were observed throughout the fibrocartilagenous tissue (Fig. 2b, c). However, differences were observed in the pattern of collagen type II staining between incompletely integrated and well-integrated samples, despite the similarity in their overall levels of collagen type II deposition. Unlike the incompletely integrated pannus-like tissue, the well-integrated tissue displayed the type of territorial collagen type II deposition that is characteristic of AC in the early stages of OA. In contrast to the fibrocartilagenous tissue, the fibrous tissue was nearly devoid of collagen type II staining (Fig. 2a). Aggrecan was abundant in all three pannus-like samples and the level of staining was comparable to the levels seen in the underlying native AC (Fig. 2d–f).

The pattern of aggrecan distribution in the well-integrated pannus-like tissue (Fig. 2f) more closely resembled the homogeneous staining typically seen in AC, whereas the staining in the incompletely integrated pannus-like tissue possessed a granular appearance (Fig. 2e). Like the aggrecan staining, collagen type I staining was observed in all three pannus-like tissue samples (Fig. 2g–i). The pannus-like tissue displayed levels of collagen type I staining comparable to the levels seen in the immediately adjacent underlying native AC, with minimal collage type I noted in the deeper layers.

Figure 3 shows the high levels of antigen specificity for the antibodies used in the detection of collagen I and II. Using the anti-collagen I monoclonal antibody, the level of staining in the no primary control (Fig. 3a) was similar to the level of staining seen in normal articular cartilage (Fig. 3b). In contrast, the anti-collagen II antibody yielded very intense staining in normal AC (Fig. 3c). When human ACL sections were incubated with the above-mentioned antibodies, the anti-collagen I antibody yielded very intense staining (Fig. 3d) while the anti-collagen II antibody showed only very faint background staining (Fig. 3e).

The osteophytes exhibited an ECM expression profile that was similar to the profile observed in the pannus-like tissue. All three samples of osteophyte cartilage displayed pronounced collagen type II staining (Fig. 4a–c). However, there was considerable variability in this staining both within and between the samples. The samples displayed evidence of the territorial localization of collagen type II typically seen in AC during the early to intermediate stages of OA [13]. A broad range of staining for aggrecan was also observed between osteophyte cartilage samples (Fig. 4d–f). Although aggrecan was present in all osteophyte cartilage samples, one sample (Fig. 4d) displayed a highly irregular aggrecan distribution. This sample contained large regions that were nearly devoid of aggrecan staining into which sharply defined, intensely staining aggrecan projections were interspersed. This was in contrast to the other two samples (Fig. 4e, f) which stained relatively evenly from the superficial to deep layers. The intensely staining osteophyte samples (Fig. 4e, f) showed a reduction in territorial staining for aggrecan that is typically associated with AC in the early stages of OA [14]. Finally, osteophyte cartilage also displayed a broad range of collagen type I deposition (Fig. 4g–i). Although some collagen type I deposition was found throughout the section displaying deep fissuring (Fig. 4g), it was predominantly associated with the most superficial layer of osteophyte cartilage. Interestingly, the depth of collagen type I staining in the sections appeared to increase as a function of structural damage.

Fig. 4 Micrographs showing the range of immunohistochemical staining for collagen type II (**a**–**c**), aggrecan (**d**–**f**), and collagen type I (**g**–**i**) in serial sections taken from three human osteophytes. Note the abundant expression of collagen type II and aggrecan staining. *Bar*=100 μm

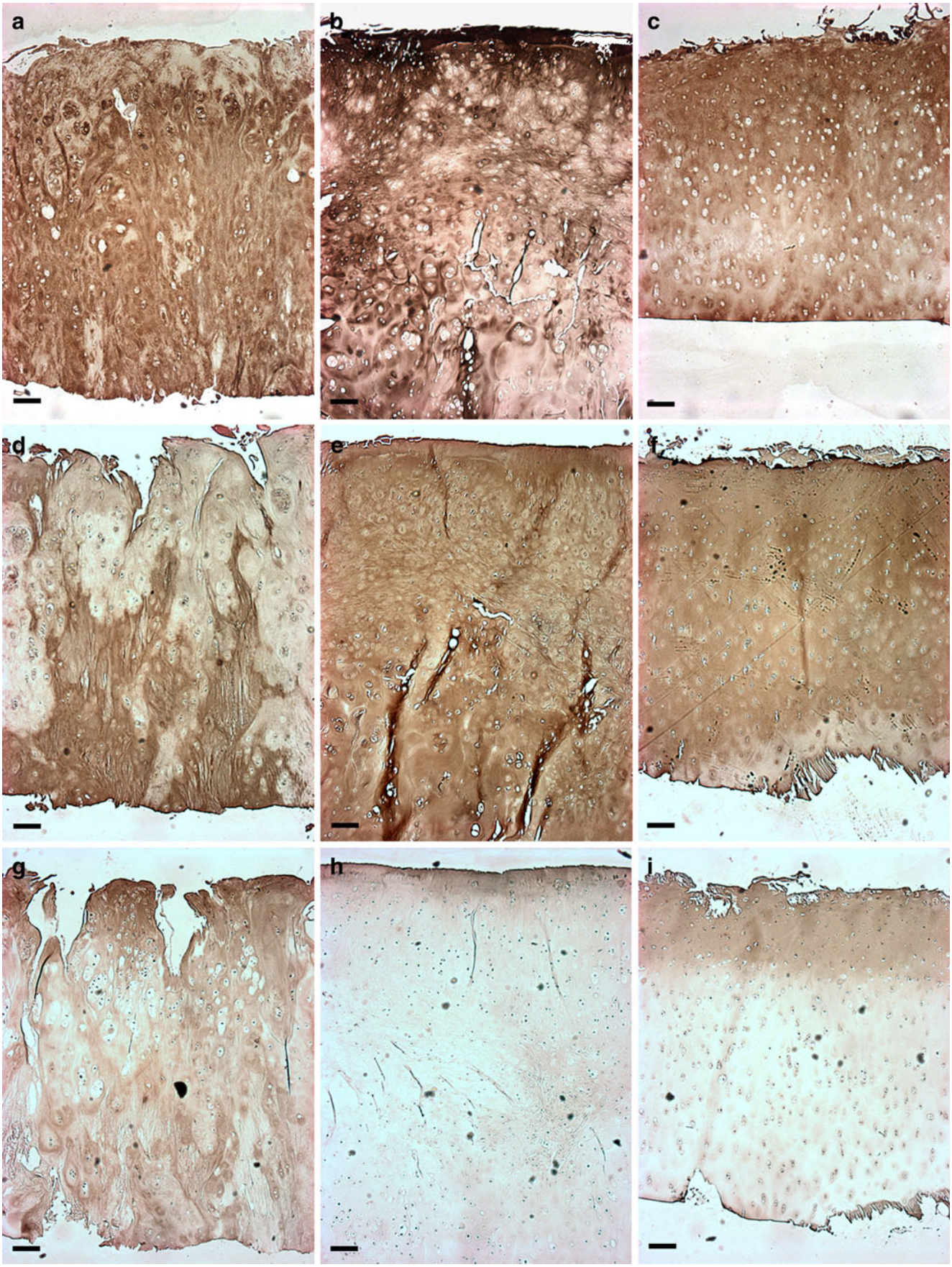
a
b
c
d
e
f
g
h
i

Discussion

The histochemical characteristics of some of the soft tissue covering AC, as observed in this study, demonstrates the considerable potential of intrinsic repair that exists in OA tissue. The pannus-like tissue varied from fibrous tissue which occupied the spaces between deep fissures in the eroded AC, to a thick layer of fibrocartilage which restored a relatively smooth surface to the previously eroded area. The extent of pannus-like tissue integration also varied considerably, but near complete integration was observed in cases of both fibrous tissue and fibrocartilage.

Histologically, the pannus-like repair tissue did not possess the structural organization characteristics of normal hyaline or osteoarthritic AC; nonetheless, it did share some of the immunohistochemical characteristics. For example, staining for collagen type II and aggrecan were surprisingly abundant, which is in contrast to the very low levels expected in fibrocartilage. These observations suggest that while repair tissue may lack the structural organization of AC, it does display an abundance of the two hallmark ECM components, collagen II and aggrecan that define AC. These findings are in contrast to the findings of Shibakawa et al. [5] who reported that pannus-like tissue showed elevated staining for collagen type I and was devoid of staining for both sulphated proteoglycans and type II collagen. Such divergent findings are difficult to explain; however, they may be related to the vascularity observed in their pannus-like tissue samples. To this end, we feel our study will benefit from further IHC characterization, particularly IHC studies for Factor VIII and its binding protein von Willebrand Factor to assess the presence or absence of vascularity as described by Petersen et al. [15], in view of the observation that a similarly avascular tissue as articular cartilage, gliding tendon, displayed characteristics of a vascular nature by expression of Factor VIII [15].

Based on the distribution of the soft tissue within this study, there appears to be a relationship between structural damage and the appearance of pannus-like tissue. In the 30 samples of OA tissue that ranged from OB-0 to OB-2, evidence of repair tissue was present in only three of them. Although one of the three samples was initially scored as OB-1, upon histological inspection, it became apparent that the tissue actually displayed evidence of damage extending into the transitional layer that was consistent with a score of OB-2. Interestingly, this damage was effectively masked by a layer of fibrocartilage that yielded a remarkably smooth surface and resulted in the underestimation of the actual AC deterioration. Even though all samples were obtained from patients undergoing TKA for advanced OA, soft/repair tissue was not found in AC with levels of tissue deterioration consistent with either OB-0 or OB-1. The association between structural damage and repair tissue synthesis suggested that tissue repair may be a localized cellular response only initiated by conditions such as structural damage or apoptosis that are common in the intermediate to late stages of OA [16]. Interestingly, the elevated anabolism that coincides with the emergence of structural damage [17] may be directly responsible for the production of the repair tissue seen in intermediate stages of OA. This surge in anabolism may temporarily permit the AC to overcome the net loss of ECM components, and the subsequent accumulation of ECM in the superficial zone could explain the observed appearance of repair tissue in structurally damaged AC. Furthermore, the accumulation of this repair tissue could account for both the improvement in patient symptoms reviewed in Buckwalter et al. [2] and the reported radiographic increases in joint space and thus may represent part of the normal course of disease progression in OA.

The origin of this pannus-like tissue in OA could arise through one of two distinct mechanisms. While it is possible that existing native AC may have been remodeled into fibrocartilage as Shibakawa et al. [5] have speculated, it is more likely that the fibrocartilage in Fig. 1c represents a de novo cartilage synthesis event. Simple remodeling of the tissue would not account for the sudden contrast in cellular distribution or the sharply delineated boundary that exists between upper fibrocartilage and the underlying native AC. Furthermore, the fact that both collagen type I and II have recently been shown to accumulate in very high levels in moderately fibrillated tissue [17], indicates that the step preceding the emergence of fibrocartilage displays the appropriate precursory levels of anabolism for the generation of de novo tissue. Therefore, it is likely that the observed de novo synthesis is merely an extension of the natural, albeit short lasting, anabolic interlude that has been described in early to intermediate OA [18–22].

Osteophytes were examined alongside pannus-like tissue to explore histological and immunohistochemical parallels between these soft/reparative tissues. Osteophyte cartilage appeared to have a wide range of features in common with the pannus-like fibrocartilage at the histological level. Both tissues shared a similar expression profile for collagen type I, collagen type II, and aggrecan. Given the organizational, histological, and IHC similarities between the cartilage associated with osteophytes and the pannus-like tissue, their development likely relies on many of the same genetic and biochemical signaling pathways. If this is true, then perhaps the pannus-like cartilage that develops in OA joints could share the same pattern of maturation as osteophytes (if provided the appropriate environment) as described by Gelse et al. [10]. In this model, pannus-like tissue would begin as fibrous tissue devoid of collagen type II and aggrecan and high in collagen type I (much like what was described by Shibakawa et al.) and progress through several

stages until the tissue resembled well-integrated fibrocartilage high in collagen type II and aggrecan (as described here). In fact, Koshino et al. [23] indirectly provided evidence for a range of maturity levels in their study on the regeneration of AC following high tibial osteotomy. They described a series of 47 eburnated OA joints that were intrinsically resurfaced, yielding a range of tissue types all the way up to hyaline-like cartilage. The study of Koshino et al. supports the concept that pannus-like repair tissue matures through a series of stages much like osteophytes and is further evidence of the commonly overlooked yet significant repair potential that exists in OA cartilage.

Finally, given that Gelse et al. [10] found that the cartilage of fully mature osteophytes very closely resembles hyaline cartilage, it is possible that the pannus-like tissue also has this potential. For this reason, the knowledge gained from a closer examination of the intrinsic repair process and the factors leading to its ultimate failure would be invaluable towards our understanding of the natural barriers that are currently impeding extrinsic repair techniques.

In this study, pannus-like tissue ranging from fibrous tissue to fibrocartilage was associated with structurally damaged OA cartilage. The pannus-like tissue was not observed in samples exhibiting the lower levels of deterioration seen in OB grades 0 or 1, suggesting that the intrinsic repair process may be highly localized (i.e., OB-0 and 1 samples did not have evidence of pannus-like tissue when OB-2 samples from the same joint did). Given that OB-2 tissue typically displays elevated levels of anabolism and that soft/reparative tissue was not observed in the predominantly degenerated OB-1 samples, it is likely that soft/reparative tissue synthesis is a direct extension of the anabolic interlude seen in later stages of OA. Finally, the osteophyte-associated cartilage and pannus-like fibrocartilage showed numerous similarities at the histochemical levels, suggesting that they may share a common evolution.

Acknowledgements This work was funded by the Edmonton Orthopaedic Research Committee.

Conflict of interest statement We declare that we have no conflict of interest.

References

1. Hunter DJ, Felson DT (2006) Osteoarthritis. BMJ 332:639–642
2. Buckwalter JA, Martin JA (2006) Osteoarthritis. Adv Drug Deliv Rev 58:150–167
3. Ledingham J, Regan M, Jones A et al (1995) Factors affecting radiographic progression of knee osteoarthritis. Ann Rheum Dis 54:53–58
4. Spector TD, Dacre JE, Harris PA et al (1992) Radiological progression of osteoarthritis: an 11 year follow up study of the knee. Ann Rheum Dis 51:1107–1110
5. Shibakawa A, Aoki H, Masuko-Hongo K et al (2003) Presence of pannus-like tissue on osteoarthritic cartilage and its histological character. Osteoarthritis Cartilage 11:133–140
6. Meachim G, Osborne GV (1970) Repair at the femoral articular surface in osteo-arthritis of the hip. J Pathol 102:1–8
7. Jeffery AK (1975) Osteophytes and the osteoarthritic femoral head. J Bone Joint Surg Br 57:314–324
8. Nakata K, Bullough PG (1986) The injury and repair of human articular cartilage: a morphological study of 192 cases of coxarthrosis. Nippon Seikeigeka Gakkai Zasshi 60:763–775
9. van der Kraan PM, van den Berg WB (2007) Osteophytes: relevance and biology. Osteoarthritis Cartilage 15:237–244
10. Gelse K, Soder S, Eger W et al (2003) Osteophyte development—molecular characterization of differentiation stages. Osteoarthritis Cartilage 11:141–148
11. Outerbridge RE (1961) The etiology of chondromalacia patellae. J Bone Joint Surg Br 43-B:752–757
12. Hunziker EB, Quinn TM, Hauselmann HJ (2002) Quantitative structural organization of normal adult human articular cartilage. Osteoarthritis Cartilage 10:564–572
13. Hollander AP, Pidoux I, Reiner A et al (1995) Damage to type II collagen in aging and osteoarthritis starts at the articular surface, originates around chondrocytes, and extends into the cartilage with progressive degeneration. J Clin Invest 96:2859–2869
14. Visco DM, Johnstone B, Hill MA et al (1993) Immunohistochemical analysis of 3-B-(-) and 7-D-4 epitope expression in canine osteoarthritis. Arthritis Rheum 36:1718–1725
15. Petersen W, Pufe T, Kurz B et al (2002) Angiogenesis in fetal tendon development: spatial and temporal expression of the angiogenic peptide vascular endothelial cell growth factor. Anat Embryol (Berl) 205:263–270
16. Thomas CM, Fuller CJ, Whittles CE et al (2007) Chondrocyte death by apoptosis is associated with cartilage matrix degradation. Osteoarthritis Cartilage 15:27–34
17. Pfander D, Rahmanzadeh R, Scheller EE (1999) Presence and distribution of collagen II, collagen I, fibronectin, and tenascin in rabbit normal and osteoarthritic cartilage. J Rheumatol 26:386–394
18. Aigner T, Bertling W, Stoss H et al (1993) Independent expression of fibril-forming collagens I, II, and III in chondrocytes of human osteoarthritic cartilage. J Clin Invest 91:829–837
19. Aigner T, Gluckert K, von der MK (1997) Activation of fibrillar collagen synthesis and phenotypic modulation of chondrocytes in early human osteoarthritic cartilage lesions. Osteoarthritis Cartilage 5:183–189
20. Eyre DR, McDevitt CA, Billingham ME et al (1980) Biosynthesis of collagen and other matrix proteins by articular cartilage in experimental osteoarthrosis. Biochem J 188:823–837
21. Lippiello L, Hall D, Mankin HJ (1977) Collagen synthesis in normal and osteoarthritic human cartilage. J Clin Invest 59:593–600
22. Young AA, Smith MM, Smith SM et al (2005) Regional assessment of articular cartilage gene expression and small proteoglycan metabolism in an animal model of osteoarthritis. Arthritis Res Ther 7:R852–R861
23. Koshino T, Wada S, Ara Y et al (2003) Regeneration of degenerated articular cartilage after high tibial valgus osteotomy for medial compartmental osteoarthritis of the knee. Knee 10:229–236

Virchows Arch (2010) 456:571–579
DOI 10.1007/s00428-010-0903-y

ORIGINAL ARTICLE

Considerations on the mechanisms of alveolar remodeling in centriacinar emphysema

Masuki Yamamoto · Shinobu Kunugi · Arimi Ishikawa · Yuh Fukuda

Received: 4 September 2009 / Revised: 20 January 2010 / Accepted: 28 February 2010 / Published online: 20 March 2010
© Springer-Verlag 2010

Abstract Chronic obstructive pulmonary disease is mainly characterized by irreversible airflow limitation, and its major pathological change is alveolar destruction and enlargement, which induces emphysema. In this study, we used stereoscopic microscopy to observe the cut surfaces of 21 surgically resected or autopsied lungs showing centriacinar emphysema. We identified columnar structures of various sizes in the cystic spaces. These columnar structures constituted two types: one that was associated with pulmonary artery and another that was not. We examined these structures in detail by light microscopy and performed statistical analyses. Columnar structures without pulmonary artery showed destruction and accumulation of alveoli, including abnormally aggregated elastic fibers. In contrast, pulmonary architecture was preserved in columnar structures with pulmonary artery. In columnar structures without pulmonary artery, statistically significant correlations were observed between the thickness of columnar structures and size of centriacinar cystic spaces and between the thickness of columnar structures and aggregation of elastic fibers in columnar structures. Electron microscopy showed that the columns were composed of aggregated elastic fibers, collagen fibers, mesenchymal cells, pigmented macrophages, and the alveolar epithelial cells covering them. Immunohistochemistry showed that the aggregated elastic fibers were positive for α-1 antitrypsin. We concluded that columnar structures without pulmonary artery are a hallmark of alveolar wall destruction seen in pulmonary emphysema.

Keywords Centriacinar emphysema · Columnar structure · Elastic fiber · Alveolar remodeling

M. Yamamoto (✉) · S. Kunugi · A. Ishikawa · Y. Fukuda
Department of Analytic Human Pathology,
Graduate School of Medicine, Nippon Medical School,
1-1-5 Sendagi, Bunkyo-ku,
Tokyo 113-8602, Japan
e-mail: masukichioji@yahoo.co.jp

Introduction

Chronic obstructive pulmonary disease (COPD) is characterized primarily by airflow limitation that is not fully reversible. A mixture of small airway disease and parenchymal destruction is thought to be the cause of this airflow limitation. Usually, this airflow limitation is progressive and associated with an abnormal inflammatory response in the lungs to noxious particles or gases, as typified by tobacco smoke [1]. Small airway disease is characterized by chronic obstructive bronchiolitis and parenchymal destruction by pulmonary emphysema. The former one is partly reversible, but the latter one is thought to be irreversible.

Pathologically, pulmonary emphysema is defined as "A condition of the lung characterized by abnormal, permanent enlargement of the airspaces distal to the terminal bronchiole, accompanied by the destruction of their walls and without obvious fibrosis" [2, 3]. Anatomical type of emphysema is classified according to the distribution within lobules. The most common one is centriacinar (centrilobular) emphysema that is characterized by focal lesions confined to the centers of the acini [4]. In an earlier study using light microscopy, the overall destruction was evaluated using a destructive index based on the recognition of alveolar wall breaks in the alveolar and alveolar duct area [5]. This technique specifically searches for the destruction of alveoli that tether to the outside of small airways. The loss of attachments, which leads to removal of radial bronchiolar support and early

airway narrowing or closure, could explain airflow limitation in patients with emphysema [5, 6]. One of the causes of alveolar enlargement in emphysema is thought to be a result of this airway narrowing and consequent air trapping [7]. But by observing the morphological changes of early and progressed stages of pulmonary emphysema, it is difficult to imagine that air trapping itself is the primary cause of alveolar enlargement because the alveolar walls themselves are usually abnormal and discontinuous.

In this study, we focused on the morphological changes in alveolar walls and the structures within the enlarged airspaces in early and progressed lesions of centriacinar (centrilobular) emphysema and analyzed the mechanism involved in the development of emphysema.

Materials and methods

Patients

Emphysematous lungs were obtained at autopsy in 17 cases and from patients who had undergone surgical resection for cancer in four cases. Patients included 19 men and two women (median age, 71 years; range, 51–85 years). Seventeen patients were smokers, one had never smoked, and the smoking history of the other three patients was unknown. All patients were from the Nippon Medical School Hospital, and they or their family (if deceased) gave approved written informed consent.

Gross examination

The lungs were removed en bloc and fixed by airway inflation with 20% formalin solution, and emphysematous lesions were selected. The surgical specimens were also fixed with 20% formalin solution, and emphysematous lesions were isolated from the cancer-affected areas.

Lung tissues were cut to a 10-mm thickness, and the fixative solution was removed gently with dry gauze. These specimens were attached to a urethane board, and cut surfaces were observed by stereoscopic microscopy (magnification ×2.1 to ×27; OLYMPUS SZX12, Tokyo, Japan). Photographs taken with a digital camera (OLYMPUS C5060, Tokyo, Japan) were used for macroscopic evaluation.

Light microscopic study

Selected formalin-fixed tissue blocks from each patient were dehydrated and embedded in paraffin. Tissue sections were cut to a 3-μm thickness and mounted on glass slides, and deparaffinized tissue sections were used. Hematoxylin and eosin (HE) or elastica Masson–Goldner (EMG) staining was performed.

Light microscopic immunoperoxidase methods for α-1 antitrypsin

Three micrometer-thick paraffin-embedded tissue sections were used. The deparaffinized and dehydrated sections were washed three times with phosphate-buffered saline

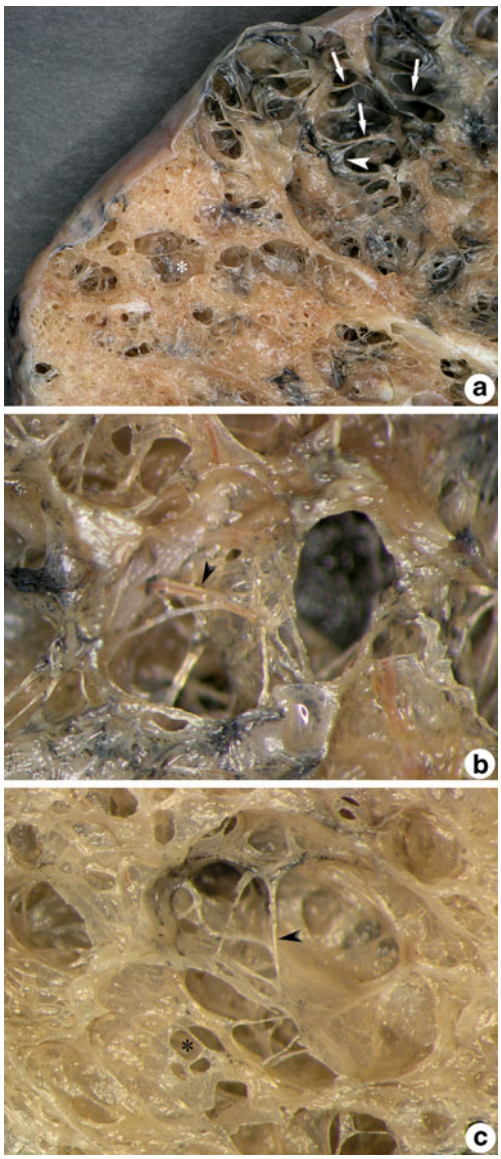

Fig. 1 Macroscopic findings observed in centriacinar emphysema. **a** There are various sized cystic spaces. In large-sized cystic spaces, thick columnar structures (*arrows*) are observed. In small-sized cystic spaces (*asterisk*), there are thin columnar structures. These varisized columnar structures connect to each other, and their tips are connected to the surrounding walls with fan-shaped membranous structure (*arrowhead*; ×4). **b** A red-colored single vessel is observed in the center of the column (*arrowhead*; ×16). **c** The high magnification of the alveolar walls which show only slight destruction in small cystic spaces. Membranous walls contain small pores (*asterisk*) and thin columnar structures (*arrowhead*) are observed (×20; stereoscopic microscope)

(PBS) and treated with 0.3% hydrogen peroxide in methanol for 30 min at room temperature to eliminate endogenous peroxidase activity. After washing three times with PBS, the tissue sections were treated with normal rabbit serum for 30 min, and they were incubated for 30 min at room temperature with goat antihuman α-1 antitrypsin antibody (Medical & Biological Laboratories Co., Ltd., Nagoya, Japan). The sections were washed three times again with PBS and probed with peroxidase-labeled rabbit antigoat IgG antibody (Histofine Simple Stain MAX-PO (G), Nichirei Co., Tokyo, Japan) for 30 min at room temperature. After a final washing of three times with PBS, the sections were reacted with a solution of 3,3′-diaminobenzidine and hydrogen peroxide for 5–8 min. The sections were counterstained with Mayer's hematoxylin and examined.

Score system

Gross and light microscopic examination revealed several characteristic findings in the emphysematous lungs, some of which seemed to be related to emphysema progression. The progression of emphysema was evaluated for the size of the enlarged airspaces that were visually seen like cysts. The cystic spaces were divided into two categories: small if the cystic space was located within the centriacinar area and large if the space was large enough to extend to the lobular septa or pleura. And then, we focused on the unique structures observed in the centriacinar area, which we termed "columnar structures". We scored some parameters of columnar structures based on light microscopic findings. To examine the relationship between emphysema progression and columnar structures, five fields were randomly selected from one EMG-stained specimen and scanned by light microscopy using a ×4 objective lens and a ×10 eyepiece and with a digital camera at 0.5-fold magnification. The parameters of columnar structures as below and size of the cystic spaces were then analyzed in pairs. The thickness of columnar structures was evaluated based on the cross-sectional diameter of columnar structures, measured on the digital photographs using the scale bar, and sorted into four classes: small <50 μm, medium 50–100 μm, large 100–200 μm, and very large >200 μm. To evaluate the role of elastic fiber degradation in alveolar remodeling, we evaluated and scored the degree of aggregation of elastic fibers in columnar structures as follows: ±/+ <25%, ++ 25–50%, and +++ >50% of the cross-sectional area. The scores were determined by visual evaluation at high-power magnification.

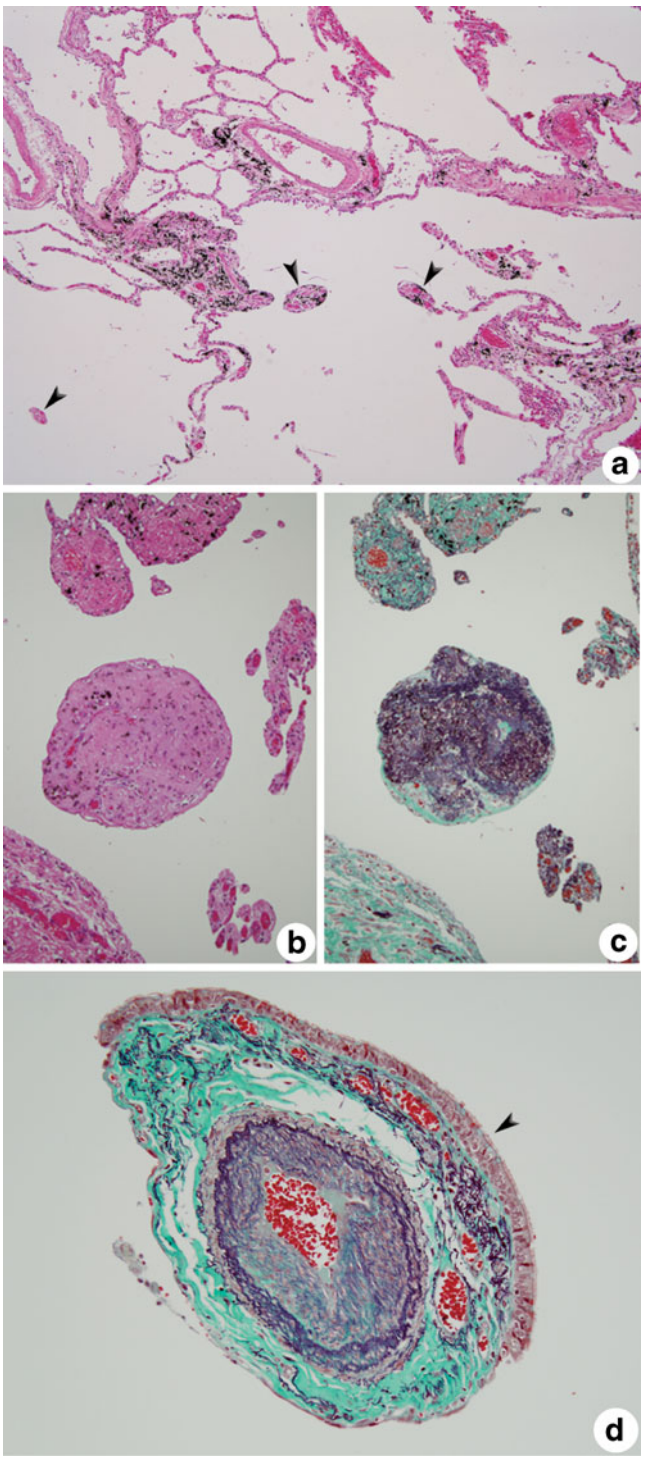

Fig. 2 Microscopic findings of typical columnar structures. **a** There are anthracotic deposits at the end of respiratory bronchiole and alveolar duct. The alveolar walls are discontinuous and fragmented. In enlarged airspace, varisized columnar structures (*arrowheads*) are observed (HE; ×32). **b** In higher magnification, a round-shaped structure is a columnar structure without pulmonary artery (HE; ×100). **c** The columnar structures have significantly aggregated elastic fibers and are surrounded by alveolar epithelial cells (EMG; ×100). **b**, **c** Serial section. **d** Columnar structure with pulmonary artery. In the center of this structure, there is a large artery. One half of the circumference of this structure is covered with ciliated bronchiolar epithelial cells (*arrowhead*; EMG). Smooth muscle and elastic layers are well preserved under the bronchiolar epithelium (×150)

Statistical analysis

The Mann–Whitney *U* test and Spearman's rank correlation test were used to evaluate the correlation between paired data from the microscopic findings observed in the emphysematous lungs. $p<0.05$ was considered statistically significant.

Transmission electron microscopic study

For electron microscopic examination, selected lung tissues were cut into small blocks and fixed with 2.5% glutaraldehyde solution in 0.1 mol/L phosphate buffer (PB), pH 7.4, overnight at 4°C. The tissue blocks were postfixed with 1% osmium tetraoxide in PB for 1 h, dehydrated in a graded alcohol series, and embedded in Epon 812 (Okenshoji Co., Ltd, Tokyo, Japan). Ultrathin sections were stained with uranyl acetate and lead citrate, or with tannic acid for elastic fibers (Kajikawa stain), and then examined by electron microscopy (model H7100, Hitachi Co, Ibaraki, Japan).

Results

Gross stereoscopic microscopic examination

In progressed pulmonary emphysema, alveolar walls were destroyed, forming cystic spaces. Many linear string-like structures were observed in these spaces (Fig. 1a). At high magnification, the string-like structures showed varying thicknesses, and their tips were connected to the surrounding walls by a fan-shaped membranous structure (Fig. 1a). They appeared similar to the columns of a Gothic cathedral. Therefore, we termed these structures, which were unique to pulmonary emphysema, as "columnar structures". Some columnar structures were connected with thicker columns and showed branching. The surfaces of these structures ranged from smooth to somewhat irregular, and the color was whitish or gray and frequently associated with black spots. In some columnar structures, a red-colored single vessel was observed in the center of the column because these structures were semitransparent (Fig. 1b). Lung tissues in which alveolar walls showed only slight destruction in small cystic spaces contained small pores, and thin columnar structures were observed between them (Fig. 1c). Taken together, the macroscopic appearance in various stage of centriacinar emphysema was as follows: The early lesions included small cystic spaces or poorly dilated pores and thin columnar structures. On the other hands, the progressed lesions included large cystic spaces and thick columnar structures.

Light microscopic study

In the centriacinar area, alveoli and alveolar ducts were dilated to varying degrees, and the tips of the alveolar septa were shortened and flattened. These lesions contained cystic lesions of various sizes. In small cysts, alveolar walls were discontinuous and fragmented (Fig. 2a). On the other hand, in large cysts, alveolar walls were thick and discontinuous, and large round masses having aggregated elastic materials were frequently observed (Fig. 2b, c). These masses may correspond to columnar structures observed with macroscopic examination. Columnar structures were typically observed as round or elliptical in shape

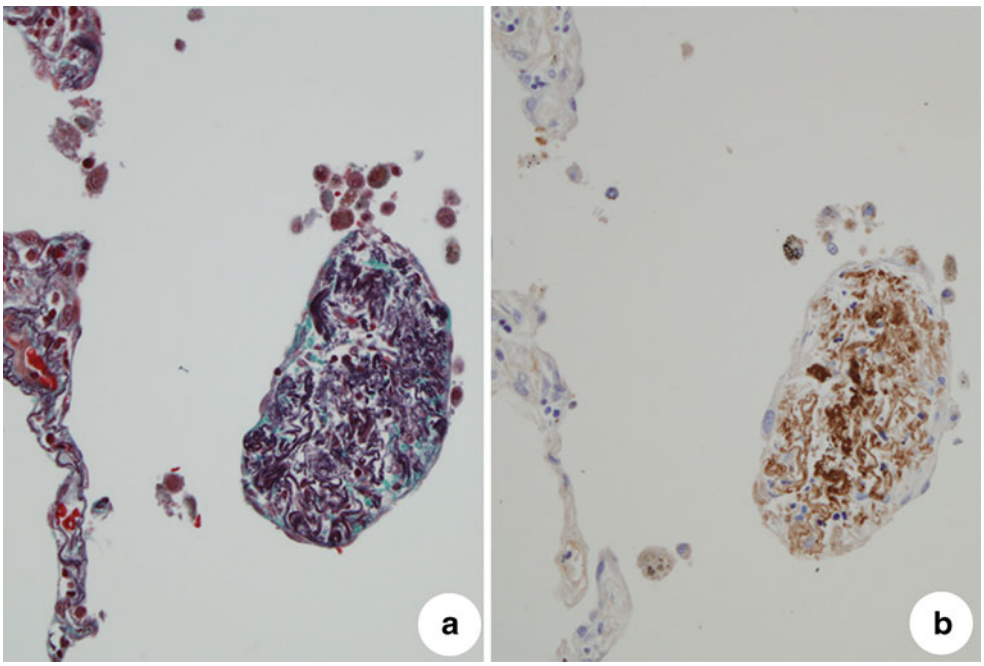

Fig. 3 The high magnification of a cross section of columnar structure. **a** This columnar structure includes aggregated elastic masses (EMG). **b** In the serial section of **a**, the aggregated elastic masses are well reacted with anti α-1 antitrypsin antibody. In contrast, the elastic framework in normal alveolar wall is not reacted with anti α-1 antitrypsin antibody (×200)

under light microscopy (Fig. 2a) [3]. These columnar structures varied in thickness, but essential components were limited and similar. Aggregated elastic fibers were usually observed, and anthracotic deposits, fibrosis, and smooth muscle cells were frequently observed in columnar structures (Fig. 2b, c). Most columnar structures were covered with alveolar epithelial cells (Fig. 2b, c).

Some columnar structures had pulmonary arteries in the center (Fig. 2d). Columnar structures with pulmonary artery were often covered not only with alveolar epithelial cells but also with bronchiolar epithelial cells (Fig. 2d). Moreover, the smooth muscle layer and some connective tissue were usually observed under these bronchiolar epithelial cells. These bronchiolar wall components were well and normally preserved in the columns with pulmonary arteries. Otherwise, columnar structures having pulmonary artery usually did not show aggregated elastic fibers.

Light microscopic immunohistochemistry for α-1 antitrypsin

Light microscopic immunohistochemistry showed that the aggregated elastic masses in columnar structures had reacted well with anti-α-1 antitrypsin antibody (Fig. 3a, b). In contrast, the elastic framework in normal alveolar walls had not reacted with anti-α-1 antitrypsin antibody. Macrophages appearing in the intra-alveolar spaces were also positive for α-1 antitrypsin. Anthracotic deposits were located within these aggregated elastic masses.

Statistical analysis

A positive correlation was seen between the size of cystic spaces and the number of columnar structures. This tendency was demonstrated in columnar structures both with and without pulmonary artery by statistical methods (Fig. 4a, b). Next, we focused on the thickness of columnar structures. A significant positive correlation was noted between the thickness of columnar structures without pulmonary artery and the size of cystic spaces ($p<0.0001$). In contrast, there was no significant correlation between the thickness of columnar structures with pulmonary artery and the size of cystic spaces ($p=0.51$; Fig. 5a, b). Moreover, comparison of the thickness between the two types of columnar structures showed that those with pulmonary artery were generally thicker than those without ($p<0.0001$; Fig. 5c).

The aggregation of elastic fibers also showed statistical significance. There was a strong correlation between the thickness of columnar structures without pulmonary artery and the degree of aggregation of elastic fibers ($p<0.0001$; Fig. 6a). In contrast, there was a poor correlation between the thickness of columnar structures with pulmonary artery and the degree of aggregation of elastic fibers ($p=0.018$; Fig. 6b).

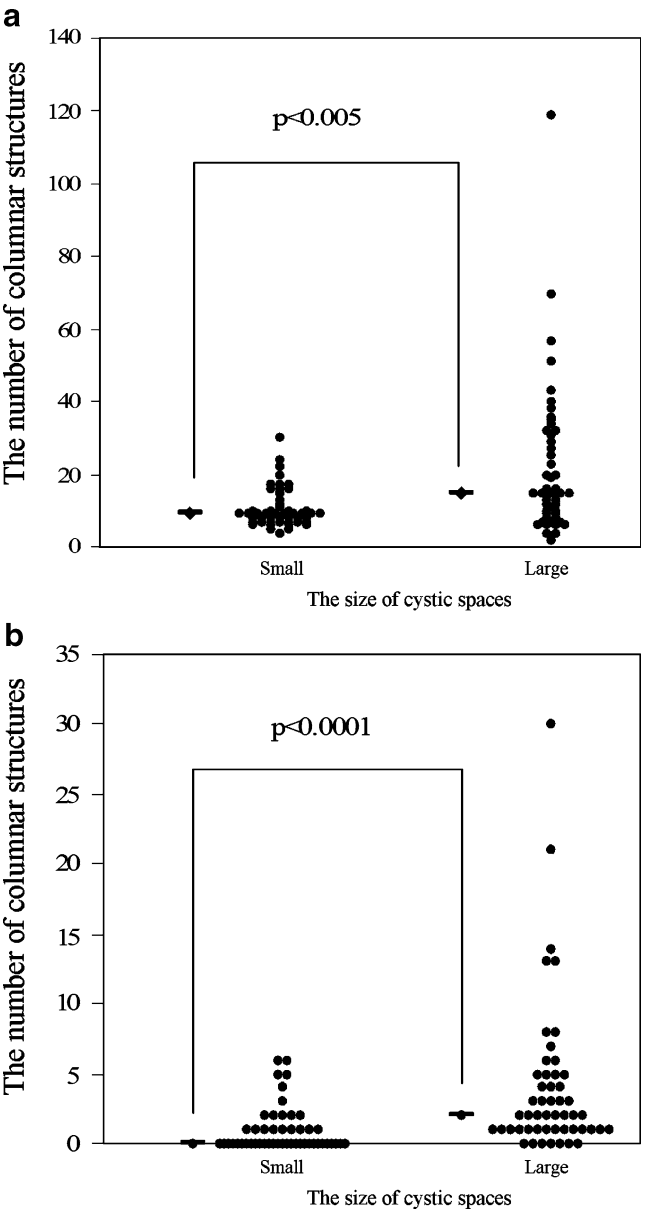

Fig. 4 The correlation between the number of columnar structures and the size of cystic spaces. Both **a** columnar structures without pulmonary artery and **b** columnar structures with pulmonary artery demonstrate statistical difference. The mean values for both groups are shown as *dots with short horizontal lines*

Finally, our examination of the epithelial cells covering columnar structures showed a significant difference between the thicknesses of columnar structures with pulmonary artery. Statistically, the columnar structures with pulmonary artery covered by both of alveolar and bronchiolar epithelial cells were thicker than those covered only by alveolar epithelial cells ($p<0.0001$). In other words, these data showed a positive correlation between the proportion of covering bronchiolar epithelial cells and the thickness of columnar

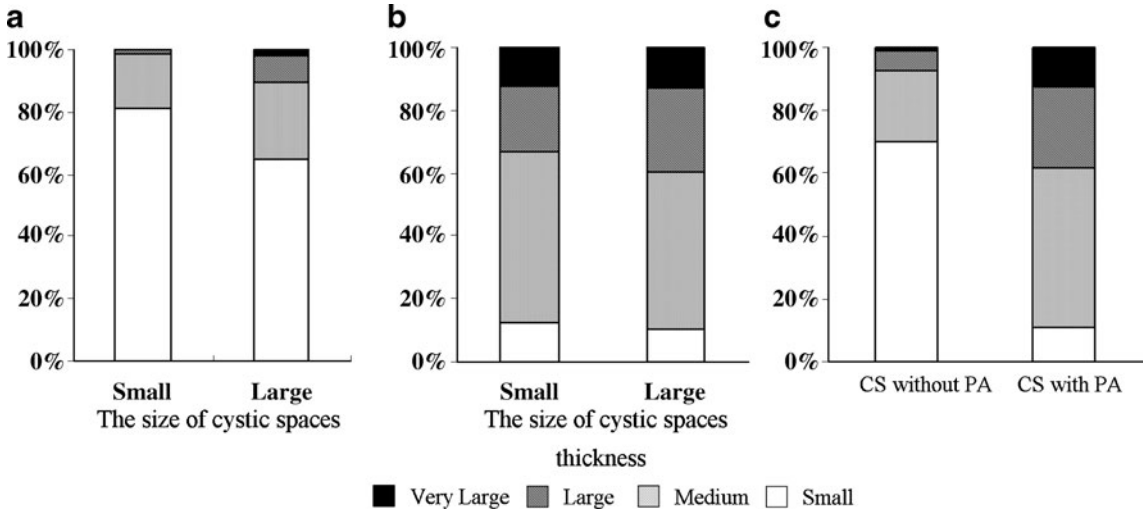

Fig. 5 The correlation between the thickness of columnar structures and the size of cystic spaces. **a** Statistically, there is positive correlation between the thickness of columnar structures without pulmonary artery and the size of cystic spaces ($p<0.0001$). **b** About the thickness of columnar structures with pulmonary artery, there are no significant differences between the small cystic spaces and the large cystic spaces ($p=0.51$). **c** The comparison of the thickness between the two types of columnar structures. Statistically, the columnar structures with pulmonary artery are thicker than those without pulmonary artery ($p<0.0001$). *CS* columnar structures, *PA* pulmonary artery

structures with pulmonary artery (Fig. 7). In this study, all columnar structures without pulmonary artery were covered only by alveolar epithelial cells.

Transmission electron microscopic findings

Columnar structures without pulmonary artery were observed on cross section as round-shaped structures covered with a single layer of alveolar epithelial cells; they were composed of aggregated thick and thin elastic fibers, increased collagen fibers, capillaries, anthracotic deposits, and macrophages (Fig. 8). Some capillaries lay adjacent to type I alveolar epithelial cells with a thin single basement membrane similar to normal alveolar walls. However, capillaries in the thicker columnar structures were frequently located in fibrous tissues.

Discussion

We identified columnar structures located in the centriacinar cystic spaces of emphysematous lungs and connected to the destroyed alveolar walls by fan-shaped structures. In mild emphysematous lesions, the remaining viable membranous alveolar walls formed small cysts with variously sized small pores. These pores were more than 20 μm in size and considered to be abnormally dilated Kohn's pores. Similar conclusions were reported by light microscopic and electron microscopic studies [6–8]. The sizes of these pores were somewhat variable, slightly varying from each other. Correspondingly, the thickness of columnar structures also varied slightly.

Types of columnar structures

Columnar structures were divided into two types, one with and the other without pulmonary artery. The type most commonly seen in centriacinar emphysema is columnar structures without pulmonary artery. This is the first report to examine these columnar structures by stereoscopic microscopy. Columnar structures without pulmonary artery were covered with alveolar epithelial cells, but no bronchiolar epithelial cells were noted. They also included capillaries, basement membrane, and varying degrees of aggregated elastic fibers and collagen fibers. Capillaries and alveolar epithelial cells with basement membranes are essential components of normal alveolar walls, and columnar structures without pulmonary artery seem to be formed within the remodeled alveoli [9, 10]. Statistically significant correlations were observed between the thickness of columnar structures and the size of cystic lesions and between the thickness of columnar structures and the degree of aggregation of elastic fibers. Occasionally, these types of columnar structures have large elastic masses surrounded by collagenous fibrous tissues. In our previous study, the large elastic masses were exclusively found in areas of severely remodeled alveolar walls in centriacinar emphysema [11]. These large elastic masses seem to be formed by coalescence of preexisting elastic fibers in areas of alveolar collapse and remodeling, possibly in association with some degree of elastin synthesis [11, 12]. Consequently, we consider the columnar structure without pulmonary artery to be closely related to the alveolar remodeling seen in emphysema.

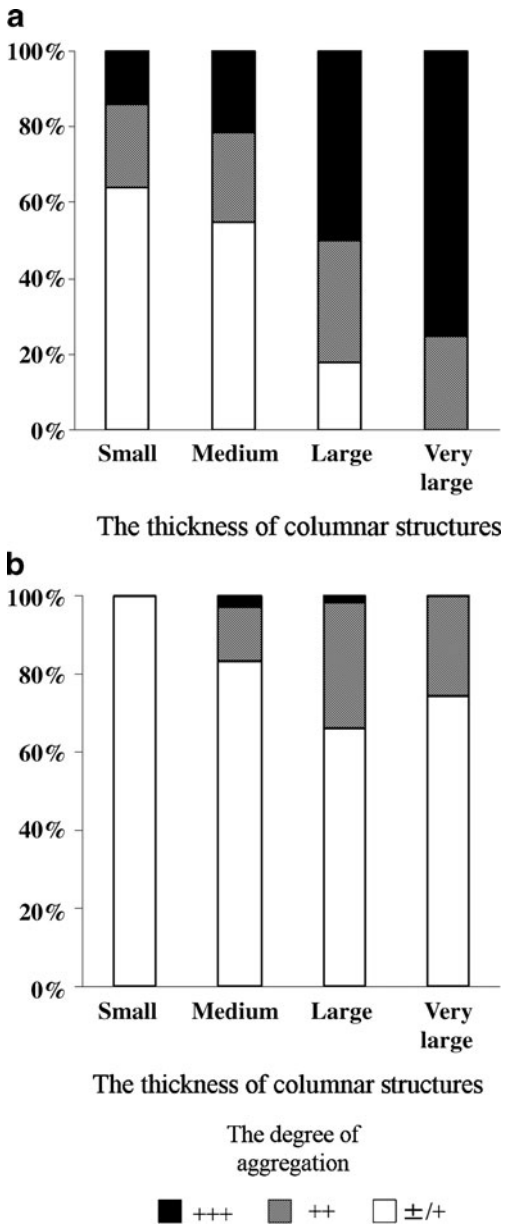

Fig. 6 The correlation between the thickness of columnar structures and the aggregation of elastic fiber. **a** There is a strong correlation between the thickness of columnar structures without pulmonary artery and the aggregation of elastic fibers ($p<0.0001$). **b** In contrasts, there is only a poor correlation between the thickness of columnar structures with pulmonary artery and the aggregation of elastic fibers ($p=0.018$)

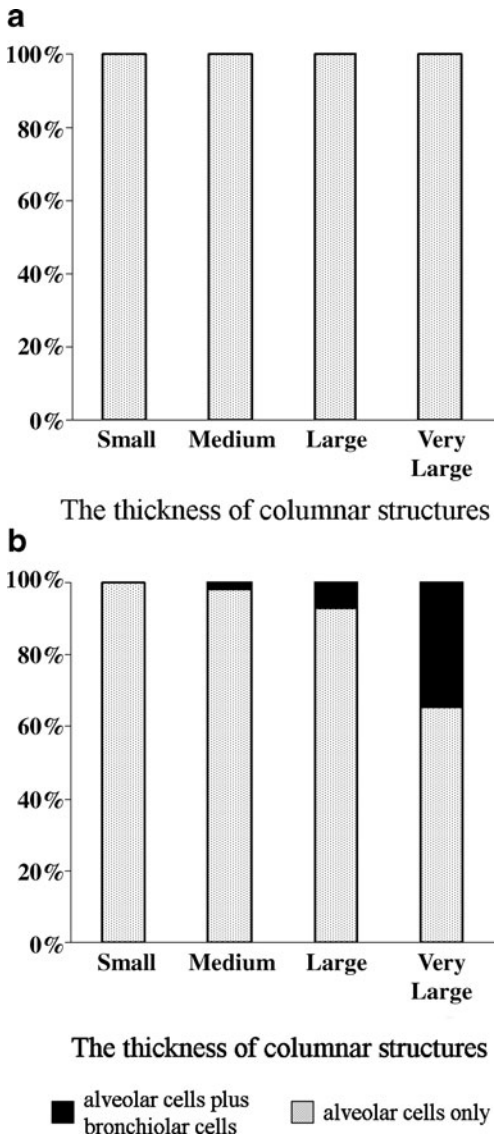

Fig. 7 The correlation between the thickness of columnar structures and the type of covering epithelial cells. **a** All columnar structures without pulmonary artery are covered only with alveolar epithelial cells. **b** In contrast, the columnar structures with pulmonary artery are covered with not only alveolar epithelial cells but also with bronchiolar epithelial cells. There is a positive correlation between the thickness of columnar structures and the proportion of covering bronchiolar epithelial cells ($p<0.0001$)

The second type of columnar structure, that is, the one with pulmonary artery, was frequently covered with bronchiolar epithelial cells. The stroma consists of a smooth muscle layer and some connective tissue, which is usually observed in the walls of respiratory bronchioles. Overall, columnar structures with pulmonary artery tended to be thicker than those without pulmonary artery ($p<0.0001$). Moreover, the thickness of columnar structures with pulmonary artery was not significantly related to the size of cystic lesions. These findings suggest that an original pulmonary artery and a part of the respiratory bronchiole combine to form these columnar structures. Columnar structures with pulmonary artery may get detached from the surrounding destroyed alveoli, while preserving their detailed structures. In earlier studies, these columnar structures were described as "remnants left in destroyed air passages" or "surviving pulmonary vessels" under macroscopic study or stereoscopic microscopy by barium sulfate precipitation [13, 14].

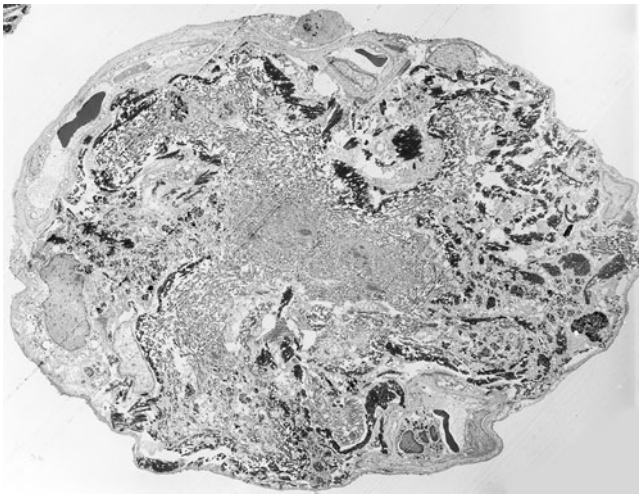

Fig. 8 Transmission electron microscopic picture of a columnar structure without pulmonary artery. The shape is elliptic form and is covered with single layered type I alveolar epithelial cells. Capillaries lie adjacent to this epithelium. Inside the columnar structure, aggregated elastic fibers, bundles of collagen fibrils, anthracotic deposits, and some inflammatory cells are observed (×1,000)

Mechanism of formation of columnar structures without pulmonary artery

The lungs of COPD patients show an imbalance between proteases that break down connective tissue components and antiproteases that protect against them [15–18]. According to this "protease–antiprotease" hypothesis, cigarette smoke causes inflammation and the subsequent release of proteolytic enzymes into the lungs in excess of their natural inhibitors. One of the major proteases is neutrophil elastase, which has potent catalytic activity against a broad array of extracellular matrix substrates, including elastin, which imparts structural stability to the lung. In contrast, α-1 antitrypsin is the major inhibitor of serine proteases, including neutrophil elastase [19, 20]. Neutrophil elastase is thought to be derived from neutrophils that are recruited to alveolar spaces by some chemokines released from alveolar macrophages [21–23]. It has been reported that neutrophil elastase activates macrophage elastase (i.e., matrix metalloprotease-12), and neutrophil and macrophage elastases enhance each other's potency by degrading each other's inhibitor [20]. In this study, we recognized well-stained α-1 antitrypsin in aggregated elastic fibers of columnar structures without pulmonary artery. In these structures, elastic masses coexisted with α-1 antitrypsin. A similar finding was reported in the emphysema-like dilated alveolar walls of lymphangiomyomatosis [24]. We also analyzed the abnormal elastic fibers in blebs and bullae seen in spontaneous pneumothorax and found similar aggregated elastic fibers [25]. These fibers also reacted with anti-α-1-antitrypsin antibody. These findings support the contention that neutrophil elastase, and α-1 antitrypsin play important roles in the degradation and aggregation of elastic fibers in the alveolar remodeling seen in pulmonary emphysema.

A possible mechanism for the formation of columnar structures without pulmonary artery is proposed. First, some proteases, including neutrophil elastase, disrupt the elastic framework of alveolar walls. The primary destruction appears to exist in the dilated Kohn's pores. Then, the frames aggregate to form early and thin columnar structures. These thin columnar structures aggregate and grow to produce thick columnar structures with large-sized cystic lesions. The growth of columnar structures is synonymous with the alveolar wall destruction associated with airspace enlargement. Therefore, the process of airspace enlargement due to air trapping in the airways may occur following alveolar wall destruction. In other words, columnar structures with aggregated elastic fibers are a hallmark of alveolar wall destruction seen in pulmonary emphysema.

Acknowledgment The authors wish to thank Mr. Takashi Arai, Ms. Mitsue Kataoka, and Ms. Naomi Kuwahara (Department of Analytic Human Pathology, Nippon Medical School) for their technical assistance.

Conflict of interest statement We declare that we have no conflict of interest.

References

1. Rabe KF, Hurd S, Anzueto A et al (2007) Global strategy for the diagnosis, management, and prevention of chronic obstructive pulmonary disease: GOLD executive summary. Am J Respir Crit Care Med 176:532–555
2. American Thoracic Society (1962) Chronic bronchitis, asthma, and pulmonary emphysema: a statement by the committee on diagnostic standards for nontuberculous respiratory disease. Am Rev Respir Dis 85:762–768
3. Snider GL, Thurlbeck WM, Bengali ZH (1985) The definition of emphysema. Report of a National Heart, Lung, and Blood Institute, Division of Lung Diseases workshop. Am Rev Respir Dis 132:182–185
4. Corrin B, Nicholson AG (2006) Diseases of the airway. In: Corrin B, Nicholson AG (eds) Pathology of the lungs, 2nd edn. Churchill Livingstone, Philadelphia, pp 87–130
5. Saetta M, Shiner RJ, Angus GE et al (1985) Destructive index: a measurement of lung parenchymal destruction in smokers. Am Rev Respir Dis 131:764–769
6. Wright JL (2005) Chronic airflow obstruction. In: Churg AM (ed) Thurlbeck's pathology of the lung, 3rd edn. Thieme, New York, pp 675–741
7. Snider GL (1989) Chronic obstructive pulmonary disease: a definition and implications of structural determinants of airflow obstruction for epidemiology. Am Rev Respir Dis 140:S3–S8
8. Pump KK (1976) Emphysema and its relation to age. Am Rev Respir Dis 114:5–13
9. Sandberg LB (1976) Elastin structure in health and disease. Int Rev Connect Tissue Res 7:159–210

10. Finlay GA, O'Donnell MD, O'Connor CM et al (1996) Elastin and collagen remodeling in emphysema. A scanning electron microscopy study. Am J Pathol 149:1405–1415
11. Fukuda Y, Masuda Y, Ishizaki M et al (1989) Morphogenesis of abnormal elastic fibers in lungs of patients with panacinar and centriacinar emphysema. Hum Pathol 20:652–659
12. Fukuda Y, Ferrans VJ, Schoenberger CI et al (1985) Patterns of pulmonary structural remodeling after experimental paraquat toxicity. The morphogenesis of intraalveolar fibrosis. Am J Pathol 118:452–475
13. Heard BE, Khatchatourov V, Otto H et al (1979) The morphology of emphysema, chronic bronchitis, and bronchiectasis: definition, nomenclature, and classification. J Clin Pathol 32:882–892
14. McLean KH (1959) The pathology of emphysema. Am Rev Respir Dis 80:58–66
15. Laurell CB, Eriksson S (1963) The electrophoretic alpha-1 globulin pattern of serum in alpha-1 antitrypsin deficiency. Scand J Clin Lab Invest 15:132–140
16. Kuhn C, Yu SY, Chraplyvy M et al (1976) The induction of emphysema with elastase. II. Changes in connective tissue. Lab Invest 34:372–380
17. Janoff A (1985) Elastases and emphysema. Current assessment of the protease–antiprotease hypothesis. Am Rev Respir Dis 132:417–433
18. Barnes PJ, Shapiro SD, Pauwels RA (2003) Chronic obstructive pulmonary disease: molecular and cellular mechanisms. Eur Respir J 22:672–688
19. Gadek JE, Hunninghake GW, Fells GA et al (1980) Evaluation of the protease–antiprotease theory of human destructive lung disease. Bull Eu Physiopathol Respir 16(suppl):27–40
20. Shapiro SD, Goldstein NM, Houghton AM et al (2003) Neutrophil elastase contributes to cigarette smoke-induced emphysema in mice. Am J Pathol 163:2329–2335
21. Betsuyaku T, Nishimura M, Takeyabu K et al (1999) Neutrophil granule proteins in bronchoalveolar lavage fluid from subjects with subclinical emphysema. Am J Respir Crit Care Med 159:1985–1991
22. Di Stefano A, Caramori G, Ricciardolo FL et al (2004) Cellular and molecular mechanisms in chronic obstructive pulmonary disease: an overview. Clin Exp Allergy 34:1156–1167
23. Betsuyaku T, Yoshioka A, Nishimura M et al (1995) Neutrophil elastase associated with alveolar macrophages from older volunteers. Am J Respir Crit Care Med 151:436–442
24. Fukuda Y, Kawamoto M, Yamamoto A et al (1990) Role of elastic fiber degradation in emphysema-like lesions of pulmonary lymphangiomyomatosis. Hum Pathol 21:1252–1261
25. Haraguchi S, Fukuda Y (1993) Histogenesis of abnormal elastic fibers in blebs and bullae of patients with spontaneous pneumothorax: ultrastructural and immunohistochemical studies. Acta Pathol Jpn 43:709–722

Virchows Arch (2010) 456:581–586
DOI 10.1007/s00428-010-0902-z

CASE REPORT

Clinico-pathological features of breast myxoma: report of a case with histogenetic considerations

Gaetano Magro · Barbara Cavanaugh · Juan Palazzo

Received: 5 February 2010 / Revised: 22 February 2010 / Accepted: 23 February 2010 / Published online: 23 March 2010
© Springer-Verlag 2010

Abstract We herein report the clinical, radiological, and pathological findings of a rare case of myxoma occurring in the breast parenchyma of a 75-year-old female. The tumor was incidentally detected at a mammographic screening and, ultrasonographically, presented as an ovoid mass. Histologically, an encapsulated hypocellular, myxoid tumor with low vascularization was evident. Neoplastic cells were round- to spindle/stellate-shaped and stained with vimentin and focally with calponin. We emphasize that morphology remains preeminent in the diagnosis of a breast myxoma, while immunohistochemistry may assist in ruling out other tumor entities. Differential diagnosis with all benign and malignant myxoid lesions, primarily occurring in the breast, is provided. The histogenesis of breast myxoma is unknown. The lack of expression of desmin, α-smooth muscle actin, CD34, CD99, CD10, bcl-2 protein, and estrogen/progesterone/androgen receptors, all markers characteristically expressed by "the benign spindle cell tumors of the mammary stroma," would suggest that breast myxoma does not fall into this tumor category and that its putative precursor mesenchymal cell resides in the interlobular stroma.

G. Magro (✉)
Department G.F. Ingrassia, Division of Anatomic Pathology,
Policlinico-Vittorio Emanuele University Hospital,
Via S. Sofia 87,
Catania, Italy
e-mail: g.magro@unict.it

B. Cavanaugh
Department of Radiology, Division of Breast Imaging,
Thomas Jefferson University Hospital,
Philadelphia, PA, USA

J. Palazzo
Department of Pathology, Division of Pathology,
Thomas Jefferson University Hospital,
Philadelphia, PA, USA

Keywords Myxoma · Breast · Imaging · Differential diagnosis · Histogenesis · Immunohistochemistry

Introduction

Myxomas are relatively uncommon, benign mesenchymal tumors that usually involve soft tissues (namely, intramuscular myxoma and juxta-articular myxoma) and heart [1–3]. It is commonly believed that myxoma can occasionally present in the breast as a sporadic lesion or in the context of the Carney complex [4, 5]. However, the lesions of the breast parenchyma in this syndrome consist of multifocal and bilateral myxoid changes (so-called myxomatosis) involving predominantly the intralobular stroma and less frequently the interlobular stroma [6, 7]. These stromal changes have also been improperly named "myxoid fibroadenoma" and "myxoid tubular adenoma" [6, 7]. In our opinion, the term "myxoma of the breast" should be restricted exclusively to those purely myxoid mesenchymal lesions which arise in the breast parenchyma, with morphological features similar, if not identical, to myxomas occurring more commonly in soft tissues [1–3]. According to this definition, only three well-documented cases of breast myxomas have been reported in the literature so far [4, 5, 8]. Although ultrastructural and immunohistochemical studies have shown that cells of myxomas are fibroblastic and, less frequently, myofibroblastic in nature, the histogenesis of this enigmatic tumor is still controversial [1]. Electron microscopy performed in one case of breast myxoma showed that the constitutive cells had a primitive mesenchymal profile, even if the presence of incomplete basement membranes, prominent intracytoplasmic microfilaments, and pinocytotic vesicles, suggested a pericytic origin [4].

We herein report the clinico-pathological features, including mammographic and ultrasonographic appearance, of a rare case of myxoma occurring in the breast parenchyma. Differential diagnosis with other myxoid tumor- and tumor-like lesions arising in the breast parenchyma is provided. Although the histogenesis of breast myxoma is unclear, it is likely that this tumor could arise from a primitive fibroblast-like cell of the mammary stroma. Histogenetic considerations about this presumptive precursor mesenchymal cell are discussed on the basis of the immunohistochemical findings.

Clinical history

A 75-year-old female presented with a 1.4-cm non-calcified focal asymmetry in her upper outer left breast detected on screening mammogram (Fig. 1a). Margins were obscured and indistinct on spot compression views. Ultrasonography showed an ovoid, hypoechoic mass with indistinct margins (Fig. 1b). There was no evidence of vascularity on Doppler analysis. The mass was not attached to the overlying skin which was unremarkable. The patient had no history of recent trauma. Twenty years ago the patient had an invasive ductal carcinoma of the left breast with associated ductal carcinoma in situ and lobular carcinoma in situ. Six years ago she had an invasive ductal carcinoma of the right breast. Sentinel and axillary lymph nodes from both axillas were negative for tumor. She had a wide local excision of the breast.

Materials and methods

The surgical specimen was submitted for histological examination in neutral-buffered 10% formalin, dehydrated using standard techniques, embedded in paraffin, cut to 5 μm, and stained with hematoxylin and eosin, alcian blue at pH 2.5 and periodic acid-Schiff (PAS). Immunohistochemical studies were performed with the labeled streptavidin–biotin peroxidase detection system using the Ventana automated immunostainer (VentanaMedicalSystems, Tucson, AZ, USA). The antibodies tested were: vimentin (dilution 1:100), α-smooth muscle actin (dilution 1:200), desmin (dilution 1:100), calponin (dilution 1:100), myogenin (dilution 1:100), S-100 protein (dilution 1:500), CD99 (dilution 1:100), CD34 (dilution 1:50), CD99 (dilution 1:100), CD10 (dilution 1:200), CD117 (dilution 1:400), pancytokeratins (dilution 1:50), EMA (dilution 1:100), p63 (dilution 1:200), and HMB45 (dilution 1:300; all from DakoCytomation, Glostrup, Denmark). Negative controls for the staining were slides stained with omission of the primary antibody.

Results

The surgical specimen was comprised of breast parenchyma measuring 3.5 cm in greatest dimension. The cut section revealed a 1.8-cm, well-circumscribed mass, whitish in color and gelatinous in appearance. Histologically, a hypocellular lesion with an abundant myxoid matrix, entirely surrounded by a thin fibrous pseudocapsule, was seen (Fig. 2a). The cellular component was represented by bland-looking, mono- or bi-nucleated round- to spindle/stellate-shaped cells with pale to eosinophilic cytoplasm (Fig. 2b, c). Some of these cells exhibited dendritic-like cytoplasmic processes (Fig. 2b). The nuclei were round to oval in shape, with one or two nucleoli (Fig. 2c). Only focally a mild degree of nuclear atypia could be seen (Fig. 2c). Mitotic activity and necrotic areas were absent. Tumor stroma was mainly composed of an abundant loose matrix positive with alcian blue at pH 2.5, but negative with periodic acid-Schiff, in

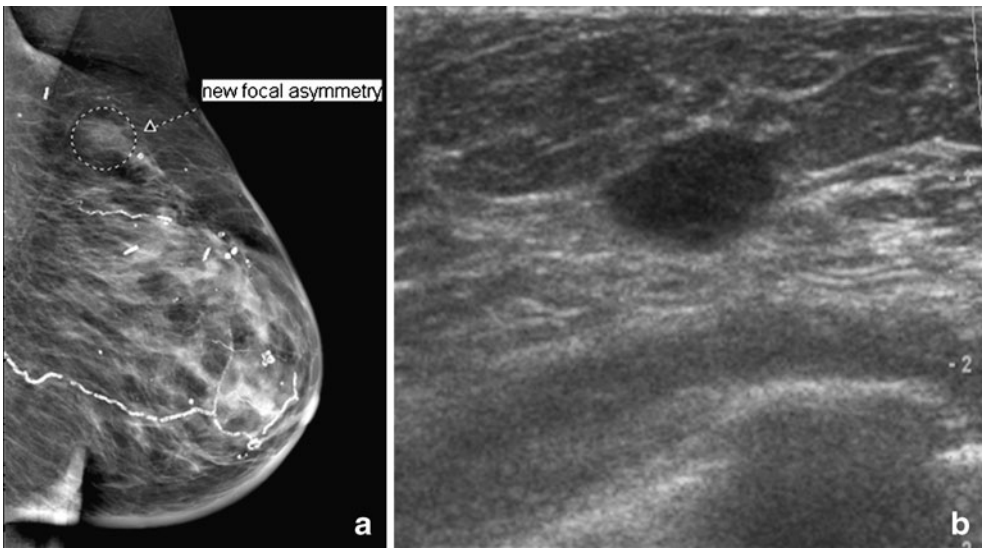

Fig. 1 **a** Mammography showing interval development of an isodense focal asymmetry. **b** Ultrasonography showing an ovoid, hypoechoic mass with indistinct borders

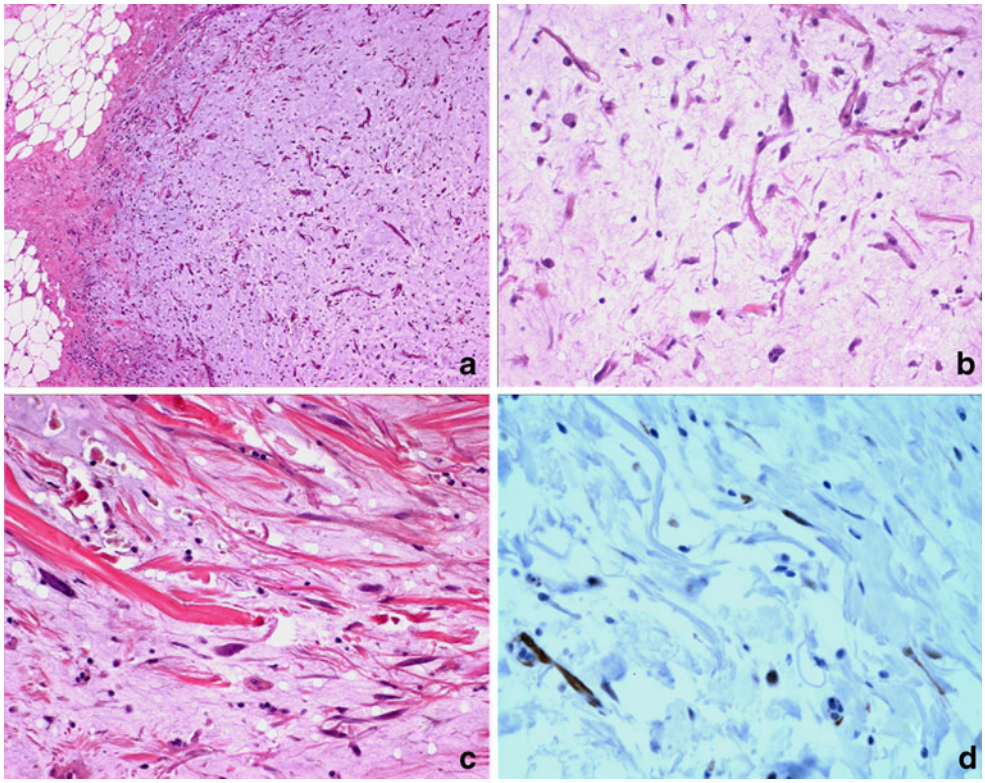

Fig. 2 **a** Low power view showing a hypocellular myxoid tumor completely surrounded by a thin fibrous pseudocapsule (H&E staining, ×50 magnification). **b** Round- to spindle- to stellate-shaped cells are embedded in abundant myxoid matrix; some cells exhibit dendritic-like cytoplasmic processes (H&E staining, ×100 magnification). Univacuolar stromal changes, simulating lipoblasts, are evident. **c** Tumor area rich in thick eosinophilic collagen bands. Mono- and binucleated cells with a mild degree of nuclear atypia are evident (H&E staining, ×100 magnification). **d** A few cells are stained with calponin (×200 magnification)

which haphazardly arranged thick eosinophilic collagen bands could be focally identified (Fig. 2c). Vacuolar stromal changes were seen throughout the tumor, sometimes simulating univacuolar lipoblasts, especially when they were close to neoplastic cells (Fig. 2b, c). In addition, fluid-filled cystic spaces, frequently containing interspersed red blood cells, were also seen; small-sized blood vessels were scattered throughout the tumor stroma. A plexiform capillary-like or a curvilinear vascular pattern was not observed. A few number of mast cells and lymphocytes were focally seen within myxoid stroma. Mammary lobules or ducts were not entrapped within tumor. No evidence of epithelial atypical lesions or cancer was observed in the breast parenchyma surrounding the myxoid lesion. Immunohistochemically, neoplastic cells were strongly and diffusely positive for vimentin and only focally for calponin (Fig. 2d). No immunoreactivity was obtained with any of the other antibodies.

Discussion

Myxomas can arise in soft tissues, bone, sinonasal cavities, maxillary antrum, and in organs or viscera [1–3]. Although a computerized literature search has revealed five cases of myxoma of the breast [4, 5, 8–10], in our opinion, only three well-documented cases are available [4, 5, 8]. In fact, one case reported with the term "myxoma of the breast" could well represent a superficial angiomyxoma, due to the close relationship with subcutis and its multinodular appearance both at gross and microscopic examination [9]. Another case of breast myxoma involved the subcutaneous tissue of a 37-year-old woman who experienced multiple local recurrences referred as "myxosarcoma" and "myxoid liposarcoma" [10]. It is likely that this case was a primary subcutaneous "myxoid sarcoma" not otherwise specified in the first diagnosis and not a true "myxoma."

Radiologic images of myxoma of the breast parenchyma are available only in one previously reported case [5]. The tumor presented as a palpable lesion which at mammography appeared as an isodense non-calcified mass with circumscribed borders, while ultrasound revealed a corresponding ovoid isoechoic and circumscribed mass [5]. On the contrary, our case shows that myxoma of the breast parenchyma may present as a solitary and asymptomatic lesion, which can be identified as a focal asymmetry and ovoid mass with indistinct margins at mammography and ultrasonography,

Table 1 Clinico-pathological features of myxoid benign and malignant lesions reported in the breast

Entity (Reference)	Site	Margins	Histology	Immunohistochemistry	Biological behavior
Myxoma (4, 5, 8, present case)	Breast parenchyma	Circumscribed; thin fibrous pseudocapsule	Round- to spindle- to stellate-shaped cells; variable number of thick collagen bands; few blood vessels; alcian blue-positive myxoid matrix; no mitoses	Variable and focal expression of muscle specific actin and calponin	Benign
Superficial angiomyxoma [8]	Subcutis; breast parenchyma; sporadic or in Carney complex	Circumscribed and multinodular; unencapsulated	Multilobular appearance; fibrous septa; spindle- to stellate-shaped cells; plexiform capillary vasculature occasionally seen; entrapped mammary lobules/ducts; alcian blue-positive myxoid matrix; no mitoses	Focal expression of s-100 protein and α-1 antichymotrypsin	Benign; potential local recurrence
Nodular mucinosis [14, 15]	Nipple; dermis–subcutis; breast parenchyma	Poorly circumscribed and multinodular; unencapsulated	Small myxoid nodules; spindle cells; entrapped mammary lobules/ducts and sweat glands; alcian blue-positive myxoid matrix; no mitoses	Variable expression of ASMA	Benign
Nodular fasciitis [16]	Subcutis; breast parenchyma	Circumscribed or infiltrative; unencapsulated	Spindle cells; short bundles; lymphocytes; extravasated eythrocytes; fibro-myxoid stroma; variable number of mitoses	Variable expression of ASMA	Benign
Myxoid myofibroblastoma [19, 20]	Breast parenchyma	Circumscribed; unencapsulated	Spindle to epithelioid cells; nuclear pleomorphism occasionally seen; variable number of thick eosinophilic collagen bands; alcian blue-positive myxoid matrix; mitoses (0–2×10 HPF)	Desmin; ASMA; variable expression of CD34, BCL-2, CD99, ER/PR/AR receptors	Benign
Myxoid neurofibroma [17, 18]	Breast parenchyma; sporadic or in NF1 patients	Circumscribed	Spindle cells with wavy nuclei; nuclear pleomorphism occasionally seen; no or only rare mitoses	S-100 protein; variable expression of CD34	Benign
Myxofibrosarcoma [21]	Breast parenchyma	Circumscribed or infiltrative; multinodular	Spindle- to stellate-shaped cells; nuclear pleomorphism; incomplete fibrous septa; curvilinear capillaries; variable number of mitoses	Variable and focal expression of muscle specific actin and ASMA	High rate of local recurrence; distant metastases dependent on histological grade and tumor depth
Myxoid liposarcoma [22]	Breast parenchyma	Circumscribed multinodular	Round- to oval-shaped cells; lipoblasts; plexiform capillary vasculature; a few number of mitoses	Variable expression of S-100 protein in non-lipogenic cells; S-100 protein in lipoblasts	Potential local recurrence and distant metastases dependent on histological grade
Mucocele-like tumors [13]	Breast parenchyma	Circumscribed and multinodular	Mucin-containing cysts in which can be identified benign (normal or hyperplastic) to in situ carcinomas to invasive mucinous carcinomas; PAS-positive mucoid material	Cells identified in mucin lakes are positive for epithelial markers (pancytokeratins; EMA)	Dependent on histological diagnosis

respectively. Unfortunately, radiologic images, including those of our case, are non-specific [5] and the diagnosis of breast myxoma is based on histological examination. The main diagnostic criteria for myxoma are: hypocellularity, abundant myxoid matrix, round- to stellate- to spindle-shaped cells, low vascularization, and lack of significant cytological atypia, mitotic activity, plexiform, and curvilinear vasculature [1–3]. Although the histological diagnosis of myxoma is usually straightforward in appropriate sites (soft tissue, heart), it is the unusual location, including breast parenchyma, that can cause some diagnostic problems. Unfortunately, there are no immunohistochemical markers helpful in confirming the morphological diagnosis of myxoma. In this regard, neoplastic cells show a variable, often focal, expression of α-smooth muscle actin, desmin, CD34, and factor XIIIa [1–3]. In our case, apart from vimentin, cells focally expressed calponin. Similar immunohistochemical findings were obtained in a myxoma of the renal capsule, suggesting a myofibroblastic nature of the constitutive cells [11].

Awareness of the possibility that myxoma may occasionally occur in the breast parenchyma is crucial to avoid confusion with a wide variety of benign and malignant lesions which could be predominantly myxoid in nature, including nodular fasciitis, reactive spindle cell nodules, solitary fibrous tumor/hemangiopericytoma, spindle cell lipoma, leiomyoma, benign fibrous histiocytoma, benign peripheral nerve sheath tumor, inflammatory myofibroblastic tumor, follicular dendritic cell tumor, dermatofibrosarcoma, leiomyosarcoma, fibrosarcoma/malignant fibrous histiocytoma, low/high grade myofibroblastic sarcoma, malignant peripheral nerve sheath tumor, rhabdomyosarcoma, fibromatosis/nodular fasciitis-like low-grade sarcomatoid/metaplastic carcinoma, and mucocele-like tumors [12–15]. Practically, however, the lesions reported in the breast with diffuse myxoid stromal changes are: superficial angiomyxoma [9], nodular mucinosis (first reported as nerve sheath myxoma) [16, 17], nodular fasciitis (myxoid variant) [18], neurofibroma (myxoid variant) [19, 20], myofibrolastoma (myxoid variant) [21, 22], myxofibrosarcoma [23], myxoid liposarcoma [24], and mucocele-like tumors [15]. A list of these lesions, including their main clinico-pathological features, is provided in Table 1. Briefly, malignant soft tissue tumors are easily ruled out on the basis of the absence of significant nuclear pleomorphism, mitotic activity, curvilinear vasculature (myxofibrosarcoma), lipoblasts, and plexiform vasculature (myxoid liposarcoma). Low-grade sarcomatoid/metaplastic carcinoma exhibiting a fibromatosis/nodular fasciitis-like pattern can be excluded with the use of immunohistochemistry for low molecular weight keratins which identify epithelial foci with spindle morphology [14]. Lastly, unlike our case, the extracellular matrix of mucocele-like tumors stains positively with PAS and contains epithelial elements which can be highlighted by pancytokeratin and EMA [15].

Among benign myxoid lesions, superficial angiomyxoma is a dermal/subcutis lesion [1] which can extend into the underlying breast parenchyma [9]. Unlike myxoma, it has a typical multilobular appearance both at gross and microscopic examination due to the presence of fibrous septa [1]. Nodular mucinosis typically occurs under the nipple, with poorly circumscribed margins due to the arrangement of myxoid stroma into small nodules [16, 17]. Nodular fasciitis (myxoid variant) is a fibro-myofibroblastic pseudosarcomatous lesion with, at least focally, infiltrative margins, composed of spindle-shaped cells which are typically positive for α-smooth muscle actin [18, 25]. A variable number of inflammatory cells, including extravasated red blood cells, are a typical feature of this reactive lesion [25]. Myxoid myofibroblastoma is a myofibroblastic tumor which typically expresses desmin and variable α-smooth muscle actin, CD34, bcl-2, CD99, CD10, and estrogen/progesterone/androgen receptors [21, 22]. Lastly, myxoid neurofibroma is a tumor that expresses S100 protein and CD34 [19].

The histogenesis of breast myxoma is still to be established. Most of the benign mesenchymal tumors of the breast belong to the category of "benign spindle cell tumors of the mammary stroma," likely arising from a common precursor fibroblast-like cell resident in the hormonally active intralobular stroma [13, 26, 27]. This is suggested by a basic common morphological and immunohistochemical profile, including the expression of desmin, α-smooth muscle actin, CD34, bcl-2 protein, CD99, CD10, estrogen, progesterone, and androgen receptors [26, 27]. Accordingly, we evaluated the expression of these markers in our case, to assess if breast myxoma falls within the spectrum of the "benign tumors of the mammary stroma." Neoplastic cells were negative for all markers and did not express any sex steroid hormone receptor, suggesting that breast myxoma is a separate entity which likely arises from a mesenchymal precursor cell resident in the interlobular stroma.

Conflict of interest statement We declare that we have no conflict of interest.

References

1. Weiss SW, Goldblum JR (2008) Enzinger and Weiss's soft tissue tumors. Mosby, St Louis, pp 1066–1080
2. Nielsen G, Stenman G (2002) Intramuscular myxoma- juxta-articular myxoma. In: Fletcher CDM, Unni KK, Metens F (eds) Tumors of soft tissue and bone. Pathology and genetics. Tumours of soft tissue and Bone. IARC, Lyon, pp 186–188
3. Allen W (2000) Myxoma is not a single entity: a review of the concept of myxoma. Ann Diagn Pathol 4:99–123
4. Chan YF, Yeung HY, Ma L (1986) Myxoma of the breast: report of a case and ultrastrucutual study. Pathology 18:153–157

5. Balci P, Kabakci N, Isil T, Canda T, Guray M, Ozfidan S (2007) Breast myxoma: radiologic and histopathologic features. Breast J 13:88–90
6. Carney JA, Toorkey BC (1991) Myxoid fibroadenoma and allied conditions (myxomatosis) of the breast. A heritable disorder with special associations including cardiac and cutaneous myxomas. Am J Surg Pathol 15:713–21
7. Courcoutsakis NA, Chow CK, Shawker TH, Carney JA, Stratakis CA (1997) Syndrome of spotty skin pigmentation, myxomas, endocrine overactivity, and schwannomas (Carney complex): breast imaging findings. Radiology 205:221–227
8. Tyler GT (1915) Report of a case of pure myxoma of the breast. Ann Surg 61:121–127
9. Arihiro K, Inai K, Kurihara K, Takeda S, Khatun N, Kuroi K, Kawami H, Toge T (1993) Myxoma of the breast: report of a case with unique histological and immunohistochemical appearances. Acta Pathol Jpn 43:340–346
10. Rudan I, RudanN SB (1996) Locally recurring primary myxoma of the breast: an evidence of malignant alteration. Acta Med Croat 50:209–211
11. Val-Bernal JF, Aguilera C, Villagrá NT, Correas MA (2005) Myxoma of the renal capsule. Pathol Res Pract 200:835–840
12. Rosen PP (2009) Benign mesenchymal neoplasms—sarcoma. In: Rosen PP (ed) Rosen's breast pathology, 3rd edn. Lippincott, Williams & Wilkins, Philadelphia, pp 829–958
13. Tavassoli FA, Eusebi V (2009) Tumours of the mammary gland, 4th Series. Armed Force Institute of Pathology, Washington, DC, pp 263–314
14. Kurian KM, Al-Nafussi A (2002) Sarcomatoid/metaplastic carcinoma of the breast: a clinicopathological study of 12 cases. Histopathology 40:58–64
15. Rosen PP (2009) Mucinous carcinoma. In: Rosen PP (ed) Rosen's breast pathology, 3rd edn. Lippincott, Williams & Wilkins, Philadelphia, pp 515–535
16. Michal M, Ludvikova M, Zamecnik M (1998) Nodular mucinosis of the breast: report of 3 cases. Pathol Int 48:542–544
17. Sanati S, Leonard M, Khamapirad T, Eltorky MA (2005) Nodular mucinosis of the breast. A case report with pathologic, ultrasonographic, and clinical findings and review of the literature. Arch Pathol Lab Med 129:58–61
18. Polat P, Kantarci F, Alper F, Gursan N, Suma S, Okur A (2001) Nodular fasciitis of the breast and knee in the same patient. AJR 178:1426–1428
19. Hock YL, Mohamid W (1995) Myxoid neurofibroma of the male breast: fine needle aspiration cytodiagnosis. Cytopathology 6:44–7
20. Gokalp G, Hakyemez B, Kizilkaya E, Haholu A (2007) Myxoid neurofibromas of the breast: mammographical, sonographical and MRI appearances. British J Radiol 80:234–237
21. Magro G, Amico P, Gurrera A (2007) Myxoid myofibroblastoma of the breast with atypical cells: a potential diagnostic pitfall. Virchows Arch 450:483–485
22. Corradi D, Bosio S, Maestri R, Mormandi F, Curry A, Eyden B (2007) A giant myxoid mammary myofibroblastoma: evidence for a myogenic/synthetic phenotype and an extracellular matrix rich in fibronectin. Histopathology 52:396–398
23. Klopcic U, Lamovec J, Luzar B (2009) Fine needle aspiration biopsy of primary breast myxofibrosarcoma: a case report. Acta Cytol 53:109–112
24. Pant I, Kaur G, Joshi SC, Khalid IA (2008) Myxoid liposarcoma of the breast in a 25-year-old female as a diagnostic pitfall in fine needle aspiration cytology: report of a rare case. Diagn Cytopathol 36:674–7
25. Hayashi H, Nishikawa M, Watanabe R, Sawaki M, Kobayashi H, Shibata A, Kikumori T, Nagasaka T, Imai T (2007) Nodular fasciitis of the breast. Breast Cancer 14:337–339
26. Magro G, Michal M, Bisceglia M (2001) Benign spindle cell tumors of the mammary stroma: diagnostic criteria, classification and histogenesis. Review. Pathol Res Pract 197:453–466
27. Magro G, Bisceglia M, Michal M, Eusebi V (2002) Spindle cell lipoma-like tumor, solitary fibrous tumor and myofibroblastoma of the breast: a clinico-pathological analysis of 13 cases in favour of a unifying histogenetic concept. Virchows Ach 440:249–260

Virchows Arch (2010) 456:587–593
DOI 10.1007/s00428-010-0893-9

CASE REPORT

First case of primary phyllodes tumor of the pancreas: case report and findings of immunohistochemical and ultrastructural studies

Kenichi Hirabayashi · Takeaki Fujihira · Hiroyuki Oyamada · Akihiko Serizawa · Tomohiro Yamashita · Kosuke Tobita · Toshihide Imaizumi · Hiroshi Kajiwara · Naoya Nakamura · Robert Yoshiyuki Osamura

Received: 5 February 2010 / Accepted: 5 February 2010 / Published online: 25 February 2010
© Springer-Verlag 2010

Abstract A 37-year-old Japanese man with a solid and cystic pancreatic mass was referred to our hospital. Computed tomography revealed a well-demarcated solid and cystic mass measuring approximately 3.0 cm in diameter in the pancreatic body. The patient underwent middle segment pancreatectomy, and the retrieved tumor specimen was found to be a well-demarcated solid and cystic lesion measuring 3.0× 3.0 cm. On histological examination, the cyst walls were found to be lined with a monolayer of non-atypical tall columnar epithelial cells. The solid areas surrounded the cystic ones and showed storiform proliferation of spindle cells that contained round, oval, or elongated nuclei and were present among abundant collagen fibers. The solid areas sent phylloid projections into the cystic spaces and the main pancreatic duct. The spindle cells were found to be diffusely positive for alpha-smooth muscle actin, desmin, and h-caldesmon on immunohistochemical analysis. Electron microscopy revealed that these cells possessed well-developed myofilaments with dense bodies, pinocytic vesicles, and basal lumina. Neither metastasis nor local invasion was detected. After the operation (4 years), tumor recurrence has not occurred. The main differential diagnoses of spindle cell tumors are leiomyomas, leiomyosarcomas, inflammatory myofibroblastic tumors, solitary fibrous tumors, extra-gastrointestinal stromal tumors, and schwannomas. However, the histological findings in the present case differed from those of these tumors. The present lesion is the first reported case of a primary pancreatic phyllodes tumor.

Keywords Phyllodes tumor · Pancreatic neoplasm · Immunohistochemistry · Ultrastructure

K. Hirabayashi (✉) · H. Kajiwara · N. Nakamura · R. Y. Osamura
Department of Pathology, Tokai University School of Medicine,
143 Shimokasuya,
Isehara, Kanagawa 259-1193, Japan
e-mail: khira@is.icc.u-tokai.ac.jp

T. Fujihira · K. Tobita · T. Imaizumi
Department of Surgery, Tokai University School of Medicine,
143 Shimokasuya,
Isehara, Kanagawa 259-1193, Japan

H. Oyamada · A. Serizawa
Division of Diagnostic Pathology, Tokai University Hospital,
143 Shimokasuya,
Isehara, Kanagawa 259-1193, Japan

T. Yamashita
Department of Radiology, Tokai University School of Medicine,
143 Shimokasuya,
Isehara, Kanagawa 259-1193, Japan

Introduction

Phyllodes tumors are composed of proliferated mesenchymal spindle cells and benign epithelial cells; these tumors commonly involve the breast. Extra-mammary phyllodes tumors have been reported in the prostate and seminal vesicles [1, 2]. Mesenchymal tumors involving the pancreas are rare, but various histological types have been reported, including leiomyosarcoma, leiomyoma, inflammatory myofibroblastic tumor (IMT), perivascular epithelioid cell tumor, schwannoma, solitary fibrous tumor (SFT), and extra-gastrointestinal stromal tumor (extra-GIST) [3–10]. However, a phyllodes tumor affecting the pancreas has not been reported. The present case is the first report of a primary pancreatic phyllodes tumor. Here, we present the histological features of this tumor along with the findings of immunohistochemical and ultrastructural studies.

Clinical history

The patient was a 37-year-old Japanese man. When he was 34 years old, he had been admitted to another local hospital for the treatment of acute pancreatitis, and a solid and cystic pancreatic mass measuring approximately 2 cm was detected. Since this mass gradually enlarged during follow-up, at the age of 37 years, he was admitted to Tokai University Hospital for the surgical removal of the mass. The patient had no symptoms, and physical examination did not reveal any abnormal findings. Further, laboratory data, including the levels of the tumor markers carcinoembryonic antigen and CA19-9, were within the normal range. Computed tomography revealed a well-demarcated solid and cystic mass measuring approximately 3.0 cm in diameter in the pancreatic body. The solid areas of the lesion showed prominent enhancement upon the injection of a contrast medium (Fig. 1a). The preoperative diagnoses included endocrine neoplasm and solid pseudopapillary neoplasm. Middle segment pancreatectomy was performed, and neither metastasis nor local invasion was detected during the surgery. Tumor recurrence has not occurred for 4 years after the operation.

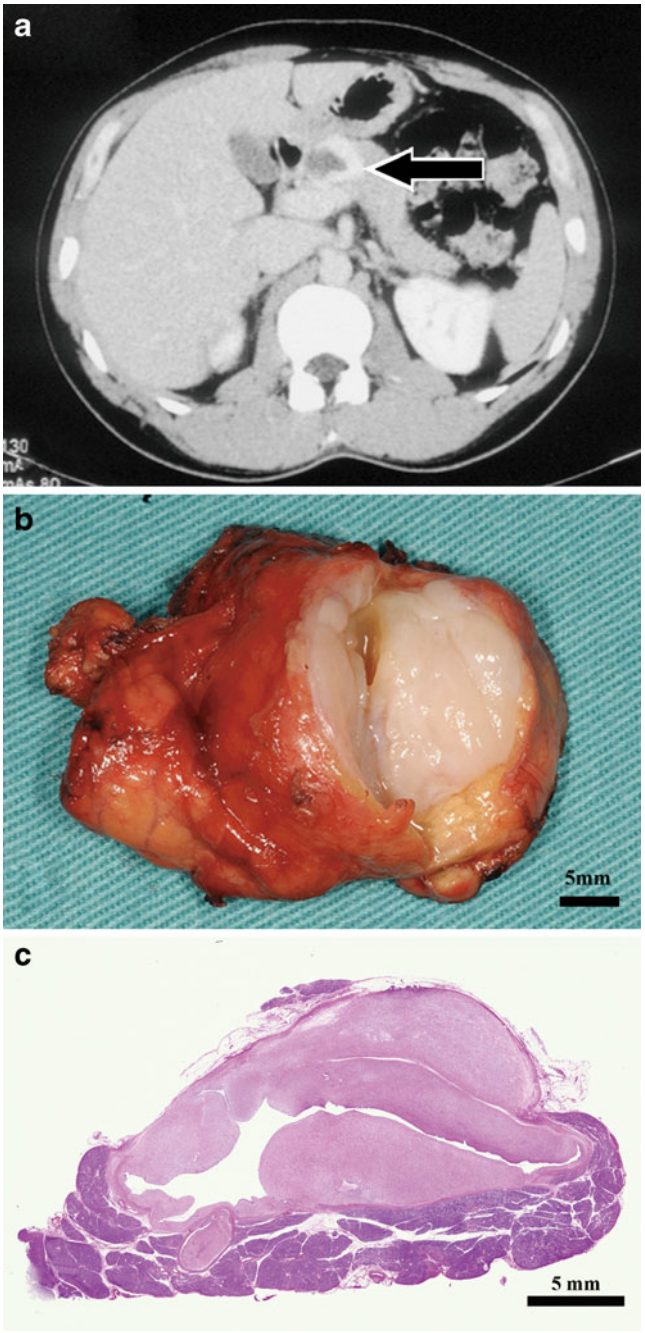

Fig. 1 **a** Computed tomography in equilibrium phase. A well-demarcated solid and cystic mass measuring approximately 3.0 cm in diameter is located in the pancreatic body (*arrow*). The *solid parts* of the mass show prominent enhancement upon contrast medium injection. **b** Macroscopic findings. The *solid parts* of the lesion are *whitish* and *elastic* and surround the cystic parts. **c**) Loupe findings. The tumor contains *solid* and *cystic* areas. The *solid area*s send phylloid projections into the cystic spaces

Materials and methods

Tissues

The tumor was fixed in 10% formalin and embedded in paraffin in the routine manner. The paraffin-embedded tissues were cut into 4-μm-thick sections and stained with hematoxylin and eosin.

Immunohistochemistry

Indirect immunohistochemical labeling was performed. The sections were deparaffinized in xylene and rehydrated through a graded ethanol series to distilled water. The primary antibodies used and their dilutions and sources are summarized in Table 1. If necessary, antigen retrieval was performed by autoclaving the samples for 15 min in a sodium citrate buffer at pH 6.0 (β-catenin, MUC1, CD99, bcl2, MUC2, MUC5AC, MUC6, vimentin, calponin, melan-A, and Ki67) or pH 7.0 (inhibin and h-caldesmon) or by treatment with 0.1% trypsin at 37°C for 30 min (CK7, CK19, CK20, and CD34). The antibodies were detected using EnVision Plus (Dako, Glostrup, Denmark; for CK7, CK19, CK20, inhibin, β-catenin, MUC1, CD99, bcl2, MUC2, MUC5AC, MUC6, vimentin, calponin, desmin, h-caldesmon, and melan-A), MAX-PO (Nichirei, Tokyo, Japan; for CD34 and Ki67), horseradish peroxidase (HRP)-conjugated polyclonal goat anti-mouse immunoglobulin (Dako; for Epstein–Barr virus (EBV), alpha-smooth muscle actin (α-SMA), HMB-45), or HRP-conjugated polyclonal goat anti-rabbit immunoglobulin (Dako; for S-100), with 3,3′-diaminobenzidine as the

Table 1 Immunohistochemical findings

	Clone	Source	Dilution	Spindle cells	Columnar cells
Pancytokeratin	AE1, AE3 and PCK26	Ventana	Prediluted	(−)	(+)
CK7	OV-TL 12/30	Dako	1:30	(−)	(+)
CK19	Ks19.1	Progen	1:20	(−)	(+)
CK20	Ks20.8	Dako	1:40	(−)	(+, focal)
MUC1	Ma695	Novocastra	1:50	(−)	(+)
MUC2	Ccp58	Novocastra	1:100	(−)	(−)
MUC5AC	CLH2	Novocastra	1:100	(−)	(−)
MUC6	CLH5	Novocastra	1:100	(−)	(+)
Vimentin	V9	Dako	1:300	(+)	(−)
α-Smooth muscle actin	1A4	Sigma	1:800	(+)	(−)
Calponin	CALP	Dako	1:50	(+)	(−)
Desmin	D33	Dako	1:200	(+)	(−)
h-Caldesmon	h-CD	Dako	1:50	(+)	(−)
S-100	Polyclonal	Dako	1:400	(−)	(−)
Inhibin	R1	Dako	1:30	(−)	(−)
β-Catenin	17C2	Novocastra	1:100	(−)	(+)
bcl2	124	Dako	1:30	(−)	(−)
Melan-A	A103	Dako	1:50	(−)	(−)
HMB-45	HMB45	Dako	1:50	(−)	(−)
c-kit	9.7	Ventana	Prediluted	(−)	(−)
Anaplastic lymphoma kinase	ALK1	Dako	1:40	(−)	(−)
CD34	QBEnd/10	Novocastra	1:50	(−)	(−)
CD99	12E7	Dako	1:10	(−)	(−)
Estrogen receptor	6F11	Ventana	Prediluted	(−)	(−)
Progesterone receptor	16	Ventana	Prediluted	(+)	(−)
Epstein–Barr virus	CS1-4	Dako	1:100	(−)	(−)
p53	DO-7	Ventana	Prediluted	(−)	(−)
Ki67	MIB1	Dako	1:200	<1%	<1%

Dako, Glostrup, Denmark; Progen Biotechnik GMBH, Heidelberg, Germany; Novocastra, Newcastle upon Tyne, UK; Ventana Medical Systems, Tucson, AZ, USA; Sigma, St. Louis, MO, USA

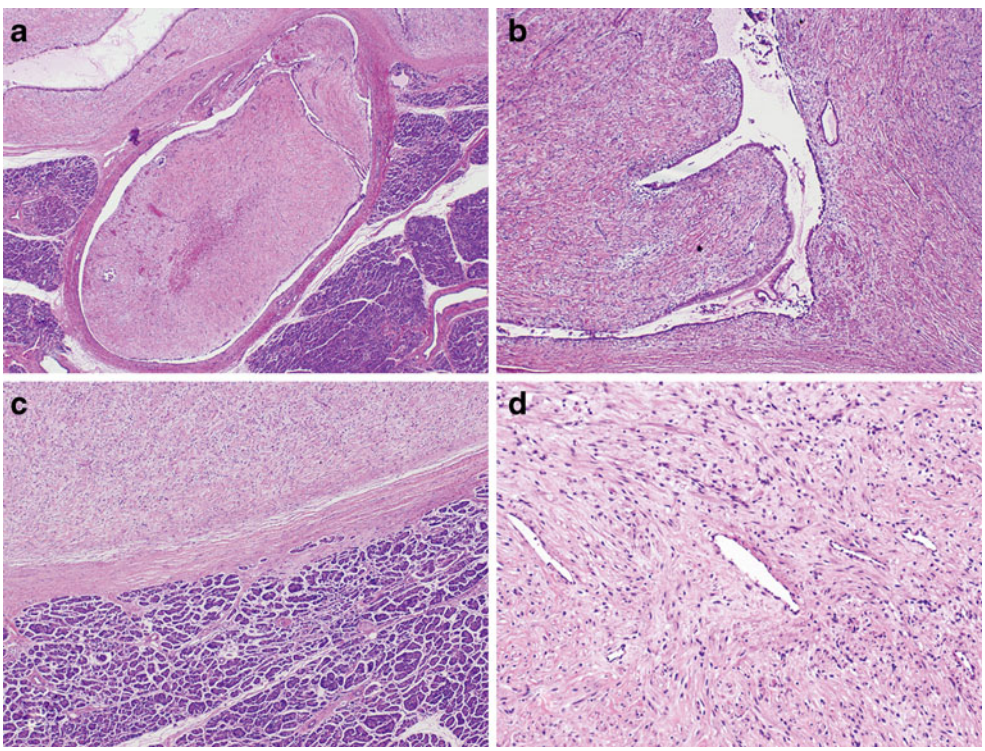

Fig. 2 Microscopic findings (low-power view). **a** The main pancreatic duct is filled with the tumor. **b** The *solid parts* of the lesion send phylloid projections into the cystic spaces. **c** The margins between the tumor and pancreatic tissues are well demarcated. **d** Many small blood vessels are embedded in the *solid areas*

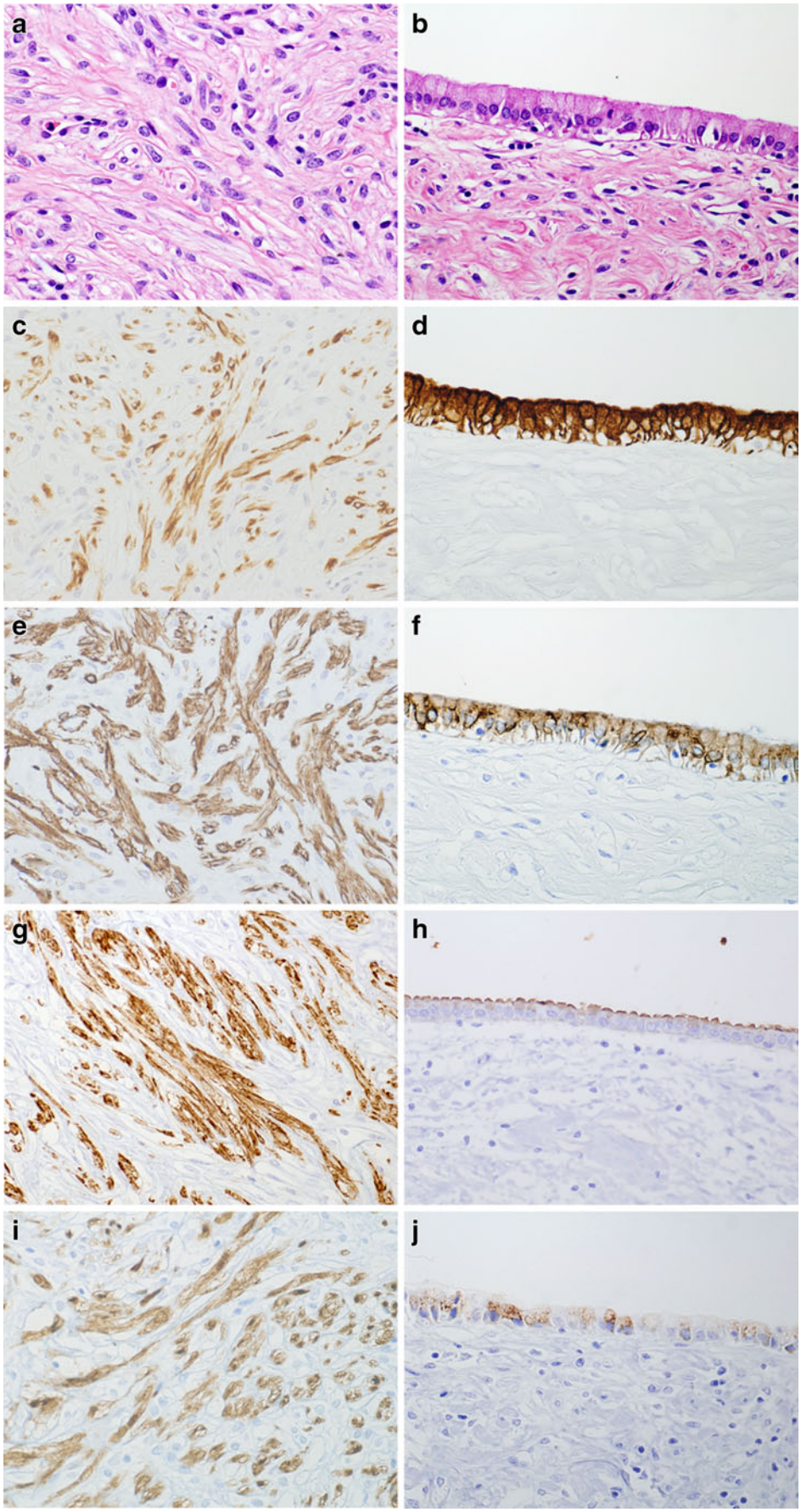

Fig. 3 Microscopic findings (high-power view) and results of immunohistochemical analysis. **a** The *solid areas* show storiform proliferation of spindle cells that contain round, oval, or elongated nuclei and are located among collagen fibers. **b** The cystic walls are lined by a monolayer of non-atypical tall columnar epithelium. The spindle cells in the solid areas proliferate under the epithelium lining the cystic walls. Immunohistochemical analysis reveals that the spindle cells are positive for desmin **c**, α-smooth muscle actin **e**, h-caldesmon **g**, and calponin **i** and that the columnar epithelium lining the cystic walls is positive for CK7 **d**, CK19 **f**, MUC1 **h**, and MUC6 **j**

chromogen. Assays for pancytokeratin, estrogen receptor (ER), progesterone receptor (PR), c-kit, anaplastic lymphoma kinase (ALK), and p53 were performed using Ventana Benchmark XT (Ventana Medical Systems, Tucson, AZ, USA) equipped with the Ultra View Detection Kit. Antigen retrieval was performed by treatment with CC1 (Ventana; for ALK1, ER, PR, and c-kit) or protease 1 (Ventana; for pancytokeratin). Appropriate positive and negative tissue control samples were used.

Electron microscopy

The tumor was also fixed in 2% buffered glutaraldehyde, postfixed in 1% osmium tetraoxide, dehydrated, and embedded in Epon for electron microscopy. Tissue sections were then prepared and stained with uranyl acetate and lead citrate.

Results

Macroscopic findings: The tumor appeared solid and cystic and measured 3.0×3.0 cm. The cystic areas contained slightly mucinous fluid; the solid areas appeared whitish and elastic, and surrounded the cystic lesions. The margins between the tumor and the adjacent normal pancreatic tissues were well demarcated (Figs. 1b, c, and 2c). Microscopic findings: The cyst walls were lined by a monolayer of non-atypical tall columnar epithelial cells (Fig. 3b). Erosions and inflammation were present in some areas of the tumor. The solid lesions surrounded the cystic ones and exhibited storiform proliferation of spindle cells that contained round, oval, or elongated nuclei and were located among collagen fibers (Fig. 3a). Many small blood vessels were found embedded in the solid lesions (Fig. 2d). The solid lesions sent phylloid projections into the cystic spaces and the main pancreatic duct (Fig. 2a and b). Few lymphocytes and plasma cells infiltrated the solid areas. No mitosis was found in the spindle cells. No other tumor lesions or inflamed areas were found in the pancreatic tissues surrounding the tumor. The results of immunohistochemical analysis are shown in Table 1 (Fig. 3c–j). Electron microscopy revealed spindle cells embedded in many collagen fibers (Fig. 4a). The spindle cells contained pinocytotic vesicles, basal lumina, and well-developed myofilaments with dense bodies. The endoplasmic reticulum was not prominent (Fig. 4b).

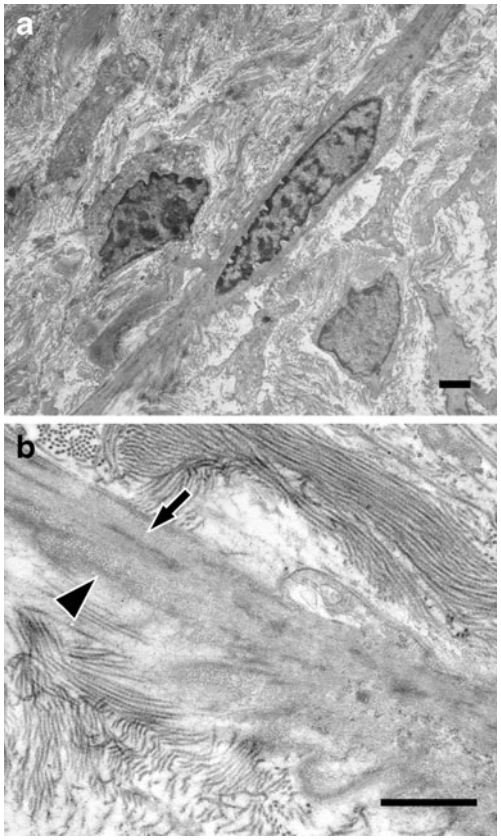

Fig. 4 The spindle cells are embedded within many collagen fibers (*bar*, 2 μm). **b** The spindle cells possess well-developed myofilaments with dense bodies (arrow), and pinocytotic vesicles (arrow head; bar, 1 μm). The endoplasmic reticulum is not prominent

Discussion

Phyllodes tumors are known to metastasize to the pancreas [11–13], but primary phyllodes tumor of the pancreas has not yet been reported. The spindle cells in mammary phyllodes tumors differentiate to muscular cells or myofibroblasts that express α-SMA [14]. In addition, mammary phyllodes tumors are positive for bcl2, CD34, PR, and β-catenin [14–16]. In the present case, the solid areas of the tumor were positive for α-SMA and PR, but not for the other proteins expressed by mammary phyllodes tumors.

The differential diagnosis includes leiomyoma, leiomyosarcoma, IMT, SFT, extra-GIST, and schwannoma. Primary pancreatic leiomyosarcomas are rare [10], and leiomyomas are extremely rare. Only two cases of pancreatic leiomyoma have been reported: one of EBV-associated leiomyomatosis with leiomyomas in multiple organs (gallbladder, liver, spleen, intestinal tract, and lung) [7] and the other of a solitary pancreatic leiomyoma that was resected by enucleation [8]. However, these two tumors did not show features of phyllodes tumors. In the present patient, no leiomyomas were detected in the other organs and no evidence of EBV infection was found. Moreover, abundant collagen fibers were observed between the spindle tumor cells—a finding that is not a typical feature of leiomyomas in other organs.

IMT is defined as the proliferation of myofibroblastic spindle cells with numerous inflammatory cells. A few cases of pancreatic IMTs have been reported [6]. These tumors express actin-associated proteins such as calponin and α-SMA and occasionally express ALK, cytokeratin, and desmin [17, 18]. They are usually negative or show very focal positivity for h-caldesmon [17]. The tumor in the present case was diffusely positive for not only α-SMA, desmin, and calponin but also h-caldesmon. Furthermore, marked inflammatory infiltration was not observed. Therefore, we considered that the present tumor was not an IMT. Moreover, we excluded the diagnoses of schwannoma, extra-GIST, and SFT because the tumor was negative for S-100; CD34 and c-kit; and CD34, CD99, and bcl2, respectively [4, 5, 9]. Mass-forming reactive lesions such as chronic fibrosing pancreatitis and the so-called inflammatory pseudotumor are also included in the differential diagnoses of spindle cell tumors. However, we think that the present lesion was a tumor and not merely a reactive change because the spindle cells were diffusely positive for muscular markers and because the margins between the lesion and the surrounding normal pancreatic tissue were well demarcated.

In the present case, we observed spindle cell proliferation and cystic spaces lined with non-atypical columnar epithelium. The epithelial lining of the cystic lesions showed no atypia, and on immunohistochemical analysis, it was found to express cytokeratins and mucins; this finding is identical to the expression pattern of normal pancreatic epithelium [19, 20]. Therefore, we concluded that the lining of the cystic lesions was normal epithelium trapped in the solid tumorous lesions. The spindle cells were found to be diffusely positive for α-SMA, desmin, and h-caldesmon on immunohistochemical analysis and to contain well-developed myofilaments with dense bodies on electron microscopy. These findings indicate that the spindle cells had differentiated to smooth muscle cells rather than myofibroblasts. We also detected myofibroblasts, which expressed α-SMA and calponin but not desmin and caldesmon, around the normal pancreatic ducts. Myofibroblasts are known to be located around the normal pancreatic duct [21]. From these findings, we speculated that in the present case, the myofibroblasts around the pancreatic duct transformed to tumor cells in the following manner: the cells differentiated to smooth muscle cells because of some trigger, proliferated, and then surrounded the dilated pancreatic ducts.

We classified the present tumor as benign because of the following findings: absence of prominent atypia in the spindle cells, low Ki-67-labeling index, smooth boundary between the normal pancreatic tissue and the tumor tissue, absence of invasion and metastasis, and lack of tumor recurrence for 4 years after the operation.

In conclusion, we have reported the case of an uncommon pancreatic tumor composed of spindle cells that differentiated to smooth muscle cells and were located around dilated pancreatic ducts, resulting in a phyllodes pattern. We believe this tumor is the first reported case of a primary pancreatic phyllodes tumor.

Acknowledgments The authors thank Johbu Itoh (Teaching and Research Support Center, Tokai University School of Medicine) for his valuable technical assistance.

Conflict of interest statement We declare that we have no conflict of interest.

References

1. Schapmans S, Van Leuven L, Cortvriend J et al (2000) Phyllodes tumor of the prostate. A case report and review of the literature. Eur Urol 38:649–653
2. Son HJ, Jeong YJ, Kim JH et al (2004) Phyllodes tumor of the seminal vesicle: case report and literature review. Pathol Int 54:924–929
3. Hirabayashi K, Nakamura N, Kajiwara H et al (2009) Perivascular epithelioid cell tumor (PEComa) of the pancreas: immunoelectron microscopy and review of the literature. Pathol Int 59:650–655
4. Hirabayashi K, Yasuda M, Umemura S et al (2008) Cytological features of the cystic fluid of pancreatic schwannoma with cystic degeneration. A case report. JOP 9:203–208
5. Luttges J, Mentzel T, Hubner G et al (1999) Solitary fibrous tumour of the pancreas: a new member of the small group of mesenchymal pancreatic tumours. Virchows Arch 435:37–42
6. Mizukami H, Yajima N, Wada R et al (2006) Pancreatic malignant fibrous histiocytoma, inflammatory myofibroblastic tumor, and inflammatory pseudotumor related to autoimmune pancreatitis: characterization and differential diagnosis. Virchows Arch 448:552–560
7. Monforte-Munoz H, Kapoor N, Saavedra JA (2003) Epstein-Barr virus-associated leiomyomatosis and posttransplant lymphoproliferative disorder in a child with severe combined immunodeficiency: case report and review of the literature. Pediatr Dev Pathol 6:449–457
8. Nakamura Y, Egami K, Maeda S et al (2000) Primary leiomyoma of the pancreas. Int J Pancreatol 28:235–238
9. Showalter SL, Lloyd JM, Glassman DT et al (2008) Extra-gastrointestinal stromal tumor of the pancreas: case report and a review of the literature. Arch Surg 143:305–308
10. Zalatnai A, Kovacs M, Flautner L et al (1998) Pancreatic leiomyosarcoma. Case report with immunohistochemical and flow cytometric studies. Virchows Arch 432:469–472
11. Ang TL, Ng VW, Fock KM et al (2007) Diagnosis of a metastatic phyllodes tumor of the pancreas using EUS-FNA. JOP 8:35–38
12. Wolfson P, Rybak BJ, Kim U (1978) Cystosarcoma phyllodes metastatic to the pancreas. Am J Gastroenterol 70:184–187
13. Yu PC, Lin YC, Chen HM et al (2000) Malignant phyllodes tumor of the breast metastasizing to the pancreas: case report. Chang Gung Med J 23:503–507
14. Dunne B, Lee AH, Pinder SE et al (2003) An immunohistochemical study of metaplastic spindle cell carcinoma, phyllodes tumor and fibromatosis of the breast. Hum Pathol 34:1009–1015
15. Lee AH (2008) Recent developments in the histological diagnosis of spindle cell carcinoma, fibromatosis and phyllodes tumour of the breast. Histopathology 52:45–57

16. Sawyer EJ, Hanby AM, Rowan AJ et al (2002) The Wnt pathway, epithelial-stromal interactions, and malignant progression in phyllodes tumours. J Pathol 196:437–444
17. Qiu X, Montgomery E, Sun B (2008) Inflammatory myofibroblastic tumor and low-grade myofibroblastic sarcoma: a comparative study of clinicopathologic features and further observations on the immunohistochemical profile of myofibroblasts. Hum Pathol 39:846–856
18. Tanaka A, Hirabayashi K, Sadahiro S et al (2010) Inflammatory myofibroblastic tumor of the ascending colon in adults manifested by positive fecal occult blood test. Gastrointest Endosc 71:214–216
19. Bouwens L (1998) Cytokeratins and cell differentiation in the pancreas. J Pathol 184:234–239
20. Nagata K, Horinouchi M, Saitou M et al (2007) Mucin expression profile in pancreatic cancer and the precursor lesions. J Hepatobiliary Pancreat Surg 14:243–254
21. Izumi M, Suda K, Torii A et al (2001) Pancreatic ductal myofibroblasts. Proliferative patterns in various pathologic situations. Virchows Arch 438:442–450

Virchows Arch (2010) 456:595–597
DOI 10.1007/s00428-010-0924-6

INVITED EDITORIAL

The ENETS and AJCC/UICC TNM classifications of the neuroendocrine tumors of the gastrointestinal tract and the pancreas: a statement

Günter Klöppel · Guido Rindi · Aurel Perren · Paul Komminoth · David S. Klimstra

Received: 13 April 2010 / Accepted: 14 April 2010 / Published online: 27 April 2010
© Springer-Verlag 2010

In 2006 a working group of the European Neuroendocrine Tumor Society (ENETS) developed and published a proposal for a TNM staging classification of the neuroendocrine tumors (NET) of the foregut (stomach, duodenum, and pancreas), accompanied by a grading system [1]. This was followed in 2007 by the publication of a TNM staging classification of the midgut and hindgut NETs (ileum, appendix, colon/rectum) from the same group [2]. These were the first TNM classifications to be developed for the NETs that took into account the distinctive growth patterns of these tumors and that differentiated these tumors from the other gastroenteropancreatic (GEP) carcinomas. These classification systems additionally supplemented the WHO classification of the GEP-NETs [3], some aspects of which had already been recognized as prognostically relevant [4]. In the years that followed the publication of these proposed TNM classifications, the classifications that concerned the foregut GEP-NETs and particularly the pancreatic NETs were validated by several studies, and their biological relevance and power to discriminate among prognostic groups was largely confirmed [5–9].

In 2009 the seventh edition of the AJCC/UICC TNM classification of the most important malignant tumors appeared [10]. It also includes new TNM staging classifications of the gastrointestinal carcinoids and of pancreatic neuroendocrine tumors, which had not previously been included in the AJCC/UICC staging classifications. However, the seventh edition of the AJCC/UICC TNM classification does not apply to high grade (large cell and small cell) neuroendocrine carcinomas and does not exactly follow the ENETS classifications for some of the anatomic sites. No data are presented to justify the use of different staging parameters. The result is that there now exist two parallel systems, each of which uses identical TNM terminology but may refer to different types and extents of disease for certain NETs. This discrepancy will lead to much confusion among clinicians and will likely limit the ability to compare research

G. Klöppel
Consultation Center for Pancreatic and Endocrine Tumors, Department of Pathology, Technical University of Munich, Munich, Germany

G. Rindi
Institute of Pathology, U.C.S.C. Policlinico A. Gemelli, Rome, Italy

A. Perren
Institute of Pathology, University of Bern, Bern, Switzerland

P. Komminoth
Institute of Pathology, Stadtspital Triemli, Zürich, Switzerland

D. S. Klimstra
Surgical Pathology Service, Memorial Sloan-Kettering Cancer Center, New York, NY, USA

G. Klöppel (✉)
Consultation Center for Pancreatic and Endocrine Tumors, Department of Pathology, Technische Universität München, Ismaningerstr. 22, 81675 Munich, Germany
e-mail: guenter.kloeppel@alumni.uni-kiel.de

Table 1 Comparison of the criteria for the T category in the ENETS and UICC TNM classifications of pancreatic neuroendocrine tumors

	ENETS TNM	AJCC/UICC TNM
T1	Confined to pancreas, <2 cm	Confined to pancreas, <2 cm
T2	Confined to pancreas, 2–4 cm	Confined to pancreas, >2 cm
T3	Confined to pancreas, >4 cm, or invasion of duodenum or bile duct	Peripancreatic spread, but without major vascular invasion (Truncus coeliacus, A. mesent. sup.)
T4	Invasion of adjacent organs or major vessels	Major vascular invasion

studies that utilize TNM staging as a prognostic factor or to stratify treatment.

Specifically, the AJCC/UICC and ENETS classifications differ in the definitions of the T stages for the tumors of the pancreas and appendix (Tables 1 and 2). In the case of the pancreatic NETs, the difference is that the AJCC/UICC applies the same TNM classification used for the exocrine pancreatic tumors to the pancreatic NETs (Table 1). To distinguish pT2 from pT3, this system requires recognition of peripancreatic soft tissue invasion, independent of tumor size, a feature very difficult to assess. According to a study presented at the last meeting of the ENETS Advisory Council in November 2009, NETs of the pancreas differ prognostically with regard to their ENETS T category, but not with regard to the corresponding AJCC/UICC T category. Publication of the aforementioned study is planned for 2010. In the case of the appendiceal NETs, the defined tumor size classes used in the AJCC/UICC system differ considerably from those in the ENETS classification (Table 1). Moreover, invasion of the mesoappendix is omitted. Instead, invasion of the cecum and ileum, a finding very rarely observed in appendix NETs, is introduced as a criterion for T2/T3.

Table 2 Comparison of the criteria for the T category in the ENETS and 7th edition- AJCC/UICC TNM classifications of appendiceal neuroendocrine tumors

	ENETS TNM	AJCC/UICC TNM.
T1	≤1 cm; invasion of muscularis propria	T1a, ≤1 cm T1b, >1–2 cm
T2	≤2 cm and <3 mm invasion of subserosa/mesoappendix	>2–4 cm or invasion of cecum
T3	>2 cm or >3 mm invasion of subserosa/mesoappendix	>4 cm or invasion of ileum
T4	invasion of peritoneum/other organs	invasion of peritoneum/ other organs

The TNM staging for the other sites in the gastrointestinal tract is similar in the two systems, although subtle differences in stage groupings persist.

For the present, the intention of this brief statement is to raise awareness about the existence of the differing criteria for staging GEP-NETs. Since the ENETS system was proposed 3–4 years earlier, it is already in widespread use in Europe. In the United States, many practitioners will be mandated to use the AJCC/UICC system. The confusion that will likely arise from these parallel systems is regrettable. When a TNM classification is being applied in practice, it is consequently important to make clear which classification is being used. Another point is that, given the differences in these two systems, it is critical to document in the pathology reports the underlying features that contribute to the T-stage classification (tumor size, extent of invasion, etc.), to allow translation between ENETS and AJCC/UICC classifications [11].

Collection of additional clinical follow-up data may help to refine the staging parameters, and it is hoped that use of such data will be the basis for future modifications of the TNM staging systems, rather than employing arbitrary criteria to modify existing classifications. The data accumulated since the proposal of the ENETS system do provide validation for the staging parameters in that system. Only time will tell whether the variations introduced in the AJCC/UICC system will confer sufficiently enhanced stratification of survival to justify the confusion this alternative classification will cause.

References

1. Rindi G, Klöppel G, Ahlman H, Caplin M, Couvelard A, de Herder WW, Eriksson B, Falchetti A, Falconi M, Komminoth P, Körner M, Lopes JM, McNicol AM, Nilsson O, Perren A, Scarpa A, Scoazec JY, Wiedenmann B, all other Frascati Consensus Conference participants (2006) TNM staging of foregut (neuro) endocrine tumors: a consensus proposal including a grading system. Virchows Arch 449:395–401
2. Rindi G, Klöppel G, Couvelard A, Komminoth P, Körner M, Lopes JM, McNicol AM, Nilsson O, Perren A, Scarpa A, Scoazec JY, Wiedenmann B (2007) TNM staging of midgut and hindgut (neuro)endocrine tumors: a consensus proposal including a grading system. Virchows Arch 451:757–762
3. Solcia E, Klöppel G, Sobin LH, (In collaboration with 9 pathologists from 4 countries) (2000) Histological typing of endocrine tumours. Second Edition. WHO international histological classification of tumours. Springer, Berlin
4. Schmitt AM, Anlauf M, Rousson V, Schmid S, Kofler A, Riniker F, Bauersfeld J, Barghorn A, Probst-Hensch NM, Moch H, Heitz PU, Kloeppel G, Komminoth P, Perren A (2007) WHO 2004 criteria and CK19 are reliable prognostic markers in pancreatic endocrine tumors. Am J Surg Pathol 31:1677–1682
5. Ekeblad S, Skogseid B, Dunder K, Oberg K, Eriksson B (2008) Prognostic factors and survival in 324 patients with pancreatic endocrine tumor treated at a single institution. Clin Cancer Res 14:7798–7803

6. Fischer L, Kleeff J, Esposito I, Hinz U, Zimmermann A, Friess H, Büchler MW (2008) Clinical outcome and long-term survival in 118 consecutive patients with neuroendocrine tumours of the pancreas. Br J Surg 95:627–635
7. Pape UF, Jann H, Muller-Nordhorn J, Bockelbrink A, Berndt U, Willich SN, Koch M, Rocken C, Rindi G, Wiedenmann B (2008) Prognostic relevance of a novel TNM classification system for upper gastroenteropancreatic neuroendocrine tumors. Cancer 113:256–265
8. La Rosa S, Klersy C, Uccella S, Dainese L, Albarello L, Sonzogni A, Doglioni C, Capella C, Solcia E (2009) Improved histologic and clinicopathologic criteria for prognostic evaluation of pancreatic endocrine tumors. Hum Pathol 40:30–40
9. Scarpa A, Mantovani W, Capelli P, Beghelli S, Boninsegna L, Bettini R, Panzuto F, Pederzoli P, Delle Fave G, Falconi M (2010) Pancreatic endocrine tumors: improved TNM staging and histopathological grading permit a clinically efficient prognostic stratification of patients. Mod Pathol doi:10.1038/modpathol.2010.58
10. Sobin LH, Gospodarowicz MK, Wittekind C (2009) UICC: TNM classification of malignant tumours, 7th edn. Wiley-Blackwell, Oxford
11. Klimstra DS, Modlin IM, Adsay NV, Chetty R, Deshpande V, Gönen M, Jensen RT, Kidd M, Kulke MH, Lloyd RV, Moran C, Moss SF, Oberg K, O'Toole D, Rindi G, Robert ME, Suster S, Tang LH, Tzen CY, Washington MK, Wiedenmann B, Yao J (2010) Pathology reporting of neuroendocrine tumors: application of the Delphic consensus process to the development of a minimum pathology data set. Am J Surg Pathol 34:300–313

Virchows Arch (2010) 456:599–607
DOI 10.1007/s00428-010-0920-x

REVIEW AND PERSPECTIVE

Would Virchow be a systems biologist? A discourse on the philosophy of science with implications for pathological research

Albrecht Stenzinger · Frederick Klauschen · Daniel Wittschieber · Wilko Weichert · Carsten Denkert · Manfred Dietel · Claudio Roller

Received: 3 February 2010 / Accepted: 1 April 2010 / Published online: 27 April 2010
© Springer-Verlag 2010

Abstract Research in pathology spans from merely descriptive work to functional studies, "-omics" approaches and, more recently, systems biology. The work presented here aims at placing pathological research into an epistemological context. Aided by Rudolf Virchow, we give an overview on the philosophy of science including the Wiener Kreis, Popper, Kuhn, Fleck and Rheinberger and demonstrate their implications for routine diagnostics and science in pathology. A focus is on the fields of "-omics" and systems pathology.

Keywords Epistemology · Philosophy of science · Pathology · Systems pathology · Rudolf Virchow

Albrecht Stenzinger and Frederick Klauschen contributed equally to this paper.

A. Stenzinger (✉) · F. Klauschen · D. Wittschieber · W. Weichert · C. Denkert · M. Dietel
Institute of Pathology, Charité-Universitätsmedizin Berlin,
Charitéplatz 1,
10117 Berlin, Germany
e-mail: albrecht.stenzinger@charite.de

C. Roller
Department of Philosophy, Philosophy of Science,
History of Science and Technology,
Innovation Center of Knowledge Research,
Technical University of Berlin,
10623 Berlin, Germany

Present Address:
A. Stenzinger · W. Weichert
Institute of Pathology,
Ruprecht-Karls-University,
Heidelberg, Germany

Introduction

It was in 1847 when Rudolf Virchow set a benchmark whose significance for pathology continues and has yielded progress since: "The standpoint, which we aim to abide, is a scientific one. Clinical medicine as applied theoretical discipline, theoretical medicine as pathological physiology is the ideal, which we shall strive to realise as far as it is in our power" [1]. This dictum has been made by a person, whom Rosai characterises as a biologist who used microscopy—the newest and most sophisticated tool of his time [2]. As Virchow said, "it must be understood that in addition to applied microscopy, there is scientific microscopy. What will in the end be of importance in the development of medicine is whether the microscope proves to be an agent merely of diagnosis or truly of (scientific) reform." [3].

Even if we do not follow this rather radical view, one has to acknowledge the fact that Virchow's scientific life provided a solid basis not only for the scientific concept of disease on which diagnostic pathology and clinical medicine heavily rely but also and particularly for biological research ([4]: cells are the fundamental units constituting all tissues, and disease is a result of failure in normal functioning [3].

Virchow also visionarily foresaw the relevance and indispensable interrelationship between clinical observation and laboratory investigation by pointing out that "the pathologist has to step out of the mortuary to the bedside" [5].

Notably, he also acknowledged (still for a century to come unrevealed) molecular alterations to possibly influence cellular behaviour without necessarily influencing morphology: "Every anatomical alteration is also physical

but does this necessarily mean that every physical alteration is always anatomical? Instead, can't it be molecular? (…) These subtle molecular changes are not the subject of anatomy but rather of physiology. They are purely functional (…)." [6].

In the age of biomarkers and gene mutation analysis influencing therapeutic regimens in oncology, it is intriguing to see the parallels to what one now calls 'translational medicine' and 'molecular pathology'.

Over the last 160 years, pathological research has extended from descriptive but nonetheless important microscopy-driven science and sophisticated molecular experimental setups to the generation of quantitative high throughput ("-omics") data and lately systems pathology [7, 8].

This rapid evolution of scientific approaches prompted and encouraged us to pause our lab work and reflect on the methodological concepts which underlie scientific work from Virchow's times until today. Our approach, however, is not a historical but a philosophical one. More specifically, it is an epistemological one which raises several questions: What is pathological knowledge? How is pathological knowledge acquired? How valid and sound is pathological knowledge?

The following discourse is not a comprehensive theoretical seminar on epistemology but aims at introducing the major different epistemological concepts to the scientifically working pathologist and ventures to liaise with the development and themes of pathological research. In this context, it is our hope that the integration of epistemological thoughts in daily scientific work becomes routine—just as decades ago the microscopy became routine in the daily diagnostic work.

To avoid any misunderstanding, it is important to note that philosophy of science and hence our work does not intend to outline a concrete 'philosophically proven' guideline for scientific work. This is charlatanry and beyond any scope of epistemology. Our work aims at shaping an enlightened self-concept of science that empowers the scientist to constantly challenge established scientific theories.

Major epistemological concepts and implications for pathology

(a) The Wiener Kreis (1922–1936) and the concept of logical empirism:

The "Wiener Kreis" was a group of philosophers and scientific theoreticians holding weekly meetings between 1922 and 1936. Moritz Schlick as well as Rudolf Carnap and the other members of the "Wiener Kreis" stuck to the idea that all metaphysical theory conceptions and metaphysical questions, i.e. all conceptions that do not rely on sensory perception exceed the horizon of experience and should thus be expelled from true science [9, 10].

The methodical ideal of experience-based or so-called "expert" knowledge relies on observations or experiments, whose verification does not bear any principal difficulties. Individual cases are used to inductively derive hypotheses, theories or even a general law of nature (inductive conclusion). Hence, the system of empirical science stands on the solid fundament of observed 'facts'. Based on 'real' observations scientists develop more new truthful theories, which comprise a timeless system of scientific knowledge that grows steadily.

[1] *At a first glance, the concept of the Wiener Kreis seems to be conclusive. Empirically based knowledge still plays an important role in research as well as in diagnostics. Induction is a fairly simple, though sometimes valuable principle to generate a novel research hypothesis but is also helpful in the diagnostic process, i.e. a certain morphological pattern of a single individual case is assigned to a certain general type of cancer. Moreover, many observations of rare histopathological entities are published as case reports, which may inductively provide the basis of the definition of a new entity.*
Implications for the concept of pathological research are as follows:
Starting with Virchow and his forefathers, pathological knowledge accumulates over time. This knowledge is based on observations, which are inductively generalized. As long as the object of observation remains unchanged and is inductively investigated, pathological theories derived thereof are correct and timelessly valid.
Virchow, however, apparently had some reservations about this scientific approach. In 1899 [11]*, he stated: "we return to the primitive state from which scientific medicine has evolved: single observations dominate and the rule emerges from the accumulation of these observations."*

The conception of the "Wiener Kreis" was based upon the validity of the inductive conclusion. All the more their point of view was delicately struck when Karl Popper formulated his powerful critique on the logic of inductive reasoning.

(b) Karl Popper (1902–1994) and his theory of falsification:

The scientific theoretician Karl Popper, who was intensively influenced by but never invited to the sessions of the "Wiener Kreis" insisted that inductive reasoning from a single specific observation to a general theorem is never eligible, since "as we all know, many observations of

[1] Philosophical relations to pathology are in italics and typeset as indention.

a white swan do not qualify for the theorem that *all* swans are white" [12].

To take Popper at his word, one cannot argue that a specific type of cancer generally harbours a gain of function mutation in gene x only because one made this observation in 'n' tumor specimens. As pointed out above, inductive reasoning is the work horse of routine diagnostics. However, with the radical view of Popper the principle of induction never provides a definite certainty whether the histomorphological pattern of a single case can be subsumed under entity y.
To be clear: According to Popper, inductive reasoning can be used to generate a hypothesis. It would wrong, however, to think that inductive reasoning leads to a timelessly valid verity.

By dismissing the principle of induction as a reliable scientific tool, Popper posed a threat to the previously unquestioned clear-cut demarcation between empirical science and the speculative creation of mind. Challenged by this problem, he proposed the principle of deduction to allow for the testing of scientific hypotheses. Basically, several observational sentences are being deduced from an already established theory. The theory is challenged if these deduced sentences fail to bear comparison with reality (*falsification*).

Popper's approach just turns the principles of empirical science upside down: deduction does not aim at the verification of theories. Theories in general do only have the status of hypotheses, which are retained unchanged until they are *falsified*. The possibility that a hypothesis can be falsified is also the criterion to discriminate between empirical and non-empirical theories.

Coming back to our previous example, one can hypothesize that all cancers of type x have a gain of function mutation in gene x. According to Popper, this hypothesis can never be verified, even if one would infinitely analyze this type of cancer for that specific mutation and even if the finding were always positive. The theory can, however, be falsified if one would find a single case of cancer x that does not harbour the mutated gene x.

Popper's approach also accentuates the dynamics of scientific theory building. As soon as a hypothesis is falsified, a new one has to take its place. The new hypothesis should incorporate the cases explainable by the old theory, as well as the falsified counter-example.

Assuming that we have sequenced several hundred cases of cancer x for that specific gain of function mutation in gene x and found one case that does not have this particular mutation, our theory is challenged and has to be adopted—provided that the applied methods are reliable and validated.
Therefore, the new theory—based on additional data—would possibly explain why all cases of cancer x have the gain of function mutation except those that do e.g. not metastasize. This theory stands in as long as it will be falsified.

According to Popper, the inherent potential of falsification improves scientific theory building. The novel theory emerging from falsification of the old one has to achieve "more" than the antecessor. It has to explain everything covered by the former theory plus it has to make new predictions. Due to the increasing amount of predictions, the new theory exhibits a higher potential of being falsified. To summarise, in contrast to what one would expect, a high number of empirically redeemable points addressable by criticism is a seal of quality of a good theory. Science should gear towards falsification.

Hence, Popper's position is not a historical or empirical one but a normative proposal: Theories *must* be falsifiable. The question whether a certain theory is truly falsified by the experimental approach contradicting the actual theoretical construct can not be answered. If inductive reasoning is dismissed, there is no "verification of a falsification".

In conclusion, it can never be conclusively determined whether a hypothesis is empirically rejected or not. However, by means of logic, we can decide whether a theory is generally falsifiable.

In contrast to the conception of the "Wiener Kreis", Popper's approach converts the starting point of gaining scientific knowledge from pure observation towards a given hypothesis and its validation (lack of falsification).

With respect to pathological research, Popper points out that scientific knowledge is not timelessly valid but falsifiable. Knowledge has only the status of a "hypothesis on call", which is true until it is falsified. This scientific self-conception is more modest than the one proposed by the Wiener Kreis.
According to Popper's claim, pathological research must steadily review its hypotheses. If these hypotheses withstand a critical analysis, they are approved. They are, however, still falsifiable.
Every falsification and subsequent development of a new hypothesis contributes to a steady enhancement of pathology. Although knowledge is not rock-solid but falsifiable, the promise of scientific enhancement is placating.

Popper also scrutinises the autonomic status claimed for the observational and the theory level, respectively: "Observations are always observations in the light of a certain theory". This statement underlines the influence of a certain theory on the read-out of any experiment.

This assertion can be readily appreciated by the fact that in diagnostic pathology as well as in research a theory-primed mind enables us to scan a tumor specimen for specific determining features that would otherwise be putatively unrecognized. However, as we will see in Fleck's approach, this also includes the risk of overlooking relevant alterations.

Thomas Kuhn (1922–1996) and his concept of scientific revolutions

This line of argument was readily taken up by Thomas Kuhn and Ludwik Fleck. However, they eventually radicalised Popper's conception by developing an epistemological theory that heavily interferes with the by then accepted idea of scientific progress, as well as with the definition of objectivity and rationality in science: Popper's proposal was deconstructed.

The central idea of Kuhn's position is the concept of the *paradigm*, which harbours two distinct denotations: First, a paradigm is the common ground on which communication among scientists and professional consensus on a specific problem is based, i.e. normative aspects such as an established and commonly accepted canon of values or formal aspects, such as accepted analogies, metaphors or definitions. Second, a paradigm stands for an established scientific concept or method which can be analogously applied to a new but related scientific field [13].

On the basis of this conception, Kuhn structures scientific practice in different phases, which are—from his point of view—pivotal for the understanding of scientific progress as a whole.

Of particular importance is the so-called phase of normal science and the occurrence of *scientific revolutions*. Kuhn defines the period of normal science by a metaphor: normal science is basically *puzzle solving*. The scientist does not aim to falsify hypotheses in terms of Popper, but tries to integrate as many phenomena as possible in a certain established paradigm. Just as working on a crossword, the phrase "puzzle solving" suggests that a definite solution exists as long as you strive hard enough. This metaphor is illustrative in as much as one can easily envisage that some parts of the puzzle do not fit in at once and have to be set aside. Another well-known strategy of solving a puzzle is to vehemently resqueeze several parts of the puzzle so that certain components of the puzzle will eventually fit in somehow.

However, a severe crisis emerges as soon as some parts of a puzzle cannot be integrated and the whole picture gets flawed and distorted. These elements, which elude proper integration, are called *anomalies*. The more these anomalies attract the attention of the scientific community the more the previously stable system of methods will be softened and a novel paradigm is about to emerge that competes with the established one.

At this point, the most remarkable process of Kuhn's approach is emerging: scientific revolution by transition from the old to the novel paradigm. Since Kuhn draws a parallel between scientific development and political revolutions, the term scientific revolution is chosen intentionally. For Kuhn, a prerequisite for revolution is the dim feeling of malfunction and collapse ultimately leading to a severe crisis of the established system. According to his conception, this holds true for both fields.

Moreover, as in politics the scientific community divides into two opponent groups: one tries to sustain the established scientific paradigm, whereas the other seeks to construct a new system. Probably the most striking parallel between political and scientific revolution is the fact that polarisation ultimately leads to a discussion which does not tolerate a paradigm-independent point of view. The consultation of an autonomous authority becomes impossible. As Kuhn points out, "Every group employs its own paradigm to defend just that paradigm." (Kuhn 106).

Due to this circulatory conclusion, the discussion between the representatives of the ancient and the novel paradigm does not have the character of a rational argument but rather of trying to persuade each other. According to Kuhn, the ancient and novel paradigms are incommensurable. This decisive and debatable but nonetheless famous thesis of incommensurability has three mainstays:

1. In different paradigms, different problem areas are considered important and different requirements are made regarding the structure of a satisfying solution. The respective paradigm determines the relevance and successful solution of a problem.
2. Second, fundamental terms are variably used in different paradigms. For example, during the change of physical concepts from "Newton's world" to "Einstein's world", the definitions of the terms space and time were amended. The novel meaning of a certain term is not necessarily obvious because the same words are still being used.
3. Finally, the perception of reality is determined by the respective paradigm. Since the paradigm only allows for a predetermined view of the world, the advocates of different scientific paradigms live in different worlds. Hence, an established and well-recognised fact is not only being interpreted in the light of a certain paradigm. In fact, insurmountable differences between scientists already arise on what is considered real—the level of data and facts—because reality is already interpreted in the context of the paradigm. It becomes clear that there is no neutral point of view and no mediation if reality is already "soaked with paradigms".

Life sciences readily adopted the term paradigm and its implications. There are numerous examples of so called paradigms (e.g. the long standing paradigm that draws a vertical line from DNA to RNA to protein, which has been recently challenged by the finding that not all RNAs are just a template for certain proteins but have a regulatory function themselves).

However, strict application of Kuhn's criteria shows that most paradigm examples that circulate in life sciences are not a paradigm in the sense of Kuhn. As one may appreciate, almost all cases lack the incommensurability between the old and the new paradigm—a central defining criterion.

A true scientific revolution (as defined by Kuhn) in the history of medicine that really parallels the change from Newton's to Einstein's world of physics or Darwin's theory of evolution is difficult to find. The finding that genetic information is encoded by DNA and the rise of molecular biology may come close to Kuhn's definition. A probably more convincing example—without which molecular biology is unthinkable—was the novel cell-based view on life and disease propagated by Virchow and his intellectual antecessors [14] *that contrasted strongly with the still established and clinically applied system of humoral pathology, the latter explaining human disease by a disordered condition of fluids and spirits of the human body. Both paradigms use a distinct terminology, predetermine a concept of disease and set the basis for research in these fields. In other words, the ancient and the novel paradigm are incommensurable*.

As a consequence of this view, one cannot assume an entirely rational decision between the old and the new paradigm by neutral comparison. A neutral level simply does not exist. Hence, shifting between paradigms is primarily triggered by persuasion. It is, however, not intended to say that rational arguments are entirely excluded from the paradigm controversy. There are certain aspects that indeed argue for the novel paradigm: the solution of exactly those problems that put the old paradigm to crisis; crucial experiments; unexpected confirmation of a prognosis regarding the outcome of an experiment; and, last but not least, aesthetic principles (e.g. simplicity).

Having discussed examples of cases in which novel scientific paradigms replaced old views in the past, a look into the future of pathology raises the question whether a transition from molecular pathology to systems pathology might similarly fulfill Kuhn's criteria of a paradigm shift. "Conventional" molecular pathology studies the relevance of, for instance, expression profiles and mutations as predictors of disease prognosis and/or the efficacy of targeted therapies by mainly correlating certain molecular conditions with clinical outcome. Systems pathology, on the other hand, aims at untangling the full complexity of diseases by performing a comprehensive functional analysis of the molecular determinants of pathological processes. The rationale behind this undoubtedly very ambitious approach is that a thorough mechanistic understanding of pathologically altered biochemical networks is a necessary precondition to overcome the current limits especially of molecular cancer diagnostics and therapeutics where the one-gene-one-drug-approach has so far brought relatively limited clinical benefit. In the sense that in different paradigms different problem areas are considered important and the focus is on different solutions structures as stated above in the first of Kuhn's three mainstays, systems pathology would certainly qualify as a novel paradigm. However, a closer look at the second and third mainstays with regard to the differences between conventional molecular and systems pathology/biology and a comparison with the historic examples may change the perspective. While the transition from classical physics to quantum mechanics or humoral pathology to histopathology implied fundamental changes of the underlying scientific and methodological concepts, the level of information used in systems pathology/biology is not conceptually different from that used in molecular biology. On the contrary, a solid systems pathology approach must be based upon the core concepts of molecular biology and even though the success of systems pathology will largely rely on modern experimental ("Omics") approaches, these technologies were developed to generate more precise, quantitative and high-throughput—but not fundamentally different—molecular data.

This said, we certainly do not want to question the potential of systems pathology to revolutionize medicine, but to point out that the systems approach is the continuous "next step", the logic consequence and natural extension of molecular pathology rather than a completely different kind of science.

Above all, the belief in a certain paradigm plays a major role when scientists have to decide on the paradigm they prefer: the belief that the new paradigm will cope with novel and more difficult problems superiorly.

Apparently, there is a contradiction between Popper's and Kuhn's ideas regarding the dynamics of scientific progress.

The self-concept of pathology would face heavy consequences if Kuhn's conception of incommensurable paradigms was applied to the dynamics of pathological theories. In contrast to Popper, Kuhn's

scientific revolution is not accompanied by scientific progress (enhancement) as there is no strong neutral criterion that allows evaluating scientific research. Obviously, this is a true affront for the critical rationalist Popper and his followers!

Within the so-called Popper–Kuhn controversy, the differences with regard to contents were discussed intensively. An effort to merge both concepts would be to consider the model of Kuhn as a descriptive explanation of knowledge formation, whereas Popper' conception refers to a normative level.

Based on this philosophical view, the obvious tensions between both concepts may be alleviated by the idea that (pathological) research is based on a certain paradigm but concomitantly seeks to discriminate a valuable scientific approach from a less valuable one by means of rational standards.
The issue of paradigm dependency is probably pursued best by thinking about the status of scientific facts.

Ludwik Fleck (1896–1961) and the impact of socio-cultural aspects on research

Ludwik Fleck, a physician by profession, opened up a stimulating account on the problem of scientific facts. Several of Kuhn's thoughts can already be found in Flecks monography from 1935 [15], correspondingly entitled: Genesis and development of a scientific fact. With regard to the recent developments in the field of life sciences, the perception of Fleck may be of special interest since his epistemological conception evolves from a medical case study.

Because biomedical research primarily aims at understanding human diseases, scientific development is focused on the abnormal rather than the normal. Systematisation of diagnostic findings is largely constructional. Moreover, there is a strong pragmatic orientation: the primary aim is to understand and master a certain disease. In this context, theoretical considerations have to take up a sub-ordinal role and are under considerable strain to improve therapeutic strategies.

For Fleck, thought collective and thought style are the major terms to describe the evolution of a (medico-) scientific fact. Thought collective is defined as scientific community that works on a certain field of research. During their medical career, young scientists will be affiliated to their research community and thus adopt the intellectual prerequisites, the thought style of the community. Predefinitions specific for the thought style are termed thought constraint and passive connections (established scientific fact shared by the thought collective) by Fleck. Opposed to thought caprice and active connections (assumptions of a thought collective) the former two ensure a focused and coherent, i.e. direct visual perception and avert unstyled non-oriented sampling. Scientists who underwent such a training know what is relevant, what to look for, how to categorise and systemise a certain observation and, last but not least, they know which method to apply for which problem.

The imagery of the direct perception of form is intimately connected to the concept of a scientific fact: direct visual perception of form means to identify scientific facts and should not be misconceived as mere construction. Accordingly, for Fleck, the hallmark of empirical sciences and hence, for the genesis of scientific facts is a maximisation of thought constraint and passive connections while minimising thought caprice. The thought style of a scientific community is a comprehensive system of shared opinions. This system of knowledge and holism, respectively, also plays a pivotal role for the development of a thought style. Although the thought collective aims to perseverate its thought style, thereby stabilising its conceptual system, changes in the thought style can occur. The latter are termed mutations of the thought style, which match or match not well with the established system of knowledge. For example, such mutations may reflect a shift in the meaning of a certain finding. Extension of these mutations potentially carries the risk that the original and the novel system of knowledge drift apart essentially leading to incommensurability of the thought styles. Although Fleck differentiates between phases of tradition and conservation ("Klassizität") and complications, the focus is not on revolutionary changes as in Kuhn's work. According to Fleck's conception such scientific revolutions are generally conceivable; his conception, however, favours a dynamic and steady shift by a multitude of small changes, additions and developments.

Moreover, the scientific community and its research output are also part of the society, which relies on a specific set of observations, thoughts, values and opinions. In this respect, the scientist is not only sharing his conceptions and thoughts with the lay public but is also part of and influenced by the society and its constituting thoughts, values and opinions.

As if he had foreseen the development of the life sciences, in 1935, Fleck pointed out that one cannot underestimate the industrial and societal–political influence on and pressure to succeed in medical research. From Fleck's point of view, these aspects play a pivotal role in shaping medical science.

Besides the obvious sociological orientation of this approach, Fleck also emphasises the historical dimension and stresses the constructing power of proto-ideas. Such

ideas may be constitutive for the development of new scientific facts and are supposed to affect all changes of a thought style. The continuous influence of proto-ideas does not favour the assumption that thought styles are superseded by radical break-ups.

Fleck does not draw so much attention to a change of paradigms rather than to the continuous process of shaping scientific facts. These are not automatically purported but have to be arduously elaborated by scientific practice. Hence, the forefront of research is not directly confronted with facts, but has to develop them. Fleck allocates this level of research to journal science, whose contributions have a provisional and preliminary character. The content of scientific work is stabilised when conveyed to a monograph or manual. The inclusion of research data and its related theories in a textbook, however, marks them as a fully established and disclosed scientific fact. By that time, the forefront of the scientific community has already relinquished this conception and has developed a new cutting-edge theory.

The system of scientific schools that rely on certain thought styles and subsequently form distinct aspects of pathology can readily be appreciated by flipping through medical history text books. Starting with Galen who believed alterations in humours to cause a certain disease, it is Vesalius who can be credited with the implementation of anatomical dissection and Morgagni who merged clinical medicine with the latter. Rokitansky, a strong advocate of pathoanatomy and founder of the Austrian school of Pathologists, was heavily criticized by Virchow for his recourse to humoral pathology in cases that did not reflect a disease by obvious macroscopic changes. Based on the work of Theodor Schwann und Henry Dutrochet, Virchow implemented the cellular view on human disease and helped to get this theory accepted. This very brief overview highlights only a few scientific schools and can easily be extended and discussed in more depth [4]. *However, one may appreciate that Fleck's concept of the thought collective and associate thought style helps to understand the basis of scientific trends.*

With respect to the pathological mechanism of a specific disease, namely diabetes, Schlich [16] *meticulously unravels the dispute between the physiologists Pflüger and the physician Minkowski on the question whether diabetes is caused by a disorder of the nervous system or can be attributed to the failure of internal secretion by pancreatic tissue. Although the outcome of this debate is very clear nowadays, this controversy nicely illustrates the concept of Fleck's thought style and provides insight into a not necessarily rational debate on a scientific problem.*

If we take Fleck's concept seriously, we will inevitably face the issue that scientific facts are not discovered by pathological research but are being created by a thought collective sharing a thought style. Concomitantly, Fleck hands in a benchmark for scientific quality control: a minimum of active connections shall be accompanied by a maximum of passive connections. In other words: a research project should be based on a minimum of theoretical assumptions while relating to as many properties of the investigated system reckoned obvious and incontrovertible ('scientific fact') within a given thought style as possible. According to Fleck, science attempts to transform these assumptions (active connections) into new scientific facts (passive connections).

Hans Jörg Rheinberger (1946–) and the role of experimental systems

Flecks considerations regarding the development of scientific facts have been picked up by Hans Jörg Rheinberger and his work on 'epistemic things' [17]. According to Rheinberger, epistemic things are things to which we apply our epistemic efforts. In other words, they are the objects of research. Characteristically, epistemic things have to be fuzzy and rather vague. According to Rheinberger, it is this fuzziness and vagueness that creates a tension, which in turn leads to scientific productivity to explore and investigate the unknown.

The background of this conception is the central role of experimental arrangements and experimental systems for scientific work. Experimental systems are knowledge generators. The practice of research reveals its own dynamic in which objects of research emerge, are shaped and modified just to be incorporated into the experimental arrangement at a later date (in this context, Fleck refers to a zigzag course of science).

From this perspective, research practice and coherence of discovery are being vindicated against the epistemological primacy of theory (as in Popper's approach).

Particularly in the age of "omics", i.e. genomics, transcriptomics, proteomics, interactomics and metabolomics, it is indeed mainly the experimental system that drives scientific knowledge acquisition. In contrast to experimental setups which are based on a certain hypothesis, the human genome project and its spin-offs are discovery-driven science, which mainly rely on inductive reasoning. Omic approaches provide quantitative data on a large scale, thereby yielding unprecedented views of the cell's inner workings.

However, while these high-throughput "omics" analyses of biological systems enable researchers to gather biolog-

ical data at an unprecedented level of detail, the mere accumulation of information does not in itself deserve to be called an inducer of a methodological/scientific "paradigm shift". The difference between conventional experimental approaches (measurements of a few constituents of biological activity) and novel "omics" approaches (analysis of many proteins, genes etc.) is gradual rather than conceptual. In principle, global gene expression profiles, for instance, could be measured conventionally by RT–PCR without gene microarrays; it is just not possible in practice. And even though the use of such novel methods facilitates data generation, it does not immediately yield insight into and produce understanding of the dynamic properties of cellular function. In this context and according to Popper's claim that a good theory should be principally falsifiable, these novel technologies per se do not conceptually improve the ability to falsify a scientific theory and therefore do not conceptually facilitate scientific theory building.

However, these limitations of the bare "omics" approaches should not lead to pessimism regarding their potential to pave the way for a new era of biomedical research. But rather than being the final answer, they are an essential but first step/building block of a more comprehensive concept commonly referred to as "systems biology". As the name may suggest, this field aims at providing the means to analyse and understand biological function at the systems level. This is achieved by integrating detailed molecular information derived from discovery- and hypothesis-driven science reflecting the multiple hierarchical levels of cellular organisation and information processing. While "omics" technologies are the work-horse for experimental data generation, the future of systems biology heavily relies on novel data analysis approaches that permit the functional reconstruction of cellular network architecture. While statistics-based methods may yield some initial insight into functional properties of cellular processes, ultimately dynamic spatio-temporal mechanistic models of molecular networks will be needed for systems biology to fulfil its ambitious promise. Systems biology will then not only be a framework of scientific tools that facilitates model/theory testing and falsification (Popper), it may be simultaneously used to generate novel hypothesis by performing computational simulations ("in-silico experiments") of the mechanistic molecular models.

In 1849, Virchow outlined a somewhat fuzzy research scheme that comes quite close to the circle of inductive bottom-up data mining and hypothesis-testing top-down data mining being used in systems biology approaches [18]*: "The scientific question is the logic hypothesis, which evolves from a known theory by analogy and induction; the answer in turn is provided by the experiment, which is encoded by the scientific question."* [19].

As it appears these days, a systemic approach, which has its origin in the pre-genomic era [20] *is unlikely a novel paradigm that is truly incommensurable with other established biological paradigms if one applies Kuhn's definition strictly. This scientific approach, however, operates novel tools that may lead our current view on cell and molecular biology into new dimensions—beyond a gene-centred world of life and disease* [21]*. With Fleck, we would expect assumed properties within a given system under study to be minimised while passive connections and its knowledge claims are being maximised. Time will tell!*

Concluding remarks

It was Virchow who, approximately 150 years ago, identified the alterations at cellular level as the driving force of disease and it is the distinguished biologist and Nobel laureate Sydney Brenner who stated in 2002 [22]: "not only is the cell the only physical locus for gene action but it is the correct level of abstraction to construct a framework for understanding functions."

Although we are unable to frame a philosophically clear-cut answer, with these quotes in mind we are tempted to conclude that if nowadays Virchow were to choose a career in pathology he would probably utilise the most promising and latest concept in these times to reinvent morphology based "Cellularpathologie" on a complex functional level: systems pathology.

Kuhn and Fleck might explain why one could follow this conclusion.

References

1. Virchow R (1847) Über die Standpunkte in der wissenschaftlichen Medicin. Arch Path Anat 1:3–19. English translation in Rather LJ (1958) Disease, life, man: Selected essays by RLK Virchow. Stanford CA, Stanford University Press, Stanford CA
2. Rosai J (2007) Why microscopy will remain a cornerstone of surgical pathology. Lab Invest 87:403–408
3. Virchow R (1855) Cellularpathologie. Arch Path Anat 8:3–39 English translation in Rather LJ (1958) Disease, life, man: Selected essays by RLK Virchow. Stanford University Press, Stanford CA
4. Nezelof C (1994) European roots of pathology. Pathol Res Pract 190:103–114
5. Virchow R (1900) Ein alter Bericht über die Gestaltung der pathologischen Anatomie in Deutschland, wie sie ist und wie sie sein muss. Arch Path Anat 159:23–39
6. Virchow R (1854) Specifiker und Specifisches. Arch Path Anat 6:3–33
7. Dietel M, Schäfer R (2008) Systems pathology—or how to solve the complex problem of predictive pathology. Virchows Arch 453:309–312
8. Faratian D, Clyde RG, Crawford JW, Harrison DJ (2009) Systems pathology—taking molecular pathology into a new dimension. Nat Rev Clin Oncol 6:455–464

9. Schlick M (1918) Allgemeine Erkenntnislehre. Moritz Schlick. Reprint in Gesamtausgabe, Abteilung I, Band 1, Springer, Wien 2009, English translation by Blumberg AE and Feige H General theory of knowledge by M Schlick Open Court Publishing 1985
10. Carnap R (1928) Der logische Aufbau der Welt. Meiner, Hamburg. English translation in George RA The Logical Structure of the World and Pseudoproblems in Philosophy by Rudolf Carnap, Open Court Classics 2003
11. Virchow R (1899) Eröffnungsansprache. In: Wangerin A, Taschenberg O (ed) Verhandlungen der Gesellschaft Deutscher Naturforscher und Ärzte. 70. Versammlung zu Düsseldorf, 19–24. September 1898. F.C.W. Vogel, Leipzig,. Theil II/2. S.4–5
12. Popper K (1959) The logic of scientific discovery. Hutchinson, London
13. Kuhn S (1962) The structure of scientific revolutions 1962 3rd edition. University of Chicago Press, Chicago
14. Mazarello P (1999) A unifying concept: the history of cell theory. Nat Cell Biol E13–E15
15. Fleck L (1935) Entstehung und Entwicklung einer wissenschaftlichen Tatsache, reprint in 1980 by Suhrkamp Verlag, Frankfurt am Main. English translation in Fleck L: Genesis and development of a scientific fact, Editors: Trenn TJ, Merton RK, Bradley F University of Chicago Press 1981
16. Schlich T (1993) Making mistakes in science: Eduard Pflüger, his scientific and professional concept of physiology, and his unsuccessful theory of diabetes (1903–1910). Stud Hist Philos Sci 24:411–441
17. Rheinberger H-J (1997) Toward a history of epistemic things: synthesizing proteins in the test tube. Stanford University Press, Stanford
18. Kitano H (2002) Computational systems biology. Nature 420:206–210
19. Virchow R (1849) Die naturwissenschaftliche Methode und die Standpunkte in der Therapie. Archiv für pathologische Anatomie und Physiologie und für klinische Medicin 2:3–37
20. Jacob F, Monod J (1961) Genetic regulatory mechanisms in the synthesis of proteins. J Mol Biol 3:318–356
21. Morange M (2009) A new revolution? The place of systems biology and synthetic biology in the history of biology. EMBO 10 (Suppl 1):S50–S53
22. Brenner S (2002) Nobel laureate speech

Virchows Arch (2010) 456:609–614
DOI 10.1007/s00428-010-0925-5

ORIGINAL ARTICLE

Early Barrett's carcinoma: the depth of infiltration of the tumour correlates with the degree of differentiation, the incidence of lymphatic vessel and venous invasion

Barbara Zemler · Andrea May · Christian Ell · Manfred Stolte

Received: 19 December 2009 / Revised: 2 April 2010 / Accepted: 16 April 2010 / Published online: 7 May 2010
© Springer-Verlag 2010

Abstract The incidence of regional lymph node metastasis in early Barrett's carcinoma is determined by the depth of infiltration of the tumour. The present study investigated the possible relationship between the depth of infiltration of the tumour, its degree of differentiation and the incidence of lymphatic vessel and venous invasion in early Barrett's carcinoma. To this end, a total of 805 endoscopically resected specimens obtained from 472 patients with early Barrett's carcinomas were analysed. The results of this analysis revealed that increasing depth of tumour infiltration is associated with an increase in the incidence of poorly differentiated carcinomas—from 0.8% for lesions limited to the mucosa (m1) to 41.4% when the depth of infiltration extended to the lower third of the submucosa (sm3). A similar correlation was also found for the incidence of lymphatic vessel invasion (m1, 0.6%; sm3, 44.8%) and for venous invasion (m1, 0%; sm3, 13.8%). All of these observations proved to be statistically highly significant ($p<0.001$). In conclusion, the results show that the degree of differentiation, as well as the incidence of lymphatic vessel and venous invasion, correlates with the depth of infiltration of the early carcinoma in Barrett's oesophagus.

B. Zemler · M. Stolte
Institute of Pathology, Klinikum Bayreuth,
Preuschwitzer Str. 101,
95445 Bayreuth, Germany

A. May · C. Ell
Department of Internal Medicine II, HSK Wiesbaden,
Ludwig- Erhard- Str. 100,
65199 Wiesbaden, Germany

M. Stolte (✉)
Kreuz 25a,
95445 Bayreuth, Germany
e-mail: prof.m.stolte@t-online.de

Keywords Barrett's carcinoma · Depth of infiltration · Degree of differentiation · Lymphatic vessel invasion · Venous invasion

Introduction

Earlier studies established that regional lymph node metastasisation of early Barrett's carcinoma is dependent upon the depth of infiltration of the tumour [1–5]. In those studies, however, a differentiation was made only between early carcinomas limited to the mucosa and those invading the submucosa, with no separate consideration being given to the individual layers of the mucosa or submucosa. More recent studies have shown that the incidence of lymph node metastasis in tumours infiltrating the various layers of the mucosa and the upper third of the submucosa is very rare, from 0% to 4.5%, while infiltration of the middle and lower third of the submucosa is associated with a marked increase in lymph node metastasis to 23% and 69%, respectively [6, 7]. Furthermore, in analogy to other regions of the gastrointestinal tract, the degree of differentiation of early Barrett's carcinomas, together with invasion of lymphatic vessels and veins, is probably a risk factor for the development of metastases.

To date, a possible connection between the depth of tumour infiltration, the degree of differentiation and invasion of the early carcinoma into lymphatics and veins has been investigated in only a few studies—which either contained relatively small numbers of patients or failed to provide any information on statistical significance—again with no differentiation being made between the various layers of the mucosa and submucosa [1, 3, 5, 6, 8, 9]. Therefore, the present study involving a relatively large number of resected early Barrett's carcinomas was under-

taken to investigate the possible presence of significant correlations between the depth of tumour infiltration and the other three suspected risk factors for the development of metastases.

Materials and methods

Patients

A total of 869 endoscopically resected specimens obtained from 472 patients with early Barrett's carcinoma were investigated. Sixty-four of these specimens were discarded, either because they were too small or because the excision had not been deep enough. Eight hundred five specimens remained for further investigation. Of the patients, 80.9% was male, 19.1% was female and their average age was 65.27±11.04 years.

Histological methods

The resected specimens were pinned to cork mats, fixed with 10% formalin and then cut into 2–3-mm-wide slices. After dehydration in an increasing series of alcohols and xylene, the material was embedded in paraffin. Subsequently, 4-µm-thick serial sections were obtained, deparaffinised and stained with haematoxylin and eosin. Lymphatic vessel invasion was identified only when lymphatic endothelial cells were unmistakably demonstrable—in questionable cases, an immunohistochemical test with the monoclonal antibody D2-40 endothelial cell marker was applied. Venous infiltration was confirmed by the Elastica van Gieson stain.

Histological classification and grading

Histological typing and grading of the adenocarcinomas was carried out in accordance with the WHO classification [10]. An early Barrett's carcinoma (pT1) was diagnosed whenever the lesion was limited to the mucosa or submucosa [11].

Using a modification of the Japanese classification of early squamous cell carcinomas of the oesophagus [12], the depth of infiltration of the early carcinomas was classified as shown below:

- m1 Carcinoma limited to the lamina propria of the Barrett's mucosa
- m2 Infiltration of the carcinoma into the newly formed (neo-)muscularis mucosae of the Barrett's mucosa
- m3 Infiltration into the original lamina propria of the oesophageal mucosa
- m4 Infiltration into the original muscularis mucosae of the oesophageal mucosa
- sm1 Infiltration into the upper third of the submucosa of the oesophageal mucosa
- sm2 Infiltration into the middle third of the submucosa of the oesophageal mucosa
- sm3 Infiltration into the lower third of the submucosa of the oesophageal mucosa

Statistical analysis

For the collection and subsequent statistical analysis of the data, SPSS 15.0.1 for Windows (SPSS Inc., Chicago, IL, USA) was used.

The relationship between depth of invasion and degree of differentiation of the tumour was investigated for significance with the Chi-square test. Because of the small number of cases in some of the different infiltration categories and the numerical disparity among the various categories, the necessary criteria for the asymptotic significance of the Chi-square test were not met, so that the Monte Carlo method had to be applied to determine the exact significance to investigate the correlation between the depth of tumour infiltration and the invasion into lymphatic vessels and veins. An additional Mann–Whitney U test confirmed the results. For all the statistical tests, the criterion of statistical significance $p<0.05$ was applied [13–15].

Results

Frequency of the parameters investigated

The frequency distribution of the depth of tumour infiltration, the degree of differentiation, lymphatic vessel invasion and venous invasion of these tumours is shown in Table 1.

The number of cases is continuously decreasing with an increasing depth of tumour infiltration from 43.9% classified as m1 to 3.6% classified as sm3. Of the 805 endoscopically resected specimens, 71.9% was well-differentiated (G1), 19.8% moderate differentiated (G2) and 8.3% poorly differentiated (G3). In 8.1% of the Barrett's carcinomas, a lymphatic vessel invasion could be found; in 1.5%, a venous invasion was detected.

Relationships between the investigated parameters

The relationship between the depth of tumour infiltration and the degree of differentiation of early Barrett's carcinomas is shown in Table 2 and Fig. 1. Increasing depth of infiltration is associated with a clearly recognisable decrease in well-differentiated tumours and an increase in poorly differentiated tumours. The percentage of well-differentiated

Table 1 Frequency distribution of depth of infiltration, degree of differentiation (G), lymphatic vessel invasion (L) and venous invasion (V) in early Barrett's carcinoma

	Frequency	Percent
m1	353	43.9
m2	126	15.7
m3	107	13.3
m4	110	13.7
sm1	61	7.6
sm2	19	2.4
sm3	29	3.6
Total	805	100.0
G1	579	71.9
G2	159	19.8
G3	67	8.3
Total	805	100.0
L0	740	91.9
L1	65	8.1
Total	805	100.0
V0	793	98.5
V1	12	1.5
Total	805	100.0

carcinomas drops from 92.9% in m1 to 17.2% in sm3. Inversely, the percentage of poorly differentiated carcinomas increases from 0.8% in m1 to 41.4% in sm3. This relationship is statistically highly significantly ($p<0.001$).

The incidence of lymphatic vessel invasion in early Barrett's carcinoma in relationship to its depth of infiltration can be seen in Table 3 and Fig. 2. With increasing depth of infiltration, the incidence of lymphatic vessel invasion increases continuously. In only 0.6% of m1 carcinomas, a lymphatic vessel invasion could be found, whereas 44.8% of sm3 carcinomas infiltrates lymphatic vessels. Again, the correlation is statistically highly significant ($p<0.001$).

The incidence of cancerous invasion into veins can be seen in Table 4 and Fig. 3. There is a highly significant relationship between depth of infiltration and venous invasion ($p<0.001$). While in m1 carcinomas no venous infiltration could be found, the percentage of carcinoma with venous infiltration increases from 0.8% in m2 carcinomas to 13.8% in sm3 carcinomas.

Discussion

The present study comprising a relatively large number of resected early Barrett's carcinomas has, for the first time, clearly revealed a statistically highly significant correlation between the depth of infiltration of these tumours and both their degree of differentiation and the occurrence of lymphatic vessel and venous invasion.

At first sight, the disparity in the numbers of early Barrett's carcinomas associated with the different levels of infiltration depth would appear to be a shortcoming of the study. This imbalance is, however, understandable since, in accordance with current recommendations, endoscopic resection is performed only when diagnostic endosonography indicates that the carcinoma is limited to the mucosa or does not extend beyond the upper third of the submucosa at the very most [6, 7, 16]. Since, however, the accuracy of the determination of the depth of infiltration achievable with 20 MHz miniprobe endosonography varies between 78%

Table 2 Relationship between depth of infiltration and degree of differentiation in early Barrett's carcinoma

			Degree of differentiation			Total
			G1	G2	G3	
Depth of infiltration (D)	m1	Number	328	22	3	353
		% of D	92.9%	6.2%	0.9%	100.0%
	m2	Number	104	20	2	126
		% of D	82.5%	15.9%	1.6%	100.0%
	m3	Number	76	23	8	107
		% of D	71.0%	21.5%	7.5%	100.0%
	m4	Number	54	34	22	110
		% of D	49.1%	30.9%	20.0%	100.0%
	sm1	Number	11	38	12	61
		% of D	18.0%	62.3%	19.7%	100.0%
	sm2	Number	1	10	8	19
		% of D	5.3%	52.6%	42.1%	100.0%
	sm3	Number	5	12	12	29
		% of D	17.2%	41.4%	41.4%	100.0%
Total		Number	579	159	67	805
		% of D	71.9%	19.8%	8.3%	100.0%

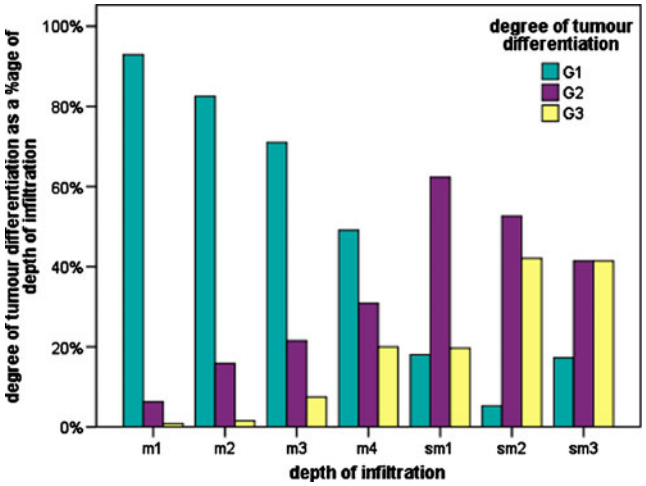

Fig. 1 Relationship between depth of infiltration and degree of differentiation in early Barrett's carcinoma

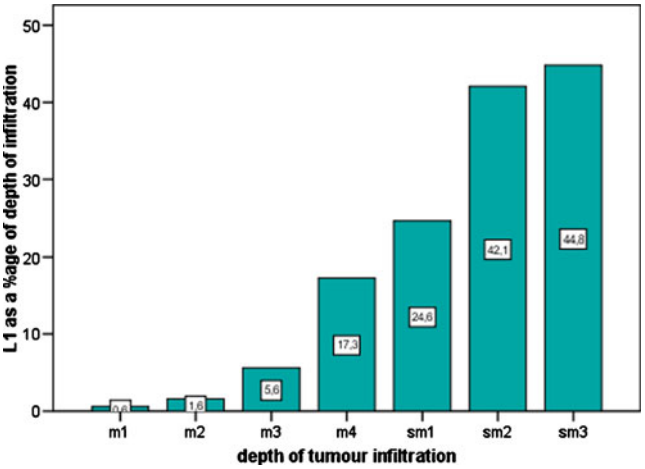

Fig. 2 Relationship between depth of infiltration and lymphatic vessel invasion in early Barrett's carcinoma

and 94% [17–19], carcinomas with depth of infiltration sm2 and sm3 are also to be found among those treated by endoscopic resection. Furthermore, some of the endoscopically resected materials originate from inoperable patients with confirmed submucosal invasion. Despite the differences in the incidence figures for the various depths of tumour infiltration, the results are statistically highly significant ($p<0.001$).

The correlation between the depth of infiltration of the tumour and regional lymphogenic metastasis is an accepted fact [1–5]. In surgical specimens, a depth of tumour infiltration to the levels m1 to sm1 has been reported to be associated with lymph node metastasis in 0–4.5% of the cases, while at the sm2 and sm3 infiltration levels, an incidence of 23–69% has been reported [6, 7].

To date, the question whether the depth of tumour infiltration has any influence on the degree of differentiation and on lymphatic vessel and venous invasion in early Barrett's carcinomas has been investigated in studies comprising only relatively small numbers of cases, and for the most part providing no information on statistical significance [1, 3, 5, 6, 8, 9].

The majority of early Barrett's carcinomas are well-differentiated lesions [1, 20]. This applies in particular to those limited to the mucosa (24–78% well differentiated), while carcinomas infiltrating the submucosa are reportedly

Table 3 Relationship between depth of infiltration and lymphatic vessel invasion in early Barrett's carcinoma

			L1	Total
Depth of infiltration (D)	m1	Number	2	353
		% of D	0.6%	100.0%
	m2	Number	2	126
		% of D	1.6%	100.0%
	m3	Number	6	107
		% of D	5.6%	100.0%
	m4	Number	19	110
		% of D	17.3%	100.0%
	sm1	Number	15	61
		% of D	24.6%	100.0%
	sm2	Number	8	19
		% of D	42.1%	100.0%
	sm3	Number	13	29
		% of D	44.8%	100.0%
Total		Number	65	805
		% of D	8.1%	100.0%

Table 4 Relationship between depth of infiltration and venous invasion in early Barrett's carcinoma

			V1	Total
Depth of infiltration (D)	m1	Number	0	353
		% of D	0.0%	100.0%
	m2	Number	1	126
		% of D	0.8%	100.0%
	m3	Number	0	107
		% of D	0.0%	100.0%
	m4	Number	5	110
		% of D	4.5%	100.0%
	sm1	Number	2	61
		% of D	3.3%	100.0%
	sm2	Number	0	19
		% of D	0.0%	100.0%
	sm3	Number	4	29
		% of D	13.8%	100.0%
Total		Number	12	805
		% of D	1.5%	100.0%

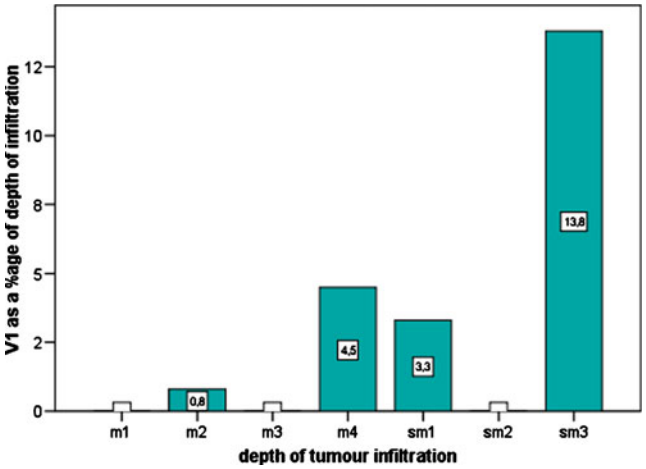

Fig. 3 Relationship between depth of infiltration and venous invasion in early Barrett's carcinoma

poorly differentiated in 44–55% of the cases [1, 5, 6, 8, 9]. In these earlier studies, however, depth of tumour infiltration was usually expressed merely as mucosal or submucosal.

In a modification of the Japanese classification of tumour infiltration of early squamous cell carcinomas of the oesophagus, Buskens et al. [6] differentiated the depth of infiltration of early Barrett's carcinomas as follows: m1 (carcinoma in situ, high-grade dysplasia in Barrett's epithelium with no penetration through the basement membrane), m2 (invasion through the basement membrane into the lamina propria), m3 (invasion into the muscularis mucosae), sm1, sm2 and sm3. The authors discovered a statistically significant decrease in tumour differentiation with increasing depth of infiltration: while all m1 tumours were well differentiated, in the case of sm3 tumours, no G1 carcinomas were found, but poorly differentiated carcinomas were seen in 62% of the lesions.

The majority of the earlier studies investigating the incidence of vascular invasion in early Barrett's carcinoma as a function of the depth of tumour infiltration only differentiate between mucosal and submucosal carcinomas but did not differentiate between lymphatic vessel and venous invasion. These studies did, however, report a relationship between depth of infiltration and vascular invasion: 0–11% of the mucosal carcinomas was associated with vascular invasion, compared with 25–42% of those infiltrating the submucosa [1, 5]. In a few studies containing small numbers of patients, the relationship between lymphatic invasion and the depth of infiltration was investigated. Ruol et al. [3] and Liu et al. [8] identified lymphatic vessel invasion in 0–18% of those carcinomas limited to the mucosa and in 25–48% of those that had already infiltrated the submucosa. These studies, however, did not distinguish between the various layers of the mucosa and submucosa.

In two more recent studies in which a differentiation was made between the various layers of the mucosa and the submucosa, mucosal infiltration was associated with lymphatic vessel invasion in 0% and 42%, respectively, sm1 infiltration with 0% and 14%, sm2 infiltration with 27% and 31% and sm3 with 21% and 92%, respectively [6, 9]. In an earlier overview published by our own working group, in which, however, significance was not calculated, the incidence of lymph vessel invasion as a function of depth of tumour infiltration was m1, 0.8%; m2 and m3, 0%; m4, 2.8%; sm1, 13.3%; sm2, 12.5% and sm3, 26.3% [21]. In the present study, in contrast, lymphatic vessel invasion was much more common, in particular when the submucosa had been infiltrated: sm1, 24.6%; sm2, 42.1% and sm3, 44.8%. In the earlier studies, however, far fewer cases had been analysed than the 805 endoscopically resected specimens harvested from 472 patients in the present report.

The literature contains only few data on venous invasion as a function of the depth of infiltration of early Barrett's carcinomas. Potet et al. [20]—who did not differentiate between the various layers of the submucosa—reported venous invasion to be associated with infiltration of the submucosa in 12.5% of the cases. In our earlier overview, comprising only a small number of cases, we found venous invasion to be associated only with sm1 involvement in 12.5%, but not with m1 to m4 or sm2 and sm3 [21]. The present study did, however, find a statistically highly significant relationship between depth of infiltration of early Barrett's carcinoma and the incidence of venous invasion.

Earlier investigations of surgical specimens clearly identified a relationship between the depth of tumour infiltration and the incidence of lymph node metastasis [1–5]. Whether, over and beyond this, the degree of differentiation, lymphatic vessel invasion and venous invasion represents independent risk factors for metastasisation has not so far been fully investigated. A few small studies showed merely that lymphatic vessel invasion is a negative prognostic factor for overall survival [1, 3, 8].

Numerous publications investigating possible risk factors for metastasisation in early colorectal and gastric carcinomas have established that both the degree of differentiation and tumourous invasion of the lymphatic vessels and veins do indeed represent risk factors for metastasisation. In all probability, this also applies to early Barrett's carcinomas, but the point needs to be clarified by further studies.

In summary, the results of this investigation confirm the existence of a highly significant statistical relationship between the depth of infiltration of early Barrett's carcinoma and both its degree of differentiation and the incidence of cancerous invasion of the lymphatics and veins. Increasing depth of infiltration is associated with a decrease

in the degree of differentiation of the tumour, while the incidence of carcinomatous invasion of lymphatic vessels and veins increases.

Acknowledgement The authors are most grateful to Dr. Reinhard Wittenberg, from the Department of Sociology and Empirical Social Research, Nuremberg, Germany, for his valuable advice on statistical analysis.

Conflict of interest The authors declare that they have no conflict of interest.

References

1. Paraf F, Flejou JF, Pignon JP et al (1995) Surgical pathology of adenocarcinoma arising in Barrett's esophagus. Analysis of 67 cases. Am J Surg Pathol 19:183–191
2. Rice TW, Zuccaro G Jr, Adelstein DJ et al (1998) Esophageal carcinoma: depth of tumor invasion is predictive of regional lymph node status. Ann Thorac Surg 65:787–792
3. Ruol A, Merigliano S, Baldan N et al (1997) Prevalence, management and outcome of early adenocarcinoma (pT1) of the esophago-gastric junction. Comparison between early cancer in Barrett's esophagus (type I) and early cancer of the cardia (type II). Dis Esophagus 10:190–195
4. Stein HJ, Feith M, Mueller J et al (2000) Limited resection for early adenocarcinoma in Barrett's esophagus. Ann Surg 232:733–742
5. van Sandick JW, van Lanschot JJ, ten Kate FJ et al (2000) Pathology of early invasive adenocarcinoma of the esophagus or esophagogastric junction: implications for therapeutic decision making. Cancer 88:2429–2437
6. Buskens CJ, Westerterp M, Lagarde SM et al (2004) Prediction of appropriateness of local endoscopic treatment for high-grade dysplasia and early adenocarcinoma by EUS and histopathologic features. Gastrointest Endosc 60:703–710
7. Westerterp M, Koppert LB, Buskens CJ et al (2005) Outcome of surgical treatment for early adenocarcinoma of the esophagus or gastro-esophageal junction. Virchows Arch 446:497–504
8. Liu L, Hofstetter WL, Rashid A et al (2005) Significance of the depth of tumor invasion and lymph node metastasis in superficially invasive (T1) esophageal adenocarcinoma. Am J Surg Pathol 29:1079–1085
9. Vieth M, Ell C, Gossner L et al (2004) Histological analysis of endoscopic resection specimens from 326 patients with Barrett's esophagus and early neoplasia. Endoscopy 36:776–781
10. Werner M, Fléjou J, Hainaut P et al (2000) Adenocarcinoma of the oesophagus. In: Hamilton SR, Aaltonen LA (eds) World Health Organization classification of tumours: pathology and genetics of tumours of the digestive system. IARC Press, Lyon, pp 20–26
11. Wittekind C, Meyer J, Bootz F, International Union Against Cancer (UICC) (2002) TNM Klassifikation maligner Tumoren, 6. Auflage. Springer-Verlag, Berlin, pp 55–58
12. Japanese Society for Esophageal Diseases (2001) Guidelines for clinical and pathologic studies on carcinoma in the esophagus, 9th edn. Kanehara & Co., Ltd., Tokyo
13. Bortz J, Lienert G, Boehnke K (1990) Verteilungsfreie Methoden in der Biostatistik. Springer-Verlag, Berlin, pp 121–158
14. Bortz J, Lienert G (1998) Kurzgefaßte Statistik für die klinische Forschung: Ein praktischer Leitfaden für die Analyse kleiner Stichproben. Springer-Verlag, Berlin, pp 71–103, 122–139
15. Lehnert U (2000) Datenanalysesystem SPSS Version 9: handlungsorientiertes und leicht verständliches Lehrbuch zur Einführung in die statistische Datenanalyse, 3. Auflage. Oldenbourg Wissenschaftsverlag GmbH, München
16. Noguchi H, Naomoto Y, Kondo H et al (2000) Evaluation of endoscopic mucosal resection for superficial esophageal carcinoma. Surg Laparosc Endosc Percutan Tech 10:343–350
17. May A, Gunter E, Roth F et al (2004) Accuracy of staging in early oesophageal cancer using high resolution endoscopy and high resolution endosonography: a comparative, prospective, and blinded trial. Gut 53:634–640
18. Murata Y, Suzuki S, Ohta M et al (1996) Small ultrasonic probes for determination of the depth of superficial esophageal cancer. Gastrointest Endosc 44:23–28
19. Simizu Y, Tsukagoshi H, Nakazato T et al (1995) Clinical evaluation of endoscopic ultrasonography (EUS) in the diagnosis of superficial esophageal carcinoma. Rinsho Byori 43:221–226
20. Potet F, Flejou JF, Gervaz H et al (1991) Adenocarcinoma of the lower esophagus and the esophagogastric junction. Semin Diagn Pathol 8:126–136
21. Vieth M, Stolte M (2005) Pathology of early upper GI cancers. Best Pract Res Clin Gastroenterol 19:857–869

Virchows Arch (2010) 456:615–623
DOI 10.1007/s00428-010-0921-9

ORIGINAL ARTICLE

Morphometric analysis of the balance between CXCR3$^+$ T cells and FOXP3$^+$ regulatory T cells in lymphocyte-rich and conventional gastric cancers

Haruo Ohtani · Osamu Yoshie

Received: 5 January 2010 / Revised: 2 March 2010 / Accepted: 4 April 2010 / Published online: 27 April 2010
© Springer-Verlag 2010

Abstract Lymphocyte-rich gastric carcinomas (Ly-rich GCs) are characterized by the formation of lymphoid stroma. Our previous study has shown abundant infiltration of CXCR3$^+$ T cells and their frequent clustering with CXCL9 (monokine induced by interferon-γ)-expressing stromal cells in the lymphoid stroma of Ly-rich GCs. Foxp3$^+$ regulatory T cells (Tregs) suppress immune responses in the peripheral tissues and play a role in the immunosuppression of cancer tissues. The present study was therefore undertaken to evaluate the significance of the balance between CXCR3$^+$ T cells and Tregs in 44 Ly-rich and 37 conventional GCs by morphometrical analyses of immunohistochemistry. Compared with the pronounced infiltration of CXCR3$^+$ T cells in the lymphoid stroma, the numbers of Foxp3$^+$ cells were relatively low in Ly-rich GCs. Therefore, the ratios of CXCR3$^+$/Foxp3$^+$ cells were much higher in Ly-rich GCs than in conventional GCs. This suggests the occurrence of T-helper type 1 (Th1)-shifted immune responses in Ly-rich GCs. On the other hand, conventional GCs were characterized by a paucity of CXCR3$^+$ T cells and a relative abundance of Tregs. Furthermore, the stroma inside the cancer was characterized by even less CXCR3$^+$ cells, suggesting a strongly immunosuppressive microenvironment. Since Tregs are known to express CCR4, we also examined the tissue distribution of cells expressing its ligand CCL22. CCL22 was not detected in conventional GCs and only sparsely detected in dendritic cells but not in cancer cells in Ly-rich GCs. To conclude, Tregs may play a more important role in conventional GCs than in Ly-rich GCs from the viewpoint of immunosuppression.

Keywords Gastric cancer · Lymphoid stroma · CXCR3 · Regulatory T cells · Tumor immunity

Electronic supplementary material The online version of this article (doi:10.1007/s00428-010-0921-9) contains supplementary material, which is available to authorized users.

H. Ohtani (✉)
Department of Pathology, Mito Medical Center,
National Hospital Organization,
Ibaraki,
Ibaraki 311-3193, Japan
e-mail: hohtani@mito.hosp.go.jp

O. Yoshie
Department of Microbiology,
Kinki University School of Medicine,
Osaka-Sayama,
Osaka 589-8511, Japan

Introduction

Human cancer tissue is associated with varying degrees of tumor-infiltrating lymphocytes (TILs). Although the significance of TILs as an indicator of host immune responses against cancer cells may not be so straightforward [1], TILs or a subset of TILs are generally associated with a better prognosis of patients in various cancers, suggesting their protective role in antitumor immunity [2–6]. As an extreme variation, some cancers are characterized by a prominent lymphocytic reaction in the stroma. Among gastric cancers (GCs), such cases are designated as "gastric cancer with lymphoid stroma" or "lymphoepithelioma-like carcinoma (LELC)." They generally show a better prognosis than conventional GCs [7, 8]. Cancer cells in typical LELC are frequently associated with Epstein-Barr (EB) virus infection [9, 10]. In the present paper, we use the term "lymphocyte-rich GCs (Ly-rich GCs)" to include typical LELC and other GCs associated with a rich distribution of lymphocytes in the stroma (for details, see the first section of "Materials and methods").

Type 1 immune responses are exerted by type 1 effector T cells (T-helper type 1 [Th1] cells, cytotoxic T cells [CTLs]) and natural killer cells (NK cells) and are important in host defense against intracellular pathogens and tumor cells. CXCR3 is one of the representative chemokine receptors for type 1 immune cells, especially Th1 cells [11, 12]. Previously, we have shown that the majority of TILs in lymphocyte-rich GCs express CXCR3, while CXCL9 (also called monokine induced by interferon-γ [MIG]), one of the cognate chemokine ligands of CXCR3, is abundantly expressed by dendritic-shaped stromal cells [13]. As a result, frequent "$CXCR3^+$ T cell–$CXCL9^+$ stromal cell clustering" was observed, which featured the lymphoid stroma of Ly-rich GCs [13]. Furthermore, $CXCR3^+$ T cells clustering with $CXCL9^+$ stromal cells are frequently positive for Ki-67, suggesting some ongoing immune responses [13].

Recent advances in tumor immunology have revealed that cancers develop by escaping the host immune responses through stepwise processes [14, 15]. Consequently, established cancer tissue is generally considered to be a strongly immunosuppressive microenvironment. In this context, our above-mentioned results from Ly-rich GCs may seem rather inconsistent to the current concept. Therefore, to understand the immunosuppressive aspect of GCs, the present study was undertaken to analyze the potential role of forkhead box protein-3 (Foxp3)-positive regulatory T cells (Tregs) as the mediator of immunosuppression [16, 17]. We compared the distribution density of $CXCR3^+$ cells and that of $Foxp3^+$ cells by morphometric analyses. We reveal here that Ly-rich GCs are characterized not only by the abundance of $CXCR3^+$ cells but also a relative paucity of $Foxp3^+$ cells, resulting in a high ratio of $CXCR3^+$ cells to $Foxp3^+$ cells (termed here as "CXCR3/Foxp3 ratio"). On the other hand, conventional GCs (i.e., GCs other than Ly-rich GCs) are characterized by a relative abundance of $Foxp3^+$ cells and a low CXCR3/Foxp3 ratio, especially within the cancer stroma. Thus, our findings may provide a new insight into the possible differences in immunosuppressive mechanisms between Ly-rich GCs and conventional GCs.

Materials and methods

Materials

We use the term "lymphocyte-rich gastric cancer (Ly-rich GC)" to include both LELC and other GCs associated with abundant TILs in the whole stroma (see [13] for details). The present study enrolled 44 cases of Ly-rich GCs (EBV^+: 35 cases; EBV^-: 9 cases) and 37 cases of conventional GCs (EBV^+: 2 cases; EBV^-: 35 cases). The 35 EBV^- cases of conventional GCs were consecutively sampled by their histopathological numbering. Intramucosal carcinoma (pTis and pT1[M]) were not included in this study, because typical lymphocyte-rich stroma is observed only when carcinoma cells have started invading the submucosa. All cases were staged as described by tumor, node, and metastasis (TNM) Classification, 7th edition [18]. The present study was approved by the ethical committee of Mito Medical Center.

Immunohistochemistry (single-labeling)

Enzyme-linked immunohistochemistry (immunoperoxidase method) was performed using formalin-fixed, paraffin-embedded tissue sections as described previously [13]. The EBV status was checked by in situ hybridization for EBER in all cases [13]. The primary antibodies used in this study were mouse monoclonal antibodies to human CXCR3 (CD183; clone 1C6, IgG1; BD, Franklin Lakes, NJ; used at 1:400=1.25 μg/mL) and Foxp3 (clone 236A/E7, IgG1; Abcam, Cambridge, MA; used at 1:100), and affinity-purified rabbit polyclonal antibody to human CCL22 (MDC) (PeproTech, Rocky Hill, NJ; used at 1:250=4 μg/mL). Tissue sections were incubated with primary antibodies overnight. The staining methods of other lymphocyte markers were described previously [13]. Heat antigen retrieval methods applied before incubation with primary antibodies were as follows: for anti-CXCR3 and anti-CCL22, 10 mmol/L Tris HCl buffer + 1 mmol/L EDTA, pH 9.0, at 95°C for 60 min; for anti-Foxp3, 1:5 dilution of DAKO (Glostrup, Denmark) high-pH buffer (S3308, DAKO), at 95°C for 60 min. Anti-mouse or anti-rabbit Envision (DAKO) was used as the secondary antibody. Diaminobenzidine (DAB; DAKO) was used as the chromogen. Endogenous peroxidase activity was inactivated by immersing tissue sections in 3% H_2O_2 for 5 min after incubation with primary antibodies.

Enzyme-linked double immunohistochemistry for CD4 or CD8 and Foxp3

The immunoperoxidase method for CD4 or CD8 detection was also performed as described above. Tissue sections were then treated with a 1:5 dilution of DAKO high-pH retrieval solution at 95°C for 20 min to inactivate antibodies and enzymes used in the first step. Then immunohistochemistry for Foxp3 was performed using a 1:40 dilution of anti-Foxp3 antibody. TrueBlue (KPL, Gaithersburg, MA) was used as the chromogen.

Morphometry

The percentage of $Foxp3^+$ cells among $CD4^+$ or $CD8^+$ cells (i.e., the labeling index of Foxp3) was determined using tissue sections double-stained for CD4 or CD8 and Foxp3.

The number of total $CD4^+$ (or $CD8^+$) cells and that of $CD4^+$ (or $CD8^+$) $Foxp3^+$ was manually counted in the same areas using an ocular grid (10×10-mm lattice) with a 400× microscopic field (40× objective lens and 10× ocular lens using a BX51 microscope; Olympus, Tokyo, Japan). The area of one lattice was 0.0625 mm^2. At least three fields were counted for each case, and the numbers were averaged. The labeling index of $Foxp3^+$ cells among $CD4^+$ (or $CD8^+$) cells was calculated by the following formula: the number of $CD4^+$ (or $CD8^+$) $Foxp3^+$ cells divided by the total number of $CD4^+$ (or $CD8^+$) cells in the same field. This analysis was performed in five representative cases of Ly-rich GCs. We also measured the distribution density of $CXCR3^+$ cells and that of $Foxp3^+$ cells in all 81 cases of GC by the same method described above. The results were expressed by the average number of three areas. In this analysis, the most densely distributed areas were selected for cell counting. The size of cancer tissues we examined were 2 to 4 cm in length.

All the statistical analyses were performed using PASW Statistics 18 (SPSS Inc., Chicago, IL), including the Fisher's exact test for the test of contingency table, the Kruskal-Wallis test for the comparison between unpaired two groups, the Pearson correlation coefficient between two variables, and the discriminant analysis to check how variables discriminate two groups. All the tests were judged to be significant when $p<0.05$.

Double-labeling immunofluorescence method for CCL22 and CD83

Tissue sections were first immersed in a 1:5 dilution of high-pH antigen retrieval solution at 95°C for 60 min. Nonspecific binding was blocked by Protein Block (X0909, DAKO). The sections were then incubated with a mixture of rabbit antihuman CCL22 (1:100) and mouse monoclonal antihuman CD83 (1:30; Clone 1H4b; Novocastra, Benton Lane, UK) overnight. Alexa fluor 488-labeled donkey antirabbit IgG (1:100=20 μg/mL; Molecular Probe, Carlsbad, CA) and Alexa fluor 555-labeled donkey antimouse IgG (1:100=20 μg/mL) were applied in a mixture for 30 min. After DAPI (Molecular Probes) nuclear staining, specimens were mounted with ProLong Gold (Molecular Probes). Immunofluorescent observation was performed with a confocal laser scanning microscope (TCS SP5; Leica Microsystems, Wetzlar, Germany).

Results

General histopathological aspects

Forty-four cases of Ly-rich GCs were composed of 25 typical LELCs (EBV^+, 22 cases; EBV^-, 3 cases) and 19 other Ly-rich GCs (EBV^+, 13 cases; EBV^-, 6 cases). LELCs were characterized by poor differentiated carcinoma cells with a syncytial appearance and abundant TILs in the whole stroma [13] (Fig. 1a, b). Of 37 cases of conventional GCs, 35 were negative for EBER. Table 1 shows the stage distribution of all the cases. There was a significant difference in the stage distribution between Ly-rich GCs and conventional GCs ($p<0.0005$, Fisher's exact test); i.e., the Ly-rich GCs were composed of cases with less advanced stages than the conventional GCs (Table 1A). Similarly, typical LELCs showed less advanced stages than other GCs (Table 1B). There was no significant correlation between the numbers of $CXCR3^+$ cells and stages or between the numbers of $Foxp3^+$ cells and stages in either Ly-rich or conventional GCs (supplementary figures).

Nearly all $Foxp3^+$ cells are $CD4^+$ cells in Ly-rich GCs

In Ly-rich GCs, $Foxp3^+$ cells were distributed relatively evenly in the whole area of the stroma. They constituted only a small part of the TILs as compared with abundantly distributed $CXCR3^+$ cells (Fig. 1c, d). Previously, we have shown that the average frequencies of $Foxp3^+$ cells among $CXCR3^+$ cells and $CCR4^+$ cells were 5.1% and 47%, respectively, in Ly-rich GCs [13]. To further characterize $Foxp3^+$ cells, we counted the Foxp3-labeling index among $CD4^+$ and $CD8^+$ cells by double staining in five representative Ly-rich GC cases (Fig. 1e, f). The Foxp3-labeling index among $CD4^+$ cells and $CD8^+$ cells were 98% and 2%, respectively. Therefore, we judged that $Foxp3^+$ cells in Ly-rich GC were mostly $CD4^+$ regulatory T cells (Tregs). This conclusion is consistent with a recent report [19].

Ly-rich GCs are characterized by a relative paucity in Tregs

We next counted the numbers of $CXCR3^+$ cells and $Foxp3^+$ cells in all GC cases. Note that we selected areas rich with TILs as described in "Materials and methods." As shown in Fig. 2a, the numbers of $CXCR3^+$ cells in Ly-rich GCs were approximately three-fold higher than those in conventional GCs, as expected from our previous study [13]. In contrast, the numbers of $Foxp3^+$ cells in Ly-rich GCs showed an approximately 1.5-fold increase (Fig. 2b). Accordingly, the CXCR3/Foxp3 ratio becomes higher in Ly-rich GCs than in conventional GCs (Fig. 2c).

We next analyzed the relationship between various parameters. When all GCs were included, the number of $CXCR3^+$ cells positively correlated with the CXCR3/Foxp3 ratio ($\gamma=0.55$, $p<0.0005$ [Pearson]; Fig. 2d) and also correlated with the number of $Foxp3^+$ cells ($\gamma=0.53$, $p<0.0005$ [Pearson], not shown). Discriminant analysis revealed that the three variables ($CXCR3^+$ cells, $Foxp3^+$ cells, and CXCR3/Foxp3 ratio) contributed to 92.6%

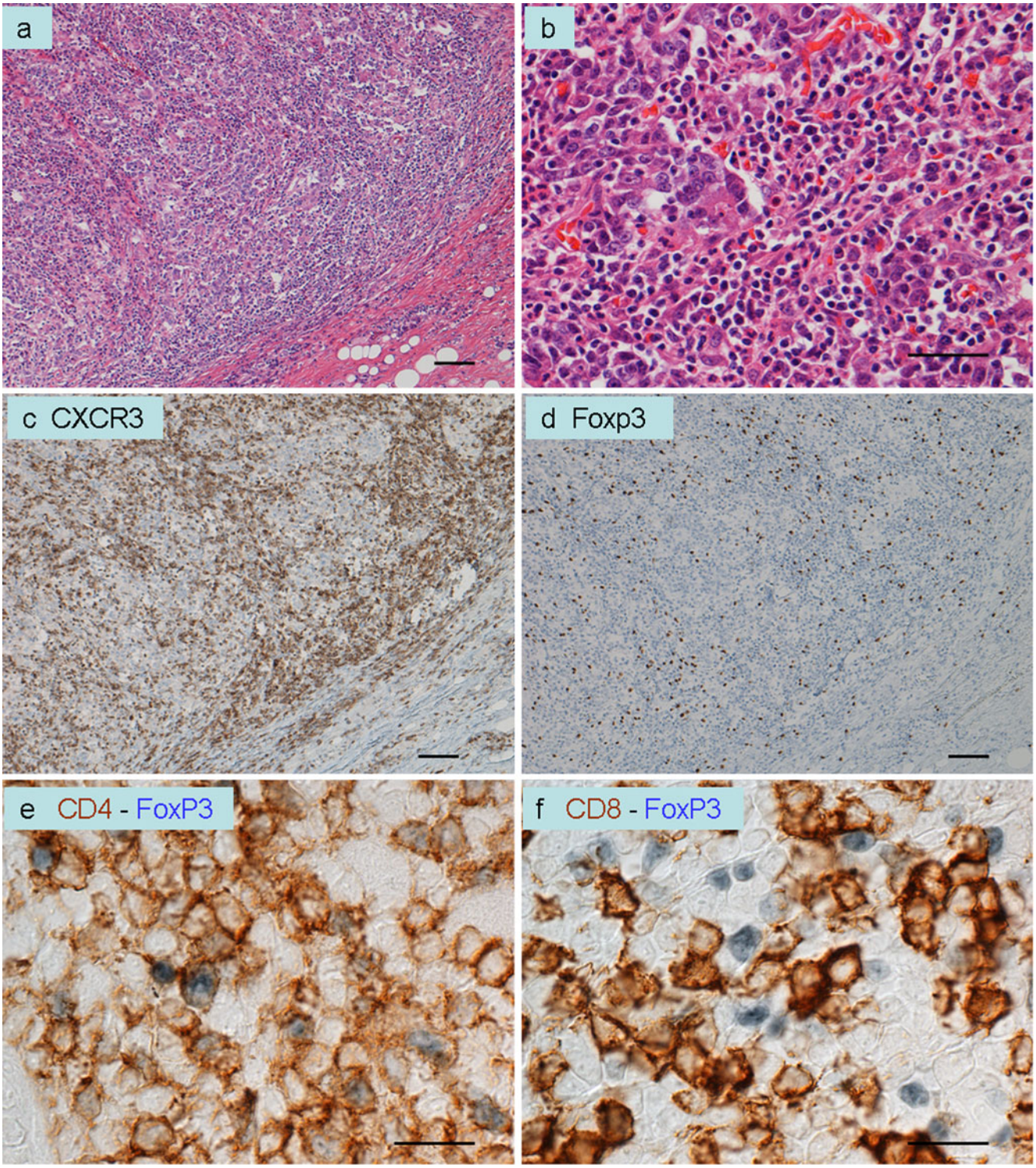

Fig. 1 **a, b** Hematoxylin and eosin staining of Ly-rich GC. The Ly-rich GCs are characterized by an abundance of TILs and a pushing margin. In typical LELCs, cancer cells show poorly differentiated morphology as in this case. **c, d** Immunohistochemistry for CXCR3 (**c**) and Foxp3 (**d**) (performed in all cases). Note the overall abundance of $CXCR3^+$ cells over $Foxp3^+$ cells. **e, f** Double immunohistochemistry for CD4 and Foxp3 (**e**) and CD8 and Foxp3 (**f**) clearly demonstrates that nearly all $Foxp3^+$ are $CD4^+$ (performed in five representative cases of Ly-rich GCs). Scale bars: 100 μm (**a**, **c**, **d**), 5 μm (**b**), and 20 μm (**e**, **f**)

Table 1 Stage distribution of cases

	I	II	III	IV	Total
A. Ly-rich vs. conventional GCs					
Ly-rich GCs (%)	21	17	5	1	44
	(47.7)	(38.6)	(11.4)	(2.3)	
Conventional GCs (%)	10	12	10	5	37
	(27.0)	(32.4)	(27.0)	(13.5)	
B. LELC (a subgroup of Ly-rich GC) vs. others					
LELC (%)	16	7	2	0	25
	(64)	(28)	(8)	(0)	
Others (%)	15	22	13	6	56
	(26.8)	(39.3)	(23.2)	(10.7)	

$p<0.0005$ (Fisher's exact test)

The distribution of stage is different from our previous paper [13] by adopting the 7th ed. of TNM classification [18]

discrimination between Ly-rich GCs and conventional GCs. The analyses here also indicated that although the numbers of $CXCR3^+$ and $Foxp3^+$ cells as a whole were in good correlation, the more $CXCR3^+$ T cells infiltrated the cancer tissue, the more $CXCR3^+$ T cells predominated over Tregs

Uneven distribution of TILs in conventional GCs

The results in the previous section also revealed that conventional GCs were characterized by a low $CXCR3^+$/Treg ratio. It should be remembered that the above morphometry was performed using areas with relatively abundant TILs. As we previously reported for colorectal cancer [20], TILs in conventional GCs also tended to be abundant along the invasive margin (cancer–host interface; Fig. 3a). The stroma inside the cancer, i.e., the cancer stroma excluding areas along the invasive margin, was usually sparse in TILs (Fig. 3b). We therefore next focused our attention on the distribution of Tregs and $CXCR3^+$ cells between these two areas. For this purpose, we selected 12 cases of conventional GCs, in which the invasive margin only contained a substantial number of TILs. The remaining 22 cases of

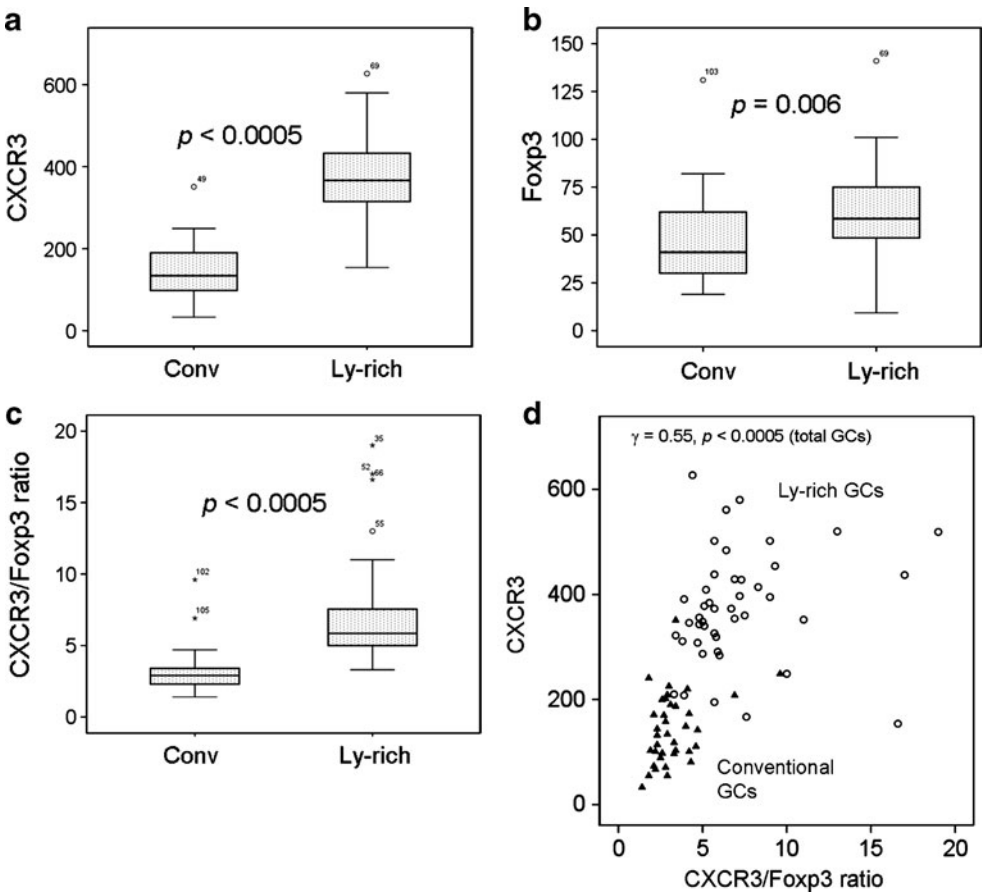

Fig. 2 **a–c** Box-whisker plots of the number of $CXCR3^+$ cells (**a**), the number of $Foxp3^+$ cells (**b**), and CXCR3/Foxp3 ratio (**c**) between Ly-rich- and conventional GCs (including all cases). All variables in (a–c) showed a statistically significant difference (Kruskal-Wallis test). **d** A scatter diagram showing the number of $CXCR3^+$ cells and the CXCR3/Treg ratio (*open circles*, Ly-rich GCs; *closed triangles*, conventional GCs; including all cases). The number of $CXCR3^+$ cells correlates with the CXCR3/FoxP3 ratio in total GCs. Also note that the Ly-rich and conventional GCs are well discriminated by these two parameters. *Vertical lines* in **a**, **b**, and **d** show the number of cells in one unit area (one lattice in a 400× field, 0.0625 mm^2)

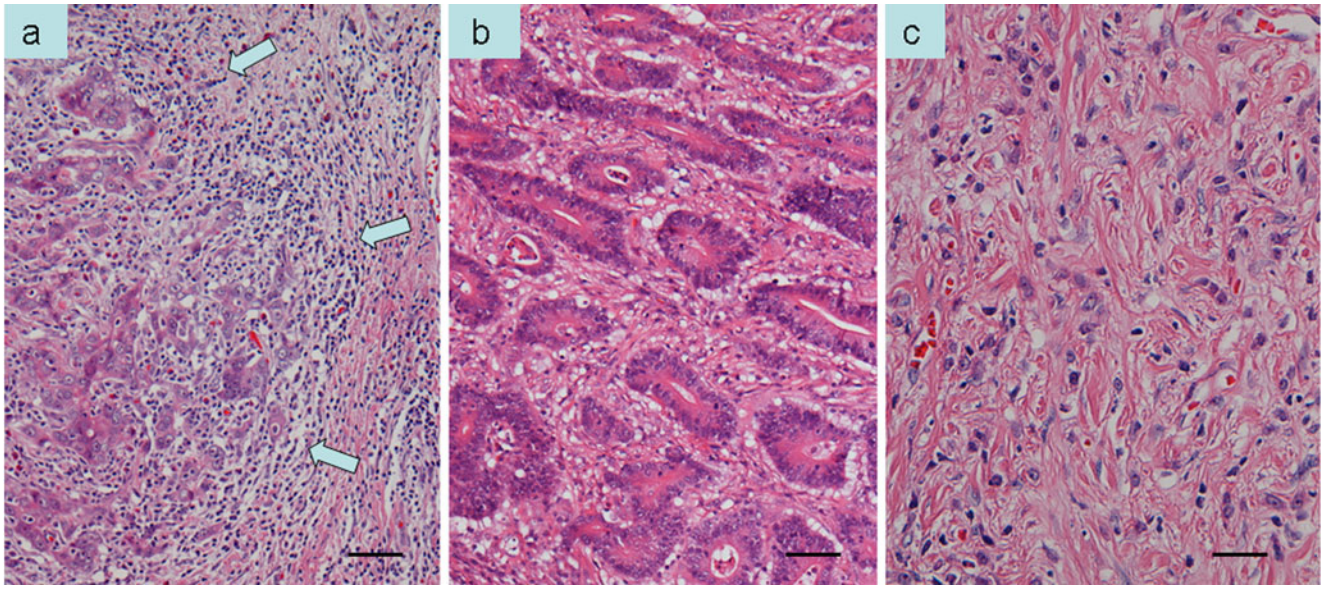

Fig. 3 **a, b** Representative hematoxylin and eosin staining of the invasive margin (**a**) and the stroma inside the cancer (**b**) in a conventional GC (tubular adenocarcinoma), showing that TILs are more abundant along the invasive margin. *Arrows* in **a** indicate the invasive margin. **c** Diffuse type GCs are usually poor in TILs. Scale bars: 50 μm (**a–c**)

conventional GCs showed either a mild increase of TILs along the invasive margin or overall scantiness of TILs. The histologic types of the selected cases were tubular and/or papillary adenocarcinoma or poorly differentiated adenocarcinoma of solid type ("por1" by Japanese classification). No scirrhous carcinomas (diffuse type by Lauren's classification [21]; "por2" or "sig" by Japanese classification [22]) were included in these 12 cases. Figure 3c shows a typical scirrhous carcinoma ("por2"), where TILs were only infrequently observed.

Stroma inside the cancer in conventional GCs is characterized by a paucity of TILs and a decrease of CXCR3/Treg ratio as compared with the invasive margin

The morphometrical analyses were done in the above-mentioned 12 cases of conventional GCs. As shown in Fig. 4, the stroma inside the cancer showed less $CXCR3^+$ cells and much lower CXCR3/Treg ratios than the invasive margin. Discriminant analysis revealed that the number of $CXCR3^+$ cells and the CXCR3/Foxp3 ratio contributed to 100% discrimination between the invasive margin and the stroma inside the cancer. The data here indicate that the stroma inside the cancer of conventional GCs is characterized by relative abundance of Tregs over effector $CXCR3^+$ cells.

Sporadic dendritic cells (DCs) express CCL22

Tregs are known to frequently express CCR4, and the chemokine CCL22 is reported to be involved in the Treg infiltration of ovarian tumors [23]. We therefore analyzed CCL22 expression in five representative cases of Ly-rich GCs and six cases of conventional GCs. As shown in Fig. 5a, CCL22 was only sparsely expressed by stromal cells in four of five Ly-rich GCs, while no such cells were detected in six conventional GCs. Cancer cells were totally negative for CCL22 in all these cases. Although the distribution density of $CCL22^+$ cells was less than that

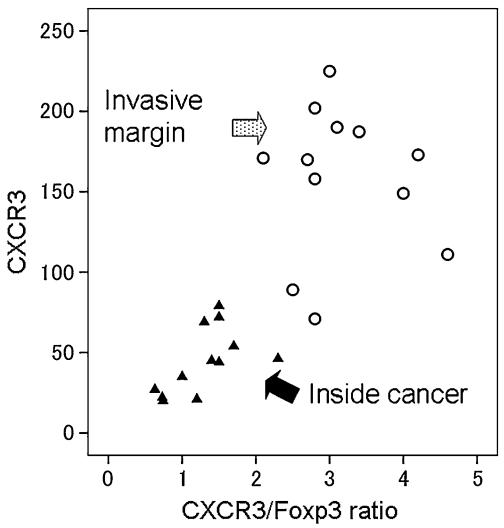

Fig. 4 Scatter diagram showing the number of CXCR3 and CXCR3/Treg ratio in 12 cases of conventional GCs. This shows that both the number of CXCR3 and the CXCR3/FoxP3 ratio were lower in the stroma inside the cancer than in the invasive margin. *Vertical line*: the number of $CXCR3^+$ cells in one unit area (one lattice in a 400× field, 0.0625 mm^2)

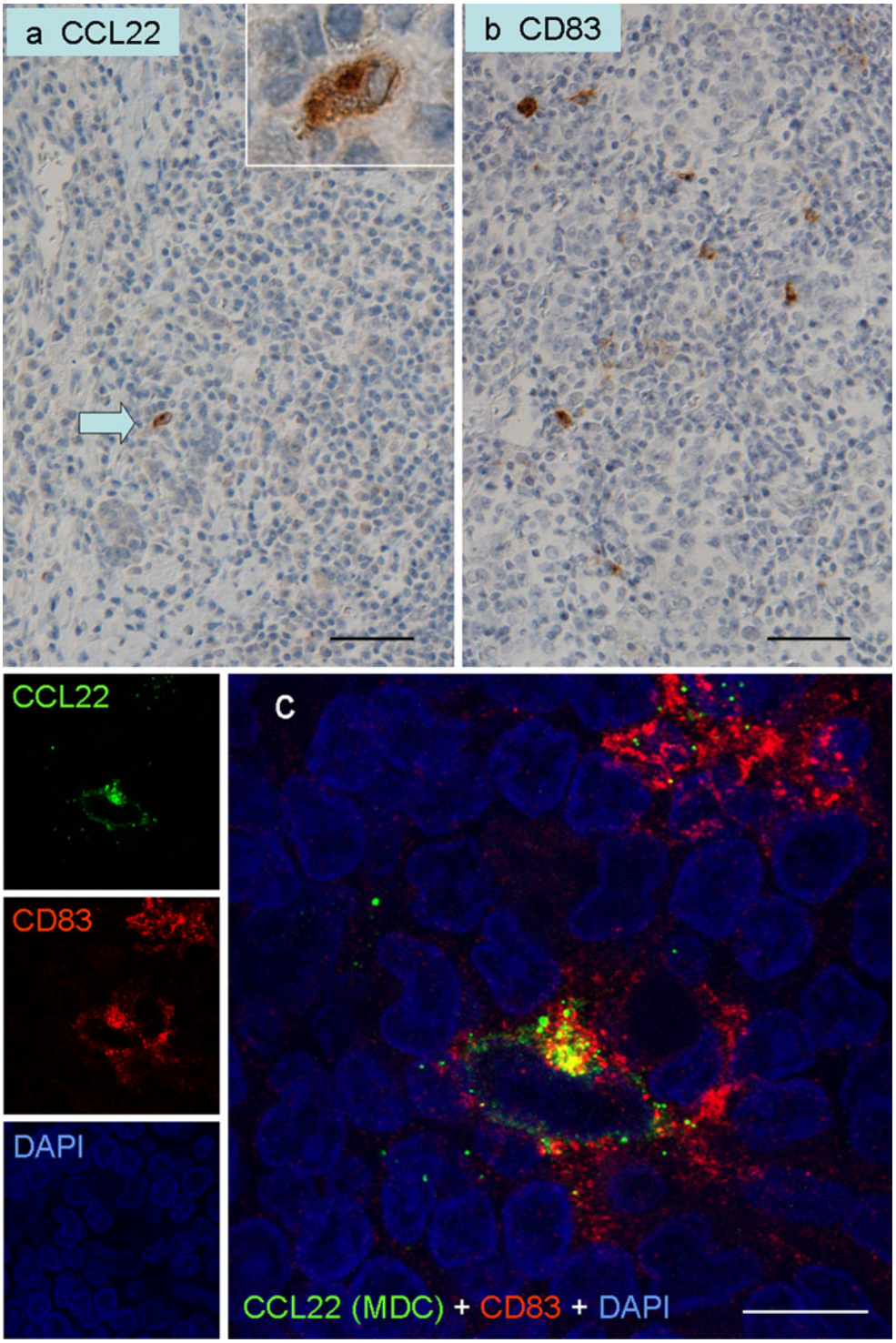

Fig. 5 **a, b** Immunohistochemistry for CCL22 (MDC) (**a**) and CD83 (**b**) in Ly-rich GCs (performed in five cases of Ly-rich GCs and six cases of conventional GCs). Note only a sporadic distribution of $CCL22^+$ cells in the stroma (*inset*, oil-immersion lens) as compared with mature DCs detected by CD83. **c** Confocal laser scanning microscopy revealed that $CCL22^+$ cells coexpress $CD83^+$, a mature DC marker (performed in two cases of Ly-rich GCs). Note the close cell-to-cell contacts of $CCL22^+$ DCs with cytoplasmic processes, labeled in *red*, with neighboring lymphocytes. Scale bars: 50 μm (**a**, **b**) and 10 μm (**c**)

of $CD83^+$ mature DCs in Ly-rich GCs (Fig. 5b), most $CCL22^+$ cells coexpressed CD83 and showed dendritic morphology together with close cell-to-cell contacts with neighboring lymphocytes, as confirmed in two representative Ly-rich GCs (Fig. 5c). The data here indicated that a small portion of mature DCs but not cancer cells expressed CCL22 in Ly-rich GCs.

Discussion

The present study has shown that the lymphoid stroma of Ly-rich GCs is characterized not only by a drastic increase in $CXCR3^+$ T cells but also by a relative paucity of Tregs, suggesting a microenvironment highly enriched with Th1 cells. In sharp contrast, conventional GCs are characterized

by a low number of CXCR3$^+$ T cells and a relative increase in Tregs, suggesting a highly immunosuppressive milieu. These results may raise an interesting issue in terms of tumor immunity and immune evasion in these two groups of GC.

Our previous report was mainly focused on Th1/Th2 responses in Ly-rich GCs and demonstrated a predominant infiltration of CXCR3$^+$ cells over CCR4$^+$ cells [13]. Tregs suppress the type 1 and type 2 immune responses and are regarded to be important for the control of immune responses [16, 17]. Tregs are also considered to participate in the immune evasion mechanism of cancer [23]. Therefore, the effector cell–Treg balance could be important for understanding the immune status of cancer tissues. In fact, a high CD8 to Treg ratio in cancer tissues was associated with a prolonged survival of patients with cancer of the ovary [4], liver [24], and kidney [25]. We therefore focused our attention on the balance between CXCR3$^+$ T cells and Tregs in Ly-rich and conventional GCs. By analyzing the CXCR3/Foxp3 ratio, our present study has shown that Ly-rich GCs are characterized by a relative paucity of Tregs in the abundance of CXCR3$^+$ TILs. This, in turn, underscores a relative abundance of Tregs along with a general paucity of TILs in conventional GCs. Therefore, Tregs may play a less major role in Ly-rich GCs than in conventional GCs as the mediator of immune evasion. The immune cell infiltrate in conventional GCs, if present, also tends to be more prominent along the invasive margin than in the stroma inside the cancer. The analysis of the 12 selected cases of conventional GCs clearly demonstrated that the stroma within the cancer is associated with even less CXCR3$^+$ T cells (i.e., less TILs) and more Tregs than the invasive margin. The results from conventional GCs are thus fully consistent with the current concept that tumor tissue is a strongly immunosuppressive microenvironment. We may regard the findings from conventional GCs as the basic feature of cancer tissue.

Concerning the function of Tregs in conventional GCs, Mizukami et al. [26] have reported that cases with diffuse distribution of Tregs are associated with a poorer prognosis than cases with peritumoral distribution of Tregs. However, Ly-rich GCs, usually associated with a better prognosis, generally show diffuse distribution of Tregs as shown in the present paper. Therefore, the balance between effector T cells and Tregs may also have a strong impact on the significance of TILs.

Tregs are known to frequently express CCR4, and Curiel et al. [23] have reported that cancer cells and tumor-associated macrophages produce CCL22 to attract CCR4$^+$ Tregs to ovarian cancer tissues. For GCs, Mizukami et al. [27] have reported that CD14$^+$ cells in the tumor stroma express CCL17 or CCL22. Our present data showed that CCL22 is only sporadically expressed by a part of CD83$^+$-mature DCs but not by cancer cells in Ly-rich GCs. The production of CCL22 by cancer cells may be dependent on the type of cancer. DC expression of CCL22 is consistent with a previous report [28]. As shown in "Results," the absolute number of Tregs is higher in Ly-rich GCs than in conventional GCs (Fig. 2b), with the number of Tregs being approximately 10% to 20% of CXCR3$^+$ T cells in Ly-rich GCs (Fig. 2d). Thus, the expression of CCL22 by a part of DCs could, at least partly, explain the increased recruitment of Tregs in Ly-rich GCs. We may need further analyses to clarify the mechanism(s) of Treg recruitment in Ly-rich GCs and conventional GCs.

Given that Tregs may not be a dominant immunosuppressive factor in Ly-rich GCs, we may need to analyze possible roles of other immunosuppressive factors such as immunosuppressive cytokines TGF-β and IL-10 in the immune evasion mechanism of Ly-rich GCs. In particular, Ly-rich GCs are frequently associated with EBV, which is known to induce IL-10 [29]. Another important issue to be addressed in the future is the possible involvement of IL-17-producing T helper (Th17) cells in Ly-rich GCs, which are known to play the major role in chronic inflammation and autoimmune pathogenesis, and selectively express CCR6 [30]. These analyses are now ongoing.

In conclusion, our present morphometrical analyses on the balance between CXCR3$^+$ T cells and Foxp3$^+$ Tregs have revealed that Ly-rich GCs are characterized by an absolute and relative abundance of CXCR3$^+$ effector T cells over Tregs in contrast to conventional GCs. On the other hand, conventional GCs, particularly in the stroma inside the cancer, are characterized by an absolute paucity of CXCR3$^+$ effector T cells and a relative abundance of Tregs. The data suggest that Tregs may play a more dominant role in conventional GCs than in Ly-rich GCs from the viewpoint of immunosuppression in cancer tissue. The present findings also highlight the unique immunologic aspect of Ly-rich GCs and the complexity of immune evasion mechanisms used by these types of cancer.

Acknowledgments We are grateful to Dr. Masaaki Miyazawa (Kinki University School of Medicine) for critical reading of the manuscript, Dr. Takashi Nakayama (Kinki University School of Medicine) for valuable discussion, Dr. Noriko Kimura (Hakodate National Hospital) and Dr. Hiroshi Naganuma (Sendai City Hospital) for supplying surgical materials, Ms. Fumiko Date (Tohoku University Graduate School of Medicine) for clerical assistance, and Ms. Megumi Maeda and Ms. Shoko Kajiwara (National Institute for Materials Science [NIM.S.]–Leica Bioimaging Laboratory) for technical assistance in confocal laser scanning microscopy. The present study was partly supported by the National Hospital Organization Collaborative Clinical Research Grant as well as the "Nanotechnology Network Project" and "HAITEKU" from the Ministry of Education, Culture, Sports, Science and Technology (MEXT), Japan.

Conflict of Interest The authors declare that they have no conflict of interest.

References

1. Yu P, Fu YX (2006) Tumor-infiltrating T lymphocytes: friends or foes? Lab Invest 86:231–245. doi:10.1038/labinvest.3700389
2. Naito Y, Saito K, Shiiba K et al (1998) $CD8^+$ T-cells infiltrated within cancer cell nests as a prognostic factor in human colorectal cancer. Cancer Res 58:3491–3494
3. Dave SS, Wright G, Tan B et al (2004) Prediction of survival in follicular lymphoma based on molecular features of tumor-infiltrating immune cells. N Engl J Med 351:2159–2169
4. Sato E, Olson SH, Ahn J et al (2005) Intraepithelial $CD8^+$ tumor-infiltrating lymphocytes and a high CD8+/regulatory T cell ratio are associated with favorable prognosis in ovarian cancer. Proc Natl Acad Sci USA 102:18538–18543. doi:10.1073/pnas.0509182102
5. Galon J, Costes A, Sanchez-Cabo F et al (2006) Type, density, and location of immune cells within human colorectal tumors predict clinical outcome. Science 313(5795):1960–1964. doi:10.1126/science.1129139
6. Sharma P, Shen Y, Wen S et al (2007) CD8 tumor-infiltrating lymphocytes are predictive of survival in muscle-invasive urothelial carcinoma. Proc Natl Acad Sci USA 104:3967–3972. doi:10.1073/pnas.0611618104
7. Watanabe H, Enjoji M, Imai T (1976) Gastric carcinoma with lymphoid stroma. Its morphologic characteristics and prognostic correlations. Cancer 38:232–243
8. Minamoto T, Mai M, Watanabe K et al (1990) Medullary carcinoma with lymphocytic infiltration of the stomach. Clinicopathologic study of 27 cases and immunohistochemical analysis of the subpopulations of infiltrating lymphocytes in the tumor. Cancer 66:945–952
9. Tokunaga M, Land CE, Uemura Y et al (1993) Epstein-Barr virus in gastric carcinoma. Am J Pathol 143:1250–1254
10. Fukayama M, Hino R, Uozaki H (2008) Epstein-Barr virus and gastric carcinoma: virus-host interactions leading to carcinoma. Cancer Sci 99(9):1726–1733. doi:10.1111/j.1349-7006.2008.00888
11. Yoshie O, Imai T, Nomiyama H (2001) Chemokines in immunity. Adv Immunol 78:57–110
12. Krieg C, Boyman O (2009) The role of chemokines in cancer immune surveillance by the adaptive immune system. Semin Cancer Biol 19:76–83. doi:10.1016/j.semcancer.2008.10.011
13. Ohtani H, Jin Z, Takegawa S et al (2009) Abundant expression of CXCL9 (MIG) by stromal cells that include dendritic cells and accumulation of CXCR3+ T cells in lymphocyte-rich gastric carcinoma. J Pathol 217:21–31. doi:10.1002/path.2448
14. Dunn GP, Old LJ, Schreiber RD (2004) The three Es of cancer immunoediting. Annu Rev Immunol 22:329–360. doi:10.1146/annurev.immunol.22.012703.104803
15. Finn OJ (2008) Cancer immunology. N Engl J Med 358 (25):2704–2715. doi:10.1056/NEJMra072739
16. Josefowicz SZ, Rudensky A (2009) Control of regulatory T cell lineage: commitment and maintenance. Immunity 30:616–625. doi:10.1016/j.immuni.2009.04.009
17. Shevach EM (2009) Mechanisms of FoxP3+ T regulatory cell-mediated suppression. Immunity 30:636–645. doi:10.1016/j.immuni.2009.04.010
18. Sobin LH, Gospodarowicz MK, Wittekind Ch (eds) (2009) TNM classification of malignant tumours, 7th edn. UK, Wiley-Blackwell, Oxford
19. Kryczek I, Liu R, Wang G (2009) FOXP3 defines regulatory T cells in human tumor and autoimmune disease. Cancer Res 69:3995–4000. doi:10.1158/0008-5472.CAN-08-3804
20. Musha H, Ohtani H, Mizoi T et al (2005) Selective infiltration of CCR5(+)CXCR3(+) T lymphocytes in human colorectal carcinoma. Int J Cancer 116:949–956
21. Lauren P (1965) The two histologic main types of gastric carcinoma: diffuse and so-called intestinal-type carcinoma. an attempt at a histo-clinical classification. Acta Pathol Microbiol Scand 64:31–49
22. Japanese Research Society for Gastric Cancer. Japanese classification of gastric carcinoma, 13th ed. Kanehara, 2001, Tokyo, Japan (in Jpn).
23. Curiel TJ, Coukos G, Zou L et al (2004) Specific recruitment of regulatory T cells in ovarian carcinoma fosters immune privilege and predicts reduced survival. Nat Med 10:942–949. doi:10.1038/nm1093
24. Gao Q, Qiu SJ, Fan J et al (2007) Intratumoral balance of regulatory and cytotoxic T cells is associated with prognosis of hepatocellular carcinoma after resection. J Clin Oncol 25:2586–2593. doi:10.1200/JCO.2006.09.4565
25. Jordanova ES, Gorter A, Ayachi O et al (2008) Human leukocyte antigen class I, MHC class I chain-related molecule A, and CD8+/regulatory T-cell ratio: which variable determines survival of cervical cancer patients? Clin Cancer Res 14:2028–2035. doi:10.1158/1078-0432.CCR-07-4554
26. Mizukami Y, Kono K, Kawaguchi Y et al (2008) Localisation pattern of $Foxp3^+$ regulatory T cells is associated with clinical behaviour in gastric cancer. Br J Cancer 98:148–153. doi:10.1038/sj.bjc.6604|49
27. Mizukami Y, Kono K, Kawaguchi Y et al (2008) CCL17 and CCL22 chemokines within tumor microenvironment are related to accumulation of $Foxp3^+$ regulatory T cells in gastric cancer. Int J Cancer 122:2286–2293. doi:10.1002/ijc.23392
28. Muthuswamy R, Urban J, Lee JJ et al (2008) Ability of mature dendritic cells to interact with regulatory T cells is imprinted during maturation. Cancer Res 68:5972–5978. doi:10.1158/0008-5472.CAN-07-6818
29. Wu MS, Huang SP, Chang YT (2002) Tumor necrosis factor-alpha and interleukin-10 promoter polymorphisms in Epstein-Barr virus-associated gastric carcinoma. J Infect Dis 185:106–109
30. Korn T, Bettelli E, Oukka M et al (2009) IL-17 and Th17 Cells. Annu Rev Immunol 27:485–517. doi:10.1146/annurev.immunol.021908.132710

Virchows Arch (2010) 456:625–633
DOI 10.1007/s00428-010-0916-6

ORIGINAL ARTICLE

Mixed-type gastric cancer and its association with high-frequency CpG island hypermethylation

Seog-Yun Park · Myeong Cherl Kook · Young Woo Kim · Nam-Yun Cho · Tae-You Kim · Gyeong Hoon Kang

Received: 4 January 2010 / Revised: 26 March 2010 / Accepted: 29 March 2010 / Published online: 27 April 2010
© Springer-Verlag 2010

Abstract Gastric carcinoma (GC) is one of the human cancers in which promoter CpG island hypermethylation is frequently found. We used the MethyLight assay to evaluate the methylation status of 16 CpG island loci that are hypermethylated in GC. We analyzed the relationship between CpG island hypermethylation of these 16 genes and the clinicopathological features in 191 advanced GCs. A significant difference was observed between the number of methylated genes in Epstein-Barr virus (EBV)-negative and microsatellite instability (MSI)-negative GCs of different histological types (Lauren classification; $P<0.01$). We found that mixed-type (MT) carcinomas, which have both diffuse-type (DT) and intestinal-type (IT) components, had more methylated genes (10.6) than either DT carcinomas (7.6 methylated genes) or IT carcinomas (6.7 methylated genes) ($P<0.001$). This trend was also observed when EBV-positive or MSI-positive GCs were excluded from the analysis (9.2, 6.9, and 4.8; $P<0.001$). When the IT and DT components were dissected from MT carcinomas and the methylation of these 16 genes was evaluated, both components had a number of methylated genes similar to MT carcinomas, (10.2 and 9.7, respectively), which was significantly higher than was found in IT and DT carcinomas ($P<0.05$). These findings indicate that MT carcinoma is distinct from IT and DT carcinomas in its enhanced CpG island hypermethylation status and implicate the enhanced promoter CpG island hypermethylation in the histogenesis of MT carcinoma.

Keywords CpG island · DNA methylation · Gastric cancer · Histologic type

Electronic supplementary material The online version of this article (doi:10.1007/s00428-010-0916-6) contains supplementary material, which is available to authorized users.

S.-Y. Park · M. C. Kook
Department of Pathology, National Cancer Center, Goyang, Gyeonggi-do, South Korea

Y. W. Kim
Department of General Surgery, National Cancer Center, Goyang, Gyeonggi-do, South Korea

N.-Y. Cho · G. H. Kang
Laboratory of Epigenetics, Cancer Research Institute, Seoul National University College of Medicine, Seoul, South Korea

T.-Y. Kim
Department of Internal Medicine, Seoul National University College of Medicine, Seoul, South Korea

G. H. Kang
Department of Pathology, 2nd Stage Brain Korea Project and Seoul National University College of Medicine, Seoul, South Korea

G. H. Kang (✉)
Department of Pathology, Seoul National University College of Medicine, 28 Yongon-dong, Chongno-gu, Seoul 110-744, South Korea
e-mail: ghkang@snu.ac.kr

Introduction

CpG islands are short DNA sequences rich in CpG dinucleotides and are found in approximately 70% of human gene promoters [1]. In normal cells, promoter CpG islands are traditionally thought to be protected from aberrant DNA hypermethylation, with the exceptions being islands on the X chromosome during inactivation or islands in genes subject to genomic imprinting. However, aberrant

hypermethylation of promoter CpG islands is frequently found in human cancer cells regardless of tissue type and is closely associated with gene expression silencing. Particularly, those genes that are expressed at low levels or not expressed in normal epithelial cells or are marked with H3K27 trimethylation in the nucleosomes are vulnerable to aberrant CpG island hypermethylation occurring in association with cancerization [2, 3]. Promoter CpG island hypermethylation is an important mechanism in human cancer tumorigenesis and can act as an alternative to genetic mutations for the inactivation of tumor suppressor or tumor-related genes. Cancer cells usually harbor both genetic changes and epigenetic changes. Recently published data indicate that epigenetic changes occur more frequently than genetic changes in human colorectal cancer (CRC) [4, 5]. Furthermore, promoter CpG island hypermethylation shows discrete cell type-specific and gene-specific patterns [6].

Gastric carcinoma (GC) is the fourth most common cancer and the second-leading cause of cancer-related death worldwide [7–9]. Histologically, GC can be classified into two major types, namely the intestinal type (IT) and diffuse type (DT) according to Lauren classification[10]; IT carcinoma consists of well-formed tubules, whereas DT carcinoma is made up of dispersed cells, minute cellular aggregates, or microglands. DT carcinoma is more aggressive than IT carcinoma, and the overall mortality rate of GC is increasing despite the decline of IT carcinoma [8, 11]. IT carcinomas are associated with intestinal metaplasia and are often preceded by sequential steps of precancerous changes, including atrophic gastritis, intestinal metaplasia, and dysplasia. DT carcinomas arise de novo and originate from gastric mucosa proper. The pathogenesis and molecular alterations leading to these two types of GC are generally considered to differ [12–14]. Several studies indicate that CpG island hypermethylation occurs more frequently in DT carcinoma than in IT carcinoma, implicating epigenetic changes in the genesis or progression of DT carcinomas [15]. In some cases, GC includes a mixture of IT and DT components; such tumors are classified as mixed type (MT) [16]. In contrast to IT and DT carcinomas, little is known about the pathogenesis and molecular alterations of MT carcinoma, particularly regarding promoter CpG island hypermethylation of tumor suppressor or tumor-related genes.

In a previous study [15], we screened 170 CpG island loci for their methylation status in paired GC and non-neoplastic gastric mucosa samples and selected 27 CpG island loci displaying a significantly higher frequency or level of methylation in GC than in non-neoplastic gastric mucosa. These 27 CpG island loci were further analyzed in another set of 25 paired GC and non-neoplastic gastric mucosal samples; of these loci, 22 were methylated in GC at levels significantly higher than those in the respective non-neoplastic gastric mucosal samples. When the methylation levels of 25 CpG island loci (including the 22 cancer-specific loci) were compared in chronic gastritis and GC, 16 CpG island loci showed higher methylation levels in GC than in non-neoplastic gastric mucosa regardless of the presence of *Helicobacter pylori* infection, indicative of cancer-related hypermethylation [17, 18]. The 16 genes include *BCL2*, *BDNF*, *CACNA1G*, *CALCA*, *CHFR*, *CYP1B1*, *DLEC1*, *GRIN2B*, *RUNX3*, *SEZ6L*, *SFRP4*, *TERT*, *THBS1*, *TIMP3*, *TP73*, and *TWIST1*. In the present study, we analyzed three histologic types (IT, DT, and MT) of GCs (n=191) for their methylation status in the 16 cancer-specific CpG island loci using a real-time PCR-based methylation-specific assay (MethyLight assay). We aimed to determine whether differences exist in the methylation frequencies of individual CpG island loci and in the overall methylation frequencies among the three histologic types. In addition, we aimed to characterize the clinicopathological features associated with enhanced CpG island hypermethylation.

Materials and methods

The study was approved by the Institutional Review Board of the National Cancer Center, Ilsan, Gyeonggi-do, Korea. A series of archived samples of advanced GCs (T2-T4) operated on at the National Cancer Center, Ilsan, Korea from February 2002 to January 2003 were taken from the files of the Department of Pathology. Cases that had neo-adjuvant therapy, other primary malignancy, or death of other causes were excluded. Hepatoid adenocarcinoma, small cell neuroendocrine carcinoma, and basaloid squamous cell carcinoma were also excluded from the study. Formalin-fixed, paraffin-embedded archival tissues from 191 GC patients were retrieved from the files of the Department of Pathology. The age of cancer patients ranged from 22 to 79 years (mean, 56.9 years; median, 59 years), and the male-to-female ratio was 2.03:1. Through gross and microscopic examination, tumor cases were evaluated for their pathological parameters: gross type (Borrmann's classification), tumor differentiation, histological type (Lauren classification), and TNM stage (American Joint Committee on Cancer) [19]. Tumor differentiation was categorized as high (≥50% glandular area) or low (<50% glandular area). Tumors were classified as MT when they showed both IT and DT components in excess of 40%. After identifying tumor areas by light microscopy, areas of approximately 1 cm^2 where tumor cells were most dense and represented the most prevalent histological type of the individual case were marked and scraped from the tissue slide with a knife blade. Non-tumorous portions in matched GC were obtained from normal gastric mucosa and were confirmed to be tumor-free by microscopy.

DNA methylation analysis

Sodium bisulfite conversion of genomic DNA was performed as described [15]. Sixteen CpG island loci were analyzed by the MethyLight assay using primers and probes targeting promoter sequences or the first exon. The oligonucleotide sequences of the primers and probes have been described [20]. Briefly, two sets of primers and probes designed specifically to bind to bisulfite-converted DNA were used in the reaction; one set of primers and a probe was designed for every methylated target to be analyzed (methylated reaction), and one set of primers and a probe was directed to the reference locus, *ALU* (normalization control reaction). The normalization control reaction refers to the methylation-independent measurement to normalize for input DNA and control for DNA amplification. We used *M.Sss*I-treated, placental genomic DNA as a constant reference sample to determine the percentage of methylated reference (PMR) at a particular locus. PMR was defined as $100\times(\text{methylated reaction/control reaction})_{\text{sample}}/(\text{methylated reaction/control reaction})_{\text{M.SssI-Reference}}$. A CpG island locus was considered methylated if the PMR value was >4. Previous studies have validated the PMR cutoff value of 4 based on the distributions of PMR values in the tested CpG island loci and the correlation of protein expression loss with methylation for *CDKN2A*, *MLH1*, and *MGMT*, where a PMR cutoff of 4 was used [21].

Microsatellite instability

The microsatellite instability (MSI) status of each tumor and normal mucosa sample was determined on the basis of an examination of five microsatellite markers (BAT25, BAT26, D2S123, D3S546, and D17S250) by a previously described method [15]. We classified tumors with instability at two or more microsatellite loci as MSI+.

Epstein-Barr virus-encoded RNA in situ hybridization

Epstein-Barr virus (EBV)+GCs were determined by the presence of the EBV-encoded small RNA *EBER1* in GC epithelial cells upon light microscopic examination of the histologic slides prepared from in situ hybridization. *EBER1* in situ hybridization was performed as described [15].

Statistical analysis

Associations between clinicopathological parameters and DNA methylation markers were analyzed using Pearson's chi-square test. To compare means between groups, analysis of variance (ANOVA) or Student's *t* test was used. Survival was measured from the date of resection of GC to the date of death or the last clinical follow-up time before 31 January 2008. The average follow-up time (from surgery to death or the last follow-up) was 46 months (range, 1–72 months). Overall survival rates were assessed using the Kaplan–Meier log-rank test, and Cox regression analysis was used to examine multivariate relationships between several clinicopathological variables and DNA methylation markers. P values of <0.05 were considered to reflect statistically significant differences.

Results

Methylation frequencies of individual loci and concordance of methylation in individual loci

We performed methylation analysis of 16 CpG island loci in 191 GC samples using MethyLight technology and calculated PMR values for each sample and MethyLight reaction. A PMR cutoff value of 4 was used to define a methylation-positive vs. methylation-negative locus, and DNA methylation frequencies (PMR>4) were calculated for each CpG island locus (Suppl. Fig. 1). The methylation frequencies of 16 CpG island loci ranged from 89% to 15%, and six (38%) of 16 CpG island loci showed methylation frequencies of ≥50%. The number of methylated genes in an individual cancer sample varied from 0 to 16, and the distribution of the number of methylated genes per sample showed a continuous pattern (Fig. 1a), which was consistently shown despite the application of variable PMR cutoff values (4, 10, or 20) to define methylation-positive status (data not shown). This continuous distribution was in accordance with previous studies in GCs [22, 23]. To examine whether DNA hypermethylation at a specific CpG island locus was coordinated with that of other loci, we determined the number of methylated loci in 15 loci (excluding the locus that was being evaluated) and evaluated whether that number changed significantly depending on the methylation status of the locus in question. All of the 16 loci showed strong associations of hypermethylation of an individual locus with hypermethylation of the other loci (Suppl. Fig. 2), indicating that DNA hypermethylation was coordinated at these 16 CpG island loci.

The relationship between CpG island hypermethylation and the clinicopathological features of GC

Because EBV infection and MSI are mutually exclusive, GCs can be grouped as EBV-/MSI-, EBV+, or MSI+. EBV+ GC and MSI+ GC show frequent hypermethylation of multiple CpG island loci [24–26]. Consistently, our study showed a higher number of methylated genes in EBV+ GC (n=16) and MSI+ GC (n=28) than in EBV-/MSI- GCs (n=

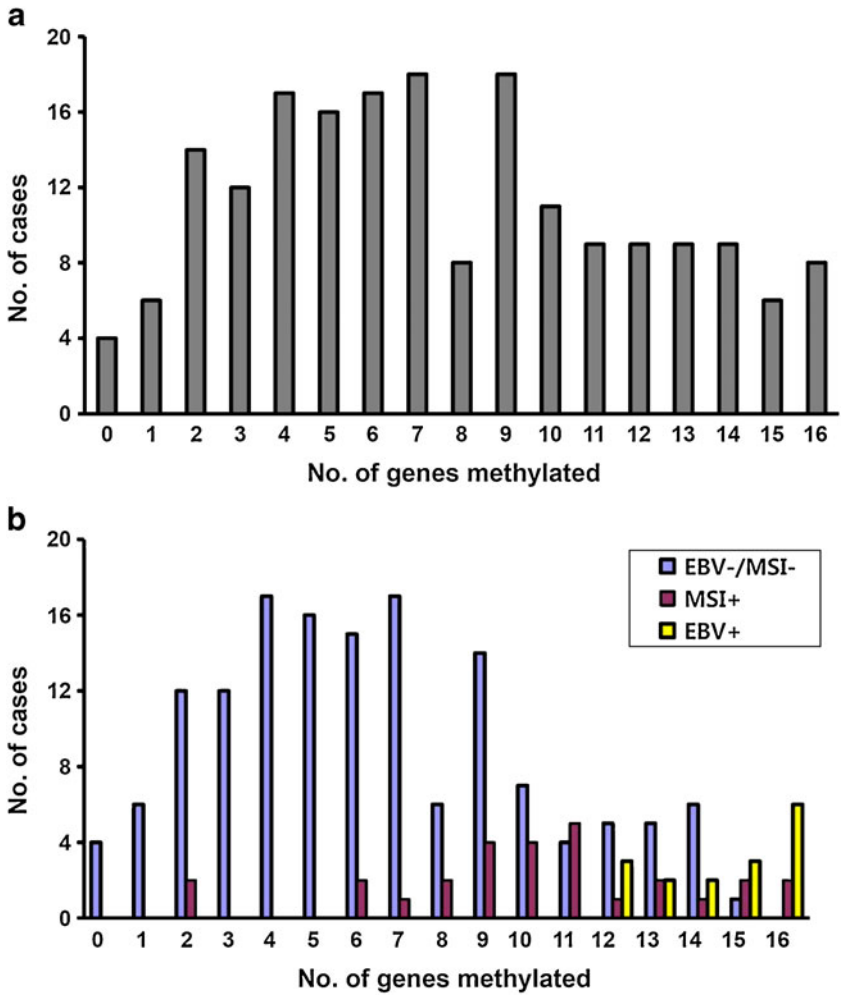

Fig. 1 Distribution of the number of methylated genes in individual gastric cancer cases (**a**). The distribution of EBV-positive (EBV+) gastric cancers was shifted to the right (**b**). *MSI+* microsatellite instability-positive, *EBV-/MSI-* EBV-negative/MSI-negative

147; 14.4, 10.1, and 6.4, $P<0.001$, ANOVA). Figure 1b presents the distribution of GC as a function of the number of methylated genes stratified by their EBV and MSI status.

A significant difference was noted in the number of methylated genes in GCs between low-grade ($n=41$) and high-grade (n=150) differentiation (5.8 vs. 8.1, $P=0.002$), while no difference was found in the number of methylated genes in GCs between male ($n=128$) and female ($n=93$) patients (7.3 vs. 8.2, $P=0.163$) and between low TNM stage (I and II, $n=73$) and high TNM stage (III and IV, $n=118$; 7.4 vs. 7.7, $P=0.574$). A marginally significant difference was also noted in the number of genes methylated between GCs of infiltrative gross types (Borrmann type III or IV, $n=152$) and GCs of fungating gross types (Borrmann type I or II, $n=39$; 7.3 vs. 8.7, $P=0.059$). However, no significant difference was noted in the number of methylated genes in GC between younger patients ($n=86$) and older patients ($n=105$; 7.7 vs. 7.5, $P=0.757$).

Because both MSI+ GC and EBV+ GC exhibit their own characteristic clinicopathological features, both tumor types might confound the analysis of the relationship between CpG island hypermethylation and clinicopathological features of GC. Thus, at this time, analysis was performed with exclusion of both MSI+ GC and EBV+ GC. A significant difference was noted in the number of methylated genes in GCs between male ($n=99$) and female ($n=48$) patients (5.8 vs. 7.5, $P=0.007$), between low TNM stage (I and II, $n=53$) and high TNM stage (III and IV, $n=94$; 5.5 vs. 6.9, $P=0.029$), and between low-grade ($n=35$) and high-grade ($n=112$) differentiation (4.4 vs. 7.0, $P<0.001$; Fig. 2). Because DT carcinoma is more frequent in male patients than in female patients, the comparison of the number of methylated genes was performed with restriction to DT carcinomas; the number of methylated genes did not differ between male ($n=48$) and female ($n=39$) patients (7.0 vs. 8.2, $P=0.157$). A significant difference was also noted in the number of genes methylated between GCs of infiltrative gross types (Borrmann type III or IV) and GCs of fungating gross types (Borrmann type I or II; 6.6 vs. 4.6, $P=0.021$). However, no significant difference was noted in the number of methylated genes in GC between younger patients ($n=70$) and older patients ($n=77$; 6.4 vs. 6.3, $P=0.901$).

When an individual CpG island locus was analyzed for the association of its hypermethylation with patient survival (with

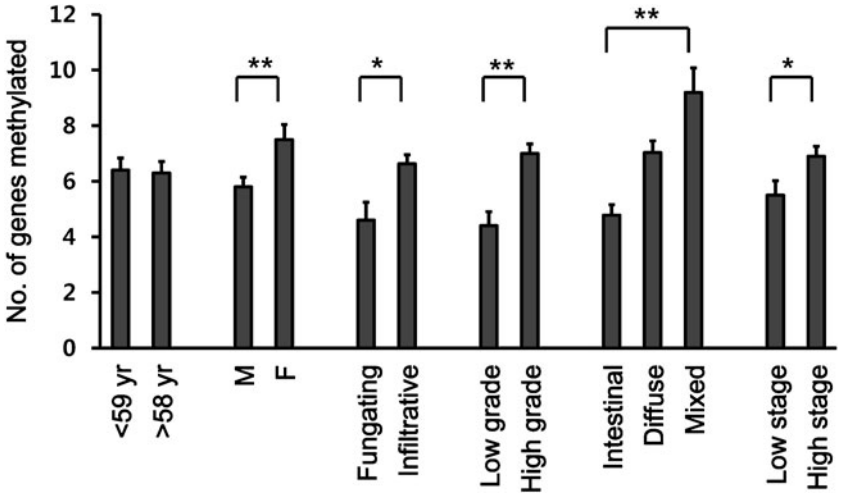

Fig. 2 Comparison of the number of methylated genes in gastric cancers according to patient age and gender as well as gross type, differentiation, Lauren's histological type and cancer stage (American Joint Committee on Cancer). *Double asterisks* and *asterisk* indicate strong statistical significance (p value <0.01) and weak significance (0.01<p value<0.05), respectively. *Error bars* indicate SEM

exclusion of EBV-positive or MSI-positive GCs), *CHFR* and *BCL2* showed significant associations between hypermethylation and decreased survival rate (P=0.0047 and P=0.0409, respectively, log-rank test; Fig. 3). However, when TNM stage and histological grade, plus *CHFR* hypermethylation and *BCL2* hypermethylation were entered into multivariate analysis to identify independent predictors of overall survival, multivariate analysis using the Cox proportional hazards model revealed that *CHFR* hypermethylation or *BCL2* hypermethylation was not an independent prognostic factor.

Lauren's histological type and CpG island hypermethylation

Clinicopathological characteristics of the three histological types are summarized in Table 1. Methylation frequencies of the individual genes were compared among different histological types of GCs, with the exclusion of EBV+ or MSI+ GCs. Eleven genes (*BDNF*, *SFRP4*, *TERT*, *TWIST1*, *RUNX3*, *CYP1B1*, *CACNA1G*, *SEZ6L*, *CHFR*, *THBS1*, and *BCL2*) were more frequently methylated in MT carcinomas than in IT or DT carcinomas (Table 2). When the number of methylated genes was compared among Lauren's histological types, MT carcinomas (n=16) were found to have more methylated genes (9.2) than DT carcinomas (n=72; 6.9 methylated genes), which had more than IT carcinomas (n=59; 4.8 methylated genes; P<0.001; Fig. 2). When we compared methylation frequencies of 16 genes in 191 GCs, including EBV+ GCs and MSI+ GCs, MT carcinomas still showed a significantly higher number of methylated genes (10.6) than DT or IT carcinomas (7.6 and 6.7, respectively; P<0.001). To determine whether the DT and IT components of MT carcinomas differed in the number of methylated genes, we microdissected 13 MT carcinomas and analyzed the individual components for their methylation status of the 16 genes. We found no difference in this regard (10.2 for IT vs. 9.7 for DT; P=0.721; Fig. 4). However, the number of methylated genes in the IT component or the DT component of MT carcinomas was significantly higher than that of either IT or DT carcinomas

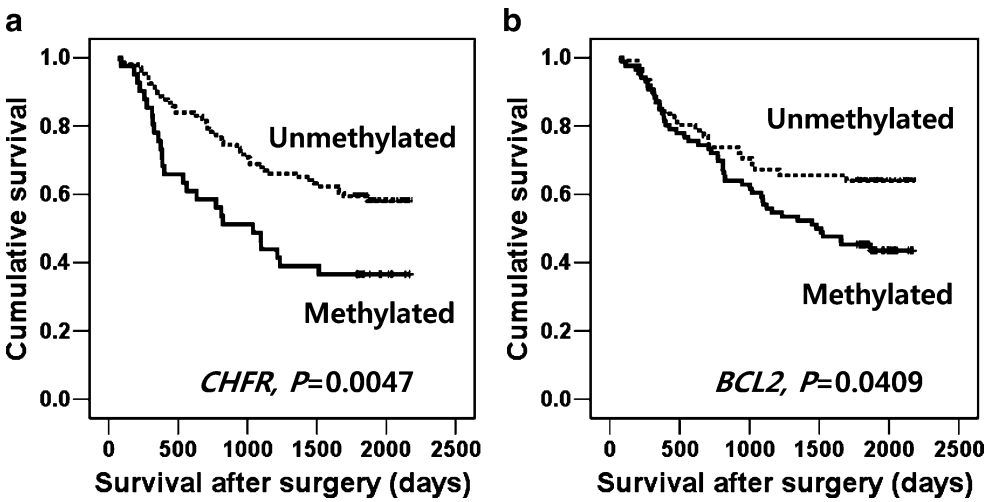

Fig. 3 Kaplan–Meier survival analysis with log-rank test. Survival analysis was performed in EBV-negative/ microsatellite instability-negative gastric cancers (n=147), and three patients were not included due to loss of follow-up. *CHFR* hypermethylation (**a**) and *BCL2* hypermethylation (**b**) were closely associated with poor survival of gastric cancer patients

Table 1 Comparison of clinicopathological features in the three histological types

		Intestinal type	Diffuse type	Mixed type	*P* value
No. of cases		79	87	25	–
Age in years (range)		58.4 (30–79)	55.2 (22–74)	57.6 (36–70)	0.199
Sex	M	64 (81.0%)	48 (55.2%)	16 (64%)	0.002
	F	15 (19.0%)	39 (44.8%)	9 (36%)	
Gross type	B1, B2	21 (26.6%)	10 (11.5%)	8 (32.0%)	0.017
	B3, B4	58 (73.4%)	77 (88.5%)	17 (68.0%)	
TNM stage	I, II	32 (40.5%)	34 (39.1%)	7 (28.0%)	0.520
	III, IV	47 (59.5%)	53 (60.9%)	18 (72.0%)	
EBV	+	8 (10.8%)	4 (4.9%)	3 (14.3%)	0.246
	–	66 (89.2%)	78 (95.1%)	18 (85.7%)	
MSI	+	12 (15.2%)	11 (12.6%)	5 (20%)	0.647
	–	67 (84.8%)	76 (87.4%)	20 (20%)	
Survival	3 years	66.7%	58.1%	72.0%	0.589
	5 years	57.7%	51.2%	60.0%	

(4.8 and 6.9, respectively; $P<0.05$). The methylation profiles of the 16 genes in the IT and DT components of MT carcinomas were comparable (Fig. 5).

Discussion

The Lauren classification divides GCs into two major histologic types: IT and DT. About 85% of GCs can be categorized as the IT or DT histologic type based on the Lauren classification, and the remaining GCs usually are comprised of a mixture of IT and DT and are thus classified as MT. Little is known regarding the molecular alterations in MT carcinomas, except for mutation of the E-cadherin gene (*CDH1*) [27] and the β-catenin gene (*CTNNB*) [28]. The morphological differences between IT and DT carcinomas can be attributed, at least in part, to differences in *CDH1* expression. Somatic mutations (intragenic deletion or point mutation) in *CDH1* have been identified in up to 80% of sporadic DT carcinomas but not in sporadic IT carcinomas [29]. In MT carcinomas, mutations in and loss of expression of *CDH1* are seen exclusively in the DT component of the tumor, suggesting that *CDH1* loss might be the genetic basis for the emergence of DT clones from an IT carcinoma [27]. However, because *CDH1* mutation is not evident in all DT or MT carcinomas, hypermethylation of the *CDH1* promoter CpG island might act as an alternative to genetic mutations to inactivate *CDH1*.

Table 2 Comparison of methylation frequencies (percent) of 16 genes in the three histological types (excludes unclassified type GC, $n=5$)

	Intestinal-type GC ($n=59$)	Diffuse-type GC ($n=72$)	Mixed-type GC ($n=16$)	*P* value
BDNF	5.1	23.6	56.3	<0.001
SFRP4	62.7	88.9	93.8	<0.001
TERT	6.8	29.2	37.5	0.002
TWIST1	72.9	91.7	100	0.002
RUNX3	20.3	38.9	62.5	0.003
CYP1B1	16.9	27.8	56.3	0.006
CACNA1G	10.2	20.8	43.8	0.009
SEZ6L	42.4	62.5	75	0.018
CHFR	25.4	23.6	56.3	0.027
THBS1	18.6	31.9	50.0	0.033
BCL2	61.0	52.8	87.5	0.036
CALCA	54.2	51.4	68.8	0.451
GRIN2B	23.7	55.6	50	0.001
TIMP3	50.8	69.4	68.8	0.078
TP73	0	13.9	6.3	0.011
DLEC1	6.8	20.8	6.3	0.043

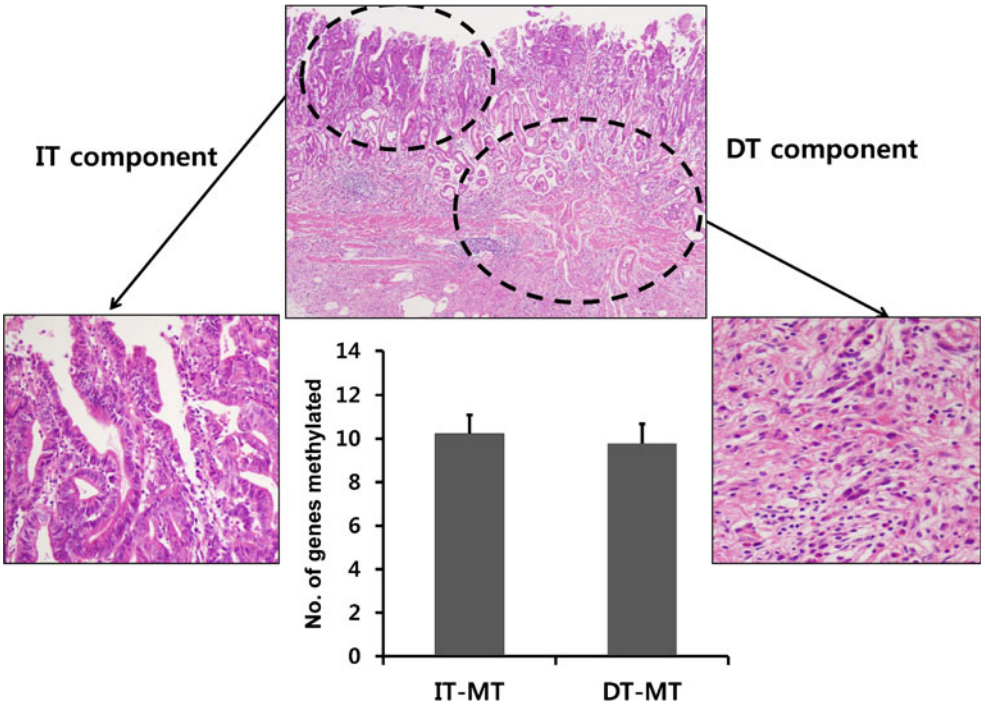

Fig. 4 Comparison of the number of methylated genes between the intestinal-type component (IT-MT) and the diffuse type component (DT-MT) of MT carcinomas. IT and DT components were dissected from MT carcinomas and analyzed for their methylation status in 16 genes. The mean number of methylated genes for each component type and the SEM (*error bar*) are shown in the graph

A study showed that *CDH1* mutation occurred only in the DT component of GC [27], suggesting that the DT component diverges from the IT component through loss of *CDH1* expression. Because DT carcinomas have higher frequencies of CpG island hypermethylation than IT carcinomas, the DT components of MT carcinomas were expected to have higher frequencies of CpG island hypermethylation than the IT components. However, our study presents two findings that contrast with this expectation. First, MT carcinomas contained a higher number of methylated genes than DT or IT carcinomas. Second, there was no difference in the number of methylated genes between the DT and IT components of MT carcinomas, which was greater than the number found in either IT or DT carcinomas. This finding indicates that, in MT carcinomas, tumor cells harbor a higher number of methylated genes regardless of whether the tumor cell arrangement is in the IT or DT form and suggests that enhanced CpG island hypermethylation, shared by both components, occurs before phenotypic divergence or in precursor cells common to both components, namely cancer stem cells. Although we do not dispute that MT carcinoma develops from IT carcinoma with the formation of DT carcinoma through *CDH1* mutation, our findings suggest that enhanced CpG island hypermethylation is also involved in the histogenesis of MT carcinoma.

A subset of GCs or CRCs exhibit hypermethylation in promoter CpG islands of multiple genes, which is referred to as the CpG island methylator phenotype (CIMP) [20, 30]. CIMP-positive CRCs have a distinct clinicopathological and molecular profile, such as associations with proximal tumor location, older age at onset, poor tumor differentiation, and high frequencies of *BRAF* mutation and microsatellite instability [20, 31, 32]. However, little is known regarding the clinicopathological features of CIMP-positive GCs, except for strong associations with EBV-positive GCs or MSI-positive GCs [22–26, 33]. One of the histological features of CIMP-positive CRCs is the presence of morphological heterogeneity as defined by the finding of two or more distinct subclones distinguished on the basis of grade of differentiation (for example, moderate and poor) or type of cancer (that is, adenocarcinoma and signet ring cell carcinoma) [22, 34, 35]. Like the close association of tumor heterogeneity with CIMP-positive CRCs, our study found a close association between enhanced hypermethylation at CpG island loci and MT carcinoma. This suggests that enhanced hypermethylation at multiple CpG island loci might be manifested as morphological heterogeneity in both GC and CRC tumors.

Both EBV+ GC and MSI+ GC constitute a major portion of CIMP+ GCs [24–26]. As revealed in our study, however, MSI+ GCs are heterogeneous in their tendency toward promoter CpG island hypermethylation, whereas EBV+ GCs are more homogeneous toward promoter CpG island hypermethylation. When we analyzed the three histological types in MSI+ GCs for differences in the number of methylated genes, MT (n=5) carcinomas showed a higher number of methylated genes (12.0) than IT (n=12; 10.5 methylated genes) and DT (n=11; 8.9 methylated genes) carcinomas, but the differences did not reach statistical

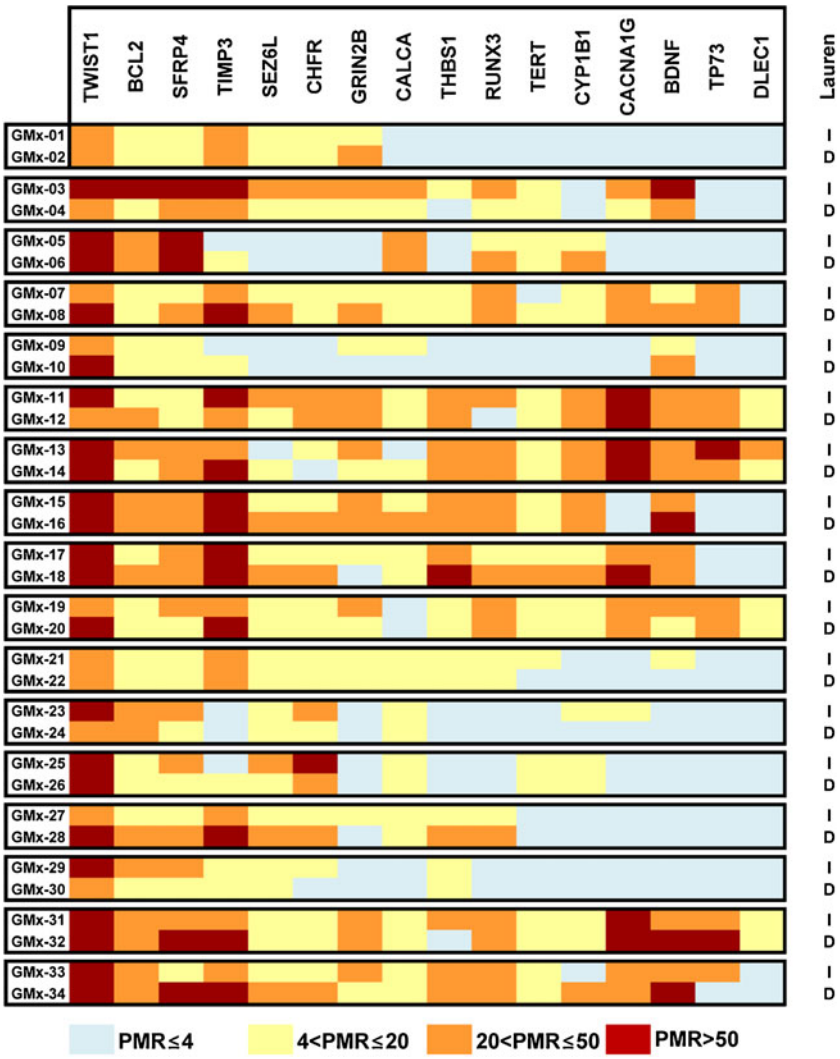

Fig. 5 Methylation map of the PMR values obtained for 16 CpG island loci in both intestinal and diffuse components of mixed-type gastric carcinoma samples (n=13) for which EBV-positive gastric carcinoma and microsatellite instability-positive gastric carcinoma were not included

significance (P=0.273), which might be attributed to the small number of cases. As such, a large-scale study is necessary to identify whether the presence of MT histology (that is, morphological heterogeneity) is a consistent feature of CIMP-induced MSI+ GCs.

In our previous studies [17, 18], we found that the number of methylated genes was not different between *H. pylori*-positive GCs and *H. pylori*-negative GCs, which is consistent with the results of Ushijima team's study [22]. In the present study, of the 191 cases, nine cases were negative for *H. pylori*, and the number of methylated genes was similar between *H. pylori*-negative and *H. pylori*-positive GCs (data not shown).

In conclusion, our study shows that of the three histological types in Lauren classification, MT carcinoma was the most highly methylated type and that both IT and DT components of MT carcinomas were similarly hypermethylated at CpG islands as compared with IT carcinomas and DT carcinomas. These findings suggest that enhanced hypermethylation is shared in cancer cells of MT carcinomas before their morphological divergence.

Acknowledgments This study was supported by a grant of the Korea Healthcare Technology R&D Project, Ministry for Health, Welfare & Family Affairs, Republic of Korea (A090126).

Disclosure The authors declare that they have no conflict of interest.

References

1. Saxonov S, Berg P, Brutlag DL (2006) A genome-wide analysis of CpG dinucleotides in the human genome distinguishes two distinct classes of promoters. Proc Natl Acad Sci USA 103:1412–1417
2. Schlesinger Y, Straussman R, Keshet I et al (2007) Polycomb-mediated methylation on Lys27 of histone H3 pre-marks genes for de novo methylation in cancer. Nat Genet 39:232–236
3. Ushijima T (2007) Epigenetic field for cancerization. J Biochem Mol Biol 40:142–150

4. Wood LD, Parsons DW, Jones S et al (2007) The genomic landscapes of human breast and colorectal cancers. Science 318:1108–1113
5. Schuebel KE, Chen W, Cope L et al (2007) Comparing the DNA hypermethylome with gene mutations in human colorectal cancer. PLoS Genet 3:1709–1723
6. Esteller M, Corn PG, Baylin SB, Herman JG (2001) A gene hypermethylation profile of human cancer. Cancer Res 61:3225–3229
7. Parkin DM, Bray F, Ferlay J, Pisani P (2005) Global cancer statistics, 2002 CA. Cancer J Clin 55:74–108
8. Crew KD, Neugut AI (2006) Epidemiology of gastric cancer. World J Gastroenterol 12:354–362
9. Leung WK, Wu MS, Kakugawa Y et al (2008) Screening for gastric cancer in Asia: current evidence and practice. Lancet Oncol 9:279–287
10. Lauren P (1965) The two histological main types of gastric carcinoma: diffuse and so-called intestinal-type carcinoma. An attempt at a histo-clinical classification. Acta Pathol Microbiol Scand 64:31–49
11. Henson DE, Dittus C, Younes M, Nguyen H, Albores-Saavedra J (2004) Differential trends in the intestinal and diffuse types of gastric carcinoma in the United States, 1973–2000: increase in the signet ring cell type. Arch Pathol Lab Med 128:765–770
12. Tahara E, Semba S, Tahara H (1996) Molecular biological observations in gastric cancer. Semin Oncol 23:307–315
13. Stadtlander CT, Waterbor JW (1999) Molecular epidemiology, pathogenesis and prevention of gastric cancer. Carcinogenesis 20:2195–2208
14. Chan AO, Luk JM, Hui WM, Lam SK (1999) Molecular biology of gastric carcinoma: from laboratory to bedside. J Gastroenterol Hepatol 14:1150–1160
15. Kang GH, Lee S, Cho NY et al (2008) DNA methylation profiles of gastric carcinoma characterized by quantitative DNA methylation analysis. Lab Invest 88:161–170
16. Zheng HC, Li XH, Hara T et al (2008) Mixed-type gastric carcinomas exhibit more aggressive features and indicate the histogenesis of carcinomas. Virchows Arch 452:525–534
17. Yoo EJ, Park SY, Cho NY et al (2008) *Helicobacter pylori*-infection-associated CpG island hypermethylation in the stomach and its possible association with polycomb repressive marks. Virchows Arch 452:515–524
18. Park SY, Yoo EJ, Cho NY, Kim N, Kang GH (2009) Comparison of CpG island hypermethylation and repetitive DNA hypomethylation in premalignant stages of gastric cancer, stratified for *Helicobacter pylori* infection. J Pathol 219:410–416
19. Greene FL (2002) The American Joint Committee on Cancer: updating the strategies in cancer staging. Bull Am Coll Surg 87:13–15
20. Weisenberger DJ, Siegmund KD, Campan M et al (2006) CpG island methylator phenotype underlies sporadic microsatellite instability and is tightly associated with BRAF mutation in colorectal cancer. Nat Genet 38:787–793
21. Ogino S, Kawasaki T, Brahmandam M et al (2006) Precision and performance characteristics of bisulfite conversion and real-time PCR (MethyLight) for quantitative DNA methylation analysis. J Mol Diagn 8:209–217
22. Enomoto S, Maekita T, Tsukamoto T et al (2007) Lack of association between CpG island methylator phenotype in human gastric cancers and methylation in their background non-cancerous gastric mucosae. Cancer Sci 98:1853–1861
23. Oue N, Mitani Y, Motoshita J et al (2006) Accumulation of DNA methylation is associated with tumor stage in gastric cancer. Cancer 106:1250–1259
24. An C, Choi IS, Yao JC et al (2005) Prognostic significance of CpG island methylator phenotype and microsatellite instability in gastric carcinoma. Clin Cancer Res 11:656–663
25. Chang MS, Uozaki H, Chong JM et al (2006) CpG island methylation status in gastric carcinoma with and without infection of Epstein-Barr virus. Clin Cancer Res 12:2995–3002
26. Kang GH, Lee S, Kim WH et al (2002) Epstein-barr virus-positive gastric carcinoma demonstrates frequent aberrant methylation of multiple genes and constitutes CpG island methylator phenotype-positive gastric carcinoma. Am J Pathol 160:787–794
27. Machado JC, Soares P, Carneiro F et al (1999) E-cadherin gene mutations provide a genetic basis for the phenotypic divergence of mixed gastric carcinomas. Lab Invest 79:459–465
28. Suriano G, Vrcelj N, Senz J et al (2005) Beta-catenin (CTNNB1) gene amplification: a new mechanism of protein overexpression in cancer. Genes Chromosomes Cancer 42:238–246
29. Grady WM, Willis J, Guilford PJ et al (2000) Methylation of the CDH1 promoter as the second genetic hit in hereditary diffuse gastric cancer. Nat Genet 26:16–17
30. Toyota M, Ahuja N, Ohe-Toyota M et al (1999) CpG island methylator phenotype in colorectal cancer. Proc Natl Acad Sci USA 96:8681–8686
31. Ogino S, Goel A (2008) Molecular classification and correlates in colorectal cancer. J Mol Diagn 10:13–27
32. Jass JR (2007) Classification of colorectal cancer based on correlation of clinical, morphological and molecular features. Histopathology 50:113–130
33. Kusano M, Toyota M, Suzuki H et al (2006) Genetic, epigenetic, and clinicopathologic features of gastric carcinomas with the CpG island methylator phenotype and an association with Epstein-Barr virus. Cancer 106:1467–1479
34. Young J, Simms LA, Biden KG et al (2001) Features of colorectal cancers with high-level microsatellite instability occurring in familial and sporadic settings: parallel pathways of tumorigenesis. Am J Pathol 159:2107–2116
35. Ogino S, Odze RD, Kawasaki T et al (2006) Correlation of pathologic features with CpG island methylator phenotype (CIMP) by quantitative DNA methylation analysis in colorectal carcinoma. Am J Surg Pathol 30:1175–1183

Virchows Arch (2010) 456:635–646
DOI 10.1007/s00428-010-0926-4

ORIGINAL ARTICLE

Immunohistochemically detectable dickkopf-3 expression in tumor vessels predicts survival in gastric cancer

Gilbert Mühlmann · Gerold Untergasser · Matthias Zitt · Marion Zitt · Hans Maier · Gregor Mikuz · Irmgard E. Kronberger · Michael C. Haffner · Eberhard Gunsilius · Dietmar Öfner

Received: 11 February 2010 / Revised: 7 April 2010 / Accepted: 16 April 2010 / Published online: 15 May 2010
© Springer-Verlag 2010

Abstract Dickkopf-3 (Dkk-3) may act as a tumor suppressor as it is downregulated in various types of cancer. Moreover, a putative role in tumor neovascularization is discussed. Here, we investigated the expression of Dkk-3 protein in gastric cancer and its potential value as a prognostic marker. Dkk-3 expression was analyzed by immunohistochemistry in 136 tumor samples and was correlated with microvessel density (MVD), tumor stage, and grading as well as the clinical outcome of the patients. Dkk-3 expression was detected in endothelial cells of the tumor vessels in 129/136 (94.9%) and in tumor cells in 85/136 (62.5%) samples. MVD was high and low in 57 (42.9%) and 76 (57.1%) specimens respectively. In tumor cells, overexpression of Dkk-3 was found in 41 (30.1%) of all cases and was correlated significantly to pT-stage ($p<0.05$) and UICC stage ($p<0.05$). Survival analysis regarding Dkk-3 expression in tumor endothelial cells showed that Dkk-3 is an independent predictor of disease-free survival ($p<0.05$). Dkk-3 expression in tumor vessels of patients with gastric cancer identifies a population of patients with relatively favorable prognosis.

Keywords Dickkopf-3 · Neoangiogenesis · Gastric cancer

G. Mühlmann · M. Zitt · I. E. Kronberger
Department of Visceral, Transplant and Thoracic Surgery,
Center of Operative Medicine, Innsbruck Medical University,
Innsbruck, Austria

G. Untergasser · E. Gunsilius
Laboratory of Tumor Biology and Angiogenesis,
Department of Internal Medicine V, Center of Internal Medicine,
Innsbruck Medical University,
Innsbruck, Austria

M. Zitt
Tyrolean Cancer Research Institute,
Innsbruck, Austria

H. Maier · G. Mikuz
Department of Pathology, Innsbruck Medical University,
Innsbruck, Austria

M. C. Haffner
Division of Medical Biochemistry, Biocenter,
Innsbruck Medical University,
Innsbruck, Austria

D. Öfner (✉)
Department of Surgery, Paracelsus Private Medical University,
Salzburger Landeskliniken, Müllner Hauptstrasse 48,
5020 Salzburg, Austria
e-mail: d.oefner@salk.at

Introduction

Despite a striking decrease in incidence especially in developed countries over the last decades, gastric cancer remains a leading cause of cancer-related death worldwide [1]. Only 50–60% of patients with newly diagnosed gastric cancer are suitable for radical surgery in curative intention, and even thereafter 5-year survival rates of 35–45% are modest [2–4].

Development of new blood vessels is an inalienable character of malignancies as mentioned by Folkman et al. [5]. During tumor development, an initial period in which the tumor is not angiogenic is followed by the switch to an angiogenic phenotype of single tumor cells [6, 7]. In a study on colorectal cancer tissue, St. Croix and co-workers were able to show enhanced expression of certain genes in tumor endothelium when compared with counterparts of normal colonic mucosa [8]. Therefore, these gene products are called tumor endothelial markers (TEMs). One of these TEMs is Dickkopf 3 (Dkk-3), a protein belonging to the

human Dickkopf (hDkk) family which again represents one of five families of extra-cellular Wnt antagonists. Wnt proteins, in turn, comprise a group of growth factors which are of particular importance in numerous processes with regard to tumor development and carcinogenesis. The hDkk family consists of Dkk-1, Dkk-2, Dkk-3, Dkk-4, and a unique Dkk-3-related protein called Soggy [9]. The five Dkk proteins share 37–50% protein identity. Human Dkk-1–4 are glycoproteins of 255–350 amino acids which possess an N-terminal signal peptide and contain two cysteine-rich domains separated by a linker region. Dkk-1, 2, and 4 have the same sphere of action by regulating Wnt signaling. Mostly their effect is inhibitory, except for Dkk-2, which was reported to show activation of Wnt signaling, too. Binding to the trans-membrane receptors Kremen 1 and 2 and lipoprotein-receptor-related protein 5/6 (LRP5/6), a co-receptor of the Wnt/Fz receptor was demonstrated as the underlying mechanism of action [10, 11].

The function of Dkk-3, which is the most divergent of the four human Dkks, is not well understood. Dkk-3 does not physically interact with LRP5/6 or Kremen and hence Dkk-3 does not seem to function in Wnt signaling. Therefore, Dkk-3 is suggested not to be involved in the beta-catenin destabilization process [12]. Nevertheless, in a variety of cancer types Dkk-3 is downregulated and its overexpression can inhibit cell proliferation [13–19]. Recently in colorectal cancer tissues, our working group was able to demonstrate distinctive Dkk-3 expression in CD31-positive microvessels of the tumor and adjacent tissue, but not in endothelial cells of normal mucosa. Therefore Dkk-3 was assumed as a putative proangiogenic protein in neovascularization [20]. Moreover, a clear association between upregulation of Dkk-3 expression in tumor blood vessels and capillary formation in vitro and in vivo with regard to micro-vessel density (MVD) was found [21].

At least to our knowledge Dkk-3 protein expression in tumor cells and the respective microvessels had not been investigated in gastric cancer specimens so far. We aimed to explore the expression and clinicopathological significance of Dkk-3 and its impact on neoangiogenesis in gastric adenocarcinomas and to elucidate the relationship between biological behavior and prognosis.

Materials and methods

Specimens construction

The study was conducted according to the regulations of the local ethics committee and Austrian law. Tumor tissues of 136 consecutive cases of adenocarcinomas of the stomach (86 men (63.7%) and 50 women (36.8%) at a mean age of 66.4 years (95% CI, 65.8–69.1)) were investigated in this study. All patients had been operated between 1993 and 2004 at the Department of Surgery, Innsbruck Medical University, Austria, with curative (n= 136) intent. Tumor tissues were routinely processed (formalin fixed and paraffin embedded) and were classified according to the guidelines of the Union Internationale Contre le Cancer (UICC) and were graded according to WHO classification [22, 23]. Adjuvant or additive chemotherapy was recommended to patients with UICC stages III and IV. Adjuvant chemoradiation as propagated by Macdonald et al. was not used routinely but carried out in selected patients [24]. Demographic data of all patients were recruited from our computerized surgical documentation system (ChiBASE). All data regarding date and cause of death were confirmed by the "Tumorregister Tirol", a cancer-register maintained by the Tyrolean government. Demographic data and tumor characteristics are summarized in Table 1.

Immunohistochemistry

Dkk-3 expression was determined by immunohistochemistry and carried out as described elsewhere [20]. Briefly, 5-μm sections were cut from recipient paraffin blocks, mounted on adhesive-coated glass slides (Instrumedics, MO, USA), deparaffinized and re-hydrated with xylene and graded alcohol series. Thereafter, antigens were retrieved by microwave treatment in citrate-buffer (10 mM, pH 6.0) and endogenous peroxidase activity was blocked with 3% H_2O_2/methanol. Sections were incubated for 45 min in blocking solution containing 10% bovine calf serum (Dako Cytomation, Copenhagen, Denmark) and then stained for 1 h with a primary polyclonal antiserum directed against human Dkk-3 (goat anti-human Dkk-3 polyclonal 1.5 μg/mL; R&D Systems Inc., Minneapolis, MN, USA). Primary antiserum was detected by incubation with a biotinylated secondary antibody (biotinylated horse anti-goat IgG, 1:150; Vector Laboratories Inc., Burlingame, CA, USA) with the Vectastain Elite ABC Kit (Vector Laboratories Inc., Burlingame, CA, USA) and the FAST DAB Tablet Set (Sigma, Vienna, Austria). Finally, slides were counterstained with Mayer's hemalaun solution (Merck, Darmstadt, Germany), clearing and mounting followed with Medite Pertex (Medite Medizintechnik, Burgdorf, Germany). Positive and negative controls were included in each run. Specificity of antiserum against human Dkk-3 was proven by blocking experiments with an excess of recombinant human Dkk-3. Simultaneously, a second section from each specimen was stained with CD31 to identify microvessels by immunostaining endothelial cells for CD31 antigen. For CD31 staining, slides were pressure cooked for 1 min in 10 mM citrate-buffer with pH 6.0.

Table 1 Patients (n=136) characteristics and clinicopathological features

		n/mean	%/min–max
Age (years)		66.4	27–94
Gender	Female	50	36.8
	Male	86	63.2
Operative procedure	Subtotal gastrectomy	47	34.6
	Total gastrectomy	71	52.2
	Resection of the gastric remnant	9	6.6
	Limited resection	9	6.6
Lymph node dissection	D0	0	0
	D1	31	22.8
	D2+D3	105	77.2
pT-category	pT1	21	15.4
	2	77	56.6
	3	33	24.3
	4	5	3.7
pN-category	pN0	58	42.6
	1	33	24.4
	2	35	25.7
	3	10	7.3
M-category	M0	124	91.2
	1	12	8.8
UICC stage	IA	19	14.0
	IB	30	22.0
	II	36	26.5
	IIIA + IIIB	29	21.3
	IV	22	16.2
R-Stage	R0	129	94.9
	R1	7	5.1
Tumor differentiation	G1–2	47	34.6
	G3–4	89	65.4
Lauren classification	Intestinal	78	57.3
	Diffuse	58	42.7
Chemotherapy	Neoadjuvant	8	5.9
	Adjuvant	14	10.3
Clinical course	Uneventful	91	67.6
	Poor[a]	45	32.4
	Loco-regional failure	8	5.9
	Distant metastases	36	26.5
	Loco-regional failure and distant metastases	1	0.7
	Death during follow-up	77	56.6
	Lost during follow-up	6	4.4

min–max lowest and highest value

[a] Poor development of loco-regional or distant relapse

Endogenous peroxidase activity was blocked with Peroxidase Block (Envision System kit, cat# K4006; Dako) for 5 min. Sections were then incubated for 60 min with anti-CD31 (clone 1A10; Novocastra–Vision BioSystems Inc., Norwell, MA, USA) diluted 1:40. Slides were then further treated with anti-mouse-labeled polymer HRP for 60 min followed by 8 min in diaminobenzidine solution (Envision System HRP, cat# K4006; Dako).

Assessment and quantification of neoangiogenesis

All CD31-positive stained microvessels from cancer tissue samples were manually counted by two independent investigators (I.K. and M.H.) at ×400 magnification in three areas within the tumor where the highest microvessel count (MVC) was assumed. Any single stained endothelial cell or cell cluster clearly separated from each other was

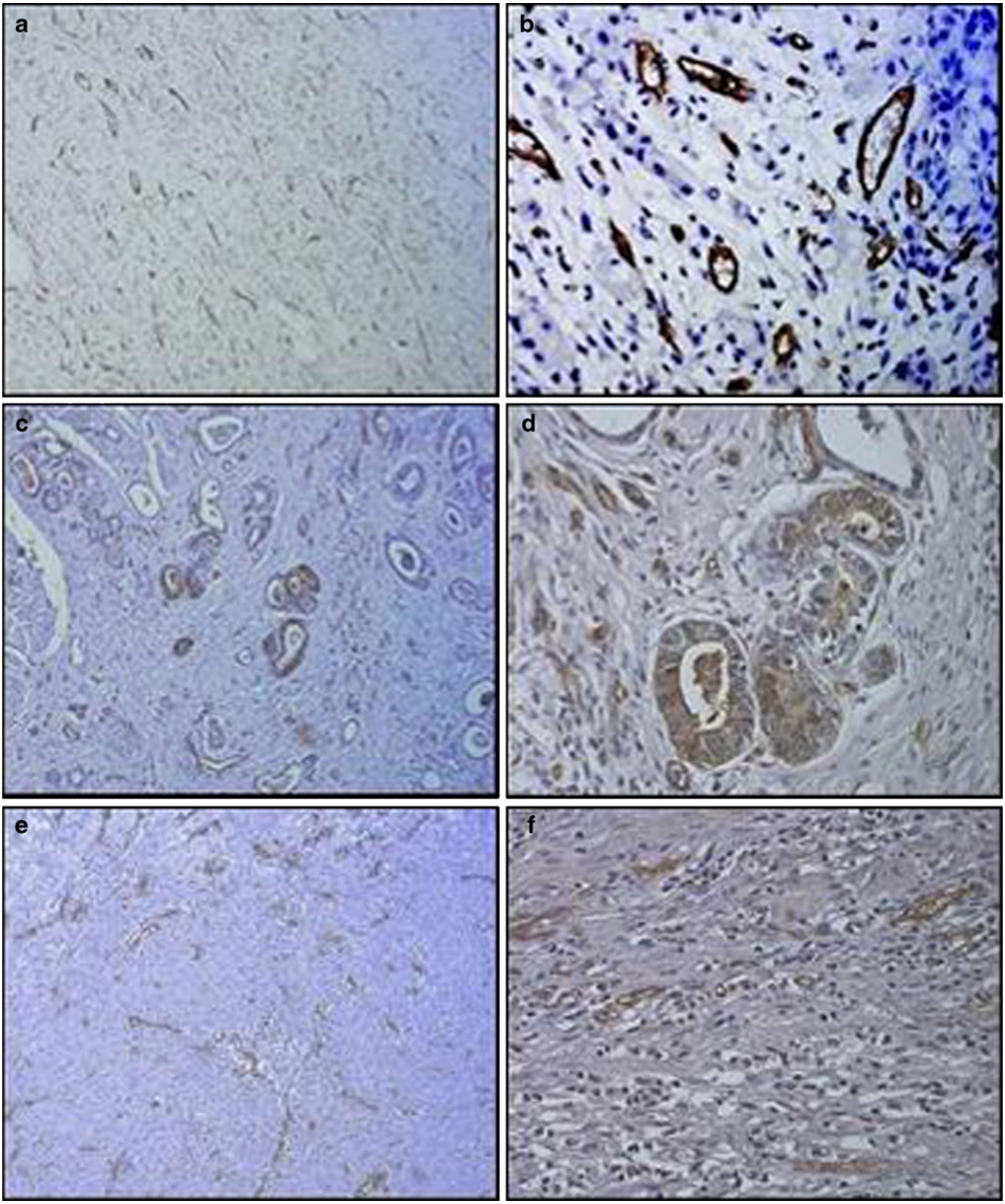

Fig. 1 Immunohistochemical staining for CD31 and Dkk-3 expression in human gastric cancer tissues. Note the homogenous membranous immunostaining of endothelial cells and tumor cells. CD31-positive microvessels in gastric cancer tissue. (**a**) Magnification, ×100; **(b)** magnification, ×400. Dkk-3-positive microvessels and Dkk-3-positive tumor cells in gastric cancer tissue. (**c**) Magnification, ×100; (**d**) magnification ×400. Dkk-3-positive microvessels in gastric cancer tissue. (**e**) Magnification, ×100; (**f**) magnification, ×400

Table 2 Distribution and intensity of Dkk-3 expression in endothelial and tumor cells in 136 gastric cancer specimens

	No.	Percent
Dkk-3 expression in endothelial cells		
Yes	129	94.9
No	7	5.1
Dkk-3 staining intensity in endothelial cells (n=129)		
Strong	27	20.9
Moderate	47	36.4
Weak	55	42.7
Dkk-3 expression in tumor cells		
Yes	85	62.5
No	51	37.5
Dkk-3 proportion score in tumor cells (n=85)		
<10%	16	18.8
10–50%	18	21.2
51–80%	20	23.5
>80%	31	36.5
Dkk-3 intensity score in tumor cells (n=85)		
Strong	14	16.5
Moderate	38	44.7
Weak	33	38.8
Dkk-3 total immunostaining score in tumor cells (n=136)		
Strong (score 9–12)	12	8.8
Moderate (score 6–8)	29	21.3
Weak or no expression (score 0–4)	95	69.9
Dkk-3 overexpression (>4 total immunostaining score) in tumor cells		
Yes	41	30.1
No	95	69.9

identified as an independent vessel. Microvessel density was calculated according to Weidner´s procedure and was defined as the mean of all MVCs [25]. Regarding MVD, three groups were performed, no microvessels, low and high MVD using the mean as a cut-off point, respectively.

Evaluation of Dkk-3 expression

Two independent investigators (H.M. and M.Z.) with no prior knowledge of the clinical data analyzed immunostained samples in parallel. Evaluation of Dkk-3 staining in endothelial cells of blood vessels was carried out using the intensity score based on a semi-quantitative Dkk-3 staining intensity estimates (0, no staining; 1, weak; 2, moderate; and 3, strong). Dkk-3 staining of the tumor cells was evaluated for each tissue sample by calculating a total immunostaining score as the product of a proportion and intensity score. The former describes the percentage of positive stained tumor cells (0, none; 1, <10%; 2, 10–50%; 3, 51–80%; 4, >80%). The total immunostaining score ranged from 0–12. Regarding the total score the tissue samples were bimodally distributed with the nadir at a total score of 3–4. Therefore, Dkk-3 "overexpression" was arbitrarily defined as a total score >4 as described previously [26].

Statistical analysis

Statistical analysis was performed using the Statistical Package of Social Science (SPSS, Version 16.0, Chicago, IL, USA). Descriptive statistics for continuous measures are given as the mean with the respective 95% confidence interval (CI) in parenthesis. For discrete data (e.g., Dkk-3 expression) frequency counts and percentages were tabulated. Results of the various estimates were compared using either the χ^2 test or one-way ANOVA. Survival curves were calculated using the Kaplan and Meier method and compared by the log-rank test. Follow-up time was censored if the patient was lost to follow-up. Patients who died without documented disease recurrence were considered censored for disease-free survival (DFS) but were included as deaths for overall survival analysis. Factors shown to be of prognostic significance in univariate models were evaluated in a

Table 3 Relationship between Dkk-3 expression in endothelial cells, tumor cells, MVD, and various clinicopathological parameters in 136 gastric cancer specimens

	All cases	Dkk-3 expression in endothelium (n=129; 94.9%)	P value	Dkk-3 overexpression in tumor cells (n=41; 30.1%)	P value
Gender					
Male	86	83 (64.3)	n.s.	25 (61.0)	n.s.
Female	50	46 (35.7)		16 (39.0)	
Lauren classification					
Intestinal	78	64 (49.6)	n.s.	28 (68.3)	n.s.
Diffuse	58	65 (50.4)		13 (31.7)	
Tumor differentiation					
Grade 1/2	47	45 (34.9)	n.s.	11 (26.8)	n.s.
Grade 3/4	89	84 (65.1)		30 (73.2)	
pT-category					
pT1	21	20 (15.5)	n.s.	1 (2.4)	0.004
pT2	77	73 (56.6)		27 (65.9)	
pT3	33	31 (24.0)		10 (24.4)	
pT4	5	5 (3.9)		3 (7.3)	
pN-category					
pN0	58	54 (41.9)	n.s.	16 (39.0)	n.s.
pN1	33	32 (24.8)		7 (17.1)	
pN2	35	33 (25.6)		11 (26.8)	
pN3	10	10 (7.8)		7 (17.1)	
M-category					
M0	124	118 (91.5)	n.s.	38 (92.7)	n.s.
M1	12	11 (8.5)		3 (7.3)	
UICC stage					
IA	19	18 (14.0)	n.s.	1 (2.4)	0.012
IB	30	28 (21.7)		10 (24.4)	
II	36	34 (26.4)		12 (29.3)	
IIIA + B	29	28 (21.7)		8 (19.5)	
IV	22	21 (16.3)		10 (24.4)	
MVD					
No	3	3 (2.3)	n.s.	1 (2.4)	n.s.
Low	76	73 (56.6)		23 (56.1)	
High	57	53 (41.1)		17 (41.5)	

multivariate Cox regression model using a stepwise backward elimination procedure. $p<0.05$ was considered statistically significant.

Results

Dkk-3 expression and MVD in gastric cancer tissue

Out of all cancer samples, Dkk-3 was immunohistochemically detected in endothelial cells of the tumor in 129 (94.9%) and in tumor cells in 85 (62.5%) specimens. Dkk-3 staining intensity in endothelial cells was found to be strong, moderate, or weak in 27 (20.9%), 47 (36.4%), and 55 (42.7%) cases, respectively. One hundred thirty-three (97.8%) out of all 136 cancer samples investigated showed CD31-positive microvessels (Fig. 1), whereas three (2.2%) did not. Regarding the first group of patients MVD was high and low distributed in 57 (42.9%) and 76 (57.1%) patients, respectively. In tumor cells, overexpression of Dkk-3 was found in 41 (30.1%; 12 and 29 cases with a total immunostaining score of 9–12 and 6–8, respectively) of all cases. Not only in tumor cells, but also in normal adjacent epithelial tissue Dkk-3 was immunohistochemically detected in 74 (54.4%) cases. For detailed description see Table 2.

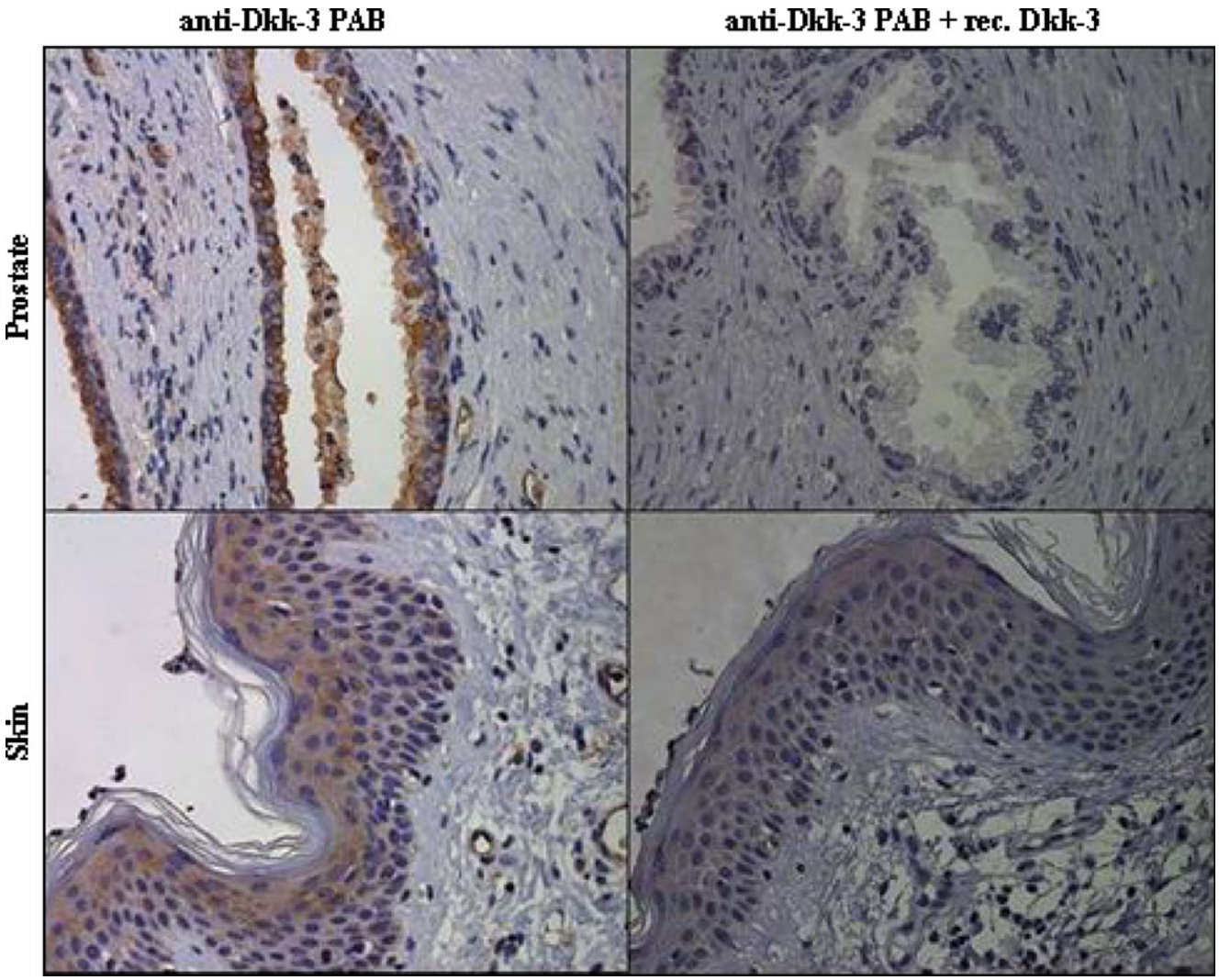

Fig. 2 Organs showing a high Dkk-3 gene expression were used as positive controls for immunohistochemical detection of Dkk-3 with a goat polyclonal antibody directed against human Dkk-3. Moreover, stainings were blocked by a 50-fold molar excess of recombinant Dkk-3 (purchased from R&D systems). The specific staining in the prostate epithelial cells, keratinocytes, and endothelial cells could be blocked by the recombinant protein. Note: Cells of the fibromuscular stroma do not stain for Dkk-3. Magnification ×400

Relationship between Dkk-3 expression in endothelial cells, MVD, and clinicopathologic features

In CD31-positive microvessels (n=133) a positive staining reaction for Dkk-3 in endothelial cells was found in 94.7% (126/133), whereas 5.3% (7/133) were Dkk-3 negative (Fig. 1). With regard to Dkk-3 positivity (n=126), 24 (19.0%) showed strong intensity, 47 (37.3%) moderate intensity, and 55 (43.7%) weak intensity. In all three tumor samples with CD31-negative microvessels, Dkk-3 showed a positive staining reaction with strong intensity (3/3).

In tumor tissues with a high MVD (n=57), 53 (93.0%) cases showed positive Dkk-3 expression. Out of these, six samples showed strong intensity, 21 moderate intensity, and 26 a weak staining reaction. Similarly, in low MVD (n=76), 73 (96.1%) samples showed immunohistochemically detectable Dkk-3 expression (strong, n=18; moderate, n=26; and weak, n=29).

Dkk-3 expression in endothelial cells lacked any statistical significant association with common clinicopathologic features (Table 3). By contrast, a statistically significant relationship between MVD and pT-stage (χ^2=25.04 ; df=6; p=0.001), nodal status (χ^2=13.19 ; df=6; p<0.05), UICC stage (χ^2=28.07 ; df=10; p<0.01), and Lauren classification (χ^2=6.65; df=2; p<0.05) was found (Fig. 2).

Relationship between Dkk-3 expression in tumor cells and clinicopathologic features

Dkk-3 overexpression in carcinoma cells was statistically significantly associated with pT-stage (χ^2=9.42 ; df=3; p<

Table 4 Prognostic factors examined in 136 adenocarcinomas of the stomach: an univariate approach to tumor relapse and cancer-specific mortality

	DFS		OS	
	X^2	*P* value	X^2	*P* value
Gender (male vs. female)	0.002	n.s.	0.56	n.s.
Age (<70 vs. >70 years)	0.38	n.s.	3.79	0.05
Lauren classification (intestinal vs. diffuse)	4.75	0.030	3.32	n.s.
Operative procedure (subt. vs. total gastr. vs. gr vs. limited)	2.52	n.s.	7.5	n.s.
Lymph node dissection (D1 vs. D2/3)	2.14	n.s.	4.8	0.042
Tumor differentiation (G1/G2 vs. G3/G4)	5.84	0.016	6.49	0.011
pT-category (pT1 vs. pT2 vs. pT3 vs. pT4)	25.12	0.001	23.46	0.001
pN-category (pN− vs. pN+)	31.57	0.001	20.48	0.001
M-category (M0 vs. M1)	13.06	0.001	24.56	0.001
UICC stage (IA + IB vs. II + IIIA/B + IV)	19.47	0.000	14.44	0.000
Residual disease (R0 vs. R1+R2)	2.23	n.s.	0.45	n.s.
Dkk-3 expression in endothelium (strong vs. m/w and no)	3.48	0.049	1.97	n.s.
Dkk-3 overexpression in tumor cells (yes vs. no)	0.2	n.s.	0.548	n.s.
MVD (high vs. low)	3.56	n.s.	0.53	n.s.

m/w moderate and weak staining intensity

0.05) and UICC stage (χ^2=9.25; df=5; p<0.05), whereas other prognostic parameters lacked any statistical significance (Table 3).

Survival analysis

Patients with strong Dkk-3 expression in tumor endothelium had a statistically significant (log rank, 3.48; df=1; p< 0.05) better disease-free survival (Table 4 and Fig. 3) compared with those with moderate or weak staining patterns. By contrast, correlation with the cancer-specific overall survival (OS) lacked statistical significance.

After excluding patients with (neo)-adjuvant treatment, survival calculations did not show significant differences in DFS and OS, nor did a subset analysis including patients treated with chemotherapy (n=22). Nevertheless, the accurate evaluation of the 22 patients indicated that patients with weak/moderate or no (n=19) expression of Dkk-3 in endothelium had a poor prognosis compared to patients with strong (n=3) expression (cancer-specific OS 32% versus 67%; not shown).

Regarding DFS and cancer-specific OS, Dkk-3 overexpression in tumor cells did not reveal statistical significance (Fig. 4). Also MVD did not show statistically significant variations in survival analysis. Univariate survival analysis with related prognostic variables are depicted in Table 3.

Multivariate survival analysis identified UICC stage, tumor differentiation, and Dkk-3 expression in endothelial cells as independent prognostic factors regarding both DFS and cancer-specific OS (Table 5).

Discussion

The present study analyzed the expression of Dkk-3 and its prognostic value in gastric cancer samples with special attention to its impact on neoangiogenesis. For the first time, we investigated Dkk-3 protein expression in tumor endothelium and tumor cells of gastric carcinoma specimens.

We recently published data on Dkk-3 expression and its impact on neovascularization in colorectal cancer tissue [20]. There we could demonstrate that in cancer samples with CD31-positive microvessels, the majority were positive for Dkk-3 whereas in samples of normal colorectal mucosa all CD31-positive microvessels showed no staining for Dkk-3. We concluded that Dkk-3 is a proangiogenic factor involved in neovascularisation during tumor growth. On the basis of this findings, we intended to investigate the behavior of Dkk-3 on the protein level in gastric carcinomas.

Regarding Dkk-3 in endothelium a positive staining reaction was found in nearly all samples with CD31-positive microvessels. Associations between Dkk-3 in endothelium and clinicopathologic parameters did not reveal significant correlations. Nevertheless, survival analysis showed a better DFS for patients with strong Dkk-3 expression in endothelium and revealed Dkk-3 as an independent prognostic feature in multivariate analysis. That does not go along with findings that only tumor vessels stained positive for Dkk-3 and that an upregulation of Dkk-3 expression in tumor blood vessels influences capillary formation in vitro and elevate the MVD in vivo [21]. MVD is reported to be one of the important prognostic factors for gastric cancer patients [27, 28].

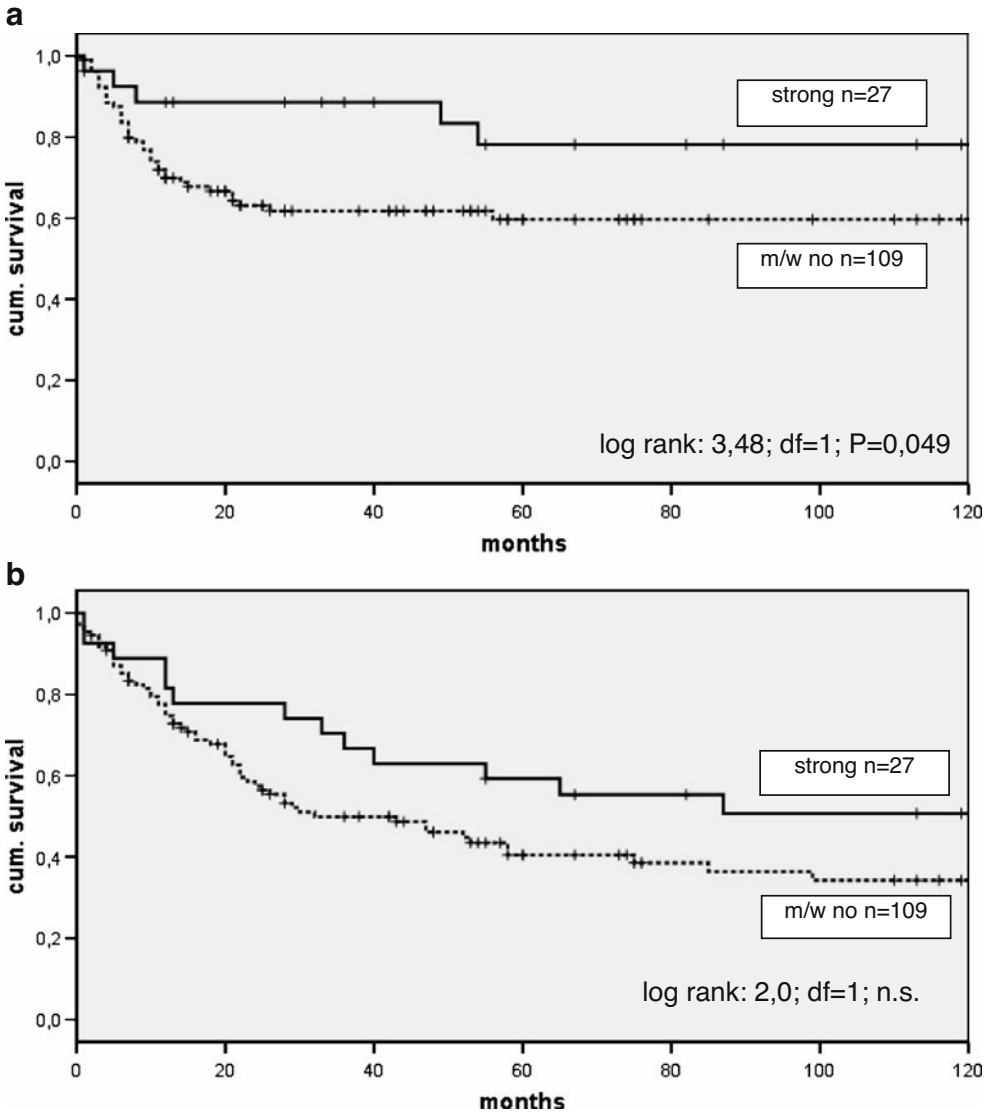

Fig. 3 Kaplan–Meier survival curves with regard to disease-free survival (**a**) and overall survival (**b**) of patients with strong Dkk-3 expression in endothelium (*line* strong; 27/136) and moderate, weak or no Dkk-3 expression in endothelium (*broken line* m/w; 109/136)

Although, Zhao et al. described MVD as an independent prognostic factor for OS, we could not confirm these results in our own study.

Similar to angiopoietin-2, Dkk-3 is probably involved in vessel maturation and stabilization processes in the tumor endothelium [29]. Thus, blood vessels adjacent to tumor cells could respond to proangiogenic destabilization signals by upregulating differentiation factors, such as Dkk-3, that in turn enhance vessel stability, thereby lowering the interstitial liquid pressure in the tumor. This in turn could lead to a better delivery of chemotherapeutics to the tumor, an effect observed with anti-vascular endothelial growth factor (VEGF) therapies [30]. This hypothesis is supported by the findings of Fong et al. in pancreatic carcinoma, where a high Dkk-3 expression in tumor blood vessels correlated with a better overall survival of patients [31]. Moreover, they were able to show that Dkk-3 overexpressing human endothelial cells were more sensitive to apoptosis induced by chemotherapeutics. Such effects on endothelial cells have also been observed in mouse models, where anti-VEGF antibodies led to increased vascular damage when combine with chemotherapy [30]. In our study, a subset analysis including patients treated with chemotherapy did not reveal statistically significant differences. That is probably due to the small number of patients in this group. Nevertheless, a trend toward an improved survival in patients with strong Dkk-3 expression in endothelial cells was evident. Taken together, our findings in gastric carcinoma also support the hypothesis that Dkk-3 over-

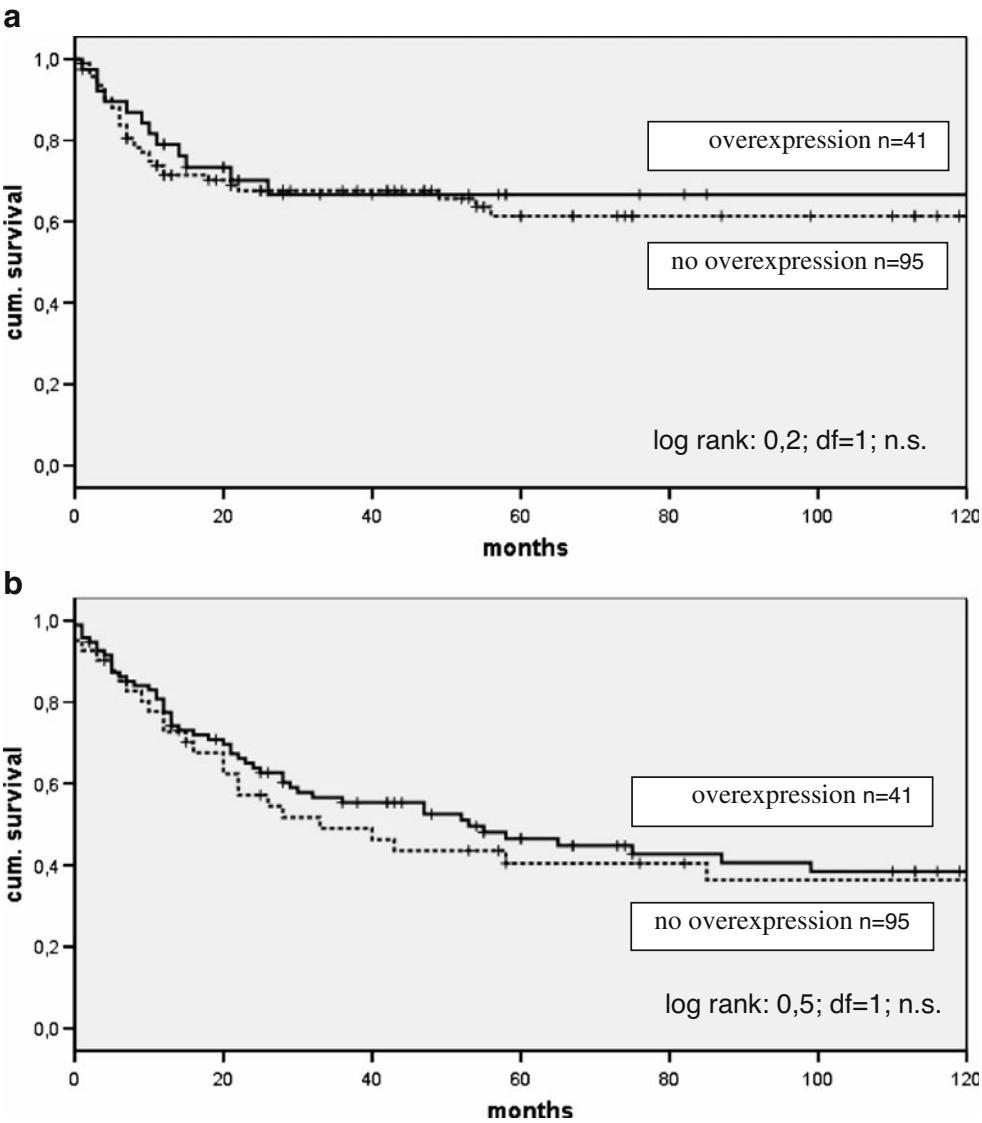

Fig. 4 Kaplan–Meier survival curves with regard to disease-free survival (**a**) and overall survival (**b**) of patients with (*line* overexpression; 41/136) and without (*broken line* no overexpression; 95/136) Dkk-3 overexpression in tumor cells

expression in the tumor blood vessel might be a prognostic marker for response to chemotherapeutics.

Unlike Dkk-1, Dkk-2, and Dkk-4, which seem to play a role in Wnt signaling and thus the beta-catenin destabilization process, Dkk-3 acts as tumor suppressor as it is downregulated in various types of cancer. Furthermore, overexpression of Dkk-3 suppresses tumor cell growth [11]. The loss of function of Dkk-3 in human cancers is attributable to promoter hypermethylation in cancer cells [14]. Downregulation of Dkk-3 has been described among others in renal clear cell carcinoma, non-small-cell lung cancer, cholangiocarcinoma, hepatocellular carcinoma, prostate cancer, melanoma, and recently in gastric cancer, where Yu et al. reported that Dkk-3

Table 5 Multivariate analysis regarding disease-free and overall survival

	DFS		OS	
	RHR (95% CI)	*P* value	RHR (95% CI)	*P* value
UICC stage				
II + IIIA/B + IV vs. IA + IB	6.71 (2.38–18.90)	0.000	2.59 (1.52–4.41)	0.001
Tumor differentiation				
G3–4 vs G1–2	2.22 (1.02–4.81)	0.038	1.93 (1.14–3.29)	0.028
Dkk-3 intensity in endothelium				
Strong vs. m/w and no	0.35 (0.14–0.89)	0.030	0.55 (0.31–0.98)	0.036

DFS disease-free survival, *OS* overall survival, *RHR* relative hazard ratio, *CI* confidence interval, *m/w* moderate and weak staining intensity

promoter methylation in primary gastric cancer correlates strongly with poor prognosis and is an independent prognostic marker of survival in multivariate analysis [13–19, 32, 33].

In contrast to colorectal cancer, not only endothelial tissue but also carcinoma cells as well as adjacent non-tumorous epithelial tissue were positively stained. Dkk-3 positivity in cancer cells could be found in more than half of cancer samples and, if including the criteria for over-expression, a rate of about 30% was detected. In univariate analysis of clinicopathologic variables, Dkk-3 overexpression correlated significantly with pT-stage, and UICC stage. In contrast, survival calculations did not show a significant relationship between Dkk-3 overexpression in carcinoma cells and DSF or OS.

Although immunohistochemically, Dkk-3 expression patterns in gastric cancer differ to other tumors reported, we can conclude that Dkk-3 is predominantly expressed in tumor microvessels and is significantly associated with favorable survival in gastric cancer. Moreover, data presented here suggest that Dkk-3 overexpression in the tumor blood vessel might be a prognostic marker for response to chemotherapeutics. However, further studies are needed to define more precisely the role of Dkk-3 in gastric cancer and to elucidate the putative role of Dkk-3 as a novel target for cancer therapy.

Acknowledgments The authors are grateful to Ms. Ines Tschörner, Ms. Daniela Pirkebner, and Ms. Martina Zimmermann for excellent technical assistance. Thanks are due to Helmut Mühlböck from the "*Tyrolean Tumorregister*" for providing survival data.

Conflict of interest No potential conflict of interest relevant to this article was reported.

Grant support Österreichische Krebshilfe-Krebsgesellschaft Tirol 2006 Grant

References

1. Hohenberger P, Gretschel S (2003) Gastric cancer. Lancet 362:305–315
2. Van de Velde CJH, Peeters KCMJ (2003) The gastric cancer treatment controversy. J Clin Oncol 21:2234
3. Cunningham D, Allum WH, Stenning SP et al (2006) Perioperative chemotherapy versus surgery alone for resectable gastroesophageal cancer. N Engl J Med 355:11–20
4. Earle CC, Maroun JA (1999) Adjuvant chemotherapy after curative resection for gastric cancer in non-asian patients: revisiting a meta-analysis of randomised trials. Eur J Cancer 35:1059–1064
5. Folkman J (1971) Tumor angiogenesis: therapeutic implications. New Engl J Med 285:1182–1186
6. Hanahan D, Folkman J (1996) Patterns and emerging mechanisms of the angiogenic switch during tumorigenesis. Cell 86:353–364
7. Poon RT, Fan ST, Wong J (2003) Clinical significance of angiogenesis in gastrointestinal cancers: a target for novel prognostic and therapeutic approaches. Ann Surg 238:9–28
8. St Croix B, Rago C, Velculescu V et al (2000) Genes expressed in human tumor endothelium. Science 289:1197–1202
9. Krupnik VE, Sharp JD, Jiang C et al (1999) Functional and structural diversity of the human Dickkopf gene family. Gene 238:301–313
10. Mao B, Wu W, Davidson G et al (2002) Kremen proteins are Dickkopf receptors that regulate Wnt/beta-catenin signalling. Nature 417:664–667
11. Niehrs C (2006) Function and biological roles of the Dickkopf family of Wnt modulators. Oncogene 25:7469–7481
12. Mao B, Niehrs C (2003) Kremen2 modulates Dickkopf2 activity during Wnt/LRP6 signaling. Gene 302:179–183
13. Kawano Y, Kitaoka M, Hamada Y et al (2006) Regulation of prostate cell growth and morphogenesis by Dickkopf-3. Oncogene 25:6528–6537
14. Kobayashi K, Ouchida M, Tsuji T et al (2002) Reduced expression of the REIC/Dkk-3 gene by promoter-hypermethylation in human tumor cells. Gene 282:151–158
15. Kurose K, Sakaguchi M, Nasu Y et al (2004) Decreased expression of REIC/Dkk-3 in human renal clear cell carcinoma. J Urol 171:1314–1318
16. Lodygin D, Epanchintsev A, Menssen A et al (2005) Functional epigenomics identifies genes frequently silenced in prostate cancer. Cancer Res 65:4218–4227
17. Nozaki I, Tsuji T, Iijima O et al (2001) Reduced expression of REIC/Dkk-3 gene in non-small cell lung cancer. Int J Oncol 19:117–121
18. Roman-Gomez J, Jimenez-Velasco A, Agirre X et al (2004) Transcriptional silencing of the Dickkopfs-3 (Dkk-3) gene by CpG hypermethylation in acute lymphoblastic leukaemia. Br J Cancer 91:707–713
19. Tsuji T, Miyazaki M, Sakaguchi M et al (2000) A REIC gene shows down-regulation in human immortalized cells and human tumor-derived cell lines. Biochem Biophys Res Commun 268:20–24
20. Zitt M, Untergasser G, Amberger A et al (2008) Dickkopf-3 as a new potential marker for neoangiogenesis in colorectal cancer: expression in cancer tissue and adjacent non-cancerous tissue. Dis Markers 24(2):101–109
21. Untergasser G, Steurer M, Zimmermann M et al (2008) The Dickkopf-homolog 3 is expressed in tumor endothelial cells and supports capillary formation. Int J Cancer 122:1539–1547
22. Sobin LH (2009) TNM classification of malignant tumours. Wiley, New York
23. WHO (2000) Classification of Tumors. Pathology and Genetics of Tumors of Digestive System. IARC, Lyon
24. Macdonald JS, Smalley SR, Benedetti J et al (2001) Chemoradiotherapy after surgery compared with surgery alone for adenocarcinoma of the stomach or gastroesophageal junction. N Engl J Med 345:725–730
25. Weidner N, Semple JP, Welch WR et al (1991) Tumor angiogenesis and metastasis-correlation in invasive breast carcinoma. N Engl J Med 324:1–8
26. Gastl G, Spizzo G, Obrist P et al (2000) Ep-CAM overexpression in breast cancer as a predictor of survival. Lancet 356:1981–1982
27. Zhao H-C, Qin R, Chen X-X et al (2006) Microvessel density is a prognostic marker of human gastric cancer. World J Gastroenterol 21:2598–2603
28. Araya M, Terashima M, Takagane A et al (1997) Microvessel count predicts metastasis and prognosis in patients with gastric cancer. J Surg Oncol 65:232–236
29. Li Y, Ye X, Tan C et al (2009) Axl as a potential therapeutic target in cancer: role of Axl in tumor growth, metastasis and angiogenesis. Oncogene 28:3442–3455

30. Ellis LM, Hicklin DJ (2008) VEGF-targeted therapy: mechanisms of anti-tumour activity. Nat Rev Cancer 8:579–591
31. Fong D, Hermann M, Untergasser G et al (2009) Dkk-3 expression in the tumor endothelium: a novel prognostic marker of pancreatic adenocarcinomas. Cancer Sci 100:1414–1420
32. Kuphal S, Lodermeyer S, Bataille F et al (2006) Expression of Dickkopf genes is strongly reduced in malignant melanoma. Oncogene 25:5027–5036
33. Yu J, Tao Q, Cheng YY et al (2009) Promoter methylation of the Wnt/beta-catenin signaling antagonist Dkk-3 is associated with poor survival in gastric cancer. Cancer 115(1):49–60

Virchows Arch (2010) 456:647–652
DOI 10.1007/s00428-010-0918-4

ORIGINAL ARTICLE

Influence of IL1B polymorphism on CpG island hypermethylation in *Helicobacter pylori*-infected gastric cancer

Eun Joo Yoo · Seog-Yun Park · Nam-Yun Cho · Nayoung Kim · Hye Seung Lee · Donguk Kim · Gyeong Hoon Kang

Received: 2 December 2009 / Revised: 30 March 2010 / Accepted: 1 April 2010 / Published online: 20 April 2010
© Springer-Verlag 2010

Abstract *Helicobacter pylori* infection can induce aberrant CpG island hypermethylation in gastric mucosal epithelial cells. Single nucleotide polymorphisms of proinflammatory cytokine genes encoding for interleukin 1B (*IL1B*), *IL6*, and *IL8* have been demonstrated to be associated with an increased risk of gastric cancer. To identify the influence of host genetic factors in CpG island hypermethylation induced by *H. pylori* infection, we analyzed *H. pylori*-infected chronic gastritis (n=111) and gastric cancer samples (n=78) for the methylation status of eight genes previously shown to be hypermethylated in chronic gastritis and single nucleotide polymorphisms of *IL1B*, *IL6*, and *IL8*. The methylation levels were then compared between different genotypes. Gastric cancers from patients with the *IL1B*-511T/T allele showed significantly higher methylation levels in five genes as compared with gastric cancers from *IL1B*-511 C carriers (P<0.05). An increased level of hypermethylation in association with the *IL1B*-511T/T allele was observed in chronic gastritis samples, but the association was not statistically significant. These findings suggest that the *IL1B*-511T/T allele is associated with enhanced hypermethylation of multiple CpG island loci, which might contribute to an increase in the risk for gastric cancer in individuals with *H. pylori* infection and *IL1B*-511T/T allele.

Keywords DNA methylation · *Helicobacter pylori* · IL1B · Single nucleotide polymorphism

E. J. Yoo · N.-Y. Cho · G. H. Kang
Laboratory of Epigenetics, Cancer Research Institute,
Seoul National University College of Medicine,
Seoul, South Korea

S.-Y. Park
Department of Pathology, National Cancer Center,
Goyang, Gyeonggi-do, South Korea

N. Kim
Department of Internal Medicine,
Seoul National University College of Medicine,
Seoul, South Korea

H. S. Lee · G. H. Kang (✉)
Department of Pathology, the Second Stage Brain Korea 21
Project and Seoul National, University College of Medicine,
28 Yongon-dong, Chongno-gu,
Seoul 110-744, South Korea
e-mail: ghkang@snu.ac.kr

D. Kim
Department of Statistics, Sungkyunkwan University,
Seoul, South Korea

Introduction

Hypermethylation of CpG islands located in the promoter regions of tumor suppressor [or tumor-related] genes is an important mechanism for gene inactivation and acts as an alternative to gene mutations for the inactivation of tumor suppressor genes or tumor-related genes in human cancers, regardless of tissue type [1]. Gastric cancer is one type of human cancers where aberrant promoter CpG island hypermethylation is frequently found. Although *Helicobacter pylori* is designated as a human class I carcinogen of gastric malignancy by the International Agency for Research on Cancer [2], the exact mechanism of *H. pylori*-associated gastric carcinogenesis remains unclear. Several studies have demonstrated enhanced hypermethylation in multiple CpG island loci in gastric mucosa of *H. pylori*-infected patients [3–6] and a reversal of methylation status of multiple CpG island loci by eradication of *H. pylori* infection [5, 7–9].

These findings suggest that aberrant promoter CpG island hypermethylation induced by chronic persistent infection of *H. pylori* may contribute to *H. pylori* infection-associated gastric carcinogenesis.

Several proinflammatory cytokines, including interleukin (IL) 1B, IL6, and IL8, are upregulated in the gastric mucosa during *H. pylori* infection and help initiate and regulate the inflammatory response to *H. pylori* infection [10–13]. IL1B and IL6 have been shown to be capable of increasing expression and activity of DNA methyltransferase 1 (DNMT1), which mediates the transfer of a methyl group from S-adenosyl methionine to cytosine of CpGs, thereby modulating CpG island hypermethylation [14–17]. Several single nucleotide polymorphisms (SNPs) in these proinflammatory cytokine genes are known to alter their expression [10, 11, 18, 19]. *IL1B* has two diallelic SNPs in the promoter at positions –511 and –31 base pairs from the transcriptional start site, which affect the gastric mucosal ILB levels in relation to *H. pylori* infection [11, 20]. These two sites (*IL1B*-31 C and *IL1B*-511T) are known to be in complete linkage disequilibrium [10]. The A allele of an *IL8* SNP in the promoter region (–251 A/T) has been shown to be associated with increased IL8 production in nonneoplastic gastric mucosa [21]. A G/C SNP in the promoter region (–174) of *IL6* affects promoter activity and alters plasma IL6 levels [19, 22, 23]. Based on these observations, it can be speculated that SNPs in these IL genes might affect CpG island hypermethylation in *H. pylori*-infected gastric mucosa through differential modulation of *DNMT1* expression.

There is a wide distribution in the number of CpG island loci hypermethylated in *H. pylori*-positive chronic gastritis patients [5, 24] that may be attributed to bacterial virulence factors, duration of *H. pylori* infection, and host genetic factors. Thus far, there is very limited information about the relationship between proinflammatory cytokine gene SNPs and CpG island hypermethylation [6]; we hypothesize that these SNPs may be a contributing factor to the variability in the number of CpG island loci with enhanced hypermethylation. In the present study, we analyzed the methylation status of eight genes in *H. pylori*-positive gastric cancer and chronic gastritis tissue samples using the MethyLight assay. We then related the methylation levels of these genes to the alleles of SNPs of *IL1B*, *IL6*, and *IL8* within the chronic gastritis and gastric cancer samples. The eight genes were selected based on the findings of our previous study in which DNA hypermethylation of 25 genes was analyzed for chronic gastritis and eight genes were found to be methylated in *H. pylori*-positive chronic gastritis at levels significantly higher than those of *H. pylori*-negative chronic gastritis samples, including *CACNA1G*, *CDH1*, *DAPK1*, *CALCA*, *CYP1B1*, *CRABP1*, *TWIST*, and *GRIN2B* [24]. Of these, six genes except for *CDH1* and *DAPK1* showed not only *H. pylori*-associated hypermethylation but also cancer-associated hypermethylation.

Material and methods

Subjects and serologic evaluation

A total of 111 tissue samples from *H. pylori*-positive chronic gastritis patients (M/F, 59:52; mean age, 53.9 years) and 78 tissue samples from *H. pylori*-positive gastric cancer patients (M/F, 64:14; mean age, 59.8 years) who had undergone an endoscopic mucosal biopsy at Seoul National University Bundang Hospital from September 2003 to March 2005 were analyzed in the present study. Duplicate blood samples from patients were evaluated for the level of anti-*H. pylori* immunoglobulin G using an enzyme-linked immunosorbent assay (Genedia *H. pylori* ELISA; Green Cross Sang A Co., Seoul, South Korea) according to the manufacturer's protocol. A modified Giemsa staining and CLO test were performed for assessment of the presence of *H. pylori*. All of the cases were positive for at least two of these three tests. The study was approved by the Seoul National University Hospital's Institutional Review Board and the Seoul National University Bundang Hospital's Institutional Review Board.

DNA isolation and bisulfite modification

Archival tissue sections (n=20) of 4-μm thickness were used for DNA extraction. After identification of tumors in the endoscopic mucosal biopsy samples through light microscopy, tumor lesions were manually dissected and the dissected tissues were pooled together in a microtube containing lysis buffer and proteinase K. Whole tissue sections were used for DNA extraction of the chronic gastritis group samples. Chronic gastritis cases showing intestinal metaplasia were excluded from the present study because intestinal metaplasia itself is associated with increased DNA hypermethylation of CpG island loci [25] and our preliminary study confirmed this finding. Sodium bisulfite conversion of genomic DNA was performed as described [26].

MethyLight assay

MethyLight technology was performed for the methylation analysis of eight CpG island loci using the iCycler Real-Time PCR Detection System (BioRad, Hercules, CA, USA). The oligonucleotide sequences of the primers and probes used have been described [24]. Two sets of primers and probes designed specifically to bind to bisulfite-converted DNA were used in each reaction; one set of

primers and probe were used for each methylated target to be analyzed (methylated reaction), and another pair of primers and probe were used for the reference locus, *ALU* (normalization control reaction). Normalization control reactions were methylation-independent measurements to control for DNA amplification and to normalize for input DNA. *M.Sss*I-treated genomic DNA was used as a reference sample for complete methylation to determine the percentage of methylated reference (PMR) at a particular locus. PMR was defined as 100× (methylated reaction/normalization control reaction)$_{sample}$/(methylated reaction/normalization control reaction)$_{M.SssI\text{-}Reference}$.

Genotyping of *IL1B*-511, *IL6*-174, and *IL8*-251

The polymorphisms of *IL1B*-511, *IL6*-174, and *IL8*-251 were analyzed by 5' nuclease PCR assay (TaqMan) using the primers and probes described in Table 1. The sequences of primers and probes were obtained from the Cancer Genome Anatomy Project SNP500 Cancer Database (http://snp500cancer.nci.nih.gov). We used genomic DNA (50 ng) in a reaction volume of 10 μl. DNA samples were amplified in a Mini Opticon System (BioRad) with cycling conditions as follows: 2 min at 50°C, 10 min at 95°C, followed by 50 cycles of 30 s at 92°C, 60°C (*IL8*-251), or 58°C (*IL1B*-511 and *IL6*-174) for 1 min.

Statistical analysis

Statistical analyses were performed using the statistics program SAS software (SAS Institute, Cary, NC, USA). To evaluate the risks of gastric cancer for each specific genotype, odds ratio and 95% confidence interval were calculated by multivariate logistic regression. The methylation levels of the examined CpG island loci were compared between alleotypes of IL genes using Student's *t* test. Comparison of the number of methylated CpG island loci between the polymorphisms of *IL* genes was also examined using Student's *t* test. A *P* value <0.05 was considered statistically significant.

Results

Genotyping of *IL1B*-511, *IL6*-174, and *IL8*-251

To compare the SNP status of *IL1B*-511T/C, *IL6*-174 G/C, and *IL8*-251T/A to the methylation levels of *CACNA1G*, *CDH1*, *DAPK1*, *CALCA*, *CYP1B1*, *CRABP1*, *TWIST*, and *GRIN2B*, we first genotyped these polymorphisms in 111 *H. pylori*-positive chronic gastritis and 78 *H. pylori*-positive gastric cancer samples.

The polymorphism *IL6*-174 was not identified in either *H. pylori*-positive chronic gastritis or gastric cancer samples using the TaqMan assay (data not shown). The genotype frequencies of *IL1B*-511 and *IL8*-251 are listed in Table 2. There were no significant differences in genotype frequencies for *IL1B*-511 and *IL8*-251 between the gastric cancer and chronic gastritis groups. Thus, there was no significant increase in gastric cancer risk associated with these *IL1B*-511 and *IL8*-251 polymorphisms.

Correlation between SNPs and CpG island hypermethylation

The relationship between differential promoter CpG island hypermethylation of the eight genes and the SNPs of *IL1B*-511 and *IL8*-251 in the *H. pylori*-infected chronic gastritis (n=111) and *H. pylori*-positive gastric cancer (n=78) samples was next assessed. In the chronic gastritis samples, *CYP1B1* and *GRIN2B* tended to show higher methylation levels in *IL1B*-511T/T than in *IL1B*-511 C carrier samples (P=0.089 and P=0.068, respectively) and there were no differences noted in methylation levels of the six other analyzed genes (Fig. 1b). On the other hand, gastric cancer with the *IL1B*-511T/T allele showed significantly higher methylation levels of five CpG island loci (in *CACNA1G*, *TWIST1*, *CYP1B1*, *GRIN2B*, and *CRABP1*) than those of *IL1B*-511 C carriers (P<0.05; Fig. 1a). For the *IL8*-251 SNP, chronic gastritis samples did not exhibit statistically significant differences in methylation levels of the CpG island loci except for a difference in *DAPK1* between the *IL8*-251 A/A

Table 1 Sequences of primers and probes for the detection of single nucleotide polymorphisms

Gene	Primer	Probe
IL1B-511 C/T	F: CAGAGGCTCCTGCAATTGACA	FAM-AGCTCCTGAGGCAGA-MGB
	R: GGTCTCTACCTTGGGTGCTGTTC	VIC-AGAGCTCCCGAGGC-MGB
IL6-174 C/G	F: TGACGACCTAAGCTGCACTTTTC	FAM-CATACATTTGATAATTCA-MGB
	R: GGGCTGATTGGAAACCTTATTAAGA	VIC-TCTTGCGATGCTAAA-MBG
IL8-251 A/T	F: GTTCTAACACCTGCCACTCTAGTAC	FAM-AGCATACATTTGATAATT-MGB
	R: CATTTAAAATACTGAAGCTCCACAATTTGGT	VIC-AAGCATACAATTGATAATT-MGB

IL1B-31, IL1B-511, *IL6*-174 and IL8-251 were genotyped by 5′ nuclease PCR assay (TaqMan)

Table 2 Comparison of *IL1B*-511 and *IL8*-251 genotype frequencies in chronic gastritis and gastric cancer samples (adjusted odds ratio)

IL1B-511					*IL8*-251				
Genotype	Gastric cancer (n=78)	Chronic gastritis (n=111)	OR (95% CI)	P value	Geno type	Gastric cancer (n=78)	Chronic gastritis (n=111)	OR (95% CI)	P value
T/T	22	29	1.25 (0.44, 3.54)	0.680	A/A	18	18	1.33 (0.55, 3.20)	0.524
T/C	45	63	1.20 (0.50, 2.90)	0.688	A/T	35	35	0.94 (0.47, 1.90)	0.873
C/C	11	19	Reference		T/T	25	40	Reference	

and *IL8*-251T carrier samples. *DAPK1* showed a higher methylation level in the T carrier than in A/A (P=0.015; Fig. 2b). In gastric cancer samples, however, five loci showed a tendency to have higher methylation levels in *IL8*-251 A/A but only *TWIST1* displayed a statistically significant difference between the *IL8*-251 A/A allele and *IL8*-251 T carrier (P=0.007; Fig. 2a).

When a PMR cutoff value of 15 was arbitrarily applied to define methylation-positive vs. methylation-negative states in individual CpG island loci, the average number of CpG island loci methylated per sample was 2.4 in gastric cancer patients with the *IL1B*-511T/T allele and was 1.6 in gastric cancer patients who were *IL1B*-511 C carriers (P=0.076, Student's t test). Gastric cancer patients with the *IL1B*-511T/T allele showed an increased odds ratio of 2.84 with respect to *IL1B*-511 C carriers for the presence of methylation at two or more genes (CI, 0.97–8.31; P=0.056). For chronic gastritis patients, the average number of methylated genes per sample was 1.0 for patients with the *IL1B*-511T/T allele and 0.7 for *IL1B*-511 C carriers (P=0.188, Student's t test).

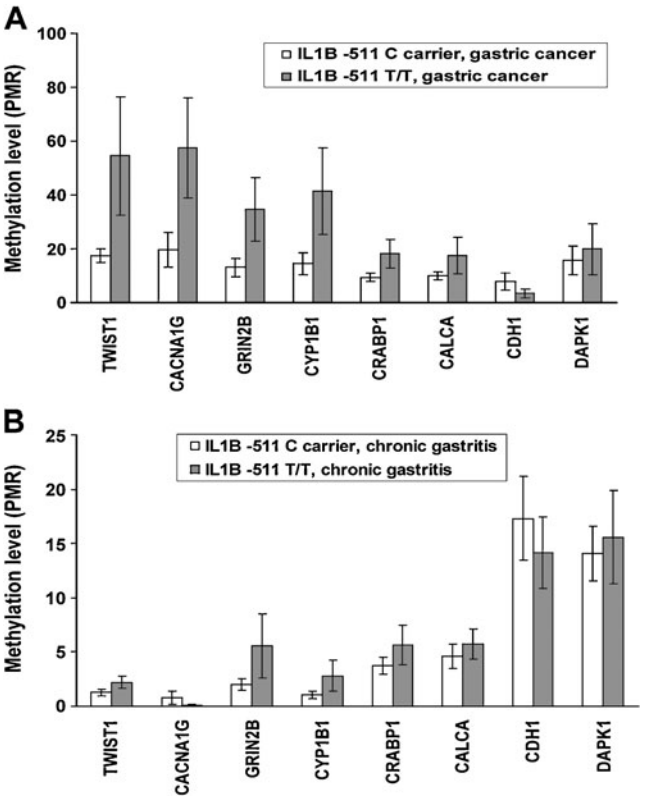

Fig. 1 Comparison of methylation levels (PMR) in eight CpG island loci between the genotypes of *IL1B*-511. Methylation levels of the promoters for the eight indicated genes were measured using the MethyLight assay in *H. pylori*-infected gastric cancer (**a**) and *H. pylori*-positive chronic gastritis (**b**) samples. *Error bars* indicate standard error of the mean (SEM)

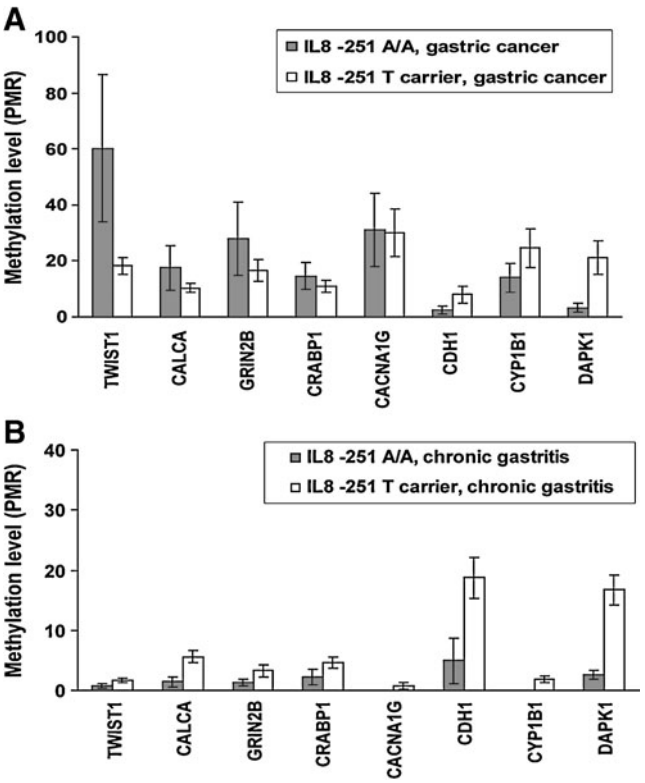

Fig. 2 Comparison of methylation levels (PMR) in eight CpG island loci for the genotypes of *IL8*-251. Methylation levels of the promoters for the eight indicated genes were measured using the MethyLight assay in *H. pylori*-infected gastric cancer (**a**) and *H. pylori*-positive chronic gastritis (**b**) samples. *Error bars* indicate SEM

Discussion

In our previous study [24] where the methylation status of 25 genes was analyzed in chronic gastritis samples using the MethyLight assay, the number of hypermethylated genes was significantly increased in *H. pylori*-infected samples than in *H. pylori*-negative samples. However, among *H. pylori*-infected chronic gastritis samples, the number of genes hypermethylated varied widely, which is consistent with other studies [5, 9]. This indicates the presence of other influential factors, including potential host genetic factors, in the susceptibility of CpG islands to *H. pylori*-provoked hypermethylation. Chan et al. [6] found that gastric cancer patients with the *IL1B*-511T/T allele showed a higher odds ratio for the presence of methylation on two or more genes compared to *IL1B*-511 C carrier gastric cancer patients, as we also observed in this study. Our quantitative results using the MethyLight assay confirm and extend the finding of Chan et al. Because we used a real-time-based methylation-specific PCR (MSP) assay that is quantitative [27, 28], we avoided the disadvantages of the traditional qualitative MSP assay—namely, variable results depending on the amount of input DNA, number of PCR cycles, and staining conditions of PCR products and the lack of discrimination between high and low methylation levels, which produces inconsistent results. In the present study, five of the eight examined genes (62.5%) showed significantly higher methylation levels in gastric cancers of patients with the *IL1B*-511T/T allele than in gastric cancers of *IL1B*-511 C carriers.

Chan et al. [6] analyzed the methylation status of four genes (*MGMT*, *CDH1*, *DAPK1*, and *p16*). However, in our previous study using MethyLight assay [26], *MGMT* was rarely methylated in chronic gastritis samples and there were no differences in *p16* methylation levels between *H. pylori*-negative and *H. pylori*-positive chronic gastritis samples. Thus, these two genes were not included in the present study. We did not find a significant difference in methylation levels of *CDH1* and *DAPK1* between *IL1B*-511T/T individuals and *IL1B*-511 C carriers in either chronic gastritis or gastric cancer samples. The discrepancies between Chan et al.'s study and the present study may be attributed to differences in ethnicity of the study populations or the methylation analysis methods used. The MethyLight assay detects a subset of DNA alleles that are heavily methylated in all CpG sites targeted by both primers and probe [29], thus it cannot detect substantially but incompletely methylated DNA alleles that can be detected by traditional MSP.

The two SNPs in *IL1B* and *IL8* studied here have been shown to alter expression of their respective genes and both SNPs have been identified as host-related risk factors for gastric cancer [10, 18, 19, 21]; however, enhanced hypermethylation was only observed with the *IL1B*-511T/T allele, but not with the *IL8*-251 A/A allele. This result may be attributed to the fact that DNMT1 enzyme activity is elevated in response to IL1B, but a response has not yet been demonstrated for IL8 [16]. Another finding in our study is that enhanced hypermethylation in association with the *IL1B*-511T/T allele was gene specific. Although little is known about factors predisposing genes toward DNA hypermethylation, recent studies have suggested that CpG island loci occupied by Polycomb repressive complexes (PRC) in embryonic stem cells or normal counterpart cells are vulnerable to aberrant hypermethylation during tumorigenesis [30–32]. *CDH1* and *DAPK1*, which did not show elevated hypermethylation in relation to *IL1B*-511T/T allele, were known to be not occupied by PRC2 in embryonal stem cells, whereas five genes showing elevated hypermethylation (*CACNA1G*, *CYP1B1*, *CRABP1*, *GRIN2B*, and *TWIST1*) harbor PRC2 occupancy in embryonic stem cells [33]. One possible interpretation of the data is that enhanced DNA hypermethylation in association with the *IL1B*-511T/T allele is dependent upon PRC2 occupancy at the gene; however, this hypothesis must be considered with caution, as a limited number of CpG island loci were examined in the present study.

In conclusion, we analyzed *H. pylori*-infected chronic gastritis and gastric cancer tissues for their methylation status at eight CpG island loci, and we correlated the methylation levels of these eight genes with SNPs of *IL1B*-511 and *IL8*-251. The *IL1B*-511T/T allele was closely associated with enhanced hypermethylation of CpG island loci in gastric cancer.

Acknowledgment Supported by the Korea Science and Engineering Foundation (KOSEF) grant funded by the Korea government (MEST, no. M10750030001-08N5003-00110), a grant from the National R&D Program for Cancer Control, Ministry of Health & Welfare, Republic of Korea (0720540), and Priority Research Centers Program through the National Research Foundation of Korea (NRF) funded by the Ministry of Education, Science and Technology (2009-0093820)

Conflict of interest There are no financial or other interests with regard to the submitted manuscript that might be construed as a conflict of interest.

References

1. Jones PA, Laird PW (1999) Cancer epigenetics comes of age. Nat Genet 21:163–167
2. IARC working group on the evaluation of carcinogenic risks to humans, schistosomes, liver flukes, Helicobacter pylori (1994) IARC monographs on the evaluation of carcinogenic risks to humans, vol 61. International Agency for Research on Cancer, Lyon, pp 1–241
3. Maekita T, Nakazawa K, Mihara M et al (2006) High levels of aberrant DNA methylation in Helicobacter pylori-infected gastric

mucosae and its possible association with gastric cancer risk. Clin Cancer Res 12:989–995
4. Chan AO, Lam SK, Wong BC et al (2003) Promoter methylation of E-cadherin gene in gastric mucosa associated with Helicobacter pylori infection and in gastric cancer. Gut 52:502–506
5. Ushijima T, Nakajima T, Maekita T (2006) DNA methylation as a marker for the past and future. J Gastroenterol 41:401–407
6. Chan AO, Chu KM, Huang C et al (2007) Association between Helicobacter pylori infection and interleukin 1beta polymorphism predispose to CpG island methylation in gastric cancer. Gut 56:595–597
7. Chan AO, Peng JZ, Lam SK et al (2006) Eradication of Helicobacter pylori infection reverses E-cadherin promoter hypermethylation. Gut 55:463–468
8. Leung WK, Man EP, Yu J et al (2006) Effects of Helicobacter pylori eradication on methylation status of E-cadherin gene in noncancerous stomach. Clin Cancer Res 12:3216–3221
9. Perri F, Cotugno R, Piepoli A et al (2007) Aberrant DNA methylation in non-neoplastic gastric mucosa of H. Pylori infected patients and effect of eradication. Am J Gastroenterol 102:1361–1371
10. El-Omar EM, Carrington M, Chow WH et al (2000) Interleukin-1 polymorphisms associated with increased risk of gastric cancer. Nature 404:398–402
11. Hwang IR, Kodama T, Kikuchi S et al (2002) Effect of interleukin 1 polymorphisms on gastric mucosal interleukin 1beta production in Helicobacter pylori infection. Gastroenterology 123:1793–1803
12. Wang M, Furuta T, Takashima M et al (1999) Relation between interleukin-1beta messenger RNA in gastric fundic mucosa and gastric juice pH in patients infected with Helicobacter pylori. J Gastroenterol 34 Suppl:10–17
13. Wallace JL, Cucala M, Mugridge K, Parente L (1991) Secretagogue-specific effects of interleukin-1 on gastric acid secretion. Am J Physiol 261:559–564
14. Hodge DR, Xiao W, Clausen PA, Heidecker G, Szyf M, Farrar WL (2001) Interleukin-6 regulation of the human DNA methyltransferase (hDNMT) gene in human erythroleukemia cells. J Biol Chem 276:39508–39511
15. Hodge DR, Peng B, Cherry JC et al (2005) Interleukin 6 supports the maintenance of p53 tumor suppressor gene promoter methylation. Cancer Res 65:4673–4682
16. Hmadcha A, Bedoya FJ, Sobrino F, Pintado E (1999) Methylation-dependent gene silencing induced by interleukin 1beta via nitric oxide production. J Exp Med 190:1595–1604
17. Wehbe H, Henson R, Meng F, Mize-Berge J, Patel T (2006) Interleukin-6 contributes to growth in cholangiocarcinoma cells by aberrant promoter methylation and gene expression. Cancer Res 66:10517–10524
18. Li C, Xia HH, Xie W et al (2007) Association between interleukin-1 gene polymorphisms and Helicobacter pylori infection in gastric carcinogenesis in a Chinese population. J Gastroenterol Hepatol 22:234–239
19. Fishman D, Faulds G, Jeffery R et al (1998) The effect of novel polymorphisms in the interleukin-6 (IL-6) gene on IL-6 transcription and plasma IL-6 levels, and an association with systemic-onset juvenile chronic arthritis. J Clin Invest 102:1369–1376
20. Chang YW, Jang JY, Kim NH et al (2005) Interleukin-1B (IL-1B) polymorphisms and gastric mucosal levels of IL-1beta cytokine in Korean patients with gastric cancer. Int J Cancer 114:465–471
21. Taguchi A, Ohmiya N, Shirai K et al (2005) Interleukin-8 promoter polymorphism increases the risk of atrophic gastritis and gastric cancer in Japan. Cancer Epidemiol Biomark Prev 14:2487–2493
22. Olomolaiye O, Wood NA, Bidwell JL (1998) A novel NlaIII polymorphism in the human IL-6 promoter. Eur J Immunogenet 25:267
23. Terry CF, Loukaci V, Green FR (2000) Cooperative influence of genetic polymorphisms on interleukin 6 transcriptional regulation. J Biol Chem 275:18138–18144
24. Yoo EJ, Park SY, Cho NY, Kim N, Lee HS, Kang GH (2008) Helicobacter pylori-infection-associated CpG island hypermethylation in the stomach and its possible association with Polycomb repressive marks. Virchows Arch 452:515–524
25. Mihara M, Yoshida Y, Tsukamoto T et al (2006) Methylation of multiple genes in gastric glands with intestinal metaplasia: a disorder with polyclonal origins. Am J Pathol 169:1643–1651
26. Kang GH, Lee S, Cho NY et al (2008) DNA methylation profiles of gastric carcinoma characterized by quantitative DNA methylation analysis. Lab Invest 88:161–170
27. Eads CA, Danenberg KD, Kawakami K et al (2000) MethyLight: a high-throughput assay to measure DNA methylation. Nucleic Acids Res 28:E32
28. Ogino S, Kawasaki T, Brahmandam M et al (2006) Precision and performance characteristics of bisulfite conversion and real-time PCR (MethyLight) for quantitative DNA methylation analysis. J Mol Diagn 8:209–217
29. Trinh BN, Long TI, Laird PW (2001) DNA methylation analysis by MethyLight technology. Methods 25:456–462
30. Ohm JE, McGarvey KM, Yu X et al (2007) A stem cell-like chromatin pattern may predispose tumor suppressor genes to DNA hypermethylation and heritable silencing. Nat Genet 39:237–242
31. Schlesinger Y, Straussman R, Keshet I et al (2007) Polycomb-mediated methylation on Lys27 of histone H3 pre-marks genes for de novo methylation in cancer. Nat Genet 39:232–236
32. Widschwendter M, Fiegl H, Egle D et al (2007) Epigenetic stem cell signature in cancer. Nat Genet 39:157–158
33. Lee TI, Jenner RG, Boyer LA et al (2006) Control of developmental regulators by Polycomb in human embryonic stem cells. Cell 125:301–313

Virchows Arch (2010) 456:653–659
DOI 10.1007/s00428-010-0907-7

ORIGINAL ARTICLE

Electronic reminders for pathologists promote recognition of patients at risk for Lynch syndrome: cluster-randomised controlled trial

L. I. Overbeek · R. P. Hermens · J. H. van Krieken · E. M. Adang · M. Casparie · F. M. Nagengast · M. J. Ligtenberg · N. Hoogerbrugge · MIPA study group

Received: 8 February 2010 / Accepted: 11 March 2010 / Published online: 9 April 2010
© The Author(s) 2010. This article is published with open access at Springerlink.com

Abstract We investigated success factors for the introduction of a guideline on recognition of Lynch syndrome in patients recently diagnosed with colorectal cancer (CRC) below age 50 or a second CRC below age 70. Pathologists were asked to start microsatellite instability (MSI) testing and report to surgeons with the advice to consider genetic counselling when MSI test or family history was positive. A multicentre cluster-randomised controlled trial (ClinicalTrials.gov, number NCT00141466) was performed in 12 pathology laboratories (clusters), serving 29 community hospitals. All received an introduction to the new guideline. In the intervention group, surgeons received education and tumour test result reminders; pathologists were provided with inclusion criteria cards, an electronic patient inclusion reminder system and feedback on inclusion. Two hundred sixty-six CRC patients were eligible for recognition as at risk for Lynch syndrome. The actual recognition was 18% more successful in the intervention as compared to the control arm (77% (120 of 156) compared to 59% (65 of 110)), with an adjusted odds ratio (OR)=2.8 (95% confidence interval (CI) 1.1–7.0). The electronic reminder system for pathologists was most strongly associated with recognition of high-risk patients, OR=4.2 (95% CI 1.7–10.1). An electronic reminder system for pathologists

The MIPA study group consists of the authors and individuals from the Radboud University Medical Centre (B. Gordijn, R.P.T.M. Grol, K.M. Landsbergen, M.F. Niermeijer, H.G. Brunner and P. van Duijvendijk en R.P. Akkermans) and from the University Medical Centre Groningen (H. Hollema, J.H. Kleibeuker and R.H. Sijmons).

L. I. Overbeek · M. J. Ligtenberg · N. Hoogerbrugge (✉)
Department of Human Genetics 849,
Radboud University Nijmegen Medical Centre,
P.O. Box 9101, 6500 HB Nijmegen, The Netherlands
e-mail: n.hoogerbrugge@antrg.umcn.nl

L. I. Overbeek · R. P. Hermens
Centre for Quality of Care Research,
Radboud University Nijmegen Medical Centre,
Nijmegen, The Netherlands

J. H. van Krieken · M. J. Ligtenberg
Department of Pathology,
Radboud University Nijmegen Medical Centre,
Nijmegen, The Netherlands

E. M. Adang
Department of Epidemiology,
Biostatistics and Health Technology Assessment,
Radboud University Nijmegen Medical Centre,
Nijmegen, The Netherlands

M. Casparie
PALGA Registry for Pathology,
Utrecht, The Netherlands

F. M. Nagengast
Department of Gastroenterology,
Radboud University Nijmegen Medical Centre,
Nijmegen, The Netherlands

N. Hoogerbrugge
Department of Medical Oncology,
Radboud University Nijmegen Medical Centre,
Nijmegen, The Netherlands

appeared effective for adherence to a new complex guideline and will enhance the recognition of Lynch syndrome.

Keywords Colorectal cancer · HNPCC · Lynch syndrome · MSI testing · Bethesda criteria

Introduction

In this era of rapidly increasing knowledge on hereditary cancer, much new evidence needs to be introduced in clinical practice, often in multidisciplinary teams including surgeons, pathologists and clinical geneticists. A commonly used method to achieve awareness is the development of guidelines for clinical practice. In recent years, many such guidelines have been published. However, approximately 30–40% of patients do not receive care according to present scientific evidence, and about 20–25% of care provided is not needed or is potentially harmful [1]. At present, little is known about effective strategies for the implementation of new guidelines in multidisciplinary teams of second-line medical care [2, 3].

Lynch syndrome, previously referred to as hereditary non-polyposis colorectal cancer [4], is the most common type of hereditary CRC and is caused by germ line inactivation of one of four DNA mismatch repair genes [5]. Although Lynch syndrome only accounts for up to 5% of CRCs [6–9], identifying Lynch syndrome is highly relevant because surveillance substantially reduces morbidity and mortality in family members carrying a mismatch repair gene mutation [10]. The identification of Lynch syndrome starts with the recognition of patients at risk for Lynch syndrome. Traditionally, this is done by the occurrence of CRC in the family. However, by using family history, only a small proportion of the expected number of patients at risk for Lynch syndrome is identified [11–14]. This is due to small families, unawareness by the patients of their own family history and suboptimal registration of family history of cancer by surgeons and gastroenterologists [11–14]. Recognising patients at risk for Lynch syndrome can effectively be improved by an additional procedure using a molecular genetic test on tumour DNA of a CRC, the so-called microsatellite instability (MSI) testing [7, 9, 15, 16]. MSI is a hallmark of a defective mismatch repair system, which results in differences in length of stretches of simple repeat sequences, called microsatellites, between normal and tumour DNA. In Lynch syndrome, virtually all CRCs show MSI. Although MSI may also occur in sporadic CRC diagnosed at relatively high age, in the group of patients suspected for Lynch syndrome, the MSI is predominantly due to genetic susceptibility [17]. Once patients at risk are identified, this will lead to identification of more patients with Lynch syndrome in a highly cost-effective way [15, 18].

A new guideline was developed using MSI testing to improve recognition of patients at risk for Lynch syndrome by a multidisciplinary team of surgeons, pathologists and clinical geneticists. In this MSI-testing-indicated-by-a-pathologist (MIPA) procedure [15], pathologists initiate MSI testing in a selection of recently diagnosed patients with one of the following criteria: (1) CRC diagnosed before age 50, (2) second CRC before age 70, (3) CRC and a Lynch syndrome associated cancer before age 70 or (4) a colorectal adenoma with high-grade dysplasia before the age of 40 years [15, 19, 20]. Pathologists report the MSI test result to the surgeon with the advice to consider referral for genetic counselling in an outpatient clinic for hereditary cancer when the MSI test was positive or the family history remained suspicious for hereditary CRC.

This guideline was proven to be feasible and cost-effective, includes modern molecular techniques for pathologists and requires more communication between surgeons, pathologists and clinical geneticists [15, 21]. To introduce the MIPA procedure in community hospitals, an implementation strategy was developed, tailored to barriers found in a feasibility study [21]. The aim of the present study was to determine the effects and costs of this implementation. The secondary aim was to determine which elements of the implementation were particularly successful.

Patients and methods

Study design

The MIPA study was a cluster-randomised controlled trial in 12 pathology laboratories and the 29 community hospitals in their catchment area, examining the effectiveness of a tailored implementation strategy for the MIPA procedure compared to standard implementation. The Committee on Research Involving Human Subjects Region Arnhem–Nijmegen approved the study and waived the need for written consent from patients (project approval 2004/156).

Patients

Patients recently diagnosed with CRC were eligible for inclusion. Selection criteria for MSI testing, the MIPA criteria, were derived from the internationally used Bethesda guidelines as described [15]. The following tumours were included as associated with Lynch syndrome: carcinomas of endometrium, ovary, small bowel, stomach, biliary tract, upper urinary tract and sebaceous gland [5]. The nationwide electronic registry for pathology in the Netherlands, PALGA [22], was used for the identification

of tumours that fulfilled the selection criteria. After closing the study, 279 patients turned out to have been eligible for inclusion between September 2005 and December 2006.

Randomisation

Randomisation was done at the level of the pathology laboratories (clusters).

Intervention

All surgeons and pathologists received written information on the new procedure for recognition of Lynch syndrome, as published articles and a guideline. In the intervention group, pathologists were also provided with electronic patient inclusion reminders (monthly), feedback on inclusion (every 3 month) and supporting materials such as small cards with the selection criteria, a list to register MSI-positive tumours and a folder to save information of MSI applications. Surgeons received a 1-h interactive small-scale education session with a lecture and discussion concerning how and when to tell a patient about a positive MSI test result. Surgeons also received reminders in the patient record, consisting of a sticker with a checklist of three items: (a) MSI result (positive or negative), (b) test result discussed with patient (yes or no) and (c) patient referred to cancer genetics clinic (yes or no).

Outcome measures

The primary outcome measure was the percentage of patients recognised to be at risk for Lynch syndrome. Recognition was defined as (1) patients with a positive MSI result who were referred to genetic counselling, or (2) patients with a negative MSI result, or (3) patients who were referred to genetic counselling without prior MSI application by a pathologist. The secondary outcome measures were the effectiveness of the elements directed to pathologists and surgeons [2].

Costs of implementation strategy

To gather data about the costs of the elements of the implementation strategy, surgeons, pathologists and the research team provided time estimates. These volumes were multiplied by standardised unit costs [23]. Because these unit costs were established in 2003, they were adjusted to 2007 by using the Consumer Price Index as published by the Central Bureau of Statistics in the Netherlands (StatLine, www.statline.cbs.nl). Overhead costs were calculated as 32% of the direct costs to approximate overhead in health care. All costs were measured on a per patient basis.

Statistical analysis

Results are reported according to guidelines for reporting cluster-randomised trials [24]. To guarantee that the laboratories and their hospitals in the intervention group did not differ in pre-randomisation performance from the laboratories and hospitals in the control group regarding the outcome measure, we retrospectively analysed in both groups ‘the percentage of patients who were referred to genetic counselling without prior MSI application by a pathologist’. This concerned patients who were recently diagnosed with CRC in the participating pathology laboratories between April and December 2004. We measured only this part of the primary outcome measure because MSI testing was not initiated by the pathologists before the start of the intervention. To examine the rate of patients referred to genetic counselling, all Dutch cancer genetics clinics were asked to check whether the patients selected by PALGA had visited their hospital. The percentage of patients who received genetic counselling was 30.2% (95% confidence interval (CI) 18.5–41.8%) in the intervention and 30.4% (95% CI 17.9–42.8%) in the control group, so the pre-randomisation performance of both groups was very comparable. To ascertain successful elements of the implementation strategy, the experiences of pathologists and surgeons with the elements scored on a six-point Likert scale were dichotomised into positive or negative experience. Odds ratios were calculated to describe univariate associations between each element of the implementation strategy and the secondary outcome measure. Statistical significance was set at 5%. Analyses were performed with the SAS system for Windows V8.2.

Results

Characteristics of clusters and participants

Two hundred seventy-nine patients were eligible for recognition at risk for Lynch syndrome. In total, 13 patients were excluded from analysis because insufficient tumour material was available (n=4); patients had been diagnosed before with either Lynch syndrome (n=5) or with familial adenomatous polyposis (n=4). Therefore, the study population consisted of 266 patients: 156 patients in the intervention arm and 110 in the control arm, treated in 17 and 12 community hospitals, respectively. The characteristics of clusters and participants in the intervention and the control arm are summarised in Table 1.

Effects of implementation strategy

In Fig. 1, a flow diagram of the recognition of patients at risk for Lynch syndrome is given. Patients were recognised

Table 1 Characteristics of study population

	Intervention	Control
Clusters:		
Pathology laboratories	6	6
Hospitals	17	12
Patients:	156	110
CRC below the age of 50 years	118 (76%)	78 (71%)
Second CRC below the age of 70 years	26 (17%)	18 (16%)
CRC and extracolonic cancer below the age of 70 years[a]	7 (4%)	2 (2%)
Colorectal adenoma with high-grade dysplasia below the age of 40 years	5 (3%)	12 (11%)
Age at diagnosis	48.2 (SD=9.8)	46.2 (SD=9.7)

[a] Extracolonic cancers: malignancies associated with Lynch syndrome (endometrial, ovaries, small bowel, stomach, sebaceous gland, biliary tract and upper urinary tract)

as at risk for Lynch syndrome significantly more often in the intervention arm compared to the control arm, 120 out of 156 (77%) patients and 65 out of 110 (59%) patients, respectively, with a for clustering adjusted OR=2.8 (95% CI 1.1–7.0). Pathologists in the intervention arm applied MSI testing to 116 out of 156 patients (74%) and pathologists in the control arm to 56 out of 110 patients (51%). This 23% difference in applying MSI testing between the intervention and control arm was significant as well, adjusted OR=4.1 (95% CI 1.3–13.2). Surgeons from the intervention arm referred as many patients with an MSI-positive tumour to genetic counselling as those in the control arm: 14 out of 19 (74%) patients and 7 out of 11 (64%) patients, respectively, OR=1.6 (95% CI 0.09–7.9).

Successful elements of implementation strategy

Five out of six pathologists experienced the electronic patient inclusion reminder system useful, but none of the pathologists thought that the feedback on inclusion every 3 months improved application of MSI testing. The pathologist who scored our electronic reminders as not effective used a self-developed electronic patient inclusion reminder system and actually meant that receiving our

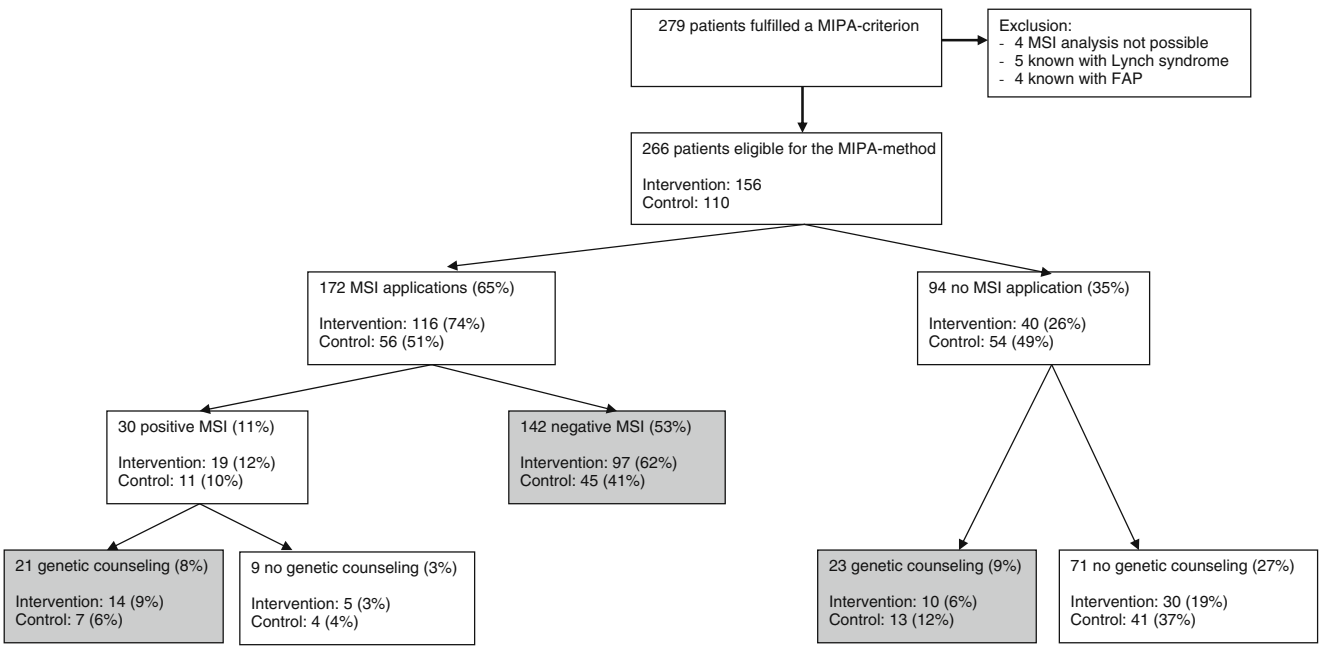

Fig. 1 Flow diagram of the recognition of patients at risk for Lynch syndrome

electronic reminders was not of additional value. Furthermore, it appeared that two pathology laboratories of the control arm had developed a reminder system very similar to the one provided in the intervention arm by themselves. The availability of an electronic patient inclusion reminder system was highly associated with the detection of patients at risk for Lynch syndrome: 156 out of 204 (76%) and 29 out of 62 (47%) with and without an electronic patient inclusion reminder system, respectively (clustering adjusted OR=4.2 (95% CI 1.7–10.1)). All pathologists agreed with the need for a reminder system because only a small subset (about 13%) of patients with CRC fulfils the criteria for MSI testing [15] and therefore referring a case for MSI testing can easily be forgotten. Nevertheless, MSI testing was applied in only 75% of eligible tumours from pathology laboratories with an electronic reminder system. According to interviews with the pathologists, barriers to application of MSI testing were time constraints and absence of the pathologist who was primarily responsible for application of MSI testing. Because the intervention directed to surgeons was not significantly effective, it was not possible to determine successful elements at this level.

Costs of implementation strategy

The costs of the elements of the intervention are presented in Table 2. The total costs per patient at risk for Lynch syndrome were €78 for the intervention and €11 for the control arm. The implementation and or running costs of the electronic patient inclusion reminder system for pathologists was €27 per patient at risk.

Discussion

This study shows that a simple electronic reminder system for pathologists markedly increases adherence to the MIPA procedure, a multidisciplinary guideline for recognition of CRC patients at high risk for Lynch syndrome. With surprisingly little effort and at low costs, multidisciplinary implementation of an entirely novel practice role for pathologists was improved. The efficiency of counselling by a clinical geneticist is greatly enhanced when patients with an MSI-high CRC are being referred for Lynch syndrome. This is due to the fact that especially patients with a positive MSI test are at very high risk to be mutation carriers, whereas a clinical geneticist has little to offer to a young patient with an MSI-negative CRC, unless the presence of polyposis or a positive family history clearly points at a hereditary defect. Our results may have a larger impact on health care because use of an electronic reminder system can increase adherence to guidelines of other hereditary diseases too.

To our knowledge, this is the first study of an implementation strategy designed to improve the recognition of patients at risk for Lynch syndrome by tumour

Table 2 Costs of development and execution of elements in euros

Elements	Total cost per element		Intervention arm	Control arm
	Total cost of development	Total cost of execution	Costs of execution per patient	Costs of execution per patient
Dissemination of MIPA method	1,586	792	1[b]	1[b]
Introduction of MIPA method	–	5,996	10[b]	10[b]
Directed to pathologists:				
Supporting materials[a]	39	164	1[c]	–
Electronic reminders	–	4,260	27[d]	–
Feedback	–	568	4[d]	–
Directed to surgeons:				
Education	2,238	6,128	20[c]	–
Reminders in surgical record	373	1,520	16[e]	–
Total	4,235	19,428	78[b]	11[b]

See "Costs of implementation strategy" in the "Patients and method" section

[a] Supporting materials include: folder, card with selection criteria, list for calling clinicians

[b] Total cost of execution of element divided by 600 patients

[c] Total cost of execution of element divided by 300 patients

[d] Total cost of execution of element divided by 156 patients

[e] Total cost of execution of element divided by 39

testing. One year before the introduction of the MIPA procedure, only 30% of the patients at risk for Lynch syndrome was recognised as such by the traditional procedure based on signalling familial occurrence of colorectal cancer [25]. This low number is in line with other studies showing that family history is insufficient for recognising patients at risk for Lynch syndrome [11–14]. After introduction of the MIPA procedure in multidisciplinary teams including surgeons and pathologists by written materials, the recognition of patients at risk for Lynch syndrome was substantially higher, namely 59%. In the tailored implementation group, this recognition was even 77%. This difference between control and intervention group is relatively large. In a review including 235 controlled studies, Grimshaw [2] studied the effectiveness of strategies to implement clinical guidelines. Overall, the majority of studies observed modest improvements in care of only 5–10%.

In the present study, the pathologists in the intervention arm obtained an overview of eligible patients only once a month. It is expected that the MSI analysis would be applied even more often, when the pathologist would get a pop-up with the possibility to initiate MSI testing at the moment of authorising the pathology report.

The surgeon-directed intervention led to 74% referrals of patients with an MSI-positive tumour. This was not significantly larger than in the control group (64%) probably because of small numbers. It is plausible that a referral rate of 74% is fairly optimal because not all patients with an MSI-positive tumour are capable or willing to receive genetic counselling at the time colorectal cancer is diagnosed and treated. Our results are in line with previous data showing that 78% of patients with CRC would accept genetic counselling shortly after diagnosis [26].

Based on the Bethesda criteria, originally four MIPA criteria have been defined. However, only two of these criteria appeared to be fulfilled within our study. Therefore, we suggest restricting the MIPA criteria to the following two criteria: (1) CRC diagnosed before age 50 and (2) second CRC before age 70.

A limitation of the study is that the patient's visit to a cancer genetics clinic for genetic counselling was measured until 6 months after the CRC diagnosis of the last patient. It is possible that more patients will receive genetic counselling in the near future. However, as it is unlikely that this effect differs between the two groups, this will not affect the conclusion that the intervention leads to a higher rate of adherence to the guideline.

Our findings indicate that a surprisingly simple and cheap electronic patient inclusion reminder system for medical specialists is effective for adherence to a complex multidisciplinary procedure for recognition of Lynch syndrome. The implications for health care can be substantially and are of course not restricted to patients at risk for Lynch syndrome. Our approach can serve as a model for implementation of guidelines in other hereditary diseases.

Acknowledgement The following pathology laboratories and Dutch hospitals are kindly thanked for their cooperation: Meander Medical Centre Amersfoort, Alysis zorggroep Arnhem, HagaZiekenhuis The Hague, Albert Schweitzer Hospital Dordrecht, Catharina Hospital Eindhoven, Medisch Spectrum Twente Enschede, Elkerliek Hospital Helmond, Medical Centre Leeuwarden, Canisius Wilhelmina Hospital Nijmegen, Medical Centre Rijnmond Zuid Rotterdam, Jeroen Bosch Hospital 's-Hertogenbosch and St Elisabeth Hospital Tilburg. The Department of Human Genetics of University Hospital Maastricht, Erasmus MC Rotterdam, University Medical Centre Groningen, University Medical Centre Utrecht and Leiden University Medical Centre are thanked for checking referrals to genetic counselling.

Conflict of interest statement We declare that we have no conflict of interest.

Funding This work was supported by a financial grant from the Netherlands Organisation for Health Research and Development (ZonMW).

Open Access This article is distributed under the terms of the Creative Commons Attribution Noncommercial License which permits any noncommercial use, distribution, and reproduction in any medium, provided the original author(s) and source are credited.

References

1. Grol R, Grimshaw J (2003) From best evidence to best practice: effective implementation of change in patients' care. Lancet 362:1225–1230
2. Grimshaw JM, Thomas RE, Maclennan G et al (2004) Effectiveness and efficiency of guideline dissemination and implementation strategies. Health Technol Assess 8:1–72
3. Shaw B, Cheater F, Baker R et al (2005) Tailored interventions to overcome identified barriers to change: effects on professional practice and health care outcomes. Cochrane Database Syst Rev 2005:CD005470
4. Jass JR (2006) Hereditary non-polyposis colorectal cancer: the rise and fall of a confusing term. World J Gastroenterol 12:4943–4950
5. Lynch HT, de la Chapelle A (2003) Hereditary colorectal cancer. N Engl J Med 348:919–932
6. Aaltonen LA, Salovaara R, Kristo P et al (1998) Incidence of hereditary nonpolyposis colorectal cancer and the feasibility of molecular screening for the disease. N Engl J Med 338:1481–1487
7. Barnetson RA, Tenesa A, Farrington SM et al (2006) Identification and survival of carriers of mutations in DNA mismatch-repair genes in colon cancer. N Engl J Med 354:2751–2763
8. Cunningham JM, Kim CY, Christensen ER et al (2001) The frequency of hereditary defective mismatch repair in a prospective series of unselected colorectal carcinomas. Am J Hum Genet 69:780–790
9. Hampel H, Frankel WL, Martin E et al (2005) Screening for the Lynch syndrome [hereditary nonpolyposis colorectal cancer]. N Engl J Med 352:1851–1860

10. Jarvinen HJ, Aarnio M, Mustonen H et al (2000) Controlled 15-year trial on screening for colorectal cancer in families with hereditary nonpolyposis colorectal cancer. Gastroenterology 118:829–834
11. Church J, McGannon E (2000) Family history of colorectal cancer: how often and how accurately is it recorded? Dis Colon Rectum 43:1540–1544
12. Grover S, Stoffel EM, Bussone L et al (2004) Physician assessment of family cancer history and referral for genetic evaluation in colorectal cancer patients. Clin Gastroenterol Hepatol 22:813–819
13. Katballe N, Juul S, Christensen M et al (2001) Patient accuracy of reporting on hereditary non-polyposis colorectal cancer-related malignancy in family members. Br J Surg 88:1228–1233
14. Sijmons RH, Boonstra AE, Reefhuis J et al (2000) Accuracy of family history of cancer: clinical genetic implications. Eur J Hum Genet 8:181–186
15. Kievit W, de Bruin JH, Adang EM et al (2005) Cost effectiveness of a new strategy to identify HNPCC patients. Gut 54:97–102
16. Niessen RC, Berends MJ, Wu Y et al (2006) Identification of mismatch repair gene mutations in young colorectal cancer patients and patients with multiple HNPCC-associated tumours. Gut 55:1781–1788
17. Overbeek LI, Kets CM, Hebeda KM et al (2007) Patients with an unexplained microsatellite instable tumour have a low risk of familial cancer. Br J Cancer 96:1605–1612
18. Vasen HF, van Ballegooijen M, Buskens E et al (1998) A cost-effectiveness analysis of colorectal screening of hereditary non-polyposis colorectal carcinoma gene carriers. Cancer 82:1632–1637
19. Rodriguez-Bigas MA, Boland CR, Hamilton SR et al (1997) A National Cancer Institute Workshop on Hereditary Nonpolyposis Colorectal Cancer Syndrome: meeting highlights and Bethesda guidelines. J Natl Cancer Inst 89:1758–1762
20. Umar A, Boland CR, Terdiman JP et al (2004) Revised Bethesda guidelines for hereditary nonpolyposis colorectal cancer [Lynch syndrome] and microsatellite instability. J Natl Cancer Inst 96:261–268
21. de Bruin JH, Kievit W, Ligtenberg MJ et al (2005) More hereditary intestinal cancer can be detected if patients with colorectal carcinoma that are selected by the pathologist are examined for microsatellite instability. Ned Tijdschr Geneeskd 149:1792–1798
22. Casparie M, Tiebosch AT, Burger G et al (2007) Pathology databanking and biobanking in The Netherlands, a central role for PALGA, the nationwide histopathology and cytopathology data network and archive. Cell Oncol 29:19–24
23. Oostenbrink JB, Bouwmans CAM, Koopmanschap MA, Rutten FFH. (2004) Handleiding voor kostenonderzoek, methoden en standaard kostprijzen voor economische evaluaties in de gezondheidszorg. 2008, College voor zorgverzekeringen
24. Campbell MK, Elbourne DR, Altman DG (2004) CONSORT statement: extension to cluster randomised trials. BMJ 328:702–708
25. Overbeek LI, Hoogerbrugge N, van Krieken JH et al (2008) Most patients with colorectal tumors at young age do not visit a cancer genetics clinic. Dis Colon Rectum 51:1249–1254
26. Porteous M, Dunckley M, Appleton S et al (2003) Is it acceptable to approach colorectal cancer patients at diagnosis to discuss genetic testing? A pilot study. Br J Cancer 89:1400–1402

Virchows Arch (2010) 456:661–670
DOI 10.1007/s00428-010-0919-3

ORIGINAL ARTICLE

Nonconventional papillary thyroid carcinomas with pleomorphic tumor giant cells: a diagnostic pitfall with anaplastic carcinoma

Juliette Hommell-Fontaine · Angela Borda · Florence Ragage · Nicole Berger · Myriam Decaussin-Petrucci

Received: 22 January 2010 / Revised: 17 March 2010 / Accepted: 1 April 2010 / Published online: 23 April 2010
© Springer-Verlag 2010

Abstract The presence of pleomorphic tumor giant cells in thyroid carcinomas of follicular cell origin is always worrisome for the pathologist as they first of all refer to anaplastic carcinoma, one of the most aggressive human malignancies. However, non-anaplastic pleomorphic giant cells are well described in other thyroid diseases, most often benign. In this paper, we describe four cases of papillary thyroid carcinoma displaying pleomorphic tumor giant cells with features that differ from those of anaplastic carcinoma. Pleomorphic giant cells were admixed with the underlying thyroid carcinoma and constituted from 5% to 25% of the tumor. Cytologically, they had an abundant eosinophilic cytoplasm with large and irregular nuclei. Compared to pleomorphic giant cells of anaplastic carcinoma, they reproduced the growth pattern of the underlying carcinoma, had a low mitotic index without necrosis or inflammation, and were reactive with thyroglobulin and thyroid-specific transcription factor-1 and strongly and diffusely positive for cytokeratin AE1/AE3. After 16–84 months of follow-up, patients are relapse-free and still alive. These cases show that pleomorphic tumor giant cells arising in papillary thyroid carcinomas do not always represent dedifferentiation and progression to anaplastic carcinoma. Distinction among these processes is critical as their treatment and prognosis are very different.

Keywords Thyroid neoplasm · Anaplastic carcinoma · Papillary carcinoma · Giant cells

J. Hommell-Fontaine · F. Ragage · N. Berger · M. Decaussin-Petrucci
Department of Pathology, Centre Hospitalier Lyon-Sud, Hospices Civils de Lyon, Université Claude Bernard Lyon I, Pierre Bénite, France

A. Borda
Department of Pathology, University of Medicine and Pharmacy, Targu Mures, Romania

M. Decaussin-Petrucci (✉)
Service d'anatomie pathologique, Centre Hospitalier Lyon Sud, 69495 Pierre Bénite cedex, France
e-mail: myriam.decaussin-petrucci@chu-lyon.fr

Introduction

Thyroid cancers account for approximately 1% of all malignancies and are the most common malignancies of the endocrine system [1]. Among thyroid carcinomas of follicular cell origin, anaplastic carcinoma is one of the most aggressive human malignancies. Three main morphological patterns exist, designed as squamoid, spindle and giant cells [1–3]. Therefore, the presence of pleomorphic tumor giant cells in thyroid lesions of follicular cell origin is always worrisome for the pathologist as they usually refer to this undifferentiated carcinoma that carries a dismal prognosis.

However, pleomorphic giant cells observed in thyroid lesions of follicular cell origin are not always tumor cells and do not always represent dedifferentiation and progression to anaplastic carcinoma. Indeed, non-neoplastic pleomorphic giant cells are sometimes observed in non-neoplastic thyroid diseases such as thyroid hyperplasia (dyshormonogenetic goiter, endemic goiter, multinodular goiter) or Hashimoto's disease [2, 4–6]. Moreover, pleomorphic tumor giant cells with bizarre nuclear features are well described in follicular adenoma and oncocytic adenoma; such atypia is not indicative of malignancy by themselves [1, 2, 7–9]. These pleomorphic giant cells with bizarre nuclear features must be

distinguished from the multinucleated giant cells of histiocytic origin described in a variety of inflammatory, hyperplastic or neoplastic thyroid diseases such as palpation thyroiditis, granulomatous thyroiditis and follicular variant of papillary carcinoma [1, 4].

Non-anaplastic pleomorphic tumor giant cells rarely occur in well-differentiated (papillary and follicular carcinomas) or poorly differentiated thyroid carcinomas, and this change is not really described in the literature. Thus, when they are incidentally found in a papillary carcinoma, pleomorphic giant cells first of all refer to the "papillary carcinoma with spindle and giant cell carcinoma" as mentioned in the last WHO classification of thyroid tumors, corresponding to a papillary carcinoma with a focal undifferentiated component [1, 10].

In this paper, we describe four cases of papillary thyroid carcinoma associated with pleomorphic tumor giant cells. The clinical, morphological, immunohistochemical and prognostic features that suggest these giant cells do not represent dedifferentiation to anaplastic carcinoma are described, and the origin of this unusual change is discussed.

Materials and methods

Four cases of thyroid carcinoma of follicular cell origin associated with pleomorphic giant cells diagnosed between 2002 and 2008 are presented. The cases were selected from the surgical files and consultation archives of the Department of Pathology, Centre Hospitalier Lyon-Sud (HCL, Lyon, France). Clinical information was obtained for each patient. Tissues have been fixed in Bouin liquid (case 1), 10% buffered formalin (cases 2 and 3) or Excell + (Microm, Francheville, France) (case 4) and embedded in paraffin. Available hematoxylin–phloxine–saffron (HPS)-stained slides were reviewed in all cases and a representative paraffin block was selected for immunohistochemistry in each case. The immunohistochemical staining was performed on 4-µm-thick sections using the labeled streptavidin–biotin method from a commercially available kit (Ventana *i*View DAB Detection Kit) on the Ventana Nexes automated stainer (Ventana, Illkirch, France). Heat-induced antigen retrieval was carried out for each antibody (except for thyroglobulin antibody) at 98°C using specific buffers. Sections were incubated for 30 minutes with the primary antibodies (Table 1). Positive and negative controls were used for each antibody. Evaluation included (i) the percentage of positively stained cells which was considered as negative (when <5%), 1+ (when 5–30%), 2+ (when 30–60%), 3+ (when >60%) and (ii) the staining intensity of the positive cells which was ranked as weak, moderate or strong.

Results

Clinical findings

The clinical findings are summarized in Table 2.

Patient ages ranged from 20 to 48 years (mean, 36 years) with a male-to-female ratio of 1:3. Three patients presented a large thyroid nodule, the other a multinodular goiter. On initial consultation, two patients had compression signs. All patients were euthyroid at the time of the diagnosis. Two patients had a fine-needle aspiration cytology: the suggested diagnosis was a follicular variant of papillary carcinoma in one case and a medullary carcinoma in the other case. All patients underwent total thyroidectomy (along with a central and jugulocarotid lymph node dissection in one of them), ^{131}I ablation and thyroid-stimulating hormone suppression therapy. All patients remain relapse-free and are still alive after 22–90 months of follow-up (mean, 52 months).

Pathologic findings

The pathologic findings are summarized in Table 3.

The nodules varied in size from 4 to 6.5 cm. They were whitish in colour, well-circumscribed, firm or soft, encapsulated, without extension to adjacent organs. One nodule contained foci of necrosis.

Histologically, all lesions were unique, encapsulated and confined to the thyroid. Surgical resection was complete in all cases. Lesions were classified according to the most recent WHO classification of thyroid tumors, taking into account the recommendations made in Turin [1, 11].

Case 1 was a poorly differentiated carcinoma arising from a papillary carcinoma. An insular pattern of growth was present in about 70% of the tumor. It was made up of well-defined nests of tumor cells, separated by artefactual clefts and associated with foci of necrosis. Tumor cells were small and uniform. The nuclei were round and lacked the conventional nuclear features of papillary carcinoma. The mitotic index was estimated at 3 mitoses per 10 HPF and atypical mitoses were present. Capsular invasion and intracapsular vascular invasion were observed. The insular pattern of growth was associated with a residual component of papillary carcinoma that displayed a papillary and follicular pattern of growth with tumor cells having conventional nuclear features of papillary thyroid carcinoma.

Cases 2 and 3 corresponded to a solid variant of papillary carcinoma. The lesions showed a solid and trabecular pattern of growth associated with areas of follicular architecture. There was no necrosis. Conventional nuclear features of papillary carcinoma were present both in the solid/trabecular and in the follicular pattern of growth. The mitotic index ranged from one to two mitoses per 10

Table 1 Antibodies used for immunohistochemical analysis

Antibody	Clone	Host species	Heat-induced antigen retrieval (buffer)	Dilution	Source
Pancytokeratin	AE1/AE3	mouse	+ (EDTA)	1:200	Dako, Carpinteria, CA, USA
Thyroglobulin	DAK-Tg6	mouse	-	1:1500	Dako, Glostrup, Denmark
TTF-1	8G7G3/1	mouse	+ (EDTA)	1:40	Zymed, San Francisco, CA, USA
Ki 67	MiB-1	mouse	+ (EDTA)	1:25	Dako, Glostrup, Denmark
HBME-1	HBME-1	mouse	+ (EDTA)	1:50	Dako, Carpinteria, CA, USA
Galectin-3	9C4	mouse	+ (citrate pH 6.0)	1:100	Novocastra, Newcastle, UK
CD 68	KP1	mouse	+ (EDTA)	1:2500	Dako, Glostrup, Denmark
p53	DO-1	mouse	+ (EDTA)	1:10	Immunotech, Marseille, France

HPF without atypical mitosis. Capsular invasion and intracapsular vascular invasion were observed in case 2.

Case 4 was a follicular variant of papillary carcinoma. Nuclei displayed the nuclear features of papillary carcinoma. The mitotic index was lower than one mitosis per 10 HPF without atypical mitosis. There was no vascular or capsular invasion.

The common feature of these four cases was the presence of pleomorphic giant cells mixed with follicular cells of the underlying thyroid carcinoma. In one case, they constituted only 5% of the tumor and were dispersed singly or in small clusters within the thyroid carcinoma (Fig. 1a). In the other three cases, they constituted between 10% and 25% of the tumor and they reproduced the same growth pattern as the underlying thyroid carcinoma (Fig. 1b, c). Pleomorphic giant cells were large, with a more abundant and eosinophilic cytoplasm than the follicular cells of the underlying thyroid carcinoma. Their nuclei were large, irregular and sometimes frankly monstrous, with clumped or smudged chromatin (Fig. 2a, b). Macronucleoli were sometimes observed (Fig. 2a). In all cases, some cells had prominent intranuclear invaginations of cytoplasm, so-called pseudoinclusions (Fig. 2b). Pleomorphic giant cells were often multinucleated. They were mixed with smaller mononuclear pleomorphic cells, whose nuclei had the same appearance as that of giant cells (Fig. 2a). In three cases, mitoses were observed in the pleomorphic giant cells, but the mitotic index was never higher than that of the underlying

Table 2 Clinical findings for four cases of pleomorphic giant cell proliferations in the thyroid

Case no.	1	2	3	4
Age (years)/sex	20/F	30/M	47/F	48/F
Clinical presentation	Thyroid nodule	Thyroid nodule	Multinodular goiter	Thyroid nodule
Compression signs	Hoarseness, dysphagia, tracheal deflection	Absent	Shortness of breath, hacking cough	Absent
Thyroid site	Right lobe	Left lobe	Left lobe	Left lobe
FNA	Medullary carcinoma	Follicular variant of PTC	ND	ND
Surgery	Total thyroidectomy + central and jugulo-carotid lymph node dissection	Total thyroidectomy	Total thyroidectomy	total thyroidectomy
Adjuvant therapy	^{131}I ablation and thyroid-stimulating hormone suppression therapy	^{131}I ablation and thyroid-stimulating hormone suppression therapy	^{131}I ablation and thyroid-stimulating hormone suppression therapy	^{131}I ablation and thyroid-stimulating hormone suppression therapy
Follow-up (total duration, months)	AWND (90)	AWND (75)	AWND (22)	AWND (22)

F female, *M* male, *PTC* papillary thyroid carcinoma, *FNA* fine-needle aspiration, *ND* not done, *AWND*, alive with no evidence of disease

Table 3 Pathologic findings for four cases of pleomorphic giant cell proliferations in the thyroid

Case no.		1	2	3	4
Macroscopy	Nodule size (cm)	6	4.2	6.5	4
	Capsule	Present	Present	Present	Present
Thyroid carcinoma	Histologic diagnosis	PD carcinoma arisen from a PTC	Solid variant of PTC	Solid variant of PTC	Follicular variant of PTC
	MI/×10 HPF	3	2	1	1
	Atypical mitoses	Present	Absent	Absent	Absent
	Necrosis	Present, focal	Absent	Absent	Absent
	Blood vessel invasion	Present, intracapsular	Present, intracapsular	Absent	Absent
	Capsular invasion	Present	Present	Present	Present
	Extrathyroidal extension	Absent	Absent	Absent	Absent
	Lymph node metastases	Absent	NA	NA	NA
Pleomorphic giant cells component	Giant cells distribution	Clusters and sheets	Patchy	Clusters and sheets	Clusters and sheets
	% of giant cells component of the total area	15	5	25	10
	MI/×10 HPF	3	0	1	1
	Atypical mitosis	Present	Absent	Absent	Absent
	Inflammation/necrosis	Absent	Absent	Absent	Absent
Non-neoplastic thyroid parenchyma		Thyroiditis	Nodular hyperplasia	Nodular and diffuse hyperplasia	Nodular hyperplasia

PD poorly differentiated, *PTC* papillary thyroid carcinoma, *MI* mitotic index, *NA* not applicable

thyroid carcinoma. In the case of poorly differentiated carcinoma arising from a papillary carcinoma, there were atypical mitoses in the pleomorphic giant cells as in the underlying poorly differentiated carcinoma. There was neither necrosis nor inflammation in the areas of pleomorphic giant cells.

The non-neoplastic thyroid parenchyma presented thyroiditis lesions in one case and nodular and diffuse hyperplasia in the other three cases. In the only case in which lymph node dissection was performed, no lymph node metastasis was found (21 lymph nodes examined).

Immunohistochemical findings

The immunohistochemical findings are summarized in Table 4.

Pleomorphic giant cells were diffusely and strongly positive for cytokeratin AE1/AE3, as the follicular cells of the underlying thyroid carcinoma (Fig. 3a).

Pleomorphic giant cells showed reactivity with thyroglobulin in all cases. The reactivity was focal both in the primary thyroid carcinoma and in the pleomorphic giant cells component, but the staining was stronger in the pleomorphic giant cells (Fig. 3b).

Due to the fixing-agent used, nuclear markers were assessed in only two cases, positive controls remaining negative in spite of repeated tests in the other two cases. Pleomorphic giant cells showed reactivity with thyroid-specific transcription factor-1 (TTF-1) in both cases. The nuclear staining was diffuse, strong in one case, weak in the other case, with the same intensity in the pleomorphic giant cells as in the follicular cells of the underlying carcinoma (Fig. 3c). The Ki-67 proliferation index was 2% in one case and less than 1% in the other one. In both cases, the Ki-67 proliferation index was not higher in the pleomorphic giant cells than in the primary thyroid carcinoma.

Three out of four cases were negative for p53, both in the pleomorphic giant cells component and in the underlying papillary carcinoma. In the remaining case (case 1 corresponding to a poorly differentiated carcinoma arising from a papillary carcinoma), moderate nuclear staining was found in 50% of the pleomorphic giant cells and in 50% of the follicular cells of the poorly differentiated component, whereas residual papillary carcinoma was negative (Fig. 3d). Non-neoplastic thyroid parenchyma was negative in all cases.

Pleomorphic giant cells were reactive with HBME-1 in all cases, as the associated thyroid carcinoma (Fig. 3e). The staining was heterogeneous in both components. Non-neoplastic thyroid parenchyma was negative for HBME-1 in all cases.

Pleomorphic giant cells showed reactivity with galectin-3 in two cases, with the same intensity as in the underlying thyroid carcinoma. The staining was focal in one case and diffuse in the other case. Non-neoplastic thyroid parenchyma was negative for galectine-3 in all cases.

Pleomorphic giant cells were nonreactive with the CD68 marker.

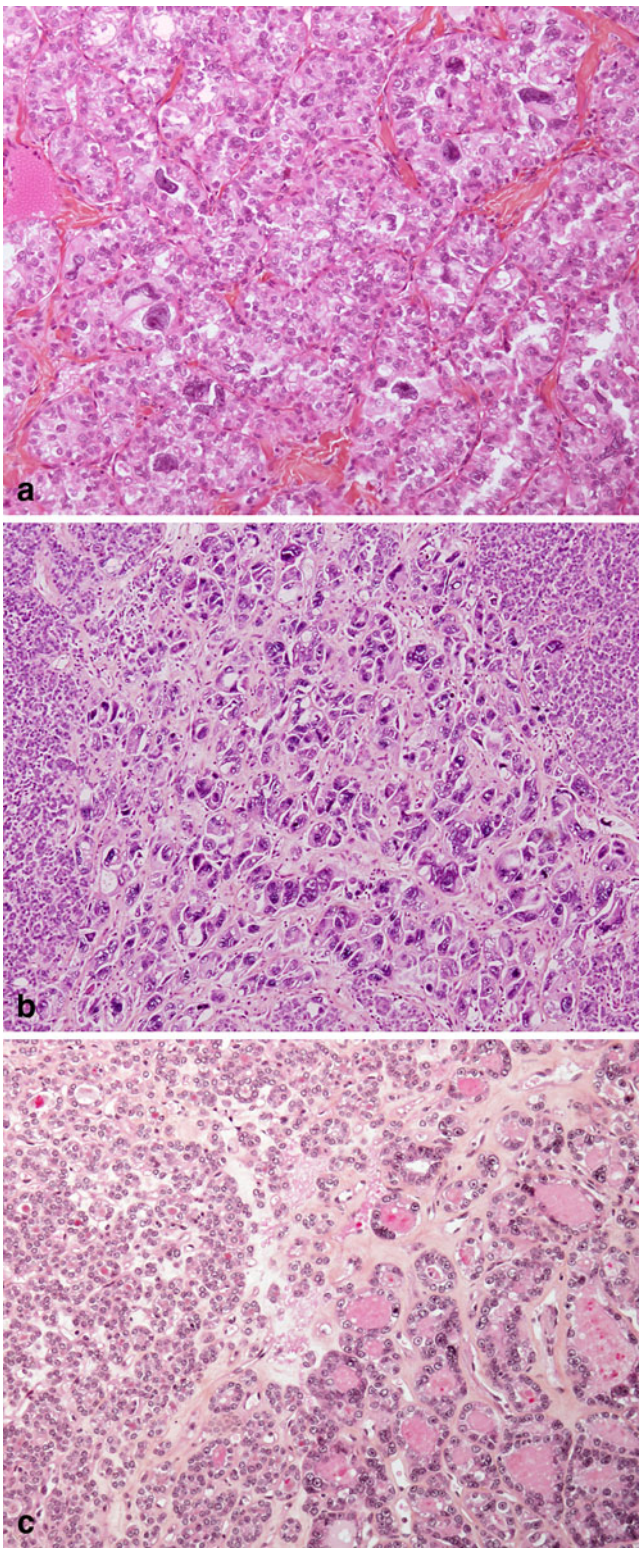

Fig. 1 Variable architectural patterns of the pleomorphic giant cells. **a** Pleomorphic giant cells are dispersed singly in a papillary thyroid carcinoma. **b** Pleomorphic giant cells are arranged in large sheets in a poorly differentiated thyroid carcinoma arising in a papillary carcinoma. **c** Pleomorphic giant cells (right) showed a follicular pattern of growth in a follicular variant of papillary thyroid carcinoma (left). HPS, ×50 (**b**) and ×100 (**a, c**)

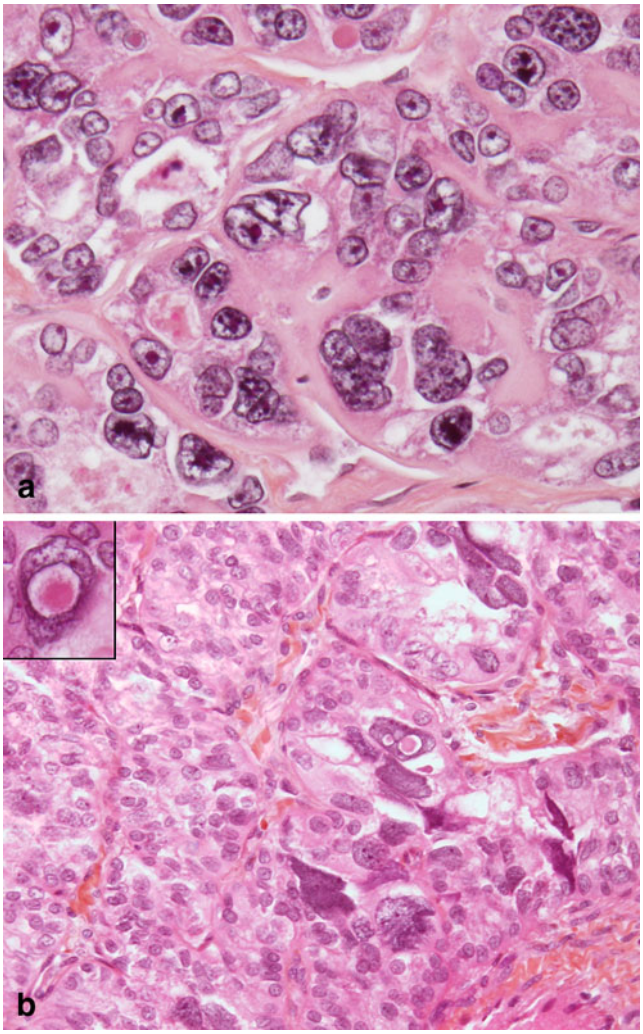

Fig. 2 Morphological patterns of the pleomorphic giant cells. **a** The pleomorphic giant cells demonstrate large and irregular (sometimes multiple) nuclei. They are mixed with smaller mononuclear pleomorphic cells. **b** Some nuclei had a smudged chromatin. A pseudoinclusion is seen in the nucleus of a giant cell (*inset*). HPS, ×200 (**b**) and ×400 (**a,** *inset*)

Discussion

The presence of pleomorphic tumor giant cells in thyroid carcinomas of follicular cell origin is always misleading and worrisome for the pathologist as it is usually associated with dedifferentiation and progression to anaplastic carcinoma, with a poor prognosis. In the giant cell variant, anaplastic carcinoma is characterized by a striking degree of pleomorphism, due to the presence of numerous pleomorphic tumor giant cells, having bizarre (sometimes multiple) hyperchromatic nuclei, abundant eosinophilic cytoplasm and a round or oval shape. These giant cells are most often mixed with smaller mononuclear tumor cells, which have otherwise similar morphological features as tumor giant cells [1–3]. Anaplastic carcinoma is

Table 4 Immunohistochemical findings for four cases of pleomorphic giant cell proliferations in the thyroid

		Thyroglobulin	TTF-1	Cytokeratin AE1/AE3	HBME-1	Galectine3	CD68	P53	Ki67 index
Case 1	Thyroid carcinoma	+ Weak	NI	+++ Strong	+++ moderate	–	–	++ Moderate	NI
	Pleomorphic giant cells component	+ Moderate	NI	+++ Strong	+++ Strong	–	–	++ Moderate	NI
Case 2	Thyroid carcinoma	+ Weak	+++ Strong	+++ Strong	+++ Strong	++ Moderate	–	–	2%
	Pleomorphic giant cells component	+ Moderate	+++ Strong	+++ Strong	+++ Strong	++ Moderate	–	–	2%
Case 3	Thyroid carcinoma	+ Moderate	+++ Moderate	+++ Strong	++ Moderate	+ Weak	–	–	1%
	Pleomorphic giant cells component	+ Strong	+++ Moderate	+++ Strong	++ Strong	+ Weak	–	–	1%
Case 4	Thyroid carcinoma	+ Moderate	NI	+++ Strong	+++ Strong	–	–	–	NI
	Pleomorphic giant cells component	+ Strong	NI	+++ Strong	+++ Strong	–	–	–	NI

–, less than 5% of positive cells; +, 5–30% of positive cells; ++, 30–60% of positive cells; +++, more than 60% of positive cells

NI not interpretable

expected to arise from a preexisting well or poorly differentiated thyroid carcinoma and it constitutes most often the bulk of the lesion. However, the component of anaplastic carcinoma may be minor, found as an incidental small focus, with the majority of the tumor mass representing a well or poorly differentiated thyroid carcinoma [3, 12, 13]. For papillary carcinoma, this variant is described in the last WHO classification of thyroid tumors and designed as "papillary carcinoma with spindle and giant cell carcinoma", corresponding to a papillary carcinoma with focal anaplastic component [1, 10]. In current literature, there is no clear guideline as how focal anaplastic should be defined. For Albores-Saavedra and Wu [10], the anaplastic component must represent less than 25% of the tumor.

In this paper, we have described four cases of papillary thyroid carcinoma with a pleomorphic giant cells component constituting from 5% to 25% of the tumor. In one case, pleomorphic giant cells were dispersed singly or in small clusters within the thyroid carcinoma. In the other three cases, they formed large ill-defined and cohesive sheets and reproduced the same growth pattern as the underlying carcinoma. However, these four cases of thyroid carcinoma do not represent dedifferentiation and progression to anaplastic carcinoma and it would be wrong to consider them as thyroid carcinomas with a focal anaplastic component.

First, the four cases described herein are very different from anaplastic thyroid carcinoma in clinical and prognostic features. Indeed, all our patients were younger than 50 years (mean, 36 years), whereas for anaplastic thyroid carcinoma the mean age at diagnosis is between 60 and 70 years with only 25% of the patients younger than 60 years [1, 2]. Concerning the prognosis, all our patients remain relapse-free and are currently alive after 22–90 months of follow-up (mean, 52 months). Yet, anaplastic thyroid carcinoma is one of the most aggressive human malignancies, with a median survival varying from 2.5 to 6 months and an overall 5-year survival ranging from 0% to 14% [1]. The prognosis of focal anaplastic carcinoma still remains uncertain [1, 10]. Some series have shown that patients with focal anaplastic carcinoma arising in well-differentiated carcinoma may have longer disease-free survival than those with classic anaplastic carcinoma [12–18]. However, some cases with focal anaplastic carcinoma having the same poor prognosis as classic anaplastic carcinoma are well described in the literature. These data usually justify local external radiotherapy after thyroidectomy [12, 14, 18, 19].

Secondly, the pleomorphic giant cells observed in our four cases are different from pleomorphic giant cells of anaplastic thyroid carcinoma in morphological and immunohistochemical features. Indeed, these pleomorphic giant cells displayed the same growth pattern as the underlying thyroid carcinoma, without necrosis or inflammatory cells. Their mitotic and proliferation indexes were never higher than in the underlying thyroid carcinoma. When atypical mitoses were observed, they were both present in pleomorphic giant cells areas and in the underlying tumor. At the opposite, an extensive necrosis, a scattering of inflammatory cells and a high mitotic activity are often present in anaplastic thyroid carcinoma [1, 2]. In immunohistochemistry, the pleomorphic giant cells described in this study were reactive with both thyroglobulin and TTF-1, indicating not only their follicular origin but above all their differentiated nature. Yet, anaplastic thyroid carcinoma is usually nonreactive with these two markers [1–3, 20, 21]. In addition, all our pleomorphic

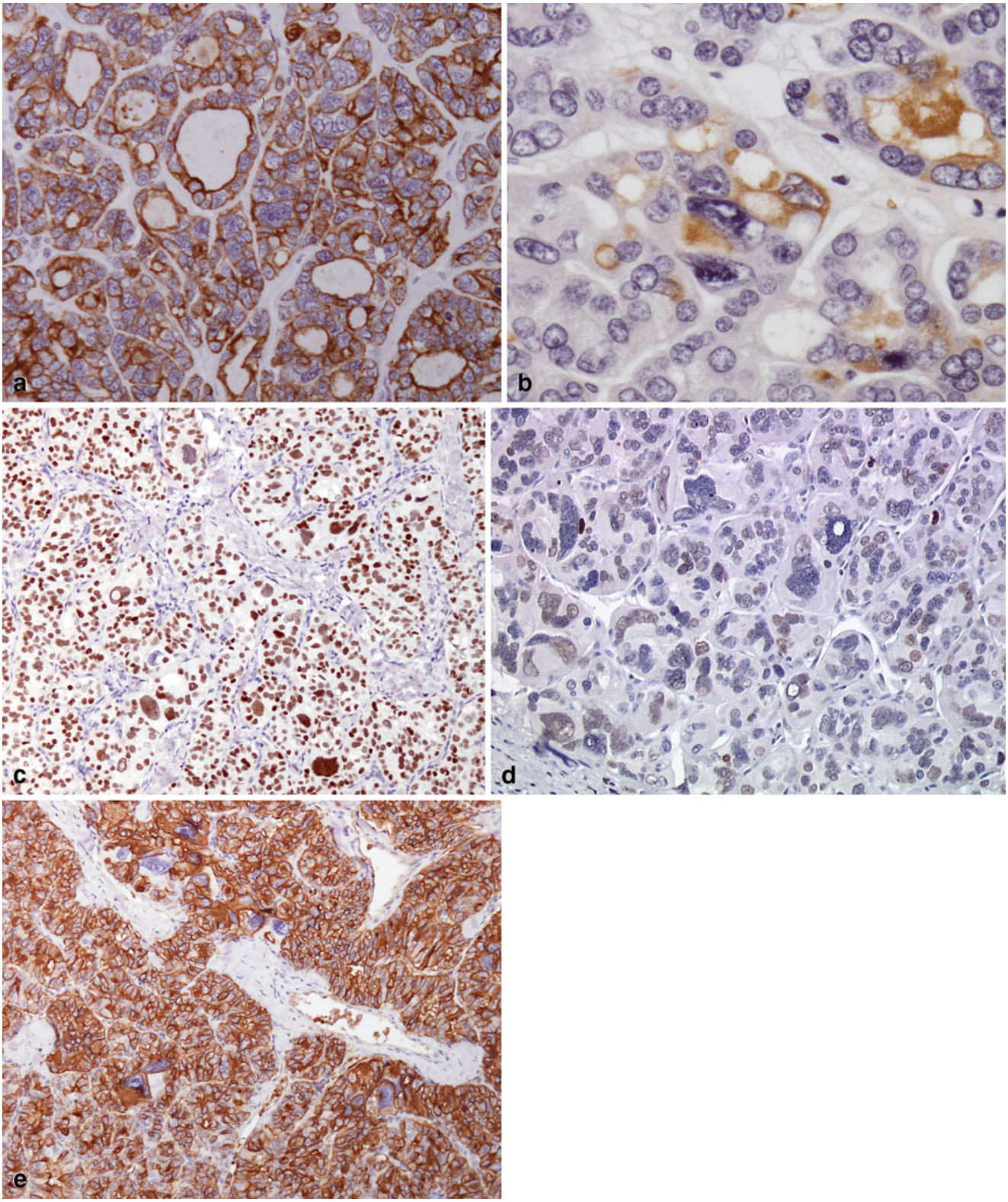

Fig. 3 Immunohistochemical analysis for AE1/AE3, thyroglobulin, TTF-1, p53 and HBME-1. **a** Pleomorphic giant cells are strongly and diffusely positive for cytokeratin AE1/AE3, with the same intensity as the follicular cells of the underlying papillary carcinoma. **b** Pleomorphic giant cells and follicular cells of the papillary carcinoma show a focal staining with thyroglobulin. **c** Pleomorphic giant cells and follicular cells of the papillary carcinoma show a strong nuclear staining with TTF-1. **d** Some pleomorphic giant cells and follicular cells show reactivity with p53 in the poorly differentiated thyroid carcinoma arising in a papillary carcinoma. **e** Pleomorphic giant cells and follicular cells of the underlying papillary carcinoma are positive for HBME-1. ×100 (**c, e**), ×200 (**a, d**) and ×400 (**b**)

giant cells were strongly and diffusely positive with the cytokeratin AE1/AE3. In contrast, expression of cytokeratin AE1/AE3 is variable in anaplastic thyroid carcinoma and the staining is usually focal in the giant cell variant [22, 23]. The pleomorphic giant cells discussed in our study were positive for HBME-1 in all cases, whereas the galectin-3 was positive only in two cases, with the same intensity both in the papillary carcinoma and in the pleomorphic giant cells component. There are few studies in the literature about the expression of HBME-1 and galectin-3 in anaplastic thyroid carcinoma. Regarding HBME-1, the negativity is the rule [24–27]. Galectine-3 is usually positive but the staining is often described as less intense than in papillary carcinoma [25, 27–34]. In the three cases of pure papillary carcinoma, pleomorphic giant cells were negative for p53. In the literature, p53 mutations are found in 0–18% of papillary carcinomas of the thyroid (mean, 5%), 17–38% of poorly differentiated carcinomas (mean, 24%) and in 20–88% of anaplastic carcinomas (mean, 59%), suggesting that p53 mutations play an important role in dedifferentiation and tumor progression of thyroid carcinomas [35]. p53 overexpression detected by immunohistochemistry is accepted to be in concordance with gene mutation in up to 95% of cases [36]. Thus, the negativity of pleomorphic giant cells in the three cases of pure papillary carcinoma confirms the differentiated nature of these cells. In the remaining case, corresponding to a poorly differentiated carcinoma arising in a papillary thyroid carcinoma, 50% of the giant cells were slightly positive for p53, but so were the follicular cells of the underlying poorly differentiated carcinoma. According to the literature, the percentage of immunoreactive cells is usually higher in anaplastic carcinoma than in poorly differentiated carcinoma [34, 37, 38]. Thus, even in this case, pleomorphic giant cells are probably not a dedifferentiation of the underlying poorly differentiated carcinoma.

Pleomorphic giant cells observed in our four cases must be distinguished from another type of giant cells described in thyroid pathology and designed as multinucleated giant cells. These multinucleated giant cells are non-neoplastic cells and have a histiocytic origin. They have been described in a variety of inflammatory, hyperplastic or neoplastic thyroid diseases, including Hashimoto's disease, multinodular goiter, follicular adenoma, granulomatous thyroiditis and palpation thyroiditis [4, 9, 39–42]. In the last WHO classification of thyroid tumors, these cells have been described as a histologic feature of the follicular variant of papillary carcinoma [1, 39, 42]. Even in anaplastic thyroid carcinoma, so-called osteoclastic-like giant cells are observed [1–3]. Both their morphological and immunohistochemical features are very different from that of pleomorphic giant cells described in our four cases. Indeed, multinucleated giant cells have multiple small nuclei devoid of atypical features and are never seen undergoing mitotic division. They are reactive with CD68 and not with cytokeratin AE1/AE3, indicating their histiocytic origin [39, 41]. However, pleomorphic giant cells described in our four cases were highly pleomorphic, with marked atypical features. They showed strong and diffuse reactivity with cytokeratin AE1/AE3 and not with CD68, indicating their epithelial origin.

Thus, pleomorphic giant cells described in our four cases are epithelial cells that neither result from a dedifferentiation to anaplastic carcinoma nor correspond to multinucleated giant cells of histiocytic origin occurring in many thyroid diseases. They seem to derive from the follicular cells of the underlying carcinoma rather than from the non-neoplastic thyroid parenchyma, so they are obviously neoplastic cells. Indeed, giant cells were intimately mixed with the neoplastic elements and reproduced their growth pattern. Moreover, the staining profile with HBME-1 and galectin-3 was the same both in the pleomorphic giant cells and in the follicular cells of the primary carcinoma, whereas it was different in the adjacent non-neoplastic thyroid parenchyma.

It is unclear why non-anaplastic pleomorphic giant cells with bizarre nuclear features develop in thyroid lesions. These changes seem to occur more often under several conditions: (i) oxyphilic cytoplasmic changes as observed in Hashimoto's disease or in oncocytic adenoma [2, 9]; (ii) after some therapies as radioactive iodine in Graves' disease or as local external radiotherapy [2, 4, 9, 43]; (iii) after fine-needle aspiration [44]. None of these conditions was present in our series. Such atypia has also been described in non-thyroid diseases, such as atypical leiomyomas [45]. For some authors, they may result from dystrophic/degenerative changes, a theory supported by the degenerative features of some of the bizarre cells [7, 9, 45]. Pleomorphic giant cells may also reflect an abnormality of DNA inherent to the neoplastic process [7].

Non-anaplastic pleomorphic tumor giant cells with bizarre nuclear features have been described in one another thyroid malignancy: the giant cell variant of medullary carcinoma [1, 2, 9, 46, 47]. This rare variant is defined by the presence of tumor giant cells with multiple nuclei and abundant eosinophilic cytoplasm. The giant cells areas are usually admixed with foci of more typical medullary carcinoma and stroma may contain amyloid deposits. These giant cells remain differentiated as they are positive for calcitonin. By analogy, the presence of non-anaplastic pleomorphic tumor giant cells in a papillary thyroid carcinoma could lead to the definition of a new variant of papillary carcinoma, the "pleomorphic giant cell variant". This variant should not be confused with the variant designed as "papillary carcinoma with spindle and giant

cell carcinoma" by the last WHO classification of thyroid tumors.

In conclusion, we have discussed that pleomorphic tumor giant cells occurring in a papillary thyroid carcinoma are not consistently synonymous to dedifferentiation and progression to anaplastic carcinoma. Clues to correct diagnosis may be obtained on morphological and immunohistological assessment. Awareness of this unusual change and its recognition are critical because treatment and prognosis are very different from those of anaplastic carcinoma.

Acknowledgement The authors would like to thank Eric Shannon for his help for the English version.

Conflict of interest statement We declare that we have no conflict of interest.

References

1. DeLellis RA, Lloyd RV, Heitz U, Eng C (2004) World Health Organization classification of tumors: pathology and genetics of tumours of endocrine organs. IARC Press, Lyon
2. Rosai J, Carcangiu ML, Delellis RA (1992) Tumors of the thyroid gland. Atlas of tumor pathology. Armed Forces Institute Pathology, Washington
3. Carcangiu ML, Steeper T, Zampi G et al (1985) Anaplastic thyroid carcinoma. A study of 70 cases. Am J Clin Pathol 83:135–158
4. Lloyd RV, Douglas BR, Young WF Jr (2002) Endocrine diseases. Atlas of nontumor pathology. Armed Forces Institute Pathology, Washington
5. Perez-Montiel MD, Suster S (2008) The spectrum of histologic changes in thyroid hyperplasia: a clinicopathologic study of 300 cases. Hum Pathol 39:1080–1087
6. Ghossein RA, Rosai J, Heffess C (1997) Dyshormonogenetic goiter: a clinicopathologic study of 56 cases. Endocr Pathol 8:283–292
7. Sato K, Shimode Y, Hirokawa M et al (2008) Thyroid adenomatous nodule with bizarre nuclei: a case report and mutation analysis of the p53 gene. Pathol Res Pract 204:191–195
8. Tzen CY, Huang YW, Fu YS (2003) Is atypical follicular adenoma of the thyroid a preinvasive malignancy? Hum Pathol 34:666–669
9. LiVolsi VA (1990) Surgical pathology of the thyroid. WB Saunders, Philadelphia
10. Albores-Saavedra J, Wu J (2006) The many faces and mimics of papillary thyroid carcinoma. Endocr Pathol 17:1–18
11. Volante M, Collini P, Nikiforov YE et al (2007) Poorly differentiated thyroid carcinoma: the Turin proposal for the use of uniform diagnostic criteria and an algorithmic diagnostic approach. Am J Surg Pathol 31:1256–1264
12. Aldinger KA, Samaan NA, Ibanez M et al (1978) Anaplastic carcinoma of the thyroid: a review of 84 cases of spindle and giant cell carcinoma of the thyroid. Cancer 41:2267–2275
13. Sugitani I, Kasai N, Fujimoto Y et al (2001) Prognostic factors and therapeutic strategy for anaplastic carcinoma of the thyroid. World J Surg 25:617–622
14. Sugino K, Ito K, Mimura T et al (2002) The important role of operations in the management of anaplastic thyroid carcinoma. Surgery 131:245–248
15. Voutilainen PE, Multanen M, Haapiainen RK et al (1999) Anaplastic thyroid carcinoma survival. World J Surg 23:975–978
16. Demeter JG, De Jong SA, Lawrence AM et al (1991) Anaplastic thyroid carcinoma: risk factors and outcome. Surgery 110:956–961
17. Pacheco-Ojeda LA, Martinez AL, Alvarez M (2001) Anaplastic thyroid carcinoma in Ecuador: analysis of prognostic factors. Int Surg 86:117–121
18. Pierie JP, Muzikansky A, Gaz RD et al (2002) The effect of surgery and radiotherapy on outcome of anaplastic thyroid carcinoma. Ann Surg Oncol 9:57–64
19. Wemeau JL, Do Cao C (2008) Anaplastic thyroid carcinoma. Ann Endocrinol 69:174–180
20. Fabbro D, Di Loreto C, Beltrami CA et al (1994) Expression of thyroid-specific transcription factors TTF-1 and PAX-8 in human thyroid neoplasms. Cancer Res 54:4744–4749
21. Miettinen M, Franssila KO (2000) Variable expression of keratins and nearly uniform lack of thyroid transcription factor 1 in thyroid anaplastic carcinoma. Hum Pathol 31:1139–1145
22. Ordonez NG, El-Naggar AK, Hickey RC et al (1991) Anaplastic thyroid carcinoma. Immunocytochemical study of 32 cases. Am J Clin Pathol 96:15–24
23. Venkatesh YS, Ordonez NG, Schultz PN et al (1990) Anaplastic carcinoma of the thyroid. A clinicopathologic study of 121 cases. Cancer 66:321–330
24. Cheung CC, Ezzat S, Freeman JL et al (2001) Immunohistochemical diagnosis of papillary thyroid carcinoma. Mod Pathol 14:338–342
25. de Matos PS, Ferreira AP, de Oliveira FF et al (2005) Usefulness of HBME-1, cytokeratin 19 and galectin-3 immunostaining in the diagnosis of thyroid malignancy. Histopathology 47:391–401
26. Mase T, Funahashi H, Koshikawa T et al (2003) HBME-1 immunostaining in thyroid tumors especially in follicular neoplasm. Endocr J 50:173–177
27. Prasad ML, Pellegata NS, Huang Y et al (2005) Galectin-3, fibronectin-1, CITED-1, HBME1 and cytokeratin-19 immunohistochemistry is useful for the differential diagnosis of thyroid tumors. Mod Pathol 18:48–57
28. Cvejic D, Savin S, Paunovic I et al (1998) Immunohistochemical localization of galectin-3 in malignant and benign human thyroid tissue. Anticancer Res 18:2637–2641
29. Fernandez PL, Merino MJ, Gomez M et al (1997) Galectin-3 and laminin expression in neoplastic and non-neoplastic thyroid tissue. J Pathol 181:80–86
30. Gasbarri A, Martegani MP, Del Prete F et al (1999) Galectin-3 and CD44v6 isoforms in the preoperative evaluation of thyroid nodules. J Clin Oncol 17:3494–3502
31. Inohara H, Honjo Y, Yoshii T et al (1999) Expression of galectin-3 in fine-needle aspirates as a diagnostic marker differentiating benign from malignant thyroid neoplasms. Cancer 85:2475–2484
32. Beesley MF, McLaren KM (2002) Cytokeratin 19 and galectin-3 immunohistochemistry in the differential diagnosis of solitary thyroid nodules. Histopathology 41:236–243
33. Herrmann ME, LiVolsi VA, Pasha TL et al (2002) Immunohistochemical expression of galectin-3 in benign and malignant thyroid lesions. Arch Pathol Lab Med 126:710–713
34. Aratake Y, Nomura H, Kotani T et al (2006) Coexistent anaplastic and differentiated thyroid carcinoma. Am J Clin Pathol 125:399–406
35. Nikiforov YE (2004) Genetic alterations involved in the transition from well-differentiated to poorly differentiated and anaplastic thyroid carcinomas. Endocr Pathol 15:319–327
36. Zafon C, Obiols G, Castellvi J et al (2007) Clinical significance of RET/PTC and p53 protein expression in sporadic papillary thyroid carcinoma. Histopathology 50:225–231
37. Pilotti S, Collini P, Del Bo R et al (1994) A novel panel of antibodies that segregates immunocytochemically poorly differentiated carcinoma from undifferentiated carcinoma of the thyroid gland. Am J Surg Pathol 18:1054–1064

38. Soares P, Cameselle-Teijeiro J, Sobrinho-Simoes M (1994) Immunohistochemical detection of p53 in differentiated, poorly differentiated and undifferentiated carcinomas of the thyroid. Histopathology 24:205–210
39. Guiter GE, DeLellis RA (1996) Multinucleate giant cells in papillary thyroid carcinoma. A morphologic and immunohistochemical study. Am J Clin Pathol 106:765–768
40. Shabb NS, Tawil A, Gergeos F et al (1999) Multinucleated giant cells in fine-needle aspiration of thyroid nodules: their diagnostic significance. Diagn Cytopathol 21:307–312
41. Tabbara SO, Acoury N, Sidawy MK (1996) Multinucleated giant cells in thyroid neoplasms. A cytologic, histologic and immunohistochemical study. Acta Cytol 40:1184–1188
42. Tsou PL, Hsiao YL, Chang TC (2002) Multinucleated giant cells in fine needle aspirates. Can they help differentiate papillary thyroid cancer from benign nodular goiter? Acta Cytol 46:823–827
43. Granter SR, Cibas ES (1997) Cytologic findings in thyroid nodules after 131I treatment of hyperthyroidism. Am J Clin Pathol 107:20–25
44. Polyzos SA, Patsiaoura K, Zachou K (2009) Histological alterations following thyroid fine needle biopsy: a systematic review. Diagn Cytopathol 37:455–465
45. Downes KA, Hart WR (1997) Bizarre leiomyomas of the uterus: a comprehensive pathologic study of 24 cases with long-term follow-up. Am J Surg Pathol 21:1261–1270
46. Kakudo K, Miyauchi A, Ogihara T et al (1978) Medullary carcinoma of the thyroid. Giant cell type. Arch Pathol Lab Med 102:445–447
47. Mendelsohn G, Baylin SB, Bigner SH et al (1980) Anaplastic variants of medullary thyroid carcinoma: a light-microscopic and immunohistochemical study. Am J Surg Pathol 4:333–341

Virchows Arch (2010) 456:671–679
DOI 10.1007/s00428-010-0922-8

ORIGINAL ARTICLE

A novel quantitative PCR of proliferation markers (Ki-67, topoisomerase IIα, and TPX2): an immunohistochemical correlation, testing, and optimizing for mantle cell lymphoma

Helena Brizova · Marketa Kalinova · Lenka Krskova · Marcela Mrhalova · Roman Kodet

Received: 27 January 2010 / Revised: 18 March 2010 / Accepted: 6 April 2010 / Published online: 24 April 2010
© Springer-Verlag 2010

Abstract A clinical course of patients with mantle cell lymphoma (MCL) is aggressive, and the disease is rarely curable. Proliferation rate is the most important prognostic factor. We developed a novel, reliable, rapid, and routinely applicable approach allowing a precise quantitative assessment of three proliferation markers, Ki-67, topoisomerase IIα, and TPX2. A total of 95 lymphoma specimens were measured in the study by real-time reverse transcription PCR (RQ-RT-PCR). We tested the reproducibility and accuracy of the assay and correlated the results with the immunohistochemical staining of the corresponding proteins. The results obtained indicated individual variability of the mRNA expression levels, reflecting heterogeneity of the proliferation rate in individual patients. In general, we observed the highest mRNA expression in the group of Burkitt lymphomas and the lowest in patients with reactive lymphadenopathies. We found increased proliferation rate in MCLs with high cyclin D1 mRNA, indicating a quantitative control of the cell cycle. We observed a correlation between mRNA expression level and the immunohistochemical staining of corresponding proteins, which significantly argues for the prognostic significance of the mRNA expression measuring. We confirmed the accuracy of the current assay for a precise quantitative examination of the proliferation activity. Real-time RT-PCR provides a novel approach applicable for clinical trials, and it represents a potent approach allowing to stratify MCL patients for entry into clinical trials according to the expression of the proliferation signature genes in their tumors. This approach may contribute to improved and individualized therapeutic options respecting the individual progression risk of patients with MCL.

Keywords Real-time PCR · Proliferation markers · Ki-67 · Topoisomerase IIα · TPX2 · Mantle cell lymphoma · Mol Pathol · Quantitative Path · Lymphoma

H. Brizova (✉) · M. Kalinova · L. Krskova · M. Mrhalova · R. Kodet
Department of Pathology and Molecular Medicine,
2nd Medical School, Charles University in Prague
and Faculty Hospital in Motol,
V Úvalu 84,
150 06 Prague 5, Czech Republic
e-mail: helena.brizova@fnmotol.cz

Introduction

Mantle cell lymphoma (MCL) is a morphologically and immunophenotypically defined B cell non-Hodgkin's lymphoma (B-NHL) [1] characterized by t(11;14)(q13;q32), leading to the cyclin D1 overexpression. MCL accounts for 3–10% of B-NHLs in adults, with a predominance in elderly males with median age at diagnosis of 65 years [1]. Generally, MCL has an unfavorable prognosis due to a more rapid disease progression than is seen in other small-cell B-NHLs and due to its resistance to conventional therapies [2]. The median overall survival is 3–4 years. However, the clinical behavior of MCL may vary. In some patients, the disease runs an aggressive course with survival of <1 year, while other patients have a relatively slow clinical evolution and survive for more than 10 years after diagnosis [3–5].

Given the relatively advanced age of MCL patients and toxicity of modern therapeutic strategies together with the survival variability, it would be advantageous to develop a methodology discriminating between patients with indolent and aggressive disease course. The predictive role of various

clinical and laboratory parameters in the MCL progression is conflicting [6–15]. Actually, based on the recent *European MCL Network's* clinicopathological study of 304 cases of MCLs, the cell proliferation was identified as a strong prognosticator [7]. In addition, multivariate analyses exposed the immunohistochemically assessed Ki-67, topoisomerase IIα, and TPX2 level as the most effective prognostic factor in MCL patients, even superior to the International Prognostic Index and other clinical and histomorphological characteristics [6, 14, 15]. The predictive role of KI-67 was also confirmed for MCL patients treated with anti-CD20 therapy, and it was reported as an important biological marker also in addition to MCL International Prognostic Index [16, 17]. Gene expression profiling of MCLs also revealed the expression of proliferation signature genes as a strong indicator of the outcome in patients with MCL [18].

Moreover, several cytotoxic agents used in the treatment of hematological malignancies target topoisomerase IIα. A high topoisomerase IIα expression might be an indicator of a better prognosis due to an increased chemosensitivity of the tumors to the topoisomerase IIα inhibitors [19–22]. The high topoisomerase IIα expression identifies the patients who should be treated more intensively [23] because the survival of such patients is dramatically shorter and their sensitivity to the topoisomerase IIα inhibitors is higher.

So far, all studies investigating the proliferation rate in MCL patients used immunohistochemistry (IHC). However, IHC allows a semiquantitative assessment of the expression levels only, it is susceptible to a subjective interpretation, and the detected protein expression is influenced by a variation in the tissue fixation and staining conditions, which decreases the interpretation reproducibility. Therefore, standardized methods to assess proliferation markers are needed for future use. The aim of the present study was to design a simple, reliable, reproducible, and routinely applicable methodology for quantitative measurement of the expression level of proliferation markers. Such an approach would provide a more precise information about the proliferation activity of lymphoma cells and may lead to a more precise stratification of MCL patients.

Materials and methods

Tissue samples

The study was approved by the Ethical Committee of the Faculty Hospital in Motol, Prague, Czech Republic, Chairman Vratislav Smelhaus, M.D. The study has been performed in accordance with ethical standards in the Czech Republic and with Helsinki declaration. All specimens included in the study were tested after an informed consent from all patients.

The mRNA level of proliferation markers was examined in 95 primary tumor specimens from 83 patients diagnosed with a variety of NHLs. The analyzed specimens are summarized in Table 1. Burkitt lymphomas (BL) are known for a very high Ki-67 expression, so they were used as positive controls in the experiment and were analyzed as a separate group. Furthermore, two reactive lymph nodes (RLN) were used as a non-neoplastic control. The diagnoses were based on a combined morphological and immunophenotypic examination using IHC and/or flow cytometry. In all MCL patients, the morphological and immunohistochemical diagnosis was supported either by interphase fluorescence in situ hybridization or by PCR demonstrating t(11;14) [24, 25]. All MCL cases also showed the cyclin D1 mRNA overexpression.

The tissue prepared for the molecular analysis was checked using morphological examination so that tissue blocks (frozen or paraffin) containing the neoplastic tissue only were processed.

Immunohistochemical analysis

The IHC staining for Ki-67, topoisomerase IIα, and TPX2 was performed using the streptavidin–biotin system. Three-micrometer-thick formalin-fixed, paraffin-embedded (FFPE) histological sections were cut and placed on the organosilane-coated slides. The specific monoclonal antibody against Ki-67 (clone MIB-1, Dako, Glostrup, Denmark A/S) and topoisomerase IIα (clone SWT3D1, Dako) was used according to the manufacturer's instructions. The IHC analysis of TPX2 was performed as previously described [14] by the use of a specific antibody Ki-S2 kindly provided by professor R. Parwaresh and dr. W. Klapper from the Department of Hematopathology and Lymph Node Registry (University Hospitals of Schleswig-Holstein, Kiel, Germany).

Because the IHC character is estimative and thus semiquantitative, the evaluation of a continuous spectrum of IHC positivities is approximate, and thus, it is of a limited use for a precise comparison of the proliferation indices. Therefore, for our correlative studies, a grouping approach adopted from the *European MCL Network* [7] was used and the tumor specimens were divided (according to their Ki-67 and topoisomerase IIα index) into three groups: samples displaying a low proliferation index as 1+ (0–10%), an intermediate proliferation index as 2+ (11–40%), and samples with a high proliferation index as 3+ (41–100%). Because the proliferation index assessed using the TPX2 staining was generally lower than the indices seen in Ki-67 and topoisomerase IIα and we observed only one MCL with TPX2 index higher than 40%, we divided the specimens into five groups: 1+ (0–5%), 2+ (6–10%), 3+ (11–20%), 4+ (21–40%), and 5+ (41–100%).

Table 1 Specimens used for the quantitative PCR analysis

Diagnosis	MCL	AML	BL	DLBCL	MZL	Per. TL
No. of patients	55	1	7	10	4	6
No. of specimens	63[a]	1	9[b]	10	6[c]	6
Fixation	46 FFPE/17 frozen	Frozen	All frozen	All frozen	All frozen	All frozen

MCL mantle cell lymphoma, *AML* acute myeloid leukemia, *BL* Burkitt lymphoma, *DLBCL* diffuse large B cell lymphoma, *MZL* marginal zone lymphoma, *Per. TL* peripheral T cell lymphoma, *FFPE* formalin-fixed, paraffin-embedded

[a] One patient with three different biopsy specimens; six patients with two different biopsy specimens

[b] Two patients with two different biopsy specimens

[c] One patient with three different biopsy specimens

RNA extraction and cDNA synthesis

RNA was extracted from ten tissue sections (5 μm thick) using Tri-Reagent (Invitrogen Ltd., Carlsbad, CA, USA) in case of frozen tissues or "High Pure RNA Paraffin Kit" (Roche, Pfenzberg, Germany) in case of FFPE tissues, both according to the manufacturer's instructions.

A reverse transcription process and control reverse transcription PCR (RT-PCR) were performed as described elsewhere [26].

Quantitative real-time RT-PCR

The detection of the cyclin D1 overexpression and β-2-microglobulin using hydrolysation probes by quantitative real-time reverse transcription PCR (RQ-RT-PCR) was performed as previously reported [26].

For the detection of the Ki-67, topoisomerase IIα, and TPX2 transcript, we designed the probes and appropriate detection primers (Table 2) using the Universal ProbeLibrary software (Roche). All probes were designed to cross a splice junction to avoid any amplification of genomic DNA. The expression levels were measured in the iQ^{TM}5 Multicolor Real-Time PCR detection instrument (Bio-Rad, Hercules, CA, USA). The reaction mixture contained 10 μl of the Fast Start TaqMan Probe Master (Roche), 1 μl of both primers (10 μM; Invitrogen), 0.2 μl of the LNA probe (10 μM; Roche), and 1 μl of cDNA in a final volume of 20 μl. Samples were amplified in duplicates. The reaction was started with 2 min at 50°C followed by the activation and pre-denaturation step at 95°C for 10 min. The reaction run consisted of 40 cycles comprising 15 s at 95°C and 1 min at 60°C.

Data analysis

The cycle at which the fluorescence of a sample rises above the background fluorescence is called the "crossing point" (Cp) of the sample. The Cp of a sample depends on the initial concentration of DNA/cDNA in the tested specimen. Samples with a higher pre-amplification target concentration show an earlier crossing point. The higher the Cp value, the lower is the expression of cyclin D1 in the specimens. The Cp values for each reaction were determined using the Bio-Rad iQ5 Optical System Software 1.0. For each amount of cDNA tested, the duplicate Cp values were averaged. As we wanted to compare whether the expression level of the proliferation markers differed between individual specimens and diagnoses, we used relative quantification using β-2-microglobulin as a normalizing transcript [27]. The normalization was used to avoid the impact of the variability in the RNA quality and quantity and the variability in the reverse transcription efficiency among samples. The normalized expression (ΔCp) was determined by subtracting the average Cp value for β-2-microglobulin from the average Ki-67, topoisomerase IIα, or TPX2 Cp value.

For statistical analysis, the JMP IN 5.1 software (SAS Institute, Cary, NC, USA) was used. The parametric Student's *t* test was used for normally distributed data, and the non-parametric Kruskal–Wallis test was used in the case of non-normal distribution.

Table 2 Primers and probes used for the quantitative detection of Ki-67, topoisomerase IIα, and TPX2 mRNAs

Analyzed transcript	Sequence of left primer (5′ to3′)	Sequence of right primer (5′ to3′)	Universal ProbeLibrary probe no.
Ki-67	gaggtgtgcagaaaatccaaa	ctgtccctatgacttctggttgt	30
Topoisomerase IIα	cagtgaagaagacagcagcaa	agctggatccctttttagttcct	43
TPX2	acatctgaactacgaaagcatcc	ggcttaacaatggtacatccctta	51

Results

RQ-RT-PCR efficacy and reproducibility within-run, between-run, in RNA and cDNA stored over time, in FFPE, and fresh frozen specimens

To asses the reproducibility of the assay, we repeated RQ-RT-PCR described above 1 week, 1 month, and 6 months after the original measurements, and we compared the Cp values individually as well as the ΔCp values for each cDNA analyzed. We tested the reproducibility of the quantitative detection by running 66, 71, and 67 samples repeatedly. We obtained highly reproducible results in 97%, 96%, and 99% of the specimens, and the median variability for the Cp values between runs was −0.55, 0.12, and 0.11 for Ki-67, topoisomerase IIα, and TPX2, respectively. Thus, there were no significant shifts in the Cp values when the cDNA analysis was repeated. Similarly, we did not observe any significant difference in the Cp values when another reverse transcription product from the same RNA extraction was used. Duplicate amplifications produced nearly identical overlapping amplification curves. We reached 97%, 94%, and 100% within-run reproducibility with the median variability of 0.27, 0.17, and 0.18 for the Ki-67, topoisomerase IIα, and TPX2 analysis, respectively. The presented results confirmed a high reproducibility and reliability of the method used.

We tested the expression level of Ki-67, topoisomerase IIα, and TPX2 in 51 fresh frozen and 46 FFPE biopsy specimens. None of the fresh frozen and FFPE specimens failed to amplify. We obtained excellent analysis efficacy and intra or inter-run reproducibility for both the fresh frozen and FFPE specimens. Additionally, to compare the expression level in FFPE tissues with those in fresh frozen tissues, we analyzed five matching MCL samples and did not find any significant difference between the ΔCp values. Thus, the method is optimized even for the routinely archived materials, such as formalin-fixed tissues. Although the formalin fixation hampers a range of molecular analyses because not all cases in paraffin yield appropriate amount of good quality RNA, the approach developed in this study circumvents this problem by using small amplicons (78, 95, and 68 nt for Ki-67, topoisomerase IIα, and TPX2), allowing the detection of fragmented and partially degraded RNA. Moreover, a potential impact of the tissue fixation is compensated by the use of the normalizing transcript.

Correlation with immunohistochemical analysis

The accuracy of the assay was evaluated at the protein level by comparing results retrieved by RQ-RT-PCR and IHC staining in the same samples. The validation of RQ-RT-PCR levels versus IHC results was performed in a blind fashion by two independent observers. As a control, we examined the Ki-67, topoisomerase IIα, and TPX2 protein expression using IHC in 97, 94, and 93 biopsy specimens, respectively. In the case of topoisomerase IIα and TPX2, we were not able to examine all the 97 specimens because the biopsy material was cut out due to an extensive preceding analysis. In one case Ki-67 and topoisomerase IIα and in three cases TPX2 IHC failed to show an interpretable result. The Ki-67 is expressed during the G1, S, G2, and M phases of the cell cycle [28]. Topoisomerase IIα and TPX2 are described to be expressed during the late S, G2, and M phases of the cell cycle [29, 30]. We found a correlation between the three proliferation indices, and as expected from their expression profiles, the topoisomerase IIα index was 10–20% lower and the TPX2 index 20–40% lower than the Ki-67 index. For correlating the RQ-RT-PCR expression with the IHC expression, we used grouping of the IHC results adopted from the *European MCL Network* [7] because a precise evaluation of a continuous spectrum of the IHC staining is not possible due to the estimative character of the IHC results reading. A statistical analysis of the Ki-67 and topoisomerase IIα protein index (Fig. 1a, b) showed significantly different mRNA levels between 2+ and 3+ and between 1+ and 3+. We observed also a difference between 1+ and 2+, but it did not reach a statistical significance, reflecting the difficulty of the precise interpretation of the "gray" zone cases. It was not difficult to reliably differentiate between tumors with the proliferation index lower than 40% and tumors with the index higher than 40%. However, it was problematic to strictly distinguish between tumors with a lower proliferation activity assessed by IHC (<10% vs. >10%), resulting in a decrease of the statistical significance. Different mRNA levels were observed between the TPX2 index groups (Fig. 1c). The difference between the groups 1+ and 3+, between 2+ and 5+, 3+ and 5+, and 4+ and 5+ reached statistical significance. The statistical significance of the analysis between the remaining groups was decreased due to a problematic evaluation of the staining results in the case of Ki-S2 antibody against the TPX2 protein. The staining result was strongly influenced by the various ways of tissue handling used in various institutions. As a result, the Ki-S2 IHC staining intensity varied and it was difficult to achieve an optimal intensity for the interpretation in all cases, which complicated the interpretation of the TPX2 index.

The correlation analysis pointed out limitations of the IHC evaluation. Nevertheless, statistically significant results were achieved. The greater the proliferation index measured by the IHC staining, the greater was the mRNA level. Thus, we have shown that the mRNA levels correspond to the IHC staining of the protein expression, indicating the reliability of the RQ-RT-PCR method for the quantitative measurement of the proliferation activity.

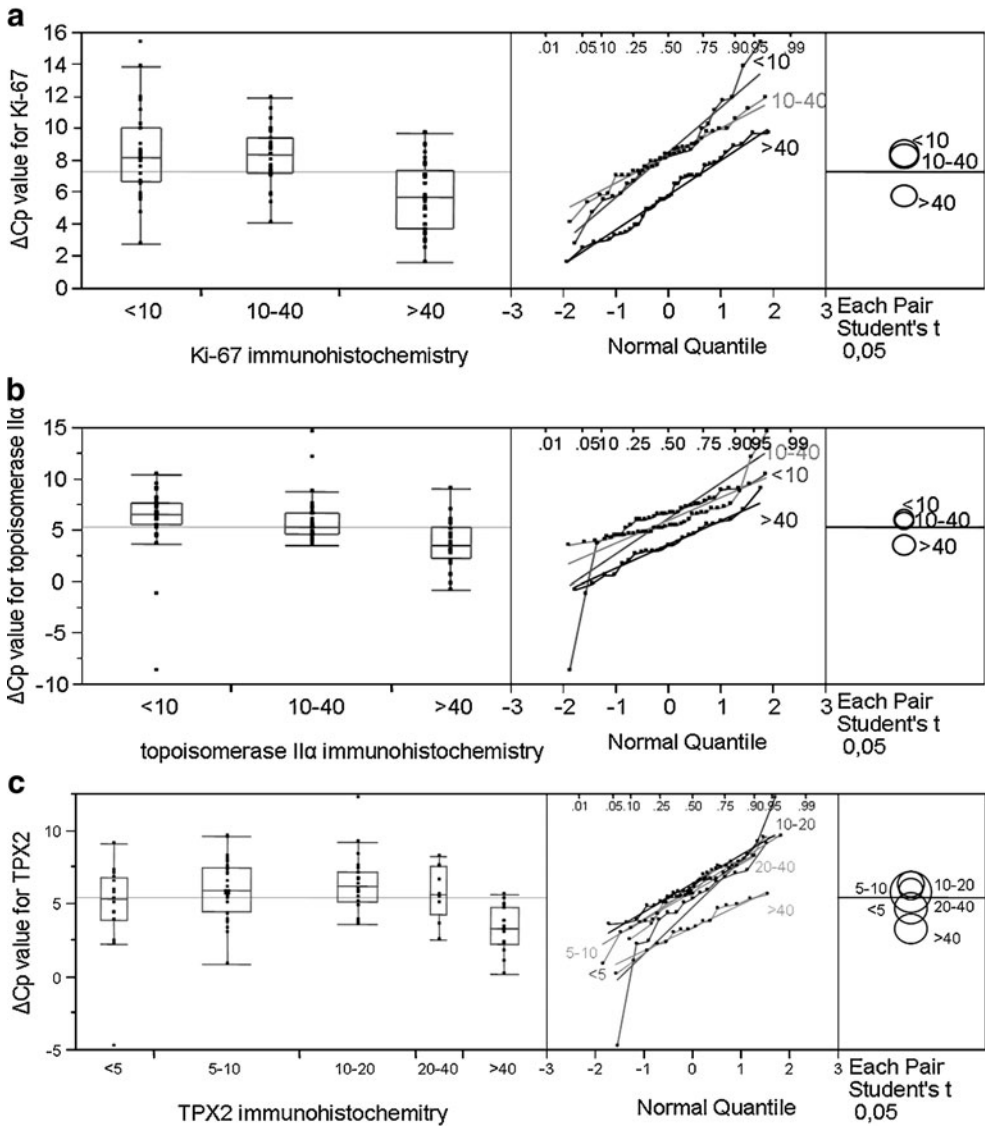

Fig. 1 Distribution and statistical comparison of the normalized ΔCp values measured by RQ-RT-PCR in the subgroups of specimens with different protein levels estimated by IHC. The greater the Cp value, the lower is the expression in the specimen. The normal quantile plot shows both the difference in the values (*vertical position*) and the variances (*slopes*) for each group. The normality is judged by how well the points follow a straight line. The standard deviations are the slopes of the straight lines. *Lines with steep slopes* represent the distribution with greater variances. **a** Ki-67 expression. Mean ΔCp values: 1+ (n=28), 8.49; 2+ (n=31), 8.28; 3+ (n=37), 5.82. Student's t test: between 1+ and 2+ (p=0.723), between 1+ and 3+ (p=0.00001), between 2+ and 3+ (p=0.00002). **b** Topoisomerase IIα expression. Mean ΔCp values: 1+ (n=33), 6.15; 2+ (n=35), 5.98; 3+ (n=25), 3.62. Student's t test: between 1+ and 2+ (p=0.805), between 1+ and 3+ (p=0.00082), between 2+ and 3+ (p=0.00150). **c** TPX2 expression. Mean ΔCp values: 1+ (n=15), 4.77; 2+ (n=28), 6.03; 3+ (n=20), 6.37; 4+ (n=11), 5.82; 5+ (n=16), 3.34. Student's t test: between 1+ and 2+ (p=0.074), between 1+ and 3+ (p=0.03060), between 1+ and 4+ (p=0.254), between 1+ and 5+ (p=0.072), between 2+ and 3+ (p=0.582), between 2+ and 4+ (p=0.806), between 2+ and 5+ (p=0.00017), between 3+ and 4+ (p=0.526), between 3+ and 5+ (p=0.00006), and between 4+ and 5+ (p=0.00763)

RQ-RT-PCR results

We achieved a strong linear correlation between the expression levels of the three proliferation markers. The Spearman's rank correlation coefficient was calculated to be 0.5831 (p<0.0001) between the Ki-67 and topoisomerase IIα mRNA level, 0.6750 (p<0.0001) between the Ki-67 and TPX2, and 0.6502 (p<0.0001) for the topoisomerase IIα and TPX2 expression levels.

The ΔCp values of the proliferation markers ranged from very high to very low in individual tumors. Results for different diagnostic groups are summarized in Table 3, and the distribution of the ΔCp values is depicted in Fig. 2. In each group of analyzed tumors, there were cases with a

Table 3 ΔCp values of proliferation markers in analyzed specimens

	Ki-67 ΔCp range	Ki-67 ΔCp median	Topoisomerase IIα ΔCp range	Topoisomerase IIα ΔCp median	TPX2 ΔCp range	TPX2 ΔCp median
RLN	11.12–8.42	9.77	6.36–3.59	4.98	7.56–6.65	7.11
MCL	15.41–2.78	8.22	14.70–8.73	6.53	12.30–4.71	5.75
NHL	9.99–3.02	7.03	7.23–0.77	5.02	8.41–0.17	5.64
BL	5.58–1.69	3.50	9.16–0.27	2.04	4.97–1.05	3.07

RLN reactive lymph node, *MCL* mantle cell lymphoma, *NHL* non-Hodgkin's lymphoma, *BL* Burkitt lymphoma

high, intermediate, and low proliferation activity. The results indicate a significant heterogeneity of the proliferation activity of individual cases.

Generally, the highest proliferation activity was observed in the BL group and the lowest proliferation activity in control RLNs. The proliferation rate of MCLs, NHLs other than MCL or BL, and control RLNs was statistically lower than the proliferation activity of BLs (Fig. 2). Moreover, MCL significantly differed from other NHLs in the expression of Ki-67 and topoisomerase IIα.

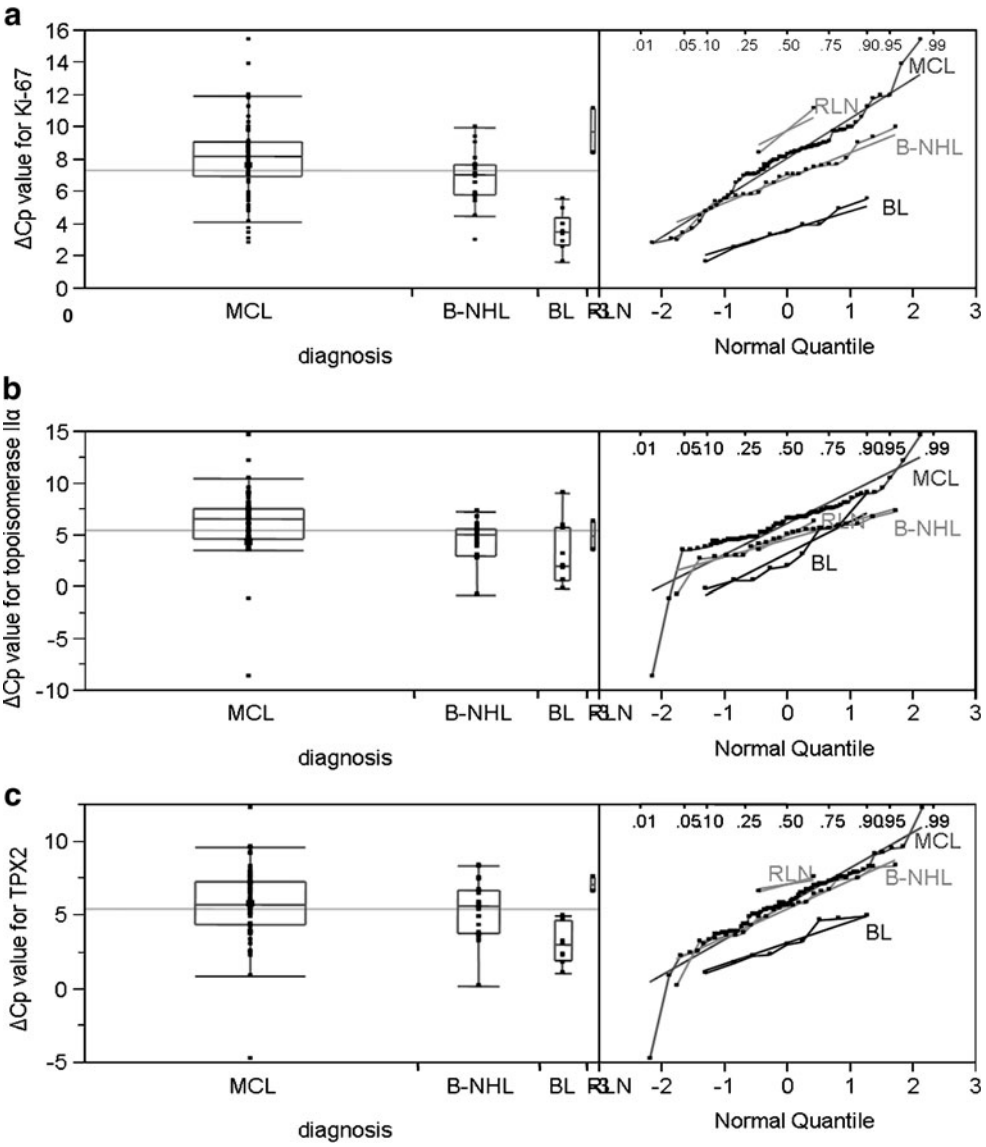

Fig. 2 Distribution and statistical comparison of the normalized ΔCp values measured by RQ-RT-PCR in MCLs, NHLs other than MCL or BL, BLs, and RLNs. The greater the Cp value, the lower is the expression in the specimen. The normal quantile plot shows both the difference in the values (*vertical position*) and the variances (*slopes*) for each group. The normality is judged by how well the points follow a straight line. The standard deviations are the slopes of the straight lines. *Lines with steep slopes* represent the distribution with greater variances. **a** Ki-67 expression. The result of the parametric *t* test was $p<0.02337$ for the difference between MCLs and NHLs other than MCL or BL; $p<0.0000001$ between MCLs and BLs; $p<0.277$ between MCLs and RLNs; $p<0.00025$ between NHLs other than MCL or BL and BLs; $p<0.070$ between NHLs other than MCL or BL and RLNs; and $p<0.00044$ for the difference between BLs and RLNs. **b** topoisomerase IIα expression. The result of the non-parametric Kruskal–Wallis test was $p<0.0012$. **c** TPX2 expression. The result of the non-parametric Kruskal–Wallis was $p<0.0017$

Correlation of proliferation markers with cyclin D1 expression

As a key regulator of the cell cycle, aberrantly expressed cyclin D1 may contribute to an increased proliferation rate of tumor cells. Therefore, we related the cyclin D1 mRNA level examined by RQ-RT-PCR to the expression level of the proliferation markers. A correlation between the cyclin D1 expression level and the expression level of topoisomerase IIα and TPX2 was found. The Spearman's rank correlation coefficients were 0.3664 ($p>0.0037$) between cyclin D1 and topoisomerase IIα and 0.2591 ($p>0.0403$) between cyclin D1 and TPX2. Thus, the cyclin D1 expression level was higher in more proliferating MCLs, as measured by the RQ-RT-PCR detection of the topoisomerase IIα and TPX2 expression. No apparent correlation between cyclin D1 and Ki-67 mRNAs was observed (Spearman's rank correlation coefficient 0.1451, $p>0.2687$).

Discussion

MCL is a disease with the poorest long-term outcome of all lymphoma subtypes [5]. However, in some of the patients, the disease runs an indolent course. These patients may be asymptomatic and with no need of therapy for a long time. It is therefore of clinical relevance to establish reliable prognostic markers useful in defining risk groups in MCL. Since it is known that a higher proliferation of the tumor cells is closely associated with a shorter survival and that the proliferation-associated genes are the major risk factors in MCL [3, 31], a better prognostic estimation may be achieved by including the assessment of the proliferation activity. Therefore, the aim of this work was to design and perform a reliable and easily applicable method for a precise quantitative measurement of three proliferation markers associated with the prognosis of MCL.

Until now, a widely accepted procedure to detect the proliferation activity is IHC using Ki-67 protein. However, in a routine pathology work, IHC is evaluated semiquantitatively and such an approach suffers from a subjective interpretation. Each investigator may differ in the evaluation of the microscopic findings and sometimes may differ in the interpretation of the result in the same case with repeated blind evaluation. The most frequent problems arise in the interpretation of "gray" zone cases. Due to these inconveniences, the immunohistochemically stained proteins are currently not applicable as a prognostic index except for research study. However, *European MCL Network* recently published the consensus guidelines for assessing the Ki-67 index. They evaluated methods to assess the Ki-67 index that included a stringent counting, digital image analysis, and estimation by eyeballing. The eyeballing estimation deviated considerably between various observers, as did the digital analysis. Although the stringent counting was published as a gold standard method, it required counting of 2 × 500 cells and specimens of a minimum size that allowed at least five independent representative areas at high magnification. Thus, it is extremely time-consuming and not available for small specimens, and therefore, it is not applicable in everyday pathology practice. Moreover, Ki-67-positive cells are not homogeneously distributed, and thus, choosing a representative area for the counting is crucial and may be a significant source of subjectivity [32]. The standardization and a precise proliferation assessment are still required for using proliferation activity as a first biologically relevant prognostic marker. Therefore, we have developed a novel approach allowing a highly effective, useful, and reproducible RQ-RT-PCR detection of proliferation markers, which is routinely applicable to both fresh frozen and formalin-fixed archived biopsy specimens in everyday diagnostic practice. Real-time PCR is a sensitive and specific approach combining the speed and ease of PCR-based system with an accurate and reproducible quantification. Therefore, disadvantages encountered with the IHC analysis are avoided.

A linear correlation between the expression of TPX2 and topoisomerase IIα was observed, which is in accordance with their similar expression patterns during the late S, G2, and M phases of the cell cycle [29, 33]. In contrast, Ki-67 is present during the G1 phase as well [34]. The length of the G1 phase may be highly variable (from a few hours to days or weeks). Consequently, if cells have a very long G1, the Ki-67 indices are higher than the actual turnover of the cells. The different expression pattern of Ki-67 led to a slightly looser (but still significant) relation between Ki-67 and topoisomerase IIα and TPX2 mRNAs. Topoisomerase IIα and TPX2 provide a better estimate of the cycling cells. Furthermore, they are described to be more important prognostic factors of the clinical outcome of MCL patients than the expression of Ki-67 [14, 15].

Among all lymphomas tested, we observed the highest proliferation activity in the group of BL as expected. Samples of BL were utilized as positive controls of the proliferation rate in the current study. In conjunction with the lowest proliferation activity of the control RLN group, we confirmed the accuracy of the current assay for the precise quantitative examination of the proliferation activity.

The individual expression of the proliferation markers varied from low to high, reflecting the heterogeneity of the proliferation activity of the tumors, which may be of a prognostic value as indicated by large multivariate analyses [7, 18]. Because 85% of the patients with MCL tested in this study were diagnosed after 2003 (70% diagnosed even after 2005), the follow-up period is not long enough to define the disease and/or event-free survival and thus to

establish the implication of this study for prognosis. To make a plausible conclusion concerning the clinical impact of the mRNA analysis, the patients need to be followed for a longer time period. However, because a tight correlation between the protein expression and survival in MCL has already been reported [7, 14, 15] and we obtained a correlation between the protein and mRNA level, we suggest that the precise quantitative measurement of mRNA by RQ-RT-PCR will be of a similar predictive value for the clinical course as the protein analysis. It is in accordance with a recently published study which demonstrates an optimized survival predictor measuring the expression levels of five genes using the RQ-RT-PCR approach [35]. Because all the described genes were involved in the proliferation process and because the five gene predictor correlated with the Ki-67 index, we consider our developed approach using a precise quantitative assessment of three proliferation markers to be routinely applicable. Moreover, the molecules used in this study are recommended to be precisely quantitatively assessed by the *European MCL Network* and the *Lymphoma/Leukemia Molecular Profiling Project* [18].

We did not find any association between the Ki-67 and cyclin D1 mRNAs because if tumor cells have a long G1 time, the high Ki-67 expression may falsely simulate a higher proliferation activity without a clinical correlation. Alternatively, the observation that the Ki-67 and cyclin D1 mRNA levels did not correlate may be explained by another compensatory mechanism governing proliferation in a way that is independent of the cyclin D1 expression. Since it was published, that the cyclin D1 knockdown did not lead to the complete cell growth retardation and its downregulation was compensated by a cyclin D2 upregulation, as an alternative D-type cyclin [36]. However, patients with high expression levels of topoisomerase IIα and TPX2 showed high expression levels of cyclin D1 mRNAs, indicating a direct relationship between the cyclin D1 level and the active cell proliferation in MCLs. Here, we report that the cyclin D1 overexpression in MCL is associated with the overexpression of the late S, G2, and M phases markers, highlighting the quantitative sensitivity of the G1/S phase transition to changes in the concentration of the D-type cyclin. Therefore, in MCLs, the cell cycle appears to be regulated by the cyclin D1 kinase complex in a quantitative way rather than by an on/off switch control activated when a threshold level of cyclin D1 is achieved.

Conclusions

To summarize, the aim of the study was to develop a quantitative measurement allowing a precise and reproducible determination of the proliferation activity of lymphoma cells. We confirmed the reliability of the RQ-RT-PCR examination for the quantitative assessment of the proliferation activity. We also showed a significant correlation between the mRNA and protein level of Ki-67, topoisomerase IIα, and TPX2. With regard to a reported prognostic significance, we expect that the precise quantitative measurement of the proliferation activity will be of a prognostic value. Recently, as it has been demonstrated that the length of the survival of MCL patients depends upon the quantitative differences in the progression from the G1 to S phase of the cell cycle, "The Lymphoma/Leukemia Molecular Profiling Project"[18] suggests incorporating the quantitative assessment of the tumor proliferation rate into clinical trials in MCL, and the PCR-based system established in this study allows such a quantitative measurement of the proliferation activity.

Acknowledgments This work was supported by the Internal grant of faculty hospital in Motol no. 9756, Grant GAUK 46/2006/C/2.LF, and the Research project of the Ministry of Health no. 00064203/6704. We thank Dr. W. Klapper and the late Prof. Dr. R. Parwaresh (Department of Hematopathology and Lymph Node Registry, University Hospitals of Schleswig-Holstein, Kiel, Germany) who kindly provided us a sample of the antibody Ki-S2 against TPX2.

Conflict of interests The authors declare that they have no conflict of interest in this study.

References

1. Swerdlow SH, Berger F, Isaacson PI et al (2001) Mantle cell lymphoma. In: Jaffe ES, Harris NC, Stein H, Vardiman JW (eds) Pathology and genetics of tumours of haematopoietic and lymphoid tissues, 1st edn. IARC, Lyon, pp 168–170
2. Weisenburger DD, Armitage JO (1996) Mantle cell lymphoma—an entity comes of age. Blood 87:4483–4494
3. Bosch F, Lopez-Guillermo A, Campo E et al (1998) Mantle cell lymphoma: presenting features, response to therapy, and prognostic factors. Cancer 82:567–575
4. Campo E, Raffeld M, Jaffe ES (1999) Mantle-cell lymphoma. Semin Hematol 36:115–127
5. Lenz G, Dreyling M, Hiddemann W (2004) Mantle cell lymphoma: established therapeutic options and future directions. Ann Hematol 83:71–77
6. Raty R, Franssila K, Joensuu H et al (2002) Ki-67 expression level, histological subtype, and the International Prognostic Index as outcome predictors in mantle cell lymphoma. Eur J Haematol 69:11–20
7. Tiemann M, Schrader C, Klapper W et al (2005) Histopathology, cell proliferation indices and clinical outcome in 304 patients with mantle cell lymphoma (MCL): a clinicopathological study from the European MCL Network. Br J Haematol 131:29–38
8. Ott G, Kalla J, Ott MM et al (1997) Blastoid variants of mantle cell lymphoma: frequent bcl-1 rearrangements at the major translocation cluster region and tetraploid chromosome clones. Blood 89:1421–1429
9. Matutes E, Parry-Jones N, Brito-Babapulle V et al (2004) The leukemic presentation of mantle-cell lymphoma: disease features and prognostic factors in 58 patients. Leuk Lymphoma 45:2007–2015
10. Orchard J, Garand R, Davis Z et al (2003) A subset of t(11;14) lymphoma with mantle cell features displays mutated IgVH genes

and includes patients with good prognosis, nonnodal disease. Blood 101:4975–4981
11. Yatabe Y, Suzuki R, Tobinai K et al (2000) Significance of cyclin D1 overexpression for the diagnosis of mantle cell lymphoma: a clinicopathologic comparison of cyclin D1-positive MCL and cyclin D1-negative MCL-like B-cell lymphoma. Blood 95:2253–2261
12. Levy V, Ugo V, Delmer A et al (1999) Cyclin D1 overexpression allows identification of an aggressive subset of leukemic lymphoproliferative disorder. Leukemia 13:1343–1351
13. Fu K, Weisenburger DD, Greiner TC et al (2005) Cyclin D1-negative mantle cell lymphoma: a clinicopathologic study based on gene expression profiling. Blood 106:4315–4321
14. Schrader C, Janssen D, Meusers P et al (2005) Repp 86: a new prognostic marker in mantle cell lymphoma. Eur J Haematol 75:498–504
15. Schrader C, Meusers P, Brittinger G et al (2004) Topoisomerase IIalpha expression in mantle cell lymphoma: a marker of cell proliferation and a prognostic factor for clinical outcome. Leukemia 18:1200–1206
16. Determann O, Hoster E, Ott G et al (2008) Ki-67 predicts outcome in advanced-stage mantle cell lymphoma patients treated with anti-CD20 immunochemotherapy: results from randomized trials of the European MCL Network and the German Low Grade Lymphoma Study Group. Blood 111:2385–2387
17. Hoster E, Dreyling M, Klapper W et al (2008) A new prognostic index (MIPI) for patients with advanced-stage mantle cell lymphoma. Blood 111:558–565
18. Rosenwald A, Wright G, Wiestner A et al (2003) The proliferation gene expression signature is a quantitative integrator of oncogenic events that predicts survival in mantle cell lymphoma. Cancer Cell 3:185–197
19. Friche E, Danks MK, Schmidt CA et al (1991) Decreased DNA topoisomerase II in daunorubicin-resistant Ehrlich ascites tumor cells. Cancer Res 51:4213–4218
20. Deffie AM, Batra JK, Goldenberg GJ (1989) Direct correlation between DNA topoisomerase II activity and cytotoxicity in adriamycin-sensitive and -resistant P388 leukemia cell lines. Cancer Res 49:58–62
21. Davies SM, Robson CN, Davies SL et al (1988) Nuclear topoisomerase II levels correlate with the sensitivity of mammalian cells to intercalating agents and epipodophyllotoxins. J Biol Chem 263:17724–17729
22. Asano T, An T, Mayes J et al (1996) Transfection of human topoisomerase II alpha into etoposide-resistant cells: transient increase in sensitivity followed by down-regulation of the endogenous gene. Biochem J 319(Pt 1):307–313
23. Korkolopoulou P, Vassilakopoulos TP (2004) Topoisomerase IIalpha as a prognostic factor in mantle cell lymphoma. Leukemia 18:1347–1349
24. Kodet R, Mrhalova M, Krskova L et al (2003) Mantle cell lymphoma: improved diagnostics using a combined approach of immunohistochemistry and identification of t(11;14)(q13;q32) by polymerase chain reaction and fluorescence in situ hybridization. Virchows Arch 442:538–547
25. van Dongen JJ, Langerak AW, Bruggemann M et al (2003) Design and standardization of PCR primers and protocols for detection of clonal immunoglobulin and T-cell receptor gene recombinations in suspect lymphoproliferations: report of the BIOMED-2 Concerted Action BMH4-CT98-3936. Leukemia 17:2257–2317
26. Brizova H, Kalinova M, Krskova L et al (2008) Quantitative measurement of cyclin D1 mRNA, a potent diagnostic tool to separate mantle cell lymphoma from other B-cell lymphoproliferative disorders. Diagn Mol Pathol 17:39–50
27. Lupberger J, Kreuzer KA, Baskaynak G et al (2002) Quantitative analysis of beta-actin, beta-2-microglobulin and porphobilinogen deaminase mRNA and their comparison as control transcripts for RT-PCR. Mol Cell Probes 16:25–30
28. Gerdes J, Lemke H, Baisch H et al (1984) Cell cycle analysis of a cell proliferation-associated human nuclear antigen defined by the monoclonal antibody Ki-67. J Immunol 133:1710–1715
29. Woessner RD, Mattern MR, Mirabelli CK et al (1991) Proliferation- and cell cycle-dependent differences in expression of the 170 kilodalton and 180 kilodalton forms of topoisomerase II in NIH-3T3 cells. Cell Growth Differ 2:209–214
30. Heidebrecht HJ, Adam-Klages S, Szczepanowski M et al (2003) repp 86: a human protein associated in the progression of mitosis. Mol Cancer Res 1:271–279
31. Argatoff LH, Connors JM, Klasa RJ et al (1997) Mantle cell lymphoma: a clinicopathologic study of 80 cases. Blood 89:2067–2078
32. Klapper W, Hoster E, Determann O et al (2009) Ki-67 as a prognostic marker in mantle cell lymphoma—consensus guidelines of the pathology panel of the European MCL Network. J Hematop 2:103–111
33. Heidebrecht HJ, Buck F, Steinmann J et al (1997) p100: a novel proliferation-associated nuclear protein specifically restricted to cell cycle phases S, G2, and M. Blood 90:226–233
34. Scholzen T, Gerdes J (2000) The Ki-67 protein: from the known and the unknown. J Cell Physiol 182:311–322
35. Hartmann E, Fernandez V, Moreno V et al (2008) Five-gene model to predict survival in mantle-cell lymphoma using frozen or formalin-fixed, paraffin-embedded tissue. J Clin Oncol 26:4966–4972
36. Klier M, Anastasov N, Hermann A et al (2008) Specific lentiviral shRNA-mediated knockdown of cyclin D1 in mantle cell lymphoma has minimal effects on cell survival and reveals a regulatory circuit with cyclin D2. Leukemia 22:2097–2105

Virchows Arch (2010) 456:681–687
DOI 10.1007/s00428-010-0911-y

ORIGINAL ARTICLE

High-resolution genome-wide analysis of chromosomal alterations in elastofibroma

Juan Luis García Hernández · Javier Ortiz Rodríguez-Parets · José María Valero · María Asunción Gomez Muñoz · M. Rocío Benito · Jesus M. Hernandez · Agustín Bullón

Received: 6 October 2009 / Revised: 9 February 2010 / Accepted: 17 March 2010 / Published online: 27 April 2010
© Springer-Verlag 2010

Abstract Elastofibroma is a rare, benign fibrous proliferation that most commonly occur in periscapular soft tissues and is characterized by accumulated elastic fibers. Although the lesion is generally regarded as a reactive process, an unusual fibroblastic pseudotumor or as a fibroelastic tumor-like lesion, its etiology remains unknown. Cytogenetic studies in these lesions detected chromosomal instability and some recurrent clonal chromosomal changes, which raised the possibility that the lesion represents a neoplastic process. Here, we report the genomic alterations detected by array-based comparative genomic hybridization (aCGH) and by multiplex ligation-dependent probe amplification (MLPA) in two cases of elastofibroma. Both cases showed losses on 1p, 13q, 19p, and 22q by aCGH. In addition, deletion of *CASR* (*3q21*), *GSTP1* (*11q13*), *BRCA2* (*13q12*) and gains on *APC* (*5q21*) and *PAH* (*12q23*) were observed by MLPA in both samples. Genomic screening studies of this fibrous proliferation may lead to identify chromosomal regions containing genes involved in the development of elastofibromas.

Electronic supplementary material The online version of this article (doi:10.1007/s00428-010-0911-y) contains supplementary material, which is available to authorized users.

J. L. G. Hernández (✉) · J. M. Valero
Research Unit, IECSCYL-Hospital Universitario de Salamanca,
Paseo San Vicente, 58,
E-37007 Salamanca, Spain
e-mail: jlgarcia@usal.es

J. O. Rodríguez-Parets · M. A. G. Muñoz · A. Bullón
Department of Pathology, Hospital Universitario de Salamanca,
Salamanca, Spain

J. L. G. Hernández · M. R. Benito · J. M. Hernandez
Centro de Investigación del Cáncer and Instituto de Biología
Molecular y Celular del Cáncer, Universidad de Salamanca-CSIC,
Salamanca, Spain

J. M. Hernandez
Department of Hematology, Hospital Universitario de Salamanca,
Salamanca, Spain

Keywords Elastofibroma · aCGH · MLPA · Genomics changes

Introduction

Benign fibrous (fibroblastic or myofibroblastic) soft-tissue tumors are a heterogeneous group of fibrous lesions with widely varied anatomic locations, biologic behavior, and pathologic features. Elastofibroma is one type of this benign fibrous tumor characterized by its almost exclusive occurrence in the periscapular region of middle-aged or older individuals and, morphologically, by an admixture of excessive collagen and abnormal elastic fibers displaying a beaded or globular appearance. The pathogenesis of elastofibroma is still unclear, but repetitive microtrauma caused by friction between the scapula and the thoracic wall may cause a reactive hyperproliferation of fibroblastic tissue. The lesion is generally assumed to be a fibrous pseudotumor or a reactive or degenerative process [1]. Interestingly, a genetic predisposition also has been described [2, 3]. The cytogenetic characterization of several "pseudo-neoplastic" or possible "reactive" or "congenital" entities such as fibroblastic or myofibroblastic tumors has been of great interest. Vanni et al. described chromosomal instability involving chromosome 1 as shown by various nonclonal structural changes [4]. Later on, additional with chromosome instability, but involving clonal chromosomal aberrations were reported [5, 6]. Comparative genomic hybridization (CGH) analysis performed in elastofibroma showed repeated chromosomal instability and a gain of DNA copy number in a chromosomal region Xq [7]. Therefore, the identification of clonal chromosomal changes has led to suggest that elastofibroma may really represent a fibroblastic neoplasm [8]. Recently developed genetic analysis techniques, such as microarray-based comparative genomic hybridization (array CGH) and

multiplex ligation-dependent probe amplification (MLPA), can be of great additional value in the study of the genomic changes present in this type of lesions. Array CGH was first published by Pinkel et al. [9] greatly improving the resolution and sensitivity of chromosome CGH. In array CGH, the target chromosomes are replaced by cloned genomic fragments of which the exact chromosomal location is known, which allows a more detailed detection of unbalanced genomic aberrations and enables to map the alterations directly onto the genomic sequence. MLPA, first described by Schouten et al. [10], is a polymerase chain reaction (PCR)-based technique capable to semi-quantitatively measure the copy number of up to 50 genes in one experiment. MLPA probe mixtures have been developed to detect gains and losses of oncogenes and tumor-suppressor genes and new mixtures are still being developed, especially for clinical diagnostic purposes. Here, we describe using array CGH and MLPA study in two cases of elastofibroma to detect the genomic changes in this type of fibroblastic lesion. We have found new chromosomal changes in both cases of elastofibroma which may be involved in the development of these benign fibrous soft-tissue tumors.

Material and methods

Cases

A 47-year-old woman from whom a mass is extirpated of 3 cm maximum diameter placed in soft tissues in the back. The second cases is a 53-year-old man with irregular elongated mass with adipose-adhered reaming measuring 5 × 3 × 0.5 cm in the back. Both cases showed localization in subscapular region. The patients denied any antecedent history of trauma. Histopathology examination revealed the lesions were composed of a mixture of a large number of fibers associated with stroma. The elastic fibber was large but fragmented into small, linearly arranged globules or screed dishes simulating beads on a string. Specific staining for elastic fibers, Orcein, confirmed their elastic fibers with the characteristic beaded or serrated edge appearance (Fig. 1a, b).

Methods

DNA isolation

Genomic DNA was extracted from paraffin-embedded tissue sections (4 μm) were deparaffinized three times in 1 ml xylene and three times in 1 ml 100% ethanol for 10 min each. After air drying, samples were suspended in 200 μl of DNA extraction buffer, containing proteinase K (both QIAamp DNA Mini kit, Qiagen GmbH, Hilden, Germany), and incubated at 55°C overnight. Normal DNA was prepared from the placenta of healthy donors. DNA was quantified using the Nanodrop spectrophotometer (ND-1000, NanoDrop Technologies, Wilmington, USA) and its quality was assessed by the 260:280 ratio and by agarose gel ethidium bromide visualization.

Array CGH

A genomic-wide analysis of DNA copy number changes of patient samples was performed using array CGH. Slides containing 5,000 bacterial artificial chromosomes (BACs) spanning the genome were produced at the "Centro de Investigación del Cáncer" (Salamanca, Spain). The particular BAC and P-1 derived artificial chromosome set used to produce this array was distributed to academic institutions by the Welcome Trust Sanger Institute (Cambridge, UK) and contains targets spaced at ≈1 Mb density over the full genome, a set of subtelomeric sequences for each chromosome arm, and a few hundred probes selected for their involvement in oncogenesis. The clone content is available in the "Cytoview" windows of the Sanger Institute mapping database site (http://www.ensembl.org/). These clones were isolated from their bacterial cultures and the DNA was extracted using the standard protocol of the Welcome Trust Sanger Institute (Cambridge, UK). A minimum of three replicates per clone were printed by *Microgrid II* (Biorobotics) on each slide (*Ultragaps Coated Slides*, Corning). Briefly, for labeling reactions, 2 μg of nonamplified genomic DNA from tumor and 2 μg of reference material (DNA of placenta) were digested separately with DpnII restriction enzyme (New England Biolabs, Beverly, MA, USA). For microarray hybridization, the digested DNAs were separately labeled using random primers (Bioprimer labeling kit, Invitrogen) and Cy3-dCTP and Cy5-dCTP fluorescent dye for paired hybridisation samples (Amersham Biosciences). The labeled nucleotide incorporation was quantified using the NanoDrop spectrophotometer (ND-1000). Labeled test and reference DNAs were mixed equitably, co-precipitated in presence of Cot-1 human DNA (Roche, Indianapolis, IN, USA) with ethanol, washed, and resuspended in hybridization solution (50% formamide, 10% dextran sulfate, 2X standard saline citrate, 10 mM Tris pH7.6, 2.7% sodium dodecyl sulfate, and 10 μg/μl of yeast tRNA). DNA mixtures were cohybridized to the arrays in the GENETAC (genomic solutions) for 48 h at 42°C according to the manufacturer's recommended protocol. Images and signal intensities were acquired using the GenePix4000B (Axon Instruments, Burlingame, CA, USA) dual laser scanner in combination with the GenePixPro4.0 (Axon Instruments) imaging software.

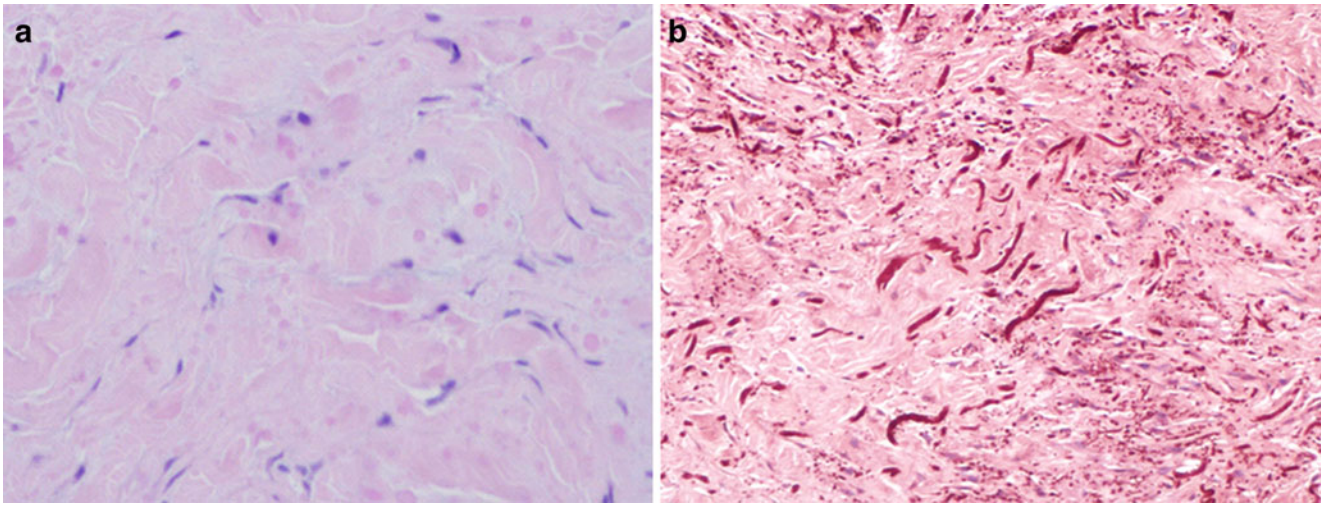

Fig. 1 **a** Microscopic of elastofibroma. **b** The presence of elastic anomalous fibers begins to be suspected by the habitual techniques (HE)

Data analysis

The Cy5/Cy3 intensity ratios of every spot were converted into $\log_2$ ratios. The $\log_2$ ratio for each clone was normalized to the median $\log_2$ ratio of ten control hybridizations, after which the median of triplicate spots was calculated. Data from two-color hybridizations for both sets of DNA were normalized using the DNMAD module of the GEPAS software [11]. Regions of copy number gain or loss from the array-CGH data were identified by creating sample-specific thresholds {Pollack 1999 57/id; Carvalho 2004 80/id}. The clones with $\log_2$ ratios above or below a control sample's threshold value were considered as gains or losses, respectively. At least two consecutive BAC clones with a $\log_2$ ratio of −0.7 or less defined genomic loss and $\log_2$ ratio of +0.7 or more defined region of genomic gain. Spots with weak Cy3 or Cy5 intensity (R^2<0.2) were excluded from analysis. In addition, clones with a SD≥0.3 of triplicate spots were also excluded. Approximately 10% of clones were excluded in each analysis. We also performed an analysis for copy error approach of Lingjaerde et al., using Asterias plataform [12]. All data sets were carefully reviewed for with the "Database of Genomic Variants" (www.project.tcag.ca/cariation) and that of chromosomal imbalances and phenotype in humans using Ensembl Resources (DECIPHER: http://www.sanger.ac.uk/PostGenomics/decipher/).

FISH analysis

Fluorescence in situ hybridization (FISH) studies were performed with the LSI 19p13/LSI19q13 Dual Color probe Set (Vysis, Dowerners Grove, IL, USA). Paraffin-embedded tissue sections (4 μm thick) were deparaffinized, dehydrated, and air-dried. The slides were placed in 2 mM EDTA (pH=9) for 15 min. After cooling, the slides were transferred to a Coplin device containing 40 ml of 0.9% NaCl (pH=1.5) and 160 mg of pepsin (Sigma) preheated to 37°C. Following incubation for 15 min, the sections were dehydrated in an alcohol series and fixed in 3:1 methanol/acetic acid for 10 min. The slides were then incubated in a Hybrite hybridization chamber (Vysis) for 12 min at 72°C, followed by 15-20 h at 37°C. After hybridization, the slides were washed in standard solutions of saline citrate. Nuclei were counterstained with DAPI (Vector Laboratories Inc). The images were captured on an Olympus BX60 epifluorescence microscope coupled with a CCD camera and were evaluated with Cytovision software (Applied Imaging). Approximately 200 non-overlapping tumor cells were evaluated.

MLPA analysis

For MLPA analysis of DNA, copy number changes the MS-MLPA probe set ME001, ME002, and ME003 kit from MRC-Holland (Amsterdam, The Netherland) which contains 41, 42, and 45 probes, respectively. DNA was isolated according to the manufacturer's protocol. In short, approximately 100 ng of DNA were denaturated at 98°C for 5 min and subsequently hybridized overnight with a mixture of probe pairs, each consisting of two oligonucleotides that recognize adjacent DNA sequences. On the next day, the adjacent hybridized hemiprobes were ligated. After denaturation, PCR was performed with two universal PCR primers amplifying all probe pairs in one reaction. Analysis of the MLPA PCR products was performed on an ABI model 3100 16 capillart sequencer (Applied Biosystems, Warrington, UK). Peak area and height were measured using GENESCAN analysis software (Applied Biosystems, Warrington, UK). The analysis was performed with Coffalyser software according to manufacturer's recommendations. Data were analyzed with Coffalyser Software (MRC-Holland). Due to overlap with and between probe set, a total of 72 genes can be analyzed for copy number aberrations by the combined use of

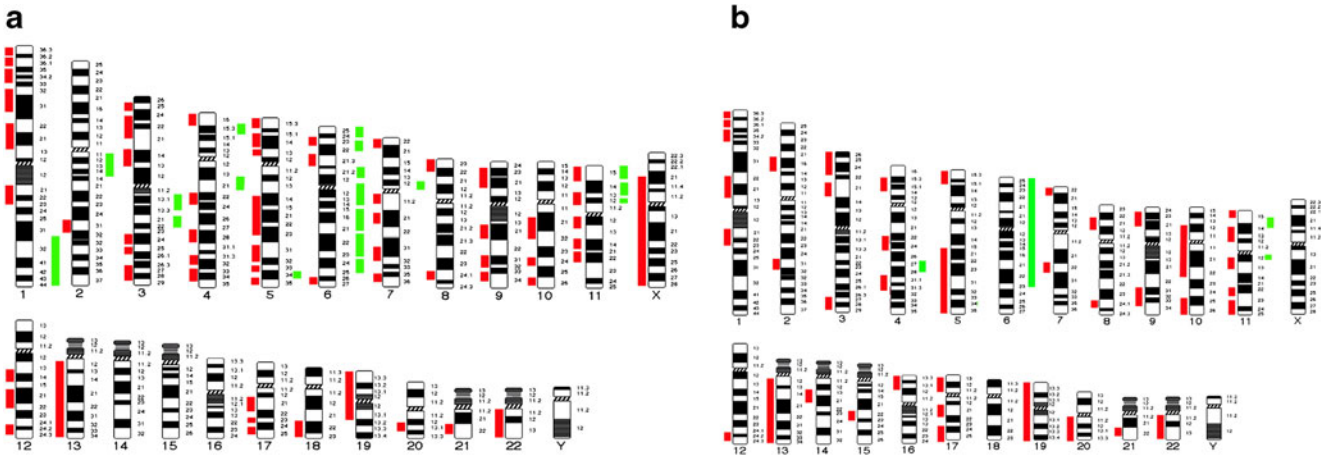

Fig. 2 Schematic representations of genomic imbalances in elastofibroma. **a** case I (p124).B) case II (p125).The *lines* show the genomic regions that exhibited gains (*right*) or losses (*left*)

both sets, So it is allowing determination of status of RARB on 3p24, PARK2 on 6q25, PTEN on 10q23, ATM on 11q22.3, BRCA2 on 13q12, and TIMP3 on 22q13 (three probes) and the rest of genes with one or two probes. For genes targeted by one probe only, values <0.7 or 1.3>were taken indicative of genomic loss and gain, respectively. For targeted by two probes, both values had to be <0.8 or 1.2> score an aberration. For genes targeted by three probes, these thresholds were set to 0.9 and 1.1.

Results

Genomic changes by aCGH

In the present study, array CGH analysis was performed in two elastofibroma. Several chromosomal gains and losses were detected in these cases. Interestingly, losses at 1p36-p31, 19p13.3-q13.3, and 22q111-q13 were recurrent in both elastofibroma. In addition, gains on chromosome 6p25-q25 were also observed in both cases (see Fig. 2 and supplementary material).

In order to confirm the genetic imbalances observed by array CGH, FISH analysis for the 19p13.1 region was performed in both cases. Loss of at 19p13 was detected in more than 40% of the cells. Analysis of MLPA showed loss genomic in STK11 and KLK3 probe on 19p13. In addition, we used MLPA analysis to facilitate identification of genes encoded in regions of genomic gains or losses. MLPA revealed that both samples showed deletions for *CASR* (*3q21*), *GSTP1* (*11q13*), and *BRCA2* (*13q12*) and gains on *APC* (*5q21*) and *PAH* (*12q23*), and in the other hand, losses on *TP73* (1p36), *DLC1* (8p23.1), *IGSFR4* (11q23), *CDH13* (16q24) and gains on *RARB* (3p24) and *TIMP3* (22q11) were observed only in patient p124. Similarly, loss of *ESR1* (6q25), *PARK2* (6q25), *ATM* (11q23), and *CHFR* (12q24)

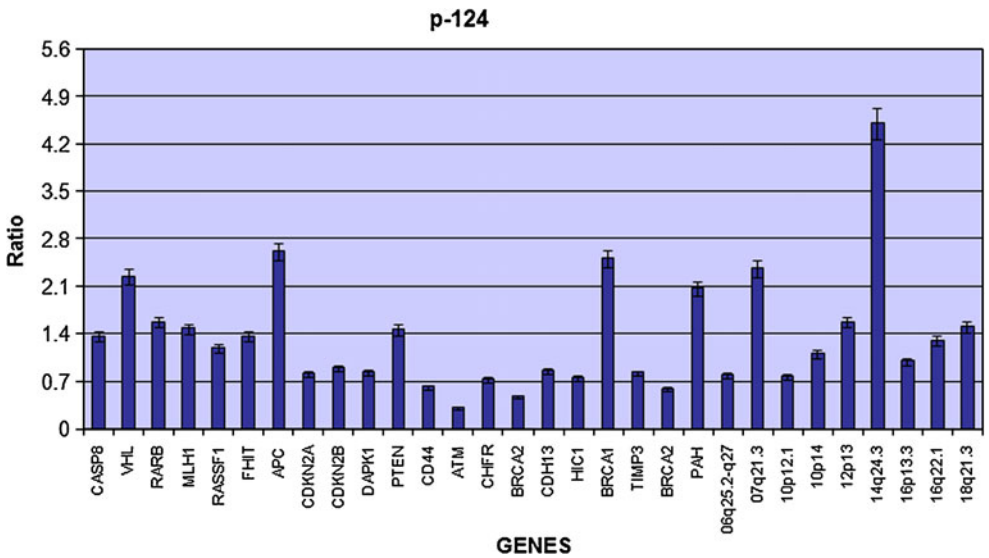

Fig. 3 Example of gains and losses of several genes by means of MLPA; case I (p124)

Table 1 Summary of samples analyzed and aberrations identified by MLPA

Gene	Chr pos	Case I (p-124)	Case II (p-125)
TP73	1p36	LOH (0.58)	
RUNX3	1p36.11	Amplification (9.46)	
PRDM2	1p36.21		Gain (1.55)
MSH6	2p16	Amplification (5.46)	Amplification (5.1)
CASP8	2q33-q34	Gain (1.34)	HO Loss (0)
FHIT	3p14.2	Gain (1.59)	HO Loss (0)
MLH1	3p21.3		
RASSF1	3p21.3		
CTNNB1	3p22	HO Loss (0.01)	HO Loss (0)
RARB	3p24	Gain (1.43)	
VHL	3p25.3		
CASR	3q13.3-q21	HO Loss (0.01)	HO Loss (0)
HLTF	3q25.1		
IL2	4q26	Amplification (3.39)	HO Loss (0)
APC	5q21	Gain (2.24)	Amplification (2.75)
SCGB3A1	5q35.3		
TNXB	6p21.3	Amplification (3.54)	Gain (2.36)
ID4	6p22.3		
ESR1	6q25.1		HO Loss (0)
PARK2	6q26		LOH (0.35)
SFRP4	7p14.1	Amplification (3.92)	
TWIST1	7p21.1		
CDK6	7q21.3	Gain (2.45)	
DLC1	8p23.1	HO Loss (0.26)	
PAX5A	9p13		
CDKN2A	9p21		
CDKN2B	9p21		
PTCH	9q22.3		
DAPK1	9q34.1		HO Loss (0)
CREM	10p12.1	Gain (1.36)	LOH (0.48)
AI651963	10p14		Gain (1.71)
PTEN	10q23.31		
SFRP5	10q24.2		
MGMT	10q26		
BNIP3	10q26.3	HO Loss (0.12)	
CD44	11p12	HO Loss (0)	HO Loss (0)
PAX6	11p13	HO Loss (0)	HO Loss (0)
WT1	11p13		Gain (2.13)
CD44	11p13		HO Loss (0)
GSTP1	11q13	HO Loss (0.01)	HO Loss (0)
ATM	11q22.3		LOH (0.58)
IGSF4	11q23	HO Loss (0.01)	Gain (1.31)
H2AFX	11q23.3		
TNFRSF1A	12p13	Gain (1.39)	
TNFRSF7	12p13	HO Loss (0)	HO Loss (0)
CDKN1B	12p13.1	HO Loss (0)	LOH (0.44)
CCND2	12p13.32		
PAH	12q23	Gain (1.95)	Amplification (2.79)
CHFR	12q24.33		LOH (0.58)

Table 1 (continued)

Gene	Chr pos	Case I (p-124)	Case II (p-125)
BRCA2	13q12	LOH (0.65)	LOH (0.34)
RB1	13q14.2		
MLH3	14q24.3		
MLH3	14q24.3		
THBS1	15q15	HO Loss (0)	
PYCARD	16p12	Amplification (8.29)	
TSC2	16p13.3		
CDH1	16q22.1	Gain (1.39)	
CDH13	16q24.2	LOH (0.52)	
PMP22	17p12	Gain (1.6)	Gain (1.34)
TP53	17p13.1		Gain (1.92)
HIC1	17p13.3		
BRCA1	17q21		
CACNA1G	17q21.33	Amplification (4.27)	Gain (1.88)
TGIF	18p11.31		Gain (1.6)
BCL2	18q21.3		Gain (1.47)
CACNA1A	19p13.13		
STK11	19p13.3	LOH (0.46)	LOH (0.38)
KLK3	19q13	HO Loss (0)	HO Loss (0)
GATA5	20q13.33	HO Loss (0)	HO Loss (0)
TIMP3	22q12.3	Gain (1.42)	

and gains on *SFR4* (11q23) and *BCL2* (18q21.3) were present in case p-125 only (see Fig. 3 and Table 1).

Discussion

The presence of an abnormally intense proliferation of fibroblastic tissue with by fragmented, thickened fibbers with serrated aspect is the typical morphological finding of elastofibroma, a lesion described in most cases in the subescapular region. Entity of benign character, the fact that it has been frequently observed in patients after performing a heavy and lasting manual work, has suggested a possible reactive nature rather than a neoplastic one

In our study, we have studied two cases of elastofibroma sample from typical location, in which the presence of elastic anomalous fibers was suspected by usual the habitual techniques and later confirmed by specific staining (Orcein satin; Fig. 1a, b).

Molecular cytogenetic studies have contributed greatly to the understanding of the histopathogenesis of a number of mesenchymal neoplasms, both benign and malignant. Of great interest has been the cytogenetic characterization of several entities considered to be" pseudo-neoplastic" or possibly "reactive" or "congenital". In case of elastofibroma, the cytogenetic studies have shown chromosomal instability, gain of DNA copy number and clonal chromosomal aberrations, suggesting that this lesion represents a true neoplasm rather than a reactive process.

Here, we report two cases of elastofibroma with genomic losses on 1p, 19p, and 22q and gains on 6p-qter, which have been detected by array CGH in both cases. Nishio et al. using CGH reported genomic changes in 33% of elastofibroma cases being the most frequent genomic changes located on chromosome X and 19 [7]. In our study, we have also observed by aCGH losses on 19p which were subsequently confirmed by FISH. In additional, losses on 22q detected by array CGH were later confirmed by deletion of genes located on 22q11 by MLPA. The 1p breakpoint has also been described in other fibrous lesions such as desmoid tumors and angiofibroma. In elastofibroma, changes on 1p have also been reported and which in accordance with chromosome instability, clonal chromosomal aberrations, and structural changes on 1p, and suggested a possible neoplastic origin for elastofibroma [4–6]. The biological significance of genetic instability is not known although it is considered to represent a precursor lesion of more stable rearrangements.

This picture of "chromosome instability" correlates well with our finding of *BRCA2* gen, detected by MLPA and deletion on whole chromosome 13 detected by array CGH in both samples of elastofibroma. *BRCA2* has been implicated in essential processes cells, including chromatin remodeling, regulation of transcription, and RAD51-mediated recombination repair, although its role in these processes remains

unclear and the mechanisms underlying tissue specificity of its tumor suppressive property unknown [13]. Also, deletion of GSTP1 (*11q13*) was detected by MLPA and by aCGH in both cases. Although the role of GSTP1 is unknown in this process, it has been recently reported that its mechanisms are involved in the genome protection and drug resistance [14].

In conclusion, our study provides more evidence supporting that elastofibroma is a clonal or a potential neoplastic process. Additional studies are needed to confirm the presence of common genomic alterations in a large series of these lesions and to characterize biological consequences of these genomic abnormalities in elastofibroma.

Acknowledgements Partially supported by grants from the Spanish Fondo de Investigaciones Sanitarias PI02/1393; Junta de Castilla y León (Refs. SAN191/SA08/06, SA053A05 and GR97).

We thank M Garayoa from Centro de Investigación del Cáncer of Salamanca, M.A. Hernández from the IECSCYL-Hospital Universitario Research Unit for their excellent technical assistance. We also thank Dr. E. Garcia (Genomics and Proteomics Unit) for microarray analyses.

Conflict of interest We declare that we have no conflict of interest.

References

1. Jarvi O, Saxen E (1961) Elastofibroma dorse. Acta Pathol Microbiol Scand Suppl 51:83–84
2. Nagamine N, Nohara Y, Ito E et al (1982) Elastofibroma in Okinawa. A clinicopathologic study of 170 cases. Cancer 9:1794–1805
3. Schepel JA, Wille J, Seldenrijk CA et al (1998) Elastofibroma: a familial occurrence. Eur J Surg 7:557–558
4. Vanni R, Marras S, Faa G et al (1999) Chromosome instability in elastofibroma. Cancer Genet Cytogenet 2:182–183
5. Batstone P, Forsyth L, Goodlad J (2001) Clonal chromosome aberrations secondary to chromosome instability in an elastofibroma. Cancer Genet Cytogenet 1:46–47
6. McComb EN, Feely MG, Neff JR et al (2001) Cytogenetic instability, predominantly involving chromosome 1, is characteristic of elastofibroma. Cancer Genet Cytogenet 1:68–72
7. Nishio JN, Iwasaki H, Ohjimi Y et al (2002) Gain of Xq detected by comparative genomic hybridization in elastofibroma. Int J Mol Med 3:277–280
8. Hisaoka M, Hashimoto H (2006) Elastofibroma: clonal fibrous proliferation with predominant CD34-positive cells. Virchows Arch 2:195–199
9. Pinkel D, Segraves R, Sudar D et al (1998) High resolution analysis of DNA copy number variation using comparative genomic hybridization to microarrays. Nat Genet 2:207–211
10. Schouten JP, McElgunn CJ, Waaijer R et al (2002) Relative quantification of 40 nucleic acid sequences by multiplex ligation-dependent probe amplification. Nucleic Acids Res 30(12):e57
11. Montaner D, Tarraga J, Huerta-Cepas J et al (2006) Next station in microarray data analysis: GEPAS. Nucleic Acids Res Web Server issue 34:W486–W491
12. Diaz-Uriarte R, Alibes A, Morrissey ER et al (2007) Asterias: integrated analysis of expression and aCGH data using an open-source, web-based, parallelized software suite. Nucleic Acids Res Web Server issue 37:W75–W80
13. Abaji C, Cousineau I, Belmaaza A (2005) BRCA2 regulates homologous recombination in response to DNA damage: implications for genome stability and carcinogenesis. Cancer Res 10:4117–4125
14. Lo HW, Stephenson L, Cao X et al (2008) Identification and functional characterization of the human glutathione S-transferase P1 gene as a novel transcriptional target of the p53 tumor suppressor gene. Mol Cancer Res 5:843–850

Virchows Arch (2010) 456:689–694
DOI 10.1007/s00428-010-0904-x

ORIGINAL ARTICLE

Mergence of partial and complete atrophy in prostate needle biopsies: a morphologic and immunohistochemical study

Athanase Billis · Luciana Meirelles · Leandro L. L. Freitas

Received: 27 November 2009 / Revised: 26 January 2010 / Accepted: 10 March 2010 / Published online: 2 April 2010
© Springer-Verlag 2010

Abstract Partial atrophy is the most common benign lesion that causes difficulty in the differential diagnosis with adenocarcinoma of the prostate. Very few studies described, illustrated, and discussed the concomitance of partial atrophy with complete atrophy in prostatic needle biopsies. The study group comprised 75 needle prostatic biopsies corresponding to 67 patients. Focal prostatic atrophy was present in all biopsies. Complete atrophy was subtyped into simple atrophy, sclerotic atrophy, and hyperplastic atrophy (or postatrophic hyperplasia). We analyzed the presence of inflammation in the atrophic foci and immunohistochemistry was performed for p63, 34βE12, and PSA. Partial atrophy and complete atrophy were present concomitantly in 47/75 (63%) biopsies. In 20/75 (27%) biopsies, there were areas with mergence of partial atrophy and complete atrophy. We illustrate morphologic transitions between these lesions in the same gland. Using immunohistochemistry, the aberrant phenotypic expression in the secretory compartment in all subtypes of complete atrophy highlighted the morphologic transitions between partial and complete atrophies in the same gland. An intriguing finding was the absence of chronic inflammation in partial atrophy foci as well as in areas of mergence between these lesions. Inflammation was present only in isolated complete focal atrophy foci. Partial atrophy seems to be part of a morphologic spectrum of focal prostatic atrophy and probably precedes complete atrophy. The question of whether the inflammation produces tissue damage and prostatic atrophy or whether some other insults like ischemia induces the tissue damage and atrophy directly, with inflammation occurring secondarily, is still unsettled.

Keywords Prostate · Atrophy · Partial atrophy · Postatrophic hyperplasia · Needle biopsy

A. Billis (✉) · L. Meirelles · L. L. L. Freitas
Department of Pathology, School of Medicine,
University of Campinas (Unicamp),
Caixa, Postal 6111, CEP 13084-971 Campinas, SP, Brazil
e-mail: athanase@fcm.unicamp.br

Introduction

The most common benign lesion that causes difficulty in the differential diagnosis with adenocarcinoma of the prostate is partial atrophy. This lesion was first reported in the periodic literature by Oppenheimer et al. [1]. Very few studies described, illustrated, and discussed the concomitance of partial atrophy to complete atrophy in prostatic needle biopsies [1–3]. In the study by Oppenheimer et al. [1], more fully developed atrophy was present simultaneously with partial atrophy in 35.35% of obtained needle cores. In their study, partial and complete atrophies were present in the same gland in 66.7% of the cases. Wang et al. [3] found that 48 of 278 (17.3%) partial atrophy cases were mixed with postatrophic hyperplasia. Przybycin et al. [2] described that complete atrophy was present but distinct from partial atrophy foci in 41/45 (91%) needle biopsies. The only image that clearly illustrates a transition between partial and complete atrophies in the same gland is in Fig. 8 of Oppenheimer's study [1].

The aim of our study is to establish the frequency of concomitance of partial atrophy to all subtypes of complete atrophy in needle cores as well as the frequency of mergence between the lesions. van Leenders et al. [4] found that many of the atrophic epithelial luminal cells in proliferative inflammatory atrophy (or postatrophic hyperplasia with inflammation) are intermediate cells. This

conclusion was based on an aberrant phenotypic expression of the secretory compartment, which is also seen in atrophic prostate acini in castrated dogs [5]. Based on our finding that partial atrophy does not show this aberrant phenotypic expression, we used immunohistochemistry to highlight the mergence of partial and complete atrophies in the same gland. Concomitance of partial atrophy to more fully developed atrophy (complete atrophy) and the mergence of partial atrophy to complete atrophy in the same gland may be a clue and an important microscopic feature for the recognition of this benign mimicker of cancer [1].

Materials and methods

The study group comprised 75 needle prostatic biopsies corresponding to 67 patients; four patients had two biopsies, and two patients had three biopsies. No patient had radiotherapy, androgen manipulation, or symptomatic prostatitis, and no biopsy showed cancer, high-grade prostatic intraepithelial neoplasia, or areas suspicious for cancer. Focal prostatic atrophy was present in all biopsies.

Partial prostatic atrophy was diagnosed according to the criteria described by Oppenheimer et al. [1]. Architecturally, it consists of crowded glands often with a disorganized growth pattern. In contrast to complete atrophy, which can typically be diagnosed at scanning magnification owing to the presence of well-formed glands with a very basophilic appearance, partial atrophy has pale cytoplasm lateral to the nuclei giving rise to pale staining glands that more closely mimic cancer (Fig. 1a). The nuclei may be slightly enlarged and irregular with occasional nucleoli. There is scant apical cytoplasm with nuclei extending to the full cell height, pale lateral cytoplasm similar to the cytoplasm seen in adjacent more recognizable benign glands, and luminal undulations as contrasted to the straight luminal borders often seen with malignant glands.

Complete atrophy was diagnosed according to criteria described by Billis [6] and Postma [7]. Three histological subtypes were identified: simple atrophy, sclerotic atrophy, and hyperplastic atrophy (or postatrophic hyperplasia).

Simple atrophy usually involves an entire lobule, although isolated acini may be affected. The acini are small, showing scant cytoplasm and decrease in the height of the epithelial cells (Fig. 1b). They may be cystic with flattened epithelium. The surrounding stroma may show fibrosis or elastosis.

Sclerotic atrophy is a distinctive lesion. There is simultaneous atrophy of the epithelium and a proliferation of the fibroblasts about the acinus. Continued proliferation results in a fibrohyaline collar frequently associated to elastosis that involves the acinus (Fig. 2a). With higher degrees of hyalinization the acini dilate, sometimes prominently, and the epithelium becomes extremely flattened and eventually can no longer be identified. In advanced stages, the lumen is replaced by loose mesenchyme-like tissue with scattered inflammatory round cells.

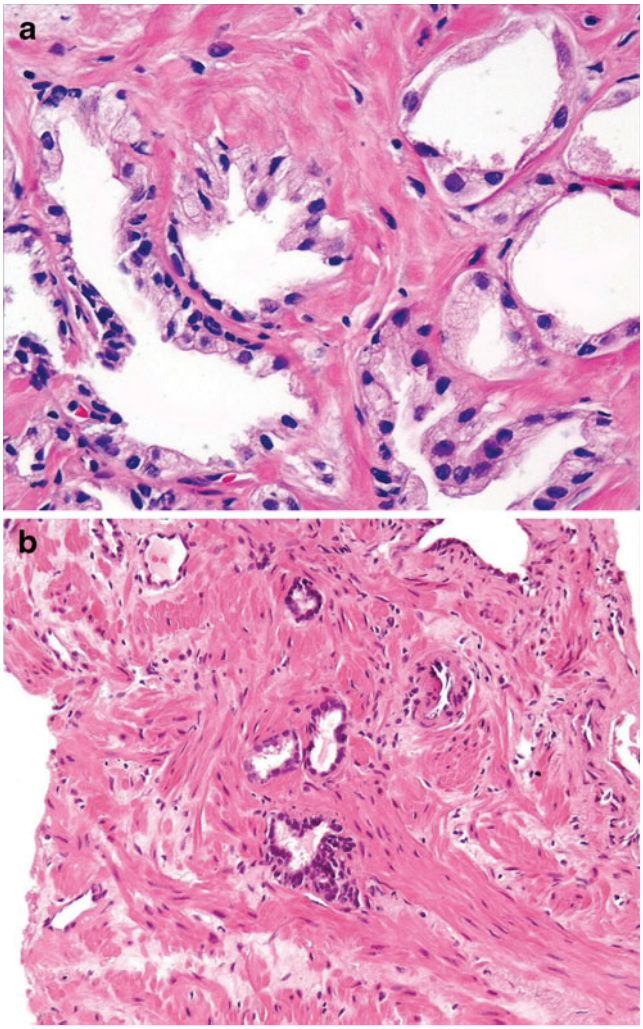

Fig. 1 **a** Partial atrophy. Acini with pale cytoplasm lateral to the nuclei giving rise to pale staining glands that more closely mimic cancer. There is scant apical cytoplasm with nuclei extending to the full cell height (H & E); **b** Simple atrophy. Isolated small acini showing crowded nuclei, scant cytoplasm and decrease in the height of the epithelial cells (H & E)

Hyperplastic atrophy (or postatrophic hyperplasia) shows small acini closely packed together and lined by atrophic epithelium. In contrast to partial atrophy, the cytoplasm is very scant, and the nuclei are crowded conferring a basophilic tinge to the lesion (Fig. 2b). When fibrosis is present in the stroma, the proliferation is irregular and can result in distortion of the acini mimicking infiltrative adenocarcinoma. The hyperplastic acini may show cystic dilatation. Hyperplastic atrophy showing a central duct or acinus with sclerotic atrophy is a very characteristic lesion of complete focal prostatic atrophy.

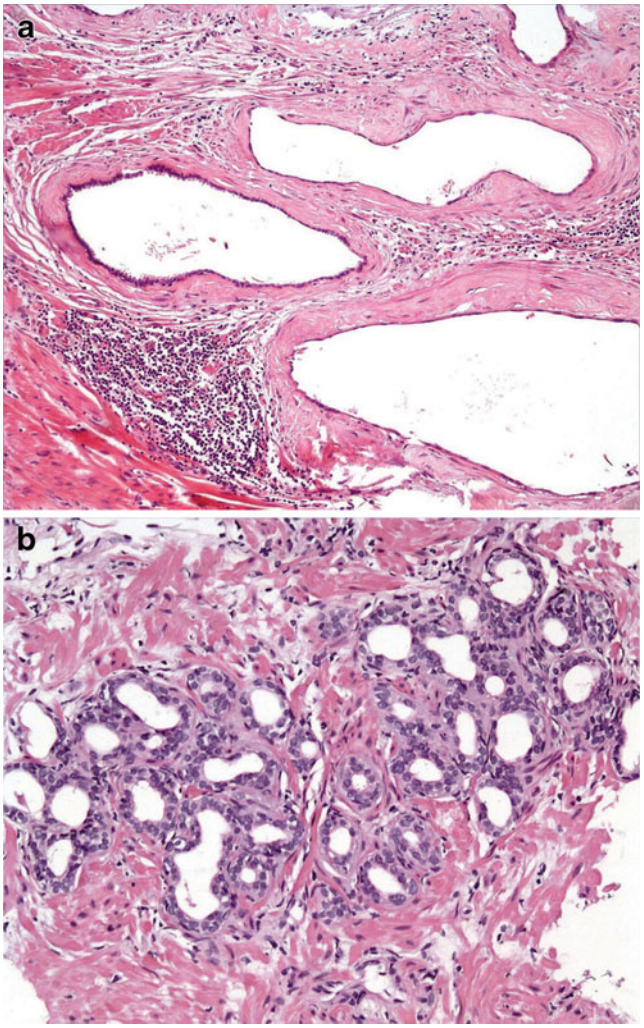

Fig. 2 **a** Sclerotic atrophy. Dilated acini, atrophy of the epithelium and a thick fibrohyaline collar involving the acinus. Presence of chronic inespecific inflammation (H & E); **b** Hyperplastic atrophy (or postatrophic hyperplasia). Small acini closely packed together and lined by atrophic epithelium. In contrast to partial atrophy the cytoplasm is very scant, and the nuclei are crowded. The stroma shows fibrosis and elastosis (H & E)

Inflammation When present in the atrophic foci was considered inactive (infiltration of lymphocytes) or active (infiltration of lymphocytes and neutrophils in the stroma). Inactive inflammation was graded as being slight, moderate or intense.

Immunohistochemistry Standard immunohistochemical techniques were used for 34βE12, p63, and PSA.

Results

The age of the patients ranged from 47 to 81 years (mean and median, 64 and 64 years, respectively). The number of cores examined for each biopsy ranged from 7 to 18 (mean and median, 9.4 and 8 cores, respectively).

Table 1 shows the several subtypes of focal prostatic atrophy present in each of 75 biopsies. In 6/75 (8%) biopsies only one subtype of prostatic atrophy was present; in 69/75 (92%) biopsies, more than one subtype were present. Partial atrophy and complete atrophy were present concomitantly in 47/75 (63%) biopsies. In 27/75 (36%) biopsies, only complete atrophy foci were seen in the cores; and, in only one biopsy, partial atrophy was the only subtype present.

Immunohistochemistry showed that basal cells in foci of both partial and complete atrophies were positive for p63 and 34βE12. The secretory cells in all partial atrophy foci were positive for PSA and negative for 34βE12, however, in all three subtypes of complete atrophy the cells of the secretory compartment showed aberrant immunohistochemical expression: PSA negative (Fig. 3a) and 34βE12 positive (Fig. 3b).

In 20/75 (27%) biopsies, we found topographical mergence of partial and complete atrophies (Fig. 4a). In these areas, we also disclosed morphologic transitions between partial and complete atrophies in the same gland. These transitions were characterized by an abrupt interruption of cells with pale cytoplasm lateral to the nuclei and scant apical cytoplasm to crowded nuclei with very scant cytoplasm (Fig. 4b). The aberrant immunohistochemistry expression of the secretory compartment in complete atrophy highlighted these morphologic transitions in the same gland (Fig. 5a and b).

Table 2 shows the presence of chronic inespecific inflammation in foci of several subtypes of focal atrophy. It was present in the foci of simple atrophy in 41/73 (56%) biopsies, in sclerotic atrophy in 12/25 (48%) biopsies, and in hyperplastic atrophy in 25/46 (54%) biopsies. The

Table 1 Subtypes of focal atrophy present in 75 needle prostatic biopsies

Subtypes	Number of biopsies (%)
P+S+H	22/75 (29.3)
P+S	16/75 (21.3)
P+S+H+SC	8/75 (10.6)
S+H+E	8/75 (10.6)
S+H	7/75 (9.3)
S+SC	6/75 (8.0)
S	5/75 (6.6)
P	1/75 (1.3)
P+S+SC	1/75 (1.3)
H+SC	1/75 (1.3)

P = partial atrophy; S = simple atrophy; SC = sclerotic atrophy; H = hyperplastic atrophy (or postatrophic hyperplasia)

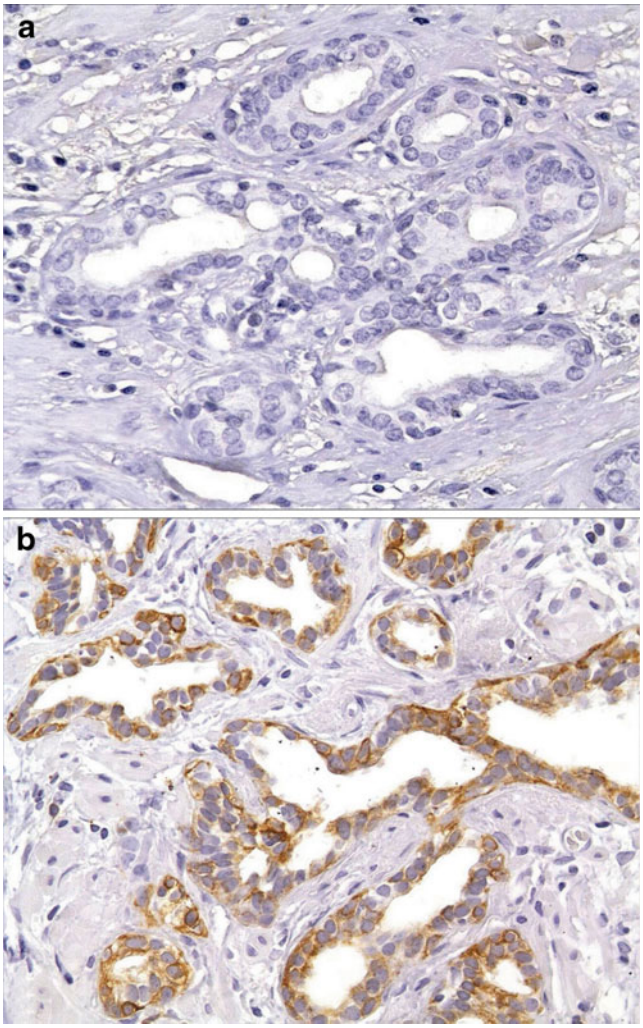

Fig. 3 Aberrant phenotypic expression in the secretory compartment of hyperplastic atrophy. **a** immunohistochemistry for PSA showing negative secretory cells; **b** immunohistochemistry for 34βE12 showing aberrant positivity in the secretory cells

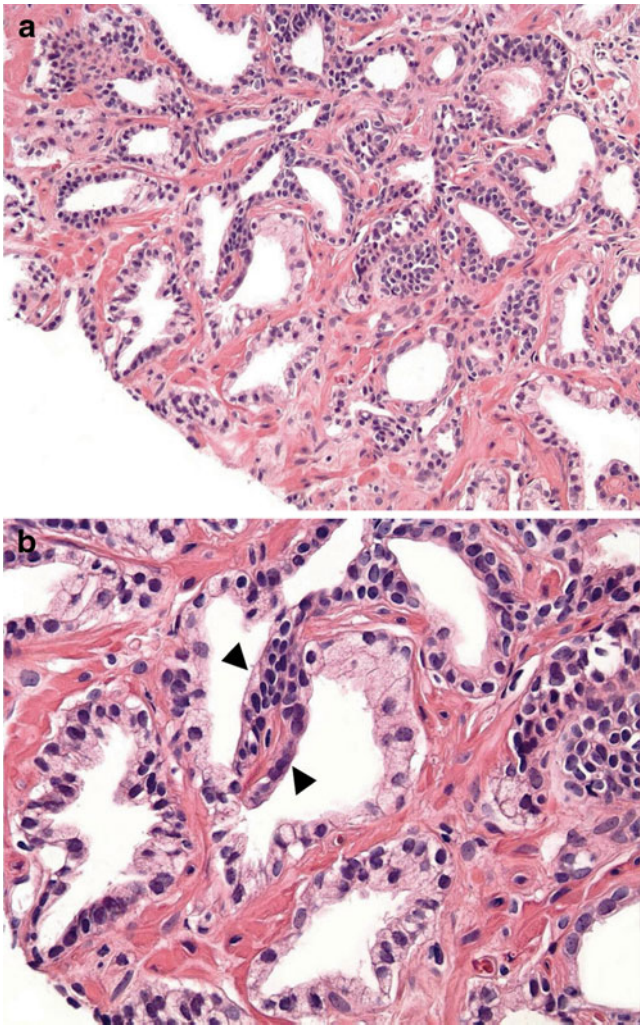

Fig. 4 **a** area showing mergence of partial atrophy and complete atrophy (H & E); **b** morphologic transitions between partial and complete atrophy in the same gland (*arrowheads* show complete atrophy) (H & E)

intensity of inflammation was slight or moderate. No case showed intense inflammation. Chronic inespecific inflammation was not seen in foci of partial atrophy either in isolated foci or in foci merging with complete atrophy. Focal active inflammation was seen in 10/75 (13%) biopsies.

Discussion

Our study showed that concomitance of partial atrophy and complete atrophy in the same biopsy is a frequent occurrence. In our study, partial atrophy and complete atrophy were present concomitantly in 47/75 (63%) biopsies. In Table 3, we compare our results with others. In the study by Oppenheimer et al. [1], partial atrophy was present simultaneously with more fully developed atrophy (complete atrophy) in 35.35% of biopsies. In the study by Wang et al. [3], 48 of 278 (17.3%) partial atrophy cases were mixed with postatrophic hyperplasia. According to the authors, this fact can help in diagnosing partial atrophy as a benign lesion in distinguishing cancer from this lesion. Przybycin et al. [2] found a much higher frequency. The authors described that complete atrophy was present but distinct from partial atrophy foci in 41/45 (91%) needle biopsies.

In 20/75 (27%) biopsies, we found topographical mergence of partial and complete atrophies. In these areas, transitions between partial and complete atrophies could be appreciated in the same gland. The aberrant phenotypic expression of the secretory compartment in complete atrophy is an aid for this recognition. We used immunohistochemistry for this purpose based on the study by van Leenders et al. [4]. These authors found that many of the

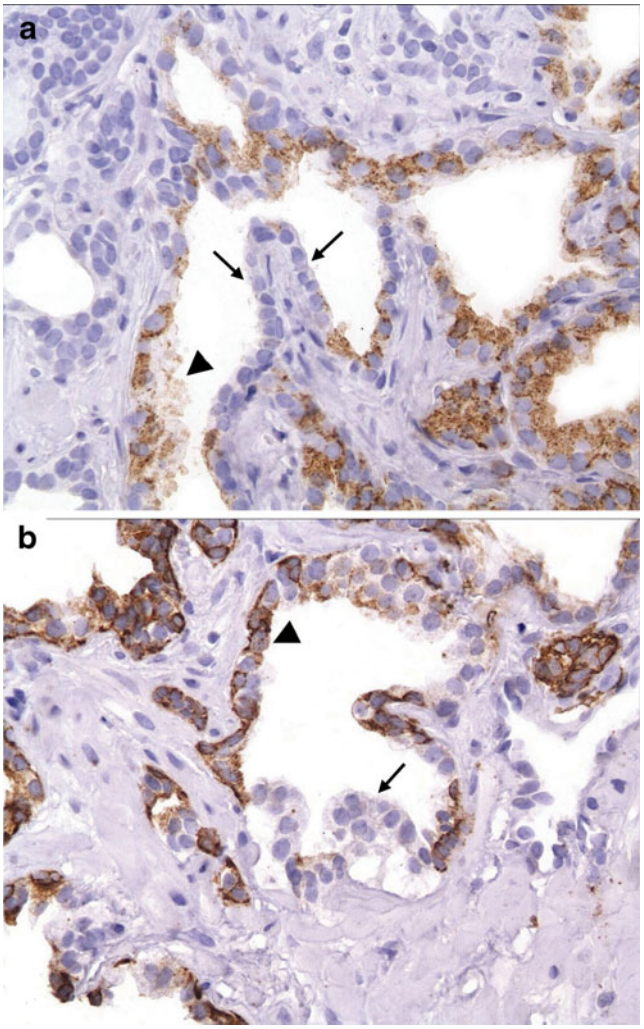

Fig. 5 Morphologic transitions between partial and complete atrophies in the same gland. **a** immunohistochemistry for PSA showing positive secretory cells in partial atrophy (*arrowhead*) and negative secretory cells in complete atrophy (*arrows*); **b** immunohistochemistry for 34βE12 showing positive secretory cells in complete atrophy (*arrowhead*) and negative secretory cells in partial atrophy (*arrow*)

atrophic epithelial luminal cells in proliferative inflammatory atrophy (or postatrophic hyperplasia with inflammation) are intermediate cells. This conclusion was based in part on the finding in these cells of weak expression of PSA and androgen receptor, high levels of cytokeratin 8/18, and lack of p63. This aberrant phenotypic expression of the secretory compartment is also seen in atrophic prostate acini in castrated dogs suggesting a pluripotentiality of response to sex hormones [5].

Table 2 Presence of chronic inespecific inflammation in foci of several subtypes of focal atrophy

Subtypes	Number of biopsies (%)
Partial	0/48 (0)
Simple	41/73 (56.2)
Sclerotic	12/25 (48)
Hyperplastic	25/46 (54.3)

Table 3 Concomitance of partial atrophy and complete atrophy in prostate needle biopsies

Study	Number of biopsies (%)
Wang et al. [3]	48/278 (17.3%)
Oppenheimer et al. [1]	18/51 (35.3%)
Przybycin et al. [2]	41/45 (91%)
Present study	47/75 (63%)

What is the significance of the mergence of partial atrophy and complete atrophy and the transitions in the same gland? According to Oppenheimer et al. [1], the transition from partial to more established atrophy, is accompanied by a parallel increase in the N:C ratio, suggesting gradual evolution from the partial form of atrophy to the more complete variety. This suggests that partial atrophy may be part of a morphologic continuum in focal prostatic atrophy. Hyperplastic type (or postatrophic hyperplasia) seems to be at the extreme end of this morphologic continuum [8]. A high cell proliferation using immunohistochemistry seems to support this hypothesis [9].

An intriguing finding in partial atrophy foci as well as in areas of topographic mergence between these lesions was the absence of chronic inespecific inflammation. On the other hand, inflammation was frequently found in complete atrophy foci: 56.2%, 48%, and 54.3%, in simple, sclerotic, and hyperplastic atrophy, respectively. In the only other study dealing with this feature, Przybycin et al. [2] found inflammation in an insignificant 1% of partial atrophy foci.

Chronic inflammation has been implicated in the development of tumors [10]. Some investigations have suggested a connection between inflammation and prostatic carcinoma. Focal prostatic atrophy, which is often associated with chronic inespecific inflammation, and less frequently to acute inflammation, has been especially suspicious. De Marzo et al. [11] proposed the term proliferative inflammatory atrophy for this type of atrophy, and suggested its implication in prostatic carcinogenesis. The question of whether the inflammation produces tissue damage and prostatic atrophy or whether some other insult like ischemia induces the tissue damage and atrophy directly, with inflammation occurring secondarily, is still unresolved [6, 12]. Hypothesizing that partial atrophy precedes complete atrophy, the absence of inflammation in the former as well as in areas of mergence between these two lesions seems to favor that inflammation in complete focal atrophy may be a secondary phenomenon.

Partial atrophy is the most common benign variant of focal atrophy that causes difficulty in the differential diagnosis with adenocarcinoma [3, 13]. Architecturally, partial atrophy consists of crowded glands often with a disorganized growth pattern. In contrast to complete atrophy, which can typically be diagnosed at scanning magnification owing to the presence of well-formed glands with a very basophilic appearance, partial atrophy has pale cytoplasm lateral to the nuclei giving rise to pale staining glands that more closely mimic cancer. An additional difficulty in distinguishing cancer from partial atrophy is the positivity for alpha-methylacyl coenzyme A racemase (AMACR) in some acini [3, 14]. The frequent concomitance of partial atrophy to more fully developed atrophy (complete atrophy) and the mergence of partial atrophy to complete atrophy in the same gland may be a clue and an important microscopic feature for the recognition of this benign mimicker of cancer [1].

In summary, partial atrophy and complete atrophy were present concomitantly in 47/75 (63%) biopsies. In 20/75 (27%) biopsies, there were areas with mergence of partial atrophy and complete atrophy. We illustrate morphologic transitions between these lesions in the same gland. Using immunohistochemistry, the aberrant phenotypic expression in the secretory compartment in all subtypes of complete atrophy, highlighted the morphologic transitions between partial and complete atrophies in the same gland. An additional and intriguing finding was the absence of chronic inflammation in partial atrophy foci as well as in areas of mergence between these lesions. Inflammation was present only in isolated complete focal atrophy foci.

Acknowledgment

Conflict of interest statement We declare that we have no conflict of interest.

References

1. Oppenheimer JR, Wills ML, Epstein JI (1998) Partial atrophy in prostate needle cores: another diagnostic pitfall for the surgical pathologist. Am J Surg Pathol 22:440–445
2. Przybycin CG, Kunju LP, Wu AJ et al (2008) Partial atrophy in prostate needle biopsies: a detailed analysis of its morphology, immunophenotype, and cellular kinetics. Am J Surg Pathol 32:58–64
3. Wang W, Sun X, Epstein JI (2008) Partial atrophy on prostate needle biopsy cores: a morphologic and immunohistochemical study. Am J Surg Pathol 32:851–857
4. van Leenders GJ, Gage WR, Hicks JL et al (2003) Intermediate cells in human prostate epithelium are enriched in proliferative inflammatory atrophy. Am J Pathol 162:1529–1537
5. Merk FB, Warhol MJ, Kwan PW et al (1986) Multiple phenotypes of prostatic glandular cells in castrated dogs after individual or combined treatment with androgen and estrogen. Morphometric, ultrastructural, and cytochemical distinctions. Lab Invest 54:442–456
6. Billis A (1998) Prostatic atrophy: an autopsy study of a histologic mimic of adenocarcinoma. Mod Pathol 11:47–54
7. Postma R, Schröder FH, van der Kwast TH (2005) Atrophy in prostate needle biopsy cores and its relationship to prostate cancer incidence in screened men. Urology 65:745–749
8. Cheville JC, Bostwick DG (1995) Post-atrophic hyperplasia of the prostate. Am J Surg Pathol 19:1068–1076
9. Ruska KM, Sauvageot J, Epstein JI (1998) Histology and cellular kinetics of prostatic atrophy. Am J Surg Pathol 22:1073–1077
10. Weitzman SA, Gordon LI (1990) Inflammation and cancer: role of phagocyte-generated oxidants in carcinogenesis. Blood 76:655–663
11. De Marzo AM, Marchi VL, Epstein JI et al (1999) Proliferative inflammatory atrophy of the prostate. Implications for prostatic carcinogenesis. Am J Pathol 155:1985–1992
12. Tomas D, Kruslin B, Rogatsch H et al (2007) Different types of atrophy in the prostate with and without adenocarcinoma. Eur Urol 51:98–104
13. Herawi M, Parwani AV, Irie J et al (2005) Small glandular proliferations on needle biopsies: most common benign mimickers of prostatic adenocarcinoma sent in for expert second opinion. Am J Surg Pathol 29:874–880
14. Worschech A, Meirelles L, Billis A (2009) Expression of AMACR (alpha-methylacyl coenzyme A racemase) in partial and complete focal atrophy on prostate needle biopsies. Anal Quant Cytol Histol 31:424–431

Virchows Arch (2010) 456:695–702
DOI 10.1007/s00428-010-0906-8

ORIGINAL ARTICLE

Cystic dysplasia of the epididymis: a disorder of mesonephric differentiation associated with renal maldevelopment

Manuel Nistal · Pilar González-Peramato · Grevelyn Sousa · Miguel Angel García-Cabezas · José Ignacio Rodríguez · Mariana M. Cajaiba

Received: 13 January 2010 / Revised: 10 March 2010 / Accepted: 11 March 2010 / Published online: 2 April 2010
© Springer-Verlag 2010

Abstract The occurrence of congenital epididymal malformations with a cystic component has not been fully characterized. Most epididymal cysts occur later in life and are likely acquired. In addition, congenital malformations of the male excretory system are extremely uncommon in fetuses and neonates, and epididymal dysplastic changes have not been reported in these cases. In this study, we report 20 cases (including 19 fetal/neonatal autopsies and one surgical specimen from an older child) showing the same spectrum of histological findings in the epididymis, characterized by cystic ductal dilation with dysplastic ducts of variable diameters and irregular shapes, with ill-defined walls. Efferent ductules also showed dysplastic features. In addition, 18 cases had either renal and/or urinary tract anomalies, including renal dysplasia (eight), pelvicaliceal dilation (eight), renal agenesis (four) and hypoplasia (one), ureteral agenesis (two) and hypoplasia (one), urethra and bladder agenesis (two), prostate agenesis (two), and autosomal recessive polycystic renal disease (two). Our observations led to the recognition of a peculiar, not previously described congenital lesion of the epididymis, and we propose the term cystic dysplasia of the epididymis for this anomaly. Similar to what is observed in other male genital system anomalies (including malformations of the rete testis, vas deferens, and seminal vesicles), most lesions occurred in association with renal and/or urinary tract malformations, suggesting a spectrum of congenital malformations. The shared embryological origin of these structures may explain their simultaneous occurrence, possibly related to disrupted mesonephric duct development.

Keywords Epididymis · Kidney · Dysplasia · Cyst · Congenital · Malformation

M. Nistal · P. González-Peramato · G. Sousa · M. A. García-Cabezas · J. I. Rodríguez
Department of Pathology, Hospital Universitário La Paz, Madrid, Spain

M. Nistal
Department of Anatomy, Histology and Neuroscience, School of Medicine, Universidad Autónoma de Madrid, Madrid, Spain

M. M. Cajaiba (✉)
Department of Pathology, University of Pittsburgh Medical Center, 200 Lothrop Street, Pittsburgh, PA 15213, USA
e-mail: cajaibamm@upmc.edu

Introduction

Congenital malformations of the male excretory system represent an uncommon finding in fetuses and neonates. These lesions are usually asymptomatic and are diagnosed incidentally later in life following orchidopexy and/or surgical exploration for hydroceles and inguinal hernias or during evaluation for infertility. Well-recognized congenital epididymal malformations include anomalous attachment of the epididymis to the testis and anomalies of number, size, and location (such as agenesis, duplication, hypoplasia, and ectopia). Anomalous attachment represents the commonest type of epididymal malformation reported and includes the diagnoses of atresia, detachment or loose attachment of one or more segments, and epididymal elongation. These anomalies are frequently found in association with undescended testes and may represent an important contributing factor for male infertility [1–5].

The occurrence of congenital epididymal malformations with a cystic component has not been fully explored, as most epididymal cysts occur later in life and are likely acquired. Cystic epididymal and testicular appendices

(embryonal remnants) which are not connected to the male excretory system should not be considered under this category. Most epididymal cysts occur after childhood and are diagnosed by ultrasound examination following palpation of a scrotal mass; they usually regress spontaneously, and anatomic pathological studies are rarely performed. A well-characterized example of acquired cysts results from obstruction of the epididymis or vas deferens leading to secondary cystic dilation of the epididymal duct, also referred to as spermatocele. An obstructive mechanism may also be responsible for the development of epididymal cysts in men with history of exposure to diethylstilbestrol, also detected later in life, and in younger patients with cystic fibrosis due to thickened secretions [4, 6–9]. In patients with von Hippel–Lindau disease (VHL), epididymal cysts are characteristically limited to the efferent ductules, have a peculiar morphology with predominance of clear cells, and often evolve into cystadenomas. In addition, they are usually diagnosed in adult patients, with no evidence of congenital lesions [10, 11].

Our observations on a series of fetal and neonatal autopsies led to the recognition of a peculiar congenital epididymal lesion characterized by architectural distortion secondary to maldeveloped aberrantly shaped efferent ductules and epididymal ducts with cystic dilation, in a pattern not previously described. Similar to what is observed in other anomalies of the male genital system (including malformations of the rete testis, vas deferens, and seminal vesicles), in most cases, these lesions occurred in association with renal and/or urinary tract malformations, suggesting a spectrum of congenital malformations. We propose the term cystic dysplasia of the epididymis (CDE) for this anomaly. In this study, we describe the morphological findings from our series and discuss the possible pathogenetic mechanisms involved.

Material and methods

Cases were retrospectively collected from the Department of Pathology files at Hospital Universitário La Paz, Madrid, Spain. The specimens were retrieved through review of 4,434 fetal and neonatal autopsy reports performed from 1966 to 2008 on male subjects, in which one of the two following criteria was present: reported epididymal anomalies (48 cases) and/or reported renal malformations (62 cases). In all cases, a full autopsy with complete dissection of the urinary tract had been performed. In addition, an orchiectomy specimen from a 4-year-old boy with renal agenesis received for consultation was also selected for review.

The archival paraffin-embedded material had been routinely processed through fixation with buffered formalin. Among the autopsy cases, representative sections from the epididymis had been submitted for histological examination according to our institutional embedding protocol: right testes/epididymides were submitted following longitudinal sectioning, whereas the left testes/epididymides were transversally sectioned. In some cases, several sections from each epididymis were submitted for histological evaluation, and others had only one available section. All H&E slides containing testis and epididymis were reviewed for each case, and morphological findings were recorded.

Results

From the 111 cases reviewed, 20 specimens were found to share the same spectrum of histological findings in the epididymis, as described below. Relevant clinical data from these cases are summarized in Table 1. The ages ranged from 27 weeks of gestation to 10 days of life for the 19 autopsy cases; the only surgical specimen corresponded to a 4-year-old boy. None of our cases had a positive history of diethylstilbestrol exposure or a family history suggestive of cystic fibrosis or VHL. However, most cases had associated systemic malformations, as summarized in Table 1.

Gross examination of the epididymis was unremarkable except for seven cases, in which the epididymal head revealed subtle surface irregularities with loss of the typical hemispherical shape. No abnormalities of size or attachment to the testis were observed, as well as any gross cystic lesions or segmental agenesis. The vas deferens was patent in all studied cases. Both right and left epididymides were available for histologic examination in 13 cases, resulting in 33 epididymal specimens from 20 studied cases; 16 out of the 33 specimens had the three anatomical segments (caput, corpus, and cauda) represented, whereas in 17 specimens, only one or two segments were available for evaluation.

Histological sections from all epididymides showed a distinctive lesion characterized by cystic ductal dilation, resulting in ducts of variable diameters and irregular shapes (Fig. 1a–d) with maldeveloped, poorly defined tubular walls (Fig. 1e) and associated abundant intertubular connective tissue (Fig. 1f). The lesion was bilateral in all 13 cases in which both epididymides were available for review. Some cases showed diffuse lesions involving the entire organ, whereas in others, the involvement was segmental (Fig. 1g) with dysplastic features present in either the caput, corpus, or cauda portions. Efferent ductules were reduced in numbers in all specimens in which the caput epididymis was involved (Fig. 1a, b) and also presented with irregularities in shape, number, and size in these cases.

Table 1 Associated findings in 20 patients with CDE: testicular pathology, renal and genitourinary malformations, and other systemic abnormalities

Case	Age	Testes		Kidneys		Urinary tract	Other
		Right	Left	Right	Left		
1	36 wga	Intra-abdominal	Intra-abdominal	No lesion	No lesion	Bilateral pyelocaliceal dilation	Cebocephaly, polydactyly, omphalocele, interatrial communication
2	38 wga	Intra-abdominal	Intra-abdominal	No lesion	Hypoplasia	Bilateral pyelocaliceal dilation + hydronephrosis	Microcephaly, sagittal suture synostosis, frontal lobes atrophy, micrognathia, low ear implantation, valgus feet
3	34 wga	Leydig cell hypoplasia	Leydig cell hypoplasia	No lesion	No lesion	Left pyelocaliceal dilation + hydronephrosis	Anencephaly
4	27 wga	No lesion	No lesion	No lesion	No lesion	Right pyelocaliceal dilation + hydronephrosis	Prematurity
5	10 days	No lesion	No lesion	No lesion	No lesion	No lesion	Trisomy 21, duodenal atresia
6	27 wga	No lesion	No lesion	No lesion	No lesion	No lesion	Prematurity
7	1 day	No lesion	No lesion	Renal dysplasia	Renal dysplasia	No lesion	Potter's sequence
8	36 wga	No lesion	No lesion	Renal dysplasia	Agenesis	Agenesis of bladder, urethra, and left ureter; rudimentary right ureter	Caudal regression syndrome, sirenomelia, complex cardiac malformations, external genitalia agenesis, renal vessels agenesis, single umbilical artery, Potter's sequence
9	1 day	Intra-abdominal	No lesion	Renal dysplasia	Renal dysplasia	Bilateral ureteral stenosis	Potter's sequence
10	38 wga	No lesion	No lesion	Renal dysplasia	No lesion	Right pyelocaliceal and ureteral dilation	Possible DiGeorge syndrome
11	35 wga	Inguinal/hypoplastic	Inguinal/hypoplastic	No lesion	Renal dysplasia	Left ureteral hypoplasia	Craniorachischisis, vertebral malformations, cleft palate, diaphragmatic hernia, pulmonary hypoplasia, nonimmune hydrops, hypospadia
12	36 wga	Intra-abdominal/ hypoplastic	Intra-abdominal/ hypoplastic	Renal dysplasia	No lesion	Agenesis of bladder and urethra, right megaureter, left pyelocaliceal dilation	Myelomeningocele, gastroschisis, cloacal exstrophy, micropenis, pulmonary hypoplasia
13	28 wga	No lesion	No lesion	Agenesis	Agenesis	No lesion	Potter's sequence
14	37 wga	No lesion	No lesion	Single ectopic kidney on pelvic midline, dysplastic		Ureteral atresia, hypoplastic bladder	Single umbilical artery, intestinal malrotation, facial anomalies, abnormal neuronal migration
15	34 wga	No lesion	No lesion	Polycystic kidneys	Polycystic kidneys	No lesion	ARPCKD, pulmonary hypoplasia
16	24 wga	No lesion	No lesion	Polycystic kidneys	Polycystic kidneys	No lesion	ARPCKD
17	33 wga	Intra-abdominal	Intra-abdominal	Agenesis	Agenesis	No lesion	Potter's sequence
18	37 wga	Intra-abdominal	Intra-abdominal	Renal dysplasia	Renal dysplasia	Bilateral hydronephrosis, prostate agenesis, posterior urethral valve	Prune belly syndrome, Potter's sequence
19	38 wga	Intra-abdominal	Intra-abdominal	Renal dysplasia	Renal dysplasia	Bilateral hydronephrosis, prostate agenesis, urethral atresia	Prune belly syndrome, Potter's sequence, single umbilical artery, intestinal duplication, prostatic agenesis
20	4 years	Cystic dysplasia of rete testis	Cystic dysplasia of rete testis	Agenesis	No lesion	No lesion	None

wga weeks of gestational age; *ARPCKD* autosomal recessive polycystic kidney disease

In some areas, dilated ductal segments were seen admixed with normal-appearing ducts. Despite the dilation and irregular shapes, the ductal epithelial components were indistinguishable from normal epididymis, with normal-appearing columnar and basal cells, and occasional clear cells. Both the normal and dysplastic ductal segments were surrounded by abundant loose mesenchymal tissue in the fetal specimens, whereas mature fibroconnective tissue without evident muscular differentiation was seen in older patients (Fig. 1h).

Among the studied 20 cases, 18 presented with either renal and/or urinary tract anomalies (Table 1); nine cases had both renal and urinary tract malformations, whereas six had only renal and three had only urinary tract malformations. The 15 cases with renal anomalies included renal dysplasia (eight cases), renal agenesis (four cases), autosomal recessive polycystic renal disease (two cases), and renal hypoplasia (one case); in nine cases, renal lesions were bilateral. The 12 cases with urinary tract anomalies consisted of pelvicaliceal dilation (eight cases), ureteral agenesis (two cases), urethra and bladder agenesis (two cases), prostate agenesis (two cases), and ureteral hypoplasia (one case). Testicular anomalies were also present in ten cases, including cryptorchidism in eight cases (Table 1). The testicular parenchyma showed normal tubular fertility index, as well as normal numbers of germ cells and Sertoli cell number per cross-tubular section; case 3 had decreased Leydig cell numbers when compared with normal age-matched controls. The tunica albuginea was normal and well collagenized in all cases. The rete testis was normal in all cases except case 20, which showed cystic dysplasia.

Discussion

All cases studied in our series share common histopathological findings characterized by irregular, segmental cystic dilation of the epididymal duct with aberrant shapes and an immature aspect, as well as an important decrease in the number of sections of efferent ductules with associated irregular cystic dilatation, resulting in architectural disruption of the organ. This peculiar epididymal lesion, referred by us as CDE, has not been previously characterized in the literature, and no similarities with other known congenital epididymal malformations were noted in any of our cases.

A remarkable feature in our cases was the presence of associated renal and/or urinary malformations in the majority of cases, similar to what has been described in other malformations of the male excretory system. The most well-characterized examples of excretory duct anomalies associated with renal and/or urinary malformations are congenital absence of the vas deferens (CAVD) and cystic dysplasia of the rete testis (CDRT) [12–15]; less frequent disorders include seminal vesicle cysts and agenesis, and ectopic deferens/mesonephric duct persistence [4, 16, 17]. Renal agenesis, usually ipsilateral to the excretory duct malformation, is the commonest type of renal malformation found in these cases; renal dysplasia, hypoplasia, ureteral duplication, and urethral stenosis have also been described. Based on these observations, screening for renal malformations is recommended in all men presenting with excretory duct malformations.

In CAVD, not only the vas deferens but other mesonephric-derived components of the male excretory system, including the epididymis (mainly corpus and cauda) and seminal vesicles, may also be absent or hypoplastic [12, 13]. Mutations in the cystic fibrosis gene, *CFTR*, have been demonstrated in the majority of bilateral cases and less frequently in unilateral CAVD, with or without a full phenotype of cystic fibrosis [18, 19]; however, renal malformations have been found in a minority of men with CAVD and *CFTR* mutation, suggesting a distinct pathogenesis [20, 21]. CDRT is a rare lesion that consists of cystic transformation of an excessively developed rete testis, which may compress the testicular parenchyma and in some cases extend through it [14, 15]. Most cases occur during infancy and childhood, in association with cryptorchidism, and must be differentiated from cystic transformation of the rete testis, which affects older men possibly as a consequence of excretory duct obstruction [22].

Epididymal cystic lesions are not part of the spectrum of CAVD or CDRT. Epididymal cysts have been reported in association with seminal vesicle cysts in adult patients with autosomal dominant polycystic kidney disease [23–26] and also in patients with seminal vesicle cysts and ipsilateral renal agenesis [16, 27]. In most cases, these cysts were diagnosed radiologically with no pathological documentation and are likely to be secondary to distal obstruction of the excretory duct. Importantly, these associations have not been reported on fetuses or young children. Although the vas deferens was patent in all of our cases and no other malformations of the excretory ducts were present, the possibility of an early manifestation of obstruction cannot be completely ruled out in this series.

To our knowledge, the association of cystic epididymal lesions and renal malformations in young patients has only been described in two isolated reports: a preterm neonate with skeletal malformations and multiple renal, epididymal, hepatic, and pancreatic cysts and a 3-year-old boy with cystically dilated epididymal channels, cystic dysplasia of the rete testis, and multicystic kidney dysplasia [28, 29]. Although the morphological description on both cases suggests some similarities with our findings, those reports lack microscopical documentation of the epididymal lesions, precluding further comparison.

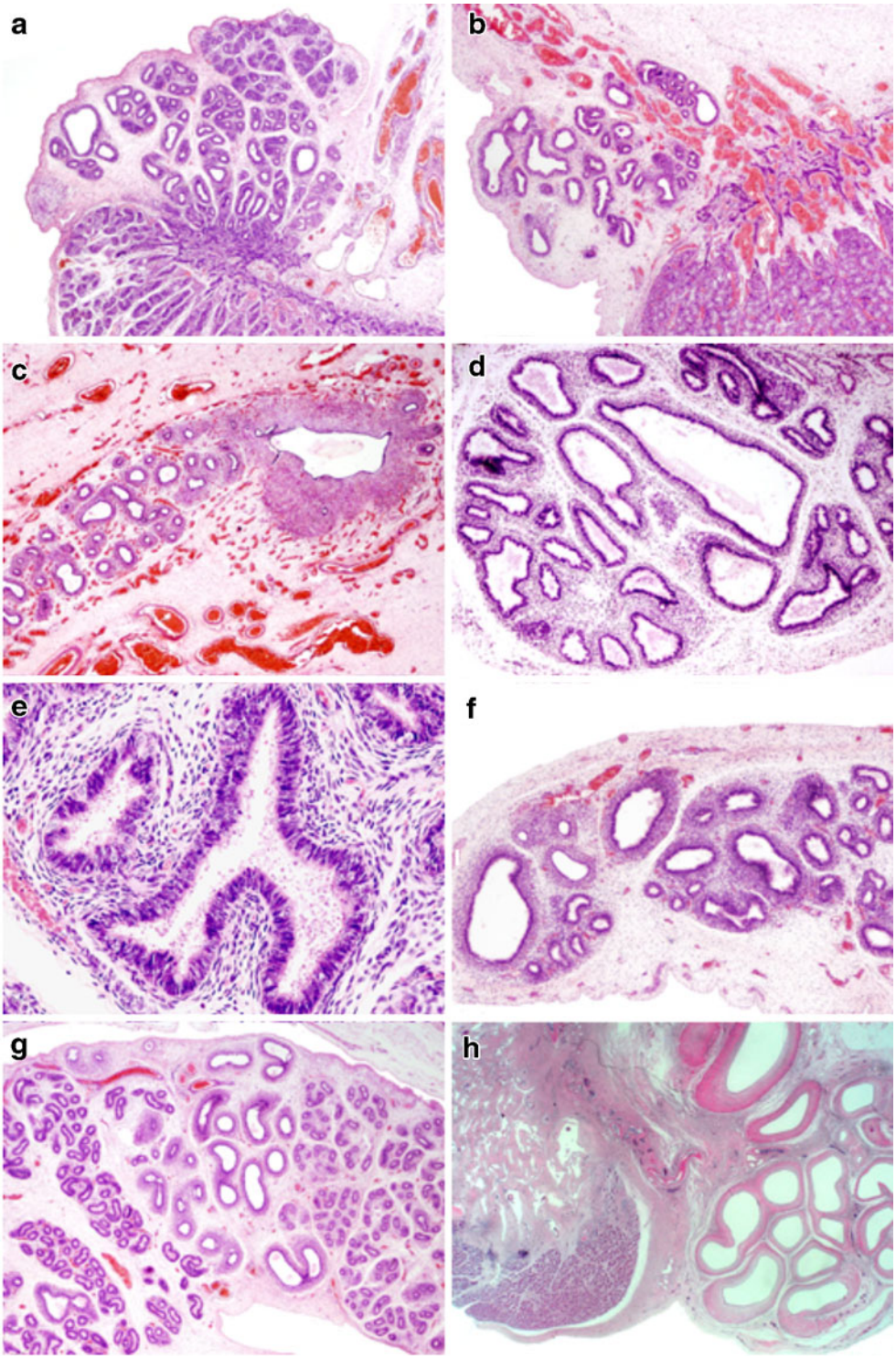

Fig. 1 Histological features in cystic dysplasia of epididymis. **a**, **b** Histological sections of caput epididymis. Abnormal efferent ductules and dilated ductal segments intermixed with normal-appearing ducts (**a**) and irregular ductal dilation with reduced number of efferent ductules (**b**). **c**, **d** Variability of size and shape of cystically dilated epididymal ducts. **e** Epididymal duct showing aberrant shapes and irregular poorly defined walls. **f** Section of corpus epididymis with abundant intertubular connective tissue surrounding an irregularly dilated epididymal duct. **g** Segmental distribution of cystically dilated sections intermixed with normal-appearing ductal sections. **h** Mature fibroconnective tissue surrounding dysplastic ductal segments with associated cystic dysplasia of the rete testis in a 4-year-old patient

It is well known that development of the male genital system and urinary tract are intimately related [30, 31]. The mesonephros, derived from the intermediate mesoderm as a component of the urogenital ridge, gives rise to the Wolffian or mesonephric duct (MD) through epithelial–mesenchymal interactions; the latter extends cranially from the pronephros to the cloaca caudally, running through the length of the urogenital ridge, and is the common source for both the reproductive ductal and collecting urinary systems (see Fig. 2). The ureteral bud arises as a diverticulum from the distal MD and grows cranially toward the metanephric blastema. After interacting with the metanephric blastema, the ureteral bud undergoes branching and gives rise to the urinary collecting system, while inducing nephron morpho-

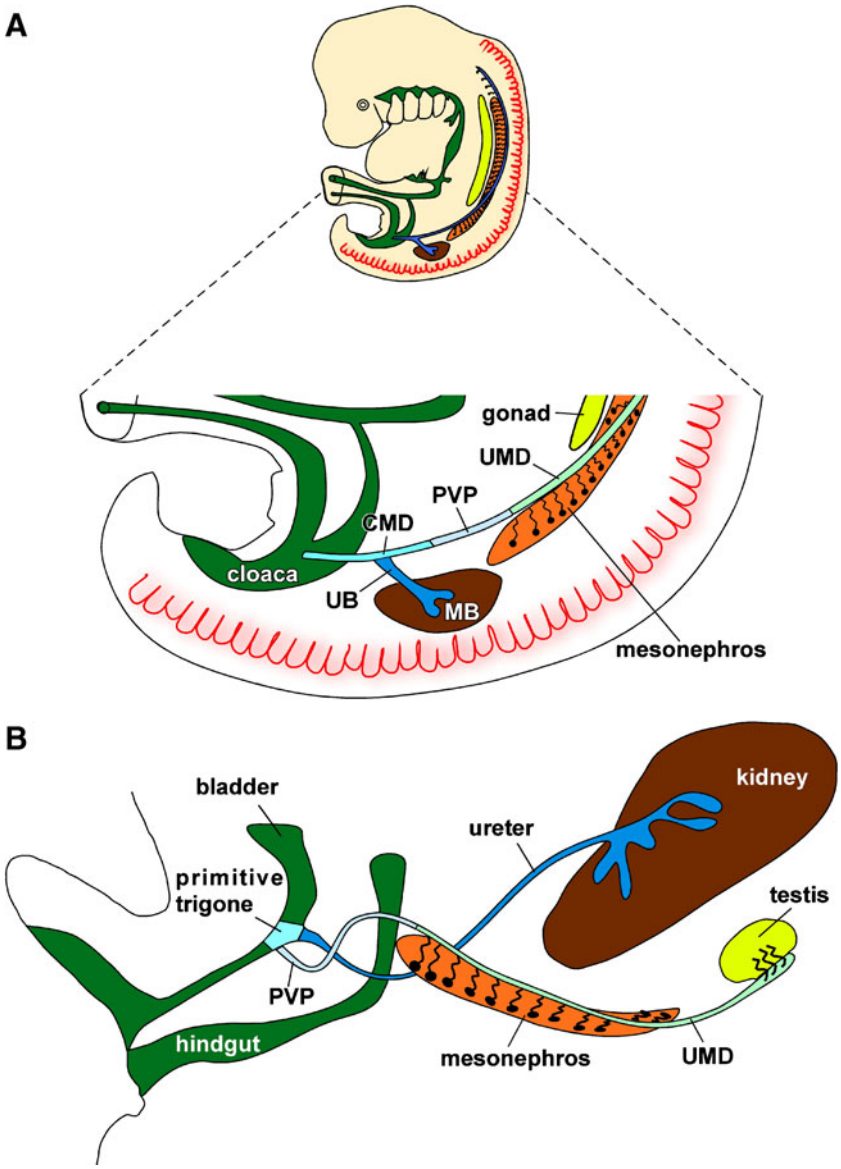

Fig. 2 Overview of male genitourinary development. **a** Sagittal drawing of a human embryo at 5 weeks of gestation. The developing genitourinary system is detailed in the lower outset. The MD is divided into three segments starting at the cloaca: common mesonephric duct (*CMD*, *light blue*), proximal vas precursor (*PVP*, *violet*), and upper mesonephric duct (*UMD*, *light green*). The ureteral bud (*UB*, *dark blue*) sprouts from the CMD and reaches the metanephric blastema (*MB*). The mesonephric ductules connect to the UMD. **b** Sagittal drawing of the genitourinary system of a human embryo at 7 weeks of gestation. The CMD has been incorporated into the urinary bladder wall and forms the primitive trigone (*light blue*). The kidney derived from the MB has ascended, and now the ureter (*dark blue*) ends in the bladder cephalad to the PVP (*violet*). The UMD will contribute to the formation of the epididymis

genesis on the overlying metanephros. The MD also induces the development of mesenchymal condensations in the adjacent mesonephros, which will give rise to the mesonephric tubules; their appearance follows a craniocaudal direction, and the most cranial tubules persist in males becoming the efferent ductules that connect the MD to the rete testis, whereas the remaining tubules regress. Subsequently, the male MD stabilizes and grows under the influence of growth factors and testosterone, regressing in females. Further differentiation of the MD into different portions (epididymis, vas deferens, and seminal vesicles) takes place under segmental expression of several different homeobox genes (Hoxa9, 10, 11, and 13 and Hoxd9, 10, and 13). Once formed, the epididymal duct undergoes extensive elongation and coiling in a proximal-to-distal pattern to acquire a convoluted configuration; this process occurs in a segmental regionalized pattern that involves rapid epithelial proliferation with associated mesenchymal quiescence.

Although the morphological features described in our cases have not been reported in other epididymal lesions in humans, a few animal models show similar pathological findings that can lead to speculations about the pathogenesis of CDE. Retinoic acid receptor mutant mice display dysplastic epididymis with alternating dilated and stenotic segments, as well as other male excretory duct defects. In addition, those mutants show renal agenesis, aplasia, or hypoplasia, always associated with ureteral abnormalities, as well as several multi-organ malformations [32]. The pathogenic mechanism in those animals likely involves target genes of retinoic acid signaling pathway. Possible targets include homeobox genes, adhesion molecules, growth factors, and growth factor receptors, all known to participate in genitourinary and renal

development. Knockout mice for leucine-rich repeat-containing G protein-coupled receptor-4, a G protein-coupled receptor with unknown ligands and possibly involved on late MD tissue remodeling, demonstrate dilated epididymal ducts surrounded by thick mesenchymal condensations accompanied by an abnormal laminin-rich basement membrane. Those animals also show rete testis dilation and multicystic and hypoplastic kidneys [33, 34]. Different from our cases, the epididymal lesions were only evident on puberal mice with normal epididymal morphology at birth, which may reflect normal differences between mouse and human development.

In summary, CDE represents a novel congenital anomaly that should be included in the spectrum of male excretory system disorders associated with renal and urinary malformations. It is possible that CDE represents an underdiagnosed condition due to the scant number of studies on fetal and newborn epididymis and also because of the high lethality associated with renal and urinary malformations. The heterogeneity of associated renal and urinary malformations merits further consideration with regards to its pathogenesis, possibly representing a wide spectrum of disrupted MD development with impairment of common key molecular pathways, suggesting that etiologic and phenotypically distinct renal malformations may share a similar pathogenic mechanism.

Conflicts of Interest Statement We declare that we have no conflict of interest.

References

1. Heath AL, Man DWK, Eckstein HB (1984) Epididymal abnormalities associated with maldescent of the testis. J Pediatr Surg 19:47–49
2. Gill B, Kogan S, Starr S et al (1989) Significance of epididymal and ductal anomalies associated with testicular maldescent. J Urol 142:556–558
3. Mollaeian M, Mehrabi V, Elahi B (1994) Significance of epididymal and ductal anomalies associated with undescended testis: study in 652 cases. Urology 43:857–860
4. Vohra S, Morgentaler A (1997) Congenital anomalies of the vas deferens, epididymis, and seminal vesicles. Urology 49:313–321
5. Kucukaydin M, Ozokutan BH, Turan C et al (1998) Malformation of the epididymis in undescended testis. Pediatr Surg Int 14:189–191
6. Gill WB, Schumacher GF, Bibbo M et al (1979) Association of diethylstilbestrol exposure in utero with cryptorchidism, testicular hypoplasia and semen abnormalities. J Urol 122:36–39
7. Whitehead ED, Leiter E (1981) Genital abnormalities and abnormal semen analyses in male patients exposed to diethylstilbestrol in utero. J Urol 125:47–50
8. Blau H, Freud E, Mussaffi H et al (2002) Urogenital abnormalities in male children with cystic fibrosis. Arch Dis Child 87:135–138
9. Homayoon K, Suhre CD, Steindhardt GF (2004) Epididymal cysts in children: natural history. J Urol 171:1274–1276
10. Glasker S, Tran MGB, Shively SB et al (2006) Epididymal cystadenomas and epithelial tumorlets: effects of VHL deficiency on the human epididymis. J Pathol 210:32–41
11. Mehta GU, Shively SB, Duong H et al (2008) Progression of epididymal maldevelopment into hamartoma-like neoplasia in VHL disease. Neoplasia 10:1146–1153
12. Van Wingerden JJ, Franz I (1984) The presence of a caput epididymis in congenital absence of the vas deferens. J Urol 131:764–766
13. Schelegel PN, Shin D, Goldstein M (1996) Urogenital anomalies in men with congenital absence of the vas deferens. J Urol 155:1644–1648
14. Nistal M, Regadera J, Paniagua R (1984) Cystic dysplasia of the testis: light and electron microscopic study of three cases. Arch Pathol Lab Med 108:579–583
15. Wojcik LJ, Hansen K, Diamond DA et al (1997) Cystic dysplasia of the rete testis: a benign congenital lesion associated with ipsilateral urological anomalies. J Urol 158:600–604
16. Van de Ouden D, Blom JH, Bangma C et al (1998) Diagnosis and management of seminal vesicle cysts associated with ipsilateral renal agenesis: a pooled analysis of 52 cases. Eur Urol 33:433–440
17. Schukfeh N, Kuebler JF, Schirg E et al (2008) Dysplastic kidney and not renal agenesis is the commonly associated anomaly in infants with seminal vesicle cyst. Br J Urol Int 103:816–819
18. Mickle J, Milunsky A, Amos JA et al (1995) Congenital unilateral absence of the vas deferens: a heterogeneous disorder with two distinct subpopulations based upon the aetiology and mutational status of the cystic fibrosis gene. Hum Reprod 10:1728–1735
19. Shin D, Gilbert F, Goldstein M et al (1997) Congenital absence of the vas deferens: incomplete penetrance of cystic fibrosis mutations. J Urol 158:1794–1799
20. Augarten A, Yahav Y, Kerem BS et al (1994) Congenital bilateral absence of vas deferens in the absence of cystic fibrosis. Lancet 344:1473–1474
21. McCallum TJ, Milunski JM, Munarriz R et al (2001) Unilateral renal agenesis associated with congenital bilateral absence of the vas deferens: phenotypic findings and genetic considerations. Hum Repr 16:282–288
22. Nistal M, Mate A, Paniagua R (1996) Cystic transformation of the rete testis. Am J Surg Pathol 20:1231–1239
23. Belet U, Danaci M, Sarikaya S et al (2002) Prevalence of epididymal, seminal vesicle, prostate, and testicular cysts in autosomal dominant polycystic kidney disease. Urology 60:138–141
24. Engelbrecht K, Bornman MS, Du Plessis DJ (1995) Multicystic epididymis and seminal vesicles in a patient with polycystic kidney disease. Br J Urol 75:554–555
25. Altiparmak MR, Pamuk ON, Toptas TK et al (2003) Psoriatic arthritis associated with adult polycystic kidney disease, seminal vesicle, and epididymal cysts. Eur J Intern Med 14:265–268
26. Orhan I, Ergin E, Koksal IT et al (2002) Infertility treatment in autosomal dominant polycystic kidney disease (ADPKD)—a case report. Andrologia 32:91–93
27. Casey RG, Stunell H, Buckley O et al (2008) A unique radiological pentad of mesonephric duct abnormalities in a young man presenting with testicular swelling. Br J Radiol 81:e93–e96
28. Leclerc JP, Canet J, Lancret P et al (1971) Polykystose hepato-pancreato-epididymo-renale et polydystrophie thoracique neonatales. Etude anatomo-clinique d'une observation. Arch Fr Pediatr 28:425–434
29. Robson WL, Thomason MA, Minette LJ (1998) Cystic dysplasia of the testis associated with multicystic dysplasia of the kidney. Urology 51:477–479
30. Hannema SE, Hughes IA (2007) Regulation of Wolffian duct development. Horm Res 67:142–151

31. Joseph A, Yao H, Hinton BT (2009) Development of the Wolffian/epididymal duct, more twists and turns. Dev Biol 325:6–14
32. Mendelsohn C, Lohnes D, Decimo D et al (1994) Function of retinoic acid receptors (RARs) during development (II). Multiple abnormalities at various stages of organogenesis in RAR double mutants. Development 120:2749–2771
33. Kato S, Matsubara M, Matsuo T et al (2006) Leucine-rich repeat-containing G protein-coupled receptor-4 (LGR4, Gpr48) is essential for renal development in mice. Nephron Exp Nephrol 104:e63–e75
34. Hoshii T, Takeo T, Nakagata N et al (2007) LGR4 regulates the postnatal development and integrity of male reproductive tracts in mice. Biol Reprod 76:303–313

Virchows Arch (2010) 456:703–710
DOI 10.1007/s00428-010-0929-1

ORIGINAL ARTICLE

Proangiogenetic molecules, hypoxia-inducible factor-1α and nitric oxide synthase isoforms in ovarian endometriotic cysts

Gaia Goteri · Guendalina Lucarini · Antonio Zizzi · Corrado Rubini · Roberto Di Primio · Andrea Luigi Tranquilli · Andrea Ciavattini

Received: 9 February 2010 / Revised: 19 April 2010 / Accepted: 23 April 2010 / Published online: 16 May 2010
© Springer-Verlag 2010

Abstract Endometriosis is a common disease characterised by ectopic growth of endometrial tissue outside the uterine cavity. Angiogenesis has been implicated in the pathogenesis of the disease; some molecules, like hypoxia-inducible factor-1α (HIF-1α) and neuronal, endothelial and inducible nitric oxide synthase isoforms (nNOS, eNOS and iNOS), are known as proangiogenetic factors. We evaluated expression of these molecules by immunohistochemistry in 32 cases of ovarian endometriomas, formalin-fixed and paraffin-embedded. Analysis was focused on the cells composing the inner layer of the cyst, constituted by the ectopic endometrial glands, stromal cells and vessels, and the outer one, constituted by a fibrous layer of fibroblasts and vessels. We found that epithelial glands and capsular vessel endothelial cells showed a correlated expression of NOS isoforms; that expression of nNOS, iNOS and HIF-1α was correlated in epithelial glands and capsular fibroblasts; that vessel endothelial cells showed a higher mean expression for all the proangiogenetic molecules in the outer layer than in the inner one; and that capsular fibroblasts showed a higher mean expression for HIF-1α, iNOS and eNOS compared to the specialised stromal cells of the inner layer. Our data seem to indicate that angiogenesis is stimulated more in the outer capsule than in the inner layer of ovarian endometriotic cysts. The knowledge of the complex mechanisms associated to angiogenesis might be useful in a therapeutic approach of ovarian endometriosis based on anti-angiogenetic drugs. The therapeutic target would be mainly the capsular vasculature, more than the vasculature of ectopic endometrial tissues.

Keywords Ovarian endometriotic cysts · HIF-1α · nNOS · eNOS · iNOS · Angiogenesis

G. Goteri (✉) · A. Zizzi · C. Rubini
Section of Anatomic Pathology, Department of Neurosciences, Polytechnic University of Marche Region,
Via Conca, 71,
60020 Torrette di Ancona (Ancona), Italy
e-mail: g.goteri@univpm.it

G. Lucarini · R. Di Primio
Department of Molecular Pathology and Innovative Therapies, Histology, Polytechnic University of Marche,
Ancona, Italy

A. L. Tranquilli · A. Ciavattini
Clinic of Obstetrics and Gynaecology, Polytechnic University of Marche Region, Ancona Salesi Hospital,
Ancona, Italy

Introduction

Endometriosis is a common disease characterised by ectopic growth of endometrial tissue outside the uterine cavity, especially on the peritoneum, ovaries and recto-vaginal septum [1]. Women are affected almost exclusively during their reproductive years, and the disease is one of the main causes of pelvic pain and women infertility [2]. The pathogenesis of the disease remains an enigma: lesions may develop either by metaplasia of the coelomic epithelium (metaplastic theory) or by the implantation of eutopic endometrium refluxed through the fallopian tubes (implantation theory) [3, 4]; according to more recent data, ovarian endometrioma could be viewed as a neoplastic process particularly in perimenopausal women [5, 6]. Several investigations were recently performed on animal, ex vivo and in vitro experimental models to study the role of angiogenesis in endometriosis, because the development of

new blood vessels is crucial to the growth and survival of endometrial tissue in ectopic locations and becomes a specific molecular target for new therapeutic strategies [7–9]. Angiogenesis in endometriosis shares common markers with tumours, but the mechanisms underlying the process remain largely unknown. Probably different mechanisms are implicated in the different locations of the disease [1, 10]. Previous studies have supported the crucial role of vascular endothelial growth factor (VEGF) in the angiogenesis occurring in endometriosis: this molecule is involved in the normal turnover of endometrium and during pregnancy; its role is to increase the permeability of endometrial blood vessels and stimulate proliferation and migration of endothelial cells [11–13]. In ovarian endometriotic cysts, VEGF is expressed in the ectopic endometrial glandular epithelium and stromal cells; either a negative or positive correlation of VEGF expression has been reported with cyst diameter [10, 14–18]. VEGF production is regulated by various stimuli, including steroid hormones, hypoxia and nitric oxide (NO) levels [19]. Hypoxia-inducible factor-1 (HIF-1) is a master transcription factor that mediates the hypoxic effect and plays a key role in VEGF-induced angiogenesis [20, 21]. Recent data indicate a possible role for HIF-1 in the pathogenesis and development of endometriosis and adenomyosis [21–23]. NO is a lipid-soluble gaseous free radical produced during the enzymatic conversion of L-arginine to L-citrulline by NO synthase (NOS) enzyme and involved in both inflammation and neoangiogenesis [24, 25]. There are three NOS isoforms: neuronal NOS (nNOS) or NOS-1, inducible NOS (iNOS) or NOS-2 and endothelial NOS (eNOS) or NOS-3—nNOS and eNOS, regarded as constitutive, are activated by intracellular calcium-dependent binding of calmodulin (CaM) and were initially identified in neurons or in endothelial cells, respectively, whereas iNOS is independent of calcium and is generally inducible in almost every cell, under stimulation mostly by inflammatory signals such as cytokines and endotoxin levels [26–29]. Several studies have demonstrated that eNOS is the predominant isoform in the uterus, expressed in endometrial glandular and surface epithelial cells and, to a lesser extent, in the stroma [30, 31]. Increased peritoneal levels of NO and higher NOS concentrations in the endometrium and in isolated peritoneal macrophages have been reported in endometriosis and endometriosis-associated infertility, suggesting a role for them in the patho-physiology of the disease [7, 32–37].

At the best of our knowledge, expression of HIF-1 and of all the three NOS isoforms has not been studied yet in ovarian endometriotic cysts at histological level and was the main aim of our investigation, in order to expand the knowledge on the potential links between NOS activity and hypoxia-mediated angiogenesis in endometriosis.

Materials and methods

Patients

This retrospective study included 32 patients who had consecutively undergone surgical excision of ovarian endometriotic cysts at the Clinic of Obstetrics and Gynaecology, Polytechnic University of Marche, Salesi Hospital, Ancona, Italy. At the time of surgery, patients were all out of therapy since at least 6 months. Eutopic endometrium was not sampled at the time of surgery.

Age of patients and some clinical features of the disease, like cyst diameter, bilaterality and adhesions to the pelvic wall or to other pelvic viscera, were retrieved from medical charts.

Pathologic examination

Surgical samples were sent fresh or in 10% buffered formalin to the Section of Anatomic Pathology of Polytechnic University of Marche, Ancona, for histologic diagnosis; specimens were rapidly processed as routinely. Pathologic description of cysts and histological slides were retrieved from the archives. Similarities were sought between epithelial lining (columnar or cuboidal) and subepithelial specialised stroma (small and spindle-shaped or plump and polygonal cells) of ectopic endometrium and the glandular and stromal components of eutopic endometrium in its proliferative or secretive phases. We also assessed cytological atypia, hyperplasia and frank malignant proliferation of the epithelial component; presence of macrophages with foamy or pigmented cytoplasm; morphologic evidence of an outer fibrous capsule with activated fibroblasts and small vessels; and preservation of an invaginated ovarian cortical layer between cyst and medulla, as previously described [38]. Representative areas of the cysts were selected for immunohistochemical investigations.

Immunohistochemistry

Immunohistochemical analysis was performed on 5-μm paraffin-embedded tissue sections on poly-L-lysine-coated glass slides. After heat-drying, sections were deparaffinised in xylene and sequentially hydrated in gradients of ethanol and treated with TUF solution (Histo-line Laboratories, Milano, Italy) at 90°C for 10 min to better unmask antigenic sites. After three washes with H_2O, they were incubated overnight at 4°C with the monoclonal antibody anti-eNOS (clone 3, dil. 1:400, BD Biosciences, USA) and with the following polyclonal antibodies: anti-HIF-1α (clone H-206, dil. 1:100, Santa Cruz Biotechnology, Santa Cruz, CA, USA), anti-nNOS (clone R-20, dil. 1:100, Santa

Cruz Biotechnology) and anti-iNOS (clone H-174, dil. 1:50, Santa Cruz Biotechnology). Antigen–antibody complex was subsequently visualised using the Envision™ Detection System kit peroxidase/DAB (DakoCytomation, Milano, Italy). Sections were then incubated with 3,3′-diaminobenzidine (0.05 diaminobenzidine in 0.05 M Tris buffer, pH 7.6 and 0.01% hydrogen peroxide; Sigma-Aldrich, Milano, Italy), counterstained with Mayer's haematoxylin (Bio-Optica SpA, Milano, Italy) and coverslipped with Paramount. Negative controls were performed by substituting the primary antibody with non-immune serum.

Quantitative analysis of immunostainings was carried out by light microscopy in epithelial cells, specialised stromal cells and vessel endothelial cells of ectopic endometrial tissue, and fibroblasts and vessel endothelia of the fibrous capsule surrounding the ectopic endometrial tissue. Immunoreactivity of ovarian cortical stroma, recognised by its woven appearance, was not analysed. The number of HIF-1α, eNOS, nNOS and iNOS immunoreactive cells was counted among at least 500 cells in the more representative fields by using a microscope at ×250 magnification and expressed as percentage. Counting was repeated three times by one of us (AZ). For statistical analysis, the mean value obtained from the repeated counts was used. Intensity of immunostaining for all markers was classified with a four-point scale: negative (neg.), faint (+), moderate (++) and strong (+++). Intra-observer variability was evaluated, and concordance was >80%.

Statistical analysis

Clinical and pathologic data were analysed by SPSS statistical package (SPSS Inc., Chicago, IL, USA). Cases were analysed based on the clinical and pathologic parameters (cyst diameter, bilaterality, adhesions to pelvic wall and viscera and histological features of ectopic endometrium). For the numerical data, we calculated mean values and SD, and differences among groups were analysed by the analysis of variance and Student's *t* test. Correlation coefficient test was used to evaluate the relationship between parameters. Significance was set at $P<0.05$.

Results

All patients were in fertile age (range, 32.14±5.34). Cysts ranged in diameter from 1 to 8.5 cm (5.20±1.66) and were bilateral in 12 patients (37.5%). Adhesions were present in 25 patients (78.1%). Histologically, the cysts exhibited an inner layer of ectopic endometrium and an outer fibrosclerotic wall recognisable in all cases, with numerous small vessels and activated fibroblasts (Fig. 1a); a third, external, layer of ovarian cortex with oocytes, follicles, functional cysts and corpora albicantes was also noted in 15 cases. The thickness of each layer varied considerably from cyst to cyst. The epithelial lining was absent in two cysts, and the specialised subepithelial stroma was markedly thinned in six. The epithelial cells forming the lining and the glands were columnar, with basal nuclei resembling those of the estrogenic phase of normal endometrium in 19 cases, and cuboidal, resembling those of the progestinic phase, in nine. Regressive atypia was found in two cysts. No hyperplastic or carcinomatous foci were detected. The endometrial-type stroma below the epithelium and around the glands showed variable thickness and numerous extravascular erythrocytes. Endometrial-type stromal cells appeared small and spindle-shaped, as in the proliferative phase, in 19 cases, and plump and even pseudo-decidualized, as in the secretory phase, in seven cases. Small vessels were recognised in the stroma in 26 cysts. Large aggregates of pigmented or foamy macrophages were present in nine cysts.

The proangiogenetic molecules studied were expressed in the cytoplasm of cells located both in the inner portion and in the outer capsule in the majority of ovarian endometriotic cysts, with variable intensity and percentage of staining (Tables 1 and 2 and Figs. 1, 2 and 3). Glands and specialised stromal cells of ectopic endometrium and fibroblasts and vascular endothelial cells of the outer capsule showed a higher immunoreactivity for all the molecules than the vascular endothelial cells in the inner ectopic endometrial tissue. Immunostaining for nNOS was stronger and more diffuse than for the other NOS and HIF-1α. Epithelial cells showed a positive correlation in the immunoreactivity for nNOS and iNOS ($r=0.534$, $P=0.0041$) and for nNOS and eNOS ($r=0.483$, $P=0.0124$). Moreover, epithelial cells and capsular fibroblasts showed a correlation in the number of cells reactive for nNOS ($r=0.694$, $P<0.0001$), iNOS ($r=0.533$, $P=0.0042$) and HIF-1α ($r=0.455$, $P=0.0131$), but not for eNOS ($r=0.353$, $P=0.06$). Epithelial cells and endothelial cells of capsular vessels showed a correlation in the number of cells reactive for nNOS ($r=0.594$, $P=0.0007$), iNOS ($r=0.545$, $P=0.0033$) and eNOS ($r=0.408$, $P=0.0311$), but not for HIF-1α ($r=0.207$, $P=0.280$). In addition, vessel endothelial cells showed a higher mean expression for all the proangiogenetic molecules in the fibrosclerotic capsule than in the ectopic endometrial tissue (paired *t* test: nNOS, $P<0.0001$; iNOS, $P<0.0001$; eNOS, $P=0.0002$; HIF-1α, $P=0.001$); capsular fibroblasts showed a higher mean expression for HIF-1α ($P=0.0006$), iNOS ($P=0.0036$) and eNOS ($P=0.025$; paired *t* test) than specialised stromal cells of the ectopic endometrial tissue. No correlations were found among immunoreactivity for proangiogenic molecules and cyst diameter, presence of adhesions and bilaterality and histological features of ectopic endometrium.

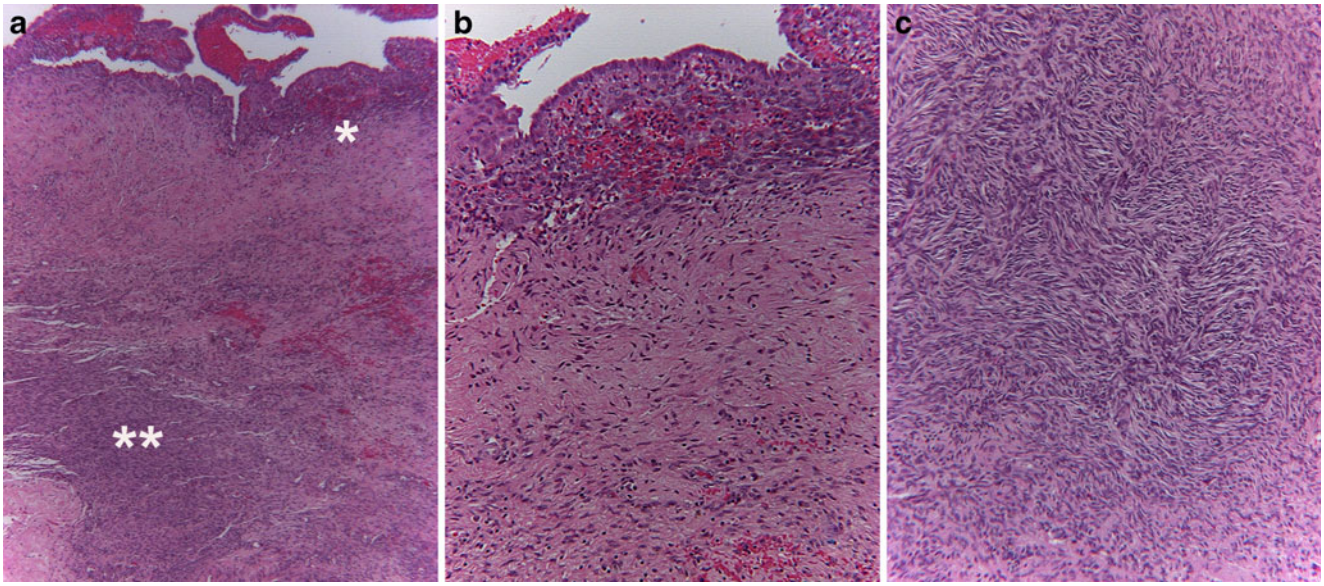

Fig. 1 Histological appearance of ovarian endometriotic cyst. **a** Low power picture showing the inner layer of ectopic endometrium with gland and stroma, and an outer layer of fibrosclerotic capsule. Cortical ovarian stroma is recognisable beneath the fibrous capsule including a corpus albicans in the lower left corner. **b**, **c** Higher magnification of the different layers of the cyst: in **b**, the inner layer of ectopic endometrium with gland and stroma and the fibrosclerotic capsule with fibroblasts haphazardly oriented and vessels are shown (*single asterisk* in **a**); in **c**, the cortical ovarian stroma shows the typical wavy and storiform hypercellular stroma (*double asterisk* in **a**)

Table 1 Staining intensity for the proangiogenetic molecules in the cell populations of the inner layer and the outer capsule of endometriotic cysts

Staining intensity	Inner layer			Outer capsule	
	Epithelial cells No. of cases	Stromal cells No. of cases	Endothelial cells No. of cases	Fibroblasts No. of cases	Endothelial cells No. of cases
nNOS					
Neg.	0	2	5	0	0
+	0	2	3	3	1
++	9	4	6	7	4
+++	21	18	12	22	27
e-NOS					
Neg.	2	4	5	2	1
+	5	4	4	6	6
++	12	8	8	6	3
+++	11	10	9	18	22
iNOS					
Neg.	2	3	9	2	4
+	8	9	7	9	5
++	7	7	4	9	6
+++	13	7	6	12	17
HIF-1α					
Neg.	5	10	12	1	2
+	12	4	6	10	8
++	6	8	6	12	18
+++	7	4	2	9	4

Table 2 Expression of proangiogenetic molecules in the inner layer and outer capsule of endometriotic cysts: range, mean values and standard deviations of cell immunoreactivity

	Inner layer						Outer capsule			
	Epithelial cells		Stromal cells		Endothelial cells		Fibroblasts		Endothelial cells	
	Range	Mean ± SD	Range	Mean ± SD	Range	Mean ± SD	Range	Mean ± SD	Range	Mean ± SD
nNOS	25–100	63.28±20.93	1–100	58.66±26.7	1–100	45.53±32.12	10–100	59.72±24.86	10–100	67.53±20.04
e-NOS	1–85	42.67±25.13	1–80	37.44±23.3	1–90	36.72±24.44	1–90	47.41±25.34	1–90	54.59±24.92
iNOS	1–90	42.04±26.36	1–90	32.31±25.99	1–70	22.19±23.10	1–100	38.09±25.97	1–90	45.31±28.41
HIF-1α	1–85	32.97±25.33	1–82	25.56±26.43	1–78	18±20.58	1–80	40.56±22.03	1–72	36.09±17.27

Discussion

Our study on ovarian endometriosis shows interesting correlations in the expression of some molecules, which are reciprocally stimulated and regulated, and involved in the process of angiogenesis. In vivo and in vitro experiments indicate that steroid hormones, hypoxia and NO are potent inducers of VEGF gene expression by enhancing HIF-1 activity and by the activation of the Akt/protein kinase B (PKB) pathway; reciprocally, VEGF induces NO

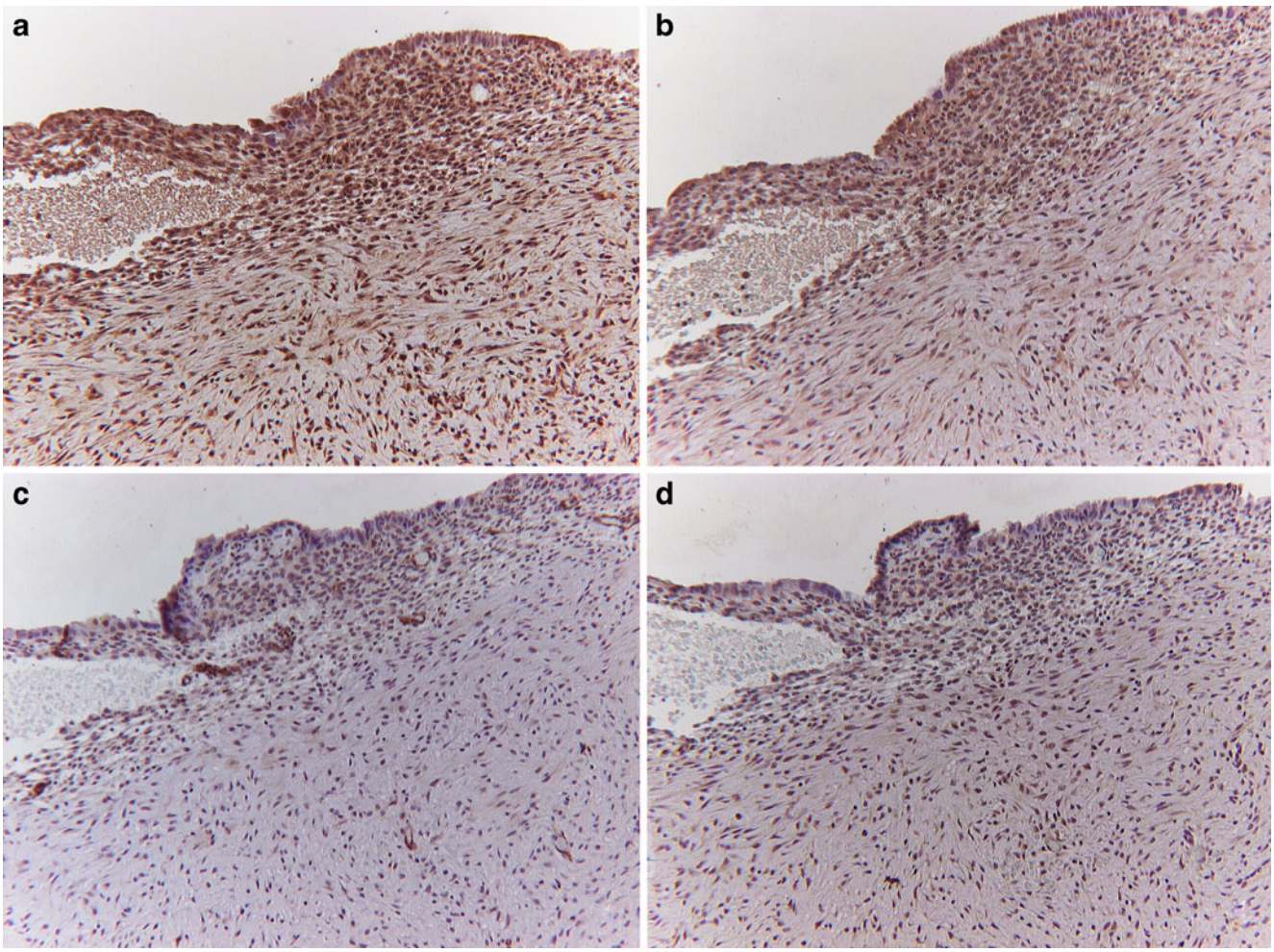

Fig. 2 Examples of immunoreactivity of proangiogenetic markers in the inner layer and in the outer capsule of endometriotic cysts. Ectopic endometrium shows high expression in the epithelial cells and stromal cells, but a low expression in vessels for the studied markers. The outer capsule shows moderate to high expression in the fibroblasts and vessels, for the studied markers: nNOS (**a**), eNOS (**b**), iNOS (**c**), HIF-1α (**d**) (immunoperoxidase, original magnification ×160)

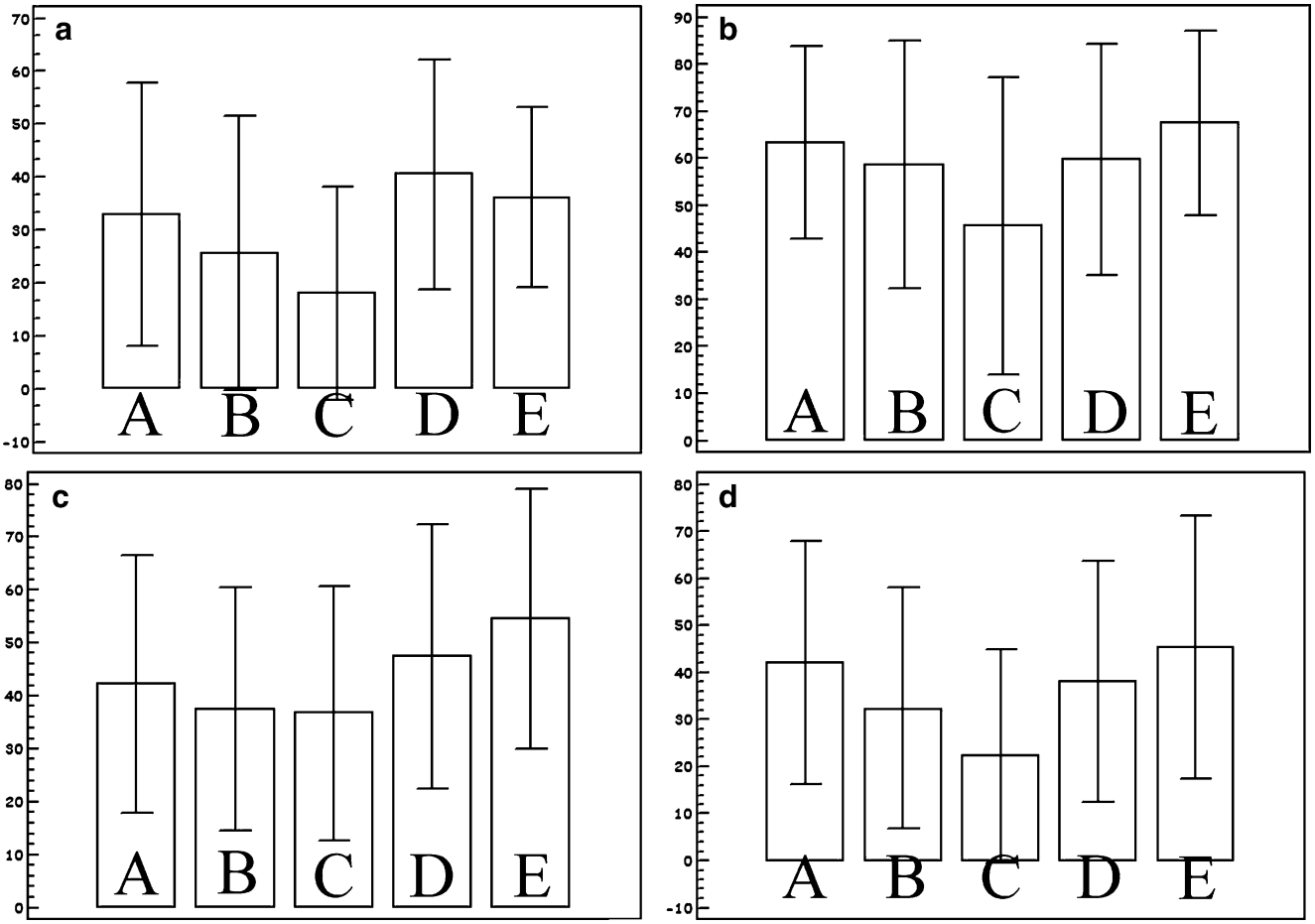

Fig. 3 Immunoreactivity for proangiogenetic molecules in cell types of ovarian endometriotic cysts. Mean values and standard deviations are reported for HIF1α (**a**), nNOS (**b**), eNOS (**c**) and iNOS (**d**). *Bars* refer to epithelial glands (*A*), specialised stromal cells (*B*) and vascular endothelial cells (*C*) of ectopic endometrium in the inner layer, and to fibroblasts (*D*) and vascular endothelial cells (*E*) of the outer fibrosclerotic capsule

production from activated eNOS involving several pathways, like Akt/PKB, Ca^{2+}/calmodulin and protein kinase C, and is regulated by HIF-1 [39–42]. In ovarian endometriotic cysts, the process of angiogenesis might be heterogeneous and different from other sites of disease [10, 18]. In a previous study, we highlighted the existence of complex interrelations between the cell components of the ovarian cysts: diffuse VEGF expression in epithelial cells was associated with larger cysts; high VEGF expression in capsular fibroblasts was associated with bilateral cysts; and expression of VEGF was found to be related in epithelial cells, capsular fibroblasts and vessels, suggesting that neoangiogenesis might especially affect the outer cyst wall, thus contributing to cyst growth [15]. We further focused on the microvasculature of the inner and outer layers of ovarian endometriotic cysts: we observed that the inner specialised stroma had the highest microvessel density but with a low expression of VEGF and survivin in endothelial cells, supporting the hypothesis that these vessels are destined to a progressive involution, lacking proliferative stimulation and apoptosis inhibition; on the contrary, in the outer fibrosclerotic capsule, the vessels were less abundant, but with a higher expression of VEGF and survivin, thus activated to proliferate and protected from programmed cell death. The hypothesis we favoured was that angiogenesis mediated by VEGF in the outer capsule contributed to the cyst growth and to the fibrosing process of adhesion [43], whereas VEGF activity was scarcely efficient on the vasculature of the ectopic endometrium. With the present work, we add further evidence to our hypotheses, by finding among epithelial glandular cells, capsular fibroblasts and vessels, a correlation in the immunoreactivity for the constitutive and inducible forms of NOS. Our results seem to indicate the existence of a cellular network that is exposed to high NO concentrations and promotes angiogenesis mediated by HIF-1 and VEGF and protected from apoptosis by the Akt/PKB and survivin antiapoptotic pathway. High NOS expression is in line with the findings of Ota et al., who reported higher eNOS levels in specimens from women with endometriosis or adenomyosis [33]. As

iNOS produces large quantities of NO, while the constitutive isoforms (nNOS and eNOS) produce lower levels [39], it is conceivable that the much higher iNOS expression observed in the capsular vessels might be associated with a high amount of NO and the consequent activation of the HIF-1 and VEGF-mediated angiogenesis and of the Akt/PKB anti-apoptotic pathway. We believe that the formation of a fibrotic capsule is reasonably not an early phenomenon in ovarian endometriomas, as its width is greatly variable from cyst to cyst; probably, angiogenesis in the ectopic endometrium might be crucial for the early development of the disease, but as we examined lesions that have already developed, we can only state that angiogenesis is more stimulated in the fibrous capsule which is the front of expansion and growth of the cysts. On the contrary, the low expression of iNOS observed in endothelial cells in the inner layer could induce a low amount of NO and, consequently, a minor activation of the HIF-1-mediated VEGF expression and a minor activation of the Akt/PKB anti-apoptotic pathway in the inner vessels. We cannot exclude, however, that in the inner layer, angiogenesis depends not only on the proangiogenetic molecules that we studied but also on the level of other molecules with anti-angiogenetic activity [44, 45].

The knowledge of the complex mechanisms associated to angiogenesis in ovarian endometriosis has not completely elucidated, but it might be extremely helpful to find the key of an optimal anti-angiogenetic therapeutic approach. We believe that anti-angiogenetic drugs could act on the capsular vasculature and block the growth of the ovarian endometriotic cysts more than have a direct effect on the vasculature of ectopic endometrial tissues. Further studies are indeed necessary to elucidate the crucial mechanisms involving aberrant angiogenesis in the development of ovarian endometriosis.

Conflict of interest The authors declare that they have no conflict of interest.

References

1. Nisolle M, Donnez J (1997) Peritoneal endometriosis, ovarian endometriosis, and adenomyotic nodules of the rectovaginal septum are three different entities. Fertil Steril 68:585–596
2. Giudice LC, Kao LC (2004) Endometriosis. Lancet 364:1789–1799
3. Jenkins S, Olive DL, Haney AF (1986) Endometriosis: pathogenetic implications of the anatomic distribution. Obstet Gynecol 67:335–338
4. Bulun SE (2009) Endometriosis. N Engl J Med 360:268–279
5. Kobayashi H (2009) Ovarian cancer in endometriosis: epidemiology, natural history, and clinical diagnosis. Int J Clin Oncol 14:378–382
6. Mandai M, Yamaguchi K, Matsumura N, Baba T, Konishi I (2009) Ovarian cancer in endometriosis: molecular biology, pathology, and clinical management. Int J Clin Oncol 14:383–391
7. Becker CM, D'Amato RJ (2007) Angiogenesis and antiangiogenic therapy in endometriosis. Microvasc Res 74:121–130
8. Groothuis PG, Nap AW, Winterhager E, Grümmer R (2005) Vascular development in endometriosis. Angiogenesis 8:147–156
9. Van Langendonckt A, Donnez J, Defrère S, Dunselman GA, Groothuis PG (2008) Antiangiogenic and vascular-disrupting agents in endometriosis: pitfalls and promises. Mol Hum Reprod 14:259–268
10. Machado DE, Abrao MS, Berardo PT, Takiya CM, Nasciutti LE (2008) Vascular density and distribution of vascular endothelial growth factor (VEGF) and its receptor VEGFR-2 (Flk-1) are significantly higher in patients with deeply infiltrating endometriosis affecting the rectum. Fertil Steril 90:148–155
11. Donnez J, Smoes P, Gillerot S, Casanas-Roux F, Nisolle M (1998) Vascular endothelial growth factor (VEGF) in endometriosis. Hum Reprod 13:1686–1690
12. Ferrara N, Davis-Smyth T (1997) The biology of vascular endothelial growth factor. Endocr Rev 18:4–25
13. McLaren J, Prentice A, Charnock-Jones DS, Smith SK (1996) Vascular endothelial growth factor (VEGF) concentrations are elevated in peritoneal fluid of women with endometriosis. Hum Reprod 11:220–223
14. Takehara M, Ueda M, Yamashita Y, Terai Y, Hung YC, Ueki M (2004) Vascular endothelial growth factor A and C gene expression in endometriosis. Human Pathol 35:1369–1375
15. Goteri G, Lucarini G, Filosa A, Pierantoni A, Montik N, Biagini G, Fabris G, Ciavattini A (2004) Immunohistochemical analysis of vascular endothelial growth factor cellular expression in ovarian endometriomata. Fertil Steril 81:1528–1533
16. Garciá-Manero M, Alcazar JL, Toledo G (2007) Vascular endothelial growth factor (VEGF) and ovarian endometriosis: correlation between VEGF serum levels, VEGF cellular expression, and pelvic pain. Fertil Steril 88:513–515
17. Ceyhan ST, Onguru O, Baser I, Gunhan O (2008) Expression of cyclooxygenase-2 and vascular endothelial growth factor in ovarian endometriotic cysts and their relationship with angiogenesis. Fertil Steril 90:988–993
18. Tuncay G, Kilic S, Yuksel B, Elmas C, Lortlar N, Erdogan D, Ozogul C (2009) Heterogeneous appearance of VEGF (vascular endothelial growth factor) immunopositivity in cyst capsules of endometrioma. Acta Histochem 111:61–67
19. Shweiki D, Itin A, Soffer D, Keshet E (1992) Vascular endothelial growth factor induced by hypoxia may mediate hypoxia-initiated angiogenesis. Nature 359:843–845
20. Ryan HE, Lo J, Johnson RS (1998) HIF-1 alpha is required for solid tumor formation and embryonic vascularization. EMBO J 17:3005–3015
21. Wu MH, Chen KF, Lin SC, Lgu CW, Tsai SJ (2007) Aberrant expression of leptin in human endometriotic stromal cells is induced by elevated levels of hypoxia inducible factor-1α. Am J Pathol 170:590–598
22. Becker CM, Rohwer N, Funakoshi T, Cramer T, Bernhardt W, Birsner A, Folkman J, D'amato RJ (2008) 2-Methoxyestradiol inhibits hypoxia-inducible factor-1α and suppresses growth of lesions in a mouse model of endometriosis. Am J Pathol 172:534–544
23. Goteri G, Lucarini G, Montik N, Zizzi A, Stramazzotti D, Fabris G, Tranquilli AL, Ciavattini A (2009) Expression of vascular endothelial growth factor (VEGF), hypoxia inducible factor-1α (HIF-1α), and microvessel density in endometrial tissue in women with adenomyosis. Int J Gynecol Pathol 28:157–163
24. Moncada S, Higgs A (1993) The L-arginine-nitric oxide pathway. N Engl J Med 329:2002–2012

25. Moncada S, Palmer RM, Higgs EA (1991) Nitric oxide: physiology, pathophysiology, and pharmacology. Pharmacol Rev 43:109–142
26. Nathan C, Xie QW (1994) Nitric oxide synthases: roles, tolls, and controls. Cell 78:915–918
27. Taguchi M, Alfer J, Chwalisz K, Beier HM, Classen-Linke I (2000) Endhotelial nitric oxide synthase is differently expressed in human endometrial vessels during the menstrual cycle. Mol Hum Reprod 6:185–190
28. Knowles RG, Moncada S (1994) Nitric oxide synthases in mammals. Biochem J 298:249–258
29. Kimura H, Esumi H (2003) Reciprocal regulation between nitric oxide and vascular endothelial growth factor in angiogenesis. Acta Biochim Pol 50:49–59
30. Telfer JF, Lyall F, Norman JE, Cameron IT (1995) Identification of nitric oxide synthase in human uterus. Hum Reprod 10:19–23
31. Telfer JF, Irvine GA, Kohnen G, Campbell S, Cameron IT (1997) Expression of endothelial and inducible nitric oxide synthase in non-pregnant and decidualized human endometrium. Mol Hum Reprod 3:69–75
32. Khorram O, Lessey BA (2002) Alterations in expression of endometrial endothelial nitric oxide synthase and $\alpha_v\beta_3$ integrin in women with endometriosis. Fertil Steril 78:860–864
33. Ota H, Igarashi S, Hatazawa J, Tanaka T (1998) Endothelial nitric oxide synthase in the endometrium during the menstrual cycle in patients with endometriosis and adenomyosis. Fertil Steril 69:303–308
34. Dong M, Shi Y, Cheng Q, Hao M (2001) Increased nitric oxide in peritoneal fluid from women with idiopathic infertility and endometriosis. J Reprod Med 46:887–891
35. Wu MY, Chao KH, Yang JH, Lee TH, Yang YS, Ho HN (2003) Nitric oxide synthesis is increased in the endometrial tissue of women with endometriosis. Hum Reprod 18:2668–2671
36. Wang J, Zhou F, Dong M, Wu R, Qian Y (2006) Prolonged gonadotropin-releasing hormone agonist therapy reduced expression of nitric oxide synthase in the endometrium of women with endometriosis and infertility. Fertil Steril 85:1037–1044
37. Osborn BH, Haney AF, Misukonis MA, Weinberg JB (2002) Inducible nitric oxide synthase expression by peritoneal macrophages in endometriosis-associated infertility. Fertil Steril 77:46–51
38. Scurry J, Whitehead J, Healey M (2001) Classification of ovarian endometriotic cysts. Int J Gynecol Pathol 20:147–154
39. Jiang BH, Liu LZ (2008) PI3K/PTEN signaling in tumorigenesis and angiogenesis. Biochem Biophys Acta 1784:150–158
40. Kimura H, Weisz A, Ogura T, Hitomi H, Kurashima Y, Hashimoto K, D' Acquisto F, Machuuki M, Esumi H (2001) Identification of hypoxia-inducible factor 1 ancillary sequence and its function in vascular endothelial growth factor gene induction by hypoxia and nitric oxide. J Biol Chem 276:2292–2298
41. Wu Y, Kajdacsy-Balla A, Strawn E, Basir Z, Halverson G, Jailwala P, Wang Y, Wang X, Ghosh S, Guo S-W (2006) Transcriptional characterizations of differences between eutopic and ectopic endometrium. Endocrinology 147:232–246
42. Matsuzaki S, Canis M, Vaurs-Barrière C, Boespflug-Tanguy O, Dastugue B, Mage G (2005) DNA microarray analysis of gene expression in eutopic endometrium from patients with deep endometriosis using laser capture microdissection. Fertil Steril 84:1180–1190
43. Goteri G, Lucarini G, Pieramici T, Filosa A, Pugnaloni A, Montik N, Biagini G, Tranquilli AL, Fabris G, Ciavattini A, Lo Muzio L (2005) Endothelial cell survivin is involved in the growth of ovarian endometriotic cysts. Anticancer Res 25:4313–4318
44. Tan XJ, Lang JH, Liu DY, Shen K, Leng JH, Zhu L (2002) Expression of vascular endothelial growth factor and thrombospondin-1 mRNA in patients with endometriosis. Fertil Steril 78:148–1453
45. Gilabert-Estellés J, Ramòn LA, Espaňa F, Gilabert J, Vila V, Réganon E, Castellò R, Chirivella M, Estellés A (2007) Expression of angiogenic factors in endometriosis: relationship to fibrinolytic and metalloproteinase systems. Hum Reprod 22:2120–2127

Virchows Arch (2010) 456:711–717
DOI 10.1007/s00428-010-0899-3

CASE REPORT

Extensive biliary intraepithelial neoplasia (BilIN) and multifocal early intrahepatic cholangiocarcinoma in non-biliary cirrhosis

Anne-Laure Rougemont · Muriel Genevay · Thomas A. McKee · Magali Gremaud · Gilles Mentha · Laura Rubbia-Brandt

Received: 23 September 2009 / Revised: 14 January 2010 / Accepted: 20 February 2010 / Published online: 29 April 2010
© Springer-Verlag 2010

Abstract Biliary intraepithelial neoplasia (BilIN), a preneoplastic condition that may precede invasive intrahepatic cholangiocarcinoma (ICC), has been compared to pancreatic intraepithelial neoplasia (PanIN), a precursor lesion of pancreatic carcinoma. Biliary tract carcinoma development and progression is associated with several gene alterations, but BilIN lesions have yet to be studied in detail by molecular techniques. We describe a case of extensive intrahepatic biliary dysplasia, with lesions ranging from BilIN-1 to BilIN-3 lesions, and multifocal microscopic ICC in hepatitis C virus (HCV)- and alcohol-related cirrhosis. The small ICC foci had remained undetected prior to transplantation. Fluorescence in situ hybridization (FISH) analysis was performed on three foci of BilIN-3 lesions and on three microinvasive ICC foci with a combination of three FISH probes directed against genes frequently altered in pancreatic and biliary tract carcinomas. FISH analysis revealed a *CDKNA2* heterozygous deletion in one BilIN-3 focus, and in one non-contiguous ICC focus, although the deletion was just above the chosen threshold. No deletions were detected in the genomic regions encoding *TP53* and *SMAD4*. This report documents for the first time the development of multifocal ICC in the setting of extensive biliary dysplasia in a patient with three risk factors, HCV infection, alcohol abuse, and cirrhosis, and suggests heterogeneous carcinogenesis in ICC and possible involvement of the *CDKNA2* gene.

Keywords Biliary dysplasia · Multifocal intrahepatic cholangiocarcinoma · FISH

A.-L. Rougemont (✉) · M. Genevay · T. A. McKee · M. Gremaud · L. Rubbia-Brandt
Division of Clinical Pathology, Geneva University Hospitals,
Rue Gabrielle-Perret-Gentil 4,
1211 Geneva 14, Switzerland
e-mail: anne-laure.rougemont@hcuge.ch

G. Mentha
Division of Visceral and Transplantation Surgery,
Geneva University Hospitals,
Rue Gabrielle-Perret-Gentil 4,
1211 Geneva 14, Switzerland

Introduction

Intra- and extrahepatic cholangiocarcinoma can arise from two main premalignant conditions, flat or low-papillary biliary dysplasia (biliary intraepithelial neoplasia, BilIN) and intraductal papillary neoplasm (IPN) [1, 2]. IPN, a macroscopically visible papillary proliferation, is considered to be a counterpart of pancreatic intraductal papillary mucinous neoplasm (IPMN) [2], while morphological and immunophenotypic similarities suggest that BilIN could be related to pancreatic intraepithelial neoplasia (PanIN) [3]. BilIN may further progress to cholangiocarcinoma with features of tubular adenocarcinoma [3], mirroring the multistep carcinogenesis progression of PanIN. The three-tiered grading system (BilIN-1 to BilIN-3) depends mainly on the degree of cytological atypia and corresponds respectively to mild, moderate, and severe dysplasia [2, 4]. Invasive adenocarcinoma defines intrahepatic cholangiocarcinoma (ICC).

Risk factors for ICC include chronic biliary disease, such as hepatolithiasis or primary sclerosing cholangitis (PSC), liver fluke infestation, biliary cysts, and bile duct dilatation (such as Caroli's disease or choledochal cyst) or Thorotrast deposition [5, 6]. A "hyperplasia–dysplasia–carcinoma" sequence has been reported in such conditions [6]. BilIN lesions have been initially described mainly in the setting of

PSC [7–9], with biliary dysplasia representing a potential marker for concomitant or later-occurring CC [10]. Several arguments point to a major role for hepatitis C virus (HCV) infection in ICC pathogenesis, including epidemiological correlations [11]; the recent identification of biliary dysplasia in HCV-related cirrhotic livers [12, 13]; the detection of HCV RNA in ICC [14]; and the detection of HCV core proteins by immunohistochemistry in ductular cells in HCV-positive patients [15]. HCV-positive patients have a 2.55-fold increased risk of ICC development, while hepatocellular carcinoma (HCC) risk is increased 15-fold [16]. HCV-positive patients are also at risk for large B cell lymphoma, albeit rarely [17]. ICC in the setting of viral hepatitis or cirrhosis mostly originates from the periphery of the liver [11, 18].

The high sensitivity of a combination of three fluorescence in situ hybridization (FISH) probes in the diagnosis of pancreatic adenocarcinoma has been recently described by our group [19]. The rationale for the choice of the three FISH probes was the frequent occurrence of mutations in the *TP53* (encoding p53), *CDKN2A* (encoding p16(INK4a) and p14(ARF)) and *DPC4*/*SMAD4* (encoding Dpc4) tumor suppressor genes in both pancreatic and biliary tract malignancy [20–23]. It is noteworthy that these gene alterations have also been described in PanIN lesions [24]. Analysis using these probes was intended to clarify the relationship between BilIN with ICC, and PanIN with pancreatic adenocarcinoma.

We describe here a case of mild to severe dysplasia BilIN lesions (BilIN-1 to BilIN-3) with microinvasive ICC foci, in the setting of HCV- and alcohol-related cirrhosis. We report on the results of a FISH analysis of this dysplasia to invasive neoplasia sequence using the *TP53*, *CDK2NA*, and *MALT1* (used as a surrogate for *SMAD4*) probes.

Clinical report

A 42-year-old man underwent liver transplantation for Child C cirrhosis. HCV conversion followed a 5-year drug abuse period, between ages 24 and 29. He had a past history of alcohol abuse. Cirrhosis complications included ascites, esophageal varices, and hepatic encephalopathy while on the waiting list for liver transplantation. Imaging was consistent with cirrhosis, but revealed no focal lesions. Liver tests during pre-transplantation evaluation were nearly within normal ranges (aspartate aminotransferase 97 U/L, alanine transaminase 57 U/L, alkaline phosphatase 85 U/L; γ-glutamyltransferase 20 U/L, total bilirubin 184 μmol/L, conjugated bilirubin 75 μmol/L). Evolution was unfavorable, with hypovolemic shock and septicemia, and the patient died 16 days after transplantation from central pontine myelinolysis, despite normal liver function.

Materials and methods

Representative sections from the liver explant were routinely processed, fixed in 10% buffered formalin and paraffin embedded. For routine histological examination, 3-μm-thick sections were stained with hematoxylin–eosin (H&E), and with the following special stains: Masson trichrome, reticulin stain, PAS with prior diastase digestion, and a Pearl's blue stain. H&E slides allowed selection of three different BilIN-3 foci and of three different ICC foci. One of each of these two lesions was selected on three different representative slides. We chose to initially focus this study on lesions with a higher degree of dysplasia, with further analysis of BilIN-1 and BilIN-2 lesions as a second step, should the initial FISH evaluation reveal major alterations.

The FISH probes were ordered from Vysis, Inc® (Downers Grove, IL). The protocol applied was the same as provided in the study by Genevay et al. [19]. Four micrometer thick tissue sections were placed on Superfrost® Plus (Menzel Glasser®) coated slides, dewaxed, rehydrated, and then immersed successively in two baths of 100% ethanol (5 min at room temperature). The slides were then dried and incubated in Vysis "pre-treatment solution" at 80°C for 15 min, washed in distilled water for 2 min, and dried at 45°C. Tissue sections were then digested with protease at 37°C 60 min for LSI-p16 (CDKN2A); 90 min for LSI-MALT1 (18q21); and 105 min for LSI p53 (17p13) and washed in distilled water for 2 min. Subsequently, they were dehydrated by successive immersions in 70%, 80%, and 100% ethanol (2 min each at room temperature). Probe mixtures were then separately prepared by mixing 1-μl probe with 7 μl hybridization buffer and 2 μl purified water. The LSI p16/CEP9 Dual Color Probe is a mixture of the LSI p16 probe labeled with SpectrumOrange and the CEP9 probe labeled with SpectrumGreen. The chromosome nine centromeric region probe (CEP9) served as an internal control. Accordingly, labeled probes specific to the pericentromeric region of chromosomes 17 (CEP17) and 18 (CEP18) were used as internal controls for the SpectrumOrange TP53 probe (CEP17) and for the SpectrumOrange MALT1 probe (CEP18), respectively. One microliter of CEP17 was placed in 10 μl of LSI-p53 probe mixture, and 1 μl of CEP18 was placed in LSI-MALT1 probe mixture. The *MALT1* gene, located at 18q21, is separated from the *SMAD4* gene by 10 Mb. The use of the commercially available MALT probe seemed reasonable, given this relatively small separation between the two genes, and since a loss of heterozygosity at 18q is described in PanIN lesions [24]. Seven microliters of probe mixture was placed onto the denatured slides and covered with glass coverslips. Hybridization was carried out in a humidified chamber at 72°C for 15 min. The

slides were then washed in post-hybridization wash buffer and incubated in wash buffer for 3 min at 75°C, then washed in distilled water. Subsequently, 7 µl of DAPI counterstain was placed on the slides, which were then mounted with glass coverslips. After hybridization, all slides were stored in the dark at −20°C. As final procedure, the slides were counterstained with DAPI.

Analysis was performed with a Zeiss® Axioplan two fluorescence microscope equipped with 10×, 20×, 60×, and 100× objectives and specific filters (Yellow simple band, Aqua simple band, DAPI simple band, and green/red double band). Image capture was provided by the IP Lab for Macintosh software (Scanalytics® Inc; Rockville, MD). FISH signal counts were repeated on three different BilIN-3 foci, and on three different ICC foci, one of each from three different representative slides. The different foci were located with the DAPI counterstaining and comparison to the original H&E slides. Hybridization signals were counted in at least 200 BilIN-3 dysplastic cell nuclei and 200 adenocarcinoma cells per focus. Genes were considered deleted or amplified when ≤1 or ≥3 nuclear signals were detected, respectively. The cutoff values defined by our group with a receiver operating characteristic (ROC) curves analysis (AUC), and providing a specificity >90% for all three probes, were applied [19]. In this previous study, the ROC curves were calculated using Medcalc® v9.6.4.0. The value for the area under the curve (AUC) had to be at least 0.5 for the test to be considered as efficient. The cutoff value (the minimum percentage of cells exhibiting deletions or amplifications required to consider the test result as positive) was chosen to maximize the test specificity (at least 90%).

Accordingly, from the results of this previous study, the following thresholds were chosen: 7% for the LSI-MALT1 and LSI-p16 probes and 17% for the LSI-p53 probe. With these criteria, a FISH sensitivity of 82% and specificity of 100% had been obtained in the diagnosis of pancreatic adenocarcinoma when ≥2 genetic modifications were observed [19]. Although no FISH data exists to date in PanIN lesions, alterations have been shown in the three selected regions in PanIN lesions [23, 25–27].

Results

Upon gross examination, the liver weighed 1,053 g and showed a micronodular cirrhosis, with no overtly malignant macronodules on cut section. Multiple white nodules measuring up to 0.5 cm in greatest diameter were observed in both lobes, mostly in peripheral locations (Fig. 1). No papillary proliferation was grossly visible in bile ducts. Upon histological evaluation, the cirrhosis was confirmed using Masson trichrome and reticulin stains, and a mainly

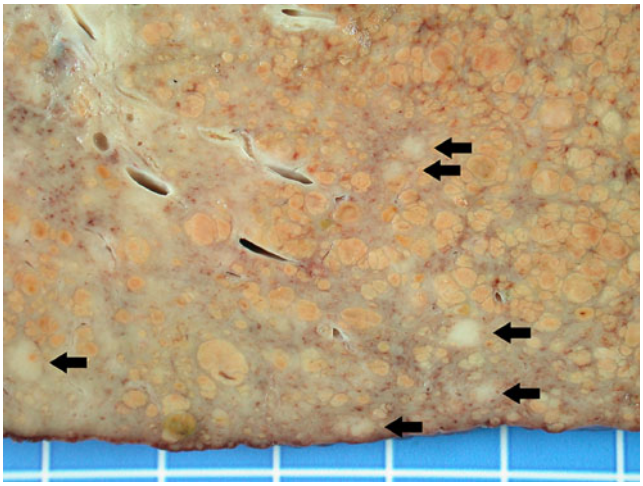

Fig. 1 Gross findings of liver cirrhosis and multiple white nodules, measuring up to 0.5 cm in greatest diameter and mostly located at the periphery (*black arrows*)

lymphocytic portal tract infiltrate with no hepatitis activity was observed (METAVIR score A0-F4) [28] with H&E. There was mild iron deposition in hepatocytes, owing to cirrhosis, and no hyaline globules. A strikingly diffuse flat or pseudo-papillary proliferation of the biliary epithelium with mucosecretion in a minority of cells involved larger intrahepatic biliary tracts and extended to the interlobular ducts (Fig. 2a). These features were observed both in peripheral and central locations, with sparing of the large perihilar bile ducts. Cytological changes ranged from mild, with basally located slightly elongated nuclei (BilIN-1), to severe, with hyperchromatic and large nuclei and loss of cell polarity (BilIN-3) (Fig. 2b–c). Additional small foci consisted of a proliferation of angular and irregular glands, surrounded by a stromal reaction consistent with stromal invasion (Fig. 2d). These ICC foci were distinguished from ductular reaction by: 1) the presence of irregular and angulated glands, with an open lumen; 2) a higher degree of cytonuclear atypia; and 3) the identification of a desmoplastic reaction. Fibrosis in such areas was prominent, and correlated with microscopic zones in some of the grossly identified fibrotic white nodules. There was no evidence of alcohol-related lesions.

FISH analysis in the 200 or more cell nuclei showed *CDKN2A* heterozygous deletion above the 7% threshold in one of the three chosen BilIN-3 foci (10% of cell nuclei) and in one of the three ICC foci (8.5% of cells) (Fig. 3). Loss of one *TP53* signal was observed in 13.8 and 15% of the nuclei analyzed in 2 ICC foci, and in 15.9% of one BilIN-3 focus, but failed to attain the previously defined cutoff value of 17%. *MALT1* showed a normal FISH signal in all the BilIN-3 and ICC foci. In view of these results, shown in Table 1, no further analysis of BilIN-1 and BilIN-2 lesions was performed.

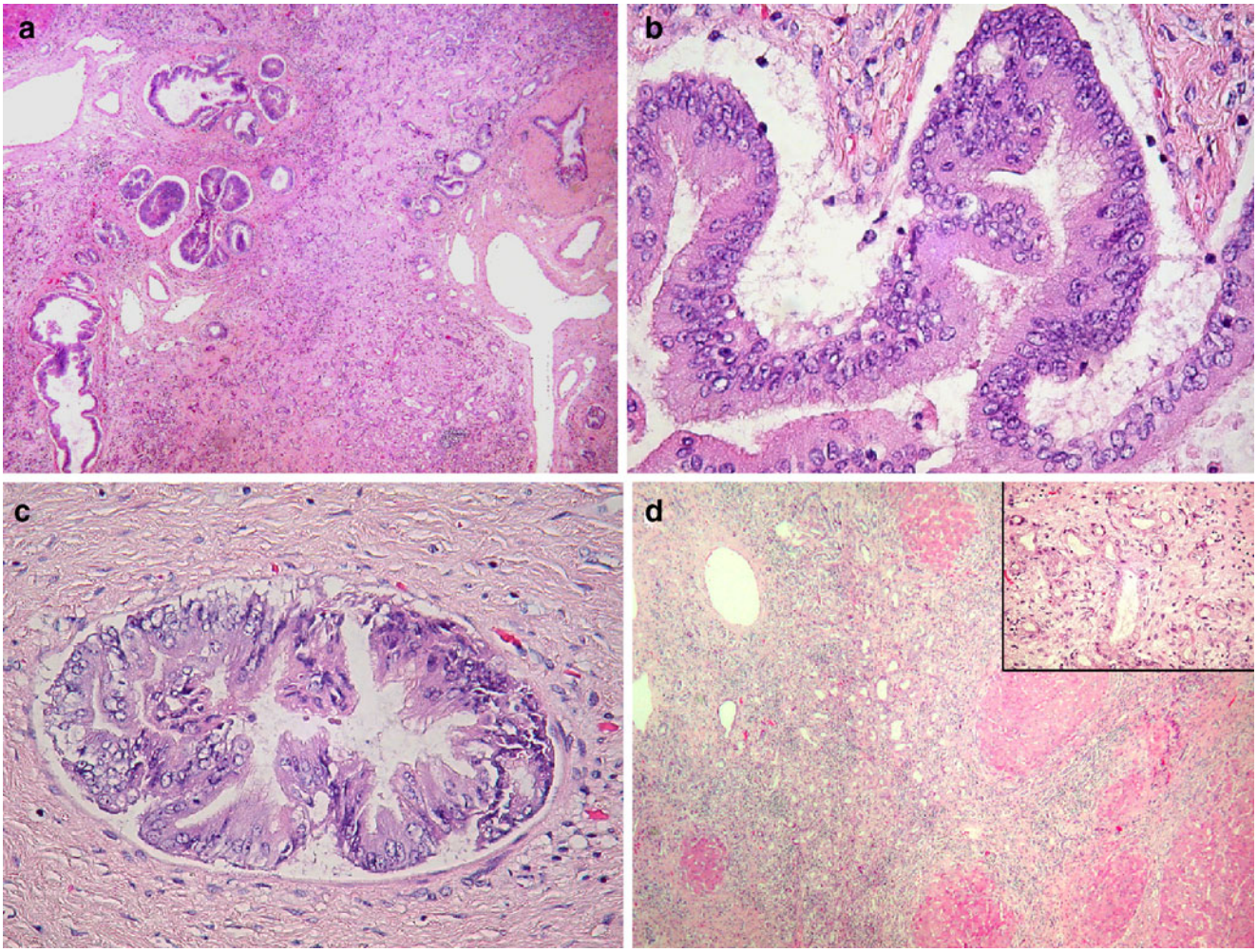

Fig. 2 Histological progression from BilIN lesions to ICC, according to the criteria by Zen et al. [2] hematoxylin & eosin (H&E). **a** Multifocal flat or pseudo-papillary proliferation of the biliary epithelium, extending from the segmental bile ducts to the interlobular ducts (original magnification 100×). **b** BilIN-2 (400×). **c** BilIN-3 (200×). **d** Microinvasive ICC focus, identified at low power (100×) and confirmed at higher power (*inset*—400×). *Inset* illustrates the distorted, angulated and branching glands, with an open lumen, and the stromal invasion

Discussion

We report here the first case of extensive BilIN lesions with multiple microscopic ICC foci, in the setting of HCV- and alcohol-related cirrhosis. BilIN lesions extended from septal-sized to interlobular bile ducts. Multiple ICC foci were located in the two lobes. A *CDKN2A* heterozygous deletion was observed in one BilIN-3 focus and in one non-contiguous ICC focus. No *TP53* or *MALT1* deletion was observed.

BilIN is a rare finding in cirrhotic livers. In a large retrospective study of 1,058 liver explants by Torbenson et al., dysplasia was observed in 1.8% of cases, and only in cirrhotic livers [12]. Addition of alcohol consumption to HCV infection increased the incidence of bile duct dysplasia from 2% (HCV infection alone) to 5% (HCV and alcohol) [12]. Multifocal dysplastic changes involved only septal-sized bile ducts [12]. In a series of 468 cases of liver cirrhosis, in patients lacking a history of cholangitis or hepatolithiasis, Aishima et al. identified two cases of high-grade biliary dysplasia with a micropapillary growth pattern and extensive spread [13]. The lesions involved the intra-hepatic septal ducts, the interlobular ducts, and the ductules of the ductular reaction, and had developed in one case in a HCV-related cirrhotic liver, with two HCC, and in the second case, in a liver with alcohol-related cirrhosis [13]. No ICC foci were described. The case presented here thus represents the third description of multifocal BilIN lesion in non-biliary cirrhotic liver, involving not only septal-sized bile ducts, but also interlobular bile ducts, and the first with co-existent ICC foci.

ICC microinvasive foci are difficult to diagnose on morphological aspects solely, and we wished to determine whether FISH techniques might be of diagnostic value. The

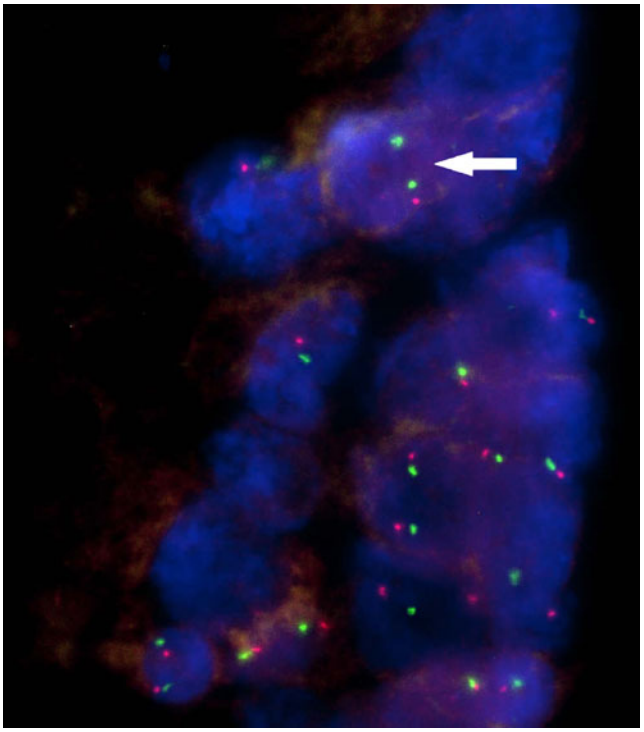

Fig. 3 FISH results, with the LSI p16 (*CDKN2A*) probe showing heterozygous deletion in a subset of the ICC cells in a BilIN-3 focus, with loss of one of the SpectrumOrange signals in a nucleus and preservation of the 2 centromeric SpectrumGreen signals (*white arrow*)

proposed relationship between these lesions and PanIN/pancreatic carcinoma justified the use of probes directed against genes involved both in pancreatic and biliary tract oncogenetic pathways [20–23]. Several studies have confirmed the importance of allelic losses at 9p21 (*CDKN2A*), 17p13 (*TP53*), and 18q21 (*SMAD4*) in pancreatic carcinoma, with loss of one or more of these loci in a vast majority of cases [29–33]. Early loss of *CDKN2A* has been shown in the PanIN to pancreatic adenocarcinoma sequence, with *TP53* and *SMAD4* being deleted later [23–27]. In invasive biliary tract tumors, or in their metastases, losses of regions harboring each of the three genes studied have been demonstrated in 64% (9p), 45% (17p), and 55% (18q) of cases [22]. This, along with the absence of deletions in the majority of lesions studied in this case, suggests molecular differences in pancreatic and biliary tract oncogenesis with chromosomal deletion, possibly occurring later in the pathway.

CDKN2A gene alterations are described in many cancer types [34]. Homozygous 9p21 deletion, encompassing the *CDKN2A* gene, was observed in 11 of 22 ICC by FISH analysis, of which 16 were sporadic and the remaining six were PSC related [35]. Homozygous 9p21 deletion has also been described in three of five PSC-related biliary dysplasia specimens [35]. We observed a *CDKN2A* heterozygous deletion in a subset of the BilIN-3 and ICC foci. These findings evoke the possibility of involvement of different molecular pathways from one ICC focus to another, as has been described in cases of synchronous multicentric HCC [36].

A progressive decrease in immunohistochemical reactivity of Dpc4 expression, the *SMAD4* gene protein product, has been observed from non-neoplastic biliary epithelium to invasive CC [37]. Despite this previous description, we observed no alteration in the *MALT1* gene, used as a surrogate for *SMAD4*, suggesting that at least part of the reduction of protein expression might result from point mutations or epigenetic inactivation.

Inactivating *TP53* mutations represent the most frequent gene alteration in human cancers [38]. *TP53* mutations have been detected particularly in the mass-forming ICC type in the setting of viral hepatitis, suggesting a relationship to ICC arising from small peripheral bile ducts [5, 39]. However, the alterations observed were missense or, rarely, nonsense mutations [39]. We observed no *TP53* alteration in the case reported here.

We described here a third case of extensive BilIN lesions in the setting of HCV- and alcohol-related cirrhosis. Multiple microscopic ICC foci were too small to allow radiological detection. BilIN has recently been described in non-biliary liver cirrhosis, and as described in PSC patients, dysplasia in liver biopsy specimens might be a marker of synchronous or metachronous ICC. However, BilIN may affect only the rarely biopsied segmental bile ducts. FISH techniques revealed a *CDKN2A* heterozygous deletion in

Table 1 FISH analysis results, in the cell nuclei of three BilIN-3 and three ICC foci, from three representative slides (foci one to three)

Significance threshold		LSI-p16 (*CDKN2A*)		LSI-MALT1 (*SMAD4* surrogate)		LSI-p53	
		7%		7%		17%	
BilIN-3	Focus 1	21/201	10%	0/202		16/155	10%
	Focus 2	3/272	1.1%	4/201	1.9%	42/264	15.9%
	Focus 3	2/213	0.9%	0/240		9/212	4%
ICC	Focus 1	8/227	3.5%	0/300		26/188	13.8%
	Focus 2	12/266	4.5%	2/201	0.9%	6/111	5.4%
	Focus 3	13/152	8.5%	0/200		38/252	15%

one BilIN-3 and in one ICC focus. We hypothesize that these *CDKN2A* alterations could represent a late event and would have been more pronounced had the lesions progressed to a more overt mass-forming ICC, in contrast to observations in PanIN, where *CDKN2A* alterations appear to be an early event. Heterogeneous findings were observed in the different BilIN-3 and ICC foci studied, evoking the possibility of involvement of different molecular pathways from one ICC focus to another, as has been described in cases of synchronous multicentric HCC. BilIN and PanIN share close phenotypic and immunohistochemical aspects, and seem to share some oncogenic mechanisms. However, the observation of heterogeneous *CDKN2A* alterations and the absence of *TP53* and *MALT1* (surrogate for *SMAD4*) deletions in the case presented here point towards different oncogenetic pathways. The study of large numbers of lesions is warranted.

Conflict of interest statement We declare that we have no conflict of interest.

References

1. Wilentz RE, Iacobuzio-Donahue CA, Argani P et al (2000) Loss of expression of Dpc4 in pancreatic intraepithelial neoplasia: evidence that DPC4 inactivation occurs late in neoplastic progression. Cancer Res 60:2002–2006
2. Zen Y, Adsay NV, Bardadin K et al (2007) Biliary intraepithelial neoplasia: an international interobserver agreement study and proposal for diagnostic criteria. Mod Pathol 20:701–709
3. Zen Y, Sasaki M, Fujii T et al (2006) Different expression patterns of mucin core proteins and cytokeratins during intrahepatic cholangiocarcinogenesis from biliary intraepithelial neoplasia and intraductal papillary neoplasm of the bile duct—an immunohistochemical study of 110 cases of hepatolithiasi. J Hepatol 44:350–358
4. Itatsu K, Zen Y, Ohira S et al (2007) Immunohistochemical analysis of the progression of flat and papillary preneoplastic lesions in intrahepatic cholangiocarcinogenesis in hepatolithiasis. Liver Int 27:1174–1184
5. Nakanuma Y, Harada K, Ishikawa A et al (2003) Anatomic and molecular pathology of intrahepatic cholangiocarcinoma. J Hepatobiliary Pancreat Surg 10:265–281
6. Shimonishi T, Sasaki M, Nakanuma Y (2000) Precancerous lesions of intrahepatic cholangiocarcinoma. J Hepatobiliary Pancreat Surg 7:542–550
7. Bergquist A, Glaumann H, Stal P et al (2001) Biliary dysplasia, cell proliferation and nuclear DNA-fragmentation in primary sclerosing cholangitis with and without cholangiocarcinoma. J Intern Med 249:69–75
8. Ludwig J, Wahlstrom HE, Batts KP et al (1992) Papillary bile duct dysplasia in primary sclerosing cholangitis. Gastroenterology 102:2134–2138
9. Martins EB, Fleming KA, Garrido MC et al (1994) Superficial thrombophlebitis, dysplasia, and cholangiocarcinoma in primary sclerosing cholangitis. Gastroenterology 107:537–542
10. Fleming KA, Boberg KM, Glaumann H et al (2001) Biliary dysplasia as a marker of cholangiocarcinoma in primary sclerosing cholangitis. J Hepatol 34:360–365
11. Kobayashi M, Ikeda K, Saitoh S et al (2000) Incidence of primary cholangiocellular carcinoma of the liver in Japanese patients with hepatitis C virus-related cirrhosis. Cancer 88:2471–2477
12. Torbenson M, Yeh MM, Abraham SC (2007) Bile duct dysplasia in the setting of chronic hepatitis C and alcohol cirrhosis. Am J Surg Pathol 31:1410–1413
13. Aishima S, Nishihara Y, Tsujita E et al (2008) Biliary neoplasia with extensive intraductal spread associated with liver cirrhosis: a hitherto unreported variant of biliary intraepithelial neoplasia. Hum Pathol 39:939–947
14. Perumal V, Wang J, Thuluvath P et al (2006) Hepatitis C and hepatitis B nucleic acids are present in intrahepatic cholangiocarcinomas from the United States. Hum Pathol 37:1211–1216
15. Uchida T, Shikata T, Tanaka E et al (1994) Immunoperoxidase staining of hepatitis C virus in formalin-fixed, paraffin-embedded needle liver biopsies. Virchows Arch 424:465–469
16. El-Serag HB, Engels EA, Landgren O et al (2009) Risk of hepatobiliary and pancreatic cancers after hepatitis C virus infection: a population-based study of U.S. veterans. Hepatology 49:116–123
17. Rubbia-Brandt L, Brundler MA, Kerl K et al (1999) Primary hepatic diffuse large B-cell lymphoma in a patient with chronic hepatitis C. Am J Surg Pathol 23:1124–1130
18. Aishima S, Kuroda Y, Nishihara Y et al (2007) Proposal of progression model for intrahepatic cholangiocarcinoma: clinicopathologic differences between hilar type and peripheral type. Am J Surg Pathol 31:1059–1067
19. Genevay M, Dumonceau JM, Pache JC et al (2010) FISH as a tool to characterize genetic alterations in pancreatic adenocarcinoma. Pancreas (in press)
20. Mahlamaki EH, Barlund M, Tanner M et al (2002) Frequent amplification of 8q24, 11q, 17q, and 20q-specific genes in pancreatic cancer. Genes Chromosomes Cancer 35:353–358
21. Schneider G, Schmid RM (2003) Genetic alterations in pancreatic carcinoma. Mol Cancer 2:15
22. Shiraishi K, Okita K, Harada T et al (2001) Comparative genomic hybridization analysis of genetic aberrations associated with development and progression of biliary tract carcinomas. Cancer 91:570–577
23. Feldmann G, Beaty R, Hruban RH et al (2007) Molecular genetics of pancreatic intraepithelial neoplasia. J Hepatobiliary Pancreat Surg 14:224–232
24. Hruban RH, Goggins M, Parsons J et al (2000) Progression model for pancreatic cancer. Clin Cancer Res 6:2969–2972
25. Luttges J, Galehdari H, Brocker V et al (2001) Allelic loss is often the first hit in the biallelic inactivation of the p53 and DPC4 genes during pancreatic carcinogenesis. Am J Pathol 158:1677–1683
26. Maitra A, Adsay NV, Argani P et al (2003) Multicomponent analysis of the pancreatic adenocarcinoma progression model using a pancreatic intraepithelial neoplasia tissue microarray. Mod Pathol 16:902–912
27. Wilentz RE, Geradts J, Maynard R et al (1998) Inactivation of the p16 (INK4A) tumor-suppressor gene in pancreatic duct lesions: loss of intranuclear expression. Cancer Res 58:4740–4744
28. Anonymous (1994) Intraobserver and interobserver variations in liver biopsy interpretation in patients with chronic hepatitis C. The French METAVIR Cooperative Study Group. Hepatology 20:15–20
29. Caldas C, Hahn SA, da Costa LT et al (1994) Frequent somatic mutations and homozygous deletions of the p16 (MTS1) gene in pancreatic adenocarcinoma. Nat Genet 8:27–32

30. Hahn SA, Hoque AT, Moskaluk CA et al (1996) Homozygous deletion map at 18q21.1 in pancreatic cancer. Cancer Res 56:490–494
31. Hahn SA, Seymour AB, Hoque AT et al (1995) Allelotype of pancreatic adenocarcinoma using xenograft enrichment. Cancer Res 55:4670–4675
32. Redston MS, Caldas C, Seymour AB et al (1994) p53 mutations in pancreatic carcinoma and evidence of common involvement of homocopolymer tracts in DNA microdeletions. Cancer Res 54:3025–3033
33. Rozenblum E, Schutte M, Goggins M et al (1997) Tumor-suppressive pathways in pancreatic carcinoma. Cancer Res 57:1731–1734
34. Ruas M, Peters G (1998) The p16INK4a/CDKN2A tumor suppressor and its relatives. Biochim Biophys Acta 1378:F115–F177
35. DeHaan RD, Kipp BR, Smyrk TC et al (2007) An assessment of chromosomal alterations detected by fluorescence in situ hybridization and p16 expression in sporadic and primary sclerosing cholangitis-associated cholangiocarcinomas. Hum Pathol 38:491–499
36. Sirivatanauksorn Y, Sirivatanauksorn V, Bhattacharya S et al (1999) Genomic heterogeneity in synchronous hepatocellular carcinomas. Gut 45:761–765
37. Nakanishi Y, Zen Y, Kondo S et al (2008) Expression of cell cycle-related molecules in biliary premalignant lesions: biliary intraepithelial neoplasia and biliary intraductal papillary neoplasm. Hum Pathol 39:1153–1161
38. Soussi T, Beroud C (2001) Assessing TP53 status in human tumours to evaluate clinical outcome. Nat Rev Cancer 1:233–240
39. Kang YK, Kim WH, Lee HW et al (1999) Mutation of p53 and K-ras, and loss of sheterozygosity of APC in intrahepatic cholangiocarcinoma. Lab Invest 79:477–483

Virchows Arch (2010) 456:719–721
DOI 10.1007/s00428-010-0923-7

LETTER TO THE EDITOR

Calcifying fibrous pseudotumor affecting the retroperitoneum: could it be a new entity within the spectrum of IgG-4 sclerosing disease?

M. J. Fernández Aceñero · Peter W. Vorwald · Sharon Cordova Yamauchi

Received: 8 March 2010 / Revised: 8 April 2010 / Accepted: 8 April 2010 / Published online: 23 April 2010
© Springer-Verlag 2010

Dear Sir:

Calcifying fibrous pseudotumor (CFP) was initially described by Fetsch in 1993 [1] as a collection of dense hyalinized collagenous tissue interpersed with scarce benign-appearing spindle cells and characterized by the presence of psammomatous calcifications and a variable infiltrate of lymphoid and plasma cells, evenly organized in lymphoid follicles. These lesions had been formerly called childhood fibrous pseudotumor with psammoma bodies by Rosenthal et al., but those lesions share enough features to be considered a unique entity. These tumors have been described in many locations, but they have a tendency to involve the extremities and also the neck area, although there are cases affecting the mediastinum and retroperitoneum. In a recent series, Kuo et al. [2] have for the first time reported the preponderance of IgG4+-plasma cells in the infiltrate in five cases of CFP associated with sclerosing angiomatoid nodular transformation of the spleen. We report a case with similar features and propose it as another possible entity to be included in the IgG4-related sclerosing disease.

A 32-year-old woman born in Colombia consulted in the Digestive System Department, Fundación Jiménez Díaz, in Madrid, Spain, on vague abdominal discomfort with bloating. A computed tomography performed during the evaluation of this symptoms revealed a 13-cm retroperitoneal mass (Fig. 1) involving the mesenteric vessels, mainly the superior mesenteric vein. She referred having been operated on in her country for a fibromatosis, but she had no medical reports regarding this surgery.

The patient was well, apart from her abdominal discomfort, and referred neither weight loss, nausea, nor vomiting. It was decided to perform a supra- and infraumbilical medial laparotomy to resect the mass. However, during surgery, the mass was found to involve the pancreatic head and the celiac axis, which made it impossible to resect the whole mass without compromising the viability of the intestines. Several small samples from the mass were obtained and sent for a frozen section study in the Pathology Department.

The histopathological analysis of these samples revealed dense collagenous, almost acellular tissue without any specific characteristics, and diagnosis was deferred until definitive study of serial sections.

The definitive histopathological analysis of the samples confirmed the presence of a dense collagenous scarcely cellular tissue. Within this tissue, there were prominent psammomatous calcifications (Fig. 2) as well as some aggregates of lymphoid cells, even constituting lymphoid follicles with clear germinal centers. Immunohistochemistry performed in the samples confirmed positivity of the lymphoid follicles for CD20 and CD3, and the presence of many plasma cells (positive for CD123). The scarce spindle cells growing within the collagenous stroma were positive for vimentin and factor XIIIa and negative for ALK, β-catenin, smooth muscle actin, and CD34. Histopathological diagnosis was calcifying fibrous pseudotumor.

The paraffin blocks were sent to Dr. Manuel Rodríguez Justo, a pathologist working at the Department of Histopathology, University College London Medical School, UK.

M. J. F. Aceñero (✉) · S. C. Yamauchi
Department of Surgical Pathology,
Fundación Jiménez Díaz (Capio Group),
Avda Reyes Católicos 2,
28040 Madrid, Spain
e-mail: mgg10167@gmail.com

P. W. Vorwald
Department of General Surgery, Fundación Jiménez Díaz,
Avda Reyes Católicos 2,
28040 Madrid, Spain

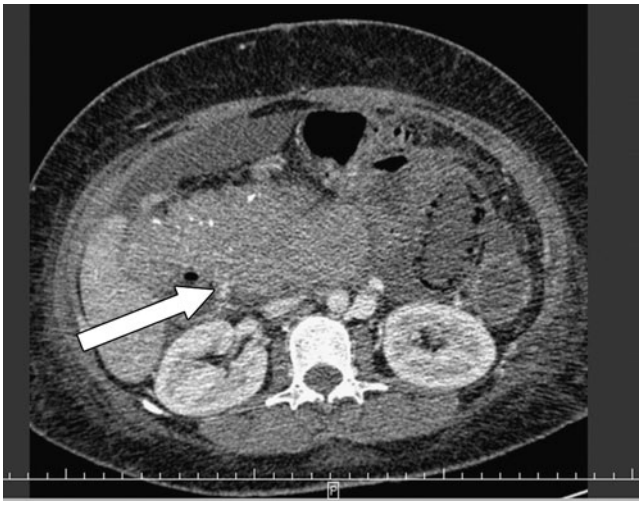

Fig. 1 Abdominal CT scan showing the large retroperitoneal mass with no specific radiological features (*arrow*)

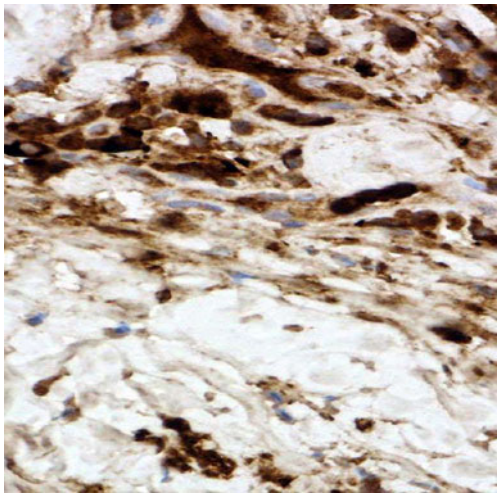

Fig. 3 Intense positivity of most plasma cells for IgG4 (immunohistochemistry for IgG4, kindly performed by Dr. Rodríguez San Justo)

He confirmed our diagnosis and also performed immunohistochemistry for IgG4 detection, showing that 80% of the plasma cells were positive (Fig. 3).

After surgery, the patient had an acute intestinal ischemia and had to be reoperated on for resection of a 30-cm small intestine segment. In this second specimen, there were no areas of fibrous pseudotumor. After this surgery, the patient has slowly recovered and is waiting for hospital discharge after a 3-month stay. No further therapy has been decided so far.

Calcifying fibrous pseudotumor is a recently described [1] tumor that seemed to originally affect more the extremities and the neck areas. However, there are recent reports on lesions of this group affecting the breast, the adrenal gland, and even the myocardium, the soft palate, and the pleura. It is defined by its histopathological characteristics, namely the diffuse collagenous paucicellular stroma, the presence of psammomatous or amorphous coarse calcifications within the stroma, and the presence of lymphoid aggregates with lymphocytes and plasma cells [1].

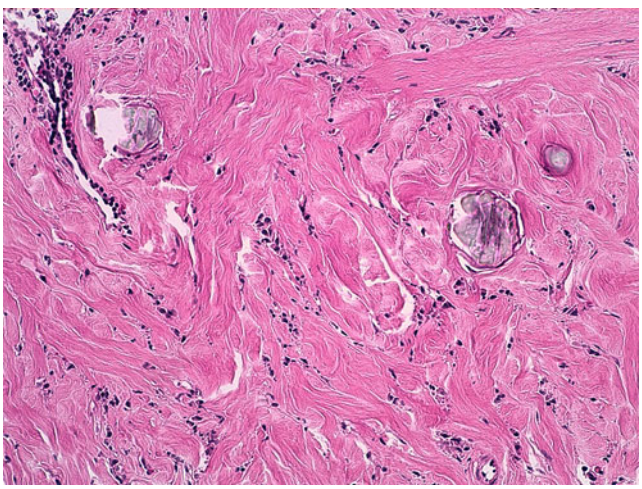

Fig. 2 High-power view confirming scarce spindle cells within the collagenous stroma and calcifications with a psammomatous conformation (H&E, ×200)

Histopathological differential diagnosis is broad. Fibromatoses are usually more cellular lesions and they usually express nuclear beta-catenin, which was negative in our case. Inflammatory myofibroblastic tumor has been related by some authors to CFP, and they have considered this latter entity as the final collagenous stage of the former. However, these tumors show a different immunohistochemical profile and a different biological behavior. The immunohistochemical detection of ALK can also help in this differential diagnosis.

Retroperitoneal fibrosis is characterized by a dense collagenous tissue that grows and encases local structures, including the kidney or the ureters that can be secondarily damaged by the infiltrative growth. This lesion is associated with other fibrosing conditions, including inflammatory pseudotumor, retractile mesenteritis, and retroorbital fibrosis. In these lesions, there are no psammomatous calcifications, as found in our case. More recently, there has been a proposal to consider all these fibrosis-inducing tumors as part of the so-called IgG4-positive multiorgan lymphoproliferative syndrome. This entity is clinically characterized by the presence of elevated serum IgG4 levels and a dense infiltration of different organs and tissues by IgG4-positive plasma cells (they must represent 50% of the plasma cells present in the infiltrate to fulfill diagnostic criteria of this entity). The patients with IgG4-positive multiorgan lymphoproliferative syndrome (also called in the literature IgG4-related sclerosing disease [3,4]) can have involvement of several target organs or just localized disease in one of them. Among the lesions that are considered part of the

spectrum of IgG4-positive multiorgan lymphoproliferative syndrome, we can mention autoimmune pancreatitis [5], sclerosing angiomatoid nodular transformation of the spleen, sclerosing cholangitis, sclerosing sialadenitis, retroperitoneal fibrosis, tubulointerstitial nephritis, and inflammatory pseudotumor. In this spectrum, there are no mentions to the calcifying fibrous pseudotumor, but a recent report by Kuo et al. [2] has shown the association of sclerosing angiomatoid nodular transformation of the spleen and CFP in five patients, and they all had a clear preponderance of IgG4-positive plasma cells in their inflammatory infiltrates. The identification in our case of the same preponderance of IgG4-positive plasma cells also speaks for the relation between this CFP and the IgG4-related fibrosing lesions. This fact can be important for some patients with this disease type who respond well to steroid therapy. In a patient like the one we report on, in whom surgical resection is impossible due to the anatomic structures involved, this can be a therapeutic option that should be explored.

There have also been recent reports on the association of CFP and some other entities, namely Castleman's disease. Besides, there are some reports on CFP affecting exclusively the gastrointestinal tract and that are associated with many diagnostic and therapeutic challenges [6].

In summary, we herein report a new case of CFP affecting the retroperitoneum in a young woman, which was not considered resectable. The immunohistochemical results showing positivity for IgG4 in plasma cell lead us to consider this could be another entity within the spectrum of IgG4-related sclerosing disease.

Acknowledgments The authors are indebted to Dr. Rodríguez Justo for the IgG4 immunostains performed in our case and to Dr. Carlos Santonja for his help in the elaboration of the present study.

Conflict of interest statement We declare that we have no conflict of interest.

Reference

1. Fetsch JF, Montgomery EA, Meis JA (1993) Calcifying fibrous pseudotumor. Am J Surg Pathol 17:502–508
2. Kuo T, Chen TC, Lee LY (2009) Sclerosing angiomatoid nodular transformation of the spleen (SANT): clinicopathological study of 10 cases with or without abdominal disseminated calcifying fibrous tumors, and the presence of a significant number of IgG4+ plasma cells. Pathol Intern 59:844–850
3. Kamisawa T, Okamoto A (2008) IgG4-related sclerosing disease. World J Gastroenterol 14:3948–3955
4. Masaki Y, Dong L, Kurose N, Kitagawa K, Morikawa Y, Yamamoto M, Takahashi H, Shinomura Y, Imai K, Saeki T, Azumi A, Nakada S, Sugiyama E, Matsui S, Origuchi T, Nishiyama S, Nishimori I, Nojima T, Yamada K, Kawano M, Zen Y, Kaneko M, Miyazaki K, Tsubota K, Eguchi K, Tomoda K, Sawaki T, Kawanami T, Tanaka M, Fukushima T, Sugai S, Umehara H (2009) Proposal for a new clinical entity, IgG4-positive multiorgan lymphoproliferative syndrome: analysis of 64 cases of IgG4-related disorders. Ann Rheum Dis 68:1310–1315
5. Zamboni G, Lüttges J, Capelli P, Frulloni L, Cavallini G, Pederzoli P, Leins A, Longnecker D, Klöppel G (2004) Histopathological features of diagnostic and clinical relevance in autoimmune pancreatitis: a study on 53 resection specimens and 9 biopsy specimens. Virchows Archiv 445:552–563
6. Agaimy A, Bihl MP, Tornillo L, Wünsch PH, Hartmann A, Michal M (2010) Calcifying fibrous tumor of the stomach: clinicopathologic and molecular study of seven cases with literature review and reappraisal of histogenesis. Am J Surg Pathol 34:271–278

Virchows Arch (2010) 456:723–725
DOI 10.1007/s00428-010-0928-2

LETTER TO THE EDITOR

Adenocarcinoma with eosinophilic cells with non-overlapping low-grade nuclei arising from heterotopic gastric mucosa in the duodenal bulb: a new tumour entity?

Eva-Maria Wolf · Ryoji Kushima · Michael Vieth · Karl Fuchs · Cord Langner

Received: 22 February 2010 / Revised: 14 April 2010 / Accepted: 22 April 2010 / Published online: 12 May 2010
© Springer-Verlag 2010

Dear Editor,

Heterotopic gastric mucosa may occur throughout the whole gastrointestinal tract and even in extraintestinal sites. Prevalence of gastric heterotopia in the duodenal bulb has been reported to be 0.5% [1]. Neoplastic progression is exceedingly rare. To the best of our knowledge, only three cases with adenomatous change, but no malignant tumours arising from heterotopic gastric mucosa, two in the duodenum and one in the rectum, have been reported in the English literature [2–4].

We recently dealt with the case of an 86-year-old female who underwent upper gastrointestinal endoscopy for unspecific abdominal discomfort. In the duodenal bulb, an irregular polyp, measuring 1 cm in largest diameter, was discovered and biopsies were taken. Upon histological examination, heterotopic gastric glands were seen at the basis of the lesion (Fig. 1a). The surface epithelium was characterised by neoplastic columnar cells with ample eosinophilic cytoplasm and non-overlapping low-grade nuclei evenly arranged below luminal cell membranes (Fig. 1b). Overall, the tumour was made up by well-differentiated tubulo-papillary glands. In parts of the lesion, however, gland fusion, cribriform glands with lateral expansion and interfoveolar spread as well as invasion of small cell clusters into the stroma were noted (Fig. 1c). Immunohistochemically, the majority of tumour cells showed gastric differentiation with extensive expression of MUC5AC (Fig. 1d) and focal expression of MUC 6 (Fig. 1e). In addition, some tumour cells expressed MUC2 and CDX-2 (Fig. 1f), thereby indicating focal intestinal differentiation. The tumour cells were diffusely positive for Keratin 7 and Keratin 19, but only focally expressed Keratin 20. MIB-1 proliferation rate was remarkably high with staining of approximately 30% of cancer cells, whereas only few nuclei were immunoreactive for p53. With antibodies directed against lysozyme, against disulfide-isomerase (detecting endoplasmic reticulum), and against the surface of intact human mitochondria, the tumour cells were intensely decorated (Fig. 1g, h). Pepsinogen-1 or proton pump-positive tumour cells were not identified within the lesion. Finally, diagnosis of a moderately differentiated adenocarcinoma with predominant gastric differentiation, originating from heterotopic gastric mucosa, was made.

Differential diagnosis includes duodenal adenomas and adenocarcinomas which usually show intestinal differentiation. Moreover, tumours originating from the ampulla of Vater can be classified as either intestinal or pancreatobiliary adenocarcinomas [5]. Finally, neoplastic lesions may arise from heterotopic pancreatic tissue located with the duodenal wall or may represent invasion of a pancreatic malignancy into the duodenal wall, ultimately extending into the lumen.

Of note, two of the three hitherto reported cases of adenomatous growth developing within heterotopic gastric mucosa were diagnosed as pyloric gland-type adenoma. In

E.-M. Wolf · C. Langner (✉)
Institute of Pathology, Medical University Graz,
Auenbruggerplatz 25,
8036 Graz, Austria
e-mail: cord.langner@medunigraz.at

R. Kushima
Institute of Pathology, National Cancer Centre Hospital,
Tokyo, Japan

M. Vieth
Institute of Pathology, Klinikum Bayreuth,
Bayreuth, Germany

K. Fuchs
Institute of Pathology, Landeskrankenhaus Vöcklabruck,
Vöcklabruck, Austria

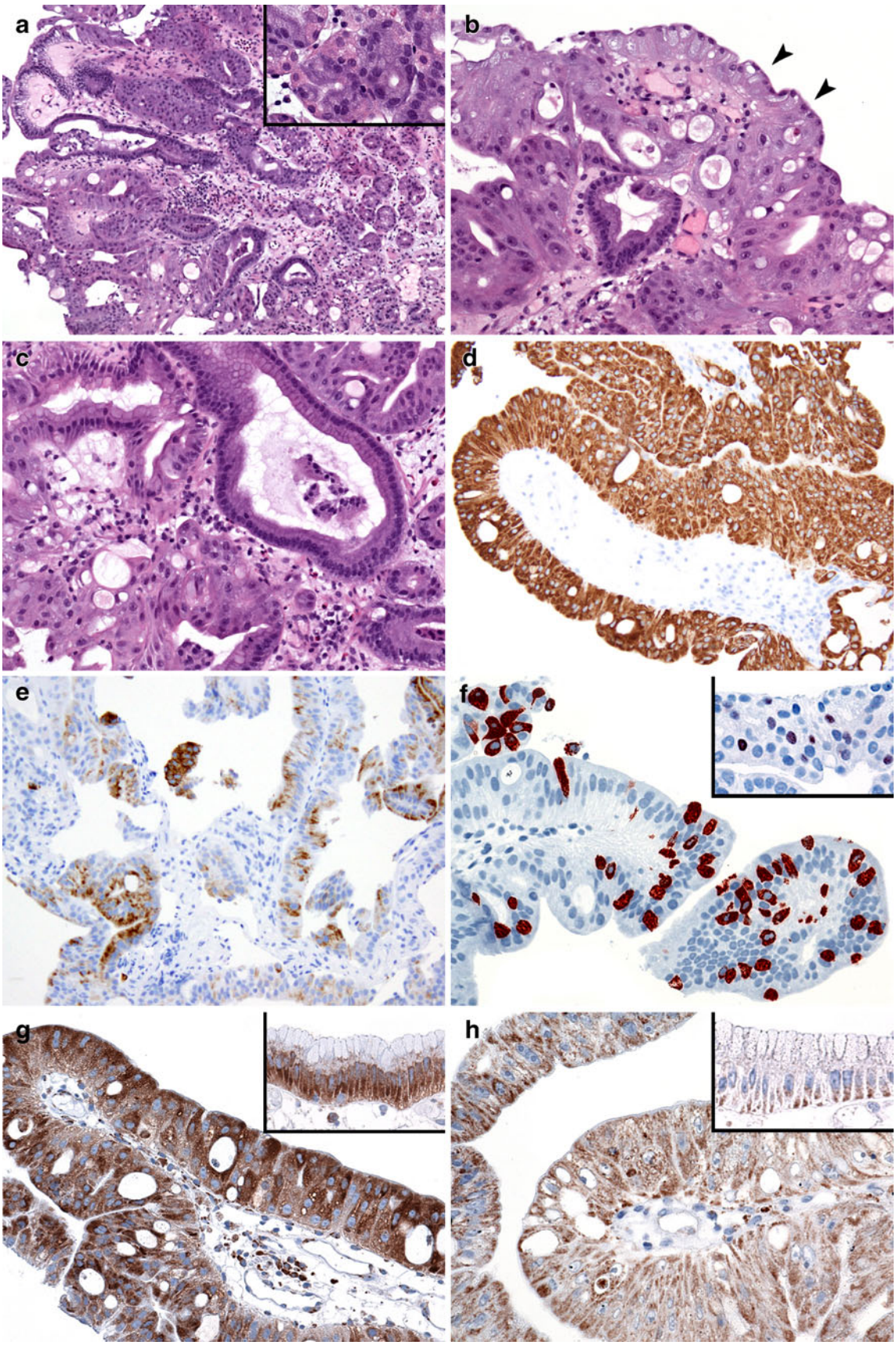
a
b
c
d
e
f
g
h

◀ **Fig. 1** Moderately differentiated adenocarcinoma of the duodenal bulb arising from heterotopic gastric mucosa (**a**, *inset*). Neoplastic columnar cells with ample eosinophilic cytoplasm and moderately atypical hyperchromatic nuclei arranged below the luminal cell membrane (**b**, *arrowheads*). Cribriform glands and invasion of cell clusters into the stroma (**c**). Gastric differentiation of carcinoma cells with extensive expression of MUC5AC (**d**) and focal expression of MUC 6 (**e**). Expression MUC2 (and CDX-2, *inset*) in single cells indicating focal intestinal differentiation (**f**). Accumulation of endoplasmic reticulum (**g**, anti-protein disulfide-isomerase, *inset* non-neoplastic mucosa for comparison) and mitochondria (**h**, *inset* non-neoplastic mucosa for comparison) in the cytoplasm of cancer cells

our case, no underlying tumour of pyloric gland type was found indicating different pathogenesis. The broadly eosinophilic cells with intracytoplasmic accumulation of both endoplasmic reticulum and mitochrondria as well as striking nuclear deviation to the luminal cell surface, as observed in our case, deserve special attention. They may represent a diagnostic clue of our lesion. However, suspected origin from parietal cells could not be proven.

In conclusion, the presented case illustrates the rare finding of an adenocarcinoma with gastric differentiation arising from heterotopic gastric mucosa in the duodenal bulb. To the best of our knowledge, no comparable case has been reported in the English literature before.

Conflict of interest statement We declare that we have no conflict of interest.

References

1. Mann NS, Mann SK, Rachut E (2000) Heterotopic gastric tissue in the duodenal bulb. J Clin Gastroenterol 30:303–306
2. Russin V, Krevsky B, Caroline DF, Tang CK, Ming SC (1986) Mixed hyperplastic and adenomatous polyp arising from ectopic gastric mucosa of the duodenum. Arch Pathol Lab Med 110:556–558
3. Kushima R, Rüthlein HJ, Stolte M, Bamba M, Hattori T, Borchard F (1999) 'Pyloric gland-type adenoma' arising in heterotopic gastric mucosa of the duodenum, with dysplastic progression of the gastric type. Virchows Arch 435:452–457
4. Vieth M, Kushima R, de Jonge JP, Borchard F, Oellig F, Stolte M (2005) Adenoma with gastric differentiation (so-called pyloric gland adenoma) in a heterotopic gastric corpus mucosa in the rectum. Virchows Arch 446:542–545
5. Chu PG, Schwarz RE, Lau SK, Yen Y, Weiss LM (2005) Immunohistochemical staining in the diagnosis of pancreatobiliary and ampulla of Vater adenocarcinoma: application of CDX2, CK17, MUC1, and MUC2. Am J Surg Pathol 29:359–367